

Lecture Notes in Civil Engineering

Moncef Nehdi · Mo Kim Hung ·
Katta Venkataramana · Jiji Antony ·
P. E. Kavitha · Beena B R *Editors*

Proceedings of SECON'23

Structural Engineering and Construction
Management

 Springer

Lecture Notes in Civil Engineering

Volume 381

Series Editors

Marco di Prisco, Politecnico di Milano, Milano, Italy

Sheng-Hong Chen, School of Water Resources and Hydropower Engineering,
Wuhan University, Wuhan, China

Ioannis Vayas, Institute of Steel Structures, National Technical University of
Athens, Athens, Greece

Sanjay Kumar Shukla, School of Engineering, Edith Cowan University, Joondalup,
WA, Australia

Anuj Sharma, Iowa State University, Ames, IA, USA

Nagesh Kumar, Department of Civil Engineering, Indian Institute of Science
Bangalore, Bengaluru, Karnataka, India

Chien Ming Wang, School of Civil Engineering, The University of Queensland,
Brisbane, QLD, Australia

Lecture Notes in Civil Engineering (LNCE) publishes the latest developments in Civil Engineering—quickly, informally and in top quality. Though original research reported in proceedings and post-proceedings represents the core of LNCE, edited volumes of exceptionally high quality and interest may also be considered for publication. Volumes published in LNCE embrace all aspects and subfields of, as well as new challenges in, Civil Engineering. Topics in the series include:

- Construction and Structural Mechanics
- Building Materials
- Concrete, Steel and Timber Structures
- Geotechnical Engineering
- Earthquake Engineering
- Coastal Engineering
- Ocean and Offshore Engineering; Ships and Floating Structures
- Hydraulics, Hydrology and Water Resources Engineering
- Environmental Engineering and Sustainability
- Structural Health and Monitoring
- Surveying and Geographical Information Systems
- Indoor Environments
- Transportation and Traffic
- Risk Analysis
- Safety and Security

To submit a proposal or request further information, please contact the appropriate Springer Editor:

- Pierpaolo Riva at pierpaolo.riva@springer.com (Europe and Americas);
- Swati Meherishi at swati.meherishi@springer.com (Asia—except China, Australia, and New Zealand);
- Wayne Hu at wayne.hu@springer.com (China).

All books in the series now indexed by Scopus and EI Compendex database!

Moncef Nehdi · Mo Kim Hung ·
Katta Venkataramana · Jiji Antony · P. E. Kavitha ·
Beena B R
Editors

Proceedings of SECON'23

Structural Engineering and Construction
Management

 Springer

Editors

Moncef Nehdi
Department of Civil Engineering
McMaster University
Hamilton, ON, Canada

Mo Kim Hung
Department of Civil Engineering
Universiti Malaya
Kuala Lumpur, Malaysia

Katta Venkataramana
Department of Civil Engineering
National Institute of Technology Karnataka
Mangalore, Karnataka, India

Jiji Antony
Department of Civil Engineering
Federal Institute of Science and Technology
Angamaly, Kerala, India

P. E. Kavitha
Department of Civil Engineering
Federal Institute of Science and Technology
Angamaly, Kerala, India

Beena B R
Department of Civil Engineering
Federal Institute of Science and Technology
Angamaly, Kerala, India

ISSN 2366-2557

ISSN 2366-2565 (electronic)

Lecture Notes in Civil Engineering

ISBN 978-3-031-39662-5

ISBN 978-3-031-39663-2 (eBook)

<https://doi.org/10.1007/978-3-031-39663-2>

© The Editor(s) (if applicable) and The Author(s), under exclusive license to Springer Nature Switzerland AG 2024

This work is subject to copyright. All rights are solely and exclusively licensed by the Publisher, whether the whole or part of the material is concerned, specifically the rights of translation, reprinting, reuse of illustrations, recitation, broadcasting, reproduction on microfilms or in any other physical way, and transmission or information storage and retrieval, electronic adaptation, computer software, or by similar or dissimilar methodology now known or hereafter developed.

The use of general descriptive names, registered names, trademarks, service marks, etc. in this publication does not imply, even in the absence of a specific statement, that such names are exempt from the relevant protective laws and regulations and therefore free for general use.

The publisher, the authors, and the editors are safe to assume that the advice and information in this book are believed to be true and accurate at the date of publication. Neither the publisher nor the authors or the editors give a warranty, expressed or implied, with respect to the material contained herein or for any errors or omissions that may have been made. The publisher remains neutral with regard to jurisdictional claims in published maps and institutional affiliations.

This Springer imprint is published by the registered company Springer Nature Switzerland AG
The registered company address is: Gewerbestrasse 11, 6330 Cham, Switzerland

Paper in this product is recyclable.

Preface

Quality and sustainability are two sides of the same coin, in which quality ensures the degree of excellence of a product and sustainability ensures the ability to maintain a process continuously over time. Hence, engineers are now educated to design facilities in the best possible way, with the least amount of waste and most effective use of resources for the entire life cycle while keeping the concept of sustainability in mind. Hence, the Seventh Annual Conference and the Fourth International Conference SECON'23 organised by the Department of Civil Engineering at the Federal Institute of Science and Technology (FISAT) in Kochi, India, in collaboration with the Indian Concrete Institute (ICI)—Kochi Chapter, the Institution of Engineers (India) (IEI)—Kochi Local Centre, the Indian Green Building Council (IGBC)—Cochin Centre, the Indian Society for Technical Education (ISTE), and the Builders Association of India (BAI)—Angamaly Centre focuses on the main theme “Quality and Sustainability in Construction Industry” as well as ten tracks that will examine breakthroughs and innovations in various fields of Civil Engineering.

Encouraging the participation of students, researchers, academicians, and industry professionals around the globe both in person or through online media the conference was held from 7 to 9 June 2023. The global-level acceptance of the conference was showcased by the participation of delegates from international and national universities. The quality of the conference is ensured at two levels: first during the acceptance of abstracts and second during the acceptance of full paper. From around 350 abstract submissions, 150 abstracts were shortlisted for full paper submission through the double-blind review process which were again screened at full paper submission stage. Finally, 89 papers were presented in the conference and are published in the Proceedings of SECON'23.

Keynote sessions by eminent speakers across the globe—Prof. Moncef L. Nehdi, Professor and Chair Department of Civil Engineering, McMaster University, Canada, Dr. Sharath S, Assistant Professor, Faculty of Engineering, Institute of Ocean Energy, Saga University, Japan, Prof. Mohammad Najafi, Director, Centre for Underground Infrastructure Research and Education, and Dr. Vinayak Kaushal, Assistant Professor of Instruction Department of Civil Engineering, the University of Texas at Arlington, Texas, USA, Dr. Albert Thomas, Assistant Professor, Department of

Civil Engineering, IIT Bombay, Dr. R Sathish Kumar, Professor and Dean School of Construction and Technology, NICMAR, Hyderabad, catalysed the glory of the conference.

On behalf of the organising committee of the conference, I express my heartfelt gratitude to the Chairman, governing body FISAT, Mr. Shimith P R, Principal, Dr. Manoj George, Head of the Department and General Convenor of the conference, Dr. Jiji Antony, core committee members Dr. Unni Kartha G, Dr. Kavitha P E, Dr. Asha Joseph, Ms. Rinu J Achison, Mr. Abin Thomas C A, Mr. Jawahar Saud S, and Mr. Sreerath S, conference advisory committee members, reviewers, authors, officials of various professional bodies, faculty members, and student volunteers of Department of Civil Engineering, FISAT for their whole hearted support for the success of the conference. Expressing my gratitude to everyone from the bottom of my heart.

Angamaly, India

Dr. Beena B R
Convenor-SECON'23

Contents

Effect of Supplementary Cementitious Materials on Properties of Self Compacting Concrete	1
Bharati Raj, Keerthy M. Simon, and Reshma Baburajan	
Landslide Susceptibility Evaluation and Hazard Zonation for Idukki district—A Case Study from Kerala, India	13
K. P. Aparna, R. N. Abhishek, T. Chaithra, M. Abhindev, and S. Jawahar Saud	
Risk Analysis in Bridge Construction	31
V. S. Fathima Nizwa, Reshma Kassim, and Sinu Philip	
Evaluation of Bituminous Concrete Using Ceramic Waste as a Filler	43
R. Adarsh, A. V. Arunkumar, Aswini Anil, K. Karthika Sreenivasan, K. K. Reshma, and Shreesh Ajaykumar	
A Case Study on the Shortage of Availability of Skilled Labour in Faridabad, Delhi—NCR	57
Ashutosh Kumar and Yaman Hooda	
An Evaluation of Road Network Vulnerability Using Geospatial Techniques	73
Cynthia Baby Daniel, Sreya Madhavan, Samson Mathew, and Subbarayan Saravanan	
Parametric Evaluation of Mechanical and Durability Properties of Graphene Concrete in Indian Context	87
Aditya Pratap Singh, Gaurav Chhokar, and Yaman Hooda	
Analysis of Causes and Effects of Critical Delay Factors in High Rise Building Projects of Kerala	103
Nilufer Noushad, S. Jawahar Saud, and Shamnas Neduvancheri	

Structural Behaviour of Square Steel Tubular Column with Deconstructable Splice Joint	117
V. G. Nehana and V. N. Krishnachandran	
Risk Assessment of Landslides During Reconstruction and Rehabilitation Phase at Iritty Taluk of Kannur District, Kerala	129
Keerthana Mohan and S. Jawahar Saud	
Environmental Sustainability Assessment of Rural Road Maintenance Using Environmental Impact Assessment Tool	145
RajiReddy Myakala and S. Shankar	
Damage Detection on Structure of Pinisi in Ship Launching Process	165
Andi Dirga Noegraha, Rudy Djamaluddin, Rita Irmawaty, and Ganding Sitepu	
Studies on Chemically Treated Rubber Tube as a Replacement for Coarse Aggregate in Concrete	177
S. Konda Reddy, R. Akhileswar Reddy, R. Subash, K. Govardhan Reddy, V. M. Bharath Nivas, S. Vanitha, and P. Karthigai Priya	
Progressive Collapse Response of Linked Column Braced Frame System	187
N. A. Fameela and R. Nikhil	
Parametric Study on Performance of Conical Shell Foundation Using FEM Modeling	197
M. K. Sheeja, T. Lamya, and Jerin Joseph	
Localized Corrosion Damage Study and Strengthening Strategies on Orthogonal Concrete Filled Steel Tubular Column	207
Drisya Dinesh and E. K. Amritha	
Study of Seismic Evaluation and Development of Innovative Curved Lateral Bracing System	221
C. S. Ansiya and E. K. Amritha	
Assessment of Structures with Floating Column on Sloping Ground Against Seismic Load	233
Yaman Hooda and Pradeep K. Goyal	
Seismic Performance Analysis of Masonry Building with Scrap Tyre Pad Isolators	243
Ancy Mathew, R. Sajeed, and M. Anandhakrishnan	

Mode Choice Modelling of Different Categories of Work Trips in Thiruvananthapuram City	251
S. Shaheem, Nisha Radhakrishnan, and Samson Mathew	
Innovative Plastic Hinge Relocation Technique in Steel Moment Connection	271
C. H. Farshad Ali and Sajan Jose	
Strength and Durability Properties of Steel Slag Incorporated Self-curing Concrete	283
Karthika Balakrishnan and Lalith Prakash Elavazhagan	
Numerical Modelling and Analysis of GGBS Mortar for Predicting Strength Parameters	295
V. Mohammed Zidan Sameer, C. Vyshakh, Geethu Elsa Thomas, and A. S. Sajith	
Study on Novel Multi-segment Replaceable Profiled Steel Shear Links	301
P. N. Nourin and Gouri S. Kumar	
Influence of Characteristics of Seismic Excitations on the Performance of Negative Stiffness and Inerter Based Systems for Apparent Weakening of Structures	311
Aayisha S. Ahamed, A. S. Sajith, and M. Azeem	
Influence of Characteristics of Ground Motions on the Behaviour of Diagrid Buildings	321
P. Rahul and A. S. Sajith	
Critical Success Factors for Post-flood Reconstruction in the Flood Affected Areas of Kerala	329
V. N. Sreelakshmi and R. Abhijith	
Experimental Investigation for Stabilization of Expansive Soil by Using Waste Materials—Eggshell Powder and Bagasse Ash	345
Moni Mishra, Ravino Mekro, Lensar Jamir, Marjom Ete, Taniya Oniya, and Ajanta Kalita	
Critical Success Factors for Sustainable Construction & Demolition Waste Management in Kochi City, Kerala	355
Hanna Salah and R. Abhijith	
Seismic Performance of Y-Braced Frame with Double Round Steel Tube	369
Fathima Manaf and Sajan Jose	
Comparative Study of Different Stabilizers for Peat Soil Stabilization: A Review	377
Torjit Elangbam and Ajanta Kalita	

Soil Stabilization Using Agro-industrial Waste	393
K. L. Anaslal, P. A. Gopika, Sneha S. Menon, and R. Sujana	
The Pozzolanic Effect of Rice Husk Ash on the California Bearing Ratio Behaviour of Arunachal Peat with Cement as Admixture	403
Nabam Jumsi and Ajanta Kalita	
Design and Modeling of a Precast Concrete Structure and Its Performance Evaluation with Conventional Structure	415
Akhil Mukundan, M. S. Anagha, Tania Thankam Mathew, Tom K. Bijoy, and Asha Devassykutty	
Wind-Induced Aerodynamic Effects on Multiple Side Setback Tall Buildings Using CFD Simulation	427
Amlan Kumar Bairagi and Sujit Kumar Dalui	
Utilization of Water Treatment Sludge as a Filler Material in Bituminous Mix Design	439
Shabnum Suhura, M. B. Syam Krishna, Sana Sudheer, A. A. Saniyamol, and K. S. Surya	
Effect of Steel Fibers in Drying Shrinkage Characteristics of Self-compacting Concrete	447
Ashika Martin and C. A. Abin Thomas	
Accessibility Analysis of Kochi Metro	457
Jeeva P. Winto, Amrutha S. Chandran, Namitha Dilip, and Sandra Shyin	
Study of Seismic Behaviour of Bent Shear Panel Dampers in Braced Steel Moment Resistant Frame	477
Aishwarya Shine and P. Anima	
Experimental Investigation on Plastic Shrinkage Characteristics of Self-compacting Concrete with Mineral Admixtures and Steel Fibers	489
V. S. Abhirami and C. A. Abin Thomas	
Study of Concrete Imperfections in T Shaped Multi-cell Composite Column	499
Akshay Murali and P. Anima	
Comparative Assessment of Geocell and Geogrid Reinforcement for Flexible Pavement: Numerical Parametric Study	515
Anjana R. Menon and Anjana Bhasi	
Experimental Study of the Shear Performance of a Beam Strengthened with Jute and Glass Fiber Hybrid Composite	525
C. S. Reshma and Jency Sara Kurian	

Numerical Analysis on Flexural Strength of Composite Slab with Inverted U-Shaped Shear Connector 539
 S. Niranjana and Milu Mary Jacob

Sustainable Transportation Indicators for Urban Areas: A Systematic Review 549
 Abdelrahman M. Farouk, Liyana Mohamed Yusof, Rahimi A. Rahman, and Azlina Ismail

Trust Issues in BIM-Based Construction Projects: A Systematic Literature Review 559
 Yusra Nur Qamarina Yushasman, Ahmad Rizal, Yong Siang Lee, and Rahimi A. Rahman

Analysis of Lateral Load Resistance of a Structural System Using Finite Element Method 567
 Sumayya Jamal, Beena Mary John, and Rajesh P. Nair

Analysis of Reinforced Concrete Structure Subjected to Blast Loads Without and with Carbon Fibres 577
 Yogeswaran Palani and R. Raghunandan Kumar

Numerical Investigation on Shear Bond Improvement of High Performance Concrete Composite Slabs Containing Recycled Aggregates 601
 B. Athulya and Milu Mary Jacob

Factors Leading to Cost Overrun and Time Overrun in Pune Metro Project 609
 V. D. Mahind and B. M. Dawari

Experimental Study on the Optimum Design and Performance of Porous Concrete with Partial Replacement of Cement with Glass Powder 619
 Mohit Yadav, Bhupender Khatana, and Haobam Derit Singh

Exploring the Perceptions of 3D Printing Through the Technology Acceptance Model (TAM) Lens 627
 Mayur Naik, Rahul Sheshadri, Tejesh Varma, Divya Jyoti, Deepansh Ade, Vaibhav Bhalme, and Vijayeta Malla

Ductility Enhancement by Incorporating Slits on Shear Resisting Frame with Haunched Beams 637
 Sarath Paul and S. P. Deepu

BIM Application for the Materials in Roadway Construction 647
 S. S. Kande and B. M. Dawari

Study on the Mechanical Properties of Glass Fibre Reinforced Aerated Concrete with Aluminium Powder as Aerating Agent	657
Nisanth Manoj, M. Gayathri Devi, and Lavanyaprakash	
Seismic Vulnerability Assessment of Baffled Elevated Water Tank with Fluid–Structure–Soil Interaction Having Variable Staging Pattern	667
T. Shahana and S. P. Deepu	
Benchmarking Existing Fire Safety Norms for Urban Villages in Noida with Best Practices	677
Prerna Sharma, Ritabrata Ghosh, Sanjay Tomar, and Amit Kumar Jaglan	
Investigating the Effects of Steel Fibre and Basalt Fibres on the Mechanical Properties of Hybrid Fibre-Reinforced High-Performance Concrete	687
Parvathy Subrahmaniam and P. Seena	
Sewage Sludge and Red Mud as Brick Materials	699
Divya S Lal and Jeena B Edayadiyil	
Experimental Evaluation of Structural Properties of Circular Scrap Tyre Pad (CSTP) Base Isolator	711
M. Anandhakrishnan, Asif Basheer, and Ancy Mathew	
Re-assessment of Existing Offshore Platform for Life Extension	723
Shikha Singh and Rajan Singh	
Mechanical Properties and Micro Structure of Graphene Oxide (GO) Cement Composites: A Review	737
S. Arya and P. Seena	
Engineering Properties of Geopolymer Concrete Incorporating Fly Ash and Clay	747
Sreedevi Lekshmi, J. Sudhakumar, and Khruvelu	
A Strategy Plan for Innovative and Sustainable Construction in Emerging Nations: A Case of India	755
Manisha Paul and Amit Kumar Jaglan	
Behaviour of SFRC Filled Cold Formed Steel Built-Up Columns	769
Nanda S. Gopan and Ajai Thampy	
Experimental Investigation on Mechanical Properties of Hybrid Polypropylene-Steel Fiber-Reinforced GGBS Mortar	779
Geethu Elsa Thomas, A. S. Sajith, and P. V. Indira	
Spatial Analysis and Comparative Study of Noise Pollution at Ernakulam City Before and During COVID-19 Using GIS	789
Meera Varghese and A. H. Amalpriya	

Sustainable Pervious Pavement Block with 3D Printed PETG Frame 811
 Keerthana Ranjith and M. V. Varkey

Experimental Study on Properties and Performance of Fibre Roofing Tile 823
 Mariamol Kuriakose, Arju M. Tomy, Ajay Emmanuel, Alwin Biju, and Roshan Benny

Studies on Seismic Performance of RC Framed Buildings Using Pseudo-optimization Method 835
 G. Priyusha, C. Shreyasvi, and K. Venkataramana

Assessing the Predictability in Rainfall Time Series—A Case Study in Wisconsin Basin 849
 P. Saravanan and C. Sivapragasam

Numerical Investigation on the Behaviour of Horizontally Curved Steel Box Girder Under Patch Loading 863
 S. P. Fathima and M. S. Ajith

Prediction of Shear Strength of Beam-Column Joint with Glass Fiber Reinforced Polymer Bars Using Response Surface Methodology 873
 Regalla Tejaswi and Greegar George

Environmental Assessment of Admixtures and Stone Powder in Cement Concrete 885
 Kiran Devi, Amit Kumar, Babita Saini, and Paratibha Aggarwal

Evaluation of Disputes in Kerala Construction Industry 893
 U. A. Devangana and Anu V. Thomas

Investigating the Characteristics of Bitumen Treated with Textile Pyrolysis Oil 907
 Yugaj G. Chaudhari, Saurabh E. Shinde, and Namdao A. Hedao

Adaptive Neuro-Fuzzy Systems and Ensemble Methods in Joint Shear Prediction and Sensitivity Analysis 917
 Shruti Shekhar Palkar and T. Palanisamy

Technology Landscape for BIM in Construction Site Safety Management 931
 Hire Shalaka, Sandbhor Sayali, and Ruikar Kirti

Numerical Analysis of Floor to Column Pounding in Series 945
 C. K. Fathima Hassan and C. Nijesh

Nonlinear Finite Element Modelling of Prestressed Concrete Railway Sleeper Using ABAQUS 955
 Kamble Yash Vijay and Greegar George

A Machine Learning Based Model to Assess Flexural Strength of Corroded Reinforced Concrete Beams	965
Arjun Sharma, Somain Sharma, and Kuldeep Kumar	
Numerical Investigation on the Behaviour of Blind-Bolted Steel Beam to CFST Column Connections	979
K. Aparna and K. N. Rajesh	
Numerical Investigation on the Behavior of Bent Shear Panel Damper on Eccentrically Braced Composite Frames	989
Reshma and K. N. Rajesh	
Effect of Length of Free Ends of Flamingo Shear Reinforcing Technique on Shear Capacity of Reinforced Concrete	1001
Asmaa Shaker Mahmood, Suhad M. Abd, and Hadee Mohammed Najm	
Effect of Ultrafine Materials on Drying Shrinkage of Concrete	1013
Jerison Scariah James, Jibin Joy Ponnappal, Aiswarya Jayan, and Elson John	
Effects of Vertical Irregularities on Seismic Response and Vulnerability of RCC Framed Structure	1027
Mohd Ubaid and Rehan Ahmad Khan	
Experimental Investigation on Microstructure-Based Quality Assessment of TMT Reinforcing Bars	1045
Ansa Varghese and Bino I. Koshy	
BaFNet: A Soil Erosion Control Net Using Banana Pseudo-stem Fibers	1055
Rolando Bitagun Jr., Angelo Lui Agustin, Noel Frederick Figueroa, Vaneza Lapangan, Princess Anne Layugan, Lester Ramirez, Marc Aeron Reyes, Frances Lorane Calapini, and Ertie Abana	
Characterisation of Pyro-oil Modified EVA and SBS Bitumen Using Variation in MSCR Test	1065
N. T. Bhagat, N. A. Hedao, and M. S. Ranadive	

Effect of Supplementary Cementitious Materials on Properties of Self Compacting Concrete



Bharati Raj, Keerthy M. Simon, and Reshma Baburajan

Abstract To avoid various environmental issues, supplementary cementitious materials (SCM) such as metakaolin, limestone powder, silica fume, rice husk ash, fly ash, ground granulated blast furnace slag (GGBS), marble powder and chalk powder are added to self compacting concrete (SCC). This paper attempts to review the effect of these SCMs have on rheological, mechanical and durability characteristics of SCC. The review shows that different SCMs have varied effects on SCC properties. Silica fume, rice husk ash and metakaolin reduce workability but improve mechanical and durability properties. Fly ash, marble powder, limestone powder require less amount of superplasticizer when compared to GGBS, chalk powder and rice husk ash. It can also be seen that the addition of mineral admixtures in optimum quantity helps to improve the packing density of SCC particles resulting in best performance in both fresh and hardened state.

Keywords Self compacting concrete · Supplementary cementitious materials · Compressive strength · Rheology · Workability

1 Introduction

Self compacting concrete (SCC) is a special concrete developed by Professor Okamura [1] in Japan. SCC is highly flowable, non-segregating concrete that fills uniformly and completely every corner of formwork by its own weight and encapsulates reinforcement without any vibration, whilst maintaining homogeneity. As

B. Raj · K. M. Simon · R. Baburajan (✉)
Department of Civil Engineering, N.S.S. College of Engineering, Palakkad, Kerala, India
e-mail: reshma211999@gmail.com

B. Raj
e-mail: bharatiraj@nssce.ac.in

K. M. Simon
e-mail: keerthysimon@nssce.ac.in

per EFNARC, SCC has been described as “the most revolutionary development in concrete construction for several decades” [2].

The amount of cement and superplasticizer (SP) dosage in SCC is very high compared to normal concrete. According to IS 10262: 2019, SCC should have characteristics like filling ability, passing ability, segregation resistance and viscosity [3]. These can be achieved by various methods which include lowering aggregate content, lowering water cement ratio, addition of mineral admixtures and SP etc.

Many research works are conducted in SCC mainly to improve its properties. This includes addition of air entraining agents, mineral admixtures, waste materials has fine and coarse aggregates, different SP dosages and mixing time. Addition of air entraining agents helps to improve freeze- thaw resistance of concrete in extreme weather condition, improve plasticity and minimize bleeding of concrete [4]. But it also leads to decrease in compressive strength of SCC mix [5].

Waste materials are used to replace aggregates and cement in SCC to improve its properties. Addition of waste marble powder and granite powder in SCC as replacement to cement leads to decreased permeability but increases carbonation depth [3]. Jain et al. uses waste granite powder as partial replacement of fine aggregate in fly ash blend SCC. By comparing the results it can conclude that in normal SCC upto 40% replacement of fine aggregate gives the best result. In fly ash blend mixture, increase in resistance against chloride, carbonation and corrosion can be obtained by 50% replacement of fine aggregate by granite powder [6]. Tomar et al. replaced fine aggregate by waste marble powder in SCC and it was found that its incorporation leads to increase in workability, best results were produced when 30% replacement [7].

As per Almalki et al. [8] increasing mixing time leads to loss of workability but increases bleeding and segregation resistance by 44% and 54% respectively for constant SP dosage of 1.5% [8]. According to de Souza et al. [9] flowability and strength characteristics are opposite when recycled aggregates are used. Also use of recycled or waste aggregate tends to increase SP dosage [10]. There are wide ranges of SCM that can be used in SCC and each one has different effect on different properties of SCC. Also combining different SCM in a single mix tends to counteract the negative effect it has on properties when they are used individually.

2 Enhancement of Properties of SCC by SCMs

SCM or mineral admixtures helps to improve the properties of SCC upto a certain percentages that are found by conducting various experiments. SCM through pozzolanic or hydraulic reactions enhances strength characteristics of SCC. Different SCM has different impacts on properties of SCC. commonly used SCM includes flyash (FA), silica fume (SF), ground granulated blast furnace slag (GGBS), metakaolin (MK), agricultural ash, marble powder (MP), limestone powder (LP), etc. Agricultural ash includes rice husk ash (RHA) and sugarcane bagasse ash.

2.1 Fly Ash (FA)

Fly ash is finely divided residue obtained from the combustion of coal and is collected using electrostatic precipitator. Flyash are most commonly used SCM in SCC. According to Kurt et al. [11], 30% replacement of cement by fly ash class F (FAF) increases workability. FA can potentially enhance the self-compatibility of fresh concrete by enhancing the flowability of the concrete and encouraging the pozzolanic reaction [12]. It reduces the friction between mortar and coarse aggregate since they act as a lubricant due to its spherical shape [4, 13].

FA also helps to increase strength of SCC. FA does account for long term strength rather than early strength gain like SF since pozzolanic reaction is slow process. Calcium hydroxide produced from the reaction between cement and water reacts with flyash to form calcium silicate hydrate, thus leading to improve strength of concrete. Hence presence of water should be present for long time leading to increased curing period. However use of FA reduces the stability of entrained air content in SCC. FA was found to increase the amount of large entrained air bubbles and due to its shape it causes unification and thus escapes of entrained air bubbles. Table 1 shows the effect of FA when used in SCC. Therefore, with a high volume of FA, a high-strength yet cost-effective SCC can be developed. FA increases fresh, mechanical and durability properties of SCC.

2.2 Silica Fume (SF)

Silica fume (SF) is an artificial pozzolans also known as microsilica or condensed silica. It is obtained as a byproduct from manufacturing of silicon or ferrosilicon alloy. SF is extremely fine spherical particles, finer than cement particles. Table 2 summarizes various research works done on SF.

SF has highest reactivity than any other SCMs. Based on amount of calcium hydroxide consumed for the formation CSH gel, the pozzolanic potential of SCMs were SF > FA > GGBS [20]. Contribution of SF to increase strength of SCC is less. They mainly plays role in improving microstructure properties due to fine size. SF blended SCC have dense packing since it act has pore filler. SF generally helps in early strength gain and stability of Interfacial Transition Zone (ITZ).

SF also helps to improve resistance to segregation and bleeding of fresh concrete. SF has the highest water demand than any other SCM. Hence the dosage of Superplasticizer is high. Also SF tends to decrease workability of SCC. This is mainly due to its high surface area.

Table 1 Properties of SCC incorporating FA

References	SCM used (replacement ratio in %)		Replacement ratio (%)		Remark
	Binary	Ternary	Binary	Ternary	
Ahari et al. [14]	FAF, FAC (4, 8, 12, 36)	GGBS (18)	4, 8, 12, 36	18	FAC needs higher amount of SP whereas FAF reduces SP dosage. Also FAF reduces V-funnel flow time and increases viscosity. GGBS addition improves plastic viscosity
Karthik et al. [15]	FAF (10, 15, 20, 25, 30)	SF (5, 7.5, 10)	10, 15, 20, 25, 30	5, 7.5, 10	FAF helps to reduce pH, and increases segregation and sulphate resistance Best mix—70% OPC + 20% FA + 10% SF
Duran-Herrera et al. [16]	FAF (15–60)	LP (0.5, 10, 15)	15–60	0.5, 10, 15	FAF increases setting time, consistency and entrapped air (9–10%). FAF decreases drying shrinkage and compressive strength. Reduction in compressive strength is counteracting by addition of limestone powder
Puthipad et al. [17]	FAF (107, 267 kg/m ³)		107, 267 kg/m ³		Increases flowability, encourage pozzolanic reactions and reduces friction
Kurt et al. [11]	FAF (20, 30, 40)		20, 30, 40		Improves fresh property of SCC. Decreases loss of workability

2.3 Ground Granulated Blast Furnace Slag (GGBS)

Ground Granulated Blast furnace Slag (GGBS), is a non-metallic industrial by-product formed by mixing impurities from iron ore with limestone, dolomite, and coal ash during the manufacture of pig iron [9]. Dadsetan and Bai [12] conducted experiments on SCC with GGBS as SCM and concluded that 20% replacement gives the best result [21].

Addition of GGBS in SCC improves workability, long-term strength and decreases heat of hydration, water demand, and permeability. It also improves durability to thermal cracks, resistance to sulphate and chloride attacks. But GGBS tends to reduce viscosity which can be found by decreased V—funnel flow time. Also superplasticizer dosage is increased. Table 3 shows various works done on GGBS as an SCM in SCC.

Table 2 Properties of SCC incorporating SF

References	SCM used		Replacement ratio (%)		Remark
	Binary	Ternary	Binary	Ternary	
Ahari et al. [14]	FAF, FAC, SF	GGBS	4, 8, 12, 36	18	SF needs higher amount of superplasticizer. SF has low plastic viscosity, reduce V funnel time. Increase in yield stress
Karthik et al. [15]	FAF	SF	10, 15, 20, 25, 30	5, 7.5, 10	Increases compressive strength, resistance to segregation, sulphate attack, chloride attack Best mix—70% OPC + 20% FA + 10% SF
Choudhary et al. [18]	MP	SF	10, 15, 20, 25, 30	5	Addition of 5% of SF in 20% of MP increases compressive strength
Benli et al. [19]	SF	FA	6, 9, 12, 15	10, 20, 30	Addition of SF increases compressive strength increase in SF helps to reduce viscosity

Table 3 Properties of SCC incorporating GGBS

References	SCM used		Replacement ratio (%)		Remark
	Binary	Ternary	Binary	Ternary	
Ahari et al. [14]	FAF, FAC, SF	GGBS	4, 8, 12, 36	18	GGBS reduce V funnel flow. Ternary systems containing 18% of GGBS shows decrease in plasticity viscosity
Dadsetan and Bai [12]	MK, FAF, GGBS		0, 20, 30		GGBS needs higher dosage of SP. Increase in compressive strength

2.4 *Metakaolin (MK)*

Metakaolin (MK) is an ultrafine pozzolan, produced by the calcination of purified kaolinite clay at moderately high temperatures of 650 to 800 °C. MK contains 50–55% silica and 40–45% Alumina. Table 4 gives summaries of works done in SCC with MK. Replacement of about 10% of RHA with cement in SCC gives an economical mix design with good fresh, mechanical and durability properties. Addition of FA and MK in self curing concrete increases its strength by 20% [4]. Rojo-López et al. [21], found that SCC with high replacement level of MK with water to binder ratio 0.45 and 0.4 gains highest strength among GGBS and FA [22].

MK shows early strength gain in SCC mainly due to its quick pozzolanic reactions, which in turn is due to higher percentage of silicon. Thus addition of MK in SCC increases compressive strength, resistance to sulphate and chloride ion attack. They also help to reduce permeability since water absorption and porosity get decreased by 46% and 45% respectively by pozzolanic reaction thus filling the voids leading to dense packing [23]. Increase in MK causes increase in water absorption due to high surface area, lower fineness modulus leading to subsequent increase in water demand. But addition of MK leads to reduced workability thus increasing the dosage of SP.

2.5 *Rice Husk Ash (RHA)*

Rice Husk Ash (RHA), a very fine pozzolanic material, is the most flexible eco-friendly SCM for concrete when combined with cement [4]. For using RHA as SCM it should be properly burned so that it has high amount of SiO₂. RHA is a widely used SCM in both concrete and SCC mainly due to its contribution to high strength and high permeability.

There is increase in compressive strength of SCC when cement is replaced with RHA. This is due to pozzolanic activity and microfilling ability of RHA. Table 5 summarizes various research works done on RHA as SCM in SCC. Chopra et al. [24], found that 15% of RHA replacement has positive effect on all properties of SCC [25]. It was found that compressive strength increases by 25% at 7 day, 33% at 28 day and 36% strength at 56 day. Similar increase in split tensile strength was also found. It is also found that RHA helps to increase resistance to sulphate and chloride ion penetration, reduces heat of hydration and permeability. Addition of RHA decreases workability since they are finer than cement particles. Finer particles have high surface area hence, amount of water absorbed get increases leading to decrease in quantity of free water in mortar.

Table 4 Properties of SCC incorporating MK

References	SCM used		Replacement ratio (%)		Remark
	Binary	Ternary	Binary	Ternary	
Ahari et al. [14]	MK	GGBS	4, 8, 12, 36	18	MK needs higher amount of superplasticizer. Plasticity viscosity highest for MK (highest 36%). Yield stress increases with addition of MK
Rojo-López et al. [21]	LP	MK	25	15	SCC containing only limestone powder decreases yield stress and plastic viscosity. Addition of MK with limestone powder increase rheological properties but decrease in mechanical properties
Gill et al. [23]	MK		5, 10, 15		Fine aggregate replaced by RHA by 10%. Decreases workability but increase in compressive strength by 27% at 28 day Best mix 10% MK and 10% RHA
Dadsetan and Bai [12]	MK, FAF, GGBS		20, 30		MK and GGBS increases SP dosage FA decreases SP dosage

2.6 Marble Powder (MP)

Marble is a metamorphic rock that is industrially processed and used for decorative purposes. In marble quarries, 20–30% of marble blocks become waste marble powder. MP is used both as SCM and as fine aggregate. When MP is used as fine aggregate, optimum quantity is found to be 10%. Table 6 summarizes various research works done on MP as SCM in SCC.

Table 5 Properties of SCC incorporating RHA

References	SCM used		Replacement ratio (%)		Remark
	Binary	Ternary	Binary	Ternary	
Gill et al. [23]	RHA	MK	30	20	RHA improves viscosity, decrease bleeding, high compressive strength, increases electrical resistivity and highest carbonation depth
Raisi et al. [10]	RHA		5, 10, 15, 20		RHA decreases workability, requires more SP amount (>20%) Splitting tensile strength, compressive strength, modulus of elasticity increases with increase in w/b ratio by keeping 10% RHA
Chopra et al. [24]	RHA		10, 15, 20		Workability & chloride ion penetration decreases with increase in RHA (lowest for 20% RHA). Optimum percent of RHA 15%. Reduces chloride ion penetration and porosity

According to Tomar et al. [7], 30% of replacement of cement with MP improves properties of SCC [7]. According to Choudhary et al. [18], 5% SF and 20% MP is an economical SCC mix [24]. Marble powder improves flowability of SCC mainly due to lower density of MP, which increases paste volume, and reduces the friction between aggregates. MP helps to reduce water content and dosage of SP needed for the mix. From various research papers it was found that by increasing the percentage of MP in SCC, passing ability can be increased. It was found that SCC with 20% MP replacement shows highest workability whereas SCC mix with 10% MP replacement shows maximum compressive strength. Thus it can be concluded that by increasing the percentage replacement of MP in SCC increases workability and segregation resistance but decreases compressive strength.

2.7 Limestone Powder (LP)

Limestone powder (LP) is a emerging non-pozzolanic material that are mainly used as fine aggregates. Limestone powder has been widely used in cement-based materials; and reportedly, can influence their properties by filler, nucleation, dilution and chemical effects [28]. Table 7 shows findings on properties of SCC with LP as SCM.

Table 6 Properties of SCC incorporating MP

References	SCMs used		Replacement (%)		Remarks
	Binary	Ternary	Binary	Ternary	
Choudhary et al. [18]	MP	SF	10, 15, 20, 25, 30	5	Addition of 5% of SF in 20% of MP increases compressive strength. Max workability—20%. MP decreases admixture dosage
Ali et al. [26]	MP	Polypropylene (PP) fibers	4, 8, 12, 16	0.1, 0.2, 0.3, 0.4	MP improves flowability and cohesiveness. Optimum amount of PP fiber—0.30%. max split tensile strength
Djebri et al. [27]	MP		10, 20, 30		Mix with 30% MP only gives workability of reference SCC. Helps in reduction of water content thus dosage of SP. improve segregation resistance. Increase in replacement and w/c decrease compressive, tensile strength
Tomar et al. [7]	MP		10, 20, 30, 40, 50		With the increment in the dose of waste marble powder, the workability of SCC is increased Optimum—30%

Recently limestone powder has been used as SCM since it increases properties of concrete, decreases cost of concrete preparation. Zhu et al. [29], conducted experiments on SCC with LP as SCM concludes that LP can be used as a replacement of cement up to 55% [29]. Addition of LP as SCM leads to improved rate of cement hydration and early strength development. LP does not show increase in compressive strength with time. SCC mixes with LP shows good surface finish, improved particle packing and water retention in fresh mixes. As the fineness of LP increases strength of SCC mixes also get increased [29]. But it increases shrinkage deformation and creep due to high paste volume. Also there is significant reduction in plastic viscosity and yield stress.

Table 7 Properties of SCC incorporating LP

References	SCM used		Replacement ratio (%)		Remark
	Binary	Ternary	Binary	Ternary	
Rojo-López et al. [21]	LP	MK	25	15	SCC containing only limestone powder decreases yield stress and plastic viscosity. Addition of MK with limestone powder increase rheological properties but decrease in mechanical properties. Ternary blended mix shows increase in durability
Zhu et al. [29]	LP, CP		55, 44, 25		Increase in compressive strength by 10–15 MPa. Finer powder give higher compressive strength
Dadsetan et al. [25]	LP		40, 80 kg/m ³		Imestone powder decreases porosity and increases resistance to chloride ion penetration, electrical resistivity

2.8 Chalk Powder

Chalk powder (CP) is an emerging non-pozzolanic SCM. Research work on CP as SCM is less. They have wide availability in educational institutions where it causes many health issues to the users. CP is a soft earthly variety of calcium carbonate that contains small amounts of silica, alumina and magnesia. As per the experiments done by Zhu et al. [29], it can be concluded that compressive strength of SCC blended with CP does not depend on its particle size [29]. Also it can be found 55% of CP in SCC mix shows highest compressive strength. CP needs higher percentage of SP when compared with SP dosage of LP blended SCC.

3 Conclusions

The following points can be concluded from previous research papers on effect of SCMs on properties of self compactability concrete.

- (1) All the SCM helps to decrease the amount of cement in traditional SCC mixes without sacrificing its requirements.
- (2) Replacement ratio of different SCM as per various experiments can be concluded as follows:

Fly ash (class F)—30%
Silica fume—12.5%
Metakaolin—10%
GGBS—20%
Rice husk ash—15%
Marble powder—20%
Limestone powder—55%

- (3) Blending of SCMs to form ternary and quaternary SCC mixes is an option to improve the properties as well as to make up for the negative effect caused by one SCM on the mix properties. For example 10% MK + 10% RHA shows increase in compressive strength by 20 MPa when compared with normal SCC mixes at 0.4 w/b ratios.

References

1. Okamura H, Ouchi M (2003) Self-compacting concrete. *J Adv Concr Technol* 1(1):5–15
2. IS 10262: 2019, Concrete mix proportioning—guidelines
3. Pereira MML, Capuzzo VMS, de Melo Lameiras R (2022) Evaluation of use of marble and granite cutting waste to the production of self-compacting concrete. *Constr Build Mater* 345:128261
4. Meko B, Ighalo JO, Ofuyatan OM (2021) Enhancement of self-compactability of fresh self-compacting concrete: a review. *Clean Mater* 1:100019
5. Attachaiyawuth A, Ouchi M (2014) Effect of entrained air on mitigation of reduction in interaction between coarse aggregate and mortar during deformation of self-compacting concrete at fresh state. *Proceeding of the Japan Concrete Institute, JCI* 36(1):1444–1449
6. Jain A, Choudhary S, Gupta R, Chaudhary S, Gautam L (2022) Effect of granite industry waste addition on durability properties of fly ash blended self-compacting concrete. *Constr Build Mater* 340:127727
7. Tomar AK, Kumar A (2018) Strength characteristics of self-compacting concrete partially replaced with waste marble powder. *J. Environ. Nanotechnol* 7(4):46–50
8. Almalki A, Zeyad AM (2020) Influence of mixing time and superplasticizer dosage on self-consolidating concrete properties. *J Market Res* 9(3):6101–6115
9. de Souza AM, de Carvalho JMF, Santos CFR, Ferreira FA, Pedroti LG, Peixoto RAF (2022) On the strategies to improve the eco-efficiency of self-compacting concrete using industrial waste: an analytical review. *Constr Build Mater* 347:128634
10. Raisi EM, Amiri JV, Davoodi MR (2018) Mechanical performance of self-compacting concrete incorporating rice husk ash. *Constr Build Mater* 177:148–157
11. Kurt M, Aydin AC, Gül MS, Gül R, Kotan T (2015) The effect of fly ash to self-compactability of pumice aggregate lightweight concrete. *Sadhana* 40:1343–1359
12. Dadsetan S, Bai J (2017) Mechanical and microstructural properties of self-compacting concrete blended with metakaolin, ground granulated blast-furnace slag and fly ash. *Constr Build Mater* 146:658–667
13. Kapoor K, Kumar S, Singh SP, Singh P, Sharma V (2022) A review on the properties of natural and recycled coarse aggregates concrete made with different coal ashes. *Clean Mater* 5:100109
14. Ahari RS, Erdem TK, Ramyar K (2015) Effect of various supplementary cementitious materials on rheological properties of self-consolidating concrete. *Constr Build Mater* 75:89–98

15. Karthik DK, Nirmalkumar K, Priyadarshini R (2021) Characteristic assessment of self-compacting concrete with supplementary cementitious materials. *Constr Build Mater* 297:123845
16. Duran-Herrera A, De-León-Esquivel J, Bentz DP, Valdez-Tamez P (2019) Self-compacting concretes using fly ash and fine limestone powder: shrinkage and surface electrical resistivity of equivalent mortars. *Constr Build Mater* 199:50–62
17. Puthipad N, Ouchi M, Attachaiyawuth A (2018) Effects of fly ash, mixing procedure and type of air-entraining agent on coalescence of entrained air bubbles in mortar of self-compacting concrete at fresh state. *Constr Build Mater* 180:437–444
18. Choudhary R, Jain A, Gupta R (2019) Utilization of waste marble powder and silica fume in self-compacting concrete. *UKIERI*, 184–194
19. Benli A, Karataş M, Gurses E (2017) Effect of sea water and $MgSO_4$ solution on the mechanical properties and durability of self-compacting mortars with fly ash/silica fume. *Constr Build Mater* 146:464–474
20. Suprakash AS, Karthiyaini S, Shanmugasundaram M (2021) Future and scope for development of calcium and silica rich supplementary blends on properties of self-compacting concrete: a comparative review. *J Market Res* 15:5662–5681
21. Rojo-López G, González-Fonteboa B, Martínez-Abella F, González-Taboada I (2022) Rheology, durability, and mechanical performance of sustainable self-compacting concrete with metakaolin and limestone filler. *Case Stud Constr Mater* 17:e01143
22. Nguyen HA, Chang TP, Shih JY, Djayaprabha HS (2018) Enhancement of low-cement self-compacting concrete with dolomite powder. *Constr Build Mater* 161:539–546
23. Gill AS, Siddique R (2018) Durability properties of self-compacting concrete incorporating metakaolin and rice husk ash. *Constr Build Mater* 176:323–332
24. Chopra D, Siddique R (2015) Strength, permeability and microstructure of self-compacting concrete containing rice husk ash. *Biosys Eng* 130:72–80
25. Dadsetan S, Shadkam HR, Sanchez LF, Tadayon M, Zakeri JA (2017) An investigation of the effects of limestone powder and Viscosity Modifying Agent in durability related parameters of self-consolidating concrete. *Constr Build Mater* 156:152–160
26. Ali A, Hussain Z, Akbar M, Elahi A, Bhatti S, Imran M, Leslie Ndam N (2022) Influence of marble powder and polypropylene fibers on the strength and durability properties of self-compacting concrete (SCC). *Adv Mater Sci Eng*, 1–12
27. Djebri N, Rahmouni ZE, Belagraa L (2017) Experimental investigation on the effect of marble powder on the performance of self-compacting concrete (SCC). *Mining Science* 24:183–194
28. Wang D, Shi C, Farzadnia N, Shi Z, Jia H, Ou Z (2018) A review on use of limestone powder in cement-based materials: mechanism, hydration and microstructures. *Constr Build Mater* 181:659–672
29. Zhu W, Gibbs JC (2005) Use of different limestone and chalk powders in self-compacting concrete. *Cem Concr Res* 35(8):1457–1462

Landslide Susceptibility Evaluation and Hazard Zonation for Idukki district—A Case Study from Kerala, India



K. P. Aparna, R. N. Abhishek, T. Chaithra, M. Abhindev,
and S. Jawahar Saud

Abstract Landslides are more common than any other geological phenomenon throughout the planet. Landslides are generally caused by geological and geomorphological processes that shape the local landscape. Previous research has found that the frequency and amplitude of landslides are increasing in many hilly or mountainous locations due to constant disruption by human activities such as urbanization, agricultural expansion, deforestation, clear-cutting, shifting agriculture, and inadequate road construction. As a result, both the internal and external factors are expected to increase the frequency, size, and volume of landslides. Furthermore, landslides are occurring more frequently and with greater intensity as a result of climate extremes in sensitive mountainous or hilly areas. It is critical to understand how the geographic distribution, frequency, amplitude, and volume of landslides affect the surrounding terrain. The significance of landslides and their effects on the natural environment is often neglected. This study investigates numerous landslides, mitigation techniques, and practical solutions for Idukki's most vulnerable regions. The study's goals include investigating the use of GIS techniques in landslide prediction and creating an ArcGIS map of landslide hazard zones and a prediction map using Analytical Hierarchy Process. A number of thematic layers, including slope, rainfall, temperature, a geology map, and a map of land use and land cover, must be constructed using GIS and remote sensing data. To perform landslide susceptibility modeling, and hazard assessment, the AHP technique combines numerous remote sensing data with other landslide-related characteristics.

Keywords GIS · Susceptibility map · AHP

K. P. Aparna (✉) · R. N. Abhishek · T. Chaithra · M. Abhindev · S. J. Saud
Department of Civil Engineering, Federal Institute of Science and Technology (FISAT),
Angamaly, Kerala, India
e-mail: aparnakp1204@gmail.com

1 Introduction

Landslides are among the costliest and damaging natural hazards in mountainous regions, triggered mainly under the influence of earthquakes and rainfall. According to Cruden and Varnes, 1996, a “landslide” is the movement of a mass of rock, debris, or earth down a slope, under the influence of gravity. It includes a wide variety of slope movements, such as soil slips, deep-seated slides, mud flows, debris flows, rockfalls, etc. [1]. Landslides mostly occur as a result of geological and geomorphological processes that control the local terrain. However, external forces including intense rainfall, earthquakes, flooding, snowmelt, stream erosion, changes in groundwater level, volcanic eruption, or any combination of these natural phenomena can cause landslides to occur on unstable slopes.

In India, the Himalayas and the Western Ghats are the regions with evidence of landslide hazards. While the Western Ghats and Nilgiris are geologically stable yet have uplifted plateau edges and unstable slopes, the Himalayan Mountain belt is composed of newer, tectonically unstable geological formations and is exposed to intense earthquake activity. The Western Ghats make up nearly 50% of Kerala State, which is situated on the southwest tip of the Indian landmass. Kerala has 14 districts, yet 13 of them are prone to landslides. Landslides, often referred to as “Urul Pottal” in local parlance, are one of the most typical and regular forms of hazards Kerala’s Western Ghats experience [2].

Landslide susceptibility studies elucidate the possibility of landslide occurrences of any chosen region in the future. In 2018, perilous rainfall and flooding severely affected all aspects of human lives in Kerala. Idukki was the worst affected district in the state, with 2219 landslides during the time period until 2018 (includes landslides reported by Kerala Disaster Management Authority and Geological Survey of India) [3]. The numbers have increased after the 2018 rainfall episode and have been causing damages both in terms of life and properties. The primary objective in the paper was to establish an explanation to the aforementioned scenario by creating and assessing a landslide hazard susceptibility map for the chosen area of study.

2 Study Area

Idukki district is the part of western ghats, bounded between the latitudes $9^{\circ} 30' 00''$ N to $10^{\circ} 00' 00''$ N and longitudes $76^{\circ} 53' 04''$ E to $77^{\circ} 15' 00''$ E. The state of Tamil Nadu borders the study region on the east, Ernakulam district on the north, Kottayam on the west, and Pathanamthitta district on the south. As far as communication is concerned, the entire district depends on roads as it is not connected to the rail network. Almost half of the district is covered in forest in Idukki, which has a sizable forest reserve area. The trees are broad-leaved tropical species with both evergreen and deciduous tendencies. Idukki is also the largest tea growing district of the state. Crops like rubber, coffee, cocoa etc. are also cultivated extensively. The study area

experiences heavy rainfall from the southwest monsoon and a tropical monsoon environment. It frequently rains during the northeast monsoon, especially in the rain shadow region to the east. Moreover, there is a definite pattern of increasing rainfall from east to west. The 2226 mm of rainfall that falls on average each year is evenly distributed over the six-month period from May to November. Winter season starts from the months of December and continues up to February. Strong cold wind blows during the months of January and February. The average annual temperature is 24.4 °C.

3 Methodology

The study begins with the identification of appropriate causative factors. These factors were identified by considering past landslides in the Idukki district and also from the available literatures [4–6]. To undertake landslide susceptibility analysis in the study area the factors considered were used to make a spatial database using spatial analytical tools in ArcGIS. All causative factors were converted into Raster Map with the coordinate system (WGS 1984 UTM 43 N). Weighted Linear Combination (WLC) approach and the outcomes of the Analytical Hierarchy Process (AHP) were used for the integration of all thematic levels into the GIS environment. These maps were further overlaid and the information was extracted using spacing analyst tool to evaluate and calculate their weightage of factors. After entering values according to the preference from 1 to 9, we computed the weightage of each factor. Based on the variables that were taken from the subjective assessments of qualities, a new weight assignment mechanism was created (Table 1). DEM/elevation is considered to have high weightage. The map was created using the CREATE MAP tool in ArcGIS. The significance of each causal component was evaluated. The created map was validated using Area Under Curve (AUC) method (Fig. 1).

Table 1 Criteria hierarchy

Factors	Weightage
DEM/elevation	17.83
Slope	15.566
Lineament density	15.133
Rainfall	11.446
Geomorphology	10.985
Drainage density	7.939
Lithology	5.481
Land use land cover	6.998
Soil	3.804
Geology	2.723
Slope aspect	2.095

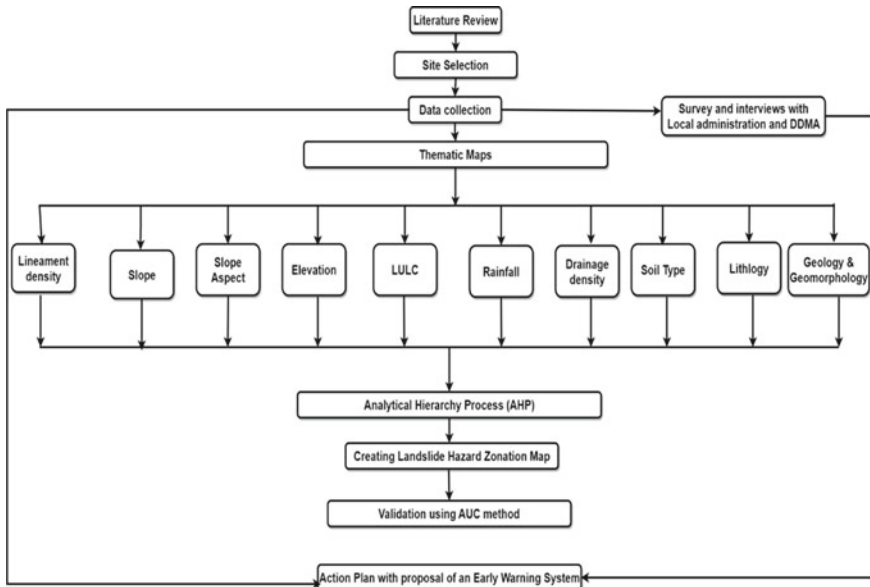


Fig. 1 Methodology

The importance of each causative factor was compared. In pairwise comparison, value differs between one and nine, if the horizontal axis factor is more important than the vertical axis factor and conversely, the value varies between 1/2 and 1/9 [7, 8] (Table 2).

Table 2 Ordinal scale representing preference of judgment [7]

Intensity of importance	Definition/degree of preference	Explanation/remarks
1	Equally important	Two activities contribute equally to the objective
3	Moderately important	Judgment and experience prefer one factor moderately over other
5	Strongly important or essential important	Judgment and experience strongly prefer one factor moderately over other
7	Very strongly or demonstrated important	A factor is strongly preferred
9	Extremely strong or absolute importance	Highest degree favors a factor over other
2, 4, 6, 8	Intermediate	Compensation between weights 1, 3, 5, 7, 9

4 Causative Factors

4.1 Rainfall

Rainfall map was derived from CRU data of resolution (0.5 × 0.5) degrees. CRU TS v.4.05 (Climate Research Unit Gridded time series) released 17 March 2021, gridded data. The gridded data was clipped to the study area. Then the Net CDF raster layer was formed. Composite bands were made for 10 years of rainfall data using 120 bands. These 120 bands were converted to one band by summation. The raster data was converted to point data and the annual rainfall map for 2011–2020 was made using interpolation and IDW method in ArcGIS (10.7.1). This is a very important factor in landslides initiation. The rainfall was measured in mm (Fig. 2).

Fig. 2 Annual rainfall

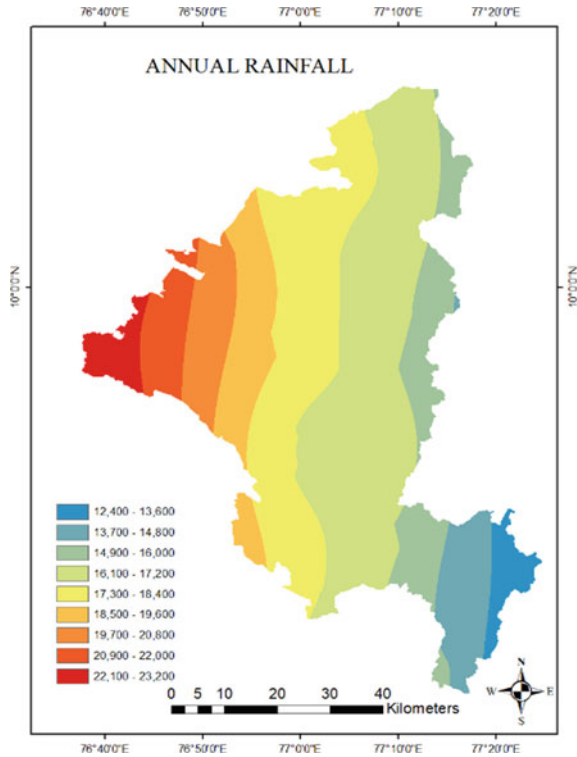
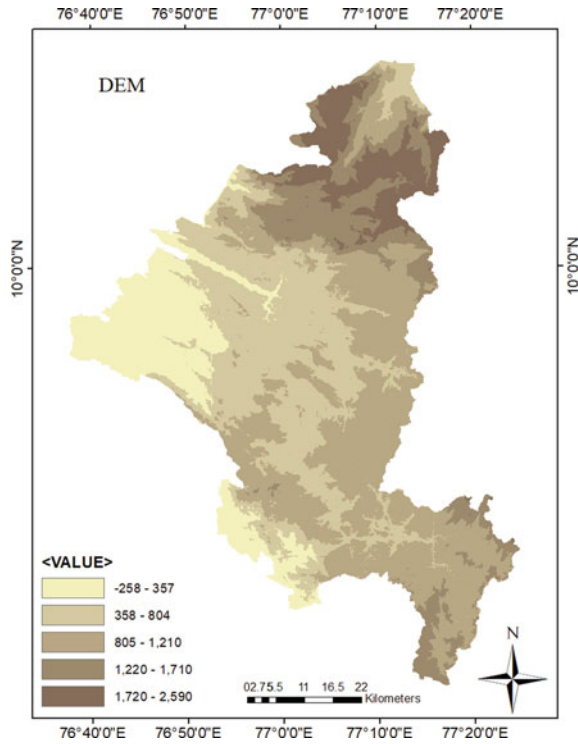


Fig. 3 DEM

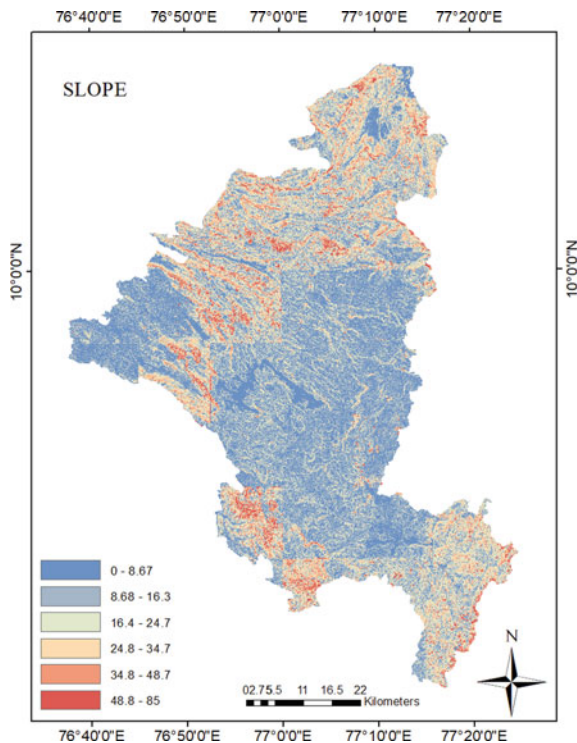


4.2 DEM

Digital Elevation Model (DEM) was downloaded from Bhuvan. The data was downloaded as DEM tiles. 4 tiles were used. These were converged by using the mosaic tool in ArcGIS and raster data was clipped to the study area. The satellite chosen was Cartosat-1. The CartoDEM Version—3 R1 of the study area was downloaded and the map was derived using ArcGIS (10.7.1). The elevation was also visualized. A classified map was derived (Fig. 3).

4.3 Slope

Slope map was derived from DEM using the spatial analyst tool from ArcToolbox of ArcGIS (10.7.1). The surface tool was chosen and slope was derived using the slope tool. The variation in slope can be noted in degrees and percentage. Slope in degrees was noted. A classified map was derived (Fig. 4).

Fig. 4 Slope

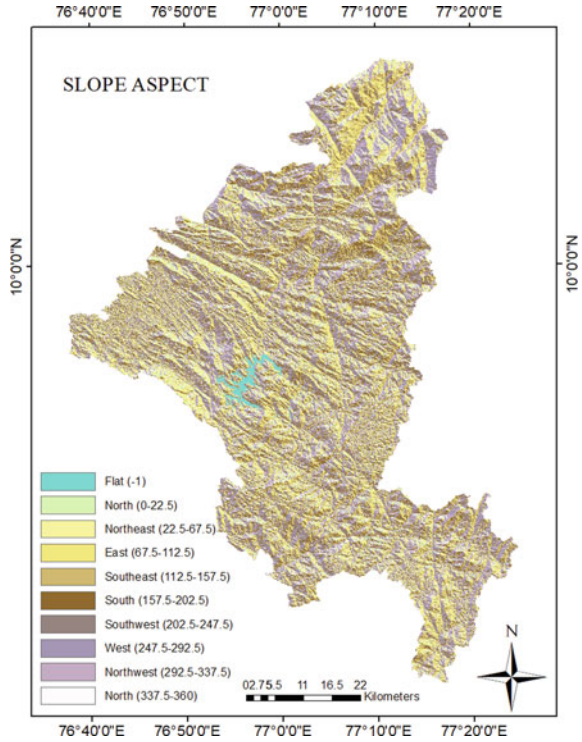
4.4 *Slope Aspect*

Aspect map was derived from DEM using the spatial analyst tool from ArcToolbox of ArcGIS (10.7.1). The surface tool was chosen and slope aspect was derived using the aspect tool from ArcToolbox ArcGIS (10.7.1). A classified map was generated. The nature of the slope was determined (Fig. 5).

4.5 *LULC*

LULC was derived from a shapefile provided by KSREC. The feature data was converted to raster data using the conversion tool in ArcGIS (10.7.1). The field was chosen from the attribute table and different types of vegetation of the study area was identified. Unique value map was formed (Fig. 6).

Fig. 5 Slope aspect

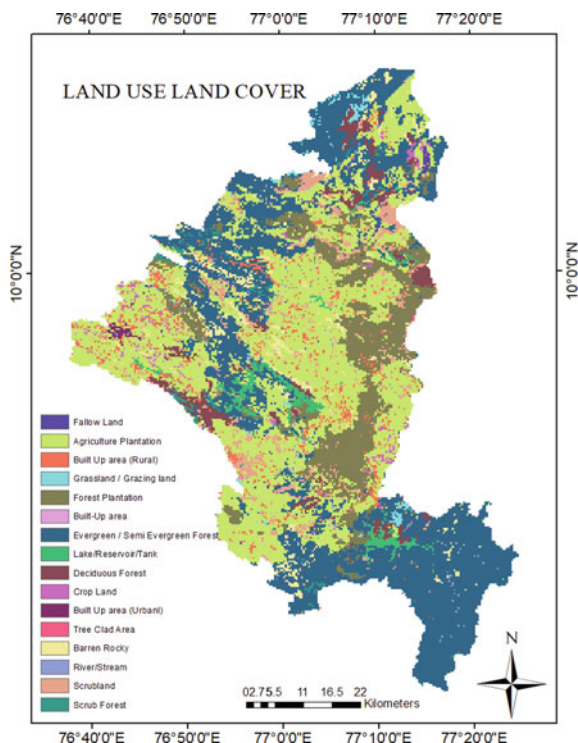


4.6 Soil Map

Soil map was derived from a shapefile provided by KSREC. The feature data was converted to raster data using the conversion tool in ArcGIS (10.7.1). The texture field was chosen from the attribute table and different types of soil of the study area was identified. The location of the water bodies were also considered. Unique value map was formed (Fig. 7).

4.7 Lithology

This map was derived from the geology map provided by KSREC. The feature data was converted to raster data using the conversion tool in ArcGIS (10.7.1). The rock group field was considered from the attribute table and the map generated showed different types of soil of the study area. Unique value map was formed (Fig. 8).

Fig. 6 LULC

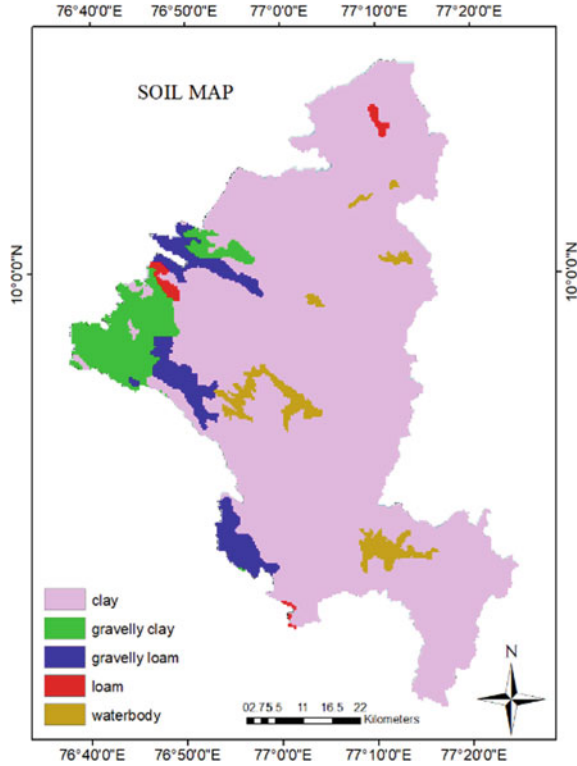
4.8 Geology

The map was derived from geology map provided by KSREC. The feature data was converted to raster data using the conversion tool in ArcGIS (10.7.1). The rock type field was considered from the attribute table. The rock types of different areas were identified. Unique value map was formed (Fig. 9).

4.9 Geomorphology

The map was derived from shapefile provided by KSREC. The feature data was converted to raster data using the conversion tool in ArcGIS (10.7.1). The field was chosen from the attribute table. Geomorphological features were identified. Unique value map was formed (Fig. 10).

Fig. 7 Soil



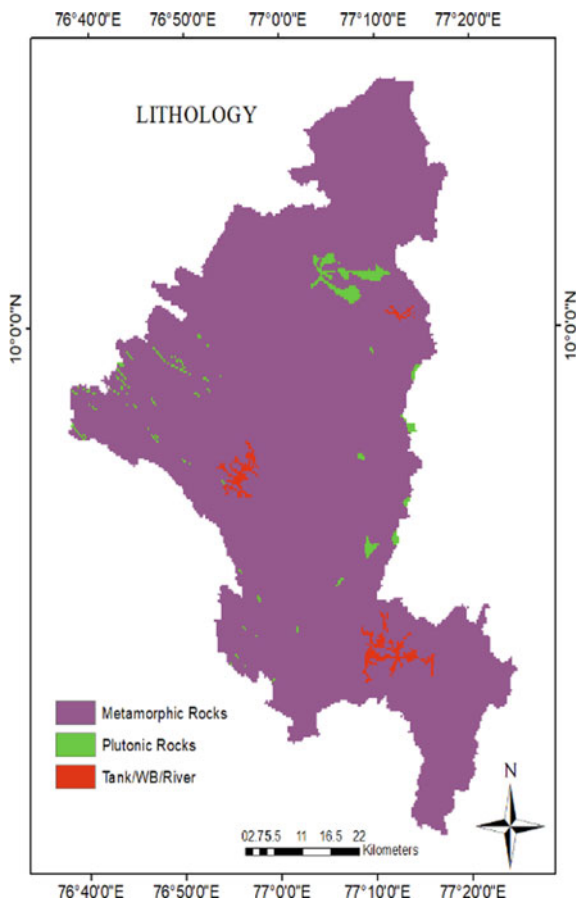
4.10 Drainage Density

The fill tool, flow direction, flow accumulation, stream order and the stream to feature tool was used to generate the stream map. By using line density tool from the spatial analyst tool in ArcToolBox, the drainage map was formed. Classified map was formed (Fig. 11).

4.11 Lineament Density

The map was derived from shapefile provided by KSREC. The feature data was converted to raster data using the conversion tool in ArcGIS (10.7.1). The field was chosen from the attribute table. Classified map was formed (Fig. 12).

Fig. 8 Lithology



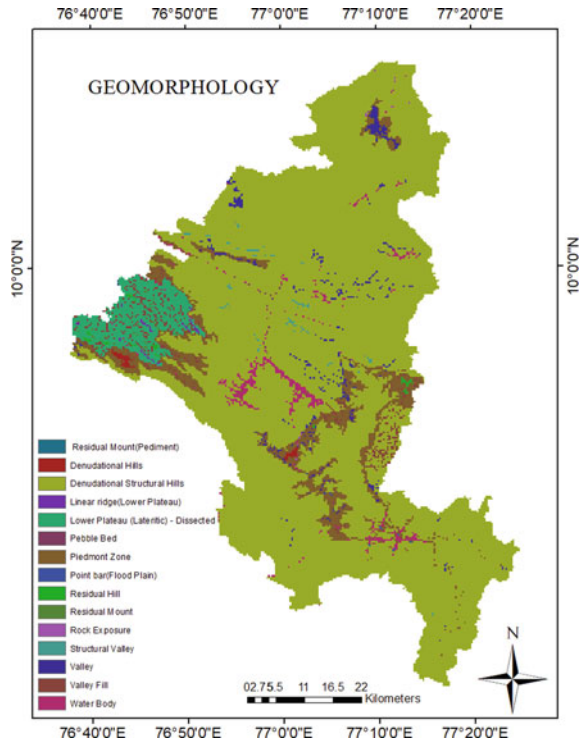
5 Thematic Maps

There were 11 factors considered; Rainfall, DEM, Slope, Slope Aspect, Geomorphology, Geology, Land Use Land Cover (LULC), Lithology, Soil type, Drainage Density, Lineament Density. All thematic layers were projected to WGS 1984 UTM Zone 43N.

5.1 Set Weights

The Landslide Susceptible Zone (LSZ) map was created by overlaying all of the index map layers with ArcGIS tools. There were different ranks assigned to each

Fig. 9 Geomorphology



class of the selected factors, as well as weights assigned to each element based on its importance on landslide incidence (Table 3).

6 Causative Factors

6.1 Landslide Susceptibility Map

The map was made using the 11 causative factors by overlaying the thematic maps in ArcGIS by using AHP (Analytical Hierarchy Process) tool. It is a decision making method, where the values of each factor is added by comparing one factor with others arranged in a table. Here a 11×11 matrix was formed. The factors were given weightage according to their relevance in a landslide.

The map depicts the high susceptible, intermediate susceptible and low susceptible areas of Idukki district (Fig. 13). From the map, we concluded Devikulam, Thodupuzha, Idukki are highly susceptible to landslides. These can be due to many human activities and hilly terrain. Perumade, Udumanchola are considered to be less susceptible to landslides. These are due to the presence of tea plantations in those

Fig. 10 Geology

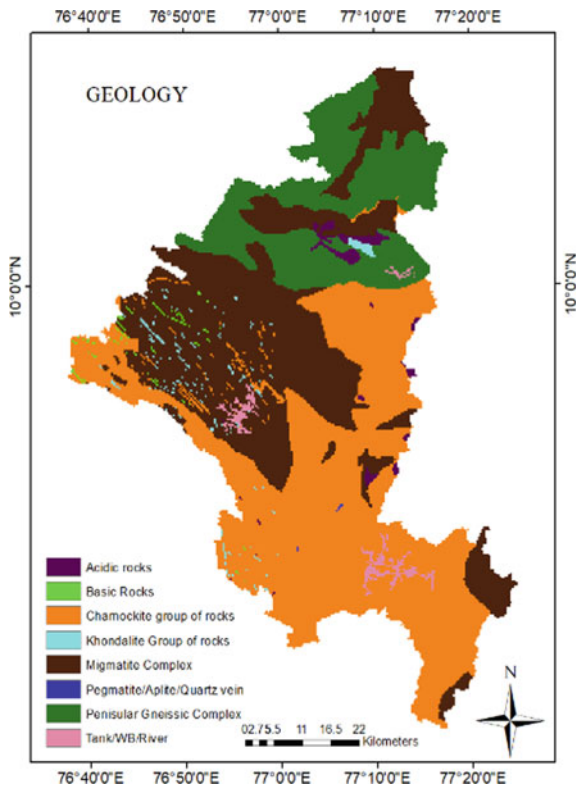


Fig. 11 Drainage density

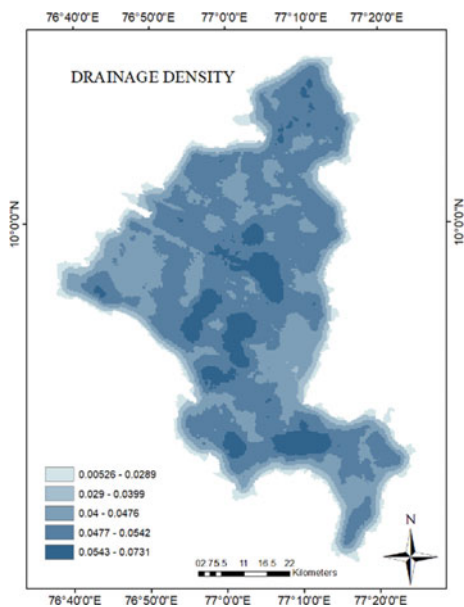


Fig. 12 Lineament density

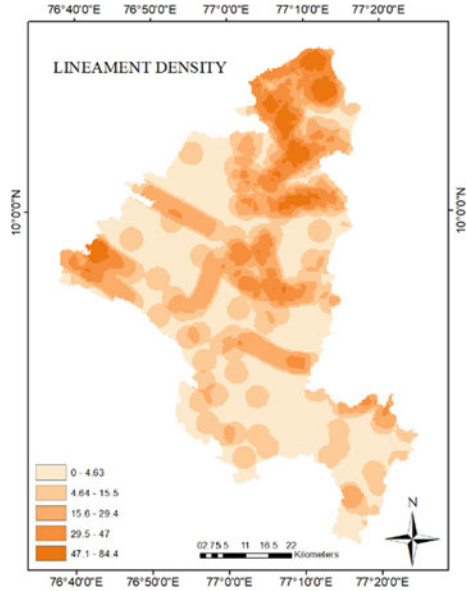


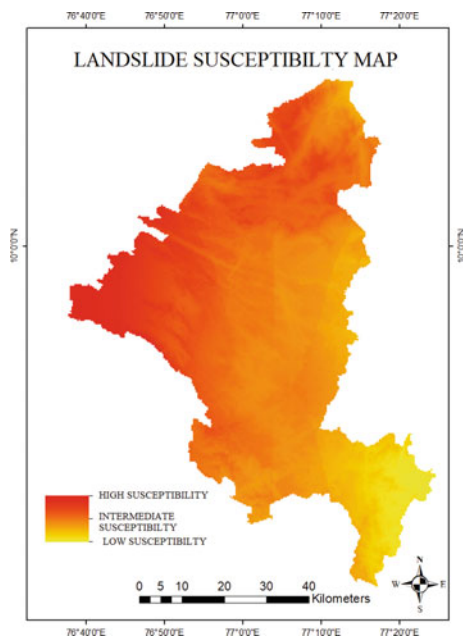
Table 3 Ordinal scale representing preference of judgment

	DEM	SLOPE	LINE	RAIN	GEOMO	DRAIN	LITHO	LULC	SOIL	GEO	SA
DEM	1	2	2	2	2	3	3	2	3	4	4
SLOPE	1/2	1	1	3	2	3	3	1	4	5	5
LINE	1/2	1	1	2	2	3	3	2	4	4	6
RAIN	1/2	1/3	1/2	1	2	2	3	2	3	4	5
GEOMO	1/2	1/2	1/2	1/2	1	2	3	3	4	4	4
DRAIN	1/3	1/3	1/3	1/2	1/2	1	2	2	3	4	5
LITHO	1/3	1/3	1/3	1/3	1/3	1/2	1	1	2	3	4
LULC	1/2	1	1/2	1/2	1/3	1/2	1	1	2	3	4
SOIL	1/3	1/4	1/4	1/3	1/4	1/3	1/2	1/2	1	2	3
GEO	1/4	1/5	1/4	1/4	1/4	1/4	1/3	1/3	1/2	1	2
SA	1/4	1/5	1/6	1/5	1/4	1/5	1/4	1/4	1/3	1/2	1

LINE-Lineament density, RAIN-Rainfall, GEOMO-Geomorphology, DRAIN-Drainage density, LITHO-Lithology, GEO-Geology, SA-Slope aspect

areas. The rainfall patterns have caused drastic changes in the terrain and it has led to many areas which were less vulnerable to landslides to areas disturbed by frequent turbulence. Many other human factors like mining, quarrying can also cause many destructions. Agriculture least affects to cause landslides [9].

Fig. 13 Landslide susceptibility map



Without model validation, landslide susceptibility maps will not be meaningful. As a result, validation of the predictive model is an important step for landslide susceptibility mapping [10, 11]. For validation, the Idukki landslide inventory map was acquired as a shape file from Bhukosh, a service operated by the Geological Survey of India, and imported into ArcGIS (10.7.1) (Fig. 14).

The ArcSDM toolbox was integrated into ArcGIS, and a ROC test was run. According to [12], a model with an AUC value above 0.5 is considered good for use in landslide susceptibility mapping [13–15]. ArcGIS calculated the AUC value and the ROC curve. The acquired AUC value is 0.613, which is a desirable value that can be used for subsequent uses. The model shows a better success rate, indicating that this susceptibility map can be used for planning schemes for hazard preparedness and land use planning with greater accuracy.

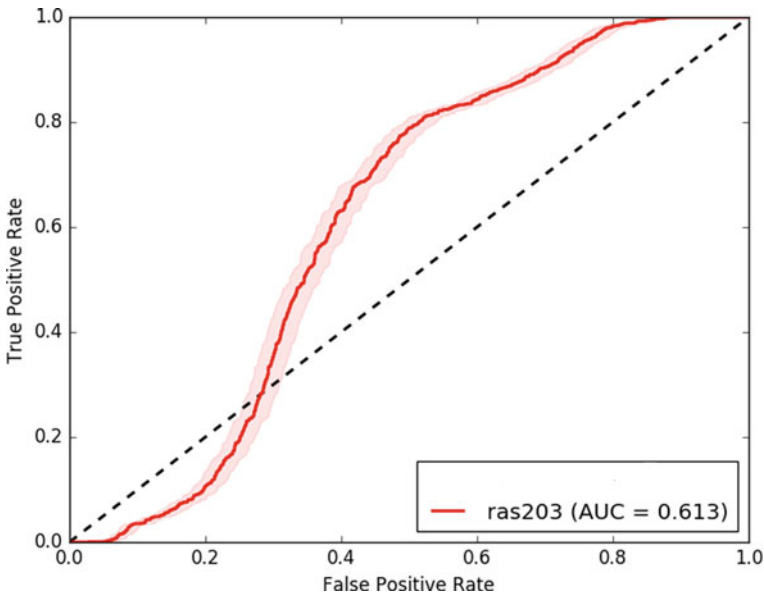


Fig. 14 AUC ROC curve

7 Conclusion

In Kerala's Western Ghats, landslides are a common threat. There have been multiple landslides in the area of the Idukki district. ArcGIS software was utilized in the study to create the susceptibility map. Analytical Hierarchy Process was the research methodology adopted. Eleven characteristics, including rainfall, DEM, slope, slope aspect, geomorphology, geology, land use and land cover (LULC), lithology, soil type, drainage density, and lineament, were chosen for the study. Assigning weight to the criteria was based on their relative importance. The study's final map divided landslides into three zones: high, intermediate, and low susceptibility. The research study aids in locating the most susceptible locations in the Idukki district. These localities include Kumaramangalam, Manakkad, Purapuzha, and surrounding areas. The central parts of the district such as, Kattappana, Periyar, Manjamala, and surrounding areas, were found to be intermediately susceptible. Kumily, Milapra, and the surrounding terrain were the least prone to landslides as per the map generated. Idukki has the fewest early warning systems, as per survey and discussions with officials of various governmental departments as part of landslide disaster management. Implementation of early warning systems in the highly susceptible areas would help in effective evacuation planning, rescue, relief and rehabilitation activities. It can help the early responders to reduce fatalities. Planners and engineers can also utilize the susceptibility map to initiate suitable mitigation measures and enforce safe land use and construction practices in the area.

References

1. Manan WAA, Rashid ASA, Rahman MA, Khanan MFA (2022) Assessment on recent landslide susceptibility mapping methods: a review. In: IOP conference series: earth and environmental science, vol 971, no 1, p 012032. IOP Publishing
2. Kuriakose SL, Jetten VG, Van Westen CJ, Sankar G, Van Beek LPH (2008) Pore water pressure as a trigger of shallow landslides in the Western Ghats of Kerala, India: some preliminary observations from an experimental catchment. *Phys Geogr* 29(4):374–386
3. Jones S, Kasthurba AK, Bhagyanathan A, Binoy BV (2021) Landslide susceptibility investigation for Idukki district of Kerala using regression analysis and machine learning. *Arab J Geosci* 14(10):838
4. Artha Y, Julian ES (2018) Landslide early warning system prototype with GIS analysis indicates by soil movement and rainfall. In: IOP conference series: earth and environmental science, vol 106, no 1, p 012012. IOP Publishing
5. Ajin RS, Nandakumar D, Rajaneesh A et al (2022) The tale of three landslides in the Western Ghats, India: lessons to be learnt. *Geoenviron Disasters* 9:16
6. Bera A, Mukhopadhyay BP, Das D (2019) Landslide hazard zonation mapping using multi-criteria analysis with the help of GIS techniques: a case study from Eastern Himalayas, Namchi, South Sikkim. *Nat Hazards* 96:935–959
7. Kumar A, Sharma RK, Bansal VK (2018) Landslide hazard zonation using analytical hierarchy process along National Highway-3 in mid Himalayas of Himachal Pradesh, India. *Environ Earth Sci* 77:1–19
8. Sarmah T, Das S, Narendr A, Aithal BH (2020) Assessing human vulnerability to urban flood hazard using the analytic hierarchy process and geographic information system. *Int J Disaster Risk Reduct* 50:101659
9. Garcia-Chevesich P, Wei X, Ticona J, Martínez G, Zea J, García V, Krahenbuhl R (2020) The impact of agricultural irrigation on landslide triggering: a review from Chinese, English, and Spanish literature. *Water* 13(1):10
10. Mersha T, Meten M (2020) GIS-based landslide susceptibility mapping and assessment using bivariate statistical methods in Simada area, northwestern Ethiopia. *Geoenvironmental Disasters* 7(1):1–22
11. Centre for Earth Science Studies, Trivandrum (1984) Resource atlas of Kerala
12. Alam E (2020) Landslide hazard knowledge, risk perception and preparedness in Southeast Bangladesh. *Sustainability* 12(16):6305
13. Popescu ME, Sasahara K (2009) Engineering measures for landslide disaster mitigation. *Landslides Disaster Risk Reduct*, 609–631
14. Addis A (2023) GIS-based landslide susceptibility mapping using frequency ratio and Shannon entropy models in Dejen District, Northwestern Ethiopia. *J Eng*, 1–14
15. Teshnizi ES, Golian M, Sadeghi S, Rastegarnia A (2022) Application of analytical hierarchy process (AHP) in landslide susceptibility mapping for Qazvin province, N Iran. In: *Computers in earth and environmental sciences*. Elsevier, pp 55–95

Risk Analysis in Bridge Construction



V. S. Fathima Nizwa, Reshma Kassim, and Sinu Philip

Abstract The construction industry is one of the most dynamic, risky, and challenging businesses. However, the industry is loaded with numerous hazards, just like other economic sectors, making it difficult to meet project objectives. A construction project has many phases, all of which involve various risks. The first step in risk management is risk identification. The goal of this research is therefore to investigate key risk factors affecting bridge construction sector based on their probability of occurrences by using Relative Importance Index (RII). This research focuses on bridge projects across Kerala. The data are collected through a survey approach by administering a questionnaire. Professionals involved in the construction of bridges identify the project risks. Software like SPSS Statistics (Statistical Package for Social Science) are adopted to evaluate the collected responses from different personnel from the construction industry. The risks were ranked and grouped into categories as financial, legal and procurement risks. The aim of this study is to find the critical factors affecting bridge projects. This research presents the factors with the highest probability and impact on any project and to check correlation between them through statistics. As a result of the study, recommendations can be suggested to improve the accuracy of their risk response technique and associated cost estimations by taking defined risk elements into account while evaluating alternative risk management approaches.

Keywords Risk analysis · RII · Bridge projects · SPSS statistics · Kerala

V. S. Fathima Nizwa (✉) · R. Kassim
Department of Civil Engineering, Saintgits College of Engineering (Autonomous), Kottayam,
Kerala 686532, India
e-mail: fathima.sm2123@saintgits.org

S. Philip
Nael Contracting Pvt. Ltd, Abu Dhabi, UAE

1 Introduction

The construction industry is one of the most dynamic, risky, and challenging businesses. Although many significant projects fail to finish on time and within budget, the sector has a very poor reputation for risk management. Weather changes, labor and plant productivity, and material quality all have a significant impact on this. Risks are way too frequently neglected or handled in an arbitrary manner; a common practice is to simply add 10% contingency to the project's estimated cost. Such a strategy is frequently ineffective in the complex construction industry and can lead to costly delays, legal action, and even bankruptcy. All construction organisations must consider risk management while making decisions. For some building projects, risk and uncertainty may have detrimental effects. Risk can have an impact on a project's productivity, performance, quality, and budget. Although risk cannot be completely removed, it can be reduced, transferred, or kept.

Risk management is not a new concept. Traditionally it has been applied instinctively, with risks remaining implicit and managed by judgment, informed by experience. The systematic approach makes the risks clear, formally describing them and making them easier to manage. In other words, systematic risk management is a management tool, which requires practical experience and training in the use of the techniques. Risk management in construction industry is an important part of the project planning and management. Various risks associated with construction projects such as financial risks, environmental risks, socio-economic and construction related risks are studied and dealt in risk management. The volatility and capriciousness of the environment in the construction industry was never hidden from anyone. It's easily influenced by external factors (technical, design, logistics, physical, operating, environmental, socio-political, force majeure et cetera) which are capable of not only derailing projects but can also create an irreparable aberration. Risk management, therefore, becomes a pivotal instrument that helps us deal with the culling out of various risks, their analyses, and the remedial steps that could be taken to avert them in a particular project. Risk management process is nothing but a series of steps that help identify and migrate the risks for the successful closure of a project. If done correctly and sincerely, construction risk management will reduce not only the likelihood of an event occurring, but also the magnitude of its impact. In the simplest terms, Risk management process is taking preemptive actions to avoid and minimize any kind of jeopardy to a project in future. This is how a typical Risk management planning progresses (Fig. 1).



Fig. 1 Risk management process in construction

2 Methodology

2.1 General

The methodology used in this research is divided into two sections which are literature review and questionnaire survey. Primary information regarding the study was collected with the help of literature survey and pilot study. By the information gathered from these a questionnaire survey was conducted to construction experts about of the risk occurrences and management in bridge construction industry. From the identified risk ranking need to be conducted from the questionnaire data. Finally using the questionnaire data, result is to be analysed using Statistical Package for Social Science (SPSS). Then this is to be represented using a case study. The framework of methodology used in the study is represented in Fig. 2.

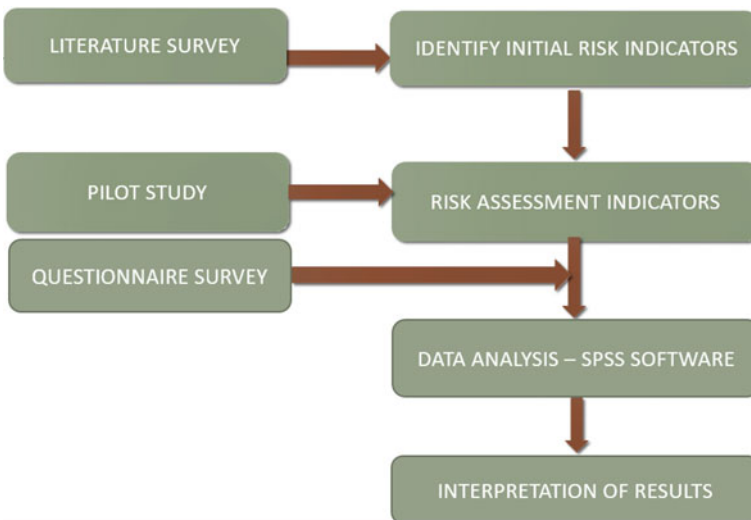


Fig. 2 Framework of methodology

2.2 *Pilot Study*

A pilot survey was carried out to identify and examine the potential problem areas and scope of the research. This study was conducted with the purpose to check the feasibility of the research and identify the variables that define the problem from construction aspect. The questionnaire was prepared with the help of the opinions from the pilot study. It includes interview with experienced professionals in construction industry and also obtained their feedback regarding their view on various variables identified from literature study. Based on the suggestions, risks were refined.

2.3 *Questionnaire Survey*

In addition, the manufacturing of other components of concrete, such as aggregate, also contributes to carbon emissions. EC also includes the emissions associated with the construction process, such as energy used on-site and the emissions from the production of construction equipment. In this study, a questionnaire survey is used to collect the necessary data required for achieving the objectives of the study. These questionnaire is prepared based on the information gathered from literature study and followed by the pilot study conducted. The questions are prepared in google forms and are sent to the target group using online platforms such as G-mails. The questionnaire mainly consist of six sections.

- Section 1—The first section of the questionnaire is of biographical information. This section collect the necessary details about the respondents such as name, email id, their field of specialization, years of experience in the construction sector, etc.
- Section 2—Second section of the questionnaire survey actually focused on understanding current situation of risk management in the construction industry. To identify the which segment of construction process the risk management is most important.
- Section 3—From this section onwards the uncertainties that happening under each process of construction is evaluated. To analyse the impact of those factors under each type of risk and level to be considered. In this section factors occurring the technical risk is included.
- Section 4—As mentioned above this section contains the factors occurring under financial risk.
- Section 5—As mentioned earlier this section contains the factors occurring under procurement risk.
- Section 6—This section contains the factors occurring under legal risk.

3 Data Analysis

In this study, the data collected from various construction experts who have first-hand experience in bridge construction in Kerala. After collecting the data, the data need to be statistically analyzed using Statistical Package for the Social Sciences (SPSS) software. In this study, the collected data are analyzed using methodologies such as reliability tests, Descriptive statistics—frequency tests, correlation analysis, normality test, Pareto analysis. From the collected data base on the responses this should be ranked using Relative Importance Index (RII).

3.1 *Relative Importance Index (RII)*

The Relative Importance Index (RII) approach used to describe the relative importance of the specific causes and effects based on the likelihood of occurrence and effect on the project using the Likert scale. It also helps to identify the most important variables based on the participant's response. One of the main objective of the study is to rank the variables that cause more impact on the performance of the bridge construction in Kerala. In this study we have identified 22 types risk that occurs in construction sector with the help of literature study and pilot study and to be ranked using RII based on the following formula Eq. (1).

$$RII = \frac{\sum W}{A \times N} \quad (1)$$

where W is the score assigned to variable by participants (1 to 4), A is the highest score (4) and N is the total number of participants (50). The higher the value of the RII, the greater its influence on the dependent variable. Note that, in this study, the RII can get a value between 0, 4–1 (0, 4: Higher—1: Ignore).

3.2 *Reliability Analysis*

Reliability analysis is an analysis technique in SPSS which is used to determine the internal consistency and to make sure that the questionnaires are reliable and suitable for the research. Reliability analysis in SPSS provides information about the relationship between individual items in the scale and also it calculates whether the scale is reliable or not. In this study, Cronbach's alpha method is used to measure the internal consistency. Cronbach Alpha is a reliability test conducted within SPSS in order to measure the internal consistency i.e. reliability of the questionnaire. It is most commonly used when the questionnaire is developed using multiple Likert scale statements and therefore to determine if the scale is reliable or not.

3.3 Descriptive Statistics—Frequency Analysis

In SPSS, the descriptives procedure computes a select set of basic descriptive statistics for one or more continuous numeric variables. The measures of variation include variance, SD, standard error, quartile, interquartile range, percentile, and coefficient of variation. Frequency measures include frequency and percent, and central tendency measures include mean, median and mode. Simple summaries of the sample and the measurements are provided. Here, frequency analysis was used because it is a crucial part of statistics that focused on the quantity and proportion of occurrences.

4 Result and Discussions

Among all construction materials concrete comes first in terms of quantity of usage. Thus, Based on the extensive literature reviews and expert's advice, the questionnaire consist of twenty eight risks fewer than five risk factors. Using a four-point ordinal scale, responses on the amount of the impact of various traits on bridge design were sought: "1" indicated "Ignore," "2" indicated "Low," "3" defined "Moderately," and "4" defined "High." Based on the research, 4 categories of risk variables that have an impact on bridge construction were identified. Although there were several risk that could affect bridge construction projects, those five risk categories were thought to be the easiest to compile all of the minor problems. The risk factors are as follows technical risk, financial risk, procurement risk, legal risk. The sub components that comes under each one are also identified and shown in Table 1.

4.1 RII Results

Firstly the RII was calculated from the response obtained within the main components of risk factors. The RII score obtained is interpreted in Fig. 3. By the RII analysis the factor which has highest score is to be ranked first. The 22 factors that identified is ranked on the basis of survey results obtained.

As seen in the Table 1, it represents the risk factors occurs during the bridge construction. By the RII analysis the factor which has highest score is to be ranked first. So from the results it's clear that TR1 i.e. incomplete project design is the most important factor which comes under technical risk and PR3 i.e. shipping accidents during transit has least impact among them. From highest mean value to lowest mean value, the ranks were produced in a hierarchical manner. Critical risk factors were ranked in a hierarchical manner in Fig. 3.

Table 1 Risk factors

	Technical risk		Financial risk		Procurement risk		Legal risk
TR1	Incomplete project design	FR1	Delay from clients	PR1	Delay in replacement of defective products	LR1	Failure to achieve satisfactory contractual arrangements
TR2	Improper specification	FR2	Unpredictable variation in raw materials	PR2	Defective product delivery	LR2	Bribery and corruptions
TR3	Late changes of design from client side	FR3	Liquidity damages penalty	PR3	Shipping accidents during transit	LR3	Breach of intellectual property
TR4	Complexity in project design	FR4	Labour charge increase	PR4	Products or material obsolete	LR4	Environmental board issue
TR5	Delays and mistakes in producing design documents	FR5	Change in law	PR5	Commodity price fluctuations	LR5	Unforeseen inclusion of contingent liabilities
TR6	Design error delivered by the owner						
TR7	Change in seismic criteria						

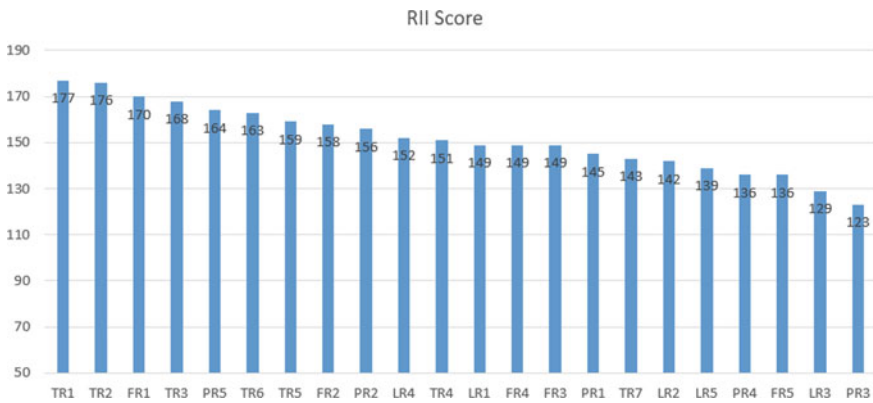


Fig. 3 Framework of methodology

Table 2 Reliability statistics

Cronbach's alpha	No. of items
0.913	22

4.2 Reliability Analysis

The Cronbach's alpha test was done for most of the questions in the questionnaire survey to test the internal consistency. The Cronbach's alpha coefficient value obtained from reliability as shown in Table 2.

The obtained alpha coefficient through reliability test for the 22 items is 0.913, suggesting that the items have relatively high internal consistency by referring the Table 2. This shows that the obtained data are highly reliable for the analysis.

4.3 Descriptive Statistics—Frequency Analysis Results

Bridges were one of the most critical components in the transportation infrastructure for safety, security and mobility. The risk in a bridge construction site was studied by adopting survey method. The data collection was conducted through questionnaire survey and Google forms and was well analysed with statistical analysis software (SPSS). In this study the questionnaire survey's respondents were total of 50 civil engineers who had rich experience in construction and strong academic background. Out of 22 factors, the questionnaires were grouped into 4 subgroups as financial risks, technical risks, procurement risks and legal risks. The statistical results, of 22 factors are shown in the Fig. 4. The ranks were formed in hierarchical order from highest mean value to lowest mean value. From the frequency analysis the top critical factor with mean greater than 3.25 is considered as the significant risk factors in this study.

4.4 Critical Risk Factors

From the statistical results, the top 5 critical factors were taken as the main factors. The ranks were formed in hierarchical order from highest mean value to lowest mean value. The Table 3 showed critical risk factors were ranked hierarchical manner.

The reasons for the risk are given below as follows.

- **Incomplete project design:** Incomplete project design with a mean of 3.54 which comes under technical risk was ranked first in risk factors. It is the most significant problem and its ranked first, as it can lead to delays, cost overruns and safety issues. Here are some of the common causes of incomplete project design: Lack of clarity in project requirements, when the project requirements are unclear, incomplete or ambiguous, it can lead to gaps in the project design. Insufficient site

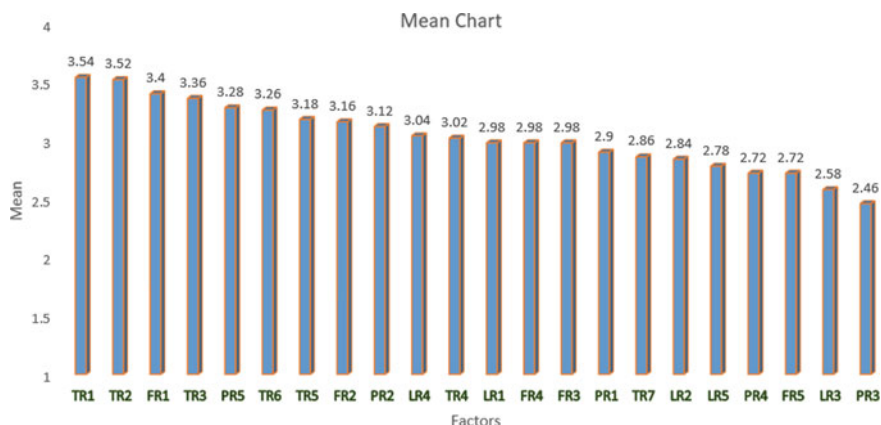


Fig. 4 Framework of methodology

Table 3 Critical risk factors

Factor ID	Factors	RII Score	Mean	Rank
TR1	Incomplete project design	177	3.54	1
TR2	Improper specification	176	3.52	2
FR1	Delay from clients	170	3.40	3
TR3	Late changes of design from client side	168	3.36	4
PR5	Commodity price fluctuations	164	3.28	5
TR6	Design error delivered by the owner	163	3.26	6
TR5	Delays and mistakes in producing design documents	159	3.18	7
FR2	Unpredictable variation in raw materials	158	3.16	8
PR2	Defective product delivery	156	3.12	9
LR4	Environmental board issue	152	3.04	10
TR4	Complexity in project design	151	3.02	11
LR1	Failure to achieve satisfactory contractual arrangements	149	2.98	12
FR4	Labour charge increase	149	2.98	13
FR3	Liquidity damages penalty	149	2.98	14
PR1	Delay in replacement of defective products	145	2.90	15
TR7	Change in seismic criteria	143	2.86	16
LR2	Bribery and corruptions	142	2.84	17
LR5	Unforeseen inclusion of contingent liabilities	139	2.78	18
PR4	Products or material obsolete	136	2.72	19
FR5	Change in law	136	2.72	20
LR3	Breach of intellectual property	129	2.58	21
PR3	Shipping accidents during transit	123	2.46	22

investigation, when the site investigation is inadequate, it can lead to inaccurate information about the site conditions. Inadequate design resources, the design team has inadequate resources, such as personnel, expertise or technology, it can lead to incomplete project design. This may be due to factors such as budget constraints, lack of qualified personnel or limited access to design tools. This can also be caused due to late changes in project scope or requirements, which occur during the project lifecycle. These changes may be due to factors such as changing market conditions, new regulatory requirements or client demands. Lack of coordination between project stakeholders, it can result in incomplete project design.

- **Improper specification:** Improper specification with a mean of 3.52 which comes under technical risk was ranked second in risk factors. It can occur at various stages of the construction process, including the design phase, material selection and construction techniques. For example, a bridge may be designed with insufficient load bearing capacity or without considering environmental factors such as seismic activity or high winds. Material selection may also be inadequate, leading to corrosion, fatigue or other structural problems. This can also lead to increased maintenance costs, cost of repairs, and replacement of materials or components and also causes potential legal liabilities. Improper specification can lead to a decrease in the lifespan of the bridge resulting in need for premature replacement. Finally there may be additional costs associated with delays or interruptions to the construction process this includes cost of rescheduling work, reordering materials and potential financial penalties for missed deadlines.
- **Delay from clients:** Delay from clients with a mean of 3.40 which comes under financial risk was ranked third in risk factors. This can occur in bridge construction projects for a variety of reasons. Some common reasons include: Changes in design, client may request changes to the bridge design during the construction process. These changes can require additional time and resources to implement, which can cause delays in the project schedule. Clients also need to obtain permits or approvals from local authorities before construction can begin. Delays in the permitting process can cause delays in the overall project schedule. Funding issues: Clients may experience funding issues that can impact construction project. For example, if a client is relying on grants or loans to fund the project, delays in receiving the funds can cause delays in the construction schedule. Insufficient access to the construction site, which can cause delays in the delivery of materials and equipment. Communication breakdowns: Clients may not communicate effectively with the construction team, which can cause misunderstandings and delays in the project schedule. It's important for clients to work closely with the construction team to ensure that any issues are addressed promptly to minimize delays in the construction schedule. Clear and frequent communication can help ensure that the project stays on track and any issues are resolved quickly.
- **Late changes of design from client side:** Late changes in design with a mean of 3.36 which comes under technical risk was ranked fourth in risk factors. During bridge construction this can be challenging and costly. However sometimes they may be necessary to ensure the safety and stability of the bridge. It becomes necessary when unexpected soil condition, changes in the project requirements or

scope or new information that was not available during the initial design phase. If changes are required, it's important to carefully consider the implications of the changes on the overall design and construction process. This may involve re-evaluating the structural integrity of the bridge, assessing the impact on the construction schedule and budget, and ensuring that any new design meets the necessary regulatory and safety standards. Careful considerations and collaboration among the project team can help to minimize the impact of any changes and ensure the project's success.

- **Commodity price fluctuations:** Commodity price fluctuations with a mean of 3.28 which comes under procurement risk was ranked fifth in risk factors. This have a significant impact on the cost of bridge construction. The price of commodities such as steel, cement and asphalt can fluctuate due to various factors such as global demand, supply chain disruptions, and geopolitical events. Steel is a crucial component in bridge construction and its price fluctuations can have a significant impact on the overall cost. Steel prices are affected by various factors, including demand from the construction industry, global trade policies and production capacity. Similarly the price of cement can also fluctuate. Asphalt is used for road surfaces on bridges, and its price can also be affected by factors such as crude oil prices, transportation costs and demand and supply. To mitigate the impact of commodity price fluctuations, bridge construction projects may use various strategies, such as hedging or locking in prices in advance, using alternative materials and adjusting project schedules to advantage of price fluctuations.

5 Conclusion

In this study, a comprehensive investigation of the main risk factors in bridge construction sector across Kerala is shown. From the questionnaire survey regulated with 50 civil engineers in Kerala who works under bridge sector, risk factors affecting the construction sector are identified by relative importance index (RII). The critical risks challenging the performance of bridge construction projects have been identified and ranked in this study.

The demographical analysis of the respondents, based on the experience of the respondents in construction were between 5 to 10 years had highest percentage of 28%. The highest respondents were from government organisations had a percentage of 45%. Based on the designation the highest respondents were contractors had a percentage of 34%.

The seven risk factors identified were analysed, the first three highest scores were considered as the most critical factors in the bridge projects in this study. The top three ranking of risk factors were as follows: Incomplete project design, Improper specification and late changes of design from client side. To avoid these factors, it is essential to follow a comprehensive and systematic design process that considers all relevant factors. Some actions that can help avoid these factors include engaging experts in bridge construction to provide insights and recommendations

on the design and construction process. Conducting a thorough review and analysis of the incomplete design to identify potential risks and develop strategies to address them. Follow established design standards and guidelines to ensure that all critical design elements are considered and that the bridge is designed to meet the required safety and quality. These also includes conducting thorough site investigations to understand the conditions, geological hazards and environmental factors. The other most important but not taking in process is of implementing quality control measures throughout the process to ensure that the bridge is built to the required specifications and standards. By following these actions it is possible to avoid the risks in bridge construction to an extent and ensure the bridge is safe, stable and meets the intended use and lifespan.

References

1. Alsaadi N, Norhayizakuan N (2021) The impact of risk management practices on the performance of construction projects. *Stud Appl Econ* 39(4):1–10
2. Boateng A, Ameyaw C, Mensah S (2020) Assessment of systematic risk management practices on building construction projects in Ghana. *Int J Constr Manag*, 1–10
3. Chandubai G, Pitroda J, Makwana A (2019) Risk management in high rise construction projects in Surat City. *Int J Tech Innov Mod Eng Sci*, 160–167
4. De Marco A, Thaheem M (2014) Risk analysis in construction projects: a practical selection methodology. *Am J Appl Sci* 11(1):74–84
5. Devi V (2018) A study on risk analysis in construction project. *Int Res J Eng Technol* 5(5):4317–4321
6. Dixit V (2022) Risk assessment of different sourcing contract scenarios in project procurement. *Int J Constr Manag* 22(8):1537–1549
7. Genc O (2021) Identifying principal risk factors in Turkish construction sector according to their probability of occurrences: a relative importance index (RII) and exploratory factor analysis (EFA) approach. *Int J Constr Manag*, 1–9
8. Iqbal S, Bukhari S, Mahmood S (2020) The assessment of risk management & engineering management practices at project planning phase on performance of construction projects. *J Bus Soc Rev Emerg Econ* 6(4):1369–1378
9. Kaffle C (2019) Correlation and regression analysis using SPSS. *OCEM J Manag Tech Soc Sci* 1(1):126–132
10. Leclezio L (2015) Pilot validation of the Tuberosus Sclerosis Associated Neuropsychiatric Disorders (TAND) checklist as a screening tool for n neuropsychiatric manifestations, Master's thesis, University of Cape Town

Evaluation of Bituminous Concrete Using Ceramic Waste as a Filler



R. Adarsh, A. V. Arunkumar, Aswini Anil, K. Karthika Sreenivasan, K. K. Reshma, and Shreesh Ajaykumar

Abstract The functional qualities of asphalt are greatly influenced by filler, which is a key ingredient in the asphalt mixture. Filler materials have the property of filling the voids between coarse aggregate and binder and improves the bond. The qualities of an asphalt mix may change if the type and quantity of filler is altered. One of the most significant building and demolition wastes with a very low potential for recycling are ceramic materials. The accumulation of ceramic waste and pavement damage can be prevented by adding ceramic waste powder as a modifier to bituminous mixture. This research aims to evaluate the effects of using ceramic dust as filler material in bituminous concrete with 25, 50 and 75% contents by total weight of the fines using conventional crushed rock fines as control material. The research work is oriented in comparing the performance of bituminous concrete using laboratory tests including Marshall stability and flow with corresponding volumetric parameters. The analysis of results proved that the value of Marshall stability was improved at all replacement ratios of the ceramic, an overall increase of 22.2% was obtained with 75% ceramic dust. This attempt not only has the potential to significantly reduce the amount of trash, but it will also reduce the usage of non-renewable resources like natural filler and in effect improves strength of flexible pavement.

R. Adarsh · A. V. Arunkumar · A. Anil (✉) · K. Karthika Sreenivasan · K. K. Reshma · S. Ajaykumar
Department of Civil Engineering, Government College of Engineering, Kannur, Kerala 670563, India
e-mail: 19b126@gcek.ac.in

R. Adarsh
e-mail: 201598@gcek.ac.in

A. V. Arunkumar
e-mail: 201619@gcek.ac.in

K. Karthika Sreenivasan
e-mail: 201569@gcek.ac.in

K. K. Reshma
e-mail: 201568@gcek.ac.in

S. Ajaykumar
e-mail: shreeshajayakumar@gcek.ac.in

Keywords Filler material · Bituminous concrete · Ceramic dust · Marshal stability

1 Introduction

Any nation's road system is the foundation of its economy. Road construction costs a considerable sum of money. Around the world, bituminous concrete mixtures are frequently utilised to construct pavements. Bituminous Concrete (BC) is a mixture used to build bituminous pavements that is created by mixing aggregate and bitumen in specific proportions. Under typical loads, conventional bituminous concrete performs well, but the environment is rapidly deteriorating. In many nations, flexible roadway pavements are the most popular type of pavement. Enhancing the qualities of the materials used to build roadways is the method utilised to stop pavement deterioration.

The third-largest tile producer in the world, India accounts for 6.2% of global tile production, or over 691 million square metres. Due to its extensive manufacture, it is now one of the materials that is used most frequently worldwide. However, manufacturing mistakes, human error, and the use of the wrong raw materials result in 30% of the daily production of ceramic materials being wasted during production. The management of garbage, particularly waste from the building industry including construction and demolition (C&D) waste, broken tiles, and sanitary ware waste, has recently been under increased public scrutiny. These waste items are now being taken to landfills, which not only take up fertile land but also pose a risk to the environment. Numerous investigations have shown that these waste products can be used to prepare concrete by substituting a portion of the construction components with the ceramic waste. Construction is therefore more affordable and the disposal problems are resolved when ceramic waste is used. Utilizing these ceramic wastes has a few benefits in addition to helping to protect the environment, such as reducing the need for raw materials, which helps to preserve natural resources. Utilizing waste materials and lowering reliance on natural resources, ceramics usage contributes to a reduction in environmental deprivation [1].

As an important ingredient of bituminous concrete, filler plays a significant role in enhancing the mechanical characteristics and boosting the durability of asphalt. Given the abundance of natural elements found in asphalt pavements, using ceramic waste as a raw material could be an innovative approach. The creation of asphalt pavements requires large quantities of natural resources including filler and natural aggregates. One practical way to achieve cleaner production is to use waste materials as aggregate or filler in the asphalt mixture. This strategy not only has the potential to significantly reduce the amount of this trash, but it may also reduce the usage of non-renewable resources like natural filler and aggregate. Majority of the well known industries pose a major threat of waste disposal without effecting surrounding environment. The significance proves the necessity of elimination of industrial and other waste by conserving to all source of natural resources [2].

The fact that the compressive strength, permeability properties, bond strength, etc. of the ceramic aggregates in concrete met the requirements set by various international standards and codes, confirming the feasibility of using ceramic waste as an effective replacement for natural aggregates in structural concrete [3, 4]. When waste ceramics are powdered, it can be used for, strengthening the stability of the expansive soil, in the construction of flexible pavement [5, 6].

From the analysis of various research studies on the utilization of ceramic dust in different domains of construction ceramic dust has the potential of improvising properties of concrete and subgrade soil. The present study was carried to observe the effect of ceramic dust on Marshall properties of Bituminous Concrete (BC). Based on the experimental results, the feasibility of using ceramic dust as filler is assessed comparing it with control mix.

2 Methods and Materials

2.1 Materials

2.1.1 Aggregates

Aggregates make up about 95% of asphalt mixtures, and they have a big impact on how well they work. Well-graded pulverised material should be used to create the finest asphalt concrete. Use of well graded aggregate aids to stability and durability in pavement construction. The maximum size of aggregate size is essential for controlling combination consistency, slide resistance, and compatibility. Higher maximal aggregate sizes result in greater stability, which is frequently attained with less bitumen. Better slide protection is also provided by the larger aggregate size (Fig. 1).

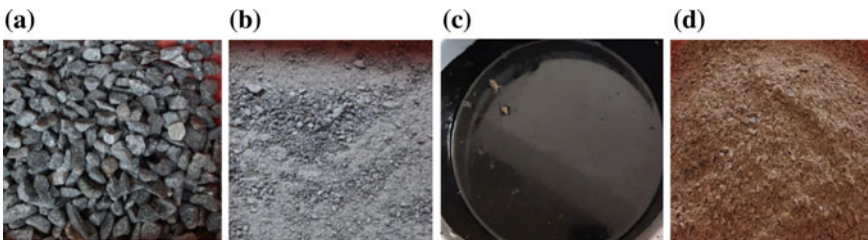


Fig. 1 a Aggregates b Quarry dust c Bitumen d Ceramic dust

2.1.2 Filler

Finely split materials, including limestone dust and other types of rock dust, must make up the filler. It must be adequately dry and basically clear of agglomeration at the time of use.

2.1.3 Bitumen

Bitumen is a cementitious, amorphous, thermoplastic material whose stiffness changes with temperature. It has a dark or black colour and can take on various shapes, such as rock asphalt or naturally occurring bitumen composed of oil. Bitumen is commonly used in road and highway building. Used in this instance is bitumen of grade VG 30 that was obtained from a college laboratory.

2.1.4 Ceramic Dust

15 to 30 metric tonnes of waste are produced yearly by the ceramics industry in India, which produces sanitary utensils, bricks, roof tiles, wall and floor tiles, and ceramic items for homes and other purposes. The remaining 70% of the waste is tossed outside, with only 30% of it being disposed of as trash. The two major garbage groups in the ceramics business are construction and demolition debris and fractured pottery from the manufacturing process. Ceramic refuse is classified as non-hazardous solid garbage because it exhibits pozzolanic properties. Materials can therefore be reused in a variety of building construction uses after reprocessing. Ceramic tile leftovers that are collected from college construction sites are meticulously pulverised to produce a gradation similar to that of conventional infill.

2.1.5 Properties of Materials

Aggregates and Filler

The physical and mechanical properties of the aggregate and filler satisfy the limits prescribed by Indian Standard code and MoRTH. Therefore it can be suitably employed in Marshall stability test analysis (Table 1).

Ceramic Dust

Specific gravity of ceramic dust = 2.65.

The specific gravity of ceramic dust slightly decrease from that of quarry dust filler.

Table 1 Table showing the properties of aggregates and its MoRTH specifications

Property	Obtained result	MoRTH specification
Impact value %	20%	Max. 24% (IS 2386 Part IV)
Crushing value %	27.7%	Max. 30% (IS 2386 Part IV)
Specific gravity	2.78	2.4–2.9
12 mm aggregate	2.76	(IS 2386 Part III)
6 mm aggregate	2.70	
Quarry dust		
Bulk density (kg/m ³)	1581.67	1200–1850
12 mm aggregate	1379	(IS 2386 Part III)
6 mm aggregate	1805.33	
Quarry dust		
Water absorption %	0.18%	Max. 2% (IS 2386 Part III)
Combined flakiness and elongation	32.92	Max. 35% (IS 2386 Part I)

Table 2 Table showing the properties of bitumen and its MoRTH specifications

Property	Obtained result	As per MoRTH
Penetration value	63 mm	50 mm-70 mm (IS 1203)
Ductility value	100 cm	Min. 75 mm (IS 1208)
Softening point	48 °C	IS 1205
Flash point	236 °C	Min 170 °C (IS 1209)
Fire point	250 °C	Min 175 °C (IS 1209)
Specific gravity	1.01	1.01 (IS 1209)

Bitumen

The physical and mechanical properties of the binder- Bitumen, satisfy the limits prescribed by Indian Standard code and MoRTH. Therefore it can be suitably employed in Marshall stability test analysis (Table 2).

Table 3 Obtained gradation

Sieve size (mm)	12 mm	6 mm	Filler	Grading	Obtained gradation
19	100.00	100.000	100.00	100	100.00
13.2	84.00	100.000	100.00	90–100	96.30
9.5	23.00	98.400	100.00	70–88	81.80
4.75	0.00	38.400	100.00	53–71	59.10
2.36	0.00	0.000	98.90	42–58	47.50
1.18	0.00	0.000	76.90	34–48	36.90
0.6	0.00	0.000	64.80	26–38	31.10
0.3	0.00	0.000	46.50	18–28	22.30
0.15	0.00	0.000	34.00	12–20	16.30
0.075	0.00	0.000	16.00	04–10	7.70

Table 4 Quantity of materials in the mix

Specimen	12 mm aggregate (g)	6 mm aggregate (g)	Filler		Number of specimens
			Quarry dust (g)	Ceramic dust (g)	
Control mix	276	348	576	0	6
C25%	276	348	432	144	6
C50%	276	348	288	288	6
C75%	276	348	144	432	6
C100%	276	348	0	576	6
Total	8280	10,440	8640	8640	30

2.2 Methods

2.2.1 Marshall Mix Design

Grading: BC Grade II.

Obtained proportion: 12 mm aggregate = 23%, 6 mm aggregate = 19%, Filler = 48% (Tables 3 and 4).

2.2.2 Marshall Test Specimen

The required value of optimum binder content was determined by Marshall, test and the mix design of Hot Mix Asphalt was done based on ASTM D1559 & IRC 111. The proportioned mixture of aggregate is heated to a temperature of 160–170 °C and binder to temperature of 140–147 °C and mixed thoroughly. Place the heated mix into the mould and provide mechanical compaction of 75 blows (for heavy traffic)

on both sides. Before Marshall stability test, keep the samples in water bath at a temperature of 60 °C for 30 min. Make specimens with 4%, 4.5%, 5%, 5.5%, and 6% bitumen content to obtain the value of optimum binder content.

2.2.3 Volumetric Parameters

The theoretical specific gravity G_t , the bulk specific gravity of the mix (G_m), the percentage of air voids (V_v), the percentage of bitumen volume (V_b), the percentage of voids in mixed aggregate (VMA), and the percentage of voids filled with bitumen (VFB) are the volumetric parameters that are relevant in Marshall analysis.

2.2.4 Marshall Stability and Flow Test

Marshall stability is the highest load needed to cause collapse. (5 cm per minute). Dial gauge is used to assess the specimen's vertical displacement as the stability test is being conducted. The Marshall flow value of the object measures the deformation at the failure spot in units of 0.25 mm.

3 Results and Discussions

3.1 Optimum Bitumen Content

The obtained values of Optimum Binder Content decreased with increase in ceramic dust. This indicates economic sustainability of ceramic dust modified bituminous concrete (Table 5).

Table 5 Table showing the Optimum bitumen content of control mix and ceramic dust modified mix

	Optimum bitumen content (%)
Control mix	5.6
25% ceramic dust	5.27
50% ceramic dust	5.23
75% ceramic dust	5.23

3.1.1 Marshall Stability

Marshall stability value increased by raising the ceramic replacement ratio (as in Table 6). At all replacement ratios of the ceramic dust, the Marshall stability was greater than that of the control specimen. A replacement ratio of 75% resulted in the highest Marshall stability, an increase of 22.2% over the specimen filled with quarry dust. According to MoRTH Table No. 500—11 for BC, the required Marshall stability is 9 kN. At all replacement ratios, the value of Marshall stability was greater than the prescribed limit. The strength of BC greatly improved due to adhesion of aggregate with bitumen (Fig. 2).

Table 6 Table showing the Marshall stability values of control mix and ceramic dust modified mix

Bitumen content (%)	Marshall stability (kN)			
	Control mix	C25%	C50%	C75%
4	6.74	7.41	7.74	9.88
4.5	8.54	9.18	9.74	10.25
5	9.86	10.45	11.35	12.05
5.5	9.75	10.71	11.20	11.58
6	8.44	9.14	9.70	10.36

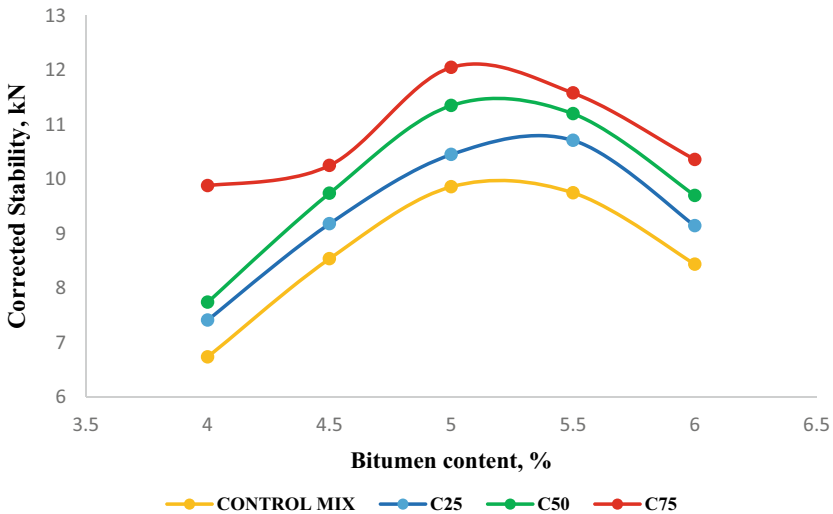


Fig. 2 Graph showing the variation of Marshall stability with bitumen content for control mix of BC and BC modified with 25, 50, and 75% ceramic dust

3.2 Marshall Flow Value

The variations in Marshall flow values for four different mixes are as shown in Table 7. The higher flow value indicates the maximum plasticity of asphalt and lower value of Marshall flow indicates the stiffness of asphalt concrete. The type of filler material has direct impact on stiffness. The analysis of results showed that specimens containing 75% Ceramic dust have the minimum flow value. It signifies increase in stiffness value. According to MoRTH Table No. 500—11, the required Marshall flow value is 2–4 mm. The results are within specified limits (Fig. 3).

Table 7 Table showing the Marshall flow values of control mix and ceramic dust modified mix

Bitumen content (%)	Flow value (mm)			
	Control mix	C25%	C50%	C75%
4	3.98	3.45	3.34	3.33
4.5	4.25	3.57	3.42	3.36
5	4.52	3.68	3.54	3.42
5.5	4.78	3.76	3.65	3.51
6	4.89	3.98	3.84	3.55

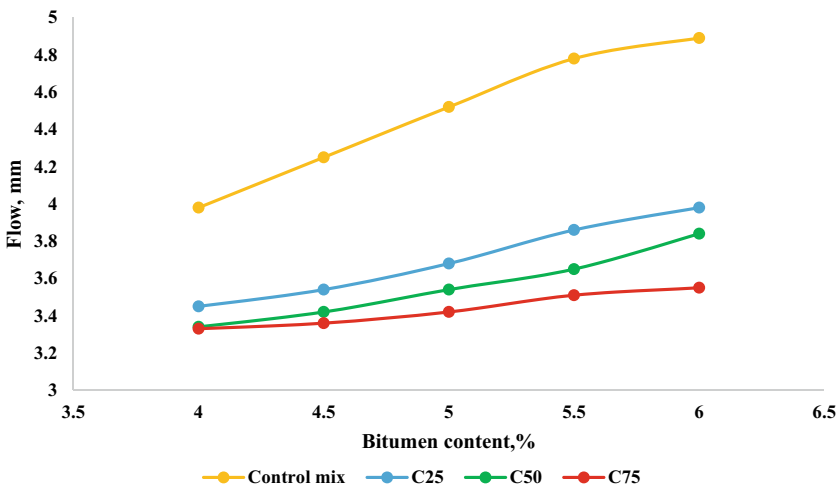


Fig. 3 Graph showing the variation of Marshall flow value with bitumen content for control mix of BC and BC modified with 25, 50, and 75% ceramic dust

3.3 Volumetric Parameters

3.3.1 Air Voids

Air voids (V_v) is the percent of air voids by volume in the specimen (Table 8 and Fig. 4).

The Air Voids is an important factor in defining asphalt mixtures. The replacement of filler with ceramic dust reduced the air voids. Ceramic dust modified bituminous concrete also have air voids within specified limits (3–5%), prescribed by MoRTH Table No. 500—11.

Table 8 Table showing the air voids in control mix and ceramic dust modified mix

Bitumen content (%)	Percentage air voids (%)			
	Control mix	C25%	C50%	C75%
4	4.928	4.720	4.62	4.540
4.5	4.783	4.622	4.225	4.119
5	3.741	3.613	3.541	3.452
5.5	3.654	3.394	3.425	3.104
6	4.074	3.861	3.112	2.988

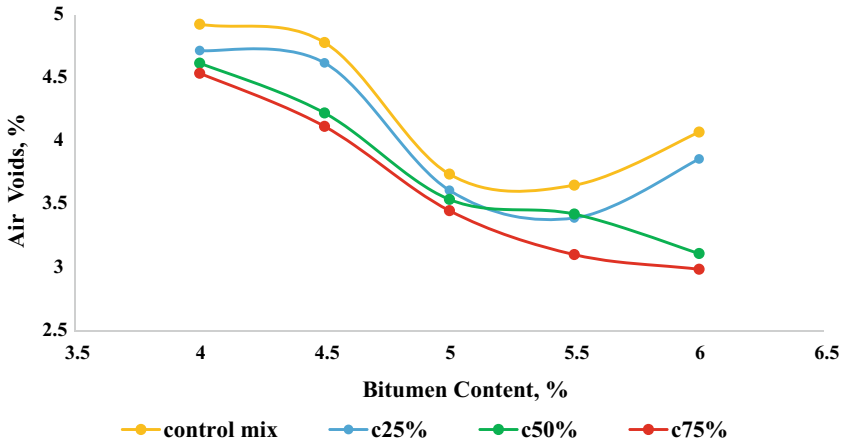


Fig. 4 Graph showing the variation of air voids with bitumen content for control mix of BC and BC modified with 25, 50, and 75% ceramic dust

Table 9 Table showing VMA of control mix and ceramic dust modified mix

Bitumen content (%)	VMA (%)			
	Control mix	C25%	C50%	C75%
4	14.14	13.94	13.91	13.89
4.5	13.80	13.74	13.72	13.67
5	13.70	13.68	13.61	13.54
5.5	13.75	13.65	13.55	13.47
6	13.60	13.45	13.32	13.20

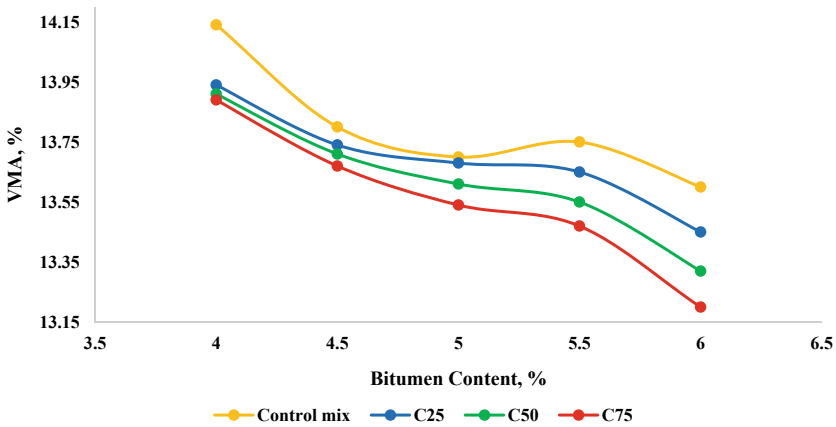


Fig. 5 Graph showing the variation of VMA with bitumen content for control mix of BC and BC modified with 25, 50, and 75% ceramic dust

3.4 Voids in Mineral Aggregate

Voids in mineral aggregate VMA is the volume of voids in the aggregates, and is the sum of air voids and volume of bitumen (Table 9 and Fig. 5).

The VMA in percentage indicates the combined percentage of voids filled with air and bitumen. Here it decreases with increase in percentage of ceramic dust due to decrease in air voids.

3.5 Voids Filled with Bitumen

VFB indicates the percentage of voids filled with bitumen. Ceramic dust modified bituminous concrete have VFB within the limits (65–75%), prescribed by MoRTH Table No. 500—11 (Table 10 and Fig. 6).

Table 10 Table showing VFB of control mix and ceramic dust modified mix

Bitumen content (%)	VFB (%)			
	Control mix	C25%	C50%	C75%
4	65.01	65.15	65.69	66.13
4.5	64.75	65.86	66.66	69.28
5	70.50	71.50	71.80	72.50
5.5	72.12	73.51	75.13	76.51
6	70.70	71.50	72.30	74.50

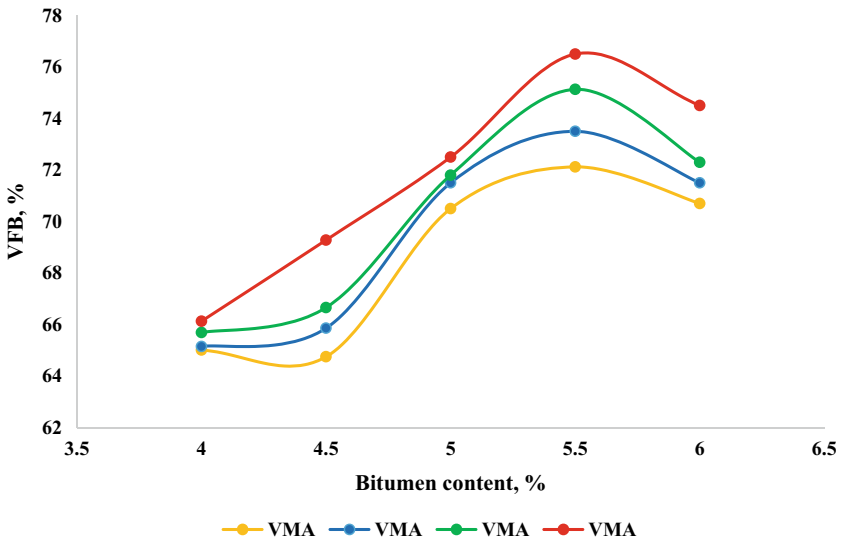


Fig. 6 Graph showing the variation of VFB with bitumen content for control mix of BC and BC modified with 25, 50, and 75% ceramic dust

4 Conclusions

The major objective of this experimental study was to evaluate the usage of ceramic waste dust as a filler material in bituminous concrete. The study proved that; the properties of ceramic dust modified asphalt mix was improved.

- Marshall stability values was increased by 7.86, 12.8%, 18.47% for the successive replacement of filler materials by 25, 50 and 75% of the control mix.
- Marshall flow value which indicates the deformation rate with the applied load reduces with increase in the amount of ceramic dust, indicates the improvement in stiffness of the mix.

- Air voids decreases with increase in ceramic dust implies the compactness of the mix.
- The volumetric properties which include Air voids, Voids in Mineral Aggregate, Voids Filled with Bitumen are within the specified limits prescribed by MoRTH.
- The obtained values of Optimum Binder Content are less than the minimum optimum value stated in MoRTH. It signifies the economic efficiency of ceramic dust modified Bituminous Concrete.
- All the volumetric parameters and stability characteristics are within standard limits with optimum binder content.
- Maximum Stability and Minimum flow were obtained with 75% replacement of quarry dust with ceramic dust.
- In addition to the enhancement in mechanical properties, the reuse of non-recyclable ceramic waste reduces the significant amount of trash and also reduce the demand of non-renewable natural resources.

5 Future Scope

- The Marshall behaviour of 100% ceramic modified Bituminous Concrete can be investigated.
- The elemental analysis on ceramic dust can be investigated.
- Spectroscopic study of ceramic dust modified specimens can be analysed.

References

1. Bhavin, Bhatt (2018) A study on the effect of ceramic tiles in flexible pavement. *Int J Adv Eng Res Dev*
2. Wozzuk A, Bandura L, Franus W (2019) Fly ash as low cost and environmentally friendly filler and its effect on the properties of mix asphalt. *J Clean Prod* 235:493–502
3. Agrawal A, Singh A, Imam A (2020) Utilization of ceramic waste as a sustainable building material. In: National conference on structural engineering, NCRASE
4. Ray S, Haque M, Sakib MN, Mita AF, Masnun Rahman MD, Tanmoy BB (2021) Use of ceramic wastes as aggregates in concrete production: a review. *J Build Eng* 43:102567
5. Chen JA, Idusuyi FO (2015) Effect of waste ceramic dust (WCD) on index and engineering properties of shrink-swell soils. *Int J Eng Mod Technol* 1(7):1–11
6. Saravanan, Sowmiya, Ramya (2013) The effect of waste ceramic on strength properties of clay soil in pavement construction. *Int J Res Civ Eng*. 1:68–74
7. Awoyera PO, Ndambuki JM, Akinmusuru JO, Omole DO (2018) Characterization of ceramic waste aggregate concrete. *HBRC J* 14(3):282–287
8. Deboucha S, Aissa Mamoune SM, Sail Y, Ziani H (2020) Effects of ceramic waste, marble dust, and cement in pavement sub-base layer. *Geotech Geol Eng* 38(3):3331–3340
9. Harun-Or-Rashid GM, Al Mamun A, Epu IE (2020) Comparative study on Marshall characteristics of bituminous mixes by partial replacement of foundry sand and ceramic tile dust as fine aggregate. *American J Mater Synth Process* 5(1):10–16

10. Kannan DM, Aboubakr SH, El-Dieb AS, Taha MR (2017) High performance concrete incorporating ceramic waste powder as large partial replacement of Portland cement. *Constr Build Mater* 144:35–41
11. Kofteci, Nazary (2020) Utilization of crushed ceramic tile waste as partial replacement of coarse aggregate in concrete production. *Int J Res Civ Eng*
12. Lekhaz DS, Sreenath R, Mohan MK, Naidu Vasudeva M (2016) A study on bituminous concrete mix with cement, GGBS, brick dust as a filler. *Int J Eng Sci Comput* 6
13. MoRTH (2013) Specifications for road and bridge works. Fifth Revision, Indian Roads Congress, New Delhi
14. Olugbenga OJ (2019) Utilization of industrial waste products in the production of asphalt concrete for road construction. *Slovak J Civ Eng* 27(4):11–17
15. Pereira LM, Freire AC, Da Costa MS, Antunes V, Quaresma L, Micaelo R (2018) Experimental study of the effect of filler on the ductility of filler-bitumen mastics. *Constr Build Mater* 189:1045–1053
16. Shamsaei M, Khafajeh R, Aghayan (2019) Laboratory evaluation of the mechanical properties of roller compacted concrete pavement containing ceramic and coal waste powders. *Clean Technol Environ Policy* 21:707–716
17. Suvama, Lokesh, Mahendra (2018) Study on the effect of stone, dust, ceramic dust and brick dust as fillers on the strength, physical and durability properties of bitumen. *Int J Appl Eng Res*
18. Subedi, Wagle, Keshav (2020) Comparative study on Marshall characteristics of bituminous mixes by partial replacement of foundry sand and ceramic tile dust as fine aggregate. *American J Mater Synth Process*
19. Sutradhar D, Miah M, Chowdhury GJ, Sobhan MA (2015) Effect of using waste material as filler in bituminous mix design. *American J Civ Eng* 3(3):88–94
20. Torkittikul P, Chaipanich A (2010) Utilization of ceramic waste as fine aggregate within Portland cement and fly ash concretes. *Cement Concr Compos* 32(6):440–449

A Case Study on the Shortage of Availability of Skilled Labour in Faridabad, Delhi—NCR



Ashutosh Kumar and Yaman Hooda

Abstract This study examined the need for skilled labour in Faridabad (Delhi-NCR) construction sector. The study's goal was to assess the current situation of the skilled labour force in the construction sector, the reason behind the low frequency of skilled workers, and their impact on the completion of construction projects. The technique used for data collecting includes the spreading of structured questionnaires. Frequency tables, percentages, mean response analysis, relative importance index, and cross-tabulation were used to analyze the data. Furthermore, the most serious causes of a labour shortage turned out to be a lack of a clear career path, the great mobility of construction employees, and low pay. According to the study, construction companies do not send their skilled personnel to training programs. The study found that the lack of trained labour was causing construction companies to overpay for labour and cause schedule delays in their construction projects. Also, the study indicated that the sampled construction trades had an ageing labour base and that the entry of young workers was quite low.

Keywords Construction industry · Skilled labours · Shortage · Mean response analysis · Delays

1 Introduction

India is a growing economy with the second-fastest economic growth in the world (8.9%) and the fourth-largest GDP (US\$ 3.6 trillion) [1]. By 2050, India crosses a population of 1.7 billion, surpassing China the country with the most people, by 400 million [2]. To meet this demand, the current infrastructure as well as the construction industry will be under a great deal of strain. The process of construction is intricate

A. Kumar · Y. Hooda (✉)

Department of Civil Engineering, Manav Rachna International Institute of Research and Studies, Faridabad, Haryana, India

e-mail: yamanhooda@gmail.com

and well-organized. It's not just a science or a business; it's also a creative art. It is a gratifying, often difficult, and demanding discipline for everyone involved, from the newest recruit to the experienced craftsman. Every worker working in the construction industry directly benefits the nation as a whole as well as the locality in which they are employed [3]. There are frequent labour shortages in the construction sector because of the relatively high rates of attrition among wage workers and subcontractors [4–7].

The skilled craft shortage is not due to less number of workers, it is a lack of workers who are competently skilled, productive, and available for particular jobs. Replacement and hiring remain difficult in the construction business since some of the most highly skilled workers must perform some of the most hazardous occupations. Lack of training, an ageing workforce, worker's negative perceptions and a field that does not appeal to many young people have all been cited as causes of the skilled labour shortage [8–11].

According to the authors of [12, 13], skill shortages are a complicated labour market phenomenon linked to business success. They went on to explain that skill gaps are typically presented as a major problem for the economy of most countries. However, the evidence regarding their incidence, reasons and effects in the Indian construction sector is shockingly scant. Still, there aren't any figures that demonstrate why there aren't enough talented craftspeople in the construction sector, construction experts and others. This study is being done in response to stakeholder concerns regarding the alleged dearth of trained labourers and the potential effects that this dearth may be having on the construction sector's capacity to achieve the rising demand for household and industrial development. Therefore, this research evaluates the situation of the Indian construction sector focusing on the Delhi-NCR Faridabad region concerning the commonness, origin & impacts on the completion of commercial projects of the skilled labour shortage. The worker's crafts used for this study were glazing, painting, tiling & bricklaying. These crafts were picked because of how much effect they have on the building construction business. A variety of factors have united to affect the shortage of building skills, some of which include; new technological developments which have developed the necessary skill [8, 14–16]. An increase in independent work & the use of workers-only subcontractors have decreased Industry support and training expenditures. The decline in trainee members and the number of self-employed craftsmen are related, as the latter cannot manage their concerns with qualification improvement. The unfavourable perception of the sector has an impact on how popular it is as a career path. Since most construction craftspeople of a wide range of ages & various levels of experience and would never suggest their line of work to their future ward, the reputation is poor among the workers themselves. Construction workers move around a lot because of their unappealing appearance, poor working conditions, unpredictable workloads, lack of respect, and lack of training possibilities. Because they were dissatisfied with the labour organisation, newly hired workers have been released, and this is specifically due to the unpredictable workload.

2 Methodology

The study looked at the workforce and state of the construction industry in Delhi—NCR focused on the Faridabad region. Preliminary data were gathered and collected by a survey to utilize in this study. This involves providing answers to a standardized questionnaire in conjunction with a personal interview. Two (2) different types of questionnaires were created and given out. Both were intended to gather information from experienced employees in various professions about their impressions of the major difficulties affecting the construction industry.

The initial survey was designed to collect data from managers of construction companies with projects in Faridabad. Construction trades used for this study were painting, glazing, tiling, and bricklaying. These trades were chosen due to their level of dominance in the construction sector. These questionnaires were distributed to reach all of the Faridabad districts. The building contractors in this district were chosen using a systematic random sampling technique, although the decision of each contractor was based on the overall number of such businesses present there.

2.1 Data Frame Size

The construction companies registered with the PWD (Public works department), Haryana state government and others working on local government projects made up the sample frame for this study. The sampling frame consisted of 125 different firms in total. For this investigation, a sample size of 40% of the sample frame, or 50 firms, was used for questionnaire type A (Questionnaire type A). 60% of the sample size was used for the second questionnaire, which was dedicated to the executives and owners of construction companies, and the tradespeople received the other form of a questionnaire (Questionnaire type B). Cross tabulation, percentage, frequency distribution, mean response analysis (MRA), and relative relevance index (RRI) are just a few of the analytical/statistical techniques that were applied to analyse the data obtained for this research study.

3 Result in Discussion and Data Analysis

The various questions asked Questionnaire I, along with their responses are depicted in the tables below.

The respondent's academic and professional qualifications are represented in Table 1 above. This demonstrates that the respondent possesses the necessary skills in the field to efficiently fill their quota in this study.

Table 1 Respondents' educational and occupational backgrounds

Description	Frequentness	Percent (%)
Matriculated	3	6
Intermediate	9	18
Diploma	19	38
Graduate	14	28
Masters	4	8
Doctorate	1	2
Total	50	100

Table 2 shows the Respondent's occupations in the construction sector. This demonstrates that the respondents are a diverse group of professionals who have the necessary understanding of the issue at hand to give their fair share.

Table 3 displays the working experience of respondents. This demonstrates that all the company's test data represent a sufficient variable in experience.

Table 4 displays the respondent sample's type of business setup. This has the consequence that all the company's test data represent small, medium, and large business operations.

The type of work performed by the individual firms examined is shown in Table 5 in more detail. Building work was completed by 44%, civil engineering work by 18%, and both building and civil engineering work by 38% of participants.

Table 2 Respondents' occupations in the construction sector

Description	Frequentness	Percent (%)
Surveyors	2	4
Architecture	7	14
Building	12	24
Civil engineering	15	30
Quantity surveying	5	10
Others	9	18
Total	50	100

Table 3 Working experience of respondents

Description	Frequentness	Percent (%)
< 2 Years	2	4
2-4 Years	20	40
5-7 Years	6	12
8-10 Years	9	18
Over 10 Years	13	26
Total	50	100

Table 4 Type of business organization

Type of business	Frequentness	Percent (%)
Individual business	19	38
Partnership	7	14
Private limited company	11	22
Public limited company	13	26
Total	50	100

Table 5 Type of work being done

Type of work	Frequentness	Percent (%)
Household works	22	44
Civil engineering works	9	18
Both household and civil engineering works	19	38
Total	50	100

The sampled construction company's total number of permanent staff is shown in Table 6. 48% had fewer than 30 staff, 34% had between 30 and 100 staff, and 18% had more than 100 staff who work as permanent employees of three different companies.

The manner of hiring used in the tested firms is displayed in Table 7. This demonstrates that the businesses employed various methods of hiring workers based on which ones suited those best.

Table 6 Number of permanent staff members

Permanent staff members	Frequentness	Percent (%)
< 30 staff members	24	48
30–100 staff members	17	34
Over 100 staff members	9	18
Total	50	100

Table 7 Hiring method

Hiring method	Frequentness	Percent (%)
Formal interviews only conducted via head office	10	20
Formal interviews only conducted via the regional office	8	16
Without a formal interview, on the spot	14	28
Combination of all of the above	18	36
Total	50	100

Table 8 Lack of skilled workers

Lack of skilled workers	Frequentness	Percent (%)
Yes	41	82
No	9	18
Total	50	100

Table 9 Skilled labour shortage in bricklaying

Description	Frequentness	Percent (%)
Yes	33	66
No	17	34
Total	50	100

Table 10 Skilled labour shortage in tile setter

Description	Frequentness	Percent (%)
Yes	37	74
No	13	26
Total	50	100

Table 8 demonstrates whether there is a skilled worker shortage in the construction sector. 50 respondents participated and the most of respondents, 82%, agreed that yes skilled workers are scarce, while only 18% disagreed. This implies the majority of managers in the construction business concur that there is a lack of trained workers in various professions.

The skilled worker shortage in the above trades examined in the construction sector is seen in Tables 9, 10, 11, and 12. A skilled labour shortage is present in 66% of the bricklaying industry, 74% of the tile setter industry, 78% of the glazing industry, and 62% of the painting industry. This demonstrates that managers were facing a skilled labour shortage in the four sampled trades.

Table 11 Skilled labour shortage in glazing

Description	Frequentness	Percent (%)
Yes	39	78
No	11	22
Total	50	100

Table 12 Skilled labour shortage in painting

Description	Frequentness	Percent (%)
Yes	31	62
No	19	38
Total	50	100

Table 13 Rate of lack of worker in bricklaying

Description	Frequentness	Percent (%)
Very low	15	30
Low	18	36
Moderate	4	8
High	4	8
Very high	9	18
Total	50	100

The rate of lack in bricklaying can be seen in Table 13. 32% of respondents thought there was a very low rate of labour shortage, followed by 38% who thought there was a low rate, while 10% thought there was a high rate and 20% thought there was a very high rate. This demonstrates that the labour scarcity rate for bricklaying has not risen to an alarming level.

The labour shortage rate for tile setters is seen in Table 14. 22% of respondents thought there was a very low rate of labour shortage, 42% thought there was a low rate, 16% thought there was a high rate, and 20% thought there was a very high rate.

The rate of the glazing labour shortage is displayed in Table 15. 18% of respondents thought there was a very low rate of labour shortage in this trade, 22% thought there was a low rate, 42% thought there was a high rate, and 18% thought there was a very high rate.

The rate of the painting labour shortage is displayed in Table 16. While 30% of the data indicates a high rate and 22% indicates a very high rate of scarcity, 30%

Table 14 Rate of labour shortage in tile setter

Description	Frequentness	Percent (%)
Very low	10	20
Low	19	38
Moderate	5	10
High	7	14
Very high	9	18
Total	50	100

Table 15 Rate of labour shortage in glazing

Description	Frequentness	Percent (%)
Very low	8	16
Low	10	20
Moderate	4	8
High	20	40
Very high	8	16
Total	50	100

Table 16 Rate of labour shortage in painting

Description	Frequentness	Percent (%)
Very low	13	26
Low	7	14
Moderate	5	10
High	15	30
Very high	10	20
Total	50	100

of the data indicates a very low rate and 16% a low rate. This demonstrates that the labour shortage rate in this industry is quite low.

Rate of lack of worker in the examined crafts was determined using RII.

The relative importance index results Rate of lack of worker in the four sampled skills is shown in Table 17 (Glazing, tile setter, bricklaying and painting). The findings indicate that glazing has the highest rate of skilled labour shortage, followed by painting, tile setter, and painting in that order.

The application of Mean Response Analysis (MRA) for the relatable reasons for the skilled labour shortage in the construction sector is shown in Table 18. High mobility of construction workers, poor earnings, dwindling programmes for educating craftspeople, and growth in self-employment were all ranked after. No clear career path in that order, with the Poor image of the industry receiving the lowest score.

The various questions asked Questionnaire II, along with their responses are depicted in the tables below:

The various trades assessed for this study are listed in Table 19. A total of hundred (100) printed and distributed questionnaires. Twenty for each of the four trades (tile setters, bricklayers, painters & glazers). 75% of respondents responded, which is sufficient for the project’s work.

According to Table 20, approximately 92% of respondents’ crafts in the construction industry in the research region were held by men. This indicates a male predominance in those crafts.

Table 21 presents the distribution of surveyed worker’s ages. Among the respondents, 2.7% were between the age of 18 and 24, 18.7% were between the ages of 25 and 34, 33.3% fell within the age range of 35 to 44, 20% were between 45 and 49 years old, and 25.3% were over 50 years old. These findings indicate that a

Table 17 Relative importance index (RII) for the rate of skilled labour shortage

Questions (13–16)	RII	Rank
Rate of lack of worker in glazing	0.64	1
Rate of lack of worker in painting	0.60	2
Rate of lack of worker in tile setter	0.54	3
Rate of lack of worker in bricklaying	0.49	4

Table 18 Analysis of the mean response for the reasons of the lack of worker

Question 17	MRA	Rank
No clear-cut career path	2.83	1
High mobility of construction workers	2.69	2
Low wages	2.67	3
Lack of tradesperson training programme	2.61	4
Increasing of self-employment	2.58	5
Not satisfied with labour organization	2.53	6
Increase in new technologies	2.47	7
Ethnic characterization	2.44	8
Safety of construction worker	2.31	9
Poor image of the industry	2.03	10

Table 19 Type/craft types

Description	Frequentness	Percent (%)
Tile setters	19	25.3
Bricklayers	20	26.7
Glazers	19	25.3
Painters	17	22.7
Total	75	100

Table 20 Gender of worker

Description	Frequentness	Percent (%)
Male	69	92
Female	6	8
Total	75	100

significant majority, specifically 78.6% of the workers, are aged 35 or above. This demonstrates how few young people are entering the construction sector, which has major implications for the future of the sector in India in terms of the need for skilled labour.

Table 21 Age of worker

Description	Frequentness	Percent (%)
18–24 years	2	2.7
25–34 years	14	18.7
35–44 years	25	33.3
45–49 years	15	20
Above 50 years	19	25.3
Total	75	100

Table 22 Place of living to site/office

Description	Frequentness	Percent (%)
On-site	8	10.7
< 5 km	22	29.3
> 5 km	45	60
Total	75	100

Table 23 Nature of employment

Description	Frequentness	Percent (%)
Permanent workers	3	4
Daily basis	31	41.3
Contract basis	25	33.3
Sub-contractor	16	21.4
Total	75	100

In Table 22, the distribution of respondents' residential proximity to their work sites/offices is presented. According to the data, 10.7% of the respondents reported living on-site, 29.3% lived within a distance of under 5 km, and the majority, 60%, lived more than 5 km away. This implies that if the firm lacks transportation options for workers to commute to the work site, the cost of transportation for employees to reach their respective locations would be higher.

The type of skilled labour employment is shown in Table 23. Only 4% of respondents worked as permanent employees for the building company, while 41.3% received daily pay, 33.3% were contract workers and 21.4% were subcontractors. The significance of this is that construction companies were not utilizing skilled workers on a permanent basis.

Table 24 displays the workers' employment qualifications. A total of 69.3% of respondents had basic qualifications while only 30.7% have desired qualifications for the construction sector. This implies that a bigger fraction of workers just have a primary school education and they may not be able to accurately fulfill orders given to them by their supervisor, Engineer & in charge.

Table 25 displays the degree to which employees are satisfied with their earnings. 18.7% of respondents believe their wages are very good, 38.7% believe they were good, 16% believe they were fair, and 25.3% believe they were poor. This implies that a higher proportion of people are dissatisfied with their salaries.

Table 26 illustrates the impact of the lack of skilled worker force. When asked if skilled workers were scarce in their trades, 64% of the respondents said yes, compared to 25.3% who said no and 10.7% who did not answer.

In Table 27, the focus was on how construction companies provide training to their employees. The respondents were asked about the frequency at which their companies send them for training. The results indicate that 21.3% of the respondents answered negatively, stating that they were not sent for training at all. On the other hand, 10.7% mentioned that they were sent for training regularly, 14.7% reported

Table 24 Qualification of worker

Description	Frequentness	Percent (%)
No response	1	1.3
No qualification	5	6.7
Up to Primary school	12	16
Primary school + Apprenticeship	15	20
Up to Secondary school	19	25.3
Secondary school + Apprenticeship	8	10.7
ITI in their trade	8	10.7
Pradhan Mantri Kaushal Vikas Yojana (PMKVY)	7	9.3
Total	75	100

Table 25 Employees level of satisfaction with received salaries

Description	Frequentness	Percent (%)
No response	1	1.3
Very good	14	18.7
Good	29	38.7
Fair	12	16
Poor	19	25.3
Total	75	100

Table 26 Skilled labour shortage

Description	Frequentness	Percent (%)
No response	8	10.7
Yes	48	64
No	19	25.3
Total	75	100

irregular training opportunities, and the majority, 53.3%, indicated that they had never been sent for training.

Table 27 Training schedule for construction's permanent staff

Description	Frequentness	Percent (%)
No response	16	21.3
Regular	8	10.7
Not regular	11	14.7
Never on training	40	53.3
Total	75	100

Table 28 Reasons why construction companies don't send staff to training

Description	Frequentness	Percent (%)
No response	22	29.3
Cost	38	50.7
Worry about switching jobs	12	16
Others	3	4
Total	75	100

Table 29 Recommendation this profession for their future ward

Description	Frequentness	Percent (%)
No response	17	22.7
Yes	18	24
No	40	53.3
Total	75	100

Table 28 displays the findings of the objective of why the construction sector didn't train their employees. When asked about reasons construction companies weren't sending workers out for training, 29.3% of respondents offered no explanation, 50.7% cited financial concerns, and 16% cited apprehension about leaving for employment with another firm.

The outcome of the recommendation of a trade or profession to respondents' children or future wards is shown in Table 29. When asked if they would advise their children to pursue this line of work, 24% of respondents said yes, compared to 53.3% who said no, and 22.7% who did not respond. This implies that tradesmen were not proud of their line of work.

When asked why this trade or profession could not be recommended for the respondents' children, 4.6% of the respondents had no response, 18% cited low pay, 16.9% cited a lack of a clear career path, 3.4% cited poor safety standards for construction work, while 43.8% cited a negative perception of the trade, and 3.4% cited reasons that were slightly different from those mentioned above (Table 30).

Tile setters comprise 0% of the workforce between the ages of 18 to 24, 5.3% between the ages of 25 to 34, 26.3% between the ages of 35 to 44, 21.1% between the ages of 45 to 49, and 47.3% above the age of 50. The conclusion of this is that no new young people entered the Tile setter sector and that the age of over 45% of Tile setters is already near 50 and continuing to rise. This has important implications for the construction sector. Bricklayers comprise 5% of the workforce between the ages of 18 to 24, 25% between the ages of 25 to 34, 40% between the ages of 35 to 44, 10% between the ages of 45 to 49, and 20% above the age of 50. The conclusion of this is that no new young people entered the Bricklaying sector and that the age of over 45% of Bricklayers is already near 50 and continuing to rise. This has important implications for the construction sector. Glazers comprise 5.3% of the workforce between the ages of 18 to 24, 15.7% between the ages of 25 to 34, 36.8% between the ages of 35 to 44, 21% between the ages of 45 to 49, and 21% above the age of 50.

Table 30 Their trade *age (cross tab)

Description		Age					Total
Type of trade		18–24 years	25–34 years	35–44 years	45–49 years	Above 50 years	
Tile setters	Count	0	1	5	4	9	19
	% within type of trade	0.0%	5.3%	26.3%	21.1%	47.3%	100.0%
	% within age	0.0%	7.1%	20%	26.7%	47.3%	25.3%
	% of Total	0.0%	1.3%	6.7%	5.3%	12.0%	25.3%
Bricklayers	Count	1	5	8	2	4	20
	% within type of trade	5.0%	25%	40%	10%	20%	100.0%
	% within age	50%	35.7%	32.0%	13.3%	21.0%	26.6%
	% of Total	1.3%	6.6%	10.6%	2.6%	5.3%	26.6%
Glazing	Count	1	3	7	4	4	19
	% within type of trade	5.3%	15.7%	36.8%	21.0%	21.0%	100.0%
	% within age	50%	21.4%	28.0%	26.6%	21.0%	25.3%
	% of Total	1.3%	4.0%	9.3%	5.3%	5.3%	25.3%
Painting	Count	0	5	5	5	2	17
	% within type of trade	0.0%	29.4%	29.4%	29.4%	11.8%	100.0%

(continued)

Table 30 (continued)

Description		Age					Total
Type of trade		18–24 years	25–34 years	35–44 years	45–49 years	Above 50 years	
	% within age	0.0%	35.7%	20.0%	33.3%	10.5%	22.7%
	% of Total	0.0%	6.7%	6.6%	6.6%	2.7%	22.7%

Table 31 Relative importance index of impact of a labour shortage

	RII	Rank
Extra compensation for labour	0.6875	1
Lack of labour results in schedule delay	0.6805	2
Experiencing cost overruns	0.6597	3

The conclusion of this is that no new young people entered the Glazing sector and that the age of over 45% of Glazers is already near 50 and continuing to rise. This has important implications for the construction sector. Painters comprise 0% of the workforce between the ages of 18 to 24, 29.4% between the ages of 25 to 34, 29.4% between the ages of 35 to 44, 29.4% between the ages of 45 to 49, and 11.8% above the age of 50. The conclusion of this is that no new young people entered the Painting sector and that the age of over 45% of Painting is already near 50 and continuing to rise. This has important implications for the construction sector.

The relative importance index for the effects of the skilled labour shortage in the construction industry is shown in Table 31. According to the results, paying more for labour was ranked first, followed by a schedule delay brought on by labour scarcity and promoting cost overruns [17].

4 Conclusion

In the evaluation of the need for skilled labour in the construction sector in the Faridabad district (Delhi-NCR), 74% of the managers polled concurred that trained labour was scarce in the four trades selected (i.e. glazing, painting, tile setter, and bricklaying), with:

- 54% of tile setters, 49% of bricklayers, 64% of glazing, and 60% of painters said skilled workers were scarce in their respective crafts.
- The most serious reasons contributing to the skilled labour shortage were the lack of a clear career path, the high mobility of construction workers, the low earnings, the ageing workforce, the perception and image of the industry, lack of

diversity and inclusivity, insufficient investment in workforce development and the declining number of programmes for craftsperson training.

- The implications of a skilled labour shortage include paying more for labour, schedule delays due to a lack of workers, and cost overruns. The results show an ageing workforce in the sampled construction professions, with over 94% of tile setters over the age of 35, 70% of bricklayers over the age of 35, approximately 78% plumbers over the age of 35, and 70% of painters over the age of 35. The study discovered an extremely low entry rate for young people between the ages of 18 and 25 into the sampled building trades.

The overall efficiency of the project depends on its timely completion, which further depends on an effective workforce in construction engineering and management [18]. With the help of the availability of skilled labour, the overall efficiency of the project may increase in terms of completion time and economics. Thus, a special clause must be put in during the finalizing the tender regarding the employment of skilled labours (partially or full) in any project so that the contractors and sub-contractors must give training to their respective man force for winning the bid for the tender and completion of the project, without any delay.

References

1. Nihlas S, Barlish KC, Kashiwagi DT (2013) Construction industry structure in India. In: RICS COBRA conference, p 9
2. DeSA U (2013) World population prospects: the 2012 revision. Popul Div Dep Econ
3. Arshad RA (1997) Training needs of Malaysian construction site managers X *
4. International Labour Organization (2019) Skills shortages and labour migration in the field of information and communication technology in India, Indonesia and Thailand
5. Buckley M, Adam Z, Biggar J, Frederiksen L, Wells J (2016) Migrant work & employment in the construction sector
6. Erlich M, Grabelsky J (2005) Standing at a crossroads: the building trades in the twenty-first century. *Labor Hist* 46(4):421–445. <https://doi.org/10.1080/00236560500266241>
7. McGrath-Champ S, Rosewarne S, Rittau Y (2011) From one skill shortage to the next: the Australian construction industry. *J Ind Relations* 53(4):467–485
8. Management and sustainable use of water at (2004)
9. Dainty ARJ, Ison SG, Root DS (2004) Bridging the skills gap: a regionally driven strategy for resolving the construction labour market crisis. *Eng Constr Archit Manag* 11(4):275–283. <https://doi.org/10.1108/09699980410547621>
10. Cardoso dos Santos Durão LF, Vinicius Di Favari Grotti M, Rafael Minetto Maceta P, de Senzi Zancul E, Tobal Berrsaneti F, Monteiro Carvalho M (2017). A review of the soft side in project management: concept, trends, and challenges. *Rev Gestão da Produção Operações e Sist* 12(2):157–176. <https://doi.org/10.15675/gepros.v12i2.1644>
11. Lill I (2017) Sustainable management of construction labour. In: ISARC 2008—proceedings from 25th international symposium on automation and robotics in construction. <https://doi.org/10.22260/isarc2008/0124>
12. McNabb DE et al (2010) Active labor market policy evaluations: adjusting to skill shortages: complexity and consequences. *Occup Labor Short Concepts Causes Conseq Cures* 18(4):1–6. <https://doi.org/10.1108/09699980410547621>

13. Sloane PJ, Healy J (2011) Active labor market policy evaluations: adjusting to skill shortages: complexity and consequences, no 171, p 33. <http://ftp.iza.org/dp6097.pdf>
14. Oseghale B, Dr Abiola-Falemu J, Oseghale G (2015) An evaluation of skilled labour shortage in selected construction firms in Edo state, Nigeria. *Am J Eng Res* 4(1):156–167. www.ajer.org
15. Agapiou A, Price ADF, Mc Caffery R (1995) Planning future construction skill requirements: understanding labour resource issues. *Constr Manag Econ* 13(2):149–161. <https://doi.org/10.1080/01446199500000017>
16. Wells J, Wall D (2003) The expansion of employment opportunities in the building construction sector in the context of structural adjustment: some evidence from Kenya and Tanzania. *Habitat Int* 27(3):325–337. [https://doi.org/10.1016/S01973975\(02\)00041-3](https://doi.org/10.1016/S01973975(02)00041-3)
17. Swami T, Hooda Y (2022) Delay assessment in construction projects using six sigma in Indian context. *NICMAR J Constr Manag* 37(IV):5–13
18. Shifnas MF, Sutha J (2016) Impact of effective workforce diversity management on employees' performance in construction sector. *Annu Int Res Conf* 2005:237–248. <http://ir.lib.seu.ac.lk/handle/123456789/1930>

An Evaluation of Road Network Vulnerability Using Geospatial Techniques



Cynthia Baby Daniel, Sreya Madhavan, Samson Mathew,
and Subbarayan Saravanan

Abstract Vulnerability in simple terms is the diminution of the quality of a network when it is subjected to failures and attacks. It denotes the consequences of a malfunction of a link or node in a network. Road networks being the most important urban infrastructure, evaluating their vulnerability becomes an essential task in understanding the performance of a network. The main objective of this study is to evaluate the robustness or vulnerability of the road network in the Central Business District of Tiruchirappalli City, South India using Geographical Information System (GIS). The critical nodes and links are identified using centrality measures to analyze their ability to withstand unpredicted and exceptional disturbances. The changes in connectivity, coverage and topology are measured using a set of indices such as alpha index, beta index, gamma index, eta index, network density, node density, edge density, grid tree pattern etc. The centre of Tiruchirappalli city is considered for this analysis and the robustness of the study area is determined. This paper focuses on computing the friability of the road network by quantifying the reduction in connectivity and efficiency of the network focusing mainly on graph theoretical parameters on removing the critical nodes and links.

Keywords Road network Robustness · Vulnerability · Critical node · Critical link · Betweenness centrality · GIS

C. B. Daniel (✉) · S. Madhavan · S. Mathew · S. Saravanan
Department of Civil Engineering, National Institute of Technology Tiruchirappalli,
Tiruchirappalli, Tamil Nadu, India
e-mail: cynthiababydaniel@gmail.com

1 Introduction

Human society depends on spatial systems and artefacts called urban infrastructures to sustain or improve the standard of living of the people. It connects spatially separated locations to people for economic efficiency and accessibility to business. The shortcoming of this dependency is that even a minor or unplanned disruption [11], in the system affects the entire network and can lead to severe consequences. These disturbances may bring back the system to its normalcy or may highly disrupt the system [15]. They worsen the users' accessibility to daily activities or even emergency medical care which can at times, be a life-threatening issue. The damages or disruption occurring to the transport system may be of varying scale and magnitude. It could range from a minor road accident or traffic jam to major environmental hazards like landslides or earthquakes, floods etc. In order to reduce the effect of these damages, critical nodes and links should be found in advance. Certain measures should be adopted to protect them, such as frequent maintenance for the critical infrastructures, and construction of new alternative parallel paths, which guarantees the reliability of the road network and reduces economic losses.

In the case of transport network models, network analysis becomes an efficient tool for transport and urban planners. Networks can be represented in many forms based on the type of study. Many researchers have depicted streets in such as primal [12, 13], dual [14, 16], axial [2, 7, 10] representations etc. A primal representation preserves the spatial layout of the road network and hence has been adopted in this study. Computing road network vulnerability is extremely vital in the planning and construction phase as well as for the management of the roads [20]. In simple terms, vulnerability can be stated as the diminution of the quality of a network due to the factors that stress it. As mentioned by [5, 6], vulnerability analysis can be grouped into two stages namely, finding the probability of the occurrence of disruptions and the consequences of the disruptions that affect the system. Friability can be defined as the overall reduction in the resilience of a network on the removal of a node or an edge [4].

Connectivity is essentially the ability of a network to maintain connections between two or more points in a spatial system and is an inherent characteristic of a network. Connectivity patterns and complex systems are vital for the improvement of the vulnerability and resilience of transport systems [15]. An understanding of network performance will help in choosing more number of acceptable options at the planning horizon and also help to cope with errors during execution. Comparatively lesser theoretical research efforts have been put into the evaluation of urban networks. Urban network evaluation has immense prospects for application projects in developing countries due to the lesser number of studies carried out [18, 19]. There has been a rising interest among researchers in utilizing GIS for complex network analysis, particularly in India in recent years, [3, 18, 19]. Network geography has been simplified to a great extent with the advancement of Geographical Information System (GIS) over the years.

This paper focuses on determining the critical nodes and links in a road network using GIS and computing the friability of the network in terms of the reduction in connectivity and efficiency of the network focusing mainly on graph theoretical parameters on removing the critical node and links.

2 Network Terminologies

A graph is a symbolic representation of a network and its connectivity. A directed graph $G = (e, v)$ consists of a set “v” of vertices or nodes and a set “e” of edges or arcs whose elements are ordered pairs of distinct nodes [1]. A road network is a directed graph where vertices (v) correspond to the junctions or street intersections and the edges (e) as road segments between them. Network measures can be categorised under three heads namely; connectivity, coverage and topology.

2.1 Critical Node

Evaluation of critical nodes can be decisive in quantifying the effect on neighbouring nodes because of damage on the critical nodes. The critical node is the most important node of a network [9] and is determined from the degree centrality method in this study.

For a directed graph, degree of a vertex $D(v)$ can be defined as the sum of its in-degree and out-degree. In-degree (D_i) is the total number of incoming links attached to the node and out-degree (D_o) is the total number of outgoing links attached to the node. For an undirected graph, the total degree is the no. of links connected to it.

Mathematically,

$$D(v) = D_i + D_o \quad (1)$$

The node with the highest degree is the most critical. The nodes are then prioritized based on node betweenness.

2.2 Critical Link

The critical link can be identified both for weighted as well as unweighted graphs. For an unweighted graph, a link is critical if the maximum number of shortest paths passes through that link. For a weighted graph, a link becomes critical if the flow value is maximum through that link. The critical link is the link with the max number of shortest paths passing through it or the link with the maximum betweenness centrality (BC) value.

$$BC(i)r = \sum_{j,k \in G - \{i\}, d[j,k] \leq r} \frac{n_{jk(i)}}{n_{jk}} \cdot W[j] \quad (2)$$

where Betweenness $BC(i)r$ is the betweenness of junction i within the search radius r , $n_{jk(i)}$ is the number of shortest paths from node j to node k that pass by node i ; $d[i,j]$ is the shortest path distance between nodes i and j and n_{jk} is the total number of shortest paths from j to k . $W[j]$ is the weight of the destination node j . The Betweenness of the edge is computed as the average betweenness of the nodes connecting it.

2.3 Connectivity Measures

Connectivity measures estimate the number of associations between road links. It refers to the directness of traversing between destination points. The connectivity of road networks can be quantified using various parameters developed by [8] based on Graph Theory. Alpha Index or meshedness coefficient, Beta Index, Gamma Index and Eta Index are indices for evaluating the connectivity of transport networks. For a graph with 'e' the number of edges or road segments and 'v' the number of vertices and $L(G)$ being the length of the graph,

Alpha index/Meshedness coefficient (α) is the ratio of the actual number of circuits to the maximum number of circuits in the network. Simple networks, for example, tree patterns will have a value of 0. The higher α , the greater will be the connectivity.

$$\alpha = \frac{e - v + 1}{2v - 5} \quad (3)$$

Beta index (β) is the number of links per node. The greater β , the more complex the network and the greater will be the connectivity.

$$\beta = \frac{e}{v} \quad (4)$$

Gamma index (γ) is the ratio of the number of observed links to the number of possible links. Higher γ indicates more connectivity.

$$\gamma = \frac{e}{3(v - 2)} \quad (5)$$

Eta index (η) is the ratio of the length of the graph to the number of edges.

$$\eta = \frac{L(G)}{e} \quad (6)$$

2.4 Coverage Measures

Coverage measures portray the density characteristic or the spread of the elements of a network, as intersections and links and are useful in ascertaining the compactness and development of transport networks. Higher values indicate a more developed network.

Network Density is the kilometres of links per square kilometres of surface.

$$\text{Network Density} = \frac{\text{Length of the network (km)}}{\text{Size of the area (km}^2\text{)}} \quad (7)$$

Node Density is the total number of nodes per square kilometres of area.

$$\text{Node Density} = \frac{\text{Number of nodes}}{\text{Size of the area (km}^2\text{)}} \quad (8)$$

Edge Density is the total number of edges per square kilometres of area.

$$\text{Edge Density} = \frac{\text{Number of edges}}{\text{Size of the area (km}^2\text{)}} \quad (9)$$

2.5 Topological Measures

Network topology uncovers underlying structures or patterns. It depicts the evolution of road networks as structured or unstructured networks. The topological indices analysed are; Grid Tree Pattern and Cyclomatic number are discussed below:

Grid Tree Pattern (GTP) is an Index for determining the pattern of the network, 0 value denoting a tree pattern to 1 denoting a grid pattern.

$$\text{GTP} = \frac{e - v + 1}{(\sqrt{v} - 1)^2} \quad (10)$$

The cyclomatic number or Maximum no. of cycles (CN) denotes the total number of closed paths in a network.

$$\text{CN} = e - v + 1 \quad (11)$$

3 Study Area and Data

Tiruchirappalli often referred to as Trichy, is an ancient city in the Indian state of Tamil Nadu. The city corporation is divided into administrative units called wards. Tiruchirappalli city consists of 4 zones consisting of a total of 65 wards. Tiruchirappalli is the fifth largest city in Tamil Nadu. The town spans 167.23 km² and is home to 916,674 people as per the 2011 Census. Trichy locates itself more or less at the geographic centre of the State and is well connected by road transport services. Trichy consists of two bus terminals: the Chatram Bus Stand and the Central Bus Station located just 6 km apart. Tiruchchirappalli railway junction is at a short distance of 1 km from the Central Bus Station. The Central Business District (CBD) area located near the Chatram Bus Stand is considered as the Central Business District and was selected for this analysis due to its economic importance and high traffic.

For the analysis of Tiruchirappalli city, the road network (Fig. 1) was digitized from Quickbird image. Only the CBD area has been selected for the vulnerability study due to its importance. The arterial, sub-arterial, collector streets and local streets are included in the analysis. As this study is a preliminary exploratory study, the road network has been considered as an undirected graph without the traffic flow values.

4 Methodology

The road network of the study area is vectorised from QuickBird image, 2012 with a spatial resolution of 2.4 m. The road network is projected to Universal Transverse Mercator (UTM) coordinate system (zone 44N) to compute the length of road segments. It is ensured that the network is free from all topological errors. The dangling nodes, overshoots, undershoots were corrected. The road network created as a shapefile is first converted into a network dataset to be used in Network Analyst. The road network has to be topologically correct in order to convert it into a network dataset. Network datasets store the connectivity of the source features, i.e. lines and points. The count of nodes and edges is obtained from the network dataset to compute the network indices. Connectivity indices are calculated using the Network Analyst extension of ArcGIS. The critical node was found using the spatial join tool to find the degree of each node. The critical link was computed as the link with the greatest betweenness centrality. UNA toolbox for ArcGIS developed by [17] was used to compute the betweenness centrality of the edges.

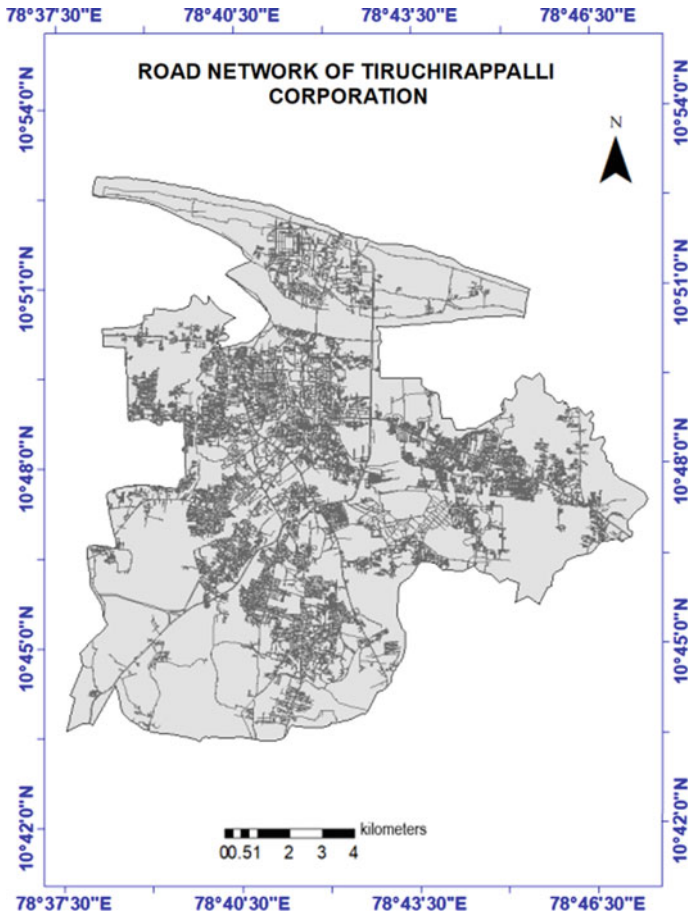


Fig. 1 Road network of Tiruchirappalli corporation

5 Analysis and Results

5.1 Critical Node Analysis

Critical node analysis is done by removing the critical node. The road network of the study area is shown in Fig. 2. While the critical node is removed, all the links associated with this node are also removed as there is no flow. The said network measures are evaluated (Case 0) and the critical node in this case is evaluated and then, removed. The network measures for this case are evaluated (Case 1). And this procedure is repeated for subsequent scenarios, Case 2 and Case 3. The analysis has been shown in Table 1. The percentage change in the network measures is represented in the graphs in Fig. 3.

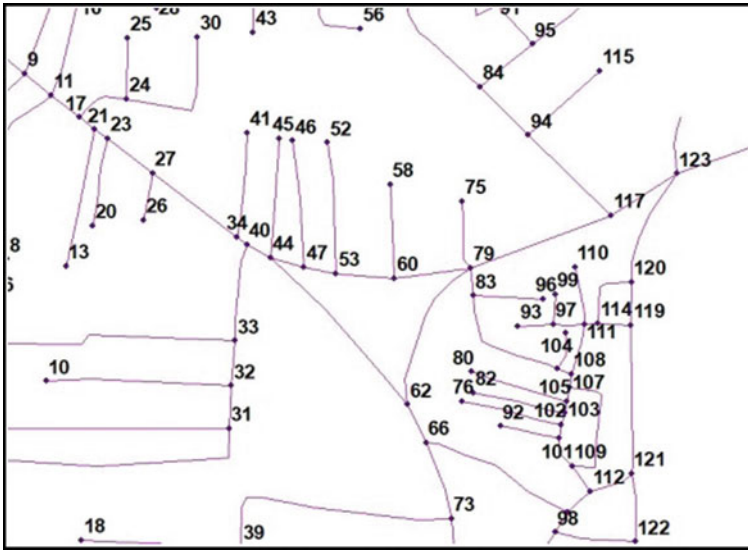


Fig. 2 Link node representation of the study area; Scale 1:12,500

From the analysis, we can infer that if a major node is removed, the connectivity that the node provides is lost. Hence, the alpha index decreases. This decrease is 21.8%. As more than three links are removed for removing one node, the beta index decreases. This decrease is 3.56%. Hence, there is a major decrease in the robustness of the network. As the number of links decreases, the gamma index also decreases, specifically by 3.49%. Most of the edges have equal lengths and more or less the same number of links are removed in each case. So, the proportion of length to the number of links is maintained. Hence, the eta index has a minor increase of 1.42%. The removal of links associated with critical nodes has disturbed the connectivity of the network by rerouting the travel paths with higher travel distances. Therefore, network density decreases by 6.07%. As the number of nodes decreases, node density also decreases by 3.97%. The decrease in number of links is much higher than that of nodes. The decrease in edge density is higher than that of node density. There is a decrease of 7.38%. Grid Tree Pattern reduces as the structure of the network gets more damaged in each of the cases. The number of cycles decreases as the number of closed paths in the network decreases i.e., by 25% here.

5.2 Critical Link Analysis

Similar to critical node analysis, critical link analysis is done by removing the critical link. Network measures are evaluated for the study area (Case 0) and the critical link here is identified and then, removed. The network measures for this case are evaluated

Table 1 Critical node analysis

Measures	Case 0: existing network	Case 1: critical node 79 is removed	Case 2: critical node 44 is removed	Case 3: critical node 40 is removed	% Reduction
Critical node	79	44	40	11	–
Critical link	44–40	44–40	40–34	79–62	–
Area (km ²)	1.17	1.17	1.17	1.17	–
Number of nodes	126	124	122	121	3.97
Number of edges	149	144	140	138	7.38
Length of edges (km)	16.40	15.90	15.51	15.40	6.07
Max. degree of nodes	5	4	4	4	20.00
Alpha index	0.0972	0.0864	0.0795	0.0759	21.84
Beta index	1.1825	1.1613	1.1475	1.1405	3.56
Gamma index	0.4005	0.3934	0.3889	0.3866	3.49
Eta index	0.1100	0.1104	0.1108	0.1116	–1.42
Network density	14.0377	13.6156	13.2817	13.1858	6.07
Node density	107.8767	106.1644	104.4521	103.5959	3.97
Edge density	127.5685	123.2877	119.8630	118.1507	7.38
GTP index	0.2296	0.2044	0.1883	0.1800	21.59
CN	24	21	19	18	25.00

(Case 4). And this procedure is repeated for subsequent cases, Case 5 and Case 6. The results are tabulated in Table 2. The percentage change in the network measures for all the scenarios obtained from the analysis is represented in the graphs (Fig. 4).

Some observations can be made from the above analysis. The effect of removing a critical link varies in the same manner as that caused by removing a critical node. If a major link is removed, the connectivity that this link provides is lost. Hence, the alpha index decreases. This decrease of 12.5% affects the robustness of the network. The beta and gamma index decreases by 2.1%. Eta index shows the proportion of length to the number of links is maintained. The same number of links are removed in each case. Hence, eta changes depending upon the length of the links removed. This increase is a minor 0.52%. The removal of critical links has disturbed the connectivity of the network by rerouting the travel paths with higher travel distances. Network density decreases by 1.5%. As the number of nodes remains the same, node density is not affected. The decrease in number of links is much higher than that of nodes. The decrease in edge density is higher than that of node density i.e., by 2.01%. Grid Tree Pattern reduces as the structure of the network gets more damaged in each

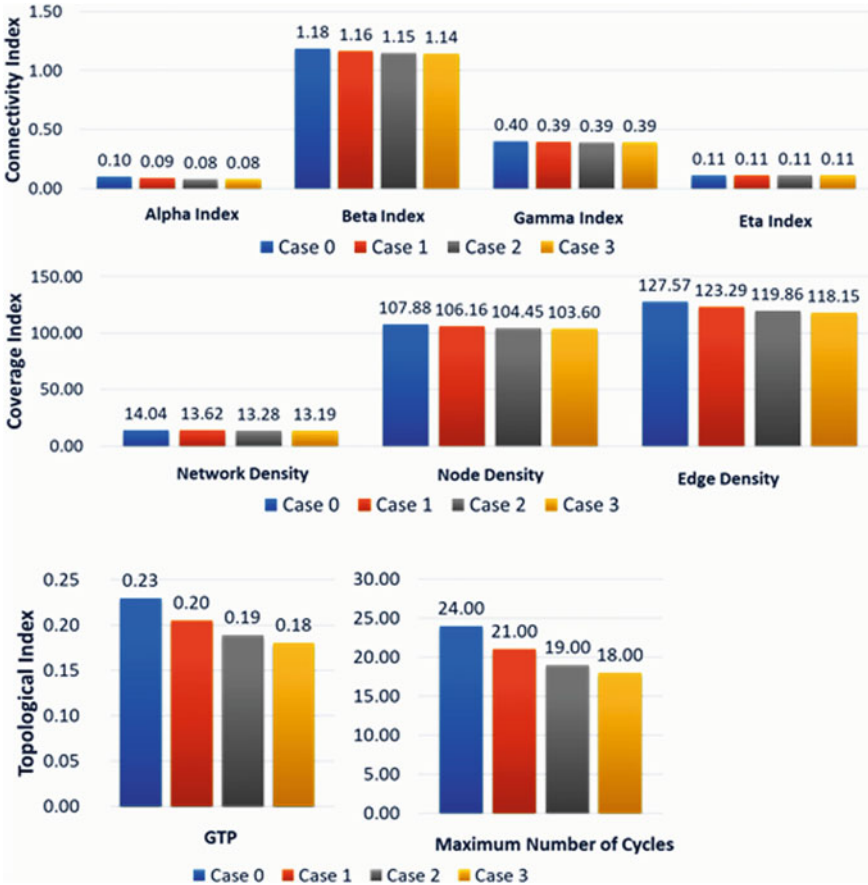


Fig. 3 Variation of network measures on removal of critical node

of the cases. This decrease is by 12.5%. The number of cycles/cyclomatic number decreases as number of closed paths in the network decreases, i.e., by 12.5%.

6 Conclusions

The Central Business District is the area where most of the economic activities happen and hence needs more focus. An attempt has been made to identify the critical links and critical nodes using GIS and to determine the vulnerability or the robustness of the network based on graph theoretical measures. This network in the study area has a close resemblance to the tree pattern as its GTP index is near to 0. Robustness of the network decreases as the critical nodes and links are removed. Connectivity, coverage and topological indices decrease if major nodes or links are removed. If

Table 2 Critical link analysis

Measures	Case 0: existing network	Case 4: critical link 44–40 is removed	Case 5: critical node 44–62 is removed	Case 6: critical node 40–34 is removed	% Reduction
Critical node	79	79	79	79	–
Critical link	44–40	44–62	40–34	79–62	–
Area (km ²)	1.17	1.17	1.17	1.17	–
Number of nodes	126	126	126	126	0
Number of edges	149	148	147	146	2.01
Length of edges (km)	16.40	16.37	16.16	16.15	1.50
Max. degree of nodes	5	5	5	5	0.00
Alpha index	0.0972	0.0931	0.0891	0.0850	12.50
Beta index	1.1825	1.1746	1.1667	1.1587	2.01
Gamma index	0.4005	0.3978	0.3952	0.3925	2.01
Eta index	0.1100	0.1106	0.1100	0.1106	– 0.52
Network density	14.0377	14.0137	13.8382	13.8271	1.50
Node density	107.8767	107.8767	107.8767	107.8767	0.00
Edge density	127.5685	126.7123	125.8562	125.0000	2.01
GTP index	0.2296	0.2200	0.2104	0.2009	12.50
CN	24	23	22	21	12.50

a major node is removed, the connectivity that the node provides is lost. Hence, the alpha index decreases. This decrease is 21.8%. If a major link is removed, the connectivity that this link provides is lost. Hence, the alpha index decreases. This decrease of 12.5% affects the robustness of the network. Coverage and topology also improve as indicated by their corresponding measures. It was concluded that connectivity decreases if major nodes or links are removed. Coverage indices also show a decrease as the density of nodes and links decreases. Topological measures also indicate a decrease in their value as the structure is damaged more and more and becomes closer to a tree-like pattern with each stage of removal of critical nodes and edges.

This study was primarily aimed at applying geospatial techniques to compute the network vulnerability. The study has not simulated traffic flow values into the road network nor considered the road characteristics and hence is a preliminary form of vulnerability analysis using GIS thus leaving scope for further research.

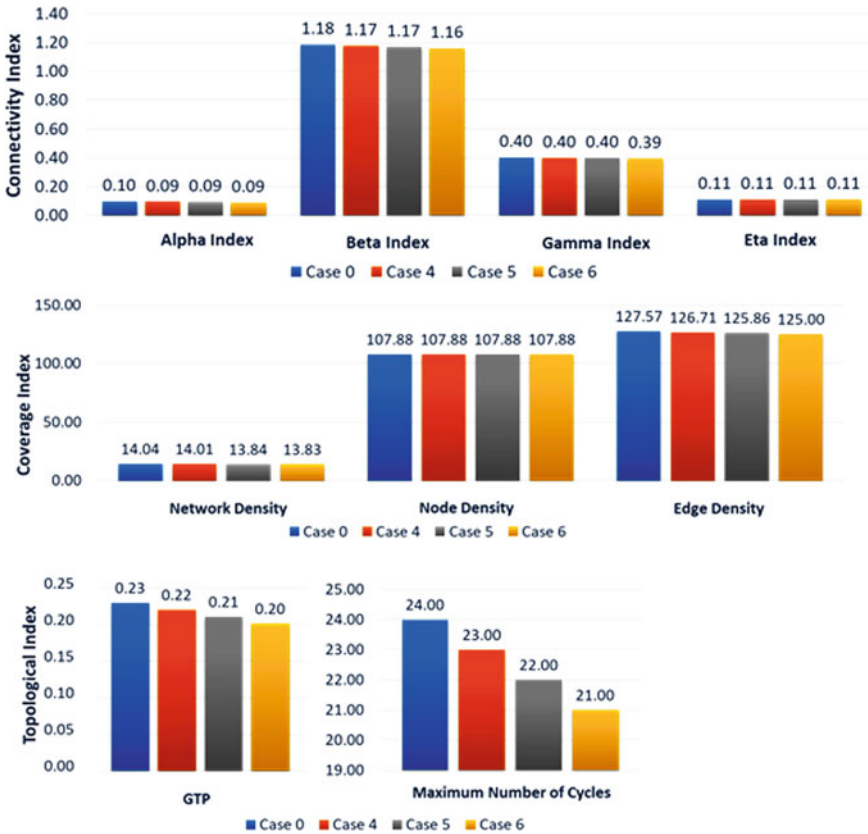


Fig. 4 Variation of network measures on removal of critical links

References

1. Ahuja RK, Magnanti TL, Orlin JB (1993) Network flows: theory, algorithms and applications. Prentice Hall, New Jersey
2. Batty M, Rana S (2004) The automatic definition and generation of axial lines and axial maps. Environ Plann B Plann Des 31(4):615–640
3. Daniel CB, Saravanan S, Mathew S (2020) GIS based road connectivity evaluation using GIS. Trans Res Lect Notes Civil Eng. https://doi.org/10.1007/978-981-32-9042-6_17
4. Ip WH, Wang D (2011) Resilience and friability of transportation networks: evaluation. Anal Optim 5(2):189–198
5. Jenelius E, Mattsson L (2006) Developing a methodology for road network vulnerability analysis. 1st Seminar Nectar Cluster (June). Available at: http://www.infra.kth.se/tla/projects/vulnerability/Paper_Molde_2006.pdf%5Cnpapers3://publication/uuid/B8E762A7-B1B6-44A1-BA00-2C3BDAAEE6C02
6. Jenelius E, Petersen T (2006) Road network vulnerability : identifying important links and exposed region (June 2014)

7. Jiang B, Chengke L (2015) Street-based topological representations and analyses for predicting traffic flow in GIS. *Int J Geograph Inf Sci* 23(9):1119–1137. <https://doi.org/10.1080/13658810701690448>
8. Kansky K, Danscoine P (1989) Measures of network structure. *Flux* 5:89–121. <https://doi.org/10.3406/flux.1989.913>
9. Lalou M, Amin M, Kheddouci H (2018) The critical node detection problem in networks : a survey. *Comput Sci Rev*. 28:92–117. <https://doi.org/10.1016/j.cosrev.2018.02.002>
10. Liu X, Jiang B (2012) Defining and generating axial lines from street center lines for better understanding of urban morphologies. *Int J Geogr Inf Sci* 26(8):1521–1532. <https://doi.org/10.1080/13658816.2011.643800>
11. Mattsson L, Jenelius E (2015) Vulnerability and resilience of transport systems – a discussion of recent research 81:16–34. <https://doi.org/10.1016/j.tra.2015.06.002>
12. Porta S et al (2009) Street centrality and densities of retail and services in Bologna Italy. *Environ Plan B: Plan Design* 36:450–466. <https://doi.org/10.1068/b34098>
13. Porta S, Crucitti P, Latora V (2006) The network analysis of urban streets: a primal approach. *Environ Plann B Plann Des* 33(5):705–725. <https://doi.org/10.1068/b32045>
14. Porta S, Crucitti P, Latora V (2006) The network analysis of urban streets: a dual approach. *Physica A* 369(2):853–866. <https://doi.org/10.1016/j.physa.2005.12.063>
15. Reggiani A, Nijkamp P, Lanzi D (2015) Transport resilience and vulnerability: the role of connectivity. *Trans Res Part A: Policy Pract Elsevier Ltd* 81:4–15. <https://doi.org/10.1016/j.tra.2014.12.012>
16. Rui Y, Ban Y (2014) Exploring the relationship between street centrality and land use in Stockholm. *Int J Geograph Inf Sci Taylor & Francis* 28(7):1425–1438. <https://doi.org/10.1080/13658816.2014.893347>
17. Sevtsuk A, Mekonnen M (2017) Urban network analysis : a new toolbox for ArcGIS. *J Geomatics Spat Anal* 10(10):1–15. <https://doi.org/10.3166/rig.22.287-305>
18. Sreelekha MG, Krishnamurthy K, Anjaneyulu MVLR (2016) Assessment of topological pattern of urban road transport system of Calicut City. *Trans Res Proc* 17:253–262–139. <https://doi.org/10.1016/j.trpro.2016.11.089>
19. Sreelekha MG, Krishnamurthy K, Anjaneyulu MVLR (2016) Interaction between road network connectivity and spatial pattern. *Proc Technol. The Author(s)* 24:131–139. <https://doi.org/10.1016/j.protcy.2016.05.019>
20. Yang L, Qian D (2012) Vulnerability analysis of road networks. *J Trans Syst Eng Inf Technol China Assoc Sci Technol* 12(1):105–110. [https://doi.org/10.1016/S1570-6672\(11\)60188-8](https://doi.org/10.1016/S1570-6672(11)60188-8)

Parametric Evaluation of Mechanical and Durability Properties of Graphene Concrete in Indian Context



Aditya Pratap Singh, Gaurav Chhokar, and Yaman Hooda

Abstract Concrete is said to be the second man – made construction material widely used in the world, and as per the studies, it will be staying at the same positions for the coming decades. With the emerging advancements in the domain of concrete technology, it's been suggested that the same must be produced with locally available materials, including natural as well as industrial waste products. For controlling the production rate of carbon dioxide using concrete mixing process, several reinforcements are being added into the mix as a partial replacement to the main ingredients of the concrete mix, with consideration of modification in the properties of the concrete in a better manner. Nanotechnology is playing an important role in the concrete industry to make it sustainable from past few years. Nanomaterials have distinct physical and chemical properties which improve the effectiveness of materials. This study focuses on the usage of Graphene Oxide as a nanomaterial reinforcement in the concrete mix with varying proportioning ranges from zero percent to 1 percent by weight of cement. The discussions were made based on the laboratory experiments performed on the fresh and hardened concrete. Durability parameters of Graphene – induced concrete were also noted. The strength of the concrete mix with 0.08% GO has shown a better result comparatively. The values of sorptivity and permeability of the concrete mixes were observed to be reduced with increasing GO content in the concrete mix.

Keywords Graphene Oxide · Mechanical properties · Durability parameters · Fresh concrete · Hardened concrete

A. P. Singh · G. Chhokar · Y. Hooda (✉)

Department of Civil Engineering, Manav Rachna International Institute of Research and Studies, Faridabad, Haryana, India

e-mail: yamanhooda@gmail.com

1 Introduction

Since 2012, there has been an increase in the amount of construction and demolition (C and D) waste generated globally, which has increased the amount of land needed to dispose of it [1]. According to the Central Pollution Control Board (CPCB) in 2017, India alone produced 15 million tonnes (MT) of C and D trash yearly, of which only 30% were reused or recycled. In order to limit the amount of trash that is disposed of in landfills, numerous researchers have been concentrating on the treatment, recycling, and reuse of these wastes in the construction sector during the past few decades. 70% of the volume of concrete is made up of aggregate [2]. Every year, there is a greater and larger demand for natural aggregate. In order to achieve a sustainable environment, it may be possible to reduce or make up for the consumption of natural aggregate in the industry by recycling and reusing concrete from C and D wastes. On the other side, India's demand for cement is skyrocketing due to the country's expanding infrastructure and urbanisation. A tonne of cement requires 1.5 to 1.7 tonnes of raw materials, 3 GJ of energy, and releases 0.8 tonnes of CO₂ into the atmosphere during production. Moreover, 350 MT of fuel are used annually to produce the 3.5 billion tonnes of cement produced globally [3]. The manufacture of cement increases the problem of global warming in the environment by a total of 6% [4, 5]. Thus, finding alternative materials or replacing OPC is a top objective to cut down on cement consumption. In order to reduce the carbon footprint, environmental pollution, fuel consumption, and landfill for waste disposal worldwide, pozzolanic materials with a pozzolanic nature, such as fly ash, silica fume (SF), metakaolin (MK), and rice husk ash (RHA), have been used to replace OPC in recent years [6].

The primary disadvantage of cement, which serves as the primary binder in concrete, is that it is brittle and has a poor tensile strength. With the introduction of steel reinforcement and fibres, these shortcomings were eventually addressed. Yet, by strengthening concrete at the nanoscale, the addition of nanoparticles to cement-based composites have improved qualities like toughness, flexural, tensile, and durability properties. Nanotechnology has demonstrated that composites can be altered or redesigned by including a small amount of nanomaterials [7–9]. The most widely used nanomaterials include carbon nanotubes (CNTs), graphene-derived materials, carbon nanofibers (CNFs), nanosilica, etc. It has been demonstrated that nanocomposites can improve the parent material's qualities. The use of nanomaterials in the concrete industry has gained popularity because of their many benefits, which range from increased mechanical strength to the ability to fill nanoscale spaces. The mechanical, thermal, electrical, optical, and other properties of cement composites have been reported to have been improved by the chemistry of cement and nanomaterials such CNTs, graphene, graphene oxide (GO), and graphene-based nanomaterials. Several researchers have studied the mechanical and durability characteristics of composites made of nano-reinforced cement. Moreover, it has consistently outperformed traditional cement composites in terms of results [10, 11]. Another nanomaterial made of carbon is graphene oxide. In 1859, Benjamin C. Brodie [12] created graphene oxide for the first time by chemically exfoliating graphite (further modified

by Hummer). The aromatic structure of graphene oxide is similar to that of graphite, but due to the chemical reactions that took place, some of the covalent bonds were broken, allowing functional groups like epoxy, carbonyl, hydroxyl, and phenol to be attached to the sp^2 aromatic monolayer structure, which is about one atom thick [13, 14]. When added to composites made of cement, the functions have their benefits. Because they are hydrophilic in nature, these oxygenated functions readily adsorb free water radicles from the produced cement composite. Large specific surface areas and greater aspect ratios characterise graphene oxide. In general, dispersibility is a major drawback for nanomaterials, but GO has an advantage over all other nanomaterials because of its oxidative characteristics, which make it simple to disperse in water. Since van der Waals forces between the GO nanosheets outweighed the repellent forces given by oxygenated functional groups at GO sheets, Chuah et al. indicate that the degree of sonication was independent for GO dispersion in water but tend to reaggregate [15]. However, the GO dispersion in cement-based composites was stabilised by a suitable surfactant (polycarboxylate ether-based). Due to its huge surface area, which tends to absorb more water molecules to get wet, and the bulky lateral size with high capacity for water retention formed by the cluster of GO nanosheets, the addition of GO in cement-based composites has a negative impact on the workability [16, 17]. Despite the disadvantage of GO that has already been mentioned, adding a little amount of GO—about 1% by weight of cement—has increased the compressive strength by 63% [18]. According to reports, adding 0.05% GO (bwoc) increased the compressive strength by 15–33% and the flexural strength by 41–58% [11, 19]. According to Shang et al., 0.04% GO addition increased the cement paste's compressive strength by up to 15.1% when compared to ordinary cement paste [19]. When 0.03% GO was added to OPC paste at 28 days after curing, the compressive strength and tensile strength rose by more than 40% [20]. Mohammed et al. came to the conclusion that the inclusion of GO improved the water sorptivity and chloride penetration values while decreasing the pore size of the GO reinforced cement paste, improving resistance to chemical intrusion [21]. According to several researchers, GO incorporation sped up the hydration process. The GO sheets with oxygenated functions make cement particles more accessible, allowing the nanosheets to serve as cement phases' nuclei, enhancing the cement's reaction with water [22]. The leaching of calcium hydroxide (CH) during the hydration phases has improved at 28 days of curing age, according to Wang et al. descriptions of the microstructure of the GO reinforced cement matrix [23]. Because of its remarkable features, the GO inclusion cement matrix is popular. Although GO is significantly less expensive than extremely expensive multi-walled CNTs, single-walled CNTs, and CNFs (which are 250, 1280, and 218 times more expensive than the price of GO per 100 g), interest in GO has increased globally in a variety of fields. GO was chosen as the top choice for this inquiry as a result. The goal of this investigation was to create a composite of GO and nano-reinforced concrete with various cement weight percentages. The workability, compressive strength, tensile strength, water permeation, sorptivity, quality of the nano-reinforced concrete composites, and cost analysis of GO inclusion in concrete (with natural coarse and fine aggregate) composites have not been studied in detail to determine whether this investigation will be

useful for practical application in the construction industry. The graphene oxide used for this study has following specifications.

- Thickness—3–5 nm
- Purity—99%
- Number of layers —3–6
- Diameter—0.8–2 nm
- Length - 5–10 μ
- Form factor—Powder.

2 Concrete and Its Components

2.1 Cement

The most important component which is required in the production of concrete is cement. The cement generally consists of oxides of several metal such as calcium, silicon, etc., which has their own functions towards the properties of the cement. Table 1 depicts the average composition of the oxides present in the cement structure. OPC cement is considered for the concrete sample production. The grade of the OPC used is OPC 43. Also, as per IS 4031, various important experiments were performed to determine the properties of the cement (Table 2).

Table 1 Properties of cement

Properties	Values obtained
Fineness of cement	7%
Specific gravity	4.03
Standard consistency	39%
Initial setting time	170 min
Final setting time	330 min
Average compressive strength at 28 days	50.56 N/mm ²

Table 2 Properties of Aggregates

Properties	Fine aggregates	Coarse aggregates
Fineness modulus	2.11	7.69
Water absorption	1.37%	3.28%
Specific gravity	2.56	2.54
Bulking	24.66%	0.395
Flakiness index	-	33.38%
Elongation index	-	6.85%

2.2 *Aggregates*

The next group of constituents of cement consists of aggregates. There are two different types of aggregates—“Fine Aggregates and Coarse Aggregates.” The aggregate size less than 4.75 mm are considered to be as “fine”, otherwise considered to be as “coarse”. Both type of aggregates is used in the production of the concrete, and thus have different roles. The amount (proportion) of the aggregates used in the concrete production depends upon the Mix Design. Similar to the cement, several experiments have to performed before using them in the concrete production as per IS 2386.

3 Methodology and Observations

3.1 *Slump Value*

Workability, also referred to as segregation or bleeding, is the ability to blend, handle, move, and set something while minimising homogeneity loss. Fresh concrete’s workability was evaluated in accordance with IS: 6461 (Part VII)—1973, and the control mix’s designed slump value, or concrete without GO content, was 100 mm. After pouring newly poured concrete into the cone in a total of four layers (1/4 of the height of the mould) and tamping each layer 25 times before raising it, the height of the coned concrete was measured and the slump value was evaluated using the slump cone test. Additionally, the impact of GO on the fluidity of composites made of nano-reinforced concrete was observed, along with the slump value for different mixes.

3.2 *Compressive Test of Concrete*

150 mm × 150 mm × 150 mm concrete blocks were made with a graphene oxide dosage of 0.00, 0.02, 0.04, 0.06, and 0.08% by weight of cement. The prepared cement mortar blocks were given time to cure. The mortar blocks were tested for compressive strength using a compression testing machine at ages of 7, 28, 56, and 90 days.

3.3 Percentage Increase in Compressive Test with Respect to Control Mix

Based on the results of compressive tests performed on specimens having dosages of 0.00, 0.02, 0.04, 0.06, and 0.08%, the percentage increase in compressive strength of the mixes at various curing ages was calculated.

3.4 Split Tensile Test of Concrete

100 mm × 200 mm concrete cylinders were made with a dose of 0.00, 0.02, 0.04, 0.06, and 0.08% graphene oxide by weight of cement. The prepared cement mortar cylinders were given time to cure and tested.

3.5 Percentage Increase in Split Tensile Test with Respect to Control Mix

Based on the split tensile test findings of the specimen having dosage of 0.00, 0.02, 0.04, 0.06, and 0.08%, the percentage increase in compressive strength of the mixes at various curing ages was calculated.

3.6 Flexure Test of Concrete

Flexure tests were performed on mixtures with dosages of 0.00, 0.02, 0.04, 0.06, and 0.08% at various healing ages.

3.7 Percentage Increase in Flexure Test with Respect to Control Mix

Based on the findings of the compressive test of the specimen having dosage of 0.00, 0.02, 0.04, 0.06, and 0.08%, the percentage increase in flexure strength of the mixtures at various curing ages was calculated.

3.8 Sorptivity Test of Concrete

The circumferential area was painted with epoxy, and polyethylene sheets were used to securely seal the circumferential and top areas to stop evaporation. The weight of the disc was determined for the initial rate of absorption at 0, 1, 5, 10, 30, 60 min, and for every 1-h interval up to 6 h after the commencement. At curing periods of 28, 56, and 90 days, plots of cumulative water absorption over time were examined for all concrete mixes, including graphene oxide (GO), at concentrations of 0, 0.02, 0.04, 0.06, and 0.08.

3.9 Chlorine Penetration Depth Test of Concrete

To determine the resistance to chloride penetration into cement-based materials, this test can be successfully used. In this procedure, samples of water-saturated cement mortar are exposed to water containing 165 g of sodium chloride per litre. After a 35-day exposure time, layers were drilled at a specific depth from the exposure front, and the dust was gathered and analysed using the right equipment to determine the chloride content. The other side of the specimen was also sprayed with AgNO₃ solution to measure the depth of the chloride front. The depth of chloride ingress to the specimen is indicated by the region that is white in colour.

4 Results and Discussion

1. Incorporating GO at various percentages by weight of cement has decreased workability. Addition of GO in cement-based composites have an adverse effect on the workability due to its large surface area that tend to absorb more water molecule to get wet and a bulky lateral size with high capacity for water retention created due to cluster of GO nanosheets. The increased surface area of nanomaterials may cause a reduction in workability since it takes more free water to moisten their surfaces (Fig. 1; Table 3).
2. The compressive strength of the concrete specimen is increased by (21–55%) when graphene oxide is added, for curing times of 28, 56, and 90 days (Figs. 2 and 3; Table 4).
3. For curing times of 28, 56, and 90 days, adding graphene oxide to concrete increases the concrete specimen's tensile strength by (16–38%) (Figs. 4 and 5; Table 5).
4. For curing times of 28, 56, and 90 days, adding graphene oxide to concrete increases the concrete specimen's flexure strength with the most effective dosage as 0.04% and sees decrease in later dosages (Figs. 6 and 7; Table 6).

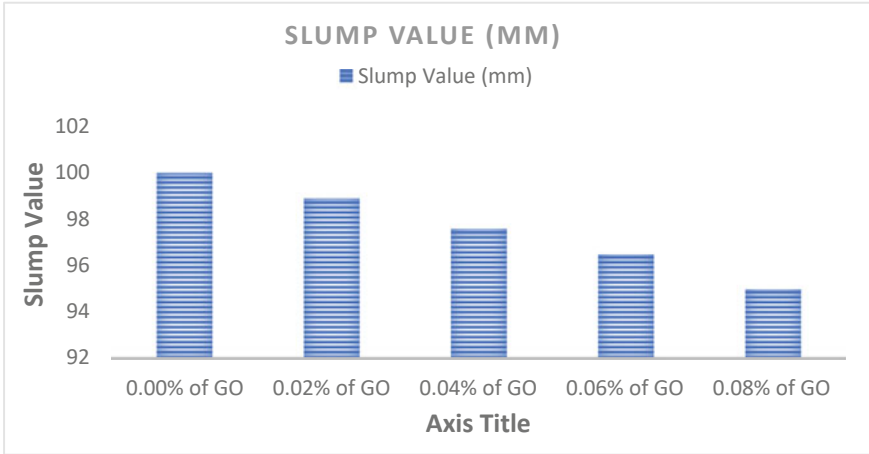


Fig. 1 Slump value

Table 3 Slump value

Grapheme oxide concentration (%)	Slump value (mm)
0.00	100
0.02	98.9
0.04	97.6
0.06	96.5
0.08	95

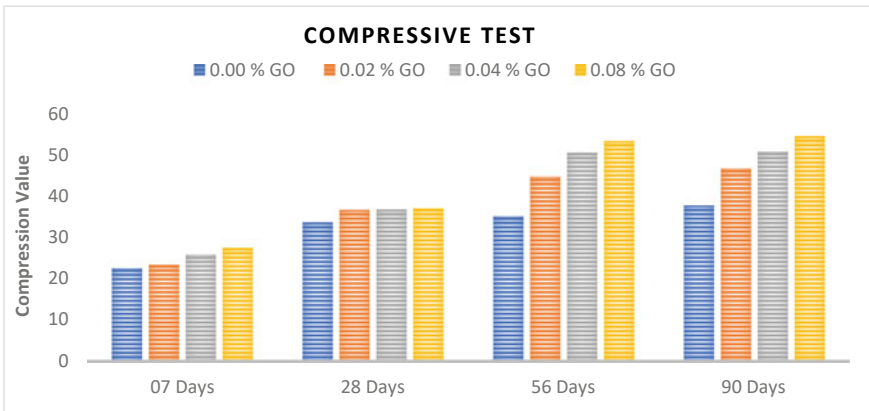


Fig. 2 Compressive value test

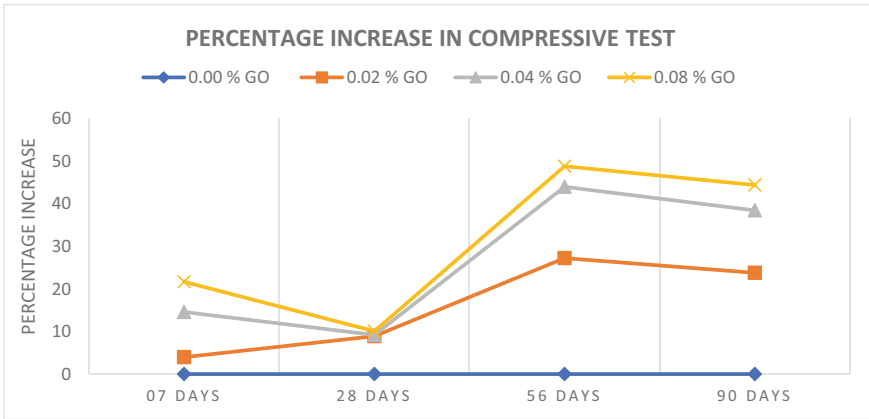


Fig. 3 Percentage increase in compressive value test

Table 4 Compressive strength obtained

Graphene oxide concentration	0.00%	0.02%	0.04%	0.06%	0.08%
<i>Number of days</i>					
07 days	22.6	23.5	25.9	27.5	29.1
28 days	33.7	36.7	36.8	37.1	38.9
56 days	35.2	44.8	50.6	53.4	54.8
90 days	37.8	46.8	50.9	54.6	55.7

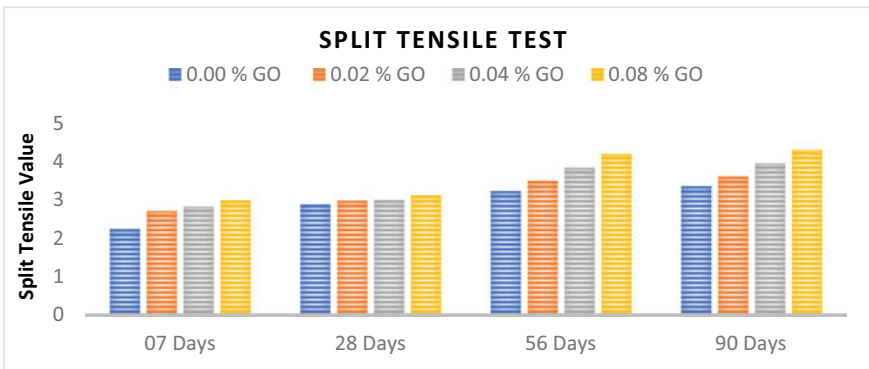


Fig. 4 Split tensile value test

- The addition of GO improved the water sorptivity and chloride penetration values while reducing the pore size of the GO reinforced cement paste, improving chemical resistance.

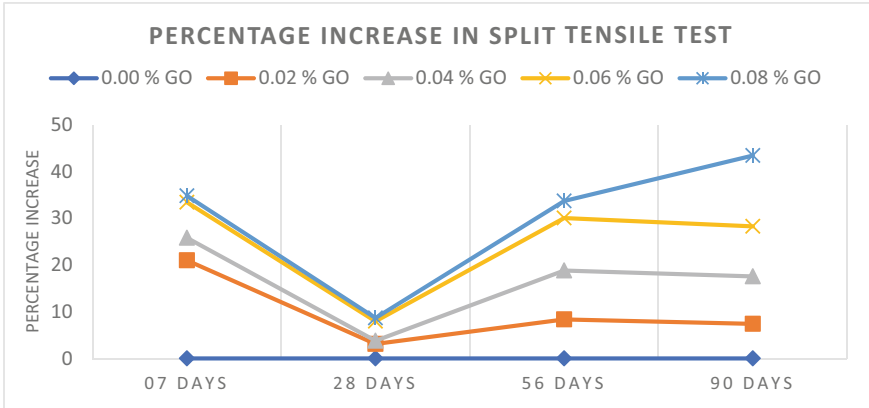


Fig. 5 Percentage increase in split tensile value test

Table 5 Split tensile strength obtained

Graphene oxide concentration	0.00 (%)	0.02 (%)	0.04 (%)	0.06 (%)	0.08 (%)
<i>Number of days</i>					
07 days	2.24	2.71	2.82	2.99	3.02
28 days	2.89	2.98	3.00	3.12	3.14
56 days	3.23	3.50	3.84	4.20	4.32
90 days	3.36	3.61	3.95	4.31	4.82

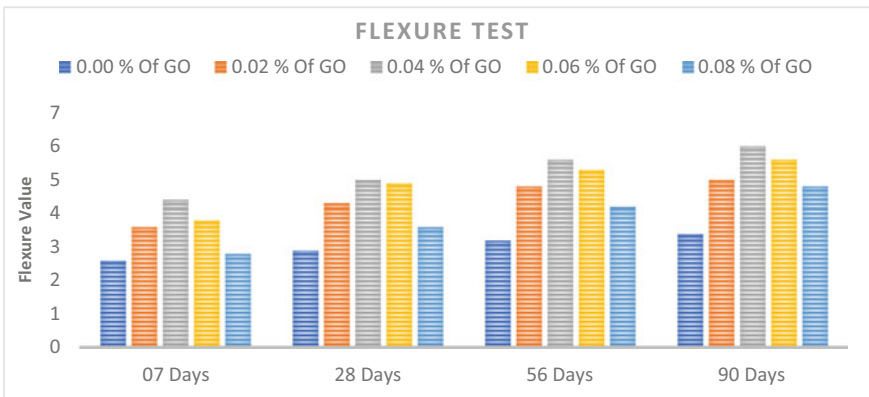


Fig. 6 Flexure value test

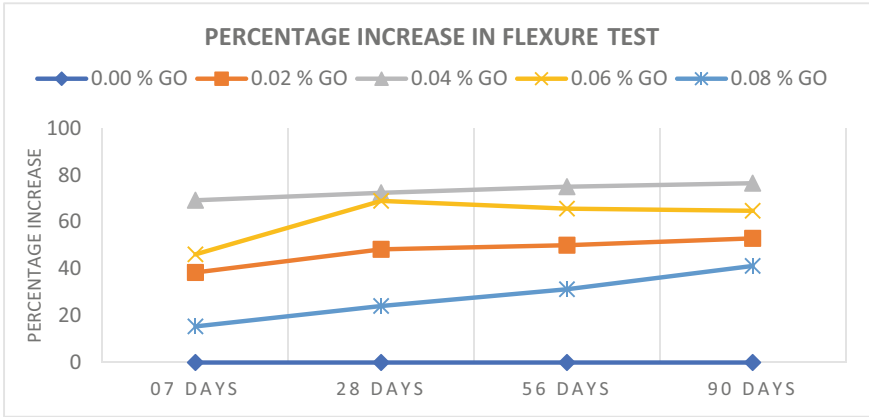


Fig. 7 Percentage increase in flexural value test

Table 6 Split tensile strength obtained

Grapheme oxide concentration	0.00 (%)	0.02 (%)	0.04 (%)	0.06 (%)	0.08 (%)
<i>Number of days</i>					
07 days	2.6	3.6	4.4	3.8	3.0
28 days	2.9	4.3	5.0	4.9	3.6
56 days	3.2	4.8	5.6	5.3	4.2
90 days	3.4	5.2	6.0	5.6	4.8

- For curing intervals of 28, 56, and 90 days, sorptivity tends to decline with rising GO content (Fig. 8; Table 7).
- In the control mix, the depth of chloride penetration was 26 mm, while it was only 5 mm in the experimental mix, which contained 0.02% by weight of chloride. By using graphene oxide, the amount of chloride infiltrating the cement material has

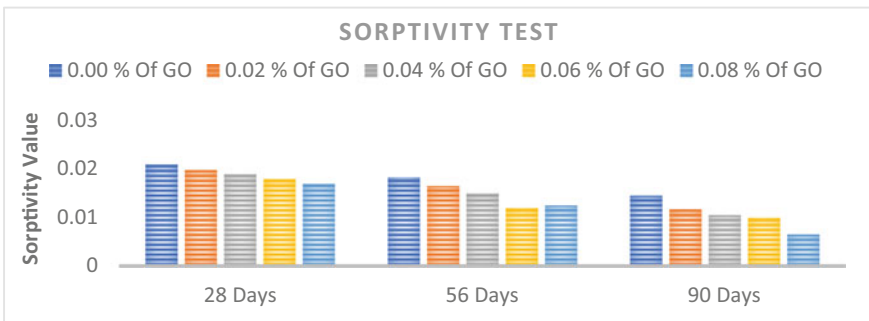


Fig. 8 Sorptivity value test

Table 7 Sorptivity value obtained

Graphene oxide concentration	0.00 (%)	0.02 (%)	0.04 (%)	0.06 (%)	0.08 (%)
<i>Number of days</i>					
28 days	0.021	0.0198	0.019	0.018	0.017
56 days	0.0183	0.0165	0.015	0.012	0.0125
90 days	0.0145	0.0117	0.0105	0.010	0.0065

been significantly decreased. The lowest chloride penetration of all the combinations is 0.02% by weight of specimen. GO sheets can be deposited to provide a protective coating that can improve corrosion resistance and stop the movement of corrosive elements. Thus, it can be inferred that adding graphene oxide to cement can prevent the entry of harmful chemicals like chlorides, improving the durability of concrete and lengthening the lifespan of structures made of the material (Fig. 9; Table 8).

- 8 The GO content of the mixture is a particularly sensitive factor to changing the transport capabilities, as evidenced by the GO cement matrix’s transport properties. Water sorptivity and chloride penetration levels have improved.
9. Effectiveness is significantly influenced by the GO fraction. It is believed that adding GO to cement matrix can significantly boost its resistance to aggressive components by forging a strong barrier that slows the transport of aggressive chemicals.

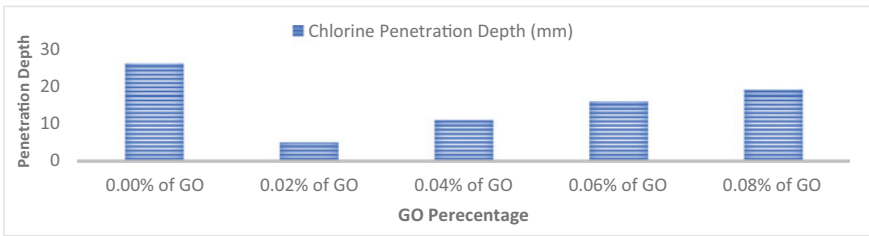


Fig. 9 Chlorine penetration value test

Table 8 Chlorine penetration value obtained

Graphene oxide concentration (%)	Chlorine penetration depth (mm)
0.00	26
0.02	5
0.04	11
0.06	16
0.08	19

5 Conclusion

Considering the M25 grade concrete, as per the latest revision of IS 10262: 2019, the proportions of the various concrete constituents are determined, and then cement were partially replaced with different dosage of graphene oxide, the study noted that:

1. Incorporating GO at various percentages by weight of cement has decreased workability. Addition of GO in cement-based composites have an adverse effect on the workability due to its large surface area that tend to absorb more water molecule to get wet and a bulky lateral size with high capacity for water retention created due to cluster of GO nanosheets.
2. The compressive strength of the concrete specimen is increased by 21–55% when graphene oxide is added, for curing times of 28, 56, and 90 days.
3. For curing times of 28, 56, and 90 days, adding graphene oxide to concrete increases the concrete specimen's tensile strength by 16–38%.
4. The addition of GO improved the water sorptivity and chloride penetration values while reducing the pore size of the GO reinforced cement paste, improving chemical resistance.
5. For curing intervals of 28, 56, and 90 days, sorptivity tends to decline with rising GO content.
6. In the control mix, the depth of chloride penetration was 26 mm, while it was only 5 mm in the experimental mix, which contained 0.02% by weight of chloride. By using graphene oxide, the amount of chloride infiltrating the cement material has been significantly decreased. The lowest chloride penetration of all the combinations is 0.02% by weight of specimen.
7. The GO content of the mixture is a particularly sensitive factor to changing the transport capabilities, as evidenced by the GO cement matrix's transport properties. Water sorptivity and chloride penetration levels have improved.
8. Effectiveness is significantly influenced by the GO fraction. It is believed that adding GO to cement matrix can significantly boost its resistance to aggressive components by forging a strong barrier that slows the transport of aggressive chemicals.

References

1. Akhtar A, Sarmah AK (2018) Construction and demolition waste generation and properties of recycled aggregate concrete: a global perspective. *J Clean Prod* 186:262–281. <https://doi.org/10.1016/j.jclepro.2018.03.085>
2. Etxeberria M, Vázquez E, Marí A, Barra M (2007) Influence of amount of recycled coarse aggregates and production process on properties of recycled aggregate concrete. *Cement Concr Res.* 37: 735–742. <https://doi.org/10.1016/J.CEMCONRES.2007.02.002>
3. Chatziaras N, Psomopoulos CS, Themelis NJ, Use of waste derived fuels in cement industry: a review. *Manag Environ Qual Int J.* 27 178–193. <https://doi.org/10.1108/MEQ-01-2015-0012>

4. Zhang J, Liu G, Chen B, Song D, Qi J, Liu X (2014) Analysis of CO₂ emission for the cement manufacturing with alternative raw materials: a LCA-based framework. *Energy Procedia* 61:2541–2545. <https://doi.org/10.1016/j.egypro.2014.12.041>
5. Vaishnav K, Lazarus GP, Bansal S, Hooda Y (2022) Review on thermal energy efficiency using gypsum integrated phase change materials in buildings. In: Gupta AK, Shukla SK, Azamathulla H (eds) *Advances in construction materials and sustainable environment. Lecture Notes in Civil Engineering*, vol 196. Springer, Singapore. https://doi.org/10.1007/978-981-16-6557-8_24
6. Behera M, Bhattacharyya SK, Minocha AK, Deoliya R, Maiti S (2014) Recycled aggregate from C&D waste & its use in concrete—a breakthrough towards sustainability in construction sector: a review. *Construct Build Mater* 68:501–516. <https://doi.org/10.1016/j.conbuildmat.2014.07.003>
7. Balaguru P, Chong K (2006) *Nanotechnology and concrete: research opportunities, Nanotechnol Concr Recent Dev Future Perspect*. Denver, Nov 7
8. Hooda Y, Bansal S, Gupta A (2022) Parametric strength of sustainable concrete using fly ash, GGBS and recycled aggregates as per taguchi's approach. In: Gupta AK, Shukla SK, Azamathulla H (eds) *Advances in construction materials and sustainable environment. Lecture notes in civil engineering*, vol 196. Springer, Singapore. https://doi.org/10.1007/978-981-16-6557-8_40
9. Dixit A, Hooda Y (2019) experimental evaluation on compressive and tensile behavior of concrete utilising GGBS, fly ash and recycled aggregates. *Int J Eng Adv Technol (IJEAT)*. 8 (5) ISSN: 2249–8958
10. Chuah S, Pan Z, Sanjayan JG, Wang CM, Duan WH (2014) Nano reinforced cement and concrete composites and new perspective from graphene oxide. *Constr Build Mater*. <https://doi.org/10.1016/j.conbuildmat.2014.09.040>
11. Pan Z, He L, Qiu L, Korayem AH, Li G, Zhu JW, Collins F, Li D, Duan WH, Wang MC (2015) Mechanical properties and microstructure of a graphene oxide-cement composite. *Cement Concr Compos*. <https://doi.org/10.1016/j.cemconcomp.2015.02.001>
12. Brodie BC (1859) On the atomic weight of graphite : Brodie B C: free download, borrow, and Streaming : Internet archive. *Philos Trans R Soc Lond* 149: 249–259. <https://doi.org/10.1098/rstl.1859.0013>. Kumar HV, Woltormist SJ (2016) Adamson DH, Fractionation and characterization of graphene oxide by oxidation extent through emulsion stabilization, *Carbon*. 98:491–495. <https://doi.org/10.1016/J.CARBON.2015.10.083>
13. Tong T, Fan Z, Liu Q, Wang S, Tan S, Yu Q (2016) Investigation of the effects of graphene and graphene oxide nanoplatelets on the micro- and macro-properties of cementitious materials. *Constr Build Mater*. 106: 102–114. <https://doi.org/10.1016/j.conbuildmat.2015.12.092>
14. Chuah S, Li W, Chen SJ, Sanjayan JG, Duan WH (2018) Investigation on dispersion of graphene oxide in cement composite using different surfactant treatments. *Constr Build Mater* 161:519–527. <https://doi.org/10.1016/j.conbuildmat.2017.11.154>
15. Li X, Lu Z, Chuah S, Li W, Liu Y, Duan WH, Li Z (2017) Effects of graphene oxide aggregates on hydration degree, sorptivity, and tensile splitting strength of cement paste. *Compos Appl Sci Manuf* 100:1–8. <https://doi.org/10.1016/j.compositesa.2017.05.002>
16. Dikin DA, Stankovich S, Zimney EJ, Piner RD, Dommett GHB, Evmenenko G, Nguyen ST, Ruoff RS (2007) Preparation and characterization of graphene oxide paper. *Nature* 448:457–460. <https://doi.org/10.1038/nature06016>
17. Li X, Korayem AH, Li C, Liu Y, He H, Sanjayan JG, Duan WH (2016) Incorporation of graphene oxide and silica fume into cement paste: a study of dispersion and compressive strength. *Constr Build Mater* 123: 327–335. <https://doi.org/10.1016/j.conbuildmat.2016.07.022>
18. Li GY, Wang PM, Zhao X (2005) Mechanical behavior and microstructure of cement composites incorporating surface-treated multi-walled carbon nanotubes. *Carbon* 43:1239–1245. <https://doi.org/10.1016/J.CARBON.2004.12.017>
19. Shang Y, Zhang D, Yang C, Liu Y, Liu Y (2015) Effect of graphene oxide on the rheological properties of cement pastes. *Constr Build Mater* 96:20–28. <https://doi.org/10.1016/j.conbuildmat.2015.07.181>

20. Gong K, Pan Z, Korayem AH, Qiu L, Li D, Collins F, Wang CM, Duan WH (2014) Reinforcing effects of graphene oxide on Portland cement paste. *J Mater Civ Eng* 27:A4014010. [https://doi.org/10.1061/\(asce\)mt.1943-5533.0001125](https://doi.org/10.1061/(asce)mt.1943-5533.0001125)
21. Mohammed A, Sanjayan JG, Duan WH, Nazari A (2015) Incorporating graphene oxide in cement composites: a study of transport properties. *Constr Build Mater* 84:341–347. <https://doi.org/10.1016/j.conbuildmat.2015.01.083>
22. Wang Q, Wang J, Lu CX, Liu B, Zhang K, Li CZ (2015) New carbon materials Influence of graphene oxide additions on the microstructure and mechanical strength of cement. *N Carbon Mater*.30: 349–356, [https://doi.org/10.1016/S1872-5805\(15\)60194-9](https://doi.org/10.1016/S1872-5805(15)60194-9)
23. Sharma S, Kothiyal NC (2016) Comparative effects of pristine and ball-milled graphene oxide on physico-chemical characteristics of cement mortar nanocomposites. *Constr Build Mater* 115:256–268. <https://doi.org/10.1016/j.conbuildmat.2016.04.019>

Analysis of Causes and Effects of Critical Delay Factors in High Rise Building Projects of Kerala



Nilufer Noushad, S. Jawahar Saud, and Shamnas Neduvancheri

Abstract The building sector is one of India's fastest expanding industries. As the number of construction companies rises, so is the number of high-rise construction projects in Kerala. As the complexity of projects such as the number of stories, size of the building, type of building, legal aspects, stakeholders, management practices, division of labour, technology used, globalization, diversity, and so on increases, so does the need to finish and deliver the project within the estimated time and budget while maintaining a higher level of work quality. The goal of this study is to quantify the top most essential elements affecting the schedule of high-rise building projects throughout Kerala, and to give relevant recommendations and remedies to reduce construction delays. For this investigation, the Delphi approach was used. There are 76 causes of delays that are congruent with the settings and situations in the state of Kerala. The surveys were distributed to other parties, including contractors, owners, designers, consultants, research scholars, architects, and so on. The data from the questionnaire survey will be analyzed using the relative importance index (RII), and the key components will be assessed based on their contribution to the delay.

Keywords Construction delays · Schedule delays · Infrastructure

N. Noushad (✉) · S. J. Saud
Federal Institute of Science and Technology, Ernakulum, Kerala, India
e-mail: nilufernoushad98@gmail.com

S. Neduvancheri
Overseas AST, Dubai, United Arab Emirates

1 Introduction

Each year, the number of construction projects grows dramatically. Many countries invest funds to build infrastructure to accelerate their economic growth. The expansion of other industries is sparked by the construction industry, which acts as an economic growth accelerator. Construction professionals' potential and performance in this business are crucial to the growth and recovery of the sector. Individual, organisational, societal, and other ad hoc factors all have an impact on the potential of the construction workforce [16]. As a result of the construction sector's influence on other related industries, it serves as a catalyst for socioeconomic growth. Because it makes up around 8% of India's GDP and is the second largest employer, the construction sector in India has grown significantly over the past ten years and is one of the most significant sectors today. Nonetheless, A construction project is typically deemed successful when it is finished on time, under budget, in accordance with specifications, and to everyone's satisfaction. The majority of the projects didn't wrap up on time or according to schedule. Instead, they were completed ahead of or behind schedule due to the unpredictable nature of events and their distinctiveness, which had a number of negative repercussions on the projects and the people involved. The term "construction delays" refers to delays in the completion or commencement of construction activities relative to the scheduled timetable or contract timeline, or to delays in the completion of construction activities relative to a set time [20]. The delay of a project means it will be finished outside the allotted time, resulting in additional penalties, inflation-based higher costs, contract termination, legal proceedings, etc., or a combination of those factors. At the planning stage, one can mitigate or limit the risk of delays in a project. A construction project is no exception to the rule that risks are inherent in every project. An early assessment of risk can allow it to be managed, minimized, shared, mitigated, or accepted. In addition, the construction industry has a lower quality of life than other occupations because of a variety of work-related problems [16].

The construction industry is one of the key individuals to growth, employment, and infrastructure enlargement in Kerala, one of the states with the fastest charge of improvement and growth. The construction industry is essential to Kerala's economic health due to its impact on industrial output, job prospects, and export earnings. The demand for the project management to finish and execute the project within the anticipated time and budgeted budget, as well as to produce work of a higher caliber, increases as infrastructure complexity of projects rises [12]. Kerala's construction industry is regarded as a key factor in the country's development since it opens up numerous chances for business in other industries and for investment. One important sign is the nation's invasive pace of construction activity. Sadly, Kerala's building industry has been beset by a number of problems that have a detrimental effect on cost, work quality, timeliness, political environment, and construction techniques. Given that the volume of construction industries is expanding, schedule performance in the Kerala construction industry is unquestionably an important area for research.

Despite several studies on the factors and causes affecting schedule and cost performance being published, the majority of them are domain specific. The applicability of such study in the context of the building industry in Kerala is still investigated. It is significant to comprehend the characteristics that lead to delays, their effects, how these characteristics are combined to form factors, and how these factors interact with one another.

1.1 Objectives

The primary goal of this study is to

- To assess the severity of the issues causing delays from the stakeholders including the owners, contractors, project managers, consultants, Research Scholars, Engineers, material suppliers etc.
- To find out the most critical factors which affect schedule and
- To propose appropriate recommendations and solutions to eliminate construction delays.

2 Study Area

Kerala, a state in southern India, is the 13th most populous state and the 21st largest state in terms of land, covering 38,863 km² (15,005 sq. m²). There are 14 districts in it. Kerala is one of the state which has numerous construction companies which is a part of their economic growth and also highly influencing the contribution to the GDP of the state. In Kerala, the number of multistory structures has also significantly increased. In total, rural areas have seen the construction of 51,539 structures for industrial-commercial use, while cities have seen the construction of 22,130 buildings [4]. Almost 300 new multistoried buildings are also on going in Kerala. Apart from that there is a variety of categories of construction which include offices, ware houses, roads, bridges, airports, etc. are also being built. However, Kerala's construction market has been afflicted with numerous complications. The necessity for the project management to finish and deliver the project within the anticipated time and intended budget, as well as to provide work of a higher calibre, increases as infrastructure complexity of projects rises. Due to severe issues with time and cost performance, Keralan construction firms are currently unable to complete projects by the required date [15]. So it is evident that the construction industry in Kerala is facing delays which need to be acknowledged. This study is exclusively intended to find out the major construction delays occurring in the construction companies across the state of Kerala in India and to analyze the crucial factors to propose appropriate mitigation measures (Fig. 1).

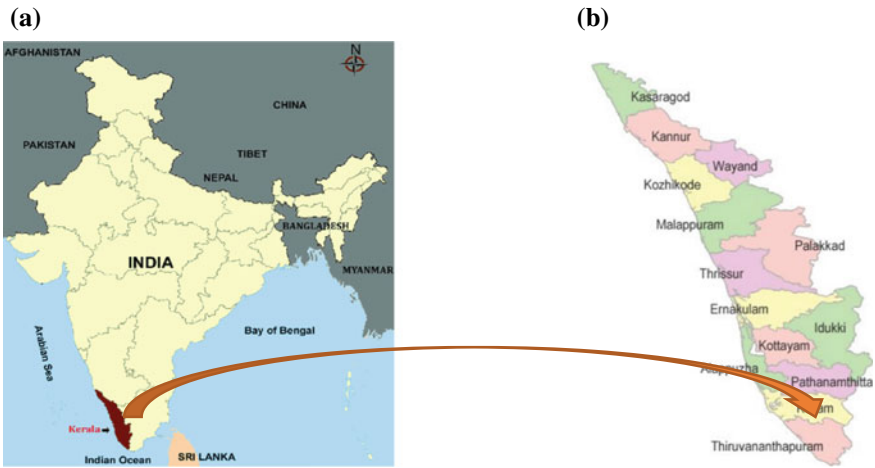


Fig. 1 a Map of India highlighting Kerala [13]. b Map of Kerala [10]

3 Methodology

This study used quantitative approach. A questionnaire survey method has been utilised to assess the impact of several variables on delay in Kerala's construction industry using data from numerous international literatures. Survey among different stakeholders of construction industry was performed. The study was focused on experts in various processes of construction industry. Delphi method is adopted for this study.

3.1 Delphi Method

The Delphi technique, also known as the Delphi method, is a structured communication technique or process that was initially created as a methodical, interactive forecasting method that relies on a panel of experts. In order to get specific answers to issues, the Delphi Method entails submitting questions to a group of specialists. It starts with the selection, placement, and validation of the Delphi panel experts [2]. It entails collecting a panel of experts, having them respond anonymously to a survey or questionnaire, and then sharing the results with the panel for discussion and comment. When an agreement is reached and the results are published, the Delphi Method is complete [17]. The panel of experts for this study was chosen from a variety of private building firms in Kerala. Respondents are selected from a varied range of experts engaged in a variety of construction projects. In the Kerala

context, high rise engineering construction projects were familiar to all of the respondents. The respondents who were identified either worked or are presently working on various construction projects around Kerala. The respondents consisted of Civil Engineers, Architects, Structural Engineers, Chartered Engineers, Project Managers, Labour Contractors, and Designers etc.

3.2 Identification of Delay Factors

There has already been a significant amount of research done on the factors that contribute to construction delays, and the literature has a collection of delay features that have been thoroughly recorded and reviewed. The many causes of building project delays have been the subject of several research. These studies range from identifying the main causes of delays in various countries and project kinds to discussing the methodology for analysing delays and potential solutions [8]. The primary goal of this research was to compile a list of delay factors relevant to building construction projects in Kerala so that they could be incorporated in a questionnaire survey. For that 76 delay causing factors were identified. The circumstances and characteristics of the delays occurring in Kerala's construction projects were used to identify and choose the delay factors. Only those aspects that are relevant to the situation in Kerala were taken into consideration after being identified in various pieces of literature. Then, these variables were separated into eight groups, including those that are related to the owner, contractor, consultant, designer, equipment, material, labour, and external influences [12, 16, 18].

3.3 Preparation of Questionnaire

The delay factors found in the literature were taken into consideration when creating the questionnaire. Two components make up the final questionnaire. Demographic information on the respondents is included in the first section which include name, contact details, job title, experience and educational qualification. The second section consists of the categorized delay factors in which the respondents have to rank the factors according to the 4 point likert scale, with a rating 1 for not important, 2 for some important, 3 for important and 4 for extremely important [12]. Additional inquiries were made to determine if there were any other causes for the delay. The participant has two additional blank fields to add any additional causes or feedback. An example of the questionnaire is shown in Appendix 1.

3.4 Data Collection and Sampling

The purpose of the questionnaire survey was to identify the most important delays' underlying causes and to quantitatively validate the list of variables collected from the interviews. To get their opinions on the things that hamper performance on construction projects, clients, consultants, designers, contractors, and project managers, among others, were given the updated survey questionnaire in person, by email, and using Microsoft forms. A total of 175 questionnaires were distributed by hand, by Personal interviews with respondents and by Microsoft forms to gather responses. With a response rate of 28.5%, 50 responses were received. Despite the sample size being rather small, the analysis was considered to be very credible due to the respondents' good comprehension of the questionnaires, their relevant industry experience, and their interactions on a personal level [7].

3.5 Demographics of Respondents

Respondents are chosen from a diverse group of professionals working in Kerala's construction industry. All of the verified responders had prior expertise engineering construction projects in Kerala. The identified respondents either had experience working on construction projects throughout Kerala or were currently doing so. The sample included labour contractors, designers, architects, structural engineers, chartered engineers, project managers, etc. The survey results shows that most of the participants responded in are undergraduate engineers and more than 60% of the respondents have more than 5 years of experience. The respondents include 62 male and 38% female, with different age groups and different educational qualification. Introductory chats and emails with each respondent were carried out in order to clarify and make the research's goals clear in order to get the best response feasible in line with expertise and skills [8].

3.6 Ranking and Computation of Relative Importance Index

The rankings of all the elements provided in the questionnaire were determined using the Relative Importance Index technique. The relative relevance index for each risk factor that increases the likelihood of schedule delays in the construction industry was determined using a 4-point Likert scale [14]. The best alternative was chosen to use RII for the objectives of this investigation. It would classify the biggest delay issues in the construction industry based on the rankings given to each source of delays. The RII has been used to assess comparative efficacy in a number of industries and to evaluate the value of various goods. Using RII, the key variable among several was identified. The formula below was used to compute the relative importance index for

each cause [9].

$$RII = \sum W/A * N \tag{1}$$

where *W* denotes the participants’ weights (ranging from 1 to 4) assigned to each component, *A* is the greatest weight (in this case, 4), and *N* denotes the total number of participants.

4 Results and Discussions

To identify the largest and smallest significant project delay factors in this industry, the relative significance index (R.I.I.) was calculated for each cause. The computed RII values for each of these parameters were used to order them. The top 10 crucial schedule affecting criteria and least 5 schedule affecting criteria were listed below in order of importance (Table 1).

Based on the results obtained from relative importance index, some recommendations and mitigation measure have been proposed for the top 5 critical factors contributing to the construction delays is given.

Table 1 Top 10 critical delay factors

Rank	Attributes	RII	Category	Source
1	Shortage of labours	0.8	Labour Related	
2	Repeated design change	0.795	Owner related	
3	Poor qualification and inadequate experience of consultants engineering staff	0.785	Consultant related	[2]
4	Delay in approving overall designs, shop drawing, sample tested materials and major changes in work	0.785	Consultant related	
5	Mistakes And Discrepancies Made In Design Documents Leads To Frequent Revisions Of Drawings/Designs	0.78	Designer related	
6	Late in revising and approving design documents	0.775	Owner related	
7	Insufficient data collection and survey before design	0.77	Designer related	[2]
8	Delay in manufacturing special building materials	0.77	Material related	
9	Conflicts in subcontractors schedule during execution	0.755	Contractor related	
10	Quality problem with procured material	0.755	Material Related	

Table 2 Least 5 factors affecting delay

Rank	Attributes	RII	Category	Source
76	Effects of social and cultural factors	0.51	External Related	
75	Nationality and language of labours	0.51	Labour related	
74	Owners lack of experience and involvement	0.53	Owner related	[2]
73	Fraudulent practices and kickbacks	0.55	Consultant related	
72	Delay in finalization of rates for extra items	0.56	External related	

4.1 Shortage of Labours

Lack of labour is recognised as the top factor affecting schedule delays in building projects after receiving the highest RII score of 0.8. In the current scenario, Kerala's construction industries are facing issues regarding the shortage of labours. Keralites have become more educated and literate, which has driven them to search outside for specialised labour and greater earnings that are occasionally seen as more respectable. The number of workers in Kerala, particularly for unskilled jobs, has decreased as a result of this. The migratory workers from other States fill this void. But over the past two years, the pandemic has affected the building industry from all sides. Some prospective employees might not want to go back to the front lines, while others might not want to go through the new immunisation or testing procedures. There may still be a disruption in family care. Since the economic shocks of 2020, many people who left the job have found possibilities in other industries, and some may have moved permanently. Even in the best-case scenarios, construction labour can be physically demanding, with demanding working conditions and more significant issues with mental health and substance misuse than other occupations. Some steps that could be performed to lessen this problem include.

- To lower the risk of an accident at work, businesses should assess their present risk control and training procedures and ensure that employees do tasks safely.
- The risks associated with a younger, less experienced workforce can be reduced by pretask planning, job site appraisal, and safety training.
- Employers who participate in employee assistance programmes are better able to attract and retain personnel. Employers can attract job prospects, improve employee satisfaction and health, and minimise burnout by offering aid with mental health and substance misuse, career counselling, and reskilling courses.
- Use construction materials which reduce the need for skilled labour.
- Expanding recruitment drive
- Enhancing the skills of present workforce.

Apart from a lack of qualified workers, the main issues with labor-related elements that need to be addressed include poor skill or productivity levels or underqualified workers. Unskilled labour is often used to describe work that does not require a specific level of training or concentrated experience. Unskilled work refers to a group of workers with a limited skill set or jobs with the lowest level of economic value. There are some suggestions made in this regard;

- Teaching current workers. Unskilled people are frequently more accessible, willing to put in significant effort, and driven to build a career. Furthermore, they are eager to learn and train. Extensive training is necessary to develop an effective staff.
- Focused hands-on training under an experienced skilled worker is the best way to quickly get these people up to speed on the relevant expertise and make them productive. The skilled worker who is providing on-the-job training will be motivated and the training schedule will move along more quickly if they are paid.
- Rotating the personnel across various departments and parts also gives the employees access to a broad range of knowledge, skills, and stimulates original thought. The employees will be inspired by field visits to successful and high-performing organisations and will realise that there is room for growth in their daily job.
- Retention of employees. It is essential for a successful organisation, among other things. Employee retention refers to the practice of encouraging employees to remain with the business for the longest possible period of time, or in some situations, until the project is finished.

4.2 Repeated Design Change by Owner

Repeated design change by owner ranked as factor no.2 after getting RII value of 0.795. Repeated design modifications would depress the designer because of the time required and raise questions about his effectiveness, which would affect the deliverables' quality. The project timeline and budget are affected by this. Ineffective risk management during design might make risks more likely to occur during execution and raise the possibility of repeating the design process to account for risks. To mitigate this factor, following measures can be taken in the construction projects in kerala

- Experienced Designer on board to take care of all possible changes during project execution phase.
- Credentials of the design team will be verified based on prior experience with projects with a similar level of value and risk. Before to hiring, previous client credentials must be confirmed.
- A suitable geotechnical baseline Report outlining all ground-related concerns must be made available to the client.

- The process for approving designs has to be reduced and made simpler. The time spent redoing the work would be saved.
- In order to reduce everyday adjustments recommended by the execution team, the designer will be based at the project site throughout the project's execution phase. Input from designers should also be considered at every step of construction.

4.3 Poor Qualification and Inadequate Experience of Consultants Engineering Staff and Delay in Approving Overall Designs, Shop Drawing, Sample Tested Materials and Major Changes in Work

With a RII value of 0.785, the consulting engineering staff's lack of training and experience, as well as the delay in approving overall designs, shop drawings, sample tested materials, and significant modifications in work, earned them ranks 3 and 4, respectively. The inadequate design management causes a lot of faults and blunders to occur during construction. It indicates that the consultants did not have a clear understanding of the project objectives when completing the feasibility study with the client when the client starts making changes during an irregular site visit. Many consultants are not familiar with the management of the design. It is a crucial consultant-side factor that negatively affects the project's advancement. On behalf of the Client, the Consultant has full authority to make changes, correct mistakes in the drawings, and issue corrections to inconsistencies in the contract document; however, the Consultant staff never knows for sure whether to make a change or issue a correction before consulting their Manager (centralization policy), in order to prevent any contractual disputes with the Client. Some engineers working for the consultant weren't involved in the initial design and lacked sufficient design expertise [5].

To mitigate this, following measures can be taken

- Consultants should always have a linear responsibility chart which generates a high volume of Data.
- To guarantee that the cash flow is not disrupted or affected, it is advised that the financial model of the project be examined, created, and authorized by the Consultant and the Client.
- To raise the level of their resident engineers' contractual and technical experience, consulting companies must set aside provisional funds or designated budgets for their design managers and supervisory team's ongoing education and professional training.

4.4 Mistakes and Discrepancies Made in Design Documents Leads to Frequent Revisions of Drawings/Designs

With a RII rating of 0.78, errors and discrepancies in design documents that cause repeated revisions of drawings and designs earned the fifth place. The performance of a project can be negatively impacted by changes and discrepancies, which frequently have a cascade effect on the numerous tasks needed to complete a project. Inconsistencies and design defects can harm a project's performance and can result in failures, accidents, and fatalities. It has been noted that sometimes what seems nice on drawings or a computer screen is challenging to create, and designers request revisions as a result in the designs during the construction phase. These differences lead to rework, quantity variations, delays, and construction flaws [6]. Some of the measures to be taken to avoid this is given.

- To enable designers to create design drawings and specifications in accordance with established criteria that are unlikely to alter significantly, the data needed by the design team must be provided at the early stage [6].
- All construction-related drawings and specifications must be properly evaluated for on-site construction operations, according to the designer and consultant. The stakeholders in a project can obtain maximum satisfaction by managing design modifications. The approving authorities take a careful approach to ensuring that disparities are kept to a minimum.
- Using the most recent construction codes, designers must be given enough time to create the drawings and requirements. They must receive compensation commensurate with their work.
- The availability of finances for the project must be carefully monitored by all parties involved, especially the owner, to reduce potential hazards that can arise during execution.

5 Conclusion

All construction projects are subject to risks of varying degrees of severity and nature, with delays being a significant industry risk. As the worldwide construction industry grows, delays and cost overruns are two of the most frequent problems affecting building projects. Due to poor management and weak organisational practises in the construction industry, which serves as a vehicle for achieving national visions and goals, project delays pose a serious threat to the economy, increase costs through significant capital expenditure, litigation, and abandoned projects, and deter foreign investors. Effective project management is crucial to the successful completion of building projects due to the complexity and inherent risks of such endeavours [1].

In Kerala, the building industry is currently dealing with a number of concerns as well, thus it's critical to research and identify the root causes. Despite the fact that numerous studies on delays in building projects have been conducted, the major objective of this study was to identify the primary delay producing variables from the perspectives of all the identified stakeholders. This study is unique because it obtains responses from all the major participants in a project, including senior engineers, contractors, project managers, consultants, designers, structural engineers, research scholars, etc. The relative importance index results showed that the most important factor was "lack of labour," which was followed by "repeated design changes by the owner," "poor qualification and inadequate experience of consultants engineering staff," "delay in approving overall designs, shop drawings, sample tested materials, and major changes in work," and "mistakes and Discrepancies Made In Design Documents Leads To Frequent Revisions Of Work." After analysing these results from a few measures to eliminate and mitigate these factors have been proposed. The fact that the top five elements have been highlighted doesn't imply that the other factors aren't significant. All the factors identified from the literature have a minor or significant impact on a construction project. Some general recommendations for reducing the chances of delay in construction projects are:

- Good communication. By establishing excellent communication between the field, the office, and the client, you may avoid delays in building projects. Instead than relying on impromptu communication channels, establish a structure for communication and stick to a schedule.
- Examine designs thoroughly. A design flaw in a project might not be obvious until the implementation stage. Resolving these issues could have a substantial impact on the project's timeline. Here is when it becomes crucial to review blueprints and confirm specifications before a project starts.
- Make the approvals procedure easier. If your team is awaiting approvals, they might not be able to move forward with a project. The good news is that by utilising automatic notifications and structured workflows, these inefficiencies may be easily avoided. Often, the person giving permission is unaware that doing so is slowing down the entire process. Give reviewers deadlines and explain how their evaluations affect the project's overall timeline in order to motivate them to complete approvals more quickly.
- Improve resource organisation. On-site productivity depends on having the right materials available at the right times. Even though every job site is different, you should consider any potential traffic jams before you begin working.
- Describe the scope of the project. Unexpected scope changes may occur in construction projects. If the owner decides to change their mind about a crucial aspect, the rest of the project may experience serious setbacks. Even though many of these adjustments are out of your control, you may encourage the project owner to have a clear grasp of the project scope before your crew gets to work. Make sure that timeframes are acceptable if revisions are necessary.
- Offer accurate estimations. Budgeting mistakes usually cost you money. Without sufficient funding, it is impossible to hire employees or purchase the required

equipment. To avoid budget-related delays, do your study before bidding to learn how much the project will cost. Automated workflow software can be used to produce regular reports on whether you're staying under your project's budget. Observe overall market developments as well. Speak with your distributor to learn what fees you can expect.

- Be prepared for weather-related delays, as some inconveniences cannot be avoided. On wet days, construction may be hindered or completely halted due to moisture-dependent tasks such as pouring concrete. To prevent your project timeline from being affected by unpredictable weather patterns, consider making your schedule more flexible. Additionally, keep necessary items like water pumps, rain suits and other safety measures near the work area in order to expedite resuming operations after unfavorable weather conditions arise. As a way to reduce outcomes of delayed work caused by adverse weather events, prefabricating components within a climate-controlled environment is also beneficial.

Appendix 1: Example of questionnaire

Category	Factors causing delay	Relative importance			
		Not imp	Some imp	Imp	Ext imp
Consultant related factors	Poor qualification and inadequate experience of consultants engineering staff				
	Delay in approving overall designs, shop drawing, sample tested materials and major changes in the work				
	Incompetent/poor management by consultant				
	Delaying in performing site inspection and testing				
	Consultants reluctance for change and their inflexibilities				

For additional comments

References

1. Alsulaiti AA, Kerbache L (2020) Analysis of critical delay factors in construction projects with a focus on Qatar. *Int J Bus Econ Res* 9(3):130. <https://doi.org/10.11648/j.ijber.20200903.16>
2. Ameyaw EE, Hu Y, Shan M, Chan APC, Le Y (2016) Application of Delphi method in construction engineering and management research: a quantitative perspective. *J Civil Eng Manag* 22(8):991–1000. <https://doi.org/10.3846/13923730.2014.945953>
3. Amrut Sisodiya K, Radhesham Karwa R, Devidas Ghadge D, Pandurang Wanjale N (2020) www.jetir.org (ISSN-2349–5162). In: JETIR2003201 J Emerg Technol Innovative Res 7(3) www.jetir.org
4. Aneesh Chandran (2019) Villages outgrowing cities in Kerala; Huge rise in number of buildings Read more at: <https://englisharchives.mathrubhumi.com/news/kerala/villages-outgrowing-cities-in-kerala-huge-rise-in-number-of-buildings-1.3949430>
5. Atout MM (n d) International conference on management and information systems factors caused by consultant engineers affecting project progress
6. Choudhry RM, Azhar S (2017) Article in journal construction developing countries. <https://www.researchgate.net/publication/315670889>
7. De Vaus D (2001) Research design in social research. *Res Des Soc Res* 1–296
8. Doloi H, Sawhney A, Iyer KC, Rentala S (2012) Analysing factors affecting delays in Indian construction projects. *Int J Project Manage* 30(4):479–489. <https://doi.org/10.1016/j.ijproman.2011.10.004>
9. Gebrehiwet T, Luo H (2017) Analysis of delay impact on construction project based on RII and correlation coefficient: empirical study. *Procedia Eng* 196:366–374. <https://doi.org/10.1016/j.proeng.2017.07.212>
10. <https://www.keralatourism.org/kerala-at-a-glance/>
11. Kumar D (2016a) Causes and effects of delays in Indian construction projects. *Int Res J Eng Technol*. www.irjet.net
12. Kramer MA (2018) A leadership profile of the successful transitional pastor: a Delphi Study
13. Lineage shift in Indian strains of Dengue virus serotype-3 (Genotype III) (2023) evidenced by detection of lineage IV strains in clinical cases from Kerala—scientific figure on research gate. Available from: https://www.researchgate.net/figure/Maps-of-a-India-andb-Kerala-The-sites-of-sample-collection-for-the-study-are-shown_fig5_235382153. Accessed 8 May 2023
14. Muneeswaran G, Manoharan P, Awoyera PO, Adesina A (2020) A statistical approach to assess the schedule delays and risks in Indian construction industry. *Int J Constr Manage* 20(5):450–461. <https://doi.org/10.1080/15623599.2018.1484991>
15. Roy BV (2018) Evaluation of cost and time overrun in government construction projects in Kerala—a case study evaluation of cost and time overrun in government construction projects—a case study. <https://www.researchgate.net/publication/326930250>
16. Soundarya Priya MG, Anandh KS, Kamal S, Shanmuga Priya S (2023) Assessing quality of working life (QWL) In: Among construction professionals in private sectors in Chennai pp 635–647. https://doi.org/10.1007/978-3-031-12011-4_51
17. Senthamizh Sankar S, Anandh KS, Rama M (2022) Examining the influence of various factors that affect construction professionals lifestyle—a case of Tamil Nadu and Kerala. In: Proceedings of SECON'22: structural engineering and construction management. International Publishing, Springer, Cham, International Publishing. pp 625–634
18. Thomas N, Saud SJ (2022) Disruption of construction industry during COVID-19 pandemic—a case study from Ernakulam, Kerala, India. *Lect Notes Civil Eng* 171:151–163. https://doi.org/10.1007/978-3-030-80312-4_13
19. Upadhyay A, Gupta V, Pandey M (2016) A case study on schedule delay analysis in construction projects In Gwalior IRJET Journal a case study on schedule delay analysis in construction projects in Gwalior. *Int Res J Eng Technol*. www.irjet.net
20. Wei KS (2010) Causes, effects and methods of minimizing delays in construction projects. A project report

Structural Behaviour of Square Steel Tubular Column with Deconstructable Splice Joint



V. G. Nehana and V. N. Krishnachandran

Abstract A steel tubular column is a vertical structural member used in construction to provide essential support. Splice joint is a method of joining two members end to end. When the material being joined cannot be obtained in the desired length, the splice joint is used. For high rise buildings the continuity of columns may break, hence splice connections are provided and columns are installed. Splice joints are deconstructable type joints as the failed parts can be repaired, reassembled or can be even removed when failure occurs. These papers focuses on developing models of square cross section of steel tubular columns with deconstructable splice joint using a finite element software ANSYS and study their structural behavior. This paper includes a parametric study on the effect of axial loading and eccentric loading by varying splice length and thickness, bolt diameter and bolt pattern of square cross section of steel tubular columns with deconstructable splice joints. Bending moment rotation curves were obtained from cyclic load testing.

Keywords Deconstructable splice joint · Local buckling · ANSYS software

1 Introduction

In addition to the benefits of high construction efficiency, good construction quality, and sustainable development associated with prefabricated steel structures, deconstructable steel structure systems enables quick disassembly and reuse of structural members following the completion of the structure. Deconstructable steel systems therefore have greater promise in the engineering field [4]. Splicing joint is made of lower square steel tubular column, upper column, four numbers of splice plates and number of high strength bolts. The splice plates are designed as four numbers

V. G. Nehana (✉) · V. N. Krishnachandran
Department of Civil Engineering, NSS College of Engineering, Palakkad, Kerala, India
e-mail: nehanavenkida@gmail.com

V. N. Krishnachandran
e-mail: vnkrishnachandran@nssce.ac.in

of independent plates in order to make sure that the splice plates well fit into the four other component plates of the column. Steel tubular constructions with distinct advantages are being employed more frequently as long span skyscrapers and high-rise buildings continue to emerge [10]. Deconstructable structural design also refers to the use of reusable materials in the design stage to create structural components that are simple to assemble and disassemble [9]. At present the research on deconstructable steel structure system is very limited. While closed section column-to-column splicing joints frequently use fully welded connections, which can't satisfy the requirements of convenient disassembly, the majority of the column-to-column joints use fully bolted connections [4]. The current study proposes square cross sections of steel tubular column with conventional high-strength bolts in order to realize deconstructable connection of closed section steel column splicing joints [1]. 3-D finite element model was built using Ansys software and further validated against the experiments, which may serve as an important reference for its use in real-world engineering applications.

2 Validation

The material properties and dimension for validation is taken from work by Fan et al. [4] as shown in Tables 1 and 2. Specimen H1 is chose for validation were splice connection is exactly placed at middle position. The square steel tubular column of size 2245 mm × 220 mm × 10 mm is taken. The type of bolt is M24 10.9 grade bolt and number of bolt is 64. The splice plate of size 785 mm × 168 mm × 14 mm is used. Boundary condition adopted is bottom fixed and top cyclic load acting. Element type used is SOLID 186(steel plates). Connector elements used is BEAM 188(Bolt). Minimum element size is 12 mm. Element shape of meshing is HEXAHERDON.

Table 1 Material properties of square steel column of thickness 14 mm

Properties	Value	Unit
Young's modulus	219,000	MPa
Poisson's ratio	0.3	
Friction coefficient	0.4	
Yield strength	385.2	MPa

Table 2 Material properties of splice plate of thickness 10 mm

Properties	Value	Unit
Young's modulus	210,000	MPa
Poisson's ratio	0.3	
Yield strength	405.2	MPa

2.1 Cyclic Loading

Loading is applied as per FEMA protocol enlisted in Table 3. As per this protocol 0.375% of drift is given first. Above 4% if a structure withstand the load without fail, then the structure is said to be seismically best suited. Hence there is no need to test above 4%. Loading Height = $6.9/0.00375 = 1840$ mm (Figs. 1, 2 and 3, Table 4).

Table 3 Cyclic loading scheme

Load step	Loading displacement (mm)	Cycle number	Storey drift angle (rad)
1	6.9	6	0.00375
2	9.2	6	0.005
3	13.6	6	0.0075
4	18.5	4	0.01
5	27.7	2	0.015
6	36.9	2	0.02
7	55.4	2	0.03
8	73.8	2	0.04

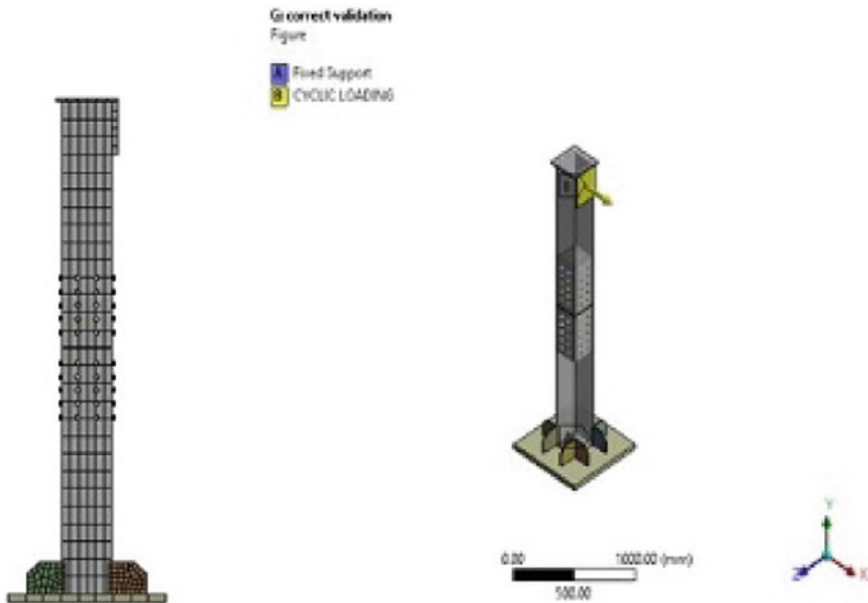


Fig. 1 Mesh and boundary conditions applied

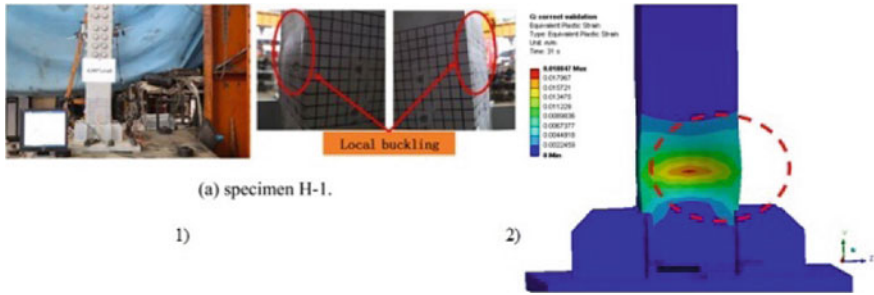


Fig. 2 Failure pattern of local buckling from experiment and validation

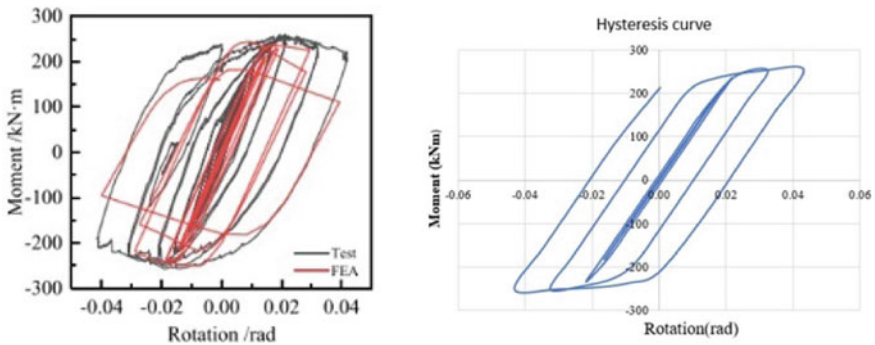


Fig. 3 Hysteresis curve obtained from experiment and from ansys

Table 4 Validation results after cyclic loading test

	Moment (KNm)	Storey drift (% rad)
Experimental (base journal)	251.77	4.1
FEA	253.9	4
% error	0.85	2.44

3 Modelling and Analysis of Square Steel Tubular Column with Deconstructable Splice Joint

The square steel tubular column with deconstructable splice joint modeled for validation is taken and tested for axial and eccentric loading and studied their failure pattern. Bottom hinged and top load is applied.

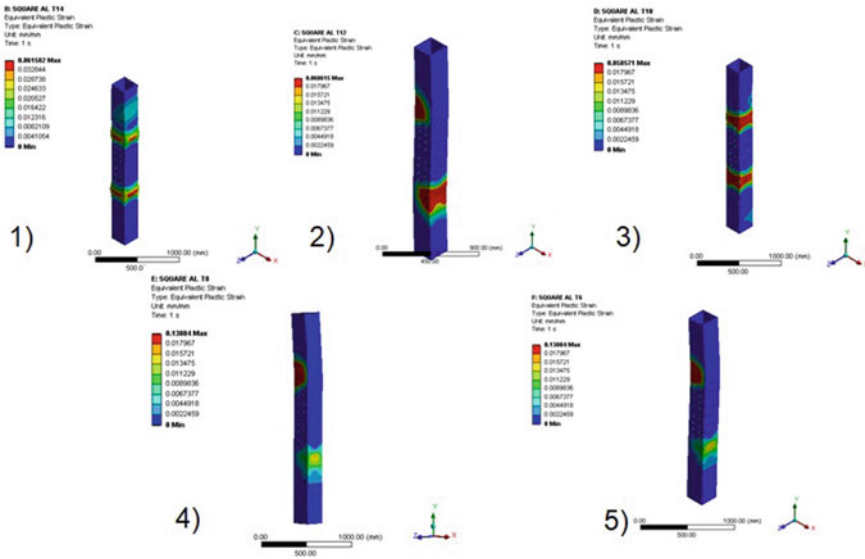


Fig. 4 Equivalent plastic strain for varying thickness of splice plate

3.1 Effect of Axial Loading by Varying Thickness of Splice Plate

Axial loading test is conducted on splice plate of thickness 14, 12, 10, 8 and 6 mm (Fig. 4).

3.2 Effect of Axial Loading by Varying Length of Splice Plate

Axial loading test is conducted on splice plate of length 785, 685 and 585 mm (Fig. 5).

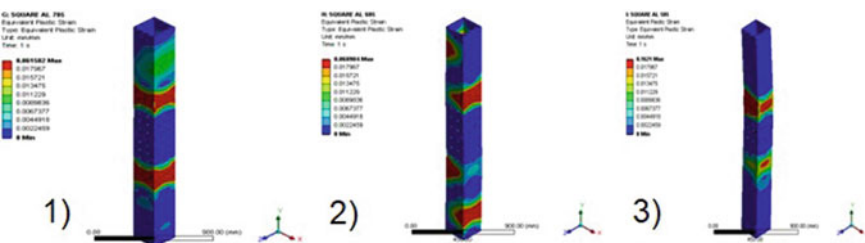


Fig. 5 Equivalent plastic strain for varying length of splice plate

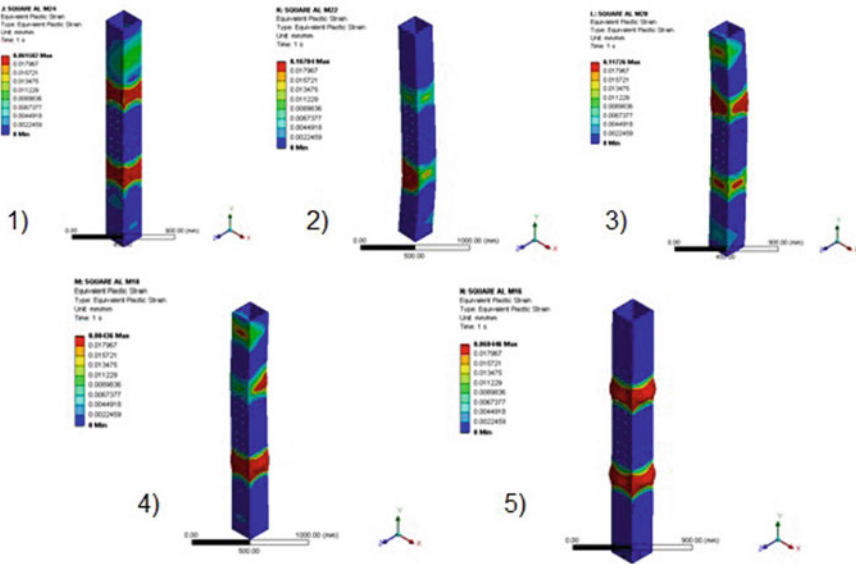


Fig. 6 Equivalent plastic strain for varying diameter of bolt

3.3 Effect of Axial Loading by Varying Diameter of Bolt

Axial loading test is conducted by changing bolt diameters as 24, 22, 20, 18, and 16 mm (Fig. 6).

3.4 Effect of Axial Loading by Varying Bolt Pattern

Axial loading test is conducted by varying bolt pattern as 64 bolts, 48 bolts and 32 bolts (Fig. 7).

3.5 Effect of Eccentric Loading on Square Steel Tubular Column with Deconstructable Splice Joint

Since the square column is a symmetric section, eccentric loading is provided along either X or Y axis only. Eccentric loading is provided at an eccentricity of 55 mm along column width of 220 mm. A parametric study is conducted for eccentric loading similar to axial loading cases by varying splice plate (thickness and length) and bolt (diameter and pattern) parameters.

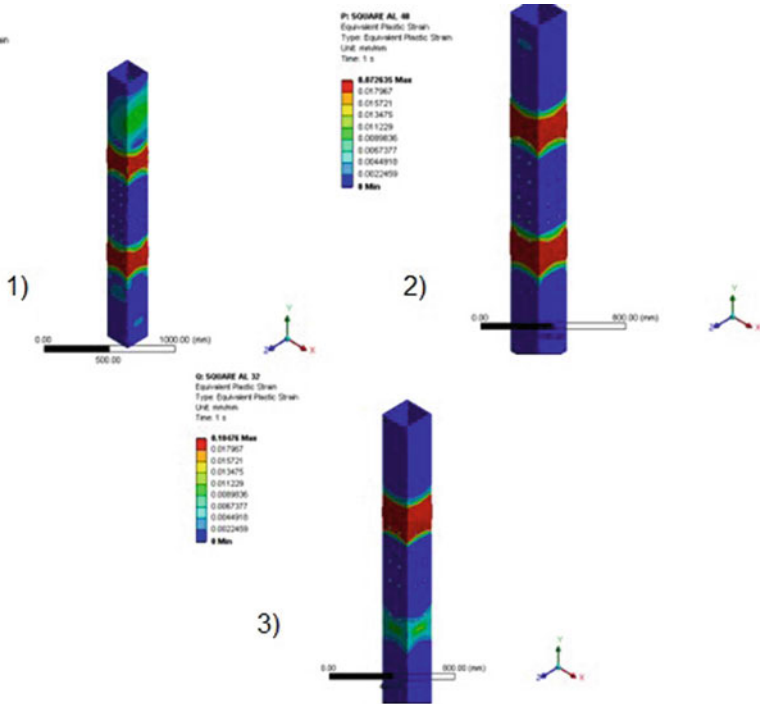


Fig. 7 Total deformation for varying bolt pattern

4 Results

From the analysis carried out using ANSYS WORKBENCH 2022 R2 Load versus Deflection curves were plotted.

4.1 Under Axial Loading

See Figs. 8, 9, 10 and 11.

4.2 Under Eccentric Loading

See Figs. 12, 13, 14 and 15.

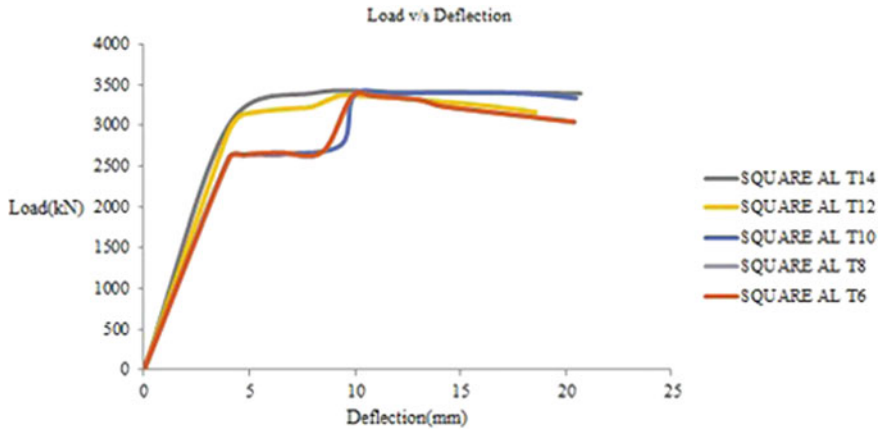


Fig. 8 Load versus deflection curve for varying splice thickness

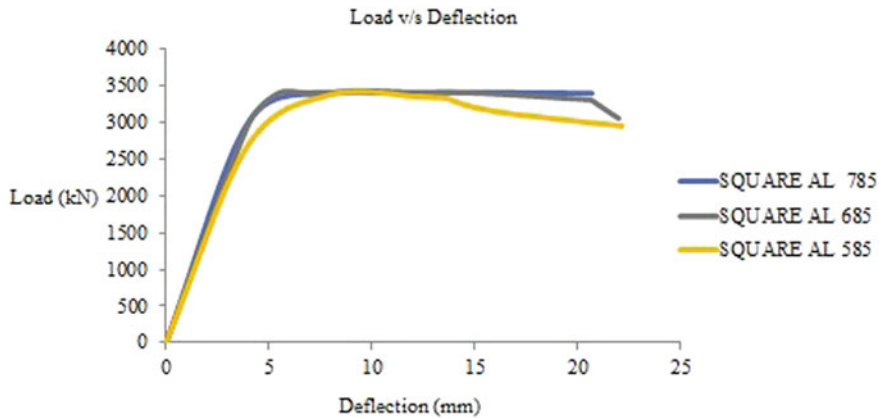


Fig. 9 Load versus deflection curve for varying splice length

5 Conclusions

Finite element analysis is an effective method to study the behavior of the connections.

The tubular columns with deconstructable splice connection with maximum load give greater strength. The section with maximum deflection gives greater ductility.

- The parametric study conducted on square cross section during both axial and eccentric loading showed local deformation buckling failure in most cases.
- Under axial loading splice thickness of 14 mm, splice length 785 mm with M24 and 64 number of bolts showed greater strength of 3412 kN. It can withstand up to a maximum deflection of 12.06 mm.

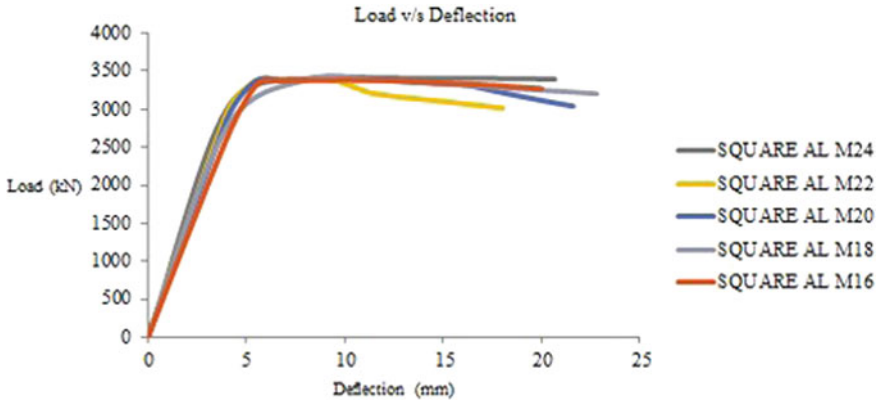


Fig. 10 Load versus deflection curve for varying bolt diameter

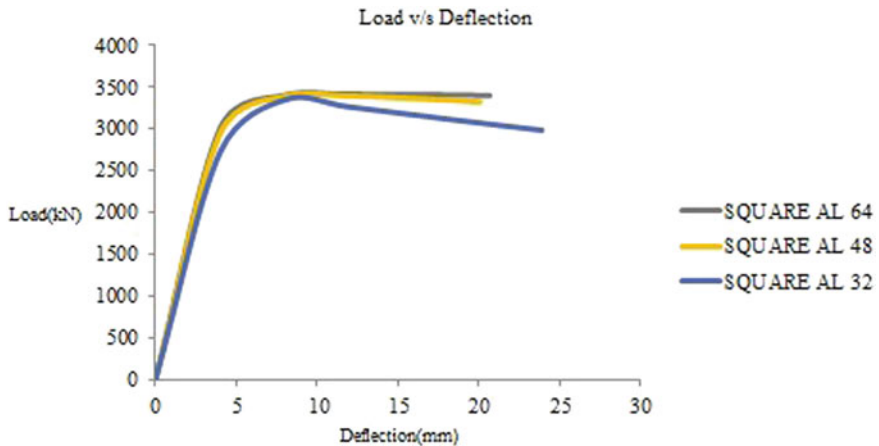


Fig. 11 Load versus deflection curve for varying bolt pattern

- Under eccentric loading splice thickness of 14 mm, splice length of 685 mm with M24 and 64 number of bolt shows greater strength of 1971.1 kN. This section can take withstand up to maximum deflection of 24.549 mm.
- Under cyclic stresses, steel columns may suffer progressive deformation, including local buckling and stiffness loss. Axial loads have the greatest influence on the column’s axial strength and deformation behaviour. Steel column behaviour under eccentric loading is determined by the size and direction of the eccentricity.
- From the parametric study conducted we can conclude that higher splice lengths generally provide increased connection strength and stiffness. A thicker splice can enhance the strength and stiffness of the joint due to increased cross-sectional area and improved load distribution. Thicker splices can better resist bending

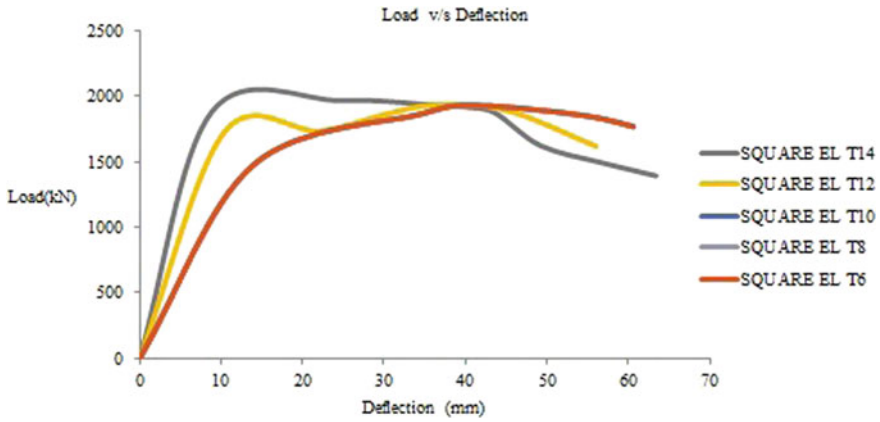


Fig. 12 Load versus deflection curve for varying splice thickness

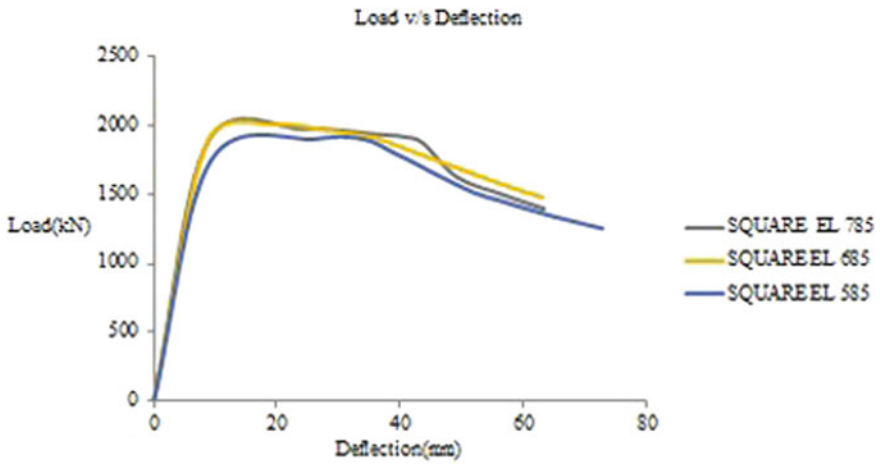


Fig. 13 Load versus deflection curve for varying splice length

and shear forces, resulting in enhanced structural behavior. Larger bolt diameters generally provide higher joint strength due to increased shear area and enhanced bolt resistance. Larger bolts also offer improved stiffness and better load transfer capabilities.

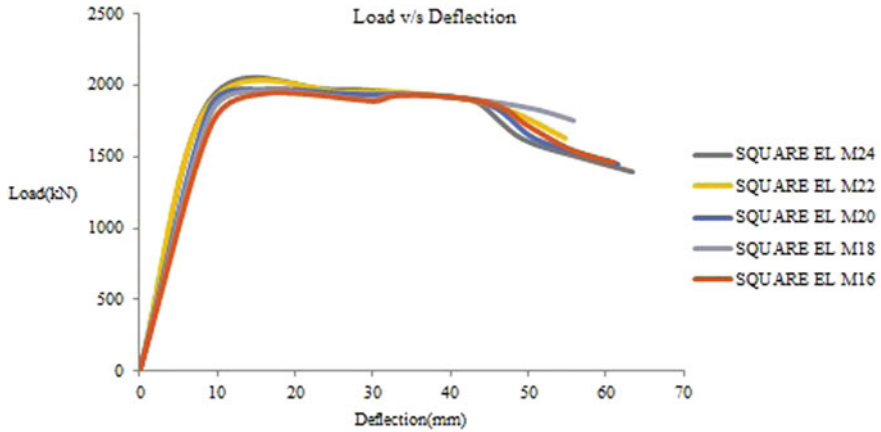


Fig. 14 Load versus deflection curve for bolt diameter

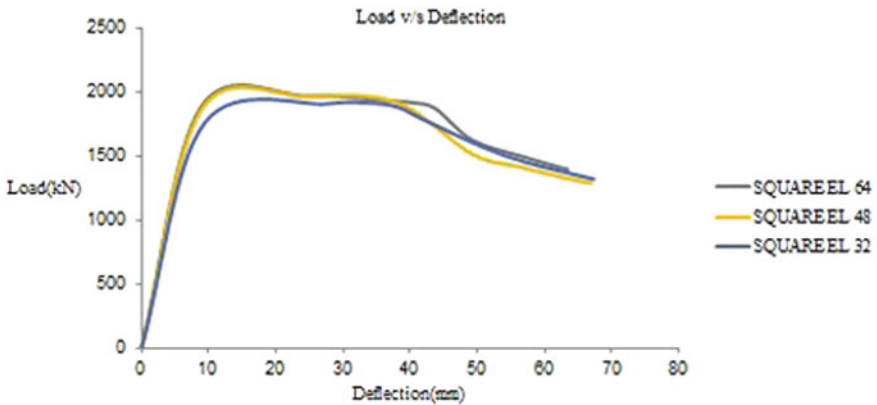


Fig. 15 Load versus deflection curve for varying bolt pattern

References

1. Ataei A, Bradford MA, Valipour HR, Liu X (2016) Experimental study of sustainable high strength steel flush end plate beam-to-column composite joints with deconstructable bolted shear connectors. *Eng Struct* 123:124–140
2. Cai Y, Quach, WM, Chen MT, Young B (2019) Behavior and design of cold-formed and hot-finished steel elliptical tubular stub columns. *J Construct Steel Res* 156
3. Chen MT, Young B (2019) Material properties and structural behavior of cold-formed steel elliptical hollow section stub columns. *Thin-Walled Struct* 134:111–126
4. Fan J, Yang L, Wang Y, Ban H (2022) Research on seismic behaviour of square steel tubular columns with deconstructable splice joints. *J Constr Steel Res* 191:107–204
5. Fan S, Xie S, Wang K, Wu Y, Liang D (2022) Seismic behaviour of novel self-tightening one-side bolted joints of prefabricated steel structures. *J Build Eng* 56:104–823

6. Liu XC, He XN, Wang HX, Zhang AL (2018) Compression-bend-shearing performance of column-to-column bolted-flange connections in prefabricated multi-high-rise steel structures. *Eng Struct* 160:439–460
7. Liu XC, Tao YL, Chen X, Chen ML (2022) Seismic performance of bolted flange splicing joints for CFST columns. *J Constr Steel Res* 196:107–412
8. Pongiglione M, Calderini C, D’Aniello M, Landolfo R (2021) Novel reversible seismic-resistant joint for sustainable and deconstructable steel structures. *J Build Eng* 35
9. Ye J, Mojtabaei SM, Hajirasouliha I, Pilakoutas K (2020) Efficient design of cold-formed steel bolted-moment connections for earthquake resistant frames. *Thin-Walled Struct* 150
10. Wang YQ, Zong L, Shi YJ (2013) Bending behavior and design model of bolted flange-plate connection. *J Constr Steel Res* 84:1–16

Risk Assessment of Landslides During Reconstruction and Rehabilitation Phase at Iritty Taluk of Kannur District, Kerala



Keerthana Mohan and S. Jawahar Saud

Abstract Certain parts of Kerala are particularly vulnerable, with landslides posing a constant threat. Kerala has experienced several landslides in recent years. Many people have died in landslides in Kerala in recent years. Although the occurrence of natural events is uncontrollable, landslides can be mitigated through good risk management. Heavy rain in Kannur district caused landslides, isolating many hilly areas from the rest of the district. More than 500 number of people have died because of disaster, and approximately 5000 number of relief camps have been established across the state. The taluk of Iritty in Kannur district was chosen for this study because it is prone to landslides. To reduce the severity of landslide and to reduce the post disaster risk in the specific area, they must estimate the extent of the disaster and there is a need to estimate the extent of risk and the various types of vulnerabilities associated with it. The study aims on risk management of landslides at Iritty Taluk during reconstruction and rehabilitation phase. The risk during the reconstruction and rehabilitation stage following the landslide is identified and a questionnaire survey is prepared. The weights are calculated using a 5-point Likert scale. Based on questionnaire surveys of professional personnel and stakeholders who are constantly engaged in risk mitigation and rehabilitation activities in Kannur district and Iritty taluk critical risk factors are identified and analyzed using the relative importance index (RII). Critical risks involved during post disaster recovery at Iritty taluk which is given least importance by the governance with an RII value ≤ 0.7 involves policy framework reconstruction, shelter reconstruction based on experience, animal care, loss of access to common resources, and unemployment is identified, restoration of environment. This statistical study focuses on risk management and aids decision-making in the control of risk during reconstruction and rehabilitation phase of landslide.

Keywords Risk assessment · Likert scale · Relative importance index (RII) · Reconstruction and rehabilitation

K. Mohan (✉) · S. J. Saud
Federal Institute of Science and Technology, Angamaly, Kerala, India
e-mail: keerthanamohan258@gmail.com

1 Introduction

1.1 General

Landslide is the displacement of earth, rock, and organic materials by gravity. The movement may be triggered by weathering or by any external mechanisms. Heavy rainfall is the primary cause of landslides during which rainwater percolates and raises hydraulic pressure, which reaches the elastic limit of the soil or rocks. The pressure developed causes the soil and rocks to loosen their elastic strengths, resulting in landslides. Every year, landslides in India pose a serious threat to human life, resulting in an annual loss of \$400 million. Economic losses from landslides have been increasing over recent decades rising construction and investment in landslide-prone areas are mostly to blame. In most mountainous regions across the world, landslides cause serious risks to human lives, belongings, resources, and natural ecosystems [1]. According to data from the Centre for Research on Disaster Epidemiology (CREDE) (Brussels, Belgium) shows that landslides are to blame for at least 17% of all fatalities from natural disasters all over the world [2]. In India study of a geological survey conducted after 2018 and 2019 indicated that the landslides prone areas have been expanded from 13,000 to 18,000 km² and possibility of landslide in India is more. Kerala is especially prone to natural disasters and shifting climatic dynamics due to its geographical position along the seacoast and steep gradients, so Kerala is one of India's most vulnerable states when it comes to mass movements about 43% of Kerala's total area is in landslide slip or landslide prone areas. In Kerala areas like Idukki, Wayanad, Kannur and Kozhikode are more prone to landslides. According to a natural hazard proneness assessment by the National Centre for Earth Science Studies 1848 km² (4.71% geographic area) in Kerala, extending along the steep slopes of the is highly prone to the occurrence of landslides. In 2019, Kerala witnessed 80 landslides in eight districts over three days and the death toll crossed 120. In 2018, about 341 major landslides were reported from ten districts. According to studies conducted in some areas of Kerala, 41% of the mud slips happened behind and around houses on slopes, 29% happened along roadways constructed by altering hill slopes, 17% on commercial lots, and 10% in plantation slopes and 3% in forest areas. Kerala is one of India's most heavily populated districts (860 persons per km²). As a result, it is much more susceptible to damage and losses as a consequence of disasters [3]. Disaster management is the process through which communities reduce vulnerability to hazards and cope with hazards. The series of steps followed by any organization to recover from a disaster is termed as a disaster management cycle. One of the phases in disaster management is the reconstruction and rehabilitation phase. The reconstruction and rehabilitation are a rebuilding measure after a disaster and the main objective is to facilitate the return of the communities to their pre-disaster condition. Recovery can take a few weeks or several years, depending on the disaster's magnitude and the reconstruction resources available and it focuses more on human and material resource development, coordinated effort towards independence, sustainability, and empowerment. Successful reconstruction projects involve

the cooperation and participation of the local communities and stakeholders in reconstruction the most vulnerable and marginalized sections like women, children, and poorest section of society are the primary stakeholders. The September 1985 Mexico City earthquake provides a good example of a participatory process for effective reconstruction that reduced future vulnerability.

The reconstruction and rehabilitation process should not ignore the importance of providing livelihood protection throughout the recovery process. Successful reconstruction and rehabilitation programs simultaneously address both the need to provide income support and the need to reconstruct [4]. Although natural phenomena are uncontrollable, prudent risk management can mitigate the effects of landslides. They must assess the degree of risk and the many forms of vulnerabilities linked with it in order to lower the risk of catastrophes in a specific location.

2 Study Area

Iritty taluk has a total area of 45.84 km² with latitude: 11° 56' 7.20.24" and 75° 55' 56.676" longitude in Kannur district, Kerala, is selected as the study area. It is an area surrounded by hills and located on the banks of the Bavali River which originates from the Wayanad passes river. Iritty Taluk has a total population of 40,369 as per the Census 2011. Out of which 48.42% of the population and females 51.58% are males that is 19543 are males while 20,826 are females. Average precipitation at Iritty taluk is about 4034 mm [5]. Figure 1 shows the landslide susceptibility map of Kannur district.

Table 1 shows the main locations in Iritty taluk where there is frequent occurrence of landslides.

3 Methodology

3.1 General

Landslides cause huge impact on humans, animals, environment, economy, social factors. The risk associated with landslide disaster reconstruction and rehabilitation is to be analyzed to reduce, or avoid, the potential losses from hazards, assure prompt and appropriate assistance to victims of disaster, and achieve rapid and effective recovery. The study focusses on the analysis of risk during reconstruction and rehabilitation phase of landslides. The methodology adopted to achieve the objectives of the work and flow chart is prepared as shown in Fig. 2.

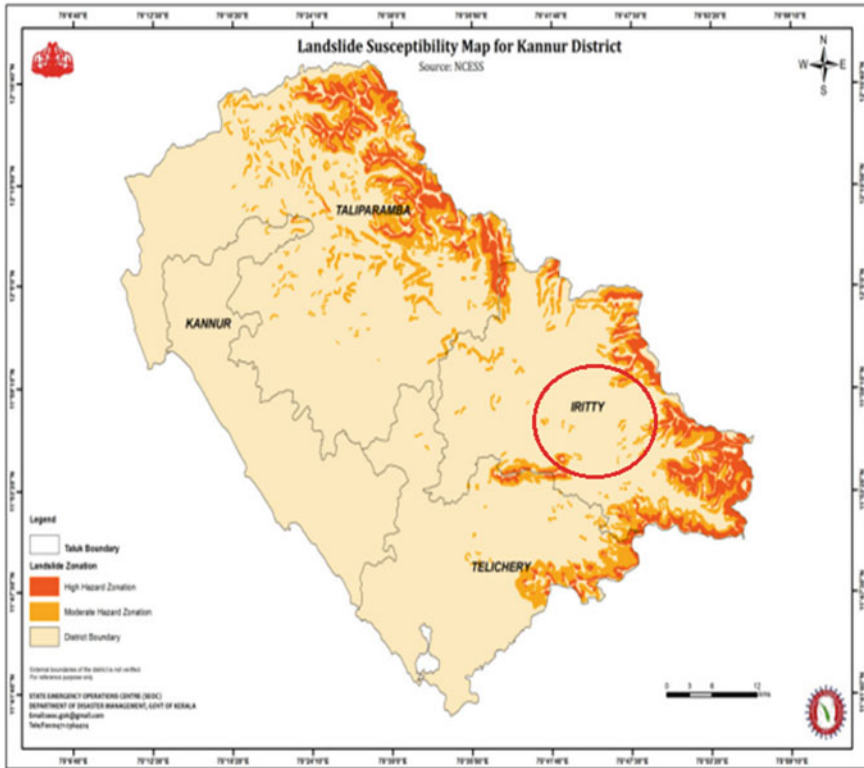


Fig. 1 Landslide susceptibility map of Kannur district [6]

Table 1 Locations at Iritty taluk where landslide frequently occur

Sl. No	Village	Location
1	Aralam	Aralam farm, Chathiroor, Mangoda, Neelayimala
2	Ayyankunnu	Parakkamala, Keezhaganam, Randamkadavu, Valathodu, Kanithattumpara, Uruppunkutti, Paalalthumkadavu
3	Kanichar	Mangulam, Erupathiettam mile
4	Keezhur	Edakkanam
5	Kelakam	Shanthigiri
6	Kottiyoor	Ambhayathodu, Panyammala, Palukachi, Chappamala, Paalchuram
7	Vayathur	Arabhikulam, Randamkai, Kalangi

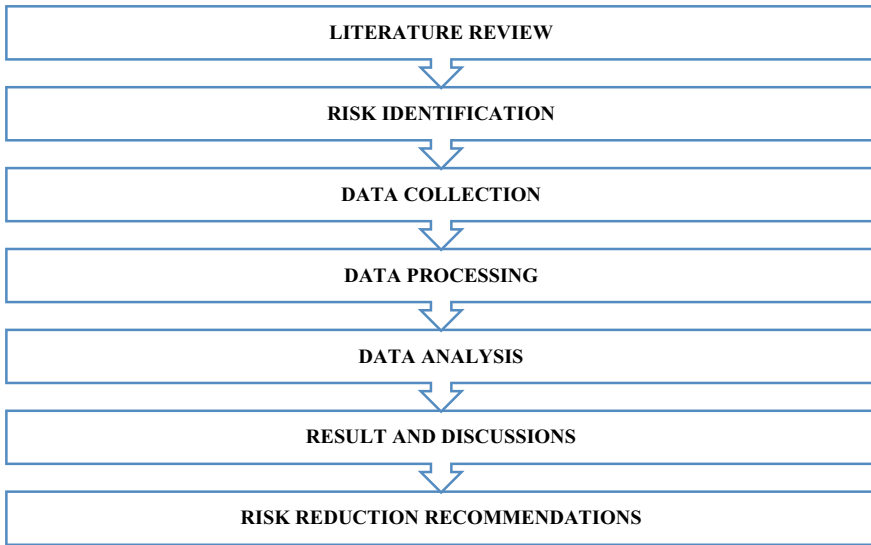


Fig. 2 Flow chart of methodology

3.2 Risk Identification

The risk during the reconstruction and rehabilitation phase of landslide is identified. Based on each risk factors questions are framed. The different risks identified through literature survey are divided into 2 sections that is, 1st is relief and rehabilitation phase and 2nd—reconstruction phase.

1 Relief and Rehabilitation Phase

- Minimum Standard of Relief
- Ex-gratia Relief
- Relief Logistics and Supply Chain Management
- Food and Essential Supplies
- Drinking Water, Dewatering and Sanitation
- Health and Mental Health Care
- Management of Relief Camps
- Veterinary Care
- Relief Employment.
- Temporary and Intermediary Shelters.

2 Disaster Reconstruction Phase

- Damage and Loss Assessment
- Post Disaster Need Assessment
- Financing Reconstruction
- Institutional mechanisms for reconstruction

Building Back Better
Reconstruction of houses
Reconstruction of infrastructure
Regeneration of ecology and environment
Livelihood Reconstruction
Learning from reconstruction and recovery.

3.3 Data Collection

Data is collected from the selected stakeholders through a group decision making process that is the Delphi method. Data is collected from stakeholders through a questionnaire survey which has 27 questions that is on the basic details of the respondents, reconstruction, and rehabilitation phase of the disaster. The Delphi method technique generally has three characteristics that make it distinct from other interaction methods: group interactions and responses, multiple rounds of questioning, and there is a provision of feedback [7]. The stakeholders selected are mainly government officials from both district level and taluk level who are mostly involved in rehabilitation and reconstruction phases.

Stake holders selected for the study are listed out are District disaster management authority (DDMA), Revenue department, Police department, Fire and rescue department, National health mission, Survey department, District supply office, Information and public relations, District employment office, District town planning office, Tahsildar, Kerala water authority, social worker, LSGD, PWD, Village officers, Village assistant, Panchayat ward members, Research scholars, Engineers, Academicians.

3.4 Data Processing

The questions on reconstruction and rehabilitation phase are done through Microsoft forms. The questionnaire survey has basically 3 sections that is Sect. 1 is the general basic details of the respondents, Sect. 2: relief and rehabilitation phase, Sect. 3: disaster reconstruction phase. The response scale is a 5-point Likert scale [8] based on level of agreement with following weightage.

Strongly agree (5)
Agree (4)
Neither agree nor disagree (3)
Disagree (2)
Strongly disagree (1).

3.5 Data Analysis

IBM SPSS Statistics 25 version software is used to check the consistency of the questionnaire through reliability analysis. The consistency of the questionnaire should be a value near to 1. Relative importance index method of analysis is done to find the important risk factor during the reconstruction and rehabilitation process during a landslide. The 5-point Likert scale was used to ascertain the relative importance index for all the risk factors that contribute during the disaster at Iritty taluk. The studies adopted relative importance index (RII) for measuring the risk factors. A 5-point Likert scale ranging from 1 (very low important) to 5 (very high important) was utilized. But the relative importance index (RII) is calculated as “Eq. (1)”

$$\text{Relative importance index} = \frac{\sum W}{A * N} \quad (1)$$

The relative importance index value should be less than 1. The more RII value, the more will be the importance of the risk factor.

4 Result and Discussion

4.1 General

The relief and rehabilitation phase provides immediate assistance to alleviate suffering and meet basic human needs such as food, drink, and shelter. The primary goal of recovery is to return quality of life and community services to pre-disaster levels. Reconstruction is a rehabilitation measure that is used following specific disasters. Building confidence, self-esteem, self-dependence, mutual support, and mutual trust are all part of the rehabilitation process, as does community rebuilding. Government officials should prioritize the primary disaster recovery phase more effectively.

4.2 Survey Response

The responses collected from selected stakeholders are about 36 numbers. Mainly the stakeholders are government officials who deal with the disaster during the reconstruction and rehabilitation phase of the landslide at Iritty taluk. The gender and experience of the respondents are collected along with the questionnaire responses. The pie chart shows the data as a percentage of total number of stakeholders. “Fig. 3 shows the survey responses”.

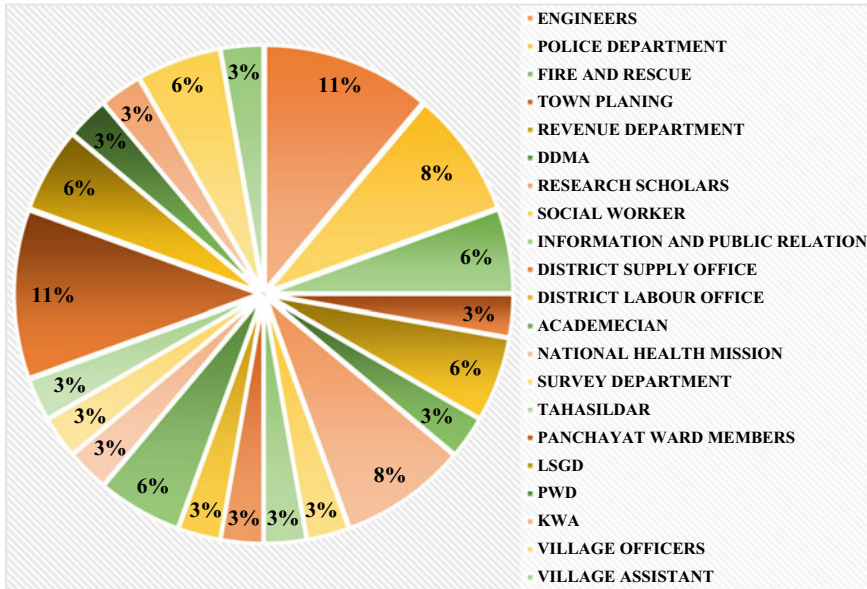


Fig. 3 Survey response

4.3 Response Analysis

Reliability analysis Reliability test gives the consistency of the questionnaire. For this study when checked the reliability of the questions through IBM SPSS statistics 25 version software the Cronbach alpha value is about 0.925 which is nearly to the maximum value which is 1. From the value of Cronbach alpha, it indicates that the questionnaire is more reliable and consistent.

Relative importance index Relative importance index method of analysis is done to find the important risk factor during the reconstruction and rehabilitation process during a landslide at Irritty taluk. Table 2 gives the relative importance index values for each factor.

The major risk during reconstruction and rehabilitation phase of landslide at Irritty taluk is assessed based on the result of relative importance index. Relative importance index (RII) value of each factor is calculated, the higher the RII value more is the importance given to the factors. The risk factors such as post disaster recovery and reconstruction, supply of drinking water, provision of standard relief during landslide at Irritty taluk, provision basic shelter, food, healthcare etc. with an RII value in the range of 0.8 is given more importance from the governance side. From the result obtained factors such as Special health care for peoples such as pregnant and lactating mothers, neo-natal, aged and those suffering from chronic diseases, reconstruction of damaged physical and social infrastructure, extra relief, following of policy or

Table 2 Relative importance index (RII) result

Sl.No	Factors	RII
1	Following of guidelines for providing standards of relief to persons affected by landslide at Iritty taluk, as provided in section 19 of Disaster Management Act [When guideline endorses norms by NDMA/SDRF/NDRF]	0.872
2	Provision of additional ex-gratia relief over and above the norms by state govt. [When State Government/UT Adm. provide additional ex-gratia relief over and above SDRF/NDRF norms]	0.772
3	Following of guidelines for the timely procurement, packaging, transportation, storage, and distribution of relief materials [Manual covers issues like -stockpiling of essential relief materials, pre tendering for supply of essential relief materials, packaging of relief materials for easy distribution, decentralized storage/transportation of relief materials, procedure for distribution of relief materials]	0.844
4	Following guidelines to deal with situations such as major disasters attract humanitarian assistance, often in kind, from all over the world, receiving, sorting, transporting, and distributing these materials to the neediest. [Guidelines are available and covers issues like receiving/sorting/ repackaging relief materials, norms for fair distribution of relief materials, transparency in distribution of relief materials, involvement of NGOs in such operations]	0.816
5	Relief practices of the govt. covers issues like minimum standards of food/cooked food to be provided to the victims, special needs of children, pregnant and lactating mothers, special needs of old, sick, NGOs for setting up community kitchens, arrangements for dry food when cooked food cannot be served, involvement of the victims for deciding choice of foods, system for feedback and monitoring for continuous improvement	0.805
6	Provision of minimum standards for supply of drinking water to people affected by landslide and assess the compliance of the standards [Alternate arrangements for supply of drinking water when normal arrangements are disrupted in disaster such as water trains, water tankers, packaged water, mechanisms to ensure that water is free from impurities and safe to drink-water purifiers, chlorination]	0.883
7	Provision of special dispensation for peoples such as pregnant and lactating mothers, neo-natal, aged and those suffering from chronic diseases [Health care arrangements for affected people, particularly for pregnant and lactating mothers, neo-natal children, senior and very senior citizens, persons suffering from chronic diseases]	0.755

(continued)

Table 2 (continued)

Sl.No	Factors	RII
8	Arrangements for expert psycho-social counselling for the people who are affected and suffering from Post-Traumatic Stress Disorder by the govt [Availability of facilities for psycho-social counselling for PTSD if facilities available to disaster affected as part of relief and rehabilitation measures, regular tie up with mental hospitals]	0.644
9	Following guidelines for the provision of basic shelter, food, water, and health care, solve the problems of people in temporary relief camps, as there are many other issues, such as privacy, safety, security, gender-based violence etc. [Based on the guidelines that have been issued and following issues are covered safety and security of camp dwellers, privacy of dwellers, particularly women dwellers, mechanism for redressing grievances, participatory management of camps, supervision, and monitoring arrangements]	0.866
10	Following and implementing any plan or guidelines by the govt. for animal care after landslide at Iritty [Based on aspects covered- evacuation and rescue of domestic animals and pets, arrangements for fodder and feed, rescue, rehabilitation, and safe passage of wild animals]	0.55
11	People affected by landslide often lose their livelihood, based on provision for relief employment or any alternative arrangement to the people of Iritty by the govt. [Alternate livelihood arrangements for affected people-relief employment such as MNREGA]	0.544
12	Following of guidelines for temporary shelter construction based on the experience of landslide [Guidelines on temporary or intermediate shelters issued, if any, experiences and practices, innovations carried out]	0.627
13	Following of initiative for relief and rehabilitation of people affected by landslide [Any innovative measures taken by the state govt. for strengthening disaster relief and rehabilitation in the state, depending on the effectiveness of such innovation]	0.7
14	Following of guidelines for assessment of the damage and losses during a landslide [Structured guidelines for assessment]	0.838
15	Approach for assessment for damages and losses human and animal lives, houses and infrastructure, production and services, livelihood, environmental assets, cultural assets, macro-economic losses, other socio-economic losses due to landslide	0.727

(continued)

Table 2 (continued)

Sl.No	Factors	RII
16	Following of guidelines for assessment of post disaster recovery and reconstruction at Iritty taluk [Based on structured guidelines for assessing needs of post-disaster recovery and reconstruction, depending on the comprehensiveness of the guidelines and quality of assessment]	0.816
17	Following of policy or framework for post-disaster recovery and reconstruction at Iritty taluk [Depending on the comprehensiveness of the framework]	0.677
18	Finance of reconstruction project, based on the period of implementation of the projects and the sources for mobilization of the fund [Methods adopted for financing post-disaster reconstruction: state budgetary allocation, central assistance, institutional finance, support of world bank, experiences with post-disaster reconstruction]	0.822
19	Approach of govt. for the implementation of reconstruction projects at Iritty taluk after a landslide [Effectiveness of institutional mechanisms for post-disaster reconstruction, when dedicated institution has been created for planning, coordination, and monitoring of reconstruction, when dedicated institution has been created for implementation as well, when reconstruction is got done through line departments]	0.722
20	Guidelines for reconstruction of damaged houses such as—disaster resistant designs and technology by the government [When there are no strategies for reconstruction of damaged houses, when well defined strategies for reconstruction of damaged houses are available, when strategies are followed: in all reconstruction projects, in some reconstruction projects]	0.611
21	Provision of material and financial support by the govt. for reconstruction of damaged houses at Iritty taluk [Support is provided by the government for reconstruction of damaged houses only as per SDRF norms, when additional support is provided by government in terms of finance, materials, technical standards of design and specification]	0.805
22	Provision and implementation of guidelines for insurance of reconstructed houses [When there is no such insurance, when houses are insured only in major reconstruction projects, when houses are insured only in major reconstruction projects]	0.577

(continued)

Table 2 (continued)

Sl.No	Factors	RII
23	Following of guidelines for reconstruction of damaged physical and social infrastructure [When there are no strategies for reconstruction of damaged infrastructure, when well defined strategies for reconstruction of damaged infrastructure are available-what are the additional elements of safety and resilience that are built in reconstruction projects]	0.766
24	Following of guidelines for strategic approach for reconstruction of damaged livelihoods [When there are no strategies for reconstruction of livelihoods of affected people and communities, when strategic approach has been developed, the effectiveness of the approach in reconstructing livelihoods of affected people in terms of reviving damaged livelihoods, creating alternate livelihoods, developing skills for alternate livelihoods, providing input and marketing support, providing credit support]	0.727
25	Implementation of any plans or guidelines by the govt. for restoring considerable damages to ecology and environment at Irritty after landslide [When there has not been any effort to repair and restore ecology and environment damaged due to disasters, when there have been efforts in this direction, effectiveness of the initiatives in terms of restoration of damaged forests and mangroves, restoration of soil, restoration of dried/contaminated water bodies]	0.561
26	Provision and following of any plans or guidelines based on the past experiences of reconstruction [Have the projects been documented, have these lessons been incorporated in the policies or guidelines, documented systematically, and incorporated in the policies or guidelines]	0.583
27	Initiative/good practice of govt for landslide recovery and reconstruction [Any innovative measures taken by the state govt. for post-disaster recovery and reconstruction in the State, depending on the effectiveness of such innovation]	0.883

guidelines for special framework for disaster reconstruction and rehabilitation etc. with an RII value in the range 0.7–0.6 indicated that these factors are given moderate importance. Factors such as relief employment, animal care after disaster, insurance of reconstructed houses, disaster resistant construction, restoration of environment and ecology after landslide etc. is given least importance from the governance side with an RII value in the range of 0.5. From the study it indicates that the factors which are long term and factors which require proper planning coordination are given least importance from the governance side. For risk reduction the factors which are given least importance during reconstruction and rehabilitation phase of landslide at Irritty taluk must be given priority. These results indicate that projects and programs for catastrophic landslide reconstruction relief and rehabilitation must be implemented

from the governance side. It is also critical to improve its financial security efficiency to achieve further outstanding results after a disaster.

Recommendations

Factors such as relief employment, animal care after disaster, insurance of reconstructed houses, disaster resistant construction, restoration of environment and ecology after landslide etc. is given least importance from the governance side with an RII value ≤ 0.7 . Iritty taluk mainly consist of people from different communities such as tribal people, women, children, old-aged people etc. Mostly the landslide prone areas of the taluk are hilly forest areas with habitations. From the result of RII, deep literature review, in depth interviews with stakeholders and common people of Iritty taluk it indicates that the factors which are long term and factors which require proper planning coordination is given least importance from the governance side. Factors which are given least importance during reconstruction and rehabilitation phase of landslide at Iritty taluk must be given priority and risk reduction methods should be adopted.

- After the landslide or before the occurrence of landslide at Iritty taluk government can make use different risk reducing new technologies for relief and rehabilitation purposes such as: unmanned aerial system, social networking system, hyogo framework for taking actions, sendai framework can be used.
- Policy framework can be developed and modified by the government for recovery and reconstruction. The effectiveness of the prepared framework can also be ensured by the government.
- Arrangements for expert psychosocial counseling must be developed by the government for improving the metal health of the people after the disaster through primary health centers.
- The resettlement plan should go beyond housing and meet other demographic needs such as social infrastructure, livelihoods, and economic activities. To eliminate re-building concerns, a more in-depth risk study, such as risk mapping, must be prepared prior to the establishment of the new site.
- Although people often possess strong economic, social, and cultural factors that influence their choice of settlement, it is critical that relocation choices and site selection be undertaken in a consultative manner with full participation of the affected populations. Before agreeing to accept voluntary relocation, communities must be prepared and informed. Appropriate mechanisms for ensuring stable land and housing tenure should be put in place.
- Hilly and forest areas of Iritty taluk have tribal communities, poor economic conditions of the people do not permit them to rebuild their houses as per the disaster resistant designs and specifications.
- Government must construct community shelters at appropriate places within the easy access of the habitations of the communities and can provide immediate protection from deaths and injuries due to the collapse of houses.

- The Bureau of standards can be revised based on the geographical context of Iritty taluk by the trained engineers of the government and design norms can followed for new constructions in the taluk.
- The building codes must be periodically reviewed and developed by the government based on historical data of landslide in the taluk, and to integrate the newest construction techniques, materials, engineering safety standards, planning and environmental regulations.
- Existing structures in the vulnerable areas of the taluk can only be retrofitted with an additional cost which the government should invest.
- Shelters constructed by the government must be spacious enough to accommodate a few people, there should be provisions of drinking water, sanitation, kitchen, etc.
- Adequate preparedness measures must be taken in strengthening the lifeline buildings in Iritty taluk such as hospitals, emergency operation centers, police control rooms etc. which plays a critical role during emergency operations.
- To reduce the consequences of landslide, transfer the risks over the last several years, “soft engineering,” that is nonstructural solutions must be used in Iritty taluk. Methods such as proper land use planning, early warning systems, awareness programs, special training, financial protection, capacity building can be developed.
- The Kerala State Disaster Management Authority can collaborate with public sector insurance companies to devise an insurance policy that would provide insurance coverage for homes hit by natural calamities. The homes of people which are located at risky vulnerable areas where landslide strikes must be insured, low-income groups are mostly vulnerable to disaster impacts, separate guidelines must be adopted for reconstruction of houses through insurance and fund.
- For restoration of the ecology and environment typical activities such as cleaning of watersheds, reforestation programs and other environmental types of interventions that are necessary to reduce future risk can be initiated by the government.
- Government should have an initiative for the welfare of animals before, during and after landslides is equally important, with reference to the moving of the animal’s safer shelters feed, safety, and shelter, as they have a significant effect on the wellbeing and productivity of the animals.
- Relief opportunities for employment can be offered to the people through agriculture and livestock production, through the supply of seeds, tools, microcredits, and other means, and small businesses through the provision of credits or different approaches.
- Economic activity will be boosted by the recovery and upgrading of productive social infrastructure such as roads and markets. Rebuilding the housing sector with local technologies, materials, and know-how to ensure that construction operations have a direct positive influence on the local economy.

5 Conclusions

Landslides are one of the most common natural incidents, affecting 15% of the landmass. It results in the loss of life and property. 13 out of 14 districts of Kerala are vulnerable to landslides. To substantially lower the damage caused by landslides, it is important to take a constructive approach to risk management. Practitioner's perspectives on the extent of landslide risk management will help to provide insight into how to boost landslide risk management practices. They also could be used as a guide for prioritizing risk management plans in the future. The risk management metrics represent operational, growth, capability, and structural measures taken to minimize vulnerability and disruptions in a geographic region, plan for a crisis, and bounce back rapidly from disasters.

The study indicates that factors which require long term planning and coordination are given least importance. Factors such as relief employment, animal care after disaster, insurance of reconstructed houses, disaster resistant construction, restoration of environment and ecology after landslide etc. have an RII value in the range of 0.5. The findings can be used to develop landslide risk management innovations in Iritty taluk, and they could be considered as a help full reference for upcoming works. The present approach can be modified and extended to other forms of natural disasters in Kerala, such as floods. However, according to the disaster situation and the local scenario, the survey questions should be modified or updated. It is also recommended that the current approach of surveying landslide risk management expectations be extended to include public perceptions, as comparing expert and public opinions will provide a more comprehensive measure of landslide risk management effectiveness.

References

1. Perera C, Jayawardana D (2018) Direct impacts of landslides on socioeconomic systems: case study from Aranayake, Sri Lanka. <https://doi.org/10.1186/s40677-018-0104-6>
2. Ajmal PK, Saud SJ (2022) Estimating landslide Risk Management Index for Nilambur Taluk, Kerala using analytic hierarchy process—a case study. *Lecture Notes in Civil Engineering* 171:205–218. https://doi.org/10.1007/978-3-030-80312-4_17
3. <https://www.onmanorama.com/news/kerala/2021/10/22/landslides-frequency-increase-kerala-climate-change-land-use-pattern.html>
4. Floods, Kerala Post Disaster Needs Assessment, and Landslides August (2018) Government of Kerala. Thiruvananthapuram, October
5. Perera ENC et al (2018) Direct impacts of landslides on socio-economic systems: a case study from Aranayake, Sri Lanka. *Geoenviron Disasters* 5(1):1–12
6. District disaster management plan Kannur 2015
7. Anderson et al (2011) Reducing landslide risk in communities: evidence from the Eastern Caribbean. *Appl Geogr* 31:590–599
8. Danner M, Gerber-Grote A (2017) Analytic hierarchy process. In: Patient involvement in health technology assessment. Springer Singapore, pp 135–147. https://doi.org/10.1007/978-981-10-4068-9_11

Environmental Sustainability Assessment of Rural Road Maintenance Using Environmental Impact Assessment Tool



RajiReddy Myakala and S. Shankar

Abstract Rural roads have been among the most prevalent types of public infrastructure across the world, and they need ongoing expenditures and upgrades to remain functional. Rural roads are also designed systems that exist in every contemporary country and have substantial effects on the economy, the environment, and society. There are a number of road sustainability evaluation techniques that have been created in an effort to encourage more environmentally friendly choices concerning rural road planning, building, and maintenance. Before selecting whether and/or how to create this instrument, as well as what innovations, legislation, and investment approach should be followed, the effects must be thoroughly considered. To examine the environmental sustainability of rural road maintenance, a thorough and trustworthy sustainability rating tool is required. An Environmental Impact Assessment (EIA) is a tool used to assess the significant impact of a project or development plan on the environment. Environmental impact studies ensure that project decision makers consider possible environmental impacts as early as possible and look for ways to avoid, reduce or compensate for these impacts. By examining the applicability and effectiveness of the sustainability assessment tool i.e., Environmental Impact Assessment (EIA), which may be used in this sense, this research attempted to provide a deeper insight into the complicated world of environmental sustainability evaluation of rural road maintenance. First, sustainability issues were determined and created environmental sustainability indicators; also, category priority was determined. Moreover, the category priority was evaluated using Delphi expert panel and sizable individuals shared their opinions. Furthermore, the environmental sustainability of real rural road maintenance work in Telangana State was computed using the employed EIA tool.

Keywords Rural roads · Sustainability rating tool · Environment · Environmental Impact Assessment · Road maintenance

R. Myakala (✉) · S. Shankar
Department of Civil Engineering, Transportation Division, National Institute of Technology
Warangal, Warangal, Telangana, India
e-mail: rr720027@student.nitw.ac.in

1 Introduction

It is well acknowledged that roads play a key role in the socio-economic growth of rural regions. Rural roads also provide access to resources for socioeconomic growth and contribute to the eradication of poverty. Rural communities can access health-care facilities, educational institutions, market facilities, and other public and private amenities when rural roads have been developed and managed properly. Whenever the roads have been properly maintained, the socio-economic advantages of a place can be enhanced; otherwise, these benefits begin to decline as a result of inadequate maintenance [29]. In addition, these remote communities' unstable access contributes to the prevalence of poverty. The populace of rural areas has decreased as a result of inadequate amenities and unstable living conditions. Since the current focus is on creating smart cities as well as urbanisation, financing for the rural sector is likely to drop or governments will run into financial difficulties trying to meet these objectives. Additionally, the construction of rural road network in developing nations may significantly affect the population it is intended to serve by promoting economic growth and reducing poverty. The development of rural road network is prioritised in emerging nations like India. Compared to urban road network, rural roads provide professionals and policymakers various considerations. Nevertheless, the construction and upkeep of rural roads is a significant global concern. Even in affluent nations like the United Kingdom (UK), rural roads have not been covered by federal resurfacing initiatives, leaving them mostly in disrepair. In addition to the claimed negative impacts, rural roads receive poor upkeep. Due to a lack of funding and ineffective building methods, almost 80% of Indian rural roads remain in poor condition. Poorly paved roads result in a loss of lives and property.

Approximately 70% of the Indian populace lives in rural regions, and approximately 70% of the country's total road infrastructure is made up of rural roads (RR), giving it the biggest and tightest road infrastructure in the world. All-weather roadways were yet inaccessible to 30% of the populace. The Indian government had launched a major initiative named the Pradhan Mantri Gram Sadak Yojana (PMGSY) in response to this deficit. The PMGSY, Rural Development Department (RDD), and the Panchayat Raj Division, a central government dept, are in charge and have the necessary power. RDD doubles as a think tank for policy. It does business through the National Rural Roads Development Agency (NRRDA), an affiliate. Additionally, in India, the word "panchayat" is used to refer to the general name for the local government. At the basic, middle, and top tiers, it has a three-tiered system. Since India seems to be an agriculture country, PMGSY was hailed as a game-changer for communities and enhanced the transportation of agricultural products. The World Bank also had increased its financial assistance for rural road construction projects. The management of the resources and the upkeep of the roadways are among the essential elements of this program. Usually, a 5-year maintenance agreement is incorporated into the rural road agreement [9].

Since it has been initially articulated in relation to forest in the eighteenth century, the idea of sustainability had undergone significant change [2, 18, 27]. Today, most people who attempt to define the term begin with the Brundtland Commission's accepted definition, which states that sustainable growth "must ensure that it serves the requirements of the current without jeopardizing the capability of forthcoming generations to satisfy their own requirements." The goal aspects of environment, economics, and society are sometimes represented graphically by three overlaying circles, to which an organizational component may be included. Various articles [28, 33] include more in-depth examinations of different sustainability principles. Tools for evaluation that are thorough, effective, and dependable are required for the shift to a better sustainable future. Sustainability assessment has been described as "a technique that may assist policy-makers as well as decision-makers decide which activities they ought or shouldn't undertake in an effort to develop society quite sustainable" by Devuyt et al. [8]. Moreover, numerous thorough models for integrated evaluation were established predicated on the four characteristics of sustainability [10]. The "Bellagio Principles" seem to be a set of operational guidance that was developed in 1996 by a cohort of investigators. They serve as a bridge between theory and practise for the entire evaluation procedure, from system layout as well as indicator recognition through field observations and compendium to explanation and interaction of outcomes [19]. Numerous ideas were produced in the previous ten years with the goal of improving the operationalization of the sustainability goal. This led to the emergence of a wide range of methodologies that assert they may be used to evaluate sustainability across several industries. The variety of impact assessment techniques, including Ecological Footprint, Life Cycle Assessment, Strategic EIA, and EIA, has grown more and more linked to sustainability evaluation [27].

1.1 Environmental Sustainability Conceptualized

The often referenced description of sustainable growth in the "Our Common Future" study [3] as well as the "triple bottom line" (TBL), which combines economic, environmental, and social sustainability, serve as common touchstones for conceptualising sustainability. But traditionally, the term "sustainability" has been used to refer solely to environmental sustainability. The fundamental goal was to keep economic expansion within the limits of the environment's holding capacity, but there has been disagreement about what constituted sustainable development and what might be supported. The many worldviews, attitudes, and philosophies that may underpin conceptions of sustainability are one area of contention. Many multi-disciplinary research areas have influenced sustainability research. These have aided in identifying important factors and relationships for evaluating sustainability in specific situations, but they haven't yet contributed to the development of a single generally applicable concept of sustainability [16]. Paradigms for sustainability have been generally constructed on the basis of a set of values as well as basic principles. The fundamentals of integrity, rejuvenation, assimilative capabilities, adaptability,

precautionary concept, inevitability and singularity of capital assets, substitutability, integration, the polluter pays concept, and limitations on resource as well as waste creation were all reflected in an initial discussion on sustainability worldviews that focused on weak vs powerful sustainability. According to [7], these ideas have been used to describe sustainability and solve environmental issues involving specific abiotic or biotic organisms, or whole ecosystems.

1.2 Sustainability Rating Tools

Infrastructure growth projects have been encouraged to make general sustainable decisions by using sustainability rating systems and tools (SRTs), which are evaluation mechanisms created predicated on best practise assessment [6]. Infrastructure SRTs promote sustainability methods by evaluating choices using a checklists or questionnaire, which depending on the instrument, may call for documentation and proof. The primary goal of this evaluation is to offer feedback in assistance of improving and modernising the overall practise; as a result, projects have been scored according to how much they contribute to the total sustainability goal specified in the scoring system as well as the selected sustainability considerations [36]. The vast majority of the SRTs that are now in use, including GreenLITES [13], Greenroads [1, 20], INVEST tool, as well as Envision, focus on broad civil engineering networks. As a result, a majority of the evaluated criteria have no direct bearing on pavement structures or paving operations [4, 36]. BE2ST-in-Highways and The Ministry of Transportation of Ontario (MTO) GreenPave [5, 19] are two tools designed exclusively for the sustainability evaluation of road projects. Network for common transportation is developed with some instruments. There are a number of additional sustainability grading systems, like CEEQUAL tool (for UK) and I-LAST (for Illinois Department of Transportation (DOT)).

1.3 Challenges in SRTs

Infrastructure sustainability grading techniques share characteristics and peculiarities that draw attention to their respective shortcomings. Every tool specifically assesses particular sustainability goals associated with infrastructure growth projects. Research has shown that the use of rating tools can affect a project's sustainability whether various tools [12], combos of tools, or a single tool has been used on several projects. The limitations of the indicators employed in existing sustainability rating tools are highlighted by distinctions in the tool data, sustainability aims, appraisal procedure, implementation requisites, and sustainability variables, reporting benchmarks and markers [12], and credit weights allocated to each attribute

Table 1 Rural road maintenance SRTs limitations

S. No	Limitations	Comment
1	Limited scope of rural road maintenance activities	Concentrating on only a few activities suggests inconsistencies in the chances found to increase rural road sustainability
2	Performance result is not defined by indicators	An EIA indicates that there is no proof of a sustainable result
3	High levels of subjectivity in the execution and process	Many indicators' points have been determined predicated on an expert's assessment of the initiative's sustainability considerations
4	Objectives and criteria weight are not properly coordinated	Rating methods give the project a general relative grade but do not offer exact numbers related to environmental sustainability
5	Indicators predicated on regionally particular behaviours and non-generalizable methods	Applying criteria for metrics like 20% recyclable material restricts creative thinking
6	Presume a particular activity significantly contributes to sustainability	Recycling may not provide in long-term environmental benefits over the course of paving life; activity metrics have been not result measures
7	Select goals are used to basis assessments	Each tool highlights the aspect of sustainability that the creator deems to be more significant and quantifiable

and marker for reporting benchmarks. The SRT's reporting guidelines' description and scope is a significant flaw. The majority of these requirements are predicated on activity measurements rather than the performance result that describes the effects of performing those activities. Table.1 indicates the limitations of rural road maintenance sustainability rating systems.

2 Literature Review

The difficulties of spatial inequities, socioeconomic discrepancies, fast urbanisation, and transportation system connectivity, which affect urban design and quality of life are addressed in each neighbourhood urban planning. The sustainability concept stands at the centre of growth; arguments on a global and local level frequently highlight its relevance in urban planning. The sustainability of neighbourhoods seems to be in doubt despite this dedication. It is believed that while cities have given substantial attention to sustainable growth, communities have, for some purpose, received less attention, particularly when it comes to the spatial dimension and its impact on sustainability. It has now become necessary to offer a variety of sustainability, a metric that can assess the level of neighbourhood sustainability efforts and the level to which this sustainability could be incorporated. A complete neighbourhood SA tool or model is developed using the core urban neighbourhood sustainable principles

and traits (Successful Neighbourhood Model (SNM)). SNM is, in theory, a tool for assessing the neighbourhood's sustainability that helps choose the best options for sustainable solutions predicated on a decision-making procedure that makes use of decision requirements, weighting techniques, relative judgement, priority of options, and incorporation of alternative solutions. However, because the air quality monitoring stations did not focus on particular neighbourhoods, they could not provide reliable performance metrics [24].

Hasan et al. [17] used the life cycle assessment technique to determine the environmental effects of a particular instance research for a 3.5 km dual lane road asphalt highway segment in Abu Dhabi all over the succeeding life cycle phases: material retrieval and manufacturing, equipment as well as materials transit, building, maintenance, and reconstruction; presuming a life span of thirty years. EIA for energy use and air emissions caused by full road construction, including earthmoving, paving, and concrete construction on barriers, traffic signs, pavements, parapets, and lighting. The minimization of environmental effect was thoroughly examined. Additionally, real-world field information for the road segment employing virgin materials, conventional asphalt manufacturing mixture for pavement operations, and Portland cement concrete for the entirety of the concrete projects have been employed as the benchmark scenario. From the standpoint of reducing the environmental effect, regular maintenance and periodical rehabilitation, which involves milling as well as repaving the worn courses every five years, were also examined. All ReCiPe midway method indications were taken into account throughout the environmental evaluation. The findings indicate that a substantial share of the environmental effects of finished roadworks is attributable to earthworks. Because of the use of artificial zeolites, the life span effect outcomes of warm- and hot-mix asphalt have been nearly similar. All measures of the results revealed a considerable reduction in environmental effect. The study found that using alternative materials and other methods for producing asphalt had larger environmental advantages than those mentioned in roadwork's research. However, this research takes more time due to implementation of large number of methods.

There are a lot of environmental emissions produced by the transportation industry. Li et al. [21] evaluate the environmental effect of the pollutants over the life span of a transport network project. The fast-tracked transport initiative in China was employed as an instance research for converting the energy as well as materials required throughout the life span into environmental pollutants. Three phases were included in the fast-track transportation research's life cycle: building, repairs and maintenance, and destruction. The transportation project's environmental effect was investigated using both quantitative as well as qualitative methods. For the creation of the EIA framework, the life cycle assessment (LCA) approach was implemented to study the contributions of each procedure in the transportation project's life cycle. The empirical findings indicate that, during the fast-track transportation project's life span, the building phase does have the greatest environmental effect, preceded by the deconstruction and maintenance stages. Steel seems to have the greatest percentage of an environmental effect during the building phase of all the materials utilised in the fast-track transportation system. This shows that the usage of steel materials during

the building phase of a fast-track transportation project has a significant negative environmental effect. By identifying the most significant environmental effect stage and material resource during the course of a transport network project, this analysis helps to reduce environmental pollutants. However, the developed method is only implemented for one country.

In the earlier, the award criterion was based on cheapest price as long as structural capability and safety have been guaranteed. Energy, environmental and long-term effects were highlighted in recent years. Unfortunately, modern pavement technology and materials (such as waste plastics) have an impact on maintenance and reconstruction procedures and need correct and timely investigations and standards. As a result, [15] offered an evaluation of an Italian urban road's environmental and energy impact and took into account several material-related situations that completely complied with developing technology. As per the ISO 14040 standard, a life-cycle methodology is used to evaluate the environmental as well as energy effects of a conventional urban road in Italy. The authors evaluated several bituminous mixture situations' energy as well as environmental profiles in further depth. Finding the scenario with the least negative effects on the energy and environment seems to be the goal of scenario assessment. In attempt to establish appropriate choices for enhancement, the contributions of every life-cycle stage to the overall consequences as well as the energy as well as environmental hazards are determined for every scenario under consideration. The analysis's findings indicate that practically each of the evaluated effect categories is important to the stage of material manufacturing, particularly raw material retrieval and resources availability. This is primarily because bitumen, a petroleum-based substance, is produced. Furthermore, the scenario assessment shows that pavement instances that employ recycled materials have less environmental as well as energy consequences since virgin raw components are saved and effects from disposal have been avoided. Furthermore, the performance needs more improvement.

In China, the region used for road building is growing quickly, which poses a problem for resource preservation. Yu et al. [37] combined material flow assessment and LCA methodologies to estimate the material stocks as well as environmental consequences of urban road network, while existing research mostly concentrated on usage at process level. Road network models were extracted from remote-sensing images. Using Nanjing like an instance, the findings indicate that: (1) arterial roads hold the biggest amount of components (42.9 million tonnes) of the whole road network; (2) macadam accounts for approximately 80% of all resource stocks; (3) an upsurge in road category corresponds with an upsurge in material shares per unit region and improves the efficacy of material utilisation; and (4) arterial roads have been overemphasised and expressways remain on a limited scale in Nanjing. This study's technique offers road planners a practical tool for managing resource depletion over the long future. Furthermore, this study needs improvement in performance and also not performed for larger scale.

Authorities and city managers have employed LCA techniques to assist in the decision-making procedure toward establishing a more stable society. While local circumstances have a significant impact on LCA and can change depending on

a number of factors, some institutions are started collaborative efforts to advance sustainable growth objectives. The environmental benefits of producing and using road components for Münster, Germany's road system were evaluated by [32]. Additionally, the author contrasted Münster's typical pavement designs with other possibilities that included more recycled asphalt pavement (RAP). Despite the fact that the example research was done in Münster, additional inquiries might make use of the information gathered and the conclusions reached in this one for comparison. Overall environmental effects, from raw materials retrieval through the completed products at the asphalt factory, were taken into account in the assessment. Global-warming potential (GWP) and non-renewable cumulative-energy-demand (nr-CED) have been employed as two environmental markers. The findings showed that employing RAP boosts energy usage while perhaps reducing the environmental effects on nr-CED as well as GWP related to the manufacture of asphalt components. However, the production phase only evaluated in this research.

In an effort to lessen most of the detrimental effects connected with the industry, construction experts and academics have been increasingly searching for sustainable building alternatives. Unaware of the interrelationships between a triple bottom line (TBL) approach made up of economic, environmental, and social, variables, it is a prevalent misperception that sustainability exclusively pertains to environmental concerns. Given that the use of particular materials may significantly vary the footprint produced over the course of a structure's life period, material selection is recognised to have a direct influence on a building's durability. When choosing which materials to use, the building industry does not currently have methods that concurrently take into consideration all three facets of sustainability. In order to select appropriate construction materials, [11] provide a paradigm for decision-making that integrates Multi-Criteria Decision Analysis (MCDA), Building Information Modelling (BIM), and Life Cycle Sustainability Assessment (LCSA). The paradigm is created using a literature study of pertinent publications to pinpoint key elements and difficulties in putting this integration into practise. Considering that the issue of material selection frequently incorporates subjectivity, unpredictability, and inconsistency, which has been best tackled using fuzzy logic, the Fuzzy Analytic Hierarchy Procedure has been chosen as the MCDA approach inside the suggested framework. In order to verify the suggested framework, a residential structure was chosen as an example study. The LCSA approach was used to encompass the building's development, operations, and end-of-life stages. Table.2 represents the reviewed literatures overview.

3 Rural Road's Environmental Sustainability

Transportation, which satisfies the three sustainability criteria, is referred to as sustainable mobility. (1) Economic sustainability: cost effective, works efficiently, provides a variety of transportation options, and facilitates a thriving economy; (2) Social sustainability: enables basic access requirements of people and communities

Table 2 Overview of reviewed existing literatures

Reference	Method	Purpose of the research	Place of the research	Merits	Demerits
[24]	Successful neighbourhood model	Sustainable growth in urban areas	N/A	It serves as the choice available for the decision-making process	It is unable to deliver trustworthy performance measurements
[17]	ReCiPe midway method	Determine the environmental effects of a particular instance	Lane road asphalt highway segment in Abu Dhabi	The approach is extensively applicable to researches on road construction	If several different procedures are being used, it takes a significant amount of time
[21]	Life cycle assessment (LCA) approach	To evaluate environmental effect of the pollutants over the life span of a transport network project	Fast-tracked transport initiative in China	The technique's analysis contributes to a decrease in environmental contaminants	The created technique is only used in one nation
[15]	Life-cycle methodology	Modern pavement technology and materials have an impact on maintenance and reconstruction procedures. To avoid this the method has been constructed	Italian urban road's	Utilizing this technique will prevent the repercussions of disposal	It is unable to deliver trustworthy performance measurements
[37]	LCA methodologies	To estimate the material stocks as well as environmental consequences of urban road network	China roads	It offers a useful tool for controlling the depletion of resources	It does not support greater dimensions and produces poor performance metrics

(continued)

Table 2 (continued)

Reference	Method	Purpose of the research	Place of the research	Merits	Demerits
[32]	LCA techniques	To assist in the decision-making procedure toward establishing a more stable society	Germany's road system	This procedure lessens the environmental impacts of the production of asphalt components on nr-CED and GWP	It solely assesses the stage of production
[11]	TBL approach	To determine the effects connected with industry, constructions and academics	N/A	It includes the creation and maintenance of buildings	This cannot be applied on bigger scales

to be fulfilled safely, in a way that is compatible with human as well as ecosystem life quality, and with shares inside and among generations; and (3) Environmental sustainability: restricts waste and pollutants within the range of the planet's capacity to ingest them, reduces usage of resources. In attempt to identify suitable management strategies for quite sustainable performance results, efforts to make rural roads sustainable must include the underlying systems and a road's effect on them. In light of this, it's critical to understand that roads had effects on environmental stability outside GHG emissions.

Other significant negative impacts involve habitat loss, energy use, and incoherence due to boundary influence, road kill, and displacement functions, water quality affects from runoff of road, which is frequently heated up and may encompass pollutants from automobiles on the road, modifications to the genetic hydrologic phase and increased storm-water runoff as a result of increased impenetrable surface zone, and air quality affects from good airborne particulates from vehicles using a road infrastructure and the equipment's employed for constructing roads and materials production [22, 25, 36]. The utilisation of innovative technology, procedures, and materials that directly improve the roadway's economic as well as environmental sustainability via decreased material usage and energy seems to be a crucial component in enhancing the road transportation sustainability [23]. By examining the environmental effects of rural road maintenance and recognizing environmental factors that could be improved in order to increase road sustainability, the function of road surface in environmental sustainability may be better comprehended.

3.1 Environmental Indicator's Categories

The indicator strategy to environmental sustainability could indeed serve as a framework for allocating environmental resources according to importance, promote mitigation as well as reconstruction efforts, and empower entities to respond to statutory requirements and public issues about environmental safety and reliability. Indicators seem to be a crucial gauge of what has been valuable and has to be preserved or safeguarded. Technically speaking, indicators create values by being derived from them. An indicator seems to be an essential tool for informational transit that permits movement from rural road maintenance activity planning as well as decision-making to execution, monitoring, and assessment. Integrating sustainable priorities as well as values has been required for this.

An Environmental Performance Indicator (EPI) seems to be a marker that gives data about a firm's environmental performance, concentrating on either maintenance/method or operations, according to the international standard organisation ISO 14031. A transportation-based environmental sustainability marker, according to [14], is a "variable, predicated on measures, which indicates prospective or real effects on the environment—or elements that might cause such effects—owing to transport, as precisely and required". The environmental effect of interest is defined using environmental markers. For instance, the capacity for global warming might

be used to gauge the effects of climate change. Indicators have been often developed by connecting environmental influences to prospective repercussions throughout the cause-and-effect chain. Performance indicators have been often divided into functional and strategic (or management) areas. At the strategic stage of maintenance, which encompasses all transportation network resources, strategic metrics are more suitable for judgments addressing a transportation regulator's manifestation of environmental responsibilities. The many aspects of a marker have been frequently developed using time and space aspects, planned use, timeframes, and operational activities of an entity, which integrate elements from different groups with the total level as well as scale indication applicability.

Therefore, a provincial or country's or its road authority's values, how these goals are prioritised, and a strategy to implement those principles and prioritise them are crucial for the analysis of environmental consequences in rural road maintenance choices to be effective. Metrics of environmental effectiveness should be developed in accordance to targets and goals that are in line with the department's overarching institutional aims for tackling the transportation network's sustainability that include rural roads. Furthermore, the following elements should be taken into account in accordance with the Environmental Protection Requirements (EPR) for Transportation Planning and Highway Construction, Design, Operations, and Maintenance:

- Cultural and built heritage landscape
- Terrestrial ecosystems
- GHG emissions and air quality effects
- Management of polluted property, waste, and surplus materials
- Water resources
- Land-use factors

It is important to take into account the planned use of marker systems such as the EIA model when evaluating their worth. A set of quantitative markers could be both essential and adequate when the goal is reporting, accounting, or efficiency enhancement. Markers for maintenance might need to directly link to policy objectives, such as concentrations or capacity restrictions. Indicators might flow into multiple decision procedures for decision assistance [35]. Making a single index was one way to accomplish this. The difficult part is combining the values of several indicators into one representative measure. For the production of reliable indicators for sustainable mobility, standards were devised [30].

4 Research Methodology

4.1 *Sustainability Evaluation in Rural Road Maintenance*

When taking decisions about managing rural roads at the project- and network-levels, sustainability in rural road maintenance means keeping in mind the requirements of society and the environment even while preserving economic viability. By maximising the rural road's sustainability properties throughout its lifetime, durable rural road maintenance strategies for road networks guarantee timely monitoring, repairs, and replacement while extending the usable lifespan of road resources. How to gauge and quantify advancements toward more viable rural road maintenance techniques is the difficult part. Recent research has concentrated on two goals for M&R programming and optimization in rural road maintenance: reducing energy usage and GHG emissions. Beyond these frequently used benchmarks for environmental sustainability, managing rural roads can have significant effects on the environment. To help rural road management make more environmentally friendly decisions, these effects require to be identified and incorporated into decision-support technologies. In order to improve environmental sustainability as well as cost-effectiveness, rural road authorities will be helped in developing the best rural road maintenance strategies by measuring the environmental performances of maintenance and operations.

4.2 *Environmental Impact Assessment (EIA)*

Since 1960s, an EIA was employed to assess the possible environmental consequences that a planned project might have in order to lessen any unfavourable repercussions. The assessment's goals are to determine whether to move forward with the plan and to develop effect mitigation strategies. An EIA seems to be the procedure of identifying, anticipating, assessing, and reducing the social, biophysical, and other pertinent impacts of development initiatives before significant decisions are created and commitments are formed, according to the International Association for Impact Assessment (IAIA) [31]. In the EU, a rule was established in 1985 that makes EIA required for any planned public as well as private initiatives (such as building projects) that have been expected to have an effect on the environments. Many other nations have also included EIA into their laws [26]. Due to these legal obligations, the EU as well as other nations has tight criteria for the EIA procedure. There were no specific EIA assessments for bioenergy initiatives in the literature.

For evaluating environmental effect, EIA as well as SRS have been utilised. There are many different operational performance markers. SRS tools have been predicated on environmental certification frameworks that emphasise best practises, akin to the LEEDS accreditation. SRS indications are given as multiple choice alternatives, numeric data, and subjective (text) data (including yes and no). The SRS assessment procedure includes a number of benefits and disadvantages. SRS is often simpler

as well as easier to execute than EIA. The chosen metrics, however, are frequently not based on real performance. Although some best practises have a relatively minor influence on sustainability effect factors, some have a much larger one. Additionally, their effects may change for road systems in various situations.

The SRS frameworks offer a more straightforward and intuitive way to quantify the advantages of sustainable projects, making it easier for more entities to grasp [34]. Simpler indications have been employed more frequently [30]. That simplicity, nevertheless, gives less visibility and necessitates greater stiffness. SRS tools might be rigorous when it pertains to rating variables and seldom enable adjustment of the evaluation criteria. This indicates that rating systems cannot be applied to every project. The most recent SRS technologies (like ENVISION, for instance) have made steps to solve this issue by allowing customisation of rating methods to project types, although the criteria still remain prescribed. Additionally, no implications have been provided for the combined impacts or connections of several activities. The EIA tool offers a guidance to evaluate the environmental effectiveness of the road lifetime taking into account numerous environmental impact classes as an option to SRS. In particular, the EIA environmental effectiveness indicators that have been documented in the research include impact criteria based on the environmental impact category of harm to the natural world, harm to human wellbeing, and resource utilization. The tool profile of EIA is indicated in Table.3.

4.3 Sustainability Issues

Examining the sustainability challenges that the EIA tool addresses is crucial for establishing the environmental sustainability of the tool for maintaining rural roads. Based on the sustainability standards for maintaining rural roads indicated in the literature, an extensive list of pertinent sustainability concerns was created with this objective in mind.

Table 4 displays the final list, arranged according to the sustainability dimensions. To maintain the functionality of the list, it has been decided not to delve into excessive information. As examples, a few indications are included.

4.4 Environmental Sustainability Indicator's Determination

The rating categories specifics are enhanced by indicators. To prevent overlap, the indicators have been carefully picked. Table 5 displays the complete set of environmental sustainability markers for each type of rural road maintenance.

Table 3 EIA's tool profile

General	Description
Tool description	A planned project's possible environmental implications are assessed using an EIA, which takes into account ecological, social, as well as economic factors. The goal is to minimise any adverse effects
Tool concept	EIA systems are in place in more than 100 nations worldwide. They have a wide range of practises and procedures. Over the previous ten years, EIA methodology and its scope have undergone significant change. Increased application to policy, strategies, as well as other operational choices, as well as a study of trade, deregulation, and structural reform activities, are all examples of advancements Site specificity is key in EIA. The majority of nations often have set of activities that call for EIAs (e.g. small or large construction works). Additionally, several nations have defined sensitive ecosystems for which EIAs have been required (such as estuaries and cultural heritage locations). Stakeholder involvement is a crucial concern in EIA
Steps involved	Although there may be different numbers of phases in an EIA process, the following stages may generally be differentiated: Screening, planning, impact analysis, reduction, reporting (EIS), evaluation, decision-making, and implementation are the first five steps
Harmonisation/ Standardisation	On general process, there has been an international consensus. Countries frequently establish their own protocol
Analysis object	A plan, policy, project or programme
Utilization frequency	EIA seems to be a recognised and widely applied instrument. EIAs are carried out in a number of nations, especially several emerging nations
Procedure/ algorithm focus	Procedure focus
Uncertainty and sensitivity	Not covered by the EIA process
Qualitative/ quantitative	Both qualitative and quantitative
Weight scores	No data are provided about the application of weight ratings

Table 4 A group of concerns about rural road maintenance' sustainability

Environmental dimension	
Indicator	Example
Soil quality	Soil erosion and compaction
Forest area	Deforestation
Energy	Energy balance
Air quality	GHG emission
Weather	Climate change

Table 5 EIA rating indicators

Category	Indicator	Note
Environment	Air quality	Air pollutants must be taken into consideration
	Ecology conservation	Restoration and protection of the natural environment must be emphasized when maintenance operations affect it
	Solid waste	Consideration should be given to the handling and distribution of substantial construction wastes
	Energy	It is important to take into account the energy used by moving vehicles
	Noise control	Building and traffic noise must be reduced using the appropriate techniques
	Weather	Maintenance tasks should be planned and performed in accordance with the temperature and weather
	Vibration control	Maintenance procedures that cause audible vibration must be planned properly and kept to a minimum

4.5 Category Priority Determination

The Delphi group of experts evaluated the category priority and produced data matrices with ordinal ratings as a consequence. The data matrix has been statistically examined to find important variations among indicators. The data were qualitative; hence a Kruskal–Wallis variance assessment has been carried out. A non-parametric technique for determining if demographic medians are identical between groups seems to be the Kruskal–Wallis analysis. However, as each individual evaluator parameter in this research only had one sample, no medians might be calculated. Environmental concerns are a subcategory in the sustainability problems data matrix.

The following individuals were asked to express their opinions on the chosen category's priority:

1. Staff from transit departments and maintenance firms;
2. Staffers of the operating crew (such as engineers as well as technicians);
3. Civil engineering instructors and students who had complete at least one training on sustainable design.

According to the findings, the environment category has obtained 0.245 as ultimate priority based on expert choice.

5 Result and Discussion

5.1 *An Example of Evaluation Process (Telangana State Rural Road)*

Ranga Reddy District Major District Road (MDR) in Telangana state was selected as a case study to illustrate the evaluation process and evaluate the application of the EIA on the environmental sustainability of an actual rural road maintenance project. Although transportation is the main role of the rural road system, it also serves as a system for infrastructures that provides houses and businesses with amenities like water and sewage. When installing, maintaining, or making modifications to these road systems, road cuts are usually needed, which reduces the lifespan of the rural roads. Examples of typical EIA report contents (i.e., assessment conclusions) are shown below:

- Sustainability issues;
- A description of strengths and weaknesses; and
- Category priority

A recently constructed rural road approximately 2 kms in length from Devarampally to Shankarpally (21.180–19.175 km) on a major district road (MDR) in Ranga Reddy District of Telangana state has been chosen as the test component for this inquiry. The study project's objectives were to perform a complete investigation and environmental sustainability study of the rural road that Telangana State's Roads and Buildings (R&B) Department developed in July 2019. Information on the study's project has been obtained from the R&B Department. Table.6 indicates overall findings of the research.

Incorporated sustainability assessment necessitates a multicriteria method since sustainability seems to be a complicated and multifaceted topic. Important sustainability challenges for rural road maintenance have been identified for this study, and their environmental viability was assessed using a Delphi panel of experts. The tool received a rating of 1 if the factor has been not resolved at all; a rating of 2 if the factor has only been partially resolved; a rating of 3 if the factor has been partially resolved using a specific methodology; a rating of 4 if the factor was thoroughly resolved but may still be markedly enhanced; and a rating of 5 if the factor in question has been fully resolved.

6 Conclusion

The difficulties in developing countries like India involve many additional different characteristics, such as varied degrees of commitment, limited financial capacities, and a lack of awareness about sustainability principles and how to solve them considering country-specific elements. Moreover, because it is intrinsically complicated,

Table 6 EIA evaluation outcomes for a MDR in Ranga Reddy district, Telangana

Category	Indicator	Sustainability issues (Delphi panel ratings)	Maximum rating	Category priority	Explanation
Environment	Air quality	4	5	57	N/A
	Ecology conservation	5	5		Existing plants have not been harmed, however some waste from the thar mix has been left on the grass next to the road
	Solid waste	4	5		Unknown was the place where waste would end up
	Energy	4	5		The traffic's pace stayed the same as it crossed the construction zone
	Noise control	2	5		N/A
	Weather	3	5		N/A
	Vibration control	1	5		N/A
Total ratings		23	35		
Earned percentage		65.71			

Note: N/A-information were not available

normative, arbitrary, and imprecise, the concept of sustainability remains fundamentally challenged. As a result, evaluating the sustainability of environmental sustainability of rural road maintenance is a difficult and complex undertaking. Nevertheless, a lot of scholars have been working to provide strategies and tools to deal with this challenging task. While many began their work with a single discipline in mind, others tried to create general equipment and tools. This has led to a wide range of methodologies. With the use of the Environment Impact Assessment (EIA) tool, this article aimed to provide a deeper understanding of the intricate realm of environmental sustainability evaluation of rural road maintenance. Initially, the environmental sustainability issues in rural road maintenance were determined. Hereafter, the environmental sustainability indicators were developed and category priority was determined based on Delphi expert panel. Moreover, Kruskal–Wallis variance assessment was conducted due to qualitative data. In addition, the presented work was tested on real rural road maintenance work in Telangana state Ranga Reddy District to illustrate the EIA assessment procedure and findings. The results demonstrated that the use of EIA to the rural road maintenance project's environmental sustainability was successful.

References

1. Anderson JL, Muench ST (2013) Sustainability trends measured by the greenroads rating system. *Trans Res Record: J Trans Res Board* 2357(1):24–32. <https://doi.org/10.3141/2357-03>
2. Becker B, Secretariat C (1997) Sustainability assessment: a review of values, concepts, and methodological approaches
3. Brundtland GH (1987) Report of the world commission on environment and development: our common future. UN
4. Bryce J, Brodie S, Parry T, Lo Presti D (2017) A systematic assessment of road pavement sustainability through a review of rating tools. *Resour Conserv Recycl* 120:108–118. <https://doi.org/10.1016/j.resconrec.2016.11.002>
5. Chan P, Tighe S, Chan S (2010) Exploring sustainable pavement rehabilitation: Cold in-place recycling with expanded asphalt mix. In: 89th annual meeting of the transportation research board, Washington, DC
6. Clevenger CM, Ozbek ME, Simpson S (2013) Review of sustainability rating systems used for infrastructure projects. In: 49th ASC annual international conference proceedings, pp 10–13
7. Cornet Y (2016) Indicators and beyond: assessing the sustainability of transport projects
8. Devuyt D, Hens L, De Lannoy W, de Lannoy W (2001) How green is the city?: sustainability assessment and the management of urban environments. Columbia University Press
9. Dolla T, Laishram B (2022) Strategies to promote collaborative governance regime in Indian rural road maintenance. *Built Environ Project Asset Manage* 12(3):365–381. <https://doi.org/10.1108/BEPAM-01-2021-0024>
10. Elghali L, Clift R, Sinclair P, Panoutsou C, Bauen A (2007) Developing a sustainability framework for the assessment of bioenergy systems. *Energy Policy* 35(12):6075–6083. <https://doi.org/10.1016/j.enpol.2007.08.036>
11. Figueiredo K, Pierott R, Hammad AWA, Haddad A (2021) Sustainable material choice for construction projects: a life cycle sustainability assessment framework based on BIM and Fuzzy-AHP. *Built Environ* 196:107805. <https://doi.org/10.1016/j.buildenv.2021.107805>
12. Griffiths KA, Boyle C, Henning TF (2017) Comparative assessment of infrastructure sustainability rating tools. In: Conference: transportation research board 96th annual meeting-transportation research board, At Washington DC, vol 17, p 01265
13. Gritsavage JS, Krekeler PK, McVoy GRM, Nelson DAN, Kolb EK (2010) Moving towards sustainability: New York state department of transportation's GreenLITES story. *Green Streets Highways* 2010:461
14. Gudmundsson H, Hall RP, Marsden G, Zietsman J (2016) Frameworks. In: Gudmundsson H, Hall RP, Marsden G, Zietsman J Sustainable transportation. Springer Berlin Heidelberg, pp 171–202. https://doi.org/10.1007/978-3-662-46924-8_7
15. Gulotta TM, Mistretta M, Praticò FG (2019) A life cycle scenario analysis of different pavement technologies for urban roads. *Sci Total Environ* 673:585–593. <https://doi.org/10.1016/j.scitotenv.2019.04.046>
16. Harley A, Clark W (2020) Sustainability science: a guide for researchers.
17. Hasan U, Whyte A, Al Jassmi H (2020) Life cycle assessment of roadworks in United Arab Emirates: Recycled construction waste, reclaimed asphalt pavement, warm-mix asphalt and blast furnace slag use against traditional approach. *J Clean Prod* 257:120531. <https://doi.org/10.1016/j.jclepro.2020.120531>
18. Huetting R, Reijnders L (2004) Broad sustainability contra sustainability: the proper construction of sustainability indicators. *Ecol Econ* 50(3–4):249–260. <https://doi.org/10.1016/j.ecolecon.2004.03.031>
19. Kazmierowski T, Navarra M (2014) Sustainability metrics of two pavement rating systems developed in Canada. Transportation 2014: past, present, future-2014 conference and exhibition of the transportation association of Canada//Transport 2014: Du Passé Vers l'avenir-2014 Congrès et Exposition de l'Association Des Transports Du Canada

20. Lew JB, Anderson JL, Muench ST (2016) Informing roadway sustainability practices by using greenroads certified project data. *Trans Res Record: J Trans Res Board* 2589(1):1–13. <https://doi.org/10.3141/2589-01>
21. Li H, Deng Q, Zhang J, Olunmi Olanipekun A, Lyu S (2019) Environmental impact assessment of transportation infrastructure in the life cycle: case study of a fast track transportation project in China. *Energies* 12(6):1015. <https://doi.org/10.3390/en12061015>
22. Li Q, Qiao F, Yu L (2017) How the roadway pavement roughness impacts vehicle emissions. *Environ Pollut Climate Change* 1(134):10–4172
23. Montgomery R, Schirmer H, Hirsch A (2015) Improving environmental sustainability in road projects
24. Moroke T, Schoeman C, Schoeman I (2019) Developing a neighbourhood sustainability assessment model: an approach to sustainable urban development. *Sustain Cities Soc* 48:101433. <https://doi.org/10.1016/j.scs.2019.101433>
25. Pellecuer L (2016) Influence of pavement maintenance strategy on road traffic social and environmental impacts and associated costs. In: TAC 2016: efficient transportation-managing the demand-2016 conference and exhibition of the transportation association of Canada.
26. Petts J (1999) *Handbook of environmental impact assessment volume 2 environmental impact assessment in practice: impact and limitations*. Blackwell Sci
27. Pope J, Annandale D, Morrison-Saunders A (2004) Conceptualising sustainability assessment. *Environ Impact Assess Rev* 24(6):595–616. <https://doi.org/10.1016/j.ear.2004.03.001>
28. Robert KW, Parris TM, Leiserowitz AA (2005) What is sustainable development? goals, indicators, values, and practice. *Environ: Sci Policy for Sustain Develop* 47(3):8–21. <https://doi.org/10.1080/00139157.2005.10524444>
29. Sarkar AK (2011) Development of a sustainable rural roads maintenance system in India: key issues. *Trans Commun Bull Asia Pacific* 36
30. Sdoukopoulos A, Pitsiava-Latinopoulou M, Basbas S, Papaioannou P (2019) Measuring progress towards transport sustainability through indicators: analysis and metrics of the main indicator initiatives. *Transp Res Part D: Transp Environ* 67:316–333. <https://doi.org/10.1016/j.trd.2018.11.020>
31. Senécal P, Goldsmith B, Conover S, Sadler B, Brown K (1999) *Principles of environmental impact assessment best practice*. Special Publication, International Association for Impact Assessment, Fargo, USA, p 86
32. Siverio Lima MS, Hajibabaei M, Hesarkazzazi S, Sitzzenfrei R, Buttgerit A, Queiroz C, Tautschnig A, Gschösser F (2020) Environmental potentials of asphalt materials applied to urban roads: case study of the City of Münster. *Sustainability* 12(15):6113. <https://doi.org/10.3390/su12156113>
33. Spangenberg JH (2004) Reconciling sustainability and growth: criteria, indicators, policies. *Sustain Dev* 12(2):74–86. <https://doi.org/10.1002/sd.229>
34. Torres-Machi C, Chamorro A, Yepes V, Pellicer E (2014) Current models and practices of economic and environmental evaluation for sustainable network-level pavement management. *Revista de La Construcción. J Construct* 13(2):49–56
35. Torres-Machi C, Nasir F, Achebe J, Saari R, Tighe SL (2019) Sustainability evaluation of pavement technologies through multicriteria decision techniques. *J Infrastruct Syst* 25(3):04019023
36. Van Dam TJ, Harvey J, Muench ST, Smith KD, Snyder MB, Al-Qadi IL, Ozer H, Meijer J, Ram P, Roesler JR (2015) *Towards sustainable pavement systems: a reference document*. United States. Federal Highway Administration
37. Yu B, Li L, Tian X, Yu Q, Liu J, Wang Q (2021) Material stock quantification and environmental impact analysis of urban road systems. *Transp Res Part D: Transp Environ* 93:102756. <https://doi.org/10.1016/j.trd.2021.102756>

Damage Detection on Structure of Pinisi in Ship Launching Process



Andi Dirga Noegraha , Rudy Djamaluddin, Rita Irmawaty , and Ganding Sitepu

Abstract The focus of the present study is to find the damaged location of the structure of the pinisi ship in the traditional ship launching system. This study uses a numerical experimental method, the analysis stage begins with designing a pinisi ship in the form of a solid three-dimensional scale in actual size, then calculated by finite element method (FEM) using explicit dynamic analysis in ANSYS software. In the launching process, the ship is given a compressive force by pulleys with an analysis time set according to the number of elements and hardware used in the analysis. Based on 3D Pinisi ship data and analysis constraints, it has been found that shear stress on the longitudinal axis and transverse axis of the ship occurs during the ship launching process. Some parts of the Pinisi ship structure experience tensile shear stress and compressive shear due to the pulley force in the launching process. The ship structure is formed from interconnected and reinforced constructions between one another from the bow to the stern of the ship. Due to the interconnected construction, longitudinal structural disturbances will impact and contribute to the lateral direction of the ship structure.

Keywords Ship launching · Finite element method · Explicit dynamics · Shear stress

A. D. Noegraha (✉)

Student of Doctoral, Department of Civil Engineering, Hasanuddin University, Makassar, Indonesia

e-mail: madn20d@student.unhas.ac.id

R. Djamaluddin · R. Irmawaty

Department of Civil Engineering, Faculty of Engineering, Hasanuddin University, Makassar, Indonesia

G. Sitepu

Department of Naval Engineering, Faculty of Engineering, Hasanuddin University, Makassar, Indonesia

1 Introduction

The process of building the wooden ship in Bulukumba is still using the traditional system from the past until now, from the beginning of laying the keel and construction of the ship's hull until the launching process is still done manually. Unlike shipbuilding in general, most ships built in Tanah Beru Bulukumba do not use design drawings [1]. That is very different from conventional shipbuilding, which requires detailed calculations and design drawings to determine the ship launching method according to the size and capacity of the shipyard. The tradition of moving ships from building berths into the seas in Tana Beru village (Bulukumba, Indonesia) is also called *Anyorong Lopi*, which is the activity of pulling or pushing the finished ship from the traditional shipyard to the beach. This process does not use modern tools, it only uses human power, so it takes a lot of energy that can reach 100 people. This activity of ship launching takes costs a lot of money and takes weeks until it has been done. In conventional ship launching, the estimated slope angle for large ships is 2.39° – 2.86° for medium-sized ships, it ranges from 3.18° to 4.76° [2]. Based on surveys obtained in previous studies, the angle of inclination of the launch at the people's shipyard in Bulukumba only ranged from 2.08° to 3.12° . Although the slope range follows conventional launching guidelines, ship launching in Bulukumba is still difficult [3]. The ground of the shipyard in Bulukumba has a rocky soil structure and also has a sloping beach contour. The condition of the beach with a slope length of only ± 40 m, and the rest of ± 200 m is flat with a relatively shallow depth. Launching a wooden ship in Bulukumba uses a system of friction between the ship's keel and the block slide. The sliding block wedge is lubricated so that the ship can slide with a frictional force with less frictional resistance. The ship is launched towards the bow by being pulled using a manual tackle at the rear end of the keel. This tackle block is pulled using the human power of about 20–30 people, some craftsmen set the sliding block using sandbags, and some other craftsmen direct the launch flow and adjust the ship's motion to remain stable when pulled (see Fig. 1).

Ship structures are particularly susceptible to cracking due to inter-construction joints, material imperfections, loading conditions, or fatigue. Most research focuses on the growth or propagation of cracks from a fatigue perspective. However, the damage itself can occur at the construction stage, after fabrication, and during the launch process, and not all can be detected and repaired [4]. Therefore, with this simulation, an overview of ship construction parts that may be damaged during the ship launching process is obtained.

2 Methods

This research uses a numerical experimental method, at the initial stage of the research is the selection of the type and size of the ship by determining the type of material used in the analysis of the launching process, then based on 2D (two-dimensional)

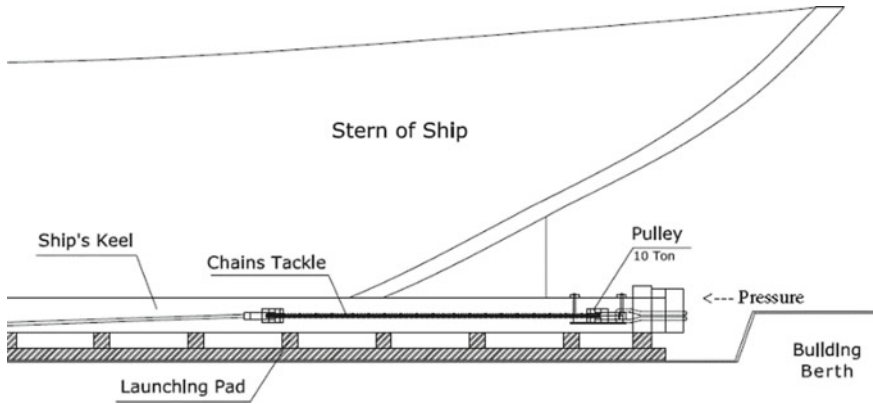


Fig. 1 Traditional system ship launching method

data the ship is made 3D solid numerical data (three-dimensional) scale 1:1 actual size using AutoCAD 3D software. After designing the 3D solid data of the pinisi ship and the launch pad, the design is inputted into Ansys software which is software that uses the Finite Element Method (FEM). The stages of analysis in Ansys begin with determining the type of material, inputting the geometry (model) of the ship and launching pad, determining the analysis limits (contact status, degrees of freedom, mesh/discretization), then determining the type of support and load in the launching process until the running solving process until the final analysis results are found.

Analysis using explicit dynamics can analyze the physical changes of elements to short-duration variables, complex structures, and large changes in body interactions. Explicit dynamic analysis can analyze loading that impacts large material deformation [5]. So, to analyze complex ship structures and dynamic loading in ship launching, we can use explicit dynamics analysis. Dynamic analysis can be done by implicit or explicit settlement methods. However, dynamic implicit analysis becomes unstable if there is a large change to the model and time, so explicit dynamic analysis becomes the solution to the problem [6]. The basic equation of dynamic analysis that describes the response of the original structure can be seen in Eq. (1).

$$[M]\{\ddot{x}\} + [C]\{\dot{x}\} + [K]\{x\} = \{F(t)\} \tag{1}$$

where M is the mass matrix (Kg), C is the damping matrix (N s/m), K is the stiffness matrix (N/m), and F is the external force vector concerning the time (t). To ensure that the explicit dynamics analysis remains stable, the Time Step Size is limited by using the CFL (Courant-Friedrichs-Lewy) condition equation [7]. Small-time steps are carried out to keep the analysis in a stable state by estimating the results in the first step can run to calculate the results in the next step, this procedure continues until the final solution in the final stage [8]. In simple terms, it can be seen in Eq. (2) time step size.

$$\Delta t \leq f * \left[\frac{h}{c} \right]_{\min} \text{ where, } c = \sqrt{\frac{E}{\rho}} \quad (2)$$

where Δt is the time step size (s), f is the safety factor ($f = 0.9$), h is the size characteristic of a finite element (m), c is the wave speed of the material (m/s), E is the value of Young's Modulus (Pa), and ρ is the density of the material (kg/m^3). The equation describes that the analysis time stage must be smaller than the time required for a compression-stress wave to pass through the smallest element of a discrete (a mesh). Therefore, the dynamic analysis time stage is controlled by the compression wave speed [9].

2.1 Sample Ship

Pinisi ship is an ancestral cultural heritage of the Indonesian people that characterizes its identity as a maritime nation. Pinisi ships are made by the hands of experts called *panrita lopi* (experts in making boats/ships) without the help of modern equipment [10]. This traditional ship of the Bugis Makassar tribe was often used by the ancestors to sail to the continents of Europe and Africa. Pinisi ships have proven their specialty by conquering vast oceans and exploring various countries in the world [11]. Pinisi ship used as the object of this research was built at the Bulukumba people's shipyard, the primary dimension data for the ship are as follows in Table 1.

The process of launching the Pinisi ship in Bulukumba with the traditional system (see Fig. 2). The image shows the research object, namely the 35.70-m-long Pinisi ship with the main dimensions as in Table 1. The ship is pulled using a pulley at the end of the stern keel towards the bow, towards the sea with a launch distance of 200 m until the ship can float freely.

Table 1 Principal dimension of the ship

Parameter	Dimension	Unit
Length of deck	35.70	m
Length of keel	25.85	m
B (Breadth)	8.50	m
H (Depth)	3.85	m
T (Draft)	2.70	m
Displacement ship	332.0	ton



Fig. 2 A sample pinisi ship launching process in Bulukumba

2.2 Real Size Modelling

Based on the design data from the Lines Plan, General Arrangement, and Construction of the Pinisi ship, 3D design data of the Pinisi Ship is made, as shown in Fig. 3. The percentage of structure and construction of real-size 3D modeling adjusts based on the conditions in the field during the launch process. When the ship launch is carried out, the main structure of the hull must be 90% complete, and the work on the part below the ship’s waterline has been completed. In launching the 35.70 m length of Pinisi ship, the condition of the engine room is still empty; the main engine (ME), auxiliary engine (AE), piping system, and electrical system have not been installed.

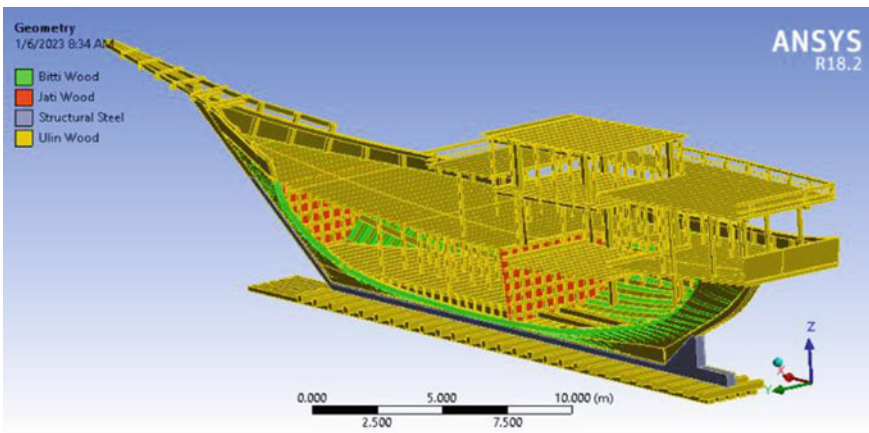


Fig. 3 Geometry of pinisi ship with materials

Table 2 Material characteristics of hull structure of the Pinisi

Type of material	Young's modulus (MPa)	Poisson's ratio	Density (kg/m ³)	Tensile/compressive (MPa)
Steel (ASME BPV Code, 1998)	2.10 ⁵	0.30	7850	250
Iron wood (E25)	25.10 ³	0.35	1040	22.9
Bitti wood (E13)	13.10 ³	0.24	740	10.4
Jati wood (E13)	13.10 ³	0.20	700	10.4

The total weight of the Pinisi ship is 99.29 tons, and the total volume of wood on the launching pad is 98.85 m³ with the ship superstructure (bridge deck and top deck). The main construction of Pinisi structures that have been completed during the launching process is the keel (stem end to stern), the plank of the ship, frames, side stringers, engine room's bulkheads, collision bulkheads, main deck, accommodation deck, and bulwark (see Fig. 3).

2.3 Materials of Ship

The main material in the hull structure of the Pinisi ship is Ulin wood or commonly called Ironwood (*Eusideroxylon Zwageri*), almost all parts of the Pinisi ship construction use Ulin Wood except for the frames, bulkhead, and ship interior [12]. Ironwood is solid wood with high durability, whereas ironwood is included in the strong category of class I and class I durability [13]. Frames on the Pinisi ship use Bitti Wood (*Vitex Cofassus*), and the bulkhead walls use Jati Wood (*Tectona Grandis*). The Pinisi ship with a keel length of 25 m has a keel shoe made of steel plate along the keel that touches the runway, connected as high as 60% of the stem bar height, and the plate covers the inside of the propeller's stern tube. The characteristics material the hull structure of The Pinisi ship used in this research can be seen in Table 2.

2.4 Boundary Conditions

In the dynamic explicit analysis with the finite element method (FEM) using several boundaries, namely the type of mesh, the limit of degree of freedom DOF (fixed support), the contact between the ship and the launching pad, the loading received by the structure, and the force applied to the ship. The type of mesh (discretization) used is curvature type with the slow transition as the meshing results, mesh size for max face size is 0.668 (default) and has 45,028 nodes with 57,975 elements (see Fig. 4). Fixed support limits are given to the base of the launching pad longitudinal beam where that part does not move during the ship launching process. The type of

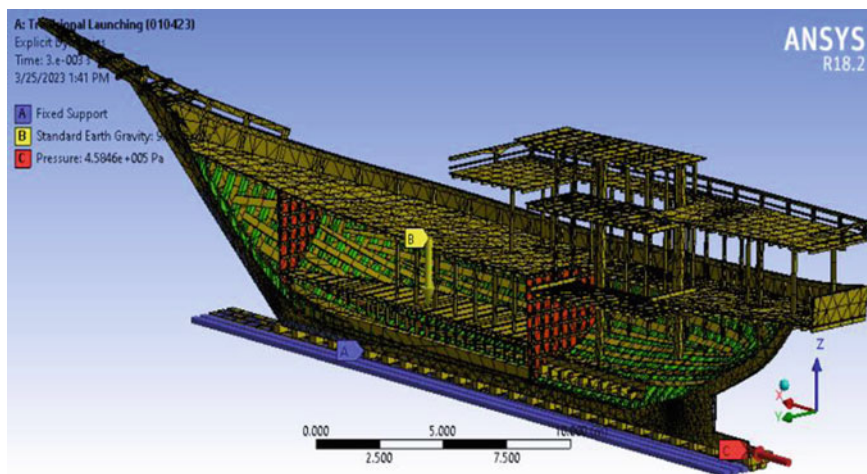


Fig. 4 Final setup with boundary conditions and pre-analyse

connection contact used between the ship (keel) and the runway is frictional, with a coefficient of friction (μ) between the keel material and the launching pad transversal beam is 0.4 [14]. However, in the launching process, the sliding block is given grease to reduce friction so that the coefficient of friction used is 0.2. The loading is given to the ship and the launch pad is a Standard Earth Gravity of 9.8066 m/s^2 , which is in the global coordinate system. Analysis of process launching is carried out without any runway inclination angle (0-degree incline) or with force without any consideration of the inclined launching pad. The force applied is the pressure force by the pulley based on the weight of the ship of 99.29 tons and the size of the pressure area on the keel of the ship 2109 cm^2 , and with the inclination of the launching platform 2.60° at the initial time of launching so that the thrust force is 0.458 MPa. The force given is the pressure of the tackle when pulled to the keel of 0.458 MPa with an analysis time of 3 ms (see Fig. 4).

3 Results and Discussion

Based on 3D pinisi ship data and analysis boundaries, the results obtained are axial stresses on the x-axis (longitudinal) and y-axis (transverse) of the ship that occurs during the ship launching process. Several parts of the Pinisi ship structure experience tensile and compressive stress due to the pulley's thrust in the launching process. The structure of the ship is formed from the existence of transverse and longitudinal constructions where the constructions are interconnected and mutually reinforcing between the constructions of each other from the bow to the stern of the ship. Due to the interconnected construction, the longitudinal structural disturbance will have

an impact and contribute to the lateral or transverse direction of the ship's structure. As shown in the analysis results, when the ship is under pressure on the stern keel at the rear end, it has an impact on the bow of the ship's structure in longitudinal and transverse construction.

In the process of launching pinisi ships with traditional systems, in addition to resulting in axial stress, there is also shear stress in the ship's structure. Shear stress is an internal stress that is mobilized by the material to resist the action of external forces, where the external force is parallel to the cross-sectional area and has a tendency to shear or break the material into two parts in opposite directions. The shear stresses that occur impact the construction of the bow section of the ship.

The longitudinal shear stress (XY plane) in the bow structure of the Pinisi ship due to the traditional launching system (see Fig. 5). As shown in Fig. 5, the maximum tensile-compressive shear stress occurs in the main deck construction in contact with the bulwark construction, planks or shell, and transverse deck beams at the bow of the ship, with a maximum tensile stress value of 5.90 MPa and maximum compressive stress of 8.50 MPa. The structures that experience significant stress are the main deck construction with a shear stress of 1.43 MPa, the bulwark construction at the bow of the ship experiences shear stress of 0.64 MPa, the construction of the ship's bow bulkhead reinforcement experiences a stress of 0.132 MPa, the ship's shell (planks) at the bow experiences stress of 0.211 MPa, and the bow keel construction (stem bar) experiences a shear stress of 1.56 MPa.

As shown in Fig. 6, the average maximum tensile shear stress is 4.81 MPa and the average maximum compressive shear stress is 4.26 MPa. In the longitudinal direction, the percentage of maximum tensile shear stress experienced in the ship structure is greater around 53% than the compressive shear stress around 47%. As shown in the graph of the relationship between tensile-compressive shear stress

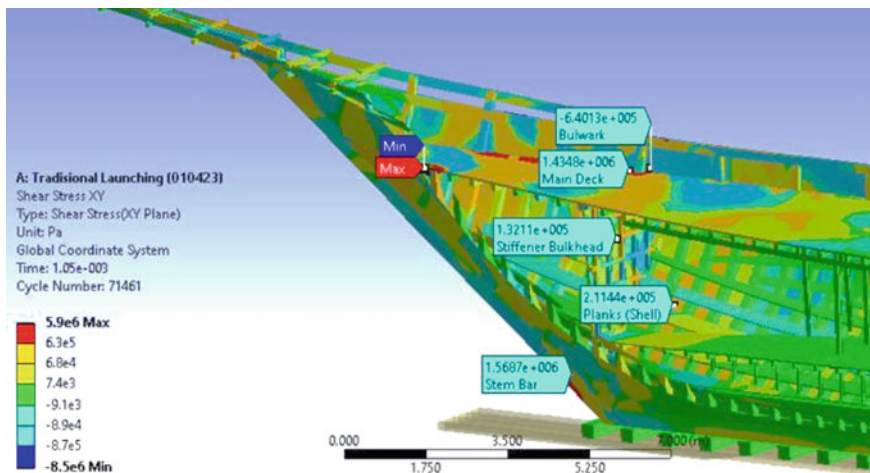


Fig. 5 Longitudinal shear stress in ship bow structure

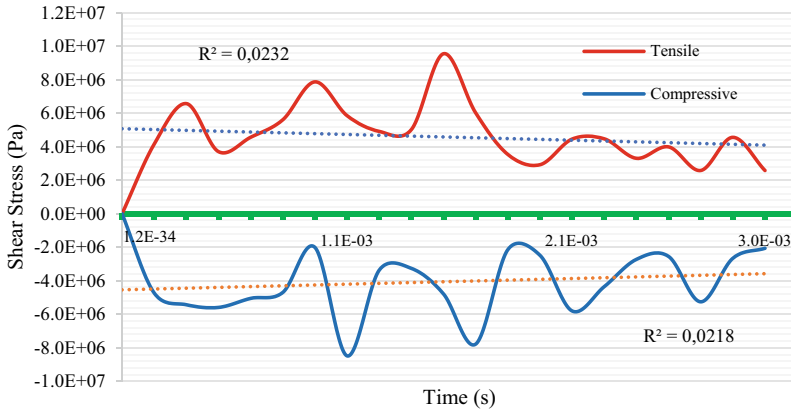


Fig. 6 Graph of maximum shear stress on the longitudinal direction

and analysis time in the longitudinal direction of the ship, the tensile shear stress trendline graph tends to decrease with a coefficient of determination (R^2) value of 0.0232, as well as the compressive shear stress trendline graph tends to decrease with a coefficient of determination (R^2) value of 0.0218. This is due to the damping of the structure experiencing tensile and compressive stresses trying to dissipate the stress or vibration into a stationary or stable condition as before the pressure from the pulley in the launch process.

The transverse shear stress (YZ plane) in the bow structure of the Pinisi ship is due to the traditional ship launching system (see Fig. 7). The maximum compressive shear stress occurs in the main deck construction in contact with the bulwark construction, planks/shell, and transverse deck beam at the bow of the ship, with a maximum compressive stress of 15.07 MPa. The maximum tensile shear stress occurs in the bulkhead stiffener construction in contact with the side stringer with a maximum tensile stress value of 12.69 MPa. The structures that experience significant stress are the main deck construction with a shear stress of 1.20 MPa, the construction of the fence at the bow of the ship experiencing shear stress of 2.30 MPa, the bow bulkhead stiffener construction experiencing a stress of 0.18 MPa, the bow skin (planks) experiencing stress of 0.113 MPa, the transverse deck beam construction (stem deck beam) experiencing stress of 1.25 MPa and the bow keel construction (stem bar) experiencing shear stress of 1.15 MPa.

Graph of the relationship between shear stress (Pa) and time (s) analyzed on the YZ (transverse) axis that occurs in the ship structure in the traditional system ship launching process (see Fig. 8). The maximum compressive shear stress occurs at the initial second when the keel is pressurized by the pulley at 0.15 ms with a value of 15.07 MPa and the maximum shear stress decreases at the final second of the pressing process at 3 ms with a value of 3.45 MPa. As shown in Fig. 8, the average maximum tensile shear stress was 7.12 MPa and the average maximum compressive shear stress was 7.62 MPa. In the transversal direction, the percentage of maximum compressive

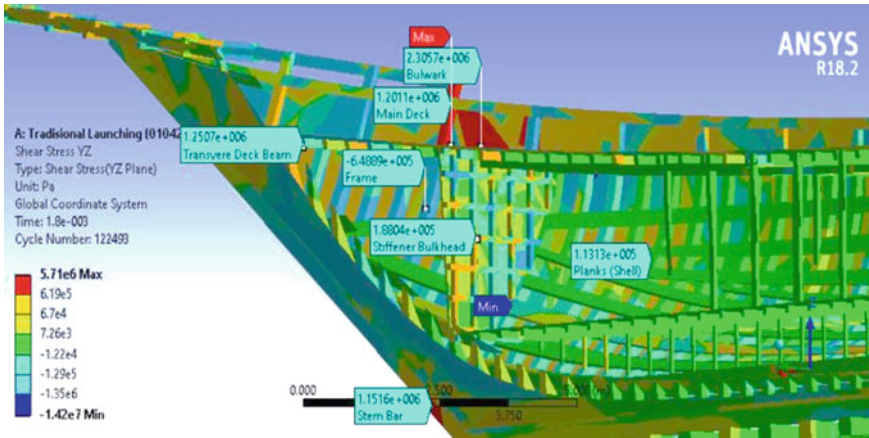


Fig. 7 Transverse shear stress in ship bow structure

shear stress suffered by the ship structure is greater around 52% than the tensile shear stress around 48%. As shown in the graph of the relationship between tensile-compressive shear stress (Pa) and time (s) analysis in the transverse direction of the ship, the tensile shear stress trendline graph tends to decrease with a coefficient of determination (R^2) value of 0.0675, as well as the compressive shear stress trendline graph tends to decrease with a coefficient of determination (R^2) value of 0.0446.

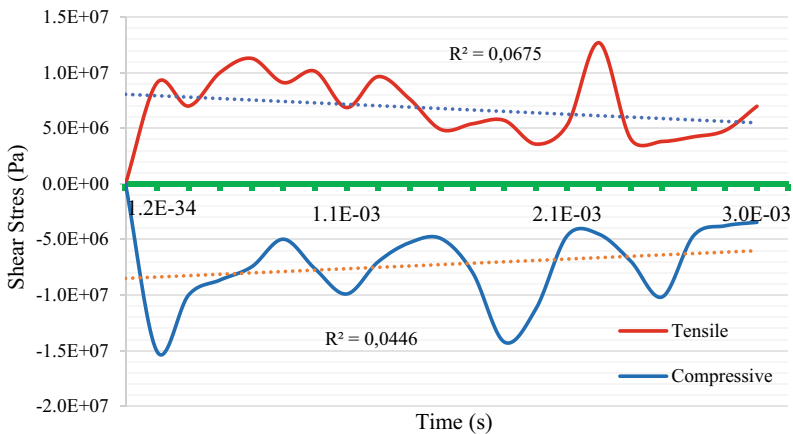


Fig. 8 Graph of maximum shear stress on the transversal direction

4 Conclusion

Damage locations have been found that can occur in the ship launching process, where the damage occurs in the bow structure of the ship. The maximum shear stress in the longitudinal and transverse directions is in the main deck construction in contact with the bulwark construction, the shell of the ship, and the transverse deck beam. In the longitudinal direction, the percentage of maximum tensile shear stress experienced in the ship structure is greater around 53% than the compressive shear stress around 47%, while in the transversal direction, maximum compressive shear stress suffered by the ship structure is greater around 52% than the tensile shear stress around 48%. The bow of the pinisi ship experiences a greater risk of damage than other parts due to the shape of the bow of the pinisi ship which is long and tapered forward, where the part has a heavy structure without any support construction so that the bow of the pinisi ship has the potential to experience great stress during the launch process.

As for the suggestions in the results of this study, in the launching of Pinisi ships with traditional systems, further calculations and analysis are needed on the dimension of the ship's construction that experiences extreme stress, or with the additional reinforcement fiber layer (FRP) of structure in the construction section that experiences maximum stress.

Acknowledgements The first author would like to thank The Indonesia Endowment Funds for Education (LPDP) at The Ministry of Finance Republic Indonesia for providing financial support for Doctoral Program (S3), research funding, and as a sponsor for this publication. The authors would like to thank The Maritime Research Centre of Lembaga Penelitian dan Pengabdian Masyarakat (LPPM), Institut Teknologi Kalimantan, for their ANSYS package software which allowing us to run the simulations.


References

1. Kinapti TT (2021) Pembuatan Kapal Melegenda Pinisi di Tanjung Bira Bulukumba. merdeka.com <https://www.merdeka.com/travel/pembuatan-kapal-melegenda-pinisi-di-tanjung-bira-bulukumba.html>
2. Bakri M, Santoso IGM, Sodjono YY (1983) Teori Bangunan Kapal, vol 3. (UPT Perpustakaan Universitas Andalas)
3. Noegraha AD (2017) Analisis penggunaan airbags Dalam Peluncuran Kapal Pada Galangan Rakyat di Bulukumba. Jurnal Multek 12:641–651
4. Nair A, Sivaprasad K, Nandakumar CG (2017) Crack assessment criteria for ship hull structure based on ship operational life 4. <http://www.editorialmanager.com/cogenteng>. <https://doi.org/10.1080/23311916.2017.1345044>
5. ANSYS (2021) Inc. ansys explicit dynamics takes over when implicit isn't enough. Ansys Explic Dyn 1–8
6. Hu H, Zhong Z (2019) Explicit-implicit co-simulation techniques for dynamic responses of a passenger car on arbitrary road surfaces. Engineering 5:1171–1178. <https://doi.org/10.2991/icst-18.2018.179>

7. Cocchetti G, Pagani M, Perego U (2015) Selective mass scaling for distorted solid-shell elements in explicit dynamics: optimal scaling factor and stable time step estimate. *Int J Numer Methods Eng* 101:700–731. <https://doi.org/10.1002/nme.4829>
8. Gattmah J, Shihab SK, Mohamed MT, Abbas AL (2021) Effects of increasing mass scaling in 3D explicit finite element analysis on the wire drawing process. In: IOP conference series materials science and engineering, vol 1076 <https://doi.org/10.1088/1757-899X/1076/1/012072>
9. Ye W, Bel-Brunon A, Catheline S, Rochette M, Combescure A (2017) A selective mass scaling method for shear wave propagation analyses in nearly in-compressible materials. *Int J Numer Methods Eng* 109:155–173. <https://doi.org/10.1002/nme.5276>
10. Akhmad, Amir, Asdi, Ali MY, Anwar (2022) The process of making a Pinisi boat in Bantobahari District, Bulukumba Regency, Indonesia. *Euro J Eng Technol Res* 7:70–75. <https://doi.org/10.24018/ejeng.2022.7.5.2837>
11. Saenong MA (2013) Pinisi : Paduan Teknologi dan Budaya. (Yogyakarta : Pen-erbit Ombak)
12. Indonesia BK (1996) Peraturan Klasifikasi dan Konstruksi Kapal Kayu, vol I. (Biro Klasifikasi Indonesia (BKI))
13. Abdurachman, Susanty FH, Ngatiman (2022) Analysis of growth and vitality class of Ulin (*Eusideroxylon zwageri* T. et B.) on Sempaja Arboretum East Ka-limantan. In: IOP conference series earth and environment science 959:012071. <https://doi.org/10.1088/1755-1315/959/1/012071>
14. McKenzie WM, Karpovich H (1968) The frictional behaviour of wood. *Wood Sci Technol* 2(2):139–152. <https://doi.org/10.1007/BF00394962>

Studies on Chemically Treated Rubber Tube as a Replacement for Coarse Aggregate in Concrete



S. Konda Reddy, R. Akhileswar Reddy, R. Subash, K. Govardhan Reddy, V. M. Bharath Nivas, S. Vanitha , and P. Karthigai Priya

Abstract Disposal of waste tires and tubes is a huge problem globally. The present study mainly focuses to study the compressive strength of chemically modified waste types in the construction. Initially the waste tubes are collected and replaced for coarse aggregate at 5%, 10%, 15% and 20% respectively without any surface modification. Results indicate the increase of waste tubes decreases 70% of its compressive strength at 20% replacement. At 5% increment of rubber, the compressive strength decreases up to 40%. The rubber tubes are then chemically treated with calcium hypochlorite and sodium hydroxide and substituted with coarse aggregate, and the results illustrate that the chemically modified rubber-based aggregates are in par with conventional concrete in compressive strength. The higher compressive strength is attained because of improved bonding between aggregate and cementitious matrix. Hence it is recommended that modified rubber aggregate can be replaced at 5% for coarse aggregate and it will be a viable option to increase the compressive strength in the concrete.

Keywords Coarse aggregate · Rubber · Chemicals · Compressive strength · Concrete

1 Introduction

Vehicular pollution is one of the major factors creating air pollution. On the other side, waste tires and tubes is one the inevitable solid waste product obtained from vehicles usage. Waste tubes are non-bio degradable materials disposed to the environment posing severe threat to ecology and environment [1]. By 2030, the waste tires production will reach 1200 million tons [1–4]. As of now the major possible option of

S. K. Reddy · R. A. Reddy · R. Subash · K. G. Reddy · V. M. B. Nivas · S. Vanitha (✉) · P. K. Priya

Kalasalingam Academy of Research and Education, Krishnankoil, Tamil Nadu 626126, India
e-mail: s.vanitha@klu.ac.in

disposing waste tires in India is land filling. Waste tire disposal causes mosquito breeding; soil pollution [5] causes serious diseases. Few cement kiln industries use waste tires as a fuel for producing carbon black [4].

In the past decade, rubber is replaced as a construction material for road construction and building construction, initially rubber is used for construction of roads. The difference in stiffness causing more stress concentration while using rubber in the pavement. Lack of compatibility within cement paste and rubber is the key reason for rubber-based construction not popularizing yet [6]. Many researches tried to replace the rubber for fine aggregate, coarse aggregate and cement paste in building construction, [4, 7, 8]. The main drawback while using rubber-based concrete is the decrease in the strength with the increase in composition of waste rubber [4, 7–9].

Liu et al. [4] studied that because of its low-density rubber is unsuitable for non-structural applications. Gerges et al. [9] used rubber as a fine aggregate in concrete, he found that softness of material initiates cracks and behaves like voids in the concrete causes less adhesion between cement paste and rubber. Ganjian et al. [10] used rubber as a coarse aggregate and as powder for replacing the cement, result found that up to 5% there are no changes in concrete properties. The increase in rubber composition decreases the workability in concrete. However, durability properties such as ductility, toughness, impact resistance, sound insulation, strain energy are desirable while using rubber in concrete. Hence it is viable option to manage environmental issues as well as to preserve existing natural resources used for construction if the strength of rubber based concrete is improved [4].

In the recent past many researches attempted to enhance the mechanical properties of rubber in concrete. He et al. [11] suggested surface modification of the rubber as cost effective, simple and very efficient in enhancing and improving the compressive strength of rubber-cement concrete. Surface treatment and surface coatings are the simple methods to facilitate the property of rubber concrete suitable for construction. Liu et al. [4] used six modifiers for minimizing the loss of compressive strength in concrete. Among these, synthetic resin increases 12% of compressive strength and 40% of split tensile strength in concrete. Pre-treatment increases the adhesion between cement paste and rubber. It is observed 20% substitution of fine aggregate and 5% of total mixture meets the safety requirement.

Banerjee et al. [7] found 5% replacement of crumb rubber is suitable for coarse aggregate but it lacks strength properties and it is overcome by adding 5% micro silica and 40% replacement of GGBS with cement. Dong et al. [12] used silane coupling agent and cementitious coating for coating the rubber, the coated rubber showed higher withstanding capacity of tensile strength to almost 10–20% more than uncoated rubber. Lu et al. [13] used two surface treatments sodium hydroxide and silane coupling agent with three types of coating techniques namely normal cement, blended cement with silica fume and blended cement with sodium silicate in the rubber. Results indicates sodium hydroxide treatment improve concrete properties than normal concrete. Xue and Cao [14] used polyvinyl alcohol dipping rubber aggregate which improves compressive strength of concrete. In this study the following objectives are made to improve the compressive strength while using rubber tubes in concrete (i) Firstly the waste rubber tube is substituted at 5, 10, 15 and 20% for

coarse aggregate in concrete (ii) The rubber tube is treated chemically with sodium hydroxide (NaOH) and calcium hypochlorite [$\text{Ca}(\text{ClO})_2$] is substituted at 5, 10, 15 and 20% for coarse aggregate in concrete (iii) The compressive strength of rubber based concrete with and without chemical addition is compared with the control specimen (iv) The micro structural characteristics of concrete specimens are studied when using chemically treated rubber tube in concrete.

2 Materials and Methods

2.1 Collection of Materials

The Ordinary Portland Cement (OPC) of 53 Grade is used in this study. Manufactured sand (M-Sand) is collected by crushing the hard granite stone. The coarse aggregate and M sand used in this study is obtained locally. The raw materials characteristics are given in Table 1.

The cement properties are tested as per IS: 4031-1: 1996 and IS: 2720-3-1: 1980. From Table 1, the specific gravity of the cement is 2.85 and the fineness of the cement is 6%. The aggregates used in the concrete are tested as per IS 2386-3: 1963. The size of M-Sand is smaller than 4.75 mm. The specific gravity of fine aggregate (M-Sand) is 2.63 and the water absorption is 0.8%. The coarse aggregate is passed through 22.5 mm sieve and retained on the 9.5 mm sieve and used for the preparation of concrete. In the total percentage, 50% of aggregates are between 10 and 12 mm size and remaining 50% of aggregates are 20 mm size. The specific gravity of coarse aggregate is 2.67 and the water absorption is 1.5%. The waste rubber is collected from automobile shop nearby and crushed into pieces. The water absorption of rubber is 2.4%. Figure 1 shows the pictorial view of rubber pieces prepared for coarse aggregate.

The concrete specimens are casted for M25 grade and the mix design for the concrete is done as per IS 10262: 2019. The materials are properly mixed till homogeneous mix proportion is attained. The 150 mm × 150 mm × 150 mm concrete cubes are casted; the specimens are properly tamped inside the cube mould. After setting

Table 1 Raw material characteristics

Physical properties	Specific gravity	Fineness (%)	Water absorption (%)
Cement	2.85	6	–
Fine aggregate	2.63	–	0.8
Coarse aggregate	2.67	–	1.5
Rubber tube	1.13	–	2.4

Fig. 1 Rubber pieces for coarse aggregate replacement



Table 2 Mix proportion of rubber as coarse aggregate in concrete

S. No	Mix ID	Replacement levels (%)	Cement (kg/m ³)	FA (kg/m ³)	Rubber (kg/m ³)	CA (kg/m ³)	Water (l)
1	R0 (control specimen)	0	383.16	663.812	–	1100.841	
2	R5	5	383.16	663.812	55.042	1045.799	213.789
3	R10	10	383.16	663.812	110.084	990.757	214.460
4	R15	15	383.16	663.812	165.126	935.710	215.134
5	R20	20	383.16	663.812	220.168	880.673	215.803

time for a period of 24 h, the concrete specimens are cured for 28 days in water. The compressive strength studies were made after the samples attained the specified curing. Table 2 shows the proportion of materials taken for mix design.

2.2 Preparation of Chemically Coated Rubber Aggregate

Chemicals such as 20% of Sodium hydroxide (NaOH) and 5% of calcium hypochlorite [Ca(ClO)₂] is taken as percentage weight of water. The rubber aggregate is soaked in the chemicals for three days so that the pores become saturated with chemicals (Fig. 2). Then the aggregate is dried for one day (Fig. 2). Now the material is ready to replace the coarse aggregate in concrete.



Fig. 2 Soaked and dried rubber particles in chemicals

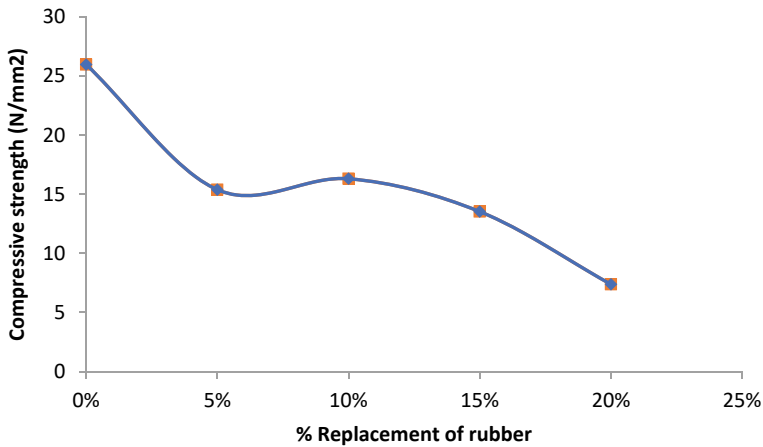
3 Results and Discussion

3.1 Compressive Strength of Untreated Rubber in Concrete

The compressive strength test for the concrete is done in accordance with IS 516: 1959. The substitution of rubber at 5%, 10%, 15% and 20%, the compressive strength results are 15.38 N/mm^2 , 16.31 N/mm^2 , 13.527 N/mm^2 and 7.38 N/mm^2 respectively and it is given in Table 3 and Fig. 3. It is observed from Fig. 3, with increase in the uncoated rubber percentage, decreases the compressive strength. On all the percentage replacements, the achieved compressive strength is less than conventional concrete specimen strength of 25.96 N/mm^2 . Notably, substitution of 5% rubber to concrete decreases the compressive strength by 10 N/mm^2 than the control specimen. From Table 3, it is evident that, almost 40% compressive strength is lost when replacing 5% of rubber aggregate to concrete and the maximum compressive strength loss of almost 75% is observed at 20% replacement. Abdulla et al. [15] replaced rubber for cement from 3 to 12% and the compressive strength decreases from 6 to 21% than normal concrete. The key possible reason for decrease in strength could be rubber aggregate is hydrophobic with cement paste creates less binding between concrete matrix which accelerates initial cracking when the external load is applied. Khern et al. [16] found formation of weak ITZ (Interfacial Transition Zone) while rubber is used as an aggregate in concrete and this problem can be solved

Table 3 Compressive strength results of replacement of rubber with coarse aggregate

Percentage replacement (%)	Compressive strength (N/mm ²)	% decrease of compressive strength from conventional concrete
0	25.96	–
5	15.38	40.00% decrease
10	16.31	37.18% decrease
15	13.53	47.89% decrease
20	7.38	71.57% decrease

**Fig. 3** Compressive strength after incorporation of rubber particles in concrete

by chemically treated aggregates. He et al. [11] found surface treatment change the hydrophobic nature of rubber aggregate with cement paste into hydrophilic thereby the adhesion is increased by 41.1%.

3.2 Compressive Strength of Chemically Treated Rubber in Concrete

The comparison of compressive strength results of concrete specimens with untreated rubber particle in concrete (RBC) and chemically treated rubber particles (CRBC) replaced at 5 and 10% for coarse aggregate can be seen in Table 4 and Fig. 4, it is found that the compressive strength tends to increase when the rubber is soaked in chemicals. At 5% replacement, the compressive strength is almost 10 N/mm² more for CRBC than RBC in concrete. Similarly, while replacing 10% with CRBC, 6 N/mm² more compressive strength is achieved than RBC in concrete. The possible

Table 4 Comparison of compressive strength in RBC and CRBC

S. No	Details	Compressive strength at percentage replacement (N/mm ²)	
		5%	10%
1	RBC	15.38	16.31
2	CRBC	24.70	22.16

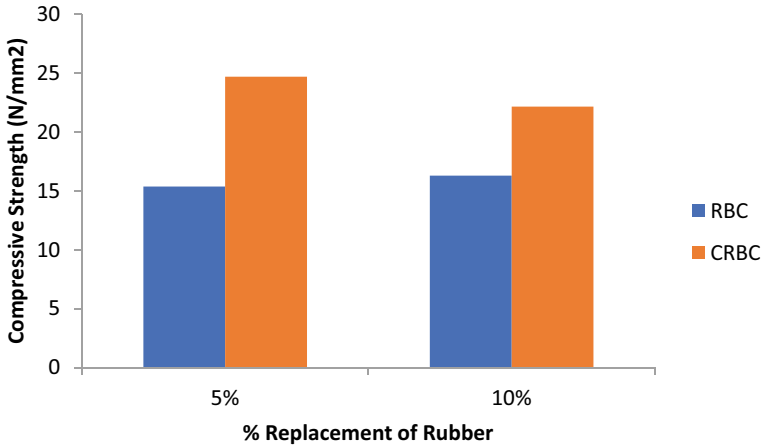
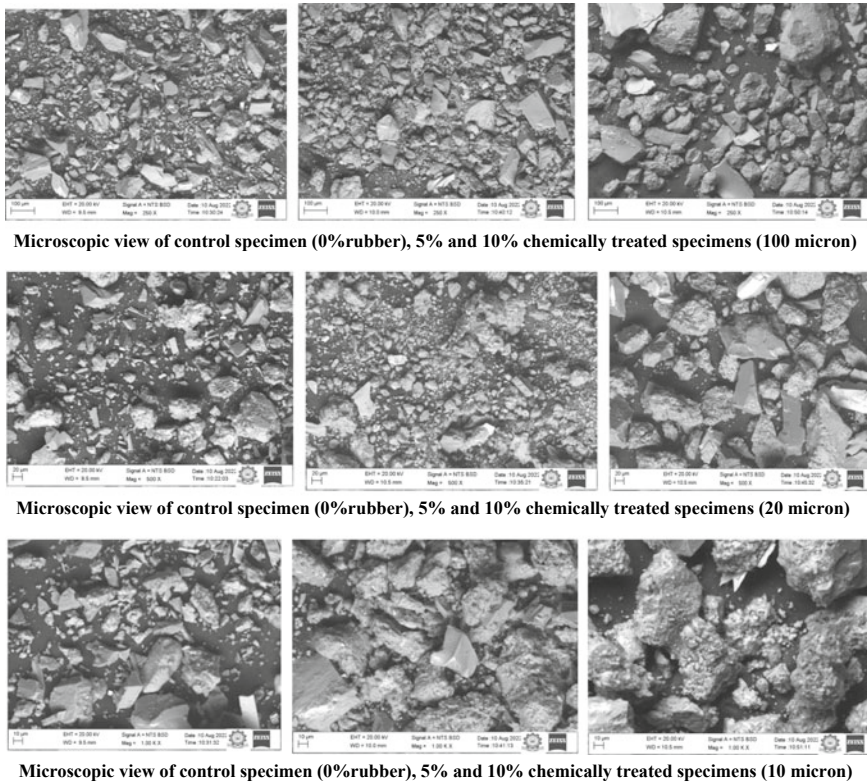


Fig. 4 Comparison of compressive strength for rubber based concrete and chemically dipped rubber based concrete

reason could be the cement is binding with chemically soaked rubber better than normal rubber particles. Another reason could be the increase in surface roughness of rubber particles makes binding strongly with cement paste. The 5% replaced chemically soaked rubber gives almost similar compressive strength value of conventional concrete. According to [13], sodium hydroxide treatment improves concrete properties than normal concrete. Lee et al. [17] found the oxidizing agent calcium hypochlorite and hydrogen peroxide promotes the binding between PET aggregate and cement paste leading to decrease the space of ITZ zone in the concrete. Additionally, the chemically treated aggregate has low Ca/Si ratio promotes the strength increment.

3.3 Micro Structural Study

Figure 5 shows the microscopic view of 100-micron, 20-micron and 10-micron size for control specimen (0%rubber), 5% CRBC and 10% CRBC. It is observed that 5% CRBC, the particles are closely arranged with each other and there are no pores between grains whereas pores are seen in conventional concrete specimen. According



Microscopic view of control specimen (0%rubber), 5% and 10% chemically treated specimens (100 micron)

Microscopic view of control specimen (0%rubber), 5% and 10% chemically treated specimens (20 micron)

Microscopic view of control specimen (0%rubber), 5% and 10% chemically treated specimens (10 micron)

Fig. 5 SEM images of control specimen and RBC specimens

to [16] the possible reason could be that there is more binding between concrete matrix and rubber and the other reason could be the surface of the rubber became rough is truly because of impregnated rubber in chemicals. It is evident that the compressive strength results show the higher value in 5% CRBC which matches with SEM results.

However, the 10% of CRBC, the particles are agglomerate with each other and formed as bigger structure and pores are seen.

4 Conclusions

The following conclusion are arrived in this study.

- (1) The compressive strength decreases while adding rubber particles to concrete. The percentage loss of compressive strength reaches up to 70% while replacing at 20% of rubber.

- (2) Addition of chemically soaked rubber particle increases the compressive strength and it is in par with conventional concrete when replaced at 5% for coarse aggregate. It is noted that the flexible rubber particles became hard and rough when it is impregnated in chemicals thus supports the cementitious matrix.
- (3) In SEM analysis it is cleared that the pores are decreased while replacing 5% chemically treated rubber based aggregate in concrete.
- (4) Overall, when untreated rubber tube is replaced in concrete up to 20%, the compressive strength gets affected and decreases. So, rubber tubes are treated chemically and replaced at 5 and 10%. Among this, 5% replacement of chemically treated rubber tube gives better results than untreated rubber tubes.
- (5) It is recommended that the rubber can be effectively used in the construction upon solving the compressive strength issue. However, detailed investigation should be carried for flexural strength, split tensile strength and durability studies while using chemically impregnated rubber particles in concrete.

5 Competing Interest

The authors declare that there is no competing interest.

Acknowledgements The authors would like to acknowledge and thank Kalasalingam Academy of Research and Education for performing the Scanning Electron Microscopy (SEM) analysis.

Funding Not applicable.

References

1. Bušić R, Miličević I, Šipoš TK, Strukar K (2018) Recycled rubber as an aggregate replacement in self-compacting concrete—literature overview. *Materials* 11(9):1729
2. Azevedo F, Pacheco-Torgal F, Jesus C, De Aguiar JB, Camões AF (2012) Properties and durability of HPC with tyre rubber wastes. *Constr Build Mater* 34:186–191
3. Eiras JN, Segovia F, Borrachero MV, Monzó J, Bonilla M, Payá J (2014) Physical and mechanical properties of foamed Portland cement composite containing crumb rubber from worn tires. *Mater Des* 59:550–557
4. Liu H, Wang X, Jiao Y, Sha T (2016) Experimental investigation of the mechanical and durability properties of crumb rubber concrete. *Materials* 9(3):172
5. Formela K (2021) Sustainable development of waste tires recycling technologies—recent advances, challenges and future trends. *Adv Indust Eng Polymer Res* 4(3):209–222
6. Shu X, Huang B (2014) Recycling of waste tire rubber in asphalt and portland cement concrete: an overview. *Constr Build Mater* 67:217–224
7. Banerjee S, Mandal A, Rooby J (2021) Performance of concrete with partial replacement of coarse aggregate with tyre chipped rubber. *Adv Civil Eng Infrastruct Develop* 665–674
8. Grinys A, Balamurugan M, Augonis A, Ivanauskas E (2021) Mechanical properties and durability of rubberized and glass powder modified rubberized concrete for whitetopping structures. *Materials* 14(9):2321

9. Gerges NN, Issa CA, Fawaz SA (2018) Rubber concrete: mechanical and dynamical properties, *Case Studies Construc Mater* 9
10. Ganjian E, Khorami M, Maghsoudi AA (2009) Scrap-tyre-rubber replacement for aggregate and filler in concrete. *Constr Build Mater* 23(5):1828–1836
11. He L, Ma Y, Liu Q, Mu Y (2016) Surface modification of crumb rubber and its influence on the mechanical properties of rubber-cement concrete. *Constr Build Mater* 120:403–407
12. Dong Q, Huang B, Shu X (2013) Rubber modified concrete improved by chemically active coating and silane coupling agent. *Constr Build Mater* 48:116–123
13. Guo S, Dai Q, Si R, Sun X, Lu C (2017) Evaluation of properties and performance of rubber-modified concrete for recycling of waste scrap tire. *J Clean Prod* 148:681–689
14. Xue G, Cao M (2017) Effect of modified rubber particles mixing amount on properties of cement mortar. *Adv Civil Eng* 1–6
15. Abdullah SR, Abidin WR, Shahidan S (2016) Strength of concrete containing rubber particle as partial cement replacement. *MATEC Web Conf* 47:01009
16. Khern YC, Paul SC, Kong SY, Babafemi AJ, Anggraini V, Miah MJ, Šavija B (2020) Impact of chemically treated waste rubber tire aggregates on mechanical, durability and thermal properties of concrete. *Front Mater* 7:90
17. Lee ZH, Paul SC, Kong SY, Susilawati S, Yang X (2019) Modification of waste aggregate PET for improving the concrete properties. *Adv Civil Eng*

Progressive Collapse Response of Linked Column Braced Frame System



N. A. Fameela and R. Nikhil

Abstract Structural integrity is one of the most important key elements considered during the planning of structures. In general, live load, dead load, and wind load is considered and impact load is not taken into account while designing structures. The action of impact load on a building affects the structural performance severely and causes progressive collapse failure as reported in several case studies worldwide. Unified Facility Criteria [3] guideline recommends various methods to increase the progressive collapse resistance capacity of buildings. The alternate load path method (APM) is one of the methods recommended in the UFC 2016 guidelines. The present work focuses on the study of the effectiveness of APM by analyzing the progressive collapse response of concentrically framed systems having linked column-braced frames (LCBF). The system comprises of braced frame system coupled with the linked column. Inverted V braces are considered for the structural analysis. The result of Pushdown analysis from SAP 2000 shows that during impact, the damage to the structural system mainly occurs in link beams which are rapidly replaceable and system performance can be retrieved.

Keywords Linked column braced frame system · Progressive collapse resistance · Alternate load path method · Unified facility criteria · Inverted brace · Impact load · Push-down analysis · Link beam · Load factor · Column removal scenario

N. A. Fameela (✉)

APJ Abdul Kalam Technological University, Thiruvananthapuram, Kerala, India

e-mail: fameela.na0@gmail.com

R. Nikhil

Universal Engineering Collage, Vallivattom, Thrissur, India

1 Introduction

The term progressive collapse is defined in the explication of the American Society of Civil Engineers Standard 7 *Minimum Design Load for Buildings and Other Structures* (ASCE 7) as “the spread of initial local failure from element to element eventually resulting in the collapse of the entire structure or disproportionately large part of it”. In general, abnormal loads are widely recognized as a significant factor contributing to structural failure. Despite their transient nature, these loads can have severe consequences. While it is impractical to design structural elements specifically to withstand abnormal loads, the Unified Facility Criteria [1] recommends several methods to mitigate progressive collapse.

One of the methods endorsed by UFC 2016 to resist progressive collapse is the Alternate Load Path Method (APM). The APM is employed in structural design to ensure that the load, acting on a failed member, can be redistributed throughout the structure, thereby preventing a complete collapse. To analyse the structure’s capacity to withstand progressive loads, a structural member is removed in lieu of applying an abnormal load.

This study focuses on the implementation of the Linked Column Braced Frame (LCBF) system as an APM approach to mitigate progressive collapse. The primary element of the LCBF system is a braced frame consisting of closely spaced Linked Columns (LC). These LCs are connected by replaceable energy-dissipating link beams. Additionally, this paper builds upon previous research published in the journal “Effect of Seismic Resistance Capacity of Moment Frame on Progressive Collapse Response of Concentrically Braced Dual System” [2]. That study estimated the progressive collapse response of a braced dual system with seismic share percentages of 25, 50, and 75%. The model described in the journal depicts a six-story residential building with four bays, measuring $24\text{ m} \times 24\text{ m}$ in plan dimension. Each story of the building has a height of 3.2 m and a span length of 6 m. The bracing configurations considered are X-bracing and inverted V-bracing, with the latter demonstrating superior resistance against progressive collapse. However, when the span length increases to 8 m, the bracing system exhibits failure in preventing progressive collapse.

2 Structural Models

The structural models analyzed in this study include an 8 m span concentrically braced dual system and an 8 m span Linked Column Braced Frame (LCBF) system. Both systems feature inverted V-bracing configurations, which exhibited superior performance in the previous journal. The applied loads on the structure consist of a dead load of 6.5 kN/m^2 , a live load of 2 kN/m^2 , and a wall load of 4 kN/m applied on the perimeter beam [2].

For the modelling and analysis of the structures, SAP 2000 ultimate version 20.2.0 was used. The columns and beams are constructed using wide flange sections with ASTM A992 steel as the material property, while the bracings employ Hollow Steel Sections (HSS) with A500 steel as the material property. Table 1 provides the member sizes for the model [2]. Additionally, Fig. 1 illustrates the elevation of the 8 m span concentrically braced frame system, while Fig. 2 depicts the elevation of the LCBF system.

Table 1 Member size of the model

Story	Column		Beam		Brace
	Internal	External	Internal	External	
1	W12X136	W12X136	W12X35	W12X22	HSS6X6X 3/8
2	W12X136	W12X136	W12X35	W12X22	HSS6X6X 3/8
3	W12X120	W12X136	W12X35	W12X22	HSS6X6X 3/8
4	W12X120	W12X136	W12X35	W12X22	HSS5X5X 5/16
5	W12X96	W12X136	W12X35	W12X22	HSS5X5X 5/16
6	W12X96	W12X136	W12X19	W12X19	HSS5X5X 5/16

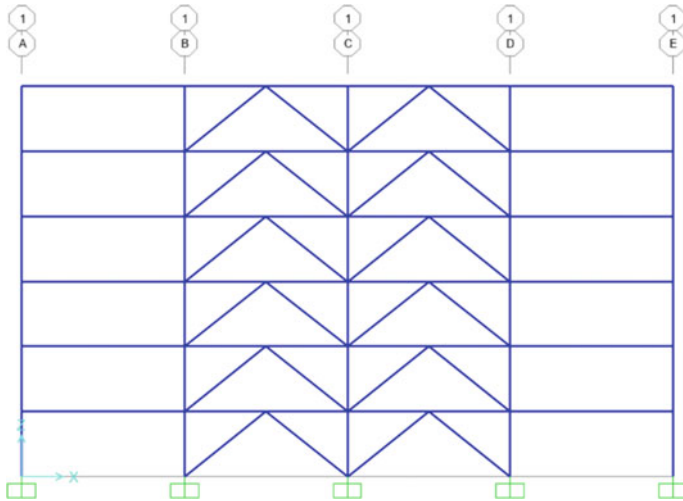


Fig. 1 Elevation of 8 m span concentrically braced frame system

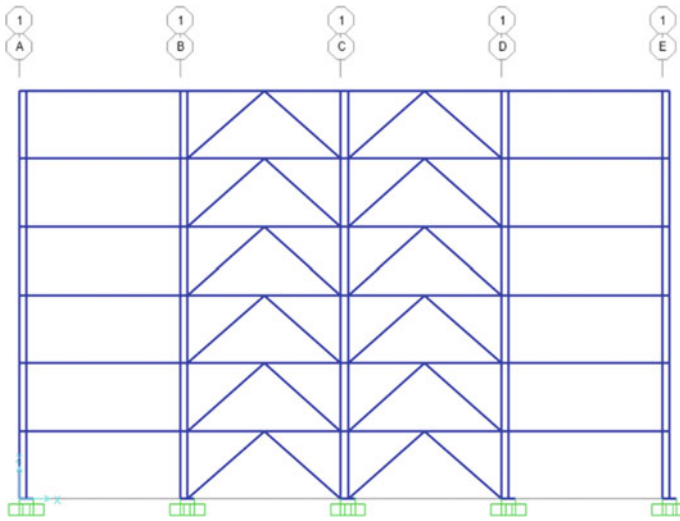


Fig. 2 Elevation of the LCBF system

3 LCBF Shear Link Design

As per Seismic Provisions for Structural Steel Buildings, the link length provided should be less than or equal to $1.6M_P/V_P$, i.e.

$$e \leq 1.6M_P/V_P \tag{1}$$

where e is the link length, M_P is the plastic moment and V_P is the plastic shear force. The value of M_P and V_P is given by the following formulae [4]

$$M_P = f_y \times t_f \times (b - t_w)(d - t_f) + \frac{f_y \times t_w \times d^2}{4} \tag{2}$$

$$V_P = \frac{f_y}{\sqrt{3}} \times t_w \times (d - 2 \times t_f) \tag{3}$$

where f_y is the yield stress, t_f is the flange thickness, b is the flange width, t_w is the web thickness and d is the height of I section.

For the analysis purpose link beam used is wide flange section W8X15. And by the calculation using Eqs. (1), (2) and (3) the link length for W8X15 should be less than or equal to 510 mm. So the adopted link lengths are 300, 350 and 400 mm.

4 Pushdown Analysis

As per the UFC [1] guideline the gravity load combination “ $\Omega_N (1.2D + 0.5L)$ ” is applied to bays adjacent to the removed column at all floors above that. The gravity load combination “ $(1.2D + 0.5L)$ ” was applied to the other bays.” Where D and L are dead and live loads, respectively. The dynamic increase factor (Ω_N) for nonlinear static analysis in steel buildings was calculated by Eq. (4).

$$\Omega_N = 1.08 + 0.76 / \left(\frac{\theta_{pra}}{\theta_y} + 0.830 \right) \quad (4)$$

where θ_{pra} is the plastic rotation angle and θ_y is the yield rotation [2]. The obtained value for the dynamic increase factor is 1.393. Then the load cases applied on the structure are $1.67D + 0.696 L$ for bays adjacent to the removed column and $1.2 D + 0.5 L$ is applied to the other bays. In the analysis, the progressive load is considered non-linear and the load application is in the vertical direction. The progressive collapse response is assessed through pushdown analysis, which uses a non-linear technique to estimate structural deformation. This approach allows for examining the sequential formation of plastic hinges in the structural members and monitoring different displacements above the removed column.

5 Results and Discussion

As per the UFC 2016 guidelines, the capability of a structure to mitigate progressive collapse is estimated by the load factor-displacement relationship. The term load factor can be defined as the ratio of applied load at the step of the pushdown analysis to total progressive collapse load. A structure is deemed capable of resisting progressive collapse when the load factor for a given pushdown step is equal to or greater than unity. Conversely, if the load factor is less than unity, the structure is considered ineffective in mitigating progressive collapse.

5.1 Braced Frame System

Figure 3a and b show the corner column and second column removal scenario of the braced frame system. From the deformation patterns depicted in Fig. 4a, it can be observed that the removal of the corner column leads to the formation of plastic hinges in the span above the failed column. On the other hand, Fig. 4b shows that removing the second column results in the formation of plastic hinges in the braces. The load factor obtained from the pushdown analysis is less than 1, indicating that the structure lacks the capability to withstand progressive collapse. The specific values

of the load factors can be found in Table 2. Therefore, to enhance the efficiency of progressive collapse resistance, an alternative method needs to be adopted, namely the LCBF system.

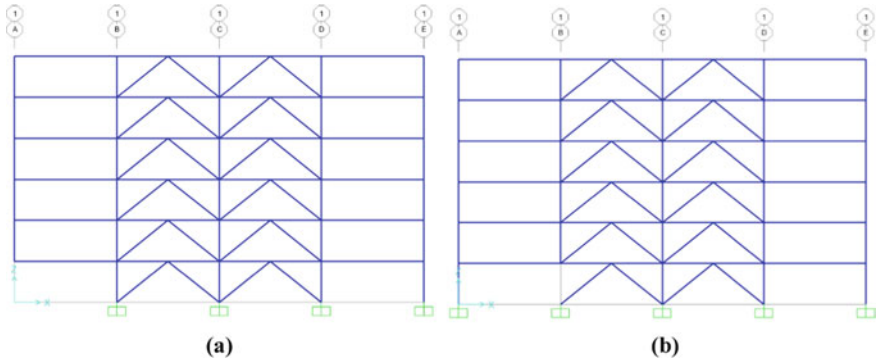


Fig. 3 Column removal scenario **a** corner column **b** second column

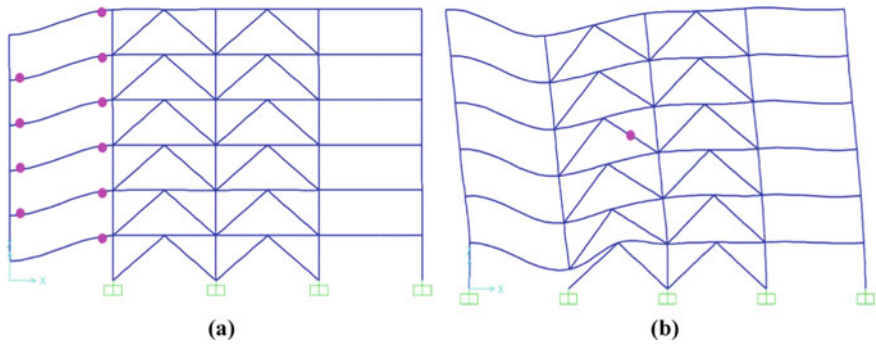


Fig. 4 Plastic hinges formation in bracing system **a** corner column removal **b** second column removal

Table 2 Result of pushdown analysis for braced frame system

Removed column	Load factor
Corner	0.496
Second	0.882

5.2 Linked Column Braced Frame System

The linked columns are provided around the perimeter of the structure. After the corner column removal and second column removal, the pushdown analysis result obtained for different link-length LCBF systems are illustrated below.

Link length 400 mm: Figure. 5a and b illustrate the formation of plastic hinges in the LCBF system with an 8 m span length and a link length of 400 mm following the removal of the corner column and the second column, respectively. Notably, the plastic hinges are observed to form within the energy-dissipating link beam itself. Load factor values for the LCBF system corresponding to the loss of the corner column and the second column are presented in Table 3. Based on the table, it can be inferred that the system does not achieve progressive collapse resistance after the removal of the corner column. However, when comparing the performance to the bracing system, the combination of the bracing system with the LC system appears to show improvement. Similarly, after the removal of the second column, a load factor value greater than 1 is obtained, indicating that the system is capable of resisting progressive collapse.

Link length 350 mm: The length of the link beam is set to 350 mm and the pushdown curve is analyzed to find the progressive collapse response of the structure. Here also perceived that the plastic hinges are formed in the link beam of the removed column as observed in the link length of 400 mm. Table 4 shows load factor values obtained by the pushdown analysis. In Table 4 it is noticed that the load factor value satisfies

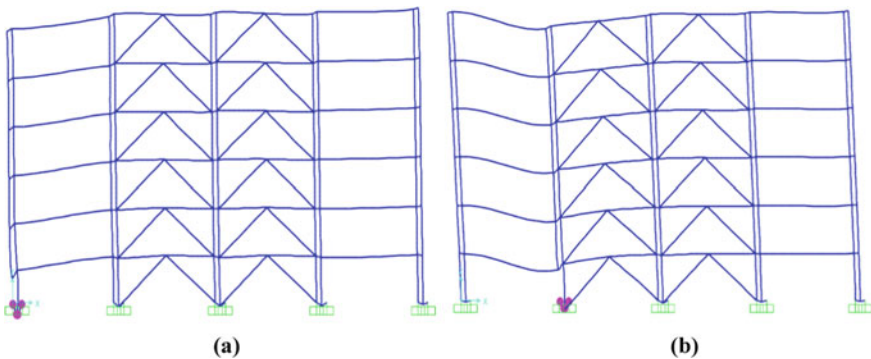


Fig. 5 Plastic hinges formation in 400 mm link length LCBF system **a** corner column removal **b** second column removal

Table 3 Result of pushdown analysis for LCBF system with link length 400 mm

Removed column	Load factor
Corner	0.891
Second	1.125

Table 4 Result of pushdown analysis for LCBF system with link length 350 mm

Removed column	Load factor
Corner	1.01
Second	1.54

Table 5 Result of pushdown analysis for LCBF system with link length 300 mm

Removed column	Load factor
Corner	1.18
Second	1.56

the UFC acceptance criterion. Furthermore, it is worth noting that reducing the link beam length results in improved progressive collapse resistance compared to the LCBF system with a 400 mm link length.

Link length 300 mm: Similar plastic hinge formation patterns are observed in this case as well. The LCBF system with a 300 mm link beam demonstrates improved performance compared to the LCBF systems with longer link beams. This indicates that reducing the link length enhances the effectiveness of the LCBF system in resisting progressive collapse. The load factor values obtained from the pushdown analysis are provided in Table 5.

6 Conclusions

This paper presents a comparative study between the braced frame system and the LCBF system regarding their performance in resisting progressive collapse. The previous journal concluded that the inverted V-braced system performs well in resisting progressive collapse over a span of 6 m. However, when the span length is increased to 8 m, the bracing system exhibits poor resistance to progressive collapse. In this scenario, the LCBF system demonstrates better progressive collapse resistance. The conclusions drawn from the pushdown analysis conducted using SAP 2000 are as follows:

- The LCBF system outperforms the bracing system in resisting progressive collapse. As the span length of the bracing system increases, its structural stiffness decreases, resulting in its failure to resist progressive collapse effectively.
- Among the three types of link length beams analyzed, the 300 mm link beam exhibits the highest ability to resist progressive collapse. A shorter link beam length corresponds to higher stiffness, thus enhancing the system's resistance.
- In comparison to the second column, the corner column displays a greater tendency towards progressive collapse failure.

- Damage to the structural system primarily occurs in the link beams. Since the link beams are replaceable, any damaged beams can be refitted, allowing the structure to retrieve its performance.

References

1. UFC (2016) Design of buildings to resist progressive collapse. Washington DC: Unified Facility Criteria
2. Musavi-Z M, Sheidai MR (2021) Effect of seismic resistance capacity of moment frames on progressive collapse response of concentrically braced dual systems. *Asian J Civil Eng* 22:23–31
3. Ciman L, Freddi F, Tondini N (2021) A retrofit method to mitigate progressive collapse in steel structures. *ce/papers* 4(2–4)
4. AISC 341 (2016) Seismic provisions for structural steel building. Chicago: Am Instit Steel Constr

Parametric Study on Performance of Conical Shell Foundation Using FEM Modeling



M. K. Sheeja, T. Lamya, and Jerin Joseph

Abstract A Shell foundation has been considered the best shallow foundation for transferring heavy load to weak soils because of the high bearing capacity values, whereas a conventional shallow foundation submits to excessive settlement. In this paper, two parametric studies were carried out on conical shell foundations using FEM software ANSYS to study the effect of the rise to radius (f/r ratio) and thickness on the strength and settlement of conical shell foundations. In the first study, various f/r ratios chosen were 0.5, 0.75, and 1. The results indicated better performances for the conical shell foundation with an f/r ratio of 1, due to its increased membrane stresses and the contact area between the shell and soil. The shell thickness was varied in the second study from 40 to 80 mm, and the results showed that as the thickness increases, the settlement reduces. The ultimate load increases up to a thickness of 70 mm, which is due to the increase in the rigidity of the foundation. From the parametric study, it was understood that f/r ratio and thickness are two main parameters that influence the behavior of shell foundations.

Keywords Foundation · Conical shell foundation · ANSYS · FEM modeling

1 Introduction

A foundation must be capable of transferring the building weight to the soil without exceeding the allowable stress limits or causing excessive settlement. When dealing with weak soils and heavy loads, shell foundations are often preferred due to their high bearing capacity values. Unlike planar structural elements such as slabs, shells use direct stress, including tension, compression, and shear, all within the shell's plane. Shell foundations are cost-effective when carrying heavy loads on weak soils,

M. K. Sheeja · J. Joseph (✉)
Albertian Institute of Science and Technology, Kalamassery, India
e-mail: jerinjoseph@aisat.ac.in

T. Lamya
Local Self Government Department, Thiruvananthapuram, Kerala, India

but large-sized foundations are required because of the low bearing capacity. Shells are more efficient and economical than bending members like flat footings because of a more uniform stress distribution. Even in smaller foundations, shells require fewer materials to support the load. However, shell construction requires more labor than conventional foundation types, including forming the shell surface, fabricating steel, and supervision. Nonetheless, cones and hyperbolic paraboloids are popular shell shapes due to their ease of construction and casting surface. The Bureau of Indian Standards has issued a code of practice for designing and constructing conical and hyperbolic paraboloid shell foundations. Therefore, shell foundations may be a suitable option in certain special situations.

1.1 Literature Review

Kurian and Devaki [8] analyzed conical, spherical, and hyperbolic paraboloidal shells to understand the influence of parameters like friction, cohesion, and internal friction angle, as well as loading conditions, on bearing capacity and settlements, comparing them to plain counterparts. Huat and Mohammed [6] utilized the non-linear finite element analysis to create finite element models of two triangular strip footings. They varied the rise to half-width ratio and compared the load-carrying capacities of the shell models with those of flat strip footings. The results indicated that the shell models had more than 40% higher load capacities and lesser settlements when compared to the flat models. Esmaili and Hataf [2] studied the ultimate load capacities of conical and pyramidal shell foundations on reinforced and unreinforced sand. Through laboratory tests and numerical analysis, they found that increasing the thickness of shell foundations made their behavior more similar to circular and square flat foundations. Fernando et al. [4] studied the bearing capacity and failure mechanism of shallow foundations in dry sand. They conducted laboratory tests on conical and pyramidal shell foundations and compared them to flat foundations. Settlement and shell gain factors were higher for conical shells, while the pyramidal shell had a lower influence zone height. The failure mechanism was similar to flat foundations. Fattah et al. [3] investigated the behavior of conical shell foundations made of reactive powder concrete mixed with different percentages of silica fume and embedded in sandy soil. They found that increasing the rise to radius (f/r) ratio for shell from 0.25 to 0.75 increased the ultimate load by about 15%. Jeyashree et al. [7] investigated funicular concrete shell foundations under ultimate loading conditions. Increasing edge beam reinforcement steel area by 40% enhanced the ultimate load capacity by 15% and reduced settlement by 26%. Thicker specimens exhibited higher load-carrying capacity. Shell foundations outperformed flat foundations with a 50% increase in ultimate load capacity. Lamy and Sheeja [9] conducted a comparative study on the performance of conical shell and flat circular foundation using FEM models. They concluded that the ultimate carrying capacity of conical shell foundation was 3 times more than the flat circular foundation. Additionally, the settlement characteristics were also in favor of the conical shell foundation. Tadyon et al. [10] conducted an

experimental study on geotechnical aspects of semi-deep shell foundations in which it was found that conical shells demonstrate higher bearing capacity than skirted hybrid foundations. After analyzing previous research, it has been determined that a shell foundation is a preferable option compared to a flat foundation. Different types of shell foundations, such as conical, hyperbolic paraboloidal, funicular, pyramidal, etc. have been investigated. However, only conical and hyperbolic paraboloidal shell foundations have been covered by the Bureau of Indian Standards code of practice. When comparing the two, a conical shell foundation utilizes a lower amount of steel and concrete compared to hyperbolic paraboloidal and flat foundations. The present study examines the structural behavior of conical shell foundations through a limited parametric analysis in which two parameters are varied. The geometric configurations i.e., change in the rise to radius (f/r) ratio and thickness of the shell foundation are varied.

2 Methodology

Two separate parametric studies were carried out to study the influence f/r ratio and shell thickness on the ultimate load-carrying capacity and settlement of the conical shell foundation. The investigation was conducted using the FEM Software ANSYS 19.0. To study the influence of f/r ratio (shell height to radius ratio), it was varied as 0.5, 0.75, and 1 and compared with a flat circular foundation. During this study, the height of the conical shell foundation was varied while keeping the radius and thickness of the shell constant at 700 mm and 60 mm thickness, respectively. The radius and thickness of the flat circular foundation were 700 mm and 60 mm thickness, respectively. The parametric study on shell thickness was carried out by varying the thickness as 40, 50, 60, 70, and 80 mm. The f/r ratio of the conical shell foundation was kept constant at 1 in this study since the results from the parametric study by varying f/r ratio had indicated optimum performance for a conical shell foundation with f/r ratio of 1. In the present study, a static structural analysis was carried out to determine the effects of steady-state loading conditions on the structure. Incremental loads were applied as vertical column loading to determine the ultimate load-carrying capacity, which was based on the strain value of concrete. The equivalent elastic strain value increased as the load increased. The load corresponding to the maximum equivalent elastic strain (at 0.002 for the foundation) was considered as the ultimate load-carrying capacity.

2.1 Material Properties, Model Geometry, and Meshing

Concrete was defined with linear isotropic property, which uses Von-mises failure criterion. Table 1 shows the material properties of foundation materials used for the

Table 1 Properties of foundation materials

Properties	Concrete	Rebars
Modulus of elasticity, E_c (kN/m ²)	2.236×10^7	2×10^8
Poisson's ratio, ν	0.15	0.3
Density (kN/m ³)	22	78.50
Tensile yield strength (MPa)	2	250
Compressive yield strength (MPa)	20	250
Tensile ultimate strength (MPa)	5	460
Compressive ultimate strength (MPa)	41	0

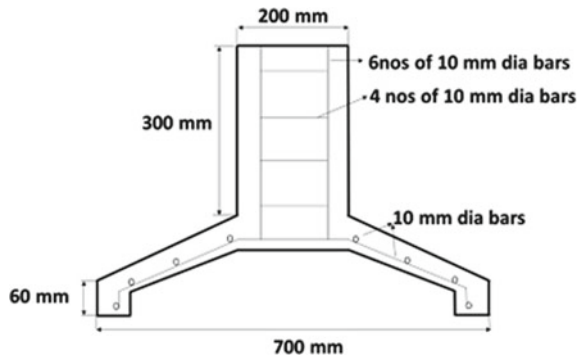
Table 2 Properties of soil

Soil properties	Value
Modulus of elasticity, E_s (kN/m ²)	25×10^3
Poisson's ratio, ν	0.3
Density (kN/m ³)	16.40
Cohesion (kN/m ²)	5
Angle of internal friction (°)	33
Dilatancy angle (°)	3

models. The properties of medium-dense sand considered for the analysis are listed in Table 2, which was adopted from Hanna and Rahman [5].

The model geometry consisted of the conical shell/circular flat foundation and the soil block on which it rests. The reinforcement details of the foundation are given in Fig. 1. A typical finite element model of the conical shell and circular flat foundation model are given in Fig. 2a and b. The dimensions of the shell foundation were varied as per the parameters taken during the parametric study. The dimension of the soil block was fixed as per the load distribution pattern. The horizontal and vertical dimensions of the soil block were kept twice the diameter of the shell.

Fig. 1 Conical shell foundation reinforcement details



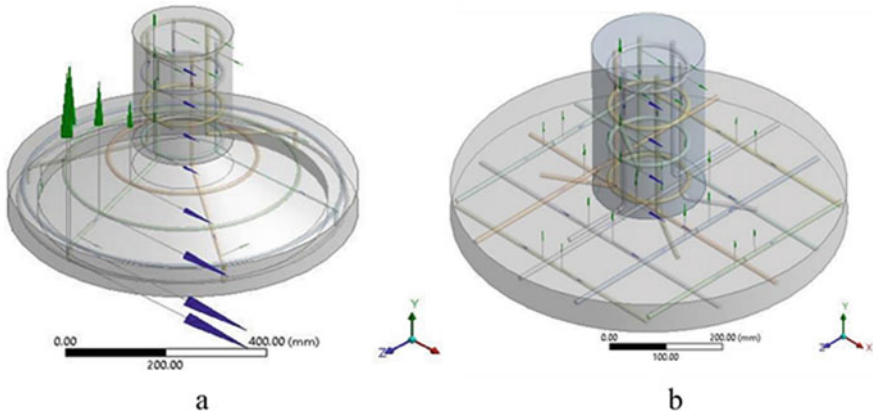


Fig. 2 Finite element model of **a** conical shell foundation **b** circular flat foundation

SOLID186, a higher-order element with 20 nodes, was chosen by the software for the analysis. The area between the inverted conical shell foundation and soil was made as bonded contact. The contact between the reinforcement bars and concrete was also made as bonded contact with the target as concrete and contact as rebars. Mesh size of 25 mm was chosen for the foundation, and 100 mm was chosen for the soil model (Fig. 3.). The tetrahedral and hexa-dominant meshing method was used for the conical shell and flat foundation respectively.

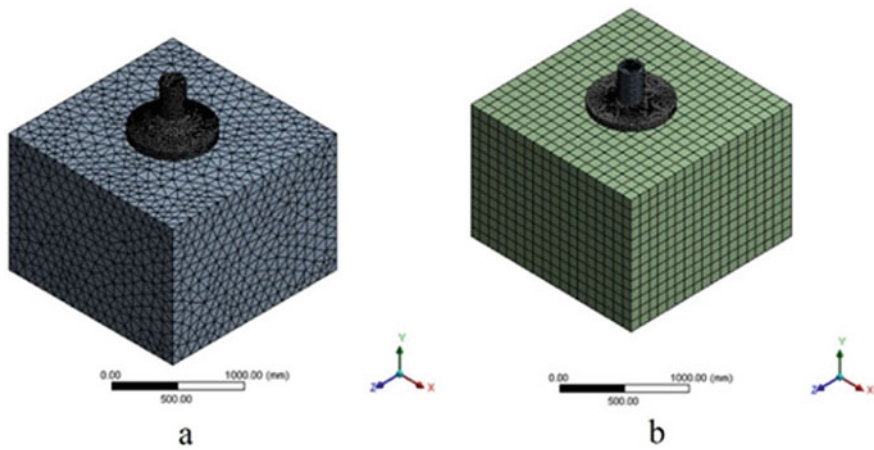


Fig. 3 FEM mesh of **a** conical shell foundation **b** circular flat foundation

Table 3 Material properties used for validation

Properties	Reinforced concrete	Medium dense sand
Modulus of elasticity, E (MN/m ²)	1.97×10^4	40
Poisson's ratio, ν	0.16	0.35
Density (kN/m ³)	24	17
Cohesion (kN/m ²)	–	5
Angle of internal friction (°)	–	35

Table 4 Comparison of results from the experimental and FEM model

Result	El-kady and Badrawi [1]	FEM model	% Error
Ultimate load	58 kN	60 kN	3.33
Settlement	35 mm	41 mm	3.81

2.2 Model Verification

The results from the experimental study conducted on folded footing by El-kady and Badrawi [1] was used to verify the model. The data corresponding to the folded footing with a folding angle of 0° was used for verification. Material properties used for the validation are listed in Table 3. A comparison of the load settlement results obtained from the experimental model and finite element results is given in Table 4. The elastic strain of the footing concrete exceeded the equivalent elastic strain limit at a load of 60 kN. It was considered the ultimate load carrying capacity, and the settlement corresponding to the ultimate load was considered the maximum settlement. The agreement between the results obtained from the literature and that obtained from the finite element model is good. Since the percentage error of both ultimate load and settlement is less than 10%, the FEM model can be considered to correctly simulate the experimental model.

3 Results and Discussion

3.1 Effect of Rise to Radius (F/r) Ratio

The structural behavior of the conical shell foundation with different f/r ratios were compared. The results show that as the f/r ratio increases, that is, as the half shell angle decreases, the ultimate load-carrying capacity increases.

The effect of f/r ratio on the ultimate load carrying capacity and settlement is given in Table 5. The ultimate load-carrying capacity of the conical shell foundation with f/r ratios 0.5, 0.75, and 1 showed an increment of 34.6, 57.7, and 84.6% than its flat counterpart, and the maximum load-carrying capacity was shown by conical

Table 5 Effect of rise to radius ration on ultimate load and settlement

f/r ratio	Ultimate load (kN)	Settlement (mm)	Settlement at 130 kN Load (mm)
0.5	175	21.64	16.08
0.75	205	24.40	15.47
1	240	23.90	12.96

shell foundation with f/r ratio 1. This shows that as the f/r ratio increases, that is, as the semi-vertical angle decreases, the ultimate load-carrying capacity increases, which is due to the increase in the membrane stresses in the shell and contact area between shell and soil.

In order to determine the effect of the variation of f/r ratio or the semi-vertical angle of the conical shell foundation on settlement, they have been subjected to a constant load value of 130 kN (which is the ultimate load-carrying capacity of the flat circular foundation of the same thickness i.e., 60 mm). As seen in Table 5, the results show that as the f/r ratio increases, settlement decreases. Settlement of conical shell foundations with f/r ratios 0.5, 0.75, and 1 is reduced by 8.52%, 12.8%, and 34%, respectively, from its flat counterpart. From this, it is clear that the smaller the angle of intersection of the foundation, the lower the measured settlement is due to the increase in the membrane stress and contact area between the shell and soil.

From the results obtained from the parametric study by varying f/r ratios, conical shell foundations with f/r ratio 1 showed better performance than others, with an increment in load-carrying capacity by 84.6% and a reduction in settlement by 34%.

3.2 Effect of Thickness

A parametric study was conducted by varying the thickness, such as 40, 50, 60, 70, and 80 mm, to analyze its effect on the ultimate load-carrying capacity and settlement characteristics. Results from the parametric study by varying f/r ratio indicated better performance of shell foundation with f/r ratio 1. Thus, shell foundation with f/r ratio one is chosen for the parametric study to determine the effect of thickness.

The load-carrying capacity of the shell foundations with thicknesses 50, 60, 70, and 80 mm showed an increment of 25.8%, 54.8%, 64.5%, and 48.3%, respectively, from that of the 40 mm thick shell foundation as shown in Table 6. This indicates that the ultimate load-carrying capacity of the foundation increases as the thickness increases due to the foundation's increased rigidity. However, at a thickness of 80 mm, the foundation displayed a slight decrease in load-carrying capacity. At a thickness of 80 mm, there was a reduction in membrane stress, and the shell structure lost its shell behavior, causing a decrease in load-carrying capacity.

In order to determine the effect of the variation of thickness of the conical shell foundation on settlement characteristics, a constant load value of 155 kN (which is the ultimate load of a 40 mm thick conical shell foundation) is subjected to the shell

Table 6 Effect of rise to radius ration on ultimate load and settlement

Thickness	Ultimate load (kN)	Settlement (mm)	Settlement at 155 kN Load (mm)
40	155	15.34	15.34
50	195	19.48	14.50
60	240	23.90	13.86
70	255	25.40	13.08
80	230	22.90	12.62

foundations with various thicknesses. A constant load value (155 kN) is chosen so as to compare the variation in settlement for shell foundations with varying thicknesses (Table 6). Vertical displacement of the shell foundations with thicknesses 50, 60, 70, and 80 mm has been reduced by 5.8%, 10.6%, 17.3%, and 21.5%, respectively, from that of the 40 mm thick shell foundation. From these results, it can be concluded that as the thickness of the foundation increases, its vertical displacement or settlement reduces, and this is because of the increase in the rigidity of the foundation. However, from the parametric study by varying thickness, it is clear that a 70 mm thick conical shell foundation showed better load-carrying capacity and settlement characteristics with an increment in load-carrying capacity by 64.5% and a decrement in settlement by 17.3%.

4 Conclusion

A Conical shell foundation exhibits different structural behavior compared to flat foundations. Factors such as load-bearing capacity, settlement characteristics, and the influence of soil-structure interaction vary in conical shell foundations. The current study helps in evaluating the performance of these foundations through a limited change in geometric configurations via a parametric study in which the effect of the rise to radius (f/r) ratio and the thickness of a conical shell foundation on the ultimate capacity and settlement of a conical shell footing. The following conclusions can be drawn from the study:

- As the f/r ratio is increased, that is as the semi-vertical angle is decreased, the ultimate load increases and settlement reduces.
- Conical shell foundations with f/r ratio of 1 showed better performances than others with an 84.6% increment in ultimate load and a 34% decrease in a settlement.
- As the thickness increases, the ultimate load also increases up to a thickness of 70 mm, showing a slight reduction in ultimate load for an 80 mm thick foundation.
- Conical shell foundation with a thickness of 70 mm showed better performances than others, with a 64.5% increment in ultimate load and a 17.3% decrement in the settlement.

Hence, it can be summarized from the parametric study that f/r ratio and thickness of the conical shell foundation are two primary parameters that have prominent effects on the behavior of the conical shell foundation.

References

1. El-kady MS, Badrawi EF (2017) Performance of isolated and folded footings. *J Comput Design Eng* 4(2):150–157
2. Esmaeili D, Hataf N (2008) Experimental and numerical investigation of ultimate load capacity of shell foundations on reinforced and unreinforced sand. *Iranian J Sci Tech* 32(5):491–500
3. Fattah MY, Waryosh WA, Al-Hamdani MA (2015) Experimental and theoretical studies on bearing capacity of conical shell foundations composed of reactive powder concrete. *Acta Geodynamica et Geomaterialia* 12(4):411–426
4. Fernando N, Sendanayake E, Sendanayake D, De Silva N (2011) The experimental investigation of failure mechanism and bearing capacity of different types of shallow foundations. *J Civil Eng Res Indust* 31(8):67–72
5. Hanna AM, Abdel-Rahman M (1998) Experimental investigation on shell foundations on dry sand. *Can Geotech J* 35(6):828–846
6. Huat BB, Mohammed TA (2006) Finite element study using FE code (PLAXIS) on the geotechnical behavior of shell footings. *J Comput Sci* 2(1):104–108
7. Jeyashree TM, Arunkumar C, Ashok KS (2017) Experimental and analytical study on funicular concrete shell foundation under ultimate loading. *Asean J Civil Eng* 18(6):863–878
8. Kurian NP, Devaki VJ (2005) Analytical studies on the geotechnical performance of shell foundations. *Can Geotech J* 42(2):562–573
9. Lamy T, Sheeja MK (2021) Analytical assessment on the behaviour of conical shell foundation. In: *Proceedings of SECON 2020: structural engineering and construction management*, vol 4, pp 307–316
10. Tadayon A, Eslami A, Fakharian K (2022) Load-displacement behavior of semi-deep shell foundations on sand by experimental study. *Int J Civil Eng* 20(7):839–855

Localized Corrosion Damage Study and Strengthening Strategies on Orthogonal Concrete Filled Steel Tubular Column



Drisya Dinesh and E. K. Amritha

Abstract Concrete-filled steel tubular (CFST) columns are widely used in the construction industry due to their high strength and durability. However, localized corrosion can significantly reduce the structural integrity of these columns, leading to potential safety hazards. This project aims to investigate the localized surface corrosion damage on 'L' shaped orthogonal CFST columns and propose effective strengthening strategies using ANSYS software. The behavior of L-shaped CFST columns under axial loading due to influence of various parameters such as Degrees of Volume loss (DoV), corrosion position and corrosion location are studied. The worst-performed model during axial loading is identified. As an effective strengthening scheme to overcome the damage according to severity, Fiber Reinforced Polymer (FRP) wrapping technique is used. Carbon Fiber Reinforced Polymer (CFRP), Glass Fiber Reinforced Polymer (GFRP), Aramid Fiber Reinforced Polymer (AFRP), and Basalt Fiber Reinforced Polymer (BFRP) are the FRPs used. A study to find out which fiber will help to regain more strength and how many layers of wrapping are needed for the same is done. The findings of this project will contribute to the development of effective strategies for mitigating the effects of localized corrosion in CFST columns and enhancing their structural performance.

Keywords Axial loading · Concrete-filled steel tube (CFST) · Localized corrosion · Fiber Reinforced Polymer (FRP) wrapping

D. Dinesh (✉)

APJ Abdul Kalam Technological University, Thiruvananthapuram, Kerala, India
e-mail: drisyadinesh481@gmail.com

E. K. Amritha

Universal Engineering College, Vallivattom, Thrissur, India

1 Introduction

Concrete Filled Steel Tubes (CFST) are composite members made of steel tubes filled with concrete having many structural advantages, including high strength, fire resistance, good ductility and high energy absorption capacity. The outer steel tubes provide a restraining effect on the concrete core, and the inner concrete core slows local buckling of the outer steel tubes. The traditional rectangular CFST column has protruding corners that not only detract from the indoor aesthetic, but also reduce the usable floor space. Columns with orthogonal (T-shaped, L-shaped, or cruciform-shaped) cross sections, are possible solutions for this. Among orthogonal CFST columns, L shaped columns are probably the most common because they can be used as corner columns in framed construction. They are generally used at the corners of buildings when the outer spans of the beams are large and generate large bending moments. However, corrosion is a challenge associated with the use of CFST columns. Localized corrosion is a type of corrosion that occurs in specific areas on a metal surface due to a variety of factors, including stress, impurities, and pollutants. Corrosion reduces the effective thickness of the steel and significantly reduces the load bearing capacity. Fiber reinforced polymer (FRP) can be used to strengthen corroded CFST columns, extending their service life. FRP wrapping allows weakened elements to be upgraded without significantly altering the appearance of the element. In addition, FRP composites are lightweight, durable, have high tensile strength, stiffness, corrosion resistance and fatigue resistance.

This study aims at performing axial loading on localized surface corrosion affected L shaped orthogonal CFST Column for varying Degree of Volume loss (DoV), Corrosion positions, and corrosion locations. The study also analyzes the strength of corroded CFST column wrapped with Fiber Reinforced Polymer (FRP) strips under axial loading by varying FRP types [Carbon Fiber Reinforced Polymer (CFRP), Glass Fiber Reinforced Polymer (GFRP), Aramid Fiber Reinforced Polymer (AFRP), and Basalt Fiber Reinforced Polymer (BFRP)] and Number of FRP layers.

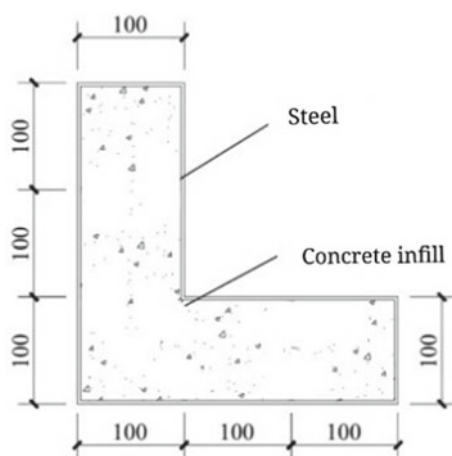
2 Finite Element Modelling

2.1 Engineering Data

The grade of concrete used to fill the steel tube is M60 and Steel yield strength is 345 MPa. The material properties are given in Table 1.

Table 1 Material properties

Material	Poisson's ratio	Young's modulus (MPa)	Tensile strength (MPa)	Thickness of fabric (mm)
Aramid (AFRP) [1]	0.3	118,000	2060	0.048
Basalt (BFRP) [2]	0.3	90,000	1700	0.032
Carbon (CFRP) [3]	0.3	91,700	1240	1.27
Glass (GFRP) [4]	0.28	71,000	2000	0.17
Steel	0.3	200,000	545	–
Concrete	0.2	36,662	4.82	–

Fig. 1 Column dimensions

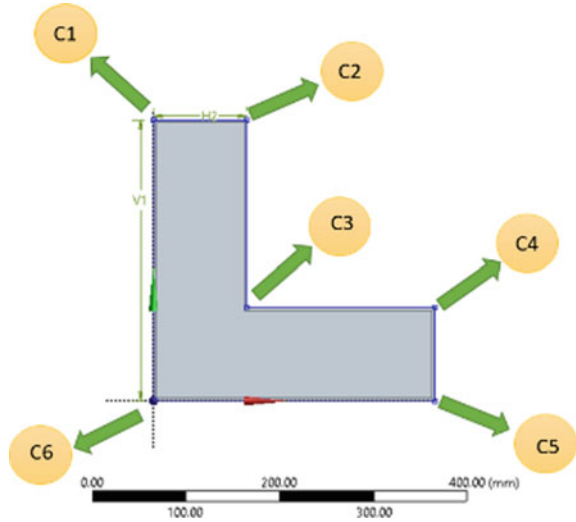
2.2 Geometry

All CFST columns were 900 mm long, with cross section shown in Fig. 1 and thickness of steel tube is 3 mm [5]. Column corners are marked in Fig. 2.

2.3 Modelling

Firstly, A total of 15 L shaped CFST columns are modeled. In this, one CFST column is modeled as control specimen. i.e, column without corrosion. It is named as Non corroded (Abbreviated as NC). The remaining 14 specimens were modeled with corrosion. Surface Corrosion is applied on the specimen as volume loss. Corrosion reduces the thickness of steel tube but density of steel remains same after corrosion.

Fig. 2 Column corners



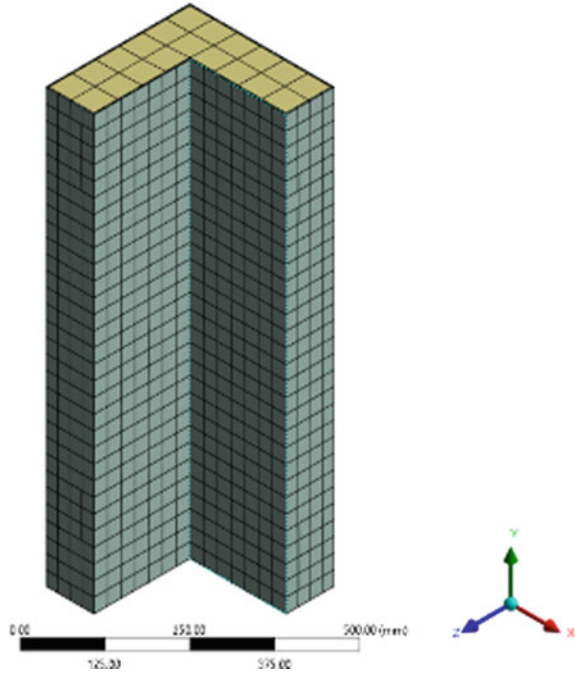
Hence volume loss is only considered in previous studies. Among these 14, 5 specimens were modeled by applying Degree of Volume loss (DoV) ranging from 0.5, 1, 1.5, 2 and 2.5% on a particular Face. DoV is applied by reducing steel thickness. Table 2 shows the thickness of steel tube lost due to corrosion on a particular Face.

3 were modeled with corrosion at 3 different positions such as top, bottom and middle on a particular face considering 2% Degree of Volume loss (DoV). Since stresses are more at corners, corner corrosion is considered for modeling 6 specimens. 2% DoV is considered and corrosion is applied on the middle position of each of the corners. The specimens are named as: specimen with corrosion on corner 1, specimen with corrosion on corner 2, specimen with corrosion on corner 3, specimen with corrosion on corner 4, specimen with corrosion on corner 5, specimen with corrosion on corner 6 and abbreviated as C1, C2, C3, C4, C5 and C6 respectively. The worst preformed specimen from the above is selected and Fiber Reinforced Polymer (FRP) wrapping is done circumferentially. 4 types of FRP are used namely AFRP, BFRP, CFRP and GFRP. The worst performed specimen is wrapped with 1, 2 and 3 layers of FRPs respectively until it reaches the strength up to Non corroded (NC). A Total

Table 2 DoV details

DoV (%)	Volume lost		
	Length (mm)	Width (mm)	Thickness (mm)
0.5	300	100	0.5454
1	300	100	1.0908
1.5	300	100	1.6362
2	300	100	2.1816
2.5	300	100	2.727

Fig. 3 Meshing of NC



of 10 specimens were wrapped. Epoxy resin is used for bonding CFST columns and the FRP.

2.4 Meshing

The model is divided into a number of Finite elements called mesh. After performing mesh sensitivity analysis here, a mesh size of 25 mm for steel and 50 mm for concrete is provided for all the CFST columns. Since concrete is crushing member a bigger mesh size than steel is given. Figure 3 shows meshing of the L shaped CFST column. Hex dominant meshing was adopted for meshing the column. Hexahedron shape was used for meshing. SOLID 186 is the element type used. It is a 20 noded 3D element.

2.5 Setup

The supports are modeled in such a way that both ends are hinged. Axial point load is applied at top of the CFST column.

3 Analysis

In this problem, static structural nonlinear analysis is considered. Displacement controlled method is used as the load method. A displacement of 5 mm is assigned to the column. The deformation and force reaction are obtained from ANSYS Workbench.

4 Results and Discussion

The load carrying capacity of the control specimen (NC) is observed as 3035.7 kN. Figure 4 shows deformation of NC. NC fails by the combination of both global and local buckling. Both the buckling is towards the outward faces. Corrosion of the steel tube reduces the confinement on the core concrete, which in turn reduces the loading capacity of the composite columns.

4.1 Degree of Volume Loss (DoV)

By Applying different Degree of Volume loss (DoV) on a Face 1 as shown in Fig. 5, the load carrying capacity of the column is observed. In all DoVs, the columns failed by the combination of both Global and local buckling but the position of local

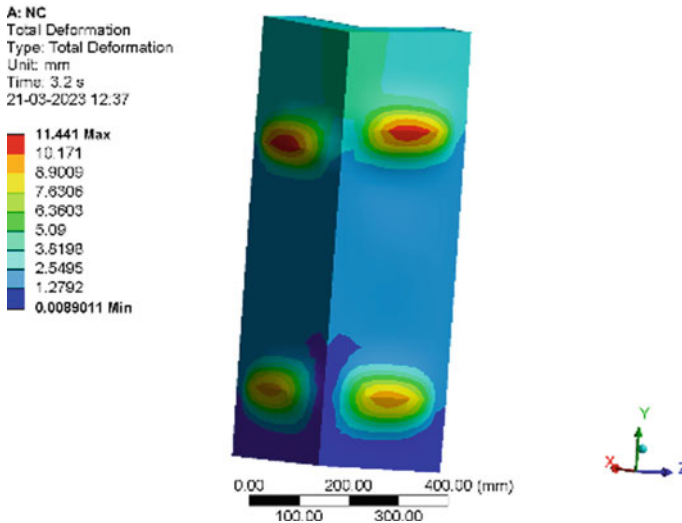
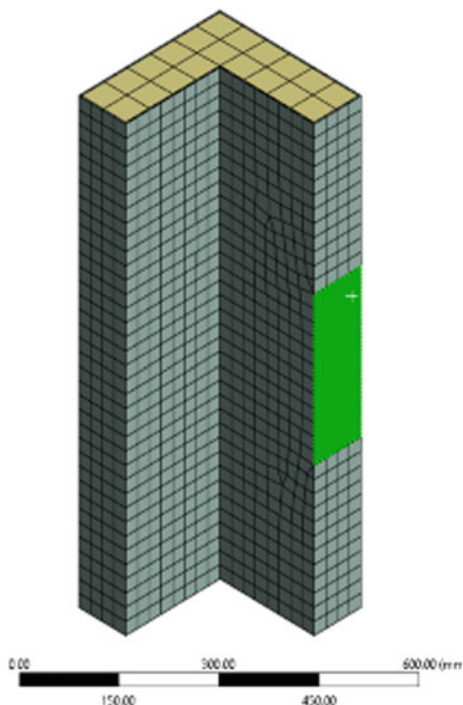


Fig. 4 Deformation of NC

Fig. 5 Corrosion at face 1

buckling varies in each case. For DoVs 0.5%, 1%, 1.5%, 2% and 2.5%, the load carrying capacities are 2886.1 kN, 2832 kN, 2826.7 kN, 2787.3 kN and 2736.1 kN respectively. The load carrying capacity of a Concrete Filled Steel Tube (CFST) column decreases as the Degree of Volume loss (DoV) increases. This is because as DoV increases, the depth of corrosion increases and the thickness of the steel tube decreases. The reduced thickness of the steel tube reduces the confinement of the concrete core, which in turn reduces the load carrying capacity of the column.

4.2 Corrosion Positions

Corrosion is applied on top, middle and bottom positions on Face 5 of the column considering Degree of Volume loss (DoV) 2% as shown in Fig. 6. Results show that corrosion at the middle is more unfavorable than at the ends. Figure 7 shows that, in the column with corrosion at the top end the local buckling is more at bottom and in column with corrosion at bottom the local buckling is more at top. However, the load carrying capacity of specimen with corrosion at top is more than specimen with corrosion at bottom. i.e., 2979.2 and 2905.5 kN. This is due to the difference in stiffness and also due to the loading conditions. Load carrying capacity of specimen with corrosion middle is 2778.1 kN and the local buckling is at the middle position

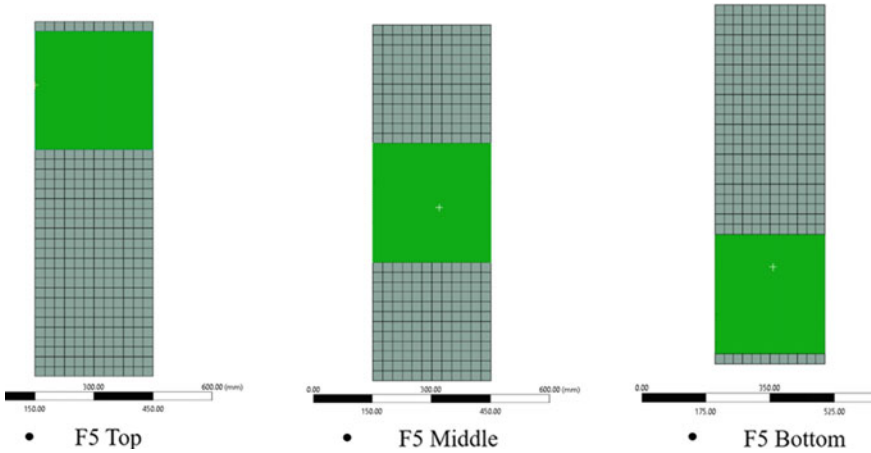


Fig. 6 Different corrosion positions on face 5

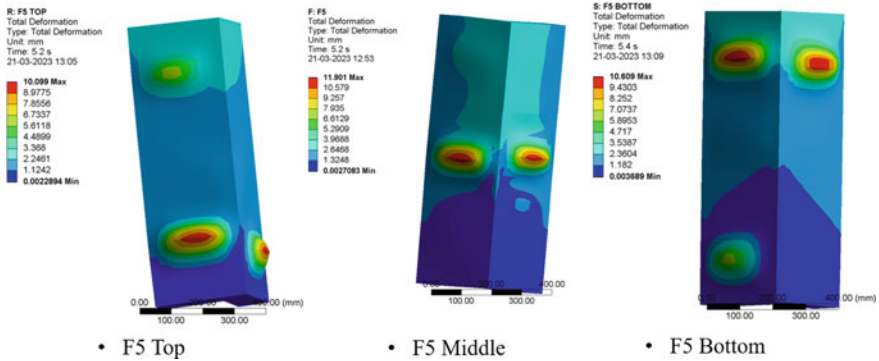


Fig. 7 Deformation of column having different corrosion positions on face 5

itself (Fig. 7). Compressive stress concentrates more at the middle compared to ends and loss of volume due to corrosion made the column unable to withstand these. Hence the load bearing capacity of the column decreased up to 8.48%.

4.3 Corrosion Locations

Since stresses are more at corners, Corrosion is applied on different corners of column considering a Degree of Volume loss (DoV) of 2% at middle position as shown in Fig. 8. Table 3 and Fig. 10 shows that Corrosion at C1 has less load bearing Capacity i.e., 2607.8 kN and C3 became the second least with 2672.7 kN load bearing capacity. C5 has the highest load carrying capacity. Since the L shaped column is unsymmetric

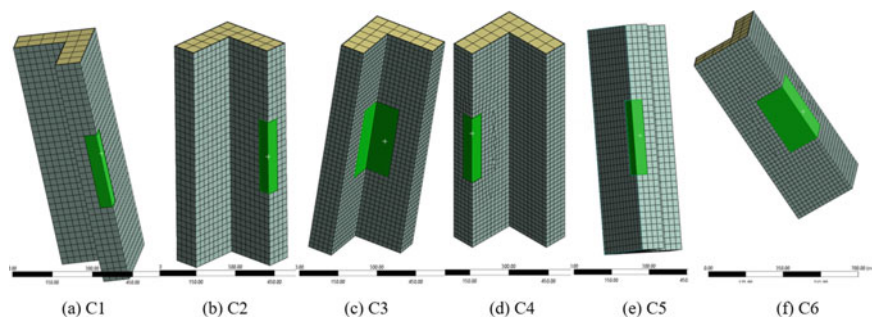


Fig. 8 Corrosion at different corners

Table 3 Percentage decrease in load due to corrosion at different corners

Name	Deformation (mm)	Load (kN)	% Decrease in load (%)
NC	11.44	3035.7	
C1	13.03	2607.8	14.096
C2	10.76	2907.6	4.220
C3	11.25	2672.7	11.958
C4	9.45	2949.2	2.849
C5	12.62	2954	2.691
C6	13.05	2879.6	5.142

in cross section, concrete-steel interaction and stiffness will be different at different locations. The differences in load bearing capacity are due to this. C1 became the worst performed model. The load bearing capacity of C1 decreased up to 14.096%.

In all the specimens buckling is the combination of both global and local buckling. However, the positions of local buckling vary (Fig. 9).

4.4 Strengthened Model

The worst performed model (i.e., C1) is wrapped with FRPs Circumferentially at 900 mm length. Comparing the load carrying capacity of specimens wrapped with 1 layer of AFRP, BFRF, CFRP and GFRP; CFRP attained more strength than non-Corroded specimen in 1 layer itself (Fig. 11). It has a load carrying capacity of 3214.2 kN, which is 5.88% more than NC. GFRP and AFRP attained strength more than corroded specimen. But couldn't attain the strength of NC. BFRP could only take a load of 1704.3 kN which is less than the strength of C1, Due to the very low thickness of the fabric.

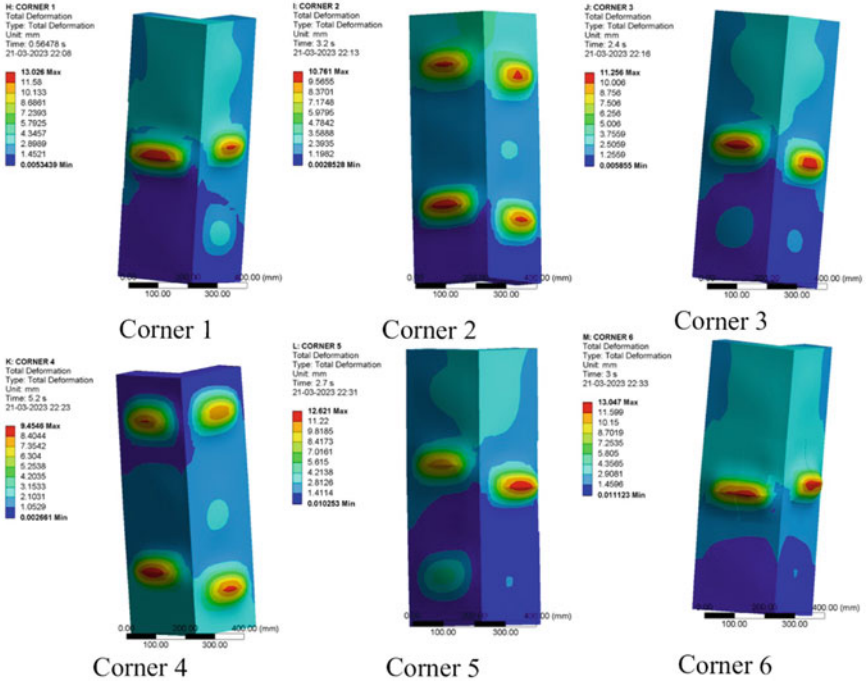


Fig. 9 Deformation of column due to corrosion at different corners

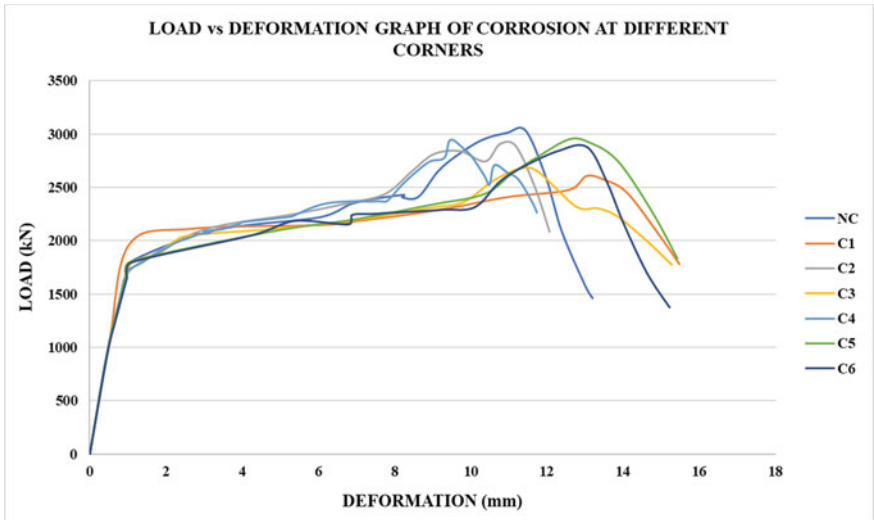


Fig. 10 Load versus deformation graph of corrosion at different corners

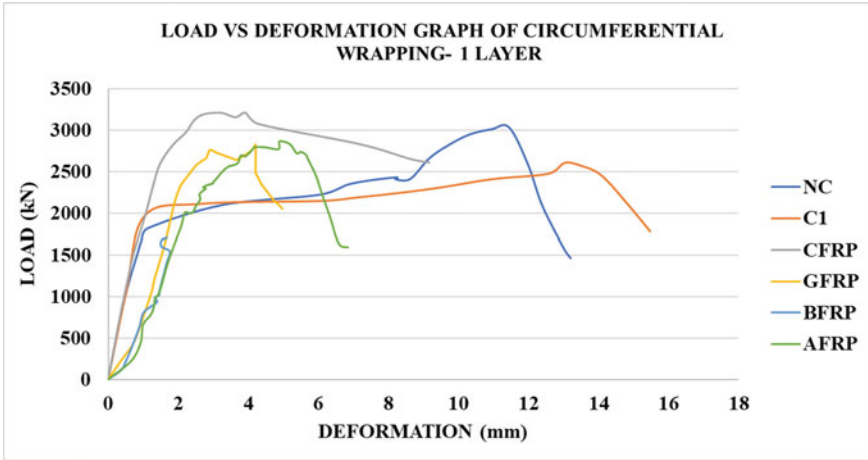


Fig. 11 Load versus deformation graph of circumferential wrapping—1 layer

On wrapping corroded columns with 2 layers of FRP, CFRP wrapping showed better results (Fig. 12). Load carrying capacity increased 36.16% than NC. GFRP attained strength of 3060.8 kN which is 0.82% more than NC, AFRP attained Strength more than C1 in 2 layers also but couldn't reach the load carrying capacity of NC. BFRP has a load carrying capacity of 2783.5 kN which is more than C1 but less than NC. Wrapping corroded column with 3 layers of AFRP increased the load carrying capacity up to 3049.9 kN which is 0.46% more than NC.

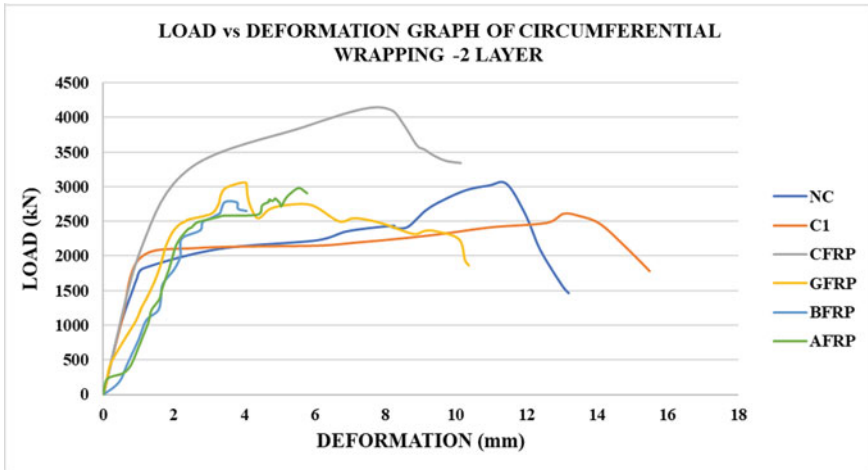


Fig. 12 Load versus deformation graph of circumferential wrapping—2 layers

Strengthening is achieved by the external circumferential wrapping of FRP sheets on the columns. Table 4 shows that CFRP wrapping showed better performance than non-corroded model and the number of layers of FRP wraps is identified as a crucial factor that governs the effectiveness of strengthening of the corroded CFST columns.

The strength of the deteriorated CFST columns can be effectively improved by wrapping FRP sheets. Figures 13 and 14 shows the deformation of a circumferential wrapped corroded column with 1 and 2 layers of FRPs respectively. Table 5 shows that the ultimate strength of the corroded CFST can be improved by 18.86% after wrapping the 1 layer of CFRP sheet. GFRP wrapping and AFRP wrapping showed better performance than non-corroded model in 2 and 3 layers respectively. The ultimate strength of the corroded CFST can be improved by 14.80% after wrapping the 2 layers of GFRP sheet and can be improved by 14.49% after wrapping the 3 layers of AFRP sheet.

FRP strengthening postponed the local buckling and reduced the stress intensity in the damage location. Thicker FRP sheets provide a stronger confinement effect to the core concrete, which can improve the strength. But in case of BFRP, 3 layers of BFRP doesn't contribute much to the load carrying capacity of BFRP. Load carrying capacity of BFRP—3 layers wrapping is less than BFRP—2 layers wrapping. This reduction in load carrying capacity is due to the over confinement around the column. Here the over confinement didn't contribute much to the increment of load carrying capacity.

Table 4 Load carrying capacity of different wrapping layers

No. of FRP layers	Load carrying capacity (kN)			
	AFRP	BFRP	CFRP	GFRP
1	2869.4	1704.3	3214.2	2822.4
2	2976.1	2783.5	4133.4	3060.8
3	3049.9	2742.2		

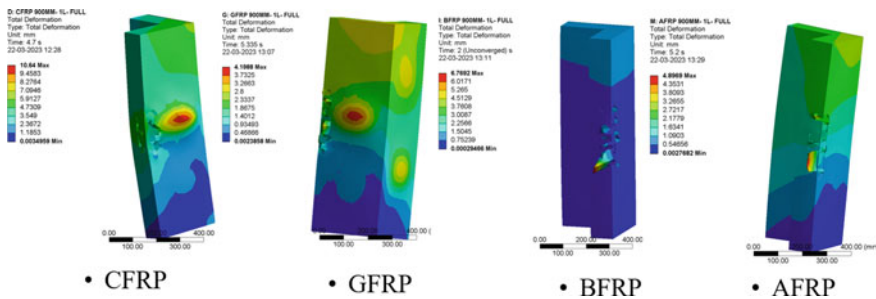


Fig. 13 Deformation of corroded column with circumferential wrapping—1 layer

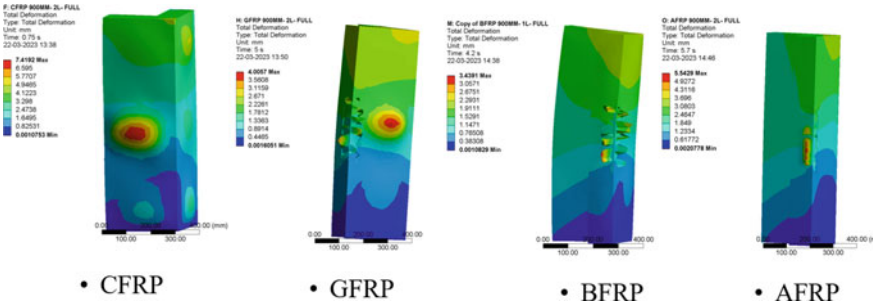


Fig. 14 Deformation of corroded column with circumferential wrapping—2 layers

Table 5 Increase in load carrying capacity

FRP	No. of layers	Load carrying capacity (kN)	% increase in load w.r.t C1 (%)	% increase in load w.r.t NC (%)
CFRP	1	3214.2	18.86	5.55
GFRP	2	3060.8	14.80	0.82
AFRP	3	3049.9	14.49	0.46

4.5 Cost Analysis

Table 6 shows the cost range of different FRPs per square meter in the Indian Market.

The Relatively low cost compared with other types of FRPs make glass fiber the most commonly used in construction industry. Aramid fibers are highly expensive compared to glass fibers and BFRP is more expensive due to scarcity in production. CFRP has excellent strength and exhibits high resistance to fatigue and creep failure between FRP composites, leading to high CFRP costs. The relatively high energy requirement to produce carbon fiber also leads to increasing costs of CFRP.

Table 6 Cost range of different FRPs [6]

Fiber type	Cost (Rs/m ²)
AFRP	850–1850
BFRP	1900–2550
CFRP	1100–2340
GFRP	140–450

5 Conclusions

These are the conclusions drawn from the study's results:

- (1) Both non corroded and corroded L shaped CFST Column fails by the combination of both global and local buckling. Both the buckling is towards the outward faces.
- (2) As Degree of Volume loss increased, Depth of corrosion increased and hence thickness of steel decreased and as a result load Carrying capacity decreased.
- (3) Corrosion site has a great impact on the load bearing capacity of the L shaped CFST Column. Corrosion at the middle position is more unfavorable than at ends. Compressive stress concentrates more at the middle compared to ends and loss of volume due to corrosion made the column unable to withstand the stress. Corrosion at Corner 1 reduces the load bearing capacity significantly. The asymmetry of column cross section resulted differences in concrete-steel interaction and stiffness at different locations.
- (4) Strengthening is achieved by the external circumferential wrapping of FRP sheets on the corroded CFST columns. FRP wrapping increases the load carrying capacity of CFST columns by providing additional confinement to the concrete core and by preventing the steel tube from buckling.
- (5) Increasing layers of FRP wraps increased the effectiveness of strengthening. However, increasing BFRP layers doesn't contribute much to load carrying capacity due to over confinement.
- (6) CFRP wrapping achieved an 18.86% increase in load carrying capacity in 1 layer itself. However, using 2 layers of GFRP wrapping seems to be economical.

References

1. Zamani-Ahari G, Yamaguchi K (2022) Experimental investigation on cyclic in-plane behavior of URM walls retrofitted with AFRP. *Case Studies Constr Mater* 17:e01558
2. Garcia-Ramonda L, Pelà L, Roca P, Camata G (2022) Cyclic shear-compression testing of brick masonry walls repaired and retrofitted with basalt textile reinforced mortar. *Compos Struct* 283:115068
3. Helal K, Yehia S, Hawileh R, Abdalla J (2020) Performance of preloaded CFRP-strengthened fiber reinforced concrete beams. *Compos Struct* 244:112262
4. Banjara NK, Ramanjaneyulu K (2017) Experimental and numerical investigations on the performance evaluation of shear deficient and GFRP strengthened reinforced concrete beams. *Constr Build Mater* 137:520–534
5. Wang Y, Guo L, Li H (2021) L-shaped steel-concrete composite columns under axial load: experiment, simulations and design method. *J Constr Steel Res* 185:106871
6. <https://www.indiamart.com/proddetail/frp-raw-materials-9460134691.html>

Study of Seismic Evaluation and Development of Innovative Curved Lateral Bracing System



C. S. Ansiya and E. K. Amritha

Abstract This study focuses on the seismic evaluation of an innovative high energy dissipative curved lateral bracing system. Unlike ordinary bracing systems, the system developed in the present study does not produce buckling, making it highly yielding, ductile, with greater load carrying capacity. The system showed appropriate initial stiffness, making it an ideal solution for structures in earthquake-prone areas. The research aims to determine the optimal thickness of the bracing and investigate the effect of span ratio on the performance of the proposed system. In addition, the study compares the performance of the proposed system with and without OGrid bracing, as well as variations in the frame and pattern of bracing. The results show that the OGrid bracing provides better performance than other bracings. The analysis of the proposed system was carried out using ANSYS Workbench 2022 R2, a finite element software tool commonly used for structural analysis. From the analysis it was found that OGrid-I bracing exhibited good ductility and load-carrying properties compared to other types of bracing. Overall, the innovative high energy dissipative curved lateral bracing system with OGrid bracing holds great promise for seismic evaluation and the findings from this project can contribute to the development of safer structures in earthquake-prone regions.

Keywords OGrid bracing system · Buckling · Curved lateral braces · Ductility · Energy dissipation · ANSYS · Lateral bracing system · Welded connection · Steel frames

1 Introduction

Seismic evaluation and the development of innovative curved lateral bracing systems are crucial considerations in earthquake engineering. The occurrence of earthquakes can lead to significant structural damage to buildings and in severe cases, even to their collapse. To minimize such damage and ensure the safety of occupants,

C. S. Ansiya (✉) · E. K. Amritha
Universal Engineering College, Thrissur, Kerala, India
e-mail: anziyasirajj@gmail.com

© The Author(s), under exclusive license to Springer Nature Switzerland AG 2024
M. Nehdi et al. (eds.), *Proceedings of SECON'23*, Lecture Notes in Civil Engineering
381, https://doi.org/10.1007/978-3-031-39663-2_17

221

seismic evaluation and retrofitting of existing buildings is essential. Lateral bracing systems are commonly used in buildings to resist lateral loads induced by earthquakes. Conventional lateral bracing systems use straight braces which can limit the architectural design of a building. In this paper an innovative curved lateral bracing systems have been developed. These systems use curved braces that not only provide lateral resistance but also enhance the structural performance of the building [1]. The OGrid bracing system which utilizes circular or elliptical-shaped braces, is an emerging approach to enhancing the seismic performance of buildings. Unlike traditional bracing systems, the OGrid bracing system is a continuous bracing type in a round shape that offers several advantages, such as improved ductility, stiffness, and stability [2]. During an earthquake, the lateral load resisting system with OGrid bracing provides the appropriate ductility and stability required to prevent structural collapse. While several authors have investigated the effect of different bracing systems on seismic and dynamic performance, Boostani [2] was the only author to introduce the concept of the OGrid bracing system. However, the shape of the frame used in that project was square, and the shape of bracing was circular.

This paper aims to provide a detailed description of the optimum thickness of bracing and the variation in frame shape and pattern of bracings. Additionally, the study compares frame designs with and without OGrid bracing systems using analytical investigation. The methodology used in this research involved modeling and analyzing the OGrid-I specimen using the ANSYS software, which is widely used for engineering simulations. Steel bracings were utilized in the study, and the results obtained were analyzed for their significance in enhancing the seismic performance of buildings. The study's findings could help to inform the development of more effective and efficient bracing systems in seismic-resistant building design. This paper provides a valuable contribution to the field of seismic evaluation and the development of innovative curved lateral bracing systems. By investigating the OGrid bracing system and comparing different thicknesses and patterns of bracings, this study advances the understanding of how to improve the seismic performance of buildings and protect occupants during seismic events.

1.1 Objectives

The main objectives of this paper is to analyze the performance of the proposed system under seismic loading and to investigate the effects of several factors, including the optimum thickness of bracing, variation in the frame, and variation in the pattern of bracings. Additionally, the project aims to compare the performance of the framed structure with and without the OGrid bracing system.

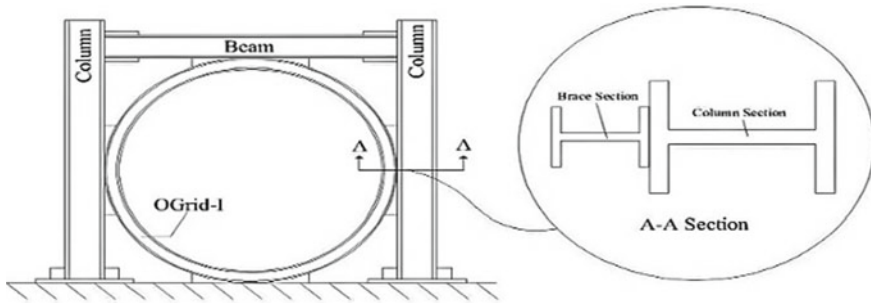


Fig. 1 Schematic representation of OGrid-I bracing system [2]

2 OGrid-I Bracing System

The O-Grid bracing system is a type of circular lateral bracing used in building construction to provide lateral stability and resistance against wind and seismic forces. The term “OGrid-I” refers to the shape of the brace section used, which is I-shaped bracing and features a series of “O-grids” along its length. This system is typically used in steel-framed buildings to resist lateral loads such as wind and seismic forces. The OGrid-I Bracing System is known for its high strength-to-weight ratio, making it an efficient solution for building bracing [1] (Fig. 1).

OGrid-I Bracing System is characterized by rigid beam-column connections, and circular shaped braces that are connected to the beams and columns using 6 mm thick connection plates welded to them [2]. It is a popular choice for building designers and engineers who are looking for a reliable and effective way to enhance the stability and safety of their structures. Additionally, it can be easily integrated into the building’s architectural design, offering an aesthetically pleasing appearance.

3 Numerical Modelling

The numerical finite element analysis was performed on OGrid bracing system. Finite element modelling of specimen is developed in ANSYS Workbench 2022 R2 to predict their seismic behavior. The element type that was used in this analysis is Solid 186 which is a 20-node solid element that provides high accuracy for stress and strain calculations. To ensure accurate results, a fine mesh was used, which means that the OGrid-I bracing was divided into a large number of small, individual elements. The mesh size has been determined through mesh sensitivity analysis, which involves running the simulation with different mesh sizes and comparing the results. The mesh size of 100 mm has been chosen for the frame, and 75 mm for the OGrid bracing.

4 Parametric Study

A parametric study is conducted to evaluate the effect of optimum thickness of OGrid bracing system. The material used in the proposed system is fe345. ISWB 450 and ISMB 400 sections were used for column and beam of the frame respectively. The dimensions and properties of the beams and columns of all specimens are shown in Table 1 [3] and the material properties of the circular bracing used in ANSYS are shown in Table 2.

4.1 Optimum Thickness of Bracing

The thickness of OGrid bracing for a structural frame was designed as per the guidelines outlined in IS code [4]. Five models were then created using various bracing thicknesses specified in the code, ranging from 6 to 12 mm, and compared against a “bare” frame without bracing (Figs. 2 and 3).

The performance of each model was evaluated under load carrying capacity, deflection and ductility were measured to determine the most effective bracing thickness for enhancing the structural integrity of the frame (Figs. 4 and 5).

The 6 mm thickness of bracing exhibits higher ductility but lower load carrying capacity. This means that the bracing is able to undergo deformation, but may not be able to withstand heavy loads. The 12 mm thickness of OGrid bracing is too stiff and has decreased deformation capability, resulting in lower ductility. This suggests that the 12 mm thickness may not be able to undergo sufficient deformation to absorb and dissipate energy during seismic events (Fig. 6).

The deformation of the 12 mm thickness is 150.02 mm, which is lower than the “bare” deformation. Bare means frame without bracing. This indicates that the 12 mm thickness of bracing is not effective in improving the structural behavior under seismic loading. However, the deformation of the 10 mm thickness is 176.04 mm,

Table 1 Dimensional details of the structural elements [3]

Structural elements	Section property	Depth (mm)	Width of the section (mm)	Thickness of web (mm)	Thickness of flange (mm)
Column	ISWB 450	450	200	9.2	15.40
Beam	ISMB 400	400	140	8.90	16

Table 2 Material properties

Youngs modulus (E)	Yielding stress (f_y)	Poisson's ratio of Steel (ν)	Density of steel (kg/m^3)
2.1×10^5 MPa	250 MPa	0.3	7850 kg/m^3

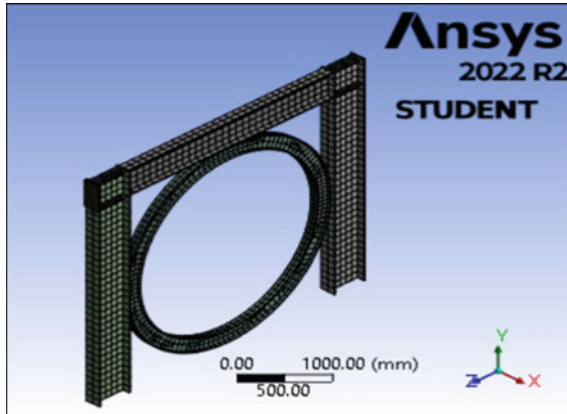


Fig. 2 Meshing of the specimen

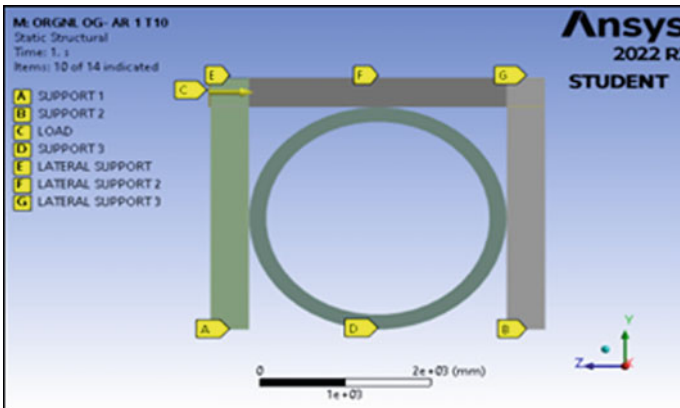


Fig. 3 Boundary condition of the specimen

which is higher than the bare deformation. This suggests that the 10 mm thickness of bracing is effective in improving the structural behavior under seismic loading (Table 3).

The yield displacement is measured based on the point at which the material or structure reaches its yield stress. Ductility displacement is evaluated by determining the ratio between the yield displacement and the ultimate displacement. The load carrying capacity of the structure is improved with the use of 10 mm thickness of OGrid Bracing system. The system is able to resist lateral loads and distribute them throughout the structure, thereby reducing the stress on individual members and also exhibits good ductility. Based on the analysis of the various thicknesses of bracings, it has been concluded that the optimum thickness of bracing is 10 mm. It provides better performance in both load capacity and ductility. This suggests that

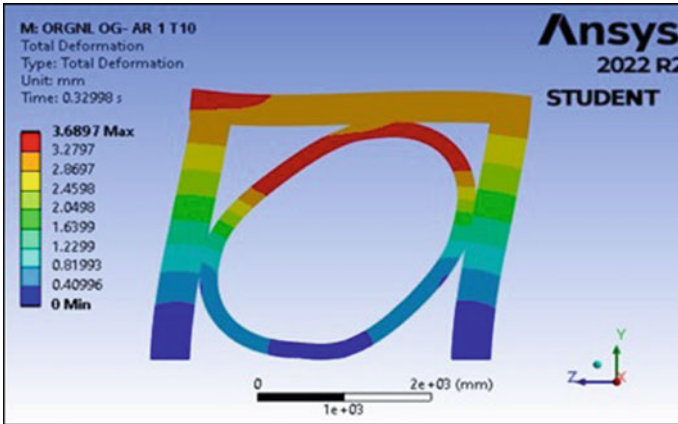


Fig. 4 Total Deformation of the specimen

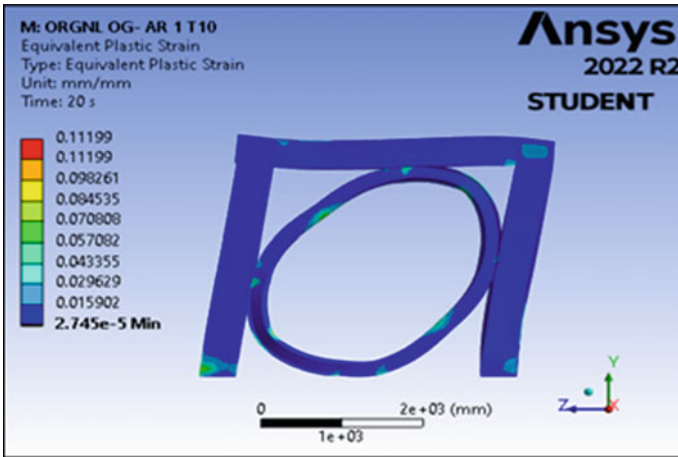


Fig. 5 Plastic strain of the specimen

this thickness is able to withstand greater loads while still allowing for deformation and ductility in the bracing. Therefore, the use of 10 mm thickness of OGrid Bracing system is recommended for seismic design of structures.

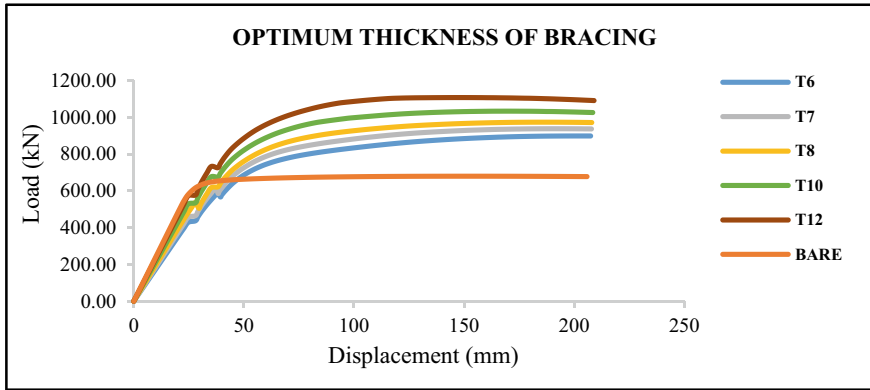


Fig. 6 Load displacement graph of OGrid bracing of various thickness

Table 3 Result Obtained from the analysis of OGrid with varying thickness of bracing

Models	Deflection (mm)	Load (kN)	Increase load (%)	Yield displacement (mm)	Ductility displacement
Bare	156.31	680.26	1	8.7029	17.960679
T6	204.33	899.22	30.7210031	22.724	8.9918148
T7	191.09	938.55	37.97	22.718	8.4113918
T8	187.01	974.23	43.2143592	22.714	8.2332482
T10	176.04	1034.2	52.0301061	22.703	7.7540413
T12	150.02	1108.2	62.9082997	24.76	6.0589660

5 Effect of Span Ratio in Curved Lateral Bracing System

The span ratio of a structural system is an important factor that affects its overall stability and resistance to lateral loads such as wind or earthquake. The pattern of bracing and frame will vary as the span ratio of ogrid bracing changes. In this study, five models of OGrid bracing system and five models of without OGrid bracing were compared, with a fixed thickness of 10 mm for the bracings. The aspect ratio of the frame was varied between 1, 1.5, 0.2, 0.75, and 0.6, as shown in Table 4. The effectiveness of the bracing system was evaluated based on the comparison of lateral deflection and overall stability of the models (Figs. 7, 8 and 9).

Figure 7 shows the model of the frame with and without the OGrid bracing system. The model with an aspect ratio of 1.5 was found to be the most effective model due to the variation in cross-section of the bracing (Figs. 10 and 11, Table 5).

The load carrying capacity was found to be greater in frames with OGrid bracing compared to frames without bracing. In terms of ductility, the frames with OGrid bracing showed more ductility compared to frames without bracing.

Table 4 Models of OGrid bracings system with varying span ratio

With OGrid bracing	Without OGrid bracing
OG L/H (1/1)—aspect ratio = 1.00	L/H (1/1)—aspect ratio = 1.00
OG L/H (3/2)—aspect ratio = 1.50	L/H (3/2)—aspect ratio = 1.50
OG L/H (4/2)—aspect ratio = 0.20	L/H (4/2)—aspect ratio = 0.20
OG L/H (3/4)—aspect ratio = 0.75	L/H (3/4)—aspect ratio = 0.75
OG L/H (2/3)—aspect ratio = 0.60	L/H (2/3)—aspect ratio = 0.60

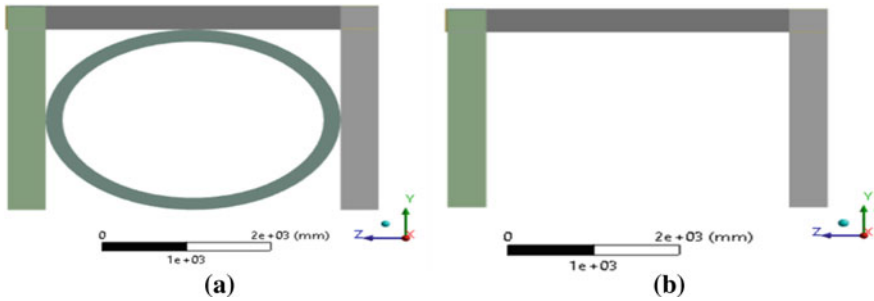


Fig. 7 Models of L/H (3/2) aspect ratio—1.5 **a** with OGrid bracing **b** without OGrid bracing

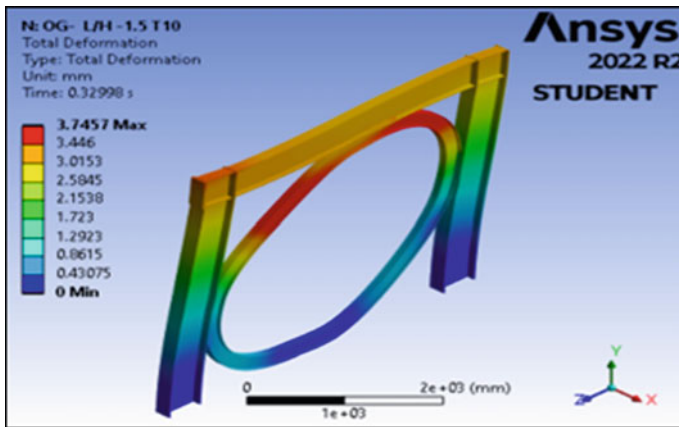


Fig. 8 Total deformation of OGrid—L/H (1.5)

5.1 Results and Discussion

The results of the study showed that the load carrying capacity was found to be greater in frames with OGrid bracing compared to frames without bracing. The deflection was greater in the frame without bracing for varying aspect ratios of the frame, except

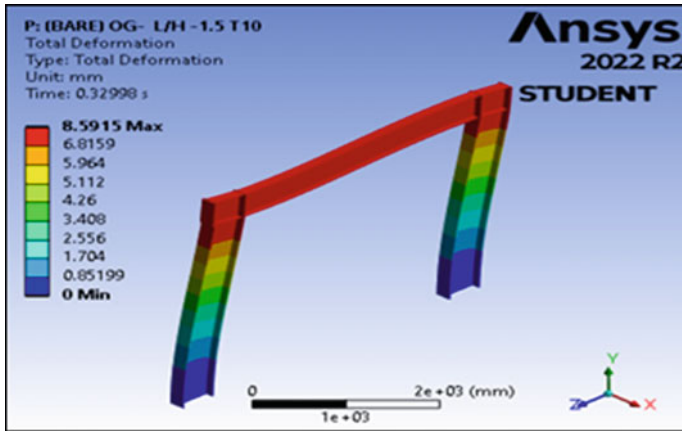


Fig. 9 Total deformation of L/H (1.5) frame

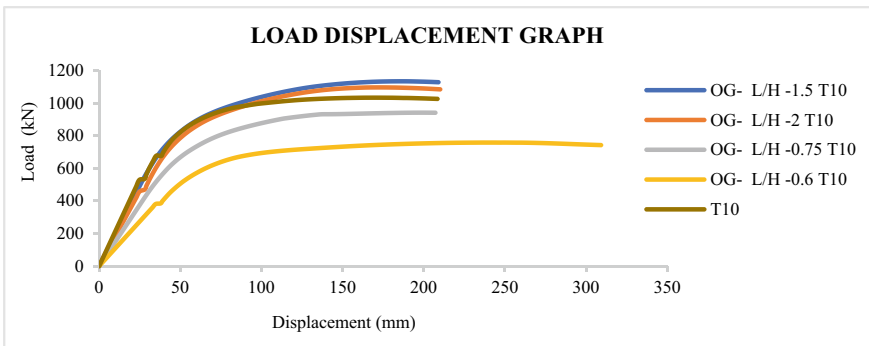


Fig. 10 Load displacement graph of frame with OGrid bracing

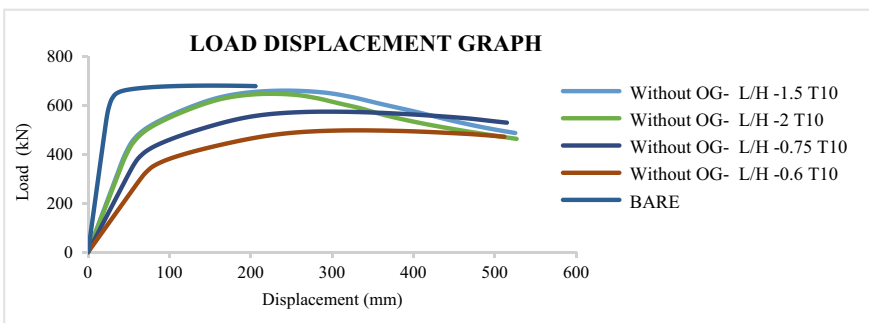


Fig. 11 Load displacement graph of frame without OGrid bracing

Table 5 Result obtained from the analysis of OGrid bracings with varying span ratio

Models	Deflection (mm)	Load (kN)	Increase load (%)	Yielding (mm)	Ductility
OG L/H –1 T10	176.04	1034.2	52.0301061	22.703	7.754041
L/H 1 T10	143.95	679.83	1	8.7029	16.54046
OG L/H –1.5 T10	187.82	1134.70	41.8612849	24.83	7.564236
L/H –1.5 T10	243.84	659.7	1	44.138	5.524491
OG L/H –2 T10	173.88	1097.20	41.0490339	24.882	6.988184
L/H –2 T10	225.89	646.81	1	44.254	5.104397
OG L/H –0.75 T10	198.8	942.12	39.0905617	30.85	6.444084
L/H –0.75 T10	293.03	573.84	1	51.51	5.688798
OG L/H –0.6 T10	243.84	758.43	34.411877	34.848	6.997245
L/H –0.6 T10	332.55	497.44	1	56.402	5.896067

in the case of OGrid bracing of aspect ratio one. This means OGrid bracing can effectively reduce the deflection of a structural frame, which is a desirable quality for a stable and resistant structural system. However, the effect of OGrid bracing on deflection may depend on the aspect ratio of the frame, as the deflection was not reduced in the case of OGrid bracing with an aspect ratio of one. Among the different aspect ratios tested, aspect ratios of 1.5 and 2 showed the highest load carrying capacity. This indicates that the use of OGrid bracing is an effective way to improve the load carrying capacity of a structural frame.

The study also found that the effective model for OGrid bracing was the model with an aspect ratio of 1.5. This is because the cross-section of the bracing varies, and as the span increases, the stiffness of the bracing increases, resulting in the shape of the bracing becoming elliptical or oval. This change in shape improves the load carrying capacity of the frame. The study suggests that the pattern of bracing and frame will vary as the span ratio of OGrid bracing changes, and the use of OGrid bracing can significantly improve the stability and resistance of a structural system to lateral loads.

6 Conclusions

Based on the analytical study, the optimum thickness of the curved lateral bracing system is 10 mm. It provides better performance in both load capacity and ductility. This suggests that this thickness is able to withstand greater loads while still allowing for deformation and ductility in the bracing. Therefore, the use of 10 mm thickness of OGrid Bracing system is recommended for seismic design of structures.

The effect of span ratio on the OGrid bracing system has also been investigated. It has been found that aspect ratios of 1.5 and 2 provide greater load carrying capacity compared to aspect ratios of 1, 0.75, and 0.6. Additionally, the OGrid bracing system with aspect ratio of one provides the highest level of ductility. Based on the results of the analysis, it was found that the OGrid bracing system was more effective in reducing lateral deflection and improving overall stability compared to the models without OGrid bracing.

In this paper the use of OGrid bracing is an effective way to improve the load carrying capacity and ductility of a structural frame. The model with an aspect ratio of 1.5 was found to be the most effective due to the variation in the cross-section of the bracing. The results of this project can be used to design more efficient and effective structural frames for seismic-resistant construction.

References

1. Rezaifar O, Gholhaki M (2018) Introduction and seismic performance investigation of the proposed lateral bracing system called OGrid. *J Struct.* <https://doi.org/10.1016/j.acme.2018.02.003>
2. Boostani M, Rezaifar O, Gholhaki M (2022) Experimental investigation of a new lateral bracing system called OGrid under cyclic loading. *J Struct.* <https://doi.org/10.1016/j.istruc.2021.11.015>
3. Reddy VR, Krishna KV (2018) Comparative study in performance of steel buildings in various seismic zones of India. *Int J Civil Eng Technol (IJCIET)* 9(6)
4. IS 1730 (1989) Steel plates, sheets, strips and flats for structural and general engineering purposes-dimensions

Assessment of Structures with Floating Column on Sloping Ground Against Seismic Load



Yaman Hooda  and Pradeep K. Goyal

Abstract The rate of construction has seen a tremendous growth in the hill-dominated topographical areas. The structures that are been constructed in the hilly areas are focusing on increasing the space at different storey levels than the usual ones, for the purpose of parking or serve as a community hall for various applications. But, one has to be very specific in designing of those buildings as the placement of the structural members (beams and columns) directly affects the strength and stiffness of the structures. With increasing tourism in the hilly areas, people are constructing the buildings with the concept of floating columns, unaware of its effects in case of seismic environment. In context to Indian topography, these areas fall under the category of highly prone seismic zones. This study will be focusing on the analysis of the structures constructed on the hill slopes with the provision of floating columns at different storey levels against seismic loads. With keeping in mind of increasing trend of constructions, different models are considered with varying sloping angle. The analysis tool used in this analysis is ETABS 20 Ultimate. Different models will be analyzed of same structural dimension with varying slope angles and discussion will be focused on feasibility of providing floating columns in high-rise structures on sloping ground. The seismic considerations are followed as per the Indian standard guidelines of IS 1893 (Part I): 2016.

Keywords Floating column · Vulnerability analysis · Sloping ground · Vertical irregularity · Pushover analysis · ETABS

Y. Hooda (✉) · P. K. Goyal
Department of Civil Engineering, Delhi Technological University, New Delhi, India
e-mail: yamanhooda_2k20phdce05@dtu.ac.in

P. K. Goyal
e-mail: pkgoyal@dtu.ac.in

1 Introduction

With the recent advancements and increasing rate of urbanisation in the domain of civil engineering, the people associated with the background of architecture and structural engineering are making continuous effort for providing enhanced facilities in a building, without compromising with its functional and aesthetics requirements. One of many common requirements applicable for both the commercial and residential structures in present era is the provision of open-space for different applications including parking, organising functions or meetings. The civil professionals researched and came to the easiest conclusion of provision of floating columns in different parts of a building, wherever the same is required and necessary [1]. As per the specifications of IS 1893-2016 (Part-I), a floating column may be defined as a normal column structural element, with its irregularity in positions at different storey levels, thus considered to be a category of “Vertical Irregularity” in structures [2]. The structural behaviour of the floating column can be understood as a point load acting on a beam. In keeping the above consideration, one must also focus on the lower resistance of the structures against the action of lateral loads [3]. Thus, the study regarding the assessment of the behaviour of the structure against lateral loads must be carried out. The situation becomes more serious when the floating columns are provided for the structure located on the sloping grounds. With different studies conducted earlier, it had been noted that even in the normal building without any plan irregularities, the structures on the sloping ground were affected more as compared to that of located on the planer surface [4]. Also, it has been noted that as the sloping angle increases, the structures get more vulnerable towards the action of the lateral forces [5].

From the latest findings of The World Economic Forum, it can be observed that there is an increase in the occurrence rate of Geo-Physical categorized disasters, which includes seismic activity. The outcomes of a seismic activity in an area result in the extensive loss of property and lives, and the severity of this loss is more when the structures are located on the hill slopes. Another thought considered while doing the study is the structures that are constructed prior to the revision in the codal provisions are more susceptible to the seismic activities as the same weren't be designed or analyzed as per the latest guidelines in the codal provisions. This study is focusing on determination of the behaviour of the structures located on the hill slopes, with varying sloping angles, when having floating column-based vertical irregularity. The study conducted by Ibrahim and Askar [6] concluded that with the provision of floating column in a G + 10 storeyed structure, the displacements observed are more as compared to the normal structural plan. The structural behaviour of the buildings situated on the sloping ground against seismic activities are analytically analysed for the determination of the structure's response dynamically [7]. When the structures located on the hill slopes with varying sloping angle from 0 to 60°, it had been observed that these structures experience a larger extent of damage [8]. This study uses ETABS 2020 ultimate edition as an analytical tool, correlating the trend of the application of different versions of STAADPro and SAP 2000 used for the analysis

and design purposes [9–11]. The building performance level of the structures are determined on the basis of the advanced analysis of the structures. The stage of advanced analysis of the structure includes the determination of the behaviour of the structure under the action of gravity loads as well lateral loads, along with the formation of plastic hinges in both structural components of beams and columns at every storey level [12]. It will be interesting to determine the combined effect of the seismic analysis of the structures with the presence of floating columns at different storey levels.

2 Methodology and Analysis

The study involves the analysis of the structures on sloping ground, with varying sloping angle from 0 to 30°; the range of angle decided as per the literature survey conducted which shows noteworthy results in this range. A building plan of 12 m × 12 m is used for the analysis to carry out the model-study behind the problem taken. G + 3 storey structure is considered with the grade of concrete M25 for the columns (400 mm × 450 mm) and beams (300 mm × 350 mm); and M20 for slab, having a thickness of 120 mm. The analytical tool chosen for the conduction of the study is ETABS 20 Ultimate. 20 models of various conditions are considered, listed in Table 1 (Fig. 1).

Floating columns in the models are provided in such a way that while considered the same, all the interior columns had been eliminated and only the effect of loading is considered on the exterior columns. The gravity loads taken on every structural members are in accordance with the Indian Standard Codal Provision of IS 875 (Part I) [13] for Dead Load and IS 875 (Part II) [14] for Live Load calculations and applications on the structural members. For the comparative analysis purpose,

Table 1 Models considered for the study

Model description	0° sloping angle	10° sloping angle	20° sloping angle	30° sloping angle
With no floating column	M0-0	M10-0	M20-0	M30-0
Floating column at ground level	M0-G	M10-G	M20-G	M30-G
Floating column at first level	M0-F	M10-F	M20-F	M30-F
Floating column at second level	M0-S	M10-S	M20-S	M30-S
Floating column at third level	M0-T	M10-T	M20-T	M30-T

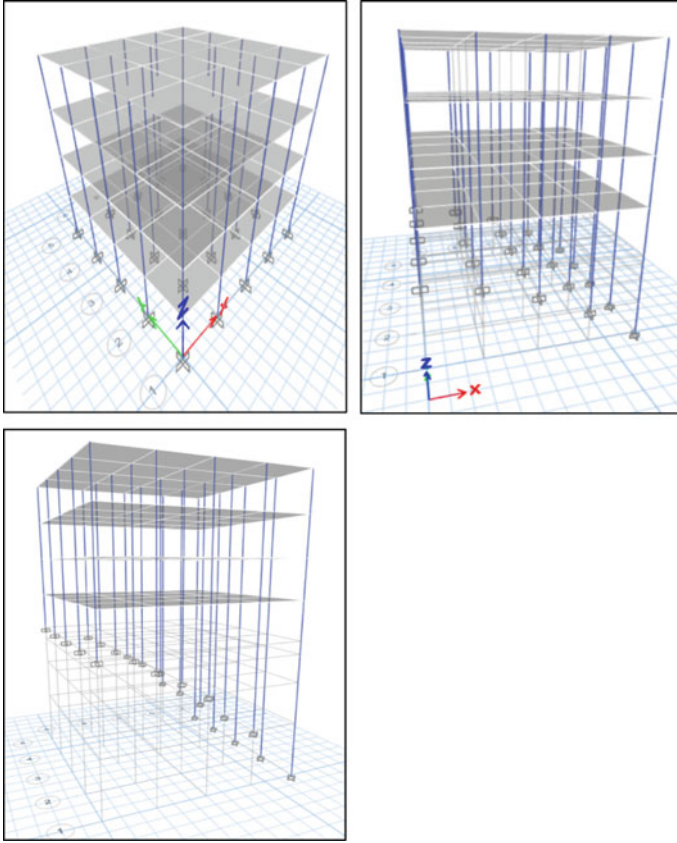


Fig. 1 M0-0, M0-10 and M0-20 models in ETABS workspace

the structural dimensions of the structural elements are kept constant. The slab is considered as a “thin-shell” membrane while assigning the properties of the same in ETABS. Separate load cases are formed for the consideration of earthquake loading on the structure as per the codal guidelines stated in IS 1893: 2016 (Part I).

The structures considered for the analysis are located on the sloping grounds, the parameters considered for the seismic analysis are as per the IS codal guidelines of IS 1893: 2016 (Part I) as “Zone V” for seismic zone and “Hard” is taken as the soil type. The type of the structure for the analysis is categorized as SMRF (Framed Structure) and thus, the value ‘5’ is taken as Reduction Factor. The importance factor is taken as ‘1’ since the category of the structure falls under “Normal Structure”. The study includes the analysis, divided into two stages. The first stage of analysis includes the modelling and application of the gravity loads on the structural members. Load cases are formed and then, modal load case is created before the application of the load on the structure for considering the effect of seismic effect on the same. Once the first stage of the analysis is completed, the second phase of the analysis is conducted,

which is based on consideration of P-Delta Effect and plastic hinge formation. The load factors considered for performing the P-Delta effect on the structures is 1.2 each for Live Load and SuperDead Load; and 1.5 for Dead Load. SuperDead Load is a load taken for consideration of load for floor finish.

After the Pushover Analysis is conducted, the next stage is to determine the Building Performance Level of each structure. The structure is divided into three different performance levels as Life Safety (LS); Immediate Occupancy (IO) and Collapse Prevention (CP). If any of the structural element crosses the CP level, then the same is of primary concern and thus, either have to retrofit or replace by a new structural element. The study will be focusing on the determination of the Building Performance Levels of all the models considered and the comparison will also be made in the same aspect. Recommendation will be provided as for the retrofitting aspects.

3 Results and Discussions

After performing the analysis on the software with all the calculations and considerations from the IS codes, the results are framed for the most important parameters through which the behaviour of the structure can be determined in different modes, Storey Displacements and Storey Drift. 'X' can be considered for the direction in which the sloping angles are provided and the transverse direction in planar configuration is considered to be 'Y' direction. It had been observed that for M0 models, the values of maximum displacement in increases till second storey and then decreases for the top storey for 'X' direction and, in contrast, the values of maximum displacement in decreases till second storey and then increases for the top storey for 'Y' direction. For M10, the maximum value for displacement is observed for normal model and floating column at top floor for 'X' and 'Y' both. For the sloping angle of 20°, the maximum displacement is observed for the case when floating column are provided at 2 and 3 storey, with no floating column also for 'X' and similar trend is observed for 'Y', excluding the case of provision of no floating column in the structure. For M30 model configuration, the maximum displacement in observed at top storey for both 'X' and 'Y' (Figs. 2 and 3).

In case of storey drift, the results observed are quite interesting. For M0-0, M0-F, M0-T the maximum drift is observed at Storey 2 and observed at Storey 1 for M0-G; Storey 3 for M0-S. But, when the sloping ground is considered for the analysis purpose, it had been observed that when the maximum storey drift is observed at base level for 10° sloping angle for all the cases considered for provision of floating column. On the same grounds, the same trend is observed for 20 and 30° sloping angle. The results obtained for the maximum storey drift is summarized as shown in Table 2.

The last stage is to determine the Building Performance Level. After the application of Pushover Analysis, the structural elements of the models considered can be visualized in categorization of three levels. These categorizations can be represented

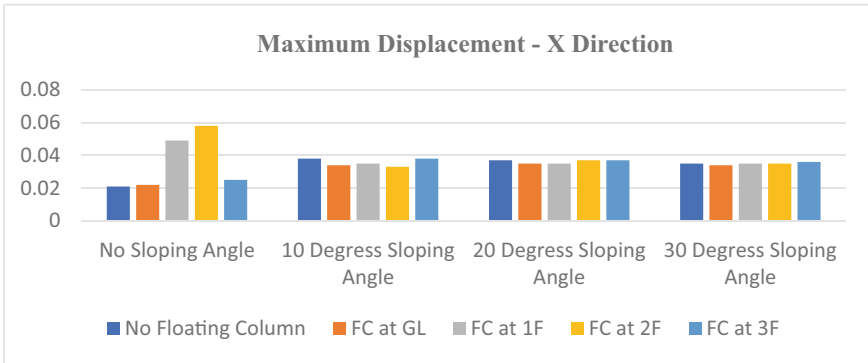


Fig. 2 Maximum displacement observed for different cases of provision of floating column for ‘X’

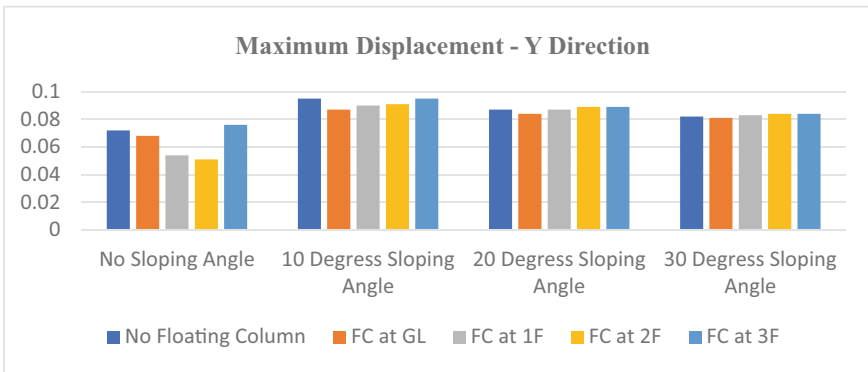


Fig. 3 Maximum displacement observed for different cases of provision of floating column for ‘Y’

Table 2 Results obtained for maximum storey drift

Type of structure	M0	M10	M20	M30
No floating column	Storey 2	Base level	Storey 1	Storey 1
Floating column at ground level	Storey 1	Base level	Base level 2	Base level 2
Floating column at first level	Storey 2	Base level	Storey 1	Storey 1
Floating column at second level	Storey 3	Base level	Storey 2	Storey 2
Floating column at third level	Storey 2	Storey 3	Storey 4	Storey 4

by different colour dots on the structural elements. The structural elements that falls beyond the “CP” benchmark are of most concern and as stated earlier, needs to be removed or retrofitted as per the current situations of the structural elements. For verification of the results, one may use the different options available of performing

Table 3 Building Performance Levels observed after performing Pushover Analysis

Type of structure	Between IO–LS level	Between LS–CP level	Above CP level
M0-0	–	–	–
M0-G	–	–	–
M0-F	–	–	–
M0-S	1	2	3
M0-T	–	–	–
M10-0	–	–	–
M10-G	–	–	–
M10-F	–	–	–
M10-S	5	2	1
M10-T	6	2	2
M20-0	–	–	–
M20-G	–	–	–
M20-F	–	–	–
M20-S	6	3	1
M20-T	8	3	2
M30-0	–	–	–
M30-G	–	–	–
M30-F	2	–	1
M30-S	10	5	3
M30-T	8	6	2

NDTs and correlating the same [15]. The results obtained for Building Performance Level is listed as shown in Table 3.

4 Conclusion

The following conclusions were made after conduction of the study:

For considering the direction in which different storey levels are provided—“X”:

- For the case of no sloping ground, the maximum storey displacement is observed for case of floating column provided at second floor.
- For the case of 10° sloping ground, the maximum storey displacement showed a similar trend for all the cases; still the maximum is observed for the case of no floating column and floating column provided at third floor.
- For the case of 20 and 30° sloping ground, the maximum storey displacement is observed similar values for all the cases taken.

For considering the transverse direction to which different storey levels are provided—“Y”:

- For the case of no sloping ground, the maximum storey displacement is observed for case of floating column provided at third floor.
- For the case of 10° sloping ground, the maximum storey displacement showed a similar trend for all the cases; still the maximum is observed for the case of no floating column and floating column provided at third floor.
- For the case of 20 and 30° sloping ground, the maximum storey displacement is observed similar values for all the cases taken.

It was observed the magnitude of storey displacement is maximum in the direction transverse to the direction to which different storey levels are provided. For determination of maximum storey drift for different cases, it can be noted that most of the values are found to be maximum for the Base Level and other storey levels above/below to it inclusively for the cases of providing floating column at ground level, first floor and second floor. For the situation of provision of floating column at third level, as the sloping angle increases, the maximum storey drift was observed with increasing storey levels. After performing the Building Performance Levels, it had been noted down, Maximum columns need to be retrofitted or get replaced is for M30-S.

Thus, while providing an open space, one needs to be very careful in removing of the structural elements. For the situation of providing the open space for the structures on sloping grounds, the placement of the floating columns needs attention in the direction transverse to the direction of the sloping ground. Also, with the results obtained, it can be noted that the space for open area must be avoided at ground level and first floor level. In regards to the Building Performance Level, more structural members fall under the category “Beyond CP” for the sloping ground of angle 30°. The future scope of the study may include the removal of floating column at every storey level and then, recommendations can be made depending upon the results obtained.

References

1. Martin WY, Malhotra M (2021) A comparative analysis on the seismic response of an irregular building with floating column and an irregular building without floating column. *Int J Sci Res Dev* 9:180–187
2. IS:1893-2016 (part 1). Criteria for earthquake resistant design of structures
3. Maitra K, Serker NK (2018) Evaluation of seismic performance of floating column building. *Am J Civ Eng* 6:55–59. <https://doi.org/10.11648/j.ajce.20180602.11>
4. Hooda Y, Goyal PK (2023) Comparative analysis of bracing configuration for retrofitting of existing structures on hill slopes. In: Marano GC, Rahul AV, Antony J, Unni Kartha G, Kavitha PE, Preethi M (eds) *Proceedings of SECON'22. SECON 2022. Lecture notes in civil engineering*, vol 284. Springer, Cham. https://doi.org/10.1007/978-3-031-12011-4_15
5. Hooda Y, Goyal PK (2023) Comparison of the vulnerability assessment of step-back configuration and set-back configuration structures on hill slopes, chap 5. In: Pal I, Shaw R (eds)

- Multi-hazard vulnerability and resilience building. Elsevier, pp 61–78. ISBN: 9780323956826. <https://doi.org/10.1016/B978-0-323-95682-6.00012-7>
6. Ibrahim A, Askar H (2021) Dynamic analysis of a multistory frame RC building with and without floating columns. *Am J Civ Eng* 9:177–185. <https://doi.org/10.11648/j.ajce.20210906.11>
 7. Singh Y, Gade P (2012) Seismic behaviour of buildings located on slopes—an analytical study and some observations from Sikkim earthquake of September 18, 2011. In: 15WCCEE, Lisboa
 8. Kumar A et al (2013) Earthquake behavior of reinforced concrete framed buildings on hill slopes. In: International symposium on new technologies for urban safety of mega cities in Asia (USMCA 2013). Report no: IIIT/TR/2013/-1
 9. Thombre P, Makarande SG (2016) Seismic analysis of building resting on sloping ground. *JETIR* 3(6). ISSN: 2349-5162
 10. Rajeswari D et al (2017) Analysis of multi store symmetrical building in zone-II on flat and sloping ground up to failure by using ETABS. *Int J Appl Res* 3(5):575–580
 11. Rajavelu K, Saravanan K (2017) Seismic analysis of RC structure in hill slope area. *Int J Res Appl Sci Eng Technol (IJRASET)* 5(XI). ISSN: 2321-9653
 12. Hooda Y, Goyal PK (2021) *IOP Conf Ser Earth Environ Sci* 796:012006. <https://doi.org/10.1088/1755-1315/796/1/012006>
 13. IS 875 (Part 1) (1987) Code of practice for design loads (other than earthquake) for buildings and structures [dead loads]
 14. IS 875 (Part 2) (1987) Code of practice for design loads (other than earthquake) for buildings and structures [live loads]
 15. Chácara C, Reátegui R, Oré Á, Suarez P, Aguilar R (2023) Integration of NDT, 3D parametric modelling, and nonlinear numerical analysis for the seismic assessment of a vaulted stone-masonry historical building. *J Build Eng* 70:106347. ISSN: 2352-7102. <https://doi.org/10.1016/j.jobe.2023.106347>

Seismic Performance Analysis of Masonry Building with Scrap Tyre Pad Isolators



Ancy Mathew, R. Sajeeb, and M. Anandhakrishnan

Abstract Earthquake has become a common natural hazard. The aftershock studies of recent earthquakes reveal that the effect of earthquakes is severe in low-rise masonry buildings too. Base isolation is an effective strategy to mitigate the effect of earthquakes on structures. The huge cost of conventional isolators makes them unaffordable for developing countries. The Scrap tyre pad isolator is an emerging low-cost technology for the seismic protection of structures. The tread portion of tyre can be cut into pads of definite size and arranged one above the other to form the isolator. In the present study, a masonry building model isolated with scrap tyre pad isolators was analyzed using the response spectrum method in ETABS. The performance was compared with that of masonry building without isolators in terms of lateral displacement, base shear and time period. The analysis results show that scrap tyre pad isolator is also effective in seismic protection of masonry structures.

Keywords Scrap tyre pad isolator · Masonry structure · Response spectrum analysis

1 Introduction

Masonry buildings are one of the common types of residential buildings adopted in India and other parts of Indian subcontinent. Even though widely used around the world, the applicability of these structures in seismic prone areas is still a question. The 2015 seismic sequence in Nepal destroyed about half a million houses and more than 250,000 buildings damaged partially. About 95% of fully damaged buildings were of low strength masonry. Out of the partially damaged buildings, 67.7% were masonry buildings [2]. Figure 1 shows the post-earthquake damage in some of the

A. Mathew (✉)

APJ Abdul Kalam Technological University, Thiruvananthapuram, Kerala 695016, India
e-mail: ancymathew129@gmail.com

R. Sajeeb · M. Anandhakrishnan

TKM College of Engineering, Kollam, Kerala 691005, India



Fig. 1 Post-earthquake damage in masonry buildings in Nepal (Rohit et al.)

historic buildings which clearly represent the seismic vulnerability of low-rise low strength masonry buildings. So, some method is to be employed to protect masonry structures from disastrous effects of earthquakes. Seismic base isolation is such a technology.

Seismic base isolation is one of the most powerful and popular tools for earthquake protection of structures [1]. During the action of an earthquake, these structural elements essentially decouple the superstructure from the substructure and thereby restrict the transfer of seismic forces into the superstructure [7]. Hence, the resultant stresses in the superstructure will be much less than that of a building without base isolation. That means, rather than increasing the capacity, the demand of the system is reduced by installing a base isolation device. But applying a conventional seismic isolator will not be a satisfactory solution as it is costly. Hence, the present study concentrates on the applicability of scrap tyre pad isolator—a low-cost sustainable initiative for seismic protection of masonry buildings.

2 Scrap Tyre as Base Isolator

The scrap tyres have been in use as a secondary material in civil engineering applications because of their excellent mechanical properties [3]. The idea of using a scrap tyre pad as a material for base isolation has evolved from the fact that it contains both rubber as well as intervening steel strands. It is expected that rubber will contribute to lateral flexibility and steel will contribute to vertical stiffness if used as an isolator [4]. The tread portion of the tyre can be cut into pads of definite size and arranged one above the other to form the isolator as shown in Fig. 2. A scrap tyre pad isolator is advantageous over conventional seismic isolation systems as there is no additional



Fig. 2 Scrap tyre pad isolator

cost for its manufacturing, ease of handling, weight reduction, and simple shear stiffness adjustment by varying the number of layers [6]. Also, the environmental issues due to the recycling of tyres can be reduced by reusing this material which is non-biodegradable.

In framed structures, isolators are provided between the plinth beam and foundation so that they are free to undergo lateral deformation. But in the case of masonry buildings, there should be two different levels of reinforced concrete beams as suggested by Thuyet et al. as shown in Fig. 3. This method is already adopted in a building in Tawang, India [5]. So, for the present study, isolators are assumed to be located between the reinforced concrete beams.



Fig. 3 Base-isolated masonry building located in Tawang, India (Thuyet et al.)

3 Methodology

The study reported in this paper includes the performance analysis of a two-storey masonry structure, with and without scrap tyre pad base isolators, using ETABS 2020. The plan area of the building is 71.04 m². The window and door openings were provided wherever required as shown in Fig. 4b. The building is assumed to be situated in seismic zone III and the soil condition is assumed to be of rock type.

The slab and wall elements were defined and assigned suitably wherever required. The geometrical simulation is done by using shell elements and the discretization of the finite element mesh is assigned entirely flat quadrilateral and triangular elements. A bilinear model is used to simulate the properties of the isolator and is adopted from the horizontal force–displacement hysteretic response of the isolators. The property is assigned using the link property element in ETABS.

3.1 Design of Isolator

The natural time period of the structure is found to be 0.0051 s from the modal analysis. In order to make the structure flexible, the target isolator stiffness is identified based on the target time period. Also, the isolator layout is fixed suitably in such a way that vertical load is distributed uniformly among the isolators. Conventional isolators can be designed and manufactured as per the requirements of a given structure. But in the case of scrap tyre pad isolators, a proper design method has not been developed yet as it is an emerging technology. So, the only solution is to adopt properties from works that have already been done.

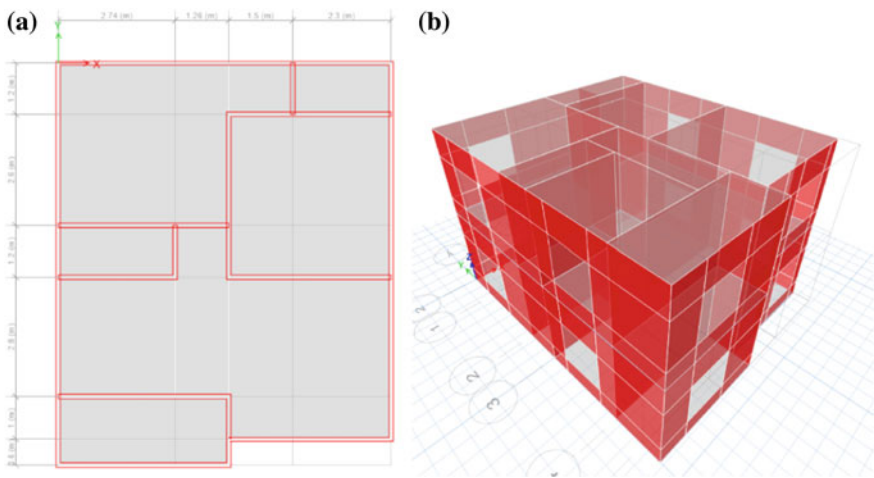


Fig. 4 a, b Plan and 3D model of the masonry building considered

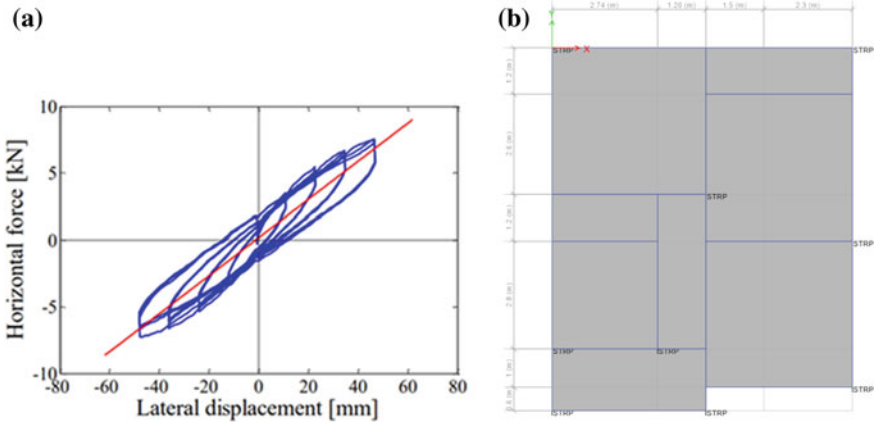


Fig. 5 a, b Load displacement hysteresis of STRP adopted (Mishra et al.)

Table 1 Isolator properties

S. No.	Isolator properties	
i	Dimensions	100 × 100 × 72 mm
ii	Effective horizontal stiffness (longitudinal)	142.5 N/mm
iii	Effective horizontal stiffness (transverse)	142.5 N/mm
iv	Number of layers	6

As per the design, the total horizontal stiffness required for the structure is estimated. Also, the individual stiffness required for the isolator is calculated. As scrap tyre pad isolators with the estimated properties are not available, it is required to use available isolators so that the total horizontal stiffness provided by the isolators matches the design stiffness. The scrap tyre pad isolator reported by Mishra et al. [4] which has a horizontal stiffness of 142.5 N/mm is adopted for the present study. Figure 5a shows the force–displacement hysteretic response of the isolators and the properties are listed in Table 1. The isolator layout is shown in Fig. 5b.

4 Results and Discussion

The masonry structure with scrap tyre pad isolators is analyzed using the response spectrum method in ETABS 2020 and compared with that of a building without isolators. Figure 6 depict the stress distribution in masonry building models with and without scrap tyre pad isolator. It is clear from the diagram that with the addition of isolators, there is a considerable reduction in stress distribution throughout the building.

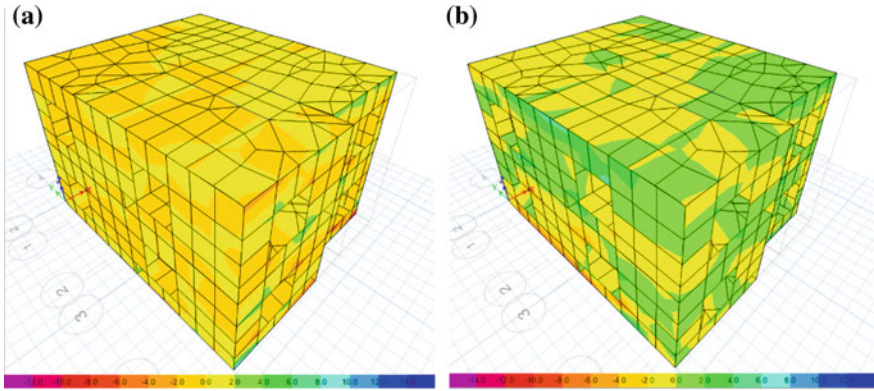


Fig. 6 Stress distribution in building model; **a** fixed base model, **b** base isolated model

It is observed that the fixed base model undergoes large lateral deformations under the action of earthquake load. But in the case of base-isolated models, the lateral deformation is comparatively high at the base level due to the action of the isolator. But, the lateral displacement of upper floor with respect to the base is found to be less. In other words, the building moves as a single unit without considerable drift. Figure 7 shows the maximum lateral displacement of building model in X and Y directions.

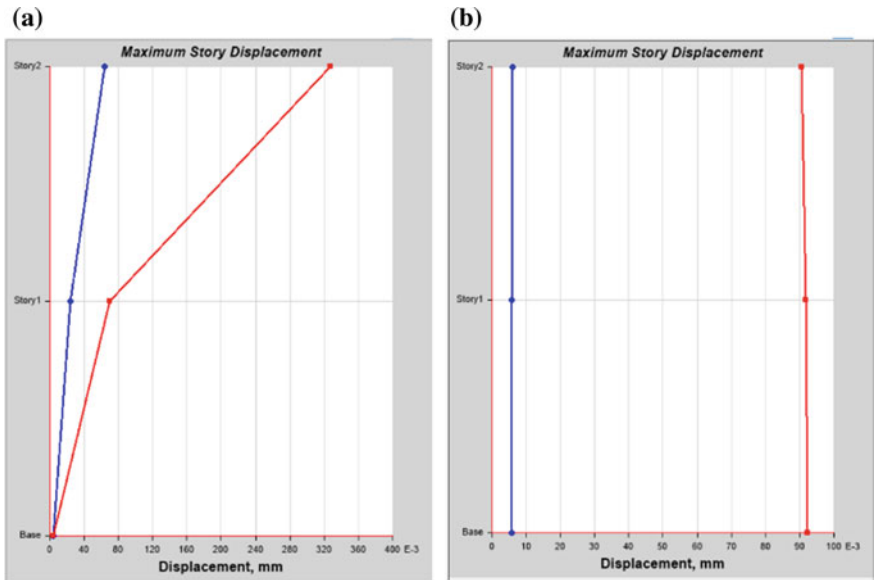


Fig. 7 Lateral displacement; **a** fixed base model, **b** base-isolated model

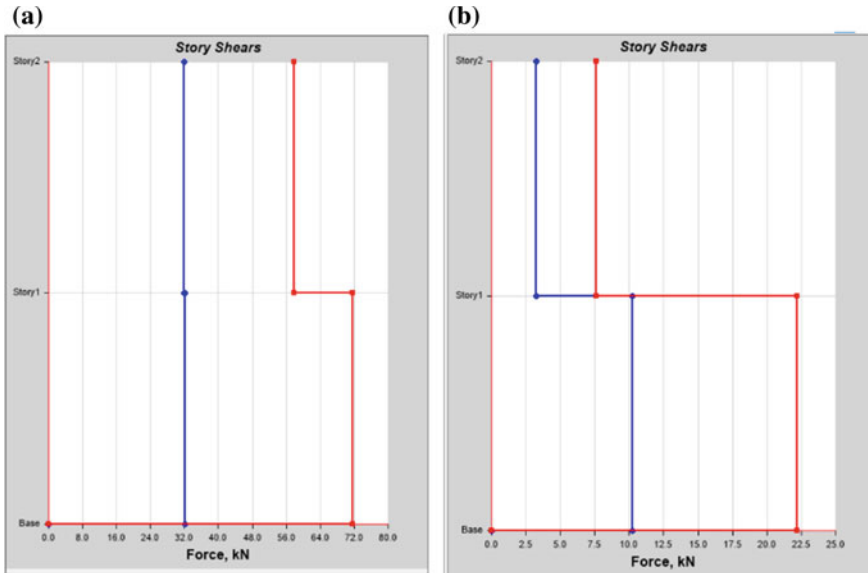


Fig. 8 Storey shear; **a** fixed base, **b** base isolated model

On comparing the storey shear, it is observed that there is considerable reduction in storey shear for base isolated models when compared to fixed base model. The reduction is about 68.75% in both X and Y directions as depicted in Fig. 8. Also, on addition of the isolator, the time period of the building model is increased to 0.0719 s from 0.0051 s.

5 Conclusions

On comparing the performance of fixed base and base isolated building models, the performance of STRP isolated model is found to be improving significantly with the addition of isolators. Also, it is observed that the base-isolated models undergo large lateral deformations at the base level along with a significant reduction in the drift at higher levels. The addition of isolators enhances the performance of the building by increasing the time period and reduce demand by reducing base shear.

Even though the numerical study proved to be effective, the practical applicability is to be checked with the help of experimental models. Also, it is worth mentioning here that the properties of STRP are adopted from the limited data available from the published literature. The performance can be further improved by adopting isolators with parameter values that exactly match the design requirements. Detailed research

on different variations of scrap tyre pad isolators is expected to provide sufficient data on the properties of scrap tyre pad isolators which in turn help the designers to devise seismic base isolators for structures with a wide range of fundamental time periods.

References

1. Antonello DL, Laura GG (2020) State of art in the worldwide evolution of base isolation design. *Soil Dyn Earthq Eng* 125:05722
2. Basar T, Deb SK, Das PJ, Sarmah M (2021) Seismic response control of low-rise unreinforced masonry building test model using low-cost and sustainable un-bonded scrap tyre isolator (U-STI). *Soil Dyn Earthq Eng* 142:0267–7261
3. Lamour M, Cecchin A (2021) Repurposed materials in construction: a review of low-processed scrap tires in civil engineering applications for disaster risk reduction. *Constr Build Mater* 293:123368
4. Mishra HM, Igarashi A, Matsushima H, Furukawa A (2012) Experimental and analytical study of unbonded and bonded scrap tire rubber pad as base isolation device. In: *Proceedings of 15th world conference on earthquake engineering, Lisbon, Portugal, 24–28 Sept 2012*
5. Thuyet VN, Deb SK, Dutta A (2018) Mitigation of seismic vulnerability of prototype low-rise masonry building using U-FREIs. *J Perform Constr Facil ASCE* 32:04017136
6. Turer A, Ozden B (2007) Seismic base isolation using low-cost scrap tire pads (STP). *Mater Struct* 4:891–908
7. Vasant AM, Jangid RS (2008) Base isolation for seismic retrofitting of structures. *Pract Period Struct Des Constr ASCE* 13:175–185

Mode Choice Modelling of Different Categories of Work Trips in Thiruvananthapuram City



S. Shaheem, Nisha Radhakrishnan, and Samson Mathew

Abstract Over the past few years, the rate of commuters using public transportation has drastically reduced, which has led to a rise in private vehicles with higher levels of traffic congestion, accidents, pollution, etc. The present study aims to identify major significant factors influencing the mode choice decisions of commuters working in Thiruvananthapuram city. The latent attributes influencing the mode choice decision were analysed using the semantic differential technique with a five-point bipolar adjective scale. In order to identify the key latent factors influencing commuters use of public transportation, exploratory factor analysis was conducted. Also, in order to statistically quantify the link between the founded latent variables and the observed variables, confirmatory factor analysis was also carried out. Latent variables integrated mode choice models were developed for different categories of work trips, such as government employees, private employees, and a combined set of employees using multinomial logistic regression. Reliability, convenience, comfort, and safety were identified as latent factors influencing the mode choice behavior of private employees and a combined set of employees. In the case of government employees, travel behavior also depends on their affinity for public transport. Latent variable integrated mode choice models were found to have a relevant role in the mode choice decisions of commuters. Mode choice models reveal that a unit percentage increase in latent variables will result in a considerable increase in the use of public transport services in Thiruvananthapuram city.

Keywords Mode choice model · Latent variables · Public transport · Exploratory factor analysis · Confirmatory factor analysis

S. Shaheem (✉) · S. Mathew
KSCSTE—NATPAC, Thiruvananthapuram, Kerala 695011, India
e-mail: shaheems@yahoo.co.in

N. Radhakrishnan
Department of Civil Engineering, National Institute of Technology Tiruchirappalli,
Tiruchirappalli, Tamil Nadu 620015, India

1 Introduction

An enormous surge in the private vehicle population on the roads is a major matter of concern. An efficient public transport system is a prerequisite for ensuring a sustainable transport system in a city. The essential requirements of a sustainable transport system are easy accessibility along with comfort and convenience. Transportation planners must take commuters attitudes, perceptions, expectations, and similar other abstract behavioural traits into account in order to plan and implement an efficient and sustainable transportation system for a medium-sized city in India. They must also consider their socio-economic characteristics and modal attributes in order to better understand their mode choice decisions. For effective planning, good knowledge of the individual contribution or share of each transportation mode and the major factors influencing individuals to choose a particular type of mode is necessary. Hence, mode choice decisions need to be properly analysed to gain insights into the factors influencing the choices made by the commuter and finally arrive at an effective policy for improving the transportation network and travel efficiency of the study region. Commuters travelling to work contribute a relevant portion of the severe traffic congestion occurring in many of the medium-sized cities in India. In this context, it is very important for the transportation planners to clearly understand the travel patterns of the working population in order to frame efficient policies to ensure a smooth traffic scenario for all the commuters.

According to Ravi Sekhar [12], a variety of social, economic, cultural, and environmental factors, such as travel time, cost, waiting time, ease of travel, personal comfort, etc., heavily influence commuters' choice of travel mode. Analysis of commuters' mode-choice decisions could be very helpful in pinpointing the specific public transportation system elements that need to be improved to entice more commuters who currently favour private vehicles to switch to the city's public transportation system. Ashalatha et al. [4] investigated commuter mode decisions in Thiruvananthapuram city using multinomial logistic regression. The study revealed that mode choice modelling using multinomial regression would be helpful to transportation planners in formulating future policies to further upgrade the prevailing public transport system. Moreover, the study observed that most of the commuters switched to private travel modes from public transport owing to the increase in travel time as well as the travel cost, both considered per unit distance.

The study conducted by Santos et al. [14] suggested that promotional policies such as a reduction in public transport fares and an increase in the frequency of buses were likely to improve public transport patronage. Dimitrios and Luis [8] investigated the influence of the mode choice on public transport network characteristics, mainly focusing on accessibility and connectivity. Chen and Naylor [7] explored how to develop an enhanced mode choice model to forecast future Bus Rapid Transit (BRT) ridership for the planning and operation of the BRT system in Santa Clara County, California. Marwa et al. [10] attempted a study on the influence of advanced Logit discrete choice models on individual mode choice decisions. Income was found to be a significant attribute affecting commuter's travel patterns. Moreover, out-of-vehicle

time, which provides an indication of accessibility, was observed to be a more influencing factor than in-vehicle time in developing countries. According to Pulugurta et al. [11], the travel mode decision taken by a trip maker involves complex human approximations that cannot be accurately determined by a Multinomial Logit model. However, artificial intelligence techniques such as Fuzzy logic can be deployed for modelling mode choice behaviour. Fuzzy logic technique was applied by Kumar et al. [9] to determine the relationship between commuter's choice of an alternate mode and their travel patterns.

Therefore, mode choice models incorporating latent variables have evolved as a promising new category of models for mode choice analysis by transportation planners. Atasoy et al. [5] presented a latent variable enriched mode choice model that comprised environmental issues as well as commuters' general attitude towards public transport. The relevance of unobservable variables in mode choice decisions was explained by the calibration of the advanced latent variable enriched mode choice models. For predicting the mode choice of a commuter with a multimodal condition, mode choice models integrated with latent variables are found to be more accurate than models using socio-demographic variables [1]. Earlier research studies have proved that the behaviour and attitude of commuters is affected by socio-demographic variables when choosing the mode of transportation for their work commute.

Chen and Li [6] identified three latent factors as the major attributes influencing the service quality of a bus transit system. The three factors comprised of service, comfort, and personnel which in turn are the key components in determining the public transport ridership. By improving the public transport characteristics like convenience, personal safety, and service environment, higher share of modal split can be achieved in public transport. Antonucci et al. [3] attempted exploratory factorial analysis and found that the level of service provided by public transport was a relevant factor influencing the travel patterns of Italian commuters. Punctuality and waiting time were found to be the most important factors determining customer satisfaction. Ren and Fan [13] investigated this by creating a structural equation model to evaluate the influencing elements of mode choice during short-distance travel in urban environments. The findings showed that the availability of traffic facilities, individual and family characteristics, and travel objectives all had a significant impact on the decision-making process when choosing a travel mode for short distances in cities.

The significant variables influencing mode choice decisions identified through the comprehensive literature review conducted for the study are travel cost, travel time, travel distance, reliability and punctuality, comfort and convenience, safety and security, frequency, waiting time, household size, gender, age, education, and monthly income. According to the literature review, commuters in medium-sized cities in developing countries tend to choose their mode of transportation based on factors affecting their travel behaviour. To the best of the author's knowledge, not many studies have been conducted in India to identify various factors influencing the quality of the public transport system and to increase patronage of public transport facilities.

The broad objectives of the present research study involve analysing the socio-economic profile and travel characteristics of commuters and identifying the major latent variables affecting the mode choice decisions of commuters in a medium-sized city. The present study also aims to develop a multinomial logit model for commuters and identify the most influential latent factors likely to enhance public transport patronage. The scope of the study is confined to the work trips in Thiruvananthapuram city.

2 Study Area

Thiruvananthapuram, one of the major cities in Kerala, South India, is situated on the Malabar Coast, the western coastal region of India. Thiruvananthapuram Corporation comprises an area of 215 km² with a population of around 9.86 lakh as per the 2011 census and is the most populated city in Kerala state. Employees working in the government sector and private sector constitute a relevant portion of the commuters in the city of Thiruvananthapuram. Kerala State Road Transport Corporation (KSRTC) plays a significant role in catering to the mobility requirements of the intra-city commuters of Thiruvananthapuram city. The majority of the intra-city buses connecting major locations within the city operate from the four bus depots located within the city. Cars and motorised two-wheelers are the two major personal modes of transport in the city.

An efficient public transport system is an ongoing need for ensuring the unhindered mobility of commuters in Thiruvananthapuram City. Moreover, there have not been many studies conducted regarding the public transport system in Thiruvananthapuram city. In addition, the proportion of working population in Thiruvananthapuram city is significantly higher than any other cities in Kerala. The ridership of public transport can be gradually increased only through the implementation of effective policies. A working population is that category of population among whom the policies can be implemented without causing considerable delay. In this context, the present study was intended to enhance public transport services in Thiruvananthapuram city by formulating policies for the working population. Figure 1 shows the map of Thiruvananthapuram City.

3 Methodology

A detailed literature review was undertaken to understand the significant factors must be considered in formulating an efficient public transport system for a city. A pilot survey was initially conducted in the study area prior to the commencement of study activities. Secondary data collection was also done, which involved previous study reports related to the public transport system in Thiruvananthapuram city. Data collection using primary surveys involved conducting questionnaire surveys



Fig. 1 Map of Thiruvananthapuram city (KSCSTE-NATPAC)

among government employees, private employees, and a combined set of employees working in Thiruvananthapuram city. Figure 2 shows the flowchart depicting the methodology of the study.

Exploratory Factor Analysis was performed as a major step to reduce the large data set of 20 indicator variables measured on a scale basis to a smaller set of latent variables. It was performed to identify the major latent variables influencing the attitude of commuters towards public transport. Confirmatory factor analysis was performed as the next step to test the hypothesis of how well the observed variables are representative of the latent factors identified through exploratory factor analysis. The analysis of mode choice decisions for work trips in Thiruvananthapuram city was done by developing separate multinomial logit models for commuters using buses, cars, autorickshaws, and motorised two-wheelers. Conventional mode choice model as well as a latent variable integrated mode choice model were developed. Latent variables were integrated with the conventional mode choice model to examine

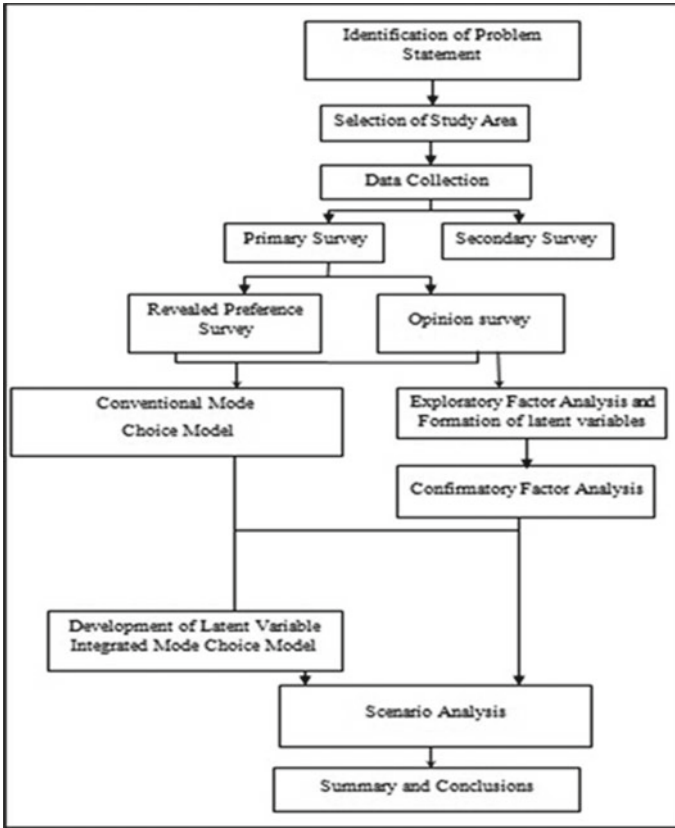


Fig. 2 Methodology of the study

the change in the explanatory ability of the model regarding the mode choice decisions made by commuters. The latent variable enriched mode choice model was used to identify various latent parameters influencing the mode choice behaviour of commuters.

4 Data Collection

The existing socio-economic as well as travel characteristics of the commuters were collected using a questionnaire survey. The third section of the opinion survey involved certain statements reflecting the attitudes of commuters towards public transport, which were to be rated by the commuters themselves on a five-point scale. Enumerators were employed for data collection after proper training. About 2046 samples were collected from government and private offices and establishments,

Table 1 Test results of two-tailed Z-test for mean household size of population

Parameter (μ_0)	Population mean of household	Sample mean age (X)	Deviation of sample (s)	Sample size (N)	Test statistic $t = \left(\frac{X - \mu_0}{S/\sqrt{N-1}} \right)$
Household size	3.94	4.01	1.93	2046	1.64 (< 1.96)

where employees commuted to and from office by road. It also involved certain statements reflecting the attitudes of commuters towards public transport, which were to be rated by the commuters themselves on a five-point scale.

In order to check whether the sample represents the population of the study area, Z-test was done for Household size of the population. It is a statistical test aimed at finding out whether the means of two populations are same with large sample size (sample size > 30) and known variances.

- Null hypothesis, H_0 : There is no significant difference between population mean and sample mean ($H_0: \mu = \mu_0$).
- Alternate hypothesis, H_1 : There is significant difference between population mean and sample mean ($H_1: \mu \neq \mu_0$).

The results of the two-tailed Z-test conducted at 5% level of significance are given in Table 1. The threshold value for the Z-test at 5% level of significance is 1.96. The results indicated the acceptance of null hypothesis, i.e., there is no difference between the population mean and the sample mean of household. Hence, it was proven that the collected data is a representative sample of the population.

5 Preliminary Analysis

The analysis of the data based on gender showed that about 58.7% of employees were female and 41.3% were male. The age of employees who participated in the survey was classified into five groups. There are mainly four different classes of employees based on the grade of employment. It was observed that 37.2% of employees were from the category of 31–40 years of age, followed by 32.8% of employees from the age bracket of 41–50. The preliminary analysis done on the collected data also indicated that majority of employees were in the employment grade of Class III, followed by Class II. Another major observation was that the majority of the employees belonging to lower income groups (72%) travelled by bus to reach their workplace. It was also observed that the majority of the employees from lower income groups chose walking as their access mode as well as egress mode (70% and 83% respectively) for their daily commute to the workplace, whereas majority of employees from higher income groups chose two-wheelers as their major mode for access trip (65%) as well as egress trip (60%). Table 2 summarises the socio-economic and travel characteristics of commuters working in Thiruvananthapuram city.

Table 2 Summary of socio economic and trip characteristics of commuters

Attributes	Statistics
Gender	41.3% males and 58.7% females
Age	21–30 (15%), 31–40 (37%), 41–50 (33%), 51–60 (14%), 61–65 (1%)
Employee grade	Class I (3%), Class II (24%), Class III (66%), Class IV (7%)
Education	Below SSLC (1%), SSLC (5%), plus two (6%), diploma (13%), degree (35%), PG (26%), professional (14%)
Monthly income level	0–10,000 Rs (2%), 10,000–20,000 Rs (20%), 20,000–30,000 Rs (32%), 30,000–50,000 Rs (30%), 50,000–100,000 Rs (15%), > 100,000 Rs (1%)
Household size	1 (1%), 2 (7%), 3 (23%), 4 (42%), 5 (18%), 6 (6%), > 6 (3%)
Vehicle ownership	Nil (17%), 1 (38%), 2 (33%), 3 (9%), 4 (3%), 5 (1%)
Driving license for two wheelers	Yes (34%), no (66%)
Driving license for cars	Yes (44%), no (56%)
Nature of attendance	Strict (90%), flexible (10%)
Accessibility to work location	Low (26%), medium (22%), high (52%)
Distance to workplace	0–5 km (31%), 5–10 km (23%), 10–20 km (20%), 20–30 km (13%), 30–50 km (9%), > 50 km (4%)
Access distance	0–100 m (30%), 100–300 m (26%), 300–500 m (20%), 500–1000 m (16%), > 1000 m (8%)
Egress distance	0–100 m (41%), 100–300 m (54%), 300–500 m (5%)
Mode of travel	Bus (41%), car (10%), auto (5%), two-wheeler (39%), walk (5%)

6 Exploratory Factor Analysis

To examine the underlying latent structure of the theoretical phenomenon, exploratory factor analysis (EFA) is used to reduce a large dataset into a smaller set of variables. It is a technique that aids in examining ideas that are difficult to quantify and does so by condensing a huge collection of indicator variables into a small number of interpretable underlying latent features. To extract a small collection of latent variables from a large collection of indicators or observed variables in the current investigation, exploratory factor analysis with the principal component approach was used. It is used to investigate the underlying connection between latent constructs and indicator variables.

From factor analysis, it is observed that each factor captures a distinct amount of the total variance in the observed attributes, and the factors are always listed according to how much variation they depict. The current study attempted exploratory factor analysis (EFA) using the principal component method on commuters' response data for 20 indicator variables regarding attitude towards public transport collected using an opinion survey for government employees and private employees. Table 3 shows

the output obtained from EFA for government employees. Loading factors higher than 0.5 shows a good correlation between item and factor are acceptable and is shown bold in the table below.

Table 3 Output obtained from EFA for government employees

	Reliability	Comfort	Safety	Convenience	Public transport affinity
Bus services are very punctual and helps to arrive at destinations on time	0.801	0.207	- 0.080	0.054	0.037
Bus services offer less vehicle time inside the bus	0.734	0.216	0.026	0.221	- 0.034
Bus services are reliable	0.702	- 0.136	0.194	0.154	0.172
Trips involving transfers keep bus usage undesirable	0.126	0.767	- 0.043	0.016	0.092
Public buses are less congested; it has comfortable seating	0.096	0.749	- 0.052	- 0.013	- 0.055
Cleanliness of public buses is very good	0.114	0.301	0.780	0.035	0.042
Public buses offer peaceful travel without harassments and insults	- 0.006	- 0.485	0.678	0.027	0.012
Public bus is a safe mode of travel	0.000	- 0.454	0.665	0.084	0.065
Frequency of bus services is good	0.094	0.054	0.060	0.890	0.065
Waiting time to get into bus is reasonable	0.269	- 0.079	0.036	0.829	- 0.003
Travel in public buses are comfortable in all weather conditions	- 0.096	0.143	0.151	0.114	0.817
Love to travel in bus transport services	0.253	- 0.120	- 0.069	- 0.052	0.783

It was observed from the rotated component matrix that there were five latent factors with Eigen values greater than or equal to 1. Only 12 variables were retained out of a total of 20 indicator variables included in the questionnaire. The five identified latent variables are grouped as follows: Reliability, Comfort, Convenience, Safety, and Public Transport Affinity.

For private employees, exploratory factor analysis utilising the principal component approach was also conducted. The Bartlett's test of sphericity's significance value was 0.00, while the KMO measure of sample adequacy was calculated to be 0.755. Four latent variables with Eigen values larger than 1 are present, according to the rotated component matrix. Based on the factor loadings and components, all the detected variables are categorised into four latent variables. These indicator variables and four latent variables identified from EFA for private employees are shown in Table 4.

Table 4 EFA results for private employees

Indicator variables	Convenience	Comfort	Safety	Reliability
Bus services offer less vehicle time inside the bus	0.920	0.166	- 0.009	0.131
Bus services take less travel time	0.892	0.152	0.004	0.194
Waiting time to get into bus is reasonable	0.752	0.026	0.003	0.320
Travel in public buses are comfortable in all weather conditions	0.091	0.861	0.000	0.115
Cleanliness of public buses is very good	0.010	0.835	0.189	0.082
Public buses offer calm and non-noisy travel	0.243	0.808	0.053	0.141
Public buses offer peaceful travel without harassments and insults	- 0.048	0.138	0.845	0.052
Public bus is a safe mode of travel	- 0.052	0.030	0.817	0.023
Public bus crew behaves properly	0.106	0.051	0.790	- 0.012
Bus services are very punctual and helps to arrive at destinations on time	0.229	0.123	0.143	0.850
Bus services are reliable	0.368	0.111	0.115	0.781
Frequency of bus services is good	0.084	0.113	- 0.127	0.697

Loading factors of EFA above 0.5 are shown in bold letters

The four latent variables identified are convenience, comfort, safety, and reliability for private employees. Exploratory factor analysis using the principal component method was also carried out for a combined set of government and private employees. The KMO measure of sampling adequacy was obtained as 0.792. All the identified variables are grouped under four latent variables based on the factor loadings and components. These indicator variables and four latent variables identified from EFA for the combined data set are shown in Table 5.

The four identified latent variables are convenience, comfort, safety and reliability for combined government and private employees.

Table 5 EFA results for combined data set

Indicator variables	Reliability	Comfort	Safety	Convenience
Bus services take less travel time	0.880	0.108	- 0.026	- 0.024
Bus services offer less vehicle time inside the bus	0.868	0.120	- 0.010	0.033
Bus services are reliable	0.752	0.160	0.079	0.166
Bus services are very punctual and helps to arrive at destinations on time	0.746	0.154	0.067	0.213
Waiting time to get into bus is reasonable	0.733	0.032	- 0.003	0.237
Travel in public buses are comfortable in all weather conditions	0.080	0.857	- 0.002	0.080
Public buses offer calm and non-noisy travel	0.248	0.854	0.034	0.069
Cleanliness of public buses is very good	0.116	0.848	0.176	0.023
Public buses offer peaceful travel without harassments and insults	- 0.001	0.067	0.866	0.066
Public bus is a safe mode of travel	- 0.005	0.020	0.841	0.086
Public bus crew behaves properly	0.064	0.090	0.763	0.013
Frequency of bus services is good	0.213	0.149	0.001	0.832
Walking to bus stop is easy	0.168	0.000	0.153	0.832

Loading factors of EFA above 0.5 are shown in bold letters

7 Confirmatory Factor Analysis

Confirmatory factor analysis (CFA) is another method used to determine whether measures of a latent construct are stable over time (factor). CFA can be used to confirm or reject the measurement theory under consideration. Model fit indices help to ascertain if the model that best represents the data reflects the underlying theory. Absolute fit indices determine how well a model fits the sample data. The Chi-squared test estimates the difference between observed as well as expected covariance matrices. Degree of Freedom (DF) gives an indication of the amount of mathematical information available to estimate model parameters. The present work obtained a value of CMIN/DF of less than 5, which in turn indicated an acceptable model fit for government, private, and combined data sets. Confirmatory Factor Analysis was carried out in AMOS 26, and the path diagram obtained for combined employees is as shown in Fig. 3.

The Root Mean Square Error of Approximation (RMSEA) value indicates the size of the standardised residual correlations. Theoretically, value ranges from 0 to 1, and a smaller value is considered acceptable when it is less than 0.06. In the present work, a value of less than 0.06 was obtained, which indicated an acceptable model fit. The value of various other model fit indices such as GFI, AGFI, NFI, and CFI ranges between 0.9 and 0.98 obtained from Confirmatory Factor Analysis for government, private, and combined data sets, which is acceptable. Hence, latent variables identified from the EFA for different categories (government, private, and combined data set) were confirmed and further considered for developing latent variable integrated mode choice models. Table 6 summarises the model fit indices obtained from CFA.

8 Mode Choice Analysis

A mode choice model of employees working in Thiruvananthapuram city was developed using multinomial regression analysis. NLOGIT software was used for mode choice analysis. Mode choice models were developed by considering the socio-demographic variables, travel attributes, and latent variables. Moreover, an attempt was also made to find out if any improvement could be observed in the model by considering the significant latent variables identified by the exploratory factor analysis which were: Reliability, Comfort, Safety, Convenience and Public transport affinity. The choice of the four modes, namely motorized two-wheeler, car, bus and autorickshaw was modeled by taking bus as the base mode. The initial command for the NLOGIT analysis was formulated by considering all the variables in the dataset. Several combinations of independent variables were tried in trial-and-error manner and were checked for variable significance and model fit. The significant variables

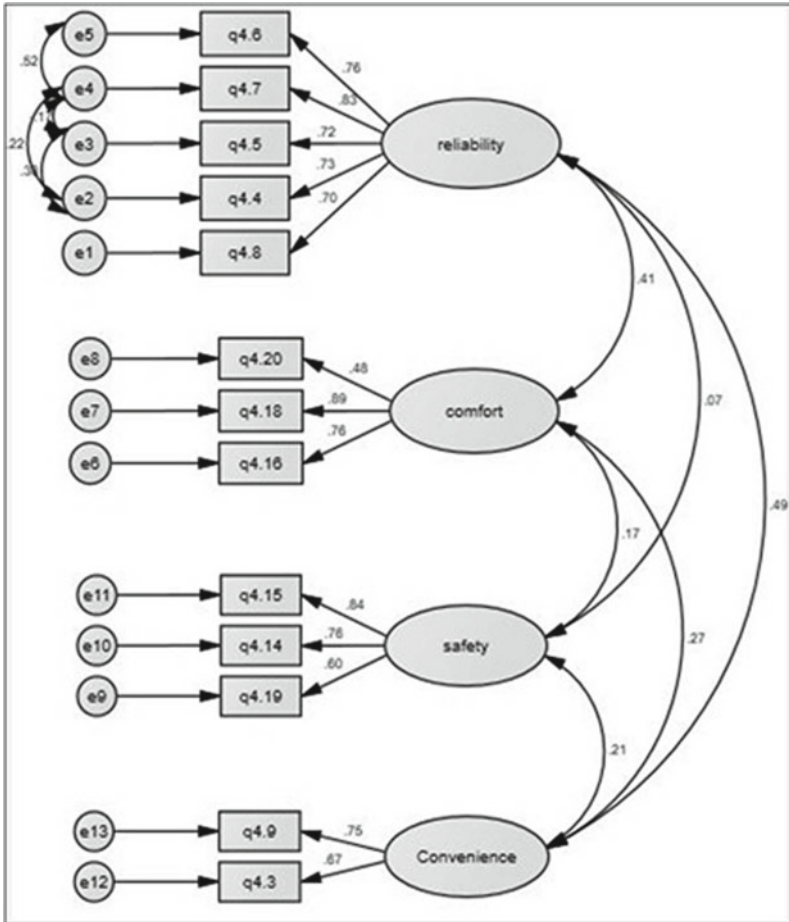


Fig. 3 Path diagram of CFA for combined data set

were identified from the initial output, and then the command was framed considering those significant variables and generic variables. Travel time per unit travel distance, and travel cost were the generic variables considered in the analysis.

8.1 Latent Variable Integrated Mode Choice Models

The following utility equations were developed using NLOGIT for government employees:

$$U(\text{BUS}) = 3.559 - 6.231 * \text{TTPERTD} + 0.829 * \text{TC} \quad (1)$$

Table 6 Model fit indices obtained from CFA

Incremental fit indices	Model fit values			Remarks
	Govt. employees	Private employees	Combined employees	
CMIN/DF value	4.58	4.04	4.97	Acceptable
RMSEA value	0.058	0.041	0.054	Acceptable
Goodness of fit index (GFI)	0.97	0.96	0.97	Acceptable
Adjusted goodness of fit index (AGFI)	0.95	0.94	0.95	Acceptable
Normed fit index (NFI)	0.93	0.94	0.96	Acceptable
Comparative fit index (CFI)	0.95	0.95	0.95	Acceptable
Tucker Lewis index (TLI)	0.92	0.92	0.97	Acceptable
Incremental fit index (IFI)	0.95	0.95	0.97	Acceptable

$$\begin{aligned}
 U(CAR) = & -6.231 * TTPERTD + 0.829 * TC - 0.242 * HHSIZE \\
 & - 0.283 * SS - 0.395 * AFF - 0.263 * REL - 5.257 * TD \quad (2)
 \end{aligned}$$

$$\begin{aligned}
 U(AUTO) = & -6.231 * TTPERTD + 0.829 * TC - 9.410 * TD \\
 & + 2.519 * GENDER - 0.817 * REL - 1.226 * VEHOWN \\
 & - 1.971 * GRADE - 0.573 * INCOME \quad (3)
 \end{aligned}$$

$$\begin{aligned}
 U(TW) = & -6.231 * TTPERTD + 0.829 * TC - 0.928 * TD \\
 & - 0.478 * PTAVAIL - 0.281 * AFF \\
 & - 0.133 * REL + 0.384 * GRADE \quad (4)
 \end{aligned}$$

where,

- U (CAR) = Utility value of car
- U (TW) = Utility value of two-wheeler
- U (AUTO) = Utility value of autorickshaw
- U (BUS) = Utility value of bus
- TTPERTD = Travel time per unit travel distance
- TC = Travel cost
- HHSIZE = Household size of the user
- MS = Marital status of the user
- GENDER = Gender of the user
- VEHOWN = Vehicle ownership

- GRADE = Employment grade of the user
- INCOME = Monthly income of the user
- TD = Travel distance
- PTAVAIL = Public transport availability
- REL = Reliability of public transport
- SS = Safety
- AFF = Public transport affinity.

All the variables used in the models were observed to have logically correct signs and with 95% significance. Reliability, safety, and public transport affinity are the latent variables found to be significantly influencing the mode choice behaviour of government employees. The major observations from the estimated model parameters of latent variable integrated mode choice model for government employees were:

1. Unit percentage increase in reliability of public transport was found to decrease the probability of choosing car, autorickshaw and two-wheeler by 0.26%, 0.82% and 0.13%, respectively.
2. Unit percentage increase in safety of public transport would decrease the probability of choosing car by 0.28%.
3. Unit percentage increase in public transport affinity would decrease the probability of choosing car and two-wheeler by 0.39% and 0.28%, respectively.

The following utility equations were developed using NLOGIT for private employees.

$$U (\text{BUS}) = - 4.999 - 0.014 * \text{TC} \tag{5}$$

$$U (\text{CAR}) = - 0.014 * \text{TC} - 2.874 * \text{GENDER} - 0.449 * \text{SS} + 1.14 * \text{EDU} - 0.605 * \text{HHSIZE} \tag{6}$$

$$U (\text{AUTO}) = - 0.014 * \text{TC} - 0.323 * \text{REL} - 0.569 * \text{INCOME} - 0.547 * \text{COM} \tag{7}$$

$$U (\text{TW}) = - 0.014 * \text{TC} + 0.06 * \text{TD} - 0.703 * \text{AGE} - 1.952 * \text{GENDER} + 0.371 * \text{COM} \tag{8}$$

where,

- TC = Travel cost
- HHSIZE = Household size of the user
- GENDER = Gender of the user
- INCOME = Monthly income of the user
- AGE = Age of the user
- TD = Travel distance

EDU = Education of the user
 REL = Reliability of public transport
 COM = Comfort
 SS = Safety.

All the variables used in the models were observed to have logically correct signs and with 95% significance. Reliability, safety, and comfort are the latent variables found to be significantly influencing the mode choice behaviour of private employees. The major observations from the estimated model parameters of the latent variable enriched mode choice model for private employees were:

4. Unit percentage increase in reliability of public transport was found to decrease the probability of choosing autorickshaw by 0.32%.
5. Unit percentage increase in safety of public transport would decrease the probability of choosing car by 0.45%.
6. Unit percentage increase in comfort will decrease the probability of choosing auto rickshaw by 0.55% and increases two-wheeler by 0.37%.

The following utility equations were developed using NLOGIT for combined data set.

$$U(\text{BUS}) = -3.883 - 3.337 * \text{TTPERTD} - 0.011 * \text{TC} \quad (9)$$

$$\begin{aligned} U(\text{CAR}) = & -3.337 * \text{TTPERTD} - 0.011 * \text{TC} - 0.225 * \text{CON} \\ & - 1.237 * \text{GENDER} - 0.243 * \text{SS} + 0.375 * \text{INCOME} \\ & - 0.331 * \text{HHSIZE} + 0.258 * \text{EDU} \end{aligned} \quad (10)$$

$$\begin{aligned} U(\text{AUTO}) = & -3.337 * \text{TTPERTD} - 0.011 * \text{TC} \\ & - 0.310 * \text{CON} - 0.906 * \text{VEHOWN} - 1.573 * \text{MS} \end{aligned} \quad (11)$$

$$\begin{aligned} U(\text{TW}) = & -3.337 * \text{TTPERTD} - 0.011 * \text{TC} - 1.872 * \text{GENDER} \\ & + 0.216 * \text{COM} - 0.069 * \text{TD} + 0.246 * \text{EDU} \\ & - 0.168 * \text{REL} - 0.352 * \text{CON} - 0.193 * \text{AGE} \end{aligned} \quad (12)$$

where,

TTPERTD = Travel time per unit travel distance
 TC = Travel cost
 HHSIZE = Household size of the user
 MS = Marital status of the user
 GENDER = Gender of the user

- AGE = Age of the user
- VEHOWN = Vehicle ownership
- INCOME = Monthly income of the user
- EDU = Education of the user
- TD = Travel distance
- REL = Reliability of public transport
- COM = Comfort
- CON = Convenience
- SS = Safety.

All the variables used in the models were observed to have logically correct signs and with 95% significance. Reliability, safety, convenience, and comfort are the latent variables found to be significantly influencing the mode choice behaviour of both government and private employees. The major observations from the estimated model parameters of the latent variable enriched mode choice model for the combined data set were:

7. Unit percentage increase in reliability of public transport was found to decrease the probability of choosing two-wheeler by 0.17%.
8. Unit percentage increase in convenience of public transport was found to decrease the probability of choosing car, autorickshaw and two-wheeler by 0.23%, 0.31% and 0.35% respectively.
9. Unit percentage increase in safety of public transport would decrease the probability of choosing car by 0.24%.
10. Unit percentage increase in comfort of public transport would increase the probability of choosing two wheeler by 0.22%.

8.2 Determining Model Fit: The Pseudo-R²

The R² statistic is calculated by the following formula:

$$\text{Pseudo } R^2 = 1 - \frac{\text{LL Estimated model}}{\text{LL Base model}} \tag{13}$$

Conventional mode choice model (Model 1) were also developed and compared with latent integrated model choice model (Model 2) for all four modes. The overall model fit was observed to be good for the two models (pseudo R² >> 0.2). According to Alvinskyah et al. [2], the acceptable R² value ranges from 0.2 to 0.4. It was also observed that pseudo R² value obtained for model 2 is greater than pseudo R² obtained for model 1, which indicated that latent variables have better explanatory ability on the mode choice decision of work trips in Thiruvananthapuram city.

9 Conclusions

The present study has focused on developing multinomial logit models for analysing mode choice decisions of employees working in Thiruvananthapuram city. It was found that the majority (72%) of the employees belonging to low-income groups travelled by bus to reach their workplace. A higher percentage of commuters from low-income groups preferring buses over other travel modes indicated that travel fare was not a major matter of concern for the lesser ridership in public transport when compared to the other modes. It was also observed that the majority of the employees from low-income groups chose walking as their access mode as well as egress mode (70% and 83% respectively) for their daily commute to their workplace, whereas majority of employees from high-income groups chose two-wheeler as the travel mode for access trips (65%) as well as egress trips (60%).

EFA identified five latent variables as the factors influencing commuter's attitudes towards public transport: reliability, comfort, safety, convenience, and public transport affinity for government employees. Reliability, convenience, comfort, and safety were identified as latent factors influencing the mode choice behaviour of private employees and a combined set of employees. The CFA performed provided a good fit as per the model fit statistics and hence confirmed the latent variables identified by the EFA.

Latent variable integrated mode choice models were developed considering socio-economic variables, travel attributes, and latent variables for government, private and combined set of employees using N-LOGIT software. The travel modes used in the study were car, autorickshaw, motorised two-wheeler and bus. The present study has also proven that models incorporating latent variables are more accurate in predicting the mode choice behaviour of commuters than the conventional mode choice models.

Latent variable integrated mode choice model is found to have a relevant role in the mode choice decisions made by commuters. It was observed that reliability, safety, and public transport affinity are the latent variables found to be significantly influencing the mode choice behaviour of government employees. A unit percentage increase in reliability of public transport was found to decrease the probability of choosing a car, autorickshaw and two-wheeler by 0.26%, 0.82%, and 0.13%, respectively, whereas a unit percentage increase in safety of public transport would decrease the probability of choosing a car by 0.28%. It was also found that unit percentage increase in public transport affinity would decrease the probability of choosing car and two-wheeler by 0.39% and 0.2%, respectively.

Reliability, safety, and comfort are the latent variables found to be significantly influencing the mode choice behaviour of private employees. A unit percentage increase in safety of public transport was found to decrease the probability of choosing a car by 0.45%, whereas unit percentage increase in the reliability of public transport were found to decrease the probability of choosing a two-wheeler by 0.32%. It was also found that a unit percentage increase in comfort of public transport, lead to the decrease in the probability of choosing a autorickshaw by 0.55% and lead to increase in the probability of choosing a two-wheeler by 0.37% respectively.

Reliability, safety, convenience, and comfort are the latent variables found to be significantly influencing the mode choice behaviour of both government and private employees. It was also found that a unit percentage increase in reliability and safety of public transport decreased the probability of choosing a two-wheeler and car by 0.17% and 0.24% respectively. Unit percentage increase in convenience of public transport was found to decrease the probability of choosing car, autorickshaw and two-wheeler by 0.23%, 0.31%, and 0.35% respectively. It was also found that a unit percentage increase in comfort of public transport, lead to the increase in the probability of choosing a two-wheeler by 0.22%.

This paper offers insights into the mode choice behaviour of work trips in a medium-sized city in a rapidly developing country. The models developed as part of the study will help transport planners and policymakers to develop policies and recommendations for different categories of work trips in medium-sized cities.

References

1. Alex AP, Saraswathy MV, Isaac KP (2016) Latent variable enriched mode choice model for work activity in multi modal condition prevalent in India. *Int J Traffic Transp Eng* 6(4):378–389
2. Alvinsyah, Soehodho S, Nainggolan PJ (2005) Public transport user attitude based on choice model parameter characteristics (case study: Jakarta busway system). *J East Asia Soc Transp Stud* 6:480–491
3. Antonucci L, Crocetta C, d'Ovidio FD, Toma E (2012) Passenger satisfaction: a multi-group analysis. *Qual Quant* 48(1):337–345
4. Ashalatha R, Manju VS, Zacharaia AB (2013) Mode choice behaviour of commuters in Thiruvananthapuram city. *J Transp Eng* 139:494–502
5. Atasoy B, Glerum A, Bierlaire M (2013) Attitudes towards mode choice in Switzerland. *disP Plann Rev* 49(2):101–117
6. Chen J, Li S (2017) Mode choice model for public transport with categorized latent variables. *Math Probl Eng* 2017:1–11
7. Chen CP, Naylor GA (2011) Development of a mode choice model for bus rapid transit in Santa Clara County, California. *J Public Transp* 14(3):41–62
8. Dimitrios P, Luis MM (2015) The role of accessibility and connectivity in mode choice. A structural equation modelling approach. *Transp Res Procedia* 10:831–839
9. Kumar M, Sarkar P, Madhu E (2013) Development of fuzzy logic based mode choice model considering various public transport policy options. *Int J Traffic Transp Eng* 3(4):408–425
10. Marwa EE, Ibrahim H, Mohamed MS, Mohamed SS (2014) Policy sensitive mode choice analysis of Port-Said City, Egypt. *Alex Eng J* 53:891–901
11. Pulugurta S, Arun A, Errampalli M (2013) Use of artificial intelligence for mode choice analysis and comparison with traditional multinomial logit model. *Soc Behav Sci* 104:583–592
12. Ravi Sekhar C (2014) Mode choice analysis: the data, the models and future ahead. *Int J Traffic Transp Eng* 4(3):269–285
13. Ren G, Fan H (2020) Study on influencing factors of urban short-distance travel mode choice based on structural equation modelling. In: *CICTP 2020*, pp 3632–3644
14. Santos G, Maoh H, Potoglou D, von Brunn T (2013) Factors influencing modal split of commuting journeys in medium-size European cities. *J Transp Geogr* 30:127–137

Innovative Plastic Hinge Relocation Technique in Steel Moment Connection



C. H. Farshad Ali and Sajan Jose

Abstract This paper presents a novel plastic hinge relocation technique in steel beam column joint with replaceable fuse connection in beam segment. The main objective of this study is to analyze the behavior of the beam member with different cross sections and orientations, and investigate the impact of removing the gap between beam segments to identify an effective specimen that can enhance the moment capacity and performance of the joint and reduce the risk of brittle failure. Finite element analysis (FEA) was conducted using ANSYS software to evaluate the performance of the proposed technique under cyclic loading conditions according to the AISC protocol (AISC in Seismic provisions for structural steel buildings, American Institute of Steel Construction, 2010 [1]), and the hysteresis curve was obtained. The results of this study provide insights into the strength and ductility of the proposed steel beam column joint with replaceable steel fuse angle connections. The proposed technique has the potential to enhance the resilience of structural systems, thereby improving public safety and reducing economic losses. The findings of this study are relevant to the civil engineering industry and can contribute to the development of innovative and resilient structural systems that can withstand extreme events and improve the safety and sustainability of modern infrastructure.

Keywords Plastic hinge relocation · Steel beam column joint · Replaceable fuse connection · Beam segment · Finite element analysis · Cyclic loading · Hysteresis curve

C. H. Farshad Ali (✉)
APJ Abdul Kalam Technological University, Thiruvananthapuram, Kerala, India
e-mail: farshadali98@gmail.com

S. Jose
Universal Engineering College, Vallivattom, India

1 Introduction

Steel beam column joints are critical components of structural systems and must be designed to withstand extreme loading conditions while maintaining their strength and stiffness [4]. In recent years, researchers have focused on developing innovative techniques to enhance the performance and resilience of steel beam column joints [2]. One such technique is the use of replaceable fuse connections in beam segments, which can significantly enhance the moment capacity and performance of the joint.

The proposed technique involves relocating the plastic hinge from the beam to the column section, which reduces the risk of brittle failure and enhances the overall ductility and performance of the joint. The Finite Element Analysis (FEA) is conducted using ANSYS software to analyze the behavior of the beam member under cyclic loading condition. The main objective of the project is to analyze the behavior of the beam member with different cross sections and orientations, and investigate the impact of removing the gap between beam segments to identify an effective specimen that can enhance the moment capacity and performance of the joint and reduce the risk of brittle failure.

2 Loading Protocol

Loading was applied as the vertical displacement at the free end of the beam in accordance with a modified loading sequence of AISC 341-10 [1]. The loading protocol is given in Table 1. After the connections reached the drift angle of 0.04, a drift angle increment of 0.01 (two cycles) was included until evident resistance deterioration was observed, and the test was terminated. In the test, the drift angle is taken as the ratio of the beam deflection to the distance between the loading tip and the centreline of the column section (i.e. 2700 mm).

Table 1 Loading protocol

Target drift angle (rad)	Target displacement (mm)	Number of cycles
0.00375	10.125	3
0.005	13.5	3
0.0075	20.5	3
0.01	27.0	4
0.015	40.5	2
0.02	54.0	2
0.03	31.0	2
0.04	108.0	2

Table 2 Material properties

Description	Yield strength, f_y (MPa)	Ultimate strength, f_u (MPa)	f_u/f_y	Fracture elongation (%)
Beam flange	299	468	1.56	29
Beam web	370	535	1.44	28
Angle	261	356	1.36	24

3 Material Properties

The beam and column made of Grade Q345 steel were built-up steel I-sections with dimensions (depth \times width \times web thickness \times flange thickness, unit: mm) of $450 \times 200 \times 8 \times 18$ mm and $350 \times 350 \times 20 \times 30$ mm respectively. The short beam segment was welded to the column, and continuity plates were provided at the centreline of the beam flange. The angles were bolted to the flange and web via five M24 and four M20 high-strength friction bolts at each side. Grade Q235 steel angles with a size of $L74 \times 96 \times 10$ (short leg length \times long leg length \times thickness, unit: mm) were installed in all test connections [3] (Table 2).

4 Modelling

The critical information on the specimens is summarised in Table 3 in terms of geometric parameters of angles and loading protocol. In general, the test parameters include the loading scenarios (i.e., cyclic test), position of the connection (i.e., a) and gap width (i.e., g). For easy reference, specimens were assigned with test codes. Specifically, the first capital letter “H” represents specimens for the cyclic test, respectively. The following number “500” stands for the position of the connection (i.e. a). The number following the hyphen, i.e. “20” represents the gap width (i.e. g). The last letter “I” stands for an initial test, respectively [3] (Figs. 1 and 2).

5 Methodology

5.1 Analyse the Beam Segment Having with Gap and Orientation

Analyze the beam segment with different orientation and find effective angle. The orientations of the beam segment are 0, 5, 10, 15°. The analysed specimens are H500 20I 0D, H500 20I 5D, H500 20I 10D, H500 20I 15D (Figs. 3, 4, 5 and Table 4).

Table 3 Information of specimens

Specimen	Position of connection, a (mm)	Gap width, g (mm)	Angle size (mm)	Inclination angle (°)	Loading protocol
H500 20I 0D	500	20	L74 × 96 × 10	0	Cyclic
H500 20I 5D	500	20	L74 × 96 × 10	5	Cyclic
H500 20I 10D	500	20	L74 × 96 × 10	10	Cyclic
H500 20I 15D	500	20	L74 × 96 × 10	15	Cyclic
ST50 H500 20I 0D	500	20	L74 × 96 × 10	0	Cyclic
ST100 H500 20I 0D	500	20	L74 × 96 × 10	0	Cyclic
H500 0I 0D	500	0	L74 × 96 × 10	0	Cyclic
H500 0I 5D	500	0	L74 × 96 × 10	5	Cyclic
H500 0I 10D	500	0	L74 × 96 × 10	10	Cyclic
H500 0I 15D	500	0	L74 × 96 × 10	15	Cyclic
ST50 H500 0I 0D	500	0	L74 × 96 × 10	0	Cyclic
ST100 H500 0I 0D	500	0	L74 × 96 × 10	0	Cyclic

5.2 Analyse the Beam Segment Having with Gap and Stepped Cross Section

Analyze the beam segment with different cross section (stepped beam section). The specimens are named as ST50 H500 20I 0D, ST100 H500 20I 0D (Figs. 6, 7, 8 and Table 5).

5.3 Analyse the Beam Segment Having Without Gap

Analyze the beam segments by removing the gap between them to find effective specimen. The specimens are H500 0I 0D, H500 0I 5D, H500 0I 10D, H500 0I 15D, ST50 H500 0I 0D, ST100 H500 0I 0D (Figs. 9, 10, 11 and Table 6).

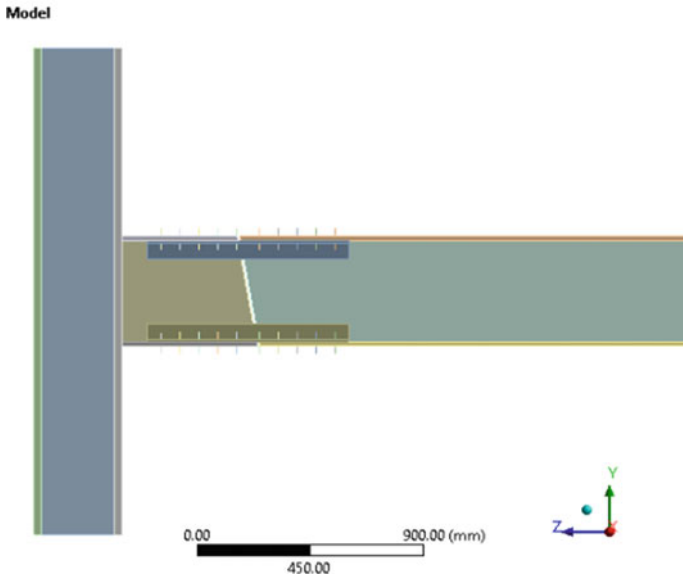


Fig. 1 Geometry of the specimen H500 20I 10D

H: H500 - 20 I 10D
Figure

- A col support 1
- B col support 2
- C cyclic anlysis

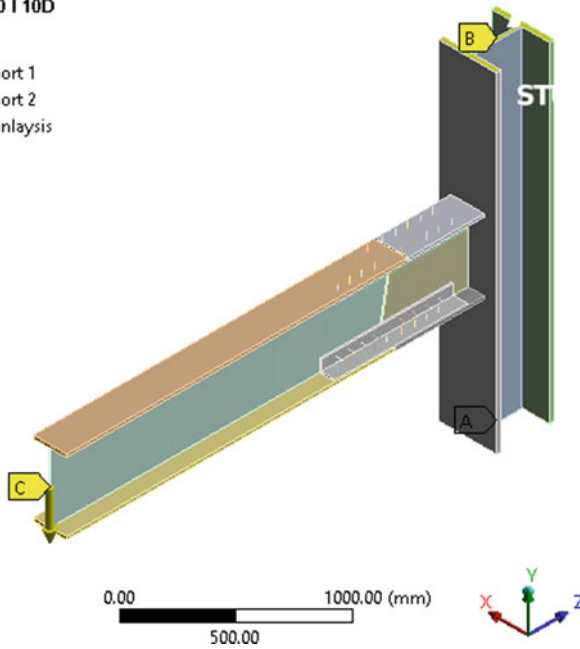


Fig. 2 Boundary condition

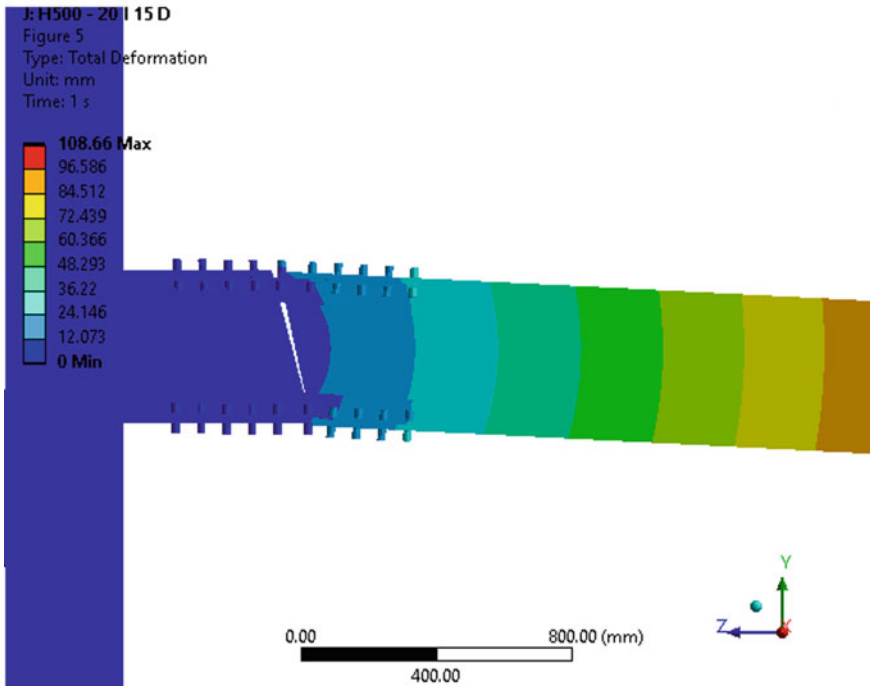


Fig. 3 Total deformation of the specimen H500 20I 10D

6 Conclusions

This study provides an analysis of the behavior of steel beam column joints with replaceable fuse connections in beam segments and relocated plastic hinges. The analysis shows that the proposed technique significantly enhances the moment capacity and performance of the joint, reduces the risk of brittle failure, and improves the overall ductility of the joint. The proposed technique has the potential to contribute to the development of innovative and resilient structural systems that can withstand extreme events and improve the safety and sustainability of modern infrastructure. The performance of the specimen can be determined by considering factors such as the failure position, moment capacity, drift, and energy dissipation. These parameters play crucial roles in assessing the overall behavior and effectiveness of the specimen.

- By analysis of different models of Beam segment having with gap and orientation, it was founded that the specimen H500 20I 10 shows better moment carrying capacity as 411.399 kN m.
- By analysis of different models of Beam segment having stepped cross section, it was founded that all models shows poor performance.

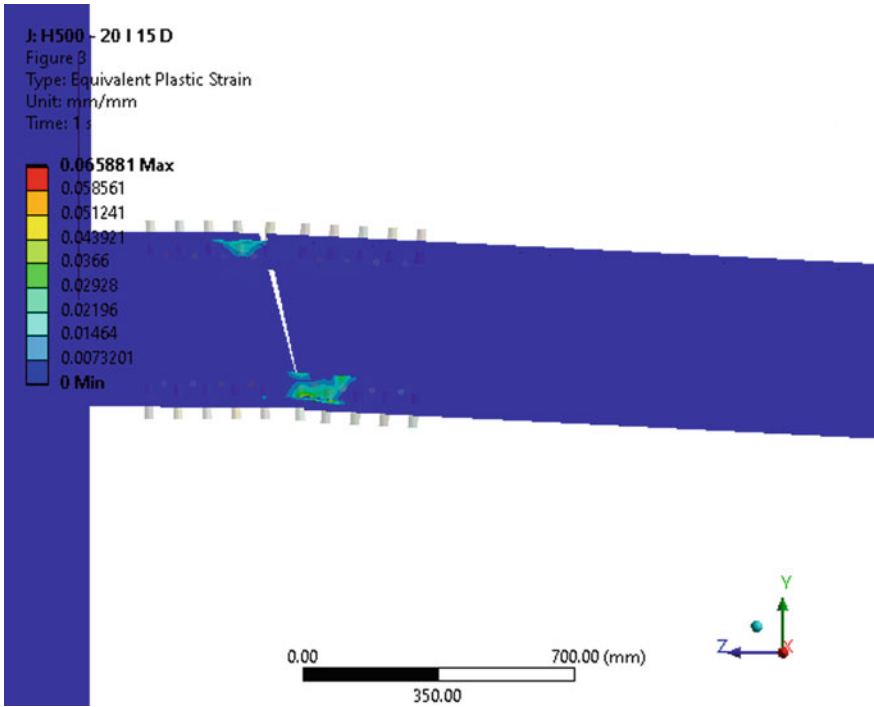
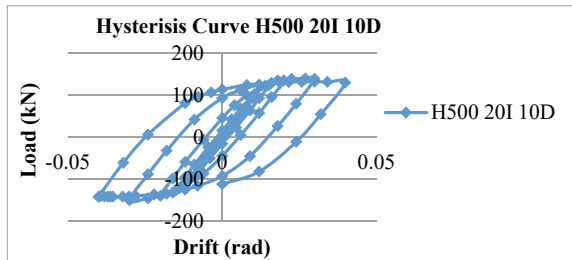


Fig. 4 Equivalent plastic strain of the specimen H500 20I 10D

Fig. 5 Hysteresis curve of specimen H500 20I 10D



- By analysis of different models of Beam segment having without gap, it was founded that the specimen H500 0I 5D, H500 0I 10D, H500 0I 15D shows higher moment capacity, energy dissipation and drift so it shows better performance.

Table 4 Performance of beam segment having with gap and orientation

Specimen	Deflection (mm)	Force reaction (kN)	Moment (kN m)	Drift (rad)	Failure	Energy dissipation (kJ)
H500 20 0I	59.728	142.53	384.83	0.022	Fuse	62.023
H500 20I 5D	109.06	128.28	346.35	0.040	Fuse	44.330
H500 20I 10D	99.046	152.37	411.39	0.036	Fuse	18.448
H500 20I 15D	108.66	139.14	375.67	0.040	Fuse	47.168

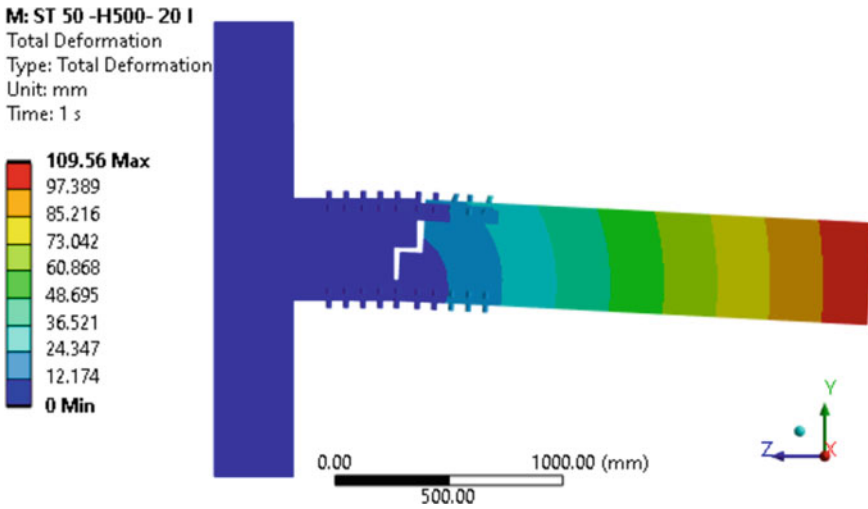


Fig. 6 Total deformation of specimen ST50 H500 20I 0D

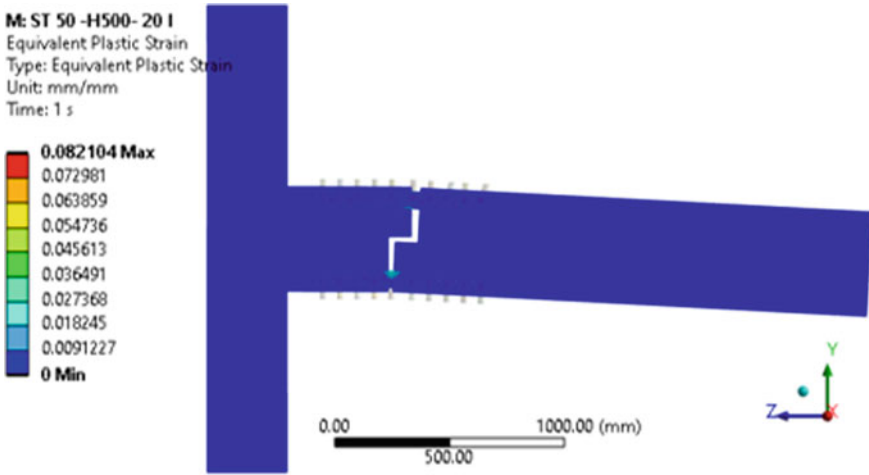


Fig. 7 Equivalent plastic strain of specimen ST50 H500 20I 0D

Fig. 8 Hysteresis curve of specimen ST50 H500 20I 0D

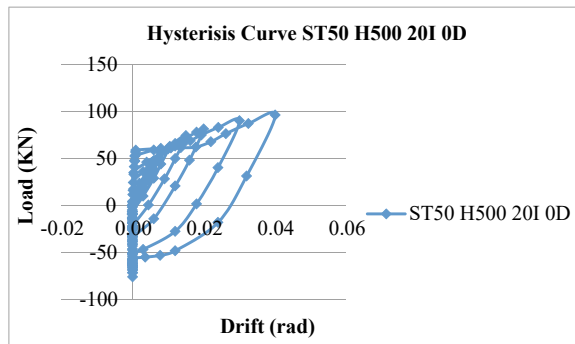


Table 5 Performance of stepped beam segment with gap

Specimen	Deflection (mm)	Force reaction (kN)	Moment (kN m)	Drift (rad)	Failure	Energy dissipation (kJ)
ST 50 H500 20I	109.56	83.27	224.829	0.0405	Fuse	18.8267
ST 100 H500 20I	109.12	98.683	266.4441	0.0404	Fuse	19.1869

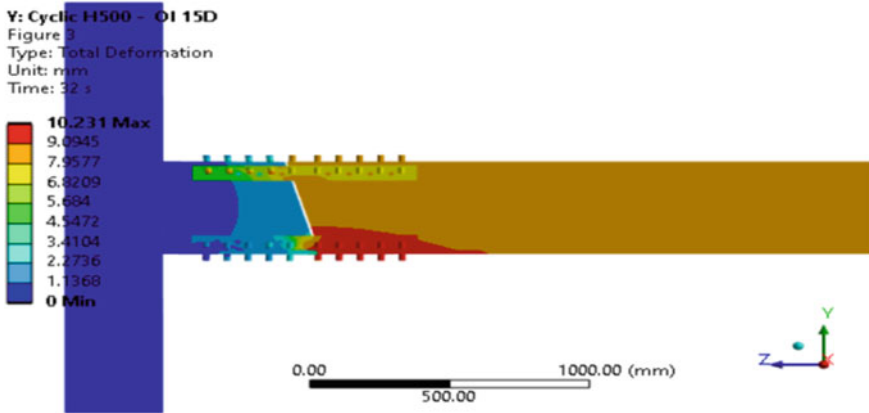


Fig. 9 Total deformation of specimen H500 OI 15D

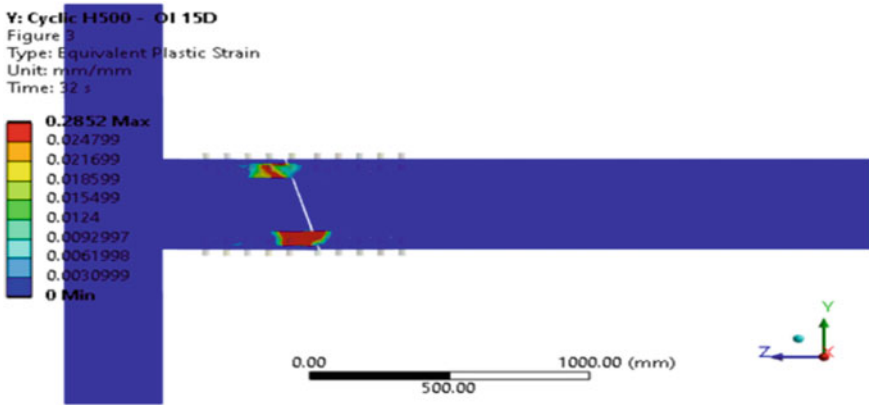


Fig. 10 Equivalent plastic strain of specimen H500 OI 15D

Fig. 11 Hysteresis curve of specimen H500 OI 15D

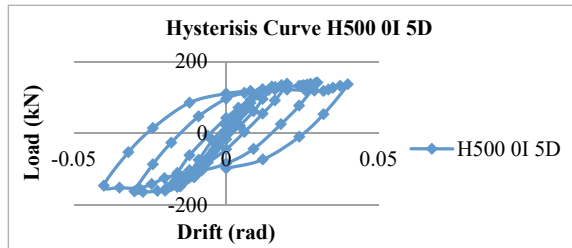


Table 6 Performance of beam segment having without gap

Specimen	Deflection (mm)	Force reaction (kN)	Moment (kN m)	Drift (rad)	Failure	Energy dissipation (kJ)
H500 0I 0D	109.75	136.54	368.658	0.0406	Fuse	42.063
H500 0I 5D	76.663	167.18	451.386	0.0283	Fuse	56.831
H500 0I 10D	109.68	157.14	424.278	0.04062	Fuse	45.506
H500 0I 15D	109.58	170.11	459.297	0.0405	Fuse	57.032
ST 50 H500 0I	109.06	229.86	620.622	0.0403	Web	32.879
ST 100 H500 0I	109.75	116.71	315.117	0.040	Fuse	18.448

References

1. AISC (2010) Seismic provisions for structural steel buildings. American Institute of Steel Construction
2. Bradford MA, Uang CM (1999) Performance-based seismic design of steel structures. J Struct Eng 125(12):1428–1435
3. He X et al (2022) Development of a connection equipped with fuse angles for steel moment resisting frames
4. Shariati M, Hejazi MM (2015) Behavior of steel beam-column connections

Strength and Durability Properties of Steel Slag Incorporated Self-curing Concrete



Karthika Balakrishnan and Lalith Prakash Elavazhagan

Abstract There is a growing global interest in SAP-treated cement-based materials due to their excellent durability, fracture resistance, wide availability, and cost-effectiveness. However, a drawback of SAP usage is the development of macropores when the polymer releases water, weakening the material's mechanical characteristics. To address this concern, steel slag, a byproduct of steelmaking, is used as a partial replacement for fine aggregate to compensate for the loss of strength. Steel slag emerges as a viable alternative as a partial replacement for natural aggregates when the natural aggregate usage in concrete fails to meet the required quantity and quality standards. This study aims to investigate the mechanical and durability properties of self-curing concrete incorporating steel slag and sodium polyacrylate, a super-absorbing polymer (SAP). The research compares the results of these properties with conventional concrete. In M30 grade concrete, the fine aggregate was substituted with steel slag in 30 and 40% proportions. The percentage of superabsorbent polymer (SAP) by weight of cement was also varied to 0.1, 0.2, and 0.3%. Concrete mix with 0.1% SAP and 40% steel slag dosage exhibited superior mechanical properties. Durability tests conducted on this mix combination revealed a better performance compared to control concrete mix.

Keywords Super absorbing polymer · Sodium polyacrylate · Steel slag · Durability · Self-curing concrete

1 Introduction

Steel slag (SS) is a residual bi-product obtained from steel production. Significant volumes of this waste are produced, posing issues and hazards for the factories and the environment. The disposal of steel slag creates environmental issues like land, air, water pollution, and soil contamination because it contains various heavy metals

K. Balakrishnan · L. P. Elavazhagan (✉)
Department of Civil Engineering, Amrita School of Engineering, Amrita Vishwa Vidyapeetham,
Coimbatore 641112, India
e-mail: e_lalithprakash@cb.amrita.edu

and other contaminants that can reach into the soil if not properly handled [1]. One of the methods for addressing the issues that this solid waste causes is recycling. Solid waste management is of particular significance due to the escalating quantities of industrial by-products [2]. Steel slag may be used in concrete as both coarse and fine aggregate, as a component of asphalt highway pavement, as clinker-making raw materials, as ballast for roadways, and as filler for a variety of excavations. Using waste materials as aggregate materials are becoming more popular, and wide-ranging research is currently underway on the utilization of a diverse range of resources as aggregate substitutes, like steel slag, coal ash, and blast furnace slag, and to lower the cost of producing concrete by using fine aggregate made from discarded steel slag. The utilization of stainless steel as a building material is becoming more popular.

Recent studies show that introducing local unprocessed steel slag in concrete has a positive impact on both compressive and tensile strength [3]. The mechanical characteristics of the concrete are enhanced when SS is used as the FA. The SS can recompense for the loss of strength that causes due to the polymer which releases the water and macropores are developed. The mechanical strength of the sample enhanced greatly, because the hydration reaction produces CSH gel due to the comparatively high CaO concentration in steel slag. These gels fill the macropores, increasing the density of the structure. When the number of mesopores increases, the number of macropores decreases noticeably. The structure becomes more compact and homogenous, giving it the appearance of a sponge. The fine particles of steel slag having sizes 1–2 mm can also act as micro fillers, occupying interstitial spaces within the concrete matrix. This micro filler effect further enhances the overall densification of the concrete and reduces the presence of macro pores.

Based on studies and research, the best results are usually obtained for substitution ratios between 30 and 50%. Using a 30–50% replacement ratio of steel slag as fine aggregate has been shown to improve the mechanical properties. It can also improve the resistance to chloride ion penetration, which can help to prevent corrosion in reinforcing cement concrete [3]. The workability of concrete is negatively affected when steel slag is substitute for fine aggregate at a ratio of 50% or higher. However, when steel slag is used as a replacement for fine aggregate, it is important to consider that the slag aggregates possess an angular structure and vary in size distribution. This characteristic results in a significant improvement in compressive strength [4].

Curing is crucial, yet in places where water availability is scarce, improper curing happens. In the process of self-curing concrete, additional internal water helps the cement to hydrate, even during the mixing process, until the required final strength is achieved, and the leftover water is retained in the concrete by the small voids. Construction activities are increasing every day in remote and desert areas. Due to the shortage of water, the construction industry is finding alternative curing methods. Self-curing concrete is a curing method that capable to meet present and future requirements for curing concrete and that can enhance strength and durability. A crucial approach to enhance the durability characteristics of concrete involves reducing its permeability through effective compaction [5].

Super absorbent polymer (SAP), which was introduced in the 1980s, is primarily intended to convenience products, food packaging, and the sanitary and medical industries. It is a polyacrylic acid that can absorb, expand, and hold onto liquid without dissolving into a solution in the area between polymer chains and crosslinks. SAPs are inherently hydrophilic. The polymer chains in SAPs contain functional groups, such as carboxyl groups ($-\text{COOH}$), that attract and interact with water molecules. When SAPs come into contact with water, the hydrophilic groups on the polymer chains attract and bind with water molecules through hydrogen bonding. This interaction causes the polymer chains to undergo a process called swelling, where they absorb water and expand in size. The swelling of SAPs is facilitated by capillary action. The interconnected network of polymer chains and crosslinks creates small capillary spaces or voids within the material. These capillaries draw water into the SAPs, allowing them to absorb water from their surroundings. SAPs have a high absorption capacity due to the presence of void spaces that can accommodate water molecules. Once water is absorbed by SAPs, it is retained within the spaces between the polymer chains and crosslinks. The polymer matrix traps the water, preventing it from easily escaping. SAP can absorb and store water, releasing it gradually over time as needed.

SAP acquires strength early in the life of the concrete and inhibits self-desiccation due to its capacity for retaining an increased amount of water equivalent to its weight. Additionally, it acts as an internal curing agent in concrete, enhancing its strength and durability. When SAP is incorporated into the concrete mix, it can absorb a certain amount of water, reducing the loss of moisture during the curing process. This leads to more complete hydration of the cement particles, resulting in a denser and stronger concrete matrix [6]. Additionally, SAP can also reduce shrinkage and cracking of the concrete, resulting in a more durable and long-lasting structure. The use of SAP at various percentages (0.1, 0.2, 0.3%) is more advantageous than normal concrete in terms of compressive strength, durability and reduced shrinkage and cracking, and reduced need for external curing methods [7]. As time progresses, the internal curing effect becomes increasingly noticeable, resulting in a continuous enhancement of strength [8].

The comprehensive study presented in this research offers a profound comprehension of the diverse attributes exhibited by self-curing concrete incorporating steel slag, allowing for a comparison between the recorded outcomes and the experimental observations of the control mixture. The optimum replacement level refers to the ideal proportion of steel slag and SAP. It is determined through mechanical testing results. Self-curing has emerged as a viable alternative technique to minimize water usage during the curing process.

Table 1 Physical properties of cement

S. No.	Characteristics	Value obtained experimentally
1	Fineness	3%
2	Specific gravity	3.15
3	Normal consistency	34%

2 Materials

2.1 Cement

Standard OPC 53 grade cement was utilized, and its physical properties were tested in accordance with the standard procedure specified by IS 12269:1989 requirements (Table 1).

2.2 Fine Aggregate

Manufactured sand is a replacement for river sand in buildings. It is produced by crushing granite stones that are known for their hardness. The size of manufactured sand (M-SAND) is smaller than 4.75 mm. The tests were carried out under IS 383-2016.

2.3 Coarse Aggregate

Following the recommendations of IS 383-1970, locally available materials coarse aggregate with a maximum size of 20 mm was used (Table 2).

Table 2 Physical properties of fine aggregate and coarse aggregate

S. No.	Characteristics	Value for fine aggregate	Value for coarse aggregate
1	Bulk density (kg/m ³)	1696.30	1696.58
2	Water absorption (%)	2.05	0.51
3	Specific gravity	2.67	2.8

Table 3 Physical properties of steel slag

S. No.	Characteristics	Value obtained experimentally
1	Specific gravity	3.25
2	Fineness modulus	3.34

Fig. 1 SAP particle

2.4 Steel Slag

Steel slag (SS) is a residual by-product that is obtained during the production of steel. Stainless steel slag of size 1–2 mm is used. The grade of steel slag is in accordance with IS 455: 1989 (Table 3).

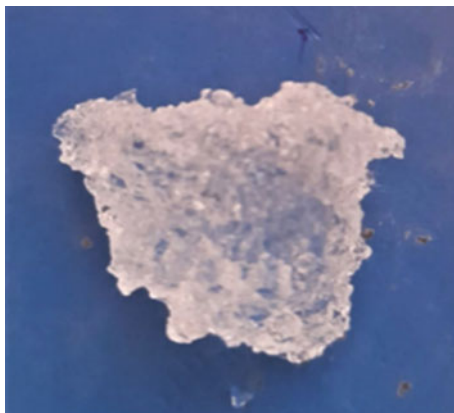
2.5 Super Absorbing Polymer

SAPs, which stands for sodium polyacrylate particles, have the unique ability to react with water, causing the polymer chains to expand and form a structure capable of absorbing water up to 200–300 times its own weight, subsequently transforming it into a hydrogel (Figs. 1 and 2).

2.6 Water

According to the Indian Standard Code, portable water is used to prepare the concrete mix. It is the basic requirement for the hydration of cement. It helps to maintain workability.

Fig. 2 SAP particle after absorption



3 Methodology

3.1 Mix Design

The mix design specifications for achieving M30 grade concrete has been prepared following IS 10262:2009, the mix design is 1:1.64:3.04 and the w/c ratio is 0.45 for maintaining workability for the control mix. The substitution ratios of steel slag were 30 and 40%, and the SAP dosages were 0.1, 0.2, and 0.3% by cement mass (Table 4).

Table 4 Mix for M30 concrete grade (kg/m³)

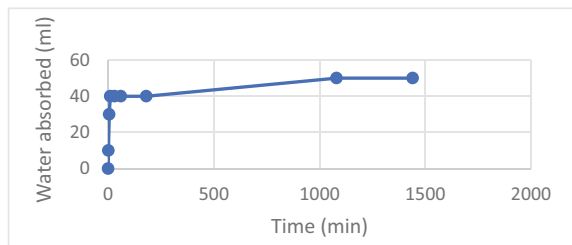
Mix	Cement	CA	FA	SS	SAP	w/c
M1 ^a	448	1366.12	735.59	0	0	0.45
M2	448	1366.12	545.13	220.76	1.36	0.45
M3	448	1366.12	441.54	294.35	1.36	0.45
M4	448	1366.12	545.13	220.76	2.73	0.45
M5	448	1366.12	441.54	294.35	2.73	0.45
M6	448	1366.12	545.13	220.76	4.09	0.45
M7	448	1366.12	441.54	294.35	4.09	0.45

^a Control mix

Table 5 Mix percentage and combinations

Mix	Cement	CA	FA	SS	SAP
M1 ^a	100	100	100	0	0
M2	100	100	70	30	0.1
M3	100	100	60	40	0.1
M4	100	100	70	30	0.2
M5	100	100	60	40	0.2
M6	100	100	70	30	0.3
M7	100	100	60	40	0.3

^a Control mix

Fig. 3 Water absorbed for 1 g of SAP

4 Tests, Results and Discussions

4.1 Tea Bag Method

As per the Recommendation of RILEM TC 260-RSC, the tea bag method is a method used for measuring the absorption behavior of SAP. The dry tea bag containing 1 g of SAP was placed in a measuring jar containing 200 ml of water and covered with a lid to minimize carbonation and evaporation. The wet tea bag with an enlarged SAP was removed from the measuring jar after 1, 5, 10, 30, 60 min, 3 h, 18 h, and 24 h. Now, observing how much water is absorbed in each period, each SAP sample was measured by three individual tea bags. The water absorption becomes constant from 18 h so the average water absorption value is taken at the end of 24 h, which was conducted on 3 samples. The average water absorption is 50 ml per gram of SAP (Fig. 3).

4.2 Flow Table Test

To assess the workability of the concrete, a flow table test was conducted in accordance with the specifications outlined in IS 1199:1959. Flow percent is calculated for

Table 6 Mechanical proper test results at 28 days

S. No.	Mix combination	Flow percent (%)	Compressive strength (N/mm ²)	Split tensile strength (N/mm ²)	Flexural strength (N/mm ²)
1	M1 ^a	34.67	31.21	2.46	3.53
2	M2	34.33	37.2	2.67	3.61
3	M3	40.67	41.33	2.88	4.1
4	M4	42.33	35.5	2.35	3.71
5	M5	51	30.41	2.45	3.8
6	M6	43.67	25.57	2.14	3.05
7	M7	47	2.61	2.38	3.7

^a Control mix

each combination, and the results obtained are shown in Table 6. The flow table test results indicate that the flow table values of the concrete produced were between 34 and 51%. The M5 mix combination has better workability compared to the control mix (M1).

4.3 Compressive Strength Test

The compressive strength of a cube with dimension 10 cm × 10 cm × 10 cm by varying the percentage at 28 days is given in Table 6. According to IS 516-1969, compressive testing equipment, UTM was used to perform a compressive strength test on three cubes. The maximum compressive strength among the trial mixes corresponds to self-curing concrete incorporated with steel slag (M3), and it is 41.33 N/mm². The compressive strength reduces with SAP dosage beyond 0.1% (Fig. 4).

4.4 Split Tensile Strength Test

The split tensile strength of concrete was evaluated following the guidelines of IS 5816-1999, and the results are presented in Table 6. For each combination, three concrete cylinders measuring 100 mm in diameter and 200 mm in height were assessed. After a hydration period of 28 days, the specimens were positioned on the testing platform of a Compression Testing Machine (CTM). A uniformly distributed load was then applied until the specimens fractured. The split tensile strength is higher for self-curing concrete incorporating steel slag compared to a control mix. The maximum split tensile strength among the trial mixes corresponds to self-curing concrete incorporated with steel slag (M3), and it is 2.88 N/mm². The control mix (M1) has a comparable strength of 2.46 N/mm² (Fig. 5; Table 6).

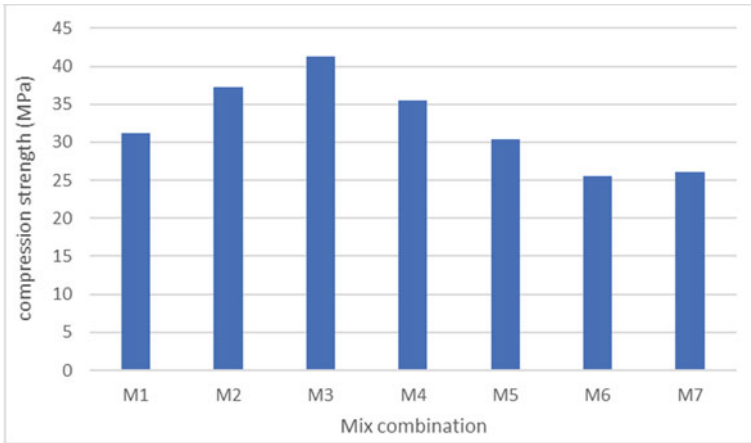


Fig. 4 Compression strength at 28 days

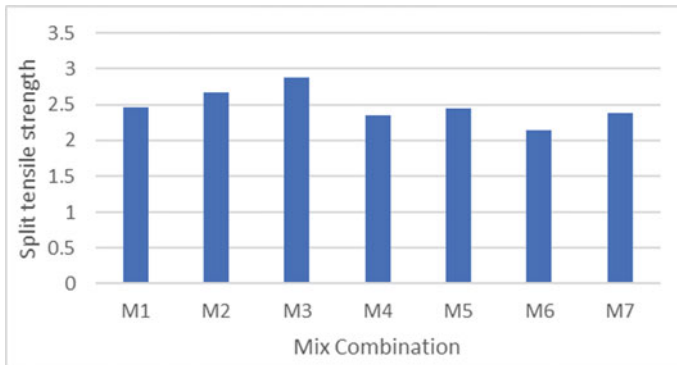


Fig. 5 Split tensile strength at 28 days

4.5 Flexural Strength Test

The flexural strength of concrete was assessed following the guidelines of IS 516-1959, and the corresponding results are displayed in Table 6. For each combination, three concrete beams measuring 100 mm × 100 mm × 500 mm were subjected to testing using a Universal Testing Machine (UTM). The maximum flexural strength among the trial mixes corresponds to self-curing concrete incorporated with steel slag (M3), and it is 4.1 N/mm² (Fig. 6; Table 6).

In all of the above tests the mix combination M3 (SS 40% and SAP 0.1%), performed well and it qualifies as the optimum mix among the tested combinations. Further, the basic durability properties, such as water absorption and sorptivity are

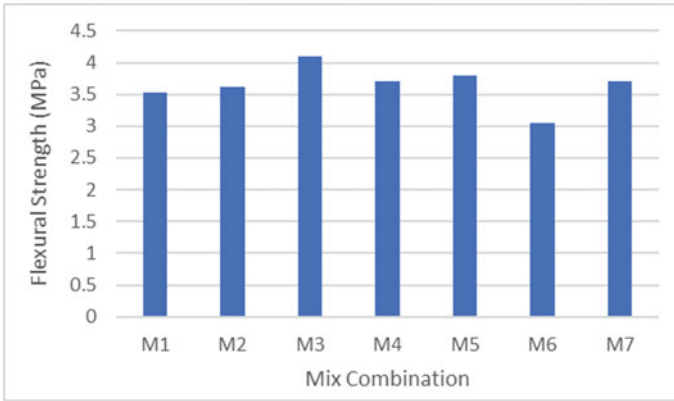


Fig. 6 Flexural strength at 28 days

Table 7 Durability performance—optimum mix versus control mix

S. No.	Mix combination	Water absorption (%)	Sorptivity ($\text{mm/s}^{0.5}$)
1	M1	4.02	0.178
2	M3	3.48	0.106

examined for this optimum mix combination (M3) and compared with the control mix.

4.6 Water Absorption Test

Water absorption tests for the cube were performed using 3 samples under IS 2185 (Part 1) 2005. A concrete specimen of size 10 cm × 10 cm × 10 cm was soaked in water for 24 h, and the wet mass of the block was measured. The cube was dried in an oven at 105 °C for at least 24 h, and the mass of the cubes after drying was recorded as shown in Table 7. Water absorption for self-curing concrete incorporated with steel slag is 3.48%, lower than the control mix of 4.02%.

4.7 Sorptivity Test

The samples were prepared according to IS 4031-Part 6. Water penetration through capillary holes from one side of the unsaturated concrete was measured using sorptivity. From the cylinder specimens, concrete discs with measurements of 100 mm × 50 mm were cut. A sealant was then applied to the top and curved surfaces of

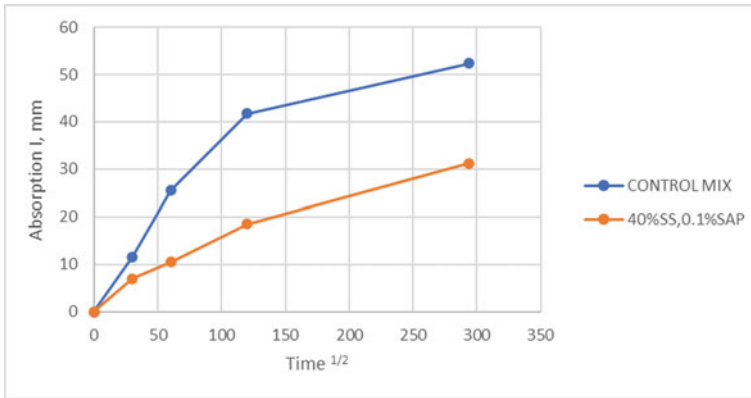


Fig. 7 Sorptivity test at 28 days

the discs, leaving the bottom surface exposed. These specimens were submerged in water, ensuring that the exposed surface made interaction with the water while maintaining a water depth of 1–3 mm. Weight was noted and shown in Table 7. Sorptivity was $0.106 \text{ mm/s}^{0.5}$ for self-curing concrete incorporated with steel slag, lower than the control mix of $0.178 \text{ mm/s}^{0.5}$. A lower sorptivity value indicates that the porosity of the concert has been reduced after the inclusion of steel slag (Fig. 7).

5 Conclusion

This paper presents the findings of an experimental investigation on the mechanical and durability properties of steel slag-incorporated self-curing concrete. Self-curing concrete is prepared by partially substituting the fine aggregate with steel slag. Based on the results, the ideal proportion of steel slag as a partial replacement in the fine aggregate is found to be 40%, while the optimal SAP dosage is 0.1%. From the research studies, the following findings were established:

- Flowability increases significantly with an increase in SAP content. Even though there is a falling trend at 0.3% SAP dosage, the values are still above the control mix.
- The optimum mix combination M3 performs better than the control mix in terms of mechanical and durability properties.
- The mixes perform better in all the test mechanical properties showing an upward trend with an increase in SAP dosage of up to 0.1%. Higher dosages beyond 0.1% affect the performance negatively.
- Mixes with higher Steel slag content exhibit better mechanical properties due to their micro filler effect.

- Compared to the control mix, self-curing concrete incorporating steel slag exhibits lower water absorption. This can be attributed to the porous characteristics of steel slag, which enable it to absorb and retain moisture. Consequently, the self-curing concrete containing steel slag demonstrates reduced water absorption, thereby enhancing the durability and moisture retention properties of the material.
- In contrast to the control mix, the self-curing concrete that incorporates steel slag demonstrates lower sorptivity. This indicates that the self-curing concrete, combined with steel slag, offers enhanced water resistance and reduced permeability. As a result, it becomes more durable and less susceptible to damage caused by water-related factors.

References

1. Qasrawi H (2014) The use of steel slag aggregate to enhance the mechanical properties of recycled aggregate concrete and retain the environment. *Constr Build Mater* 54:298–304
2. Prasad VD, Prakash EL, Abishek M, Dev KU, Kiran CS (2018) Study on concrete containing waste foundry sand, fly ash and polypropylene fibre using Taguchi method. *Mater Today Proc* 5(11):23964–23973
3. Qasrawi H, Shalabi F, Asi I (2009) Use of low CaO unprocessed steel slag in concrete as fine aggregate. *Constr Build Mater* 23(2):1118–1125
4. Gencil O, Karadag O, Oren OH, Bilir T (2021) Steel slag and its applications in cement and concrete technology: a review. *Constr Build Mater* 283. <https://doi.org/10.1016/j.conbuildmat.2021.122783>
5. Sathyan D, Anand KB (2019) Influence of superplasticizer family on the durability characteristics of fly ash incorporated cement concrete. *Constr Build Mater* 204:864–874
6. Yang J, Guo Y, Shen A, Chen Z, Qin X, Zhao M (2019) Research on drying shrinkage deformation and cracking risk of pavement concrete internally cured by SAPs. *Constr Build Mater* 227:116705
7. Desineni BOR, Kommineni HR (2020) An experimental study on strength characteristics of self-curing concrete with manufacture sand using super absorbed polymer. *Mater Today Proc* 33:333–337. <https://doi.org/10.1016/j.matpr.2020.04.117>
8. Lokeshwari M, Pavan Bandakli BR, Tarun SR, Sachin P, Kumar V (2020) A review on self-curing concrete. *Mater Today Proc* 43:2259–2264. <https://doi.org/10.1016/j.matpr.2020.12.859>

Numerical Modelling and Analysis of GGBS Mortar for Predicting Strength Parameters



V. Mohammed Zidan Sameer, C. Vyshakh, Geethu Elsa Thomas, and A. S. Sajith

Abstract Cement production is a significant source of carbon dioxide (CO₂) emissions and is responsible for around 8% of global greenhouse gas emissions. New studies recommend replacing cement with other supplementary cementitious materials such as Ground Granulated Blast Furnace Slag (GGBS), fly ash, etc. The use of these materials can also help to reduce waste, as they are typically disposed of in landfills. GGBS is an industrial waste product that is produced as a by-product during the production of iron. The disposal of GGBS can potentially pose environmental hazards if it is not appropriately managed. GGBS can improve durability and strength when used as an ingredient in concrete. The use of GGBS reduces the amount of cement needed for construction, which in turn reduces the amount of CO₂ emission associated with cement production. This study numerically models GGBS mortar which is a combination of 50% cement and 50% GGBS considering economy and strength parameters. ABAQUS CAE 2020 is used for the finite element modeling of the GGBS mortar. The numerical model is validated using the experimental results from the literature. This study provides useful contributions toward sustainable construction practices.

Keywords Ground granulated blast furnace slag · Finite element modelling · Sustainable construction

1 Introduction

Mortar is a mixture of cement, fine aggregates, and water in a specific amount to achieve a specific strength. The mortar mix design aims to reach the highest levels of compressive strength and durability without sacrificing quality [1]. One of the most widely used materials for construction is Ordinary Portland cement, and demand is rising as infrastructure work picks up speed. One of the main directions of low-carbon materials is the reuse of waste or byproducts, which has the tremendous

V. Mohammed Zidan Sameer (✉) · C. Vyshakh · G. E. Thomas · A. S. Sajith
Department of Civil Engineering, National Institute of Technology Calicut, Kozhikode, India
e-mail: mohammedzidanv@gmail.com

potential [2]. The construction industry should develop novel methods and materials. To lower the cost of building materials by utilizing locally available materials, various researchers are looking at the usage of alternative materials instead of standard traditional materials. It lowers the price of producing concrete and will lower the price of constructing buildings. Cement is the most essential component of concrete. The use of cement alone as a binder substance generates a high heat of hydration. Because the production of this raw substance emits a significant amount of CO₂. Many studies have been conducted recently to decrease CO₂. The use of industrial byproducts or supplementary cementing materials such as Ground Granulated Blast Furnace Slag (GGBS), Fly Ash, Silica Fume, and Metakaolin is an effective method of reducing CO₂ emissions from the cement industry [3]. The current experimental effort attempts to replace cement with GGBS. Thomas et al. [4–6] studied the mechanical and durability performances of cement mortar when partially replaced with GGBS. GGBS was tested for various proportions, in the mortar mix and was found to enhance the performance of the system. The authors identified that a mix with 50% GGBS and 50% cement is the most efficient in terms of durability, impact resistance, and other strength parameters and this mix is termed GGBS mortar.

Experimental analysis has always been a tedious, time-consuming, and costly process. Numerical analysis is preferred over experimental analysis due to the above-mentioned concerns. Concrete and mortar models are successfully modeled numerically using Finite Element (FE) Analysis software like ABAQUS and ANSYS. Abaqus uses the Concrete Damage Plasticity (CDP) model to numerically model concrete. Many concrete models have been analyzed and validated using ABAQUS previously [7, 8].

The present study attempts to develop a FE model for the GGBS mortar mentioned in the literature [5]. The FE model for the GGBS mortar beam is modeled using ABAQUS CAE 2020, and the flexural behavior of the beam is studied under a three-point bending test. This model is validated by the experimental results in the literature [5].

2 Material Properties

GGBS mortar was modeled in Abaqus using the concrete damage plasticity model [9]. The material properties and the CDP model parameters are shown in Table 1.

3 Modelling in ABAQUS

In this research, the ABAQUS finite element program was used to simulate the behavior of the experimental beams. ABAQUS CAE was chosen for this simulation because of its user-friendly UI and support for parametric modeling. The study is analyzed using dynamic explicit analysis. ABAQUS offers three concrete material

Table 1 Material properties and CDP parameters

Material properties	Value
Density	2100 kg/m ³
Modulus of elasticity	19,700 MPa
Poisson's ratio	0.19
Dilation angle	38°
Eccentricity	1
F _{b0} /f _{c0}	1.12
K	0.667
Viscosity parameter	0

models: the smeared crack model, the damaged plasticity model, and the cracking constitutive model. The concrete damage plasticity (CDP) model is used to model the beam specimen. The three-dimensional finite element model of the beam of dimension 160 × 40 × 40 mm has been developed. The gauge length is taken as 120 mm. Figure 1a shows the GGBS mortar beam geometry made. Figure 1b shows the meshed model of the beam. The total number of elements in meshing is 2048. The C3D8R eight-node continuum elements are based on a Lagrangian explanation of behavior where the element deforms together with the material deformation. Figure 1c shows the boundary condition and load applied on the beam. The boundary condition is encastre. The load applied is 2.226 mm/s in the vertical direction.

4 Results and Discussions

The beam is modeled and tested under a three-point bending test under dynamic explicit analysis. Figure 2 shows the concentration of the stress in the beam under the three-point bending test. Figure 3 illustrates the load–deflection graphs for the experimental and numerical findings. The FEM-modeled beam exhibited an ultimate load value of 2470 N with a displacement value of 0.52 mm. Table 2 shows the comparison of the ultimate loads obtained from the experimental and numerical results. The studies from Thomas et al. [4] also exhibited an ultimate load value of 2500 N with a displacement value of 0.56 mm. From the result, it is clear that the modeled FEM model is in good agreement with the experimental value with an error of 1.2%.

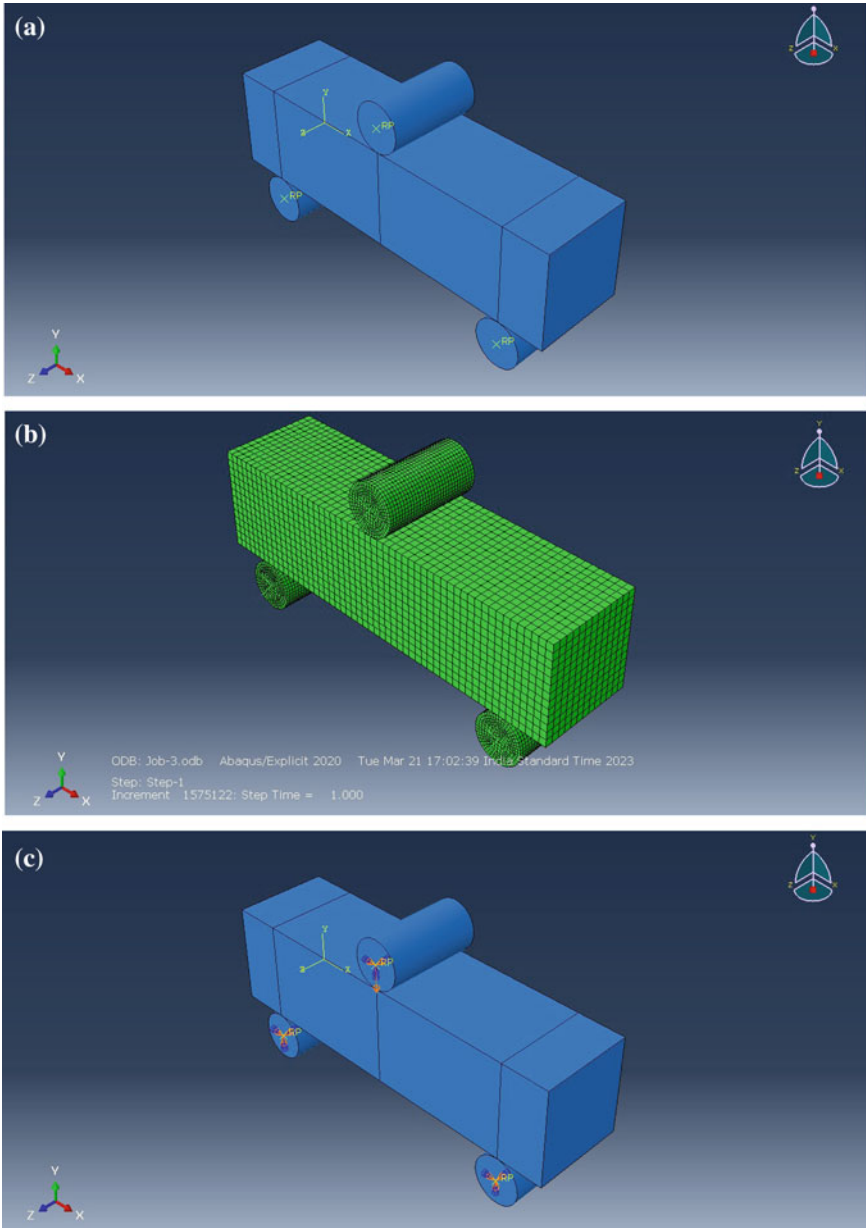


Fig. 1 a Geometry of the beam. b FEM meshed model. c Defining boundary condition

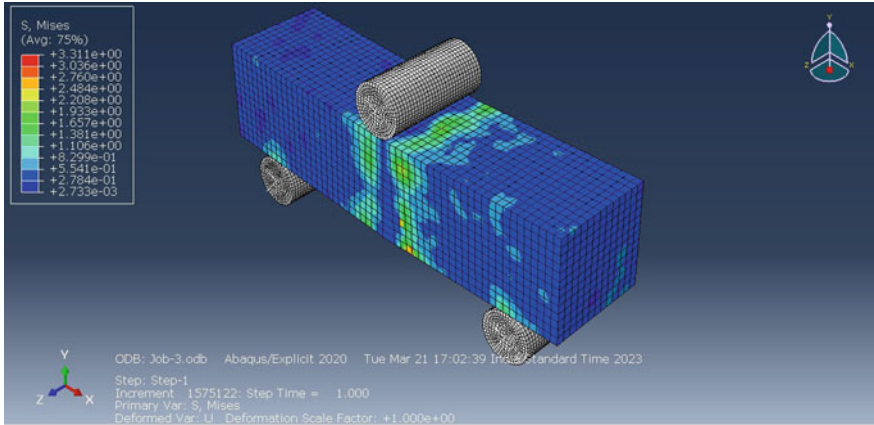


Fig. 2 Stress concentration diagram

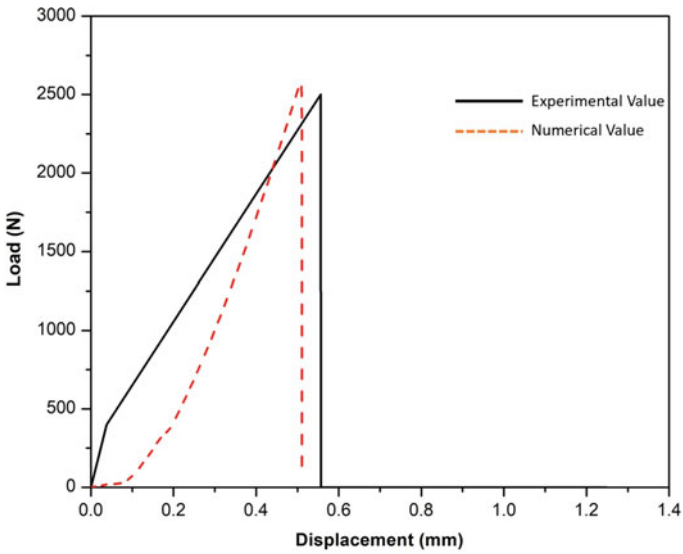


Fig. 3 Comparison of the load–deflection curves

Table 2 Comparison of results

Ultimate load (N)		
Experimental value	Numerical value	Error (%)
2500	2470	1.2

5 Conclusion

The research adds to the development of a new eco-friendly concrete binder i.e., GGBS. Based on the strength parameters and economy, it has been discovered that replacing up to 50% of ordinary Portland cement with GGBS yields the best performance. The results were found to be in good agreement with the experimental values when the experimental results and the numerical results acquired from the ABAQUS CAE 2020 were compared. These numerical modeling capabilities allow us to get extremely near to the Load–Deflection diagrams produced by laboratory tests. However, selecting an optimized procedure/methodology for determining material attributes is difficult. Further research will be conducted by the authors in this area.

References

1. Shanmuga Priya D, Sakthieswaran N, Ganesh Babu O (2021) Experimental study on mortar as a partial replacement using sawdust powder and GGBS. *Mater Today Proc* 37:1051–1055
2. Ravinder R et al (2018) Study on compressive strength of concrete on partial replacement of cement with ground granulated blast furnace slag (GGBS). In: National conference on water and environment society
3. Kumar A, Deep K (2023) Experimental investigation of concrete with cementitious waste material such as GGBS & fly ash over conventional concrete. *Mater Today Proc* 74:953–961
4. Thomas GE, Indira PV, Sajith AS (2022) Enhancement of mechanical properties of cement mortar using ground granulated blast furnace slag as a partial replacement. In: Recent trends in civil engineering: select proceedings of ICRAE 2021. Springer Nature Singapore, Singapore, pp 171–180
5. Thomas GE, Indira PV, Sajith AS (2022) Structural performance of ground granulated blast furnace slag mortar under impact loading. In: Recent advances in structural engineering and construction management: select proceedings of ICSMC 2021. Springer Nature Singapore, Singapore, pp 813–820
6. Thomas GE, Indira PV, Sajith AS (2022) Experimental investigations on durability characteristics of ground granulated blast furnace slag mortar. *E3S Web Conf* 347:02007
7. Sangeetha SP, Aravind Raj PS (2018) Study on finite element analysis of reinforced concrete beams with GGBS using ANSYS. *Int J Pure Appl Math* 118(5):881–887
8. Thomas GE, Indira PV, Sajith AS (2022) Numerical studies on seismic behaviour of RC structures incorporated with shape memory alloy—a review. In: Proceedings of SECON'21: structural engineering and construction management, pp 955–962
9. Jankowiak T, Lodygowski T (2005) Identification of parameters of concrete damage plasticity constitutive model. *Found Civ Environ Eng* 6(1):53–69

Study on Novel Multi-segment Replaceable Profiled Steel Shear Links



P. N. Nourin and Gouri S. Kumar

Abstract The shear link consists of a central shear link connected to two linked beams through dismountable connections at its two ends, forming a multi-segmental shear link that is replaceable. The replaceable shear link serves as the structural fuse which is connected to the dual steel columns by some specialized connections to be replaced readily after earthquake. The multi-segment shear link helps to energy dissipation at the time of earthquake. The central shear link is designed as the primary fuse, while the linked beams act as a secondary fuse. This study is intended to enhance the seismic resilience of structures by designing an innovative linked columns frame system that can effectively dissipate energy during an earthquake consisting of dual steel columns and the multi-segment profiled replaceable steel shear link. The multi-segment replaceable profiled shear link is composed of a corrugated central shear link connected to two linked beams. To examine the behaviour of multi-segment corrugated shear link the nonlinear finite element model of the proposed link was developed and results were compared with multi-segmental shear link which designed by central link made of flat web plate with stiffeners and without stiffeners. The study indicates that proposed links show higher shear performance and better load carrying capacity. Finite element analysis software ANSYS is used for the analysis. The design parameters include the link length ratio, thickness, and height of the corrugated central shear link. The results are compared in the terms of link rotation, drift angle, shear capacity and strength.

Keywords Multi-segment shear link · Earthquake resilience · Energy dissipation · ANSYS · Corrugated link · Replaceable

P. N. Nourin (✉)

APJ Abdul Kalam Technological University, Thiruvananthapuram, Kerala, India

e-mail: nourinnaushad1999@gmail.com

G. S. Kumar

Universal Engineering College, Vallivattom, India

1 Introduction

The primary objective of engineering structures is to prevent collapse and avoid casualties under the action of seismic forces. Earthquake-resilient structures are designed to withstand the forces generated by earthquakes, minimizing the risk of damage and collapse. To achieve earthquake resilience, structural engineers utilize a range of techniques and technologies. The target of earthquake resilience is that the structure should quickly restore its function after the earthquake. To achieve the target of earthquake resilience the structure concentrates the damage on replaceable members [1]. One of the critical components of an earthquake-resilience structure is the use of replaceable members. Replaceable members are structural components that are designed to absorb the forces generated during an earthquake and can be easily replaced if damaged. The use of replaceable members ensures that the structure can be repaired quickly and at a lower cost after an earthquake, reducing the downtime of the building and the associated economic losses.

The multi-segment shear links serve as “fuse” components connected to the dual steel columns by some specialized connections that can be easily replaced after an earthquake [2]. The multi-segment steel shear link is a combination of a central shear link and two linked beams, which are connected at the ends of the central shear link [2]. During a seismic event, the central shear link is usually built to yield in a controlled way, dispersing a large amount of seismic energy and sparing the remainder of the building from severe damage. In this sense, the central shear link can be seen as the primary fuse of the structure. Linked beams stay elastic during an earthquake, providing added strength to structures. If the central shear link exceeds its limit, linked beams will yield and dissipate seismic energy, acting as a secondary fuse to protect the building [2]. A new type of replaceable links was developed to improve seismic behaviour and achieve the rapid return to occupancy under predetermined levels of lateral load [3]. In particular, the seismic strengthening performance of the entire structure demonstrates that the plastic deformations mainly concentrate on the replaceable shear links to protect other structural components.

This paper introduces novel multi-segment replaceable profiled steel shear links which consist of a trapezoidal corrugated central shear link connecting to linked beams at its ends by dismantlable connections. This method converts the flat plate central shear link to a corrugated plate central shear link, which supports the steel plate out-of-plane without the need for additional stiffeners or restraint plates. Figure 1 shows the modified column frame composed of dual columns and multi-segment replaceable profiled steel shear link and the isometric view of the multi-segment replaceable profiled steel shear link. The research work presented in this paper focuses first on investigating and analyzing the geometry characteristics and deformation mechanism of the modified linked column frame in terms of parametric study. The parameters considered in this study are link length ratio, thickness and height of the corrugated plate and secondly choose an optimum model of multi-segment replaceable profiled steel shear link and compare it with multi-segment

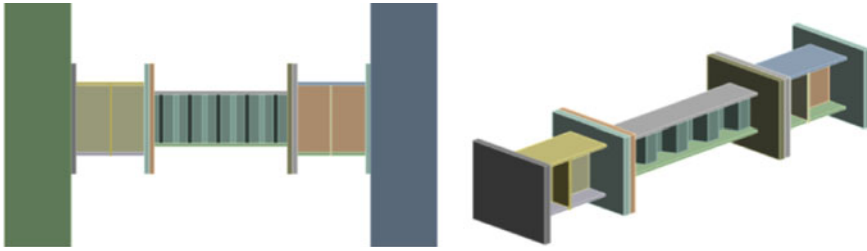


Fig. 1 Schematic view of multi-segment replaceable profiled shear link

replaceable shear link designed by central link made of flat web plate with stiffeners and without stiffeners. Finite element analysis software ANSYS is used for the analysis of numerical models of specimen.

2 Modelling of Multi-segment Replaceable Shear Link

The two numerical models were developed in finite element software ANSYS Workbench 2022. First one the multi-segment replaceable shear link of flat web plate with stiffeners. Second one of the multi-segment replaceable shear links of flat web plate without stiffeners. The optimization of models is carried out by trial-and-error method. The optimum model is selected based on its strength and shear capacity. For these models the central shear link and linked beams are I section. The dimension of the central shear link is $300 \times 150 \times 10 \times 18$ mm and linked beams are $400 \times 200 \times 10 \times 18$ mm (Figs. 2 and 3).

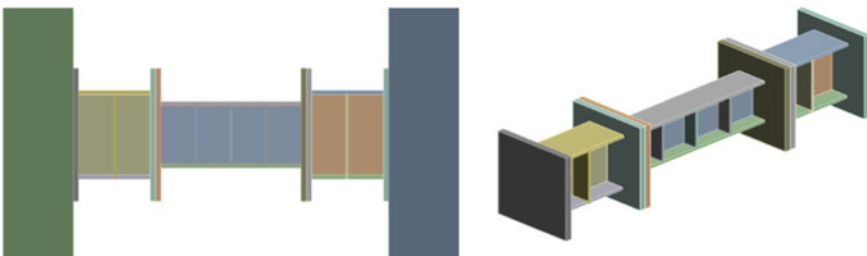


Fig. 2 Multi-segment shear link with flat web

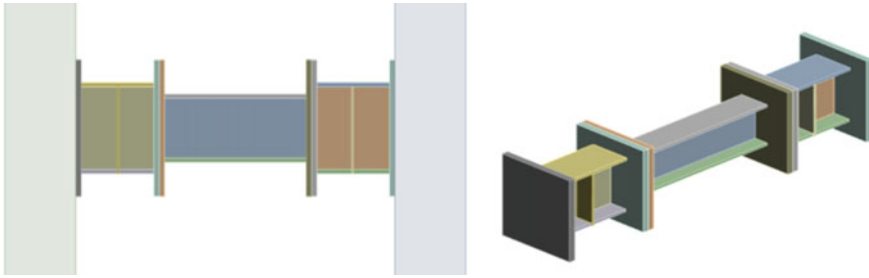


Fig. 3 Multi-segment shear link with flat web without stiffeners

3 Finite Element Analysis of the Multi-segment Replaceable Profiled Shear Links

3.1 Parametric Studies

Finite element (FE) models were created by using ANSYS Workbench 2022 R2 to perform some of parametric studies aimed to examining the mechanical behaviour of the multi-segment replaceable profiled shear link, as the experimental specimens were limited and expensive. Intention of this study to design an optimum model of the multi-segment replaceable profiled shear link that has a higher shear capacity and strength. The parameters include link length ratio, thickness and height of the corrugated plate.

$$\rho = \frac{e}{(M_p/V_p)} \quad (1)$$

Equation (1) defines the central link ratio (ρ). Where, e is the central link length; M_p and V_p are the plastic flexural strength and shear strength of the central links. Links that have a length ratio of $\rho < 1.6$ are known as short links in this system. These links demonstrate stable, ductile, and predictable shear behaviour when subjected to cyclic loading [2]. The link length ratios of models of multi-segment replaceable profiled shear link are less than 1.6 to achieve the shear behaviour. The link length ratios of 6 FE models consisted of 0.6, 0.72, 0.85, 0.97, 1.09 and 1.21, were evaluated in this study.

Other key parameter is the thickness and height of corrugated plate used in central shear link, which effect the strength and entire behaviour of shear link. With the increasing thickness of plate the stiffness of plate increases. Increasing stiffness results cause reduction in link rotation. So the thickness of corrugated plate must keep in limit to achieve a better shear behaviour. 4 FE models are evaluated with thickness of 6 mm, 8 mm, 10 mm and 12 mm respectively and 3 FE models are evaluated with varying height of corrugated plate of 15 mm, 30 mm and 60 mm respectively.

Table 1 Material properties

Material	Modulus of elasticity, E_s (10^5 MPa)	Yield strength, f_y (MPa)	Ultimate strength, f_u (MPa)
Q235	2.11	291.7	441.7
Q345	1.99	391.7	538.3

3.2 Model Overview

Figure 1 shows the FE model of multi-segment replaceable profiled shear link. In this model created by changing the flat plate central shear link to a corrugated plate central shear link, which supports the steel plate out-of-plane without the need for additional stiffeners or restraint plates. The shear link is made up of I section. Q235 steel type is used for web plates and Q345 steel type is used for flange plates (Table 1).

3.3 Optimization of Proposed Link

About 11 models were analysed using trial and error method with varying link length, thickness and height of the corrugated central link to find an optimum model. The model should have a higher load bearing capacity and shear performance. Link rotation γ , structure inter-storey drift angle θ and horizontal angle of central shear link θ_α are indicates the shear performance of the link. The results from the study the effect of multi-segment profiled shear link by changing the length, thickness and height of central link given in Table 2.

From these models analysed the better shear performance shows for CW 600 \times 60 \times 10 mm. This model shows a higher link rotation value when compared to a flat web plate multi-segment shear link and its strength has also improved to a great extent.

4 Results and Discussion

The analysis results of total deformation and equivalent plastic strain of optimum of proposed link, multi-segment link with stiffener and without are given below. The equivalent plastic strain of proposed link is high at the central corrugated web. The material undergoes significant plastic deformation as it is shaped into the corrugated pattern, which results in a higher value of equivalent plastic strain. The high equivalent plastic strain value of corrugated plates is results of deformation and it is beneficial in applications that require high strength and energy absorption capabilities.

Table 2 Load and shear performance of proposed links

	Length (mm)	Thickness (mm)	Height (mm)	θ (rad)	θ_α (rad)	γ (rad)	Load (kN)
CW 1000 × 60 × 6	1000	6	60	0.1461	0.1006	0.2468	648.27
CW 900 × 60 × 6	900	6	60	0.1557	0.1226	0.2783	692.12
CW 800 × 60 × 6	800	6	60	0.1927	0.1885	0.3813	761.36
CW 700 × 60 × 6	700	6	60	0.2004	0.2284	0.4289	793.92
CW 600 × 60 × 6	600	6	60	0.1812	0.2293	0.4105	832.29
CW 500 × 60 × 6	500	6	60	0.1767	0.1650	0.3417	877.5
CW 600 × 60 × 8	600	6	30	0.1802	0.2275	0.4077	829.61
CW 600 × 60 × 10	600	6	15	0.1888	0.2438	0.4326	829.65
CW 600 × 60 × 12	600	8	60	0.1583	0.1880	0.346	870.35
CW 600 × 30 × 6	600	10	60	0.1346	0.1489	0.2836	924.54
CW 600 × 15 × 6	600	12	60	0.1106	0.1133	0.2240	969.75

Figure 4a shows the total deformation of flat web plate with stiffeners, Fig. 4b shows the total deformation of flat web plate without stiffeners and Fig. 4c shows the total deformation of corrugated web plate. The maximum value of total deformation of shear link of flat web with stiffeners, shear link of flat web without stiffeners and shear link of corrugated web plate are 502.92, 502.97 and 333.36 respectively. The total deformation of shear link of corrugated web plate is less than other two models because corrugated shape introduces additional rigidity and strength to the structure, allowing it to resist deformation more effectively. The maximum value of equivalent plastic strain of shear link of flat web with stiffeners, shear link of flat web without stiffeners and shear link of corrugated web plate are 0.17754, 0.24086 and 0.52697 respectively. The corrugated shear link shows more plastic strain than other models due to some factors are stress concentrations, increased contact area and redistribution of stresses. The higher value of equivalent plastic strain indicates that it can undergo greater plastic deformation before failure. This enhances the improved ductility, increased energy dissipation, structural performance and weight reduction (Figs. 5, 6 and 7).

From the load versus link rotation graph shown in Fig. 8, the final stiffness of corrugated web plate is greater than other two models and initial stiffness is slightly

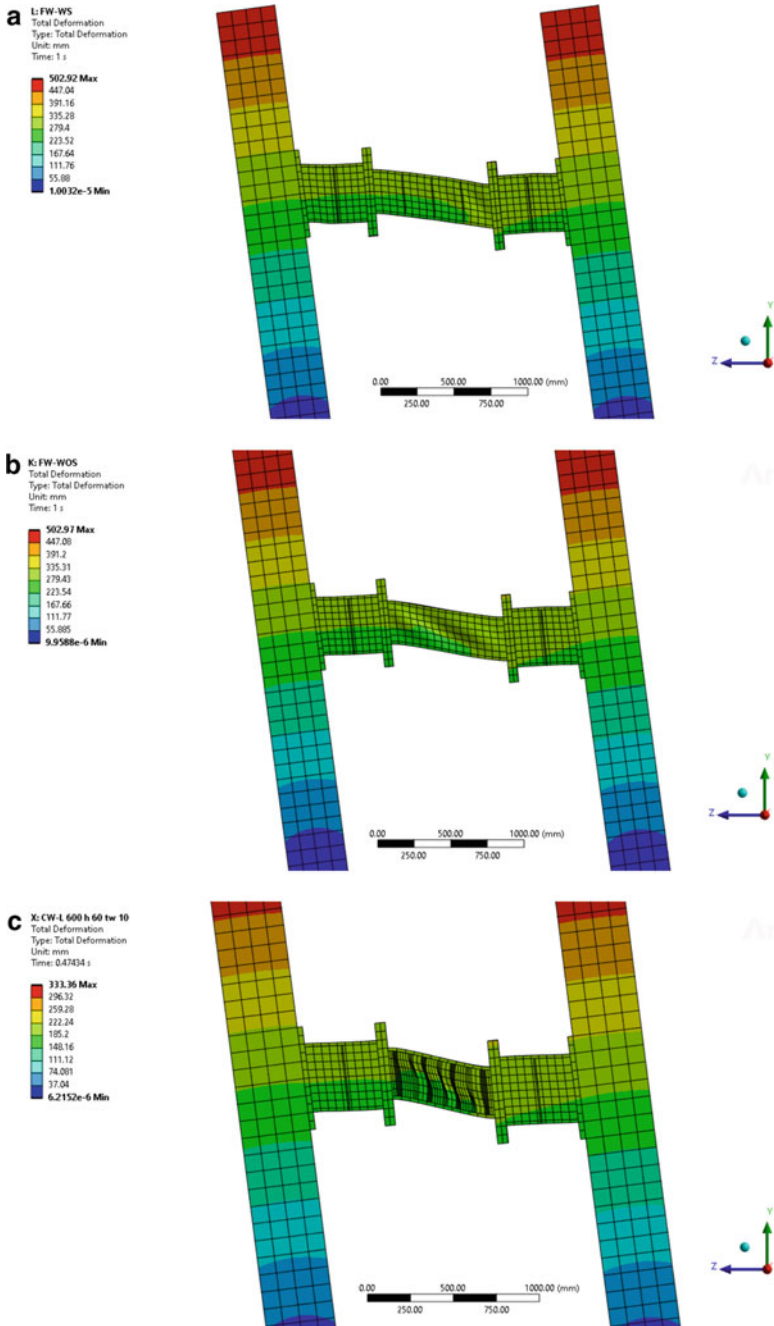


Fig. 4 Total deformation of (a) Flat web plate with stiffeners, (b) Flat web plate without stiffeners (c) Corrugated web plate

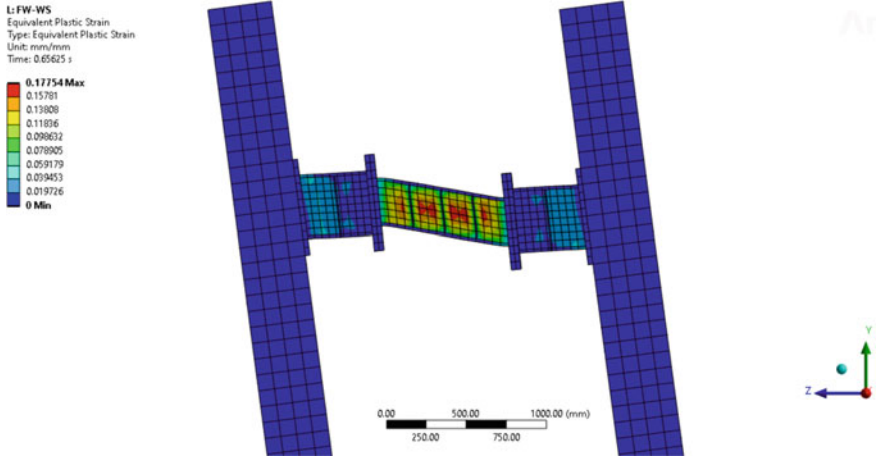


Fig. 5 Equivalent plastic strain of flat web plate with stiffeners

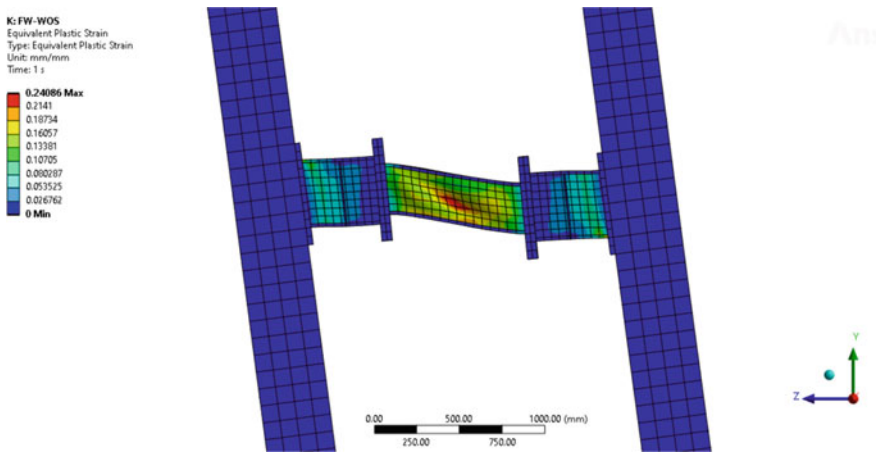


Fig. 6 Equivalent plastic strain of flat web plate without stiffeners

less than flat web plate without stiffeners. Final stiffness value of corrugated web plate is higher than others. Because when loading on corrugated web shear link increases the material begins to undergo strain hardening which leads to an increase in stiffness. From values in Table 3 the corrugated web plate shows better result in shear and load bearing capacity.

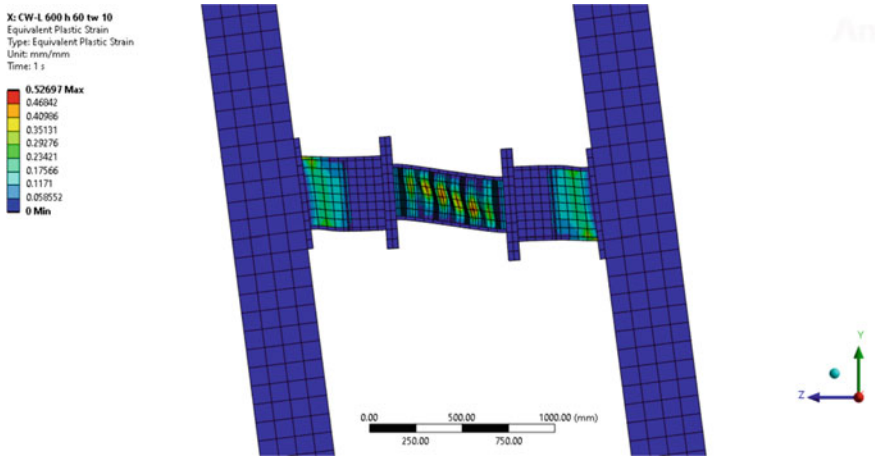


Fig. 7 Equivalent plastic strain of corrugated web plate

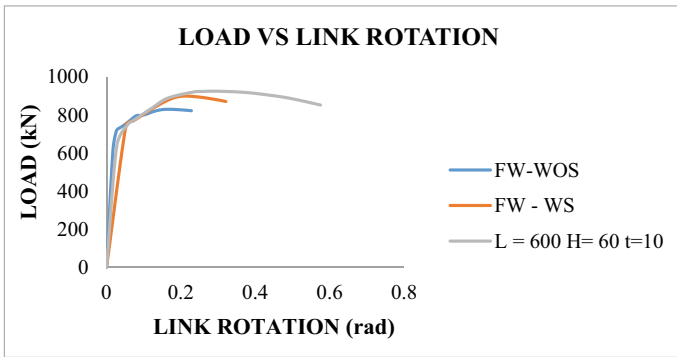


Fig. 8 Load versus link rotation graph

Table 3 Results comparison

	θ (rad)	θ_{α} (rad)	γ (rad)	Load (kN)	Total weight of the link (kg)
FW-WOS	0.1340	0.0381	0.1722	829.37	47.849
FW-WS	0.1184	0.0932	0.2116	899.05	44.367
CW L = 600, H = 60, t = 10	0.1346	0.1489	0.2836	924.54	45.602

5 Conclusions

This study proposed a novel multi-segment profiled steel shear links. The multi-segment replaceable profiled shear links is used to meet the architectural function requirement and enhance its seismic performance. These links act as structural fuses and are designed to withstand specific levels of lateral load. By replacing the flat plate central shear link to the corrugated plate central shear link can avoid the stiffeners and extra connections cause benefits in weight loss. FE numerical analysis conducted to investigate behaviour of proposed link in shear and lateral loading. The main findings are

- By using corrugated web plate it improves overall shear performance of shear link. The corrugated plate reduces the stress concentration will leads to increase the shear resistance of the shear link.
- The multi-segment corrugated shear link gives higher link rotation other than two types of multi-segment flat shear link and also shows better values in drift angle, horizontal angle of central shear link. Which indicates proposed links is better in shear capacity.
- The load carrying capacity of proposed link is 924.54 kN, which is greater than other two specimens. The proposed link shows 2.83% of increased load carrying capacity than shear link of flat web with stiffeners and 11.47% of increased load carrying capacity than shear link of flat web without stiffeners.
- The total weight of proposed link is lesser than shear link of flat plate with stiffeners and flat plate without stiffeners.
- The graph shows the initial stiffness of proposed link is greater than multi-segment flat shear link without stiffeners and little smaller than the multi-segment flat shear link with stiffeners. The final stiffness is greater than other two specimens.




Overall the multi-segment replaceable shear link is best replacement of existing shear link. Which give more strength and withstand at specified levels of lateral load, also improves the shear capacity in the terms of link rotation. Additionally the high surface area of the corrugated plate allows for greater energy absorption in the event of an impact or other loading event, making it a preferred material for impact-resistant applications. Corrugated shear links can achieve comparable or higher strength and performance while potentially reducing the weight of the structural element. The corrugated designs allows for material optimization, eliminating excess material where it is not necessary, which can lead to weight savings and cost efficiency.

References

1. Men J, Xiong L, Wang J, Zhang Q, He P (2021) An experimental study on the seismic behavior and replaceability of the replaceable steel shear links. *Structures* 33:2334–2348
2. Men J, Xiong L, Wang J, Zhang Q (2022) Experimental and numerical study on the behavior of novel multi-segment replaceable steel shear links. *J Constr Steel Res* 194:107–314
3. Men JJ, Deng DP, Lan T, Xiong LQ, Ren RY (2021) Replaceability evaluation method of shear link for RCS hybrid frame. *Structures* 33:2085–2098

Influence of Characteristics of Seismic Excitations on the Performance of Negative Stiffness and Inerter Based Systems for Apparent Weakening of Structures



Aayisha S. Ahamed , A. S. Sajith , and M. Azeem 

Abstract Structures have effectively incorporated passive energy dissipation or supplemental damping systems to reduce excessive vibrations caused by seismic excitation. Negative stiffness devices (NSDs) and inerter-based devices are two passive device types that are gaining popularity in the field of vibration isolation and suppression because they both help to lower structure's natural frequency, which in turn helps to regulate the acceleration of the structure. Despite their similarities, the mechanical behaviour of these two passive devices clearly differs from one another. NSD can produce a force that is in the same direction of induced displacement and would alter the stiffness of structure-device assembly, thus generating apparent yielding. Inerter-based device is a vibration control device which achieves a large inertance-to-mass ratio. This study attempts to illustrate the effectiveness of a single degree of freedom (SDOF) structure-NSD and SDOF structure-inerter assembly in response reduction in a better perspective. The variability in the seismic input is considered by choosing a wider range of earthquake ground movements that include both near-fault (NF) and far-fault (FF) records. The study indicates that the response control of the SDOF structure is highly dependent on the characteristics of the input earthquake ground motion.

Keywords Negative stiffness device · Inerter

A. S. Ahamed (✉) · A. S. Sajith · M. Azeem
National Institute of Technology Calicut, Kozhikode, India
e-mail: aayishasahamed26@gmail.com

1 Introduction

An essential feature in the design procedure of structures is controlling undesirable vibration, especially for structures that might be vulnerable to seismic excitations. Negative stiffness devices (NSDs) and inerter-based devices are two passive device types that are gaining popularity in the field of vibration control because both help to lower structure's natural frequency, which in turn helps to regulate the acceleration of the structure.

Diverse dampers with negative stiffness have been developed and studied to attain control performance comparable to that of active controllers [1]. Numerous techniques for attaining negative stiffness have been devised, including pre-compressed springs, pre-buckled beams, magnets, geometrically nonlinear structures, composite structures, and metamaterials. NSD considered for the present study was developed by Sarlis et al. which depend on pre-compressed spring for achieving negative stiffness [2].

Smith first suggested the idea of inerter to establish the “force current analogy” between mechanical and electrical networks [3]. The control force of an inerter is proportional to the relative acceleration across its two terminals, and this proportionality constant is inertance [3]. The rack and pinion inerter, the ball and screw inerter, and the hydraulic inerter are a few of the inerter types that have already been proposed [4].

Aim of the current study is to comprehend how a single degree of freedom (SDOF) structure with NSD and an SDOF structure with an inerter respond to different earthquake ground motions and to understand the dependency of the system's behaviour on the characteristics of the input ground motion.

2 Negative Stiffness Device

A new method of retrofitting by “weakening” the existing structures, was proposed by Reinhorn et al. to control the maximum acceleration coming on to a structure [5]. The increased displacement which would be produced could be controlled with the help of a supplemental passive device. Even though this approach was efficient, this would lead to permanent deformations in the structure. A supplemental “Negative stiffness device (NSD)” was introduced to produce an apparent weakness in the structural system by simulating the global system's yielding and drawing attention away from the primary structural system. NSD, a passive device capable of demonstrating real negative stiffness without an external power source, was introduced. When a spring has true negative stiffness, force should facilitate motion rather than resist it, as it would with a positive stiffness spring. The force needed to push the structure is produced by a pre-compressed spring, and the force is amplified by a lever mechanism in NSD. The pre-compressed spring concept is modified along with

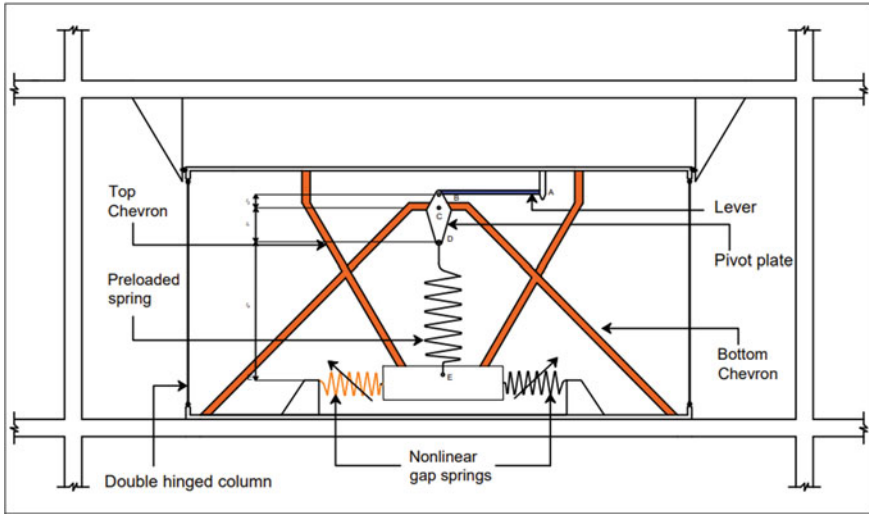


Fig. 1 Schematic diagram of NSD

a dual amplification mechanism to produce the required level of forces to simulate a yielding system. Figure 1 shows a schematic diagram of NSD.

NSD introduced in the structure would help to reduce both acceleration and base shear coming on to the structure. But incorporating NSD alone might result in an increased displacement in the structure. So, to overcome this drawback an adaptive system was developed [6]. Here, depending on the properties of the structure an adaptive NSD was designed that could change stiffness during lateral displacement. After that, a passive damper design is added to the assembly to reduce the displacements caused by the apparent weakness. The combination of NSD and passive damper was termed as Adaptive Negative Stiffness System (ANSS). The governing differential motion of a structure-NSD assembly is given by Eq. (1).

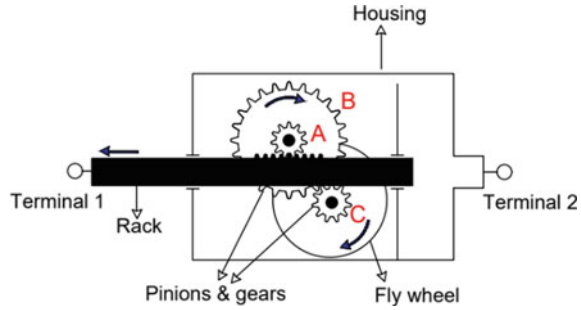
$$m\{\ddot{u}\} + c\{\dot{u}\} + (k - k_{NSD})\{u\} = -m\{\ddot{u}_g\} \tag{1}$$

where, m , k and c are the mass, stiffness and damping matrices of the structure, and \ddot{u}_g is the ground acceleration corresponding to the seismic loading. k_{NSD} is the stiffness produced by NSD.

3 Inerter Based System

Although conventional passive vibration control methods have proven to be efficient and often used in practise, there are certain built-in restrictions. The control performance of this method is highly dependent on ratio of masses of secondary structure

Fig. 2 Schematic diagram of rack and pinion inerter



and primary structures. Inerter, the two-terminal element was proposed in analogous with the capacitance and would produce a force proportional to relative acceleration between two of its terminals [3]. The constant of proportionality was called “inertance” and had kilogram as its unit. The most common inerter configuration consists of a rack, pinions, flywheels and gears. The flywheel is rotated by the rack, which can slide inside the housing and is driven by pinions and gears. The most attractive characteristic of inerter is its mass amplification effect. Gearing enables the effective mass of inerter devices to be much greater than the actual mass of the device. Figure 2 gives a schematic diagram of rack and pinion inerter. Equation (2) provides the force generated by the inerter.

$$F_{inerter} = b(\ddot{u}_1 - \ddot{u}_2) \tag{2}$$

where, inertance $b = I \cdot \eta^2$ and gear ratio $\eta = \frac{r_2}{r_1 r_3}$ in which r_1, r_2, r_3 are the radii of Gears A, B and C, respectively, and I is flywheel’s mass moment of inertia [7].

The equation of motion of a SDOF model with an inerter subjected to earthquake loading is given in Eq. (3).

$$(m + b)\{\ddot{u}\} + c\{\dot{u}\} + k\{u\} = -m\{\ddot{u}_g\} \tag{3}$$

4 Seismic Response of SDOF Structure Under Various Earthquake Ground Motions

4.1 Structure-NSD Assembly

A SDOF system with mass, 10,000 kg, stiffness of the system, $k = 1.579 \times 10^6$ kN/m and damping constant, $c = 5024$ kNs/m was considered for the study. The properties of ANSS assembly were considered according to research carried out by Sarlis et al.

[2]. To account for the diversity in the seismic input and to understand the effectiveness of the structure-NSD assembly in response reduction, an ensemble of earthquake ground movements, including both near-fault (NF) and far-fault (FF) recordings, is chosen. The properties of earthquake data considered are given in Table 1. The structural responses of SDOF structure with NSD subjected to earthquake ground motion was then obtained using a MATLAB code.

The responses of the assembly are analysed for the above earthquakes. The displacement and acceleration response of the assembly when subjected to Imperial Valley Elcentro, 1940 earthquake ground motion is given in Fig. 3.

The analysis was also carried out for the rest of the ground motions. The Root Mean Square (RMS) value of both acceleration and displacement of the structure was found for these ground motions. The acceleration response and displacement response of structure under FF earthquake ground motion is given in Fig. 4a, b for the base structure, structure with NSD and, ANSS.

Table 1 Earthquake ground motions and their properties

Earthquake	Station	Fault type
Imperial Valley, 1940	Elcentro array #9	NF
Imperial Valley, 1979	Elcentro array #6	NF
Landers, 1992	Lucerne	NF
Morgan Hill, 1984	Gilroy	NF
San Fernando, 1971	Pacoima Dam	NF
Landers, 1992	Silent Valley	FF
Sierra Madre, 1991	Tarzana	FF
Loma Prieta, 1989	Lower Crystals Spring Dam	FF
Loma Prieta, 1989	Sunol Fire station	FF
Morgan Hill, 1984	SF intern airport	FF

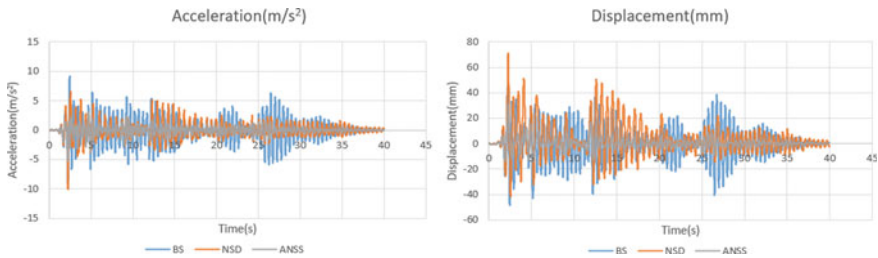


Fig. 3 Acceleration/displacement response of base structure, structure with NSD and structure with ANSS under Imperial Valley, 1940

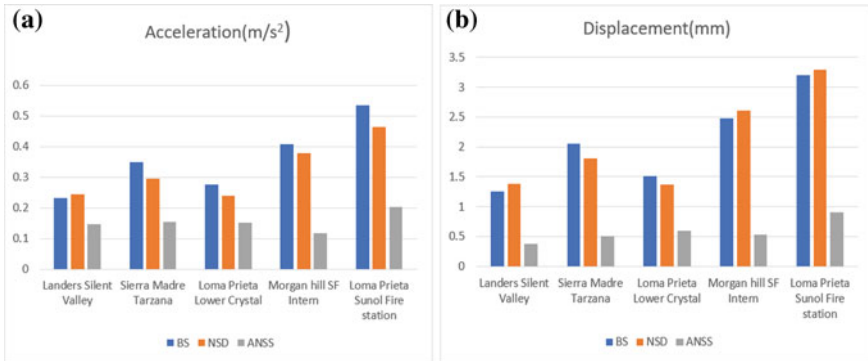


Fig. 4 **a** RMS acceleration of the structure-ANSS assembly under FF earthquake ground motions. **b** RMS displacement of the structure-ANSS assembly under FF earthquake ground motions

Reduction in the acceleration response of a structure with NSD under FF ground motions varies from 6.9% under Morgan Hill, SF intern airport, 1984 ground motion to 16% under the Sierra Madre, Tarzana, 1991 ground motion. Under Landers’ 1992 ground motion, the acceleration response increased slightly. The reduction in the acceleration response of the structure with ANSS under FF ground motions varies from 36% under Landers Silent Valley 1992, ground motion, to 70% under Morgan Hill, SF intern airport, ground motion, 1984. When subjected to FF ground motion, structure incorporated with NSD alone displayed a varying trend in case of displacement response. Structure with ANSS assembly showed a decrement in displacement ranging from 60 to 78% for Loma Prieta Sunol Fire station and Morgan Hill SF intern airport ground motions.

For NF ground motion scenarios, a response reduction of around 13% and 47% is observed for structure-NSD assembly under Landers Lucerne, 1992, and Morgan Hill Gilroy, 1984, respectively. With the introduction of ANSS, a significant response reduction ranging from 34 to 75% was observed. In case of NF ground motions an expected increase in displacement was observed for structure-NSD assembly except for San Fernando, Pacoima Dam 1971. Structure with ANSS assembly showed a decrement in displacement ranging from 38 to 78% for Landers Lucerne and Morgan Hill Gilroy ground motions. The acceleration response and displacement response of structure under NF earthquake ground motion is given in Fig. 5a, b.

4.2 Structure-Inerter Assembly

The properties of SDOF system used in Sect. 4.1 was considered here also for the structure-inerter assembly. An inerter with flywheel mass = 500 kg and radius ratio = 3 was considered. The structure-inerter assembly was then subjected to earthquake ground motions given in Table 1. The structural responses of SDOF structure and

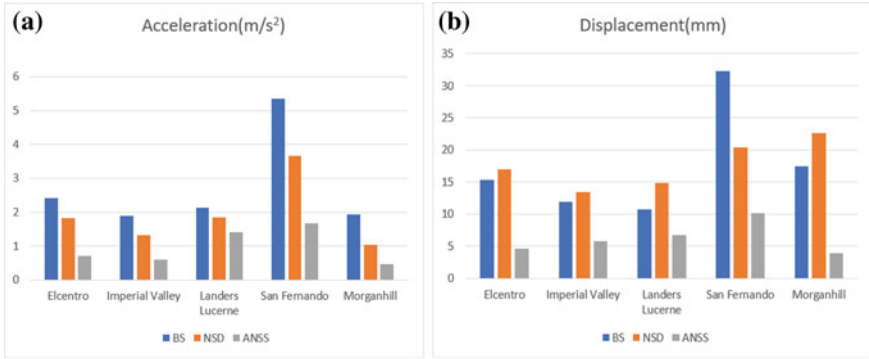


Fig. 5 a RMS acceleration of the structure-ANSS assembly under NF earthquake ground motions. b RMS displacement of the structure-ANSS assembly under NF earthquake ground motions

structure with inerter subjected to earthquake ground motion was then obtained using a MATLAB code. The displacement response and acceleration response of the assembly when subjected to Imperial Valley Elcentro, 1940 earthquake ground motion is given in Fig. 6.

The analysis was carried out for the remaining ground motions also. RMS value of both acceleration and displacement of the structure was found for these components. The obtained seismic response of structure under FF earthquake ground motion is given in Fig. 7a, b for the base structure and the structure with inerter.

The obtained response of structure under NF earthquake ground motion is given in Fig. 8a, b.

Reduction in the acceleration response of structures with inerter during FF ground motions approximately ranges from 31% under the Loma Prieta, Sunol Fire station, 1989, ground motion to 59% under the Morgan Hill, SF intern airport, 1984, ground motion. In the case of NF ground motion cases, a response reduction ranging from 2 to 31% is seen under Landers, Lucerne 1992 and Imperial Valley, 1979 respectively. But the acceleration response increased a little under Morgan Hill, 1984 ground

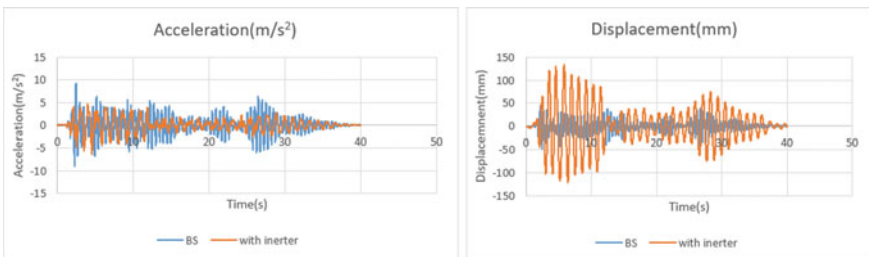


Fig. 6 Acceleration/displacement response of base structure, structure with inerter under Imperial Valley, 1940

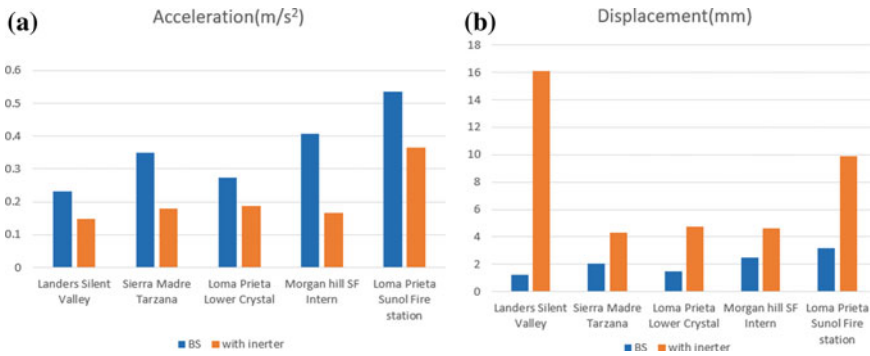


Fig. 7 a RMS acceleration of the structure-inerter assembly under FF earthquake ground motions. b RMS displacement of the structure-inerter assembly under FF earthquake ground motions

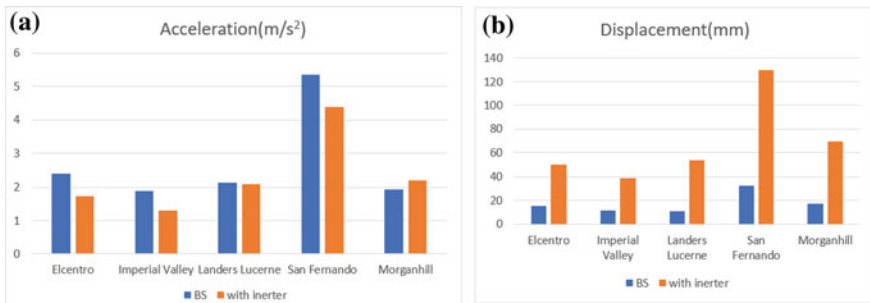


Fig. 8 a RMS acceleration of the structure-inerter assembly under NF earthquake ground motions. b RMS displacement of the structure-inerter assembly under NF earthquake ground motions

motion. In all the cases displacement response of the structure was increased when incorporated with an inerter.

5 Conclusion

Negative stiffness devices (NSD) and inerter-based devices are two passive device types that are gaining popularity for vibration isolation and suppression because they both help to lower the structure’s inherent frequency, which in turn helps to control the structure’s acceleration. Both SDOF-NSD assembly and SDOF-inerter assembly was subjected to a varied range of earthquake ground excitations. The structure-NSD assembly when subjected to both FF and NF ground motion showed a decrease in acceleration except for one case. A significant decrease in acceleration was observed in case of SDOF-ANSS assembly. When structure was subjected to both NF and FF earthquake records the displacement response control showed a mixed trend in case

of SDOF-NSD assembly, but an evident decrement was observed in case of SDOF-ANSS assembly. In case of SDOF-inerter assembly a decrease in acceleration was observed for both NF and FF ground motions, but the displacement response showed an increment. It was understood that both the passive devices had a strong dependency on input ground motion and further study has to be conducted to understand the relationship between system-assembly parameters in the effectiveness of response control.

References

1. Iemura H, Pradono MH (2005) Simple algorithm for semi-active seismic response control of cable-stayed bridges. *Earthq Eng Struct Dyn* 34(4–5):409–423
2. Sarlis AA et al (2013) Negative stiffness device for seismic protection of structures. *J Struct Eng* 139(7):1124–1133
3. Smith MC (2002) Synthesis of mechanical networks: the inerter. *IEEE Trans Autom Control* 47(10):1648–1662
4. Ma R, Bi K, Hao H (2021) Inerter-based structural vibration control: a state-of-the-art review. *Eng Struct* 243:112655
5. Reinhorn AM, Viti S, Cimellaro GP (2005) Retrofit of structures: strength reduction with damping enhancement. In: *Proceedings of the 37th UJNR panel meeting on wind and seismic effects*
6. Pasala DTR et al (2013) Adaptive negative stiffness: new structural modification approach for seismic protection. *J Struct Eng* 139(7):1112–1123
7. Ul Islam N, Jangid RS (2022) Optimum parameters and performance of negative stiffness and inerter based dampers for base-isolated structures. *Bull Earthq Eng* 1–28

Influence of Characteristics of Ground Motions on the Behaviour of Diagrid Buildings



P. Rahul  and A. S. Sajith 

Abstract The diagrid structural system, employed in constructing buildings and roofs, can be characterised as diagonal members built as a framework produced by joining various materials such as metals, concrete, or wooden beams. Today's high-rise constructions and large-span structures typically employ diagrid, particularly for complex geometries and curved shapes. Triangles have a natural tendency to remain stable, as has been known since the earliest days. There is still much research being done in this area to get the finest results with improved performance and dependability despite its recent rise in popularity. As a result, experts have utilised them frequently and are well-liked by engineers and architects. Concrete-Filled Steel Tubular (CFST) diagrids can rectify the main disadvantage of diagrid structures over conventional buildings as they are less brittle and more ductile. The poured concrete effectively keeps the steel tube in the CFST from buckling inward. The steel tube causes a tri-axial state of stress in the concrete, which improves the concrete's compressive strength. The steel tube also serves as longitudinal and lateral reinforcement for the concrete core. This paper aims to study the behaviour of CFST diagrid buildings of different heights subjected to earthquake ground motions. The focus is to investigate the influence of ground motion characteristics on the behaviour of steel diagrid buildings and CFST diagrid buildings when subjected to ground motions of varied classes. The response parameter considered is top-storey displacement.

Keywords Concrete-filled steel tubular diagrid · Time history analysis · Seismic performance

P. Rahul (✉) · A. S. Sajith
National Institute of Technology Calicut, Calicut, India
e-mail: rahulpannikottil@gmail.com

1 Introduction

Residential buildings rose in height due to the rapid urban population increase and lack of available land. As a building's height rises, the lateral load-resisting system takes precedence over gravitational-resisting system [1]. When designing tall buildings in the late nineteenth century, people realised how well diagonal bracing components resisted lateral forces. Diagrid is an example of an external lateral load-resisting system where the system is located at the outer periphery of the structure [2]. Since ancient times, humans have been aware of the inherent stability of triangles, which has led to a wide range of uses and high popularity among engineers and architects. Due to its structural effectiveness and aesthetic potential, offered by the system's distinctive geometric configuration, the diagrid structural system is now widely employed for high-rise buildings. Diagrid members replace the conventional vertical columns along the perimeter in this design [2]. In both gravity and lateral load resisting systems, the diagrids participate. Diagrids withstand the forces of gravity and lateral loads due to their triangulated structure by creating axial forces in their constituent members. They bear lateral shear by the axial action of diagonal elements, which is also more effective in minimising shear deformation [3].

Steel, concrete, or wood are the most common materials used to build diagrids. Due to excellent tensile and compressive strengths, steel is the material that is utilised most frequently nowadays. A different option is Concrete Filled Steel Tubular Diagrids (CFST Diagrids), which have benefits such as increased strength for a given cross-sectional area, increased stiffness, reduced slenderness, increased buckling resistance, high fire resistance, better ductility and confining effect on concrete [2]. The usage of CFST beams and columns in construction technology is becoming more and more common because of their structural advantages. Additionally, during concrete infilling, the steel tube of the CFST member can be used as formwork. Inward local buckling typically happens in bare steel tubes, however, CFST successfully prevents and eliminates this problem [3].

To establish the benefit of CFST over hollow steel tubes, a CFST diagrid building is examined in this study, along with its comparison to hollow steel diagrid buildings.

2 Time History Analysis

2.1 Building Configuration

The CFST diagrid structure is a 12-storey building of plan dimension 24 m \times 24 m and having a uniform storey height of 3.6 m [3]. The plan and elevation of the diagrid building are shown in Fig. 1. The angle of inclination of diagrids (74.5°) is kept uniform throughout the height. This value has been adopted from literature as an optimum value giving best performance for the diagrid [4]. The slab thickness is 150 mm. At 6-m spacing along the perimeter, the diagrids are provided.

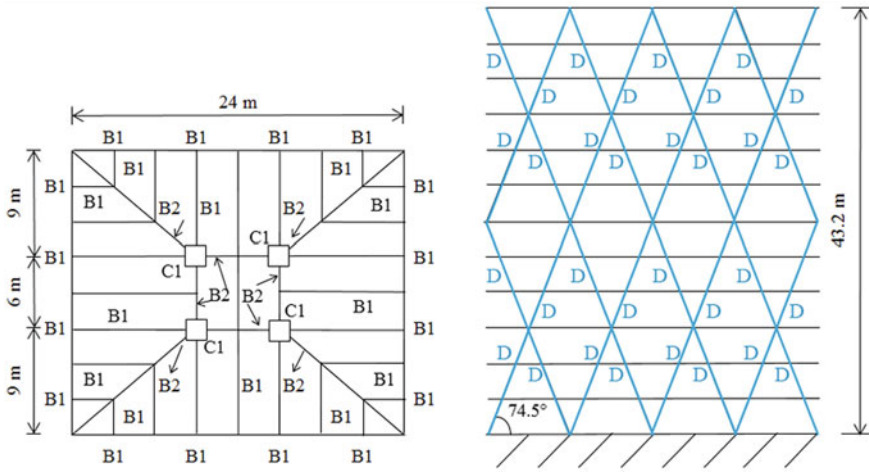


Fig. 1 Plan and elevation of 12-storey diagrid building [3]

The floor slab is subjected to a design dead load of 3.75 kN/m² and a live load of 2.5 kN/m². With a base wind speed of 30 m/s and terrain category III, the dynamic wind loading is calculated following IS:875 (Part 3): 2015. Calculating the design earthquake load considers the zone factor of 0.16, an importance factor of 1, a response reduction factor of 5, and medium soil [1]. This is done in accordance with IS: 1893-2016 requirements. Truss elements are used to model diagrids, while beam elements are used to simulate beams and columns. It is considered that the support conditions are hinged. The IS: 800-2007 requirements are applied for the design of members. ETABS software is used for modelling and analysis. Table 1 gives details of members.

Steel diagrid building is modelled with the exact dimensions as CFST diagrid building. The CFST diagrid is replaced with a hollow steel tube with a size of 375 mm external diameter and 12 mm thickness [3]. The increase in total weight of the CFST diagrid structure compared to the steel diagrid structure is 3.79% which is neglected and the two buildings are considered having comparable structural mass. Moreover, it is important to note that despite the slight increase in weight, there won't be a significant impact on the overall costs of the CFST diagrid structure when compared to the steel diagrid structure. The additional costs associated with the use of CFST

Table 1 Details of various members forming the diagrid

Member name	Description
B1	ISMB550
B2	ISWB600 with top and bottom plates of 220 mm × 50 mm
C1	1500 mm × 1500 mm
D	375 mm diameter and 12 mm thick filled in with M20 concrete

Table 2 Ground motion properties

ID	Name	Magnitude	EpiD in km	Fault type
EQ01	Duzce, Turkey, 1999	7.14	1.61	NF
EQ02	Cape Mendocino, 1992	7.01	4.51	NF
EQ03	Chi-Chi, Taiwan, 1999	7.62	4.96	NF
EQ04	Kocaeli, Turkey, 1999	7.51	5.31	NF
EQ05	Iwate, 2008	6.90	2.52	NF
EQ06	El Mayor-Cucapah, 2010	7.20	126.17	FF
EQ07	Landers, 1992	7.28	121.92	FF
EQ08	Montenegro, Yugo., 1979	7.10	124.33	FF
EQ09	Hector Mine, 1999	7.13	124.69	FF
EQ10	Kern County, 1952	7.36	125.81	FF

materials and construction techniques are outweighed by the advantages and benefits they offer in terms of structural integrity, durability, and other performance factors.

2.2 Ground Motion Characteristics

For the time history analysis of the structure ten ground motion data are chosen out of which five are near-fault (NF) and five are far-fault (FF). All the ground motions selected are those of high intensity earthquakes with a magnitude greater than 6.5. Details of the selected ground motions are shown in Table 2.

Time history analysis is carried out for all ten ground motion data for both CFST diagrid and Steel diagrid buildings using ETABS software. The top storey displacement in mm is plotted versus time in seconds and this is used for the comparison study.

3 Analysis Results

3.1 Near-Fault Earthquakes

The CFST and steel diagrid buildings are analysed using the ground motion data in Table 2. Figure 2a shows the top-storey displacement of CFST diagrid and steel diagrid to time when subjected to the Duzce, Turkey, 1999 earthquake and Fig. 2b shows the same when subjected to Kocaeli, Turkey, 1999 earthquake.

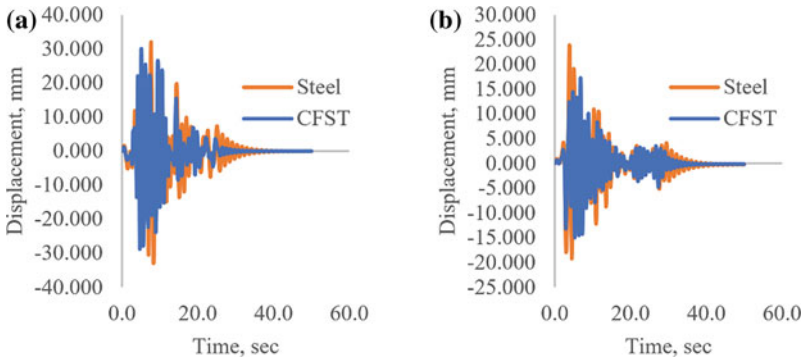


Fig. 2 Displacement response of CFST diagrid and steel diagrid subjected to **a** Duzce, Turkey, 1999 earthquake and **b** Kocaeli, Turkey, 1999 earthquake

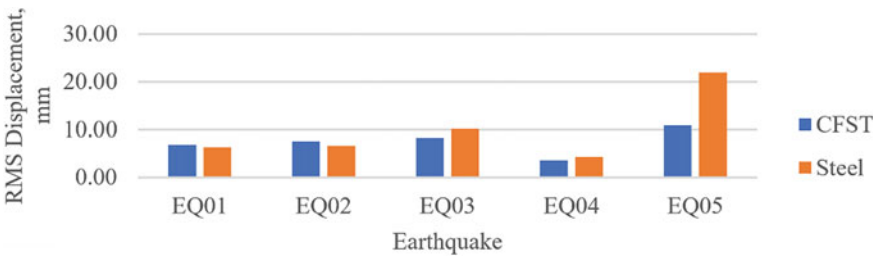


Fig. 3 RMS displacement of CFST diagrid and steel diagrid under NF earthquake ground motion

The time history analysis for the remaining NF earthquake ground motions are also carried out. The Root Mean Square (RMS) values of the displacements are calculated and the response is plotted as a bar chart as shown in Fig. 3 for CFST diagrid and steel diagrid for NF earthquake ground motion.

The displacement increases by 7.63% and 13.69% in CFST diagrid compared to steel diagrid under EQ01 and EQ02. However, when the buildings are subjected to EQ03 and EQ04, the displacement of CFST diagrid decreases by 17.73% and 16.50% compared to steel diagrid. In the case of EQ05, the decrease in displacement for CFST diagrid is 50.69%. The study primarily focuses on analysing the behaviour of diagrid buildings under near fault and far fault conditions. While variations in results for EQ01 and EQ02 may be influenced by other characteristics of the ground motions, it is important to consider their potential impact. Similarly, in the case of EQ05, where the displacement is highest despite the lowest earthquake magnitude, the emphasis lies in understanding behaviour across different fault distances, while acknowledging the significance of other earthquake characteristics.

3.2 Far-Fault Earthquakes

FF earthquake ground motion data from Table 2 is used for the analysis of CFST diagrid and steel diagrid. The displacement response of CFST diagrid and steel diagrid with time when subjected to Hector Mine, 1999 earthquake and Kern County, 1952 earthquake ground motion is shown in Fig. 4a, b, respectively.

The CFST and steel diagrid are analysed for the remaining FF earthquake ground motions. The RMS values of displacement responses for CFST diagrid and steel diagrid are calculated and are as shown in Fig. 5.

From the results, the displacement of CFST diagrid is decreasing in all five cases compared to steel diagrid. The displacement response of CFST diagrid dropped by 34.42%, 39.28%, 31.69%, 43.98% and 40.99% when subjected to ground motions EQ06, EQ07, EQ08, EQ09 and EQ10 compared to steel diagrid. The observed variation in response can be attributed to several factors, including changes in magnitude and differences in fault distance. The study is specifically focused on investigating the influence of fault distance, considering two scenarios: near fault and far fault.

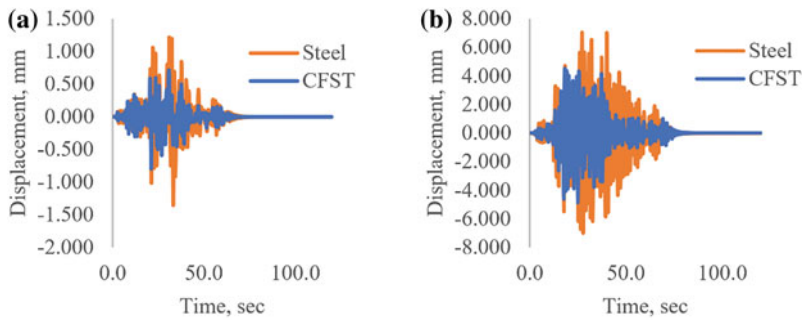


Fig. 4 Displacement response of CFST diagrid and steel diagrid subjected to **a** Hector Mine, 1999 earthquake and **b** Kern County, 1952 earthquake

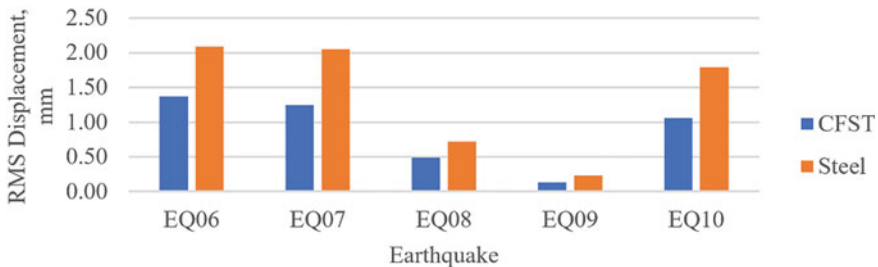


Fig. 5 RMS displacement of CFST diagrid and steel diagrid under FF earthquake ground motion

4 Conclusion

The time history analysis of 12-storey CFST diagrid and steel diagrid uses ETABS software for five high-intensity NF earthquakes and five high-intensity FF earthquake ground motions. The RMS values of top-storey displacement responses are calculated, and the results are compared. It is found that for NF earthquake ground motion, the displacement increases by around 7–14% for two cases of ground motion and decreases for the rest of the three instances of ground motion. A distinct pattern is not observed for the displacement response from the five NF earthquake ground motions. However, the displacement of CFST diagrid decreased in all five FF earthquake ground motion cases compared to steel diagrid. The decrease in displacement response is around 30–45%, which clearly shows the better performance of CFST diagrid under FF earthquake ground motion when compared to steel diagrid. It is understood that when the top-storey displacement is compared, the CFST diagrid performs much better than the steel diagrid when subjected to high-intensity FF earthquake ground motion.

It is important to acknowledge that the observed variations in some of the results may be attributed to the influence of other ground motion characteristics. However, the study primarily focuses on the classification based on fault distances, specifically NF and FF earthquakes. The comprehensive analysis of these additional ground motion characteristics falls outside the scope of this study and warrants future research endeavours. Recognizing the significance of other ground motion characteristics, further studies are needed to explore their influence on CFST diagrid and steel diagrid responses, particularly under high-intensity NF earthquake ground motions, using a broader range of ground motion data. Such investigations will enhance the understanding of the structural behaviour and facilitate informed design practices in seismic regions.

References

1. Jani K, Patel PV (2013) Analysis and design of diagrid structural system for high rise steel buildings. *Proc Eng* 51:92–100
2. Minu AP, Sajith AS, Praveen N (2017) A review of diagrid systems for lateral load resistance of structures. *Appl Mech Mater* 857:19–23
3. Minu AP, Sajith AS, Nagarajan P (2018) Comparison of the performance of concrete-filled steel tubular and hollow steel diagrid buildings. In: *IOP conference series: materials science and engineering*, vol 330, no 1. IOP Publishing
4. Panchal NB, Patel VR, Pandya II (2014) Optimum angle of diagrid structural system. *Int J Eng Techn Res* 2(6):150–157

Critical Success Factors for Post-flood Reconstruction in the Flood Affected Areas of Kerala



V. N. Sreelakshmi and R. Abhijith

Abstract In 2018, 2019, and 2022 the state experienced its highest level of monsoon rainfall of 2346.6 mm, leading to the worst flooding in the past 100 years. 24,536 houses were partially or completely damaged in the flood and 10,000 km of roads were damaged. Kerala's flood rehabilitation efforts have had varying degrees of success and failure. In light of this context, this study investigates the factors that lead to the implementation of post-flood construction projects in Kerala that are successful by evaluating the crucial success factors for post-disaster construction and planning through the use of questionnaire surveys from identified stakeholders and the identification of various UN sustainability goal 11 criteria that are appropriate for the reconstruction and planning of a flood-affected city through case studies. Finally, formulation of planning policies by identifying indicators through literature review and expert surveys. Structured questionnaires will be the instruments used to survey the various stakeholders involved in Kerala's post-disaster development projects to collect the necessary data. The study aids in identifying project management skills that require development for Kerala's post-disaster housing projects to be implemented successfully. As a result, the research findings can be used to develop project management plans that are suitable for PDR projects in Kerala.

Keywords Critical success factors · Construction project management success traits · Post-disaster reconstruction

V. N. Sreelakshmi (✉)

Structural and Construction Management, Federal Institute of Science and Technology (FISAT),
Angamaly, Kerala, India
e-mail: sreelakshmivn98@gmail.com

R. Abhijith

Department of Civil Engineering, Federal Institute of Science and Technology (FISAT),
Angamaly, Kerala, India
e-mail: abhijithr@fisat.ac.in

1 Introduction

Kerala, the most southern state of India, is situated on its southwest coast and is susceptible to several disasters, including cyclones, earthquakes, floods, landslides, and so forth. Large-scale destruction has been caused by floods since the dawn of civilization. As a result of urbanization brought on by population growth, there is deforestation and a large percentage of paved surfaces, which prevents rainwater from penetrating the ground. Less infiltration causes heavy runoff, which causes the hydrograph peak to rise more quickly. Climate change is predicted to increase the frequency, regional extent, length, intensity, and timing of extreme weather extremes. Since flooding is a natural occurrence that cannot be stopped, effective flood mitigation is currently required to reduce damage in flood-prone locations. Safe, financially viable, environmentally friendly, and socially acceptable expansion are all components of sustainable development. It is necessary to grow sustainably in the field of reducing flood risks. Riverine flooding is a frequent occurrence caused by severe or persistent rainfall that exceeds the ability of the soil to absorb water and the flow capacity of streams and rivers. This results in a watercourse overflowing onto a flood plain, defined as a relatively flat area of land next to a natural water course mostly made up of sediments transported by the associated stream and periodically flooded.

Flood plains are consequently “flood prone” and dangerous if the amount of development there goes above what is reasonable. Rainfall, channel slope, the relative height of banks, stream bank materials, and land use in flood plain all have a role in how frequently an area is inundated. In many states, reclamation, and settlement in floodplain regions are major contributors to flood damage. Innovative disaster management techniques to deal with emergencies are more important since the damaging effects of both natural and man-made catastrophes on communities and built environments are anticipated to rise in the future. Due to resource limitations, choosing the most important post-disaster restoration projects from among those that are accessible is a difficult decision.

Numerous critical success factors (CSFs) that are likely to affect the performance of rebuilding projects have been discovered by researchers in light of the distinctive characteristics of catastrophe reconstruction project environments. It has been noted that the method of acquiring and managing the house is the cause of the poor performance of many post-disaster housing reconstruction projects, and poor planning and implementation of reconstruction projects can also lead to the failure of these projects by increasing the community’s vulnerability to disasters. A project-oriented strategy for PDR has been promoted in India by the National Policy on Disaster Management in 2009 and the National Disaster Management Plan in 2016. As a result, project management was supported as a crucial activity throughout the recovery phase by the Kerala State Disaster Management Policy 2010 and best practices from the state’s prior project management experience were advised. Due to changes in environmental circumstances, the nature of the project, and the project management organization,

every project has a unique set of success elements that may not be transferrable to other projects. The implementing authorities must be ready to efficiently plan and carry out the rehabilitation efforts since Kerala is especially sensitive to disaster-related loss. The most important criteria that determine project success in Kerala's post-disaster rehabilitation, however, have barely ever been identified. In light of this context, the research defined the following objectives:

1. To evaluate various factors affecting post-flood reconstruction in Kerala.
2. To analyze and identify the critical success factors of post-flood reconstruction in Kerala.

2 Research Context: Reconstruction Projects in Kerala After the 2018 Flood

As per IMD, TVM, The average annual precipitation in Kerala State is roughly 3000 mm. The South-West and North-East monsoons regulate the amount of rain that falls in the State. The six monsoon months account for almost 90% of the annual rainfall. All of the rivers get substantial flows as a result of the frequent, high-intensity storms that occur during the monsoon season. The steep and undulating terrain's constant and heavy precipitation makes its way into the main rivers via many streams and water courses. From June 1 to August 19, 2018, Kerala had unusually heavy rains. This led to significant flooding in 13 of the State's 14 districts. Due to the constant rain starting on June 1st, the water levels in various reservoirs were virtually at Full Reservoir Level (FRL). During a second period of heavy rain that began on August 14 and lasted until August 19, 13 out of 14 districts were devastated by floods. The depths of rainfall reported from August 15–17, 2018 were equivalent to the severe storm that struck in the year 1924, according to the IMD's rainfall data.

Nearly all of Kerala's rivers experienced unprecedented and extremely significant flooding in 1924. There have been reports of significant losses in terms of life, property, crops, etc. The people of Kerala were still reeling from the wrath of the 1924 flood levels in most of the rivers, and the year 1961 also saw severe floods and an increase in reservoir water levels. Highways and other significant infrastructure were mostly flooded. After a brief respite, the monsoon returned by the middle of July, worsening in the northern regions of the State. Rainfall totals were 56% above average. The floodwaters had caused catastrophic and extensive destruction. We know that 115 individuals perished as a result of floods and landslides. Around 115,000 acres of paddy were badly impacted, along with over 50,000 fully and partially destroyed homes [1].

Comprehending these issues and the potential solutions to them is key to comprehending Kerala's road to recovery and reconstruction. In Kerala society, there is a strong desire to rebuild to higher standards of quality. Although moving is a viable choice, it must emerge realistically as the sole one after other possibilities have been considered. Rebuilding is a significant and crucial problem that represents a turning point in the State's modern history. However, it must be accomplished and conveyed in Kerala's style and manner, based on its unique creative inclinations.

To give the flood-affected populations permanent homes, many solutions were developed. The post-flood recovery effort has been slow to move forward; of the 17,000 destroyed homes, less than 2000 have been taken on by the state administration for restoration 2000 households who lost their homes in the first phase were to be rehabilitated as part of the Cooperation Department's "Care Home" initiative. Under the "Care Home" initiative of the Cooperation Department, as many as 2000 households were renovated. Out of the 13,311 families whose houses were fully damaged in the flood, 8881 were ready to take up construction on their own with government aid. Rebuild Kerala, which was launched by the government for gathering information on the damage caused to buildings and other properties in the floods. Without asking the community for suggestions on the placement of the new neighborhood or housing unit, the housing units were randomly allocated to the qualified recipients. After 1992, there has never been a tragedy of such magnitude as the 2018 flood in Kerala, hence the state was unable to handle the difficult restoration tasks. As a result, programs for post-flood restoration that were sponsored and carried out by national and international entities using various governance structures and implementation methods experienced several difficulties. The primary difficulties originally faced by state-level disaster management organizations included a lack of institutional backing, insufficient human resources, implementation agencies' lack of expertise and managerial abilities, and delays in developing these factors. The donor-driven housing projects for the flood-displaced residents of Kochi cooperation, Adoor Thaluk, and Kuttanad Thaluk were viewed as an ideal case study for determining the factors of project success in post-disaster situations in Kerala after the reconstruction project scenarios had been established [2, 3].

3 Theoretical Approach

The research's main goal was to group the crucial success variables under project management success attributes and examine how they affected Kerala's post-flood housing developments. The study made a correlation between CSFs and certain success features that define main project management aspects based on a thorough examination of pertinent literature on CSFs for rebuilding projects.

3.1 Critical Success Factors for Post-disaster Reconstruction Projects: An Overview

Numerous CSFs were found in the research, either tailored to certain catastrophe conditions or various forms of the reconstruction effort. Based on a literature review of project key success factors (CSF) and rebuilding projects and processes in various countries, Egbu [4] investigated and recorded challenges and variables that affect the success of reconstruction. The study reviewed recent research on the factors that influence reconstruction success and the challenges faced there. Based on the literature evaluation, this study has found 32 challenges with the rebuilding process. Nyamagere Gladys Sospeter et al. (2020) In the study, the Critical Success Factors (CSFs) for PDRP implementation in Angola are analyzed. The paper used both interviews and a survey. Participants in the study from the planning ministry, province government office, and local government in Angola provided the data that was gathered. The purpose of this study was to identify key success factors for managing PDRPs in Angola. Using the One Sample t-Test, nine out of the twenty success variables were identified. According to the findings, crucial success factors of PDRPs in Angola include adequate funding, effective planning, qualified project managers, good communication, active stakeholder and community involvement, a well-written contract, enough resources, economic stability, knowledge gained from prior experience, and top management support. Key project stakeholders can use the findings to assure success since they provide an understanding of the best practices in this context, which calls for the collaboration of all key project stakeholders. Using the analytical hierarchy process, Golz et al. [5] assessed and evaluated the physical flood susceptibility of various building structures. Eleven evaluation criteria, including ones related to durability, physics, and building statics are examined in the research. The notion of residential construction that is flood resistant as well as the modern techniques developed and used internationally was examined by Rasim Navas1 et al. (2019).

These factors for project success or failure were compiled from a survey of the literature. The subsequent section makes an effort to group these components under key success qualities (Table 1).

According to various studies, using structured project management techniques will enhance project outcomes for PDR initiatives, which are by their nature complicated. Activities employed in post-disaster project management are essentially modified versions of non-disaster activities. Best practices for project management and expertise in regular (non-disaster) constructions may also be helpful in disaster scenarios. However, because they differ in scope and purpose, it might not be possible to evaluate how each CSF would affect a project's success. There are few attempts in the literature now in existence to categorize CSFs universally into success attributes for PDR projects. However, in the case of construction projects that did not result

Table 1 Critical success factors (CSFs) for (PDR) projects

Sl. No	Critical success factors	References
1	Community empowerment	Shaw et al. (2002)
2	Community participation	Moe and Pathranarakul (2006)
3	Communication and information dissemination	Ahmed (2011)
4	Community culture and beliefs	Hidayat and Egbu (2011, 2013)
5	Support from local Government	Yi and Yang (2013)
6	Transparency and accountability	Jordan and Javernick-Will (2014)
7	Appropriate reconstruction strategy	Toor and Ogunlana (2005)
8	Good coordination and communication	Chan et al. (2004)
9	Sufficient funding availability	Gudiene et al. (2013)
10	Gathering trust from the community	Belassi and Tukul (1996)
11	Project managers competence	Yong and Mustafa (2013)
12	Clear project plan	Choudhary and Mehmood (2013)
13	Improvement in design management	Gudiene et al. (2013)
14	Enhancement of coordination at the planning stage	Belassi and Tukul (1996)
15	Senior management support	Moe and Pathranarakul (2006)
16	Project management skill	Ahmed (2011)
17	Training of human resources on disaster-resilient construction	Hidayat and Egbu (2011, 2013)
18	Monitoring and feedback by project participants	Ahmed (2011)
19	Rapid evaluation of contractor's qualification	Hidayat and Egbu (2011, 2013)
20	Land availability	Yi and Yang (2013)
21	Temporary units	Jordan and Javernick-Will (2014)
22	Waste management	Moe and Pathranarakul (2006)
23	Political support	Ahmed (2011)
24	The synergy between government and non-governmental agencies	Hidayat and Egbu (2011, 2013)
25	User participation and satisfaction	Ahmed (2011)

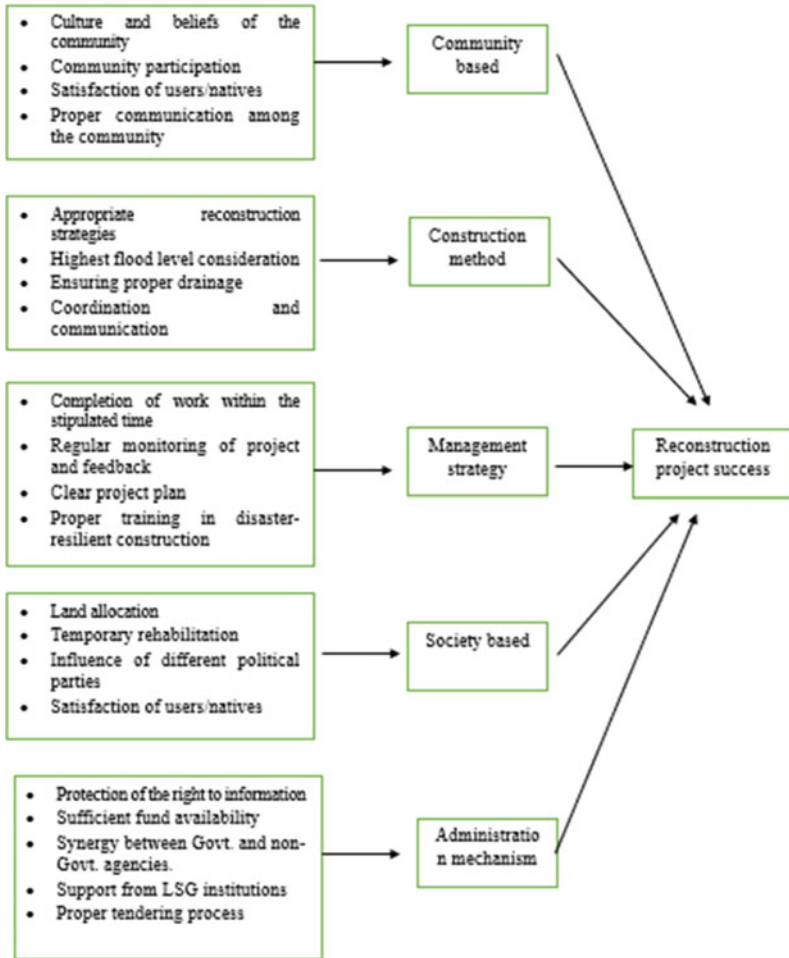
in a disaster, CSFs have been combined under certain success qualities, characterizing project management dimensions as crucial elements of project success. However, because PDR projects are not typically constructed environments, these model categories of CSFs cannot be immediately applied to PDR projects. In light of this, we categorized often reported CSFs for post-disaster projects under 5 core project management dimensions, which are essential qualities for project management success. We did this by drawing on the classification of success factors for typical construction project situations.

Reconstruction Strategy: A suitable rebuilding strategy offers higher chances to repair damaged buildings and boost catastrophe resistance. When recovery methods take into account local needs and local capabilities, they can help accomplish long-term recovery goals including social equity and hazard reduction. Risk management, monitoring, and assessment of the organization's capacities, as well as a system to coordinate their participation, must also be part of the rebuilding strategy. Strategies for reconstruction must strike a balance between cost-effectiveness, technological viability, and quality of life.

Management strategy: Implementation techniques in catastrophe scenarios offer recommendations for how rebuilding should be carried out to produce effective project results. Although risk mitigation and community recovery measures are in place, they must be implemented effectively and efficiently for recovery objectives to be met. Effective project execution requires the application of building rules, open need assessment, efficient logistics and resources, enough technical assistance, a framework for quality control, and prompt feedback.

Administration Mechanism: The community, local government, the commercial sector, NGOs, international funding organizations, and others must all participate in reconstruction. Stakeholder involvement has been demonstrated to be essential for post-disaster restoration initiatives to succeed. Project efficiency is a result of stakeholders' good coordination and engagement in the reconstruction process as well as their awareness of their respective roles. However, a significant problem that hinders governance during a disaster is assuring cooperation and coordination among many parties.

Social Preference: The capacity to address the governance concerns that emerge in post-disaster settings will determine whether rebuilding initiatives are successful or not. The best approach to addressing governance challenges is through an adequate institutional structure. Establishing a single organization at each level of government is a typical feature of institutional systems for disaster management. Activities for reconstruction were carried out in Kerala and across all of India by creating independent Extraordinary Mechanisms.



Conceptual framework for reconstruction project success

The institutional mechanism's nature and purpose are influenced by several elements. A good institutional arrangement is characterized by the quality of its leadership, planning, and organization for repair. The success or failure of a reconstruction program is determined by local authorities' capability, resource knowledge, leadership, and ability to act. An effective institutional process following catastrophes also depends on political will, the availability of resources, the needs of international financial institutions, and the style of bureaucratic and political leadership. And last, in post-disaster settings, government assistance is a key role in promoting inclusive planning procedures.

The conceptual model combined the characteristics of effective project management and prospective project management steps required for the efficient execution of rebuilding projects. This model offers a set of project management procedures that must be carefully considered when a disaster has occurred. Furthermore, the National Disaster Management Agency (NDMA), Sphere Standards, the National Building Code, and other organizations now provide unduly technical post-disaster rehabilitation standards with a product-oriented approach. Rather, this paradigm emphasizes a process-oriented approach to reconstruction while attempting to understand the “management processes.”

4 Research Methodology

According to the research, institutional mechanism, reconstruction strategy, project execution, and stakeholder management are the four key project management success attributes that have the most impact on PDR project success. Through the review of the literature, CSFs were identified and consolidated. To determine the extent to which the various CSFs had been used during the reconstruction of the Flood-displaced community in Kerala, a primary survey employing a structured questionnaire was used. To verify the project management success attributes and examine their impact on project success, statistical analysis using SPSS (Statistical Software for Social Science) was used. In prior studies that looked at CSFs in disaster-related initiatives, this method of merging qualitative and quantitative methodologies was also discovered.

4.1 Stakeholder Population of the Study

This study, which focused on several stakeholders heavily involved in the conception and execution of home reconstruction projects, was designed to comprehend the project-oriented success factors that were applied during Kerala’s post-flood housing rebuilding projects. However, community leaders from different resettlements were given fair consideration throughout the sample selection because they were representatives of the project’s users. Given the challenges in getting in touch with stakeholders in particular completed projects, the poll focused on stakeholders generally involved in relocating flood-affected communities. the officers of district administrations, taluk offices (an administrative division within a city or town that serves as its administrative center, with possible additional towns and usually several villages), village offices, architects, and engineers; state and local government officials involved in the planning and policy-making for disaster reconstruction. As part of the implementation of various infrastructure services, officers from various line departments,

including state housing boards, town planning departments, public works departments, water authorities, elected officials, local civic network leaders, community representatives, members of religious organizations, and active women groups, and community leaders from various relocated settlements were also surveyed.

4.2 Data Collection Method

The population's size was unclear because there are no official records of the participants in post-flood restoration operations. As a result, the survey used a snowball sampling method, in which the first respondents assisted in identifying further possible respondents. Data were gathered through a combination of online and in-person surveys. To determine the degree to which the project management measures had been employed or prioritized throughout house rebuilding, a five-point Likert scale with anchors—5 = Strongly agree, 4 = agree, 3 = neutral, 2 = disagree, and 1 = strongly disagree—was used. Through the study, responses to 93 questions were gathered. This sample size meets the requirement for factor analysis that the item-to-respondent ratio be at least 1:5. The sample consisted of 15.1% structural engineers, 10.8% contractors, 11.8% project managers/site engineers, 12.9% policymakers, 34.4% natives of flood affected area and 15.1% others. Since the sample fairly represented all relevant parties, responses were consistent and reliable.

4.3 Data Analysis Method

Initially using SPSS software (version 27.0), each measuring item was examined for consistency and reliability using Cronbach's alpha, item-total correlation, and factor loading from the principal component analysis. The Cronbach's alpha value reveals how closely connected the collection of measurement items is overall. Item-total statistics offer an evaluation of how closely measurement items on a scale are evaluating the same content. The link between each variable and the underlying latent component is shown by the factor loadings of measurement items. Following the first inspection of the data for consistency and reliability, the measurement items were purged by the acceptable fit statistics. The credible measuring items for the four main latent components were then used using SPSS. The link between the model variables, including the higher-order construct of project success, was simultaneously evaluated throughout the data analysis. In the end but not least, the model fitness was evaluated using the acceptable cut-off values for the goodness of fit indices: Tucker-Lewis index (TLI) [0.9, the goodness of fit index (GFI), comparative fit index (CFI), and root mean square error of approximation (RMSEA) 0.08.

5 Analysis and Findings

The model validation procedure is described in the following subsections utilizing factor analysis. The project management success attributes were conceptualized in the study as first-order latent constructs impacted by the measurement items (CSFs), which in turn controlled the second-order construct, total project success. The measurement items (CSFs) were initially examined for reliability and validity, and the findings are shown in Table 2.

The study validated and strengthened the CSFs' validity and reliability. With composite reliability better than 0.7 and average variance larger than 0.5, the model parameters' reliability and validity were determined. The research also demonstrated the significance of the CSFs associated with the model's first-order dimensions, since the factor loading is above the cut-off value of 0.5. Numerous validity and reliability tests performed on the data gathered show that the success factors proposed in the study are related to projecting the aforementioned managerial success attributes. The mean score of all key factors identified is calculated in SPSS and the factors having a mean score greater than the average of all mean score is identified as critical success factors for PDR (Table 3).

Influence of different political parties: More remote inaccessible and marginalized areas which don't have any resources, and that cannot articulate their feelings, are often worst affected but they are neglected, uncared for, and taken for granted and the political leaders with vested interest divert the material to their areas and misuse them.

Temporary rehabilitation: Immediate temporary rehabilitation is provided to the natives without considering their needs and are withdrawn once the emergency is under control often the health and sanitation facility of refugees in the relief camps and rehabilitation centers are not properly taken care of.

Highest flood level consideration: During the design and reconstruction activities the highest flood level is often neglected which becomes a barrier in flood resilient reconstruction.

Appropriate reconstruction strategies: Reconstruction is a rebuilding measure that is applicable after certain disasters. The reconstruction involves building confidence, self-respect, self-esteem, self-dependency, mutual support, mutual trust, and rebuilding of communities [6].

Project managers enhancing coordination from the planning stage: Often there is a drawback in the post-flood reconstruction activities due to the lack of coordination and communication among various stakeholders involved in the PDR.

Clear project plan: A project plan is a more necessary element in the PDR activities to satisfy the disaster's prevention, mitigation, response, and recovery phases.

Community participation: The lack of community participation in the PDR activities is the cause of reducing the success percentage of the reconstruction. The community should be given prime importance in decision-making at each stage.

Table 2 Critical success factors and their reliability measures

Dimensions	Measurement item	Alpha ($\alpha > 0.6$)	Kaiser–Mayer–Olkin, KMO (> 0.50)	Factor loading ($k > 0.5$)
Community-Based	Empowerment of the community	0.813	0.881	0.55
	Community participation			0.76
	Proper communication among the community			0.72
	Culture and beliefs of the community			0.77
	The trust of the local community/ affected people			0.43
Reconstruction Strategy	Appropriate reconstruction strategies	0.813	0.785	0.551
	Highest flood level consideration			0.544
	Ensuring proper drainage			0.519
	Coordination and communication between Stakeholders			0.511
	Proper waste management			0.471
Project Implementation	Completion of the work within the stipulated time	0.852	0.866	0.786
	Regular monitoring of the project and feedback			0.495
	Clear project plan Improvement in the design management			0.566
	Project managers enhance coordination from the planning stage			0.641

(continued)

Table 2 (continued)

Dimensions	Measurement item	Alpha ($\alpha > 0.6$)	Kaiser–Mayer–Olkin, KMO (> 0.50)	Factor loading ($k > 0.5$)
	Proper support from senior management			0.649
	Proper training on disaster resilient construction			0.519
Society based	Land allocation	0.79	0.53	0.624
	Temporary rehabilitation			0.738
	Involvement of different political parties			0.763
	The satisfaction of the users/ natives			0.726
Institutional Mechanism	Protection of the right to information	0.67	0.785	0.478
	Sufficient fund availability			0.544
	The good synergy between the government and non-government agencies			0.757
	Support from the LSG institutions			0.672
	Proper tendering process			0.519

Source SPSS output

Regular monitoring of the project and feedback: Monitoring entails collecting and reviewing information that reveals how an operation is proceeding and what aspects of it, if any, need to be adapted as the program progresses. Monitoring occurs throughout the operation. A baseline study is usually conducted before the operation begins.

Training to workers on disaster resilient construction: Training to the workers regarding the use of locally existing ecologically friendly, low-cost materials should be made and all the available local resources, local talents, subsidies, and various schemes of the governments should be made use of.

Table 3 Critical Success Factors and Ranks

Rank	Critical success factors
1	Influence of different political parties
2	Temporary rehabilitation
3	Highest flood level consideration
4	Empowerment of the community
5	Appropriate reconstruction strategies
6	Project managers enhance coordination from the planning stage
7	Clear project plan
8	Community participation
9	Proper communication among the community
10	Support from the LSG institutions
11	Regular monitoring of the project and feedback
12	Protection of the right to information
	<i>Less critical success factors</i>
1	Proper support from senior management
2	Training to workers on disaster-resilient construction
3	Improvement in design management
4	The trust of the local community/ affected people
5	Completion of the work within the stipulated time
6	Proper tendering process
7	Proper Drainage
8	Proper waste management
9	Satisfaction of users
10	The good synergy between the government and non-government agencies
11	Culture and beliefs of the community
12	Land allocation
13	Sufficient fund availability

5.1 Discussion

The objective of the research was to properly group the CSFs under the project management success aspects. Community-based, construction-based, management-based, society-based, and administration-based are the five strategic project management aspects to which the various CSFs for housing reconstruction projects are linked. The empirical results and subsequent analysis served to further investigate how much these success factors were emphasized in Kerala's post-flood scenario. Through a single-window method, an effective institutional framework might hasten the building process by enabling group decision-making. To meet the urgent requirements of the disaster-affected people, project execution cannot proceed at its usual

pace. Developing methodologies and processes that facilitate a quick project implementation process is essential during post-disaster rebuilding. For the most part, housing rebuilding projects were identified, chosen, executed, and monitored using a top-down method. The hierarchical bureaucratic structure of governance was used to create and carry out numerous restoration programs. The communities who were forced from their original homes by the flood experienced communal isolation and disintegration as a result of housing development in the lack of an effective housing restoration strategy. The outcomes of this empirical investigation supported current discoveries regarding the performance-related aspects of Kerala's post-flood resettlement initiatives. The study demonstrated that several project management success elements throughout the rebuilding phase are responsible for the projects' success. Despite the Kerala Disaster Management Policy's support for a project-oriented approach to reconstruction, the disaster management plan for 2016 lacks any methods for communicating this to prospective stakeholders. This study also provides ample evidence of Kerala's disaster management systems and policy shortcomings in dealing with the demands of post-disaster rebuilding management. Therefore, this can offer a basis for study to develop project management best practices and knowledge domains and integrate them into Kerala's reconstruction efforts after a disaster.

6 Conclusion

This study aimed to understand different crucial success elements for post-disaster rehabilitation projects in the context of strategic project management. With the use of factor analysis, the effect of these success characteristics on post-flood housing developments in Kerala was further examined. The results show that project management success characteristics such as Community-based, Construction based, Management based, Society based and Administration based may be largely responsible for the successful implementation of housing projects. But the research showed that these success factors weren't taken into proper consideration during rebuilding. The results might aid in prioritizing project management regions that require development for sustainable housing provision in Kerala during future crisis circumstances. The corpus of knowledge on project management in a catastrophe setting should benefit from this study. The study primarily combined the CSFs for PDR projects under special project management parameters. Such a categorization offers enormous promise for the effective rehabilitation of damaged infrastructure because the project management methodology is well-recognized for post-disaster projects. The conceptual model created for this study emphasizes a process-oriented approach to post-disaster shelter creation while comprehending the management process.

The research does have certain restrictions, though. The study made an effort to investigate and simulate the success variables that define project management dimensions. However, a project's scale, cost, design, functioning, and context (political, environmental, as well as pre-and post-disaster socioeconomic situation), among other things, may also have an indirect or direct impact on a project's success. Similarly to this, CSFs for various success attributes may correlate, and the success of a project may be influenced by a mix of CSFs. Future studies can look at how many other elements interact and support the success of PDR projects.

References

1. Ecosystem-based Recovery: The Case of the 2018 Kerala Floods (n.d.)
2. Adu-Boateng K, Oppong BM (2011) Post-disaster reconstruction activities: a case study in Ghana. *Trans Built Environ* 119:1743–1778. <https://doi.org/10.2495/DMAN110>
3. Afkhamiaghda M, Elwakil E (2022) Challenges review of decision making in post-disaster construction. *Int J Constr Manag*. <https://doi.org/10.1080/15623599.2022.2061751>
4. Egbu C, Lou E (2011) Association of researchers in construction management. www.em-dat.net
5. Golz S (2016) Resilience in the built environment: how to evaluate the impacts of flood resilient building technologies?
6. Samuel AM (2018) A project work on introduction Christian ethics (as a requirement for grading) topic: reconstruction of Kerala state after recent flood of 2018 in socio-economic

Experimental Investigation for Stabilization of Expansive Soil by Using Waste Materials—Eggshell Powder and Bagasse Ash



Moni Mishra , Ravino Mekro , Lensar Jamir , Marjom Ete , Taniya Oniya , and Ajanta Kalita 

Abstract The poor strength and cyclical swell-shrink behaviour of expansive soil make it a problematic soil for civil engineers. Most foundation failures are commonly caused by these soils. Given the increasing need for infrastructure expansion, avoiding these soils for future construction may not be feasible. As such, it is advised to take strengthening measures for expansive soils before constructing any structure. In this study, we have explored the modification of expansive soil by adding eggshell powder and bagasse ash, both of which are waste materials, as stabilisers. A total of 24 groups of stabilised soil samples were prepared by incorporating varying proportions of eggshell powder and bagasse ash as stabilisers. With respect to the dry soil, ESP was added at weight ratios of 6%, 9%, 12%, and 15%, while BA was added at weight ratios of 4%, 6%, 8%, and 10%. The result showed that as the content of eggshell powder increased, there was a notable decrease observed in both the plastic and liquid limits. While the addition of ESP (12%) to the untreated soil sample resulted in a maximum reduction of both the plastic and liquid limits, respectively. In contrast, a rise in the BA concentration resulted in a rise in the plastic and liquid limits. At 4% BA, a maximum reduction in the plastic limit was observed. Furthermore, it was observed that the soil exhibited improved performance when treated with a combination of 15% ESP and 10% BA, representing the optimum percentage of the admixture. The combined use of eggshell powder (ESP) and bagasse ash (BA) admixture was found to be highly effective in enhancing the engineering properties of expansive foundational soil and strengthening the subgrade soil. Additionally, both eggshell powder and bagasse ash have the potential to be used not just for soil stabilisation purposes but also as construction materials.

Keywords Expansive soil · Eggshell powder · Bagasse ash · Plastic limit · Liquid limit

M. Mishra (✉) · R. Mekro · L. Jamir · M. Ete · T. Oniya · A. Kalita
Department of Civil Engineering, NERIST, Nirjuli, Arunachal Pradesh, India
e-mail: moni13mishra@gmail.com

1 Introduction

Expansive soils are composed of swelling clay minerals, such as montmorillonite, that change in volume based on water content. As these soils absorb more water, their volume increases, and some of the most expansive clays can expand by up to 10%. To determine whether a soil has the potential to be expansive, physical properties such as plasticity, clay content, and soil structure are evaluated during the reconnaissance and preliminary stages of a site investigation [1]. Due to their low strength and tendency to undergo cyclic swell-shrink behaviour, expansive soils can pose significant problems for civil engineering projects. For this reason, it is recommended to take strengthening measures before constructing any structures on such soil.

Over the years, many researchers have conducted studies on various methods of soil stabilisation to improve soil properties and ensure their suitability for construction projects. Among the different approaches explored, one promising option involves employing waste materials such as brick dust [2], bagasse ash [3], quarry dust [4], fly ash [5], plastic waste [6], and eggshell powder [7] for stabilising expansive soil.

Eggshells have the potential to be used as a raw material or admixture in a variety of construction projects because they are predominantly composed of calcium carbonate. The environmental problems brought on by open waste disposal may be lessened by recycling or using such waste as construction materials, and the effective use of eggshell, a waste material, creates an opportunity for a sustainable solution. Anoop et al. [8] had recommended utilising eggshell powder as an alternative to commercial lime for stabilising expansive soil.

Bagasse ash consists of silica (SiO_2), magnesium (MgO), calcium (CaO), iron (Fe_2O_3), and alumina (Al_2O_3) [9], of which silica is the main component and makes up more than half of the total chemical composition. Bagasse ash is largely used as fertiliser or disposed of in landfills, which can negatively affect the environment. In recent years, bagasse ash has been utilised as construction material, which not only enhances the qualities of the materials used but also aids in lowering the amount of agricultural waste dumped in the environment. Bagasse ash demonstrates pozzolanic characteristics and is frequently utilised as a supplementary cementitious material. [10–13] conducted the study on using bagasse ash for stabilising expansive soil, and they found that it significantly improved expansive soil's engineering qualities. Eggshell powder and bagasse ash are also found to be efficient in increasing the CBR value of clayey soil [14].

The primary objective of this paper is to thoroughly explore the impact of these waste materials on the consistency properties of expansive soil.

2 Materials and Mix Designation

2.1 Soil

The soil sample utilised in this study was collected from a depth of 1.5 m below the surface in Visakhapatnam, Andhra Pradesh. Additionally, a table listing the soil’s geotechnical properties is provided below (Table 1).

The soil’s particle size analysis was carried out in compliance with the standards specified in IS-2720 (Part-IV)-1985. For particles larger than 75 μm, wet sieve analysis was employed; for particles smaller than 75 μm, a hydrometer test was conducted. The particle size distribution curve for particle size lesser than 75 μm is shown in Fig. 1. According to the results, the natural soil exhibits high plasticity characteristics, with a plasticity index of 24.09%, a liquid limit of 57.06%, and a plastic limit of 32.97%. These measurements suggest that the soil contains a significant amount of montmorillonite clay mineral.

Table 1 Geotechnical properties of expansive soil

Sr. No	Description	IS Code	Values
I	Optimum Moisture Content (%)	IS: 2720 PART VII (1980)	26.51
II	Maximum Dry Density (kN/m ³)	IS: 2720 PART VII (1980)	14.70
III	Specific Gravity	IS: 2720 Part III/SEC I (1980)	2.39
IV	Liquid Limit (%)	IS: 2720 Part V (1985)	57.06
V	Plastic Limit (%)	IS: 2720 Part V (1985)	32.97
VI	Plasticity Index (%)	IS: 2720	42.09
VII	Soil Classification	IS: 1498 (1970)	CH

Fig. 1 Particle size distribution curve of expansive soil

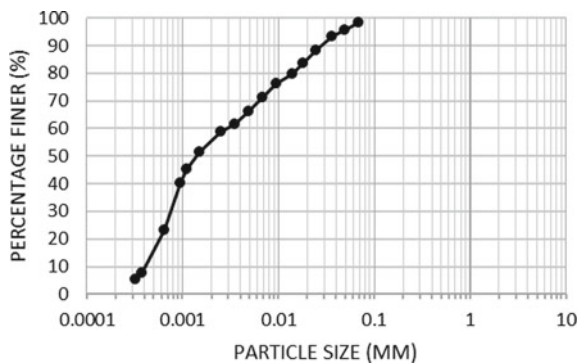


Table 2 Eggshell powder's chemical composition [15]

Sl. No	Composition	Weight (%)
I	CaO	76.9922
II	C	21.1286
III	MgO	0.9261
IV	P ₂ O ₅	0.4149
V	SO ₃	0.3264
VI	Na ₂ O	0.1046
VII	K ₂ O	0.0542
VII	SrO	0.0396
IX	Fe ₂ O ₃	0.0132

2.2 Eggshell Powder

The egg shells were collected from the hostel mess, and thoroughly cleaned with water to remove any odour or dirt. Once clean, it was left to dry under the sunlight before being ground into a fine powder using a grinding machine. The powder was then passed through a 75-micron sieve to ensure its consistency, and ultimately used as an admixture. Amal and Yamuna [15] used an x-ray fluorescence spectrometer to determine the chemical composition of the eggshell powder. Table 2 presents the findings.

2.3 Bagasse Ash

Bagasse ash was collected from different parts of Arunachal Pradesh, and then dried in the sunlight for a week to remove any remaining moisture. Next, it was burned on a steel surface until it was completely converted into ash. Finally, the resulting ash was used as an admixture in the expansive soil. The bagasse ash chemical composition was analysed by [16]. Table 3 presents the findings.

2.4 Mix Designation

In this study, different mixed specimens were represented by following specific mix designations, with letters used to indicate the different materials used. ES represented Expansive Soil, ESP represented Eggshell Powder, and BA represented Bagasse Ash. For example, a mixed specimen represented as ES + 12% ESP + 6% BA denoted a combination of expansive soil with 12% eggshell powder and 6% bagasse ash.

Table 3 Chemical composition of bagasse ash [16]

Sl. No	Oxide	Weight (%)
I	SiO ₂	78.34
II	Al ₂ O ₃	8.55
III	Fe ₂ O ₃	3.61
IV	CaO	2.15
V	Na ₂ O	0.12
VI	MnO	0.13
VII	TiO ₂	0.50
VIII	MgO	1.65
IX	BaO	< 0.17
X	P ₂ O ₅	1.07
XI	K ₂ O	3.46

3 Experimental Programs

3.1 Liquid Limit Test

Liquid limit tests as per IS 2720 (Part V)—1985 (Reaffirmed 2015) were performed on expansive soil and treated soil samples. In the expansive soil samples, varying amounts of eggshell powder (6%, 9%, 12%, and 15%) and bagasse ash (4%, 6%, 8%, and 10%) were carefully mixed to make 24 groups of treated soil samples.

3.2 Plastic Limit Test

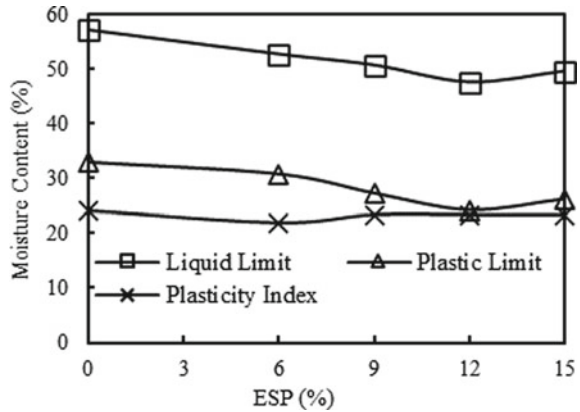
Plastic limit tests were performed according to IS 2720 (Part V)—1985 (Reaffirmed 2015) on untreated and treated soil samples. In the untreated soil samples, varying amounts of eggshell powder (6%, 9%, 12%, and 15%) and bagasse ash (4%, 6%, 8%, and 10%) were carefully mixed to make 24 groups of treated soil samples.

4 Results and Discussions

4.1 Effect of Eggshell Powder on Expansive Soil

It can be observed from Fig. 2 that the LL and PL of the soil sample decreases with an increase in the concentration of ESP. This is due to the presence of lime in the ESP, which affects the moisture content through cation exchange between the soil

Fig. 2 LL, PL, and PI variation with different %ESP



and lime, causing cementation between the soil particles. This results in a slightly reduced plasticity index of the soil. The addition of ESP at 12% reduced the LL from 57.06% to the lowest value of 47.51%, indicating the optimal mixture of ESP. However, the LL of the soil increased further with the addition of 15% ESP; this is due to the extra water required by the excess lime present in ESP, which makes the soil swell.

4.2 Effect of Bagasse Ash on Expansive Soil

It can be observed from Fig. 3 that the plastic limit drops from 32.97% to 29.5% when 4% BA is added to the untreated soil sample. However, with the addition of more BA, both the LL and PL increase. This is because BA has a low specific gravity and a larger specific area. This results in a varied plasticity index, where it slowly increases with the addition of BA and is maximum at 4% BA concentration, but after which there is a steady decline of the plasticity index with increasing concentration of BA from 6%, 8%, and 10%.

4.3 Effect of Combined Admixture of Eggshell Powder and Bagasse Ash on Expansive Soil

Figure 4a–d show that the addition of 6%, 9%, 12%, and 15% ESP by varying the amount of BA in increasing concentration from 4%, 6%, 8%, and 10% increases both the LL and the PL. The plasticity index shows a decrease at higher concentration of ESP at 15%, when blended with 10% BA. The presence of lime in ESP creates cementation between the soil particles, which is more effective when the surface area of the soil is higher. At all variations of ESP concentration, there is a decline in the

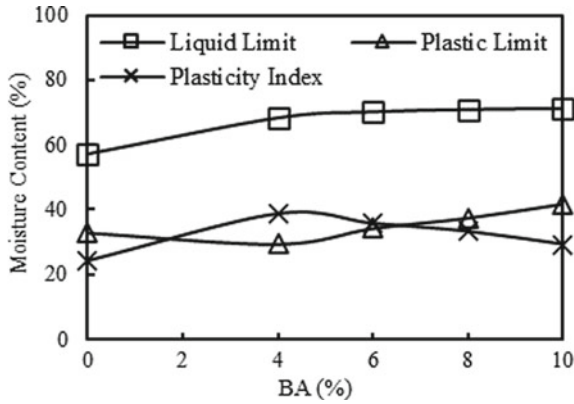


Fig. 3 LL, PL, and PI variation with different %BA

plasticity index at 10% BA. This can be attributed to the BA's surface area being larger than the soil's surface area.

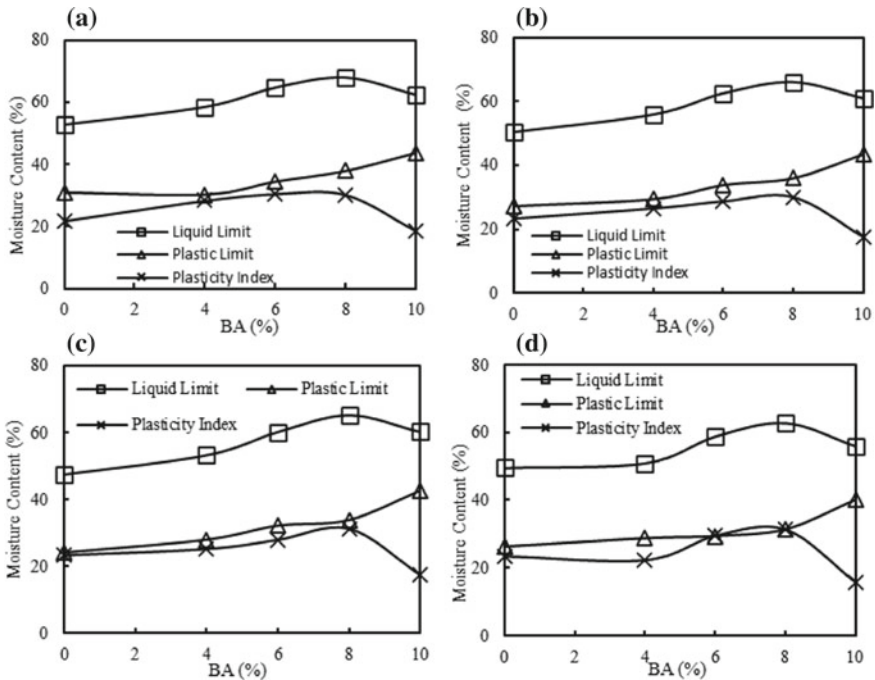


Fig. 4 a LL, PL, and PI variation with different %BA for ES + 6%ESP, b LL, PL, and PI variation with different %BA for ES + 9%ESP, c LL, PL, and PI variation with different %BA for ES + 12%ESP, d LL, PL, and PI variation with different %BA for ES + 15%ESP

5 Conclusions

The following conclusions can be drawn from the results of various tests and the analyses done:

- The addition of eggshell powder led to a decrease in both the liquid limit and the plastic limit, resulting in a lower plasticity index.
- At 10% bagasse ash concentration, the addition of eggshell powder to the mixture resulted in a decrease in the plasticity index.
- Desirable results were observed when the soil was treated with a combination of 15% eggshell powder and 10% bagasse ash, representing the optimum percentage of the admixture.
- Eggshell powder and bagasse ash can be used as an affordable and eco-friendly alternative to chemical stabilisers and cement. The utilisation of these materials not only provides a cost-effective solution but also addresses environmental concerns associated with their disposal, making them a sustainable option for soil stabilisation.
- In addition to their use in soil stabilisation, eggshell powder and bagasse ash have the potential to be utilised as construction materials.

The scope for future work

- To assess the effectiveness of these admixtures in enhancing the strength of a road subgrade, the California Bearing Ratio (CBR) test can be conducted.
- A more detailed study can be conducted to further explore the utilisation of eggshell powder and bagasse ash as reinforcement materials for various soil types.

References

1. Dakshanamurthy V, Raman V (1973) A simple method of identifying an expansive soil, Japanese society of soil mechanics and foundation engineering, vol 13, no 1
2. Teja S, Kumar S, Needhidasan S (2018) Stabilisation of expansive soil using brick dust. *Int J Pure Appl Math* 119(17):903–910
3. Khan S (2019) Use of gypsum and bagasse ash for stabilization of low plastic and high plastic clay. *J Appl Res Ind Eng* 6(3):251–267
4. Samuthiram M, Ravi E, Sashikkumar M (2016) Stabilization of expansive soil with eggshell powder and quarry dust. *J Adv Chem* 12(23)
5. Devi T, Prasad D (2016) Stabilization of expansive soil using aluminium chloride and fly ash. *IOSR* 13(3):78–82
6. Alzaidy M (2019) Experimental study for stabilizing clayey soil with eggshell powder and plastic wastes. *IOP Conf Ser: Mater Sci Eng*. <https://doi.org/10.1088/1757-899X/518/2/0220082>
7. Veerabrahmam K, Prasad D (2021) A review on the effect of eggshell powder on engineering properties of expansive soil. *Indian J Sci Technol* 14(5):415–426
8. Anoop et al (2017) *Int J Adv Eng Res Sci* 4(8). <https://doi.org/10.22161/ijaers.4.8.15>

9. Faria K, Gurgel R, Holanda J (2010) Characterization of sugarcane bagasse ash for use in ceramic bodies. In: *Materials science forum*, vol 660. Trans Tech Publications Ltd, pp 1049–1052
10. Surjandari N, Djarwanti N, Ukoi N (2017) Enhancing the engineering properties of expansive soil using bagasse ash. *J Phys: Conf Ser*. <https://doi.org/10.1088/1742-6596/909/1/012068>
11. James J, Pandian P (2018) Bagasse ash as an auxiliary additive to lime stabilization of an expansive soil: strength and microstructural investigation, Hindawi. In: *Advances in civil engineering*. <https://doi.org/10.1155/2018/9658639>
12. Singh M, Malik M (2020) Stabilization of expansive soil using bagasse ash and bamboo fiber as reinforcement. *Int Res J Eng Technol* 7
13. Sharma T, Singh S (2021) Experimental study on stabilisation of clayey soil using cement and bagasse ash. *IOP Conf Ser: Earth Environ Sci*. <https://doi.org/10.1088/1755-1315/889/1/012010>
14. Carlina M, Apriyanti Y, Fahriani F (2021) The effect of addition of bagasse ash and eggshell powder on CBR value of clay soil. *IOP Conf Ser: Earth Environ Sci*. <https://doi.org/10.1088/1755-1315/926/1/012102>
15. Amal S, Yamuna M (2015) Characterization of raw eggshell powder (ESP) as a good bio-filler. *J Eng Res Technol* 2(1):56–60
16. Cordeiro G, Filho R, Fairbairn E, Tavares L, Oliveira C (2004) Influence of mechanical grinding on the pozzolanic activity of residual sugarcane bagasse ash. In: *Use of recycled materials in building and structure*

Critical Success Factors for Sustainable Construction & Demolition Waste Management in Kochi City, Kerala



Hanna Salah and R. Abhijith

Abstract Construction and Demolition waste (C&D) as a direct consequence of rapid urbanization is increasing around the world. C&D waste generation has been identified as one of the major issues in the construction industry due to its direct impacts on the environment as well as the efficiency of the construction industry. It is estimated that an overall 35% of C&D waste is landfilled globally; therefore, effective C&D waste management is crucial to minimize detrimental impacts on the environment. C&D waste management must be implemented successfully since the industry cannot continue to operate if the resources it depends on are depleted. Considering the environmental, socio-economic, and sustainability impact, sustainable C&D waste management practices have been started globally. The 3R (Reduce, Reuse, Recycle) method is the base for sustainable C&D waste management practices. This study focuses on sustainable C&D waste management in Kochi City and helps in evaluating critical success factors (CSFs) by examining the effectiveness of C&D waste management in Kochi. A survey was conducted and survey results were analyzed using SPSS and Microsoft Excel. Descriptive analysis was carried out in SPSS to find CSFs and the results were also validated by using RII analysis done in Microsoft Excel.

Keywords Construction and demolition waste · Landfilling · Detrimental impacts · Critical success factors · Descriptive analysis

H. Salah (✉)

Structural Engineering and Construction Management, Federal Institute of Science and Technology (FISAT), Angamaly, Kerala, India
e-mail: salahhanna256@gmail.com

R. Abhijith

Department of Civil Engineering, Federal Institute of Science and Technology (FISAT), Angamaly, Kerala, India

1 Introduction

1.1 General

India is the second-largest urban system in the world, with about 11% of the world's urban population (NITI Aayog 2020). Urban growth is expected to contribute to 73% of the total population increase by 2036 (MoHFW 2019). Thus the construction sector in India is developing day by day as it is expected to gross \$1.4 trillion in 2025 (World Economic Forum 2016). India generates an estimated 150 million tonnes of construction and demolition (C&D) waste every year, but the official recycling capacity is a meager 6500 tonnes per day (TPD) i.e., just about 1% (Building Material Promotion Council (BMPTC) 2020) [1].

1.2 Quantification of C&D Waste

- a. Activity-wise C&D waste quantification by Technology Information, Forecasting and Assessment Council's (TIFAC)
 - 40–60 kg per m² of C&D waste will be generated during new construction,
 - 40–50 kg per m² of C&D waste will be generated during building repair,
 - 300–500 kg per m² of C&D waste will be generated during the demolition of buildings [2].
- b. C&D waste quantification by Local Self Government Department (LSGD)

10% of total Municipal Solid Waste generated in the Local Self Governments may be taken as the approximate quantity of C&D waste generation for planning purposes [3].

1.3 Study Area: Kochi City, Kerala

As solid waste management is a big concern for the state, the Kerala government is planning to develop an elaborate system to recover and recycle the increasing construction and demolition (C&D) waste that is currently deposited in water bodies and open spaces. The study focuses on the management of C&D waste in Kochi, Kerala, in compliance with a set of guidelines issued by the central and state governments. The total amount of C&D waste generated in Kochi city is 55 TPD and the estimated cost for recycling is 3.3Cr/year. The study area starts from Kalamassery and extends to Edapally, Kaloor, Vyttyla, Kakkanad & Thripunitura (Fig. 1).



Fig. 1 Study area (<https://www.mapsofindia.com/maps/kerala/kochi.htm>)

1.4 Objectives of the Study

- To identify various parameters affecting C&D waste management globally.
- To evaluate and analyze critical success factors for C&D waste management in Kochi city.

2 Critical Success Factors (CSFs) for C&D Waste Management in Kerala

2.1 Introduction

Kerala's fast urbanization has resulted in a considerable volume of construction and demolition debris in recent years. Although India has implemented various waste management documents and policies, these documents are neither operational nor thorough enough to guide practices further. Critical success factors (CSFs) that could contribute to the successful development of building and demolition waste management in Kerala are essential. The study's findings would most likely inspire Kerala policymakers to examine useful CSFs to improve the performance of building and demolition waste management.

2.2 Methodology

Based on the literature reviews, several parameters were identified which are categorized under different phases like Construction, Planning, Designing and Management. A questionnaire was prepared based on the identified parameters and the questionnaire is finalized after professional assessment by some experts. The questionnaire after expert supervision involves 31 tentative success factors as shown in Table 1 [4].

The survey was conducted with the involvement of researchers, policymakers, contractors, engineers, workers, and laymen affected by C&D waste in Kochi. Participants were required to evaluate the importance of the 31 potential CSFs in the successful development of construction and demolition waste management in Kochi, using a 5-point Likert scale. A value of 1 denotes extremely unimportant, 2 moderately unimportant, 3 neutral, 4 moderately important, and a value of 5 means extremely important. A total of 86 participants from Kochi participated in the survey. For 93% of respondents, C&D waste is a big issue in Kerala and about 95.3% are aware of the problems caused by its illegal dumping. The whole process lasted for approximately 1 month, from February to March 2023.

2.3 Analysis Using SPSS

The questionnaire's reliability is assessed by entering survey results into SPSS 19.0 and calculating Cronbach's Alpha of the questionnaire's contents. Cronbach's Alpha was $0.938 > 0.70$, indicating that the questionnaire has good structural reliability [5].

Table 1 Tentative success factors for C&D waste management

No	Factors for C&D waste management
<i>Section 1. Construction</i>	
1	Separating used or excess materials from construction sites for reuse and recycling
2	Lack of space on the job site for material separation on C&D waste management
3	Take back arrangements with suppliers (i.e. Packaging of excess)
4	Improving conventional construction practices
5	Implementing low-waste construction technologies
6	Precise supervision on construction materials and works
7	High cost and labor availability in separating C&D wastes
<i>Section 2. Planning and designing</i>	
1	Material selection in waste generation
2	Lack of planning during design stage
3	Inefficient storage of construction material
4	On-site C&D waste supervision system (e.g. Storage zoning)
5	Proper planning and techniques for dismantling of structures
6	Selection of high-quality construction materials while designing
7	Usage of project management and building information software
7	Accurate estimation of materials before ordering
8	Inefficient storage of construction material
9	Electrical safety and fire safety during demolition
<i>Section 3. Management</i>	
1	Lack of knowledge and education
2	Lack of legislation to manage C&D waste
3	Lack of standardized waste collection systems
4	Requirement of waste management/waste recycling centers
5	Implementation of polluter pays penalties
6	Providing subsidies for recycling activities
7	Setting guidelines for recycling of materials
8	Setting standards for recycled products
9	Simplifying construction and demolition waste recycling project approval procedures
10	Setting of necessary qualifications for demolition companies
11	Awareness of proper C&D waste management among common people
12	Providing vocational training to various construction personnel
13	Proper collaboration among various stakeholders
14	Cost of transportation between worksites and waste recycling plants
15	Proper guidelines for landfilling using C&D waste

The mean score and standard deviation of each of the 31 factors are then calculated in SPSS. And ranking all of the factors based on their mean score values. If two or more factors have the same mean score, the factor with the lower standard deviation is assigned to a higher rank. Table 2 shows the ranking results. The 18 elements with mean values greater than the average of all values (4.03) were chosen as critical success factors (CSFs) for C&D waste management [6].

2.4 Analysis Using Excel

For evaluating the relative importance, an index value for each factor is calculated using the RII method. RII or Relative Importance Index of each factor is calculated using the following equation and the factors with the highest RII are ranked accordingly as shown in Table 3.

$$RII = \frac{\sum W}{A \times N}$$

W—Weighting is given to each question by the respondent ranging from 1 to 5.

A—Highest weight in the study i.e. 5.

N—Total number of respondents.

2.5 Results

The SPSS and Excel results clearly show the important success factors for construction and demolition (C&D) waste management in Kochi. After assessing 31 parameters in both SPSS and Excel, 18 factors were identified as critical. The results of both analyses are identical, implying that the results are more accurate. The 18 identified critical success factors (CSFs) are shown in Table 4.

2.6 Discussion and Findings

CSF 1—Lack of planning during design stage. Design changes primarily include design drawing changes caused by the correction of design errors, client requirements, or noncompliance with new design standards. Some suggestions for reducing design changes include properly preparing feasibility study reports, improving design management, better coordination among all designers, close communication between designers and contractors, and improving joint check-ups of drawings to find and solve any problems on the drawings as early as possible.

Table 2 Rank of success factors for C&D waste management

No	Tentative factors	Mean	Std. deviation	Rank
1	Lack of planning during design stage	4.5395	0.70125	CSF 1
2	Awareness of proper C&D waste management among common people	4.5233	0.68129	CSF 2
3	Accurate estimation of materials before ordering	4.5132	0.70225	CSF 3
4	Lack of knowledge and education	4.4767	0.77803	CSF 4
5	Requirement of waste management/waste recycling centers	4.4535	0.74608	CSF 5
6	Precise supervision on construction materials and works	4.3816	0.79945	CSF 6
7	Cost of transportation between worksites and waste recycling plants	4.3605	0.71805	CSF 7
8	Selection of high-quality construction materials while designing	4.3553	0.84386	CSF 8
9	Providing vocational training to various construction personnel	4.3462	0.78669	CSF 9
10	On-site C&D waste supervision system (e.g. Storage zoning)	4.3421	0.82547	CSF 10
11	Lack of standardized waste collection systems	4.3372	0.84867	CSF 11
12	Lack of legislation to manage C&D waste	4.3023	0.81269	CSF 12
13	Setting standards for recycled products	4.2500	0.81854	CSF 13
14	Proper guidelines for landfilling using C&D waste	4.1512	0.78990	CSF 14
15	Implementation of polluter pays penalties	4.1279	0.90484	CSF 15
16	Proper planning and techniques for dismantling of structures	4.1053	0.87299	CSF 16
17	High cost and labor availability in separating C&D wastes	4.1053	0.96026	CSF 17
18	Electrical safety and fire safety during demolition	4.0658	0.91412	CSF 18

(continued)

Table 2 (continued)

No	Tentative factors	Mean	Std. deviation	Rank
19	Lack of space on the job site for material separation on C&D waste management	4.0000	0.71181	
20	Providing subsidies for recycling activities	3.9877	0.81385	
21	Setting guidelines for recycling of materials	3.9873	0.80851	
22	Separating used or excess materials from construction sites for reuse and recycling	3.9868	1.11347	
23	Take back arrangements with suppliers (i.e. Packaging of excess)	3.9868	0.95907	
24	Implementing low-waste construction technologies	3.9737	0.93771	
25	Inefficient storage of construction material	3.9620	0.86888	
26	Improving conventional construction practices	3.9605	0.82366	
27	Proper collaboration among various stakeholders	3.9481	0.84130	
28	Simplifying construction and demolition waste recycling project approval procedures	3.9359	0.84269	
29	Setting of necessary qualifications for demolition companies	3.8974	0.87668	
30	Material selection in waste generation	3.8289	0.97143	
31	Usage of project management and building information software	3.7895	0.94256	

CSF 2—Awareness of proper C&D waste management among common people.

Awareness of proper C&D waste management among common people is another important factor. Common people need to get aware of environmental issues caused due to illegal dumping and the common people's participation can produce a great impact.

CSF 3—Accurate estimation of materials before ordering. A building estimator or a quantity surveyor with adequate experience in the construction sector needs to quantify the materials required in a construction site before the start of work. The accurate estimation of materials prevents the segregation of waste and thus it helps in the proper management of C&D waste.

Table 3 Ranking of factors based on RII

No	Factors	RII	Rank
1	Lack of planning during the design stage	0.907895	1
2	Awareness of proper C&D waste management among common people	0.904651	2
3	Accurate estimation of materials before ordering	0.902632	3
4	Lack of knowledge and education	0.895349	4
5	Requirement of waste management/waste recycling centers	0.890697	5
6	Precise supervision of construction materials and works	0.876316	6
7	Cost of transportation between worksites and waste recycling plants	0.872093	7
8	Selection of high-quality construction materials while designing	0.871053	8
9	Providing vocational training to various construction personnel	0.869230	9
10	On-site C&D waste supervision system (e.g. Storage zoning)	0.868421	10
11	Lack of standardized waste collection systems	0.867441	11
12	Lack of legislation to manage C&D waste	0.860465	12
13	Setting standards for recycled products	0.85	13
14	Proper guidelines for landfilling using C&D waste	0.830232	14
15	Implementation of polluter pays penalties	0.825581	15
16	Proper planning and techniques for the dismantling of structures	0.821053	16
17	High cost and labor availability in separating C&D wastes	0.821053	17
18	Electrical safety and fire safety during demolition	0.813158	18
19	Lack of space on the job site for material separation on C&D waste management	0.8	19
20	Providing subsidies for recycling activities	0.797530	20
21	Setting guidelines for recycling materials	0.797468	22
22	Separating used or excess materials from construction sites for reuse and recycling	0.797368	21
23	Take back arrangements with suppliers (i.e. Packaging of excess)	0.797368	23
24	Implementing low-waste construction technologies	0.794737	24

(continued)

Table 3 (continued)

No	Factors	RII	Rank
25	Inefficient storage of construction material	0.792405	25
26	Improving conventional construction practices	0.792105	26
27	Proper collaboration among various stakeholders	0.789610	27
28	Simplifying construction and demolition waste recycling project approval procedures	0.787179	28
29	The setting of necessary qualifications for demolition companies	0.779487	29
30	Material selection in waste generation	0.765789	30
31	Usage of project management and building information software	0.757895	31

Table 4 Critical success factors

No	Critical Success Factors (CSFs)
CSF1	Lack of planning during design stage
CSF 2	Awareness of proper C&D waste management among common people
CSF 3	Accurate estimation of materials before ordering
CSF 4	Lack of knowledge and education
CSF 5	Requirement of waste management/waste recycling centers
CSF 6	Precise supervision on construction materials and works
CSF 7	Cost of transportation between worksites and waste recycling plants
CSF 8	Selection of high-quality construction materials while designing
CSF 9	Providing vocational training to various construction personnel
CSF 10	On-site C&D waste supervision system (e.g. Storage zoning)
CSF 11	Lack of standardized waste collection systems
CSF 12	Lack of legislation to manage C&D waste
CSF 13	Setting standards for recycled products
CSF 14	Proper guidelines for landfilling using C&D waste
CSF 15	Implementation of polluter pays penalties
CSF 16	Proper planning and techniques for dismantling of structures
CSF 17	High cost and labor availability in separating C&D wastes
CSF 18	Electrical safety and fire safety during demolition

CSF 4—Lack of education and knowledge. It never occurred to the construction site management and technical team that resource conservation and environmental preservation could be accomplished through C&D waste management. According to them, C&D waste management usually means higher project costs and a reduction

in company profits. It is necessary to provide proper education for construction practitioners.

CSF 5—Requirement of waste management/waste recycling centers

It is necessary to have both stationary and mobile recycling plants. The fixed ones are typically more technologically advanced than the mobile ones, containing sorting equipment for the removal of unwanted fractions. Mobile recycling operations typically recycle lesser amounts of C&D waste in temporary demolition sites and using simple technologies. States with a population of more than one million people should have C&D waste recycling facilities in all cities.

CSF 6—Precise supervision on construction materials and works. On construction sites whether large or small, supervision has a key role in managing C&D waste. Workload planning and assignment, decision-making, performance and compliance monitoring, leadership, and adequate worker participation are all part of supervision. Contractors should have clear supervision of materials as well as works to reduce waste generation.

CSF 7—Cost of transportation between worksites and waste recycling plants.

Transportation cost between worksites and waste recycling plants is one of the main reasons leading to illegal dumping. The agencies that generate C&D waste in bulk quantity have to deliver the C&D debris to the recycling plant. Government incentives can solve the issue to a certain limit. Also setting up waste collection points as well as recycling plants at convenient locations can solve the problem.

CSF 8—Selection of high-quality construction materials while designing. The usage of high-quality construction materials promotes reusing and also in the case of recycling, it helps in the increased production of high-quality products. This is considered an important contribution to close construction materials cycles, as it decreases the amount of residual C&D waste to be managed, increases the economic value of the recycled component, and reduces the number of natural aggregates used.

CSF 9—Providing vocational training to various construction personnel. The skill level of workers in construction has a significant impact on C&D waste generation. Workers involved in reinforcing, welding, blasting, and tower crane operation, in particular, require proper training. Vocational training in construction project management, construction technologies, building materials, construction site supervision, project evaluation, and construction safety can be provided by government-approved training agencies. The training sessions might also include sustainable development and C&D waste management skills.

CSF 10—On-site C&D waste supervision system (e.g. Storage zoning). On-site awareness is an important factor. It is important to allocate specific areas in a site to satisfy storage requirements and this will help the employees to be aware of where specific substances are placed. Deliveries can also cause problems on busy construction sites. Proper supervision is needed for checking the quality and quantity

of materials on delivery and monitoring stock holdings. A proper storage system prevents damage to construction materials.

CSF 11—Lack of standardized waste collection systems. C&D collection centers have to be set up for small quantity generators of C&D waste who can deliver the C&D debris. Collection points can be provided so that a small quantity generator of C&D waste is not required to transport the debris to a distance of more than 2.5–3.0 km.

CSF 12—Lack of legislation to manage C&D waste. Current C&D waste management regulations have no obvious effects, and the main issue is that most current regulations are insufficiently specific to guide and enforce C&D waste management. Cities' municipal governments should implement more functional C&D waste management policies, and each region should develop its precise legislation, norms, and standards to guide sorting, reduction, reuse, recycling, and disposal. Also, penalties for illegal waste dumping are rarely enforced in Indian towns and panchayats.

CSF 13—Setting standards for recycled products. The experience in Delhi and Ahmadabad indicates that the market for recycled products made from C&D waste in India is still fairly limited due to poor quality. In India, a high goods and services tax (GST) of 18% is levied on recycled products, making them more expensive than traditional ones. A GST exemption for C&D waste recycled products should be examined. When a city's C&D waste recycling plant is operational, it may become necessary for all construction operations to use a certain percentage of building construction materials made from recycled debris.

CSF 14—Proper guidelines for landfilling using C&D waste. Construction and demolition waste disposal in landfills is substantially less expensive than recycling. High-landfill-charge initiatives could reduce landfilling. Increase demand for recycling and reusing wastes through measures such as demonstration and knowledge transfer, beginning with public-sector projects involving C&D waste diversion.

CSF 15—Implementation of polluters pays penalties. Charging for C&D waste dumping is a common waste reduction strategy. According to the 'polluter-pays principle,' waste producers must manage waste throughout its entire life cycle and pay for the environmental costs incurred as a result of their actions. The concept assigns financial responsibility for any environmental harm and initiates appropriate waste-reduction strategies. However, when disposal fees are low, it is impossible to force waste producers to prevent waste generation and landfilling.

CSF 16—Proper planning and techniques for dismantling of structures. Deconstruction is the careful dismantling of buildings to recover valuable components for reuse and recycling. Systematically selected demolition, sometimes known as "construction in reverse" or "deconstruction," is rarely used in India but has enormous potential. The key difference between conventional demolition and modern demolition is waste separation, which allows for the separation and sorting of building

components and materials on-site. It can be used to recover useable resources and drastically reduce waste.

CSF 17—High cost and labor availability in separating C&D wastes. Segregation of C&D waste on site is highly labor intensive. Materials that can be reused at the same site should be kept in separate heaps from those which are to be carried for recycling. Thus, additional labor charges seem to be a problem for contractors on sites.

CSF 18—Electrical safety and fire safety during demolition. Hazardous demolition operations need the services of qualified emergency response personnel like firefighters to ensure fire safety and electrical safety supervisors to ensure electrical safety.

2.7 Conclusions

An extensive assessment of available global publications on sustainable C&D waste management was carried out and various parameters influencing the C&D waste management were identified. Among them, 31 parameters were identified to be appropriate in the Kerala scenario. The questionnaire was prepared based on the identified parameters and the survey was conducted among professionals from multiple occupations involved in construction and demolition. The survey results were then analyzed using SPSS and Microsoft Excel. In SPSS, descriptive analysis was carried out and 18 factors were determined as Critical Success Factors. Lack of planning during the design stage was ranked first followed by factors like awareness of proper C&D waste management among common people, accurate estimation of materials before ordering, lack of knowledge and education, requirement of waste management/waste recycling centers, precise supervision of construction materials and works, cost of transportation between worksites and waste recycling plants, selection of high-quality construction materials while designing, providing vocational training to various construction personnel, on-site C&D waste supervision system (e.g. storage zoning), lack of standardized waste collection systems, lack of legislation to manage C&D waste, setting standards for recycled products, Proper guidelines for landfilling using C&D waste, implementation of polluter pays penalties, proper planning and techniques for the dismantling of structures, high cost and labor availability in separating C&D wastes and electrical safety and fire safety during demolition and these results are also validated by using RII analysis done in Microsoft Excel.

References

1. Guidelines on Environmental Management of C&D wastes, 2017 (Issued by Central Pollution Control Board)
2. Construction and Demolition Waste Management Rules (2016) (Issued by Ministry of Environment, Forest & Climate Change)
3. Guidelines for managing C&D waste in Kerala, Dated: 30-07-2022 (Issued by Local Self Government Department)
4. Strategy on Resource Efficiency in Construction & Demolition Sector, NITI Aayog (Issued by Ministry of Housing & Urban Affairs) (2019)
5. Liu J, Wang Y, Lin Y (2012) Critical success factors for construction and demolition waste management in Pearl River Delta of China. *Appl Mech Mater* 174–177:3245–3252 (ResearchGate)
6. Lu W, Yuan H (2010) Exploring critical success factors for waste management in construction projects of China. *Resources Conserv Recycling* 55:201–208 (ResearchGate)

Seismic Performance of Y-Braced Frame with Double Round Steel Tube



Fathima Manaf and Sajan Jose

Abstract Seismic performance of Y-braced frame with double round steel tube aims to study the performance of the Y shaped bracing in a frame under seismic forces. The project involves the designing of the double round steel tube which act as a damper in the frame. The optimum size of the damper or the double round steel tube is to be identified by varying the dimensions in terms of height, thickness, diameter and length. Any one of the parameters is changed keeping all others constant to find the better resulting one. All most 20 combinations were done to find the optimum sized one. Optimization aims to achieve the best yielding damper to be placed. After optimization, the performance of the damper under seismic load is analyzed. The evaluation includes analysis and result comparison of the frame with and without double round steel tube. The finite element analysis software ANSYS is used to find the optimum size of damper and analyze the frames.

Keywords Y-Brace · Damper · Double round steel tube · Ansys · Finite element analysis · Seismic forces · Cyclic loading

1 Introduction

Earthquake is nowadays found to be the most often heard and threatening disaster that not only destroys the structures but also take away the lives of many people. It is caused when the rocks in the underground breaks suddenly and releases the seismic waves or energy which shakes the surface ground [1]. Today the technology has improved so much that many seismic energy absorbers have been found. Steel braced frame structures is now being used widely in construction. We can see tall building all around is due to the increased population and increased land rates. When the height of the buildings increases the lateral load resistance mechanism is to be

F. Manaf (✉) · S. Jose
Universal Engineering College, Thrissur, Kerala, India
e-mail: fathimamanaf7@gmail.com

taken into consideration. To enhance the seismic performance of the structures, a wide variety of controlling methods are found. These methods include active, semi-active and passive control methods [2].

Double round steel tube is a damper which dissipates the seismic energy that effects the structure and helps the maintain the building [3]. The structural design makes sure that bearing capacity of the double round steel tube is lower than that of the bearing capacity of the braced bar. During the action of the seismic waves the double round steel tubes yields first protecting the bracings from buckling. The deformation of the damper can dissipate the earthquake energy. Low yielding steel is used as the material for the damper as compared to the bracings. This damper was chosen as a part of validating the journal 1 in references. Also, this damper is a metallic damper. The model is compared with the parameters like load bearing, ductility and energy dissipation. Yield strength and ductility are the two important factors of a structural component as it enhances the service safety of the structure [4].

In this paper the seismic performance of the Y-braced frame is analysed. Then the optimum size of the damper is found out by trial-and-error method. After optimization of the damper, it is placed to the frame with Y-bracing and cyclic loading is provided to the frame. Both the frames are analysed and compared. Optimization of the damper and analysis of the frame is done using the engineering software ANSYS 2022.

2 Analysis and Design of Y-Braced Frame (Without Damper)

The modelling of the y-braced frame is done using ANSYS Workbench 2022 R2. The frame which has a height of 3.3 m and span of 6 m is modelled and loading is applied to the frame for analysis [1]. The dimensions of the y-bracings were selected from the journal 2 in the reference. The maximum load taken by the frame and the corresponding displacement is observed. The specimen is having a mesh size of 50 mm. The boundary conditions are fixed at the bottom and a displacement is applied laterally to the frame (Table 1).

Table 1 Results of Y-braced frame

	Deflection (mm)	Load (kN)	Yielding	Ductility	Type of failure
Brace	29.144	995.81	10.279	2.835	Buckling of brace

Table 2 Properties of the damper [2]

Yield strength (MPa)	Young's modulus (MPa)	Poisson's ratio
300	$2.1e + 5$	0.3

3 Optimization of Damper

The aim of this paper is to design an optimum model of the damper that has a higher load bearing capacity and ductility and to place that damper to the Y-braced frame. The initial size of the damper has an outer diameter of 500 mm, inner diameter of 300 mm, 100 mm height and rib have 10 mm thickness [2]. These dimensions are varied accordingly to get the optimum sized damper which takes maximum loads. About 20 models were analysed to get the optimum sized one. The one which takes more load is selected to be placed in the frame. The material of the damper is low yielding steel of 300 MPa. The properties of the damper are shown in the Table 2.

From these models analysed load carrying capacity and ductile performance has increased simultaneously for damper size **500 × 100 × 100 × 9 mm**. This model shows a higher load bearing capacity when compared to other models and its ductility has also improved to a great extent. The type of failure is commented on the basis of the failure pattern of the damper (Table 3).

When dampers are installed in to a structure its damping property increases. Dampers are used in structures to improve its overall ductility by reducing the likelihood of catastrophic failure during earthquake [5].

4 Analysis and Design of Y-Braced Frame (with Damper)

After the optimization of the damper, the damper of size $500 \times 100 \times 100 \times 9$ mm is placed where all the three braces of the Y-braced frame meet. The cyclic loading is given to the frame and made to analyse (Figs. 1, 2, 3, 4 and 5).

5 Results and Discussion

With the comparison of the 2 models, the specimen with and without damper, we can see that the load taken by the frame with damper is more as compared to the frame without damper. There was a increase of 7.06%. Also, the energy dissipation of the frame with damper is much greater with a percentage increase of 605.065. Greater energy dissipation results in increased seismic resistance of the frame leading to less damage to the structure (Fig. 6; Table 4).

Table 3 Damper models analysed

Model	Deflection (mm)	Load (kN)	Yielding	Ductility	Type of failure
500 × 100 × 300 × 10	185.45	974.91	40	4.63	Connection failure
500 × 100 × 200 × 10	139.14	943.46	40	3.47	Connection failure
500 × 100 × 100 × 10	192.10	1154.30	38.58	4.97	Connection failure
500 × 75 × 300 × 10	176.62	973.62	40	4.41	Connection failure
500 × 75 × 200 × 10	146.64	950.50	40	3.66	Connection failure
500 × 75 × 100 × 10	138.07	1025.70	45.53	3.03	Yielding of damper
500 × 50 × 300 × 10	165.46	965.96	40	4.13	Damper brace connection failure
500 × 50 × 200 × 10	149.86	877.62	40	3.74	Connection failure
500 × 50 × 100 × 10	261.43	888.36	21	12.44	Yielding of damper
1S-500 × 100 × 200 × 10	34.00	924.98	20	1.7	Buckling of brace
1S-500 × 75 × 200 × 10	32.90	923.69	14	2.35	Buckling of brace
1S-500 × 50 × 200 × 10	50.50	887.65	40	1.0.26	Buckling of brace
1S-500 × 100 × 200 × 5	213.23	958.30	15	14.2	Connection failure
1S- 500 × 75 × 200 × 5	318.33	850.34	28	11.36	Buckling of brace
1S- 500 × 50 × 200 × 5	262.00	830.21	30	8.7	Connection failure
1S-500 × 100 × 200 × 6	79.97	879.36	21	3.8	Connection failure
500 × 100 × 100 × 9	201.63	1066.20	41.39	4.87	Yielding of damper
500 × 75 × 100 × 9	165.38	941.15	45.28	4.87	Yielding of damper
500 × 100 × 100 × 8	236.49	955.00	41.95	5.63	Connection failure
500 × 75 × 100 × 8	220.21	848.44	17.50	12.58	Connection failure

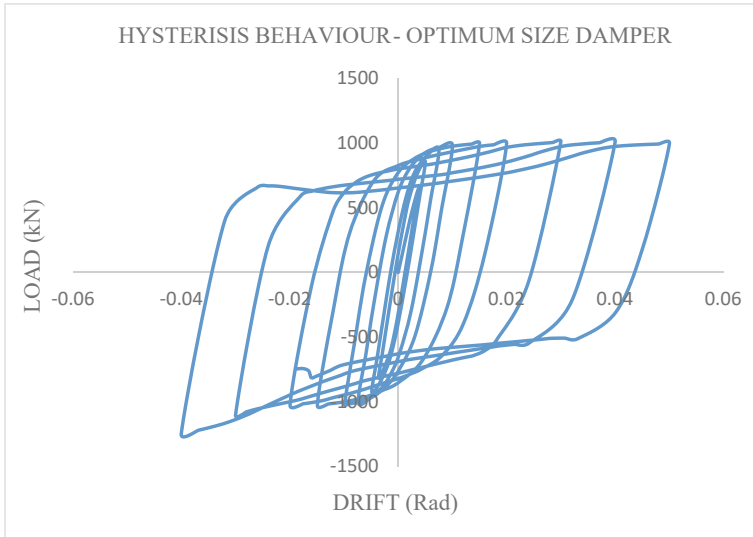


Fig. 1 Hysteresis curve of frame with optimum size damper

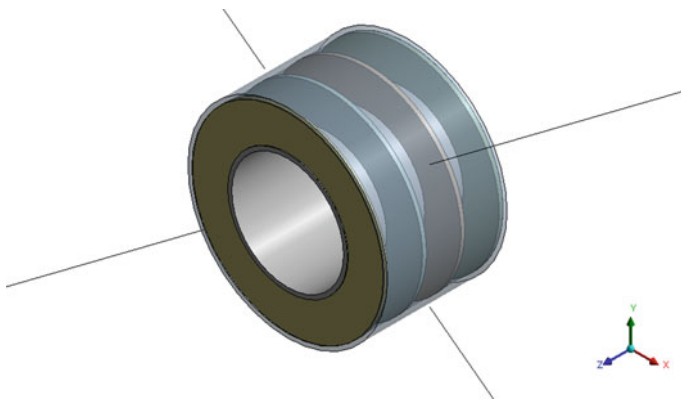


Fig. 2 Double round steel tube (damper)

6 Conclusions

In this study, the optimum double round steel tube in braced steel moment resistant frame was designed. Optimum damper was selected on the basis of the load carrying capacity and the ductility of damper placed in the frame. Initially a frame having Y-bracing is analysed and analysis of the frame with double round steel tube were done. The optimization of the damper was done before the placement to the frame on the bracing. With the introduction of the damper the load carrying capacity and the ductility of the frame increased. The load carrying capacity increased by 7.06%

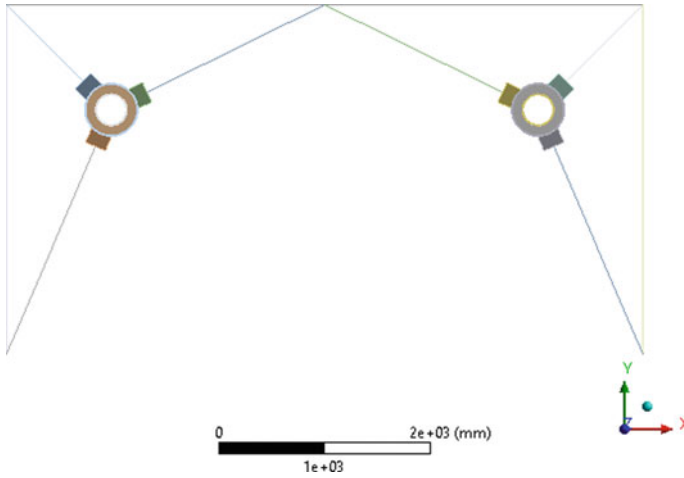


Fig. 3 Damper placed on the frame

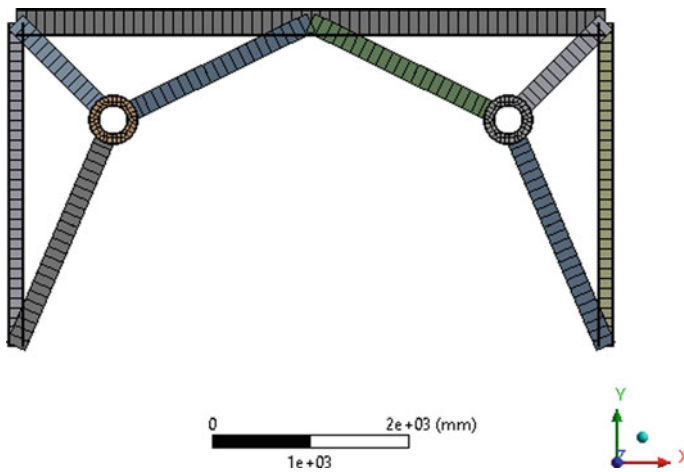


Fig. 4 Mesh of the specimen

and ductility by 71.78%. Also, through the comparison of the model it is evident that the model with damper have a high energy dissipation rate by 605.065%. Increased rate of energy dissipation helps to take up a greater amount of seismic waves that hit on the structure and hence protects the structure.

The results obtained from this study suggest that the use of double round steel tube dampers can significantly enhance the seismic performance of steel frames. Along with load bearing capacity ductile behaviour is also improved. By dissipating energy and reducing forces, dampers may help prevent the structure from failure as the dampers yield thereby protecting the bracings.

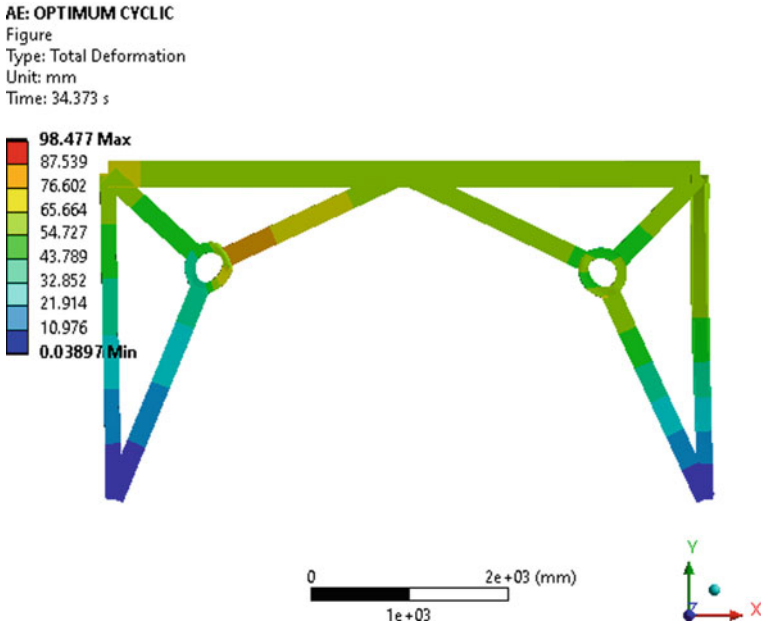


Fig. 5 Total deformation of the specimen

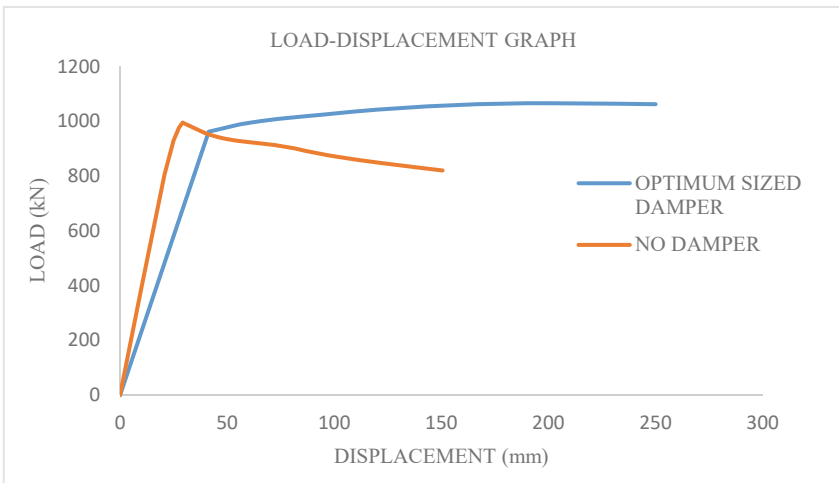


Fig. 6 Comparison chart of the models

Table 4 Comparison of the specimens

	Load (kN)	Energy dissipation (kJ)	% Improvement
Brace	995.81	174.011	1
Brace with damper	1066.20	1226.89	605.065

Overall, this study helps to the advancement of research in the field of earthquake engineering and can serve as a precious information for researchers and practitioners in the field of structural engineering. The results gained from this project can be used to design more earthquake-resistant steel structures, ultimately contributing to the safety and well-being of communities in earthquake-prone regions.

References

1. Majid Zamani S, Vafaei A et al (2012) Experimental investigation of behavior of steel frames with y-shaped concentric bracing. *J Constr Steel Res* 70:12–27
2. Zheng L, Dou S, Wang W et al (2022) Seismic performance of braced frame with double round steel tube. *J Constr Steel Res* 193:107297
3. Majid Zamani S et al. (2012) Experimental investigation of steel frames with single bays of symmetrical y-shaped concentric bracings. *Scientia Iranica Trans A: Civil Eng* 19:195–210
4. Annan CD, Youssef MA, El Naggar MH (2009) Experimental evaluation of the seismic performance of modular steel-braced frames. *Eng Struct* 31:1435–1446
5. Shahiditabar A, Moharrami H et al (2021) Development and experimental verification of self-centered y-shaped braced frame. *Structures* 34:1312–1325

Comparative Study of Different Stabilizers for Peat Soil Stabilization: A Review



Torjit Elangbam  and Ajanta Kalita 

Abstract With the increase in population, there is a dearth of land suitable for infrastructure development. Due to poor engineering properties, many areas of land remain unutilized which also slows down rapid development. Areas containing peat soil are among the most unutilized land in many regions of the world. Total area covered by peat soil is 4.23 million km² (Xu et al. in *Catena* 160:134–140, 2018 [1]). Peat deposits have been discovered to be widespread throughout the world, taking up between 5 and 8% of the planet's geographical area (Mesri and Ajlouni in *J Geotechn Geoenviron Eng* 133:850–866, 2007 [2]). Peat soils are formed from partially decomposed plant material under anaerobic water saturated conditions. They are categorised based on their level of humification. These peat soils are characterised by high moisture content, low bearing capacity, high porosity, and high compressibility. Different stabilisers used for peat soil stabilization can be broadly categorised into cementitious material (Portland cement, fly-ash C, slag cement etc.), geopolymer and other non-conventional material (envirotac, effective microorganism etc.). Different studies have demonstrated that the unconfined compressive test performed on every type of peat sample with varying quantity of each stabiliser shows a significant increase in the compressive strength. The optimum strength of each stabiliser obtained in different research have been compared in this study. Results of Permeability and UU triaxial tests are also studied by some researchers. It is also found that various places have different peat soil depending on their humification level and environmental condition, thus suitable stabiliser for that place can be found after extensive research with an emphasis on locally available materials. In this article, results of several studies conducted on peat soil are reviewed to understand the improvement of engineering properties of peat soil after stabilization. Each stabilizer is studied thoroughly to understand its feasibility in peat soil stabilization and impact on environment.

Keywords Geopolymer · Cementitious material · UCS

T. Elangbam (✉) · A. Kalita
Department of Civil Engineering, North Eastern Regional Institute of Science and Technology,
Nirjuli, Arunachal Pradesh 791109, India
e-mail: torjitelang@gmail.com

A. Kalita
e-mail: ajanta@nerist.ac.in

1 Introduction

Peat soils are mostly found in peatlands (also called bogs or mires). Peatlands cover about 3% of the earth's land mass; they are found in the temperate (Northern Europe and America) and tropical regions (Southeast Asia, South America, South Africa and the Caribbean). A high distribution of peatlands can particularly be seen in the northern hemisphere (including Canada, Russia, and Finland). In Japan the peat deposits are mainly found on Hokkaido Island (the northernmost of Japan's four main islands), yet a minor distribution exists in other islands as well. In Hokkaido, around 2000 km² is occupied by peat deposits, which has been reported to be approximately 6% of the flat land in Hokkaido (Noto 1991). Peat is soil that has an organic content greater than 35%, according to scientists studying soil. All soils with an organic content of more than 20% are considered organic soils by geotechnical engineers, and peat is an organic soil with an organic content of more than 75%. The mechanical characteristics of the soil serve as the foundation for the engineering definition. It is well accepted that the mechanical parameters of typical mineral soil (silt and clay) can no longer be typically applied to soils with a higher than 20% organic content. Moisture content and temperature both have an impact on peat formation. Microorganism's ability to decompose plant matter is hindered in extremely saturated anaerobic soils, leading to excessive carbon buildup. In colder climates, microorganisms take longer to decompose plant matter, which speeds up the creation of peat. Peatland is a significant carbon storage area on the earth's surface due to the carbon concentration of its peat soils. Its significance in battling climate change cannot be overstated for this reason.

Peat develops from the accumulation and decomposition of organic materials (derived from plant residues) in an oxygen-poor, moist environment, peat soil is one of the most difficult types of soil to work with in civil and environmental engineering (O'Kelly 2015). As indicated in Table 1, plant remnants in peat can be found at various levels of decomposition, from undecomposed to highly decomposed. As a result, the peat soil frequently has a dark brown to black color, a spongy consistency, and a characteristic odor. Warm, humid climates are ideal for the growth of peat, but peat may also grow in chilly places like Siberia, Canada, and Scandinavia. The inadequate breakdown of the remnants of organisms results in the creation of peat. The beginning of peat formation in bogs dates back around 12,000 years. Since peatlands store a lot of rainwater or are also fed from groundwater, they are saturated with water. Most decomposing organisms cannot live and do their work under these conditions or can do so only poorly. For this reason, an increasingly thick layer of plant material accumulates in bogs over time. This is reinforced by the establishment of very high acidity in some types of peatlands. Since this deposited plant material consists largely of carbon compounds, peatlands are rightly considered giant and important CO₂ reservoirs that remove carbon dioxide from the atmosphere. However, when peat is used it is released again to the environment fueling the greenhouse effect.

Table 1 Classification according to humification

Degree of humification	Nature of matter extruded on squeezing	Nature of plant structure in residue
H1	Clear colourless water; no organic soil squeezed out	Unaltered, fibrous, undecomposed
H2	Yellowish water; no organic soil squeezed out	Almost unaltered, fibrous
H3	Brown turbid water; no organic soil squeezed out	Easily identifiable
H4	Dark brown turbid water; no organic soil squeezed out	Visibly altered but identifiable
H5	Turbid water and some organic soil squeezed out	Recognisable but vague, difficult to identify
H6	Turbid water; 1/3 of the sample squeezed out	Indistinct, pasty
H7	Very turbid water; 1/2 of sample squeezed out	Faintly recognisable; few remains identifiable, mostly amorphous
H8	Thick and pasty; 2/3 of sample squeezed out	Very indistinct
H9	No free water; nearly all of sample squeezed out	No identifiable remains
H10	No free water; all the sample squeezed out	Completely amorphous

Source Abdel-Salam [3]

Peat is frequently acknowledged in geotechnical engineering as a material with high compressibility and limited bearing capacity, making it unsuitable for use as foundation materials for any construction operations (Adnan et al. 2007). But the quick economic growth and rapid development in many nations have led to significant infrastructural growth. In order to find ways to build infrastructure like roads, housing, drainage, and other types of construction, further research into the properties of soil in areas with unfavorable ground conditions, like peat, is motivated by the fact that these developments are hampered by a lack of suitable land for development.

Stabilization of a soil can be defined as the process of improving the properties of a soil to make it suitable for construction purposes. It is the process to improve the strength characteristics of the soil. There are different types of admixture or additives that can be added to soil. One of the most common additives is cement. Chemicals like cement and lime do improve the strength of soil but it also has its drawbacks. These materials are chemicals and production of these materials harms the environment due to their pollution in the process of production. The new trend in soil stabilization is to look for alternative solutions where waste materials or naturally available material are used in soil stabilization. Geopolymer succour the purpose of sustainability. Geopolymer and other materials have their drawbacks in ineffectiveness when compared to cementitious materials.

2 Literature Review

Peat soil stabilization has been conducted by many researchers using different types of materials on different types of peat. The use of cementitious materials in soil stabilization is observed in many papers for different soils. The use of geopolymer in soil stabilization is increasing as geopolymers are made from industrial by products. In this review, the literature reviews are broadly categorized as stabilization of peat using cementitious materials, geopolymer related and stabilization of peat using non-conventional materials.

2.1 Stabilization of Peat Soil Using Cementitious Material

Author(s)	Description	Results
Hauashdh et al. [4]	OPC, fly ash, and bottom ash were added; Before and after the stabilization of peat soil, UCS and FESEM were conducted; 60% of the admixture is composed of peat soil, 18% is fly ash, 14% is bottom ash, and 8% is OPC	UCS (Unconfined Compressive Strength) strength improvement with longer dry curing times; voids between stabilized peat became smaller
Boobathiraja et al. [5]	Lime and cement are added to the soil sample in percentages of 10%, 30%, and 50% to achieve the highest possible dry density	Increase in UCS strength with increase in content of lime and cement
Zambri and Ghazaly [6]	In accordance with BS standard 1377:1990(part 7), all disturbed samples were evaluated using a direct shear test in drained condition for untreated and treated peat sample (peat + 10% lime, 20% lime, 10% cement and 20% cement)	With an increase in lime and cement content, it is discovered that the angle of shear resistance and the cohesiveness of peat both dramatically rise. In terms of the shear strength of peat soil, lime performs better than cement
Radwan et al. [7]	PPF, fly ash, and cement were added in varied amounts	OMC, MDD and PH increase with increase in percentage of cement; The UCS and CBR of cement-treated peat soil improved significantly with increasing cement content

(continued)

(continued)

Author(s)	Description	Results
Abdel-Salam [3]	Mixture 1 has 20% clayey diatomite, 27% calcium carbonate, 13% lime, and 41% water. Mixture 2 contains 25% cement, 33% calcium carbonate, 14% lime, and 28% water.; another 2 mixtures were prepared with peat	The strength of peat increases significantly with increase in curing period in mixture 2
Yacob and Som [8]	Ordinary Portland cement (OPC) and magnesium oxide serve as the binder (MgO); Filler: sand and garnet	The findings of the UCS test indicate that applying MgO to cement stabilised peat soil improved the peat's strength. The engineering characteristics of peat soils were changed by the filler addition of wasted garnet
Wong et al. [9]	Cement, slag and well graded siliceous sand were used as admixtures for stabilization of peat soil	Improvement in compressive strength; Increase in undrained shear strength at first and reduction in strength with increase in curing period
Wong et al. [10]	For the peat stabilisation, Portland Composite Cement, Calcium Chloride, Kaolin, and Silica Sand were chosen as the components	The test specimen with 10% partial kaolin replacement has the maximum unconfined compressive strength, which is more than the minimum necessary unconfined compressive strength of 345 kPa.; Permeability reduces significantly
Dehghanbanadaki et al. [11]	All stabilised peat samples utilised in this investigation had original natural moisture contents of around 495% ($\pm 5\%$); filler materials included coarse poorly graded sand, fine poorly graded sand, and poorly graded gravel	The compressive strength of cement peat significantly decreases when combined with different dosages of poorly graded gravel, coarse poorly graded sand, and fine poorly graded sand, except for when addition of well graded sand is made at a dosage of approximately 125 kg/m ³ of weight of wet peat
Kalantari and Prasad [12]	Unaltered samples as well as peat samples stabilised with various OPC doses were used in the UCS tests (15%, 30%, and 50%); samples were cured in different modes (moist, air, moist with surcharge load of 10 kPa)	Increase in UCS strength; strength increase in different types of curing were compared
Paul and Hussain [13]	Cement (OPC) is use as binder to stabilized peat collected from Manipur, Assam and Tripura	Ph and EC increase with increase in cement content; UCS strength increase with increase in cement content; increase in organic content decreases the strength of stabilized soil

(continued)

(continued)

Author(s)	Description	Results
Ghasem Ghanbari et al. [14]	Cement and basalt fibres were used as additives; sample are test after curing with different length of basalt fibre and cement content	Compared to basalt fiber, UCS strength rises as cement content increases; Increase in basalt content improves ductility
Ahmad et al. [15]	Silica fume and cement were added as additives	Increase in the density of stabilized peat; evidence of morphological alteration in stabilized peat

2.2 Soil Stabilization Using Geopolymer

As much research cannot be found for peat soil stabilized with geopolymer materials, the study includes research performed on other types of soil using geopolymer and geopolymer related studies.

Author(s)	Description
Yang et al. [16]	This study gathered a large amount of bibliometric data on GPC from the Scopus database and then used the right software to perform a scient metric analysis. The scient metric analysis found the top publications, frequently used keywords in the published articles, authors and papers with the most citations, and active regions
Razali et al. [17]	Vinyl Acetate-Acrylic Copolymer (VAAC) was used as main stabilizer for this study. Sand, lime and cement were also used as binder material. The results showed that peat soil stabilized with VAAC increases their strength significantly up to 14 days of curing. The binder doesn't show any positive effect
Muhammad et al. [18]	This study assessed the geotechnical properties of laterite soil using metakaolin as an additive. UCS strength and MDD increases with increase in metakaolin content
Wang et al. [19]	This study used a blend of quicklime and sodium bicarbonate as an alkali activator to create the geopolymer binder using metakaolin as a precursor. Soil made of silty clay is then used to stabilize the geopolymer. The compressive strength improved positively
Esparham et al. [20]	This study assessed the effect of alkaline activated solution in improving the strength of fly ash based geopolymer. NaOH and KOH are used as alkaline solutions along with Na ₂ SiO ₃
Ruzaidi et al. [21]	The study assessed the changes in clay substrate due to coating by kaolin based geopolymer. The specimens were prepared into 2 types namely sintered and unsintered. It is seen that the sintered specimen produced better results
Jais et al. [22]	Geopolymer Flexible Activator (Geo Flex A) and fly ash were used as alternative solutions to improve the strength of peat soil. The Geo Flex A was kept constant and fly ash percentage was increased. UCS strength increases with increase in fly ash

(continued)

(continued)

Author(s)	Description
Wibisono et al. [23]	Fly ash based geopolymer used as binder along with cement to increase the strength for peat soil. The results after 7 days of curing show positive result
Parthiban et al. [24]	The paper reviewed different types of geopolymer used in strengthening engineering property of soil. It also analyzed the effectiveness of using geopolymer in reducing environmental impact
Duxson et al. [25]	The study investigated the basic structural and chemical features of geopolymers made from metakaolin, fly ash, and slag in order to determine how the choice of raw material affects the characteristics of geopolymer composites. The setting behavior, workability, and chemical and physical properties of geopolymer products are demonstrated to be highly dependent on the raw components and processing circumstances
Den Hamer et al. [26]	This paper studied peat Sinification, in which the peat soil properties are improved using silicate layers. During the silicification procedure, a cationic surfactant, a binding agent (a sodium meta silicate solution), and molasses to encourage microbial fermentation are all added
Khanday et al. [27]	This paper analyzed the feasibility of rich husk ash geopolymer in enhancing the properties of Indian peat. The paper also examined the effectiveness of additives with respect to organic content. The alkaline used in making geopolymer ranges from 3 to 9 molarity

2.3 Stabilization of Peat Using Non-conventional Materials

Most of the research for peat soil stabilization relates to cementitious material and geopolymer. Therefore, few research papers are available in this part.

Author(s)	Description
Norazam et al. [28]	Envirotac is a distinctive product that controls dust, erosion, and soil stabilisation. Envirotac is typically a liquid that is white in colour. It creates a transparent plastic and resin link that holds the soil particles together while they are drying. This material is used to stabilize the peat soil from 15 to 45%. There is increase in strength compressive strength and increase in shrinkage with respect to envirotac percentage
Yusof et al. [29]	This paper examined the use of effective microorganisms in stabilization of peat soil. EM were added in 2 conditions (controlled and uncontrolled moisture). The result shows an increase in controlled moisture content,
Kolay et al. [30]	This paper studied the feasibility of pond ash in stabilization of peat soil. The pond ash is added in varying quantity and the sample is tested after curing. The compressive strength increases with increase in pond ash and curing period
Khanday et al. [31]	The authors reviewed different types of additives used in peat soil ranging from conventional like lime and cement to non-conventional like ggbs, slag, magnesium chloride etc

(continued)

(continued)

Author(s)	Description
Moayed and Nazir [32]	This paper reviewed the different types of peat soil available in Malaysia and their recent developments in peat soil stabilization. It is also found that different areas have different types of peat soil
Devi and Kumar [33]	The utilization of lime, cement, plastic trash, industrial waste, fiber, mushroom waste, wet olive pomace, and other materials in soil stabilization was discussed in this work. The engineering qualities of soil were greatly enhanced using additives

2.4 Analysis of Findings from Literature Review

Unconfined compressive strength

UCS test is performed in almost every paper of peat soil stabilization. Every type of additive discussed above has a positive impact on peat soil. The magnitude of effectiveness is the main issue.

Significant improvement in peat soil due to cementitious material (Table 2)

As it can be seen from the table, the percentage increase of UCS at 30% Cement content along with fly ash and PPF is enormous. The peat soil used in this test is collected in Kuala Lumpur, Malaysia.

Table 2 UCS strength comparison

Untreated peat	Cement		Flyash + Cement		PPF + Cement	
	Cement content	UCS improvement (%)	Fly ash content (%)	UCS improvement (%)	PPF content (%)	UCS improvement (%)
95 kPa	10	43.2	10	93.7	0.10	46.3
			20	143.2	0.15	51.6
			30	147.4	0.20	48.4
95 kPa	20	105.3	10	155.8	0.10	115.8
			20	208.4	0.15	135.8
			30	216.8	0.20	124.2
95 kPa	30	319	10	352.6	0.10	377.9
			20	422.1	0.15	475.8
			30	429.5	0.20	427.4

Source [7]

Significant improvement in peat soil due to geopolymers (Fig. 1)

This is the significant improvement of peat soil compressive strength due to increase in VAAC, a type of polymer. The binder materials added along with VAAC does not help in improving the compressive strength of soil. The peat soil is collected in Johor, Malaysia.

Significant improvement in peat soil due to non-conventional materials (Table 3)

The value of compressive strength increases when the envirotac content increases. The shrinkage of the peat soil will, however, accelerate when the additive substance interacts with it. 30% is the ideal amount of Envirotac in peat soil. The peat soil

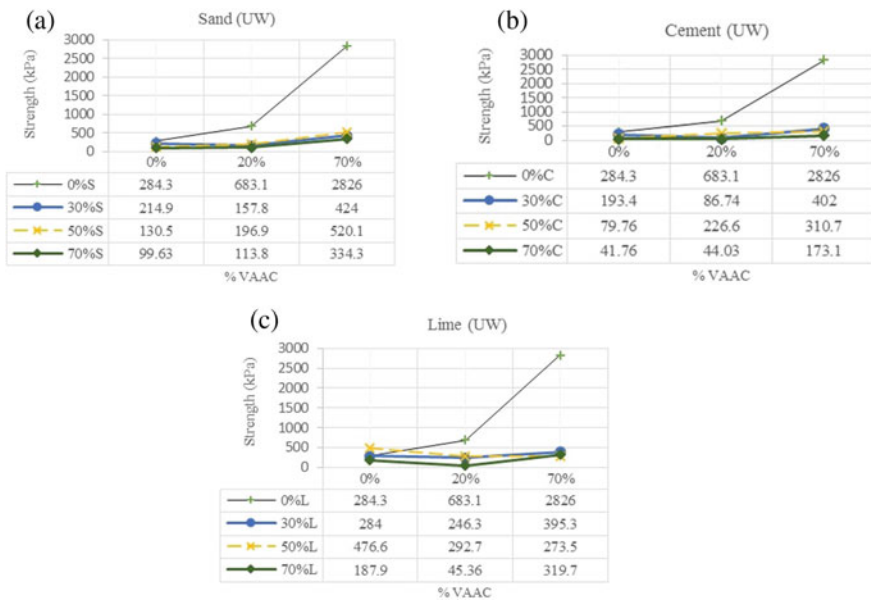


Fig. 1 Strength variation in treated peat soil due to VAAC using **a** Sand (UW), **b** Cement (UW), **c** Lime (UW). *Source* [17]

Table 3 Improvement of peat soil with increase in envirotac content

Types of soil	Additives	Unconfined compressive strength (kPa)		
		7 days	14 days	21 days
Peat soil	Blank	42.46	44.84	46.31
	15% Envirotac	175.81	405.53	501.27
	30% Envirotac	241.87	537.34	561.72
	45% Envirotac	422.95	560.55	573.89

Source [28]

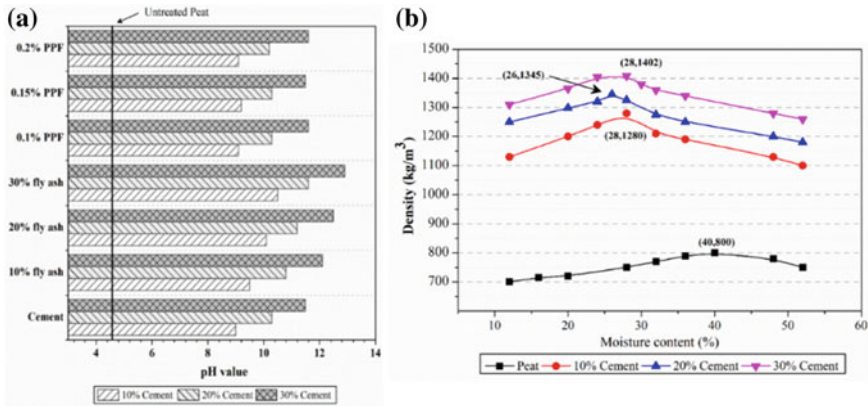


Fig. 2 a pH; b OMC and MDD of treated and untreated soil. Source [7]

has the highest strength of the Envirotac, at 45%. However, it has seen much more shrinkage than the 30% Envirotac in the peat soil.

Effect of curing in compressive strength

The strength of stabilized peat increases with the increase in curing period. However, it is not the same for all types of peat soil. It does not follow any specific trend. The rate of increases in compressive strength is also different according to range. Many studies have shown that the strength increases significantly up to 14 days and there is slow growth after 14 days. The strength increases due to curing occurred in all types of stabilizers.

OMC, MDD, PH and permeability

The pH increases when the peat soil is treated with any type of mentioned additive. This signifies that bacterial action will reduce in stabilized soil. This can be seen in source [13]. There is also mention of reduction in pH with increase in curing period of cement stabilization (source [13]). Furthermore, MDD is increased in stabilized peat soil. The Untreated peat was found to have a 6.43 to 106 times higher rate of permeability than stabilised peat (source: [10]). As for peat stabilized using geopolymer, there is dependent on the molarity of the alkaline solution, most probably NaOH solution. There is an increase in pH with increase in molarity up to some limit (source [27]). The MDD increases with decrease in OMC in stabilized peat soil. Moreover, Permeability also improves with increase in stabilizer up to some limit (Fig. 2).

2.5 Microstructural Analysis

Microstructural analysis of peat soil treated with cement (Figs. 3 and 4)

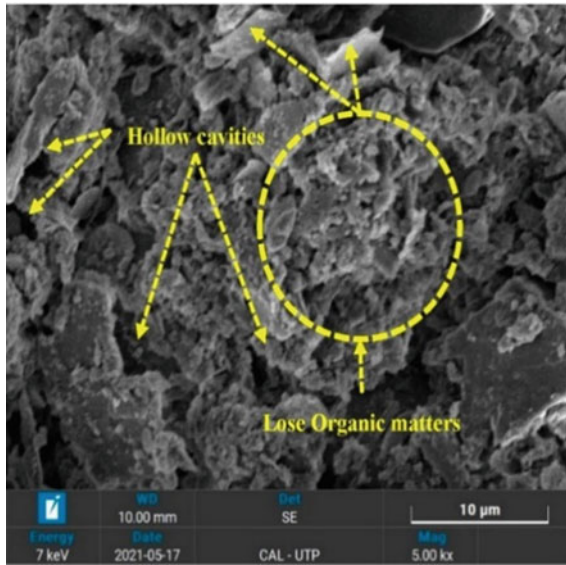


Fig. 3 SEM image of untreated peat. Source [15]

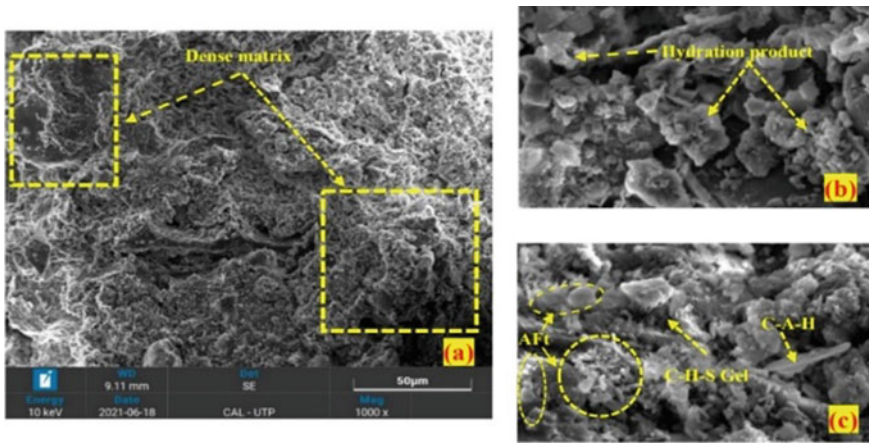


Fig. 4 SEM image of 28-day cured OPC stabilized peat a 1000×, b 8000×, c 10,000×. Source [15]

As shown in the figures above, when peat soil is stabilized with cement, it becomes denser. This is a result of the cement hydration process. The stabilized peat has become denser as a result of the creation of calcium silicate hydrate (C–S–H) gel, calcium aluminate hydrate (C–A–H), and ettringites (Aft), which filled the peat soil’s microscopic holes.

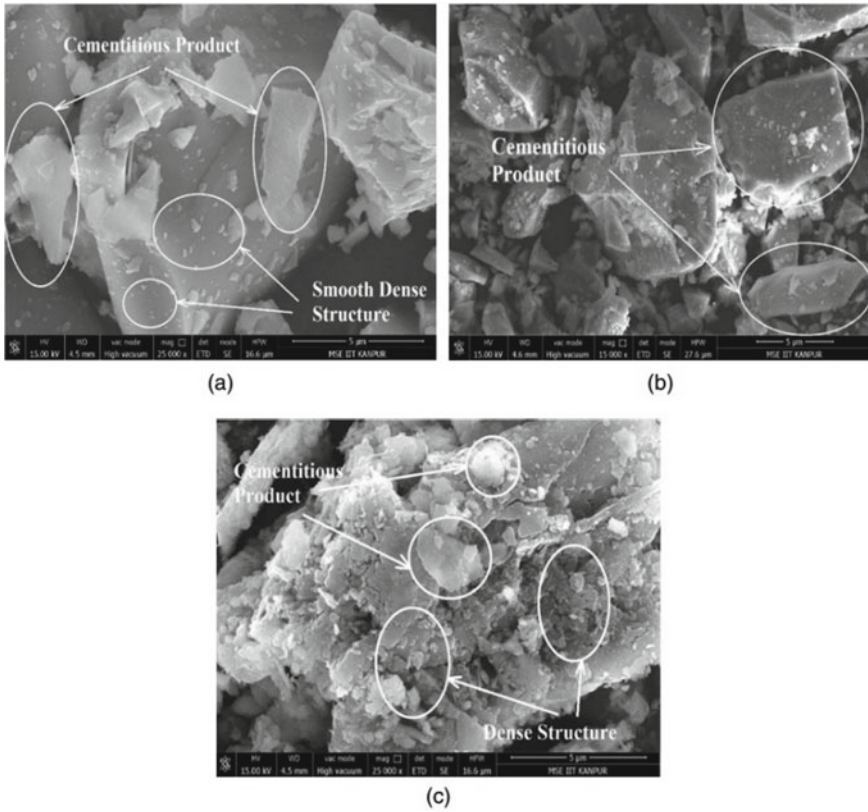


Fig. 5 FESEM of treated peat: **a** sapric; **b** fibric; and **c** hemic after 28 days of curing. *Source* [27]

Microstructural analysis of peat stabilized with geopolymer (Fig. 5)

The formation of denser stabilized peat due to geopolymer is due to the formation of cementitious product from Si and Al rich materials with the help of alkaline activator. It involves a 3-step process as explained in (source [27]).

3 Conclusion

The following conclusions can be made from the above studies: -

- (1) Peat soil is very problematic as mentioned in all the papers. It has low bearing capacity, high compressibility, high permeability, high organic content etc. Further, there are many types of peat soil. This is due to different levels of humification. Peat soil is distributed in many parts of the world. The research conducted is on peat soil collected from many parts including India, Malaysia etc. Peat soil

available in India is distributed in different parts. It can be found in Manipur, Assam, Tripura and Arunachal Pradesh. According to the Indian Council of Agricultural Research (ICAR), peat covers about 88,756 km² (2.17%) of the entire country. There has not been proper research to improve the utility of peat soil in India. Although few laboratories' findings have been made, there is a huge gap when it comes to real in situ application.

- (2) The UCS findings denotes that peat soil stabilization is possible with many types of binder material starting from cementitious to geopolymer. There has been results showing a significant increase in UCS strength from every category of geopolymer. The effectiveness of a stabilizer depends on its longevity of stabilization, percentage of improvement and conditions in which the soil is tested. Effective microorganisms (EM) succeed in improving strength of peat soil in controlled moisture content only, as for uncontrolled moisture content, it does not improve the strength of peat soil as mentioned in source [29]. Furthermore, the highest strength increase is seen on combination of more than 2 binders instead of using only a single binder. As for polymer VAAC as mentioned in source [17], the strength kept on increase with increase in polymer content but after a limit, it impacts on permeability.
- (3) Other tests including pH, Electric conductivity, CBR, permeability shows positive improvement in any kind stabilizer. Although this is true up to some limit. Due to lack of research in geopolymer stabilization of peat soil, comparison of findings cannot be studied. Further, stabilization of peat soil due to cementitious material focuses more on UCS test.
- (4) As for microstructural analysis, there is improvement in morphological structure of peat soil with cementitious material and geopolymer. Although there is reduction in density of cement stabilized peat soil with increase in curing period as mentioned in source [13]. There is lack of microstructural analysis in other types of non-conventional stabilizers (envirotac, Effective microorganism, magnesium chloride etc.)
- (5) Cement is considered as the best binder for construction purposes, but it has many drawbacks causing air pollution and ecological imbalance. Concrete is the 2nd highest consumer material in world, right after water. In the process of mining raw materials for cement, it causes destruction in flora and fauna. There is consensus in the scientific community to find an alternative solution in finding an alternative. On the other hand, the use of geopolymer benefits greatly to the environment as its raw material are industrial by-products (fly ash, ggbs, silica fume etc.). As these material content has silica and alumina content, they can be made into geopolymer using alkaline activator. The by-products do not have many uses and using them in soil stabilization improves the environment and serves the goal of sustainability. In terms of improving engineering properties of peat soil, they have shown to be quite effective but geopolymers take time to harden. Even with few drawbacks, geopolymer can become a very effective stabilizer of peat soil with proper elaborate research on it. Finally, there should be extensive research on peat soil with geopolymer and other additives.

References

1. Xu J, Morris PJ, Liu J, Holden J (2018) PEATMAP: Refining estimates of global peatland distribution based on a meta-analysis. *CATENA* 160:134–140
2. Mesri G, Ajlouni M (2007) Engineering properties of fibrous peats. *J Geotechn Geoenviron Eng* 133(7):850–866
3. Abdel-Salam AE (2018) Stabilization of peat soil using locally admixture. *HBRC J* 14(3):294–299
4. Hauashdh A, Mohamed RMSR, Jailani J, Abd Rahman J (2020) Stabilization of peat soil using fly ash, bottom ash and Portland cement: soil improvement and coal ash waste reduction approach. In: IOP conference series: Earth and environmental science, vol 498, no 1. IOP Publishing, p 012011
5. Boobathiraja S, Balamurugan P, Dhansheer M, Adhikari A (2014) Study on strength of peat soil stabilised with cement and other pozzolanic materials. *Int J Civil Eng Res* 5(4):431–438
6. Zambri NM, Ghazaly ZM (2018) Peat soil stabilization using lime and cement. In: E3S web of conferences, vol 34. EDP Sciences, p 01034
7. Radwan MK, Lee FW, Woon YB, Yew MK, Mo KH, Wai SH (2021) A study of the strength performance of peat soil: a modified cement-based stabilization agent using fly ash and polypropylene fiber. *Polymers* 13(23):4059
8. Yacob LS, Som AM (2020) Stabilisation of peat soil using magnesium oxide: a preliminary study. *Malays J Anal Sci* 24:578–586
9. Wong LS, Hashim R, Ali FH (2008) Strength and permeability of stabilized peat soil. *J Appl Sci* 8(21):3986–3990
10. Wong LS, Hashim R, Ali F (2013) Improved strength and reduced permeability of stabilized peat: focus on application of kaolin as a pozzolanic additive. *Constr Build Mater* 40:783–792
11. Dehghanbanadaki A, Ahmad K, Ali N (2013) Influence of natural fillers on shear strength of cement treated peat. *Gradevinar* 65(07):633–640
12. Kalantari B, Prasad A (2014) A study of the effect of various curing techniques on the strength of stabilized peat. *Transp Geotech* 1(3):119–128
13. Paul A, Hussain M (2020) Cement stabilization of Indian peat: an experimental investigation. *J Mater Civ Eng* 32(11):04020350
14. Ghasem Ghanbari P, Momeni M, Mousivand M, Bayat M (2022) Unconfined compressive strength characteristics of treated peat soil with cement and basalt fibre. *Int J Eng* 35(5):1089–1095
15. Ahmad A, Sutanto MH, Ahmad NR, Mohamad ME, Bujang M (2023) Microstructural characterization of fibric peat stabilized with Portland cement and silica fume. *Materials* 16(1):18
16. Yang H, Liu L, Yang W, Liu H, Ahmad W, Ahmad A, Joyklad P et al (2022) A comprehensive overview of geopolymer composites: a bibliometric analysis and literature review. *Case Stud Constr Mater* 16:e00830
17. Razali SNM, Zainorabidin A, Bakar I, Mohamad HM (2018) Strength changes in peat-polymer stabilization process; an introduction of new material for peat condition. *Int J Integr Eng* 10(9)
18. Muhammad A, Yusuf A, Umar M (2020) Assessment of lateritic soil stabilized using metakaolin. *J Geotechn Stud* 5(1):15–26
19. Wang S, Su J, Wu Z, Ma W, Li Y, Hui H (2021) Silty clay stabilization using metakaolin-based geopolymer binder. *Front Phys* 657
20. Esparham A, Moradikhoh AB, Jamshidi Avanaki M (2020) Effect of various alkaline activator solutions on compressive strength of fly ash-based geopolymer concrete. *J Civil Eng Mater Appl* 4(2):115–123
21. Ruzaidi CM, Al Bakri AM, Binhussain M, Salwa MS, Alida A, Faheem M, Muhammad Faheem MT (2014) Study on properties and morphology of kaolin based geopolymer coating on clay substrates, vol 594. Trans Tech Publications Ltd, pp 540–545

22. Jais IM, Abdullah N, Ali MM, Johar MA (2019) Peat modification integrating Geopolymer and fly ash. In: IOP conference series: materials science and engineering, vol 527, no 1. IOP Publishing, p 012021
23. Wibisono G, Kamaldi A, Olivia M (2019) Peat soil mass stabilization using geopolymeric hybrid material in early age. In: MATEC web of conferences, vol 276. EDP Sciences, p 05003
24. Parthiban D, Vijayan DS, Koda E, Vaverkova MD, Piechowicz K, Osinski P, Van DB (2022) Role of industrial based precursors in the stabilization of weak soils with geopolymer—a review. *Case Stud Constr Mater* e00886
25. Duxson P, Fernández-Jiménez A, Provis JL, Lukey GC, Palomo A, van Deventer JS (2007) Geopolymer technology: the current state of the art. *J Mater Sci* 42:2917–2933
26. Den Hamer DA, Venmans AAM, Van Der Zon WH, Olie JJ (2009) Stabilization of peat by silica based solidification. In: Proceedings of the 17th international conference on soil mechanics and geotechnical engineering, vols 1, 2, 3 and 4). IOS Press, pp 2224–2227
27. Khanday SA, Hussain M, Das AK (2021) Rice husk ash–based geopolymer stabilization of Indian peat: experimental investigation. *J Mater Civ Eng* 33(12):04021347
28. Norazam PNFI, Bakar I, Siang AJLM, Herman HS (2017) Stabilization of peat soil by using envirotac. In: MATEC web of conferences, vol 103. EDP Sciences, p 07014
29. Yusof NZ, Samsuddin NS, Hanif MF, Osman SS (2018) Peat soils stabilization using Effective Microorganisms (EM). In: IOP conference series: earth and environmental science, vol 140, no 1. IOP Publishing, p 012088
30. Kolay PK, Sii HY, Taib SNL (2011) Tropical peat soil stabilization using class F pond ash from coal fired power plant. *Int J Civil Environ Eng* 3(2):79–83
31. Khanday SA, Hussain M, Das AK (2021) A review on chemical stabilization of peat. *Geotech Geol Eng* 39(8):5429–5443
32. Moayedi H, Nazir R (2018) Malaysian experiences of peat stabilization, state of the art. *Geotech Geol Eng* 36(1):1–11
33. Devi K, Kumar ACA (2020) Soil improvement using waste materials: a review. *J Build Mater Sci* 2(01)

Soil Stabilization Using Agro-industrial Waste



K. L. Anaslal, P. A. Gopika, Sneha S. Menon, and R. Sujana

Abstract Stabilization of soil is essential to create strong foundations for infrastructure. Studies are being conducted to evaluate the efficacy of existing methods and to develop novel methods in the domain of soil stabilization. Though economy, efficiency and sustainability are the key aspects to be considered in any stage of a project, most of the existing practices fails to fulfil these altogether. Using refuse and industrial wastes as additives in ground improvement can help preserve the environment and promote sustainable practices. The present study aims at using agro-industrial wastes viz. eggshell powder and sugarcane bagasse ash as stabilizing materials. Due to the pozzolanic characteristics of these materials, they can be used as a good substitute for industrial lime also. The effect of adding eggshell powder and bagasse ash on the strength and settlement properties of soft soil will be evaluated based on various laboratory tests such as unconfined compressive strength test, permeability test, compaction test, CBR test etc. The best additive proportion was determined based on test outcomes, which assisted in analyzing how soil qualities improved in the presence of additives.

Keywords Soil stabilization · Bagasse ash · Eggshells · Agro-industrial wastes

1 Introduction

This study aims to understand the effect of stabilizing additives such as egg shells and sugarcane straw ash on the soil properties. The materials were used since they were affordable and easily accessible in the area. Sugarcane bagasse ash is a pozzolanic material because it is a burned product of sugarcane bagasse, which has a high silica concentration. Egg shell powder can be used as a substitute for lime-based soil stabilizers due to its high level of calcium, protein, and lime. Studies were carried out using a series of laboratory experiments, including fundamental soil tests and strength tests, which determined the soil to be weak soil. Repeating the same tests

K. L. Anaslal · P. A. Gopika (✉) · S. S. Menon · R. Sujana
Sahrdaya College of Engineering and Technology, Kodakara, Thrissur, India
e-mail: gopika.appukuttan2000@gmail.com

© The Author(s), under exclusive license to Springer Nature Switzerland AG 2024
M. Nehdi et al. (eds.), *Proceedings of SECON'23*, Lecture Notes in Civil Engineering
381, https://doi.org/10.1007/978-3-031-39663-2_32

393

with a mixture of eggshell powder and bagasse ash in different ratios (3%, 6%, and 9%) of plain soil was necessary to determine the various strength properties of the soil with the additives and compare them to those of plain soil. Stabilization of soils using Agro-industrial waste products results in safe disposal and increased strength and stability of soil.

Carlina et al. (2021) found that adding bagasse ash and eggshell powder increased the CBR value of clay soil, due to their silica content and calcium content binding water to clay [1]. Kiran et al. (2013) found that bagasse ash and additives increased the CBR and UCS values of black cotton soil [10]. Kharade et al. (2014) found that partial replacement of Bagasse Ash improved maximum dry density, but increased moisture content, leading to weak bonds and less strength [7]. Wubshet et al. (2016) found that additives such as 3% lime, 15% bagasse ash and 3% lime plus 15% bagasse ash increased the optimum moisture content of soil mixes from 32.2% to 41.0%, 43.2% and 52.2% respectively [6]. Hitesh et al. (2016) found that the addition of bagasse ash can significantly improve the engineering properties of black cotton soil, making it a viable option for stabilization in construction projects [3]. Basack et al. (2021) studied the geotechnical properties of soil treated with bagasse ash and stone dust, including compaction, shear strength, and permeability. Additionally, they analyzed the cost-effectiveness of using these additives for soil stabilization and for transport infrastructure projects [4]. Beegom et al. (2017) found that egg shell powder can be a potential alternative to lime for soil stabilization, offering favorable engineering properties and environmental benefits [5]. Ali et al. (2014) found that the addition of marble dust and bagasse ash can effectively improve the engineering properties of expansive soils, reducing their susceptibility to volume changes and also contributes to sustainable and cost-effective methods for stabilizing expansive soils in construction projects [9].

2 Materials and Methodology

2.1 Materials

Clay soil. The required laboratory tests were carried out on soil utilized in the study in order to ascertain its fundamental characteristics a strength. Table 1 displays the results of various index and engineering properties of the soil. From the sieve analysis and gradation data, it can be inferred that soil is poorly graded sand.

Egg Shell Powder. Due to its chemical similarity to lime, eggshell powder (ESP), which has not been used as a stabilizing material, could be a potential replacement for industrial lime. Chicken eggshell is a domestic waste product and egg shell powder largely contains the minerals CaO, Al₂O₃, SiO₂, Cl, Cr₂O₃, MnO, and CuO [8]. The waste eggshell that would be utilized in the test was initially washed, dried, and crushed. From the specific gravity test conducted, the specific gravity of the eggshell powder was determined as 1.86.

Table 1 General properties of soil

Properties	Results
Specific gravity of soil	2.15
Effective size, D_{10}	0.286 mm
Uniformity coefficient, C_U	3.185
Coefficient of curvature, C_c	0.815
Coefficient of permeability, K	0.0246 cm/s
Optimum moisture content	9%
Maximum dry density	18.63 kN/m ³
CBR value	1.74
Unconfined compressive strength,	1.765 kN/m ²
Liquid limit	48.5%
Plastic limit	33.33%
Plasticity index	15.17%

Bagasse. Bagasse is the fibrous, dry substance that is left over after the juice from sugarcane or sorghum stalks has been extracted. It was first sun-dried for two days before being reduced to ashes and utilized for the test. From the specific gravity test conducted, the specific gravity of the Bagasse ash was determined as 1.82.

2.2 Methodology

Preparation of sample. For the collected soil sample, fundamental laboratory tests (Atterberg’s limit, specific gravity, sieve analysis) were performed to determine the basic soil properties. Then the stabilization of soil with bagasse ash (BA) and egg shell powder is accomplished by blending the soil with various proportions of these two ingredients (3%, 6%, and 9%), after which the optimum percentage of bagasse ash and egg shell that can be added has been established [2]. Then laboratory experiments (compaction, California bearing ratio, unconfined compressive strength, and permeability test) were carried out to evaluate the strength behavior of the soil containing bagasse ash and egg shell powder.

Table 2 displays the various percentage combinations that are used when conducted the laboratory tests:

Table 2 Percentage combinations for determining the strength characteristics

Percentages	Composition of materials in soil sample
3	Soil + 1.5% BA + 1.5% ESP
6	Soil + 3% BA + 3% ESP
9	Soil + 4.5% BA + 4.5% ESP

Table 3 Results obtained after specific gravity test

% composition of additives	Specific gravity
0	2.15
3	2.21
6	2.34
9	2.43

3 Results and Analysis

3.1 Specific Gravity

Specific gravity is a fundamental property of soils and other construction materials. This dimensionless unit is the ratio of material density to the density of water and is used to calculate soil density, void ratio, saturation, and other soil properties.

The soil's Specific Gravity without additives was 2.15, which is a relatively low value. As demonstrated in Table 3, the specific gravity value rises with the addition of Bagasse ash and Eggshell powder.

3.2 Light Compaction

The purpose of the IS light compaction test is to ascertain the relationship between the water content and the dry density of compacted soil and to derive the Maximum Dry Density (MDD) and Optimum Moisture Content (OMC) from this test.

Figure 1 and shows the change of optimum moisture content with different percentage of sugarcane bagasse and eggshell powder. It is found that the optimum moisture content increases with addition of sugarcane bagasse ash and eggshell powder.

Figure 2 shows the variation in dry density with different percentage addition of sugarcane bagasse ash and egg shell powder. It is found that dry density drops down with increase in the additives.

3.3 Atterberg Limits

Atterberg limits experiments measure the moisture contents at which fine-grained clay and silt soils change between the solid, semi-solid, plastic, and liquid phases. Table 4 shows the Atterberg limit values obtained in various percentage of additives.

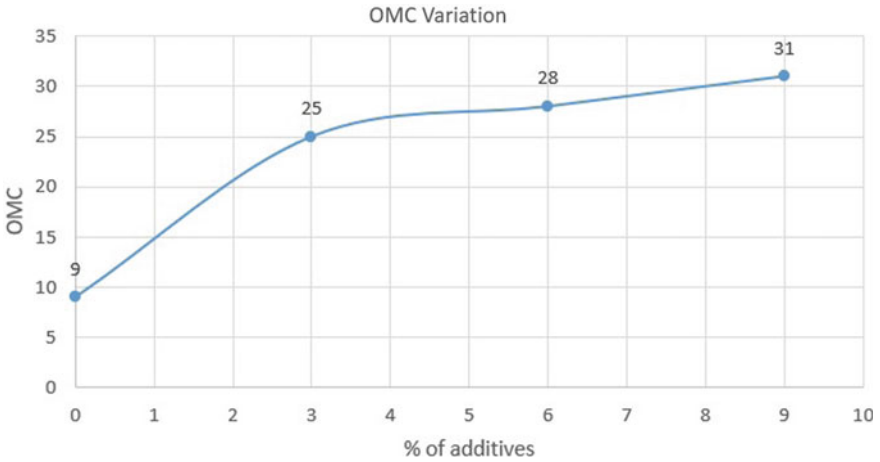


Fig. 1 OMC variation with various percentage of additives

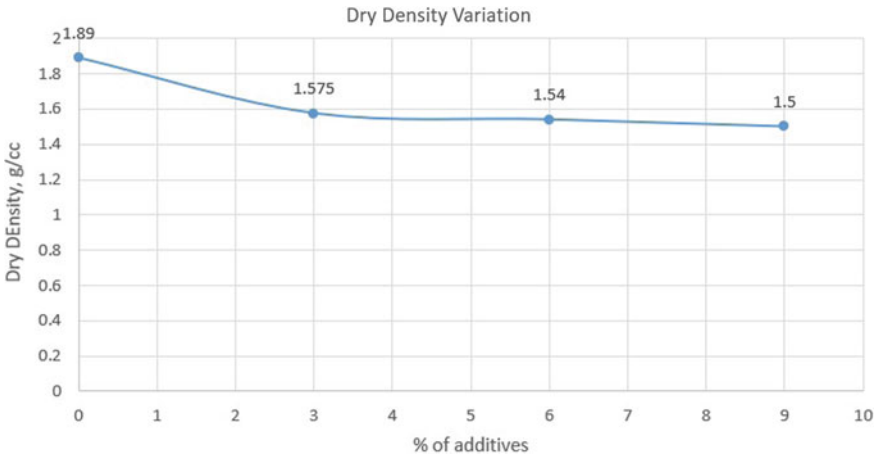


Fig. 2 Maximum dry density variation

Table 4 Atterberg limit value with varying percentage of additives

Percentage composition of additives in soil (%)	Liquid Limit (LL) (%)	Plastic Limit (PL) (%)	Plasticity Index (PI)
0	48.5	33.33	15.17
3	46.7	38.4	8.3
6	42.5	36.2	6.3
9	43.2	34.9	8.3

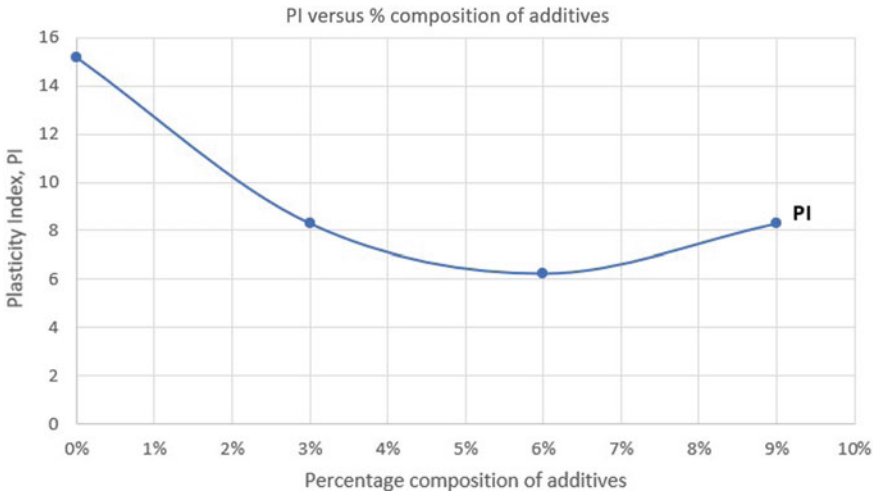


Fig. 3 Plasticity index value at various percentage of additives

According to Fig. 3, we can infer that up to 6% of the soil’s weight, the plasticity index value decreases. Hence, stabilizing it with bagasse ash and eggshell powder which makes up 6% of its weight can provide the soil the needed strength.

3.4 California Bearing Ratio

It is a penetration test that is primarily used to assess the subgrade strength of roads, pavements, and foundations. The soil’s subgrade strength and bearing capacity are evaluated using the CBR value. According to Fig. 4, soil CBR value increases when additives are added up to the optimal level (6%) and then starts to decline at 9%.

Table 5 demonstrates how the addition of bagasse ash and eggshell in varying ratios has raised the CBR value. The value rises up to 6% before falling at 9%. Thus, 6% is the optimum value.

3.5 Permeability

The permeability test evaluates how easily a liquid pass through a sample of soil.

According to Fig. 5, the coefficient of permeability value declines at 3%, increases somewhat at 6%, and then drops again at 9%. As a result, the permeability reduces with increasing sugarcane bagasse and eggshell powder contents.

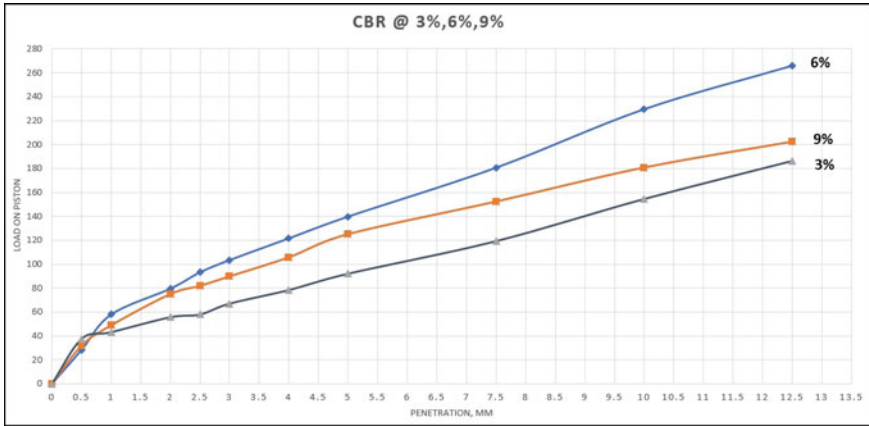


Fig. 4 CBR value at 3%, 6%, 9% of additives

Table 5 CBR value of soil with different percentage of additives

Percentage of additives added (%)	CBR value
0	1.74
3	4.6
6	6.8
9	6.08

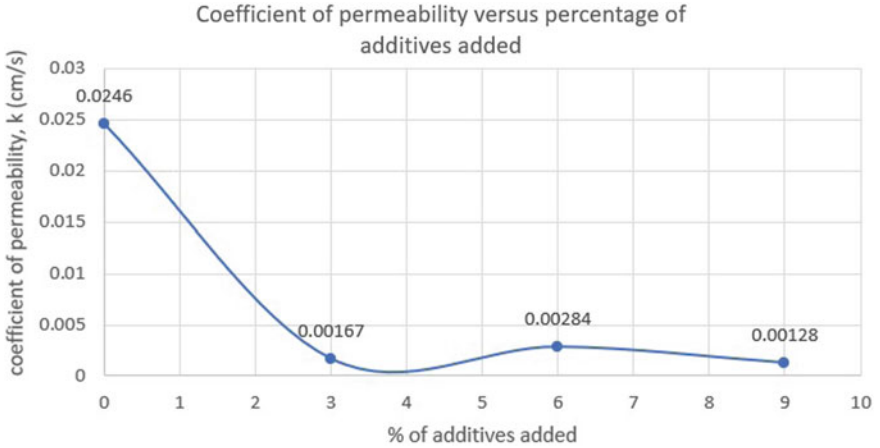


Fig. 5 Coefficient of permeability value at various percentage of additives

Table 6 Unconfined compressive strength at different percentages of additives

% composition of additives	Unconfined compressive strength kN/m ²
0	1.765
3	24.5
6	36
9	34

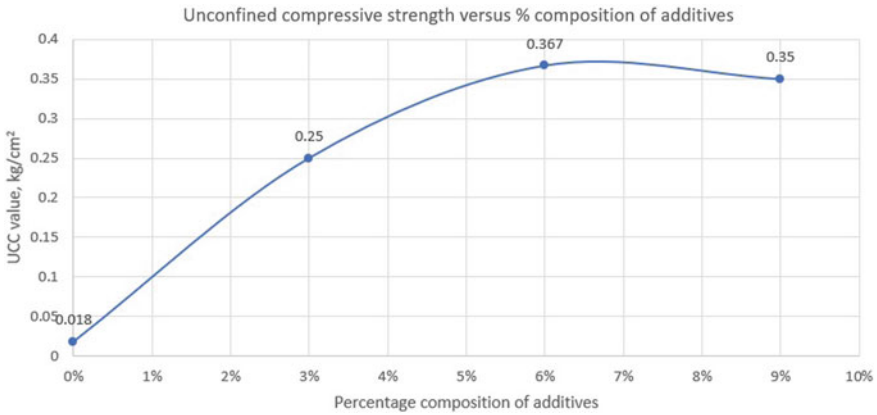


Fig. 6 Unconfined strength value at various percentages of additives

3.6 Unconfined Compressive Strength

The unconfined compression test (UCT) is a simple laboratory testing procedure to evaluate the mechanical characteristics of rocks and fine-grained soils.

Table 6 and Fig. 6 indicate the change in unconfined compressive strength at various additive percentages. Unconfined compressive strength is found to rise as additives are added, with a slight decrease occurring after a certain percentage.

3.7 Sieve Analysis

Sieve analysis identifies the particle size distribution of a specific soil sample, making it simple to identify the mechanical characteristics of the soil.

Based on the gradation curve shown in Fig. 7 and results from Table 7. It can be inferred that as the percentage of additives is increased, the C_u and C_c values are improving shifting the property of soil towards well gradation.

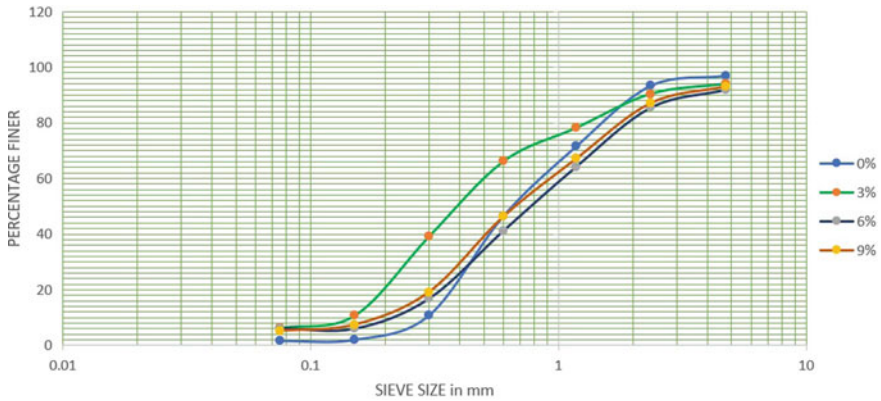


Fig. 7 Gradation curve of soil

Table 7 Values of C_c and C_u obtained after sieve analysis

Percentage of additives (%)	C_u	C_c
0	3.185	0.8156
3	3.904	0.872
6	5.269	0.969
9	5.349	0.979

4 Conclusion

The objectives of the study were to enhance the geotechnical characteristics of soil and look into the strength of the soil sample when combined with agro-industrial waste. After performing fundamental soil tests and various strength tests such as Atterberg Limit Test, CBR Test, and Unconfined Compression Test etc. to ascertain the strength and stability properties of the soil sample, it can be concluded that the inclusion of additives increases the soil’s quality and strength.

1. Based on the specific gravity test, the value for raw soil was 2.15 and with the addition of additives, the value rises to 2.43 up to 9%.
2. The soil’s optimum moisture content rises as the proportion of additives is increased, and maximum dry density decreases with additives. This can be due to the presence of organic material or fibres which leads to the reduction of contact between the particles.
3. The pozzolanic action of bagasse ash can lead to improved particle bonding and reduced soil plasticity. Atterberg limit tests led to the conclusion that the plasticity index value decreases up to 6% before increasing at 9%.

4. Eggshell powder and bagasse ash can possibly raise soil's CBR value, indicating better soil strength and load-bearing capabilities. CBR value rises up to 6.8 at 6% of additives and slight fall was observed at 9% of additives. Therefore, optimum value was observed at 6% of additives.
5. A more compacted soil matrix may develop as the additive content rises, which might hinder water movement and based on the permeability test conducted, coefficient of permeability value had decreased by adding additives but a slight increase was observed at 6% and at 9%, the value again decreases.
6. Based on UCC test, the strength increased from 1.765 kN/m² to 36 kN/m² up to 6% of additives and at 9% the strength falls. This may be due to the pozzolanic and cementitious property of bagasse ash and the particle interlocking property of eggshell powder.
7. Based on sieve analysis and gradation curve obtained, the soil group classification at 0% of additives was poorly graded sand, and as additive percentage increases, the soil gradation improves towards well graded nature.
8. Maximum dry density of the soil was found to be decreasing with increasing percentage of additives still, the CBR and Unconfined compressive strength was found to be increasing up to 6% of additives.

Based on the analysis of results, 6% of additives was determined to be the ideal amount to be added in order to improve the strength and characteristics of soil.

References

1. Carlina M, Apriyanti Y, Fahriani F (2021) The effect of addition of bagasse ash and eggshell powder on CBR value of clay soil. IOP Conf Ser: Earth Environ Sci 926:012102. <https://doi.org/10.1088/1755-1315/926/1/012102>
2. Singh ML, Sharma R, Abhishek (2017) Soil stabilization using industrial waste (wheat husk and sugarcane straw ash)
3. Hitesh Sant RM, Jain S (2016) Stabilization of black cotton soil with bagasse ash. Int J Eng Res Technol (IJERT) 4
4. Basack S, Goswami G, Khabbaz H, Karakouzian M, Baruah P, Kalita N (2021) A comparative study on soil stabilization relevant to transport infrastructure using bagasse ash and stone dust and cost effectiveness Civil Eng J 7:1947–1963
5. Anoop P, Beegom H, Johnson J, Midhula J, Tharis Muhammed TN, Prasanth S (2017) Potential of egg shell powder as replacement of lime in soil stabilization. Int J Adv Eng Res Sci 4:86–88
6. Wubshet M, Tadesse S (2016) Stabilization of expansive soil using bagasse ash lime. Afr J Online (AJOL) 32
7. Kharade AS, Suryavanshi VV, Gujar BS, Deshmukh RR (2014) Waste product 'bagasse ash' from sugar industry can be used as stabilizing material for expansive soils. Int J Res Eng Technol 03:506–512
8. Paul AH, Moideen FM, Jose JK (2014) Studies on improvement of clayey soil using egg shell powder and quarry dust
9. Ali R (2014) Expansive soil stabilization using marble dust and bagasse ash. Int J Sci Res (IJSR) 3:2812–2816
10. Kiran RG, Kiran LK (2013) Analysis of strength characteristics of black cotton soil using bagasse ash and additives as stabilizer. Int J Eng Res Technol 2

The Pozzolanic Effect of Rice Husk Ash on the California Bearing Ratio Behaviour of Arunachal Peat with Cement as Admixture



Nabam Jumsi  and Ajanta Kalita 

Abstract Peat is Geotechnically problematic for any infrastructure as it contains a lot of moisture, low shear strength, and high compressibility. This paper particularly focuses on the improvement of peat in Ziro valley, Arunachal Pradesh using cement and rice husk ash. An environmentally responsible replacement to final disposal using rice husk ash as a soil stabiliser because it is a waste product from the rice industry with pozzolanic qualities. By adjusting the amount of rice husk ash put to the peat soil during all of the usual laboratory procedures as 6, 8, and 12% by weight of soil and cement as 5, 10, 15, 20 and 25%. The strength of peat is greatly enhanced by cement, neutralises the impact of organic matter content, and lessens the impact of acidity. with an increasing amount of cement material, the dry density increases and the optimum water content decreases. With increase in RHA content, MDD decreases but OMC increases. Both unsoaked and soaked CBR test were carried out on peat mixed with cement and RHA. For the test specimen made up of soil, cement, and rice husk ash, it was noticed that the mixture of peat-cement-RHA significantly improved the strength characteristic of parent peat soil. S + 25C and S + 25C + 8RHA can be recommended for treating subgrade.

Keywords Rice husk ash · Cement · CBR · OMC · MDD · Peat soil

1 Introduction

Due to its extreme low bearing capacity and severe primary and secondary compression peat is one of the most challenging soil kinds. Peat is referred to be an extremely soft soil with a high organic content that is created by the accumulation of half or completely decaying plant or animal remains over an extended period of time in

N. Jumsi (✉) · A. Kalita
NERIST, Nirjuli, Arunachal Pradesh 791109, India
e-mail: nabamjumsi45@gmail.com

A. Kalita
e-mail: ajanta@nerist.ac.in

an anaerobic environment. The most recent analysis indicates that the world's peat land covers an area of about 4.23 million km². According to the new global peat land map, India's total land area is around 88,756 km². (Indian council of agricultural research, ICAR). The peat related survey in India has been finished only in few parts of India which includes South-western, eastern and northern region. Abhinaba Paul¹ and Monowar Hussain² conducted a study concerning the peat from three North-eastern states of India (Assam, Tripura and Manipur), nevertheless, no such research has been done to yet, which highlights the Arunachal Pradesh peat. There are many recommended treatments for peat, but the employment of chemical binders, including fly ash, cement, lime was the most successful [1, 2]. The most popular treatment method for any soil is by using cement as binder, which shows improvement in geotechnical characteristics of a soil. cement as binder can be use in both powder and semi-liquid form [3, 4]. The hydration of the cement in the soil-cement treatment method produces calcium silicate hydrates (CSH), calcium aluminates (CAH), and calcium aluminium silicate hydrates (CASH), these are essential for development of substantial strength [5, 6].

When rice husks are burned to produce energy, they produce rice husk ash (RHA), Which is both an industrial and agricultural waste. It is exceedingly difficult to dispose of rice husk due to its high silica concentration, abrasive, woody, and rough nature [7]. In a study it was found that coal impacts global warming 34 times more than burning rice husk to produce 1 MJ of electricity [8]. India is the second largest country after China and produces around 20 million tons yearly [9]. This enormous amount of RHA, if not consumed effectively, can cause various environmental hazards [10]. Therefore, burning rice husk to generate electricity at zero net carbon production is a very practical and cost-effective solution in light of growing environmental concerns [11, 12]. Rice husk ash is the substance left over after burning rice husk, the main component is amorphous silica (> 90–95% by weight) [13, 14].

Given the foregoing, the authors looked into the utilisation of rice ash husk as a stabiliser to lessen this geotechnical issue. The investigation of the Indian, Arunachal Pradesh peat is the main emphasis of the current study, which also provides a workable solution for its applicability.

2 Materials Used

2.1 Peat Soil

The Peat soil was collected from Siro village (27.51°N, 93.84°E) at Ziro valley in Arunachal Pradesh, it was collected from a depth of about 1 m. The peat soil was oven dried before testing. The index properties of soil are mentioned in Table 1. According to IS-2720 (part-IV)-1985 the grain size distribution of peat was analysed, and peat was identified as the dominant soil type (OH) the curve in Fig. 1 depicts the peat's grain size distribution.

Table 1 Index properties of the peat soil

Properties	Value
Sieve analysis	
Gravel size (> 4.75 mm)	0%
Sand size (0.075–4.75 mm)	16.4%
Silt (0.075–0.002 mm)	15%
Clay (< 0.002 mm)	68.6%
IS soil classification	OH (peat)
Specific gravity	1.33
Liquid limit	52.08%
Plastic limit	37.13%
Plasticity Index	Medium plastic
Water content	67.3%

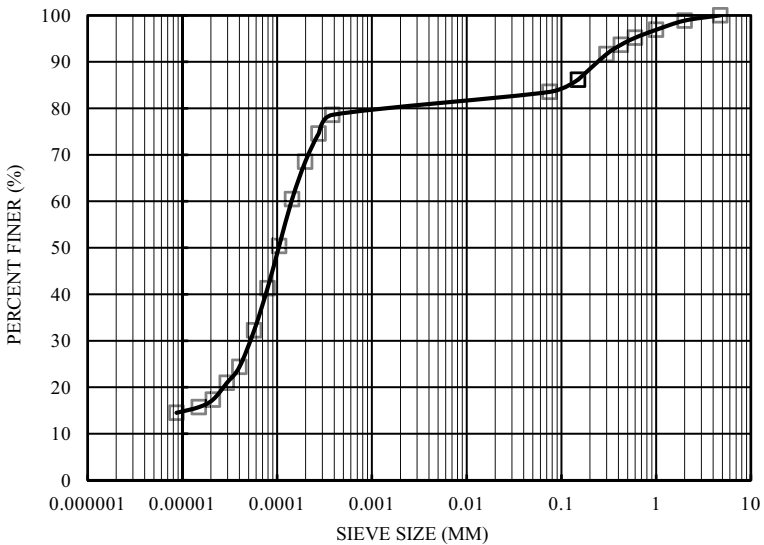


Fig. 1 Grain size distribution curve of peat soil

Microstructure Analysis: Scanning electron microscope (SEM) micrographs of untreated Arunachal Pradesh peat are displayed in Fig. 2a–d. SEM test were done on dry sample without curing. Figure 2a displays fibres that are in decomposed state. Clearly visible voids can be seen in the micrographs Fig. 2b, d.

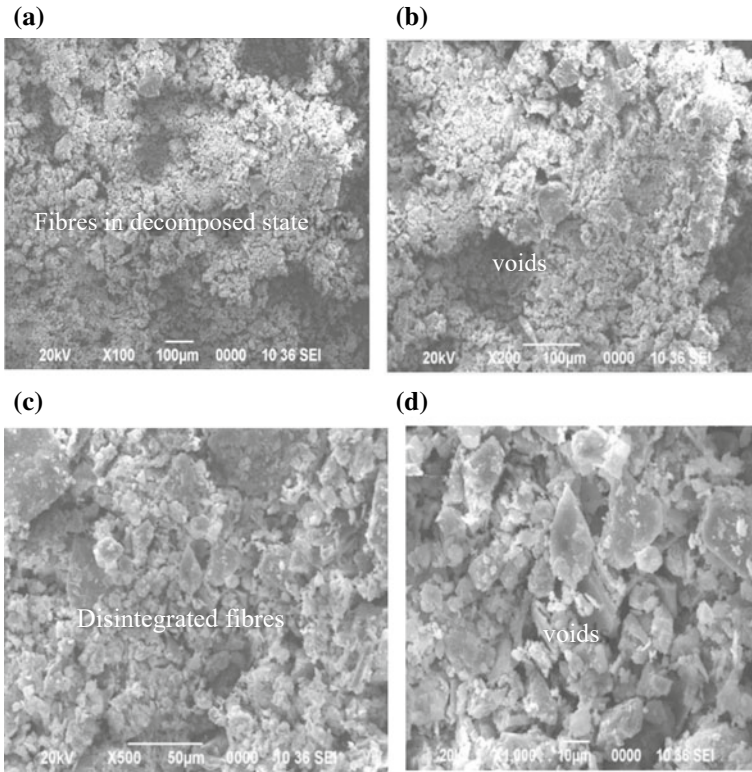


Fig. 2 SEM images of untreated peat

2.2 Rice Husk Ash

Rice husk was collected locally, and burned into ashes. The burned temperature for RHA was 600 °C in muffle furnace for 5 h. The temperature was controlled. Rice husk is a by-product created during the production of puffed rice. Table 2 displays the chemical composition of rice husk ash as based on studies using energy dispersive X-ray diffractors (EDX). The main component is silicon dioxide.

Table 2 Chemical composition of Rice husk ash

Standard	Composition (%)
SiO ₂	66.8
Al ₂ O ₃	5.2
Fe ₂ O ₃	0.94
CaO	1.39
MgO	1.71

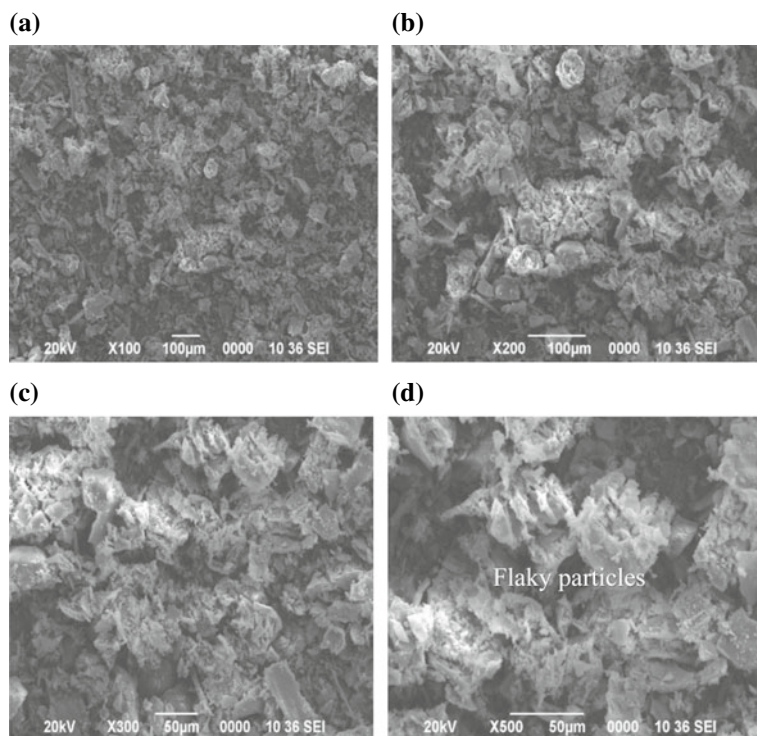


Fig. 3 SEM of Rice husk ash

Microstructure Analysis: Figure 3a–d show the scanning electron microscopy (SEM) micrographs of RHA. Both the presence of crystalline particles and flaky particles are seen, which indicate the presence of silica.

2.3 *Cement*

Ordinary Portland cement (OPC) of 53 grade has been utilised in the investigation conforming to Indian standard BIS specification IS:12269-1987. All samples are prepared and cured using regular water.

2.4 *Designation of the Mixes*

In this present study, S stands for soil, RHA for rice husk ash, and C stands for cement. These letters were assigned to each of the materials used.

3 Experimental Programs

3.1 *Compaction Tests*

Standard proctor compaction tests in accordance with IS 2720 (part VII)-1992 had been carried out on the untreated and treated peat in order to explore the cement's impacts and as a stabilising agent RHA was used to observe the strength properties of peat. To create a uniform mixture, different percentages of cement 5, 10, 15, 20 and 25% and rice husk ash 6, 8 and 12% of the weight of the oven dried soil were carefully blended into the treated samples.

3.2 *California Bearing Ratio (CBR) Test*

After 14 days of curing with varied percentage of soil- cement mixes, soil-RHA mixes, and soil-cement-RHA mixes, the California bearing ratio (CBR) tests were done on the peat sample in accordance with IS 2720 (Part 16)-1987 (reaffirmed 2022). A sequence of unsoaked and soaked CBR experiments were performed on various amounts to assess the effect of rice husk ash on the CBR behaviour of cement stabilized soil. In order to prepare the CBR test, the soil with various combinations were compacted, and the OMC and MDD values obtained for a mixed specimen were determined. After draining the surplus water, CBR tests on the moulds that had been submerged in the water for 96 h were conducted.

4 Results and Discussions

OMC and MDD were 29.89% and 14.48 kN/m³, respectively for the following standard proctor compaction test of parent peat soil. The next sections discuss how different values of MDD and OMC were varying with cement and Rice husk ash.

4.1 *Compaction Behaviour of Peat-Cement Mixes*

Figure 4, Demonstrate that when cement concentration increases, OMC decreases and MDD increases. The cement process, which involves significant water consumption, heat generation, and moisture loss owing to evaporation, is what causes the drop in OMC with addition of cement since cement is so dense, it fills in the gaps in porous peat structures, raising the density values and contributing to the rising value of MDD

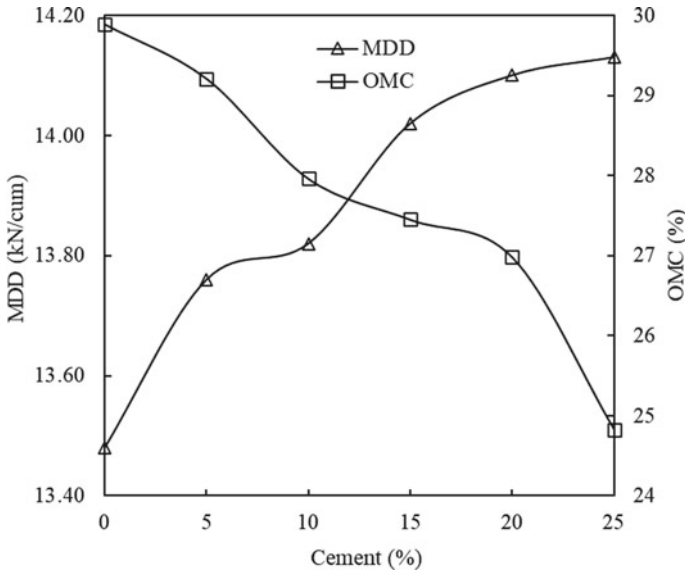


Fig. 4 Variation of MDD and OMC of peat-cement mixes

4.2 Compaction Behaviour of Peat-Rice Husk Ash

A rise in the OMC and MDD reduces when the percentage of rice husk ash rises, as can be seen in Fig. 5. The difference in the specific gravities of the peat and rice husk ash may be the reason behind the decline in MDD [15]. OMC is due to excess absorption by RHA, since it has high porous properties, as reported in [16]. The OMC and MDD for the 6% RHA sample was 30.24% and 13.40 kN/m³ respectively. For 8% RHA, the OMC AND MDD calculated was 30.65% and 13.23 kN/m³. Similarly, the OMC and MDD for 12% RHA was 31.18% and 12.12 kN/m³ respectively.

4.3 Compaction Behaviour of Peat-Cement-Rice Husk Ash Mixes

It is observed from Fig. 6 that when 15% cement was blended with 6% and 8% RHA, the MDD decreases and OMC increases. The same characteristic is noticed also when 20% and 25% cement was blended with 6% and 8% RHA. The optimum moisture content increases probably due to RHA’s porous characteristic, which allow for greater water absorption than other materials [16]. Mostly, rise in dry density indicates the improvement of soil. But unfortunately cement and RHA reduces the dry density. The decreasing in dry density take place due to the peat’s specific gravity, particle size, and stabiliser [15].

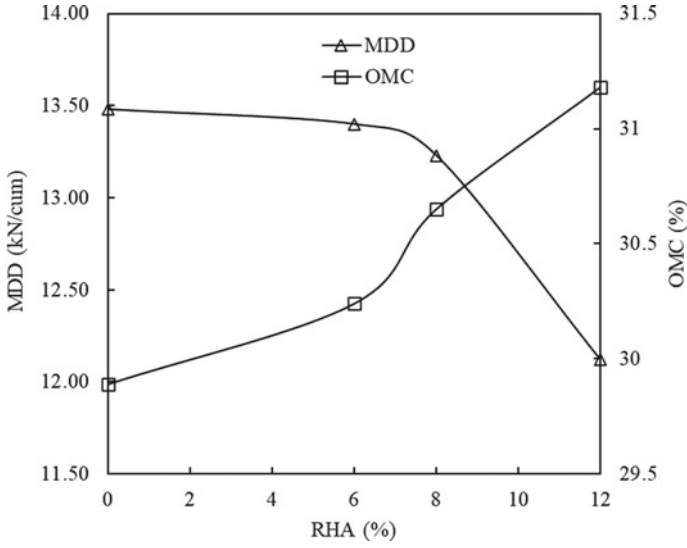


Fig. 5 Variation of MDD and OMC of peat-RHA mixes

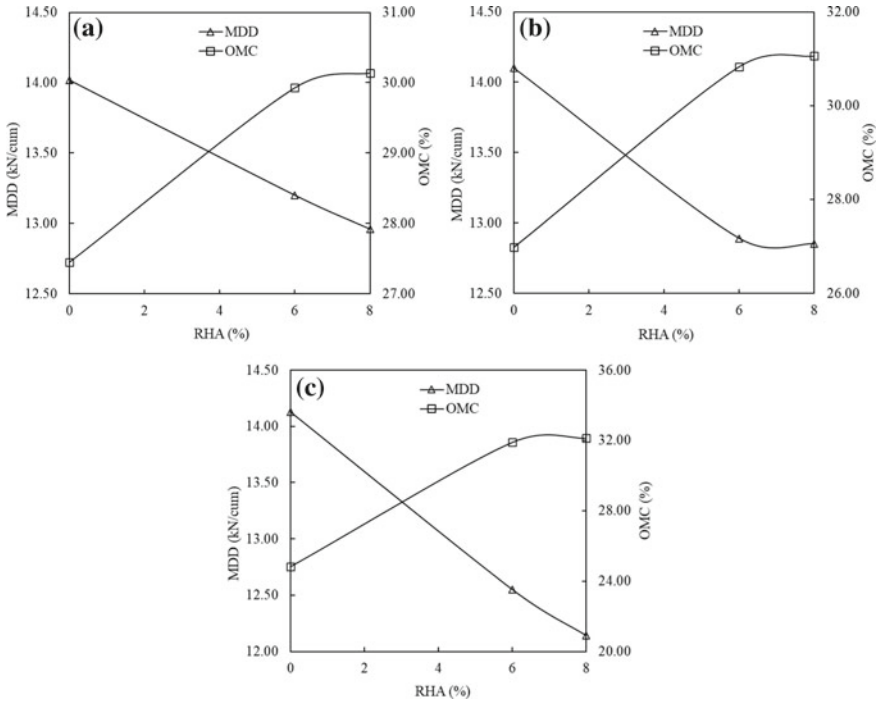


Fig. 6 a Variation of MDD and OMC for S + 15C + different % RHA, b variation of MDD and OMC for S + 20C + different % RHA, c variation of MDD and OMC for S + 25C + different % RHA

4.4 CBR Behaviour of Peat and Cement Mixes

The unsoaked and soaked CBR values for untreated peat is found to be 4.63 percent and 3.163% respectively. Figure 7 shows that the CBR values rise with increase in cement percentage in both soaked and unsoaked situations. The presence of surface tension forces, which additional increases penetration resistance, may be the cause of the higher CBR value in the unsoaked condition. The hydration process, in which cement generates silicate gel, is what causes the increase in CBR values when cement was added. As cement is added, silicate gel creation likewise increases. This accelerates the rate of growth of the CBR values. Table 3 shows percentage increase CBR (soaked) values of peat- cement mixes. It is noticed that the CBR value of peat-cement mixes increases from 3.56 to 6.02 with percentage increase from 26.24% to 113.47%.

Fig. 7 Variation of unsoaked and soaked CBR of Peat-cement mixes

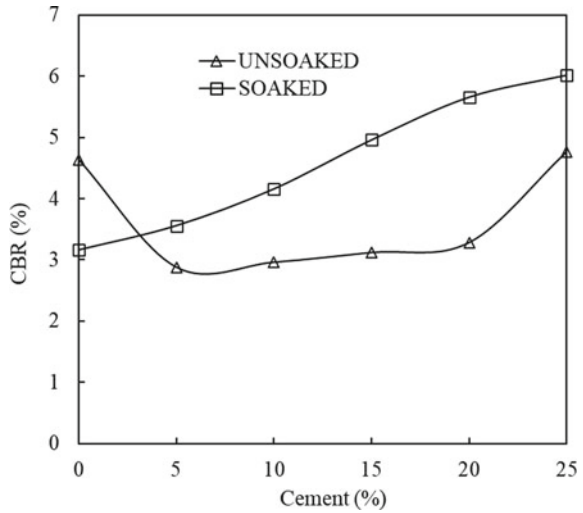


Table 3 CBR values of the peat-cement mixes and percentage increase CBR

Mix proportion	CBR value % (unsoaked)	CBR value % (Soaked)	%Increase CBR (soaked)
S	3.18	2.82	—
S + 5C	2.88	3.56	26.24
S + 10C	2.96	4.16	47.51
S + 15C	3.12	4.98	76.59
S + 20C	3.28	5.66	100.70
S + 25C	4.76	6.02	113.47

4.5 CBR Behaviour of Peat, Cement and RHA Mixes

Test specimen were made by mixing 15, 20, 25% of cement with 6% and 8% RHA in order to observe the impact of RHA on the strength characteristic of the peat. According to Fig. 8 adding RHA to the peat significantly boosts CBR strength relative to the untreated sample. It is observed that the CBR values are improved by 8 percent RHA to a level that is suitable for design objectives, and that further increase in RHA percentage beyond this point maybe not validated. S + 25%C + 8RHA is the mixture that results in the greatest improvement in CBR, with CBR values of 4.90 and 6.34 for unsoaked and soaked respectively. The pozzolanic reaction, which have increased, could be blamed for the increase in CBR. Table 4 shows percentage increase CBR (soaked) values of peat- cement-RHA mixes. It is noticed that the soaked CBR value of peat-cement-RHA mixes increases from 4.38 to 6.34 with percentage increase from 55.32% to 124.82%.

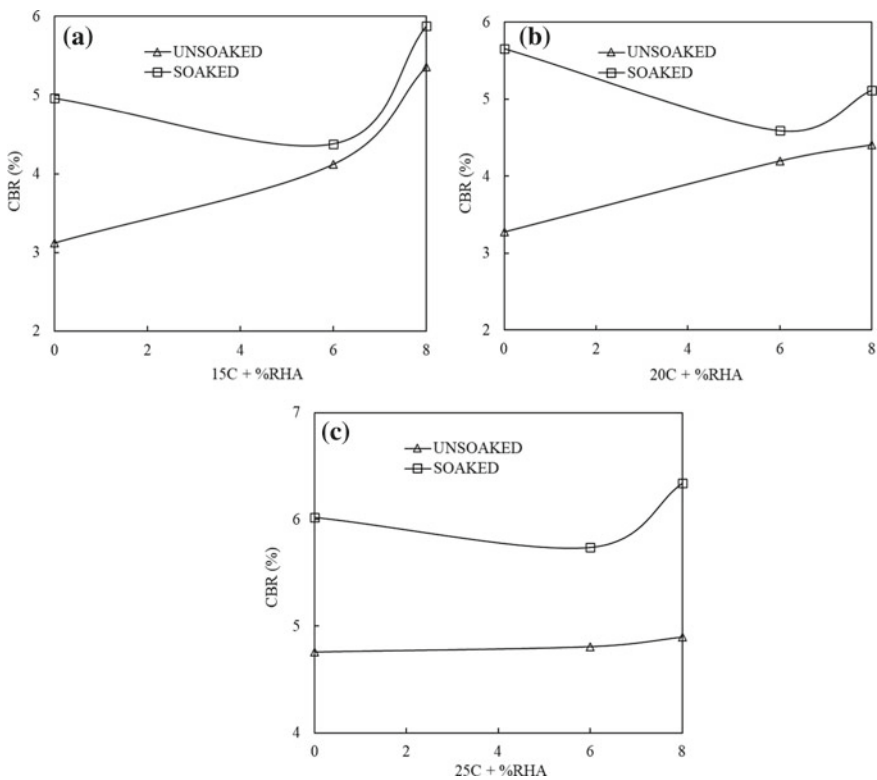


Fig. 8 a Variation of unsoaked and soaked CBR of S + 15C + %RHA, b variation of unsoaked and soaked CBR of S + 20C + %RHA, c variation of unsoaked and soaked CBR of S + 25C + %RHA

Table 4 CBR values of peat-cement-RHA mixes and percentage increase

Mix proportion	CBR value % (unsoaked)	CBR value % (Soaked)	%Increase CBR (soaked)
S	3.18	2.82	–
S + 15C + 6RHA	4.12	4.38	55.32
S + 15C + 8RHA	5.36	5.88	108.51
S + 20C + 6RHA	4.20	4.59	62.76
S + 20C + 8RHA	4.41	5.12	81.56
S + 25C + 6RHA	4.81	5.74	103.54
S + 25C + 8RHA	4.90	6.34	124.82

5 Conclusions

The efficiency of cement and rice husk ash as a stabiliser in enhancing the strength qualities of Arunachal Pradesh Peat has been investigated in the current study. Based upon the experimental results, the following conclusions are made.

- With an increase in cement percentage in peat-cement mixes the OMC decreases and MDD increases.
- OMC value increases as RHA percentage increases in peat-RHA mixes, whereas MDD decreases as RHA percentage increases.
- For both the unsoaked and soaked conditions, an increase in CBR value was seen with increase in cement content in peat-cement mixes. CBR value of S + 25C mix considerably improved the parent soil under unsoaked and soaked from 3.18% and 2.82% to 4.76% and 6.02% respectively, i.e. percentage increase CBR is 113.47%.
- It has been noticed that in peat-cement-RHA mixes, CBR value increases as RHA percentage increase. 8% RHA mixed with peat-cement mixes increases the CBR values to a level suitable for design purposes. It was observed that the mixture containing S + 25C% + 8%RHA performed better improvement. This mixture considerably improved the unstablized samples under unsoaked and soaked CBR value of 3.18% and 2.82% to 4.90% and 6.34% respectively, i.e. percentage increase CBR is 124.82% than the parent peat soil.
- Utilization of S + 25%C and S + 25%C + 8%RHA can be recommended for treating subgrade.

References

1. Hoikkala S, Leppänen M, Lahtinen P (1996) Mass stabilization of peat in road construction. XII Nordiska Geoteknikermötet NGM, Reykjavík 1:26–28
2. Den Haan EJ (1998) Cement based stabilizers for Dutch organic soils. In: Problematic soils, pp 53–56
3. Bergado DT, Anderson LR, Miura N, Balasubramaniam AS (1996) Soft ground improvement in lowland and other environments. ASCE
4. Evans J, Ruffing D, Elton D (2021) Fundamentals of ground improvement engineering. CRC Press
5. Sherwood P (1993) Soil stabilization with cement and lime. H.M stationery office, London, p 153
6. Porbaha A, Shibuya S, Kishida T (2000) State of the art in deep mixing technology. Part III: geomaterial characterization. In: Proceedings of the institution of civil engineers-ground improvement, vol 4, issue 3, pp 91–110
7. Chaudhary DS, Jollands MC (2004) Characterization of rice hull ash. *J Appl Polym Sci* 93(1):1–8
8. Quispe I, Navia R, Kahhat R (2019) Life cycle assessment of rice husk as an energy source. a Peruvian case study. *J Clean Prod* 209:1235–1244
9. Paul A, Hussain M (2020) Sustainable use of GGBS and RHA as a partial replacement of cement in the stabilization of Indian Peat. *Int J Geosynthetics Ground Eng* 6:1–15
10. Jittin V, Bahurudeen A, Ajinkya SD (2020) Utilisation of rice husk ash for cleaner production of different construction products. *J Clean Prod* 263:121578
11. He J, Jie Y, Zhang J, Yu Y, Zhang G (2013) Synthesis and characterization of red mud and rice husk ash-based geopolymer composites. *Cem Concr Compos* 37:108–118
12. Nimwinya E, Arjham W, Horpibulsuk S, Phoo-Ngernkham T, Poowancum A (2016) A sustainable calcined water treatment sludge and rice husk ash geopolymer. *J Clean Prod* 119:128–134
13. Chaudhary DS, Jollands MC, Cser F (2004) Recycling rice hull ash: a filler material for polymeric composites? *Adv Polym Technol: J Polym Process Inst* 23(2):147–155
14. Nair DG, Jagadish KS, Fraaij A (2006) Reactive pozzolanas from rice husk ash: an alternative to cement for rural housing. *Cem Concr Res* 36(6):1062–1071
15. Rahman MA (1987) Effects of cement-rice husk ash mixtures on geotechnical properties of lateritic soils. *Soils Found* 27(2):61–65
16. Zhang MH, Lastra R, Malhotra VM (1996) Rice-husk ash paste and concrete: some aspects of hydration and the microstructure of the interfacial zone between the aggregate and paste. *Cem Concr Res* 26(6):963–977

Design and Modeling of a Precast Concrete Structure and Its Performance Evaluation with Conventional Structure



Akhil Mukundan, M. S. Anagha, Tania Thankam Mathew, Tom K. Bijoy, and Asha Devassykutty

Abstract The use of precast concrete technology is increasing day by day due to its easier installation technique, time saving and money saving benefits. Precast concrete construction is cheaper due to fewer labour. The difference between precast concrete construction and conventional construction is found by analyzing the materials and loading conditions. Outline of the study is to illustrate the process involved in the implication of precast concrete products in the construction industry and compare the same with conventional construction methods. It focuses on various issues related to it directly and indirectly. Various factors affecting the construction process are analyzed and addressed. The design involves identifying the loads which acts upon a structure and the forces and stresses which arise within that structure due to those loads. The design of precast concrete elements such as wall, column and beam are done using Tekla Tedds Software according to Eurocode 2 [1].

Keywords Precast concrete · Tekla Tedds · Conventional system

1 Introduction

The precast technology's benefit is that it expedites the construction process while simultaneously improving the final product's quality. It also facilitates expanding the carpet area. Concrete goods are perfect for a number of applications since they are ready to use, simple to install, and have strong resistance to corrosive elements and inclement weather for a longer period of time [2]. Precast structures also have a very appealing finish. Highrise, lowrise, villas, commercial buildings, parking lots, etc., the precast panels can be swiftly and with little site interruption built on the job site.

A. Mukundan (✉) · M. S. Anagha · T. T. Mathew · T. K. Bijoy · A. Devassykutty
Sahrdaya College of Engineering and Technology, Kodakara, India
e-mail: akhilmukundan06835@gmail.com

1.1 History of Precast Concrete Technology

Concrete was used by ancient Roman builders, who quickly poured the substance into moulds to create their intricate system of aqueducts, culverts, and tunnels. Pre-cast technology is now used for a wide range of architectural and structural applications, including individual components or even entire building systems. Liverpool, England, made the first precast panel buildings in the modern era in 1905. John Alexander Brodie, a brilliant city engineer who also came up with the concept for the football goal net, created the method. Following in 1906 were the tram stables at Walton in Liverpool. In Britain, the proposal did not receive much attention. But it caught on everywhere, especially in Scandinavia and Eastern Europe.

Precast is a material that is frequently utilised today while building a building's superstructure or frame. It's also frequently used as architectural cladding to imitate the appearance of more expensive materials like limestone, granite, or stone due to its adaptability in shape, texture, and colour [3]. The ability of precast concrete to function as both the structural and architectural component at the same time, resulting in a fully precast concrete building, is likely its greatest advantage.

1.2 Objectives

- To study precast construction and erection methodology.
- Comparison between conventional and precast construction.
- Design of precast concrete structures.

Precast concrete, which is used to make products like tilt-up wall panels and precast beams, is created by pouring concrete into a reusable mould or "form" before curing it under controlled conditions and moving it to the construction site. Precast concrete is used in interior and exterior applications, including tilt-up and high-rise building construction as well as highway, bridge, and hi-rise projects. Precast concrete is produced in a controlled atmosphere, giving the precast concrete the chance to cure properly and be carefully observed by plant staff. Precast concrete systems have a number of possible benefits over onsite casting. Precast concrete manufacturing can be done on the ground, maximising casting safety. Higher levels of material quality control are in place, and compared to a construction site, precast plants have better workmanship. In terms of cost per unit of formwork, precasting is frequently less expensive than onsite casting because the forms used there can be reused hundreds to thousands of times before they need to be replaced. Molds for precast concrete can be created from a variety of synthetic materials, each of which produces a different finish. Also, a variety of surface finishes, such as those that mimic ashlar stone and horizontal boards, are available for the four varieties of precast wall panelling: sandwich, plastered sandwich, inner layer, and cladding panels. The quantities and size of the aggregate as well as the addition of colour to the concrete mix can alter the final concrete surface's appearance and texture.

Elements of precast structures

- Precast Slabs
- Precast Beam and Girders
- Precast Columns
- Precast Walls
- Precast Stairs.

2 Design Concepts for Precast Concrete Buildings

- (1) All loads and restraint circumstances, from casting through final use of the structure, should be taken into account in the design of precast members and connections. The tensions that formed in precast elements between casting and final connection may be more important than the stresses caused by service load. The procedures for dismantling, storing, transporting, and installing precast elements require special consideration.
- (2) When precast members are used in a structural system, the forces and deformations that occur in and around connections (in neighbouring members and throughout the entire structure) should be taken into account. Precast elements may behave structurally very differently from comparable members that are cast in place monolithically. Design of connections to transmit forces resulting from creep, shrinkage, temperature changes, elastomeric deformation, wind forces, and earthquake forces calls for specific consideration. To guarantee that precast constructions work as intended, such connection details are very crucial.
- (3) Precast members and connectors should be made to adhere to tolerance standards. Tolerances affect how precast members and connectors behave. Design should account for the effects of unfavourable combinations of fabrication and erection tolerances. Contract documents should include a list of the tolerance requirements, which can be further defined by making reference to recognised standards. Tolerances that depart from accepted standards should be noted as such.
- (4) On the contract documents created by the architect/engineer of record or on the shop drawings provided by the contractor, all details regarding reinforcement, connections, bearing elements, inserts, anchors, concrete cover, openings, and lifting devices, as well as the specified strength of concrete at critical stages of fabrication and construction, should be shown. Depending on the terms of the contract documents, either the shop drawings or the contract paperwork must include this information [4]. All of the specifics of the precast concrete members and embedded components should at the very least be shown in the shop drawings. The contract documents may state that the shop drawings must also include details of connections that are located outside of the member. The contract documents could also mandate that the contractor submit designs for the connections, or members. The contract agreements should outline the loads that must be taken into account when designing the precast concrete components

of the project, as well as any unique needs or tasks (such as seismic loads, movement allowances, etc.) that must be taken into account by the contractor. In this instance, full information of the connections involved should be included in the shop drawings.

Need for precast technology in India

India's housing demand cannot be fully satisfied due to an enormous shortage. The urban development and housing ministry's report estimates the current demand at close to 27 million units and notes that shortages of qualified labour are one of the difficulties in carrying out projects. It also acknowledges that the current capacity for doing so using conventional brick and mortar is extremely constrained [5]. According to a report from the urban development and housing ministry, the present demand is close to 27 million units, and one of the challenges in completing projects is a lack of qualified labour. It also acknowledges how limited the present ability to do so using traditional brick and mortar [6].

These are the major reasons for going precast construction of houses and buildings:

1. Precast requires less time to implement, so construction is completed quickly.
2. These are produced in facilities with automated quality control.
3. These goods were produced using less labour by machines.
4. Allows load bearing concrete structures in place of framed walls.
5. 5. These are weather resistant and help build the house at any time of the year.

3 Importance of Precast Construction

Precast concrete is comfortable

The material has intrinsic properties of thermal inertia (allowing a more constant temperature both in cold and hot regions) and acoustic insulation.

Precast concrete is safe

Concrete does not ignite, as is common knowledge. Concrete construction not only prolongs the structural stability but also stops fires from spreading from one building to another. It has enough strength to withstand blows, impacts, and natural disasters like floods, cyclones, and earthquakes [7].

Precast concrete is versatile

A broad variety of surface finishing, colour palettes, and unique shapes are all possible with factory production. Another benefit of precast concrete is its ability to be molded, allowing architects and designers to replicate traditional features like keystones and caps or replicate the appearance of materials like weathered stones. The local precast concrete market offers a huge selection of colours and aesthetic effects and has access to a broad range of aggregates [8].

Precast concrete is optimized

In comparison to concrete that is cast on site, precasting factories' use of advanced technologies results in products of higher quality (e.g., thinner sections, reduced tolerances, and engineered solutions). Before a unit is installed into a building or site project, the quality can also be checked.

4 Design of Precast Elements Using Tekla Software

Trimble is an industrial technology company transforming the way the world works by delivering solutions that enable our customers to thrive. Core technologies in positioning, modeling, connectivity and data analytics connect the digital and physical worlds to improve productivity, quality, safety, transparency and sustainability. Tekla Tedds has been the go-to document and design solution for engineers. This a powerful structural analysis software which reduces repetitive hand calculations, and offers dependable multi-material element design because of its extensive, easy-to-inspect quality assured library of calculations. As a specialist solution for civil and structural engineers, structural analysis software Tekla Tedds has been designed by engineers for engineers. Tekla Tedds automates calculations, improving engineering productivity and quality by replacing tedious, time-consuming hand calculations. The software not only has a quality assured library of multi-material code compliant calculations, but also gives users the flexibility to create additional calculations and elegant, engaging design documents. The software follows Eurocode 2 EN 1992 which includes rules and concepts required for designing concrete structures. Table 1 gives the difference between precast system and conventional system.

5 Design Details and Parameters

Precast concrete beam design

Section reinforcement details: 2 reinforcement bars of diameter 12 mm at the top, 3 reinforcement bar of 12 mm diameter at the bottom and 2 shear reinforcement bars of 6 mm diameter (Figs. 1, 2 and 3).

- Length of beam: 2800 mm
- Distance between lifting points: 1500 mm
- Section type: Rectangular
- Width: 250 mm
- Depth: 300 mm.

Table 1 Difference between precast system and conventional system [9]

Precast system	Conventional system
The manufacturing of elements takes done in a controlled casting environment, making it simpler to manage the mix, positioning, and curing	Column, slab etc. elements are cast on site and hence it is difficult to control mix, placement and curing in cast-in-situ concrete
Construction using precast concrete can be completed quickly because there is no need to wait for the material to strengthen	In situ concrete construction is slow as gaining of strength requires time
Controlling and maintaining quality is simple	Quality control and maintenance are difficult
The ability to cast elements in advance and store them till the time of the need, saves time	Elements cannot be cast in advance
Weather conditions has no effect on casting work [10]	Weather conditions can delay the casting work
Precast concrete is a cheaper form of construction if large structures are to be constructed	In situ concrete is a cheaper form of construction for small structures
Elements of varying lengths and shapes can be developed	There is a constraint in length and shape of the element
Less labours are required	More labours are required

Precast concrete wall design

Thickness of wall: 200 mm
 Vertical reinforcement: 16 mm diameter at 200 centre to centre spacing
 Horizontal reinforcement: 10 mm diameter at 250 centre to centre spacing
 Design axial load: 30 kN/m
 Cover to outer layer: 20 mm
 Fire resistance period: 60 min
 Concrete strength class: C40/50.

Precast concrete column design

Length of column: 3000 mm
 Dimension: 300 × 300 mm
 Distance between lifting points: 2000 mm
 Cover to reinforcement: 30 mm
 Design axial load: 75 kN
 Concrete strength class: C 40/50
 Fire resistance period: 60 min.

RC PRECAST BEAM DESIGN

In accordance with EN1992-1-1:2004 incorporating Corrigenda January 2008 and the recommended values

Tedds calculation version 3.3.03 - Development

Design summary

Overall design utilisation 0.671
 Overall design status PASS

Section 1

Description	Unit	Provided	Required	Utilisation	Result
Top reinforcement	mm ²	226	0	0.000	PASS
Bottom reinforcement	mm ²	339	204	0.601	PASS
Shear reinforcement	mm ² /m	377	253	0.671	PASS

Lifting check

Description	Unit	Provided	Required	Utilisation	Result
Moment neg (1.3 kNm)	mm ²	226	115	0.510	PASS
Moment pos (-0.9 kNm)	mm ²	339	115	0.340	PASS
Shear (2.9 kN)	mm ² /m	377	253	0.671	PASS

Concrete details (Table 3.1 - Strength and deformation characteristics for concrete)

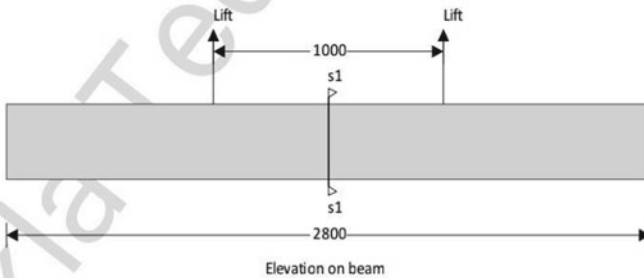
Concrete strength class C40/50 Char. comp. cylinder strength $f_{ck} = 40 \text{ N/mm}^2$
 Design comp conc. strength $f_{ovd} = 26.7 \text{ N/mm}^2$ Maximum aggregate size $\eta_{agg} = 20 \text{ mm}$
 Design compressive conc str $f_{cd} = 26.7 \text{ N/mm}^2$ Tensile strength coefficient $\alpha_{ct} = 1.00$
 Design tensile strength of conc. $f_{ct,d} = 1.64 \text{ N/mm}^2$

Reinforcement details

Char. yield strength of reinf. $f_{yk} = 500 \text{ N/mm}^2$ Partial factor for reinf. steel $\gamma_s = 1.15$
 Design yield strength of reinf. $f_{yd} = 435 \text{ N/mm}^2$

Nominal cover to reinforcement

Nominal cover to top reinf $c_{nom,t} = 35 \text{ mm}$ Nominal cover to bottom reinf $c_{nom,b} = 35 \text{ mm}$
 Nominal cover to side reinf $c_{nom,s} = 35 \text{ mm}$



Rectangular section details

Section width $b = 250 \text{ mm}$ Section depth $h = 300 \text{ mm}$

Fig. 1 Precast beam design using Tekla Tedds software

PRECAST WALL DESIGN (EN 1992)

In accordance with EN1992-1-1:2004 incorporating corrigendum January 2008 and the recommended values

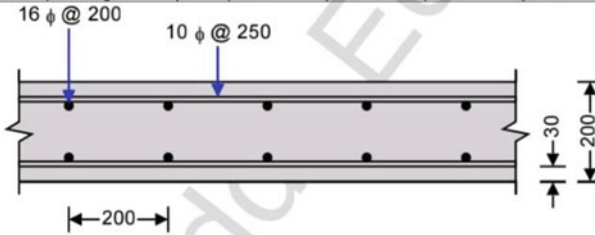
Tedds calculation version 1.1.0'

Design summary

Description	Unit	Allowable	Actual	Utilisation	Result
Moment capacity	kNm/m	100.28	32.63	0.33	PASS
Crack width	mm	0.30	0.12	0.38	PASS

Design summary - lifting checks

Description	Unit	Provided	Required	Utilisation	Result
Top reinf. - y axis - Lifting	mm ²	942	903	0.958	PASS
Bot reinf. - y axis - Lifting	mm ²	942	903	0.958	PASS
Shear cap. - y axis - Lifting	kN	309.9	25.2	0.081	PASS
Top reinf. - x axis - Lifting	mm ²	2011	555	0.276	PASS
Bot reinf. - x axis - Lifting	mm ²	2011	555	0.276	PASS
Shear cap. - x axis - Lifting	kN	217.4	25.2	0.116	PASS
Punching shear cap. - Lifting	N/mm ²	0.63	0.09	0.141	PASS



Wall input details

Wall geometry

- Thickness **h = 200 mm**
- Length **b = 1000 mm/m**
- Clear height between restraints **l = 3000 mm**
- Stability about minor axis **Braced**

Concrete details

- Concrete strength class **C40/50**
- Partial safety factor for concrete (2.4.2.4(1)) **γ_c = 1.50**
- Coefficient α_{cc} (3.1.6(1)) **α_{cc} = 1.00**
- Maximum aggregate size **d_a = 20 mm**

Reinforcement details

- Reinforcement in outer layer **Horizontal**
- Nominal cover to outer layer **c_{nom} = 30 mm**
- Vertical bar diameter **φ_v = 16 mm**
- Spacing of vertical reinforcement **s_v = 200 mm**

Fig. 2 Precast wall design using Tekla Tedds software

6 Result and Analysis

RC Precast concrete beam

The overall design utilisation for steel was obtained as 0.671 which lies in the limit and the overall design status was obtained as pass. In case of lifting check of the beam, design negative moment and design positive moment was obtained as 1.3 kNm and – 0.9 kNm respectively. The utilisation of steel requirement for top, bottom and shear reinforcements lies in the limit.

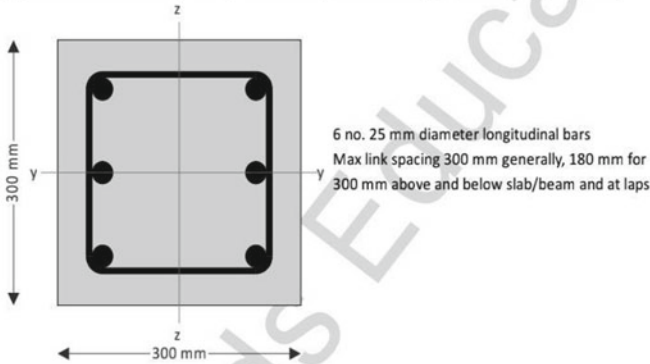
PRECAST COLUMN DESIGN (EN 1992)

In accordance with EN1992-1-1:2004 incorporating Corrigendum January 2008 and the recommended values

Tedds calculation version 1.4.02 -

Design summary - PASS

Description	Unit	Provided	Required	Utilisation	Result
Moment capacity (y)	kNm	144	77	0.54	PASS
Moment capacity (z)	kNm	163	52	0.32	PASS
Biaxial bending				0.86	PASS



Column geometry

Overall depth (perp y)	h = 300 mm	Overall breadth (perp z)	b = 300 mm
Stability in the z direction	Unbraced	Stability in the y direction	Unbraced

Concrete details

Cylinder strength of concrete	$f_{ck} = 40 \text{ N/mm}^2$	Safety factor for concrete	$\gamma_c = 1.50$
Coefficient α_{cc}	$\alpha_{cc} = 1.00$		
Maximum aggregate size	$d_g = 20 \text{ mm}$		

Reinforcement details

Nominal cover to links	$c_{nom} = 35 \text{ mm}$	Longitudinal bar diameter	$\phi = 25 \text{ mm}$
Link diameter	$\phi_v = 8 \text{ mm}$	Total no. of longitudinal bars	N = 6
No. bars per face parallel y axis	$N_y = 2$	No. bars per face parallel z axis	$N_z = 3$
Area of longitudinal reinf	$A_s = 2945 \text{ mm}^2$	Safety factor for reinforcement	$\gamma_s = 1.15$
Modulus of elasticity of reinf	$E_s = 200000 \text{ MPa}$		

Fire resistance details

Fire resistance period	R = 30 min	Exposure to fire	Exposed one side only
Ratio of fire design axial load to design resistance		$\mu_{fi} = 0.70$	

Axial load and bending moments from frame analysis

Design axial load	$N_{Ed} = 330.0 \text{ kN}$		
Moment about y axis at top	$M_{topy} = 75.0 \text{ kNm}$	Moment about y axis at btm	$M_{btmy} = 75.0 \text{ kNm}$

Fig. 3 Precast column design using Tekla Tedds software

RC Precast concrete wall

The moment capacity of the designed wall was obtained as 32.63 kN/m which is less than allowable moment capacity. A crack width of 0.12 mm was attained which is less than the allowable crack width 0.3 mm. The shear capacity along x axis and y axis, punching shear capacity in case of lifting check was found to be a safe value.

RC Precast concrete column

The moment capacity along y axis and x axis was obtained as 144 kNm and 163 kNm respectively. The design bending moments about y axis is found as obtained as 77.5 kNm and about z axis as 52.5 kNm. The moment capacity about the y axis and z axis exceeds the design bending moments for both y axis and z axis. Thus the design was resulted as a safe design.

7 Conclusion

The main aim of the project is to understand and study the precast construction technology and compare it with that of conventional construction. The design of precast concrete structures like beam, column and wall were done using Tekla Tedds Software by Trimble. A beam of span 2.8 m is required in the construction residential structure. Design shear force of the precast concrete beam was obtained as 3 kN with a design shear stress 0.048 N/mm^2 . In the design of precast concrete wall, moment capacity was found to be 100.28 kNm with a crack width of 0.3 mm which is found to be in limit. For the design of precast concrete column, the design moment capacity about y and z axis exceeds the design bending moment for an axial load of 75 kN. The utilisation factor, which defines the steel requirement for all elements was obtained in limit which shows there is no excess of steel or wastage of material. The outputs for each precast concrete element was obtained as a safe design. In the upcoming construction activities, precast concrete structures are going to play a major role in the civil engineering field.

References

1. Raghvani S, Harwande N, Khose P, Ubale N, Ray S (2022) Review on comparative study of international codal provision for precast construction. *Int J Sci Res Publ*
2. Murari S, Joshi A (2017) Precast construction methodology in construction industry
3. Polat G (2010) Precast concrete systems in developing vs. industrialized countries. *J Civ Eng Manag* 16(1):85–94
4. Pheng LS, Chuan CJ (2001) Just-in-time management of precast concrete components. *J Constr Eng Manag* 127(6):494–501
5. Nanyam VN, Basu R, Sawhney A, Vikram H, Lodha G (2017) Implementation of precast technology in India—opportunities and challenges. *Proc Eng* 196:144–151
6. Nagaraju Kaja AJ (2021) Review of precast concrete technology in india. *Int J Eng Res Technol (IJERT)* 10
7. Kurama YC, Sritharan S, Fleischman RB, Restrepo JI, Henry RS, Cleland NM, Ghosh S, Bonelli P (2018) Seismic-resistant precast concrete structures: state of the art. *J Struct Eng* 144(4):03118001
8. Tam VW, Tam CM, Zeng S, Ng WC (2007) Towards adoption of pre-fabrication in construction. *Build Environ* 42(10):3642–3654

9. Agrawal A, Sanghai S, Dabhekar K (2021) Comparative studies between pre-cast and conventional cast-in-situ structural systems. In: IOP conference series: materials science and engineering, vol 1197, no 1. IOP Publishing
10. Yu H, Al-Hussein M, Nasser R, Cheng RJ (2008) Sustainable precast concrete foundation system for residential construction. *Can J Civ Eng* 35(2):190–199

Wind-Induced Aerodynamic Effects on Multiple Side Setback Tall Buildings Using CFD Simulation



Amlan Kumar Bairagi and Sujit Kumar Dalui

Abstract The present study considers different types of setback tall building models and compares the aerodynamic study with the 1:1:2 regular-shape tall building model. The setback height is considered at $h/2$, and $2h/3$ levels from the base of the model. The setback distances are arranged on the single side, double side, and around the building at the considered $h/2$ and $2h/3$ levels. This study was conducted by Computational Fluid Dynamics (CFD) method. The drag and lift coefficients of the building due to wind load are correlated. Power spectral density (PSD) at the top and setback roofs are also compared. Finally, this study concludes that the model has setbacks around the building efficiently reducing 89% torsional moment compared to the regular square shaped model. The reduced frequency decrease on the setback model has a setback around it. Finally, this study suggests that setback distance and increase of setback number around the model can easily handle the wind velocity and control the torsional moment due to wind.

Keywords Computational fluid dynamics (CFD) · Power spectral density (PSD) · Dynamic analysis · Setback building · Wind load

1 Introduction

Wind load on tall buildings continuously challenges researchers for reliable design. Calculation of aerodynamic effects on irregular shaped tall buildings is difficult to compare to regular shaped tall building models. Several international codes have already guided the calculation procedure of wind load for conventional shape-building models and suggested wind tunnel studies for unconventional shaped building models. The analysis of wind load on wind tunnel testing is expensive and

A. K. Bairagi (✉) · S. K. Dalui
Department of Civil Engineering, Indian Institute of Engineering Science and Technology,
Shibpur, Howrah, India
e-mail: amlan.bairagi.rs2016@civil.iiests.ac.in

S. K. Dalui
e-mail: sujit@civil.iiests.ac.in

protracted. Therefore, researchers have considered Computational Fluid Dynamics (CFD) study to simulate the different aerodynamic effects on the prototype model. The irregular shape and asymmetric shape of the tall buildings are always conspicuous. But this type of irregularly shaped tall building aids to damage the structure due to wind load. Continuous change and modification of tall building shapes can control the wind effect. A large number of tall buildings have already introduced setbacks for the alluring architectural appearance. Kim et al. [1] considered various configurations such as corner modifications, taper, setback, openings, and twists tall building models for the aerodynamic and pedestrian level wind characteristics. Kim et al. [2] studied seventeen different types of super-tall building models such as basic and corner modification with corner cut, chamfered, oblique opening, tapered, inversely tapered, bulged, and helical with twist angles and observed the aerodynamic effects for the different wind angles. Wang and Zhang [3] noticed the crosswind displacement response of the chamfered tall building when the ratio is increased to 5% or the rounded ratio increased to 12.5%. Bairagi and Dalui [4] studied 48 setback tall building models and optimized them by genetic algorithm. Finally selected a single model which reduces 45–65% drag and 25–60% lift compared to the regular shape 1:1:2 square model. Several researchers already studied the 1:1:2 models in the wind tunnel [5, 6] and CFD [7–9] study. The present study considers 1:1:2 regular plan shaped tall buildings and six different types of setback tall buildings to compare the aerodynamic effects at the rooftop and setback roof of the buildings. Computational Fluid Dynamics (CFD) study has been employed for the study. The multiple levels and multiple setback models have drastically reduced the aerodynamic effect and the number of setbacks. Variation of setback distances can play an important role to cut back on the frequency of the structure.

2 Numerical Method

The present study considered the renormalization group (RNG) k - ε method for the simulation technique. The transport equation of the RNG k - ε model as shown in Eqs. (1–3) [8, 10]:

$$\frac{\partial}{\partial t}(k) + \frac{\partial}{\partial x_i}(\rho k u_i) = \frac{\partial}{\partial x_j} \left(\alpha_k \mu_{eff} \frac{\partial k}{\partial x_j} \right) + G_k + G_b - \rho \varepsilon - Y_M + S_k \quad (1)$$

$$\begin{aligned} \frac{\partial}{\partial t}(\rho \varepsilon) + \frac{\partial}{\partial x_i}(\rho \varepsilon u_i) &= \frac{\partial}{\partial x_j} \left(\alpha_\varepsilon \mu_{eff} \frac{\partial \varepsilon}{\partial x_j} \right) + C_{1\varepsilon} \frac{\varepsilon}{k} (G_k + C_{3\varepsilon} G_b) \\ &\quad - C_{2\varepsilon} \rho \frac{\varepsilon^2}{k} - R_\varepsilon + S_\varepsilon \end{aligned} \quad (2)$$

where k is the turbulence kinetic energy, ε is the turbulent eddy dissipation, G_k is the generation of turbulence kinetic energy due to the mean velocity gradients, G_b is the generation of turbulence kinetic energy due to buoyancy, Y_M is the contribution of

the fluctuating dilatation in-compressible turbulence to the overall dissipation rate, α_k , and α_ε are the inverse effective Prandtl numbers for k and ε respectively, S_k and S_ε are user-defined source terms.

The scale elimination procedure in RNG theory results in a differential equation for turbulence viscosity:

$$d \left[\frac{\rho^2 k}{\sqrt{\varepsilon \mu}} \right] = 1.72 \frac{\hat{v}}{\sqrt{\hat{v}^3 - 1 + C_v}} d\hat{v} \quad (3)$$

where, $\hat{v} = \frac{\mu_{eff}}{\mu}$, $C_v \approx 100$. For an accurate description of the variation of effective turbulence transport for effective Reynolds number, integrate $\mu_t = C_\mu \rho k^2 / \varepsilon$. For the high Reynolds number limit, the constant $C_\mu = 0.0845$ was used to calculate the turbulence viscosity (μ_t). The other constants used in RNG theory are $\sigma_\varepsilon = 0.719$, $C_{1\varepsilon} = 1.42$, $C_{2\varepsilon} = 1.68$.

3 Description of the Models

This study considers seven square plan shaped models. It initially considered a square plan shape tall building model (SQ) of length (l) = 250 mm, breadth (b) = 250 mm, and height (h) = 500 mm. Therefore, the $l:b:h$ is 1:1:2. Similar type of six different setback tall building models are considered for the study. The models are considered setbacks at different levels and on different sides of the models. According to the setback location from the base of the model, the setback models are considered in two groups. The first group is considered a single setback and the second group is a double setback. The first group has three different models and setbacks at the $h/2$ level from the base. The second group of setback models has three different models at setback levels $h/3$ and $2h/3$ from the base. At first, the study considered the single side single setback model (SB1_a) considered the setback at the $h/2$ level as shown in Fig. 1. The setback distance is considered at $0.2l$ distance from the edge. That is 20% of the length of the building. Similarly, model (SB1_b) has two setbacks at the $h/2$ level on the opposite side of the building. Here, the 20% setback distance is divided on the opposite side of the model. Therefore, the setback distance of the double-side single setback model is $0.1l$. The SB1_c model has a setback around the model at $h/2$ height. Therefore, the setback distance is $0.1l$ around the model. In this similar way, the SB1_a model allowed for a single side double setback at level $h/3$ distance from the base and $2h/3$ distance from the base. So, the 20% setback distance is equally divided at the different levels. Therefore, the setback distance of the single-side double setback model (SB2_a) is $0.1l$. In this similar fashion, the SB2_b and SB2_c models have considered setback distance $0.1l$ at $h/3$ and $2h/3$ levels. The setback distances are placed on the opposite side for the SB2_b model and around the building for the SB2_c model. The flow of 0° wind is considered along the y -axis and 90° wind along the x -axis.

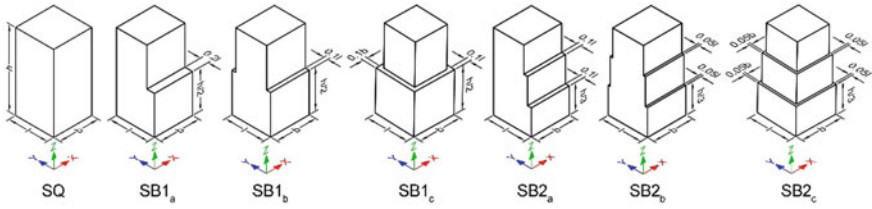


Fig. 1 Regular shape square building and different multiple-side setback building models

4 Domain and Meshing

The present study considered Computational Fluid Dynamics (CFD) method using ANSYS 2019 fluent package. The considered models are placed inside the domain for the analytical study. The inlet and both sidewalls are considered as $5h$ from the extreme edge of the model. The outlet of the model is placed at a $15h$ distance from the back side of the model for proper flow at the back side of the model. The top of the domain is placed at $6h$ from the base of the model as shown in Fig. 2a. The size of the domain is considered according to the guideline of the Architectural Institute of Japan (AIJ) [11]. This study considered 1:300 scale of the prototype model. The blockage ratio of the domain is 5%, which satisfies the AIJ guideline. The boundary conditions are selected as free-slip for the sidewalls of the domain and no-slip for the model walls. Tetrahedron meshing is considered around and inside the domain. The growth rate selected is 1.2 and the y^+ value is 3, which is less than 5 [12]. Mesh detail of the SQ model inside the domain is shown in Fig. 2b.

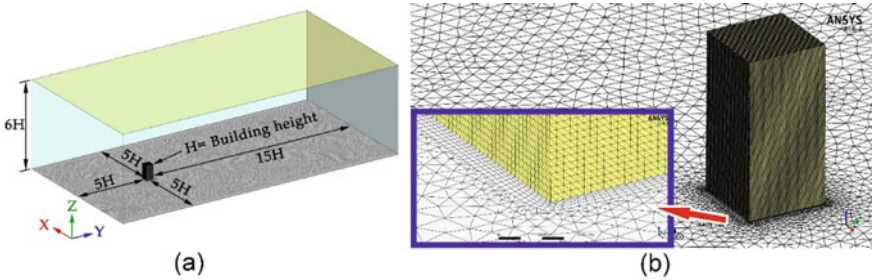


Fig. 2 a Dimension of the domain, b mesh diagram of SQ model inside the domain

5 Grid Sensitivity and Validation of the Study

This study considers the RNG k - ε turbulence model for the simulation purpose. The equation of fluctuation velocity (U), turbulence intensity (I), and turbulence energy (k) inside the domain are presented by Eqs. (4–6) [11].

$$U = U_h \left(\frac{Z}{Z_h} \right)^\alpha \quad (4)$$

$$I = \frac{u_u(z)}{U} = 0.1 \left(\frac{Z}{Z_g} \right)^{(-\alpha-0.005)} \quad (5)$$

$$k = \frac{u_u^2(z) + u_v^2(z) + u_w^2(z)}{2} \cong u_u^2(z) = (I \times U)^2 \quad (6)$$

where U_h is the boundary layer velocity, which was 10 m/s; $\alpha = 0.133$ is the power-law index for terrain category 2, Z_g is the boundary layer height determined by terrain category, u_u is the root-mean-square (RMS) value of velocity fluctuation in the streamwise direction. A similar type of experimental study of the same 1:1:2 building model was conducted by [4, 5, 13].

In Computational Fluid Dynamics (CFD) simulation, the grid sensitivity study is an important part [12]. In this study, the regular shaped square model was considered for the study. The SQ model was placed inside the domain and studied with tetrahedral meshing. A similar type of meshing has already been considered for past CFD studies and a good quality results have been found [14–16]. Coarse grid (Gr1), intermediate grid (Gr2), and fine grid (Gr3) are used in this study. The node number and element numbers of the model and domain continuously increase with the increase of the number of edge divisions [17]. The pressure, force, and moment coefficient of the SQ model was simulated with the Gr1, Gr2, and Gr3 grid conditions and presented in Fig. 3a. Grid size-wise node numbers are considered to present the pressure (C_p), force (C_f), and moment (C_m) coefficients of the SQ model. Here, it is clear that the C_p , C_f , and C_m of the SQ model are continuously increasing with the increase in grid size [18]. Furthermore, this study compares the C_p and C_f of the SQ model for the adopted grid Gr3 with the pre-calculated values from the different international codes [19–22]. The pre-calculated values of C_p and C_f are adopted according to the considered aspect ratio (i.e., 1:1:2) of the SQ model. The simulated value of the SQ model has a good agreement with the considered international codes as shown in Fig. 3b. Therefore, this study adopted the Gr3 grid for further study of setback models.

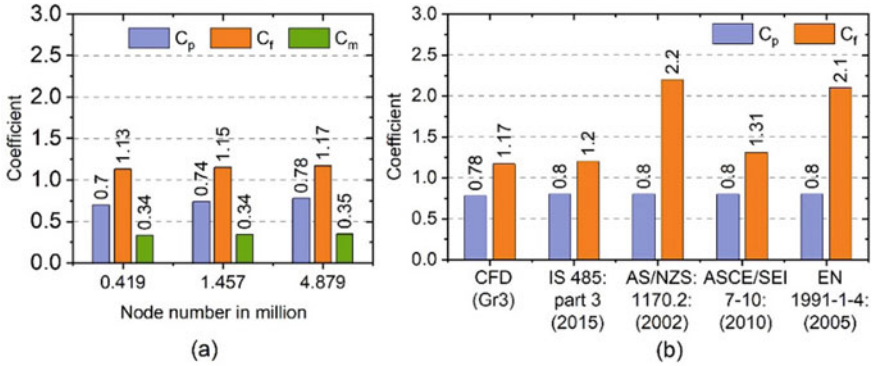


Fig. 3 **a** Grid sensitivity study of SQ model and **b** Comparative study of pressure and force coefficient between CFD and different international codes

6 Results and Discussions

6.1 Moment Coefficient Calculation

The models are experienced with the moment due to the flow of wind along the x and y axes. Simultaneously, the torsional moment about the z-axis is also calculated for the 0° and 90° wind angles. Moments about the x and y axes are represented as C_{mx} and C_{my} . The torsional coefficient is considered about the z-axis and represented as C_{mz} . The moment coefficients are calculated as [7]:

$$C_{mx} = \frac{F_x}{0.5\rho U_h^2 \cdot A_x} = \frac{\sum_i C_p A_j \sin \alpha_j}{\sum_i A_j \sin \alpha_j} \quad (7)$$

$$C_{my} = \frac{F_y}{0.5\rho U_h^2 \cdot A_y} = \frac{\sum_i C_p A_j \cos \alpha_j}{\sum_i A_j \cos \alpha_j} \quad (8)$$

$$C_{mz} = \frac{F_z}{0.5\rho U_h^2 \cdot A_z} = \frac{\sum_i C_p A_j \cos \alpha_j}{\sum_i A_j \cos \alpha_j} \quad (9)$$

$$C_m = \sqrt{C_{mx}^2 + C_{my}^2} \quad (10)$$

where A_j is the supplementary area of point j ; $\sin\alpha$ and $\cos\alpha$ are the direction vector of the point j along the x, y, and z axes. C_p is the pressure coefficient and C_m represents the global moment coefficient of the building. The global moment coefficient (C_m) of the buildings is calculated on the x and y axes for the 0° and 90° wind angles. Maximum values of torsional coefficients ($C_{mz,max}$) are considered between 0° and 90° wind angles as shown in Fig. 4.

The fluctuation of the global moment coefficient (C_m) and torsional moment coefficient ($C_{mz,max}$) are compared according to the initial SQ building model. Here, the

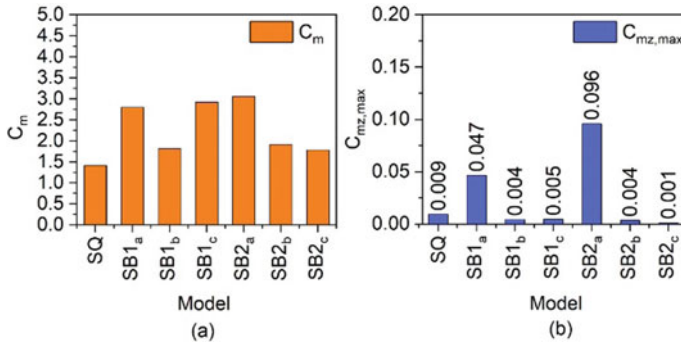


Fig. 4 Comparison of **a** global moment coefficient (C_m) and **b** maximum torsional moment coefficient ($C_{mz,max}$) between the square and setback building models

study considers the C_m of the SQ model as the datum to compare the other considered models. A comparison of the percentage increase of the global moment and torsional moment coefficient is shown in Table 1. Upward (\uparrow) and downward (\downarrow) arrow marks behind the percentage data of Table 1 are represented the increase and decrease of C_m and $C_{mz,max}$ of the respective model compared with the initial SQ model. As the SQ model is considered a datum of the comparative study, the comparative value of the SQ model in Table 1 is 0%. The model SB2_c represented the minimum (20.58%) global moment coefficient compared to other setback models. Whereas, the SB2_a model is experienced with maximum (53.65%) global moment coefficient. In this similar fashion, the torsional moment coefficient of setback buildings is compared with the SQ model. Here an interesting point is noticed. The SB2_c model experienced a minimum torsional moment coefficient (0.001), which is 89% less than the SQ model. This type of variation of the global moment and torsional moment of setback models happens due to the setback distance and setback location. The setback of the SB2_c model is considered around the building at the $h/2$ level. Therefore, the wind flows around it for 0° and 90° are similar. The SB2_a has a double setback on a single side. According to the geometry of the model, the wind flow variation for 0° and 90° wind is different. Due to this reason, the SB2_a model experienced the maximum torsional moment coefficient.

6.2 Normalized Velocity Spectra

The energy spectra of velocity or power spectral density (PSD) $S_u(f)/\sigma^2$, (u = oscillating signal at the measuring point, f = frequency in Hz, σ = standard deviation of energy variation) was compared to the setback roof and top roof of the models. Another non-dimensional part Strouhal number ($S_u = fb/u$) was introduced here to evaluate the location of the peak of the dimensionless energy. One interested can follow the previous study [7, 23] for a detailed derivation of PSD and Strouhal

Table 1 Comparison of percentage increase of global moment coefficient (C_m) and torsional moment coefficient ($C_{mz,max}$) according to the SQ model

Model	Increase of global moment (C_m) compared with SQ mode	Increase/decrease of the torsional moment ($C_{mz,max}$) compared with SQ mode
SQ	0%	0%
SB1a	49.43% (↑)	80.85% (↑)
SB1b	22.03% (↑)	44.45% (↓)
SB1c	51.57% (↑)	55.56% (↓)
SB2a	53.65% (↑)	90.63% (↑)
SB2b	26.02% (↑)	44.45% (↓)
SB2c	20.58% (↑)	88.89% (↓)

number. The points are considered adjacent to the leeward face of the modes to observe the response of the spectral density [24]. Tapping points are considered at the edge of the rooftop for all the models. Another tapping point is fixed at the setback roof of double setback building models (SB1_a, SB2_b, and SB2_c). The tapping point locations that are demarcated are R1 and R2 for the first and second setback roof. According to the different shapes of the models, this study preferred normalized spectral density for 0° and 90° wind flow as shown in Figs. 5 and 6.

Variations of normalized velocity spectra for 0° wind angle at the rooftop of the SQ and Setback models are shown in Fig. 5a. The SQ model reflects the low-velocity spectral variation at the roof compared to the other setback models. The normalized PSD at the first setback region of the SB1_a model represented the low variation due to its maximum setback distance as shown in Fig. 5b. Whereas Fig. 5c–d represented the normalized PSD of velocity at the first and second setbacks of the SB2_a, SB2_b, and SB2_c models. Here SB2_c model is reflected a lower value compared to the SB2_b and SB2_a. This type of variation is due to the setback distance (0.1*l*) of the SB2_a model. Whereas, the other two models (SB2_b and SB2_c) have a setback distance of 0.05*l*. On the other hand, the normalized PSD of velocity is less at both setbacks of the SB2_c model. This model produces low frequency at the setback region due to the proper distribution of setbacks around the model.

For the 90° wind angle, no such alteration of normalized PSD of velocity at the rooftop was noticed on the setback buildings as shown in Fig. 6a. An interesting point was noticed in the SB2_a and SB2_c models for 90° wind flow conditions. The normalized PSD for the velocity at the first and second setback region of the SB2_a and SB2_c modes are just opposite to the 0° wind flow condition as shown in Fig. 6b–c. The frequency of the SB2_c model decreases at both the setback roof portion due to the uniform distribution of setbacks around the SB2_c model. The 90° wind flow attacks the flat face of the SB2_a model. Therefore, the fluctuation of wind flows attacks the setback region of the considered tapping points adjacent to the leeward face. But the SB2_c model has a setback face for 90° wind flow. Therefore, the fluctuation of flow decreases due to the setback in the windward direction. Finally, the study came to the conclusions that, the setback around the building model may take an important

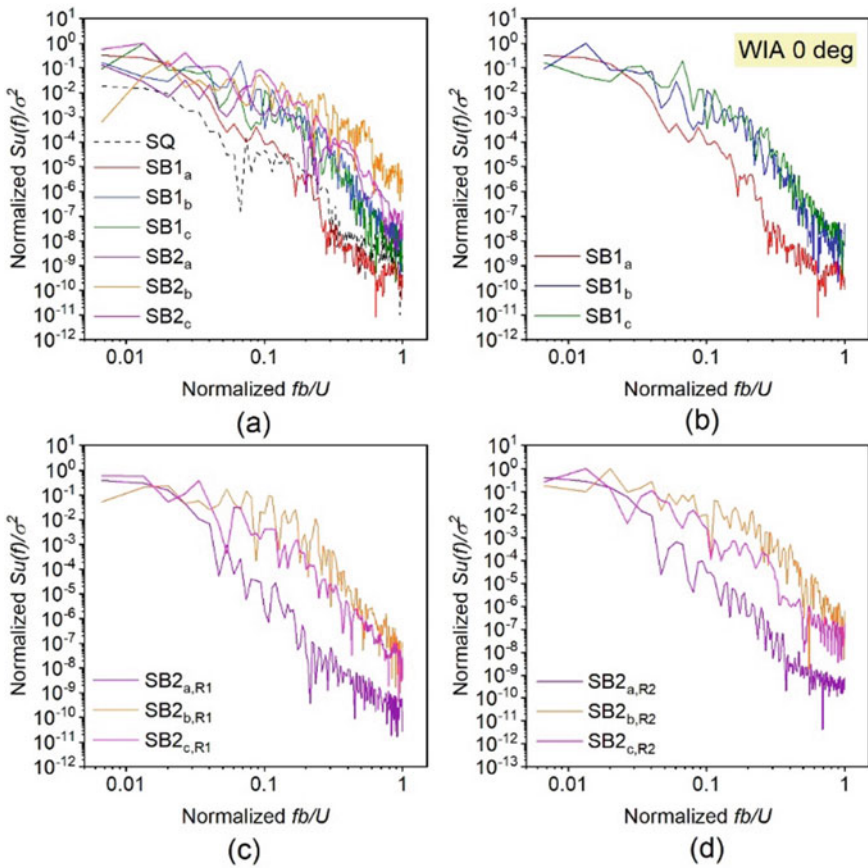


Fig. 5 Variation of the spectral density of velocity at the **a** top roof, **b** setback roof of single setback models, **c** setback roof (R1) of double setback model, **d** setback roof (R2) of double side setback model for 0° wind angle

role to reduce the aerodynamic effects on the setback buildings. Furthermore, the number of setbacks also plays an important part to reduce the frequency of velocity on the buildings.

7 Conclusions

This study focuses on the aerodynamic variation on the multiple numbers and multiple side setbacks of tall buildings and compared it with the regular square plan shape (1:1:2) building model. The study was conducted with the CFD simulation

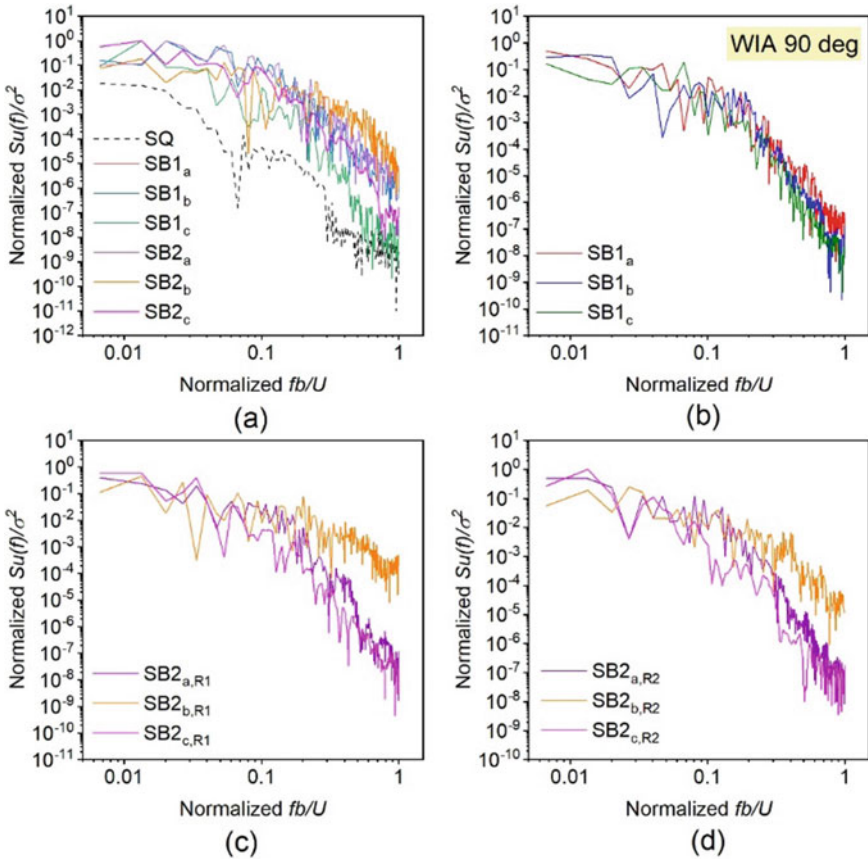


Fig. 6 Variation of the spectral density of velocity at the **a** top roof, **b** setback roof of single setback models, **c** setback roof (R1) of double setback model, **d** setback roof (R2) of double side setback model for 90° wind angle

along and across wind flow conditions. The following conclusions are established from the study.

1. The double setback building (SB2_c) model has setbacks around the model. This model experienced the same aerodynamic effects along and across wind conditions due to its geometry. Therefore, this model has a minimum torsional moment coefficient and is 89% less compared to the regular shape square (SQ) model.
2. The single-side double setback model (SB2_a) efficiently reduces the frequency at the setback region for 0° wind flow, but it increases the frequency for the 90° wind angle due to the uniform windward face.
3. The SB2_c model is very efficient to reduce the frequency of the velocity at the setback locations due to its uniform geometrical shape.

4. Finally, this study concluded the setback around the building model may take a foremost to reduce the aerodynamic effects on the setback buildings.
5. The number of setbacks also plays an important part to reduce the frequency of velocity on the building.
6. In this study, the conclusions are made according to the 1:1:2 (*l:b:h*) building models. Therefore, the results are suitable for the models have similar aspect ratio.
7. This study may further improve with the increase of setback distance and number. Also, it may be studied for different aspect ratios.

Acknowledgements The authors would like to express his gratitude to Sagata Jana, Assistant Teacher, at Ichapur Northland High School for her valuable guidance to modify the manuscript. The authors thank the editor for deciding on the manuscript in the reputed conference proceedings and book chapter. The authors also thank the reviewers for their valuable comments on the manuscript.

Funding The authors declare no specific funding for this work.

References

1. Kim YC, Xu X, Yang Q, Tamura Y (2019) Shape effects on aerodynamic and pedestrian-level wind characteristics and optimization for tall and super-tall building design. *Int J High-Rise Build* 8(4):235–253. <https://doi.org/10.21022/IJHRB.2019.8.4.235>
2. Kim W, Yoshida A, Tamura Y (2019) Wind-induced aerodynamic instability of super-tall buildings with various cross-sectional shapes. *Int J High-Rise Build* 8(4):303–311. <https://doi.org/10.21022/IJHRB.2019.8.4.303>
3. Wang L, Zhang W (2023) The influence of chamfered and rounded corners on vortex-induced vibration of super-tall buildings. *Appl. Sci.* 13
4. Bairagi AK, Dalui SK (2022) Minimization of wind load on setback tall building using multiobjective optimization procedure. *Wind Struct Int J* 35(3):157–175
5. Meng Y, Hibi K (1998) Turbulent measurements of the flow field around a high-rise building. *J Wind Eng* 76:55–64. https://doi.org/10.5359/jawe.1998.76_55
6. Kim YC, Kanda J, Tamura Y (2011) Wind-induced coupled motion of tall buildings with varying square plan with height. *J Wind Eng Ind Aerodyn* 99(5):638–650. <https://doi.org/10.1016/j.jweia.2011.03.004>
7. Bairagi AK, Dalui SK (2021) Prediction of pressure coefficient on setback building by artificial neural network. *Can J Civ Eng.* <https://doi.org/10.1139/cjce-2020-0100>
8. Bairagi AK, Dalui SK (2021) Wind environment around the setback building models. *Build Simul* 14(October):1525–1541. <https://doi.org/10.1007/s12273-020-0758-3>
9. Khaled MF, Aly AM, Elshaer A (2021) Computational efficiency of CFD modeling for building engineering: an empty domain study. *J Build Eng* 42(May):102792. <https://doi.org/10.1016/j.jobe.2021.102792>
10. Ansys 15 (2013) ANSYS fluent theory guide
11. Tominaga Y et al (2008) AIJ guidelines for practical applications of CFD to pedestrian wind environment around buildings. *J Wind Eng Ind Aerodyn* 96(10–11):1749–1761. <https://doi.org/10.1016/j.jweia.2008.02.058>
12. Franke J, Hellsten A, Schlünzen H, Carissimo B (2010) The best practise guideline for the CFD simulation of flows in the urban environment: an outcome of COST 732. In: The fifth international symposium on computational wind engineering, pp 1–10

13. Bairagi AK, Dalui SK (2020) Estimation of wind load on stepped tall building using CFD simulation. *Iran J Sci Technol Trans Civ Eng*. <https://doi.org/10.1007/s40996-020-00535-1>
14. Wijesooriya K, Mohotti D, Amin A, Chauhan K (2021) Comparison between an uncoupled one-way and two-way fluid structure interaction simulation on a super-tall slender structure. *Eng Struct* 229:111636. <https://doi.org/10.1016/j.engstruct.2020.111636>
15. Singh J, Roy AK (2019) Wind pressure coefficients on pyramidal roof of square plan low rise double storey building. *Comput Eng Phys Model* 2(1):1–16. <https://doi.org/10.22115/cepm.2019.144599.1043>
16. Weerasuriya AU, Zhang X, Lu B, Tse KT, Liu CH (2021) A Gaussian process-based emulator for modeling pedestrian-level wind field. *Build Environ* 188:107500. <https://doi.org/10.1016/j.buildenv.2020.107500>
17. Bairagi AK, Dalui SK (2018) Comparison of aerodynamic coefficients of setback tall buildings due to wind load. *Asian J Civ Eng* 19(2):205–221. <https://doi.org/10.1007/s42107-018-0018-3>
18. Bairagi AK, Dalui SK (2022) Prediction of pressure coefficient of setback building using backpropagation neural networks. Springer Singapore
19. IS 875 (part-3) (2015) Design loads (other than Earthquake) for buildings and structures-code of practice
20. AS/NZS 1170.2 (2011) Structural design actions—part 2: wind actions, vol 2
21. ASCE/SEI 7.10 (2010) Minimum design loads for buildings and other structures
22. EN 1991-1-4 (2005) Actions on structures—part 1–4: general actions—wind actions
23. Gavin HP (2016) Random processes, correlation, and power spectral density. Duke University, pp 1–28. https://doi.org/10.1007/978-1-4615-3406-8_43
24. Kim Y, Kanda J (2010) Characteristics of aerodynamic forces and pressures on square plan buildings with height variations. *J Wind Eng Ind Aerodyn* 98(8–9):449–465. <https://doi.org/10.1016/j.jweia.2010.02.004>

Utilization of Water Treatment Sludge as a Filler Material in Bituminous Mix Design



Shabnum Suhura, M. B. Syam Krishna, Sana Sudheer, A. A. Saniyamol, and K. S. Surya

Abstract The water supply of densely populated Ernakulam City of Kerala is carried out from Water Treatment Plant in Aluva, working under Kerala Water Authority. The plant with a capacity of 200 MLD, produces abundant sludge, which is usually disposed by pumping it into the river Periyar. As a sustainable method, utilization of water treatment sludge in pavement design is considered for the study. The water treatment sludge can be effectively used as a filler material in bituminous mix. Conventional filler material is replaced by sludge in 25, 50, 75 and 100% by mass. Trial specimens are prepared by incorporating the sludge in varying percentages. To study the optimum binder content and stability, Marshall Stability flow value test is conducted. The adhesion properties of the mix are understood through the Cantabro test. Comparing the results of Marshall stability test and Cantabro test, bituminous mix with 25% sludge replacement proves sufficient property to be implemented in public works, which can be considered as a sustainable alternative to the current method of disposal.

Keywords Water treatment sludge · Bituminous mix · Pavement design · Sustainable disposal method

1 Introduction

Highway construction requires a significant financial expenditure. A precise engineering plan could result in significant financial savings and ensure that the in-service highway performs reliably. The design of the pavement and the mix design are two key factors in this respect. The considerations for mix design are highlighted in the project. An effective bituminous mix design should produce a material that is both cost-effective and environmentally favorable while also being sufficiently strong, resilient, and resistant to fatigue and permanent deformation. Through numerous tests on the mix with various proportions of material combinations, attempts to

S. Suhura · M. B. S. Krishna · S. Sudheer · A. A. Saniyamol · K. S. Surya (✉)
Adi Shankara Institute of Engineering and Technology, Kalady, Ernakulam, Kerala, India
e-mail: suryaks69378@gmail.com

© The Author(s), under exclusive license to Springer Nature Switzerland AG 2024
M. Nehdi et al. (eds.), *Proceedings of SECON'23*, Lecture Notes in Civil Engineering
381, https://doi.org/10.1007/978-3-031-39663-2_36

439

meet these criteria and to choose the best one are done. A novel idea of using the water treatment sludge as filler for the bituminous mix is being considered. A partial replacement for the filler is to be done by the sludge [1]. Materials such as stone dust, hydrated lime and OPC are traditionally used as filler. Filler plays dual role in bituminous mixes. It effectively fills in the spaces left by the coarser particles while also giving the mixture strength and impermeability. Filler materials typically have a fine texture and can pass through a 0.075 mm sieve. It also gives the bituminous mix binding qualities. The sludge effectively satisfies both of these requirements [2]. Sludge serves as a more effective filler replacement in the initial evaluation. By using sludge as a filler in bituminous mix it becomes an effective way of sludge disposal.

2 Detailed Methodology

The sludge generated in the water treatment plants is usually disposed back into the river, which is an environmentally unhealthy practice [3]. Lack of efficient, convenient and sustainable way of sludge disposal paved way for the formulation of the objective of the study to use the water treatment sludge as a partial replacement of filler material in bituminous mix. For grounding the knowledge on the topic, a series of literature review was done. Several journals, books and other articles were referred. Knowledge regarding the mix design, tests on the specimen, expected strength etc. were achieved from the literature review.

Fillers are generally used in bitumen mix for the better adhesion of the particles and to fill up the voids in the mix. Sludge can satisfy both the requirements. A bituminous mix is made by replacing the conventional filler material by water treatment sludge in varying percentages. The designs are done as per IRC 111 [4] and ASTM D 1559 [5] since these are proposed to be used in public works.

Optimum binder content is found out for the conventional filler specimen by conducting the Marshall test. 4, 6 and 8% binder content is tested and the optimum binder content is selected. Standard bitumen mix is prepared using the conventional filler and the already obtained optimum binder content. After which project specimens are made by replacing conventional filler with sludge using the optimum binder content which is already found. The conventional filler is replaced by 25, 50, 75 and 100% by mass with sludge. Marshall Stability and flow value test and Cantabro test are done on all the specimens and the results are tabulated and compared with the standard specimen. The specimen with acceptable properties is selected for the design of pavement.

Fig. 1 Powdered WT sludge

3 Materials Used for the Experiment

Bitumen and aggregates typically make up a bituminous mix. Depending on the size of the particles, the aggregates are typically divided into coarse, fine, and filler portions. The description of the bitumen, fillers, coarse aggregates, and fine aggregates used in this research can be found in the sections that follow.

Coarse aggregate: The Coarse aggregate needs to be impact, abrasion, and crashing resistant. Its purpose is to absorb wheel-related pressures. It resists deterioration from traffic's rough action.

Fine aggregate: The fine aggregate must pass through 600 μ sieve and be retained on a 75 μ sieve. Its purpose is to close up the gaps left by the coarse gravel.

Fillers: The fillers should be inert substances that can clear a sieve of 75 μ . Fillers are used to cover voids. In this study stone dust and water treatment sludge are used as filler.

Bitumen: It serves as both a binding and a waterproofing substance.

Water treatment sludge: Dewatered sludge cakes are required for the study. But dewatering facilities and drying beds are not available in Aluva WTP. So the sludge which was deposited on the clarifier is collected, sun dried and crushed to get the raw material. Powdered sludge is shown in Fig. 1.

4 Optimum Binder Content Determination

Marshall Stability testing setup is used in this study project. To ascertain the Marshall stability, flow value, and optimum bitumen concentration, tests are conducted. To determine the optimum bitumen content, three specimens with diameters of 101.6 mm and thicknesses of roughly 63.5 mm are made for bitumen contents of 4, 6, and 8%. Figure 2 represents a set of samples made for the experiments. According

to ASTM D1559, the material preparation, compaction, and testing are carried out (Marshall Mix Design Method). The bitumen and aggregates are quickly combined to produce a mixture with a consistent bitumen spread. According to ASTM D 2041 [6] and D 2726 [7], respectively, the bulk specific gravity and theoretical maximum specific gravity are calculated. The compacted specimens are placed in a thermostatically regulated water bath that is kept at a temperature of 60 °C for 30 min after their specific gravities have been determined. Each specimen then undergoes a Marshall Stability and Flow test on a measuring apparatus. An electrically powered compression testing equipment is the Marshall testing machine. The test specimens are subjected to a constant rate of load application through cylindrical segment testing heads until the maximum load is attained. According to ASTM D 3203 [8], the maximum load resistance and corresponding flow value are noted, and the percentage of air voids is calculated. Table 1 shows the average Marshall properties of standard samples with 4, 6 and 8% bitumen content. From the results the optimum binder content is found out to be 5.33%.

Fig. 2 Sample specimen



Table 1 Properties of the mix

Bitumen %	Theoretical specific gravity, G_t	Bulk specific gravity, G_m	Percentage air voids ($V_v\%$)	Voids in mineral aggregate (VMA%)
4	2.5	2.39	4	13
6	2.62	2.5	4.84	13.87
8	2.36	2.25	4.66	16.14

Table 2 Results of tests on standard specimen

Test	Value
Marshall stability test	930.25 kg
Flow value test	2.8 mm
Cantabro test	6.45%

5 Tests on Standard Bituminous Specimen with Conventional Filler

Bituminous mix specimens with conventional filler material are casted. Marshall stability flow value test and cantabro test are conducted. Marshall stability flow test is conducted to find the maximum load that the standard specimen can withstand and is carried out as specified in Sect. 4. Cantabro test is conducted to find the adhesive characteristics. It is used to determine the loss of weight the specimen will undergo after the abrasion test in Los Angeles machine as per ASTM C-131 [9] standards. The specimen is inserted into the machine drum without steel balls and is then rotated at speeds 30–33 rpm. The percentage loss in weight is then calculated. The results of these experiments are given in Table 2.

6 Tests on Sludge Replaced Specimens

The conventional filler in the bitumen mix is replaced by the Water Treatment sludge in varying percentages i.e. 25, 50, 75 and 100% by adding the optimum binder content already found. Marshall Stability test is conducted on the specimens to determine the optimum percentage of sludge added to the mix that is more efficient in satisfying the functionality. Cantabro test is conducted to find the adhesion properties of these specimens. Figure 3 shows the morphology of specimens after cantabro test. Table 3 and Fig. 4 depict the results of Marshall stability test and comparison between them. Table 4 and Fig. 5 illustrate the results of Cantabro test and the comparison between the results.

7 Conclusions

As per MoRTH specifications, for heavy traffic the stability value should be > 910 kg and for medium traffic it should be between 545 and 910 kg. Since we expect a medium traffic with high load vehicles, Marshall stability value > 910 kg is considered. The comparison of weight loss during Cantabro test shows that the value of weight loss is the smallest at 25% sludge replacement and is the highest at 100%.

Fig. 3 Morphology of specimen after Cantabro test



Table 3 Results of Marshall stability-flow value test

Sludge replacement (%)	Stability value (kg)	Flow value (mm)
25	918.28	5
50	830.25	6
75	723.58	7
100	584.56	8

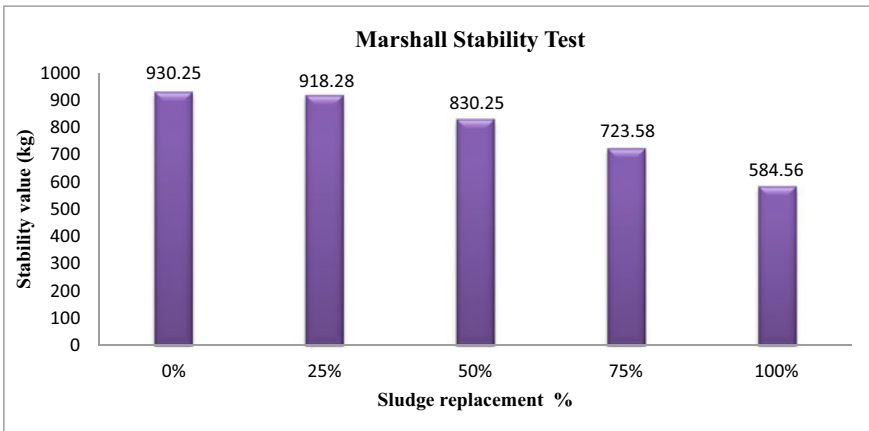
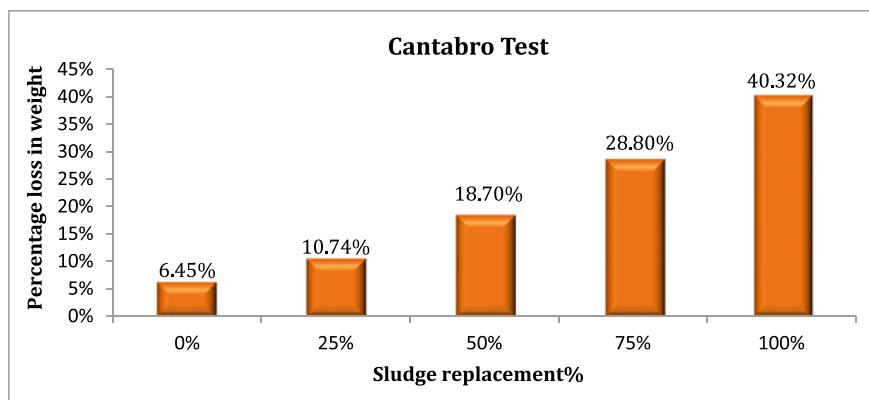


Fig. 4 Comparison of stability value of the sludge replaced specimens

Table 4 Results of Cantabro test

Sludge replacement (%)	Percentage loss in weight of specimen (%)
25	10.74
50	18.7
75	28.8
100	40.32

**Fig. 5** Comparison of weight loss during Cantabro tests

Thus 25% sludge replacement is considered for pavement design and as a sustainable alternative to the current method of water treatment sludge disposal.

References

1. Abiero ZG, Owili D (2016) Suitability of sewage sludge ash as a filler material in asphalt concrete. *J Multidiscipl Eng Sci Stud* 2:925
2. Tenza-Abril A, Saval JM, Cuenca A (2013) Using sewage-sludge ash as filler in bituminous mixes. *J Mater Civil Eng ASCE* 13:1–9
3. Lucena LCFL, Jucá JFT, Soares JB, Marinho Filho PGT (2014) Use of wastewater sludge for base and subbase of road pavements. *Transp Res D* 33:210–219
4. IRC 111
5. ASTM D 1559
6. ASTM D 2041
7. ASTM D 2726
8. ASTM D 3203
9. ASTM C-131

Effect of Steel Fibers in Drying Shrinkage Characteristics of Self-compacting Concrete



Ashika Martin and C. A. Abin Thomas

Abstract Self-compacting concrete has the ability to compact and be placed by its own weight and no other external vibrations are required. They show high performance and help with faster construction. The aim of this project is to study the drying shrinkage of self-compacting concrete (SCC) in which the supplementary cementitious material used is fly ash about 30% and the concrete mix design is carried out for M30 grade with a water-cement ratio of 0.4. Then to the optimized SCC mix the hooked end steel fibers of 30 mm with an aspect ratio of 60 are added at different dosages of concrete volume fraction of 0.5, 1.0, and 1.5% and the compression test and drying shrinkage test is carried out. The test results of SCC with fly ash and different dosage of steel fibers were compared.

Keywords Concrete · SCC · Fly ash · Steel fibers · Drying shrinkage

1 Introduction

Concrete is a construction material that is used worldwide as it has the ability to mold and shape. Concrete has some deficiencies like low impact strength, low post cracking, low ductility, low tensile strength, etc. The cracks can occur in a plastic state or hardened state. The cause of each cracking depends on many factors and excessive cracking can lead to the failure of structures to comply with the code. Therefore we have to face the issue of concrete shrinkage during the construction and necessary actions to be taken to minimize the impact on the durability of concrete. Shrinkage is the change in volume over time in a way it decreases the dimensions of the concrete. During the hardening of concrete, the volume changes due to the effect

A. Martin (✉)

Structural and Construction Management, Federal Institute of Science and Technology (FISAT),
Angamaly, Kerala, India
e-mail: ashikamartin@gmail.com

C. A. A. Thomas

Department of Civil Engineering, Federal Institute of Science and Technology (FISAT),
Angamaly, Kerala, India

Table 1 Physical properties of OPC 53 grade cement

Physical properties	
Specific gravity	3.15
Fineness	6%
Standard consistency	34%
Initial setting time	92 min
Final setting time	412 min

of the hydration of cement and concrete drying with the loss of water in the paste. This project aims to evaluate the drying shrinkage of self-compacting concrete mixes and focuses on investigating the use of steel fibers in reducing the drying shrinkage of self-compacting concrete.

2 Experimental Investigation

2.1 Materials

The materials used for the current experiment are 53 grade OPC cement, Fine aggregate, coarse aggregate, supplementary cementitious materials, steel fibers and superplasticizer [1].

2.1.1 Cement

Ordinary Portland cement of grade 53 conforming to IS 12269:2013 is used. Cement tests are done as per IS 4031:1988 and the results are analyzed using IS 12269:2013. The test conducted on cement are standard consistency test, initial setting time, final setting time and specific gravity test. The physical properties of cement are shown in Table 1.

2.1.2 Coarse Aggregate

A sample of not < 2000g of the aggregate shall be tested. The sample shall be thoroughly washed to remove finer particles and dust, drained and then placed in the wire basket and immersed in distilled water as per IS 2386 (part 3)-1963. Average specific gravity of coarse aggregate vary from 2.5 to 2.9 for the given sample the specific gravity is 2.853. Stones having low specific gravity are generally weaker than those with higher specific gravity values. The obtained water absorption of coarse aggregate is 1.462% which lies in between 0.1 and 2%. Properties are shown in Table 2.

Table 2 Physical properties of coarse aggregate

Properties	
Specific gravity water absorption	2.853
	1.462%

Table 3 Physical properties of fine aggregate

Properties	
Specific gravity	2.8
Fineness modulus	3.36
Water absorption	1.01%

2.1.3 Fine Aggregate

The fine aggregate used is M. Sand. Tests on fine aggregates are conducted confirming to IS 2386:1963 (part 1 and part 3). Tests conducted on fine aggregate is sieve analysis and specific gravity. Physical properties are shown in Table 3.

2.1.4 Fly Ash

Fly Ash is the most widely used SCM in concrete and is a byproduct of coal combustion in electric power generating plants [2]. Fly ash can compensate for fine materials that may be lacking in sand quantities and can be very beneficial in improving the flow ability and finish ability of concrete mixtures. The two designations for fly ash used in concrete are Class C and F and are described in ASTM C618. Class C Ash: high calcium contents with low carbon and good pozzolanic and cementitious properties lend this material to use in higher-performance mixtures where early age strength is important. Class F Ash: low calcium ash effectively moderating heat gain during concrete curing and therefore ideal for mass placement conditions and high strength mixtures or use in hot weather climates; Here the Fly Ash used is class F (Table 4).

Table 4 Physical properties of Fly Ash

Properties	
Specific gravity	2.2
Specific surface area	649.9 m ² /kg
Particle size	22.2 μm

Table 5 Physical properties of superplasticizer

Properties	
pH	Minimum 6
Specific gravity	1.19–1.20
Dosage	0.3–0.4%
Colour	Brown liquid

Table 6 Properties of steel fibers

Properties	
Fiber length	30 mm
Specific gravity	7.86
Diameter	0.50 mm
Tensile strength	1186 MPa
Aspect ratio	60

2.1.5 Superplasticizer

Super plasticizers are the essential ingredients in the concrete mix, as they increase the efficiency of cement paste by improving workability of the mix and there by resulting in considerable decrease of water requirement. It disappears cement particles more rapidly in the concrete mix by reducing the surface tension of water and imparting repelling charges to the ions in the solution. This makes the concrete highly workable and flowable even at lower water cement ratios, resulting in increased strength. The superplasticizer used is CONFLO L N which is brown in colour liquid (Table 5).

2.1.6 Steel Fibers

The new alternative for the conventional steel bars or welded fabric is the Steel fibers mixed into the concrete. Here we use the cold drawn hooked end steel fiber which is manufactured by quality base steel bar, which has excellent mechanical properties including high tensile strength. Owing to high strength and uniform distribution of fibers, stresses can be fully dispersed and cracking propagation be effectively controlled [3] (Table 6).

2.2 Mix Proportion of SCC Mixes

The mix proportion was done in accordance with IS 10262: 2019 guidelines [4]. Mix proportions with mineral admixtures and steel fibre is tabulated in Table 7.

Table 7 Mix proportions of various mixes

Mix	SCM	S F (%)	Cement	SCM	F A	C A	S P	Water	Flow diameter (mm)
			kg/m ³						
MF30	Fly ash	–	311	134	938	808	2.67	200	670
M0.5FS30	Fly ash	0.5	311	134	938	808	2.67	200	650
M1FS30	Fly ash	1	311	134	938	808	2.67	200	650
M1.5FS10	Fly ash	1.5	311	134	938	808	2.67	200	630

2.3 Assessment of Rheological Properties of the Mix

To ensure the rheological properties of SCC flow ability, passing ability and segregation resistance tests were performed on control SCC and Steel fibre SCC mixes according to IS 10262:2019 guidelines. Slump flow and T500 slump flow time tests for filling ability, V-funnel test for the viscosity and segregation resistance, L-box and U-box test to assess the flow of concrete and passing ability were performed to study the workability of the mix.

2.4 Drying Shrinkage Tests

Drying shrinkage, in its simplest definition, is the contraction of concrete (either young or mature) due to moisture/water loss to the environment. This very nature also implies the fact that drying shrinkage can happen in any concrete structure as long as there is direct exposure to drier conditions. The magnitude of drying shrinkage depends on the concrete (quality) itself and the characteristics of the environment it is exposed to. Established knowledge so far has acknowledged the effects of such as mix design (e.g. type and quantity of binders, amount of mixing water, type, and grading of aggregates, the presence of shrinkage-reducing admixtures, etc.), curing conditions, size-shape of the members and environmental conditions (e.g. temperature and temperature fluctuation, relative humidity, wind speed, etc.) on its intensity and development over time. The Fig. 1 shows the length comparator machine which is used to measure the drying shrinkage of concrete. Used to measure the length variation of cement specimens, the unit comprises a steel frame with an adjustable height beam, and an analog dial indicator ranging 5×0.002 mm. Drying shrinkage is a long-term loss of moisture in hardened concrete. When concrete shrink, it will gain stress, and when the stress exceeds strength, it will cause a crack (ASTM C157). The drying shrinkage mould is of size $40 \times 40 \times 160$ mm is used to make the mould and let the mixture hardened for 24 h. Take out the specimen from the mould and loosen the knob and set the dial gauge to zero. Place the specimen between the stud for measurement as the initial reading. Rotate the specimen twice to get a consistent reading. Record the dial gauge reading and Immerse the specimen in a curing tank



Fig. 1 Drying shrinkage mould and length comparator. When $L_1 > L_2$; Shrinkage = $\frac{(L_1 - L_2)}{L_1} \times 100\%$ [5]

for 28 days. Take the specimen out and keep it for 24 h outside. Place the reference rod again before keeping the specimen to ensure the readings don't change. Then place the specimen and record the dial gauge reading.

2.5 Compressive Strength

The bearing surface of the testing machine shall be wiped clean and any loose sand or other material shall be removed from the surfaces of the specimen which are to be in contact with the compression platens. The concrete cubes of size $150 \times 150 \times 150$ mm were casted. The specimen shall be placed in the machine in such a manner that the load shall be applied to opposite sides of the cubes as cast, that is, not to the top and bottom. The axis of specimen shall be carefully aligned with the centre of thrust of the spherically seated platen. The load shall be applied without shock and increased continuously at a rate of $\sim 14 \text{ N/mm}^2/\text{min}$ until the resistance of the specimen to the increasing load breaks down and no greater load can be sustained. The maximum load applied to the specimen shall then be recorded and the appearance of the concrete and any unusual features in the type of failure shall be noted. The measured compressive strength of specimen shall be calculated by dividing the maximum load applied to the specimen by cross sectional area of the specimen. The cubes were tested for its compressive strengths for different mixes after curing periods of 7 and 28 days. Average of the results of three cubes was taken for the study.

$$\text{Compressive Strength} = \text{Load at failure} / \text{Cross-sectional Area}$$

Table 8 Rheological properties of the SCC mix

Mix	SF (%)	Slump flow (mm)	T50 (s)	V-funnel (s)	L-box	U-box (mm)
MF30	–	670	1.5	1.3	1.31	30
M0.5FS30	0.5	650	2	1.5	1.20	30
M1FS30	1	650	2.5	2.5	1.022	25
M1.5FS10	1.5	630	2.5	2.7	1.00	20

3 Experimental Results and Discussions

3.1 Rheological Properties of the Mix

In case of the workability of SCC mix various tests like slump flow, T500 time, V funnel, L box and U box for normal Fly ash replaced SCC mix and SCC mix with 0.5, 1 and 1.5% of steel fibre along with replacing cement with Fly ash were conducted. The rheological properties of the mix are given in Table 8 and the test result should fall within the rage as given in IS 10262: 2019.

3.2 Compressive Strength

The compressive strength test were conducted on concrete cube specimen of size 150 × 150 × 150 mm. the results obtained for different mixes were tested after curing periods of 7, 14 and 28 days. From Fig. 2 as the percentage of steel fibers increased the compressive strength also got increased.

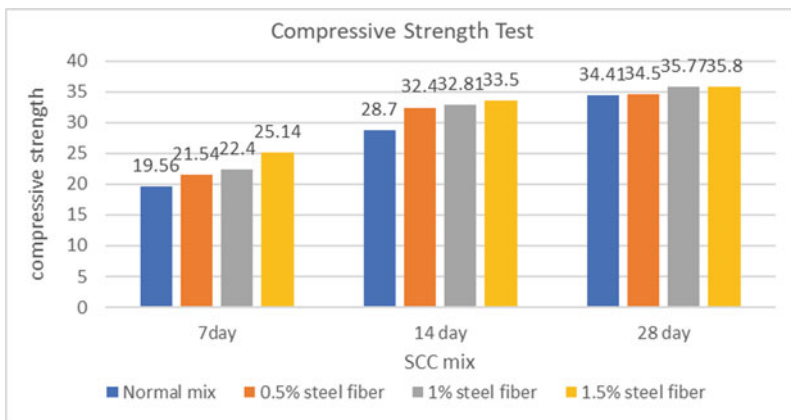


Fig. 2 Compressive strength of concrete mix

Table 9 Calculation of drying shrinkage

SCC mix	S F (%)	Trials (mm)	% Shrinkage	Average
MF30	–	A. 0.035	0.125	0.175
		B. 0.030	0.25	
		C. 0.034	0.15	
M0.5FS30	0.5	A. 0.035	256	43
		B. 0.034		
		C. 0.036		
M1FS30	1	A. 0.037	216	31
		B. 0.037		
		C. 0.036		
M1.5FS30	1.5	A. 0.038	239	36
		B. 0.038		
		C. 0.039		

3.3 Drying Shrinkage

The test results of drying shrinkage of specimens are tabulated below. After the commencement of drying, the shrinkage rate developed rapidly. The chance of drying shrinkage of self-compacting Steel fiber reinforced concrete was also influenced by complex effect of binder materials and steel fibers [5]. The increased binder to coarse-aggregate ratio and fine aggregate ratio had negative effects on the reduction of drying shrinkage of self-compacting SFRC due to the weakness of aggregate skeleton and inevitable loss of free water from macro and micro pores of concrete. Oppositely the steel fibers reduce the drying shrinkage of SCC SFRC. Generally, with the aid of expansive agent, the self-compacting SFRC had a reduced drying shrinkage than normal SCC. As the percentage volume fraction of steel fiber increased the drying shrinkage percentage got decreased from the study (Table 9).

4 Conclusions

With the premise of ensured workability of a fresh mixture, this study of drying shrinkage and mechanical properties of hardened self-compacting SFRC with varying volume fraction of steel fibers. The following conclusion can be drawn from the current experimental study.

- By the addition of more volume fraction of steel fibers in concrete reduces the workability of SCC and significantly affect the compressive strength.

- The mechanical properties of normal self-compacting concrete and SCC -SFRC were improved with the incorporation of 30% Fly Ash and Steel fibers. With the increase in volume fraction of steel fiber from 0.5, 1 and 1.5% the cube compressive strength for 28 days are 34.41, 34.5, 35.77 and 35.8.
- The drying shrinkage percentage of normal SCC, SCC with 0.5, 1 and 1.5% are 0.175, 0.125, 0.0833 and 0.04167.
- The drying shrinkage of self-compacting concrete with and without steel fibers shows a greater difference in drying shrinkage. As the percentage volume fraction of steel fibers increased the drying shrinkage got reduced.
- Thus we can optimize the percentage of steel fiber as 1% to reduce the drying shrinkage in SCC.

References

1. Kashania A, Ngo T (2020) Production and placement of self-compacting concrete. *Self-compact Concr Mater Proper Appl Sci Direct* 12:65–81
2. Gaziantep University Turkey (2013) Performance of self-compacting concrete (SCC) with high-volume supplementary cementitious materials (SCMs). *Eco-Efficient Concrete*. <https://doi.org/10.1533/9780857098993.2.198>
3. Alrawashdeh A, Eren O (2022) Mechanical and physical characterisation of steel fibre reinforced self-compacting concrete: different aspect ratios and volume fractions of fibres. *Results Eng* 13:100335. <https://doi.org/10.1016/j.rineng.2022.100335>
4. IS 10262 (2019) Concrete mix proportioning: guidelines. Bureau of Indian Standards. <http://www.bis.org.in/>
5. Maghfouri M, Alimohammadi V, Gupta R, Saberian M, Azarsa P, Hashemi M, Asadi I, Roychand R (2022) Drying shrinkage properties of expanded polystyrene (Eps) lightweight aggregate concrete: a review. *Case Stud Constr Mater* 16:e00919. <https://doi.org/10.1016/J.Cscm.2022.E00919>
6. Qin D, Dong C, Zong Z, Guo Z, Xiong Y, Jiang T (2022) Shrinkage and creep of sustainable self-compacting concrete with recycled concrete aggregates, fly ash, slag, and silica fume. *Am Soc Civil Eng* 34:22236. [https://doi.org/10.1061/\(ASCE\)MT.1943-5533.0004393](https://doi.org/10.1061/(ASCE)MT.1943-5533.0004393)
7. Chen W, Xie Y, Li B, Li B, Wang J, Thom N (2021) Role of aggregate and fibre in strength and drying shrinkage of alkali activated slag mortar. *Constr Build Mater* 299:124002. <https://doi.org/10.1016/j.conbuildmat.2021.124002>
8. Sinha DA, Verma AK (2017) Investigation on the effect of varying dosage of steel fibre on the strength and workability properties of high strength concrete. Kalpa Publications in civil engineering
9. Yousefieh N, Joshaghani A, Hajibandeh E, Shekarchi M (2017) Influence of fibers on drying shrinkage in restrained concrete. *Constr Build Mater* 148:833–845. <https://doi.org/10.1016/j.conbuildmat.2017.05.093>
10. Gueciouer D, Youcef G, Tarek N (2019) Rheological and mechanical optimization of a steel fiber reinforced self-compacting concrete using the design of experiments method
11. EFNARC (2002) Specifications and guidelines for self-compacting concrete. EFNARC, Association House. www.efnarc.org
12. IS: 4031 (1996) Method of physical tests for hydraulic cement: specification. Bureau of Indian Standards, New Delhi. <http://www.bis.org.in/>

Accessibility Analysis of Kochi Metro



Jeeva P. Winto, Amrutha S. Chandran, Namitha Dilip, and Sandra Shyin

Abstract Kochi metro is one of the most thriving transit systems in Kerala, as it is a rapid transit mode that helps in fast and efficient movement of the public. Accessibility of Kochi metro still remains a challenge at some point, though it is a necessary factor to make the metro service more convenient and attractive to the public. Moreover, it is generally perceived that land-use examples and traffic designs are firmly connected through changes in availability. In this work, we survey a group of Kochi metro commuters to study their metro convenience preferences. This study mainly concentrates on three pertinent areas, which are accessibility analysis of Kochi metro, that takes into account both to-metro accessibility and from metro accessibility in order to assess and categorize the performance of the metrosystem, formulation of accessibility index with the data collected and development of mobile application for improving the ease of accessing metro for commuters. A switch from private to public modes of transportation has always been necessary due to expanding urbanization, population growth, and traffic. The study aims to improve the level of accessibility for commoners, to flourish the public transit systems connecting metro stations and regions around and also to reduce the economic woes in most practical ways. After the study, an application embracing relevant information on accessibility of metro stations including nearest public transit systems and their corresponding details will be developed.

Keywords Accessibility · Kochi metro · LOS · Accessibility index

J. P. Winto · A. S. Chandran (✉) · N. Dilip · S. Shyin
Department of Civil Engineering, Adi Shankara Institute of Engineering and Technology, Vidya
Bharati Nagar, Mattoor, Kalady, Kerala, India
e-mail: amruthasubrahmanian@gmail.com

N. Dilip
e-mail: namithadilip2k@gmail.com

S. Shyin
e-mail: sanshyinammu@gmail.com

1 Introduction

1.1 General

Transportation systems are viewed as the foundation of development of any city systems and have a big impact on how efficiently and quickly things move through the facility. Human existence and development have always depended on the movement of people, goods, and services from one location to another. The infrastructure of transportation must play a crucial part in this growth for successful advancement as the world becomes increasingly globalized and organized. The transfer of goods and passengers between two locations by a single transport operator using various modes of transportation is known as multimodal transport. It investigates how to coordinate the employment of two or more modes of transportation for swift, secure, enjoyable, and comfortable passenger mobility in metropolitan areas and hence more connections and options are available. Inter connected travel by means of public transportation, railroads, waterways, bicycles, and foot travel can all be considered under multimodal mobility.

Urban rapid rail transit networks are crucial components of contemporary urban transportation infrastructure, especially in densely populated big cities. Their accessibility has a significant impact on the layout of cities, how people move around, and how comfortable urban environments are. Therefore, the purpose of this study is to assess how accessible an urban rapid transit network is in. It also appears that the creation of the metro network has been considered as one of the most effective ways to address the problems with urban transportation. In the state of Kerala, Kochi is the most potential region for growth-oriented development. In the past twenty years, the city and its surroundings have undergone rapid development. The deterioration of the urban environment and the growing traffic congestion in Kochi City are the most obvious problems. The Kochi City Region is expanding quickly and could become a metropolitan city within the plan period, which could demand reviewing the development plan that includes the metropolitan region. KMRL recognizes the importance of transportation services in a city for access to education and economic opportunities, and are constantly working for improving the services for Kochi residents. KMRL also recognizes the importance of effective information communication in making the metro more accessible. Metro is a quick, dependable, practical, effective, contemporary, and cost-effective form of urban transportation. Elevated Metro Rail is safe and environmentally sustainable, taking up only around 1.80 m of the road's width and uses one fifth of the energy per passenger km as compared to systems based on roads.

Accessibility, particularly refers to the qualities of transportation modes across various regions via a transportation network, has indeed been frequently used to assess the connectivity and structure of a transportation network. Accessibility is influenced by a variety of factors, including mobility (physical movement), the effectiveness and cost of available transportation options, the interconnection of transportation networks, mobility aids, and land use patterns. Accessibility can be

assessed from a variety of angles, including the viewpoint of a certain group, mode, place, or activity. Some of these considerations and viewpoints are frequently overlooked and undervalued in conventional planning. A more thorough consideration of accessibility during planning broadens the range of feasible fixes for transportation issues. The objectives identified are to:

- Qualitatively assess and categorize the performance of the Kochi metro system [1]
- Develop an accessibility index [2]
- Develop a mobile application for Kochi metro users.

2 Methodology

2.1 Study Area

One of the main port cities in the West Indian coastal regions is Kochi. This city shown in Fig. 1 is found in Kerala's Ernakulam district and is bordered by the Arabian Sea, frequently referred to as Ernakulam. This second-largest city in Kerala is regarded as the state's top location for drawing both domestic and foreign tourists. This bustling metropolis is renowned for offering breath taking views of Kerala state. Aside from that, this city serves as the state's industrial and commercial hub. Kochi is situated between north latitude $9^{\circ}56'23''$ and east longitude $76^{\circ}15'36''$. The city has 94.88 km^2 of densely inhabited land. According to official Census India report, Kochi's population in 2011 was 602,046 with an average population density of 6287.

The study areas chosen were Aluva shown in Fig. 2a, Edappally shown in Fig. 2b, and Ernakulam South shown in Fig. 2c metro stations. Aluva is the starting point of metro having high passenger flow because of the availability of nearby transportation facilities like railway stations, KSRTC and private bus stands and Cochin International airport. The Edappally metro station is situated above the Edappally crossroads, one of Kerala's busiest road intersections.

Due to its proximity to important sites like Edappally Church and Lulu Mall, it is one of Kochi Metro's busiest stops. Ernakulam South station situated near Ernakulam Junction railway station which is one of the biggest railway stations in Kochi. This metro station is also located near to KSRTC bus stand.

2.2 Study Parameters

After researching the variety of accessibility measures, various researchers have put forth fundamental requirements that the accessibility measure must satisfy. As a result of the fact that our study is focused on metro accessibility, we were able to extract the data using ten different parameters. Firstly, origin and destination, time

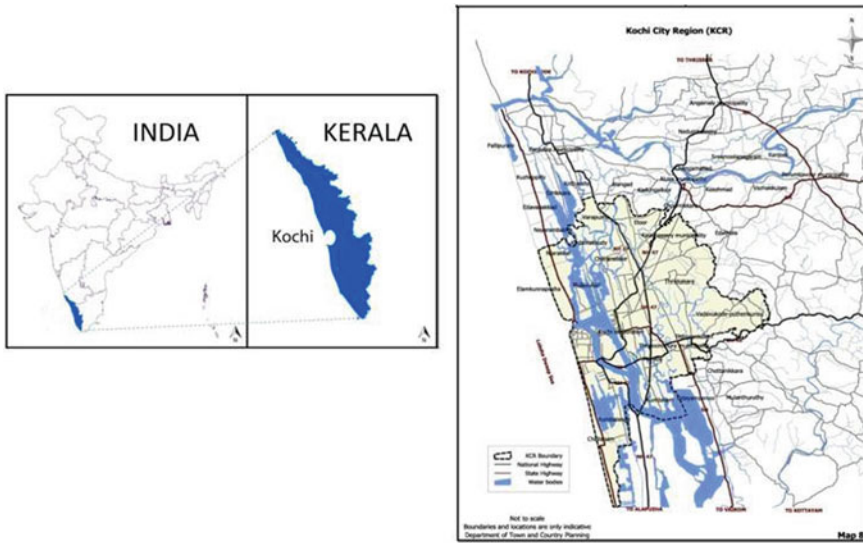


Fig. 1 Location map of Kochi City

and distance for travel, personal details of the commuters which includes their age, occupation, gender, mode of travel to reach metro station. Parking facilities, accuracy and punctuality as well as coordination of metro trains were also taken as parameters as it affects the accessibility. Following are the major parameters that are needed for assessing accessibility [3]: Determining the time travel by the metro, time travel by the Bus, distance covered by the metro, time taken for reaching the hubs by the metro (from ALUVA), time taken for reaching the hubs by the bus, transfer time from metro to hub (From nearest metro station), transfer time from bus to hub.

2.3 Data Collection

The study is being done to find out how easy it is for the general public to access the Kochi Metro and to identify the most economical mode of intermediate transit to reach metro as well as their desired destination. Through a questionnaire survey [4], the accessibility index is determined. Questions for the survey are formulated based on parameters upon which the accessibility depends. Survey is conducted at four different metro stations.



Fig. 2 a Aluva; b Edappally; c Ernakulam South

3 Pilot Survey Approach

Passenger survey form was created and pilot-tested before it was completed in two phases: online and in-person. Questionnaire prepared was based on the parameters that affected [3] the accessibility. Conducted a pilot study [5] for assessing the survey’s readability and understandability and to monitor the average amount of time required to complete the survey. These participants suggestions incorporated into the final version. The pilot survey took < 5 min to complete. Also created a QR code for commuters to scan and enter the data by themselves. A total of 17 questions

were framed as questionnaire. Anonymous responses were collected for both the online and in-person versions of the survey. About 100 responses were obtained of which 89 valid responses are evaluated, due to incomplete responses received through online survey. A pilot survey is a miniature survey that the researcher conducts with a smaller sample size than the intended audience. One can forecast participant response patterns and adjust the research as necessary by gathering data from a convenience sample. The primary goal is to test the research instruments, such as the survey questions, layout, and distribution methods. Also, it is easier to find any instances of exclusion in the survey questions and design based on the input given by pilot phase respondents. If done properly, it aids in identifying difficulties that may impair the main data collection procedure.

After identifying the parameters questionnaire was prepared in a platform called **JotForm**. It is San Francisco based company which enables to create free online forms, collect responses directly to mail and creates fillable PDF forms. It is easy to use for professional works as it is more versatile than google forms.

Following were the questions included for pilot survey questionnaire:

1. Personal information (Name, Age, Gender, Employment status).
2. Are you differently abled?
3. Where are you coming from and going to?
4. How often do you use metro in a week?
5. Purpose of travel?
6. Mode of transport used to reach metro station.
7. Are you satisfied with parking facility provided?
8. Have you faced any discrimination?
9. 5 scale preference rating on comfort, safety, timing, behavior of staff, facilities inside station and cleanliness.
10. Any suggestions.

4 Rating Survey

Several conclusions were made after conducting pilot survey at different metro stations. It was identified that a few of the parameters are to be changed and questionnaire was to be formulated accordingly. Vyttila metro station was eliminated, and a new study area, Edappally metro station, was added. The Vyttila metro station has a low volume of passengers compared to Edappally, MG road, and Maharajas college. Additionally, the Vyttila metro station features similar transit amenities as the Aluva metro station, including a local mobility hub and water metro. To improve the questionnaire, awareness about feeder bus services from metro and to metro question was added. The final questionnaire was administered in English and consisted of 30 questions includes demographic, socioeconomic, and choice-set questions. Survey was conducted similarly as pilot survey and 450 samples were collected from these three desired metro stations. Every Tuesday, Saturday and Sunday, during peak and non-peak hours, the survey was completed at the targeted stations from the month

of November (2022) to March (2023). From the responses obtained through questionnaire survey accessibility index was formulated. Following were the questions included in questionnaire survey:

1. Personal information (Name, Age, Gender, Employment status).
2. How often do you commute?
3. Purpose of travel.
4. Trip origin (home, office, hospital, educational institutes etc.).
5. Boarding station.
6. Mode of ticket (counter ticket, E-ticket, Kochi one card).
7. Time taken to board metro.
8. Mode of transport used to reach metro station.
9. Time taken to reach boarding station.
10. Approximate distance travelled to reach metro station.
11. Alight station.
12. Time taken to get out of metro (after reaching station).
13. Trip destination (home, office, educational institute etc.).
14. Mode of transport used to reach trip destination from alight station.
15. Time taken to reach trip destination from alight station.
16. Other mode used to reach destination (if not boarding on metro).
17. Approximate distance travelled to reach destination.
18. Are you satisfied with the parking facility provided?
19. Are you aware about KMRL feeder bus?
20. If yes, do you use feeder bus service?
21. 5 scale rating on metro services provided (comfort, safety, timing, behavior of staff, facilities inside station, cleanliness and availability of signage).
22. 5 scale rating of intermediate transit system from metro stations (auto, bus, cab service, train).
23. Any suggestions for improving existing services at metro station?

This QR code was provided to commuters as a part of online survey (Fig. 3).

Fig. 3 QR code scanner



4.1 Level of Service

A concept called level-of service (LOS) [6] of a traffic system was developed to link the level of service provided by a given flow rate to that flow rate. HCM introduced the concept of “Level-of-Service” to describe the level of quality one can have from a location under various conditions of operation and traffic volume [7]. HCM suggests using the letter “LOS” to denote a variety of operational circumstances for a certain kind of facility. HCM defines six LOS levels from A to F, in which A stands for best service quality and F for the lowest based on measures of effectiveness of that facility. LOS is based on the factors such as speed, travel time, density, delay etc. For each of the LOS levels there is a corresponding service volume known as service flow rate. Service flow rate is defined as the greatest number of vehicles, people and other similar objects that can be carried by a specific facility or system under specific circumstances at a specific LOS. Various indicators that were used to assess the quality of metro are comfort, safety, timing, behavior of staff, facilities, cleanliness and availability of signage.

5 Evaluation of LOS

LOS can be determined by multiplying the user score for each indication by the relevant weightage, then dividing that result by overall weightage. The user score can be calculated as the average of all survey response scores.

The formula for calculating overall LOS is shown in Eq. (1) [1] below.

$$LOS = \frac{\text{User score} \times \text{weightage}}{\text{Total weightage}} \tag{1}$$

The end result will be a number that ranges between 1 and 5, and the LOS assessment will be given as a grade between A and D. The determined LOS and rating grade are shown in Table 1 [1].

Table 1 LOS grading [1]

Calculated LOS	Grade
4–5	A
3–4	B
2–3	C
1–2	D
0–1	E

5.1 Accessibility Index

The main purpose of the accessibility index is to serve as a measure of accessibility [8]. An area is considered to be more accessible if its accessibility index is greater. There are several ways to define [3] and assess a location's accessibility for travelers on business, leisure, or social travels. These include accessibility via various modes as influenced by trip duration, cost, geographic coverage, and service frequency; travel safety or privacy; comfort and dependability during travel; and the availability of services seven days a week and around-the-clock. Accessibility also refers to the ability for people with disabilities to properly use the facilities offered. Accessibility measurement techniques have been developed and are in use. In transportation studies, isochrons have frequently been used to highlight accessibility. These quantify the convenience of utilizing public transportation routes, typically from residential locations, in terms of time and distance without taking the intention, destination, or cost of the trip into account. Special features of the accessibility indices are as follows:

- (a) Public transportation, private vehicles, and other modes of transportation are directly compared, taking into account elements that represent local and regional efforts to reduce reliance on private vehicles, such as elevated parking fees, bus prioritization, ticket structuring, and related measures.
- (b) The idea of equality in transportation is a crucial foundation for comparing modes.
- (c) The indices have no weighting or other elements that would make them difficult for non-technical individuals to grasp because they are directly related to travel duration and prices.

6 To and from Accessibility Between Nearby Bus Stops and Point of Interests (POIs)

- (a) *Point of Interest (POI)*: Metro stations where the level of accessibility will be evaluated [2].
- (b) *Service Access Point (SAP)*: The nearest bus stations serve as service access points for public transportation [2].
- (c) *Walk Time (WT)*: Time required for pedestrians to walk from closest bus stations to a metro station [9].
- (d) *Average Waiting Time (AWT)*: Time frame when a passenger enters at an SAP until the requested service comes [9].
- (e) *Scheduled Waiting Time (SWT)*: Half the amount of time between transit vehicle arrivals at a stop [2].
- (f) *Total Access time (TAT)*: $WT + AWT$ [2]

- (g) *Equivalent door-step frequency (EDF)*: The concept is to apply the access time as a hypothetical average waiting time since the route was available close to the chosen POI [2].
- (h) *Public Transport Accessibility Level (PTAL)*: The PTAL [10] is a tool used in the UK for development planning that shows the density of the public transport system in a given area and evaluates the accessibility of various geographic areas to public transport.

The following is a basic explanation of the accessibility index calculation method [2].

The nearby bus stops (SAP) for each metro station (POI) were determined. After that WT between the POI and SAP was manually computed. In Eq. (2), AWT was calculated using the frequency of services on all of the valid bus routes during peak hours. Since the SWT is assumed to be half the headway, the hourly frequency (f) in the calculation is reduced by half. A reliability factor (K), which is 2 min for buses, is added to the SWT to make the computations more accurate.

$$AWT = 0.5 \frac{60}{f} + K \tag{2}$$

“Equation (3) [2] shows the estimated minimum TAT for each route at each SAP”.

$$TAT = WT + AWT \tag{3}$$

Next step includes conversion of TAT into EDF by dividing TAT with 30 as depicted in “Eq. (4)” [2].

$$EDF = \frac{30}{TAT} \tag{4}$$

The route with the highest frequency, known as the most dominant route, was given a weighting value of 1.0; all other routes were given a weighting factor of 0.5. Consequently, the AI is determined using “Eq. 5” [2] for a certain transport mode (m).

$$AI_m = EDF_{max} + 0.5 \sum_{\text{all other routes}} EDF \tag{5}$$

“Equation (6)” [2] describes how to calculate the accessibility index for a POI.

$$AI_{POI} = \sum_m AI_m \tag{6}$$

Eight bands of PTAL are assigned to the AIs obtained for each POI as shown in Table 2 [2].

Table 2 PTALs [2]

PTAL	Range of index	Description
1a (low)	0.01–2.50	Very poor
1b	2.51–5.00	Very poor
2	5.01–10.00	Poor
3	10.01–15.00	Moderate
4	15.01–20.00	Good
5	20.01–25.00	Very good
6a	25.01–40.00	Excellent
6b (high)	40.01 +	Excellent

6.1 APP Development

A user-friendly mobile application called “GOMET” has been created that may be used to find touristic, recreational and other important locations nearby the selected metro station using flutter. A thorough passenger survey was conducted at Aluva, Ernakulam South and Edappally metro stations to gather data and content for our application. Based on factors that affect accessibility, survey questions for developing the app’s features were created. The origin and destination of the passengers, the distance travelled, the time spent travelling and the reason for the trip were all chosen as evaluation criteria. Parking facilities were also included, as were out vehicle travel time which comprises access, waiting and egress times. All feeder services offered at the metro stations and in the user’s, areas are included in our app along with the time and distance taken to reach the destination. The commuter is helped by the app to reach their destinations in the most affordable way. By guaranteeing that passengers will arrive at their destination to and from the metro station in safety and comfort, this app promotes the idea of improving metro accessibility.

7 Results and Discussion

7.1 Pilot Study

Figure 4 shows that most of the Kochi metro commuters, that is about 72.73% are using metro services for < 3 times a week, and about only 2.27% commuters are using it frequently for about 6–10 times a week.

Figure 5 illustrates the mode of public transport the commuters have used for reaching their metro stations. Here it is observed that 50.56% users have opted buses as their mode of transport to reach their desired metro stations, whereas, about only 1.12% have used cab services to reach their stations.

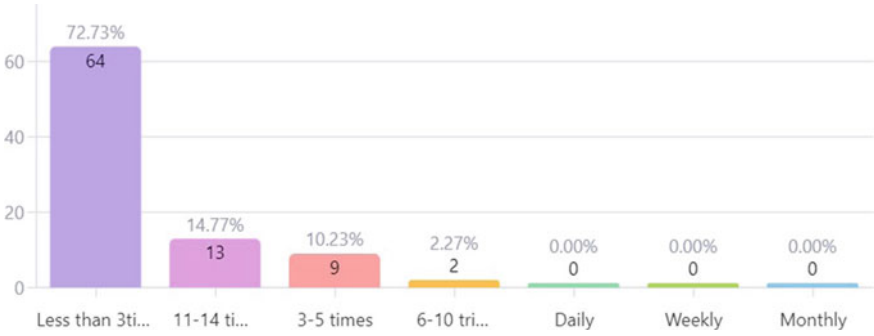


Fig. 4 How often metro is used in a week

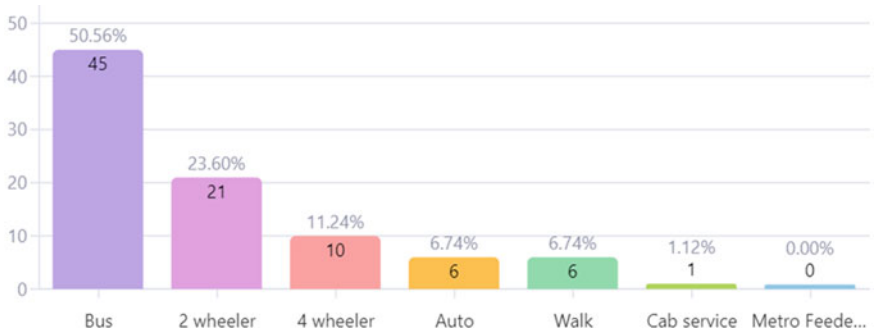


Fig. 5 Mode of transport used to reach metro station

In the following, Fig. 6a, b, age range as well as their gender is shown. Most of the metro users were in the age range of about 21–30 years while only 2.22% were above 60 years and also in the second figure about we can see that most of the commuters were female.

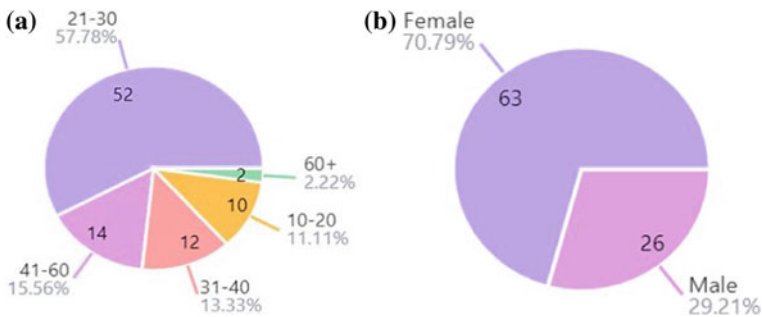


Fig. 6 a Age range; b Gender

Table 3 Satisfaction of present parking facilities

Data	Response	Percentage (%)
Yes	58	65.17
No	31	34.83

Table 4 Employment status of commuters

Data	Response	Percentage (%)
Student	53	58.89
Employed full time	23	25.56
Homemaker	5	5.56
Unemployed	4	4.44
Self-employed	3	3.33
Employed part time	1	1.11
Retired	1	1.11

Here in this Table 3, it is observed that out of the total responses only 58 commuters were satisfied with the parking facilities provided by the Kochi metro service system, and about 31 commuters were facing several problems while using the parking facilities provided.

Table 4 shows that most of the commuters that preferred to use metro services were students and only about a few percentages of users were retired.

7.2 Rating Study

From Fig. 7a it is understood that 22.95% of all commuters took the metro at least once each month, and only 10.23% were using it occasionally. According to Fig. 7b, 25.19% of the commuters used the metro as their means of transportation to go to their workplaces.

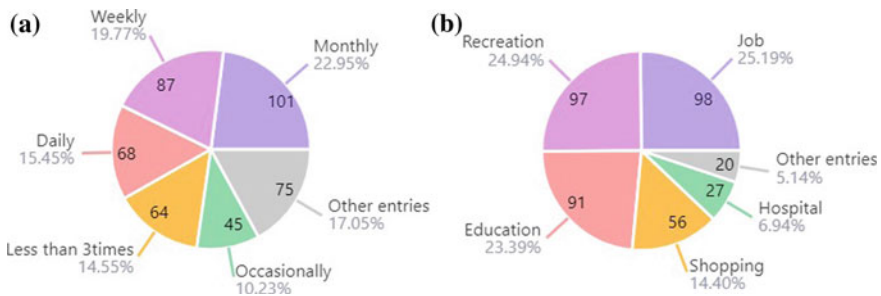


Fig. 7 a How often do you commute; **b** Purpose of travel

Table 5 Mode used to reach metro station

Data	Response	Percentage (%)
2-Wheeler	129	28.67
Bus	106	23.56
Walk	91	20.22
Auto	59	13.11
4-Wheeler	47	10.44
Other entries	18	4.00

Out of 450 responses, Table 5 indicates that 129 users chose to travel by two-wheeler to go to their targeted metro stations, and only a total of 18 users were travelling using other modes of transport to reach their destination.

From the following Fig. 8 it can be inferred that most of the metro users were taking only a maximum time of 10 min to reach metro stations.

The data in Table 6 reveals that many passengers used foot travel to get from one metro station to their desired destination.

From Table 7 it is inferred that, 46.43% of the travelers took just under 10 min to get to their destination from the corresponding metro stations, and about 0.82% of the users took about 40–60 min to reach their location.

Table 8 indicates that 152 passengers used public transportation, such as buses, to get to their destination rather than preferring other means of transportation.

Fig. 8 Time taken to reach boarding station

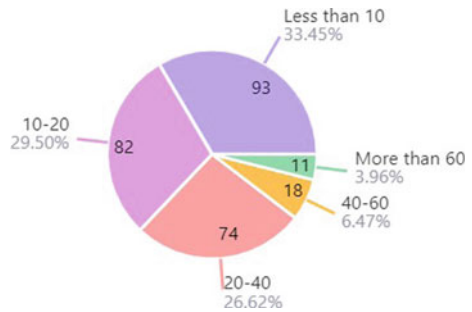


Table 6 Mode used to reach trip destination (from alight station)

Data	Response	Percentage (%)
Walk	117	31.97
Bus	101	27.60
Auto	85	23.22
Two-wheeler	22	6.01
Cab service	20	5.46
Other entries	21	5.74

Table 7 Time taken to reach trip destination (from alight station)

Data	Response	Percentage (%)
< 10 min	169	46.43
10–20 min	118	32.42
20–40 min	67	18.41
40–60 min	7	1.92
More than 60 min	3	0.82

Table 8 Other mode used to reach trip destination

Data	Response	Percentage (%)
Bus	152	41.64
Two-wheeler	70	19.18
Four-wheeler	61	16.71
Cab service	42	11.51
Train	21	5.75
Other entries	19	5.21

7.3 LOS of Kochi Metro

Figure 9a–c depicts cleanliness, timing and comfort respectively, shows that all the three service qualities were having an excellent rating which ranges from 69.40 to 72.28%.

It was able to deduce from the responses to the questionnaire survey that about 296 passengers gave the behavior of the employees an excellent rating, as shown in Fig. 10a, and ~ 278 passengers gave the amenities available inside the station as shown in Fig. 10b.

A 5-star rating was given by ~ 45.58% of the commuters for the accessibility of the station’s signage as shown in Fig. 10c, while a 73.83% response rate was obtained from survey respondents for safety as in Fig. 10d.

Table 9 gives an overall weighted average of LOS for 7 different parameters as listed, for 3 different metro stations such as Aluva, Edappally and Ernakulam South.

7.4 Accessibility Index of Kochi Metro

Only buses were taken into account while calculating the accessibility index because other forms of transport also offer door to door services. Four alternative bus routes were chosen for each metro station (SAP) and the equivalent door frequency of the buses along these routes was calculated. The accessibility index was created by adding the EDF value for each route multiplied with the appropriate weighting factor and integrating all the routes together. Table 10 shows the accessibility indices of

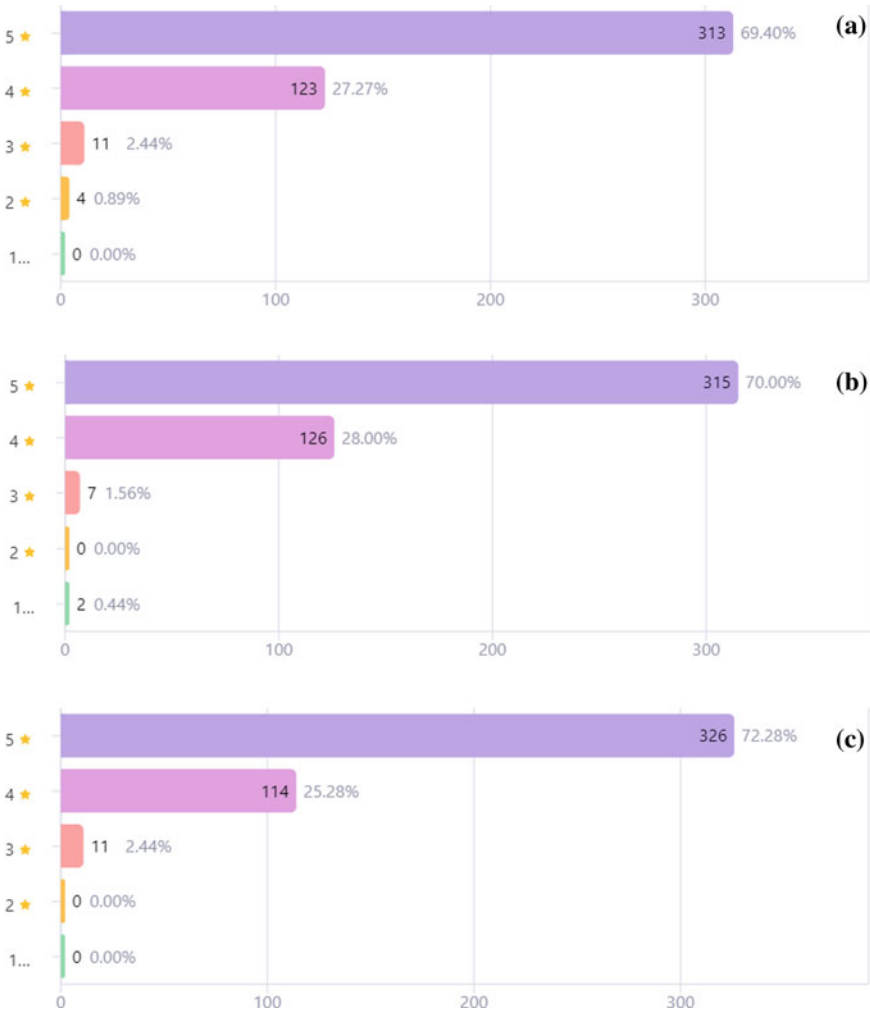


Fig. 9 a Cleanliness; b Timing; c Comfort

metro stations Aluva, Edappally and Ernakulam South respectively. From these three indices a single accessibility index is determined, which brings us to a conclusion that Kochi metro is highly accessible to everyone.

Accessibility index of Kochi metro (Point of Interest) is given by:

$$AI_{POI} = 10.115 + 12.42 + 13.62 = 35.797$$

The result lies in the index range of 25.01–40.00 corresponding to the PTAL grade of 6a, which indicates excellent.



Fig. 10 a Behavior of staff; b Facilities inside station; c Availability of signage; d Safety

Table 9 Calculated LOS of Kochi Metro

Metro stations	LOS
Aluva	4.59
Edappally	4.58
Ernakulam South	4.57

Table 10 Calculated AI of Kochi Metro

POI	Accessibility index
Aluva	10.115
Edappally	12.42
Ernakulam south	13.262

7.5 GOMET Mobile Application (Version 1.0.0)

The programme allows to easily travel to a locus by one click and displays fare to that destination by different modes of transport. This app helps to find the information right away to avoid searching unfamiliar places. The station icon on the home page links to a page that shows the three stations. Any station can be selected to display neighboring hotels, restaurants, and tourist attractions. The cost to travel there via various means is displayed when choosing any of the locations on the page. The primary goal of the app is to persuade users to shift from using private to using public transit (Fig. 11).

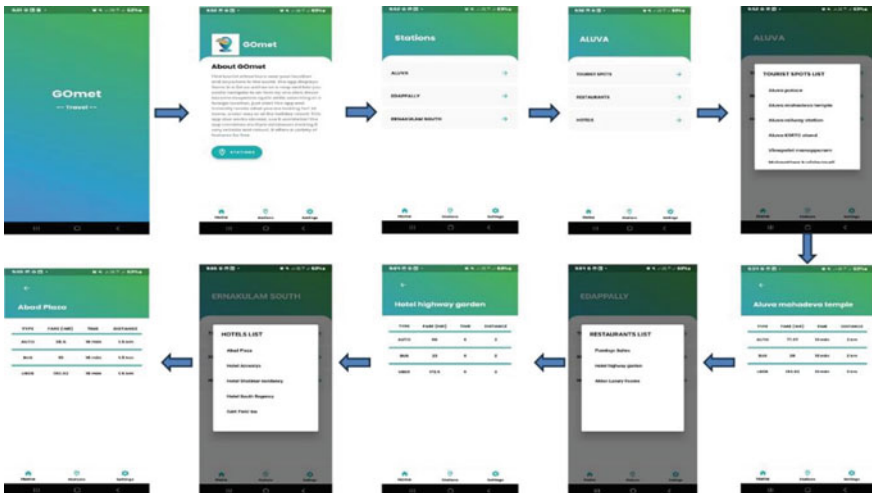


Fig. 11 GOMET App

8 Conclusion

It's important to make travel safe and comfortable for people of all abilities, which is what accessibility aims to achieve. Accessibility is becoming more acknowledged as a crucial component of a rising, effective, and sustainable transportation system. Accessibility analysis is divided into two parts (a) to-metro and (b) from-metro. To-metro accessibility is the ease of reaching a station from a given location and from-metro accessibility is the ease of reaching destination from the station. The findings of the pilot study indicates that Edappally metro station is also needed to be included among the study areas as it is difficult to access metro and other public transit modes due to heavy traffic flow, which helps in improving the accessibility analysis study.

It is noticed that online surveys were easier for youngsters and difficult for elder community. Changes were made in the questionnaire after identifying several other parameters which is an aftermath of pilot study. This study enabled to enhance the research and to assess more about the difficulties of commuters in to-metro and from-metro accessibility. Rating survey or main survey questionnaire was prepared after applying the changes in the pilot survey questionnaire. Study area was also changed which previously included 3 metro stations. Edappally metro station was added in place of Vyttila along with Aluva, and Ernakulam South metro stations.

After conducting pilot and rating survey, we came to a conclusion that most of the metro users were female passengers. It was also found that most of their commuters were of the age range 21–30. Due to the metro's proximity to the city's main thoroughfare, it has become a convenient and affordable means of transportation for those seeking to travel along this route. From the survey it was noticed that the commuters travelled within the time range of ten minutes. LOS and accessibility index were developed from the combined data obtained through surveying. The results showed that the quality of service provided by the metro was rated 'A' along with an accessibility index that was acquired as excellent.

Mobile applications are widely used in this modern era. Every service offered to public now has an online version. A mobile application was built using Flutter Software which showcases the features that helps in improving accessibility of metro. The software can be altered in the future to suit the needs, and the research area can be expanded to include all metro stations.

References

1. Amal Krishna KA, Haritha B, Shilpa Mol TO, Sriganesh V, Winto JP (2021) Shortest path analysis and service levels of emergency services in Kalady. *Int J Eng Res Technol* 10(06):15694
2. Shah J, Adhvaryu B (2016) Public transport accessibility levels for Ahmedabad, India. *J Public Transp* 19:19–35. <https://doi.org/10.5038/2375-0901.19.3.2>
3. Litman T (2008) Evaluating accessibility for transportation planning. Victoria Transport Policy Institute, Victoria

4. Bajaj G, Singh P (2019) Understanding preferences of Delhi Metro users using choice-based conjoint analysis. *IEEE Trans Intell Transp Syst* 128:1–10. <https://doi.org/10.1109/TITS.2958259>
5. Schoon JG, McDonald M, Lee A (1999) Accessibility indices: pilot study and potential use in strategic planning. *Transp Res Rec* 1685(1):29–38. <https://doi.org/10.3141/1685-05>
6. Cyril A (2021) Level of service test on public transport facilities in Trivandrum city. *Int J Recent Technol Eng* 8:319
7. Highway Capacity Manual (HCM) (2000)
8. Mamun S, Lownes N (2011) A composite index of public transit accessibility. *J Public Transp* 14:69–87. <https://doi.org/10.5038/2375-0901.14.2.4>
9. Yang R, Liu Y, Jingtian S, Gan V (2019) Comprehensive public transport service accessibility index: a new approach based on degree centrality and gravity model. *Sustainability* 11:5634. <https://doi.org/10.3390/su11205634>
10. Cooper S (2006) Measuring public transport accessibility levels: sub matter 5b parking strategy, transport for London. <http://sharepoint.bromley.gov.uk/Public%20Docs/APPENDIX%20L.pdf>

Study of Seismic Behaviour of Bent Shear Panel Dampers in Braced Steel Moment Resistant Frame



Aishwarya Shine and P. Anima

Abstract Shear Panel Dampers (SPDs) can be mounted vertically in frames to effectively increase its load bearing capacity and ductile performance. Through plastic deformation, SPD can dissipate the energy in the frames under seismic conditions. Vertically installed dampers may impose an additional bending moment on the middle of the primary beam, which results in significant damage of the concrete slab. A novel type of SPDs with bent web panels (BSPDs) were developed to overcome this limitation, where the end plate of the Bent Shear Panel Damper (BSPD) is connected to the web of the beam. Here, the bending moment resulting from the SPDs can be minimized, thereby reducing the damages caused to the concrete slab. The aim of introducing BSPD in a braced steel moment resistant frame (SMRF) is to enhance the seismic resilience of the braced SMRF. This study involves the design, optimisation, and assessment of the damper's performance under seismic loading. Finite element analysis software ANSYS was used for the analysis and optimization of the damper. The design parameters include the thickness, length, and breadth of the damper. The goal of the optimization is to achieve the best energy dissipation performance. The stress, strain, and deformation properties of the dampers under seismic load are assessed. After the optimization of damper, time hysteresis analysis was done by installing the damper in a 5 storied frame.

Keywords Shear panel damper · Seismic resilience · Energy dissipation · ANSYS · Braced steel moment resisting frame · Cyclic loading

A. Shine (✉) · P. Anima
Universal Engineering College, Thrissur, Kerala, India
e-mail: aishwaryashineaish@gmail.com

1 Introduction

An earthquake is a quick natural calamity that can release a lot of energy and cause the earth's crust to vibrate. Property and human lives are seriously threatened by every earthquake. In recent decades, a wide variety of structural control systems have been applied to enhance the seismic performance of engineered structures. Dampers are one among them.

Many methods have been put forth to improve the energy dissipation and deformation capabilities of conventional steel structures and to minimise the damages caused to the structure. Chan et al. [1] researched on shear panel dampers (SPDs), which are often adopted as energy dissipation tool to improve the seismic performance of a structure. The most common kind of dampers used are metallic ones. The advantages of metallic dampers include their reasonable price, easy fabrication and availability. The energy dissipation capacity of metallic dampers is mainly determined by the hysteretic performance obtained through the inelastic deformation of the dampers. A new type of metallic damper was suggested by Chen et al. [2], graded yield metal damper possessing two yield points. The novel damper is effective at reducing responses to earthquakes of various intensities as well as structural damage to buildings. Shayanfar et al. [3] performed a numerical simulation to examine eccentrically braced frame structures with multiple vertical links, the results indicated that by using several vertical linkages, the link size can be lowered while retaining the structure's seismic performance. Rahnavard et al. [4] used ABAQUS software to create the finite element model of a composite frame with one and two vertical linkages and to undertake seismic performance assessments. The findings showed that EBCFs with two vertical connections exhibit higher energy dissipation capacity and can more successfully accomplish the desired ductile failure mode than frames with a single link. Zhao et al. [5] focused on hysteresis dampers known as bent shear panels, which may effectively absorb seismic energy to reduce damage to the main structural elements. They are frequently employed in seismically active areas to withstand wind or earthquake stresses. The boost in structural energy dissipation capacity brought on by the steady hysteretic behaviour is the main advantage of using bent shear panel dampers.

This study involves the design and optimization of the bent shear panel damper (BDSP) and the evaluation of its performance under seismic loading. The BSPD is a type of damper that is commonly used in steel frame buildings to mitigate the effects of earthquakes. It consists of a steel plate that is bent into a sinusoidal shape and attached to the bracing members of the frame. When an earthquake occurs, the plate undergoes cyclic deformation, dissipating energy and reducing the overall seismic force on the building. The optimization of the BSPD was carried out using Ansys software. Ansys is a finite element analysis software package widely used for engineering simulations. The performance metrics considered included the maximum deformation, maximum stress, load bearing capacity and ductility performance of

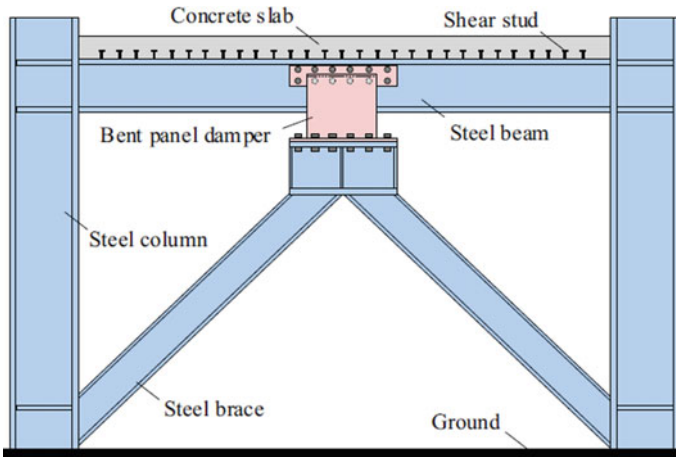


Fig. 1 Configuration of BSPD [5]

the damper. This paper provides a detailed description of the optimization process, including the methodology used, the results obtained, and their significance. Overall, the project has significant implications for the safety and durability of steel frame buildings in high seismically active regions (Fig. 1).

2 Analysis and Design of Braced SMRF (Without Damper)

A braced steel moment resistant frame of 9 m × 4 m span without a damper was modelled, analysed and designed. The overall performance of braced SMRF was noted using ANSYS Workbench 2022 R2. Table 1 gives the load bearing capacity and ductility performance of a braced SMRF without dampers (Figs. 2 and 3).

Mesh size is a crucial factor in finite element analysis (FEA), as it determines the level of detail and accuracy of the simulation. In this case, the mesh size of 50 mm was provided. The meshing process involves creating a finite element model of the structure, which consists of small elements that are connected to form a mesh.

Table 1 Results of braced SMRF

Configuration	Deflection (mm)	Load (kN)	Ductility factor
Brace	16.43	4355.20	4.10

Fig. 2 Meshing of the specimen

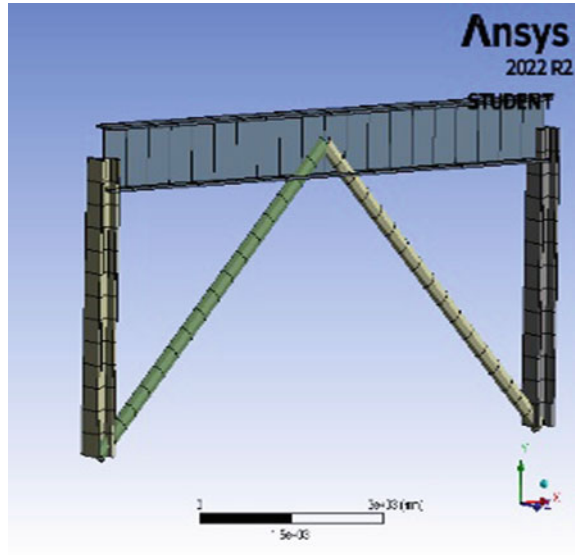


Fig. 3 Total deformation of the specimen

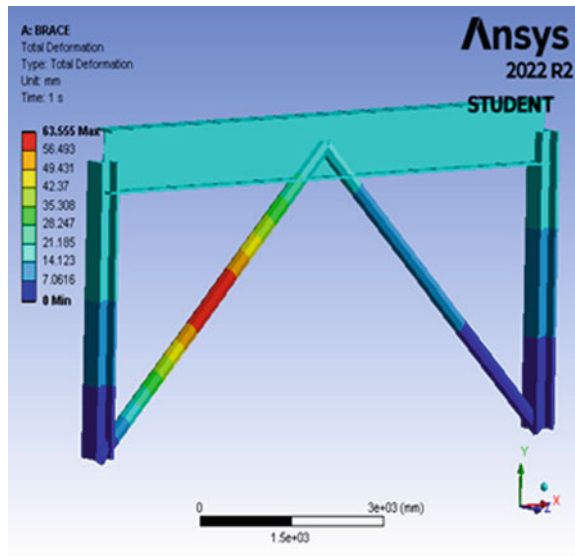


Fig. 4 Geometry of BSPD

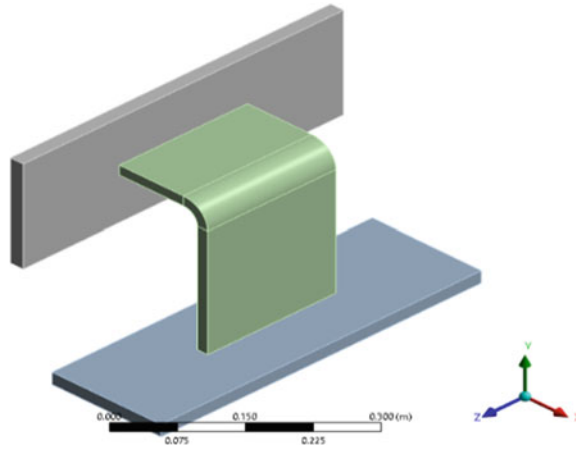


Table 2 Material properties

Material	E_s (GPa)	f_y (MPa)	f_u (MPa)	Elongation (%)
LY 160	203	154	295	37.2
Q345	203	285	455	25.5

3 Analysis and Design of BSPD

3.1 Material Properties

The Low Yield Point (LYP) steel, LY160, which has a yield strength of 160 MPa and is used to give the best material support for energy dissipation devices, was used to design the damper. After the yield stage, it possesses good ductility and steady cyclic characteristics that are appropriate for SPDs to assure superior seismic performance (Fig. 4, Table 2).

3.2 Validation

Base journal adopted for validation was ‘Experimental and Numerical study on Bent Shear Panel Damper made of BLY160 Steel’ by, Ji-Zhi Zhao, Mu-Xuan Tao, Liang-Dong Zhuang in 2022. For validation, BSPD was analysed using ANSYS Workbench R2 and the results obtained were compared with the base journal results (Table 3).

Table 3 Results of validation

Configuration	Load (kN)	Deformation (mm)
Current study	279.51	16
Experimental (base journal)	277.70	16.51
Difference (%)	0.64	3.03

The load bearing capacity and deformation of BSPD obtained by finite element analysis method is approximately close to the results obtained from the base journal.

3.3 Parametric Analysis of BSPD

Parametric analysis was done to find the optimum damper which has higher load bearing capacity and ductility. The optimization of BSPD was done using ANSYS Workbench 2022 R2. 18 models were analysed to find an optimum model with higher load bearing capacity and ductile performance. The models were specified as BP 700 × 200 × 200-10 (mm), where BP stands for Bent Panel, 700 × 200 is the length, 200 is the breadth and 10 is the thickness. Models were analysed using trial and error method in which length varies from 700 to 200 mm, breadth from 500 to 200 mm and thickness from 50 to 10 mm.

From all the models analysed it was found that load bearing capacity and ductile performance have increased simultaneously for BP 500 × 300 × 500-30. This model showed a higher load bearing capacity when compared to a braced SMRF and its ductility has also improved to a great extent.

4 Design and Analysis of BSPD

In this case a mesh size of 50 mm was provided to the frame and 20 mm was provided to the damper. The meshing process involves dividing the structure into a finite number of smaller elements, each of which is represented by a finite number of nodes. The nodes act as points of connection between the elements, and their positions are determined by the software based on the chosen element type and meshing size (Figs. 5, 6, 7 and 8).

Figure 6 shows the boundary conditions provided. Boundary conditions refer to the restrictions imposed on a structure at its edges or boundaries. The BSPD is a type of structural member used in buildings to resist lateral forces such as wind or earthquake loads to protect the structure from damages. Here, fixed support was provided. The fixed supports ensure that the structure remains stable and does not undergo significant deformation under the applied loads (Figs. 9 and 10).

Fig. 5 BSPD

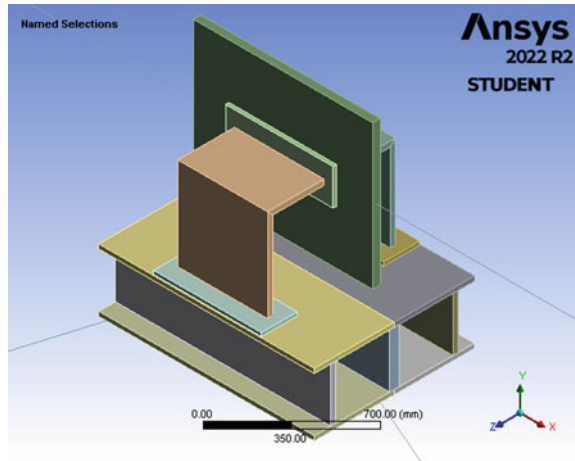
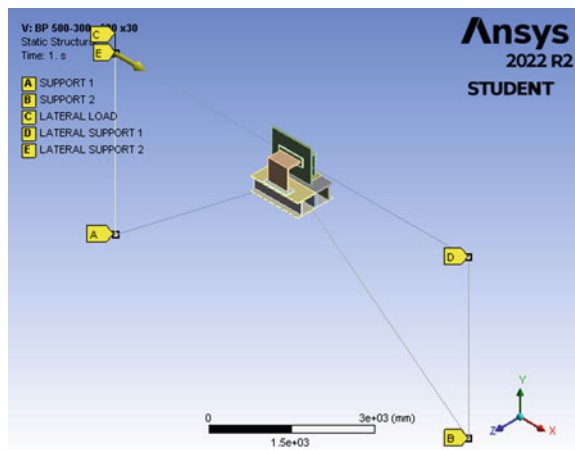


Fig. 6 Boundary condition in the specimen



5 Results and Discussion

By analysing 18 models it was found that the load bearing capacity ranges from 1876.80 to 5564.1 kN and ductility from 6.92 to 87.53. The results obtained are summarised in Table 4. The load bearing capacity and ductility have simultaneously increased only for BP 500 × 300 × 500-30 when compare to braced SMRF. Hence, it was selected as the optimum model.

Table 3 shows the results of dampers designed by trial-and-error method. The load bearing capacity and ductility factor of dampers with different dimensions are given. From Fig. 11 it can be concluded that when dampers are installed in a braced frame its ductile performance increase.

Fig. 7 Meshing of the specimen

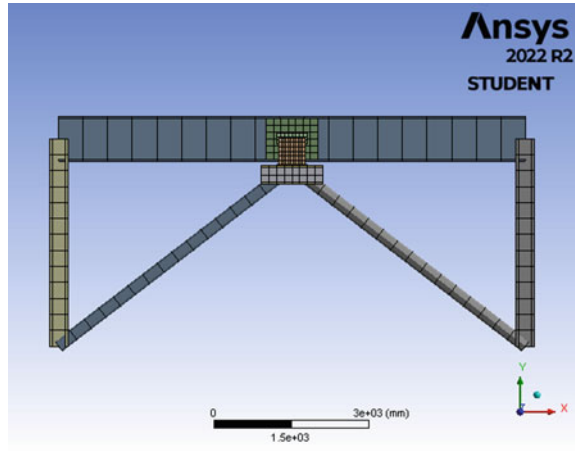


Fig. 8 BSPD in a frame

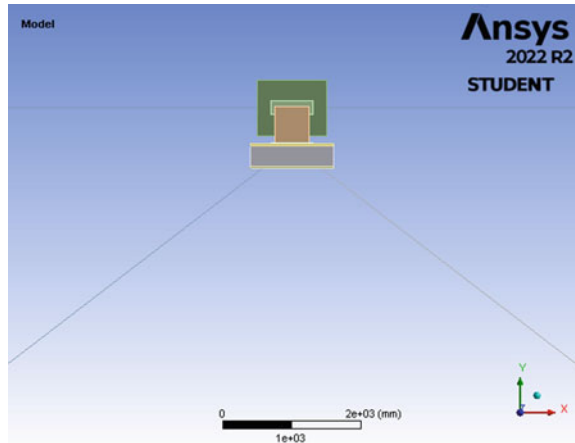


Fig. 9 Total deformation of the specimen

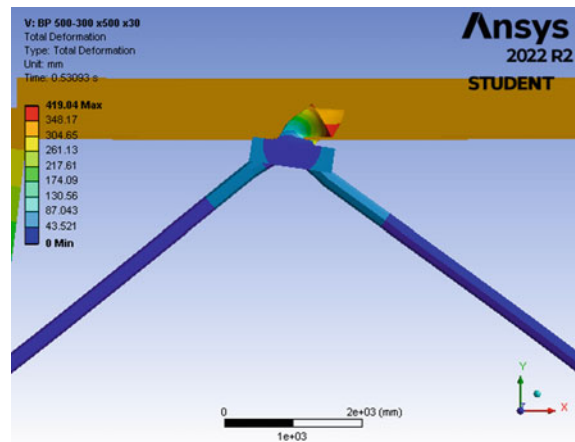


Fig. 10 Plastic strain of the specimen

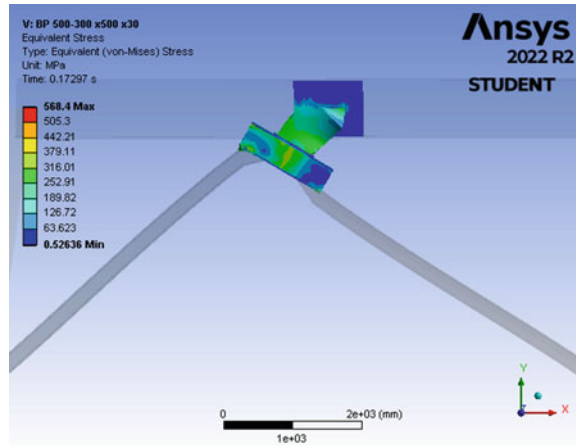


Table 4 Load and ductility of the specimens

Configuration	Load (kN)	Ductility factor
BP 700 × 200 × 200-10	1876.80	77.68
BP 700 × 200 × 300-10	1967.80	80.75
BP 700 × 200 × 400-10	2181.30	87.53
BP 700 × 200 × 500-10	2270.90	18.29
BP 700 × 200 × 500-20	3139.30	38.36
BP 700 × 200 × 500-30	4058.41	31.65
BP 700 × 200 × 500-40	4647.10	9.72
BP 700 × 200 × 500-50	4719.61	11.15
BP 500 × 200 × 500-40	5564.10	28.05
BP 500 × 200 × 500-30	4484.81	29.98
BP 500 × 200 × 500-25	3843.21	28.62
BP 500 × 100 × 500-30	444.71	22.97
BP 500 × 300 × 500-30	4362.40	34.21
BP 600 × 200 × 500-40	5118.60	26.78
BP 700 × 300 × 500-40	4751.70	9.61
BP 700 × 100 × 500-40	4754.70	6.92

6 Performance of BSPD in a 5-Storey Frame

The optimum BSPD was installed in a 5-storey frame to analyse its seismic behaviour through time hysteresis analysis. Real earthquake data from El Centro was adopted to analyse the seismic behaviour of the frame. The 5 storied frame was modelled with bracings alone and was compared to a 5 storied frame with dampers. From analysis it was found that the acceleration, storey displacement, base shear and time period

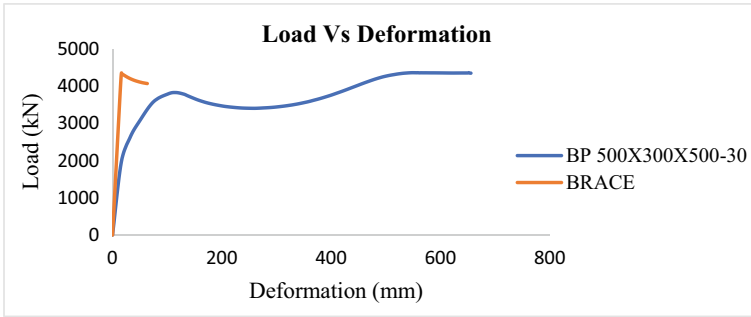


Fig. 11 Load-deformation curve

have decreased when bent shear panel dampers are installed in to the structure. When compared to a 5-story frame with bracings, the 5-story frame with BSPD is more earthquake resistant (Figs. 12, 13 and 14).

Table 5 gives the results of time hysteresis analysis, when real earthquake data is applied to the entire structure. During the time of earthquake, braced frame with damper has a higher load bearing capacity than a braced frame without dampers. In a braced frame with BSPD, the base shear, storey displacement and acceleration are less when compared to braced frame without dampers. As the acceleration and storey displacement of a structure is reduced during earthquake the damages caused to the structure also reduces.

Fig. 12 Total deformation with bracings

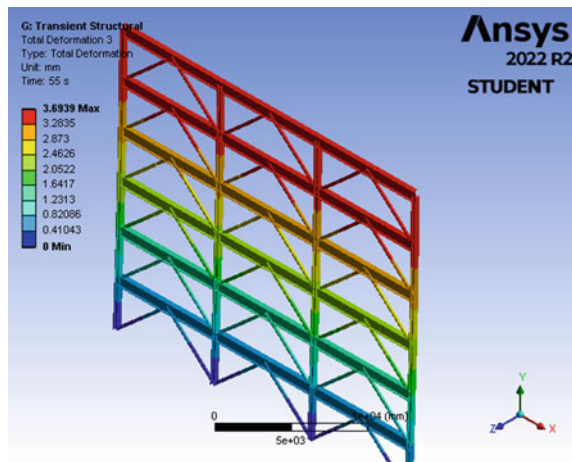


Fig. 13 Total deformation with dampers

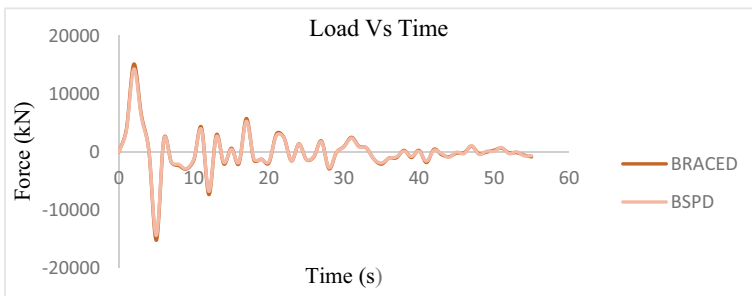
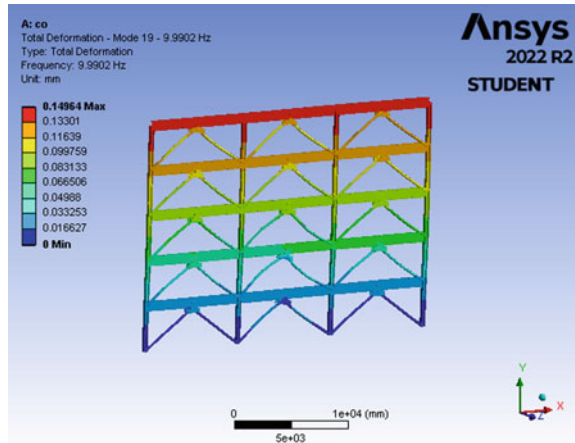


Fig. 14 Base shear graph

Table 5 Results of time hysteresis analysis

Configuration	Frequency (Hz)	Time period (s)	Base shear (kN)	Storey displacement (mm)	Acceleration (m/s ²)
Braced	8.989	0.111	15,213.000	65.661	819.940
BSPD	9.990	0.100	14,383.000	56.468	728.141

7 Conclusions

This study contributes to the advancement of knowledge in the field of earthquake engineering and can serve as a valuable resource for researchers and practitioners in the field of structural engineering. The insights gained from this project can be used to inform the design of more resilient and earthquake-resistant steel structures, ultimately contributing to the safety and well-being of communities in earthquake-prone regions.

Here, the optimum bent shear panel damper in braced steel moment resistant frame was designed. Optimum damper was selected based on the load bearing capacity and ductility performance of the frame. It has provided valuable insights into the effectiveness of this type of damper in increasing the load bearing capacity of steel frames. Through the comparison of the load bearing capacity of a frame with and without the damper, it was found that the:

- A frame incorporating a bent shear panel damper (BSPD) could resist heavier loads and performed better when subjected to seismic loading.
- The load bearing capacity of braced SMRF with BSPD is 1.65% higher than that of braced SMRF without BSPD.
- The ductile performance of braced SMRF with BSPD is 88% higher than braced SMRF without BSPD.
- In time hysteresis analysis, real earthquake data was applied in the 5-storied building, BSPD in SMRF has better performance when compared to braced SMRF.
- The analytical results obtained from this study suggest that the use of bent shear panel dampers can significantly enhance the seismic performance of steel frames. Along with load bearing capacity, ductile behaviour was also improved.
- When dampers are installed in a structure, its base shear, acceleration, storey displacement reduces which reduces the damage caused to the building.
- Further studies can be conducted on energy dissipation of BSPD, cyclic analysis can be done to know more about energy dissipation curve.

References

1. Wang W, Song J, Wang W et al (2022) Experimental investigation of the seismic behavior of low-yield-point corrugated steel plate dampers. *J Struct Eng* 147:04020335
2. Chan RWK, Albermani F, Williams MS (2009) Evaluation of yielding shear panel device for passive energy dissipation. *J Constr Steel Res* 65(2):260–268
3. Rahnavard R, Hassanipour A, Suleiman M, Mokhtari A (2017) Evaluation on eccentrically braced frame with single and double shear panels. *J Build Eng* 10:13–25
4. Chen Y, Chen C, Jiang H, Liu T, Wan Z (2019) Study of an innovative graded yield metal damper. *J Constr Steel Res* 160:240–254
5. Zhao JZ, Tao MX, Zhuang LD (2022) Experimental and numerical study on bent shear panel damper made of BLY160 steel. *Eng Struct* 260:114–229

Experimental Investigation on Plastic Shrinkage Characteristics of Self-compacting Concrete with Mineral Admixtures and Steel Fibers



V. S. Abhirami and C. A. Abin Thomas

Abstract The aim of this work is to evaluate the effectiveness of mineral admixtures and steel fibers on the plastic shrinkage of Self-compacting concrete (SCC). SCC is a highly flowable concrete without any segregation used in both dynamic and static states. For the production of sustainable SCC, appropriate supplementary cementitious materials (SCMs) are added. An optimum percentage of Fly ash, GGBS, Silica fumes, and steel fibers are incorporated. The workability test and compressive strength test of SCC mixes were done. ASTM C1579-based mould is used for the plastic shrinkage test is also carried out. Plastic shrinkage is the volumetric contraction of fresh concrete due to the escape of water from the surface of the concrete. The test results of normal conventional SCC and SCC with optimum SCMs incorporated with steel fibers were compared. CRR (crack reduction ratio) was determined and it was 83, 78 and 73% respectively for MFS30, MGS30, MSS30 compared to that MF30, MG30, MS10 respectively.

Keywords Concrete · SCC · Fly ash · GGBS · Silica fumes · Steel fibers · Plastic shrinkage

1 Introduction

The onset of energy crisis and environmental consciousness has led to a rapid growth in the construction industry. Also, the worldwide depletion of natural resources and the simultaneous accumulation of generated industrial wastes are increasing

V. S. Abhirami (✉)

Structural Engineering and Construction Management, Federal Institute of Science and Technology (FISAT), Angamaly, Kerala, India
e-mail: abhiramivs1048@gmail.com

C. A. A. Thomas

Department of Civil Engineering, Federal Institute of Science and Technology (FISAT), Angamaly, Kerala, India

at alarming rates. The sustainable development in the construction industry with major emphasis on the utilization of innovative and non-conventional industrial by-products to replace the natural resources used in concrete along with the recycling and reuse of waste materials. The development of Self-Compacting Concrete (SCC) with the unique property of flowing under its own weight by Okamura was with the prime aim of solving the problem of honeycombing and giving better finishes to structures, especially where congestion of reinforcement occurs. One way to enhance the sustainability of SCC is to partially replace the mineral aggregates in SCC with industrial waste materials such as rice husk ash, marble dust, recycled aggregates, silica dust, scrap rubber, glass aggregates, and fly ash to produce sustainable concrete [1].

Structures that complied with code requirements still fail due to excessive cracking. Shrinkage is primarily responsible for such failures. The earliest crack formation can already occur right after concrete placement and compaction, i.e., before initial setting, when concrete has lost its fluidity but has not yet achieved any appreciable cohesion. Structures that complied with code requirements still fail due to excessive cracking. Shrinkage is primarily responsible for such failures. Hence a main focus of maintaining a durable structure is based on its shrinkage properties. Shrinkage in concrete can be broadly classified into two different stages, namely early age and later age. At early ages of concrete when the concrete is still moist there are difficulties of measuring the fluid material. These difficulties have hindered comprehensive physical testing of shrinkage in plastic concrete [2, 3]. This project aims at evaluating the plastic shrinkage of different self-compacting concrete mixes. This study focuses on investigating and quantifying the effectiveness of using Fly Ash, GGBS and Silica Fumes on reducing shrinkage in concrete and the effect of Hooked End Steel Fibres on shrinkage of concrete.

2 Experimental Investigation

2.1 Materials

The experiment was carried out using powder materials as OPC 53 grade cement (IS: 12269, 1987) and commercially available mineral admixtures (Fly Ash, GGBS, Silica Fume) [4]. The physical properties of cement are presented in Table 1.

The physical and chemical properties of mineral admixtures are as shown in Table 2. A Ligno-sulphate based superplasticiser with a specific gravity of 1.19 is used at a dosage of 0.3–0.8% by weight of cement to improve workability. As per IS 383:1970 the grading for fine aggregate and different zones are provided and the fine aggregate used is manufacture sand belongs to zone 2. Coarse aggregate used is of 12.5 mm downsize nominal size.

Table 1 Physical properties of OPC 53 grade cement

Physical properties	
Specific gravity	3.15
Fineness	6%
Standard consistency	34%
Initial setting time	92 min
Final setting time	412 min

Table 2 Physical and chemical properties of mineral admixtures

Physical properties	Fly ash	GGBS	Silica fume	Chemical properties	Fly ash	GGBS	Silica fume
Specific gravity	2.2	2.5	2.9	SiO ₂ (%)	63.8	37.28	90.26
Surface area (m ² /kg)	649.9	758.5	12,387	Al ₂ O ₃ (%)	21.3	17.11	5.84
Average particle size (μ m)	45	16	1	CaO (%)	2.9	36.47	1.11
Form	Powder	Powder	Powder	Fe ₂ O ₃ (%)	0.39	0.12	0.01

Rather than these Hooked End Steel fibres used of the brand Go Green Products having a fibre length of 30 mm and diameter of 0.50 mm. the specific gravity, aspect ratio and tensile strength are 7.8, 60 and 1186 Mpa respectively.

2.2 Mix Proportion of SCC Mixes

The mix proportion was done in accordance with IS 10262: 2019 guidelines. Mix proportions with mineral admixtures and steel fibre is tabulated in Table 3.

2.3 Assessment of Rheological Properties of the Mix

To ensure the rheological properties of SCC flow ability, passing ability and segregation resistance tests were performed on control SCC and Steel fibre SCC (GFSCC) mixes according to IS 10262:2019 guidelines [5]. Slump flow and T500 slump flow time tests for filling ability, V-funnel test for the viscosity and segregation resistance, L-box and U-box test to assess the flow of concrete and passing ability were performed to study the workability of the mix [6].

Table 3 Mix proportions of various mixes

Mix	SCM	S F (%)	Cement	SCM	F A	C A	S P	Water	Flow diameter (mm)
			kg/m ³						
M _{F30}	Fly ash	–	311	134	938	808	2.67	200	670
M _{G30}	GGBS	–	311	134	950	817	2.67	200	690
M _{S10}	Silica fume	–	396	44	975	824	2.67	200	610
M _{FS30}	Fly ash	1	311	134	938	808	2.67	200	650
M _{GS30}	GGBS	1	311	134	950	817	2.67	200	680
M _{SS10}	Silica fume	1	396	44	975	824	2.67	200	600

2.4 Plastic Shrinkage Tests

Plastic Shrinkage appears on the surface of fresh concrete soon after it is placed and while it is still plastic. Primary cause of plastic shrinkage is the rapid evaporation of water from the surface of the concrete. Figure 1 shows the mould for plastic shrinkage measurement is designed and fabricated in accordance with ASTM C1579. Plastic shrinkage is measured using a steel mould of 600 × 200 × 100 mm size with three stress risers. The central riser is with a height of 63.5 mm which is used to provide maximum stress concentration on the central area and promote cracking. The other two risers of height 32 mm each are used to provide restrain in concrete.

The mould is made out of cast iron and transparent acrylic sheet is provided on one side; this is to make the crack visible which is formed along the depth of the mould. 10 bolts of 5 mm diameter are provided at both ends to increase the restrain. During testing the formation of the full-length plastic shrinkage crack was observed with naked eyes and the test is terminated at final setting time or when full length crack forms. The crack was formed above the central riser throughout the depth and across



Fig. 1 Plastic shrinkage mould based on ASTM 1579

the width of the mould. The crack width, time of occurrence of the initial centre line crack and propagation time of the crack on the concrete surface was recorded. The crack width measured is used to calculate the crack reduction ratio (CRR) [7].

$$CRR = \left[1 - \frac{\text{Average crack width of Fibre reinforced Concrete}}{\text{Average crack width of control concrete}} \right] \times 100$$

2.5 Compressive Strength

The bearing surface of the testing machine shall be wiped clean and any loose sand or other material shall be removed from the surfaces of the specimen which are to be in contact with the compression platens. The concrete cubes of size 150 × 150 × 150 mm was casted. The specimen shall be placed in the machine in such a manner that the load shall be applied to opposite sides of the cubes as cast, that is, not to the top and bottom. The axis of specimen shall be carefully aligned with the centre of thrust of the spherically seated platen.

The load shall be applied without shock and increased continuously at a rate of approximately 14 N/mm²/min until the resistance of the specimen to the increasing load breaks down and no greater load can be sustained. The maximum load applied to the specimen shall then be recorded and the appearance of the concrete and any unusual features in the type of failure shall be noted. The measured compressive strength of specimen shall be calculated by dividing the maximum load applied to the specimen by cross sectional area of the specimen.

$$\text{Compressive Strength} = \text{Load at failure} / \text{Cross-sectional Area}$$

The cubes were tested for its compressive strengths for different mixes after curing periods of 7, 14 and 28 days. Average of the results of three cubes was taken for the study.

3 Experimental Results and Discussions

3.1 Rheological Properties of the Mix

In case of the workability of SCC mix various tests like slump flow, T500 time, V funnel, L box and U box for normal Fly ash replaced SCC mix and SCC mix with 1% steel fibre along with replacing cement with Fly ash, GGBS and Silica fume test were conducted. The rheological properties of the mix are given in Table 4 and the test result should fall within the range as given in IS 10262: 2019.

Table 4 Rheological properties of the SCC mix

Mix	SF (%)	Slump flow (mm)	T500 (s)	V-funnel (s)	L-box	U-box (mm)
M _{F30}	–	670	1	1	1.31	30
M _{FS30}	1	650	2	2	1.022	25
M _{GS30}	1	680	4	5	0.984	27
M _{SS10}	1	600	5	8	0.846	12

3.2 Compressive Strength

The compressive strength tests were conducted on concrete cube specimens of size 150 mm as per IS: 516-1959, Clause 5. The compressive strength of concrete is affected by many factors, most of them being interdependent, such as the W/C ratio, cement compressive strength, properties of the aggregates (shape, grading, surface texture mineralogy, strength, stiffness, and maximum grain size), air-entrainment, curing conditions, testing parameters, specimen parameters, loading conditions, and test age.

From Fig. 2 Silica fume SCC Mix with steel fibres showed increase in strength. Since the pozzolanic reactions of silica fume are slow and depend on the calcium hydroxide availability, the strength gain takes longer time for fly ash and concrete mixes.

Pozzolanic reaction of silica fume can begin as early as 12 h. The higher the w/c ratio, the greater the silica fume reaction at early ages. Fly ash is found to depress calcium hydroxide formation at 12 h. The pozzolanic reaction can begin at 3 days, but significant reaction does not occur until after 7 days. Consequently, incorporation of steel fiber (SF) improves concrete’s compressive strength as well as its toughness and

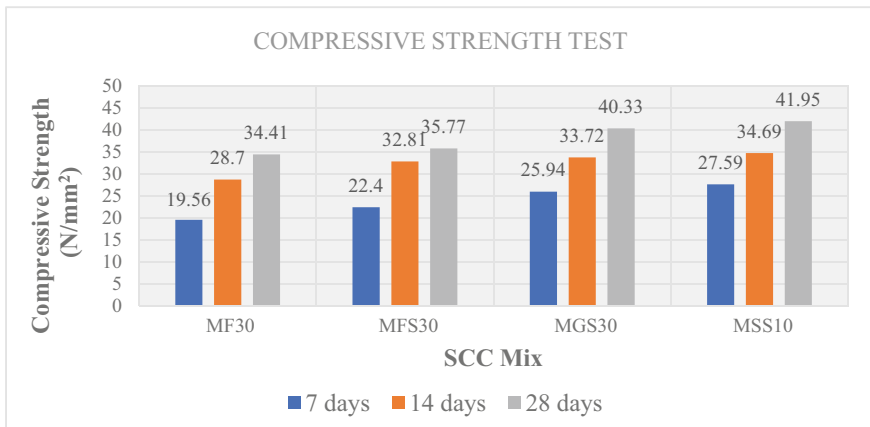


Fig. 2 Compressive strength of concrete mix

fracture resistance [8, 9]. Concrete's durability can be improved by adding different percentage of steel fibre and further study is required for the same.

3.3 Plastic Shrinkage

The plastic shrinkage test was conducted using ASTM C1579 based mould. During testing, the crack width, the time of occurrence of initial centre line crack and centre line full length crack was noted. The time of occurrence of the initial centre line crack and the time of propagation of crack indicates the plastic shrinkage behaviour of the concrete. The time of propagation of crack is taken as the time difference between the time of occurrence of centre line full length crack and centre line initial crack.

The full-length crack and vertical crack of the specimen of concrete formed in mould during testing is formed in Fig. 3. Time of occurrence of centre line initial crack and time for crack propagation of mixes with various SCC Mixes are tabulated in Table 5.

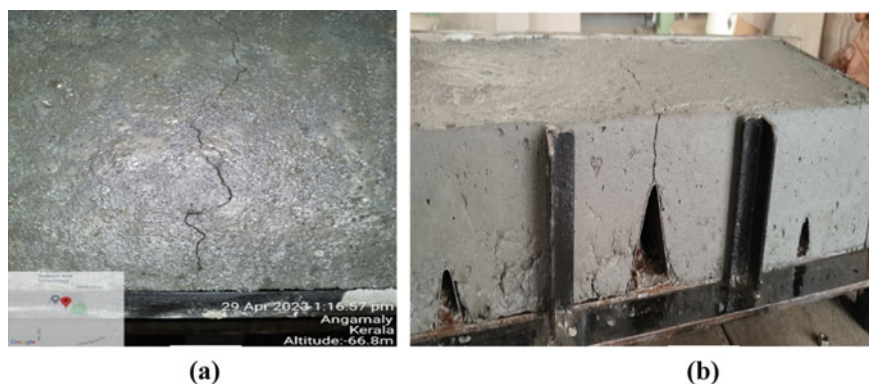


Fig. 3 a Top view and b Side view of full-length crack evolution in specimen

Table 5 Plastic shrinkage behaviour of various concrete mixes

SCC mix	S F (%)	Time for initial crack (min)	Time for full length crack (min)	Time for crack propagation (min)	Crack width (mm)
M _{F30}	–	170	203	33	0.46
M _{FS30}	1%	213	256	43	0.08
M _{G30}	–	185	216	31	0.4
M _{GS30}	1%	203	239	36	0.09
M _{S30}	–	178	210	32	0.49
M _{SS10}	1%	192	233	41	0.136

In the case of SCC mixes with different SCM; results seem to suggest that initial crack and the propagation of crack occurs fast. So, this cannot be considered purely as a plastic shrinkage crack, instead this can be a settlement crack or an interaction of plastic settlement and shrinkage crack. The chance of concrete prone to plastic settlement crack is there, since there is a central triangular insert and there is a 40 additional provision of 5 mm diameter bolts in the ASTM C1579 based mould which can act as a restrain and initiate the differential settlement crack [10, 11].

The results show that fly ash had a positive effect in reducing the plastic shrinkage. This may be attributed by some of the properties that fly ash possess. When fly ash is added, filling effect of admixture turns big pores in the structure of concrete into small voids lowering permeability of the free water. As a result of this synergistic effect there is a lower bleeding rate and hence drying shrinkage decreases. Retarding effect of pozzolanic reaction of fly ash helps in a delayed shrinkage strain. The higher amounts of SO₃ which result in Ettringite which is expansive in nature also compensate the shrinkage [12]. Figure 4 shows the time for initial and full-length crack propagation.

The delayed crack occurred with SCC mix with steel fibres since they act as crack arresters and gives positive effect on the plastic shrinkage of SCC. Silica fume can be used to increase the strength of SCC mix and to reduce the permeability. It is observed that the increase in strength causes an inverse in plastic shrinkage of the concrete. Increasing the percentage of silica fume in a concrete mix will also increase the plastic shrinkage. The fineness of the silica, as represented by its specific surface area and bulk density, is a strong indicator of its potential to increase plastic shrinkage cracking. SCC with GGBS showed comparatively fast crack propagation time that Fly ash and Silica Fume [13, 14].

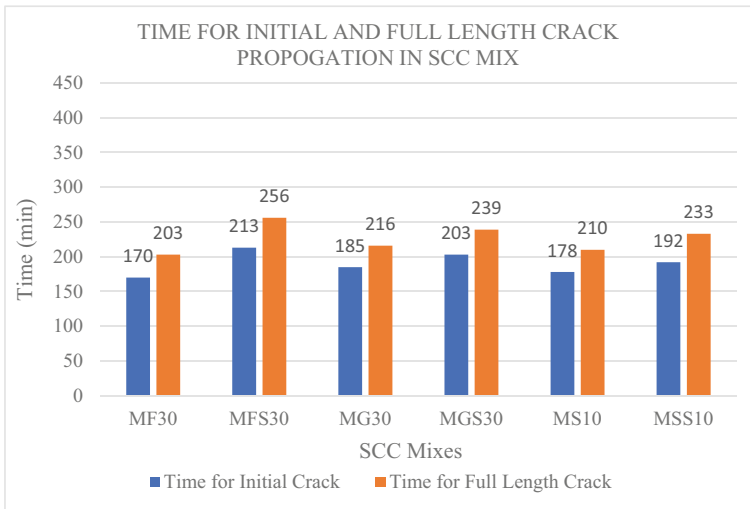


Fig. 4 Time for initial and final propagation of crack

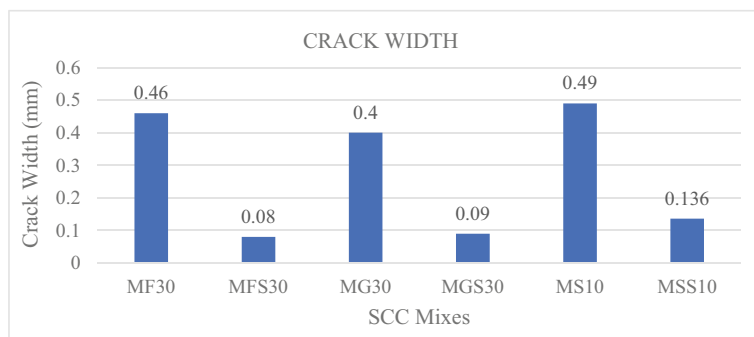


Fig. 5 Variation of crack width in different concrete mixes

The crack width is measured with the help of a Brinell microscope. It is observed that with the addition of Steel fibres the width of the crack gets reduced. And crack width increased for Silica fume SCC Mix following Fly Ash and GGBS Mix, this is observed because of silica content of Admixture. Since, Silica Fume contain more amount of silica and GGBS has low silica content crack width is observed accordingly. Further studies are needed to confirm these assumptions. And controlled amount of silica fume could give better effect plastic shrinkage properties of SCC mix [15].

Variation of crack width with various SCC mix is shown in Fig. 5. SCC mix with different SCM shows increase in width of crack. The graph shows that the fly ash mix efficiently reduces the crack width on adding steel fibres in it and all mix shows reduction crack width on addition of steel fibres. It is so evident that crack reduces by adding steel fibres and further reduction crack may be observed when varying the volume fraction of steel fibres added to the mix since they act as crack arrestors. CRR (crack reduction ratio) was determined by equation and it was 83, 78 and 73% respectively for MFS30, MGS30, MSS30 compared to that MF30, MG30, MS10.

4 Conclusions

The early age shrinkage properties of different SCC mixes with and without steel fibre are studied. Compressive Strength of SCC mixes were done and values obtained for 28 days are 34.41 N/mm² for Normal SCC and 35.77, 40.33, 41.95 N/mm² Fly Ash, GGBS and Silica Fume with 1% of Steel Fibres respectively. Adding Steel fibre in concrete reduces the workability of SCC and had showed significant effect on the compressive strength. Fly ash had a positive effect in reducing the plastic shrinkage. When Steel fibres were added the initial cracking time, maximum crack length and crack width was considerably reduced. Thus, from the above Plastic Shrinkage test the crack reduction ratios are 83, 78 and 73% for Fly Ash, GGBS and Silica Fume respectively.

References

1. Kristiawana SA, Taib M, Aditya M (2015) Effect of high-volume fly ash on shrinkage of self-compacting concrete. *Proced Eng* 125:705–712. <https://doi.org/10.1016/j.proeng.2015.11.110>
2. Combrinch R, Steyl L, Boshoff WP (2018) Interaction between settlement and shrinkage cracking in plastic concrete. *Constr Build Mater* 185:1–11. <https://doi.org/10.1016/j.conbuildmat.2018.07.0280>
3. Wu L, Farzadni N, Shi C, Zhang Z, Wang H (2017) Autogenous shrinkage of high performance concrete: a review. *Constr Build Mater* 149:62–75. <https://doi.org/10.1016/j.conbuildmat.2017.05.064>
4. IS: 4031 (1996) Method of physical tests for hydraulic cement: specification. Bureau of Indian Standards, New Delhi. <http://www.bis.org.in/>
5. IS 10262 (2019) Concrete mix proportioning: guidelines. Bureau of Indian Standards. <http://www.bis.org.in/>
6. EFNARC (2002) Specifications and guidelines for self-compacting concrete. EFNARC, Association House. www.efnarc.org
7. Sayahi F, Emborga M, Hedlund H (2017) Plastic shrinkage cracking in concrete: influence of test methods. In: Proceedings of the 2nd international RILEM/COST conference
8. Pelisser F, Neto ABSS, La Rovere HL, Pinto RCA (2010) Effect of the addition of synthetic fibers to concrete thin slabs on plastic shrinkage cracking. *Constr Build Mater* 24(11):2171–2176. <https://doi.org/10.1016/j.conbuildmat.2010.04.041>
9. Sinha DA, Verma AK (2017) Investigation on the effect of varying dosages of steel fibre on the strength and workability properties of high strength concrete. *ICRISET Civil Eng* 1:352–356
10. Turcry P, Loukili A (2006) Evaluation of plastic shrinkage cracking of self-consolidating concrete. *ACI Mater J* 103:272–280
11. Suprakash AS, Karthiyaini S, Shanmugasundaram M (2021) Future and scope for development of calcium and silica rich supplementary blends on properties of self-compacting concrete: a comparative review. *J Mater Res Technol* 15:5662–5681. <https://doi.org/10.1016/j.jmrt.2021.11.026>
12. Zhao Y, Gong J, Zhao S (2017) Experimental study on shrinkage of HPC containing fly ash and ground granulated blast-furnace slag. *Constr Build Mater* 155:145–173. <https://doi.org/10.1016/j.conbuildmat.2017.07.020>
13. Ghafari E, Ghahari SA, Costa H, Júlio E, Portugal A, Durães L (2016) Effect of supplementary cementitious materials on autogenous shrinkage of ultrahigh performance concrete. *Constr Build Mater* 127:43–48
14. Khan SU, Nuruddin MF, Ayub T, Shafiq N (2014) Effects of different mineral admixtures on the properties of fresh concrete. *Sci World J* 2014:11. <https://doi.org/10.1155/2014/986567>
15. Golaszewski J, Golaszewska M (2022) The effect of shrinkage reducing admixture and expansive admixture on properties of mortars with Portland and slag cement. *Arch Civil Eng PAS* 13:337–353

Study of Concrete Imperfections in T Shaped Multi-cell Composite Column



Akshay Murali and P. Anima

Abstract Orthogonal composite column is a structural element that consists of two or more individual columns arranged in a perpendicular fashion. This composite column is created by connecting the individual columns with a steel or concrete beam at their intersection. They are often used in high-rise buildings where they provide increased structural stability and load-bearing capacity. This analytical study focuses on investigating the effect of two common types of concrete imperfections, namely Interfacial gap and Cap gap, on the strength of T shaped multi-cell composite column. For this study, the preparing and analysing models of T shaped column without concrete imperfections is to be done and compared with column with imperfections and to study their behaviour. This paper aims to determine the impact of the concrete imperfections on the strength and failure patterns of T shaped composite column using ANSYS software. The results of this study provide valuable insights into the behaviour of T shaped multi-cell composite column with different types of concrete imperfections. The findings can be used to improve the design and construction practices of these structures and enhance their structural integrity and safety.

Keywords Concrete imperfections · Load-bearing capacity · Interfacial gap · Cap gap

1 Introduction

Composite columns are structural columns that are made up of two or more materials with different physical and mechanical properties. The primary purpose of using composite columns is to increase their load-carrying capacity, improve their stiffness, and reduce their weight. The most common type of composite column is a concrete-filled steel tube (CFST) column. In this type of column, a steel tube is filled with concrete.

A. Murali (✉) · P. Anima
Universal Engineering College, Vallivattom, Kerala, India
e-mail: akshaymurali027@gmail.com

With favourable static and seismic performance, special-shaped CFST cross-sections (L, T, +, etc.) has recently drawn significant attention in the construction of residential buildings. Besides the benefits offered by traditional steel tubes filled with concrete, incorporating orthogonal composite columns can eliminate the columns that project out from the walls, resulting in a larger usable space in a room and facilitating furniture placement.

A T-shaped multi-cell composite column is a structural member used in building construction that consists of a vertical stem or web and one or more horizontal flanges. The stem and flanges are made of steel and concrete, that work together to resist loads. These columns are constructed by welding three steel tubes of rectangular or square shape, and then pouring concrete into them.

However, due to the influence of multiple factors like non-compaction vibrating, concrete shrinkage, temperature difference effect, etc., the interface between the hollow steel section (HSS) and the concrete core of the CFST members may exhibit varying degrees of debonding behaviour known as concrete imperfections. The two types of concrete imperfections considered for this study are Interfacial gap imperfection and Cap gap imperfection. The existence of the gap defects would weaken the confining effect, leads to reductions in the load bearing capacity, stiffness, and ductility.

Several researchers conducted multiple experimental investigations and analysis on CFST members with concrete imperfections to determine the impact of gap defects on the behaviour of CFST members. Wang et al. [1] researched the impact of load eccentricity and the gap between the spherical-cap on the compressive strength, ductility, failure modes, and distribution of strain in CFST short columns with spherical-cap gaps. Shen et al. [2] studied the impact of gaps on the efficiency of ECFT stub columns under axial loading was uncovered. Han et al. [3] examined how the gap affects the efficiency of CFST columns subjected to eccentric loads. Liao et al. [4] performed a study to examine the behaviour of CFST stub columns with circumference gap or spherical cap gap when subjected to compressive forces. Xue et al. [5] examined the impact of debonding on circular CFST stub columns examined, both physically and computationally. [6] studied the response of multi-cell composite T-shaped concrete-filled steel tubular columns when subjected to compression under biaxial eccentricity, in which the position and angle of the eccentric loading influenced the ultimate load-bearing capacity. [7] explored how gaps impact the performance of CFST columns loaded eccentrically and the key parameters investigated in the tests were type of gap (circumferential or circular-segment) and the gap ratio. [8] conducted a nonlinear analysis on CFST stub columns subjected to axial compression, considering cases with a circumferential gap or a spherical-cap gap. [9] conducted study on the effect of debonding on circular CFST stub columns by a combination of experimental and numerical approaches and parameters examined were ratio of debonding arc-length, the level of confinement and the applied load mode. [10] investigated how gaps impact the compressive and flexural performance of CFST members and the primary variables examined in these tests were the type of gap (circumferential or spherical-cap) and ratio of the gap.

Table 1 Material properties [1]

Material	Young's modulus (Mpa)	Compressive strength (Mpa)	Yield strength (Mpa)	Poisson's ratio
Concrete	38,730	60	–	0.12
Steel	205,000	–	345	0.3

Currently, there is insufficient research on special-shaped CFST members that are frequently utilized in practical engineering. The majority of the research has focused on symmetrical-shaped members such as elliptical and circular shapes. Additionally, the majority of research has been conducted on short columns with gaps.

This study focuses on the performance and behaviour of T shaped column with concrete imperfections and to identify the maximum load carried by the column in comparison with column having no imperfections.

2 Analytical Study

2.1 Modelling

In this study, T shaped columns with breadth (B) of 100 mm and depth (D) of 200 mm were modelled and the thickness (t) of the steel tube and height (H) of the column are 2.3 and 1600 mm respectively (Table 1).

The analysis was done using ANSYS software. The meshing was done with 25 mm mesh size and boundary conditions were provided at top and bottom of the column. The element type used for the analysis was Solid 185 and the element shape of meshing is Hexahedron. The loading provided was axial compressive loading (Figs. 1, 2, 3 and 4).

3 Behaviour Characteristics of Column

3.1 Column Having no Gap

The analysis of the T shaped column with no imperfection or gaps was done by applying axial load. The maximum load carried by the column was found out (Fig. 5).

Fig. 1 Dimension of the specimen

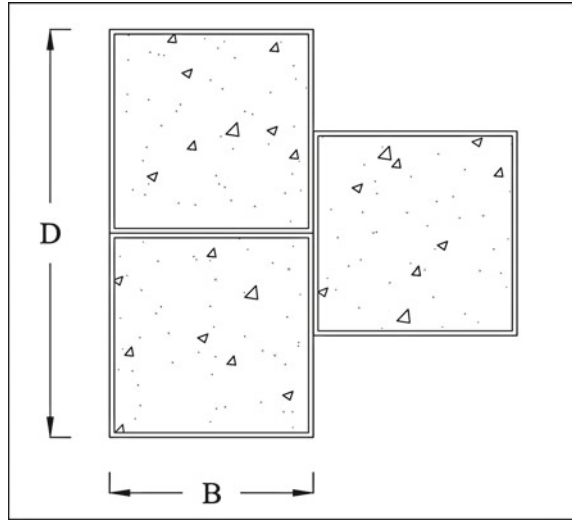
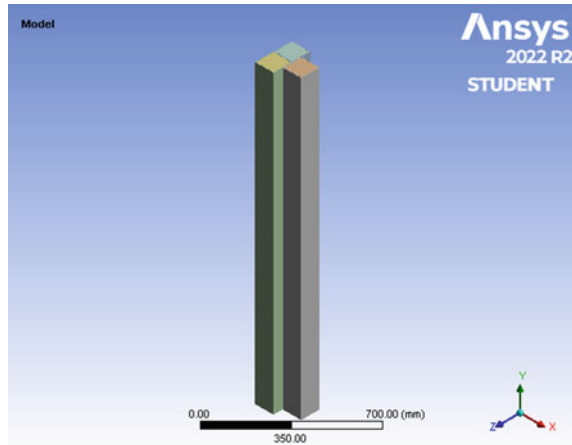


Fig. 2 Geometry of the specimen



3.2 Column Having Interfacial Gap Imperfection

The interfacial imperfections are minute gaps that are formed at the faces of the column between the steel and the concrete faces. The column was provided with interfacial gap of 1 mm at different faces of the column. Interfacial gaps were denoted as IG.

In Fig. 6, the interfacial gaps IG 1, IG 2, IG 3, IG 4, IG 5, IG 6, IG 7 represents different locations in T shaped column where the interfacial gaps are provided. These gaps are provided by considering symmetry with respect to X-axis (IG 2, IG 4, IG 5, IG 6, IG 7) and independent interfaces (IG 1, IG 3). Each case of the column

Fig. 3 Meshing of the specimen

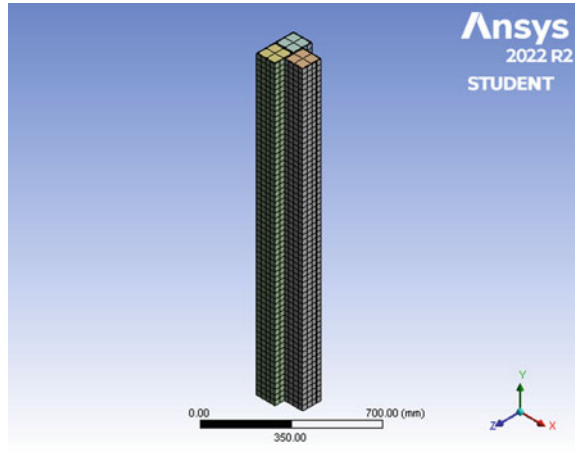
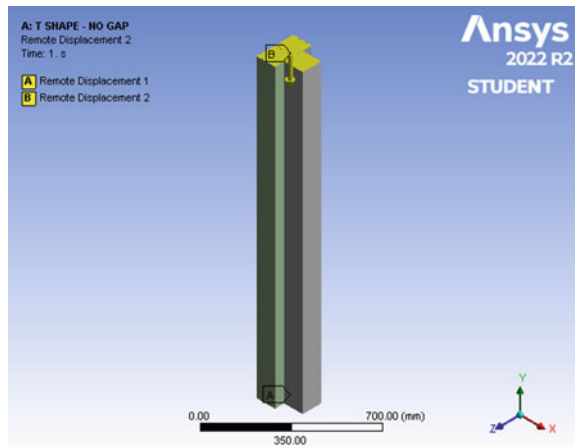


Fig. 4 Boundary conditions of the specimen



model was prepared and analysed separately to identify the gap formation at which face causes the decrease in load carrying capacity of the column and the percentage decrease in load carrying capacity was compared with the column having no gap.

3.3 Column Having Cap Gap Imperfection

Cap gap imperfections are slightly larger void formed at the corners of the orthogonal composite column between the concrete and the steel. The column was provided with cap gap of 25 mm at different corners of the column. Cap gaps were denoted as CG.

Fig. 5 Column having no gaps

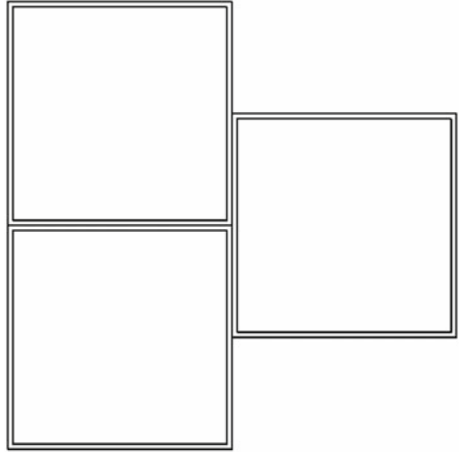
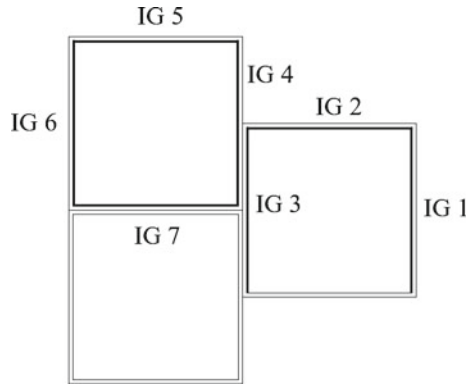
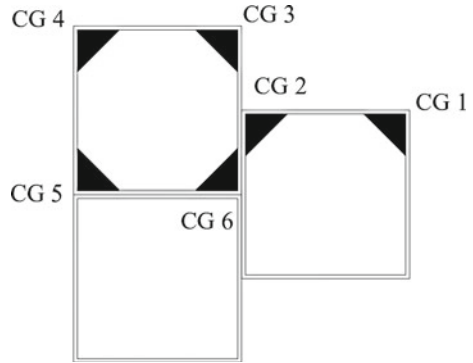


Fig. 6 Column with interfacial gaps provided



In Fig. 7, the cap gaps CG 1, CG 2, CG 3, CG 4, CG 5, CG 6, represents gaps provided at different corners inside the column. These gaps are provided by considering symmetry with respect to X-axis, as cap gaps are likely to occur in corners. Each case of the column model was prepared and analysed separately to identify the gap formation at which corner causes decrease in load carrying capacity of the column and the percentage decrease in load carrying capacity is compared with the column having no gap.

Fig. 7 Column with cap gaps provided



4 Results and Discussion

4.1 Effect of Axial Load on the Behaviour of Column Having No Gap

When the column is subjected to an axial load, it experiences compressive stress along its length, which can cause it to buckle or deform if the load exceeds its capacity [3] (Fig. 8).

From the analysis result, the maximum load carrying capacity of the column is obtained to be 3105.80 kN (Fig. 9 and 10).

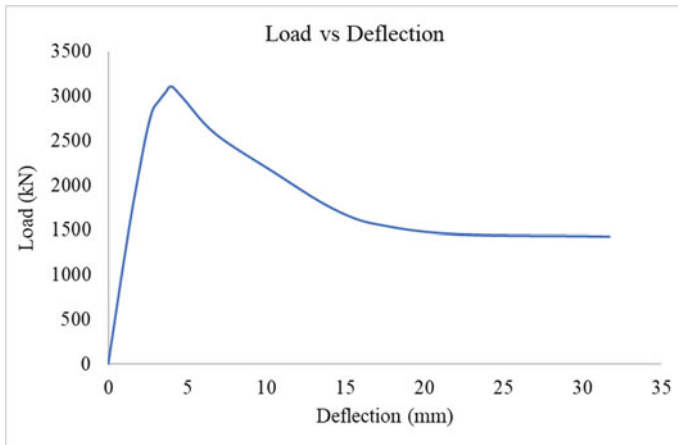


Fig. 8 Load versus deflection curve

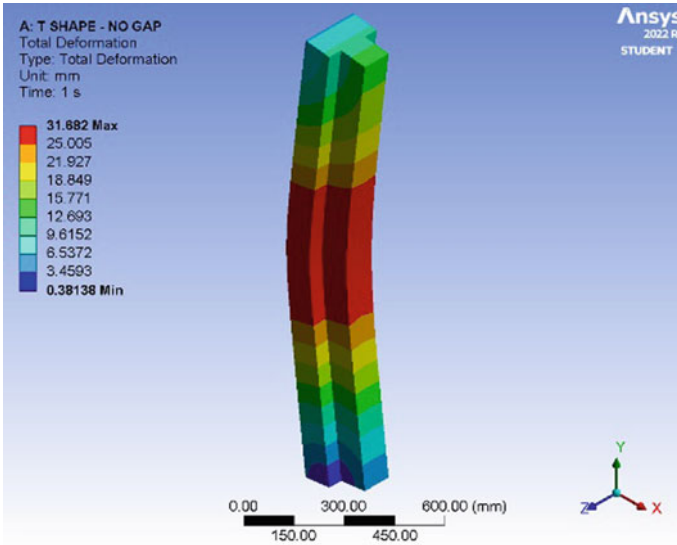


Fig. 9 Total deformation of the column

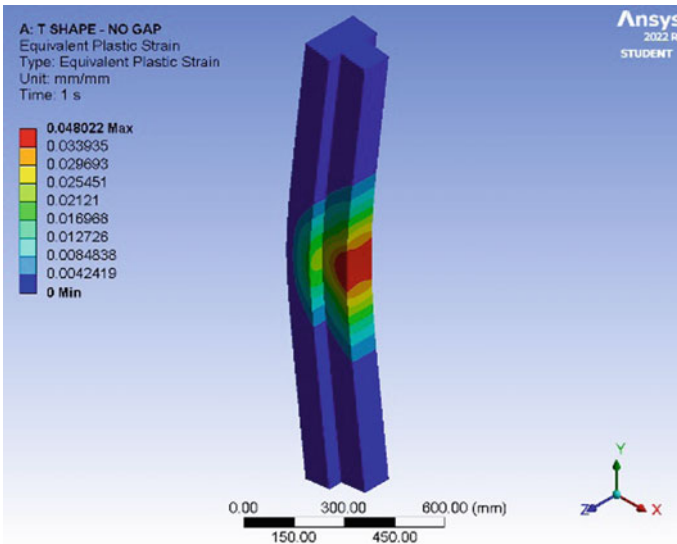


Fig. 10 Equivalent plastic strain of the column

4.2 Effect of Axial Load on the Behaviour of Column Having Interfacial Gap

From the analysis, the model IG 5 of the column has the least load carrying capacity when compared with column having no gap and the location of the interfacial gap in the worst model is given in Fig. 11. From comparison the percentage decrease in load carrying capacity of the column with interfacial gap ranges from 4 to 5.69% (Figs. 12, 13 and 14, Table 2).

The worst model of the column with interfacial gap obtained after analysis is IG 5, having a percentage decrease in load of 5.69% and the load carried by the column is 2929.2 kN. Failure due to Interface gap in composite columns occurs due to gaps between the steel and concrete, resulting in a weakened bond strength causing slip or separation between the steel and concrete when subjected to axial compressive loading, ultimately leading to the failure of the composite column. Additionally, if interfacial gaps are present, the load transfer between the steel section and the concrete core may not be efficient, which can lead to premature buckling of the steel section and subsequent column failure. The interfacial gaps create a weak bond between the steel and concrete, reducing the load-carrying capacity of the column and causing it to fail at lower loads. In a composite column, the concrete provides confinement to the steel section, enhancing its strength and ductility. However, interfacial gaps disrupt the transfer of confinement pressure from the concrete to the steel, resulting in a loss of confinement. This loss of confinement reduces the ductility of the column, especially under lateral loading. The presence of interfacial gaps allows

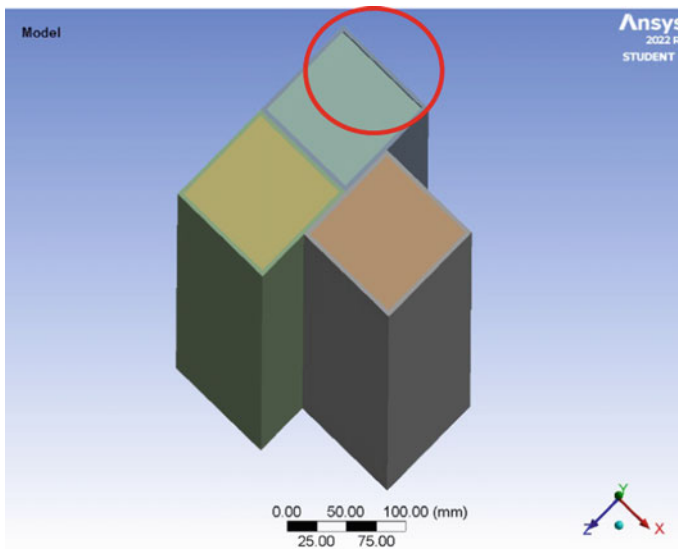


Fig. 11 Location of interfacial gap of the worst model IG 5

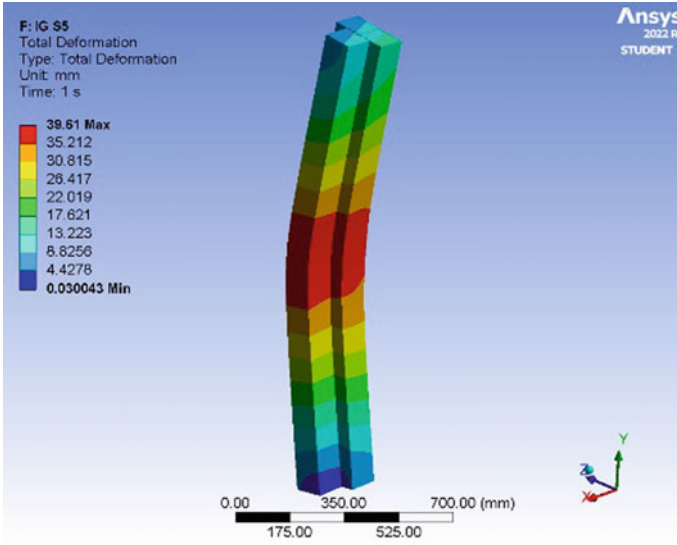


Fig. 12 Total deformation of model IG 5

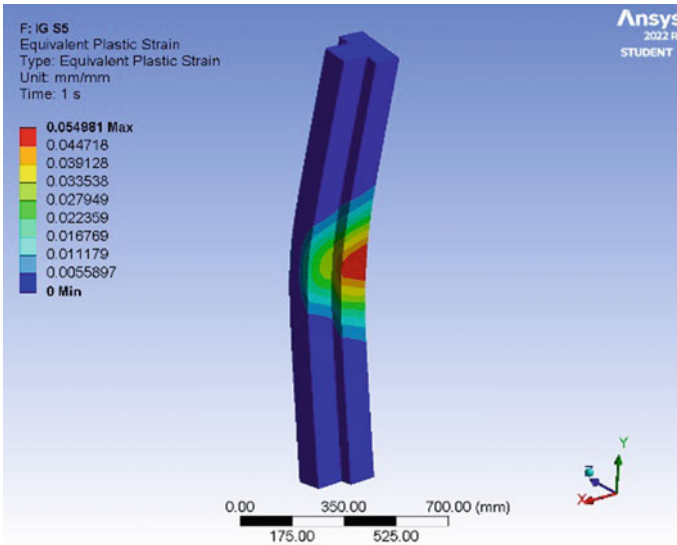


Fig. 13 Equivalent plastic strain of model IG 5

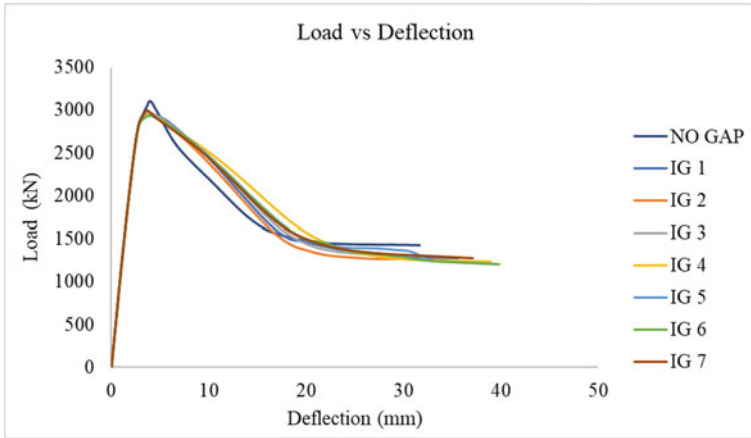


Fig. 14 Load versus deflection curve of IG in column

Table 2 Percentage decrease in load in each case of IG in column

Columns	Deflection (mm)	Load (kN)	% Decrease in load
No Gap	4.01	3105.80	0
IG 1	4.08	2947.10	5.11
IG 2	3.98	2967.20	4.46
IG 3	3.78	2981.7	4.00
IG 4	4.06	2951.2	4.98
IG 5	4.05	2929.2	5.69
IG 6	4.22	2940.9	5.31
IG 7	3.68	2995.5	3.55

relative movement between the steel and concrete sections of the column under load, leading to increased deformation and deflection and can affect overall stability of the column. Furthermore, interfacial gaps prevent the transfer of load between the steel and concrete, resulting in a lack of composite action, and its absence significantly reduces the load-carrying capacity of the column.

4.3 Effect of Axial Load on the Behaviour of Column Having Cap Gap

From the analysis, the model CG 4 of the column has the least load carrying capacity when compared with column having no gap and the location of the cap gap in the worst model is given in Fig. 15. From comparison the percentage decrease in load

carrying capacity of the column with cap gap ranges from 4.98 to 7.37% (Figs. 16, 17 and 18, Table 3).

The worst model of the column with cap gap obtained after analysis is CG 4, having a percentage decrease in load of 7.37% and the load carried by the column is

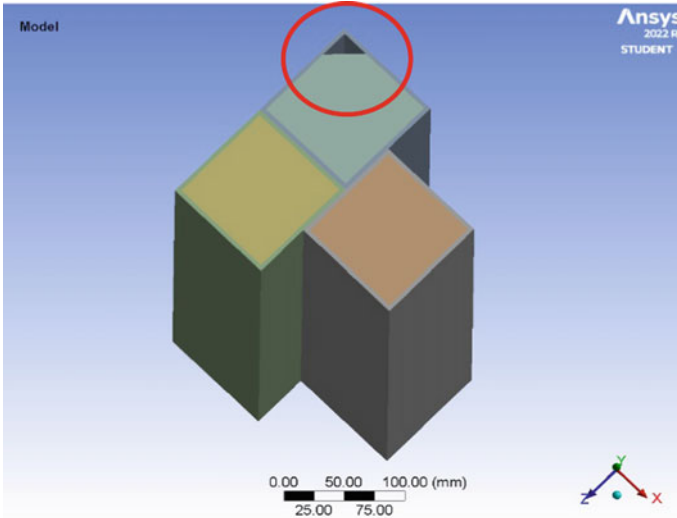


Fig. 15 Location of cap gap of the worst model CG 4

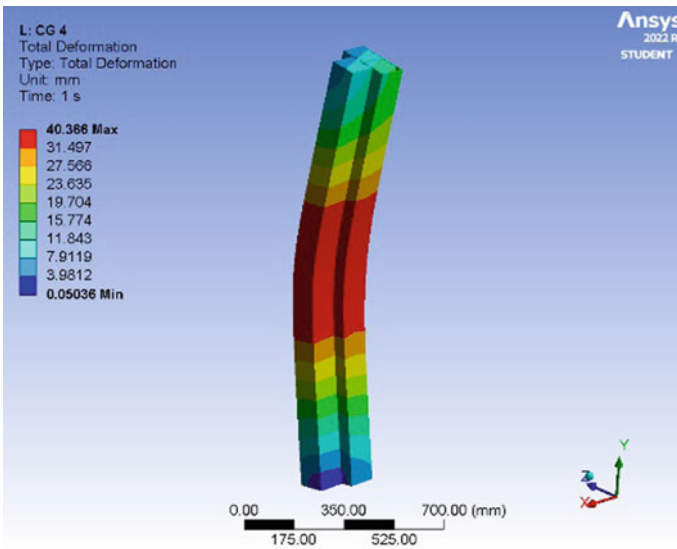


Fig. 16 Total deformation of model CG 4

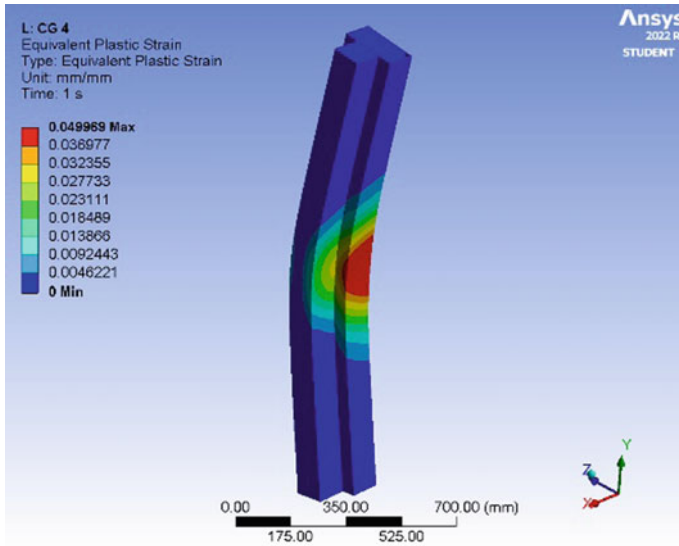


Fig. 17 Equivalent plastic strain of model CG 4

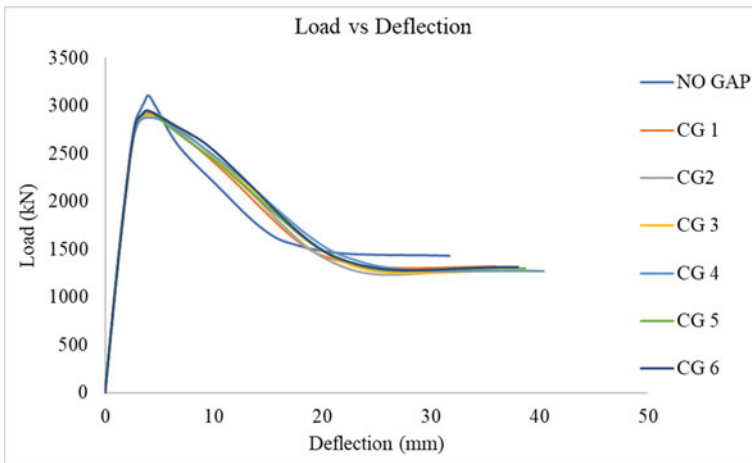


Fig. 18 Load versus deflection curve of CG in column

2877 kN. Cap gap imperfection diminish the effective cross-sectional area that can resist compressive loads, resulting in a weakened column with reduced load-bearing capacity. Consequently, the column becomes more vulnerable to failure under axial compression. Another detrimental effect of cap gap is the loss of composite action in composite columns. If the gaps within the concrete encasement are substantial, they can impair the effective composite action between the core and the encasement. This

Table 3 Percentage decrease in load in each case of CG in column

Columns	Deflection (mm)	Load (kN)	% Decrease in load
No gap	4.01	3105.90	0
CG 1	4.38	2909.30	6.33
CG 2	4.04	2944.30	5.20
CG 3	4.68	2889.40	6.97
CG 4	3.69	2877.00	7.37
CG 5	4.13	2936.50	5.45
CG 6	3.97	2951.20	4.98

loss of composite action diminishes the column's ability to carry loads, increasing the risk of failure. Moreover, the presence of cap gaps within the concrete can lead to a non-uniform distribution of compressive forces throughout the column leading to localized high stresses around the gaps, which can result in cracking and eventually lead to the failure of the column. Furthermore, cap gaps can also have adverse effects on the overall stability of the column, making it more susceptible to buckling. The reduced effective cross-sectional area and the decreased stiffness caused by voids can contribute to buckling failure. Additionally, the presence of cap gaps can adversely affect the stiffness of the composite column, leading to increased deformations under axial compression.

5 Conclusions

The studies of concrete imperfections in T-shaped multi-cell composite columns have shown that the concrete imperfections have a significant impact on the strength and behaviour of the columns. To address these issues, it is important to develop reliable methods for detecting and assessing concrete imperfections in T-shaped multi-cell composite columns. Furthermore, the development of advanced computational models and simulation techniques can provide a better understanding of the structural behavior of these columns with imperfections. This can help engineers and designers to optimize the design and construction process and ensure the safety and reliability of these structures.

- The maximum load carried by T shaped multi-cell composite column having no gap under axial load is 3105.80 kN. In conclusion, axial compressive load significantly influences the behavior of T-shaped composite columns by affecting the load-carrying capacity, stability buckling, deformation, strain and load redistribution.
- By analysing different models of T shaped column having interfacial gap, it was found that the model IG 5 appeared as the worst model having a load carrying capacity of 2929.2 kN and the percentage decrease in load when compared with column having no gap was found out to be 5.69%. In conclusion, interface gap

imperfection in composite columns between the steel and concrete weakens the bond strength. This leads to slip or separation under axial compressive loading, causing column failure. Interfacial gaps reduce load transfer efficiency, resulting in premature buckling and lower load-carrying capacity. Loss of confinement reduces ductility, especially under lateral loading. Interfacial gaps allow relative movement, increasing deformation and deflection, compromising overall stability. Lack of composite action hinders load transfer, significantly reducing the column's load-carrying capacity.

- By analysing different models of T shaped column having cap gap, it was found that the model CG 4 appeared as the worst model having a load carrying capacity of 2877 kN and the percentage decrease in load when compared with column having no gap was found out to be 7.37%. In conclusion, cap gaps in columns diminish the column's cross-sectional area and load-bearing capacity, making it more prone to failure under compression. Cap gaps also lead to the loss of composite action in composite columns, reducing their ability to carry loads and increasing the risk of failure. This gaps also make the column more susceptible to buckling due to reduced cross-sectional area and stiffness. Furthermore, they increase deformations under compression, compromising structural integrity and overall stability of the structure.

References

1. Wang J, Cheng A, Shen Q, Li G, Xiao Q (2022) Eccentric compression behaviour and assessment of CFET short columns offering spherical-cap gaps. *J Constr Steel Res* 197:107–476
2. Shen Q, Li J, Wang J (2022) Experimental, numerical and design investigations on the performance of axially-loaded ECFT stub columns with spherical-cap gaps. *Structures* 46:109–127
3. Yu P, Ren Z, Yun W, Zhao Y, Xu J (2022) Performance of bolt-welded CFST short columns with different initial imperfections: experimental and numerical studies. *Buildings* 12:1352
4. Zheng Y, Liang W, Ma S, Zeng S (2022) Behaviour of stiffened and multi-cell L-shaped CFST column under eccentric compression. *Thin-Walled Struct* 174:109–156
5. Guo C, Lu Z (2019) CFST rib with circumferential gap and SWS composite defects. *Iran J Sci Technol* 45:1441–1456
6. Sui Y, Tu Y, Zhang J, Ke F (2019) Study on the behavior of multi-cell composite T-shaped concrete-filled steel tubular columns subjected to compression under biaxial eccentricity. *J Constr Steel Res* 159:215–230
7. Han LH, Ye Y, Liao FY (2016) Effects of core concrete initial imperfection on performance of eccentrically loaded CFST columns. *J Struct Eng* 142:12
8. Liao FY, Han LH, Tao Z (2013) Behaviour of CFST stub columns with initial concrete imperfection: analysis and calculations. *Thin-Walled Struct* 70:57–69
9. Xue JQ, Briseghella B, Chen BC (2012) Effects of debonding on circular CFST stub columns. *J Constr Steel Res* 69:64–76
10. Liao FY, Han LH, He SH (2011) Behaviour of CFST short column and beam with initial concrete imperfection: experiments. *J Constr Steel Res* 67:1922–1935

Comparative Assessment of Geocell and Geogrid Reinforcement for Flexible Pavement: Numerical Parametric Study



Anjana R. Menon  and Anjana Bhasi 

Abstract Development of highways and railways play crucial role in a nation's economic growth. While rigid concrete pavements are durable with high load bearing characteristics, growing economies mostly rely on flexible pavements which enables easier and economical construction. The strength of flexible pavement is based on the strength of subgrade and load distribution characteristics of intermediate granular layers. In this scenario, to simultaneously meet economy and strength criteria, it is imperative to strengthen and stabilize the load-transferring layers, namely subbase, and base. Geosynthetic reinforcement in planar and cellular forms has been proven effective in improving soil stiffness and providing a stable load transfer platform. The present study investigates the efficiency of geocells over single/multiple layer geogrid reinforcements by a series of three-dimensional model analyses of a flexible pavement section under a standard repetitive wheel load. The geocell network modeled with actual curvature is assumed to be embedded in the granular base with hard contact without separation. Stress transfer mechanisms and deformation profiles under various reinforcement configurations are also studied. Geocell reinforcement is observed to take up a higher proportion of stress caused by the traffic loads compared to single and double-layer geogrid reinforcements. The efficiency of single geogrid reinforcement reduces with an increase in embedment depth. The contribution of lower geogrid is insignificant in the case of the double-geogrid reinforced system.

Keywords Geocell · Geogrid · Flexible pavement · Repetitive wheel load · Numerical analysis

1 Introduction

Growing infrastructure demand and the scarcity of stable ground profiles compel engineers worldwide to utilize poor ground conditions with suitable modifications. Flexible pavements being easier and more economical than rigid pavements, are

A. R. Menon (✉) · A. Bhasi
NIT Calicut, Kattangal, Kerala 673601, India
e-mail: anjana5193@gmail.com

© The Author(s), under exclusive license to Springer Nature Switzerland AG 2024
M. Nehdi et al. (eds.), *Proceedings of SECON'23*, Lecture Notes in Civil Engineering
381, https://doi.org/10.1007/978-3-031-39663-2_42

515

prevalent in growing economies like India. However, the strength of flexible pavement is based on the strength of subgrade and load distribution characteristics of intermediate granular layers. Hence, a strong pavement with high service life demands a moderate to hard subgrade beneath thick granular layers. In this scenario, to simultaneously meet economy and strength criteria, it is imperative to strengthen and stabilize the load transferring layers, namely subbase and base. Amongst the various ground modification techniques that evolved, geosynthetic reinforcement remains the most versatile and effective method for bearing capacity enhancement and settlement control. Studies have proven that Geosynthetic reinforcement in granular layers improves the stress carried by the granular layer and offers uniform and wider stress distribution, thus lowering the pressure on the subgrade. Ibrahim et al. [1], Leonardi et al. [2], and Dessouky et al. [3] enhancing the potential for using soft subgrades for pavement construction. Most past studies focused on the reinforcing effect of geogrid and geotextile reinforcement. However, the last few decades have witnessed a growing trend in studies on cellular geosynthetics, namely geocells, in various applications, including pavements. These cellular structures offer an additional confining effect, resulting in a soil-geocell mat with improved rigidity. It has been reported that geocells perform better than their planar counterparts in reducing the deformation of underlying layers and improving the load distribution pattern [4, 5].

The present study analyses a flexible pavement for the stress transfer and deformation pattern under different geosynthetic reinforcement configurations viz-a-viz single geogrid, multiple geogrid, and geocell in the granular layer. Three-dimensional numerical analysis is performed using finite element package ABAQUS to compare the performance of geocell over geogrid in terms of the stress in subgrade and settlement under a standard single axle wheel load. The behaviour of pavement layers under cyclic loads such as standard traffic can be effectively simulated using finite element analyses [2]. The influence of various parameters like geosynthetic stiffness and strength of subbase and subgrade are investigated in this study. The model details and the parametric study is explained in the subsequent sections.

1.1 Materials and Model Geometry

The study considers a 5-m by 5-m section of fictitious flexible pavement composed of a thin layer of asphalt wearing course over a well-graded granular base of 0.7 m thickness laid over the subgrade. The thickness of the granular layer in the model is 0.7 m which is chosen based on IRC 37 guidelines [6] for cumulative traffic of 100 MSA. The granular layer is reinforced using a geosynthetic material in planar and cellular forms. Table 1 lists the properties of different pavement components. Geocells are manufactured by cutting strips of geotextile/geogrid in the required length and height. The adjacent strips are suitably jointed at regular intervals to form uniform series of honeycomb-shaped pockets. The exact load transfer pattern is simulated in the numerical model by developing the actual cell geometry using carefully extracted coordinates of a real-time geocell sample.

Table 1 Properties of materials used in the analysis

Material/layer	Density (kg/m ³)	Elastic modulus E (× 10 ³) (kPa)	Poisson's ratio (μ)	Friction angle φ (°)	Cohesion (kPa)
Asphalt	2230	1000	0.35	–	–
Granular base	1550	42	0.33	40	1
Subgrade	1450	10.6	0.3	5	120
Geosynthetic	200	33,000	0.45	–	–

1.2 Loading and Boundary Conditions

Pavements are mostly subjected to cyclic loads due to traffic and wheel loads. The distribution and magnitude of stresses and strains in pavement layers largely depend upon the tire configuration and resultant contact pressure [3]. Since flexible pavements are designed based on Burmister's layer theory, only the wheels on one side shall be considered for design [7]. The present study considers two tires (of length 0.22 m and width 0.15 m) arranged in a single axle single wheel assembly. The configuration under a load of 40 kN generates a contact pressure of 595 kPa on each tire situated at an axle distance of 1.5 m [7]. The exact elliptical profile of the tire contact area can be simplified to a rectangle with an equivalent area [8], as given in Fig. 1.

The vehicular traffic is simulated by applying the calculated load in the equivalent contact area in a repetitive fashion of 1000 cycles with a cycle length of 0.01 s [2]. Total fixity was assumed at the subgrade bottom, whereas the lateral boundaries were permitted to deform only in the vertical direction. The geosynthetic reinforcement was embedded in the granular base with hard contact without separation. General contact with zero slip and zero separation conditions were assigned to connect the individual pavement layers [9].

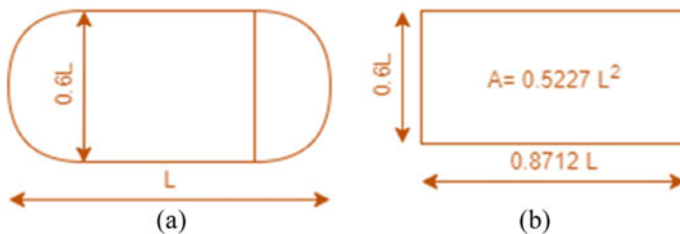


Fig. 1 a Actual wheel contact area and b equivalent rectangular area

1.3 Mesh and Element Configurations

The granular base and subgrade were modelled using 8-noded linear brick elements with reduced integration (C3D8R), assuming linearly elastic perfectly plastic behaviour under the Mohr–Coulomb failure criterion. The wearing asphalt course and geosynthetic material are modelled as perfectly elastic materials. The actual behaviour of geosynthetic reinforcement is simulated by adopting the membrane elements (M3D4R), which possess stiffness only along the fabric plane with zero bending stiffness.

1.4 Parametric Study

The study primarily focuses on comparing the performance of geocell reinforcement with single or multiple layers of geogrid placed in the granular base. With single geogrid reinforcement, three cases are considered by changing the embedment depth of geogrid in the granular layer. The height of the geocell wall being 0.5 m, the optimum location for placing the geocell is at the center, because this leaves a marginal gap of 0.1 m each at the top and bottom. Since the geogrid reinforcement is to be compared with Geocell, the embedment depth is varied from the top to bottom of Geocell location, i.e., 0.1 (top of geocell), 0.35 (center of geocell) and 0.6 m (bottom of geocell). For double layer geogrid, the spacing is considered equal to the height of the geocell, so as to replicate a planar equivalent of Geocell. The performance of different reinforcement configurations is compared in terms of stress transferred to the subgrade, vertical deformation of subgrade and the stress deformation response of geosynthetic reinforcement. Observations from the numerical analyses are explained in the subsequent sections.

2 Results and Discussion

2.1 Stress Transfer

The geosynthetic reinforcement acts as a membrane in tension and takes up stresses induced by the wheel loads. As a result, the effective stress transferred to the subgrade is lowered. The stress transfer mechanism in the case of geocell reinforced subbase and that of single- and double-layer geogrid reinforced subbase is shown in Fig. 2. It can be seen that the stress transferred to the subgrade is least in the case of the geocell reinforced system. The contribution of vertically jointed geocell walls results in this additional stress reduction. While there is a sharp increase in stress at the wheel contact area in the geogrid reinforced system, the stress distribution pattern is much more uniform in the Geocell reinforced sub-base case. It indicates that the geocell

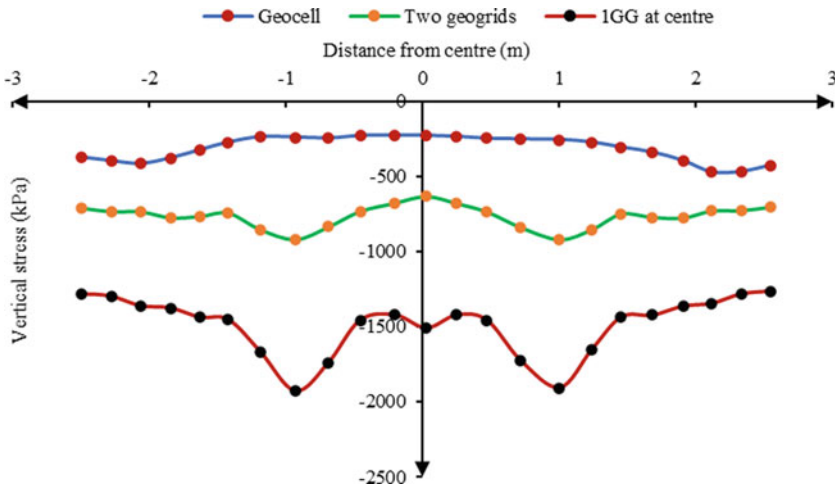


Fig. 2 Vertical stress transferred to subgrade with different forms of geosynthetic reinforced sub base

takes up a higher proportion of stress and distributes it more evenly. The magnitude of stress transferred is improved by providing a double-layer geogrid system, but cellular confinement is the most effective in the magnitude and distribution of stress transfer.

Figure 3 shows the effect of placement depth of geogrid on the stress transfer pattern. It can be seen that the distribution pattern is similar in all cases, but the magnitude of stress transferred to the subgrade is least in the case of geogrid placed at an embedment depth of 0.1 m from the top of the granular base layer. The Geosynthetic reinforcement reduces the stress transfer by sharing a proportion of stress and widening the angle of distribution of load to the underlying layers. A reduced embedment depth implies the distribution angle is widened at shallow depth, which in turn increases the effective area of load distribution at the subgrade surface. As a result, the stress transferred to the subgrade is low. In other words, the reinforcing effect decreases with an increase in the embedment depth of geosynthetic.

2.2 Stress-Deformation Response of Geosynthetic Reinforcement

The reinforcing action of geosynthetic reinforcement in different forms is explained through the shear stress developed on the membrane and deformation mobilized at the surface of the geosynthetic (Figs. 4, 5 and 6). The stress on the geocell is distributed among the whole pocket area in a nearly uniform manner with very little stress concentration on the pockets near wheel contact area. When a single geogrid is used

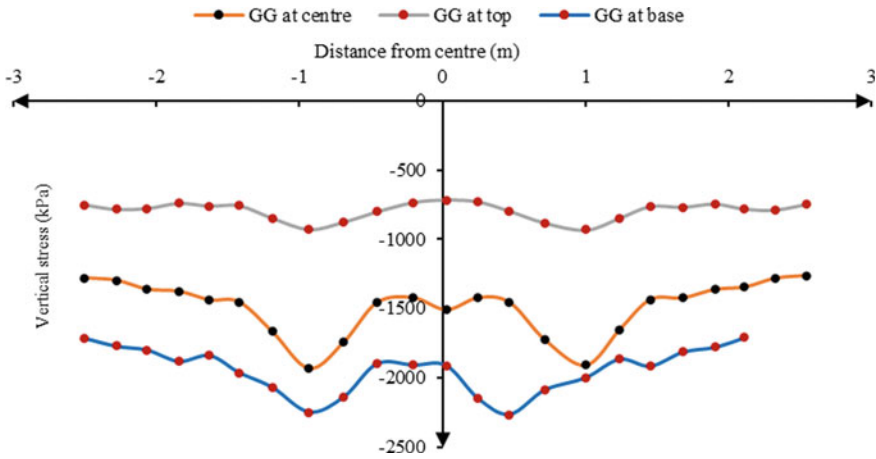


Fig. 3 Effect of geogrid placement depth on vertical stress transferred to subgrade

as reinforcement, the shear stress developed at the sides is more owing to the tensioned membrane effect. The stress concentration is less when two geogrids are used. The magnitude of stress developed is slightly higher, with a significant proportion taken up by the upper geogrid. The stress distribution on lower geogrid is almost uniform. This observation aligns with the higher stress transfer efficiency in the case of geogrid placed at the top compared to other locations (Fig. 4). The stress distribution and deformation pattern indicate that the contribution of lower geosynthetic is not much significant. The geocell network distributes the strain among a wider area. Hence the magnitude of maximum deformation is less than the geogrid reinforced systems. The deformation of lower geogrid is lower than upper geogrid (Fig. 6) due to the less stress transferred to the lower reinforcement.

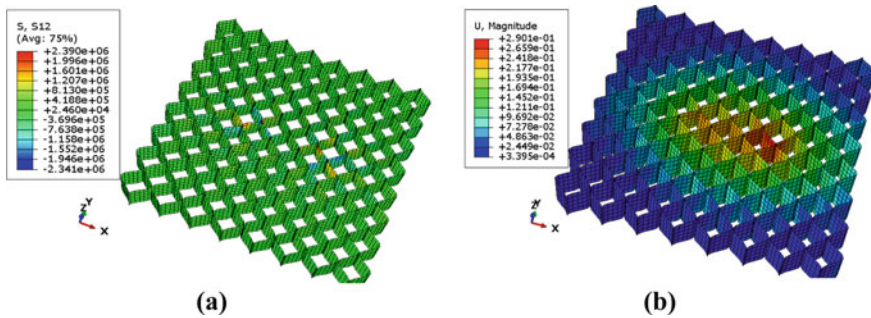


Fig. 4 a Shear stress developed; b deformation in geocell

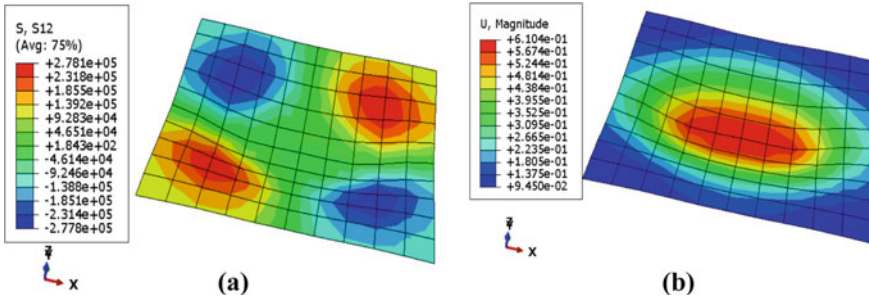


Fig. 5 a Shear stress developed; b deformation in a single geogrid placed at the centre

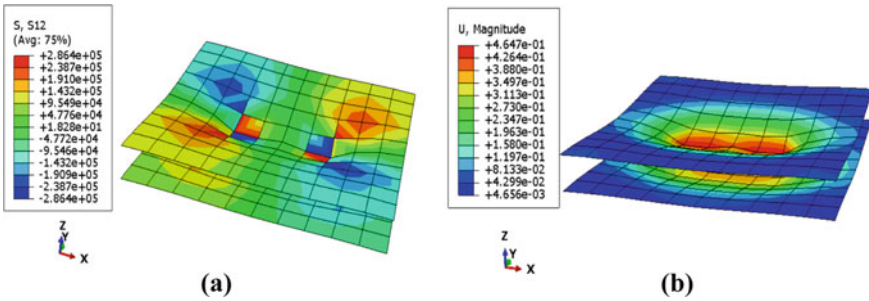


Fig. 6 a Shear stress developed; b deformation in double geogrid

2.3 Subgrade Deformation

The reduction in subgrade settlement evaluates the reinforcement efficiency in the pavement layer. In this study, the vertical deformation after 1000 cycles of loading is analyzed for different reinforcement configuration sin planar and cellular forms (Fig. 7). The stress transfer pattern is reflected in the deformation of the subgrade as well. Since the geocell takes up higher stress, the stress transferred to the subgrade is less in magnitude and more evenly distributed. Thus, the resultant deformation at the subgrade surface is less. The double layer geogrid reinforced pavement exhibits lower subgrade deformation among the geogrid reinforced cases. Still, the profile is undulating due to the stress concentration at the sides of the membrane. The single geogrid reinforcement is most effective when placed at a shallow depth (Fig. 8), where the stress is distributed evenly along the membrane surface. Hence the subsequent stress transfer towards underlying layers become uniform. As the depth of placement increases, the subgrade deformation profile becomes undulating, reflecting longitudinal cracking and alligator cracking on the surface.

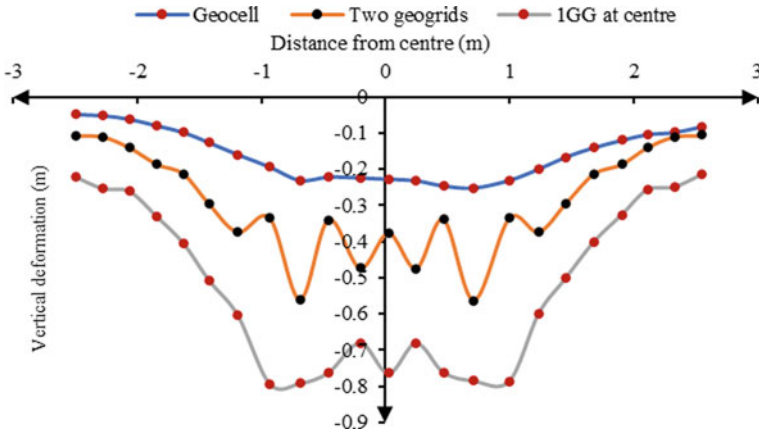


Fig. 7 Vertical deformation profile of subgrade with different forms of geosynthetic reinforced sub base

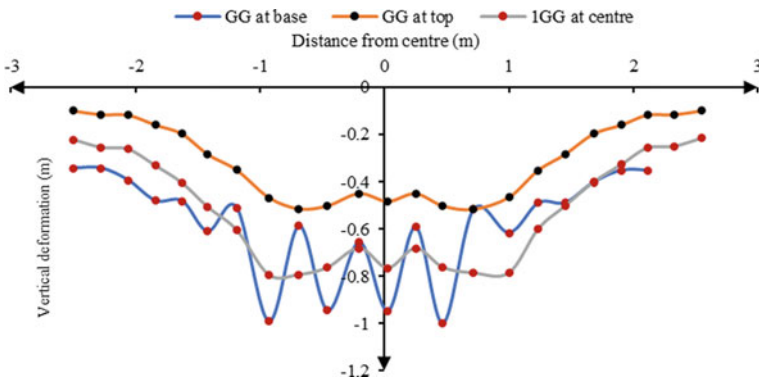


Fig. 8 Effect of geogrid placement depth on vertical deformation profile of subgrade

3 Conclusions

Three-dimensional numerical analyses were done to assess the relative performance of geocell reinforced flexible pavement with that of single and multiple geogrid reinforced pavements. The behaviour was analyzed regarding the stress deformation response of various pavement components. The observations from the study lead to the following conclusions.

- Cellular confinement provided by Geocell walls enables more uniform distribution of stress than the geogrid reinforced system. As a result, the stress transferred by the geocell reinforced sub-base to the underlying subgrade is less in magnitude and smooth in pattern than Geogrid reinforced sub-base.

- A single-geogrid reinforced subbase is effective when embedded at a shallow depth in the granular layer. As embedment depth increases, stress taken up by the planar geogrid reduces. Moreover, the stress distribution fluctuates at higher depths with a stress concentration at the wheel contact area.
- The interconnected pockets in the geocell enable broader distribution of stresses and strains along the geocell. Hence the efficiency of reinforcement is improved. In the planar reinforcement, the lateral boundaries tend to bend under the wheel load, generating stress concentration at the sides. As a result, the deformation profile also fluctuates. Due to less contribution of lower geogrid, multiple geogrid reinforcements create insignificant improvement.
- The stress transferred and resultant deformation of the subgrade is the least in the case of the geocell-reinforced subbase. Unlike geogrid reinforcement, the geocell network creates a rigid platform generating a uniform deformation profile at the underlying layers.

The study is purely numerical, the material properties of which are based on laboratory tests performed as per relevant standards. The presented results on material behavior have been validated by the authors by performing detailed model studies using the mentioned material parameters [10, 11]. The results shall be verified by extending the results to extensive field studies and model analyses incorporating the dynamic behavior of the materials.

References

1. Ibrahim EM, El-Badawy SM, Ibrahim MH, Gabr A (2017) Azam, A: Effect of geogrid reinforcement on flexible pavements. *Innov Infrastruct Solut* 2(1):1–15. <https://doi.org/10.1007/s41062-017-0102-7>
2. Leonardi G, Lo Bosco D, Palamara R, Suraci F (2020) Finite element analysis of geogrid-stabilized unpaved roads. *Sustainability* 12(5):19–29. <https://doi.org/10.3390/su12051929>
3. Dessouky SH, Al-Qadi IL, Yoo PJ (2014) Full-depth flexible pavement responses to different truck tyre geometry configurations. *Int J Pavem Eng* 15(6):512–520. <https://doi.org/10.1080/10298436.2013.775443>
4. Venkateswarlu H, Ujjawal KN, Hegde A (2018) Laboratory and numerical investigation of machine foundations reinforced with geogrids and geocells. *Geotext Geomembr* 46(6):882–896. <https://doi.org/10.1016/j.geotextmem.2018.08.006>
5. Zhou H, Wen X (2008) Model studies on geogrid-or geocell-reinforced sand cushion on soft soil. *Geotext Geomembr* 26(3):231–238. <https://doi.org/10.1016/j.geotextmem.2007.10.002>
6. IRC:37–2001 (2018) Guidelines for the design of flexible pavements. Indian roads congress, New Delhi, pp 19–37
7. Arvin MR, Rezaei E, Bahmani Shoorijeh M (2018) Numerical evaluation of geocell-reinforced flexible pavements under traffic loads. *Sci Iran* 25(2):493–504
8. Huang YH (2004) Pavement analysis and design. Pearson Prentice Hall Inc., Upper Saddle River, pp 8–530
9. Sheikh IR, Mandhaniya P, Shah MY (2021) A parametric study on pavement with geocell reinforced rock quarry waste base on dredged soil subgrade. *Int J Geosynth Ground Eng* 7(2):275

10. Menon AR, Konnur S, Bhasi A (2021) Model tests on coir geotextile-encased stone columns with tyre crumb-infilled basal coir geocell. *Int J Geosynth Gr Eng* 7(2):38. <https://doi.org/10.1007/s4089102100274x>
11. Menon AR, Bhasi A, Konnur S (2023) Experimental and numerical investigation of column-supported soft clays reinforced with basal geocell. *Transp Infrom Geotech* 157:1–28. <https://doi.org/10.1007/s40515023002933>

Experimental Study of the Shear Performance of a Beam Strengthened with Jute and Glass Fiber Hybrid Composite



C. S. Reshma and Jency Sara Kurian

Abstract In beams shear failure occurs when the shear capacity is less than the flexural capacity. Shear strengthening has to be provided under such conditions. The common methods of enhancing the shear capacity of RC beams are Steel plate jacketing, Near mounted surface strengthening method using steel or FRP bars, Externally bonded fiber reinforced polymer strips or laminates. However due to the advantages of Fiber Reinforced Polymer (FRP) composites over other conventional techniques, it has now become a very popular method of shear strengthening. In this paper a total of 3 numbers of shear deficient Reinforced Concrete (RC) beams are designed. A hybrid composite of glass and jute fiber FRP's is made. Hand layup technique is used to prepare the hybrid composites. These composites are then externally wrapped in beams to enhance the shear capacity. The study is conducted to understand the effect of various wrapping configurations, i.e. full and strip wrapping on the shear strengthening of RC beams. The mechanical properties of glass and jute fiber hybrid composites are determined and the load deflection behavior and ultimate failure load of the beams are analyzed experimentally.

Keywords Shear strengthening · Steel plate jacketing · Near surface mounted surface strengthening · FRP · RC beams

1 Introduction

One of the most essential components of concrete buildings is the concrete beam. The shear and bending behaviors of concrete must therefore be optimized, which calls for greater research on these members particularly the shear performance of structures

C. S. Reshma (✉) · J. S. Kurian
Department of Civil Engineering, Amal Jyothi College of Engineering, Kanjirappally, Kerala,
India
e-mail: reshmachempilayil9@gmail.com

J. S. Kurian
e-mail: jencysarakurian@amaljyothi.ac.in

in challenging conditions [1]. In the last several years, the construction industry has been increasingly concerned about FRP (fibre reinforced polymer)-reinforced concrete beams because of their resilience to harsh climatic conditions. One of the main challenges in the design of such beams is the occurrence of shear cracks in FRP-reinforced concrete beams during the course of their service life. The strength of these beams is greatly decreased by these shear cracks. Also, the change in the structure's functions may increase the shear force on the concrete beams. So, it is inevitable that these beams will need their shear characteristics to be repaired and strengthened [2].

The majority of research works on strengthening and repairing reinforced concrete (RC) structures concern the exterior bonding of FRP strips applied to RC structures [3]. Current advancements in the field of composite materials, together with their inborn characteristics such as high specific tensile strength, good fatigue and corrosion resistance, and are simple to utilize offers a great substitute for any other retrofitting method in the field of strengthening and repairing of concrete elements [4]. The combination of matrix and reinforcing materials is referred to as a composite material. For the manufacturing of composite materials, researchers primarily employ the hand layup method. Reinforcing materials include fibres made of glass, carbon, basalt, flax, cotton, hemp, jute, sisal, kenaf, pineapple, ramie, and bamboo. The most common matrix materials are polyester, vinyl ester, and epoxy [5–7].

Due to attractive physical and chemical properties of natural fibers, they can be used to manufacture fiber reinforced polymer composites thereby reducing the use of synthetic fibers such as glass, carbon, basalt etc. which are toxic to the environment. Although the use of synthetic fibers along with polymer epoxy as the matrix material has its own disadvantages, we cannot neglect the benefits they offer such as durability, less moisture absorption etc. [8].

Fewer studies have been conducted on the use of natural and artificial fibre hybrid composites. The goal of this experiment is to adopt a more sustainable practice of making composite materials by reducing CO₂ emissions and thereby achieving carbon neutrality. Although natural fibers are considered more sustainable, eco-friendly and non-toxic but they have a lower tensile strength as compared to artificial fibers. Therefore fully replacing glass fibers with jute is not possible. By using glass-jute composite, partial replacement of glass fibers is possible.

In this experiment a hybrid composite of jute and glass fibers are made and they are used to strengthen beams which are shear deficient. A total of 3 numbers of shear deficient beams were designed and casted. The FRP composites are then externally wrapped in beams to enhance the shear capacity. The study is conducted to understand the effect of various wrapping configurations, i.e. full and strip wrapping on the shear strengthening of RC beams. The mechanical properties of glass and jute fiber hybrid composites are to be determined. The load deflection behavior and ultimate failure load of the beams are to be studied.

2 Fabrication and Testing of FRP Composites

For this experiment woven jute and glass fiber sheets were used. Araldite Standard Epoxy Resin which consists of Araldite AW 106 Standard Epoxy Resin and Araldite Hardener HV 953 IN were used for fabrication of the composites. These resin and hardener were mixed in the ratio 1:1. Hand lay-up technique was adopted for composite fabrication. A plastic bit mold was used for the casting of the composites. A mold releasing agent was used for the easy removal of the composite sheets. The resin and hardener were thoroughly mixed in the ratio 1:1 by using a glass rod to minimize the air entrapment. The fiber sheets were cut according to required sizes. A thin layer of epoxy was applied over the mold and were evenly spread. This was followed by placing one type of fiber mat i.e. glass fiber mat on top the epoxy. The entrapped air was removed using a roller. Epoxy was poured on to the fiber mat and they were evenly spread. Jute fiber mats were then placed and the process continues until the required thickness is obtained. The two types of fibers were placed in alternate configuration. To obtain a good surface finish a matrix coating was provided over the last fiber mat layer. Finally a releasing sheet was placed over the last layer and rolled using a roller. A weight was applied over the composite and was air cured for 24 h.

Tensile strength test was conducted as per ISO 527-4:1997(E) for woven glass, jute and hybrid of glass and jute composites. The specimens were cut in dog bone shape. The composites were laid in 4 layers in order to achieve a minimum thickness of 4 mm. The tensile strength test was conducted on a universal testing machine with at most loading rate of 100 kN by applying a uniaxial load through both the ends of the specimen. Load was applied until the specimen breaks and the corresponding breaking load was noted. Four samples were tested for each composite types and the average tensile strength value was calculated.



Fig. 1 Jute composite



Fig. 2 Glass composite

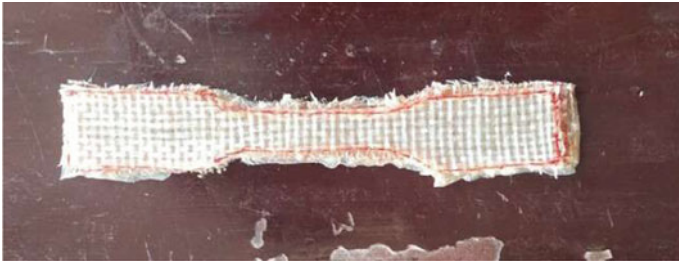


Fig. 3 Glass-jute composite



Fig. 4 Testing of composites

Table 1 Typical properties of epoxy

Properties	Araldite
Young’s Modulus, E (GPa)	1.32 GPa
Poisson’s ratio	0.380
Ultimate tensile stress	23–24 MPa
Ultimate yield stress	21 MPa
Density	1.15 kg/L

Table 2 Tensile strength of glass, jute and glass-jute FRP composites

Type of FRP	Peak tensile load (kN)	Cross sectional area (mm ²)	Average peak tensile load (kN)	Average tensile strength (N/mm ²)
Jute	4.2	60	4.6	76.67
	4.8	60		
	4.6	60		
	4.8	60		
Glass	17.8	76	17.55	230.92
	17.6	76		
	17.2	76		
	17.6	76		
Glass-jute	7.6	80	7.5	93.75
	7.8	80		
	7.6	80		
	7	80		

3 Shear Strengthening of RC Beams Using Glass-Jute FRP

The applicability of glass-jute FRP composite as a shear strengthening material for reinforced concrete beam is evaluated in this chapter. Glass-jute FRP composite is wrapped to the concrete beams and they were tested under two-point loading to determine their load–deflection behaviour and ultimate failure load.

3.1 Materials

For this experiment, Portland Pozzolana Cement was used. The maximum size of coarse aggregate used was 12 mm. The grade of material used was M25 concrete and Fe 500 steel. The concrete mix was designed as per IS 10262-2009 for a designed water-cement ratio of 0.49. The mix proportion by weight of cement: fine aggregate: coarse aggregate was found to be 1:1.64:2.68. Woven glass and jute fibers were used

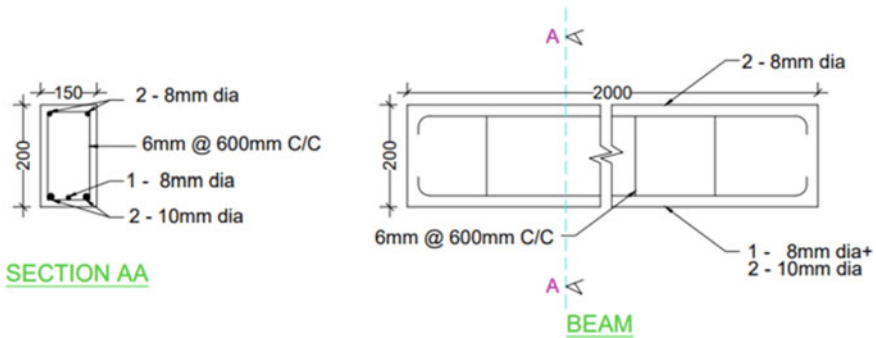


Fig. 5 Reinforcement details of RC beam

for composite preparation. Araldite Standard Epoxy Resin which consists of Araldite AW 106 Standard Epoxy Resin and Araldite Hardener HV 953 IN were used for the fabrication of the composites.

3.2 Design of Reinforced Concrete Beams

The experimental program consists of 3 sets of beams, one control beam and two test specimens. All the beams were designed to fail in shear by providing additional flexural reinforcements and increasing the stirrup's spacing. The size of the beams were $2000 \times 200 \times 150$ mm. The design of RCC beam was carried out as per IS 456:2000. The reinforcement details of the beams is shown in Fig. 5. The reinforcements provided were two no's of 10 mm diameter bar and one 8 mm diameter bar at the bottom face and two no's of 8 mm diameter bar at the top face. 2 legged 6 mm diameter stirrups were provided at 600 mm c/c. The beams are designed such that shear failure precedes the flexural failure. Hence the beams were strengthened in flexure, by providing additional flexural reinforcement. It was made sure that the design of the beam remained under-reinforced even after providing extra flexural reinforcement. All the test specimens were used for evaluating the effect of shear strengthening due to wrapping of glass-jute FRP composite. The control beam was not strengthened and it was used for comparative study purpose.

3.3 Shear Strengthening of Reinforced Concrete Beam with Glass-Jute FRP Composite

Two configurations of composite wrapping was adopted in this experiment. They are full wrapping on two sides of the beam (configuration A) and strip wrapping i.e., U wrap provided on the three sides of the beam (configuration B). In U wrapping

only 50% of the total area was used for strengthening. FRP strip cut at a width of 10 cm were placed over the beams. The clear distance between two consecutive strips were 10 cm. The FRP sheets together with epoxy were arranged in 4 layers thus making a thickness of approximately 4 mm. The fiber sheets were placed in the order glass-jute-glass-jute. The surface of the beams were prepared by grinding the 3 sides of the beam with a grinding machine. This was done to obtain good bonding of the composite. After grinding all the excess dust and loose particles were removed. Epoxy resin and hardener mixed in the ratio 1:1 was evenly spread over the beam. FRP sheets were then placed over the beam. The excess resin was squeezed through the roving of the fabric with the help of a roller. Air bubbles entrapped between the fabrics were carefully eliminated. The strengthened beams are shown in Fig. 6a, b.



(a)



(b)

Fig. 6 a Fully wrapped beam; b 3 sided U wrapped beam

3.4 Experimentation

The beam was loaded under two point loading for the determination of ultimate failure load using a hydraulic jack of 1000 k N size for the application of load. A loading cell of 1000 kN capacity was used to measure the applied load. Two steel columns were erected over a girder placed on a rigid footing. The column head placed with an arrangement on one side is roller and another side as hinge with two plates and a pin at the centre. The supports were provided at a distance of 350 mm from both the ends of the beam. The effective span for which the beams were tested was 1.3 m. Load was applied at one-third spans. At one-third points two round rods were placed and over them a steel girder was placed. Exactly at the centre between two round rods on the girder a hydraulic jack was placed. The top of the hydraulic jack was fixed with a proving ring with dial gauge of capacity of 10t. A potentiometer was placed exactly at the middle touching the bottom face of the beam to note the deflections. In this arrangement the load was applied manually through hydraulic jack. The experimental set up is shown in Fig. 7a-c.

4 Results and Discussions

All the beams were tested to find out their ultimate shear strength capacity and different types of failure modes were observed. The failure modes along with crack pattern are studied.

4.1 Fracture Study

It was found that the control beam had lesser load carrying capacity as compared to the beams strengthened fully and partially. The control beam failed perfectly in shear.

Fully wrapped beam exhibited higher ultimate shear strength than the partially wrapped beam.

5 Fracture Study of Un-strengthened Beam

The un-strengthened beam failed in pure shear. This ensures that the beam was deficient in shear. Diagonal cracks were developed at the support and it extends towards the load at 45° angles. Figure 8 depicts the clear representation of the failure mode of the beam.



(a)



(b)



(c)

Fig. 7 Experimental set up of two point loading on (a) control beam (b) test specimen having FRP on two sides (c) test specimen with partially wrapped FRP



Fig. 8 Diagonal shear failure of un-strengthened beam

6 Fracture Study of Fully Wrapped Beam

The beam failed by the rupture of FRP. The beam failed in shear and the ultimate load carrying capacity was very much higher than the other beams. At higher loads sudden debonding of the FRP was observed. Sudden debonding of FRP occurs on both the two lateral sides of the beam. Shear cracks were observed at the supports and they extended towards the load. These shear cracks were visible after the debonding of the FRP from the beam faces. Figure 9 depicts the clear representation of the failure mode of the beam.



Fig. 9 Debonding of FRP from the surface of the beam

7 Fracture Study of Partially Wrapped Beam

It was observed that the ultimate load carrying capacity of the partially wrapped beam was higher than the un-strengthened beam but was lower than the fully wrapped beam. At higher loads flexural cracks were observed. The beam failed in flexure. No cracks were developed on the FRP. The FRP did not undergo any sort of debonding from the surface of the beam. Figure 10 depicts the clear representation of the failure mode of the beam.

7.1 Load Deflection Behaviour

From the experimental studies, load deflection graphs of all the beams were plotted. The mid-span deflections of strengthened beams were compared with that of the un-strengthened beam. The mid-span deflections were higher in the case of fully wrapped beams due to its higher ultimate load at failure as compared to partially wrapped beams. Both the strengthened beams showed an increase in their ultimate shear strength. The un-strengthened beam had an ultimate failure load of 36.709 kN. Fully wrapped beam exhibited an ultimate failure load of 98.83 kN, whereas partially



Fig. 10 Failure of partially wrapped beam

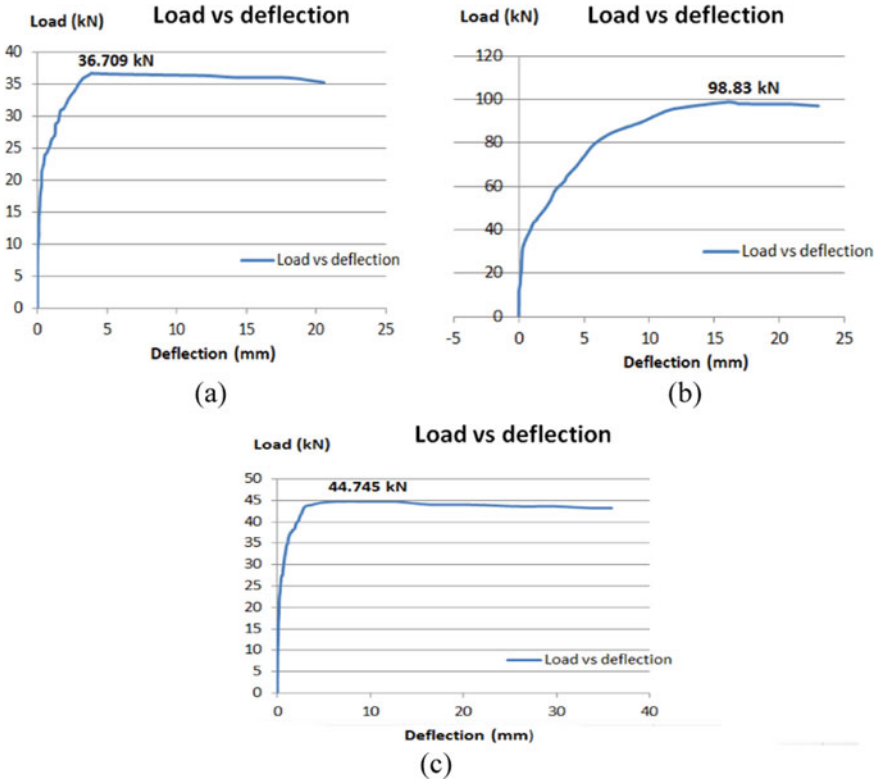


Fig. 11 Load—deflection graph of: (a) un-strengthened beam. (b) Fully strengthened beam. (c) Partially strengthened beam

wrapped beam showed an ultimate failure load of 44.745 kN. The load deflection graphs are shown in Fig. 11a–c.

8 Conclusion

On determining the mechanical properties of glass FRP composite, jute FRP composite and glass-jute FRP composite it was observed that glass composite exhibited higher tensile strength. Glass-jute composite exhibited an increase in tensile strength than jute FRP composite but less than that of glass FRP composite. Although natural fibers are considered more sustainable, eco-friendly and non-toxic but they have a lower tensile strength as compared to artificial fibers. Therefore fully replacing glass fibers with jute is not possible. By using glass-jute composite, partial replacement of glass fibers is possible.

Experimental results showed that wrapping the shear deficient beams with FRP composite is an effective method of shear strengthening. Both full wrapping and strip wrapping increased the ultimate shear strength of the beams. The ultimate shear strength of the retrofitted beams were higher than that of the control beams. Beam with wrapping of 4-layer hybrid composite on both the sides of the beam have an increase of 169.23% in ultimate shear strength, while beams partially wrapped with FRP i.e. strip wrapping showed an increase in ultimate shear strength by 21.89%.

References

1. Draiche K, Bousahla AA, Tounsi A, Alwabri AS, Tounsi A, Mahmoud SR (2019) Static analysis of laminated reinforced composite plates using a simple first-order shear deformation theory. *J Comput Concr* 24(4):369–378
2. Hussein ME, Yousef AA, Tarek HA, Abdulhafiz OA, Husain A (2019) Experimental and numerical study on FRP-upgraded RC beams with large rectangular web openings in shear zones. *Constr Build Mater* 194:322–343
3. Tran CTN, Nguyen XH, Nguyen HC, Le DD (2021) Shear performance of short-span FRP-reinforced concrete beams strengthened with CFRP and TRC. *Eng Struct* 242:112548
4. Yan L, Kasal B, Huang L (2016) A review of recent research on the use of cellulosic fibres, their fibre fabric reinforced cementitious, geo-polymer and polymer composites in civil engineering. *Compos B Eng* 92:94–132
5. Ceroni F (2010) Experimental performances of RC beams strengthened with FRP materials. *Constr Build Mater* 24(9):1547–1559
6. Al-Amery R, Al-Mahaidi R (2006) Coupled flexural–shear retrofitting of RC beams using CFRP straps. *Compos Struct* 75(1–4):457–464
7. Sengun K, Arslan G (2022) Parameters affecting the behaviour of RC beams 212 strengthened in shear and flexure with various FRP systems. *Structures* 40:202
8. Sen T, Reddy HJ (2014) Efficacy of bio derived jute FRP composite based technique for shear strength retrofitting of reinforced concrete beams and its comparative analysis with carbon and glass FRP shear retrofitting schemes. *Sustain Cit Soc* 13:105–124

Numerical Analysis on Flexural Strength of Composite Slab with Inverted U-Shaped Shear Connector



S. Niranjana  and Milu Mary Jacob 

Abstract Steel–concrete composite slab utilizes the advantages of steel as well as concrete and also reduces the overall dead loads. Flexural failure, vertical shear failure and longitudinal shear failure are the three major failure modes of a composite slab. The most prominent mode of failure is the longitudinal shear failure which is denoted by the horizontal slip between steel sheet and the concrete layer. In order to reduce slip, inverted U shaped shear connectors are introduced. This study focuses to improve the flexural strength of composite slab by using High-Performance Concrete (HPC), which also incorporated the usage of construction and demolition waste as recycled coarse aggregates. Numerical study is conducted on simply supported one-way slab. Parameters varied and studied are different configurations of inverted U-shaped connectors and overall depth of the slab. The composite slab with inverted U-shaped connector is expected to have more load carrying capacity and flexural strength than composite slab with shear studs.

Keywords Composite slab · HPC · Finite element analysis · Flexural strength · Shear connectors

1 Introduction

Steel–concrete composite slabs are a type of structural system that combines the advantages of steel and concrete to create a high-performance and sustainable building solution. Steel–concrete composite slabs are structural elements consisting of a concrete layer and a steel sheet that are connected and act together to resist loads. The concrete layer is typically poured onto the top of the steel sheet, and the

S. Niranjana · M. M. Jacob (✉)
Department of Civil Engineering, Saintgits College of Engineering, Kottayam, Kerala, India
e-mail: milu.mary@saintgits.org

S. Niranjana
e-mail: ns.sm2123@saintgits.org

two materials are mechanically bonded through various means, such as mechanical fasteners (e.g. headed studs or shear connectors), welded studs, or profiled sheeting with embossments or ribs. The composite action between the concrete and steel sheet provides several advantages, including increased strength and stiffness, enhanced resistance to bending and deflection, improved fire resistance, and reduced construction time, raw material use, overall dead load and costs. Composite slabs are commonly used in various types of buildings and structures, such as office buildings, industrial facilities, bridges, and parking garages.

Three major types of failure that occurs in a composite slab are flexural failure, horizontal shear failure between steel and concrete and vertical shear at support. Although flexural failure is the preferred mode of failure due to its better load bearing capacity, horizontal shear failure is the most prevalent failure mode among the three. Concrete and steel sheets should operate as a good composite to prevent failure. The composite action can be accomplished through chemical adhesion, mechanical interlocking, and frictional interlocking, i.e. via embossments and intermediate stiffeners, shear screws, shear studs, etc. [1]. The longitudinal shear transfer mechanism at the point where the concrete and steel meet greatly contribute to the strength of the composite slab. The connector type, connector spacing, and concrete strength influences the performance of the composite deck slab [2]. Different forms of mechanical interlocks, for example shear embossments, holes, transverse wires, and other shear connection devices, which give the composite action of concrete and steel sheets, are used to bind steel and concrete [3].

Providing shear connectors throughout the deck [4] can improve the composite action between the concrete and steel sheets, leading to increased load carrying capacity and stiffness. This is because the connectors transfer the shear forces and bending moments between the two materials, reducing the slip between them and ensuring they act together as a composite system [5]. In this study, to reduce slip between concrete layer and the steel sheet, inverted u-shaped shear connectors are installed throughout the deck. Various arrangements of these connectors are analysed and the configurations with higher load carrying capacities are further studied by varying overall depth of the slab [6].

2 Concrete

For high performance concrete, M60 grade is selected. OPC 53 grade cement is partially replaced by GGBS to ensure higher compressive strength [7]. To ensure sustainability, the concrete waste is used as recycled coarse aggregates. Preliminary experiments on materials used, i.e. cement fine aggregates, coarse aggregates and recycled concrete aggregates, are conducted. Compressive strength of concrete cubes with 40% GGBS replacement of cement and 30% recycled concrete aggregates replacement of coarse aggregates is determined experimentally and is found to be 60.68 N/mm².

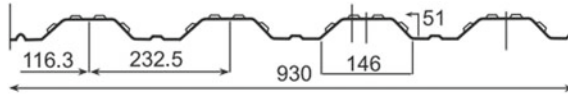


Fig. 1 Sheet dimensions from manufacturer

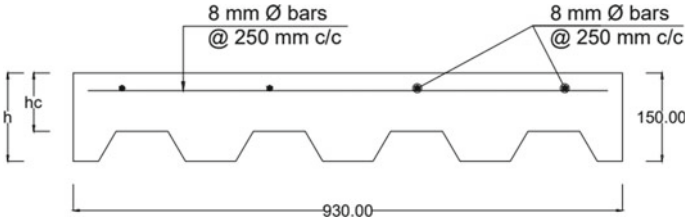


Fig. 2 Reinforcement detailing of composite slab

3 Numerical Analysis

3.1 Modelling

The designed composite deck slab is modelled in ANSYS Workbench (2021) software and imported to Abaqus/CAE (2019) software to determine the load, deflection and slip [8]. The specimen with total length of 2500 mm, width of 930 mm and overall depth of 150 mm are primarily analysed. The deck sheet with 1 mm thickness and M60 concrete with 30% replacement of coarse aggregates with recycled concrete aggregates are used. The top surface is provided with mesh reinforcement of 8 mm ϕ bars @ 250 mm c/c. The cross-sectional dimensions of steel deck are shown in Fig. 1 and reinforcement detailing after design as per Eurocode 4 [6] is shown in Fig. 2.

Various configurations of inverted U-shaped shear connectors are considered for the numerical study. Long and short type inverted U-shaped connectors are provided in staggered as well as parallel arrangements. The short type connectors are also placed longitudinally and transversely across the deck. The shear connectors are spaced at 500 mm c/c along the rib. The cross-sectional dimensions of long and short inverted U-shaped connectors are demonstrated in Fig. 3a, b. The details of models are given in Table 1.

3.2 Finite Element Analysis

Modelled elements are imported to Abaqus. Different configurations of inverted U-shaped shear connectors are modelled and analysed and the configurations with greater load carrying capacity is adopted for further study. The depth of concrete layer

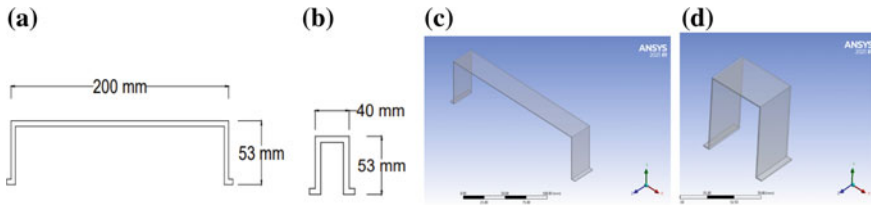


Fig. 3 a, b Cross sectional dimensions of long and short inverted U-shaped shear connector respectively. c, d Long and short inverted U-shaped shear connector modelled respectively

Table 1 Description of models

Name	Type of connector	Position of connector
Staggered U0	Short inverted U-shaped shear connector	Transverse direction, staggered arrangement
Parallel U0	Short inverted U-shaped shear connector	Transverse direction, parallel arrangement
Staggered U90	Short inverted U-shaped shear connector	Longitudinal direction, staggered arrangement
Parallel U90	Short inverted U-shaped shear connector	Longitudinal direction, parallel arrangement
Long U	Long inverted U-shaped shear connector	Transverse direction, staggered arrangement
Shear studs	Shear studs	Staggered arrangement

is varied from 100 to 150 mm for the selected configurations, in order to determine the variation in load carrying capacity various configurations tried are shown in Fig. 4.

The properties of concrete and steel used for the composite slab are provided in Tables 2 and 3 respectively.

The parts are assembled, and material properties are assigned for each element. The concrete, steel sheet, shear connectors and the reinforcement bars are modelled as 3D deformable parts. Concrete section is defined as homogeneous solid while deck sheet is defined as homogeneous shell. Top surface of concrete is partitioned at a distance of $1/3$, i.e. 867 mm, from either ends to provide load as per the four-point bending test. Bottom surface of deck sheet is similarly partitioned at 100 mm from either ends to provide support conditions. The bottom surface of concrete and top surface of steel deck are provided with friction contact with friction coefficient 0.45. The shear connectors are connected to deck sheet by tie constraint and that with concrete by embedded region. The reinforcement bars are also provided with embedded region constraint. Reference points are coupled with the nodal lines of partition for distribution of line load. Displacement value is entered at U2 point in negative direction (downward) for the load application. Mesh size of each elements

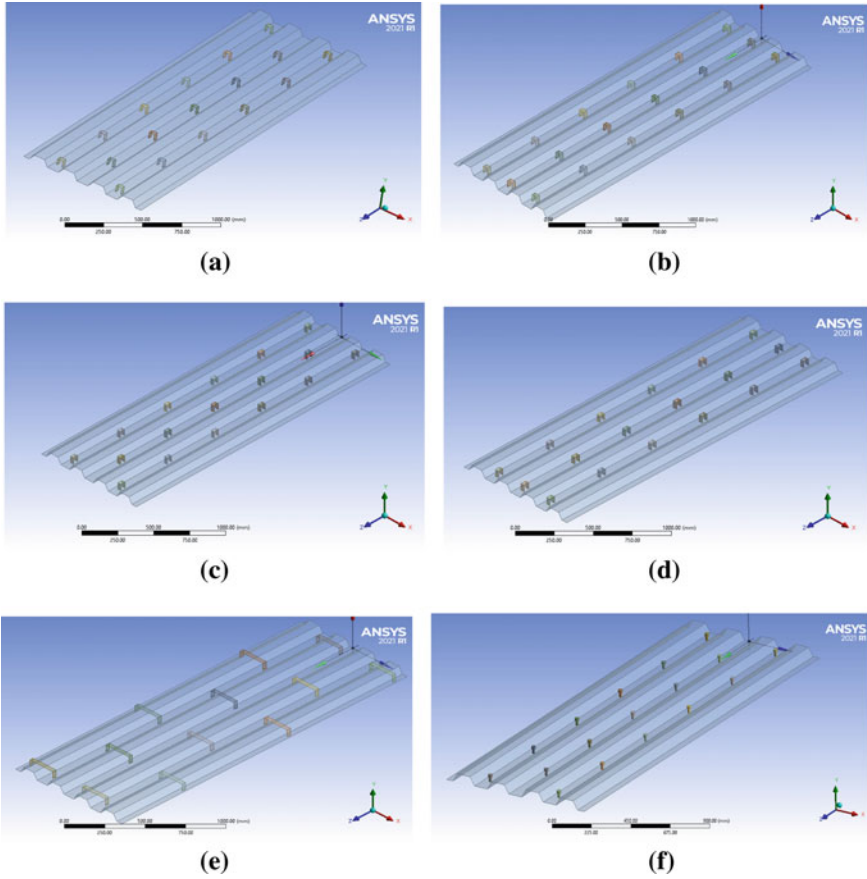


Fig. 4 **a** Staggered U0 model. **b** Parallel U0 model. **c** Staggered U90 model. **d** Parallel U90 model. **e** Long U model. **f** Shear stud model

Table 2 Properties of steel deck sheet

Parameter	Values
Thickness	1 mm
Yield strength	240 N/mm ²
Density	7850 kg/m ³
Young's modulus	200,000 N/mm ²
Poisson's ratio	0.3

are adopted by conducting mesh dependency study. As mesh size reduces, the accuracy of result increases but the computation time tremendously increases, as shown in Table 4. The adopted mesh size of various elements provided is given on Table 5.

Table 3 Properties of concrete

Parameter	Values
Density	2400 kN/m ³
Characteristic compressive strength	60.68 N/mm ²
Young's modulus	38,948.68 N/mm ²
Poisson's ratio	0.18

Table 4 Mesh dependency study

Trial No	Concrete (element size)	Deck (element size)	Reinforcement (element size in mm)	Shear connector (element size in mm)	Number of elements	Deformation (mm)
1	24	24	8	4	37,528	2.822
2	22	22	6	3	52,202	2.791
3	20	20	5	2	77,116	2.750
4	18	18	4	1	147,366	2.746

Table 5 Mesh size provided

Elements	Mesh size	Type of element
Concrete	20	C3D8R (linear hexahedral elements)
Steel deck	20	S4R (linear quadrilateral)
Shear connectors	2	S4R (linear quadrilateral)
Reinforcement	5	T3D2 (linear line elements)

4 Results

The models are analysed by Abaqus/CAE and the models staggered U0 and long U found to have greater load carrying capacities compared to that of other models. So, these 2 models are further analysed for smaller concrete depths. Overall slab depth is varied as 100, 125 and 150 mm. The load deflection curve for various shear connectors are shown in Fig. 5 and load displacement values in Table 6.

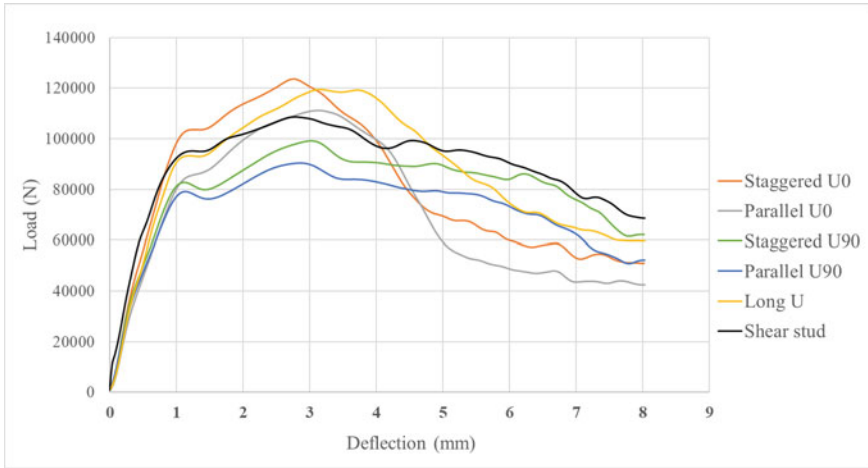


Fig. 5 Load deflection graphs of various shear connectors

Table 6 Load displacement values

Type of connector	Maximum load (kN)	Displacement (mm)	Slip (mm)
Staggered U0	123.62	2.75	1.92
Parallel U0	111.16	3.11	2.71
Staggered U90	99.23	2.68	2.17
Parallel U90	90.49	2.87	2.76
Long U	119.51	3.15	2.23
Shear stud	108.52	2.80	2.62

5 Conclusion

Finite element analysis was employed to investigate the load and deflection characteristics of different configurations of inverted U-shaped shear connectors. By placing the connectors along the ribs of the steel deck, the load-carrying capacity of the composite slab is significantly improved. The connectors placed in staggered arrangement has higher load carrying capacities than the parallel arrangement. Staggered U0 and Long U models possess highest load carrying capacity and flexural strength than the other models. Staggered U0 performed better than Long U. This may be because long U connectors, due to its greater length and thinner sections undergo failure earlier than that of Staggered U0 connectors. It was also be noted that the staggered arrangement of connectors exhibited more load carrying capacity than the parallel arrangement. This can be due to the more evenly distributed contact between the steel and concrete in the staggered arrangement. In the parallel arrangement, every other trough or section lacked the same level of contact between the steel

and concrete, leading to potential stress concentrations and reduced load carrying capacity in those areas. This non-uniform contact could result in localized failures and decreased overall performance of the composite slab. The following conclusions can be drawn from the study. Load displacement graphs of staggered U0 connector is shown in Figs. 6 and load deflection graphs of long U connector is shown in Fig. 7.

- Staggered U0 model shows 13.91% increase in the ultimate load value than shear studs and 26.71% reduction in slip.
- Long U model shows 10.13% increase in the ultimate load value than shear studs and 14.88% reduction in slip.
- The ultimate load values and the deflection corresponding decrease with decrease in overall depth of slab.

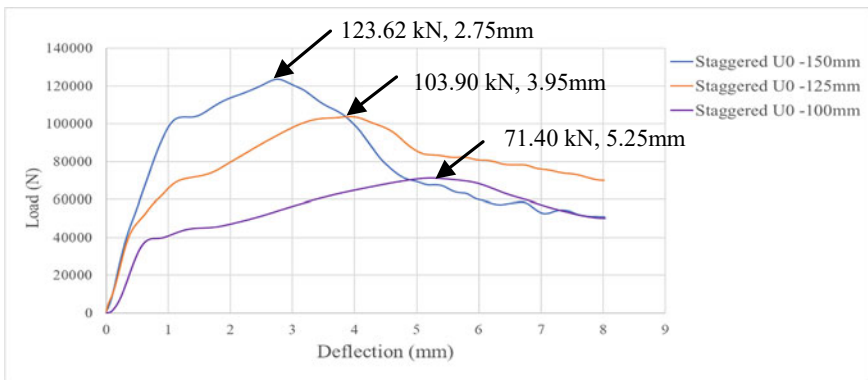


Fig. 6 Load deflection graphs of staggered U0 with various overall depths

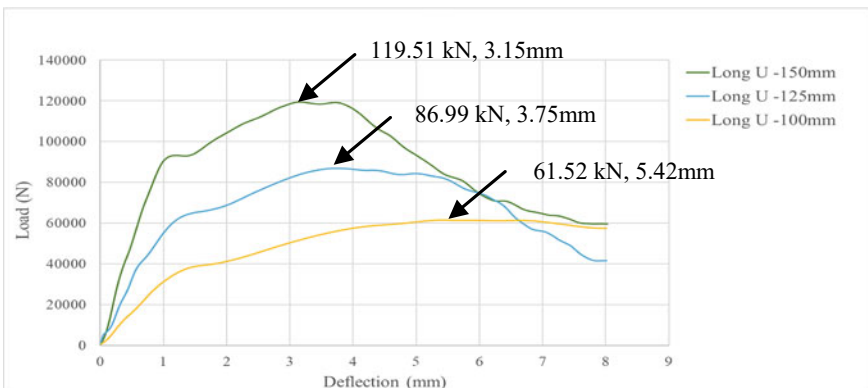


Fig. 7 Load deflection graphs of long U with various overall depths

- Composite slab of depth 125 mm with staggered U0 connectors have 15.95% reduction in load carrying capacity while slab with 100 mm depth have 42.24% reduction in load carrying capacity.
- Composite slab, with long U connectors, of depth 125 mm have 25.91% reduction in load carrying capacity while slab with 100 mm depth have 47.60% reduction in load carrying capacity.

References

1. Shirgaonkar AA, Patil YD, Patil HS (2021) Influence of stiffeners and pattern of shear screws on behaviour of cold formed profiled deck composite floor. *Case Stud Constr Mater* 15:1–16
2. Lakshmikandhan KN, Sivakumar P, Ravichandran R, Jayachandran SA (2013) Investigations on efficiently interfaced steel concrete composite deck slabs. *J Struct* 147:1–10
3. Eltobgy HH, Abdelkareem KMM, Bakhoum MM (2021) Experimental study on shear bond behavior of composite deck slab equipped with shear connectors. *Int J Sci Technol Res* 10(5):76–85
4. Burnet MJ, Oehlers DJ (2001) Rib shear connectors in profiled slabs. *J Constr Steel Res* 57:1267–1287
5. Dar MA, Subramanian N, Dar AR, Ghowsi AF, Siddiqui F, Fayaz S, Mir MS (2020) Comparison of various shear connectors for improved structural performance in CFS concrete composite slabs. *Eng Struct* 220:1–15
6. Eurocode 4 (1994) Design of steel and concrete composite structures. EN1994 1-1 & 1-2
7. Buddhe N, Barsagade D, Bhende S, Petkule A, Borkar T, Lanjewar PS (2020) High performance concrete using recycled aggregates. *Int Res J Eng Technol* 07:1421–1425
8. Hossain KMA, Attarde S, Anwar MS (2019) Finite element modelling of profiled steel deck composite slab system with engineered cementitious composite under monotonic loading. *Eng Struct* 186:13–25

Sustainable Transportation Indicators for Urban Areas: A Systematic Review



Abdelrahman M. Farouk , Liyana Mohamed Yusof ,
Rahimi A. Rahman , and Azlina Ismail 

Abstract Sustainable transportation is crucial for promoting long-term health, well-being, and economic prosperity of individuals, societies, and economies. Transportation is responsible for significant greenhouse gas emissions, air pollution, and environmental degradation. To identify sustainable transportation indicators in urban areas, this study conducted a systematic review of 23 published articles related to sustainable transportation indicators in urban areas, analyzing the articles thematically to identify five main themes: Accessibility, Environment, Infrastructure, Performance, and Economic. The most commonly mentioned subthemes were Gas Emissions, Energy Consumption, and Monthly Fuel Price. The findings also emphasize the importance of considering multiple indicators and subthemes for a coordinated approach to sustainable transportation that maximizes sustainability improvements in urban areas. This study contributes to the ongoing discourse on sustainable urban development and transportation planning by identifying and analyzing key indicators that can be used to measure sustainability in urban transportation systems.

Keywords Sustainable transportation · Urban transportation · Systematic review · Thematic analysis · Indicators

1 Introduction

Sustainability, defined as meeting the needs of the present without compromising the ability of future generations to meet their needs [1], is a critical consideration in transportation planning. Sustainable transportation planning raises significant issues that impact the definition of sustainability and sustainable transportation. Additionally, how goals and objectives are defined, evaluated and the decision-making process is

A. M. Farouk · L. M. Yusof (✉) · R. A. Rahman · A. Ismail
Universiti Malaysia Pahang Al-Sultan Abdullah, Lebu Persiaran Tun Khalil Yaakob, 26300
Kuantan Pahang, Malaysia
e-mail: liyanam@ump.edu.my

critical to achieving sustainable transportation. Sustainability requires comprehensive and integrated planning considering a broad set of economic, social, and environmental impacts, including those that are difficult to measure [2]. Failing to account for the impact of transportation on various sectors can result in missed opportunities to create sustainable transportation systems that benefit everyone. Neglecting to recognize the interconnectedness of environmental, social, and economic issues can lead to incomplete solutions and missed opportunities to create genuinely sustainable transportation systems.

A narrow definition of sustainability can exacerbate these problems and create gaps between finding solutions and solving problems. Urban transportation faces many sustainability issues that pose significant challenges for cities. One of the primary concerns is the over-reliance on private vehicles, which contributes to traffic congestion, air pollution, and carbon emissions [3]. The sprawling nature of many cities exacerbates these problems, requiring people to travel long distances to access goods and services. This further increases reliance on automobiles and adds to environmental degradation. Additionally, the lack of priority given to public transport, walking, and cycling is a significant issue, which leads to inadequate infrastructure and facilities for these modes of transport. Furthermore, the subsidization of private vehicles through road infrastructure and taxes only reinforces car dependency and adds to the economic and environmental burdens associated with unsustainable transportation [4]. These challenges highlight the need for comprehensive and integrated planning that prioritizes sustainable transportation solutions to address the complex and interconnected issues facing urban areas.

A possible solution to the challenges of sustainable transportation is the identification of sustainable transportation indicators. These indicators can be used to evaluate the performance of transportation systems in terms of environmental, social, and economic sustainability [5]. By incorporating sustainability indicators into transportation planning and decision-making, it is possible to create more diverse and economically efficient transportation systems, as well as more compact land use patterns that reduce dependence on private vehicles. Sustainable planning can help to reduce resource consumption and harmful environmental impacts while supporting economic growth [6]. However, it is important to acknowledge and address the gaps that exist between finding solutions and implementing them in order to ensure a sustainable future for all.

In order to address the current issues and find solutions for sustainable transportation, the study was conducted to identify the indicators of sustainable transportation. A systematic review of 23 articles on sustainable transportation indicators in urban areas was carried out using thematic analysis. The findings of this study can serve as a guide for policymakers and transportation planners to develop effective strategies to address the issues of unsustainable transportation in urban areas. The study's findings provide valuable insights for policymakers, transportation planners, and researchers, highlighting the importance of considering a comprehensive set of indicators for sustainable transportation planning and decision-making in urban areas.

2 Methodology

The study aimed to identify sustainable transportation indicators through a systematic review (SLR). The SLR is a thorough and methodical approach to analyzing all available evidence related to a research question to provide a reliable and unbiased summary of existing knowledge. The SLR is a commonly used and accepted methodology in research [7–10]. The first stage is the search using Scopus's Title/Abstract/keyword (T/A/K) feature. Scopus was chosen because it covers a broader range of literature in different areas compared with Web of Science, Google Scholar, and PubMed [11]. The search was conducted on 10/2/2023. The search string was as follows: (TITLE-ABS-KEY (“sustainable transport*” AND urban AND indicator)) AND (LIMIT-TO (SRCTYPE, “j”)) AND (LIMIT-TO (PUBSTAGE, “final”)) AND (LIMIT-TO (DOCTYPE, “ar”)) AND (LIMIT-TO (LANGUAGE, “English”)). Also, the search was done in the last decade, from (2012–2023). The initial search yielded around 98 articles. The search string included journal articles in English.

In the second stage, a visual examination was conducted on 98 articles to remove unrelated articles. A total of 24 articles were concluded from the second stage. In the third stage, a full-text check was conducted on the 24 articles to check if it falls within the scope of the research aim. The stage resulted in 12 articles in total. Due to the limited number of articles snowballing technique was adopted, which was the last stage. The snowballing technique included both forward and backward. Forward snowballing is going through references, and backward snowballing is going through references. Moreover, the snowballing went through journal and conference papers within the time range for more results. The snowballing resulted in a total of 11 more articles. The final total number of articles is 23 articles.

3 Results

After identifying the 23 articles, the next step was thematic analysis. Thematic analysis is a robust technique that aims to identify patterns or themes within the data that provide insights into the research question or topic being studied. It is widely used in qualitative data analysis, such as SLR data [12–14]. This thematic analysis aimed to identify indicators of sustainable transportation. The analysis identified five main themes: Accessibility, Environment, Infrastructure, Performance, and Economic. Under the Accessibility theme, subthemes included Disabled Access, Non-motorized Vehicles, Public Transport, Pedestrian and Cyclist Areas, and Plan Coverage. The Environment theme had subthemes such as Green Transport, Gas Emissions, Renewables and Alternative Fuels, and Energy Consumption. The Infrastructure theme included subthemes such as Airport Traffic, Cycling, Inland Ports, Parking, Pavement and Road Roughness Index, Transport Fleet Age, and Pedestrian Infrastructure. The Performance theme had subthemes such as Data Availability, Safety and Security, Transport Quality and Reliability, Transport Speed, Transport

Comfort, Passenger Transport, and Traffic Congestion. Finally, the Economic theme had subthemes such as Freight Income, Newly Registered Cars, Transport Revenue, Public Transport Investments, Car Ownership, Monthly Fuel Price, and Transport Expenses.

4 Discussion

The following section discusses the key themes of sustainable transportation: accessibility, environment, infrastructure, performance, and economic. These themes are interrelated and provide a comprehensive understanding of sustainable transportation. Table 1 below summarizes the research findings related to the key themes of sustainable transportation: accessibility, environment, infrastructure, performance, and economic. This table provides a quick reference guide to the key sub-themes influencing sustainable transportation choices and highlights the interrelated nature of these themes.

4.1 Accessibility

Accessibility refers to the ease individuals can access transportation modes and services. It is a crucial factor in promoting sustainable transportation as it encourages people to choose alternative modes of transport with less environmental impact. Disabled access is a vital subtheme as it ensures that transportation services are accessible to people with disabilities, promoting inclusivity. Non-motorized vehicles such as bicycles and walking are sustainable transportation modes that encourage active travel and reduce reliance on fossil fuels. Public transport has the most mentions with eight times and indicates its importance in the Accessibility theme. In this subtheme, buses and trains provide an efficient means of transportation for many people. Pedestrian and cyclist areas encourage active travel and promote public health. Finally, plan coverage is a subtheme that ensures that sustainable transportation options are considered in the planning stages of new developments, encouraging sustainable transportation choices.

4.2 Environment

The environment theme focuses on the impact of transportation on the environment. Green transport is a subtheme that encourages using environmentally friendly modes of transportation, such as electric vehicles or hybrid cars. Gas emissions are the most mentioned subtheme, with a total of sixteen times. This emphasizes the need to reduce harmful emissions from transportation that affect the environment and is a

Table 1 Research findings

Theme	Subtheme	References	Mentions
Accessibility	Public transport	[9–16]	8
	Plan coverage	[10, 12, 13, 16, 17]	5
	Pedestrian and cyclist areas	[10, 12–14]	4
	Non-motorized vehicles	[10, 12, 18]	3
	Disabled access	[11, 12]	2
Environment	Gas emissions	[8, 9, 11–13, 15–25]	16
	Energy consumption	[8–10, 12, 13, 15, 17, 18, 22, 23, 25–27]	13
	Renewables and alternative fuels	[9, 10, 12, 13, 15, 17, 18, 24]	8
	Green transport	[10, 12, 13, 15, 17]	5
Infrastructure	Cycling	[10, 12, 21, 24]	4
	Parking	[9, 12, 23, 24]	4
	Pedestrian infrastructure	[10, 12–14, 24]	4
	Transport fleet age	[12, 24, 28]	3
	Airport traffic	[12, 21]	2
	Inland ports	[12, 21]	2
	Pavement and road roughness index	[12, 21]	2
Performance	Safety and Security	[8, 9, 11, 12, 15, 17, 18, 22, 24, 26, 27, 28]	12
	Traffic congestion	[13, 15–17, 19–21, 24, 26]	9
	Transport speed	[12–15, 17, 23–25]	8
	Transport quality and reliability	[12, 15–17, 24, 26]	7
	Passenger transport	[3–6, 18, 20, 25]	7
	Transport size and comfort	[3–6, 18, 20]	6
	Data availability	[3, 4, 20, 30]	4
Economic	Monthly fuel price	[9, 10, 12, 13, 15, 17, 18, 21, 24, 29]	10
	Public transport investments	[9, 10, 12–14, 16, 17, 21, 29]	9

(continued)

Table 1 (continued)

Theme	Subtheme	References	Mentions
	Transport expenses	[8, 12, 13, 15, 17, 29]	6
	Freight income	[12, 13, 17, 21, 25]	5
	Newly registered cars	[12, 13, 17, 21]	4
	Transport revenue	[8, 12, 13, 17]	4
	Car ownership	[12, 13, 17, 24]	4

primary contributor to greenhouse gas emissions and air pollution. Renewables and alternative fuels such as biofuels or hydrogen can replace fossil fuels and significantly reduce the impact of transportation on the environment. Energy consumption is a subtheme that emphasizes the need to reduce the energy consumed by transportation; It is the 2nd most mentioned subtheme under environment theme. Overall, reducing energy consumption in transportation has several benefits, including mitigating the effects of climate change by lowering greenhouse gas emissions, conserving finite resources, improving cost efficiency, promoting healthier communities by reducing air pollution, and enhancing safety [19].

4.3 Infrastructure

The infrastructure theme focuses on the physical infrastructure that supports sustainable transportation. Airport traffic is a subtheme that emphasizes the need to reduce the environmental impact of air travel. Cycling is a crucial subtheme that encourages active travel and provides secure bicycle parking. Inland ports are an alternative to traditional seaports, reducing the environmental impact of long-haul shipping. Parking is a subtheme that emphasizes the need for efficient use of parking space, reducing congestion, and encouraging alternative modes of transportation. The pavement and road roughness index is a subtheme that emphasizes the need for well-maintained roads and infrastructure, reducing the impact of transportation on the environment. The transport fleet age is a vital subtheme emphasizing the need for newer, more efficient vehicles. Finally, pedestrian infrastructure is a subtheme emphasizing the need for safe and accessible pedestrian infrastructure, encouraging active travel [6].

4.4 Performance

The performance theme focuses on the quality of transportation services. Data availability is a vital subtheme as it provides information on the performance of transportation services, which can be used to improve efficiency and reduce the environmental impact. Safety and security is a subtheme emphasizing the importance of safe transportation services. It is the 3rd most mentioned overall and the most under the Performance theme. A safe and secure transportation system can contribute to economic growth and development by improving access to goods and services. By contrast, unsafe and insecure transportation systems can lead to accidents, injuries, loss of life, and damage to infrastructure and property. Transport quality and reliability are important subthemes that encourage using high-quality transportation services. Transport speed is a subtheme that encourages efficient transportation services, reducing the environmental impact of transportation. Finally, transport size and comfort is a subtheme that emphasizes the need for efficient use of space in transportation, reducing the environmental impact of transportation.

Furthermore, it encourages comfortable transportation services, promoting sustainable transportation choices. Therefore, passenger Transport is one of the most essential sub-themes in transportation performance. Traffic congestion is a subtheme that emphasizes the need to reduce traffic congestion, which can be achieved through improved transportation infrastructure [22, 31].

4.5 Economic

The economic theme focuses on the financial aspects of sustainable transportation. This theme includes sub-themes such as freight income, newly registered cars, transport revenue, public transport investments, car ownership, monthly fuel price, and transport expenses. These sub-themes help in understanding the economic benefits and costs of sustainable transportation. For example, public transport investments and the share of public transport indicate the level of investment in sustainable transportation and the degree to which people use public transport, which is often more sustainable than private transport. Car ownership and newly registered cars can indicate the overall demand for private vehicles, while monthly fuel prices and transport expenses can indicate the costs associated with private transport. Monthly fuel price, in particular, was the 4th most mentioned subtheme with a total of 10 times. Monthly fuel price is an important indicator of sustainable transportation for several reasons. High fuel prices can lead to higher transportation costs, reducing people's travel ability and decreasing economic activity [25, 32].

5 Conclusion

The study aims to identify sustainable transportation indicators through the SLR approach. The SLR consisted of four stages. The first stage involved a search using Scopus's T/A/K feature. The initial search yielded around 98 articles. In the second stage, a visual examination was conducted to remove unrelated articles, and a total of 23 articles were concluded from the second stage. In the third stage, a full-text check was conducted on the articles to check if they fall within the scope of the research aim. Finally, in the fourth stage, a data extraction process was conducted to extract relevant information from the 23 articles. The study identified sustainable transportation indicators based on five themes: Accessibility, Environment, Infrastructure, Performance and Economic. These themes are broken down into subthemes, which provide a comprehensive understanding of sustainable transportation indicators. The study's findings have practical implications for policymakers and transportation planners, who can use the identified indicators to prioritize investment in sustainable transportation and achieve the most significant economic impact. Additionally, the study has theoretical implications for future researchers interested in sustainable transportation. Although the research aim was successfully achieved, this study has several limitations. Firstly, the study was limited to urban areas, and the findings may not apply to rural or suburban areas. Secondly, while the study used Scopus as the primary database for the search, snowballing helped overcome this limitation. Lastly, this study aimed only to identify sustainable transportation indicators from the current literature, and future studies can focus on finding the gap within the literature.

Acknowledgements This work is supported by Universiti Malaysia Pahang [RDU220321].

References

1. Farouk AM, Rahman RA, Romali NS (2021) Non-revenue water reduction strategies: a systematic review. *Smart Sustain Built Environ* 12(1):181–199. <https://doi.org/10.1108/SASBE-04-2021-0071>
2. Wey W-M (2019) Constructing urban dynamic transportation planning strategies for improving quality of life and urban sustainability under emerging growth management principles. *Sustain Cit Soc* 44:275–290
3. Hbiak I, Adidi A, Nicolas JP (2019) Choice of indicators of sustainable urban mobility for Casablanca and calculation of some indicators using a geographical information system
4. Syahbandi M, Mardiah ANR, Wijaya SE (2022) Designing sustainable transportation strategy in Covid-19: jabodetabek commuter community movement in Indonesia. *Int J Disast Dev Interf* 2(1):20
5. Perra V-M, Sdoukopoulos A, Pitsiava-Latinopoulou M (2017) Evaluation of sustainable urban mobility in the city of Thessaloniki. *Transp Res Proced* 24:329–336
6. Ogryzek M, Adamska-Kmieć D, Klimach A (2020) Sustainable transport: an efficient transportation network: case study. *Sustainability* 12(19):8274

7. Farouk AM, Rahman RA, Romali NS (2021) Economic analysis of rehabilitation approaches for water distribution networks: comparative study between Egypt and Malaysia. *J Eng Des Technol* 21(1):130–149
8. Rani HA, Farouk AM, Anandh KS, Almutairi S, Rahman RA (2022) Impact of COVID-19 on construction projects: the case of India. *Buildings* 12(6):762
9. Farouk AM, Romali NS, Rahman RA (2023) Cost-benefit analysis of rehabilitation approaches for water distribution networks. In: AIP conference proceedings, vol 2688
10. Farouk AM, Omer MM, Rahman R, Romali NS (2023) Effective approaches to water distribution network rehabilitation: fuzzy synthetic evaluation. In: AIP conference proceedings, vol 2688
11. Falagas ME, Pitsouni EI, Malietzis GA, Pappas G (2008) Comparison of PubMed, scopus, web of science, and google scholar: strengths and weaknesses. *FASEB J* 22(2):338–342. <https://doi.org/10.1096/fj.07-94921sf>
12. Farouk AM, Nasuha AN, Rahman R, Zakaria Z, Haron AT (2023) Design coordination in BIM: decision criteria for determining tolerances. In: AIP conference proceedings, vol 2688
13. Farouk AM, Romali NS, Rahman RA, Seman MA (2021) Optimization techniques for rehabilitating water distribution networks. *IOP Confer Ser Earth Environ Sci* 641(1):12019
14. Farouk AM, Zulhisham AZ, Lee YS, Rajabi MS, Rahman RA (2023) Factors, challenges and strategies of trust in BIM-based construction projects: a case study in Malaysia. *Infrastructures* 8(1):13
15. Illahi U, Mir MS (2022) An indicator-based integrated methodology for evaluating sustainability in transportation systems using multivariate statistics and fuzzy logic. *J Sci Technol Policy Manag* 13(1):43–72
16. Sdoukopoulos A, Pitsiava-Latinopoulou M (2017) Assessing urban mobility sustainability through a system of indicators: the case of Greek cities. *WIT Trans Ecol Environ* 226:617–631
17. Munira S, San Santoso D (2017) Examining public perception over outcome indicators of sustainable urban transport in Dhaka city. *Case Stud Transp Policy* 5(2):169–178
18. Chakhtoura C, Pojani D (2016) Indicator-based evaluation of sustainable transport plans: a framework for Paris and other large cities. *Transp Policy* 50:15–28
19. Regmi MB (2020) Measuring sustainability of urban mobility: a pilot study of Asian cities. *Case Stud Transp Policy* 8(4):1224–1232
20. Miller P, de Barros AG, Kattan L, Wirasinghe SC (2016) Analyzing the sustainability performance of public transit. *Transp Res D Transp Environ* 44:177–198
21. Sdoukopoulos A, Pitsiava-Latinopoulou M, Basbas S, Papaioannou P (2019) Measuring progress towards transport sustainability through indicators: analysis and metrics of the main indicator initiatives. *Transp Res D Transp Environ* 67:316–333
22. Bandeira RAM, D'Agosto MA, Ribeiro SK, Bandeira APF, Goes GV (2018) A fuzzy multi-criteria model for evaluating sustainable urban freight transportation operations. *J Clean Prod* 184:727–739
23. Nadi PA, Murad A (1879) Modelling sustainable urban transport performance in the Jakarta city region: a GIS approach. *Sustainability* 11(7):2019
24. Nadi PA, Murad A (2017) Review of methods and indicators in sustainable urban transport studies overview from 2000 to 2016. *Commun Sci Technol* 2(2):1576
25. Buzási A, Csete M (2015) Sustainability indicators in assessing urban transport systems. *Period Polytech Transp Eng* 43(3):138–145
26. Haghshenas H, Vaziri M (2012) Urban sustainable transportation indicators for global comparison. *Ecol Indic* 15(1):115–121
27. Nathan HSK, Reddy BS (2013) Urban transport sustainability indicators—application of multi-view black-box (MVBB) framework. *Int J Environ Sustain Dev* 12(3):285–312
28. Ali N (2021) Evaluating sustainable urban transport systems: a review study for the identification of smart mobility indicators. *Trans Transp Sci* 12:16–23
29. Haghshenas H, Vaziri M, Gholamialam A (2015) Evaluation of sustainable policy in urban transportation using system dynamics and world cities data: a case study in Isfahan. *Cities* 45:104–115

30. Illahi U, Mir MS (2020) Development of indices for sustainability of transportation systems: a review of state-of-the-art. *Ecol Indic* 118:106760
31. PriorFilipe R, Heath A, McCullen N (2022) The path to sustainable and equitable mobility: defining a stakeholder-informed transportation system. *Sustainability* 14(23):15950
32. Yatskiv I, Budilovich E (2017) A comprehensive analysis of the planned multimodal public transportation HUB. *Transp Res Proced* 24:50–57

Trust Issues in BIM-Based Construction Projects: A Systematic Literature Review



Yusra Nur Qamarina Yushasman, Ahmad Rizal, Yong Siang Lee,
and Rahimi A. Rahman

Abstract Building Information Modelling (BIM) is known as one of the digital tools that can transform and improve the construction industry in terms of project organization and execution. However, with the emergence of new BIM technology in the construction industry, trust issues arise among team members involved in construction projects. The lack of understanding of the new digital technology or misinterpretation of the construction flow can lead to trust issues. Therefore, this study aims to explore trust issues among team members in BIM-based construction projects. In terms of research methodology, a systematic literature review (SLR) was conducted on published articles using preferred reporting items for systematic review. The result of this study portrays a list of identified trust issues in BIM-based construction projects. From there, a theoretical model of trust issues will be developed. This outcome of this study will provide insights into trust issues among industry practitioners to improve BIM-based construction projects for the successful delivery of the project.

Keywords Trust · Building information modelling (BIM) · Construction

1 Introduction

The life cycle of a construction industry project is complicated and fragmented in nature. Building information modeling (BIM), as a digital innovation, has been advocated worldwide for its transforming power to improve the productivity of the whole construction industry [1]. Besides, BIM allows project teams to develop a virtual model that can be examined and altered. The BIM Software used is first used to create a three-dimensional virtual model, which can be used to manage the construction planning in terms of cost and time [2]. Other than that, several project benefits have been documented with the application of BIM, including lower

Y. N. Q. Yushasman · A. Rizal (✉) · Y. S. Lee · R. A. Rahman
Faculty of Civil Engineering Technology, Universiti Malaysia Pahang Al-Sultan Abdullah, Lebu
Persiaran Tun Khalil Yaakob, 26300 Kuantan, Pahang, Malaysia
e-mail: arizal@umpsa.edu.my

expenses, faster project timelines, higher quality, and fewer coordination mistakes [1, 3]. In this BIM-based construction industry, it has been found that existing research regarding benefits mainly focused on intangible advantages such as construction productivity, faster timelines, and lower expenses [3]. However, with the emergence of new BIM technology in the construction industry, trust issues arise among team members involved in construction projects. The lack of understanding of the new digital technology or misinterpretation of the construction flow can lead to trust issues. Therefore, this study aims to explore trust issues among team members in BIM-based construction projects. To achieve that aim, a systematic literature review was conducted on published articles using preferred reporting items for systematic review. A theoretical model will be developed based on the identified trust issues in BIM-based construction projects.

2 Research Overview

2.1 Building Information Modelling

Building Information Modelling (BIM) is a technology that is extensively embraced across the globe, and it functions as a revolutionary technology that may revolutionize the way structures are created, built, and maintained [4]. BIM also helps save project costs, improves project affordability, and helps the construction team retain data for subsequent operations and maintenance tasks as well as making planning and construction processes run more effectively in construction projects. However, in the construction industry, projects are managed in a collaborative setting spanning several disciplines and different team members, causing trust concerns, and producing a lack of clarity about duties, responsibilities, and interoperability. The implementation of BIM added significant benefits to the construction industry, but at the same time, it has a significant impact on its current practices, contractual policy, and business model [2]. According to [5], they found that implementation of BIM requires the urgent development of trustworthy tools for information exchange between various software tools while also enabling effective and direct coordination and monitoring processes between project participants and team members employed for the project from different companies and using various software sets.

2.2 Issue BIM-Based in Construction Project

The study presented herein started with a review of the available literature relating to issues in BIM-based construction projects. According to past researchers they had found a few issues regarding trust in BIM-based construction projects. These include the lack of knowledge, lack of skill, lack of collaboration and high-cost expenses. In

past research, insufficient training also led to issues in lack of knowledge of BIM, especially when it comes to fresh graduates that are just aware of the BIM-based construction project. This training regime is still in its infancy, and therefore, it is incumbent upon educators to treat collaboration skills as a central element of their BIM-related curricula [6]. Besides, the lack of highly skilled staff that can manage BIM technology also leads to a significant issue, and it causes most industry players to be unable to see how BIM benefits them [7]. In terms of combination, the non-user-friendly format combined with the lack of skills and experience is a major concern.

3 Methodology

In this study, a systematic review was conducted to identify and analyze the optimization methods and techniques for trust issues in BIM-based construction projects. This systematic review consisted of three stages. In the first stage, a comprehensive search is conducted under “T/A/K (title/abstract/keyword).” Scopus was used for this study since it searches a variety of databases and has high-impact journals. The search involves the following keywords: (1) “trust”; and (2) “Building Information Modelling” OR “bim” OR “building information modeling.” Then, this study is limited to the English language only. The full search code is:

TITLE-ABS-KEY (trust AND “Building Information Modelling” OR bim OR “building information modeling”) AND (LIMIT-TO (LANGUAGE, “English”)).

The first search was on 13/9/2022, with 94 results. In the second stage, a visual examination is conducted on the title, abstract, and conclusion to choose related papers for the systematic review, which results in a total of 21 articles. Then, articles that are referenced in the related collected papers are gathered. This method is conducted to identify articles outside of the designated databases but still relevant to the topic. The process of identifying the articles involves going through the list of references of the collected papers. This process is repeated using the articles that have been collected to identify another set of articles until there are no new articles to be found. Lastly, a total of 32 articles are identified for further analysis. These articles are subjected to the analysis to aim trust issues in BIM-based construction projects. Figure 1 summarizes the methodology used in this paper.

4 Result and Discussion

Table 1 represents the trust issues in BIM-Based construction projects from the 32 articles. In summary, there are 18 trust issues that have been analysed and tabulated.

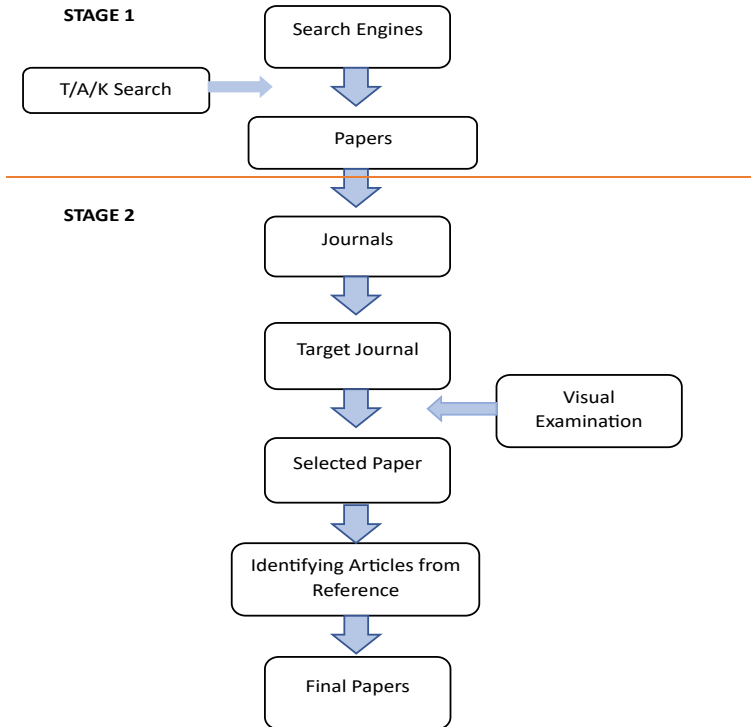


Fig. 1 Methodology flowchart to identify trust issues in BIM-based construction projects

4.1 Trust Issue in BIM-Based Construction Project

From the finding result, there were 18 trust issue BIM-based construction projects that were analyzed. According to the analysis of trust issues in BIM-based construction projects in Table 1, the first issue with code TI1 is a lack of knowledge. Most construction parties were distrusted in BIM-based construction projects due to poor knowledge and lack of training [8]. The next trust issue is a lack of skill with the code of TI2. From this case, lack of skills can be related to less competence in BIM and unwillingness to learn BIM practices [19]. Other issue is called a lack of collaboration with the code of TI3 where if contractors do not take any performance risk in ensuring project efficiency the client may not want to collaborate again with the contractors due to delay, and rework caused by contractors' careless [3].

Accessibilities issues also led to a distrust of the construction team in BIM. This issue was categorized in the code of TI4. According to past researcher, [27] the cost is the main trust issue in BIM-based construction projects and categorised as TI5. In BIM-based construction projects, utilization of BIM software purchasing is quite expensive and requires higher BIM adoption costs with training expenses

Table 1 Identify trust issues on BIM-based construction project

Code	Issue	References
TI1	Lack of knowledge	[1, 2, 5, 7–21]
TI2	Lack of skill	[1, 2, 6, 7, 12, 14, 15, 19, 20]
TI3	Lack of collaboration	[1, 3, 5, 6, 8, 10, 13, 22–25]
TI4	Accessibility issue	[5–7, 13, 19, 26]
TI5	High-cost expenses	[5, 13, 14, 19, 21, 23, 27]
TI6	Software limitation	[5, 6, 14, 20, 23, 27]
TI7	Model ownership issue	[1, 6, 16, 24, 26–28]
TI8	Poor communication	[14, 25, 29]
TI9	Standardization issue	[6, 14, 28, 30]
TI10	Immaturity of BIM-based technologies	[1, 10, 13, 14, 26]
TI11	Contractual issue	[21, 22, 31, 32]
TI12	Missing information	[10, 27]
TI13	Highly time-consuming in BIM	[1, 5, 6, 15, 19]
TI14	Limited material taking-off	[14]
TI15	Data security	[6, 26]
TI16	Legal liabilities issue	[13, 24]
TI17	Procurement issue	[24]
TI18	No enforcement from the client	[19]

[5, 13, 14, 19, 21]. Next, the software limitation is one of the trust issues in BIM-based construction with a code TI6. Some tools compass the industry, such as file format and software, are not compatible with the BIM open formats [3, 6, 14]. There are a few limitations of 3D/4D modelling software tools and information management that cause some distrust between in their own team construction group. In this analysis model ownership issue was categorized as code TI7. In some events, model ownership issues or barriers can trigger some of the construction parties' trust in BIM implementation in construction projects [24, 26, 27].

The next analysis is poor communication which was categorized as code TI8. This barely happened as some of the parties have different BIM capabilities, and they will argue about what they adapt and trust from BIM practices. Thus, it is difficult for them to communicate well [22]. The other trust issue is the standardization issue, and it is categorized as the code of TI9 in this analysis. In the utilization of BIM, the “lack of a standard for the description of BIM objects and a coding system” is what have been researching. The one trust issue which can be related to the BIM-based technology was categorized as TI10. The complexity of the current technology, such as BIM practice with design authoring tools, could be included in this kind of trust issue [10].

The contractual issues which were categorized as code TI11 in this trust of BIM regarding digital data protocols, coordination and reliance, project responsibilities

and risks, copyright, and the utilization of documents [32]. In other to achieve collaboration and trust among construction parties, legal and contractual issue obligations need to be done and solved [22]. Another issue related to digital tools of BIM is missing data information. This issue was categorized as TI12. According to Tan et al. [27], the barriers to trust in BIM could be lack of data, and insufficient transmission [10].

The highly time-consuming was analyzed and categorized as code TI13 in this study. Since building trust in BIM-based is time-consuming, the beginning of distrust would trigger the unending cycle of further team behaviors and expectations [1]. Besides, BIM software also leads to time-consuming learning of how to use the software and develop the model [5, 19]. In terms of the construction team, the senior and job site engineers require substantial time and assistance to edit knowledge feedback in the BIM environment [15]. In this trust issue, it was categorized as TI14, and mostly the capability of BIM was limited for material tacking-off. BIM-extracted quantities are frequently inaccurate and hence unreliable. Their accuracy varies depending on the modeling strategy employed for various model geometries, and for some geometry, the derived numbers are unreliable irrespective of the modeling strategy [14].

In this finding, data security was analyzed as in code TI15 for this study. The past researcher stated that in other, to put trust in BIM technologies, data security is one of the challenges for implementing trust in BIM-based construction projects [26]. The BIM data is at risk of being missing, which could damage the project financially, physically, economically, or reputationally. Most BIM experts claim that using the Cloud to host BIM data is unsafe and subject to hacking due to bad authentication component of the access data. The code for legal liabilities issue is TI16, and the liabilities arise from the utilization of BIM in construction projects. Legal liabilities usually happen usually when the virtual modeling is wrong and incomplete data [13] This could lead to high exposure of liabilities among the design team and general contractor. Next, trust issue that is categorized as TI18 is no enforcement from the client. This usually occurs from small companies of clients that are not demanding the use of BIM in construction projects even though the government enforcing BIM for publicly funded work [19].

5 Conclusion

This paper has identified major trust issues in BIM-based construction projects by systematically examining thirty-two (32) articles in past research and result shows eighteen (18) trust issues have been identified. All these trust issues are essential to act as a reference for various parties. In summary, all parties involved in BIM-based construction projects can benefit from addressing trust issues. In summary, the research suggests that further studies can be conducted to identify strategies that can improve trust issues in BIM-based construction projects.

Acknowledgements The authors would like to thank Universiti Malaysia Pahang for supporting this study through financial grant RDU223420 and the industry practitioners that agreed to participate in this work.

References

1. Chen G, Chen J, Tang Y, Ning Y, Li Q (2022) Collaboration strategy selection in BIM-enabled construction projects: a perspective through typical collaboration profiles. *Eng Constr Archit Manag* 29(7):2689–2713. <https://doi.org/10.1108/ECAM-01-2021-0004>
2. Al-Ashmori YY et al (2020) BIM benefits and its influence on the BIM implementation in Malaysia. *Ain Shams Eng J* 11(4):1013–1019. <https://doi.org/10.1016/j.asej.2020.02.002>
3. Guo X, Chen Y (2020) Perceived trust of contractors in building information modeling assisted projects
4. Lan HK, Omran A, Hanafi MH, Khalid SSM, Zainee SNBS, Hooi LB (2015) Building information modelling (BIM): level of understanding and implementation among civil and structural engineers in Penang. *Ann Fac Eng Hunedoara Int J Eng* 169
5. Migilinskas D, Popov V, Juocevicius V, Ustinovichius L (2013) The benefits, obstacles and problems of practical bim implementation. *Procedia Eng* 767–774. <http://doi.org/10.1016/j.proeng.2013.04.097>
6. Oraee M, Hosseini MR, Edwards DJ, Li H, Papadonikolaki E, Cao D (2019) Collaboration barriers in BIM-based construction networks: a conceptual model. *Int J Project Manage* 37(6):839–854. <https://doi.org/10.1016/j.ijproman.2019.05.004>
7. Zahrizan Z, Ali NM, Haron AT, Marshall-Ponting A, Hamid ZA (2013) Exploring the adoption of building information modelling (BIM) in the Malaysian construction industry: a qualitative approach
8. Harris BN, Alves T (2020) Building information modeling and field operations: opportunities and challenges. *Can J Civ Eng* 47(2):153–164. <http://doi.org/10.1139/cjce-2018-0415>
9. Darabseh M, Martins JP (2020) Risks and opportunities for reforming construction with blockchain: bibliometric study. *Civ Eng J (Iran)* 6(6):1204–1217. <https://doi.org/10.28991/cej-2020-03091541>
10. Che Ibrahim CKI, Mohamad Sabri NA, Belayutham S, Mahamadu A (2019) Exploring behavioural factors for information sharing in BIM projects in the Malaysian construction industry. *Built Environ Proj Asset Manag* 9(1):15–28. <http://doi.org/10.1108/BEPAM-02-2018-0042>
11. Lee CY, Chong H-Y, Wang X (2018) Enhancing BIM Performance in EPC projects through integrative trust-based functional contracting model. *J Constr Eng Manag* 144(7). [http://doi.org/10.1061/\(asce\)co.1943-7862.0001521](http://doi.org/10.1061/(asce)co.1943-7862.0001521)
12. Singh S, Chinyio E, Suresh S (2018) The implementation of stakeholder management and building information modelling (BIM) in UK construction projects
13. Alreshidi E, Mourshed M, Rezguy Y (2017) Factors for effective BIM governance. *J Build Eng* 10:89–101. <https://doi.org/10.1016/j.jobe.2017.02.006>
14. Aibinu A, Venkatesh S (2014) Status of BIM adoption and the BIM experience of cost consultants in Australia. *J Prof Issues Eng Educ Pract* 140(3). [http://doi.org/10.1061/\(ASCE\)EI.1943-5541.0000193](http://doi.org/10.1061/(ASCE)EI.1943-5541.0000193)
15. Ho SP, Tserng HP, Jan SH (2013) Enhancing knowledge sharing management using BIM technology in construction. *Sci World J* 2013. <http://doi.org/10.1155/2013/170498>
16. Dounas T, Lombardi D, Jabi W (2021) Framework for decentralised architectural design BIM and blockchain integration. *Int J Archit Comput* 19(2):157–173. <https://doi.org/10.1177/1478077120963376>

17. Zhang J, Wu W, Li H (2018) Enhancing building information modeling competency among civil engineering and management students with team-based learning. *J Prof Issues Eng Educ Pract* 144(2). [http://doi.org/10.1061/\(ASCE\)EI.1943-5541.0000356](http://doi.org/10.1061/(ASCE)EI.1943-5541.0000356)
18. Yahya Al-Ashmori Y, Bin Othman I, Bin Mohamad H, Rahmawati Y, Napiah M (2019) Establishing the level of BIM implementation—a case study in Melaka, Malaysia. In: IOP conference series: materials science and engineering. Institute of Physics Publishing. <http://doi.org/10.1088/1757-899X/601/1/012024>
19. Memon AH, Rahman IA, Memon I, Azman NIA (2014) BIM in Malaysian construction industry: status, advantages, barriers and strategies to enhance the implementation level. *Res J Appl Sci Eng Technol* 8(5):606–614. <https://doi.org/10.19026/rjaset.8.1012>
20. Ghaffarianhoseini A et al (2017) Building information modelling (BIM) uptake: clear benefits, understanding its implementation, risks and challenges. *Renew Sustain Energy Rev* 75:1046–1053. <http://doi.org/10.1016/j.rser.2016.11.083>
21. Ahmed S (2018) Barriers to implementation of building information modeling (BIM) to the construction industry: a review. *J Civ Eng Constr* 7(2):107. <https://doi.org/10.32732/jceec.2018.7.2.107>
22. Liu Y, van Nederveen S, Hertogh M (2017) Understanding effects of BIM on collaborative design and construction: an empirical study in China. *Int J Project Manage* 35(4):686–698. <https://doi.org/10.1016/j.ijproman.2016.06.007>
23. Roorda D, Liu MK (2008) Implementation of building information modeling (BIM) on the renovation of the art gallery of Alberta in Edmonton, Alberta
24. Fan SL, Lee CY, Chong HY, Skibniewski MJ (2018) A critical review of legal issues and solutions associated with building information modelling. *Technol Econ Dev Econ* 24(5):2098–2130. <https://doi.org/10.3846/tede.2018.5695>
25. Wu W, Issa RRA (2014) BIM education and recruiting: survey-based comparative analysis of issues, perceptions, and collaboration opportunities. *J Prof Issues Eng Educ Pract* 140(2). [http://doi.org/10.1061/\(ASCE\)EI.1943-5541.0000186](http://doi.org/10.1061/(ASCE)EI.1943-5541.0000186)
26. Lee C-Y, Chong H-Y, Tanko BL, Klufallah M (2022) Effect between trust in communication technology and interorganizational trust in BIM-enabled projects. *J Constr Eng Manag* 148(8). [http://doi.org/10.1061/\(asce\)co.1943-7862.0002299](http://doi.org/10.1061/(asce)co.1943-7862.0002299)
27. Tan JH, Loo SC, Zainon N, Aziz NM, Mohd Rahim FA (2022) Potential functionality and workability of blockchain within a building information modelling (BIM) environment. *J Facil Manag.* <http://doi.org/10.1108/JFM-10-2021-0131>
28. Azhar S, Khalfan M, Maqsood T (2012) Building information modeling (BIM): now and beyond. *Australas J Constr Econ Build* 12(4):15–28. <https://doi.org/10.5130/ajceeb.v12i4.3032>
29. Gao Y, Guo Q, Zhang S, Zhang J (2022) Understanding the effect of BIM capability imbalance on opportunistic behavior: the case of the Chinese construction market. *J Manag Eng* 38(3). [http://doi.org/10.1061/\(asce\)me.1943-5479.0001028](http://doi.org/10.1061/(asce)me.1943-5479.0001028)
30. Kensek K (2015) BIM guidelines inform facilities management databases: a case study over time. *Buildings* 5(3):899–916. <https://doi.org/10.3390/buildings5030899>
31. Harty J, Laing R (2011) Trust and risk in collaborative environments. In: Proceedings of the international conference on information visualisation, pp 558–563. <http://doi.org/10.1109/IV.2011.106>
32. Jay W (2009) Legal and business implications of building information modeling (BIM) and integrated project delivery (IPD)

Analysis of Lateral Load Resistance of a Structural System Using Finite Element Method



Sumayya Jamal, Beena Mary John, and Rajesh P. Nair

Abstract High rise structural systems are subjected to different types of loading conditions including dynamic loading where the seismic ground motions are oscillatory which induces inertia forces that varies with time. The response of the structure towards earthquake loading will be different for different structural configuration. In the present study the behaviour of structural configuration towards the earthquake ground motion is evaluated, along with considering the soil structure interaction effects. A realistic approach has been followed by taking into account the soil profile and foundation above which the building structures are resting. A finite element software PLAXIS 3D is used for conducting the analysis. The response of four structures having different aspect ratio and slenderness ratio has been analysed, when it is subjected to ground motion. The ground motion is provided by means of a real time history data of a past earthquake happened in Bhuj, Gujarat, 2001. In India, according to some paleo seismic studies conducted the Kutch region which is recorded as the second most seismically active region in the Himalayan ranges are more prone to experience earthquakes in the coming future which makes this study more relevant. A real soil profile situated in an earthquake susceptible region of Kutch was considered for the study. The dynamic analysis performed in PLAXIS 3D on the structure by taking into account the soil-foundation- structure interaction determines the impact of seismic loading on structures which are situated in seismically active regions in a more precise way. From the results obtained, as the aspect ratio changes from 1 to 1.75 there was a 23% increase in the acceleration response of the structure at the roof level. Similarly when the slenderness ratio was changed by increasing the number of floors considered there was an increase of 4.2% in the acceleration response of the structure towards seismic loading at the roof level making it clear that, with the increase in aspect ratio and slenderness ratio of the structure the displacement, as well as the acceleration response of the structure towards earthquake loading has increased. This shows the influence of configuration parameters of the structures towards its response during dynamic loading condition.

S. Jamal (✉) · B. M. John · R. P. Nair
Cochin University of Science and Technology, Kochi, Kerala, India
e-mail: sumayyajamal4@gmail.com

Keywords PLAXIS 3D · Seismic ground motions · Aspect ratio · Soil structure interaction

1 Introduction

A structural system is an assembly of various elements which are subjected to different types of loading conditions. The lateral loads including wind, earthquake ground motion, and dynamic forces from equipment generate vibration in structures. Earthquake loading is considered as a displacement-type loading predominantly through the horizontal axis which consists of the inertial forces of the building mass that results from the shaking of its foundation by a seismic disturbance which generates random oscillatory movements. The induced ground motion of earthquake drags the building foundation along with it, but the superstructure prefers to stay at rest. One of the major challenge related to the design of earthquake loading is that it is not possible to estimate with precision the maximum displacement imposed under the building [1]. Describing the strong ground motion is quite a complicated process. But the typical ground motion records are in the form acceleration-time histories which contains tremendous amount of information using which a more credible response of the structure towards the loading can be determined.

All structures are considered as vertical cantilevers projecting out from the earth's surface. The seismic waves generated due to earthquake cause the ground to vibrate and create severe natural disasters. It is evident to make sure that the designed structure is well adequate to resist the ground displacements. For creating an earthquake-resistant design of structures there are mainly four aspects on which the engineer or the architect should work, namely seismic structural configuration, lateral stiffness, lateral strength and ductility, in addition to other aspects like form, aesthetics, functionality and comfort of building. Among these four virtues lateral stiffness, lateral strength and ductility of the structure can be ensured by strictly following most seismic design codes. But for good structural behaviour towards the lateral loading it is required to ensure good structural configuration by the designer especially in the seismically active regions. Good seismic structural configuration simply implies no choice of architectural form of the building that is detrimental to good earthquake performance and that does not introduce newer complexities in the building behaviour than what the earthquake load is already imposing [1].

Along with the structural qualities it is important to understand the behavior of soil during devastating earthquakes. The relevance of the study lies in the fact that intensity of a shock from earthquake is directly related to the soil type and also the soil stratification [2]. So along with studying the characteristics of structure which is subjected to earthquake loading, it is also important to understand the soil ground and the foundation in which the structure has been constructed. The soil structure interaction has a significant role in inducing increased lateral deflection thereby changes the performance level of the structure during earthquakes which may be safety threatening. The seismic excitation experienced by the structures

depends on various factors including soil structure interaction, local soil properties and earthquake characteristics [3]. Depending upon the soil type, level of water table, proximity of hard rock and other geological features, soil at a particular location possesses certain natural frequency at which it vibrates under a dynamic force. When a structure is constructed on the ground, the system of soil-structure will possess a natural frequency, perhaps different from that of soil alone depending on the factors including the type of material used for the structure and the type of the foundation. If the predominant frequency of an earthquake is close to the natural frequency of the system of soil-foundation-structure, the condition similar to resonance may occur, even if the earthquake motion is of short duration and random in nature.

2 Methodology

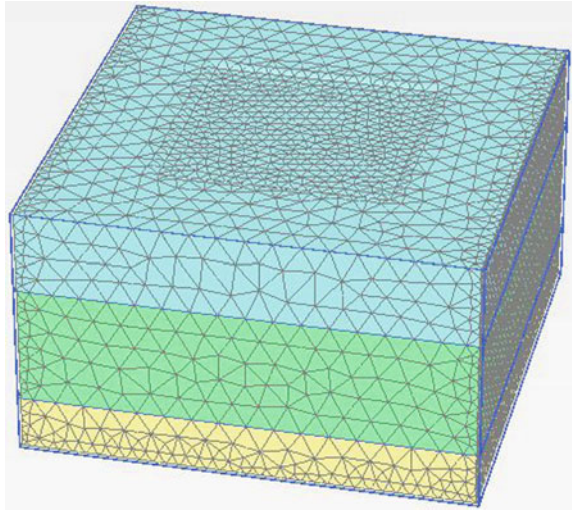
The response of structural system along with foundation and soil above which it is resting when subjected to seismic excitations that are random in nature are analysed using a geotechnical software PLAXIS 3D. A real soil profile of Kandla port is considered for the study which was earlier affected by the 2001 Bhuj earthquake. The soil profile in Kandla port consists of three layers with an upper layer of depth up to 9.1 m consisting of soft plastic clay, middle layer of depth up to 22.1 m consisting of silty sand and the lower layer consisting of reddish clay up to a depth of 28.5 is taken for the study. The Mohr–Coulomb constitutive model available in the PLAXIS library has been used for the soil profile and the corresponding soil parameters used are presented in Table 1. Four different structures having different aspect ratio and height has been considered for evaluating the influence of structural configuration in the dynamic response. The same soil strata is used for all the four structures analysed. For structures having rectangular plan area, the x and y dimensions considered is 67.2 × 38.4 m and for structures having square plan area, the dimensions considered is 50 × 50 m. The soil model generated is presented in Fig. 1.

For all the four structures, the foundation used is piled raft foundation which is a composite system of foundation comprising of pile and raft. A total of 25 piles with

Table 1 Soil parameters of Kandla port soil profile

	Soft plastic clay	Silty sand	Reddish clay
	Drained	Drained	Drained
c_{ref} (kN/m ²)	5	12	10
ϕ	25	23	0
ψ	0	0	0
Saturated unit weight (kN/m ³)	16	17	16
Unsaturated unit weight (kN/m ³)	16	17	16
E (kN/m ²)	25×10^3	13,000	11,000

Fig. 1 The three layered soil profile of Kandla port



each pile of length 15 m is used in each model. The concrete raft is assumed to be placed at the ground level which has a thickness of 1.5 m. The modulus of elasticity of concrete used in raft is 3.4×10^7 kN/m² while the Poisson's ratio and density of concrete considered in structural models are 0.2 and 25 kN/m³ respectively. A total of 25 circular concrete piles of 0.75 m diameter are located under the raft for each building structure. Modulus of elasticity of pile material is taken as 2.35×10^7 kN/m² while its density is considered as 25 kN/m³ [4]. The slenderness ratio (L/D) of the piles is taken as 20. In PLAXIS 3D, piles are modelled as embedded pile element and raft is modelled as plate element.

Out of the four structures, two six storeyed structures are having an aspect ratio of 1 and 1.75. The structures analysed are RC buildings. Six storeyed structure comprises of a ground basement floor and five storeys above it. The basement floor has a height of 6 m and the rest of the floors has a height of 3 m. Even if the structures considered have different aspect ratios, buildings have nearly the same plan area. The structural system above the raft comprises of columns and slabs. The structural system of all floors consists of flat concrete slab type of 200 mm thickness and 25 kN/m³ density with modulus of elasticity and poisson's ratio considered are 3.4×10^7 kN/m² and 0.2 respectively. The plan dimension of square raft is 25 m \times 25 m with overhang of 2.5 m while the plan dimension of rectangular raft is 19.2 m \times 33.6 m with overhang of 2.4 m. Modulus of elasticity of concrete columns is assumed as 3.4×10^7 kN/m² while concrete Poisson's ratio and density is considered in structural models as 0.2 and 25 kN/m³ respectively [5]. The slabs are modelled using plate elements and columns are modelled using beam elements in PLAXIS 3D. The column dimensions used are presented in Table 2. Different column dimensions are considered for outer and inner columns of the structure considering the loads taken by them.

For evaluating the effect of height in the response of structures when subjected to ground motions two structures of ten storey and fifteen storey are considered having

Table 2 Dimensions of columns

Building shape	Column dimensions (m × m)		
	C1	C2	C3
Square	0.65 × 0.65	0.75 × 0.75	0.9 × 0.9
Rectangular	0.65 × 0.65	0.75 × 0.75	0.9 × 0.9

a square plan similar to that of six storey [6]. All the properties of the structural elements are similar to that of the six storeyed structure. The typical floor plans and foundation plans having raft with pile location of square and rectangular shaped building is shown in Fig. 2.

The seismic loading is applied using a real time history data of Bhuj earthquake [7] which is shown in Fig. 3. Radiation damping is often referred to as the geometric damping/attenuation which is the transport of structural vibration energy to the far field. In reality radiation waves travel towards infinity but due to computational limitations of finite model, radiation damping is automatically included in the 3D geotechnical FE analysis by means of Rayleigh material damping in combination with absorbing boundaries. The value of damping chosen was 5% which is a typical value for the geotechnical material [8, 9]. Lateral boundaries provided are the free field boundary conditions in the X-direction and the compliant base in Z direction. A 10 node tetrahedral mesh is generated in PLAXIS 3D [10]. For the four structures considered, fine mesh with average element size of 70 cm is used. For the rectangular structure, a fine mesh having 26,432 elements and 64,298 nodes were generated.

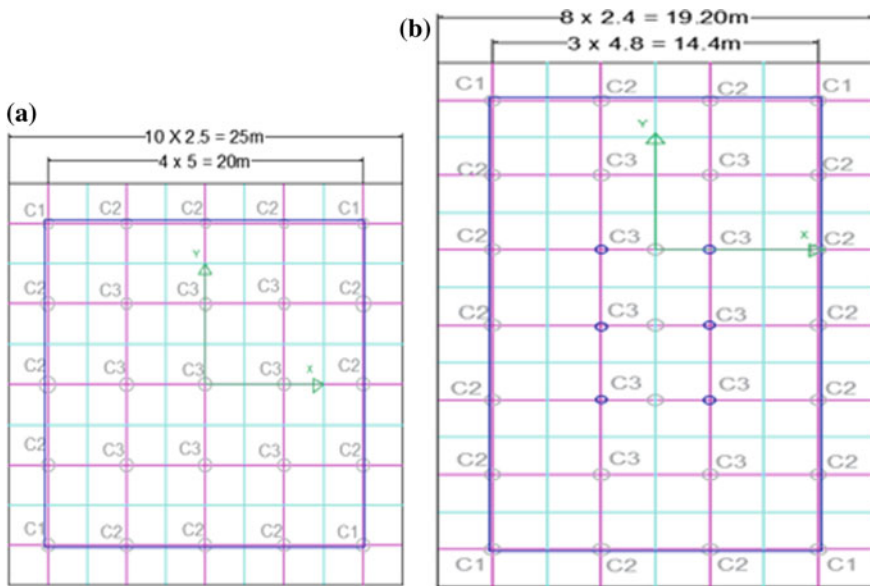


Fig. 2 Floor and raft plan. **a** Square structure, **b** rectangular structure

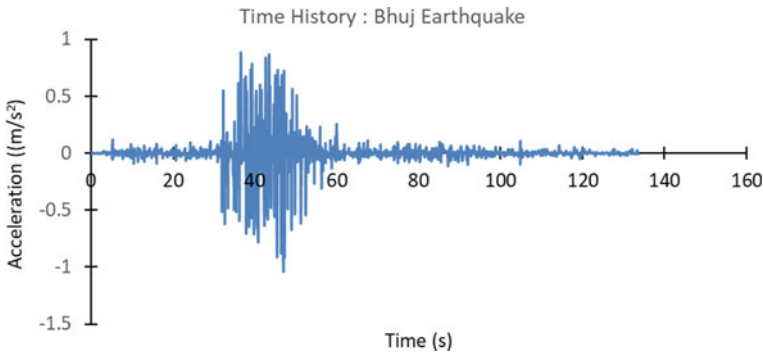


Fig. 3 Time-history data of Bhuj earthquake

In the case of square structure, a fine mesh of 23,234 elements and 5524 nodes were generated. For the other two structures ten storey and fifteen storey, fine mesh is generated. For the ten storey structure 26,628 elements and 63,935 nodes were generated. For the fifteen storey structure 35,236 elements and 77,322 nodes were generated. The four structures created for the analysis having different heights and different aspect ratio is depicted in Fig. 4.

3 Results and Discussion

The acceleration response as well as the displacement response of the four structures considered are evaluated and the results are tabulated in Tables 3 and 4. Four structures, among which two six storeyed structures having different aspect ratios were considered and the results shows that the square structure with minimum aspect ratio shows the least response. The structure shows an acceleration of 0.713 m/s^2 and a displacement of 0.081 m at the roof level when subjected to ground motion. Change in slenderness ratio also influences the response of structure towards seismic loading. As the number of storeys is increased from 10 to 15 acceleration response of the structure had seen an increase 0.17 m/s^2 .

The presented results indicate the influence of structural configuration towards the behavior of structures when it is subjected to seismic ground motions.

The displacement and acceleration results indicates that the structure having an aspect ratio of 1 with a square plan shows better performance towards the dynamic loading conditions than the one with higher aspect ratio. Also, as the height of the structure is increasing, the structure shows more tendency to get displaced in the top floors. The response of the square structure having aspect ratio 1, has been presented in Fig. 5.

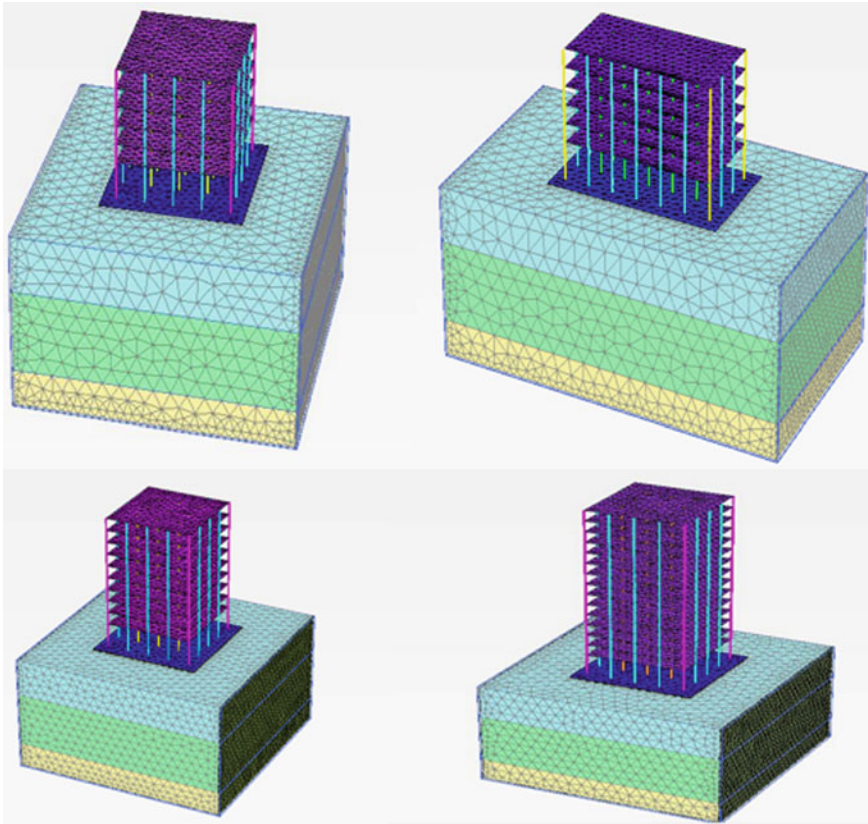


Fig. 4 Four structures modelled in PLAXIS 3D

Table 3 Result comparison of acceleration response of structures

	Structure	Acceleration response (m/s^2)		
		Roof	Intermediate	Basement
Aspect ratio	6 storey rectangle	0.874	0.425	0.342
	6 storey square	0.713	0.449	0.304
Slenderness ratio	10 storey square	0.872	0.571	0.290
	15 storey square	1.042	0.774	0.283

4 Conclusions

The influence of structural configuration when subjected to lateral loading has been evaluated using the analysis. The present study focused on the possibility of analyzing a structure using real-time history data and understanding the deformation caused

Table 4 Result comparison of displacement response of structures

	Structure	Displacement response (m)		
		Roof	Intermediate	Basement
Aspect ratio	6 storey rectangle	0.0905	0.0840	0.081
	6 storey square	0.081	0.077	0.075
Slenderness ratio	10 storey square	0.106	0.095	0.081
	15 storey square	0.155	0.107	0.077

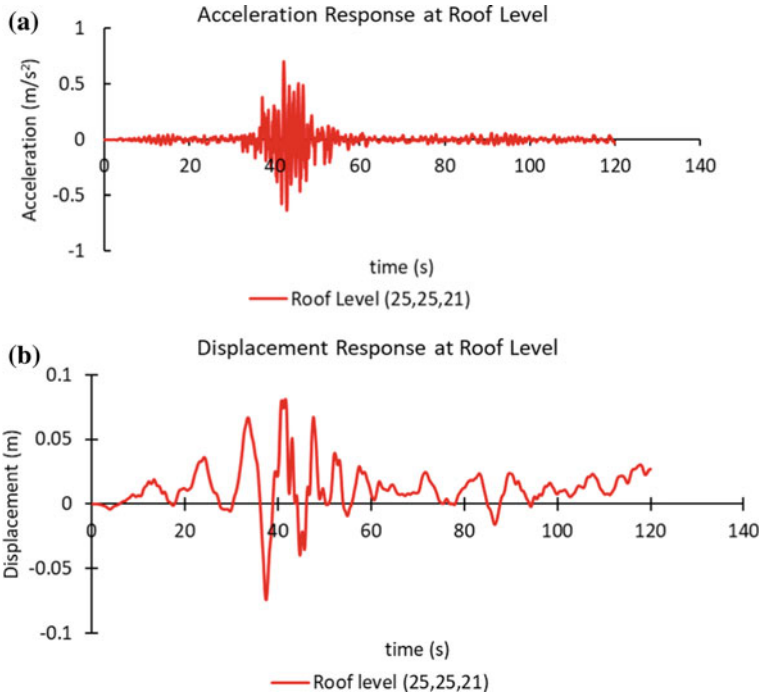


Fig. 5 Response of six storey square structure. **a** Acceleration response, **b** displacement response

in the structure due to the load. Along with the structure, the soil as well as the foundation characteristics has also been taken into account as part of a realistic approach. Soil strata of seismic prone area has been considered above which structures having different aspect ratio and slenderness ratio has been considered. Four structural configurations resting on piled raft foundation when subjected to seismic conditions using a real time history data of a past earthquake was evaluated. When the aspect ratio of a six storey structure has been increased from 1 to 1.75 the response of the structure towards the loading conditions also increased at different floor levels. There was an increase of 23% in the acceleration response of structure at the roof level. The intermediate level, as well as the basement level also shown an increase in

response with the increase in aspect ratio. Along with the acceleration, the displacement response also shown an increase with the variation in structural configuration. As the response of the structure towards dynamic loading is highly visible in roof level, the influence of slenderness of the structure when subjected to seismic conditions is understood by considering a 10 storeyed and 15 storeyed structure. The acceleration response of 10 storeyed structure at the roof level is 0.872 m/s^2 whereas for 15 storeyed structure it was 1.042 which shows an increase of 4.2% in the acceleration response of the structure towards seismic loading at the roof level making it clear that, with the increase in aspect ratio and slenderness ratio of the structure the displacement, as well as the acceleration response of the structure towards earthquake loading has increased. So a structure with less aspect ratio and slenderness ratio can be considered ideal for an earthquake prone subjected to lateral loading conditions.

References

1. Goswami R, Murthy CVR, Vijayanarayanan AR, Mehta VV (2012) Some concepts in earthquake behavior of buildings. Gujarat State Disaster Management Authority, Government of Gujarat
2. Sitharam TG, Govindaraju L (2004) Geotechnical aspects and ground response studies in Bhuj earthquake, India. *Geotech Geol Eng* 22(3):439–455
3. Hokmabadi AS, Fatahi B, Samali B (2013) Seismic response of superstructure on soft soil considering soil-pile-structure interaction. In: 18th international conference on soil mechanics and geotechnical engineering: challenges and innovations in geotechnics. In: ICSMGE 2013
4. Visuvasam J, Chandrasekaran SS (2019) Effect of soil–pile–structure interaction on seismic behaviour of RC building frames. *Innov Infrastruct Solutions* 4(1):1–19
5. Ahmed M, Mohamed MH, Mallick J, Hasan MA (2014) 3D-analysis of soil-foundation-structure interaction in layered soil. *Open J Civ Eng* 4(04):373
6. Sheth V, Panchal VR, Wankawala A (2017) Comparative study of different structural systems. Kalpa Publications in civil engineering, vol 1, pp 508–513
7. https://strongmotioncenter.org/vdc/waveform_data/india/200101260317/ahmdgl.dat
8. Chopra AK (1995) Dynamics of structures theory and application to earthquake engineering. Prentice Hall
9. Kumar A, Choudhury D, Katzenbach R (2016) Effect of earthquake on combined pile–raft foundation. *Int J Geomech* 16(5):04016013
10. Brinkgreve RBJ, Engin E, Swolfs WM (2013) PLAXIS 3D 2013 user manual. Plaxis bv, Delft

Analysis of Reinforced Concrete Structure Subjected to Blast Loads Without and with Carbon Fibres



Yogeswaran Palani and R. Raghunandan Kumar

Abstract In the past few decades, the terrorist attack on buildings has significantly increased. Blast loads due to explosions cause severe damage to the building's structural and non-structural elements which may also lead to progressive collapse of the building. Hence, there is a need for the structures to be analysed and designed for blast loads in addition to the conventional loads. An investigation is undertaken to minimize the damage of a G+3 storied building and by improving the mechanical properties such as compressive strength, nonlinear behaviour of M40 grade concrete by adding carbon fibres in different dosages. A finite element model of G+3 storied building has been created using Ansys/LS Dyna to analyse the structure subjected to a blast load with charge weights of 50 kg, 100 kg, 150 kg at 3000 mm standoff distance. The lateral deflections and strains of the structure are determined for different charge weights to study the behaviour of the structure when subjected to blast loads. The addition of carbon fibres has improved the behaviour of structure by reducing the strains and deflections and optimum dosage of fibres is also determined in this paper.

Keywords Blast loads · RC structure · Carbon fibres · Strain rates · Stresses

1 Introduction

A rapid or sudden burst of a chemical or a gas is called as explosion. Based upon the nature of blast, explosions can be classified as physical, chemical and nuclear explosions. Energy released from the failure of cylinder of compressed gas, or volcanic explosions are called as physical explosions. The energy released from nuclear fission and fusion reaction can be called as nuclear explosion.

Y. Palani (✉) · R. Raghunandan Kumar
Department of Civil Engineering, Christ University, Bangalore, India
e-mail: yogeswaran0807@gmail.com

R. Raghunandan Kumar
e-mail: raghunandan.kumar@christuniversity.in

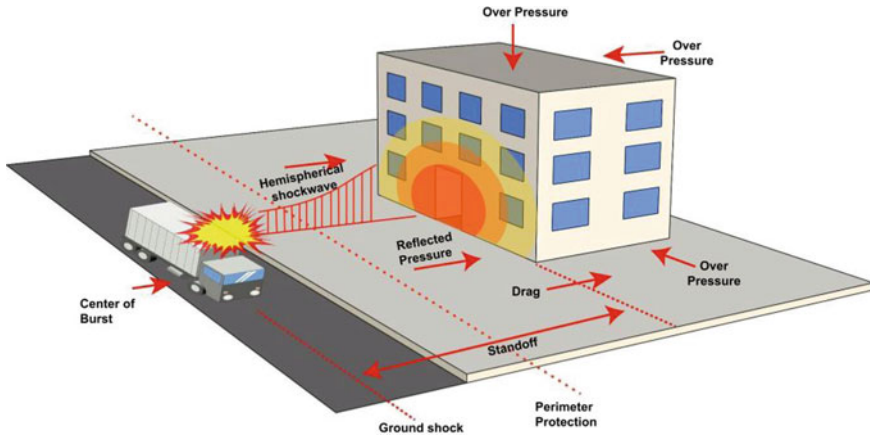


Fig. 1 Typical blast wave due to explosion

The explosive materials are classified into solids, liquids, and gases in which the solid explosives are known for their blast effects.

Mercury fulminate and lead azide are examples of primary explosives and trinitrotoluene (TNT) and ANFO are examples of secondary explosives. Secondary explosives when detonated, create blast waves which results in widespread damage to the surroundings [1]. Figure 1 shows a typical blast occurring outside a building.

2 Blast Phenomenon

The pressure surrounding the element is initially equal to the ambient pressure P_0 , and it undergoes an instantaneous increase to a peak pressure P_{s0} at the arrival time t_A , when the shock front reaches that point.

The time needed for the pressure to reach its peak value is very small and for design purposes, it is assumed to be equal to zero. The peak pressure P_{s0} is also known as side-on overpressure or peak overpressure. The value of the peak overpressure as well as the velocity of propagation of the shock wave decrease with increasing distance from the detonation centre.

After its peak value, the pressure decreases with an exponential rate until it reaches the ambient pressure at $t_A + t_0$, being called the positive phase duration. After the positive phase of the pressure–time diagram, the pressure becomes smaller (referred to as negative) than the ambient value and finally returns to it. The negative phase is longer than the positive one, its minimum pressure value is denoted as P_{s0}^- and its duration as t_0^- . Figure 2 shows the variation of the positive and negative pressure with respect to time.

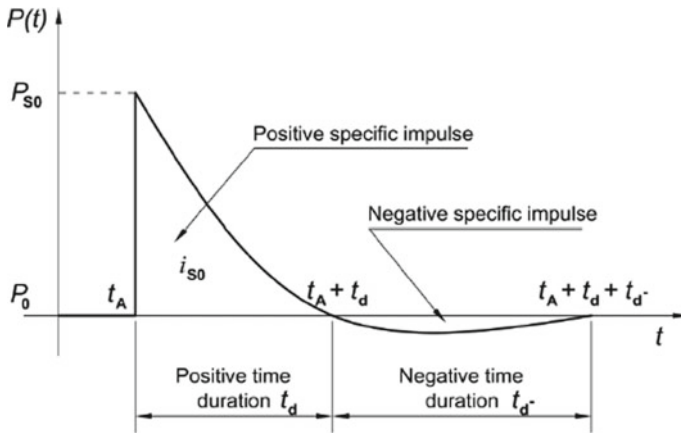


Fig. 2 Ideal blast wave's pressure time history [1]

3 Types of Blast

There are two types of blast. They are confined and unconfined blasts.

3.1 Confined

The blast which occurs inside the building is confined blast. These blast waves cause refraction in the structure. There are three types of confined blast viz., Fully vented, partially vented and fully confined (Fig. 3).

Fully vented is in case where the blast waves move outward and affects only a small portion of the structure whereas partially vented means the blast waves partially flow through the vents and cause more damages. When it is fully confined, the blast waves have no way to cross over rather than confined inside the building and creates the worst damages to the building.

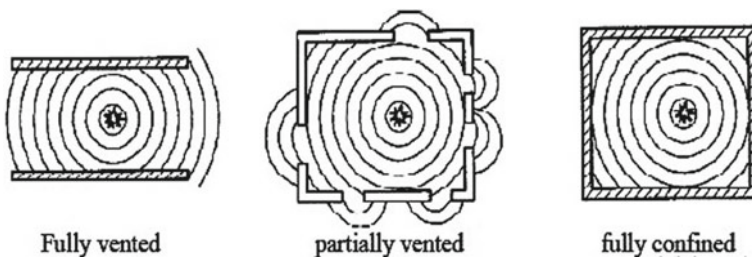


Fig. 3 Types of confined blast [2]

3.2 Unconfined

This is a type in which blast occurs outside the structure. As shown in Fig. 4, it is distinguished into three basic types, which depend on the relative position of the explosive source and the structure to be protected.

Three explosion types are:

3.2.1 Free-Air Bursts

The explosive charge is detonated in the air, the blast waves propagate spherically outwards and impinge directly onto the structure without prior interaction with other obstacles or the ground.

3.2.2 Air Bursts

The explosive charge is detonated in the air, the blast waves propagate spherically outwards and impinge directly onto the structure after having interacted first with the ground.

3.2.3 Surface Bursts

The explosive charge is detonated almost at the ground surface, the blast waves immediately interact locally with the ground and they next propagate hemi spherically outwards and impinge onto the structure.

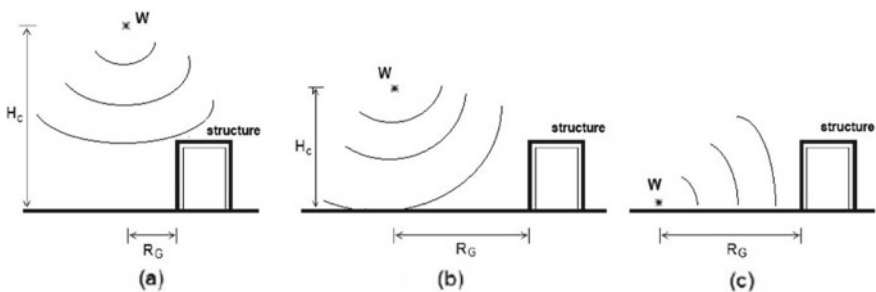


Fig. 4 Types of blast explosion [3]

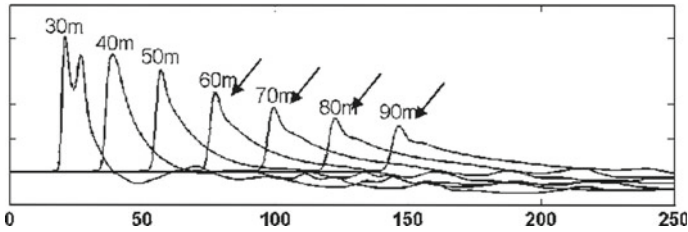


Fig. 5 Influence of distance on the blast positive pressure phase

4 Blast Scaling Laws

Scaling laws are one of the important parameters for blast loading computations. One of the most common scaling laws was introduced by Hopkinson-Cranz and Sachs.

According to Hopkinson-Cranz and Sachs, a dimensional scaled distance is introduced,

$$Z = R/(W)^{1/3} \quad (1)$$

where,

R is the distance from the detonation point to the point of interest

W is the charge weight of the explosive.

The peak pressure value and the velocity of the blast wave, decrease rapidly as the distance of the blast source and target surface increases which is shown in Fig. 5.

5 Effects of Blast on the Structure

Explosions cause dynamic loading on the structural elements. Since the rate of loading is very high, structural elements undergo huge distress. The behaviour of structural elements largely depends on the nonlinear inelastic property of material for proper dissipation of the energy. Initially the outer most (façade) elements are subjected to high stress which may also lead to progressive collapse of the structure. Primary effects of the blast cause shear or flexural failure to the individual structural members. Localized shear failures can occur in the form of spalling and fragmentation of the members. The secondary effects may occur due to the flying debris which may cause further damage to the structure or to the people.

6 Review of Related Literature

Ngo et al. [1] have studied the phenomenon of the blast. The detonation of an explosive produces hot gases with a pressure of up to 300-kbar and a temperature of about 3000–4000 °C. When the hot gas expands, it pushes out the volume it occupies, forming a layer of compressed air in front of it.

Ismail et al. [4] have investigated the response of G+4 RC structure against blast loading using ABACUS. To investigate the effects of blast, a 1-tonne weight of TNT is blasted at a distance of 5 m from an external column. As compared to a standard RC structure, the columns with external steel casing have greater durability, absorb more energy, and protect the structure.

Ibrahim et al. [5] have considered three blast loads caused by 0.7 tonne of TNT at distances of 14 m, 13 m, and 12 m from the buildings. The authors use nonlinear dynamic time-history analysis with Seism Struct to investigate the response of RC structures when composite columns are used instead of traditional reinforced concrete (RC). From the results it is noted that the models with composite columns performed well during the blast. It is also noted that the columns having more toughness and ductility are more resistant to the blast pressure.

Bhosale et al. [6] used Staad-Pro to investigate the dynamic behaviour of a G+5 storey RC Frame Structure subjected to Blast Loadings. Wave scaling laws are used to evaluate the blast load parameters. According to their findings, Peak Reflected Overpressure rises with increasing blast charge weight and decreases with increasing standoff distances. As we progress from the ground to the upper stories, the effect of the peak Reflected Over Pressure decreases.

Fu [7] used a 3-D computational model with direct blast load simulation to investigate the actual behaviour of a 20-story tall building under blast loading. On the 12th floor, a 15 kg package bomb charge was detonated. The plastic strain of the column near the blast was detected, indicating the start of column yielding. The shear capacity and ductility of the column must be increased to prevent the building from gradually collapsing under blast load. The majority of slab cracks are found near the blast site. There were no gaps in the building's interior slabs. When the distance between the blast and the target increases, the blast load decreases rapidly.

Bhatt et al. [8] used ETABS to compare the output of a G+3 storey building subjected to blast and earthquake loading. The amount of concrete needed for a blast-resistant building is 40% higher than for an earthquake-resistant building, owing to the need for larger sections in the blast case.

Kumar et al. [9] analysed a G+3 RC structure subjected to blast loads without and with steel fibres using ANSYS. Steel fibre reinforced concrete with 0.5%, 1%, 1.5% and 2% of steel fibres are compared. This result demonstrates that high strains and deformations are more prevalent near the beam-column joints. The results obtained for 1% and 1.5% steel fibres with an aspect ratio of 50 indicate that the optimum percentage of fibres is between 1% and 1.5 that respond well to blast loads.

Suaris et al. [10], it is clear that the addition of carbon fibres improves the flexural strength by 85%, flexural toughness by 205%.

Fig. 6 Carbon fibres

Thakur et al. [11], added carbon fibres with different volume fractions to study the effect of carbon fibres on the mechanical properties of concrete. The carbon fibres of length 30 mm and (0.6% of cement content) shows better results of concrete.

Tabatabaei et al. [12], added long carbon fibres to improve the spalling resistance of concrete under blast loads. From the research work, it is clear that the long carbon fibre reinforced panel decreases the amount of material lost during blast loads by a factor of 10 times.

Tabatabaei et al. [13] have developed long carbon fibres—fibres 75 mm or longer to improve the resistance of reinforced concrete to dynamic loadings, such as blasts and impact. The impact test slab size of 1.2×1.2 m is made with two types of carbon fibres. It was concluded that fibre panels were much more ductile, resulting in greater energy absorption and thus higher capacity. In the case of carbon fibre panels, there is also low deformation for the same load, resulting in low strains. It has been determined that twined carbon improves the spalling resistance of conventional reinforced concrete significantly.

From the above research work, it is inferred that the addition of carbon fibres improves the mechanical properties of concrete and also improves the ductility of concrete significantly. The current study is done with addition of short carbon fibres with dimensions of 1 mm in diameter and 12 mm in length (Fig. 6).

7 Methodology

The research work is carried out in two phases.

The first phase entails casting concrete specimens with and without carbon fibres and measuring properties like density, modulus of elasticity, and Poisson's ratio. It also includes using existing empirical methods to calculate blast parameters such

as peak overpressure, reflected pressure, time duration, and temperature during the blast.

The second phase entails creating a G+3 structure finite element model for blast load analysis of normal RC structures as well as RC structures with various percentages of carbon fibres, charge weights, and standoff distances. High strains, variation of displacements, stresses, and strain rate with respect to variation in carbon fibre percentage, different charge weights, and standoff distances will be determined in this phase. ANSYS/LS-DYNA is used to create the finite element model.

8 Experimental Investigation

The experimental investigation is carried out for M40 grade concrete in addition to carbon fibres. The carbon fibres are added in 4 different dosages as 0.5%, 1%, 1.5%, and 2% of the volume of cement.

8.1 Materials

The cement used for the research work is OPC 53 grade cement and the specific gravity of cement is 3.1. Manufactured sand is used as fine aggregate whose specific gravity was found to be 2.8 and the water absorption was 1.56%. The coarse aggregate used had a specific gravity of 2.8 and the water absorption was 0.2%.

8.2 Mix Proportion

The mix proportion was determined as per IS 10262:2019. The mix proportion for 1 m³ of concrete is as follows,

Weight of coarse aggregate = 1193.11 kg/m³

Weight of fine aggregate = 671.126 kg/m³

Weight of cement = 465 kg/m³

Water content = 186 L/m³.

8.2.1 Dosage of Superplasticizers

Without Carbon fibres: From various trial mixes, it was found that for the nominal concrete mix 0.318% of superplasticizers is optimum for achieving 75 mm of slump.

With Carbon fibres: From various trial mixes, it was found that for the 0.5%, 1%, 1.5%, and 2% of carbon fibres the dosage required is 0.57%, 0.7%, 0.9%, 0.95% of superplasticizers which was found to be optimum for achieving the slump of 60 mm.

8.3 Casting of Concrete Specimens

The size of the cubes used was 100 mm × 100 mm × 100 mm. The size of the cylinder used was 100 mm in diameter and 200 mm in height. This size is as per ASTM C39—Standard Test Method for Compressive Strength of Cylindrical Concrete Specimens. Three samples of each was used for 7-days, 14-days testing and 28-days testing.

The size of the beam used was 700 mm × 150 mm × 150 mm, and the reinforcements provided was 2 no of HYSD 550 MPa 12 mm bar at top and bottom with 8 mm bar as stirrups at 150 mm c/c spacing.

8.4 Hardened Properties of Concrete

Compressive test, split tensile test and Flexure test of the concrete samples were conducted by using the universal testing machine which has a maximum capacity of 1000 kN as shown in Fig. 7.

8.4.1 Density of Concrete

The Density of concrete with different dosage of fibres are shown in Table 1. From the table, it is clear that the density of concrete increases with an increase in the dosage of fibre.

8.4.2 Compressive Strength of Concrete

Table 2 shows the compressive strength values obtained for M40 grade concrete with different dosages of fibres. It is observed that the compressive strength of concrete increases till 1% of carbon fibres and the value dropped beyond 1% of carbon fibres. As the fibre dosage increases the rate of hydration of cement is slowed and that appears to be the reason for the reduced compressive strength of concrete at higher dosage of fibres. The results obtained concur with research work done by Chen et al. [14].



Fig. 7 Universal testing machine

Table 1 Density of concrete

Sample	Density kN/m ³
M40 concrete	23.85
M40 + 0.5% of carbon fibres	23.9
M40 + 1% of carbon fibres	23.95
M40 + 1.5% of carbon fibres	24
M40 + 2% of carbon fibres	24.05

Table 2 Compressive of strength of concrete

Sample	Compressive strength N/mm ²
M40 concrete	45.1
M40 + 0.5% of carbon fibres	49.7
M40 + 1% of carbon fibres	53.7
M40 + 1.5% of carbon fibres	49.25
M40 + 2% of carbon fibres	48

Table 3 Young's modulus of concrete

Sample	Young's modulus MPa
M40 concrete	33,580
M40 + 0.5% of carbon fibres	35,250
M40 + 1% of carbon fibres	38,200
M40 + 1.5% of carbon fibres	35,089.17
M40 + 2% of carbon fibres	34,640

Table 4 Poisson's ratio of concrete

Sample	Poisson's ratio
M40 concrete	0.17
M40 + 0.5% of carbon fibres	0.206
M40 + 1% of carbon fibres	0.24
M40 + 1.5% of carbon fibres	0.26
M40 + 2% of carbon fibres	0.267

8.4.3 Young's Modulus of Concrete

Table 3 shows the shows young's modulus values obtained for M40 grade concrete with different dosages of fibres. It was observed that young's modulus of concrete increased till 1% of carbon fibres and the value dropped beyond 1% of carbon fibres.

8.4.4 Poisson's Ratio of Concrete

Table 4 shows the shows Young's modulus values obtained for M40 grade concrete with different dosages of fibres. The Poisson's ratio is increased as the dosage of carbon fibres increases.

8.4.5 Tensile Strength of Concrete

Table 5 shows the shows split tensile strength values obtained for M40 grade concrete with different dosages of fibres. It is observed that the maximum value of split tensile strength of concrete is at 1% of carbon fibres and the value drops beyond 1%.

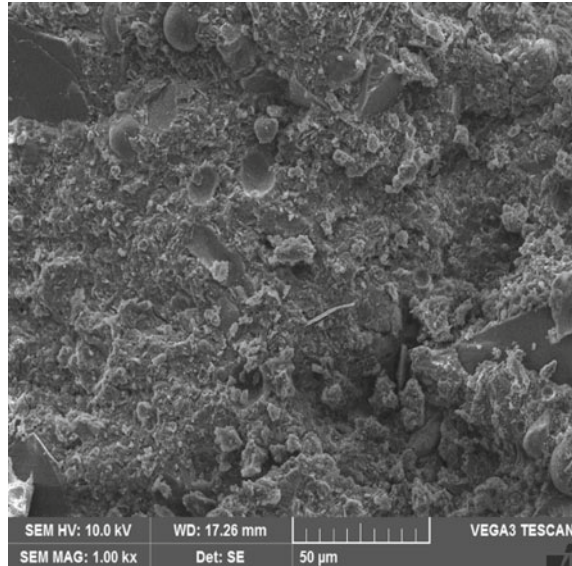
8.4.6 Scanning Electron Microscope (SEM) Images of Concrete Samples

The following images show SEM images of M40 grade concrete with different dosages of fibres. The addition of fibres increases the ductility of concrete by bridging

Table 5 Split tensile strength of concrete

Sample	Split tensile strength MPa
M40 concrete	2.92
M40 + 0.5% of carbon fibres	2.95
M40 + 1% of carbon fibres	3.05
M40 + 1.5% of carbon fibres	3.03
M40 + 2% of carbon fibres	2.76

Fig. 8 M40



the micro cracks which are visible in these images. A microcrack is bridged by at least one carbon fibre.

Figure 8 shows the SEM image of M40 grade concrete.

Figure 9 shows the SEM image of M40 + 0.5% of CF where the carbon fibre bridges a micro crack (Figs. 10 and 11).

In 1% of CF, there is a proper bond between the fibre and concrete but in Fig. 12 due to higher dosage of CF (2%), there is a gap between fibre and concrete resulting in poor bonding. Proper bonding of fibres shows improved mechanical properties.

8.5 Blast Parameters

The blast load parameters were calculated as per “Unified Facilities Criteria-3-340-02”, released by the Department of Defence of the United States of America (Fig. 13).

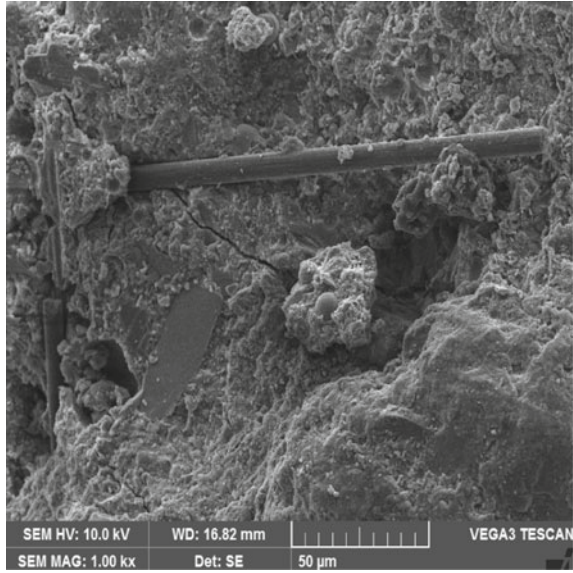


Fig. 9 M40 + 0.5% CF

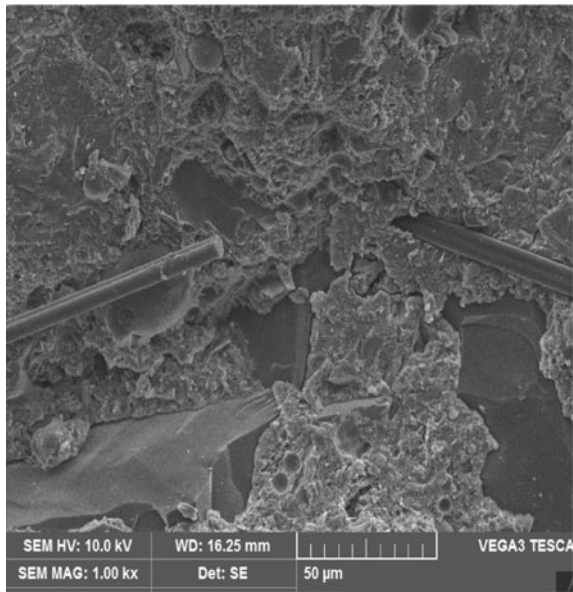


Fig. 10 M40 + 1% CF

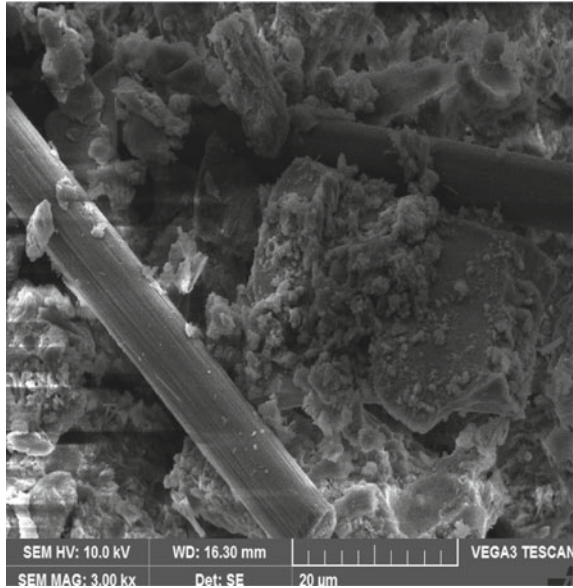


Fig. 11 M40 + 1.5% CF

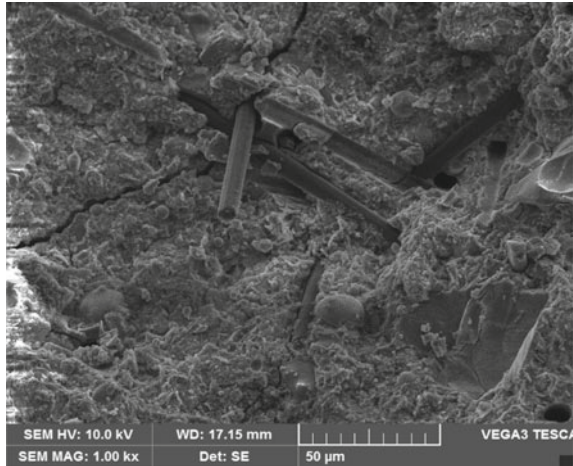


Fig. 12 M40 + 2% CF

8.5.1 Blast Load Parameters for 50 kg Charge Weight of TNT and 3000 mm Standoff Distance

$Z = R/(W)^{1/3}$, where R is the standoff distance and W is the charge weight.

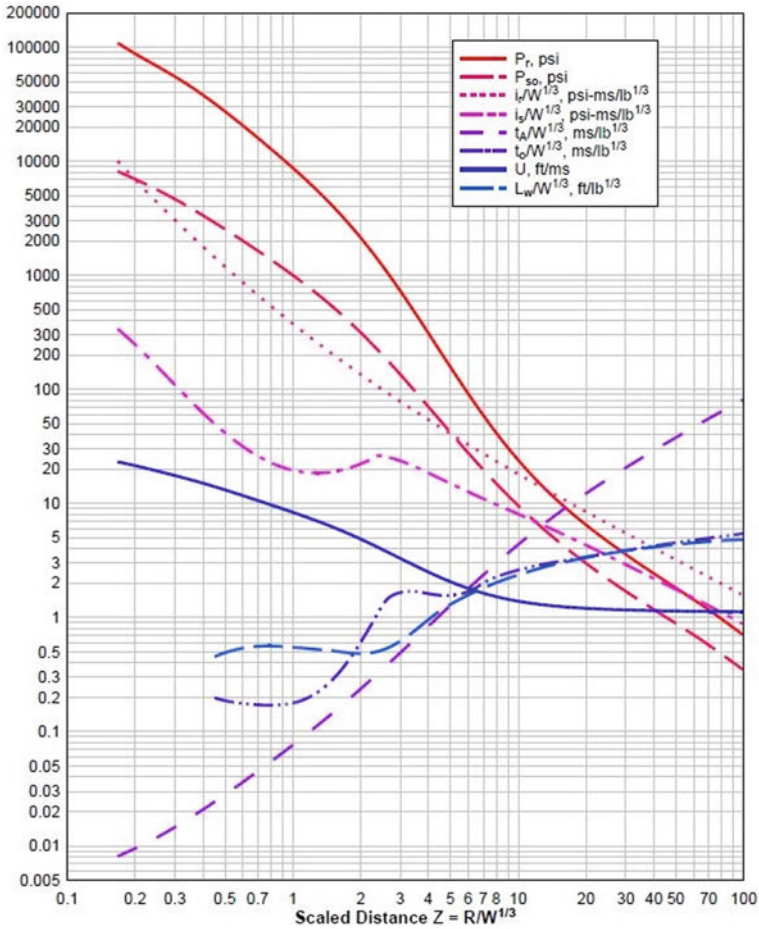


Fig. 13 Positive phase parameters of the blast wave [15]

$$Z = 3/(50)^{1/3}$$

$$Z = 2.055 \text{ ft/lbs}^{1/3}.$$

Peak blast equivalent overpressure $P_{so} = 300 \text{ psi} = 0.3 \text{ ksi} = 0.3 \times 6.895 = 2.068 \text{ MPa}$.

$$t_a/W^{1/3} = 0.25 = 1.19 \text{ ms}.$$

$$t_o/W^{1/3} = 0.6 = 2.87 \text{ ms}.$$

Figure 14 shows the variation of blast pressure with respect to time.

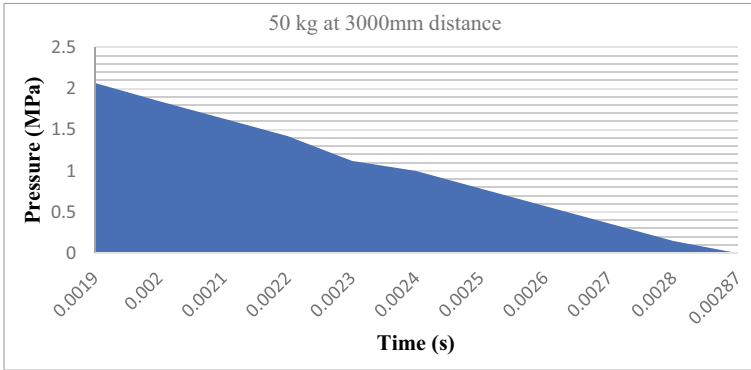


Fig. 14 50 kg at 3000 mm

8.5.2 Blast Load Parameters for 100 kg Charge Weight of TNT and 3000 mm Standoff Distance

$$Z = R/(W)^{1/3}$$

$$Z = 3/(100)^{1/3}$$

$$Z = 1.6318 \text{ ft/lbs}^{1/3.5}$$

Peak blast equivalent overpressure $P_{so} = 559 \text{ psi} = 0.559 \text{ ksi} = 0.559 \times 6.895 = 3.85 \text{ MPa}$.

$$T_a/(W)^{1/3} = 0.1556 = 1 \text{ ms.}$$

$$T_o/(W)^{1/3} = 0.3816 = 2.3 \text{ ms.}$$

Figure 15 shows the variation of blast pressure with respect to time.

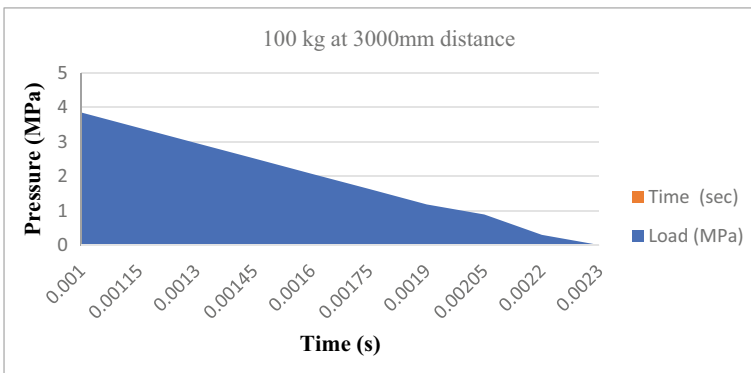


Fig. 15 100 kg at 3000 mm

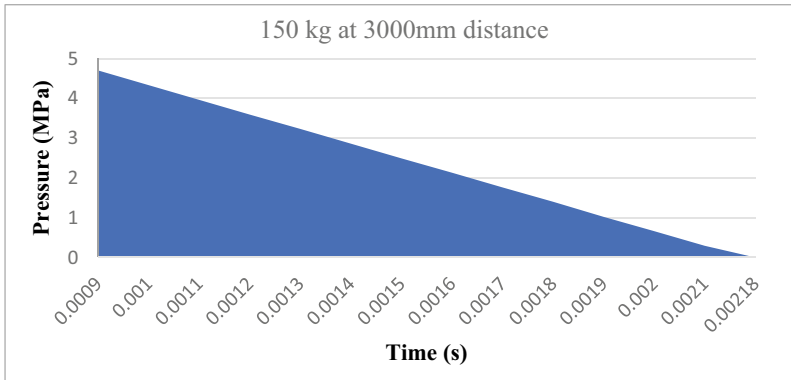


Fig. 16 150 kg at 3000 mm

8.5.3 Blast Load Parameters for 150 kg Charge Weight of TNT and 3000 mm Standoff Distance

$$Z = R/(W)^{1/3}$$

$$Z = 3/(150)^{1/3}$$

$$Z = 2.055 \text{ ft/lbs}^{1/3}.$$

Peak blast equivalent overpressure $P_{so} = 702.5 \text{ psi} = 0.7025 \text{ ksi} = 0.7025 \times 6.895 = 4.84 \text{ MPa}.$

$$T_a/(W)^{1/3} = 0.131 = 0.9 \text{ ms}.$$

$$T_o/(W)^{1/3} = 0.316 = 2.18 \text{ ms}.$$

Figure 16 shows the variation of blast pressure with respect to time.

9 Finite Element Modelling

9.1 Modelling

The finite element model was developed using ANSYS/LS-DYNA (Workbench 19.1) for a Ground+3 storied building.

Firstly, the columns were modelled and then the beams and slabs using workbench 19.1. For all the members, 20-noded Solid 186 element was used which supports plasticity, hyper elasticity, creep, stress stiffening, large deflection, and large strain capabilities. Pressures are input as surface loads on the element faces.

Since it is a reinforced concrete structure, contacts are defined as bonded contacts and fixed supports are assigned to the base of the column. Live Loads on the structure

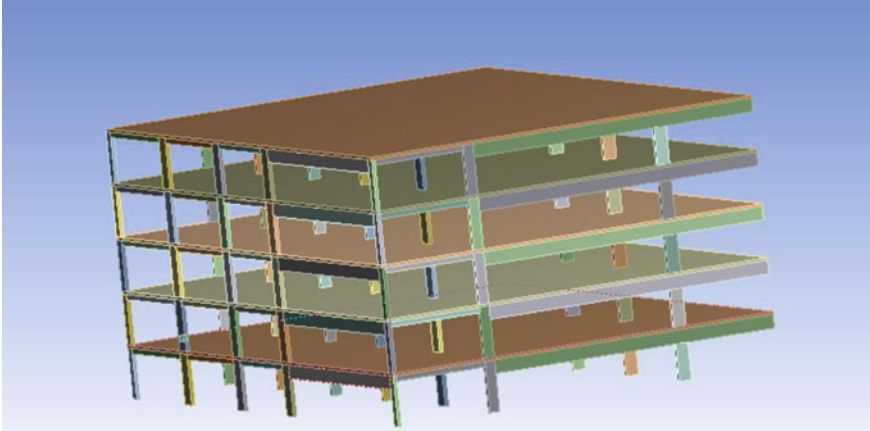


Fig. 17 Geometric model

are provided as per IS.875 part-2. Standard earth gravity with $g=9.81 \text{ m/s}^2$ was defined to apply the dead load to the structure.

Though in the model the infill walls are not shown, however, the load coming from walls are applied as a uniformly distributed load on the beams.

Explicit Dynamics was used for the analysis of the structure (Fig. 17).

9.2 Discretization of Finite Element Model

All the elements are discretised as a 20-noded quadrilateral element. The size of the element used is $150 \text{ mm} \times 150 \text{ mm}$. Meshing is done in such a way that the compatibility of nodes is satisfied. To reduce the computation time, the building is modelled in half symmetry (Fig. 18).

10 Results and Discussions

10.1 50 kg at 3000 mm

Table 6 shows the lateral deflections and strains of the structure subjected to blast load of 50 kg at 3000 mm respectively.

It is observed that the lateral deflections and strains reduce till 1% of fibres and the lowest lateral deflection is observed at the 1% of carbon fibres. The maximum value strain is observed in the ground floor column and the strain values decrease as the storey height increases.

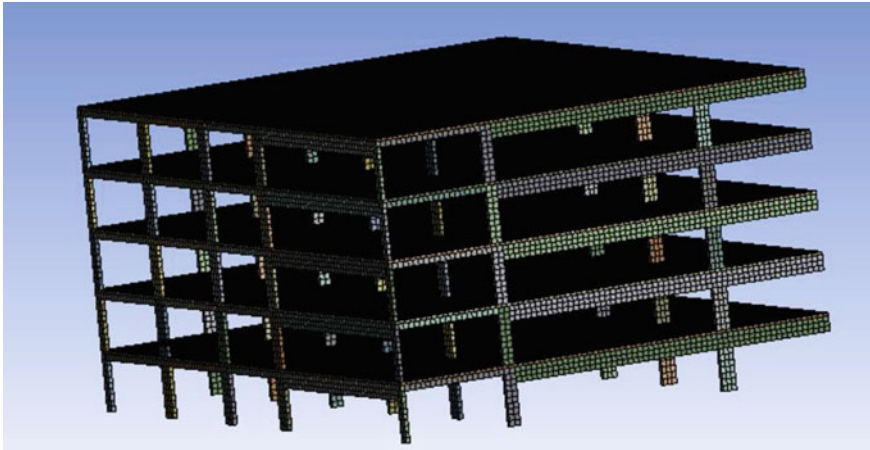


Fig. 18 Meshed structure

Table 6 Lateral deflections and strains for 50 kg at 3000 mm

Sample	Lateral deflections (mm)	Strains
M40 concrete	129.51	0.0014
M40 + 0.5% of carbon fibres	124.74	0.0023
M40 + 1% of carbon fibres	117	0.0012
M40 + 1.5% of carbon fibres	126	0.002
M40 + 2% of carbon fibres	127.5	0.0041

10.2 100 kg at 3000 mm

Table 7 shows the lateral deflections and strains of the structure subjected to blast load of 100 kg at 3000 mm respectively.

It is observed that the lateral deflections and strains reduce till 1% of fibres and the lowest lateral deflection is observed at the 1% of carbon fibres. Similar to 50 kg

Table 7 Lateral deflections and strains for 100 kg at 3000 mm

Sample	Lateral deflections (mm)	Strains
M40 concrete	178	0.0054
M40 + 0.5% of carbon fibres	175	0.0076
M40 + 1% of carbon fibres	167.9	0.0033
M40 + 1.5% of carbon fibres	175	0.0064
M40 + 2% of carbon fibres	187	0.0081

of charge weight, the maximum value strain is observed in the ground floor column and the strain values decrease as the storey height increases.

10.3 150 kg at 3000 mm

Table 8 shows the lateral deflections and strains of the structure subjected to blast load of 150 kg at 3000 mm respectively.

It is observed that the lateral deflections and strains reduce till 1% of fibres and the lowest lateral deflection is observed at the 1% of carbon fibres and the lateral deflections and strains does not significantly improve from 100 kg of blast but the strains due to 150 kg of charge weight are more distributed in all the ground floor columns than 100 kg of charge weight. Figures 19 and 20 shows the distribution of strains with 100 kg and 150 kg of charge weight respectively.

Table 8 Lateral deflections and strains for 150 kg at 3000 mm

Sample	Lateral deflections (mm)	Strains
M40 concrete	185.9	0.0056
M40 + 0.5% of carbon fibres	176.3	0.0078
M40 + 1% of carbon fibres	172.54	0.0035
M40 + 1.5% of carbon fibres	178	0.0068
M40 + 2% of carbon fibres	189	0.0085

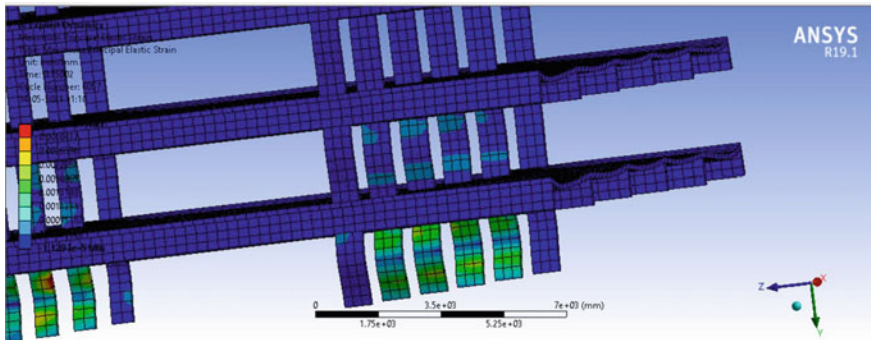


Fig. 19 Distribution of strain in 100 kg at 3000 mm

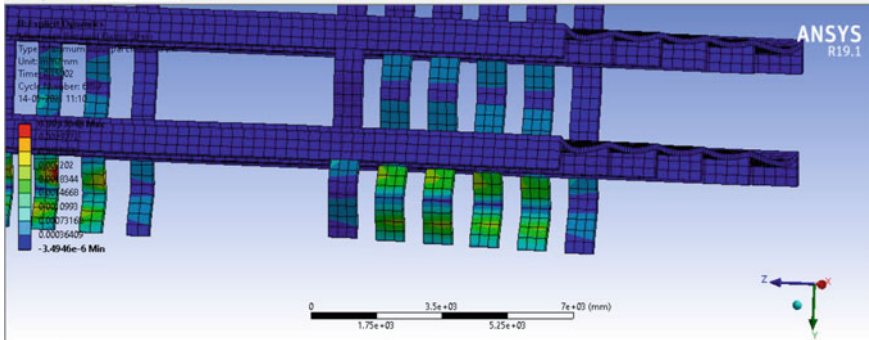


Fig. 20 Distribution of strain in 150 kg at 3000 m

10.4 Lateral Deflections of the Structure

From the above figure, it is inferred that the lateral deflections of the structure increases as the charge weight increases which does follow the Hopkinson-Cranz law (Fig. 21).

Due to the addition of fibres, there is an improvement in Young’s modulus of the structure and as a result, the deflection of the structure decreases till the addition of 1% of carbon fibres. And as the dosage increase, Young’s modulus of concrete drops and as a result, the deflection increases.

In the finite element model, it is observed that the lateral deflection is maximum in the ground floor and the lateral deflection reduces as the storey height increases which also obeys the Hopkinson-Cranz law.

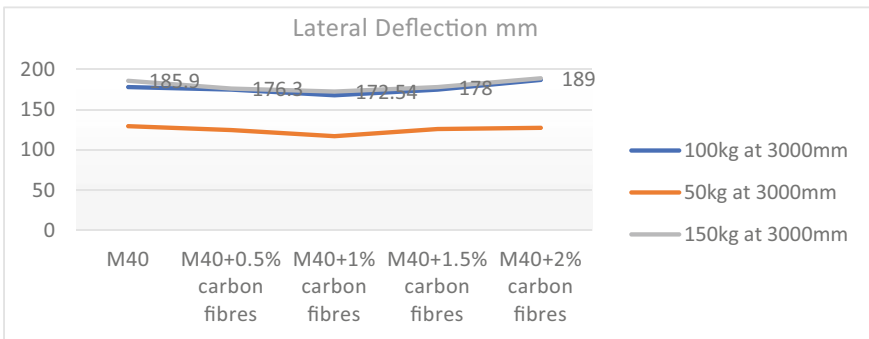


Fig. 21 Lateral deflections of the structure

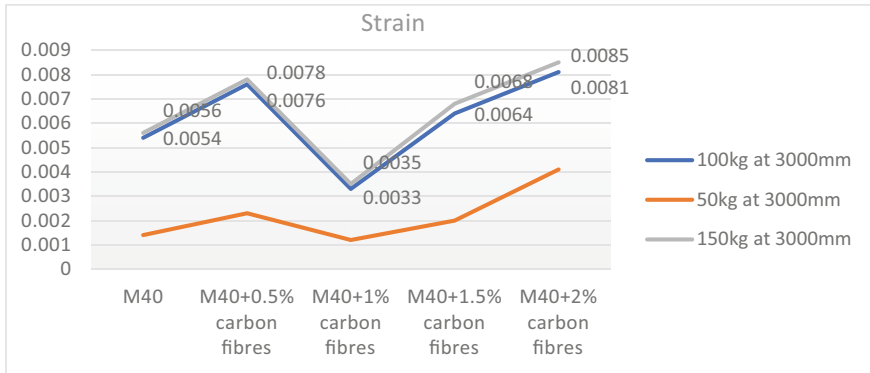


Fig. 22 Strains of the structure

10.5 Strains of the Structure

From the above figure, it is evident that the strains of the structure increase as the charge weight increases (Fig. 22).

In the finite element model, it is observed that the maximum value of strain is in the ground floor columns and the strains reduce as the storey height increases.

As stated earlier, the strain does not significantly increase from 100 to 150 kg but the strains are more distributed in 150 kg charge weight and more columns in the first floor also have more value of strains in 150 kg charge weight.

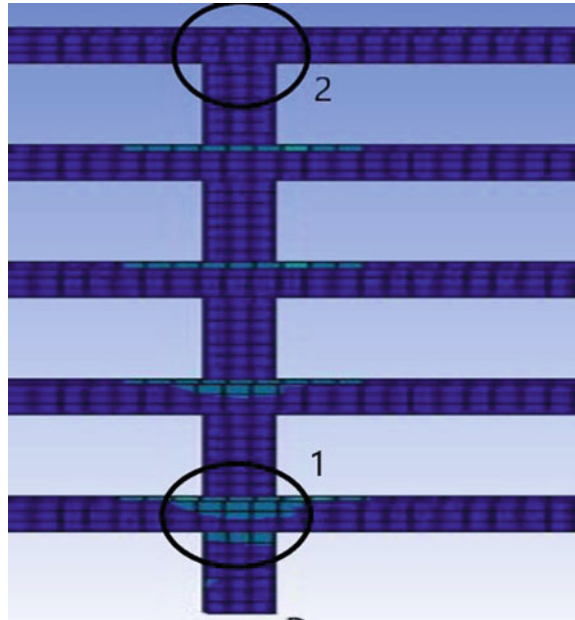
As the storey height increases the distribution of the maximum value of strains got reduced which is observed from Fig. 23. This is also shown by Bhosale et al. [6]. The values of strain in the ground floor (at location 1) is 0.0009 but the strains in the top floor (at location 2) is 0.00014 which got reduced significantly.

11 Conclusions

The following conclusions are drawn from the research work undertaken,

1. From the experimental results, it is clear that the mechanical properties of concrete improved with the addition of carbon fibres till 1% dosage of fibres. Adding more dosage of fibres does not help in improving the mechanical properties.
2. The density of concrete increased by 0.2%, 0.6%, 0.8%, and 1% with addition of carbon fibres of 0.5%, 1%, 1.5% and 2% respectively.
3. The compressive strength of concrete increased by 10%, 19%, 9%, and 6.5% with addition of carbon fibres of 0.5%, 1%, 1.5% and 2% respectively.
4. The Young’s modulus of concrete increased by 4.9%, 13.7%, 4.5%, and 3.1% with addition of carbon fibres of 0.5%, 1%, 1.5% and 2% respectively.

Fig. 23 Distribution of strains in the upper story



5. The Poisson's ratio of concrete increased by 21%, 41%, 52%, and 57% with addition of carbon fibres of 0.5%, 1%, 1.5%, and 2% respectively.
6. The addition of carbon fibres increases the tensile strength of concrete by a percentage of 5%.
7. The overall ductility of concrete improved by adding carbon fibres.
8. The Peak blast equivalent overpressure (P_{so}) increases with an increase in the charge weight of the blast and also decreases with the increase of standoff distance which is shown from the calculations of blast parameters.
9. Effect of peak Reflected overpressure reduces as we move from ground story to upper story.
10. The distribution of the maximum value of strains was observed in ground floor columns and the distribution got reduced as the storey height increases.
11. The lateral deflections and strains were least in the M40 + 1% Carbon Fibre mix.
12. From the results obtained for 1 mm × 12 mm carbon fibres, it is observed that the addition of 1% of carbon fibres performs well for the blast loads.

From the above investigations, it can be concluded that the addition of carbon fibres which is an industrial by-product, improves the mechanical properties of concrete and also improves the resistance of structure, by reducing the lateral deflections and strains, when subjected to blast loads.

Acknowledgements The authors wish to acknowledge the encouragement and the facilities provided by CHRIST (Deemed to be University), while undertaking this research.

References

1. Ngo et al (2007) Blast loading and blast effects on structures—an overview. *EJSE Spec Issue Loading Struct* 76–91
2. Koccaz Z et al (2008) Architectural and structural design for blast resistant buildings. In: *The 14th world conference on earthquake engineering*
3. Karlos, Solomos (2013) Calculation of blast loads for application to structural components. *JRC technical reports. Blast Simulation Technology Development, European Laboratory for Structural Assessment*
4. Ismail MA et al (2017) Response of A 3-D reinforced concrete structure to blast loading. *Int J Adv App Sci* 46–53
5. Ibrahim et al (2020) Mitigation of blast load risk on reinforced concrete structures considering different design alternatives. *Arch Civ Eng* 225–238
6. Bhosale et al (2016) Dynamic behaviour of frame structure subjected to blast loadings. *Int Adv Res J Sci Eng Technol* 245–249
7. Fu F (2013) Dynamic response and robustness of tall buildings under blast loading. *J Constr Steel Res* 299–307
8. Bhatt et al (2016) Comparative study of response of structures subjected to blast and earthquake loading. *J Eng Res Appl* 62–66
9. Kumar et al (2018) Response of reinforced concrete structure subjected to blast loads without and with steel fibres. *Int J Civ Struct Eng* 124–137
10. Suaris W et al (1982) Strain-rate effects in fibre-reinforced concrete subjected to impact and impulsive loading. *Composites* 153–159
11. Thakur P et al (2018) Effect of carbon fiber on different mixes of concrete. *Int Res J Eng Technol* 3996–3999
12. Tabatabaei ZS et al (2013) Experimental and numerical analyses of long carbon fibre reinforced concrete panels exposed to blast loading. *Int J Impact Eng* 70–80
13. Tabatabaei ZS et al (2015) Development of long carbon fibre-reinforced concrete for dynamic strengthening. *J Mater Civ Eng* 1446–1455
14. Chen P-W et al (1992) Concrete reinforced with up to 0.2 vol% of short carbon fibres. *Composites* 33–52
15. Unified facilities criteria-3-340-02. Department of Defence of United States of America

Numerical Investigation on Shear Bond Improvement of High Performance Concrete Composite Slabs Containing Recycled Aggregates



B. Athulya  and Milu Mary Jacob 

Abstract Composite slab with profiled metal decking provides economical solutions for floors of steel framed building systems particularly due to its reduced dead weight. The ability of the slabs to act compositely is governed by the shear interaction between the concrete topping and the profiled steel deck. The longitudinal shear bond failure is reported to be the most common failure mode in composite slabs. Significant end slips occur between concrete and profiled steel sheeting interfaces even before reaching its ultimate bending capacity. The present study aims at investigating various bond improvement methods for a composite slab with High Performance Concrete (HPC) topping containing recycled aggregates from demolition waste. The materials for longitudinal shear bond improvement under consideration includes nitobond, saw toothed steel and eye hooks. Percentage replacement of recycled coarse aggregates were first optimised and the analysis of composite slab after bond improvement is done numerically for different configurations of various shear connectors from which shear strength is computed using codal m-k method. The composite slab under consideration exhibits better performance in terms of load carrying capacity and shear strength compared to normal concrete composite slab. It also reflects in a reduced deflection and end slip.

Keywords HPC topping · End slip · Bond improvement · Longitudinal shear

1 Introduction

A composite slab is a slab structure made of hardened concrete and profiled metal sheet that works as fixed formwork during construction phase and as tensile support during the composite stage. The main components of a composite slab are a steel

B. Athulya (✉) · M. M. Jacob
Department of Civil Engineering, Saintgits College of Engineering, Kottayam, India
e-mail: athulya.sm2123@saintgits.org

M. M. Jacob
e-mail: milu.mary@saintgits.org

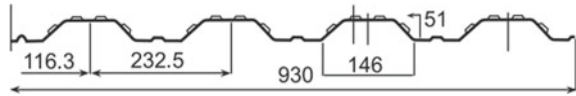
deck and a concrete slab; the concrete slab portion of a composite slab is frequently supplemented by steel mesh on the top side. The main advantage is that the amount of concrete and consequently the total dead loads can be decreased by utilising the geometry of the profiled steel sheet [1]. A composite slab with a contoured deck can fail under stress in three different ways. The first failure type of composite slabs is flexure failure, the second failure type is vertical shear fractures at the support, and the third failure type is horizontal shear failure at the steel–concrete sheet interface [2, 3]. Horizontal shear is the most common kind of failure in composite slabs and has a considerable impact on the shear strength of the slab [4]. To guarantee that the composite action of composite slab is achieved, the profiled sheeting must be able to transmit longitudinal shear to concrete across the interface. In addition to conveying longitudinal shear, the profile sheet must be built to resist vertical separation. Composite behaviour between profiled sheeting and concrete is expected to improve either by mechanical interlocking, frictional interlocking and also by adhesion [5, 6].

High performance concrete has received increased attention as a result of the expansion of infrastructure, including buildings, industrial structures, hydraulic structures, bridges, and roads [7]. There has been minimal study done to forecast the behaviour of composite slabs with different profiles of steel sheeting and recently created high performance concrete, despite the fact that many research publications have focused on the structural performance of composite slabs with traditional concrete. By analysing the performance of a composite deck slab made using HPC and a sufficient quantity of recycled aggregate acquired from demolition waste, this study aims to improve the conservation of resources and make optimal use of demolition products. The study also examines the effects of various materials, such as saw toothed steel, nitobond, and eye hooks, on the improvement of the longitudinal shear bond. Analytical method mentioned in Eurocode called the m-k method is used for the determination of shear strength.

2 Preliminary Study

Preliminary tests were done on all raw materials like OPC grade 53 cement, coarse aggregates sized 20 mm, fine aggregate and recycled aggregates of size 20 mm collected from demolition waste. Ground Granulated Blast furnace Slag (GGBS) was used as admixture and super plasticizer used is poly carboxylate ether. All these raw materials were used to develop the required High Strength Concrete (HPC) of grade M60. In order to finalise the HPC mix proportions for numerical investigation GGBS and recycled aggregates were first optimized. The optimization results showed that 40% GGBS and 30% recycled aggregated replacement contributed to the target strength achievement.

Fig. 1 Cross sectional dimensions of deck sheet



3 Numerical Investigation

The prime objective of the present study is to analyse the longitudinal shear bond improvement of a profiled deck composite slab modelled using 2 different types of shear connectors—saw tooth blade and eye hooks. The composite slab is studied under different configurations of these connectors as well as under different shear span and the effect of the said differences are compared. For this purpose 2 different softwares are used—Ansys for modelling and Abaqus for analysis.

3.1 Modelling

Ansys workbench 2021 is used for modelling the profiled deck composite slab. The trapezoidal profiled deck is modelled as per the data sheet from the supplier Deva Steels, Cochin. The sheet had an overall width of 930 mm and trough height of 51 mm as shown in Fig. 1. Overall span of composite slab modelled is 2500 mm and depth 150 mm. Reinforcement bars of 8 mm diameter is provided on top as compression bars. For the purpose of comparison the composite slab is modelled with and without shear connectors. Saw tooth blades and eye hooks were used as shear connectors and these connectors were provided throughout the trough in each model as in Fig. 2a, b. Saw tooth connectors were modelled with a total height of 5 cm and length of these connectors were kept varying in each configuration. 100 mm, 200 mm and 300 mm blade lengths were considered. Similarly eye hook connectors of 5 mm thickness and 32 mm overall diameters were modelled with their spacing being 200 mm and 300 mm respectively in each model. Each of these components of the composite slab are modelled separately and are exported to Abaqus as a step file for analysis. Details of each model with saw tooth connectors and eye hook connectors are enlisted in Tables 1 and 2.

3.2 Analysis

The components modelled in ansys are assembled in abaqus for analysis. Material properties were assigned to each of the components and the contacts are provided between each component as listed in Table 4. Mesh dependency study is done, results given in Table 3 and the mesh size chosen are 20 mm for concrete (linear hexahedral) and deck (linear quadrilateral), 5 mm for reinforcement (linear line element) and

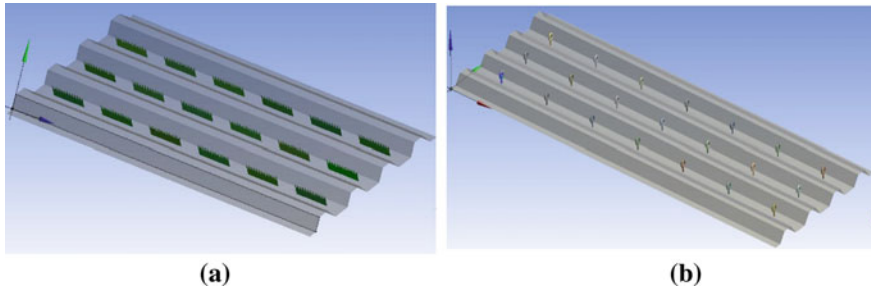


Fig. 2 a, b Deck sheet modelled using sawtooth blades and eye hooks respectively

Table 1 Various configurations of saw tooth connectors

S. No.	Saw tooth configuration	Blade length (mm)
1	Staggered	100
2	Staggered	200
3	Staggered	300
4	Parallel	200

Table 2 Various configurations of eyehook connectors

S. No.	Eye hook configuration	Spacing
1	Staggered	200
2	Parallel	200
3	Staggered	300

2 mm for connectors (linear quadrilateral). The type of contact provided between each component is enlisted in Table 3. Analysis of each model is done in simply supported condition with line loading. One model of each connector was again analysed by providing varying shear spans of 575, 525, 475 and 425 mm. This is done in order to analyse the effect of shear span on the load carrying capacity of the composite slab as well as to determine the shear strength of the selected models using m-k method.

Table 3 Mesh dependency study

Set No.	Concrete (Element size)	Deck (Element size)	Reinforcement (Element size in mm)	Shear connector (Element size in mm)	Deformation (mm)
1	24	24	7	4	4.05
2	22	22	6	3	3.48
3	20	20	5	2	2.34
4	18	18	4	1	2.30

Table 4 Interactions provided between various components

S. No.	Region	Contact
1	Concrete—deck	Friction
2	Concrete—connector	Embedded
3	Connector—deck	Tie constraint
4	Concrete—reinforcement	Embedded
5	Reference point—nodal line	Coupling

4 Results and Discussion

All models were initially analysed with a shear span of $l/4$ which is 575 mm. From the initial analysis it is clear that the staggered arrangement of shear connectors performed better than parallel arrangement in terms of load carrying capacity. This variation can be identified from Fig. 3a, b. In the case of saw tooth connectors the model with the greatest blade length of 300 mm showed an ultimate load of 146.52 kN.

The analysis of composite slab models containing eye hook connectors showed that the configuration with least spacing of eye hooks had greater load bearing

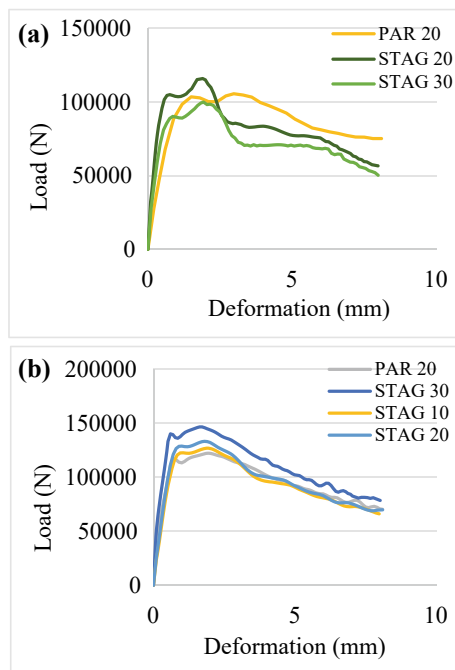
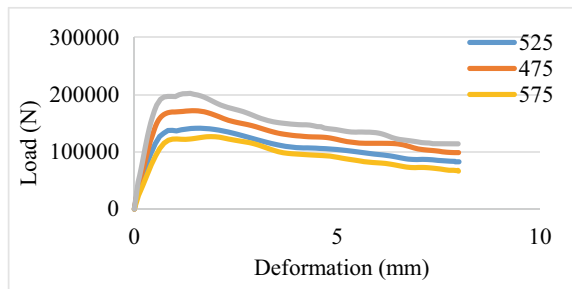


Fig. 3 a Load deformation curve for various configurations of sawtooth connectors. **b** Load deformation curve for various configurations of eye hook connectors

Table 5 Ultimate load and displacement values for various configurations of shearconnectors

S. No.	Connector	Configuration	Ultimate load (kN)	Deformation
1	Saw tooth	STAG-20	132.56	0.87
2	Saw tooth	PAR-20	121.97	2.31
3	Saw tooth	STAG-30	146.52	2.37
4	Saw tooth	STAG-10	126.51	1.89
5	Eye hook	STAG-20	122.65	2.09
6	Eye hook	PAR-20	115.36	1.79
7	Eye hook	STAG-30	99.98	1.89

Fig. 4 Load versus deformation curve for various shear spans of saw tooth connectors



capacity which is 122.65 kN and the corresponding deformation was 2.09 mm. The ultimate load value and corresponding deformation after the analysis of each model is enlisted in Table 5.

4.1 Shear Span Variation

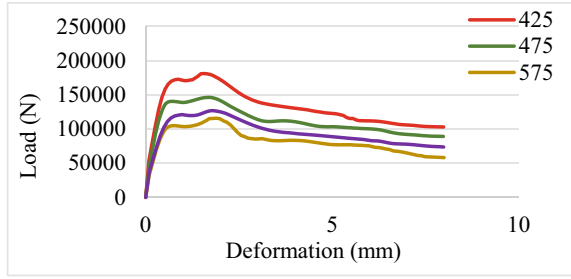
One model containing saw tooth connector and one containing eye hook connector were chosen for studying the effect of variation in shear span. The results obtained are represented graphically in Figs. 4 and 5. The shear spans considered for analysis are 575 mm, 525 mm, 475 mm and 425 mm respectively.

The results showed that the ultimate load carrying capacity increased as the shear span reduced from 575 to 425.

4.2 Shear Strength

Shear strength of composite slab containing saw tooth connectors as well as eye hook connectors were calculated using m-k method mentioned in Eurocode 4 [8] by using the datas obtained from the graph in Figs. 4 and 5. Shear strength is computed using

Fig. 5 Load versus deformation curve for various shear spans of eye hook connectors



Eq. (1)

$$\tau_u = m(A_p/bL_s) + k \tag{1}$$

where m and k are the slope and intercept respectively of the curves shown in Fig. 6a, b, the values of which are found using linear regression. The results obtained using m-k method of evaluation is tabulated in Table 6.

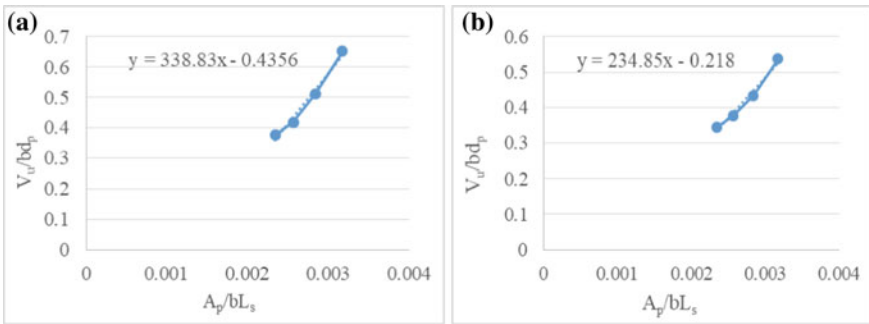


Fig. 6 a Load versus deformation curve for various shear spans of saw tooth connectors. **b** Load versus deformation curve for various shear spans of eye hook connectors

Table 6 Longitudinal shear strength computed using m-k method

Shear span L_s (mm)	V_u/bd_p		A_p/bL_s	Longitudinal shear strength, τ_u (N/mm ²)	
	Eyehook	Saw tooth		Eyehook	Saw tooth
575	0.34	0.37	0.0023	0.33	0.35
525	0.37	0.42	0.0025	0.38	0.43
475	0.43	0.51	0.0028	0.44	0.52
425	0.53	0.65	0.0031	0.52	0.63

5 Conclusion

Finite element analysis was done to investigate the longitudinal shear behavior of composite slab made using high strength concrete containing recycled aggregates. Two different types of shear connectors namely saw tooth and eyehook connectors were used and the results were compared. One model from each type was analysed by varying the shear span in order to monitor the effect of shear span on the load bearing capacity of the slab and the results were used to formulate the longitudinal shear strength of the composite slab.

- In the case of composite slabs modelled using saw tooth connectors the loadcarrying capacity increased with increase in blade length.
- For composite slabs modelled with eye hook connectors the load bearing capacity reduced with increase in spacing between the connectors.
- The ultimate load value increased with decrease in shear span for both type of connectors.
- Load carrying capacity improved by more than 50% by introducing shear connectors throughout the trough.
- Longitudinal shear strength was found to be greater for the smallest shear span in both cases.

References

1. Ahmed IM, Tsavdaridis KD (2019) The evolution of composite flooring systems: applications, testing, modelling and eurocode design approaches. *J Constr Steel Res* 155:286–300
2. Jacob MM, Praveen A, Kurian SA (2022) Investigations on geometrical modifications for profiled decking of composite slabs. *Mater Today Proc* 65:2007–2015
3. Siva A, Senthil R, Swaminathan S (2016) Assessment of longitudinal shear strength of composite deck slab. *Int J Innov Sci Res* 24:277–284
4. Bai L, Li Y, Hou C, Zhou T, Cao M (2020) Longitudinal shear behaviour of composite slabs with profiled steel sheeting and ECC. *Eng Struct* 205:110085
5. Alsarayreh AIM, bin Sulaiman A, Siang TC, Mansour H (2022) Recent improvements in the longitudinal shear resistance in composite slabs: a review. *J Algebraic Stat* 13(3):2863–2872
6. Eltobgy HH, Abdelkareem KM, Bakhom MM (2021) Experimental study on shear bond behavior of composite deck slab equipped with shear connectors. *Int J Sci Technol Res* 10
7. Hossain KMA, Alam S, Anwar MS, Julkarnine KMY (2016) High performance composite slabs with profiled steel deck and engineered cementitious composite—strength and shear bond characteristics. *Constr Build Mater* 125:227–240
8. Eurocode 4, Design of steel and concrete composite structures, EN1994 1-1 & 1-2

Factors Leading to Cost Overrun and Time Overrun in Pune Metro Project



V. D. Mahind and B. M. Dawari

Abstract The success of any infrastructure construction project rely on cost and time aspect of project. Execution of infrastructure project within given timeline and budget is really challenging. It is of essential to study the issues that can arise while project is ongoing. Metro construction sector is currently the one with utmost investment. Pune Metro construction project is such a project that aims to provide a rapid transit system for the growing population of Pune city in India. However, like many other construction projects, it has been plagued by cost and time overruns. In this paper, we have studied factors related Metro construction which lead to cost and time overrun through literature and then validated with the pilot study. Responses of various stakeholders working on project were recorded on the Likert's scale for each factor considering their overall impact on cost and time aspect of project. Factors are then ranked with relative importance index method for each aspect and the reliability of responses is checked through Cronbach's alpha test. Through this research, primary causes which affected cost of project most are found as material cost, land acquisition and price escalation while Covid-19 pandemic, land acquisition affected the time schedule of project most. This paper discusses methodology opted by Pune Metro to tackle these risks and recommendations about measures to be taken for avoiding these overruns which were found out through personal interactions with stakeholders and site visits. This study can turn out to be guide for future Metro construction projects, both in India and globally, and help to lower down likelihood of cost and time overruns risk in these complex and important infrastructure projects.

Keywords Pune metro · Cost overrun · Time overrun · Risk

V. D. Mahind (✉) · B. M. Dawari
Department of Civil Engineering, College of Engineering Pune, Pune, India
e-mail: mahindvd21.civil@coep.ac.in

B. M. Dawari
e-mail: bmd.civil@coep.ac.in

1 Introduction

The Pune Metro is public transport system which intends to link different areas of the city reliably, efficiently, and affordably. The project was started in 2017 and is expected to be completed in phases by 2025. The estimated cost of project is around Rs. 11,400 crores (\$1.5 billion) [1]. However, the project has faced various challenges, including cost and time overruns. According to recent reports, the project is currently running three years behind schedule, and the cost has increased by 20%. This research paper aims to identify the factors that have led to these overruns and possible solutions to mitigate their impact.

India is country with significantly growing in infrastructure. As we know, Construction industry is dynamic, complex in nature and is characterized by uncertainty [2] and with scale of project it magnifies. Out of the 1673 infrastructure projects (project cost more than ₹150 crores) which are overseen by MoSPI, 445 projects are cost overran and 557 projects are time overran. Total cost overrun shown by these projects is around of ₹4.4 Lakh Crores which is greater than GDP of some nations.

According to Pune Metro's Rail Project's Detailed Project Report (DPR) published in 2017, the estimated completion date for Phase 1 of the project was December 2021. However, because of several reasons such as land acquisition, COVID-19 pandemic, and the delay in getting permissions, the project got delayed. The new estimated completion date for Phase 1 of the Pune Metro project is December 2024.

Narayanan et al. [3] studied time and cost overrun in mega infrastructure construction in India. Around 30 mega projects were studied. The most frequent reasons were delays in land acquisition, delays in clearing forests, law and order issues, general price increases, high capital costs, contractor performance issues, and delays in the delivery of equipment. Additionally, the impact on both parameters is explored.

Abd El-Karim et al. [4] prepared probabilistic model of risk. The political sub-criteria were determined to be the most likely and impacted element, and the owner sub-criteria to be the least likely and impacted one. Paper concludes by noting that while risk management is critical for the successful completion of construction projects.

Larsen et al. [5] used the Relative Importance Index (RII) method to examine the impact of the variables schedule delay, cost overrun, and quality level. The study examines, first, using a questionnaire survey of industry experts in construction, how project execution is impacted by construction delays, and, second, through an empirical approach, how costs and completion times are impacted.

The main objective of this research is to point out the factors leading to cost and time overrun in Pune Metro, to check how they are being addressed and to find out extent of overruns. The paper identifies numerous elements that lead to cost and schedule overruns on the Pune Metro project in order to pinpoint best practises and potential remedies for these problems. Policymakers, Government Organisations, Contractors, and commuters are just a few of the stakeholders involved in the Pune Metro project that will find the research's conclusions to be extremely valuable.

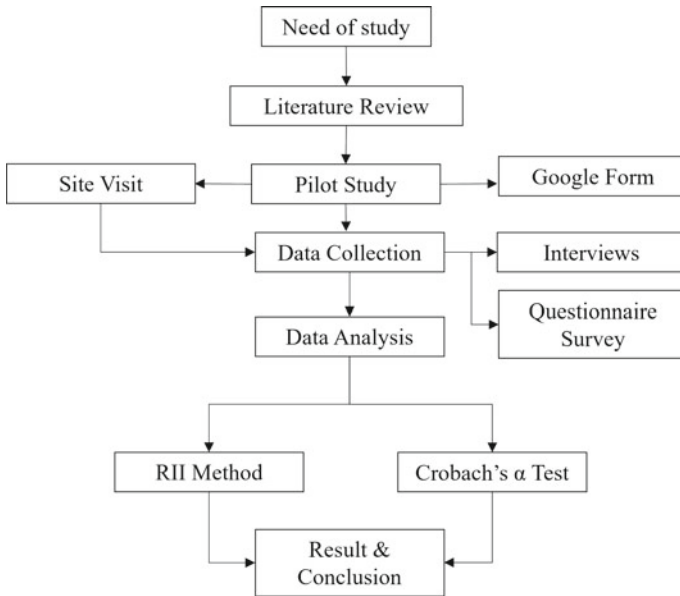


Fig. 1 Research methodology

Ultimately, this study aims to add to the existing conversation on infrastructure development in India with an emphasis on the difficulties encountered by massive initiatives like the Pune Metro. Insights on potential solutions and best practises for managing and completing similar projects in the future is also included in the paper.

2 Research Methodology

See Fig. 1.

3 Data Collection

The case study of the Pune Metro Project is considered for this research work. The study is primarily quantitative, and data has been collected through questionnaire survey and interviews with project managers, contractors, and other stakeholders involved in the project. The study also involved a review of project documents, including project reports, budgets, and timelines.

3.1 Pilot Study

The pilot study is carried out initially to find out key factors that affect the cost and duration of project and also to validate the previous listed factors from literature and observation. Factors considered are strictly related to infrastructure project. While conducting pilot study, around twenty responses were recorded which were from the various stakeholders involved in Pune Metro project. Questionnaire of main study is redesigned after conducting pilot study. This study is conducted through two modes via Google Form as well as through actual site visits.

3.2 Factors Found Out Through Previous Literature Available and Pilot Study

See Table 1a, b.

3.3 Questionnaire Survey

The questionnaire survey is conducted for collection of data. As all questions were pre-defined and same for all, it was structured questionnaire survey. Questionnaire survey method is said to be best method of collecting data from large set of samples. It along with Likert scale enable the easy analysis of data. The required data is collected through google forms and site visits. This survey include several sections wiz general information, factors affecting the cost and factors affecting the duration of project. Sections have several factors and respondent rate the factors on Likert scale from 1 to 5 depending on the impact that particular factor causes on cost or time of project. Likert scale ranges from 1 for mild impact to 5 for extreme impact. 43 responses were recorded from the ones working on Pune Metro project (Fig. 2).

4 Data Analysis

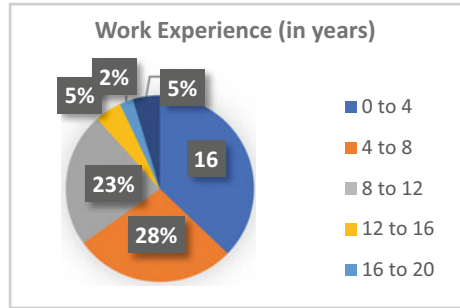
Relative Importance Index method is selected for analysis purpose. The ranks are allotted to factors according to their RII. Previously this method is used by Niazi and Painting [6] to rank causes of cost overrun in Afghanistan construction projects.

$$RII = \frac{\sum_{i=1}^5 W_i}{A \times N},$$

Table 1 (a) Factors affecting cost, (b) Factors affecting time

(a)	
<i>No.</i>	<i>Cost factors</i>
1	Material cost
2	Labour cost
3	Transportation cost
4	Environmental conditions
5	Land acquisition
6	Government permits and approvals
7	Stakeholder conflicts
8	Contractor performance
9	Inflation and currency fluctuations
10	Design changes
11	Unforeseen site conditions
12	Covid-19 pandemic
13	Poor site management
14	Poor inventory management
15	Price escalation
16	Realignment of route
(b)	
<i>No.</i>	<i>Time factors</i>
1	Funding issues
2	Covid-19 pandemic
3	Land acquisition
4	Material availability
5	Labour availability
6	Availability of equipment and machinery
7	Unforeseen site conditions
8	Complexity of project
9	Government permits and approvals
10	Poor site management
11	Change in project scope
12	Contractor performance
13	Unforeseen rain
14	Handing over of land to contractor
15	Realignment of route

Fig. 2 Work experience of respondents



where, RII = relative importance index, W_i = weightage given to particular factor by respondent from 1 to 5, A = max. weightage value (here it is 5), N = Total no. of responses recorded.

Furthermore, Cronbach’s alpha test is used to check consistency or reliability of data. Cronbach α coefficient lies between 0 to 1. Closer the value of coefficient to 1, higher is the consistency and reliability [7].

$$\text{Coefficient of Cronbach}(\alpha) = \frac{K}{K - 1} \times \left(1 - \frac{\sum V_i}{V_{total}} \right)$$

where, K = Number of factors, V_i = Sum of the variance of all factors, V_{total} = Variance of the total score.

5 Results and Discussion

After finding RII of each factor, top 10 ranked factors affecting cost and duration each are selected and ranked accordingly.

Of the top 10 factors that affect cost from Table 3a, material cost was found to be highest impacting followed by land acquisition and price escalation with RIIs 0.897, 0.841 and 0.837 resp.

Of the top 10 factors that affect duration from Table 3b, Covid-19 pandemic was found to be highest impacting followed by land acquisition and government permits and approvals with RIIs 0.804, 0.781 and 0.758 resp.

Values got are shown in Table 3c and verified with the help of Table 2. The Cronbach’s α coefficient for the cost factors is 0.765 and that of time factors is 0.792 which implies the acceptable consistency. This result validated the consistency and reliability of data collected.

Table 2 Cronbach's alpha thumb rule

Cronbach's alpha	Internal consistency
$\alpha \geq 0.9$	Excellent
$0.9 \geq \alpha \geq 0.8$	Good
$0.8 \geq \alpha \geq 0.7$	Acceptable
$0.7 \geq \alpha \geq 0.6$	Questionable
$0.6 \geq \alpha \geq 0.5$	Poor
$0.5 > \alpha$	Unacceptable

Table 3 (a) Ranking of cost factors according to RII, (b) Ranking of time factors according to RII, (c) Cronbach's alpha test results

(a)		
<i>Rank</i>	<i>Cost factors</i>	<i>RII</i>
1	Material cost	0.897
2	Land acquisition	0.841
3	Price escalation	0.837
4	Covid-19 pandemic	0.786
5	Unforeseen site conditions	0.781
6	Design changes	0.762
7	Contractor performance	0.758
8	Poor inventory management	0.753
9	Labour cost	0.749
10	Realignment of route	0.716
(b)		
<i>Rank</i>	<i>Time factors</i>	<i>RII</i>
1	Covid-19 pandemic	0.804
2	Land acquisition	0.781
3	Government permits and approvals	0.758
4	Handing over of land to contractor	0.753
5	Material availability	0.73
6	Labour availability	0.726
7	Contractor performance	0.72
8	Change in project scope	0.716
9	Complexity of project	0.711
10	Funding issues	0.702
(c)		
	<i>Cost factors</i>	<i>Time factors</i>
Cronbach's alpha	0.765	0.792

6 Methodology Adopted by Pune Metro to Overcome Cost and Time Overrun

6.1 Deployment of Experienced Staff

The Pune Metro project has appointed experienced staff to supervise the construction work and to ensure the smooth implementation of the project. Those with less relative experience have been trained for the job. Teams are formed in such a way that each team is mix of freshers and experienced ones. These people are involved extensively in planning and monitoring so as to keep project efficient, safe and sustainable.

6.2 Use of Precast Structures

Most of the structures used in Pune Metro are precast structures like elevated viaducts, pier, walls. For underground Metro line precast tunnel lining is used. Precast elements allowed Pune Metro for rapid progress of construction and also mitigated down the requirement of space on site. Precast structures also allowed better quality of work [8].

6.3 Use of 5D BIM Softwares

Use of BIM technology increase value creation and cost savings by facilitating several services on single platform [9] (Fig. 3).

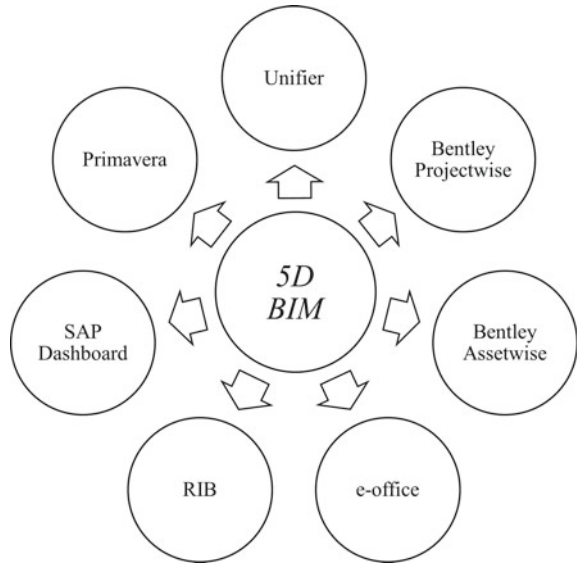
6.4 Use of GGBS (Ground Granulated Blast-Furnace Slag) in Concrete

GGBS is by product of the iron and steel industry and its use in concrete production reduces the amount of cement needed which in result reduces the cost [10]. Also use of GGBS reduces amount of waste. GGBS is used in Pune Metro for construction of columns.

Based on the study carried out following remedial measures can be adopted to tackle risk of cost and time overrun:

- Effective project planning is crucial for ensuring effective completion of project [4]. The detailed project plan should have covered each aspect of project. Timely updation of plan should be done if any changes arise.

Fig. 3 Softwares used for 5D BIM



- It is essential to have a clear and effective risk management plan in place to minimize the potential impact of risks on the project as risks can never be completely eliminated [4].
- Maintaining good relation with vendors is required for timely material supply. This can be achieved by creating strong communication channels and by negotiating favourable contracts.
- Contracts should be well negotiated, formulated and documented according to project schedule [11].
- Regular monitoring of project progress should be done with site visits and meetings in order to check if there is any delays or cost overruns. Solutions for issues should be given immediately to avoid further delays or cost increases.
- If any unforeseen circumstances arises, there should be enough resources so that they can be reassigned whenever needed.
- All the stakeholders involved should be given updates regarding the progress of work [12].

7 Conclusions

It is found that like most of the infrastructure projects, Pune Metro have also been cost and time overrun. It has been found that factors leading to cost and time overrun in context of Metro construction, the extent of overruns and addressment of issues by the parties involved.

The project is delayed for almost 3 years to December 2024 from it’s estimated completion in December 2021 mostly because of Covid-19 pandemic and delayed

land acquisition. Although Metro work didn't stop during the Covid-19 pandemic but it slowed down the progress significantly. The cost of project has risen to Rs. 13,636 crores from its estimated cost of Rs. 11,400 crores i.e. cost overrun of Rs. 2236 crores and the main reasons for it are rising cost of materials over the time and land acquisition cost which was pretty high than the one estimated. Several attempts mentioned above are applied by Pune Metro to overcome the risk. Still cost overrun could only be limited up to 20% as of now. Some of the issues like land acquisition are occurring frequently almost in every infrastructure project that needs to be addressed properly with adapting some new and more effective strategies.

Currently 22 Metro construction projects are ongoing in India out of which 5 are in construction phase, 13 in planning stage and 4 projects are in proposal phase So this research can directly help these projects for their efficient and effective completion. This study can also be helpful in guiding other similar infrastructure projects in future.

References

1. Website: <https://www.puneMetrorail.org/>
2. McCord J, McCord M, Davis PT, Haran M, Rodgers WJ (2015) Understanding delays in housing construction: evidence from Northern Ireland. *J Financ Manag Prop Constr* 20(3):286–319. <https://doi.org/10.1108/JFMPC-07-2015-0028>
3. Narayanan S, Kure AM, Palaniappan S (2019) Study on time and cost overruns in mega infrastructure projects in India. *J Inst Eng (India) Ser A* 100(1):139–145. <http://doi.org/10.1007/s40030-018-0328-1>
4. Abd El-Karim MSBA, Mosa El Nawawy OA, Abdel-Alim AM (2017) Identification and assessment of risk factors affecting construction projects. *HBRC J* 13(2):202–216. <http://doi.org/10.1016/j.hbrj.2015.05.001>
5. Larsen JK, Shen GQ, Lindhard SM, Brunoe TD (2016) Factors affecting schedule delay, cost overrun, and quality level in public construction projects. *J Manag Eng* 32(1). [http://doi.org/10.1061/\(asce\)jme.1943-5479.0000391](http://doi.org/10.1061/(asce)jme.1943-5479.0000391)
6. Niazi GA, Painting N (2017) Significant factors causing cost overruns in the construction industry in Afghanistan. *Procedia Eng* 510–517. <http://doi.org/10.1016/j.proeng.2017.03.145>
7. Mahind SD, Patil D (2023) COVID-19—assessment of economic and schedule delay impact in Indian construction industry using regression method. In: Ranadive MS, Das BB, Mehta YA, Gupta R (eds) *Recent trends in construction technology and management*. Springer Nature Singapore, pp 283–297
8. Tomek R (2017) Advantages of precast concrete in highway infrastructure construction. *Procedia Eng* 176–180. <http://doi.org/10.1016/j.proeng.2017.07.188>
9. Kumar B, Cai H, Hastak M. An assessment of benefits of using BIM on an infrastructure project
10. Meng W, Valipour M, Khayat KH (2017) Optimization and performance of cost-effective ultra-high performance concrete. *Mater Struct/Mat Constr* 50(1). <http://doi.org/10.1617/s11527-016-0896-3>
11. Prasad KV, Vasugi V, Venkatesan R, Bhat NS (2019) Critical causes of time overrun in Indian construction projects and mitigation measures. *Int J Constr Educ Res* 15(3):216–238. <https://doi.org/10.1080/15578771.2018.1499569>
12. Mezher TM, Tawil W (1998) Causes of delays in the construction industry in Lebanon. *Eng Constr Architectural Manag* 5(3):252–260. <http://doi.org/10.1108/eb021079>

Experimental Study on the Optimum Design and Performance of Porous Concrete with Partial Replacement of Cement with Glass Powder



Mohit Yadav, Bhupender Khatana, and Haobam Derit Singh

Abstract Given the concrete jungle of the metropolitan cities resulting to increasing carbon footprint in the global atmosphere, the need for reduction in carbon emission is the need of the hour. Construction and its allied activities accounting for more than 38% of global carbon emission need to take part in mitigating as such. Many such metropolitan cities saw improper design and town planning resulting to water logging and drainage issues, which are a main concern. One such mitigation strategy is to implement the use of Porous Concrete on light traffic pathways. Porous concrete are construction materials that allows for seepage of water through the appropriate voids in its form without compromising its strength. Porous concrete as pavement materials will also address the drainage issues that the main Indian cities like Delhi and Mumbai are facing. It is so designed to recharge ground water as well by its seepage action. This study focused on the optimum design for strength parameters of Porous Concrete partially replaced with glass powder in 0%, 10%, 15% and 20%. The fresh and hardened properties of the porous concrete are conducted and compared with the nominal sample (controlled sample) of M25 grade porous concrete.

Keywords Porous concrete · Glass powder · Fresh properties · Hardened properties

M. Yadav · B. Khatana · H. D. Singh (✉)
Department of Civil Engineering, Manav Rachna International Institute of Research and Studies,
Faridabad, Haryana, India
e-mail: haobamderitsingh@gmail.com

© The Author(s), under exclusive license to Springer Nature Switzerland AG 2024
M. Nehdi et al. (eds.), *Proceedings of SECON'23*, Lecture Notes in Civil Engineering
381, https://doi.org/10.1007/978-3-031-39663-2_51

619

1 Introduction

The need for reduction in carbon emission should be viewed as a highlight in the construction and its allied activities given the accountability of 37–39% of energy plus process-related CO₂ emissions over the past few years (as per the Global Status Report) out of which eleven percent were the output of manufacturing building materials and its allied products including glasses, Cement etc. With the activities of construction alone, accountability of 85% global emission of CO₂ has been pinpointed to cement industry [1]. Given these stances, it is also a concern to be noted that given the concrete jungle of the metropolitan cities and its changing shift to increasing carbon footprint in the global atmosphere, the need for reduction in carbon emission is the need of the hour. Construction and its allied activities accounting for a significant percentage of carbon emission need to take part in mitigating as such. The search to remedy such issue has been increasing over the past few decades through innovative research as well as replacement of materials by greener constituents [2–6]. One such innovation in the field of concrete study is pervious/porous concrete. Porous/Pervious concrete are construction materials that allows for seepage of water through the appropriate voids in its form without compromising its strength. The improper and or/lack of drainage system in Indian cities that resulted to flooding can be tackled to an extent with porous concrete. Porous concrete as pavement materials will also address the drainage issues that the main Indian cities like Delhi and Mumbai are facing. It is so designed to recharge ground water as well by its seepage action. Porous concrete is obtained with the use of aggregate in larger size (with zero to little FA). Studies conducted over the years stated this concrete type is plausible as a usage for pavement while also ensuring road traffic stability in regions of heavy showers [7–9]. It is a probable remedy for runoff of stormwater elimination to atleast some extent, owing to its interconnected-macroporosity in higher levels. The search for greener aspects in concrete technology is a work in progress and the need of the hour. This paper attempt to experimentally study the performance of optimum designed porous/pervious concrete partially replaced with glass powder (0%, 10%, 15% and 20%). Usage and effect of replacement by glass powder for concrete ingredient proved to be beneficial in concrete fields through various reliable studies [10–13]. Some studies deduced that optimum% usage of glass resulted to increase in mechanical properties, stating that the age of curing affected hugely in development of strength on such concrete containing glass-powder and as such compressive strength is ensured to increase in long term through pozzolanic reactivity in association with the glass-powder [14].

2 Methodology

This experimental study was undergone to conclude the optimum design percentage of porous concrete partially replacing the cement by glass-powder in the percentage of 0%, 5%, 10% and 20%. The mix for the concrete were formed as below and methodology deduced as a flow chart highlighted in Fig. 1:

- Cement: Experimental study was conducted through incorporation of OPC53 grade, wherein the test on cement were conducted.
- Aggregates: Selection of crushed aggregates i.e., 12.5 mm sieve size passing and 10 mm retained on sieves were considered and tested for physical requirements.
- Preparation of Mix/Concrete Mix Design: M25 mix proportions were chosen for the purpose of the study. The subset for this were made in such a way that first subset was made as a controlled sample of nominal mix design (0% replacement) for porous concrete whereas the second subset was conducted through the usage of glass powder with different proportions (10%, 15%, 20%) partially replacing the cement. The testing of the prepared mixed were deduced at 7 days and 28 days for each mix%.

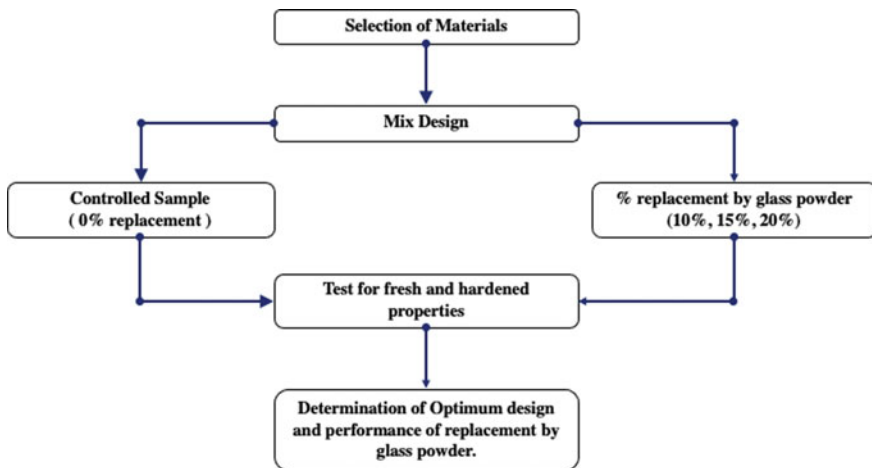


Fig. 1 Methodological procedure adopted for the study

Table 1 Fresh properties of concrete

S. No.	% of replacement by glass powder	Slump value for M20 grade	Compaction factor for M20 grade
1	0	33	0.932
2	10	50	0.948
3	15	55	0.950
4	20	60	0.965

3 Results and Discussions

3.1 Laboratory Experiments for Concrete Ingredients

The Cement's maximum compressive strength thus found as per tested specimen was 56 MPa (as per IS: 12269-2013, minimum-53 MPa), with a 3.14 value of Specific Gravity. The specific gravity of the coarse aggregates is 2.60 and 1% is noted as water absorption. The mix designing is performed as per the IS codal provisions IS 10262: 2019; with the value obtained 452 kg/m³, 1114 kg/m³ and 0.3 for cement, coarse aggregates, and W/C ratio respectively.

3.2 Porous Concrete (Fresh Properties Test) Under Consideration

The experimental results obtained are summarized in Table 1.

3.3 Porous Concrete (Hardened Properties Test) Under Consideration

3.3.1 Compressive Strength

The results deduced below where the valuations averaged from six specimens each cured and undergone testing at 7 and 28 days (Fig. 2; Table 2).

3.3.2 Split Tensile Strength

The results deduced below where the valuations averaged from six specimens each cured and undergone testing at 7 and 28 days (Fig. 3; Table 3).

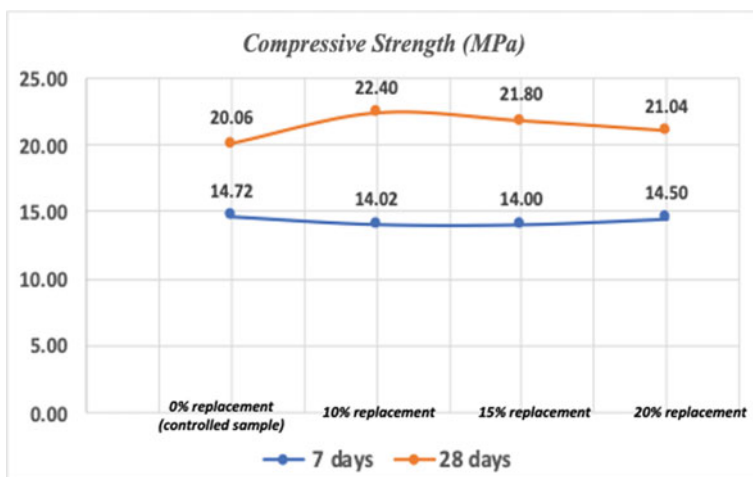


Fig. 2 At 7 and 28 days (Compressive strength test)

Table 2 Compressive strength

Age of concrete	At 0% (Controlled sample)	At 10%	At 15%	At 20%
7 days	14.72	14.02	14.0	14.50
28 days	20.06	22.40	21.80	21.04

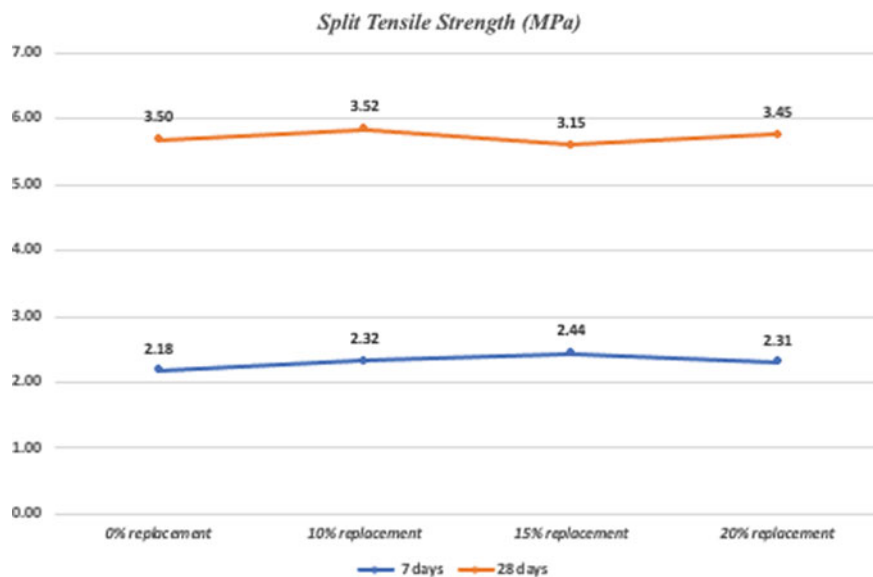


Fig. 3 At 7 and 28 days (Split tensile test)

Table 3 Split tensile strength

Age of concrete	At 0%	At 10%	At 15%	At 20%
7 days	2.18	2.32	2.44	2.31
28 days	3.50	3.52	3.15	3.45

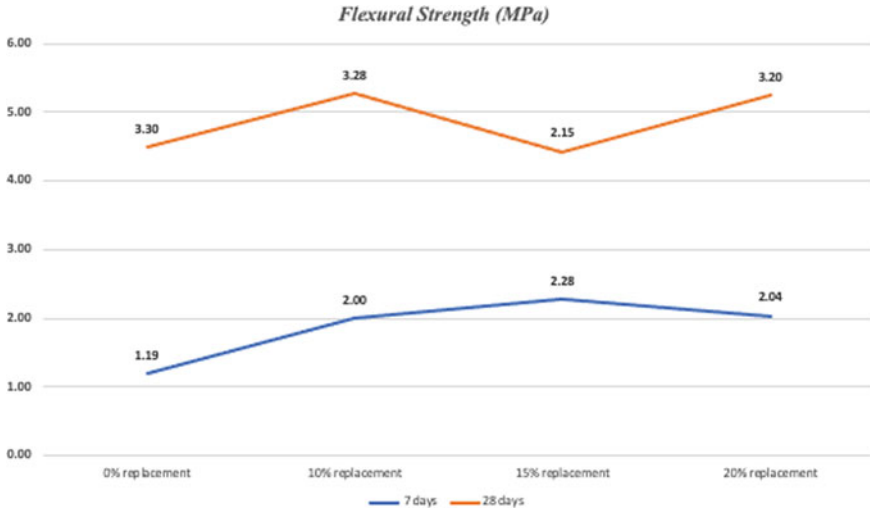


Fig. 4 At 7 and 28 days (Flexural strength test)

Table 4 Flexural strength

Age of concrete	At 0%	At 10%	At 15%	At 20%
7 days	1.19	2.0	2.28	2.04
28 days	3.30	3.28	2.15	3.20

3.3.3 Flexural Strength

The results deduced below where the valuations averaged from six specimens each cured and undergone testing at 7 and 28 days (Fig. 4; Table 4).

4 Conclusion

Based on this study, glass powder usage as a substitute for cement in the mix of concrete effects the overall concrete’s strength. With the usage of glass powder in variation of 0%, 10%, 15% and 20%, there was an increase in the concrete’s strength aged at 7 days and 28 days. Obtained results are concluded as below:

- (a) Compressive strength was found to be maximum at 10% replacement with a value of 22.40 MPa, when compared to its partial replacement with 0%, 10%, 15% and 20% cement by glass powder at 28 days with consideration of 7 days result found from the test specified, wherein the strength decreased as we increased the percentage from 10% onwards of partial replacement by glass powder.
- (b) Tensile Strength was attained to be maxed at 10% replacement with a value of 3.52 MPa, when compared to its partial replacement with 0%, 10%, 15% and 20% cement by glass powder at 28 days with consideration of 7 days result found from the test specified, wherein the strength decreased as we increased the percentage from 10% onwards of partial replacement by glass powder.
- (c) Flexural strength was found to be maximum at 0% replacement with a value of 3.30 MPa, in comparison to partially replaced with 0%, 10%, 15% and 20% cement by glass powder at 28 days with consideration of 7 days result found from the test specified, wherein the strength decreased as we increased the percentage of partial replacement by glass powder.

Hence, it can be concluded that the with regards to maximum values from strength of compressive and tensile tests of porous concrete partially replaced with glass powder, the optimum design percentage thus concluded is 10% as compared to 0%, 10%, 15% and 20%. Though, the flexural strength was found to be decreased with percentage increment of glass powder.

References

1. Andrew RM (2018) Global CO₂ emissions from cement production. *Earth Syst Data Sci* 10
2. Dixit A, Hooda Y (2019) Experimental evaluation on compressive and tensile behavior of concrete utilising GGBS, fly ash and recycled aggregates. *Int J Eng Adv Technol (IJEAT)* 8(5):2249–8958
3. Yao A, Ding H, Zhang X, Hu Z, Hao R, Yang T (2018) Optimum design and performance of porous concrete for heavy-load traffic pavement in cold and heavy rainfall region of NE China. *Adv Mater Sci Eng* 2018
4. Hooda Y, Bansal S, Gupta A (2022) Parametric strength of sustainable concrete using fly ash, GGBS and recycled aggregates as per Taguchi's approach. In: Gupta AK, Shukla SK, Azamathulla H (eds) *Advances in construction materials and sustainable environment. Lecture notes in civil engineering*, vol 196. Springer, Singapore. http://doi.org/10.1007/978-981-16-6557-8_40
5. Vaishnav K, Lazarus GP, Bansal S, Hooda Y (2022) Review on thermal energy efficiency using gypsum integrated phase change materials in buildings. In: Gupta AK, Shukla SK, Azamathulla H (eds) *Advances in construction materials and sustainable environment. Lecture notes in civil engineering*, vol 196. Springer, Singapore. http://doi.org/10.1007/978-981-16-6557-8_24
6. Sukh AV, Hooda Y, Singh HD (2023) Relative experimental evaluation of properties of concrete with addition of super—plasticizers. *Mater Today Proc.* ISSN 2214-7853, <http://doi.org/10.1016/j.matpr.2023.03.507>
7. Drake J (2014) Winter effluent quality from partial-infiltration permeable pavement systems. *J Environ Eng* 140(11)
8. Muda MM, Legese AM, Urgessa G, Boja T (2023) Strength, porosity and permeability properties of porous concrete made from recycled concrete aggregates. *Constr Mater* 3(1)

9. Turkey FB, Beddu SB, Ahmed AN, Al-Hubboubi SK (2022) Effect of high temperatures on the properties of lightweight geopolymer concrete based fly ash and glass powder mixtures. *Case Stud Constr Mater* 17
10. Junior JKQ, Kankam CK, Dzivenu CK, Akortia VK (2022) Strength characteristics of concrete partially replaced with glass powder and palm kernel shells. *J Eng Res Rep* 23(12)
11. Harshith SD, Ahmad E (2020) Experimental investigation of porous concrete for concrete pavement. *Int J Eng Tech Res* 9
12. Shashi Kumar VN (2021) Study on properties of concrete with boron glass powder as cement. *Int Res J Modernization Eng Technol Sci* 3
13. Najaf E, Abbasi H (2022) Using recycled concrete powder, waste glass powder, and plastic powder to improve the mechanical properties of compacted concrete: cement elimination approach. *Adv Civ Eng* 2022
14. IS 12269: 2013, Ordinary Portland cement, 53 grade—specifications

Exploring the Perceptions of 3D Printing Through the Technology Acceptance Model (TAM) Lens



Mayur Naik , Rahul Sheshadri , Tejesh Varma, Divya Jyoti, Deepansh Ade, Vaibhav Bhalme, and Vijayeta Malla 

Abstract The existing situation and prospects of implementing digital technologies in construction are the subject of this study. The central notion of digital technology is the transition from “paper-based” technologies to computer-aided design tools and then to information modelling of construction things. Digital technologies are studied in experimental and field investigations, the interaction with mathematical modelling is demonstrated, and the current challenges raised in the area are highlighted. 3D printing (3DP) is a civil engineering invention that adds to automation and provides design, greenness and efficiency benefits. The extant studies lack focus on understanding the perceptions of the use of 3D printing in the AEC industry. The current research explores the perceptions of construction stakeholders through the theoretical lens of the technology acceptance model (TAM). The study adopts a qualitative approach through semi-structured interviews of practitioners possessing 3D printed construction. Subsequently, the transcribed interviews are coded and thematically analyzed using a text-mining tool. The findings include the themes generated from the TAM framework that serves as a conceptual model for prospective practitioners who aim to develop careers in the 3D printing domain.

Keywords Digital construction · 3D printing · Technology acceptance model (TAM) · Smart materials

1 Introduction

Computerized development is using advanced devices to work on the conveyance and activity of the constructed climate. The advantage of computers in virtual space construction leads to the expansion of imaginative space and three-dimensional shaping to express construction creativity in digital construction, which is based on conventional construction. Construction digitalization is a complicated topic

M. Naik · R. Sheshadri · T. Varma · D. Jyoti · D. Ade · V. Bhalme · V. Malla (✉)
NICMAR, Hyderabad, India
e-mail: vijayeta.malla@gmail.com

that entails many digital technologies being used to solve numerous issues in the construction sector. 3D printing technology is one of the latest such digitalization tools.

In the automated additive manufacturing technique known as three-dimensional printing (3DP), successive layers of material are applied to create three-dimensional objects. Using CAD software, a three-dimensional model is created to start the procedure. The model is then sent to the 3D printer as a Stereo lithography Language (STL) file for saving. The use of 3D printing technology will speed up production while also lowering expenses. Nowadays, mass customization and assembly of any kind of open-source design are increasingly being done using 3D printing technology.

One of the models that is used the most frequently and help predict how new information resources will be used is the technology acceptance model (TAM). According to the TAM, when clients are given new technology, various factors influence their decision about how and when to employ it. A theory that coordinates with information systems is called the Technological Acceptance Model (TAM). This model was created by Fred Davis in his 1989 article, which was widely read. This model is currently one of the most frequently mentioned in the development of scattering space. For the past twenty years, client appropriateness of development has been an essential subject of assessment. Yet many models expect structure dispersing, the Technology Acceptance model is the one species that revolves solely around information systems.

2 Literature Review

Advanced development utilizes innovation and computerized apparatuses in the development processes, similar to configuration, an amalgamation of materials, and undertaking arranging. Any kind of advanced programming or innovation utilized as a component of a development interaction can be viewed as computerized development [1]. 3-D printing is an additive manufacturing (AM) technique for fabricating a wide range of structures and complex geometries from three-dimensional (3D) model data. The process consists of printing successive layers of materials that are formed on top of each other [2]. Recent developments also allow for 4D printing. 4D printing permits the production of the expected shape with controllable power by consolidating the size and the time. Late forward leaps in an astute plan, novel printers, transformation procedures, and numerical displaying have significantly improved the plausibility of 4D printing [3]. The development business is encountering mechanical changes from Industrial 4.0 that will meaningfully alter the manner in which undertakings are carried out, driven by advances, for example, construction, BIM, computerized and automated machines, remote sensors, and 3D printing. Opposing advancement is quite difficult for the business. There are a couple of instances of eagerness to involve the force of new advancements with regard to development [4]. 3D printing advancement has so far offered unparalleled chances for new creations in various domains [5]. In the aerospace industry, 3D printing advancement might

potentially make numerically advanced and perplexing lightweight parts that can reduce the necessity for energy and resources. In the auto business, the 3D Printing strategy has done wonders to bring new light, considering more straightforward and additional confusing plans in a faster time. In the development business, 3D printing innovation can be utilized to print a whole structure or to make building parts. The development of the portrayal of the Building Knowledge of the practical and actual elements can share data and information about the 3D design. It can shape a dependable wellspring of choice throughout its life cycle, from origination to destruction to building or developing a structure [5].

Technology Acceptance Model (TAM) theorizes the usage behavior of computer technology [6]. The TAM was adopted from another popular theory called the theory of reasoned action (TRA) from the field of social psychology, which explains a person's behavior through their intentions [7].

The most notable application of the Technology Acceptance Model (TAM) is the prediction and explanation of end-user reactions [8].

The fundamental designs of TAM are perceived value—"how much an individual accepts that carrying out a specific program can work on their exhibition of work", perceived usability—"how much an individual accepts that applying a specific program would be easy", behavioral goal to utilize—"the reason for clients to involve the framework later on", actual framework use—"genuine utilization of framework clients in performing undertakings" [6].

3 Research Methodology

As the research study entails novel domain, a qualitative approach suits appropriate to understand the in-depth analysis. Two objectives were proposed in this study. Initial first objective included content analysis of per-reviewed journal articles, and online firm specific documents, and reports available in open media. The second objective is to obtain thematic analysis through semi-structured interviews. Analysis of the literature review on smart materials for 3D printing is covered in objective one, along with the framing of hypotheses based on TAM theory (technology acceptance model). The second goal includes qualitative research using semi-structured interview questions, thematic analysis of the results, and developing themes, concepts, and connections to the data gathered (Fig. 1).

4 Data Collection

To understand the Perception of 3D Printing technology in the Construction Industry, Semi Structured interviews are conducted. Invitations to Six Construction and Research based expertise were sent sufficing the criteria: (1) Expertise who has a fair knowledge of 3D Printing and directly or indirectly has been a part of 3D printing

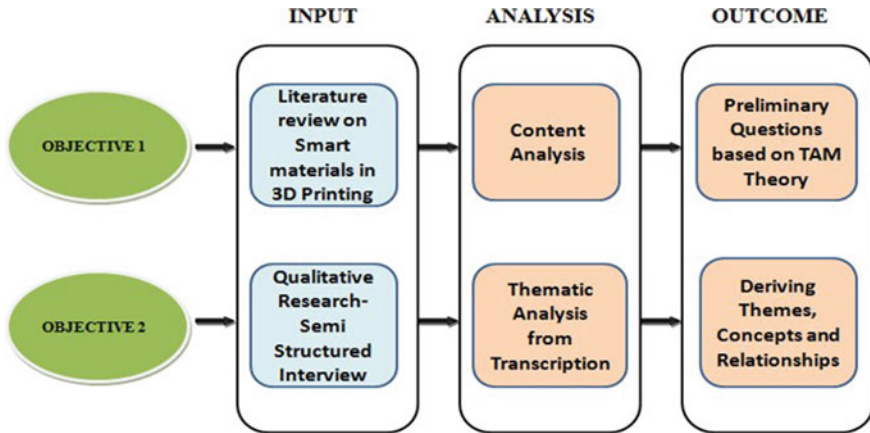


Fig. 1 Research flow

work, (2) Expertise with more than 4 years of experience and who have worked in departments of Automotive, Robotics, etc. Four out of seven agreed to the interview, few of which were telephonic, and also, few responses were obtained via mail the following were the interview questions.

1. What are your views on 3D printing technology in the industry?
2. In the Indian construction industry, will employees and labor accept this modern technology over the traditional method of construction?
3. What was their behavior during the training period of employees in learning 3-D printing technology?
4. What were the barriers to adopting this technology, and how much did these barriers affect the whole process?
5. What were their perceptions of using this technology over traditional on the basis of ease of use, productivity, quality, and efficiency?
6. How is 3D printing going to help in Indian construction economy?
7. How will smart materials such as 3D printing material change the various industries (construction, medical, aviation, etc.) as an innovative approach?
8. What other new innovations or modifications are possible in 3D printing technology?
9. What was the outcome satisfaction, and does this satisfaction encourage an individual to use this technology?

5 Data Analysis

The interview responses to the questions, which were converted to the transcript, were studied, and the important and impactful words were highlighted in every question for all the interviews obtained the same were imported to Word and a word Cloud

Fig. 2 Word cloud of outlook of 3D printing from the practitioners



was created for every question as performed thematic analysis [9, 10] as shown in the figure below.

The first question concentrated on knowing how well all the interviewees/participants were familiar with the 3D Printing concept, and it was observed that the common responses included: how 3D printing works, how helpful it is in cost reduction with the effective outcome, awareness about labor shortage and the innovations are possible with this technology.

Second Question was about the acceptance of technology in the Indian Construction Industry, the word cloud of which is shown in Fig. 2, that explains technology plays a dynamic role of 3D construction, and mass construction works which is inevitable thing that will be accepted later or now.

The Third question response included the behavior towards acceptance of this technology in the industry, which explained how heavy training it usually requires for the team to understand the operation due to which it is not complex but different from usual automation, though a number of labors required is less in 3D printing execution. The requirement of skilled labor or workforce requirement is of greater importance (as shown in Fig. 3), However, barriers such as design constraint, material availability, and awareness were specified by the participants.

The acceptance of this technology explained that there are barriers to overcome, so what are these barriers and how much does it affect the whole process was interviewed the Fourth question. The common barriers are availability, area or the space requirement, wind/temperature influence, automation, and special rebar. As the construction process itself is unique, the exposure of the concrete surface is open to the environment, unlike conventional concrete pouring, which is protected by formwork apart from this, the acceptance of this work by the consumers is of concern too (as shown in Fig. 4).

Fig. 3 Word cloud of the determinants to accept 3D printing



Fig. 4 Word cloud of behavior towards acceptance of 3D printing



The stakeholder’s acceptance, employees, and labor getting used to the technology became a bigger task, overshadowing the advantage of 3D printing. The productivity and efficiency of this were not praised much compared to the conventional type by the industry persons (as shown in Fig. 5),

Thoughts on how the use of this technology be helpful for the Indian Economy were interviewed in sixth question. This would help in population migration, rapid urbanization and affordable housing for all concept can be benefited as the required time of construction is very less and also this can result into less wastage lowering the labour and Resource cost (as shown in Fig. 6).

Fig. 5 Word cloud of barriers to adoption of 3D printing



Fig. 6 Word cloud of perceived advantage of 3D printing



How the usage of smart materials makes a change in a different field, the response to this question contained: the use of nanomaterials influencing the elasticity of the structure, increasing its durability, direct use of carbon fibre in automotive reducing the weight of the material and resulting in better mileage and efficiency—superhydrophobic material in aircraft resulting lesser fuel consumption. So, the overview of this was that using Smart materials in 3D Printing could result in flexibility, strength, and durability. Eradication of the design constraint will give more room for innovation (Fig. 7).

Fig. 7 Word cloud of benefits to national economy



6 Conclusion

From the interviews conducted with industry practitioners, it is understood that although 3D printing is applicable and implemented in various sectors such as automation, medical, aerospace, aviation, etc. Yet, there is still a need to investigate and educate people about 3D printing in the building industry. The study developed themes from a qualitative approach themes using technology acceptance model (TAM) such as “practitioner’s purview of 3D printing” (that novel approaches such as 3D printing will propel innovation in the technophobic industry, hence emphasized technology as the lever to 3D printing adoption), “technological acceptance” (owing to faster completion of projects, one of the approaches deemed to be 3D printing that enables mass construction work in less duration), “behavioral” (vigorous training of workforce, as it is a niche area), barriers (the aspects such as availability, area or the space requirement, wind/temperature influence, automation, and special rebar), perceived advantage from practitioners’ points of view (increased productivity and quality outcomes owing to lessened human intervention), contribution to national economy (construction of affordable housing at lesser duration and cost). Nevertheless, this study has limitations wherein the results cannot be generalized as more sampling population of the interviews needed to be considered and another issue is the subjectivity induced outcomes from the interview participants. Further research can be extended by considering more interviews and a longitudinal case-study to bolster the results from qualitative approach.

References

1. Ngo TD, Kashani A, Imbalzano G, Nguyen KT, Hui D (2018) Additive manufacturing (3D printing): a review of materials, methods, applications and challenges. *Compos B Eng* 143:172–196
2. Gokhare VG, Raut DN, Shinde DK (2017) A review paper on 3D-printing aspects and various processes used in the 3D-printing. *Int J Eng Res Technol* 6(06):953–958
3. Zhang Z, Demir KG, Gu GX (2019) Developments in 4D-printing: a review on current smart materials, technologies and applications. *Int J Nano Mater* 53(19):68–82
4. Olsson NO, Arica E, Woods R, Madrid JA (2021) Industry 4.0 in a project context: introducing 3D printing in construction projects. *Proj Leadersh Soc* 2:1–10
5. Shahrubudin N, Koshy P, Alipal J, Kadir MHA, Lee TC (2020) Challenges of 3D printing technology for manufacturing biomedical products: a case study of Malaysian manufacturing firms. *Heliyon* 6(4):e03734
6. Venkatesh V, Davis FD (2000) A theoretical extension of the technology acceptance model: four longitudinal field studies. *Manag Sci* 46(2):186–204
7. Rauniar R, Rawski G, Yang J, Johnson B (2014) Technology acceptance model (TAM) and social media usage: an empirical study on Facebook. *J Enterp Inf Manag* 27(1):6–30
8. Holden RJ, Karsh BT (2010) The technology acceptance model: its past and its future in health care. *J Biomed Inform* 43(1):159–172
9. Malla V, Jagannathan M, Kumar Delhi VS (2022) Identification of BIM dimension-specific contract clauses in EPC turnkey projects. *J Leg Aff Disput Resolut Eng Constr* 14(1):04521040
10. Malla V, Jagannathan M, Delhi VSK, Nair BS (2022) BIM-specific prequalification criteria in construction projects: exploring the nature and timeline of their inclusion. *J Legal Aff Dispute Resolut Eng Constr* 14(2):04522008

Ductility Enhancement by Incorporating Slits on Shear Resisting Frame with Haunched Beams



Sarath Paul and S. P. Deepu

Abstract Earthquake are one of the most devastating disasters the world is facing from decades and constant researches are conducted for providing various solutions to improve the seismic performance by using the idea of ductility and stiffness in appropriate manner. Ductility enhancement is one of the key principles of seismic design. Various techniques are introduced to improve the ductile behaviour of the buildings in past decades. Reduced web sections are one of the older concepts that follows the idea of predetermined failure at determined weak regions. Incorporating slits allows the weakening of slits thus utilizing plastic strain capacity of material which results in dissipating energy and improving ductile ability of structures. This study focuses on improving the ductile behaviour and energy dissipation characteristics of shear resisting frame with haunched beams by using slits at the shear link. Shear resisting frame (SRF) is an innovative concept where failure occurs by shear yielding. SRF is suitable for low span to depth ratio's where moment resisting frames can't be used. SRF with haunched beam is used in this study to prevent sudden transition from prismatic beam to link and thus avoiding sudden discontinuity. The parametric study was conducted on the link separately to avoid the computational time and the link with better performance was attached to the frame to analyze the seismic behaviour of the shear resisting frame with haunched beams (SRFH). Effect of aspect ratio of slits, orientation and number of slits on improving the ductile characteristics of the frame were studied. Slits improved the ductile behaviour of the frame by 75% and energy dissipation increased by more than 100%. Rotation capacity of the links were also improved thus improving the over all seismic performance of the frame.

Keywords Shear resisting frame with haunched beams (SRFH) · Slits · Energy dissipation · Ductility factor

S. Paul · S. P. Deepu (✉)

Department of Civil Engineering, Government College of Engineering Kannur, Kannur, India

e-mail: deepusp@gcek.ac.in

1 Introduction

For the past several decades the impact of earthquake is immense including loss of life and property in countless numbers. Several techniques have been evolving and immense research is being conducted in making buildings seismic resistant. Lateral load resisting systems are used for improving the seismic behaviour of structures by enhancing energy dissipation capability and ductility characteristics. Eccentrically Braced frames and Moment Resisting Frames are the most effective lateral load resisting frames known so far. While comparing with shear resisting frame eccentrically braced frame undergoes more rotational tendency of link beam and much higher displacement of link and offers architectural constraints due to the bracing provided which creates space limitations [1]. The main limitation offered by moment resisting frame is that it can't be used for span/depth ratio $< 5-7$, according to AISC Seismic provisions [2]. For short spans flexural hinge formation does not occur properly and lead to beam column joint failure. In such scenarios shear resisting frame proves its advantage [1].

Payam Ashtari et al., conducted a study on T Resisting Frames with both horizontal plate girders and prismatic beams [3, 4]. It was found that shear yielding of haunched frame results in higher ductility and more energy dissipation characteristics. Ductility factor also improved when haunched girders were used in T resisting frames. Mohammad Rahnemoun et al., introduced a shear resisting frame with haunched beam with a shear fuse at center so that shear fuse act as a suiciding agent [5]. The study shows the effective seismic performance of SRFH than moment resisting frame and eccentrically braced frame SRFH having better base shear, ductility and overall seismic performance for the same span to depth ratio. Shear resisting frame is advantageous for low span conditions where moment resisting frame can't be executed. For the same drift ratio SRF has better lateral stiffness and better ductility compared to all conventional lateral load resisting frames [5]. Seyed Saeed Askariani et al. conducted a study on the application of slit link beams in eccentrically braced frames. It was found out that slit link beam improved the energy dissipation almost double the amount when compared to beams without slits [6]. The failure point was shifted to the slit openings at the slit ends. Using slits also reduces the material amount and also improves the rotation capacity of the links [7]. This study focusses on improving the ductile behaviour and energy dissipation by incorporating slits on the shear link of the SRFH to achieve better seismic performance.

2 Numerical Modelling

A numerical model was developed using the commercial finite element software ANSYS 2022 R2 to simulate the shear resisting frame subjected to cyclic loading conditions. As shear link is the main component that acts as an energy dissipation device two numerical models were simulated, one a shear resisting frame with

Table 1 Material properties of SRFH and shear link

Material properties	Shear resisting frame with haunched beam	Shear link
Yield stress	245 MPa	291 MPa
Ultimate stress	565 MPa	538.3 MPa
Elongation	0.27	0.425

haunched beam and second the shear link alone subjected to cyclic loading conditions to ease the analysis time and reduce the computational time. The shear link with better seismic performance was finally attached to the frame.

2.1 Material Modelling

Material properties were obtained from tensile coupon test conducted by Mohammad Rahnemoun et al. on shear resisting frame with haunched beam [5]. Table 1 shows stress strain properties of shear resisting frame and shear link. The material properties of the shear link were referred from the experimental test conducted by Jinjie Men et al. on multi-segment replaceable shear link [8].

2.2 Finite Element Modelling

Finite element model was developed from the experimental setup [5] conducted by Mohammad Rahnemoun et al. on SRFH. Figure 1a show the finite element model of the shear resisting frame developed in ANSYS 2022 R2 along with the boundary conditions. The dimensions of the specimen are listed in Table 2. 20 noded, Solid 181 element was used for modelling. Multilinear Kinematic Hardening parameter was used in ANSYS for material calibration. Mesh size of 20 mm was used for the shear link and 50 mm for the frame, so that more accurate results could be obtained on the link itself as shown in Fig. 1b. Cyclic loading conditions were provided by push and pull action according to AISC341-16 cyclic qualification controls consisting of 8 amplitudes applied at the top flange level of the beam represented by G and F. Bottom of the frame was pinned at both ends as shown as A and B and to prevent out of plane deformation lateral buckling was restrained along the beam length denoted by E, D, C in Fig. 1a.

As the parametric study was conducted on the shear link, FEM model was developed to validate the shear link from the experimental setup conducted by Jinjie Men et al. on multi-segment replaceable fuse [8]. Figure 2 shows the meshed diagram of the shear link with a mesh size of 25 mm selected for analysis after convergence

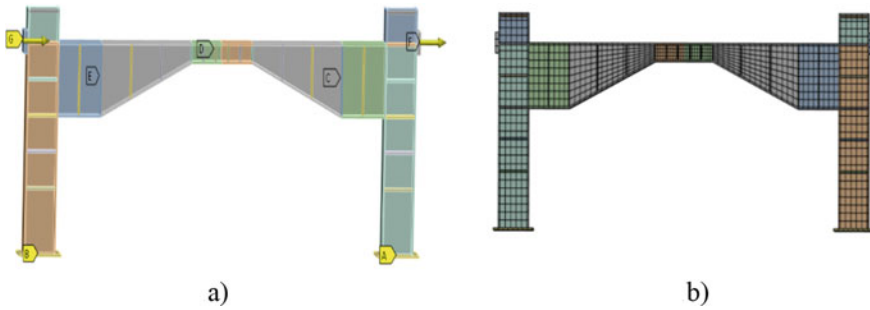


Fig. 1 a Finite element model of SRFH, b meshed model of SRFH

Table 2 Dimensions of the shear resisting frame with haunched beams

Geometrical parameters	Dimensions (mm)
Length of prismatic beam	300
Length of haunched beam	630
Length of shear link	420
<i>Shear link</i>	
Thickness of web	4
Thickness of flange	10
Depth of shear link	90
Width of flange	75
<i>Prismatic beam</i>	
Thickness of web	5
Depth of prismatic beam	320
<i>Stiffeners</i>	
Spacing at shear link	84
Spacing of haunched beam	150
Spacing of prismatic beam	300

study under monotonic loading. Multilinear Kinematic Hardening was used as hardening parameter for analysis purposes. Loading was applied as push/pull along the end plates in vertical direction.

3 Validation

Two validations were done, one for SRFH and another for shear link as a single member in order to conduct the parametric study. SRFH was validated for the shear force versus link rotation curve from the experimental results conducted by Mohammad Rahnemoun et al. on shear resisting frame with haunched beam [5]. The

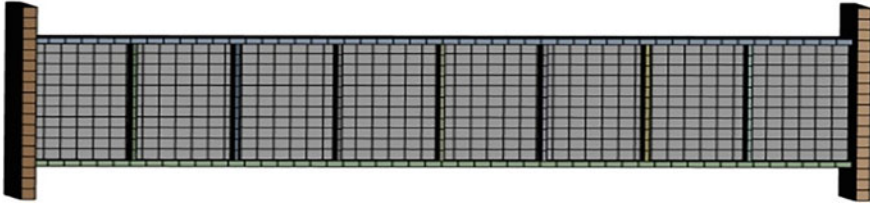


Fig. 2 Meshed model of shear link with end plates

shear link curve for shear force versus link rotation was validated from the experimental results conducted by Jinjie Men et al. on multi-segment replaceable shear link [8]. Figure 3a shows the validation curve for SRFH and shear link. The result obtained from numerical study showed a close match with experimental one differing by only 4% for both shear link and SRFH. Figure 3b shows the equivalent plastic strain diagram of both models where the SRFH shows the link failure thus validating the concept of link and for shear link failure was observed at the link ends.

4 Parametric Study

The validated models are further extended for detailed parametric analysis. The first parameter considered was the effect of orientation of slits either being horizontal or vertical. The width of slits was fixed at 5 mm as per [6] which can be from 4 to 8 mm. The second parameter considered was the aspect ratio of slits, namely the height to width ratio of slits. The third parameter considered was the effect of number of slits by observing the seismic performance of the link by increasing the number of links. Finally, the link with the stable seismic performance was attached to the frame to find out the performance of shear resisting frame with the effect of slits.

4.1 Effect of Orientation of Slits

The size of the slits to find out the effect of orientation of slits was taken as 60×5 mm in both horizontal and vertical direction. Horizontal slits showed higher energy dissipation and ductile behaviour than vertical slits. Although horizontal slits had better seismic performance than the vertical ones, pinching behaviour was observed but considering the high variation in energy dissipation horizontal slits performed better than the vertical ones. Figure 3 shows the failure behaviour of both horizontal and vertical slits. Horizontal slits failed at a rotation of 0.33 rad, while the vertical ones capable to take up to 0.235 rad. Table 2 shows the ductility and energy dissipation characteristics for both type of slits. Figure 4 shows the force envelope curve for orientation of slits (Table 3 and Fig. 5).

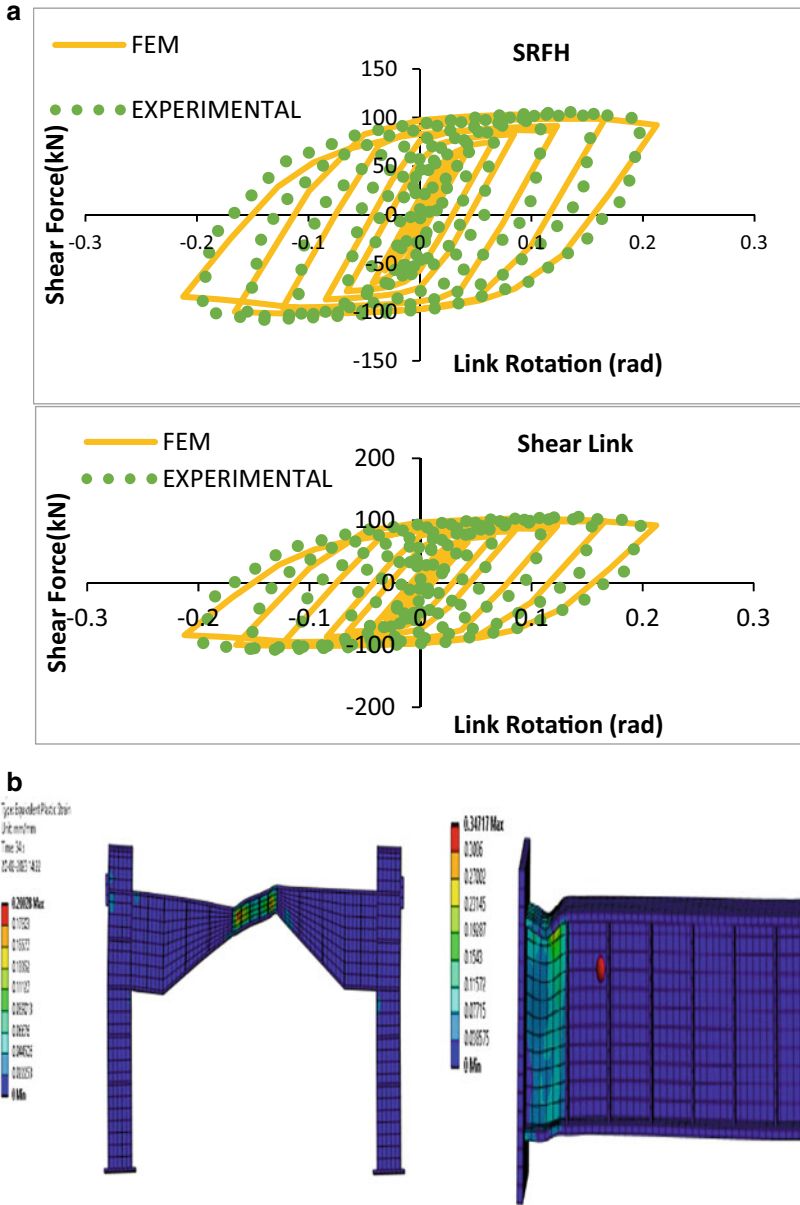


Fig. 3 **a** Validation diagrams of SRFH and shear link, **b** equivalent plastic strain diagram of SRFH and shear link

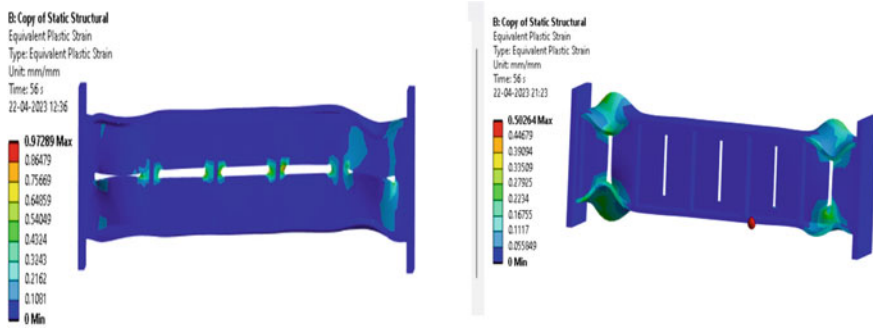
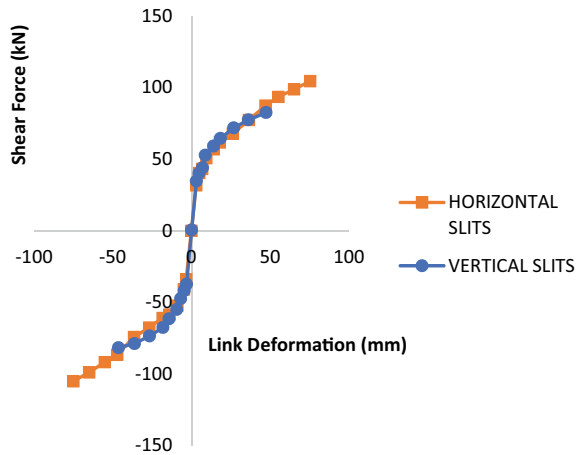


Fig. 4 Failure diagram when horizontal and vertical slits were provided

Table 3 Seismic behaviour of vertical and horizontal slits

	Horizontal slits	Vertical slits
Ultimate displacement	75.09 mm	55.404 mm
Ductility factor	12.01	11.0366
Energy dissipated	127.32 kJ	61.32 kJ

Fig. 5 Force envelope curve with orientation of slits



4.2 Aspect Ratio of Slits

Variation in seismic behaviour for height/width ratio of slit was studied. The width of slit was fixed at 5 mm. The length of the slit was varied from 20 to 60 mm. No significant changes were observed for aspect ratio up to 10. As the length of the slit was varied from 50 to 70 mm significant ductile behaviour and improvement in link rotation was observed. Energy dissipation was also improved significantly almost double the condition without slits. Ultimate displacement also increased as

Fig. 6 Cumulative energy dissipation with aspect ratio of slits

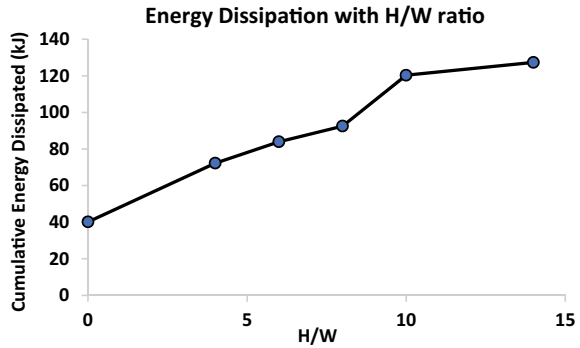


Table 4 Comparison of seismic performance of link with slit length 60 mm

	No slit	Slit length 60 mm
Plastic rotation angle (rad)	0.143	0.319
Ultimate displacement	35.94 mm	75.23 mm
Ductility factor	8.04	16.86
Energy dissipated	46.58 kJ	124.56 kJ

the aspect ratio of slit increases which shows the improvement in ductile behaviour. Link rotation improved from 0.2 to 0.33 rad which also improves the rotation carrying ability of the links. Figure 6 shows the variation in cumulative energy dissipated with aspect ratio of slits. Energy dissipation increased by 118% when height of the slit reached 60 mm. So, the size of the slit was fixed at 60 × 5 mm (Table 4 and Fig. 7).

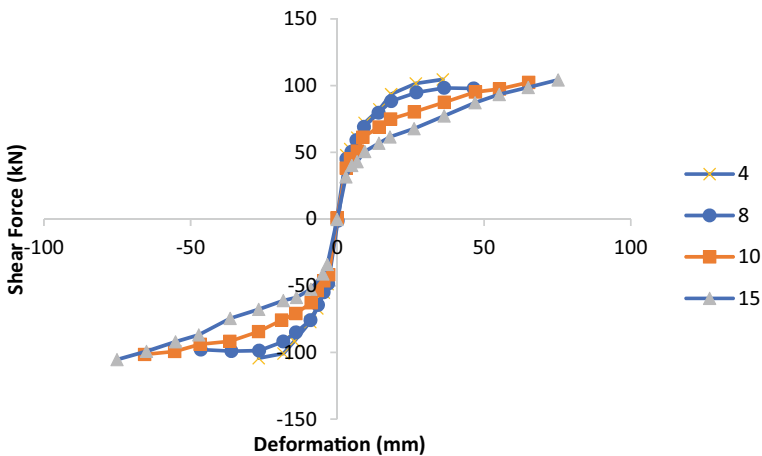
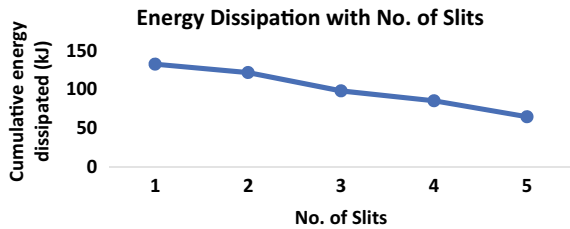


Fig. 7 Force envelope curve for various aspect ratio of slits

Fig. 8 Energy dissipation versus number of slits curve



4.3 Effect of Number of Slits

Figure 8 shows the variation in energy dissipated with number of slits. As the number of slits increased energy dissipation decreased from 2 to 5 numbers. But significant variation is observed when a single slit is observed. When more slits are used shear force capacity is reduced significantly by about 30–40%. Energy dissipated tremendously reduced with increase in slit number. The more the slits ultimate load carrying capacity is reduced and thus stiffness degradation is observed. A single slit can perform well in terms of both stiffness and ductility characteristics. Figure 6 shows the variation in energy dissipated with number of slits. Ductility factor reduced from 16 for single slit to 8.6 for slit number five. Similar behaviour was observed in case of ultimate displacement, number of loops absorbed, plastic rotation capacity and stiffness of the link.

4.4 Influence of Slits on Shear Resisting Frame with Hunched Beams

Slits of size 60 × 5 mm with horizontal orientation was incorporated into the SRFH to study the seismic performance under cyclic loading conditions. Pinching behaviour was found when slits was used, but energy dissipation and ductility was found to be maximum. Link rotation also improved from 0.2 to 0.338 rad when slits were used. Energy dissipation increased by 118% and ductility factor increased by 25% which shows the effect of slit on SRFH on improving the seismic performance of the frames.

	SRFH with slits	SRFH without slits
Yield displacement	5.295 mm	4.103 mm
Ultimate displacement	75.121 mm	46.235 mm
Ductility factor	14.1871	11.268
Energy dissipated	92.36 kJ	42.35 kJ
Link rotation	0.338 rad	0.21 rad

5 Conclusion

This study investigates the effect of slits on shear link on improving the seismic performance of the shear resisting frame. The effect of orientation of slits, aspect ratio of slits and number of slits were studied. The following conclusions can be made,

- (1) Incorporating slits into the SRFH improved the seismic performance by increasing the ductile characteristics and energy dissipation behaviour of the frame.
- (2) The failure region shifted from end of the links to the slit openings where failure initiation was observed
- (3) Ductility factor increased by 25% and ultimate displacement by 63% which significantly shows the effect of slits
- (4) Energy dissipation also improved significantly almost around 110%, when slits were provided. Incorporating slits improved the plastic deformation of links thus utilizing most of the energy.
- (5) The rotation capacity of link also increased from 0.2 to 0.3 rad which shows the increased ductile yielding of the links
- (6) Increasing the number of slits decreases the energy dissipation capacity and unstable seismic behaviour is obtained by decreasing the force carrying ability of the links.
- (7) Link performs well when slits are oriented perpendicular to the loading. Better dissipation characteristics were observed when slits are arranged horizontally.

Thus slits improved the overall behaviour of SRFH and more study regarding the influence of slits can be done extensively to improve the behaviour of the frames.

References

1. Rahnemoun M, Tabrizi SK, Ashtari P (2021) In-depth cyclic and monotonic assessment of innovative shear resisting frames with haunched beams (SRFHBs). *Iran J Sci Technol Trans Civ Eng* 1–25
2. AISC (2016) Seismic provisions for structural steel buildings, AISC/ANSI 341-16. American Institute for Steel Construction (AISC), Chicago
3. Ashtari P, Rahnemoun M, Rasouli I (2020) Experimental and numerical evaluation of innovated T-resisting frames with haunched horizontal plate girders. *Adv Struct Eng* 23(8):1669–1682
4. Ali M (2021) Development of a novel haunched link for eccentrically braced frames. *Eng Struct* 245
5. Rahnemoun M, Tabrizi SK, Ashtari P (2022) Experimental and numerical study on innovated steel shear resisting frame with haunched beams (SRFHBs). *J Constr Steel Res* 197:745–759
6. Askariani SS, Garivani S, Aghakouchak AA (2020) Application of slit link beam in eccentrically braced frames. *J Constr Steel Res* 170
7. Lu J, Yu S, Xia J, Qiao X, Tang Y (2018) Experimental study on the hysteretic behavior of steel plate shear wall with unequal length slits. *J Constr Steel Res* 147:477–487
8. Men J, Xiong L, Wang J, Zhang Q (2022) Experimental and numerical study on the behavior of novel multi-segment replaceable steel shear links. *J Constr Steel Res* 194

BIM Application for the Materials in Roadway Construction



S. S. Kande and B. M. Dawari

Abstract To efficiently manage all parts of roadway construction projects, a comprehensive and integrated strategy is required. Building Information Modelling (BIM) may provide a comprehensive solution for road widening projects. This article focuses on the use of BIM to determine the influence on materials in road widening construction. The research begins with a literature survey on BIM applications in infrastructure projects. The BIM for the roadway widening project is then discussed, which included the development of a 3D model using BIM and the incorporation of Total station data for analysis and visualization. Monitoring road construction by hand is time-consuming and laborious, and sorting and retrieving data from numerous components gets perplexing. So, the primary goal of this project is to investigate the impact on various materials with respect to the cost overrun of road construction. The study concludes with recommendations for future research on the use of BIM for road infrastructure projects, highlighting the importance of these technologies continuous development and use in the industry.

Keywords Building information modelling (BIM) · Roadway construction

S. S. Kande (✉) · B. M. Dawari
Department of Civil Engineering, College of Engineering, Pune 411005, India
e-mail: kandess21.civil@coep.ac.in

B. M. Dawari
e-mail: bmd.civil@coep.ac.in

1 Introduction

With the current demographic situation in India, which has led to significant industrialization, following urbanisation, and changes in human lifestyle, rapid, efficient, and effective urban infrastructure development is necessary to fulfil all the demands of the general populace. Road is the first significant component that connects multiple areas; thus, we need it on top of all other types of infrastructure work that must be constructed. In order to make a country expand and develop, roads contribute to economic development, growth, and social gain. Moreover, roads offer social, health, and educational services as well as job, making the road network crucial in the battle against poverty. The nation's economy depends on the highways that act as its arteries to function. As road transportation accounts for 4.8% of India's GDP, it is the dominant sector by report of Ministry of Statistics and Programme Implementation (MOSPI). The second-largest road network in the world, which transports 90% of India's total passenger traffic and 64.5% of the nation's total freight, is an important aspect of the country's development. In the construction sector, there is a wide variety of such customized software that may be modified to meet any unique personal needs. The usage of this software provides high quality construction while also protecting the contractor from cost and schedule overruns. The use of planning and scheduling software is now limited to projects costing crores of rupees by international corporations; as a result, even though Indian construction projects cost thousands of rupees, appropriate planning and scheduling are not used in most of these projects. The use of building information modelling (BIM) can present a variety of choices for enhancing the materials used in the construction of roads. By exchanging information and models on a shared platform, BIM may help designers, engineers, contractors, and material suppliers collaborate more effectively. As a result, stakeholders can make more informed decisions and optimise material selection, resulting in better road construction materials. BIM makes it possible to see and simulate the building of the highway in 3 dimensions, which may be useful for spotting potential issues and assessing the performance of various materials before they are applied during the construction phase.

Digital technology called as Building Information Modelling (BIM) has been widely used in the building sector [3]. It entails developing and maintaining digital representations of a facility or infrastructure's structural and functioning elements. The design, construction, and operation of buildings and infrastructure projects, like constructing roads, can be made more efficient with the support of BIM. Modelling and managing construction materials can be done with BIM in the context of building roads. Materials including asphalt, concrete, aggregates, and subgrade soils are included in this, as well as their selection, purchase, delivery, and installation. BIM can aid in waste reduction, material utilization optimization, and general project efficiency and sustainability enhancement. BIM can help identify prospective maintenance concerns and lower long-term maintenance costs by assisting in the analysis and visualisation of materials performance over time. The project team, which consists of designers, contractors, owners, and maintenance staff, can share

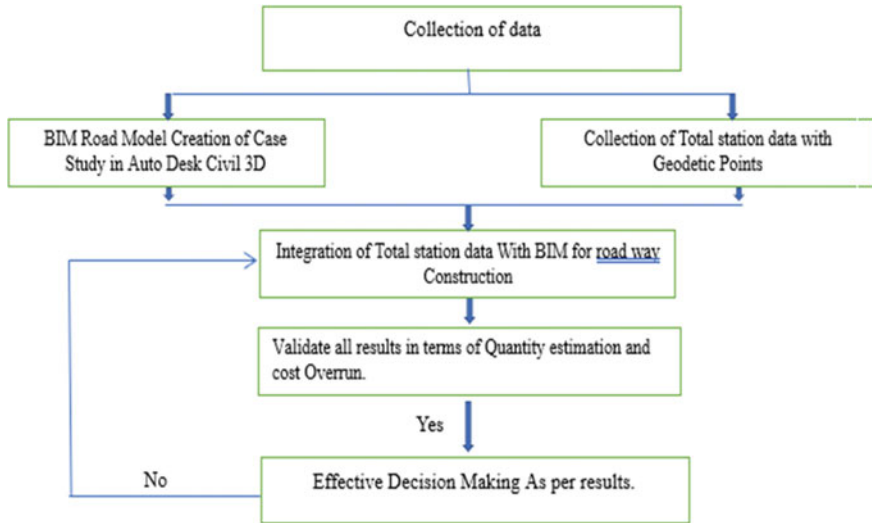


Fig. 1 Application flowchart

this information, enhancing teamwork and project results [2]. BIM is becoming an increasingly valuable technology in the construction industry since it can be used to improve project quality, save costs, and increase sustainability in the context of roadway construction [1]. In order to provide significant reference value for bridge construction management safety, the application of BIM technology in the safety management of highways and bridges is examined in this study in order to effectively improve the quality and efficiency of construction safety management measures.

2 Application Flow

The methodology for using BIM to assess the impact of roadway construction on materials typically involves several steps. These steps can vary depending on the specific project and the objectives of the study, but the following are some common steps (Fig. 1):

3 Case Study

The length of the road project is 14.2 km. The current road is typically one lane wide with earthen shoulders on either side. The horizontal alignment of most of the road along the Manchar to Belhe Roadway length is typically in accordance with IRC

Table 1 Features of road case study

Project details	
Name of project	Improvement of Manchar to Belha SH-112 78/000 km to 92/200 Dist. Pune
Name of client	North Division, Public Works Department, Pune, Maharashtra
Contract value	₹3.4 Crore for chainage of 78/000 km to 83/000 km
The total length of the project road	14.2 km
Avg. daily axial load	10,584 Mega Ton

standards. 14.2 km of total road, of which 5 km from chainage 78/000 km to 83/000 km have been selected for this investigation (Table 1).

3.1 Details of Existing Roads

The majority of the project road's sites have deficient pavement and varied cross-section widths. Moreover, most of the alignment has poor geometrics. There are a few isolated sections of the road in better condition. Several communities are located along the proposed route alignment. Together with large agricultural regions, the road's whole length travels through a mix of built-up and rural areas. On the project route, there are significant built-up regions with notable urban settlements, making it challenging to enlarge the road beyond the already available land width in these places. Major junctions are also present at these places.

	Chainage length	Existing width (meter)	Proposed width (meter)
1	78/00 to 83/00	3.75	5.5
2	83/00 to 84/400	3.75	7.5 (Bituminous pavement)
3	84/400 to 92/200	3.75	7.5 (Earthen embankment)

3.2 Details of Proposed Road

According to traffic demand during the planning phase, a Two-lane undivided carriageway is suggested for the project length. The construction of typical cross-sections considered the needs and conditions of the location. Different cross-sections would be appropriate for various building route segments (Fig. 2 and Table 2).



Fig. 2 Detailed design of flexible pavement

Table 2 Design summary of flexible pavement

Layer	Thickness (in mm)
Sub-grade	500
Granular Sub-Base (GSB) (Grading IV)	200
Wet Mix Macadam (WMM) Grp.1	75
Wet Mix Macadam (WMM) Grp.2	75
Bituminous Macadam (BM)	50
Bituminous Concrete (BC)	30

4 Data Collection with Analysis

1. **Survey Point data collection from site:** With the Autodesk Civil 3D 2022 software, a 3D model must be developed before BIM can be used for that data from the site for the survey must be collected. A total station, a surveying tool used to gather geodetic data, can be used to collect survey points like easting, northing and Elevation which describe the geographical Cartesian coordinates of each point from a location.
2. **BIM model of Case Study:** This application utilises Autodesk Civil 3D 2022 as a platform to create a BIM model. Making informed choices about cut and fill amount estimation and different quantities for road widening can benefit from this information. To analyse the real influence on the quantity of road building, it is necessary to acquire the various cross sections of the road. This needs programme load assembly in short intervals of the road (Fig. 3 and Table 3).

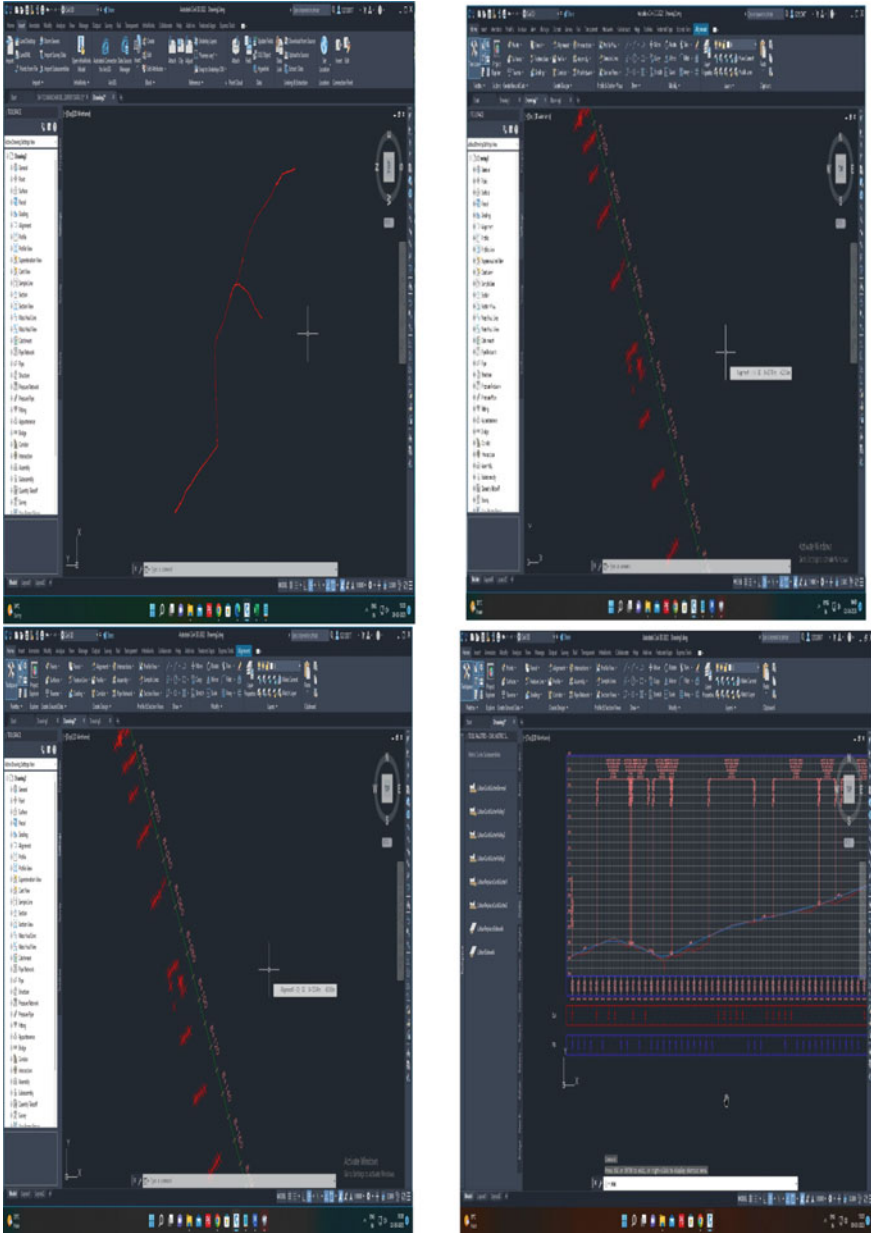


Fig. 3 BIM model creation process of project road

Table 3 A sample data of total station from PWD Dept. Pune

S. No.	Northing	Easting	Elevation
1	2,107,229.892	408,863.916	625.493
2	2,107,229.894	408,863.925	625.492
3	2,107,228.272	408,872.916	625.489
4	2,107,230.982	408,872.967	625.520
5	2,107,230.866	408,873.378	625.493
6	2,107,228.298	408,873.156	625.468
7	2,107,227.683	408,873.077	624.803
8	2,107,231.813	408,864.255	625.539
9	2,107,231.857	408,864.355	625.258
10	2,107,228.036	408,866.836	625.258
11	2,107,229.664	408,865.728	624.892
12	2,107,230.008	408,865.638	624.145
13	2,107,226.088	408,866.316	624.722
14	2,107,229.089	408,869.820	624.812
15	2,107,235.470	408,871.943	624.922
16	2,107,241.047	408,870.198	624.928
17	2,107,235.570	408,870.659	624.948
18	2,107,235.459	408,871.458	624.804
19	2,107,235.144	408,871.433	624.898
20	2,107,235.115	408,863.764	624.928
21	2,107,234.776	408,864.309	625.110
22	2,107,234.975	408,874.546	625.139
23	2,107,234.876	408,872.915	625.234
24	2,107,234.536	408,873.690	625.127
25	2,107,234.393	408,873.766	625.027

5 Conclusion

Urban infrastructure must be built quickly and effectively given the increase in global population and the tendency of people to live in cities. Roads are the most important prerequisite for this design. In order to make a country expand and develop, roads contribute to economic development, growth, and social gain. Moreover, roads offer social, health, and educational services as well as jobs, making the road network crucial in the battle against poverty. The globalisation wave transformed rural regions into towns and small towns into cities. The infrastructure must constantly be upgraded. We require careful planning and prompt execution of the infrastructure improvements to close this gap.

Building information modelling is a practical method for calculating the impact on the quantity of materials required in road development (BIM). By creating a digital model of the path, BIM allows experts in the construction industry to exactly predict the amount of materials needed for the project. Utilizing this information will help the building process run more smoothly, reduce trash, and ultimately save money. BIM can help identify possible conflicts or design flaws so that changes can be made before the building begins. BIM is a powerful instrument that can increase the efficiency, accuracy, and viability of road construction projects. This tool creates BIM models using Autodesk Civil 3D 2022 as a platform. Making informed judgements on cut and fill amount estimation and varied quantities while widening a road might benefit from this information. A designer using a BIM model will benefit from the quantity take-off of previously saved quantities, automatic generation of cross sections for newly constructed assemblies, and drawing of those cross sections.

The total excavation for a finished road, including dressing the section to the required grade camber and side slopes, is 7103 m^3 . The precise quantity required to dig a roadway in any form of earth soil, including sand, gravel, or soft murum, as well as dress the section to the required grade camber and side slopes is 6970 m^3 . This precise value is obtained by utilizing the Auto Desk Civil 3D dynamo program load assembly.

However, Building Information Modelling (BIM) can have a few limitations when calculating the impact on the quantity of materials needed in road building as follows:

- I. **Data Accuracy:** The quantity estimates could be off if the BIM model is missing crucial details about the road design, such as the thickness of the pavement layers or the kind of subgrade material. It could be challenging to combine BIM data with other project information since BIM software and hardware are not always compatible with other software and systems used in the building of roads.
- II. **Updating Software:** It is possible that quantity estimations may not always consider BIM model changes, which might result in differences between the model and the actual materials utilized.
- III. **Budget and timeline restrictions:** For some road construction companies, the expense of BIM hardware and software as well as the training necessary to utilise it successfully can be a major hurdle.

The suggestion for further investigation into the use of BIM for projects involving the construction of road infrastructure and the significance of its ongoing advancement and usage in the sector is one that is valid and has the potential to spur innovation and enhance the effectiveness and sustainability of infrastructure development.

References

1. Jian S (2020) The application of BIM technology in road and bridge construction management. IOP Conf Ser Earth Environ Sci 587(1)
2. Oreto C, Massotti L, Biancardo SA, Veropalumbo R, Viscione N, Russo F (2021) Bim-based pavement management tool for scheduling urban road maintenance. Infrastructures 6(11)
3. Puusaag E, Palmi A (2021) Implementing Building Information Management (BIM) in Estonian transport administration. IOP Conf Ser Mater Sci Eng 1202(1)

Study on the Mechanical Properties of Glass Fibre Reinforced Aerated Concrete with Aluminium Powder as Aerating Agent



Nisanth Manoj, M. Gayathri Devi, and Lavanyaprakash

Abstract The demand for novel technology for manufacturing lightweight concrete has increased in the global construction industry. Therefore, studies that explore alternative lightweight concrete systems for structural applications are urgently needed. The objective of this study is to develop Fibre Reinforced Aerated Concrete (FRAC) by the addition of 1%, 1.5%, 2% and 2.5% of glass fibres. Fibre Reinforced Aerated Concrete is examined under compressive, flexural, and splitting tensile strengths. The foaming agent used is aluminium powder. Aerated Concrete was strengthened by replacing cement with fly ash and the properties of the Aerated Concrete were enhanced by the addition of glass fibres. The addition of glass fibres will enhance the strength of aerated concrete in compression, Tension and in Flexure. The strength of aerated concrete is maximum for 2% of fibres than other fibre percentages. The study mainly focuses on the comparison of the ability of Glass Fibres in increasing the mechanical properties of the Aerated Concrete (AC) compared to the control specimen.

Keywords Fibre reinforced aerated concrete (FRAC) · Foaming agent · Lightweight concrete · Aerated concrete (AC)

1 Introduction

Aerated concrete (AC) is light weight concrete having a density range 400–1600 kg/m³ is developed by the addition of aluminium powder which is the aerating agent [1]. Aerated concrete is made of cementitious mortar enclosing randomly spaced, disconnected air bubbles, with the air often filling up more than half the volume. The gas that forms in the mortar or the foam that is added to the mortar mixture is what causes the air bubbles. These applications make use of cellular concrete's

N. Manoj (✉) · M. Gayathri Devi · Lavanyaprakash
Department of Civil Engineering, Saintgits College of Engineering (Autonomous), Kottayam,
Kerala, India
e-mail: nisanth.sm2123@saintgits.org

lighter weight, lower strength, superior fire protection, or insulating ability [2]. The Lightweight property of aerated concrete blocks makes it easier in handling and transport during the time of construction. The time required for construction will be less as compared to other concrete blocks.

Also, the manufacturing process of aerated concrete generates fewer greenhouse gas emissions compared to traditional concrete, making it a more sustainable option. Cellular concrete's special properties make it a suitable material for sound barriers and firewalls, structural backfill, foundations, building panels, and lightweight base or geotechnical fill. Additional uses for the material's energy-absorbing properties include mine plugs, ballistic range targets, vehicle arresters on airport aprons, and roadway crash barriers [3]. Concrete's weaknesses include significant shrinkage, poor durability, quick microcrack propagation, and weak strength characteristics. Although aerated concrete has a compressive strength of 2 MPa, it must have a compressive strength of at least 10 MPa and a density of at least 1200 kg/m³ to be used for load-bearing purposes. We can utilise fibres as reinforcement to make the aerated concrete stronger. Strength is the main constraint of aerated concrete for using it in load-bearing purposes. The project's major goal is to make aerated concrete stronger by adding glass fibres which boost the material's strength. The fibre type, dosage, aspect ratio, and length are the primary variables that contribute to the strength of concrete. In this project, the percentage of fibre such as 1%, 1.5%, 2% and 2.5% of cement weight is varied [4]. Glass fibre of 12 mm in length is taken for the experiment. Also, we are replacing 20% fly ash instead of cement to increase the strength of aerated concrete.

2 Experimental Details

The investigation make use of OPC 53 for the preparation of the specimens. The detail of the cement is shown in the Table 1.

Aluminium powder is used as the aerating agent which aerated the concrete by forming hydrogen bubbles in contact with water. The Chemical composition of the aluminium powder is given in Table 2.

Fly ash (class F) of 20% is replaced with cement to strengthen the aerated concrete as per Amran et al. (Table 3).

Table 1 Specifications of OPC 53

Tests	Result
Specific gravity	3.07
Standard consistency	32%
Initial setting time	40 min
Final setting time	9 h
Fineness of cement	3%

Table 2 Components of aluminium powder

Components	Minimum percentage (%)
Assay	99.50
Arsenic (As)	0.0005
Lead (Pb)	0.030
Iron (Fe)	0.50

Table 3 Properties of fly ash Class-F

Property	Result
Specific gravity	2.2
Standard consistency	30.5%
Initial setting time	45 min
Fineness of cement	5.6%

Table 4 Properties of glass fibre

Specific gravity	2.68 g/cm ³
Softening point	860c
Modulus of elasticity	72 GPa
Tensile strength	1100–1700 MPa
Length	12 mm
Diameter	14 μm

Glass fibre of 12 mm in length having an aspect ratio of 850 is used for reinforcement. Table 4 shows the properties of glass fibre. A polycarbonic ether-based superplasticizer is applied for the fabrication of a flexible and sufficiently flowable mixture. 4% of superplasticizer is used as per Amran et al. to prepare the mix of uniform flow. The fine aggregate used is of zone II is an important factor in the mix proportion (Table 5). The details of the trial mixes are shown in Table 4.

Table 5 Properties of fine aggregate

Tests	Results
Specific gravity	2.52
Water absorption	0.91%
Grading zone	Zone II
Tests	Results
Specific gravity	2.52

2.1 Flexural Tensile Strength Test

Flexural Strength Test was conducted for Fibre Reinforced Aerated concrete specimens and control specimens to determine the Modulus of Rupture as per IS 516-1959. Figure 1a shows the test setup for the flexural test. A concrete mix of desired strength was prepared and three prisms of size 500 mm × 100 mm × 100 mm were cast. The specimens were cured for 28 days and tested immediately after removing from the water. The load was applied until the specimens failed. Flexural Tensile Strength or Modulus of Rupture was calculated using Eq. (1)

where, b = width

$$\text{Flexural Tensile Strength} = \frac{PL}{bd^2} \quad (1)$$

d depth

L length of the span

P maximum load applied to the specimen.

2.2 Split Tensile Strength Test

A Split tensile strength test was conducted for all the specimens as per IS 5816-1959. The test setup for split tensile strength is shown below (Fig. 1b). Cylinders of size 150 mm × 300 mm were cast and cured for 28 days. The load was applied continuously until the specimens fail using CTM. Split Tensile Strength was calculated using Eq. (2)

$$\text{Split Tensile Strength} = \frac{2P}{\pi DL} \quad (2)$$

where

P Maximum applied load

D Diameter

L Length.

2.3 Compressive Strength Test

A compressive strength test was conducted for all the specimens as per IS 516-1959. The ingredients of concrete were weighed accurately and mixed thoroughly in a mechanical mixer until a uniform colour was obtained. The concrete was filled in the mould of size 150 mm × 150 mm × 150 mm whose inner surface was oiled in three equal layers and compacted thoroughly. The specimens after demolding were



Fig. 1 a Test setup for flexural strength test. b Test setup for resistance measurement of split tensile test. c Test setup for resistance measurement of compressive strength

cured in water for 28 days. Then they were tested on a compression testing machine as shown below (Fig. 1c).

3 Preparation, Mixing, Fabrication

The Aerated Concrete is produced by the performing method, by the addition of aluminium powder to the concrete mix. The aluminium powder which comes in contact with the water will produce hydrogen bubbles, which will make the concrete into a porous structure. In lightweight concrete, 50% of the volume is occupied by air voids which is the reason for the decrease in the density of concrete.

The mix consists of Cement, Fine aggregate, fly ash, aluminium powder, glass fibre, superplasticizer, and water, which are mixed for 2 min to get a homogenous mixture. After 10 min of mixing the aeration process of the concrete will take place, as the concrete mix increases its volume. Cube ($150 \times 150 \times 150$ mm), cylinder (300×150 mm) and beam ($500 \times 100 \times 100$ mm) are cast to study the Compressive, Tensile and Flexural strength of the concrete. Only 1/3 portion of the mould is filled with concrete, as the volume will increase. Trial mixes are done initially to develop a concrete mix of suitable density. The trail mix is given in Table 6.

The Study progresses with the use of trial mix 19, which is used as the control mix. The percentage of fibres varied to study the mechanical properties. The Quantities of materials required for the casting of 1 m^3 of the sample are shown in Table 7. The following figures show the mixing and casting of samples (Fig. 2a). The flow table test for each fibre percentage is conducted. There is a uniform flow obtained for all the fibre percentages, showing each mix is of having workability (Fig. 2b).

These casted samples (tube, cylinder and beam) are cured in water for 7 days, 14-day and 28 days for strength gain. The specimens are then tested in a Compression testing machine and Flexure testing machine to obtain the mechanical properties of Glass Fibre Reinforced Aerated concrete.

The figure shows the results of the flow table test. All the mix is of uniform flow with an average diameter of 20 mm. The mix is having good workability.

4 Results and Discussions

Test values of Compression, Tension and Flexure is as shown in the figures below.

Figure 3a shows the compressive strength values for different fibre contents, The addition of fibres will increase the strength of aerated concrete. The increase in strength is due to the confinement effect of fibres. The strength is increased by 5% by the addition of 2% of fibre. The maximum strength is obtained for 2% of fibre and then the strength got decreased for 2.5% of fibre which is due to the clogging of the fibres in the concrete. Thus, we can say that percentage of fibre greater than 2%

Table 6 Trial mix proportions

Trial	Cement: fine aggregate	Fly ash (%)	Water cement ratio	Aerating agent (%)	Super plasticizer (%)	Avg weight of cube (kg)	Density (kg/m ³)	Compressive strength (MPa)
Trial 1	1:2	20	0.5	0.5	0.4	0.663	1886	10.54
Trial 2	1:2	20	0.5	0.75	0.4	0.657	1869	10.33
Trial 3	1:2	20	0.5	1	0.4	0.644	1832	10.71
Trial 4	1:2	20	0.6	0.5	0.4	0.655	1863	10.49
Trial 5	1:2	20	0.6	0.75	0.4	0.648	1844	10.15
Trial 6	1:2	20	0.6	1	0.4	0.599	1705	9.18
Trial 7	1:2	20	0.62	1.5	0.4	0.537	1526	8.95
Trial 8	1:2	20	0.62	1.2	0.4	0.581	1653	8.75
Trial 9	1:2	20	0.5	1.2	0.4	0.632	1798.50	10.2
Trial 10	1:2	20	0.55	1	0.4	0.636	1810.19	9.48
Trial 11	1:2	20	0.55	1.2	0.4	–	–	–
Trial 12	1:2	20	0.57	1.2	0.4	0.620	1764.34	9.35
Trial 13	1:2	20	0.59	1.2	0.4	0.598	1702.20	9.19
Trial 14	1:1:1	20	0.6	1	0.4	0.581	1652.64	8.69
Trial 15	1:1:1	20	0.6	0.75	0.4	0.627	1782.1	9.93
Trial 16	1:1:1	20	0.62	1	0.4	0.584	1662.42	8.93
Trial 17	1:1:1	20	0.62	1.2	0.4	0.595	1693.34	9.05
Trial 18	1:2	20	0.63	1.2	0.4	0.589	1676.43	8.95
Trial 19	1:2	20	0.64	1.2	0.4	0.537	1526.01	8.89

Table 7 Quantity of materials required for 1 m³

Materials	Quantity (kg/m ³)
Cement	435
Fine aggregate	1072
Fly ash	95
Aluminium powder	5.7
Water	295
Super plasticizer	1.9



Fig. 2 a Casting of samples. b Flowability check on the mix with 0%,1%,1.5% and 2% glass fibre

can lead to a decrease in compressive strength. Here in this experiment, we can take 2% of fibre based on compressive strength.

Figure 3b shows the tensile strength of the samples after 7, 14 and 28 days of curing. The addition of fibre increases the tensile strength. There is an increasing pattern of tensile strength till 2% of fibre and then it gets decreased for 2.5% fibre. The tensile strength increased by 40% with the addition of 2% of fibre. The increase in strength is due to the bridging action of fibres present in the concrete. The 2% fibre will give a tensile strength of 1.51 MPa after 28 days of the curing process.

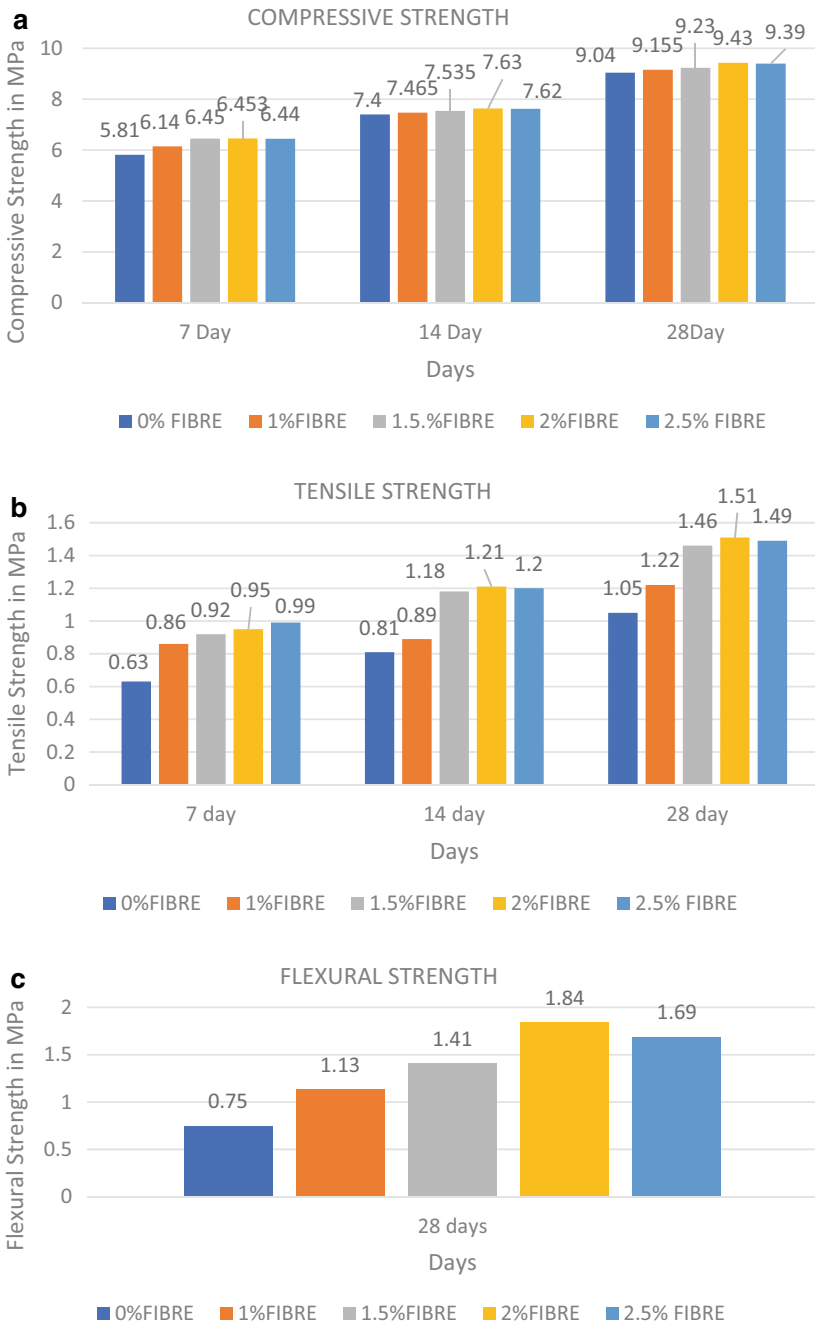


Fig. 3 **a** Graphical representation of compressive strength for different fibre content. **b** Graphical representation of tensile strength for different fibre content. **c** Graphical representation of compressive strength for different fibre content

The addition of fibre has a significant effect in increasing the Flexural strength of concrete. The bridging action of fibres is the reason for the increase in Flexural strength. Figure 3c clearly shows the increase in strength. The flexural strength is maximum for 2% fibre.

The 2.5% fibre shows lower flexural strength than 2% fibre, it is due to clogging of fibres in the concrete.

5 Conclusion

- The trial number 19 is taken as the control mix based on the density obtained, which is satisfactory.
- The maximum compressive strength is obtained for 2% of fibre. The increased compressive strength is due to confining effect of the glass fibres. The compressive strength is then decreased for 2.5% fibre, due to clogging of fibres in the specimen.
- The tensile and flexural strength is also maximum for 2% fibre which is due to bridging action of the glass fibres. The strength then decreased for 2.5% fibre is due to clogging of fibres which is observed from the tested specimen.

References

1. Amran M, Fediuk R, Vatin N, Lee YH, Murali G, Ozbakkaloglu T, Klyuev S, Alabduljabber H (2020) Review fibre-reinforced foamed concretes: a review. *Materials* 13:4323
2. Demir I, Sevim O, Ogdü MK, Dogan O, Demir S (2021) Mechanical and physical properties of autoclaved aerated concrete reinforced using carbon fibre of different lengths. *ISSN 1330-3651*
3. Geetha S, Selvakumar M (2016) Flexural behaviour of steel fibre reinforced aerated concrete beam. *IJRET Int J Res Eng Technol* 5(20)
4. Zhang J, Jiang N, Li H, Wu C (2018) Study on mix proportion design of cement foam concrete. *Mater Sci Eng* 439:042053

Seismic Vulnerability Assessment of Baffled Elevated Water Tank with Fluid–Structure–Soil Interaction Having Variable Staging Pattern



T. Shahana and S. P. Deepu

Abstract The damages found in the elevated water tank from previous earthquake events confirm that the failures occur mainly in the staging of the water tank. It is essential to quantify these damages to investigate its performance. Fluid–structure–soil interaction plays an important role in the investigation of structural performance of baffled elevated water tank. With the use of performance-based earthquake engineering, in this study the performance level is investigated by utilizing spectral acceleration as intensity measure and the engineering demand parameter is the top drift of staging. With the use of SAP2000 software various models were developed by considering variations in water level and staging configuration of baffled elevated water tank by considering fluid–structure–soil interactions. Non-linear dynamic analysis were conducted following FEMA P695 guidelines by considering five ground motions with gradually increasing intensities in increments of 0.1 g up to failure and IDA curves were obtained. Fragility curves were made from the IDA curves according to three performance limit states for assessing seismic risk. For evaluating safety margin against collapse, collapse margin ratios were obtained. It shows that cross staging is having a safety margin of 32.5% higher than radial and basic staging. From the result it shows that hard soil is having a safety margin of 99% higher than soft soil and medium soil has 25% higher safety than soft soil. The seismic fragility analysis by considering variation in water level shows that half-filled water level shows more critical condition than Full and Empty condition.

Keywords Elevated water tank · SAP2000 · Fluid structure soil interaction · Fragility curves

T. Shahana (✉) · S. P. Deepu
Government College of Engineering Kannur, Department of Civil Engineering, Kannur 670563,
India
e-mail: Shahanat2016@gmail.com

1 Introduction

Elevated water storage tanks are used to store water for both fire protection and potable drinking purposes within a specific area or neighborhood. Due to the gravitational force of gravity, elevated tanks enable the system's water pressure to remain constant throughout. Depending on the intended usage and needs of the distribution zone, elevated water tanks can be created using a wide range of designs, sizes, and materials.

Several research were done in past to study the performance of elevated water tank. Mansour et al. [1] conducted Seismic assessment of elevated water tanks incorporating the fluid–structure interaction with variable staging pattern. It was found that when compared to radial staging, the cross-staging configuration offers more initial lateral rigidity. The cross configuration performs better in terms of ductility than the radial configuration by offering higher ductility factors. The seismic fragility of the cross and radial layouts was superior to that of the basic staging type. Rebouillat et al. [2] conducted fluid structure interaction in partially filled liquid containers. They discussed the problems related to modelling the free surface of fluid and fluid solid interface. They discussed that near the still water level, most severe impact pressure occurs. A study of fluid structure interaction modelling of liquid sloshing in the flexible tank was conducted by Nicolici et al. [3]. They mainly focussed on sloshing phenomena and coupling computational fluid dynamics analysis with finite element analysis for the prediction of convective mode frequency, sloshing wave amplitude and pressure on walls. They showed that two-way model provided more realistic results by considering amplification of impulsive pressure, but more computational time than one-way model [4]. From their results it understood that coupled lumped fluid mass model is more appropriate for assessing the reaction force at anchoring points. A study on seismic design on frame-supported elevated water tanks incorporating fluid–structure interaction was conducted by Mansour et al. [5] and found that the damage sustained by EWTs as a result of static lateral stress was primarily concentrated in the lower part of the staging based on the creation of plastic hinges in RC-MRFs. Bansode et al. [6] conducted study on seismic response of overhead water tank with different staging system. It was found that under both full and empty tank conditions, base shear also increases when the lateral bracing level rises from no lateral bracing to lateral cross bracing and from lateral cross bracing to lateral radial bracing. For a particular type of baffle, the response of pressure on the tank side wall during a major earthquake was comparable. Jin et al. [7] shows that a perforated baffle's slots can successfully lessen the influence of sloshing liquid on it. Liu et al. [8] conducted study on water tank with baffles having three-dimensional sloshing. They showed that the vertical baffle was a more efficient technique for lowering the sloshing amplitude as compared to a horizontal baffle. They also recreated the intense liquid sloshing in both baffled and un baffled tanks under surge and sway excitations. Strong turbulence and fractured free surfaces are present in the sloshing. Investigation of the pressures and free surface displacements revealed that vertical baffles can significantly lower the impulse pressure [9].

Investigations on the non-linear seismic response of EWTs having baffles with fluid–structure–soil interaction were not studied using probabilistic and deterministic approaches. Previously no studies were found on the performance of elevated water tank with varying staging pattern against the quantifiable damage states.

Hence this study focused on the non-linear seismic response of EWTs having baffles with fluid–structure–soil interaction using probabilistic and deterministic approaches.

2 Methodology

The numerical model has to be developed by using finite element software SAP2000. The numerical model is going to validated against the data by Mansour et al. [5]. For assessing the dynamic behavior of Elevated Water Tank following methodology was adopted. With the consideration of water level condition and staging pattern the configuration of elevated water was produced. The system has to be developed using spring mass mechanical model for the elevated liquid tank system. The modeling of soil structure interaction is using equivalent springs. This consists of nonlinear analysis. The incremental dynamic analysis was used to develop fragility curves for analyzing structural performance of elevated water tank. The structural modeling has to be followed is shown in Fig. 1.

The parameter to be studied are effect of water levels, effect of soil types and effect of staging configuration of elevated water tank with baffles with incorporating fluid structure soil interaction. Different configuration of elevated water tank to be used for the study is shown in Fig. 2.

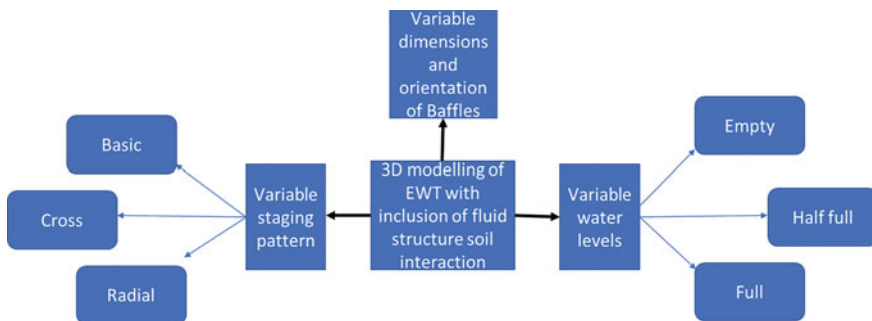


Fig. 1 Structural modeling of elevated water tank

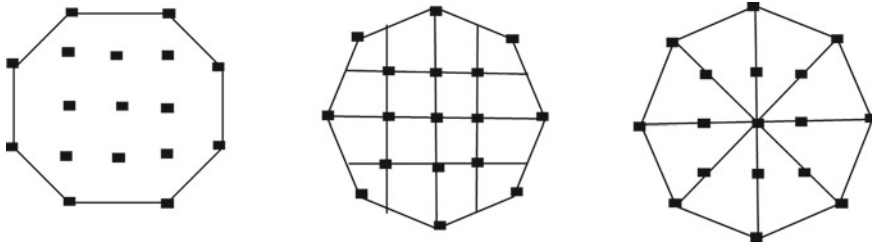


Fig. 2 Different staging configurations (basic, cross and radial)

Table 1 Geometric properties of elevated water tank [1]

Geometry		Value in meters
Tank	Height (H)	5.4
	Diameter (D)	15.66
	Wall thickness	0.5
	Roof slab thickness	0.35
	Base slab thickness	0.175
	Top beams	0.6 × 0.5
Supporting structure	Height	19.3
	Columns	0.6 × 0.6
	Beams	0.6 × 0.35
Liquid	Height	5.13 (Almost full: 0.95H) 2.7 (Half full: 0.5H)

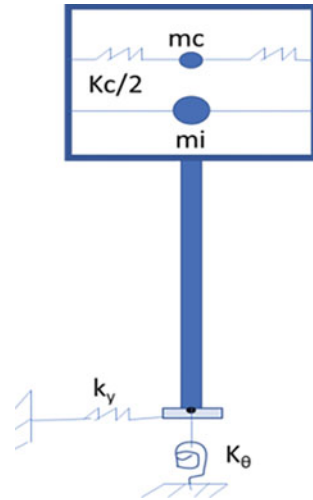
2.1 Geometric Modeling

The dimensions for the modelling of water tank are represented as shown in Table 1. For the modelling, study conducted by Mansour et al. [5] was considered.

2.2 Modeling of Fluid Structure Soil Interaction

The spring mass model of an elevated water tank is given in Fig. 3, where m_c stands for convective mass and m_i for impulsive mass, both of which are permanently coupled to the tank wall by a spring with stiffness (K_c). The water tank model for RC overhead tanks can also be idealised into a two-mass model, which has two degrees of freedom and is more accurate. As seen in Fig. 4.1, Housner introduced the two-mass model theory for an overhead water tank in 1963. The spring mass model parameters are m_i , m_c , K_c , and K_s . The soil springs were applied to the raft foundation as per Richart

Fig. 3 Spring mass model for fluid structure soil interaction



and Lysmer 1970. Hard, Medium and Soft Soil springs are applied as joint spring in SAP2000.

2.3 Incremental Dynamic Analysis

The incremental dynamic analysis was conducted to assess the seismic performance of baffled elevated water tank having fluid structure soil interaction with variations in staging patterns and water level. Five earthquake events were selected from PEER Ground motion data and these are listed in Table 2.

The structure is subjected to seismic records to increasing intensities in increments of 0.1 g of Spectral acceleration. Drift ratio is used as a function of Spectral

Table 2 Ground motion records

Label	Ground motion event	Station	Component	Magnitude
G1	Loma Prieta [1989]	Gilroy Array Station 3, CA-Sewage plant	90	7.0
G2	Landers [1992]	Joshua Tree, CA, FireStation	90	7.3
G3	Imperial Valley [1979]	El Centro, CA Array station 5	230	6.5
G4	Northridge [1994]	San Fernando Valley, CA-Arleta	90	6.7
G5	Kobe [1995]	Port island, Japan	0	6.9

acceleration. The fragility curves were developed based on IDA and probabilistic analysis were conducted according to immediate occupancy (IO), Life safety (LS), and Collapse Prevention (CP) as per vision 2000.

3 Results and Discussion

3.1 Validation

Manual calculation was done by using ACI 350.3-06 for calculating impulsive period and convective period. Results obtained from the manual calculation for time periods were compared with the result from the analysis by Mansour et al. [5].

Impulsive period,

$$T_i = 2\pi \sqrt{\frac{m_s + m_i}{K_S}} = 2\pi \sqrt{\frac{1372051}{26123 \times 10^3}} = 1.44 \text{ s} \tag{1}$$

Convective period,

$$T_c = \frac{2\pi}{\sqrt{3.68 \tanh\left[3.68\left(\frac{H_c}{D}\right)\right]}} \sqrt{\frac{D}{g}} = \frac{2\pi}{\sqrt{3.68 \tanh\left[3.68\left(\frac{5.13}{15.66}\right)\right]}} \sqrt{\frac{15.66}{9.81}} = 4.53 \text{ s} \tag{2}$$

From Table 3, shows that a deviation of 1.98% was found between the result of FE analysis and ACI 350.3-06 and 0.216% error was found between the result of FE analysis and Mansour et al. [5] for convective mode and a deviation of 5.5% was found between the result of FE analysis and ACI 350.3-06 and 3.8% error was found between the result of FE analysis and Mansour et al. [5] for impulsive mode.

Table 3 Result analysis for convective and impulsive mode

Modes	Natural Periods (s)		
	FE analysis	Mansour et al. [5]	ACI-350
1	4.62	4.61	4.53
2	4.62	4.61	4.53
3	1.52	1.57	1.44
4	1.5	1.57	1.44

3.2 Variation in Soil Type

Hard, medium and soft soil were analyzed by keeping the ratios of height of baffles to height of water level as 0.5 ($h_b/h_w = 0.5$) at full water level condition. Taking the probabilities at 0.6 g of spectral acceleration, the probability of exceeding the damage state at collapse prevention (CP) state is analyzed. It shows that for hard soil the probability is 24%, for medium soil probability is 24.3% and for soft soil it is 94%. Hence it shows that the probability of exceeding the damage state for soft soil is more than hard and medium soil.

Collapse Margin Ratio is the ratio of intensity measure that causes damage of 50% of ground motion to intensity measure of maximum considered earthquake. For the design return period of 475 years, 0.424 g of spectral acceleration is considered. From the result it shows that hard soil is having a safety margin of 99% higher than soft soil and medium soil has 25% higher safety than soft soil as shown in Table 4 (Fig. 4).

Table 4 Collapse margin ratio and P[D/Sa] of different soil type

Soil type	Intensity measure at 50% collapse [g]	Intensity measure at MCE [g]	Collapse margin ratio	Probability of damage state [%]
Hard	1	0.424	2.35	24
Medium	0.8	0.424	1.88	24.3
Soft	0.5	0.424	1.18	94

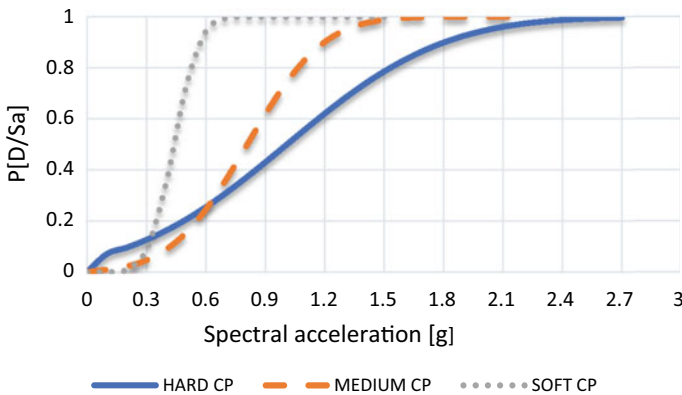


Fig. 4 Collapse fragility curve

Table 5 Collapse margin ratio and P[D/Sa] of different staging

Staging type	Intensity measure at 50% collapse [g]	Intensity measure at MCE [g]	Collapse margin ratio	Probability of damage state [%]
Cross	0.66	0.424	1.55	66
Radial	0.5	0.424	1.17	94.3
Basic	0.5	0.424	1.17	89.9

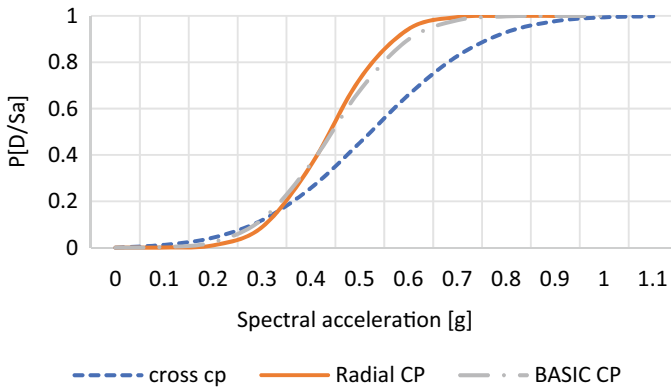


Fig. 5 Collapse fragility curve

3.3 Variation in Staging Pattern

Cross, Radial and Basic staging pattern were analyzed keeping the ratios of height of baffles to height of water level as 0.5 ($h_b/h_w = 0.5$) at full water level condition and soft soil type. It shows that cross staging has a probability of exceeding damage state as 66%, Radial staging has 94.3% and Basic staging has 89.9%. Hence it shows that the probability of exceeding the damage state for radial staging is more than cross and basic staging type.

From the result of Collapse Margin Ratio, it shows that cross staging is having a safety margin of 32.5% higher than radial and basic staging as shown in Table 5 (Fig. 5).

3.4 Variation in Water Level

Full, Half-filled and Empty water level conditions were analyzed keeping the ratios of height of baffles to height of water level as 0.5 ($h_b/h_w = 0.5$) having soft soil type. It shows that Full water tank has a probability of exceeding damage state as 94.3%, for half-filled water tank as 98.6% and empty water tank as 45%. This shows that

Table 6 Collapse margin ratio and P[D/Sa] of different water level

Water level	Intensity measure at 50% collapse [g]	Intensity measure at MCE [g]	Collapse margin ratio	Probability of damage state [%]
Full	0.5	0.424	1.179	94.3
Half-filled	0.45	0.424	1.06	98.6
Empty	0.65	0.424	1.53	45

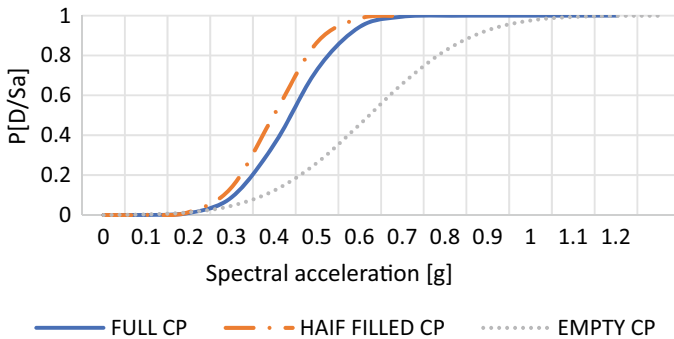


Fig. 6 Collapse fragility curve

half filled water tank is found to be more critical. From the result of Collapse Margin Ratio, it shows that Empty water level is having a safety margin of 44% more than Half-filled and 29% more than Full water level as shown in Table 6. Hence it shows that half-filled water level condition is more critical (Fig. 6).

4 Conclusions

In this study, the performance baffled elevated water tank under fluid structure soil interactions is investigated with varying water level, soil type and staging configuration. Damage states were investigated according to Vision 2000. The probability of damages was evaluated with the use of fragility curve and Collapse Margin Ratio. Following conclusions were made:

1. The seismic fragility analysis by considering variation in staging configuration shows that cross staging shows better performance than radial and basic staging. It shows that cross staging is having a safety margin of 32.5% higher than radial and basic staging. This is because cross staging is having more stiffening beams than other staging type, hence provides more structural stability.
2. The seismic fragility analysis by considering variation in soil type shows that hard soil shows better performance than medium and soft soil type. From the result it shows that hard soil is having a safety margin of 99% higher than soft

soil and medium soil has 25% higher safety than soft soil. Soft soil shows more flexibility at the bottom of the structure, which creates more displacement at the top than hard soil condition. This shows the importance of having inclusion of fluid structure soil interaction in the analysis.

3. The seismic fragility analysis by considering variation in water level shows that half-filled water level shows more critical condition than Full and Empty condition. It shows that Empty water level is having a safety margin of 44% more than Half-filled and 29% more than Full water level. In half filled condition sloshing will be more due to more displacement of water inside the water tank.

References

1. Mansour AM, Kassem MM, Nazri FM (2021) Seismic vulnerability assessment of elevated water tanks with variable staging pattern incorporating the fluid-structure interaction. In: Structures, vol 34. Elsevier, pp 61–77
2. Rebouillat S, Liksonov D (2010) Fluid–structure interaction in partially filled liquid containers: a comparative review of numerical approaches. *Comput Fluids* 39(5):739–746
3. Nicolici S, Bilegan RM (2013) Fluid structure interaction modeling of liquid sloshing phenomena in flexible tanks. *Nucl Eng Des* 258:51–56
4. Jogi P, Jayalekshmi BR (2022) Effect of soil-structure interaction on the seismic response of elevated water tank. In: Recent advances in earthquake engineering. Springer, Singapore, pp 237–248
5. Mansour AM, Nazri FM (2021) On the influence of fluid–structure interaction and seismic design on frame-supported elevated water tanks. *Struct Eng Int* 1–15
6. Bansode P, Rajemahadik C (2019) Seismic response of overhead water tank with different staging system. In: Proceedings of national conference on advances in structural technologies (CoAST-2019), vol 1, p 3
7. Jin H, Calabrese A, Liu Y (2021) Effects of different damping baffle configurations on the dynamic response of a liquid tank under seismic excitation. *Eng Struct* 229:111652
8. Liu D, Lin P (2009) Three-dimensional liquid sloshing in a tank with baffles. *Ocean Eng* 36(2):202–212
9. Minnekanti M, Alapati M (2020) Effect of baffle wall parameters on the modal responses of elevated rectangular water tank. In: International conference on emerging trends in engineering (ICETE). Springer, pp 27–38

Benchmarking Existing Fire Safety Norms for Urban Villages in Noida with Best Practices



Prerna Sharma , Ritabrata Ghosh, Sanjay Tomar, and Amit Kumar Jaglan

Abstract The formation of urban villages is an integral phenomenon of growing cities in India. Such villages become extremely important in the perspective of urban areas as they offer an affordable solution to the needs of many city dwellers. However, it is a hard reality that urban villages lack the availability of services and infrastructure essential to offer a safe living environment to the inhabitants which leaves them at a high-risk level. Fire is recognized as one of the most fundamental services under the 12th schedule of the constitution of India. Fire prevention and firefighting are the subject matter of states and union territories and urban local bodies. Studies have shown that there is a strong disconnect between the policies formed at National, regional & local levels that leaves urban villages at their fate without giving much recognition in planning. The study region, Noida came into existence when the need to develop planned urban centers in proximity to Delhi was realized and hence a lot of villages were engulfed in the development and got converted to urban villages. The development norms applicable in Noida do not highlight the holistic development and planning strategies required for the safety of urban villages. This study presents a benchmarking of policies and norms in Noida, India (southeast Asia) with the case studies identified to understand the key indicators of improvement in existing policies. This study will help the policymakers, planners, and building authorities to position the existing norms with international standards.

Keywords First Keyword · Second Keyword · Third Keyword · Forth Keyword · Sixth Keyword

P. Sharma (✉) · R. Ghosh
Amity University, Noida, India
e-mail: ar.sharmaprerna@gmail.com

S. Tomar
Delhi Fire Service, New Delhi, India

A. K. Jaglan
School of Planning and Architecture, New Delhi, India

1 Introduction

Urban villages formation is an outcome of the process of urbanization in any developing country. Farmlands are acquired by the government agencies for developing cities and urban encroachment leads to conversion of rural character of villages to urban. The coining of urban villages is a solution to urban demands that resolves the consumption-based needs resulting from the urbanization process [1]. However, these villages often lack availability of basic infrastructural facilities from the state authorities which results in high vulnerability towards disasters. It has been researched that the gaps in the policies at state and center level for urban villages is one of the major reasons for this situation. While their lands are acquired, no other means of livelihood is offered to the inhabitants and hence for the income, rural houses are converted to multistorey structures with commercial activities. These land-use conversion and construction are not under the check by authorities and users does not seek necessary approvals before construction and expansion. The villages experience haphazard growth with no upgradation of infrastructure required for the high-density villages [2].

Fire is one of the many disasters that can occur and is the fourth most disruptive risk according to the India Risk Survey 2021 [3]. The unorganized growth of urban villages in India leaves them at high risk of fire incidents, where not only property but also the lives of people are at stake. The norms and codes laid down for the development of Indian cities do not holistically recognize urban villages as a distinctive identity different from regular building typologies. They also lack in addressing life safety norms and measures specific to urban villages [4].

If we look at a global scenario, one of the reasons for the gap in fire safety of urban villages is the lack of emphasis on preventive measures, such as reducing the risk of ignition sources and creating fire breaks. Still systems rely on reactive measures, such as firefighting, which can be costly and often insufficient [5]. Urban villages are densely populated areas that often lack basic infrastructure and services such as water supply, sanitation, and waste management. Due to the inadequate infrastructure, these areas are more prone to fires. However, there is a gap in fire policy at the global level that specifically addresses the needs of urban villages.

One of the major reasons for this gap is the lack of attention paid to urban villages in policymaking. Most fire policies focus on urban areas and do not adequately consider the unique challenges faced by urban villages. In many cases, policies do not account for the lack of access for emergency vehicles in narrow streets and alleys, which can impede firefighting efforts. Furthermore, the lack of resources in urban villages poses a challenge in implementing fire prevention and firefighting measures. Many urban villages do not have access to firefighting equipment, and the lack of resources makes it difficult for residents to take proactive measures such as fire safety training and evacuation planning [6].

To address this gap, there is a need to develop fire policies that specifically target the needs of urban villages. These policies should account for the unique challenges faced by these areas, such as narrow streets and lack of resources. They should also prioritize preventive measures such as fire safety training and building code compliance. Additionally, it is important to involve local communities in policymaking to ensure that policies are tailored to the specific needs of each urban village.

The study area, known as New Okhla Industrial Development Authority (NOIDA), was established to create planned urban centers near Delhi that could provide alternative sites for the development of small and medium-sized industrial units. In 1976, 36 villages in the “Yamuna-Hindon-Delhi Border Regulated Area” were designated as NOIDA with the goal of providing land for 10,000 small industrial units that would employ 41,000 workers and create a suitable living and working environment for them, thereby reducing stress on Delhi’s industries. Currently, NOIDA encompasses 81 revenue villages and a total of approximately 20,316 hectares of land. In 1991, NOIDA was granted Census Town status, and its population grew to 181,003 with a growth rate of nearly 400%. The Census Town of NOIDA, including 29 “urban villages,” accounted for a population of 146,514, while the remaining 34,489 people lived in the rural area of the Notified Area [7].

Although there is a growing awareness regarding fire and life safety due to the realization of the significant losses caused by fires, there are still gaps in the regulations that govern fire safety in the study area. The authorities have acknowledged the issues faced by urban villages and recognize the need for a comprehensive study to evaluate the current state of the physical infrastructure in these areas in Noida. This study will enable the governing authorities to identify areas that require improvement and suggest solutions to address these issues.

Benchmarking of existing norms can provide an opportunity to the policy makers to identify areas of improvement to ensure a safe living environment to urban village also as it is provided to the urban areas of the city. This research aims at service level benchmarking of fire safety norms related to urban villages in Noida with the best practices. Since services like water supply, electrification, roads etc. plays a vital role in fire safety hence benchmarking has been done based on service level indicators. The study identifies services performance indicators as per the ministry of urban development, Government of India and compares the existing norms for urban villages with the case studies.

2 Benchmarking Process

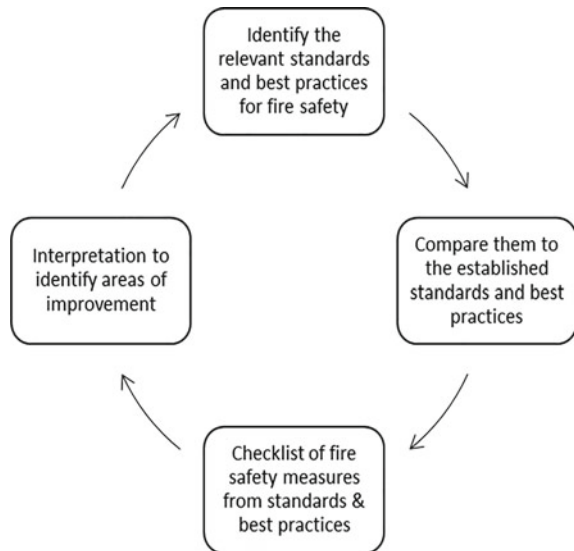
Benchmarking is a process of comparing the performance of an organization or system against industry standards or best practices. In the context of fire safety norms, benchmarking refers to evaluating the adequacy of a building’s fire safety measures by comparing them to established standards and best practices [5, 8].

The benchmarking process for fire safety norms involves several steps. The first step is to identify the relevant standards and best practices for fire safety. This involves reviewing national and international codes and regulations, as well as industry standards and guidelines. After reviewing the policies and codes, the next step is to compare them to the established standards and best practices. This includes developing a checklist of fire safety measures and evaluating compliance with each item on the checklist.

The benchmarking process also involve evaluating the emergency response procedures and training programs. This can include assessing the effectiveness of evacuation plans, identifying potential hazards, and ensuring that staff are adequately trained in fire safety procedures. Once the benchmarking process is complete, the results can be used to identify areas where improvements are needed. This may involve making recommendations for changes to the building’s fire safety measures, such as installing additional fire alarms or improving the building’s fire escape routes.

Overall, the benchmarking process for fire safety norms is an important tool for evaluating the adequacy of fire safety measures. By comparing a fire safety measures to established standards and best practices, one can identify areas where improvements are needed and ensure that their fire safety measures remain effective over time (Fig. 1).

Fig. 1 Benchmarking process for fire safety



3 Benchmarking Indicators of Fire Safety in Urban Villages

Identification of indicators is an important process for evaluating the level of fire safety provisions available to the residents of these areas. Urban villages often have inadequate fire safety provisions, and benchmarking can help to identify gaps in the provision of fire safety measures and establish targets for improvement [8].

The following are some benchmarking indicators of fire safety in urban villages:

1. Availability of fire stations: The availability of fire stations in urban villages is a critical indicator of fire safety. The number of fire stations in the area, their location, and the availability of firefighting equipment can help determine the level of fire safety provision.
2. Fire incidence rate: This measures the frequency of fires that occur in a particular area over a period.
3. Fire loss ratio: This measures the ratio of losses incurred due to fire to the value of the property.
4. Fire hydrants: The availability of fire hydrants is another important benchmarking indicator of fire safety. The number and location of fire hydrants can help determine the level of fire safety provision in an urban village.
5. Fire safety training: The level of fire safety training provided to residents is also an important benchmarking indicator. Fire safety training can include education on fire prevention, fire safety drills, and the use of fire extinguishers.
6. Building codes: Building codes and regulations play an important role in ensuring fire safety in urban villages. Compliance with building codes can be used as a benchmarking indicator of fire safety provision.
7. Smoke detectors and fire alarms: The availability of smoke detectors and fire alarms in buildings is another important benchmarking indicator of fire safety provision. The number and location of smoke detectors and fire alarms can help determine the level of fire safety provision in an urban village.
8. Emergency response time: The emergency response time of fire-fighting personnel is a critical benchmarking indicator of fire safety provision. The response time can be evaluated based on the time taken to reach the location of the fire, as well as the time taken to control the fire.

By benchmarking these indicators of fire safety provision, it is possible to identify areas for improvement and establish targets for progress.

4 Case Studies

Land is a critical resource especially in countries with large population to support. To understand urban village scenario in other parts, China has been considered as a case study area which relates to the contextual understanding for Indian cities. Urban villages in China are also recognized as a social and spatial phenomenon

closely related with rural-to-urban transformation [9]. As in case of Indian cities, in China also, urban villages support the vulnerable groups of the urbanization process: the floating migrant population and the native farmers of rural village. On similar lines as Indian cities, urban villages in China also does not fall under the purview of government agencies.

The case studies discussed in this section include urban villages in Beijing, Guizhou and Shenzhen.

4.1 Redevelopment Approach in Xidian Village, Beijing

Beijing city has around 1700 urban villages with 3.7 million residents, mostly migrant population of the city. Redevelopment projects of 50 selected pilot villages have been implemented since 2010 to resolve issues of urban villages in Beijing. Like the case of Noida, villagers in urban villages of Beijing have constructed high-density low and medium-rise housing units on land meant for their personal residential needs, and this becomes their means of livelihood by leasing to migrants at a low price [10].

The redevelopment model of Xidian village focused on keeping intact the rural identity while upgrading the infrastructure to match with the rest of the urban fabric of the city with improved infrastructure and standardising the plots to three storey mixed use buildings. redevelopment model was led by village committee instead of municipal officials. As per the model, 50 m² of space per person was allocated for residential units and 50 m² of floor space per person for commercial or industrial development.

During the redevelopment of Xidian Village, the local government implemented a range of fire safety measures to protect the historic buildings and ensure the safety of the residents. The measures taken included [10]:

Installation of fire hydrants: The government installed fire hydrants throughout the village to provide a reliable source of water in case of a fire. This allowed firefighters to quickly access water to extinguish any fires that occurred.

Upgrade of electrical systems: The electrical systems in the historic buildings were upgraded to reduce the risk of electrical fires. The new systems were designed to be safer and more efficient, reducing the risk of fire caused by faulty wiring.

Implementation of fire safety regulations: The government implemented fire safety regulations that required residents to maintain their homes and buildings to a high standard. This included regular inspections of electrical systems, chimneys, and other potential fire hazards.

Fire safety training: The government provided fire safety training to the residents, including information on how to prevent fires and how to respond in case of a fire. The training helped to increase awareness of fire safety and reduce the risk of fires occurring.

The fire safety measures implemented during the redevelopment of Xidian Village were successful in reducing the risk of fires and protecting the historic buildings. The installation of fire hydrants and the upgrade of electrical systems provided a reliable source of water and reduced the risk of electrical fires. The implementation of fire safety regulations and training helped to increase awareness of fire safety and reduce the risk of fires occurring.

4.2 Land Readjustment Approach in Guizhou

In Guizhou, a province located in southwestern China, land readjustment is being used to revitalize urban villages and improve the living conditions of their residents [11]. Urban villages in Guizhou are typically low-income areas with inadequate infrastructure and services. The land readjustment approach involves pooling together small plots of land owned by different individuals and redistributing them to create larger and more efficient land parcels [12]. The process also involves providing basic infrastructure, such as roads, water supply, and sewage systems, to the area.

The land readjustment approach has several benefits for urban villages in Guizhou. First, it enables the development of larger and more functional land parcels that can accommodate a variety of land uses, such as residential, commercial, and public facilities. The land readjustment approach in Guizhou has several benefits for fire safety. First and foremost, it allows for the implementation of modern fire safety measures in urban villages that may not have had adequate fire safety infrastructure previously. Secondly, land readjustment helped to reduce the risk of fires in urban villages by improving the overall layout of the area. This involves reconfiguring streets and buildings to create larger and more functional land parcels, reducing the risk of overcrowding and congestion that can contribute to the spread of fires [12].

4.3 Fire Safety Provisions in Urban Villages of Shenzhen, China

Urban villages in Shenzhen, China, are densely populated areas with a high risk of fire. These areas are typically characterized by narrow streets, informal building structures, and inadequate fire safety infrastructure. The lack of fire safety measures in these urban villages is a major concern, as fires can quickly spread and result in significant loss of life and property [13].

To address this issue, the government of Shenzhen has implemented several measures to improve fire safety in urban villages. These measures include the installation of fire hydrants, sprinkler systems, and smoke alarms, as well as the construction of wider roads and improved access points for emergency vehicles [14]. In addition to these physical measures, the government has also worked to increase community

awareness of fire safety. This has included the distribution of educational materials and the organization of training programs for residents on how to prevent fires and respond to emergencies.

The government of Shenzhen has implemented several measures to improve fire safety in urban villages which includes installation of Fire Safety Equipment, Construction of Wider Roads, Community Education and Training, Building Code Regulations, Inspection and Enforcement, Fire Safety Drills etc.

5 Mapping Existing Fire Norms of Noida with Case Studies and Best Practices

Fire Stations: As per SFAC guidelines in India, one Fire Station should be provided in an area of 10 km² in urban area; and 50 km² in rural area. As per this, since Noida is completely urbanized, there must be 20 fire stations considering area of Noida as 203 km². This clearly shows the gap in infrastructure existing in Noida as presently there are only 4 fire stations available. Due to this gap, not only the developed sectors but the urban villages are also at high vulnerability [15].

UK has the third largest firefighting organization in the world, with 111 Fire Stations from which it operates across the 1587 km². The fire station services provided in different countries may vary based on several factors such as the population density, geography, climate, and available resources. In developed countries like the United States, Canada, and the United Kingdom, fire station services are typically well-equipped and staffed with highly trained personnel. These countries also have a robust emergency response system that coordinates with various agencies, including the fire department, police, and medical services.

Fire incidence rate: As per the National Crime Records Bureau (NCRB), there were 7389 fire accidents in Uttar Pradesh in 2019, including residential, commercial, and industrial incidents. From January to April 2022, 626 fire incidents were reported in Gautam Buddha Nagar, where Noida is located. Official data shows that there were 1372 fire incidents in 2021, 1246 in 2020, 1729 in 2019, and 2017 in the preceding year [4]. However, a study conducted in Xidian village showed a significant decrease in fire incidents after the redevelopment approach was implemented, with no fire incidents reported since the new buildings were constructed, and fire safety measures were put in place. This highlights the importance of effective fire safety measures in reducing the risk of fire incidents and protecting lives and property.

Fire loss ratio: Not enough literature is available to understand the fire loss ratio in Noida, but it is important to have effective fire safety measures in place, such as regular fire safety audits, installation of fire safety equipment, and training of personnel to handle fire emergencies. Additionally, public awareness campaigns and community involvement in fire safety efforts can also help reduce the fire loss ratio.

Fire hydrants: Presently there is no Fire hydrant system in Noida neither does the building byelaws suggest any upgradation of the fire infrastructure in this regard [7]. The installation of fire hydrants in urban villages may pose some logistical challenges due to narrow streets and limited space. In all the 3 case studies mentioned above, external fire hydrant system was incorporated once road widening was done. This helped in drastically reducing the number of fire cases.

Inclusion in Building codes and byelaws: At present, urban villages are kept out of purview of building authorities and are not liable to seek approvals before any construction. This is one of the most critical reasons for the haphazard growth of the villages and needs most urgent attention. In the above stated case studies one of the most fundamental steps was to implement an agency for the responsible expansion of the village. This will significantly reduce the number of fire incidents in urban villages [2].

Emergency response time: The SFAC norms prescribe response time for the first fire tender to be 3, 5, and 7 min respectively based on the risk category A, B, and C in urban areas and 20 min in rural areas. Developed countries have varying response times, such as Germany with 8–15 min in urban areas, Japan with 5–10 min depending on the building location, the USA with (3–4) to 8 min, and the United Kingdom with 5–8 min. The response time can differ based on factors like the location, infrastructure, and risk assessment [16].

6 Conclusion

Benchmarking compares fire safety measures to established standards and best practices, identifying areas for improvement, and ensuring effectiveness for emergency response and staff training. Benchmarking indicators of fire safety in urban villages is a critical process to evaluate the level of fire safety provisions available to the residents of these areas. The identification of gaps in the provision of fire safety measures and the establishment of targets for improvement can be done through benchmarking. Indicators of fire safety in urban villages can include the availability of fire stations, fire incidence rate, fire loss ratio, fire hydrants, fire safety training, building codes and regulations, smoke detectors and fire alarms, and emergency response time. Through benchmarking, it is possible to identify areas for improvement and establish targets for progress. Case studies from China have demonstrated successful approaches to urban village redevelopment, including implementing fire safety measures such as installation of fire hydrants, upgrading electrical systems, implementing fire safety regulations, and providing fire safety training.

Noida, an urban area of 203 km², requires 20 fire stations as per SFAC guidelines, but there is a clear gap in infrastructure. The fire incidence rate in Uttar Pradesh was 7389 in 2019, and there were 626 incidents in Gautam Buddha Nagar from January to April 2022. Effective fire safety measures and community involvement can help reduce the risk of fire incidents. Currently, there are no fire hydrants in

Noida, and urban villages are kept out of building codes and byelaws. The response time for fire tenders varies from country to country based on factors such as location, infrastructure, and risk assessment.

Further this research can be taken forward to do an on-ground pilot study of existing infrastructure and collect real-time data to understand the gaps in fire safety services of urban villages in Noida.

References

1. Masoumi Z, van Genderen JL, Maleki J (2019) Fire risk assessment in dense urban areas using information fusion techniques. *ISPRS Int J Geo-Inf* 8(12). <https://doi.org/10.3390/ijgi8120579>
2. Kumar B, Bhaduri S (2018) Disaster risk in the urban villages of Delhi. *Int J Disaster Risk Reduct* 31(April):1309–1325. <https://doi.org/10.1016/j.ijdrr.2018.04.022>
3. P, FICCI (2021) India risk survey report
4. NCRB (2020) Place of occurrence-wise number of fire accidents, Persons Injured and Died during 2016 Accidental Deaths & Suicides in India 2016. p 16900 [Online]. Available: https://ncrb.gov.in/sites/default/files/adsi_reports_previous_year/Table-1.10_2019.pdf
5. Grandison A, Galea ER, Patel MK (2001) FIRE MODELLING STANDARDS/BENCHMARK Report on SMARTFIRE Phase 2 Simulations by Grandison AJ, Galea ER, Patel MK Fire Safety Engineering Group. University of Greenwich London SE10 9LS. for Dr David Peace Head Fire Research And Development Group. Home Office (1)
6. Macke J, Casagrande RM, Sarate JAR, Silva KA (2018) Smart city and quality of life: Citizens' perception in a Brazilian case study. *J Clean Prod* 182. <https://doi.org/10.1016/j.jclepro.2018.02.078>
7. Noida development authority (2020) Noida master plan - 2031 1
8. BIS (2016) National Building Code of India, 2016 Volume 1. *Natl Build Code India 80:1 v.* (various pagings)
9. T. P. R. of C (2014) Development Research Center of the, China's urbanization and land: a framework for reform. *Urban China Toward Inclusive Sustain Urban* 263–336. https://doi.org/10.1596/978-1-4648-0206-5_ch4
10. G. Y. Ua, "of Xidian Village , Beijing."
11. Zhang L, Yu H, Zhou Z, Yi F, Li D (2023) National big data experimental area and the unexpected booming of the housing Price in Guiyang of Guizhou Province of China. *Land* 12(2). <https://doi.org/10.3390/land12020453>
12. Number P (2017) People's Republic of China: Guizhou rocky desertification area water management project (6)
13. Zhou H (2014) ScholarWorks @ UMass Amherst Redevelopment of Urban Village in Shenzhen (8)
14. Hao P, Sliuzas R, Geertman S (2011) The development and redevelopment of urban villages in Shenzhen. *Habitat Int* 35(2):214–224. <https://doi.org/10.1016/j.habitatint.2010.09.001>
15. Government of India Ministry of Home Affairs Directorate General FS, CD & HG Compilation of Minutes of the Meetings of the Standing Fire Advisory Committee/Council from 1 st Meeting to 38 th Meeting
16. Directorate General NDRF & Civil Defence (Fire) (2011) Fire hazard and risk analysis in the country for revamping the fire services in the Country final report-state wise risk assessment, infrastructure and institutional assessment of pilot states, [Online]. Available: www.rmsi.com

Investigating the Effects of Steel Fibre and Basalt Fibres on the Mechanical Properties of Hybrid Fibre-Reinforced High-Performance Concrete



Parvathy Subrahmaniam and P. Seena

Abstract This paper presents the development of hybrid fibre reinforced high-performance concrete (HFRHPC) using basalt fibre and steel fibre. The basalt fibre and steel fibre were used to improve the mechanical properties of the concrete. Both fibres were used to improve the tensile strength of the concrete. In this study, the mix proportions of M60 grade HPC has been arrived based on the method proposed by Prof. Aitcin which was derived from the guidelines given by ACI 211.1 The Hybrid fibre-reinforced High-performance concrete was obtained by adding different volume fractions of basalt and steel fibres. The percentages of steel fibres considered include 0.5, 1, 1.5 and 2%. Whereas the percentages of basalt fibres considered include 0.1, 0.3 and 0.5%. An attempt was made to obtain the relation between the various engineering properties with the percentage of fibres added. In general, the addition of fibres improved the mechanical properties of both HPC and HFRHPC. However the increase was found to be minimal in the case of while adding basalt fibre. The outcome of this investigation will be useful in structures subjected to stress reversals.

Keywords High performance concrete · Hybrid fibre reinforced high performance concrete · Steel fibres · Basalt fibres

1 Introduction

High-performance concrete (HPC) is a type of concrete that is designed to possess superior mechanical and durability properties compared to traditional concrete. One way to enhance the mechanical properties of HPC is by reinforcing it with Fibres. Steel Fibres have been commonly used as a reinforcing material in concrete, but there has been growing interest in using basalt Fibres as well due to their unique properties.

P. Subrahmaniam (✉) · P. Seena
Government Engineering College, Thrissur, India
e-mail: tcr21cese13@gectcr.ac.in

The aim of this study is to investigate the effects of steel and basalt Fibres on the mechanical properties of hybrid Fibre-reinforced HPC. The hybrid Fibre reinforcement is expected to provide better performance compared to using just one type of Fibre. The mechanical properties that will be investigated include compressive strength, tensile strength and flexural strength.

The study will involve preparing different mixtures of HPC with varying percentages of steel and basalt Fibres. The samples will then be tested for their mechanical properties and compared to samples without Fibres as well as samples with only one type of Fibre. The results will provide insight into the potential benefits of using hybrid Fibre reinforcement in HPC and the optimal mixture of Fibres for achieving the desired mechanical properties.

2 Experimental Program

2.1 Materials and Mix Proportions

Ordinary Portland Cement (OPC) of 53 Grade conforming to IS: 12,269-1987 (reaffirmed 2004) [1] was used and the properties are shown in Table 1. M. sand passing through 4.75 mm IS sieve conforming to grading zone II of IS: 383-1970 (reaffirmed 2002) [2] was used as fine aggregates. The maximum size of coarse aggregates was limited to 20 mm. Physical properties of fine and coarse aggregates are presented in Tables 2 and 3. The properties of mineral admixtures class F fly ash and silica fume provided by the suppliers are given in Tables 8 and 9. To obtain the required workability for the mix Conplast SP 430 from Fosroc Chemicals, was used. Properties of super plasticizer provided by the manufactures are given in Table 4. In the present paper, the hybrid mixes were prepared with the use of steel and basalt fibres. The volume fraction and properties of basalt fibres are shown in Tables 5 and 6 [3]. The hooked end steel fibres having a length 30 mm and diameter 0.5 mm were used for the present study and properties of steel fibres are shown in Table 7 (Figs. 1 and 2).

Table 1 Physical properties of OPC (Grade-53)

Sl. No	Properties	Values		Requirements as per IS:12,269-1987 (reaffirmed 2004)
1	Specific gravity	3.107		–
2	Standard consistency	30%		–
3	Initial setting time	135 min		Not less than 30 min
4	Final setting time	215 min		Not more than 600 min
5	Compressive strength	3 days	27.5 MPa	Not less than 27 MPa
		7 days	37.8 MPa	Not less than 37 MPa
		28 days	54.2 MPa	Not less than 53 MPa

Table 2 Physical properties of fine aggregate

Sl. No	Properties	Values
1	Particle size distribution	Zone II
2	Specific gravity	2.67
3	Water absorption	1.5%

Table 3 Physical properties of coarse aggregates

Sl. No	Properties	Values
1	Bulk density	1.5 g/cc
2	Specific gravity	2.88
3	Water absorption	0.82%

Table 4 Properties of super plasticizer

Product name	ConplastSP430
Specific gravity	1.22 at 30 °C
Chloride content	Nil to IS 456
Air entrainment	1–2% additional air is entrained

Table 5 Properties of basalt fibre

Particulars	Observed value
Length of fibre (mm)	12
Specific Gravity	0.91
Diameter of fibre (mm)	0.015
Density	2670 kg/m ³
Tensile strength (MPa)	4100–4840
Elastic modulus (GPa)	100

Table 6 Composition of basalt fibres [3]

SL. NO	Chemical name	Percentage (%)
1	SiO ₂	51.6–59.3
2	Al ₂ O ₃	14.6–18.3
3	CaO	5.9–9.4
4	MgO	3.0–5.3
5	Na ₂ O + K ₂ O	3.6–5.2
6	TiO ₂	0.8–2.25
7	Fe ₂ O ₃ + FeO	9.0–14.0
8	Others	0.09–0.13

Table 7 Properties of steel fibre

Length of fibre	30 mm
Diameter of fibre	0.5 mm
Aspect ratio	60
Density	7850 kg/m ³
Ultimate tensile strength	800 MPa

Table 8 Properties of fly ash

Specific gravity	2.40 (%)
Silica, SiO ₂	55.39
Iron oxide, Fe ₂ O ₃	9.80
Alumina, Al ₂ O ₃	23.20
Calcium oxide, CaO	5.58
Magnesium oxide, MgO	1.31
Sulphate, SO ₃	1.80
Potassium oxide, K ₂ O	2.92

Table 9 Properties of silica fume

Specific gravity	2.10
SiO ₂	90.36%
Moisture content	0.60%
Retained on 45 microns sieve	0.40%
Bulk density	640 kg/m ³

Fig. 1 Basalt fibre

Fig. 2 Hooked end steel fibre



Table 10 Mix proportions of HPC

Cement (Kg/m ³)	Fly ash (Kg/m ³)	Silica fumes (Kg/m ³)	Fine aggregate (Kg/m ³)	Coarse aggregate (Kg/m ³)	Water (Kg/m ³)	Super plasticizer (Kg/m ³)
405	110	45	680	1042	172	12.62

In this study, the mix proportions of M60 grade HPC had been arrived based on the method proposed by Prof. Aitcin which was derived from the guidelines given by ACI211.1 [4]. The final mix proportions were obtained by carrying out trial and error with different combinations of materials in the laboratory. Details of mix proportions for M60 grade HPC are shown in Table 10.

Fibres generally tend to stiffen a concrete mix by reducing its workability. Chemical admixture was adjusted for different volume fractions of fibres to maintain constant workability of compacting factor 0.9. The dosage of super plasticizer for each mix was decided after carrying out sequential trials between dosage of super plasticizer and volume fraction of fibres.

2.2 Methodology

The freshly mixed HPC, Steel fibre reinforced HPC and Hybrid fibre reinforced HPC was poured layer by layer, into standard cubes of size 150 × 150 × 150 mm for compressive strength test, 150 × 300 mm cylinders for splitting tensile test and into 100 × 100 × 500 mm prisms for finding modulus of rupture. The total number of specimens were cast consists of six cubes, six cylinders and six prisms.

After 24 h the specimens were demoulded and then immersed in curing tank for a period of 7 and 28 days. The details of specimens are given in Table 11. The 3000 kN Compression Testing Machine was used to determine the compressive strength of the cube specimens. Cube specimens were tested for compressive strength after 28 days of curing, as per IS: 516-1959 (reaffirmed 2004) [5]. Split tensile strength test was carried out on cylindrical specimens of placed horizontally between the loading surfaces of the compression testing machine, as per IS 5816: 1999 (reaffirmed 2004) [6]. The flexural strength test was as per IS 516-1959(reaffirmed 2004) [5]. The specimen was mounted on the universal testing machine as and third-point loading was applied until failure. Figure 3 shows the specimen ready for testing.

Table 11 Experimental programme of HFR-HPC

Sl No	Mix	Mix Designation	Fibre proportion	
			Steel fibre	Basalt fibre
1	HPC – M60	HPC	0	0
2	HPC + Steel fibre	SFRHPC 0.5	0.5	0
3	HPC + Steel fibre	SFRHPC 1.0	1.0	0
4	HPC + Steel fibre	SFRHPC 1.5	1.5	0
5	HPC + Steel fibre	SFRHPC 2.0	2.0	0
6	HPC + Steel fibre + Basalt fibre	HFRHPC 0.1	1.5	0.1
7	HPC + Steel fibre + Basalt fibre	HFRHPC 0.3	1.5	0.3
8	HPC + Steel fibre + Basalt fibre	HFRHPC 0.5	1.5	0.5

Fig. 3 Specimens ready for testing



3 Results and Discussions

3.1 Hardened Properties

Table 12 presents the test results of HPC, SFRHPC and HFRHPC. Each test result was the average of 3 specimens tested after 7 and 28 days. From the table it is clear that the compressive strength, splitting tensile strength and modulus of rupture increased with as the fibre volume fraction increases (Figs. 4 and 5).

Table 12 Test results

Sl No	Mix	Average compressive strength (MPa) (f_{ck})		Average split tensile strength (MPa) (f_t)		Average flexural strength (MPa) (f_r)	
		7th day	28th day	7th day	28th day	7th day	28th day
1	HPC	42.22	60.92	3.53	4.25	5.28	6.46
2	SFRHPC 0.5	45.62	62.43	4.18	5.46	5.42	7.22
3	SFRHPC 1.0	49.26	65.06	4.86	5.65	5.8	8.02
4	SFRHPC 1.5	53.11	68.27	5.48	6.52	7.84	9.16
5	SFRHPC 2.0	52.26	67.12	5.21	6.07	7.65	8.78
6	HFRHPC 0.1	51.33	65.56	6.17	6.98	8.05	8.95
7	HFRHPC 0.3	52.06	66.75	6.48	7.05	8.38	9.42
8	HFRHPC 0.5	51.92	66.60	6.62	7.12	8.74	9.77

Fig. 4 Compressive strength test of cube



Fig. 5 Flexural strength test

Compressive strength (f_{ck})

The Compressive strength was obtained by dividing the maximum load by the area of cross section of the specimen.

$$\text{Compressive strength} = P/A \quad (1)$$

where, P = the failure load A = area of cross section of specimen.

Referring to Table 12, it may be observed that, rate of strength development is higher for SFRHPC and HFRHPC compared to HPC. The reason may be due to the bridging effect of fibres and thereby it delays the crack propagation in concrete. The maximum increase is about 12.07% for SFRHPC and 9.60% for HFRHPC. Figure 6 shows the comparison of compressive strength of HPC with SFRHPC and HFRHPC it may be noted from the figure that the maximum and minimum compressive strength was obtained for SFRHPC is 68.27 MPa and 62.43Mpa respectively. Whereas it was 66.75 MPa and 65.56 MPa for HFRHPC.

Split tensile strength (f_t)

The Split tensile strength was obtained by using the equation.

$$\text{Split tensile strength} = 2P/\pi DL \quad (2)$$

where: P = failure load, D = diameter of cylinder, L = length of cylinder.

Referring to Table 12, it may be observed that, rate of tensile strength development is higher for SFRHPC and HFRHPC compared to HPC. During testing the bridging action of fibres at the crack was noted in all specimens containing steel fibres and

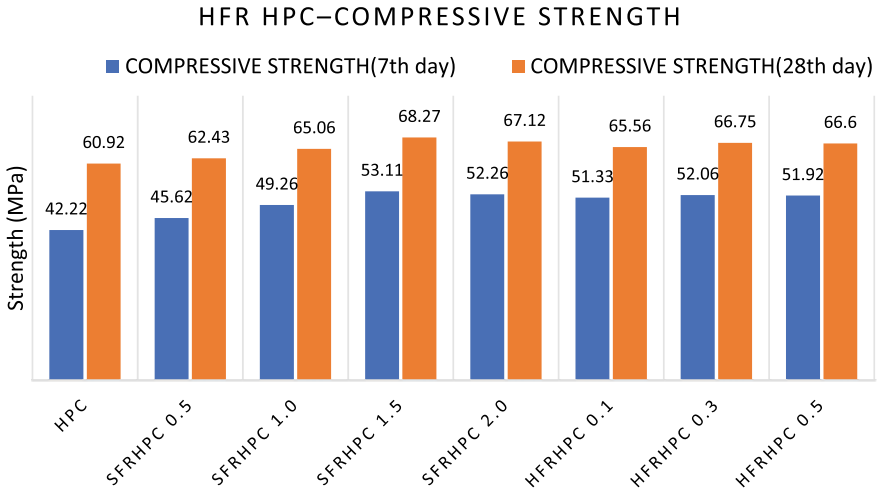


Fig. 6 Compressive strength test results

basalt fibres. The failure mode was brittle in the case of HPC but the failure mode of SFRHPC and HFRHPC did not completely split into two halves at failure. The addition of Basalt fibre into the steel fibre enhances the tensile strength of the specimen for about 9.20%. The maximum increase is about 53.41% for SFRHPC and 67.53% for HFRHPC. Figure 8 shows the comparison of split tensile strength of HPC with SFRHPC and HFRHPC it may be noted from the figure that the maximum and minimum split tensile strength was obtained for SFRHPC is 6.52 MPa and 5.46 MPa respectively. Whereas it was 7.12 MPa and 6.98 MPa for HFRHPC (Fig. 7).

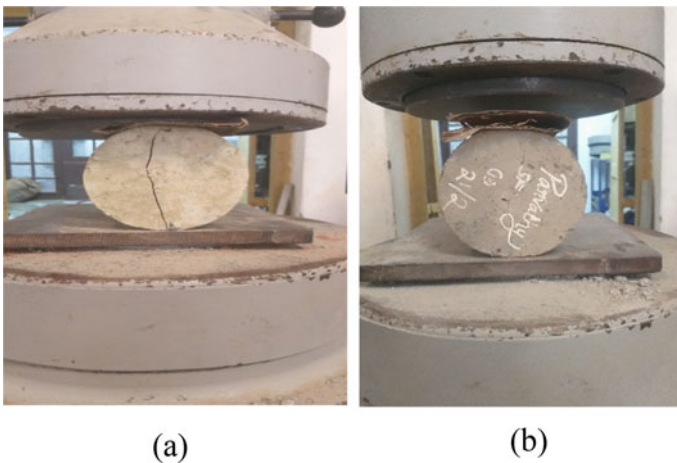


Fig. 7 Split tensile strength test **a** HPC specimen after testing **b** HFR HPC specimen after testing

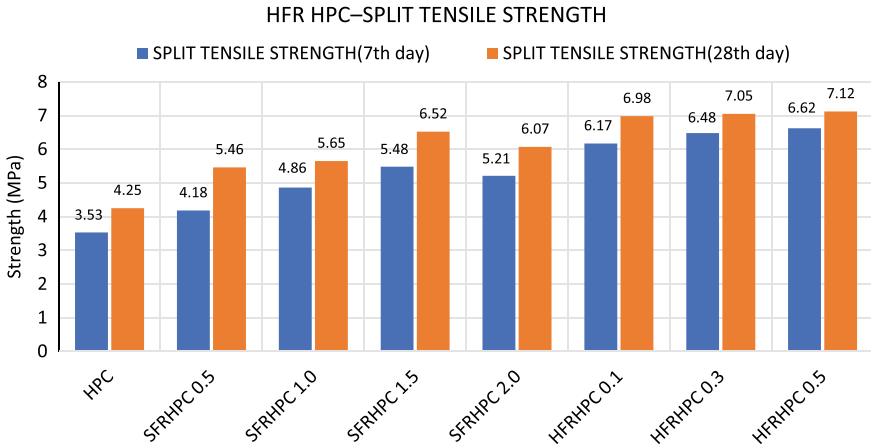


Fig. 8 Split tensile strength test results

Flexural strength (f_r)

The Flexural strength was obtained by using the equation.

$$\text{Flexural strength} = Pl/bd^2, \text{ when } a > 133 \text{ mm} \tag{3}$$

$$\text{Flexural strength} = 3Pa/bd^2, \text{ when } 110 < a < 133 \text{ mm} \tag{4}$$

where: P = failure load, a = the distance between the line of fracture and the near support measured on the central line of the tensile side of the specimen, L = length of specimen between supports, b = width of the specimen, d = depth of specimen.

Referring to Table 12, it may be observed that, rate of flexural strength development is higher for SFRHPC and HFRHPC compared to HPC. From the Fig. 9 it can be noted that as the volume fraction of fibres increases, f_r gradually increases and there is significant improvement in the value of f_r in the case of HFRHPC. These trends can be explained using the same concept of fibre bridging and crack propagation. The maximum increase is about 41.80% for SFRHPC and 51.24% for HFRHPC. Figure 9 shows the comparison of Flexural strength of HPC with SFRHPC and HFRHPC it may be noted from the figure that the maximum and minimum flexural strength was obtained for SFRHPC is 9.16 MPa and 7.22 MPa respectively. Whereas it was 9.77 MPa and 8.95 MPa for HFRHPC.

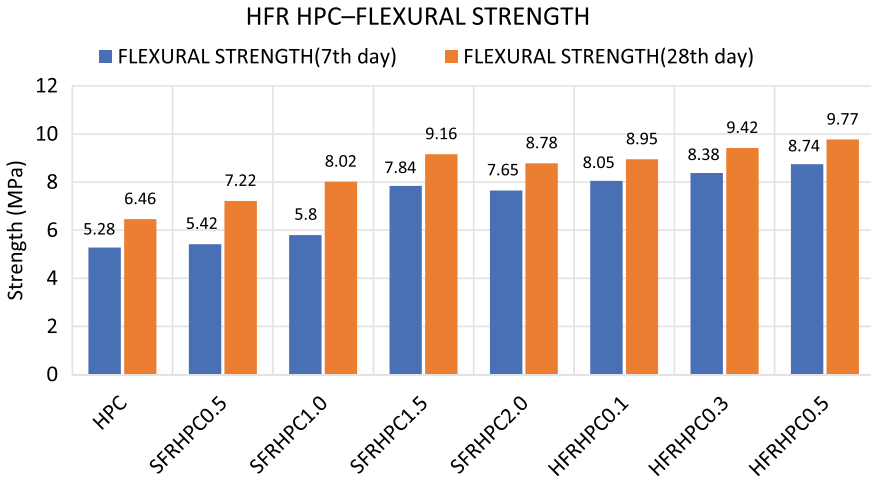


Fig. 9 Flexural strength test results

4 Conclusion

Based on the research conducted on the effects of steel and basalt Fibres on the mechanical properties of hybrid Fibre-reinforced high-performance concrete, the following conclusions can be drawn:

1. The addition of both steel and basalt Fibres to high-performance concrete (HPC) resulted in improved mechanical properties, including compressive strength, tensile strength, and flexural strength. The hybridization of steel and basalt Fibres in HPC showed superior results compared to using only one type of Fibre.
2. The optimal dosage of Fibres for both steel and basalt was found to be 1.5 and 0.5% by volume of concrete.
3. The use of hybrid Fibres led to enhanced post-cracking behavior of HPC. The addition of Fibres resulted in a reduction in the brittleness of HPC.
4. Compressive strength at 28 days is maximum for SFRHPC1.5 (HPC + 1.5%SF), is increased by 12.07% andHFRHPC0.3 (HPC + 1.5%SF + 0.3%BF) is increased by 9.60%with respect to normal HPC.
5. Split tensile strength at 28 days for SFRHPC1.5 (HPC + 1.5%SF) is increased by 53.41% andHFRHPC0.5 (HPC + 1.5%SF + 0.5%BF) is increased by 67.53%with respect to normal HPC.
6. Flexural strength at 28 days for SFRHPC1.5 (HPC + 1.5%SF), is increased by 41.80% andHFRHPC0.5 (HPC + 1.5%SF + 0.5%BF) is increased by 51.24%with respect to normal HPC.
7. The steel Fibres were found to be more effective in enhancing the compressive strength and flexural strength of HPC, while basalt Fibres were more effective in improving the split tensile strength of HPC.

Overall, the findings of this study suggest that the use of a hybrid combination of steel and basalt Fibres in HPC can significantly enhance the mechanical properties of concrete and improve its performance and is useful in structures subjected to stress reversals.

References

1. BUREAU OF INDIAN STANDARDS IS 516–1959 (2002) Indian standard methods of tests for strength of concrete
2. Junwei Z, Shijie L, Hongjian P (2021) Experimental investigation of multiscale hybrid fibres on the mechanical properties of high-performance concrete. *Constr Build Mater* 299
3. Ayub T, Shafiq N, Nuruddin MF (2014) Effect of chopped basalt Fibers on the mechanical properties and microstructure of high performance fiber reinforced concrete. *Adv Mater Sci Eng* 14:587686
4. Aitcin PC (2004) High performance concrete 2nd edition. Taylor and Francis e-Library
5. BUREAU OF INDIAN STANDARDS, IS 383 (1970) Specifications for coarse and fine aggregates
6. BUREAU OF INDIAN STANDARDS IS 456 (2000) Indian standard –plain and reinforced concrete

Sewage Sludge and Red Mud as Brick Materials



Divya S Lal and Jeena B Edayadiyil

Abstract Sludge resulting from wastewater treatment plants has disposal problems. Generally, this sludge is disposed by spreading on the land or by landfilling. However, for cities which are urbanized, sludge disposal by landfilling might not be appropriate due to limited area. Incineration can create very big amount of ash and that must be disposed by other means. With growing social awareness about toxic incinerator emissions and the increasing concern over the disposal of sludge onto agricultural land, it seems obvious that the recovery of sewage sludge as a building and construction material can be considered as an important step in the right direction. The use of sludge in construction industry is considered to be the soundest option both economically and environmentally. Sludge produced in the treatment plant can be effectively used in manufacture of bricks and the quantity of waste produced can be minimized. Red mud (RM) is a by-product from alumina production through Bayer process. The production of RM was estimated about four billion tons. Recycling of this big amount of alkaline waste is considered to be a serious challenge. Utilizing RM as a raw material to make bricks seems like a promising option. Also, there are substances in RM which can lower the sintering temperature of bricks. The current research focuses on the effective utilization of sewage sludge and red mud in clay bricks to minimize the impact of massive dumping of these materials on the environment. Also the study aims to create a material with quality and economy. From the study, it is understood that even though the high organic content will decrease the mechanical properties, it can give out bricks which are environmentally sustainable. As these bricks are third class bricks, it can be effectively used in non-load bearing structures.

Keywords Sewage sludge · Sustainable · Red mud

D. S. Lal (✉) · J. B. Edayadiyil
Department of Civil Engineering, Amal Jyothi College of Engineering, Kottayam, Kerala, India
e-mail: divyaslal@ce.ajce.in

J. B. Edayadiyil
e-mail: jeenabedayadiyil@amaljyothi.ac.in

1 Introduction

Urban areas produce an enormous amount of sewage sludge, thus it's important to develop an effective and environmentally friendly technique of treating municipal wastewater [1]. Sludge cannot be disposed of directly since it may have negative environmental effects. High levels of pathogens, heavy metals, and unstable organic components are present in sewage sludge. The proper disposal of large amounts of sewage sludge is still a significant problem. Reusing it in construction could help create greener products and lessen the negative environmental effects of sludge creation [2]. Four billion tonnes of RM were produced globally, with output rising at a rate of 150 million tonnes year. This obviously calls for the creation and application of large-scale RM reuse. However, due to its high alkalinity and trace amounts of radioactive and heavy metal components, this enormous amount of alkaline waste is thought to pose a severe problem to the alumina industry and should be addressed in research on RM recycling [3]. The production of bricks using RM as a supplementary raw material can completely utilize practically all of the created waste. Additionally, RM contains a variety of chemicals that can reduce the sintering. However, the variables (heavy metals, alkalinity, radioactivity, etc.) that caused issues during its landfill remain in the RM. Therefore, proof that these materials do not provide a risk to the environment or health is required before they can be successfully used (in increased quantities) in bricks [3].

The valorization of sewage sludge from wastewater treatment plants as a raw material in the production of red ceramic bricks by extrusion is found to be highly feasible. It was also found that sewage sludge does not present environmental risk in terms of the leachability of heavy metals [4]. Without having any negative impacts on the health of those who use the finished products, the procedure of inerting sludge on clay bricks might be applied. The ceramic sector has a significant potential for using WWTP sewage sludge in the industrial process because of its enormous productivity [5]. However, compressive strength can be lower as a result of the introduction of larger sludge additive percentages. This was explained as being caused by samples with large sludge proportions having lower silica (SiO_2) contents, which are responsible for the produced specimen's mechanical strength [6]. Water absorption of the fired product was also found to be affected by the presence of sludge [7]. It is found to be difficult to determine how sewage sludge affects the characteristics of bricks. The brick's rough surface, which was brought about by the burning of big sewage sludge particles, appears to have reduced its compressive strength, although fewer micro pores in the microstructure increased resistance to freeze–thaw [8]. The most amount of sludge that could be added while still producing clay bricks that meet the requirements for mechanical strength and water absorption was 15 wt%. [6].

It is quite feasible to manufacture sintered bricks with RM [9] Red mud brick shows greater characteristic performances than regular brick. Water absorption is also greater but within limits, size changes, and weight losses of red mud bricks are found to be minimal [9]. Many researches shows that utilizing red mud in the construction industry is a better option as it reduces the damages the red mud causes when it remains in landfills. Cost, compared to conventional brick production can be reduced as incorporating these wastes into the bricks.

In this research, different dosages of SS (5, 10, 15, 20%) on clay bricks is analyzed and an optimum percentage of 15% has been chosen. Analysis was later done on the effect of different dosages of red mud (5, 10, 15%) with a constant percentage of SS. Study was conducted on how the variables affected the compressive strength and microstructure of the finished SS and RM incorporated bricks. To assess the effects of RM and SS recycling in bricks, analyses of water absorption and efflorescence were performed.

2 Materials and Methodology

2.1 Materials Used

Materials which were used in the tests are sewage sludge (SS), Red mud (RM) and clay. Sewage sludge was collected from the waste water treatment plant of Amal Jyothi College of Engineering, Kanjirappally. Red mud was collected from a local supplier and clay from a privately operated brick factory near Neyyattinkara, Thiruvananthapuram. It was found that the sewage sludge has a specific gravity of 1.18 g/cm^3 , red mud has 2.8 g/cm^3 and clay has 2.36 g/cm^3 . As collected, sludge additive was in an aqueous impure form. It had a water content approximately of 70%. Collected sewage sludge was dried in sun for about a month. After the procedure of drying, it was sieved to remove coarse particles. Then it was crushed using a jaw crusher followed by sieving so that the particles are less than 1.36 mm. Dried, filtered and powdered Sewage sludge, Red mud and Clay were characterized and mentioned in Tables 1, 2, 3 and 4.

Table 1 Properties of sewage sludge used

	Sludge properties
Optimum moisture content	53%
Dry density	$6.535 \times 10^{-4} \text{ kg/cc}$
Liquid limit	132%
Plastic limit	52%
Specific gravity	1.081 g/cm^3

Table 2 Properties of red mud used

	Red mud properties
Optimum moisture content	34%
Dry density	1.229×10^{-3} kg/cc
Liquid limit	45%
Plastic limit	32%
Specific gravity	2.8 g/cm ³

Table 3 Properties of clay used

	Clay properties
Optimum moisture content	26%
Dry density	1.481×10^{-3} kg/cc
Liquid limit	45%
Plastic limit	25%
Specific gravity	2.113 g/cm ³

Table 4 Chemical composition

Chemical compounds	Clay (%)	SS (%)	RM (%)
SiO ₂	44.4	14.20	14.4
TiO ₂	0.95	0.66	5.59
Al ₂ O ₃	27	6.29	21.5
MnO	0.03	0.05	–
Fe ₂ O ₃	6.87	4.62	43.59
CaO	0.25	14.50	1.89
MgO	0.32	1.44	–
Na ₂ O	0.1	0.38	11.6
K ₂ O	0.99	1.07	0.18
P ₂ O ₅	0.09	2.90	0.12
Cl	–	0.66	–
SO ₃	–	9.96	0.42
LOI	0.77	42.86	0.054

2.2 Sample Preparation

Table 5 provides the amount and ratios of mixtures. Including the reference mixture, it was decided on 5 mixtures. Stirring for 10 min gave a homogenous dispersion between materials. Standard sized Brick samples (19 × 9 × 9 cm) were prepared using a laboratory hydraulic press. Samples were kept in room temperature for 48 h

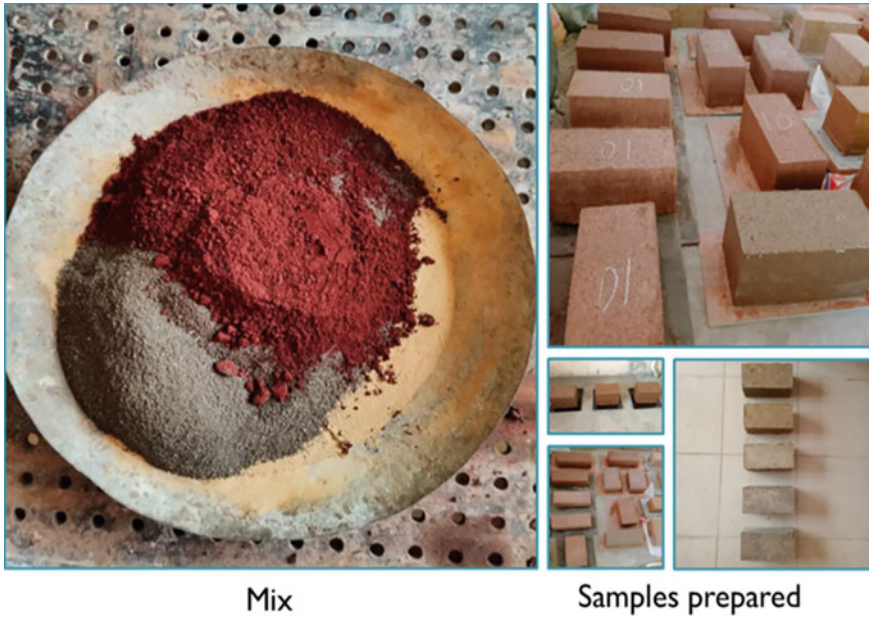


Fig. 1 Sample preparation

Table 5 Mix proportions of materials

Mixtures of test samples (%)		
Clay	SS	RM
100	0	0
85	15	0
80	15	5
75	15	10
70	15	15

followed by oven drying for 48 h. Curing temperature of 900 °C had been chosen. Samples were heated until the temperature reached to 900 °C and maintained the temperature for 2 h. After the internal temperature of the furnace reached down to room temperature, samples were removed from it. Figure 1 represents the mixture preparation and final product.

2.3 Tests on Samples

Tests are performed on the processed bricks. Water absorption, compressive strength, efflorescence and microstructure analysis were done on the specimens according to

Indian testing standards. To ensure the accuracy, three trials were performed on each tests and the mean value was selected.

3 Results and Discussion

3.1 Compressive Strength

Compressive strength of specimens made with sewage sludge, red mud and clay are analysed to check whether they conform to standards. It is checked to obtain the load carrying capacity of bricks. It was tested under universal testing machine (UTM). It was analysed in reference to IS: 3495 (Part I) and IS 1077 (1970). The result obtained from brick specimens with various proportions is given in Table 6. Compressive strength test showed a decrease in strength as the red mud content increased. It is understood that the addition of 15% SS and 10% RM were the maximum found to still produce bricks with compressive strength that attend the standards. When the red mud addition was 10%, compressive strength was noted as 38.167 kg/cm² which is in the limits. However, it reduced when the red mud addition was raised to 15%. As the diversity of waste increases, it has been found that the compressive strength of bricks reduces. This might be due to the lower SiO₂ content as the waste percentage increase. This will reduce the friction between particles leading to open pores. It might be reason to lower mechanical properties. The reduction in the proportion of earth will affect the crystalline structure and thus the compressive strength will be reduced in sludge added bricks.

3.2 Water Absorption

The water absorption test on bricks was conducted to determine the durability property of bricks. The results of burnt bricks are obtained to compare its resistance to absorption. It is tested for water absorption in accordance with IS: 3495 (Part II) and IS 1077 (1970). The results obtained from the bricks are given in Table 7. Water absorption is highly related to the pores present in it. This property highly affects the durability of bricks. Pores are closed when the sintering occurs. It is understood that the specimens made have water absorption value less than 20% and within limit. So they are safe to use.

3.3 Efflorescence

Efflorescence test is usually done to determine the presence of alkalinity in bricks. Presence of alkalinity can even cause corrosion. Therefore it is important to check. It is done in accordance to IS: 3495 (Part III). Table 8 provides the efflorescence results. It is understood that specimens without red mud shows slight efflorescence. Samples with red mud content up to 10% exhibit a moderate efflorescence while samples above 10% exhibit heavy efflorescence on the other hand (Table 8).

Table 6 Compressive strength test results

Mixtures of test samples (%)			Compressive strength	
Clay	SS	RM	N/mm ²	kg/cm ²
100	0	0	5.723	58.357
85	15	0	4.327	44.123
80	15	5	4.123	42.042
75	15	10	3.743	38.167
70	15	15	3.392	34.588

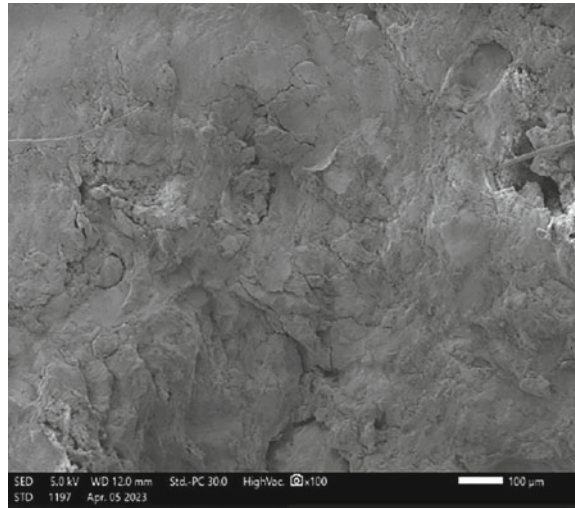
Table 7 Water absorption test results

Mixtures of test samples (%)			Water absorbed in %
Clay	SS	RM	
100	0	0	13.654
85	15	0	16.753
80	15	5	18.965
75	15	10	19.892
70	15	15	20.205

Table 8 Efflorescence test results

Mixtures of test samples (%)			Observation	
Clay	SS	RM	Efflorescence in %	Classification
100	0	0	Below 10	Slight
85	15	0	Below 10	Slight
80	15	5	Below 25	Moderate
75	15	10	Below 25	Moderate
70	15	15	Above 25	Heavy

Fig. 2 SEM image of reference sample



3.4 *Microstructure*

The final mechanical and durability capabilities of tested materials are directly influenced by their structural characteristics. Here, SEM was employed to characterize the bricks' constituents. The textural behaviour was provided via SEM.

SEM images of specimens are given in Figs. 2, 3, 4, 5 and 6. It is clear that the sewage sludge generally disrupts the structure of bricks. Bonding of particles is also less in sludge incorporated specimens. SEM micrographs show that RM has a significant degree of agglomeration and irregular particles. However it improves the microstructure to a degree compared to the control mix. Even though it was observed that the glassy structures are forming as we incorporated red mud, it doesn't give much result in compressive strength compared to reference specimen. It does give a hint about properties not being changed positively because of waste diversity.

Fig. 3 SEM image of control mix

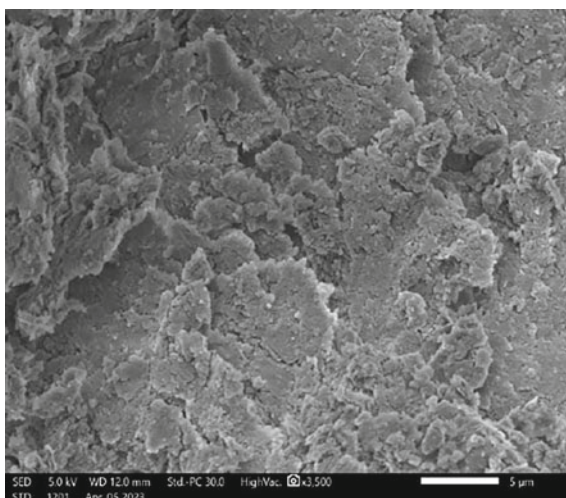


Fig. 4 SEM image of 5% red mud incorporated specimen

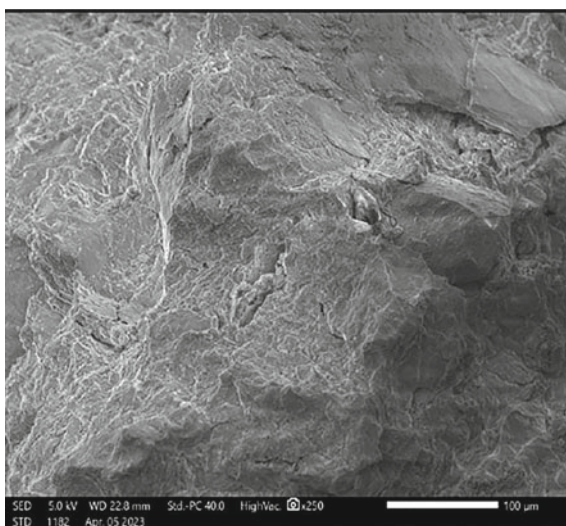


Fig. 5 SEM image of 10% red mud incorporated specimen

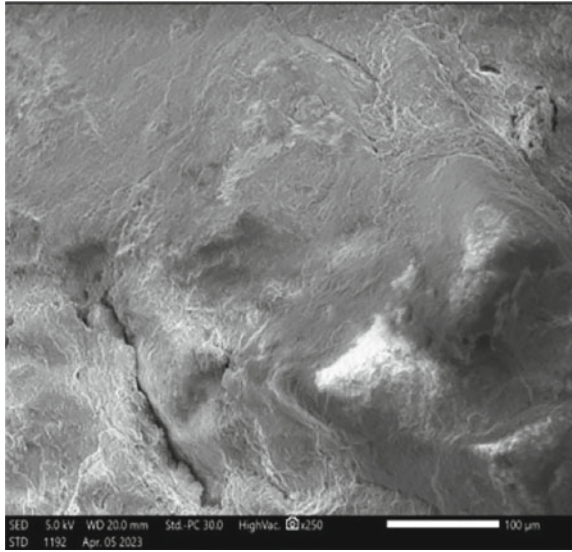
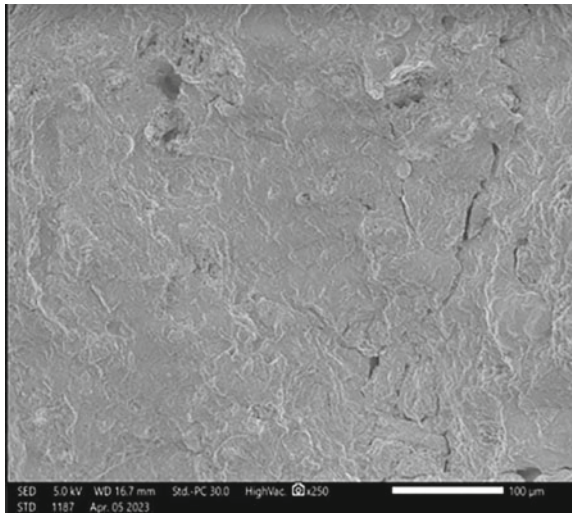


Fig. 6 SEM image of 15% red mud incorporated specimen



4 Conclusion

It has been investigated as a potential alternative to dumping sewage sludge into landfills to use it as a raw material for creating clay bricks. Due to the widespread usage of ceramic materials in the construction industry, it has been demonstrated that this alternative is both practical and intriguing. However, it runs into certain environmental problems and some user prejudice. In comparison to traditional burnt

bricks, the use of Red Mud as a brick-making material is an economically and environmentally sound choice. It is found that bricks with sludge and red mud additions can be used for construction works. As these are third class bricks, it can be used in non-load bearing structures. The strength of bricks reduces as the percentage of waste increases. An addition of 10 wt% red mud was the maximum found to still produce clay bricks that attend the standards of compressive strength. Since it is a third class brick, we can only use it for non-load bearing structures. It is acknowledged that the specimens produced have a water absorption value that is below 20% and acceptable. Samples with red mud content up to 10% showed a moderate efflorescence, whilst samples with a red mud content of more than 10% show significant efflorescence. Red mud was an excellent addition to the mixture because it reduced flaws. It is evident that sewage sludge generally messes with the bricks' structural integrity. Particle bonding is also less evident in specimens with sludge incorporation. SEM micrographs demonstrate that RM contains substantial amounts of irregular particles and agglomeration. In contrast to the control mix, it does improve the microstructure. Red mud was added, and although glassy structures were seen to emerge, the compressive strength of the material was not considerably good from the reference specimen. It does provide a suggestion that the diversity of waste may not have a good impact on certain properties. It is found that red mud incorporation of 10% with a sewage sludge content of 15% in clay bricks can be beneficial for both humanity and nature.

References

1. Gürtekin E (2019) Experimental and numerical design of renewable-energy-supported advanced biological wastewater treatment plant. *Int J Environ Sci Technol* 16:1183–1192
2. Li Y, Zhuge Y, Chow CW, Keegan A, Li D, Pham PN, Siddique R (2020) Utilization of drinking water treatment sludge in concrete paving blocks: microstructural analysis, durability and leaching properties. *J Environ Manag* 262:110352
3. He H, Yue Q, Su Y, Gao B, Gao Y, Wang J, Yu H (2012) Preparation and mechanism of the sintered bricks produced from Yellow River silt and red mud. *J Hazard Mater* 203:53–61
4. Zat T, Bandiera M, Sattler N, Segadas AM, Cruz RCD, Mohammed G, Rodriguez ED (2021) Potential reuse of sewage sludge as a raw material in the production of eco-friendly bricks. *J Environ Manag* 297(2021):113238
5. Luo L, Li K, Fu W, Liu C, Yang S (2019) Preparation, characteristics and mechanisms of the composite sintered bricks produced from shale, sewage sludge, coal gangue powder and iron ore tailings. *Constr Build Manag* 232(2020):117250
6. Houssame Limami AC, Imad Manssouri A, Khalid Cherkaoui B, Khaldoun A (2021) Recycled waste water treatment plant sludge as a construction material additive to ecological lightweight earth bricks. *Cleaner Eng Technol* 2(2021):100050
7. Areias IOR, Vieira CMF, Colorado HA, Delaqua GCG, Monteiro SN, Azevedo ARG (2020) Could city sewage sludge be directly used into clay bricks for building construction? A comprehensive case study from Brazil. *J Build Eng* 31(2020)101374
8. Chen Y-C, Kuo J (2016) Potential of greenhouse gas emissions from sewage sludge management: a case study of Taiwan. *J Cleaner Prod* 129(2016):196–201

9. Arroyo F, Luna-Galiano Y, Leiva C, Vilches LF, Fernández-Pereira C (2020) Environmental risks and mechanical evaluation of recycling red mud in bricks. *Environ Res* 186:109537
10. Khanlari A, Tuncer AD, Sozen A, Şirin C, Gungor A (2020) Energetic, environmental and economic analysis of drying municipal sewage sludge with a modified sustainable solar drying system. *Solar Energy* 208(2020):787–799

Experimental Evaluation of Structural Properties of Circular Scrap Tyre Pad (CSTP) Base Isolator



M. Anandhakrishnan, Asif Basheer, and Ancy Mathew

Abstract Base isolation systems have conventionally been used as a tool for mitigating the impacts of earthquakes on civil structures and to attenuate their seismic responses. Optimal design of base isolator has a vital role in the performance of a structure in response to earthquake. The study focuses on the development of low-cost circular scrap tyre pad (CSTP) base isolator in unbonded configuration. The compression and shear properties of isolators were investigated to check the vertical stiffness and lateral flexibility. The study also investigates the effect of shape factor and vertical pressure on structural properties of isolator. The result reveals that the shape factor and vertical pressure has a considerable effect on the lateral performance of the CSTP base isolator.

Keywords Base isolation · Circular scrap tyre pads · Shape factor · Lateral performance

1 Introduction

Recent earthquakes in developing nations demonstrate the significance of low-cost seismic isolation systems. Conventionally the lead rubber bearings, steel-reinforced elastomeric isolators (SREIs), friction pendulums (FPS) etc. were used to isolate the structure from seismic response. The studies suggest that sliding type of isolation systems like the friction pendulum, FPS [1] and its modifications like the variable friction pendulum systems, VFPS [2], the multiple friction pendulum system, MFPS [3] and double concave friction pendulum, DFPS [4] are effective in base isolation. But the cost associated with the manufacturing and implementation of these systems

M. Anandhakrishnan (✉) · A. Basheer
TKM College of Engineering, Kollam, Kerala 691005, India
e-mail: anandhan1618@gmail.com

A. Mathew
APJ Abdul Kalam Technological University, Thiruvananthapuram, Kerala 695016, India

makes it uneconomical for developing countries to afford. Steel-reinforced elastomeric isolators (SREI) are expensive owing to their high production costs resulting from labour-intensive manufacturing and vulcanization processes [5–7].

In comparison to a fixed base, the base isolation system can significantly increase the structure's lifespan and reduce base shear by up to 75%. The researches indicate that steel strands in scrap tyre pads (STPs) behave similarly to steel plate in rubber-based isolators, RB [8]. The studies conducted on unbonded and bonded conditions of STPs suggest that because of the roll-over deformation occurring in the unbonded system, a much longer time period can be achieved due to the reduction in contact area. After full rollover, there is an abrupt increase in stiffness that serves as a safety mechanism against large displacements during earthquakes [9]. The rollover deformation also lowers stress demand on rubber material. Hence, the peeling stress on the interface between rubber and fibre will be considerably reduced and the STP can show a stable hysteresis loop and good energy dissipation and damping characteristics [10]. The vertical stiffness of the STP isolator is found to be adequate to bear the structural weight load of buildings and prevent the structure from seismic loads [11]. The performance of a three-story shear structure isolated at the base with scrap tyre pad (STP) bearings has been investigated and studied [12]. The feasibility study of the unbonded STPs to be used as an isolation device is carried out by Basar et al. [13].

Being a waste material, Scrap Tyre Pads (STPs) can be considered as a cost-effective option for seismic isolation. The STPs are light in weight, easily available and are having good damping properties, as compared to the conventional base isolation systems. The possibility of using Scrap Tyre Pads as base isolators has been studied by various researches [14, 15]. The presence of steel strands within the tyre layers not only prevents the lateral bulging but also permits the lateral movements. A crucial parameter for a base isolator is the ratio of vertical to horizontal stiffness. The ratio of vertical to horizontal stiffness of STPs is proportional to their shape factor. The shape factor is the ratio of the top area to the free to bulge area, which varies with respect to the number of layers. In order to design the STP base isolator with the required utility, it is necessary to determine the effect of the change in vertical and horizontal properties with respect to the change in shape factor. In previous studies, rectangular-shaped scarp tyre pads were used as base isolators, while conventional isolators like lead rubber bearings had a cylindrical shape with a circular top area. Hence this study focuses on the evaluation of scrap tyre pads in circular shape under unbonded condition.

1.1 Specimen Details

The standard sized tyres of 185/65/R15 are selected for the study. 185 indicates the width of the tyre in millimeters and the aspect ratio of the tyre is 65. 15 represents the inner circle diameter of the tyre in inches. Circular shaped samples of diameter 145 cm



Fig. 1 Circular scarp tyre sample

were cut from the tyre. The average thickness of the sample was found to be 9.6mm when measured with a vernier caliper. Figure 1 represents CSTP the specimen.

2 Methodology

Figure 2 depicts the methodology of the study. Based on reviews from the relevant literatures, it is found that STPs can be utilised as a cost-effective method for mitigating the effects of earthquakes on superstructures. The details of the collected sample are described in Sect. 1.1. The scrap tyre samples consist of steel strands within the rubber. To design an isolator, it is necessary to determine the damping ratio, horizontal stiffness, and vertical stiffness. Hence to evaluate the structural behaviour, diameter of the specimen selected is 145 mm and the performance is studied with respect to the change in shape factor. The shape factor is varied by changing the number of layers and the number of layers used are 4, 6, 8 and 10. The specimen's vertical stiffness can be determined by compression testing, and its horizontal stiffness and damping ratio by cyclic shear testing.

3 Experimental Setup and Test

The scrap tyre pad isolator was formed by stacking circular shaped tyre pads one over the other without any bonding agents. The number of layers is varied to study the effect of shape factor on compression properties. In case of cyclic shear test the shape factor is varied in the same manner as explained and performance is analyzed for 1, 2 and 3 MPa (Table 1).

Fig. 2 Methodology of the study

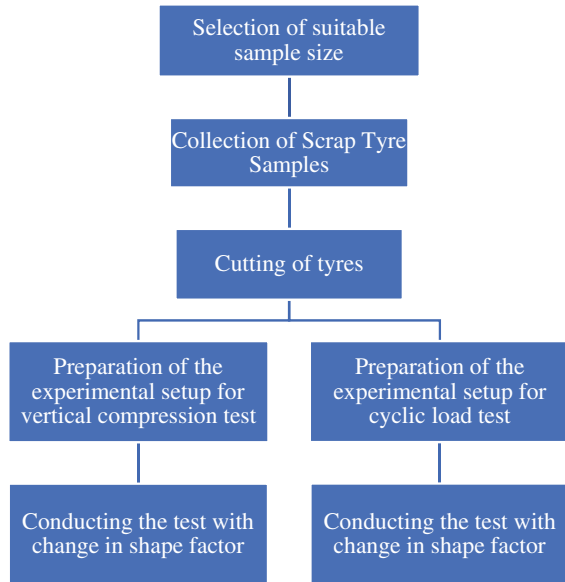


Table 1 The relationship between plane area, height, number of layers and shape factor

Sl. No.	Plan area	Height	Number of layers	Shape factor
1	16,504.625	38.4	4	0.944
2	16,504.625	57.6	6	0.629
3	16,504.625	76.8	8	0.472
4	16,504.625	96	10	0.377

3.1 Compression Testing

In a computer-controlled universal testing apparatus, isolator specimens were subjected to compression tests (Fig. 3a, b). The STPs are equipped with two steel plates at the top and bottom to evenly distribute the applied load.

The specimen was loaded up to approximately 300 kN of force. The scrap tyres consist of steel strands within itself, which contributes to the vertical compression characteristics of the specimen. Hence, the load at which breaking sound of the steel strand observed is taken as the breaking load of the sample. After each trial, specimens were replaced with a fresh batch. Using software created by Fuel Instruments and Engineers Pvt. Ltd., the corresponding load and deformation were recorded digitally on a computer.



Fig. 3 a Experimental setup for compression testing, b CSTP specimen loaded in the compression machine

3.2 *Cyclic Loading Test*

The horizontal shear performance of the CSTP specimen is found by applying a constant vertical pressure and noting the lateral load required for corresponding displacements. The study is conducted to analyze the performance under 1, 2 and 3 MPa vertical pressures. Keeping the vertical pressure constant, using a push pull jack horizontal load is applied. Linear Variable Differential Transformer (LVDT) is used for measuring the horizontal displacement corresponding to the load applied and the value of the displacement is obtained by the means of a digital displacement indicator. The load applied by the push pull jack can be figured out by the means of load indicator. The experimental setup for cyclic loading is as shown in the Fig. 4.

Figure 5a–c represents the behavior of 8 layer specimen under 2 MPa pressure on cyclic loading action. From the experiment it is observed that during the horizontal displacement the specimen is acting as a single unit without any layer separation. Figure 5a, c shows the rollover behaviour of the sample under the loading.

4 Results and Discussion

The shape factor is an important parameter for accessing the properties of the CSTP isolator that depends on the height of the isolator specimen. Hence the study is conducted by keeping the plan area of the considered specimen constant and height of the specimen is increased by increasing the no of layers. The compression test and cyclic loading test is performed by varying the shape factor.



Fig. 4 Experimental Setup for cyclic loading



Fig. 5 a 8 Layer 2 MPa Specimen (+ 18 mm displacement), b 8 Layer 2 MPa Specimen, c 8 Layer 2 MPa Specimen (- 18 mm displacement)

4.1 *Compression Test*

The compression testing of the specimen is done as explained in the Sect. 3.1. The vertical stiffness of a damper is an important parameter which decides whether the specimen can be used as a base isolator or not. The specimen should have enough stiffness under the vertical action of load to be considered as a base isolator.

The load–displacement relation of the CSTP specimen is depicted in Fig. 6. The samples shows a low stiffness value in the initial stages of loading which is due to the curved shape of the tyre pads. But a considerable increase in vertical stiffness is observed after a certain loading for all cases under consideration. The slope of the curves seen decreasing with increase in number of layers. The 4 Layer sample had the highest slope which shows that the isolator had behaved rigidly.

Effect of shape factor on vertical stiffness. The slope of the linear portion in the plot provides the vertical stiffness of CSTP specimen as shown in Fig. 7. The slope of the specimen with change in shape factor is found to understand the effect of shape factor in vertical stiffness. The 10 layer sample with a shape factor of 0.377 found to have the least stiffness among the all cases under consideration [13].

$$\text{Stiffness, } K = \Delta F / \Delta l$$

where, ΔF = change in the load
 Δl = change in the displacement.

Fig. 6 Load versus displacement plot for the CSTP specimens

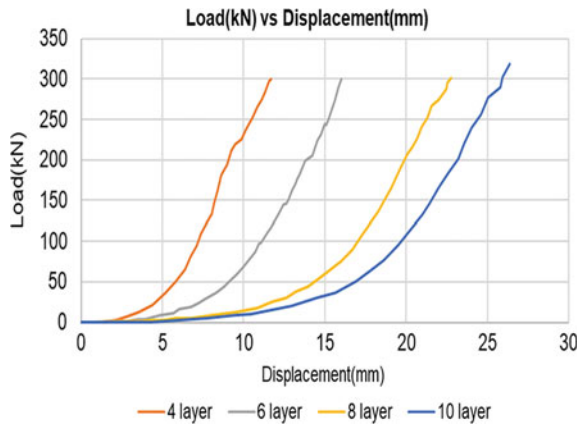
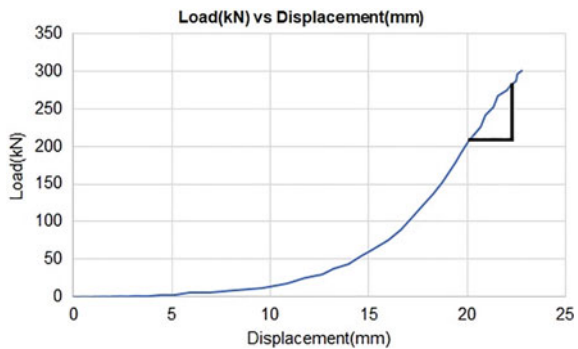


Fig. 7 Load versus displacement plot for the 8 layer CSTP specimen



The variation of the vertical stiffness with shape factor is plotted as shown in the Fig. 8. It shows that with the increase in shape factor the vertical stiffness is found to increase.

Effect of shape factor on compressive strength. The isolator properties depend on the height of the isolator which is a function of shape factor. Hence to study whether the shape factor has an effect on variation of compressive strength, analysis is conducted. The load at which the breakage observed is taken as the load for the calculation of compressive strength and the compressive strength is observed to be in the range of 8.25–8.5 MPa. From the experiment, it is also observed that even after the initial breakage of the steel strands, the specimen where able to take higher loads. The variation of compressive strength with respect to increase in shape factor is plotted as shown in Fig. 9. From the graph it can be observed that with respect to increase in shape factor the compressive strength is also increasing but the variation is negligibly small.

Fig. 8 Variation of vertical stiffness with change in shape factor

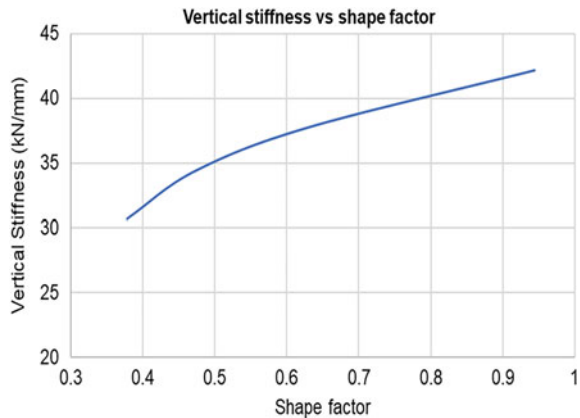
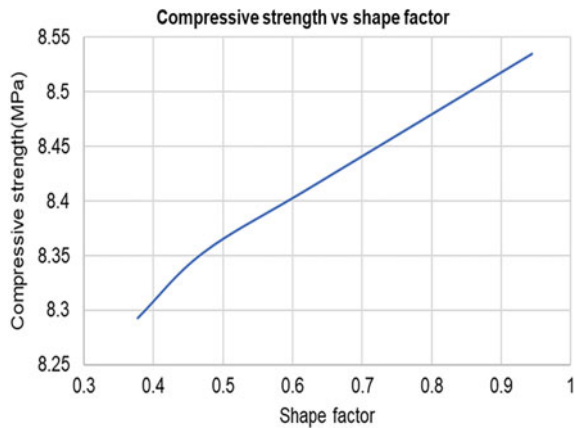


Fig. 9 Variation of compressive strength with shape factor



4.2 Cyclic Load Test

The base isolator should have good level of horizontal flexibility to safeguard the structure above it from seismic damages. The cyclic shear test estimates the horizontal stiffness and damping characteristic of the CSTP isolator specimen.

Effect of shape factor on horizontal Stiffness of CSTP Isolator. The horizontal stiffness is a very important parameter in the design of the CSTP isolator as it influences the effectiveness in the base isolation capability of the damper. It can be obtained by taking the slope of the hysteresis loop from the cyclic load test (Fig. 10). The stiffness seems to decrease in each cycle of loading, so the effective horizontal stiffness can be taken corresponding to the outer loop. The isolator’s effective horizontal stiffness corresponding to each load cycle of the test can be calculated based on the peak lateral loads and the peak lateral displacements as follows [13].

$$K_{eff} = \frac{F_{max} - F_{min}}{\Delta_{max} - \Delta_{min}}$$

where, K_{eff} = Horizontal stiffness of STP isolator

F_{max} = peak value of positive horizontal load

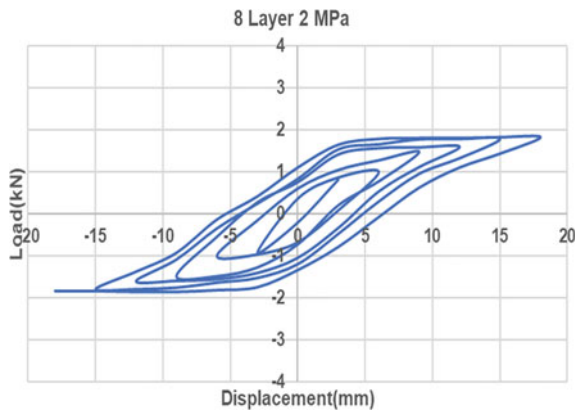
F_{min} = peak value of negative horizontal load

Δ_{max} = peak value of positive horizontal displacement

Δ_{min} = peak value of negative horizontal displacement.

The horizontal stiffness of the CSTP isolator with change in shape factor is tabulated in Table 2 and is graphically represented as shown in Fig. 11. Figure 11 shows the influence of vertical pressure on the performance of the isolator. The horizontal stiffness seems to be increasing with respect to increase in vertical pressure from 1 to 3 MPa. Even though the 1 MPa cases yields a lower horizontal stiffness, the separation between the layers is observed during the experiment, particularly when lower

Fig. 10 Load displacement curve obtained from cyclic load test



shape factors are used. Hence it is desirable to use higher vertical load combinations for more stability.

Effect of shape factor on the effective damping of CSTP isolator. The effective damping is a measure of energy absorption capacity of the CSTP isolator, which can be measured by taking the area of the hysteresis loop obtained from the cyclic shear test. The change in damping factor with respect to change in shape factor is plotted in the Fig. 12. The effective damping (β_{eff}) of an isolator shall be calculated for each cycle of loading by the formula [13]

$$\beta_{\text{eff}} = \frac{\left(\frac{2}{\pi}\right) * E \text{ loop}}{(|\Delta^+| - |\Delta^-|)^2 * K_{\text{eff}}}$$

β_{eff} = Effective damping

E loop = Energy dissipated per cycle of the loading

K_{eff} = Horizontal stiffness of STP isolator

Δ^+ = peak value of positive horizontal displacement

Δ^- = peak value of negative horizontal displacement.

Table 2 Relationship between shape factor, vertical pressure, effective stiffness and damping factor

Shape factor	1 MPa		2 MPa		3 MPa	
	Effective Stiffness, K_{eff} (kN/m)	Damping ratio	Effective Stiffness, K_{eff} (kN/m)	Damping ratio	Effective Stiffness, K_{eff} (kN/m)	Damping ratio
0.944	90.56	0.204	118.33	0.163	166.67	0.119
0.629	83.89	0.227	107.78	0.183	161.67	0.134
0.472	80.56	0.229	101.67	0.196	144.44	0.138
0.377	78.33	0.233	97.22	0.199	130.56	0.141

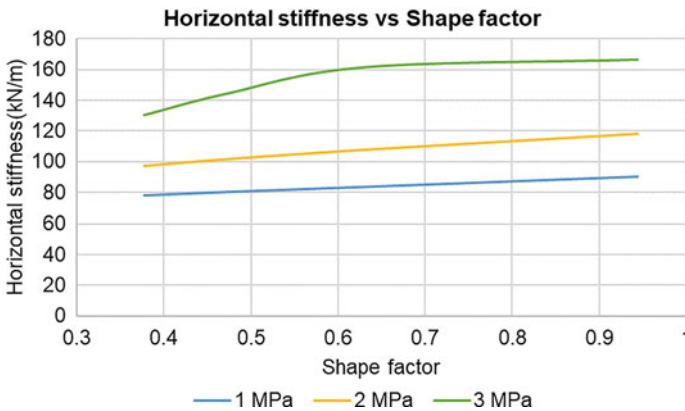


Fig. 11 Relationship between horizontal stiffness and shape factor

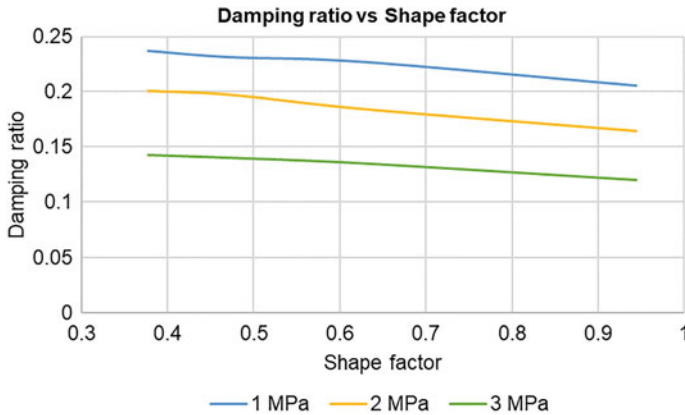


Fig. 12 Relationship between damping ratio and shape factor

From the Fig. 12 it can be inferred that the damping factor is decreasing with respect to the increase in the shape factor and vertical pressure. The experiment results show that the CSTPs can offer a damping factor in range of 0.12–0.25.

5 Conclusion

Experimental study on the unbonded scrap tyre pads are carried out to determine the effect of change in shape factor to the change in vertical stiffness. A total of 12 combinations were used to analyze the horizontal stiffness as mentioned in the Table 2. The study is conducted based on the change in shape factor, therefore the diameter of the specimen can be varied to meet the practical constraints keeping the shape factor constant. The selection of the isolator of a particular shape factor depends on desired horizontal stiffness. But it can be suggested that the isolator combinations under 3 MPa vertical pressure is better because lesser number of isolators will be required to transfer the vertical load of the superstructure. The conclusion from the study can be summarized as below.

- The CSTP specimen were able perform well under vertical load even after initial breakage of steel strands.
- The compressive strength of all CSTP combinations were found to be in a range of 8.25–8.5 MPa. Hence the variation of shape factor doesn't have a considerable effect on the compressive strength.
- Shape factor is found to have considerable effect on both the vertical stiffness and horizontal stiffness. The vertical stiffness is observed to increase with the increase in shape factor but it is not a linear relationship. Under low shape factor the scrap tyre pad performs more rigidly.

- The horizontal stiffness of CSTP is found to be easily modifiable by varying the shape factor. With the increase in shape factor, lateral stiffness increases for all cases.
- Damping factor is observed to decrease with increase in shape factor and with increase in vertical pressure.
- With decrease in shape factor stability issues due to sliding is observed especially with lower vertical pressure
- At higher vertical pressure, the isolator performed more stiff. Hence, lateral stiffness is comparatively high for 3 MPa vertical pressure.
- The ratio of vertical to horizontal stiffness in case of CSTP is found to be greater than 150 hence it can be used as a base isolator (Eurocode 8 2004)

References

1. Zayas VA, Low SS, Mahin SA (1990) A simple pendulum technique for achieving seismic isolation. *Earthq Spectra* 6(2)
2. VR Panchal, RS Jangid (2009) Seismic response of structures with variable friction pendulum system. *J Earthq Eng* 13(2)
3. CS Tsai, Chiang T-C, Chen B-J (2005) Experimental evaluation of piecewise exact solution for predicting seismic responses of spherical sliding type isolated structures. *Earthq Eng Struct Dyn* 34(9)
4. Fenz DM, Constantinou MC (2006) Behaviour of the double concave friction pendulum bearing. *Earthq Eng Struct Dyn* 35(11)
5. Kelly JM (2002) Seismic isolation systems for developing countries. *Earthq Spectra* 18(3)
6. P Pan, D Zamfirescu, N Nakashima, N Nakayasu, H Kashiwa (2009) Base-isolation design practice in Japan: introduction to the post-Kobe approach. *J Earthq Eng* 9(01)
7. Rahnavard R, Thomas RJ (2019) Numerical evaluation of steel-rubber isolator with single and multiple rubber cores. *Eng Struct* 198
8. Turer A, Özden B (2008) Seismic base isolation using low-cost Scrap Tire Pads (STP). *Mater Struct* 41
9. Sistla S, Mohan SC (2021) Parametric studies and application of fibre reinforced elastomeric isolators to low-rise buildings. *Structures* 34
10. Shirai K, Park J (2020) Use of scrap tire pads in vibration control system for seismic response reduction of buildings. *Bull Earthq Eng* 18
11. Mishra HK, Igarashi A, Matsushima H (2013) Finite element analysis and experimental verification of the scrap tire rubber pad isolator. *Bull Earthq Eng* 11(2)
12. Raj JCI, Suppiah S (2021) Seismic isolation using scrap tire rubber pads. *Mater Today: Proc* 43
13. Basar T et al. (2021) Seismic response control of low-rise unreinforced masonry building test model using low-cost and sustainable un-bonded scrap tyre isolator (U-STI). *Soil Dyn Earthq Eng* 142
14. Mathew A, Devangana UA, Anandhakrishnan M, Sajeed R (2023) A shake table investigation on low-cost seismic isolation using unbonded scrap tyre pad isolators. *Mater Today: Proc*
15. Mathew A, Firdouse FS, Sajeed R (2020) Experimental and analytical studies on the compression properties of scrap tyre pad base isolators. *IOP Conf Ser: Earth Environ Sci*

Re-assessment of Existing Offshore Platform for Life Extension



Shikha Singh and Rajan Singh

Abstract Majority of offshore steel platforms in Mumbai High Field in Arabian Sea as well as around the world are about to reach their design life. To continue to operate the platforms after their design life, existing offshore platforms requires re-certification. Also change in design criteria, addition of new facility and damages of the structure may lead to a need for assessment. Underwater and topside surveys are carried out to collect sufficient information about the present condition of the structures for their engineering assessment. The method normally used for assessment of existing offshore structures is In-place analysis based on Design level and Ultimate level check. In-place analysis of the jacket structure has been carried out using SAC's software to evaluate the structural adequacy of the jacket structure in accordance with code API-RP2A criteria's for life extension. In-place analysis is based on working stress and considers only linear analysis for the jacket structure. If Jacket structure does not pass design level criteria, advance analysis such as ultimate strength analysis needs to be carried out as per criteria of API-RP-2A to study failure mechanism of the structure and determine Reserve Strength Ratio (RSR). In ultimate strength analysis both material and geometrical nonlinearity is considered and incremental loading is applied to study the behaviour of the structure. This paper intends to provide Re-assessment of existing fixed offshore steel platform and results from the investigation are discussed and conclusions are drawn about the applicability of the proposed framework.

Keywords Offshore steel platforms · Life extension · API RP 2A · In-place analysis · Reserve strength ratio · SACS

S. Singh (✉)

Structural Engineering, Delhi Technological University, New Delhi, India

e-mail: shikha.sgsits@gmail.com

R. Singh

Offshore Engineering Department, EIL, New Delhi, India

1 Introduction

Offshore activities primarily involve the installation of structures in a sea environment for the production of oil and gas. Mainly comprises of extracting oil and gas from the sea and transporting it to land for use after some amount of processing. Fixed offshore steel platforms are commonly used to provide support for oil and gas exploration and production facilities. Majority of offshore steel platforms in Mumbai High Field in Arabian Sea as well as around the world are of fixed type installed at sea having shallow water depths, it comprises of mainly three parts, Jacket—Underwater Structure, Deck—Topside Structure and foundation.

Re-assessment of existing platforms is performed to extend service life of the over lived jacket structures. Also change in design criteria, addition of new facility and damages of the structure may lead to a need for assessment. From a commercial point of view, the use of existing platform in many cases is given preference, compared to installation of new platform. This will be acceptable for many platform structures even with major modifications. The purpose of the assessment of an existing platform is to ensure that the structure has an acceptable level of safety as compared to new designed platform. This paper intend is to provide Re-assessment methodology of Jacket structure of the fixed offshore steel platform for life extension which is located in the Mumbai High Field in Arabian Sea [1].

1.1 Indian Western Offshore—Overview

- ONGC operates around ~ 250 fixed offshore platforms in western offshore.
- Water depth ranges from 55 to 90 m.
- Designed based on API code for the design life of 25 years.
- More than 40% of the platforms have exceeded their design life. As a result, Life extension studies are therefore required to ensure their fitness for purpose for the extended life.

1.2 Components of Typical Fixed Platform

Components of typical fixed offshore platform are described in following points with the help of schematic of platform shown in Fig. 1.

- Tubular space frame structure to support platform topsides.
- Fixed to the seabed by driving piles through main legs or skirt piles around the legs.
- Typically used up to water depths of 120–150m.
- Self-weight of the jacket is governed by Water depth, Topside Weight, Environmental conditions.

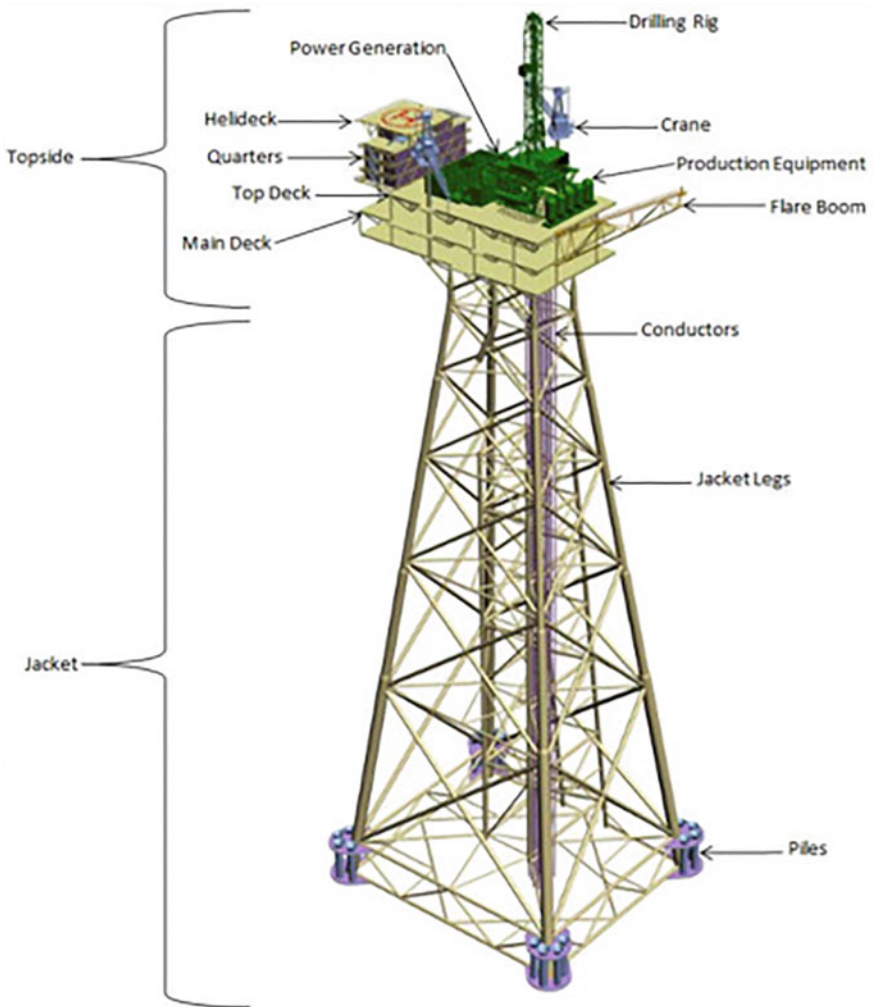


Fig. 1 Schematic of a generalized fixed offshore platform

- Top portion of a fixed platform which sits on the jacket and consists of the decks, accommodation and facilities required for processing oil/gas/water injection.
- Mudmat is present at bottom-most level and prevents tilting of jacket due to settlement of seabed.
- Conductors are installed inside the jacket with guide frames at different levels, which assist in drilling and provide casing pipes through which oil/gas is taken out.

1.3 Need of the Assessment

Platform design life is 25 years and the majority of the platforms around the world have exceeded their design life. API-RP-2A requires an assessment of an existing platform if any of the following indicators exists:

- Changes in design codes resulting in increased environmental loading.
- Damages such as dents/holes/cracks/parting of members.
- Additional facilities like clamp-on wells, riser, deck extension etc.
- Use of structure beyond design life.
- Structure is subjected to increased loading due to modifications in structures.

1.4 Objective of the Assessment

The objectives of assessment can be outlined as follows:

- The method normally used for assessment of existing offshore structures is In-place analysis based on Design level and Ultimate level check. In-place analysis of the jacket structure has been carried out using SACS software to evaluate the structural adequacy of the jacket structure in accordance with code API-RP2A criteria for life extension.
- To perform inelastic pushover analysis to calculate RSR of fixed platform with respect to metocean data to assess the ultimate capacity of the platform. RSR is defined as the ratio of a platform's ultimate lateral load carrying capacity to its 100-year environmental condition lateral loading.

Based on the above analyses this study intends to provide Re-assessment of existing fixed offshore steel platform and results from the investigation are discussed and conclusions are drawn about the applicability of the proposed framework to give an up-to-date picture of platform strength. Then this picture is used to assess if the existing platform is still "fit-for-purpose", and to decide the suitability of structures for an extended lifetime.

2 Methodology

2.1 Assessment Methodology

The two different analysis of the platform should be carried out to give an extended up-to-date picture of platform strength and to confirm the suitability of structures for a lifetime.

2.1.1 In-Place Analysis

In-place analysis is to be performed based on the 3-dimensional model of the platform structure including the topsides, substructure and piles. Extreme storm loading conditions is considered. Design level analysis considering linear static methodology is very conservative and do not utilize the reserved strength of jacket. Design level analysis is done to assess the integrity of structure for present condition. The strength is expressed the maximum of all unity checks.

2.1.2 Pushover Analysis

A pushover analysis is carried out using the SACS software. This program uses a large deflection; iterative direct stiffness solution technique to solve for the geometric and material non-linearity's associated with the ultimate strength of a structure. A progressive collapse analysis is performed to establish the residual strength. Reserve Strength Ratio is the load factor applied to the design environmental load just before the collapse or to obtaining maximum displacement. Overall Reserve Strength Ratio is the minimum RSR for all directions analysed. RSR is a measure of platform strength when compared to design strength. The strength is measured in terms of the total load that can be resisted as shown in Fig. 2 [2].

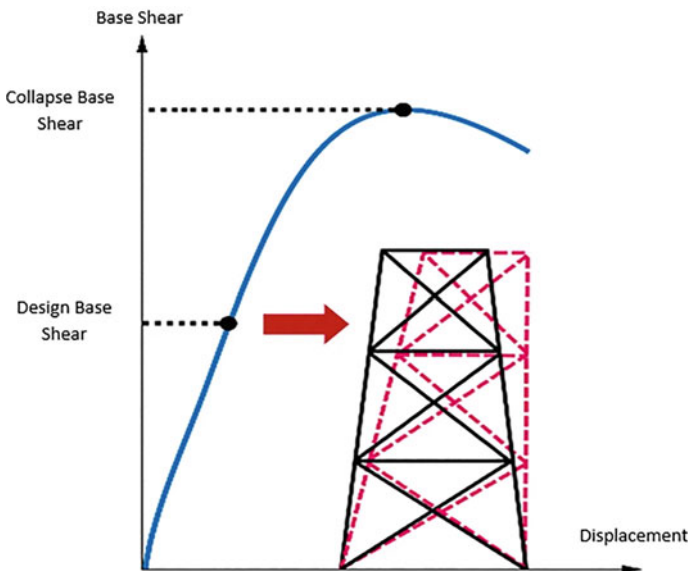


Fig. 2 Base shear from pushover analysis [2]

Gravity loadings are applied first to the model. The storm load case has been applied by factoring the environmental loading until the structure turns into a mechanism or any of defined failure criteria occurs. The environmental loading is applied to the structure in increments. The nodal deflection and member forces are calculated for every load step and the stiffness matrix is reformed at every step. When the stress in the member reaches the yield stress, plasticity occurs in the member. The presence of plasticity reduces the stiffness of the structure and additional loads due to subsequent load increments will be re-distributed to members adjacent to the members that have plasticity. This is continued until the whole structure is collapsed or pushed over.

2.2 Validation Scheme

A vertical cylindrical structural member of an offshore structure with diameter 1.0m is installed at a site where the water depth is 150m and the mean current is negligible as shown in Fig. 3. The design wave for the structural member has a height of 8m and period of 12 s.

The result obtained for maximum wave induced horizontal force is compared here for manual calculation method and SACS software (Table 1).

Fig. 3 Vertical cylindrical member (SACS software model)

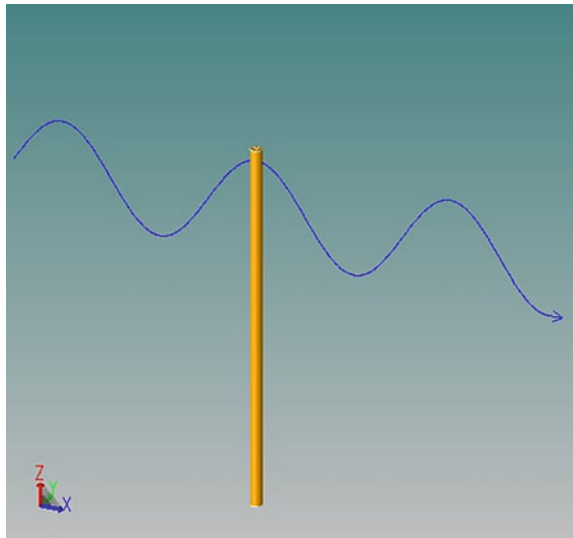


Table 1 Maximum wave induced horizontal force

Manual calculation	SACS software	Error (%)
72.82 kN	79.48 kN	8.37

From comparison we can see that the values obtained by manual calculation and SACS software do not differ too much. So, SACS software is reliable to be used for the further study.

2.3 Proposed Analysis Procedure

Assessment of existing fixed offshore steel platform is carried out in SACS software as per criteria of API-RP-2A [3] in three stages. The SACS software presents the structural response in terms of member's stress utilization ratio and joint utilization ratios. The structure is defined as code compliant if all members have stress utilization ratio of less than 1.0. First stage involves In-Place analysis which is carried out to simulate the behaviour of the structure as close as possible to give the response of the structure during its service and it is performed with 85% of environmental load at design level and overstressed Joints/Members are identified from the analysis.

Further in second stage, these overstressed members and joints are to be checked in In-place analysis with 100% of environmental load at ultimate level. In the final stage overstressed joints and members identified in ultimate level check are further assessed by performing Non-linear analysis in SACS, where incremental environmental loading is applied on the structure till it collapses and reserve strength of the structure is achieved. If RSR of the structure is less than the desired criteria of API RP 2A, then strengthening of overstressed members and joints identified during ultimate analysis is provided to achieve the desire Reserve strength ratio (RSR) [4].

2.4 Structural Model

The Jacket structure analysed is comprised of a four legged Well platform in Mumbai high field. It is located in a water depth of 76.00m.

Topside consists of three decks, Main deck at (+ 23.00m), Cellar deck at (+ 18.00m) and Helideck at elevation (+ 33.00 m) w.r.t. chart datum. The cellar and the main deck framing is 28×17 m in plan. Jacket consists of four legs and five horizontal framings; top dimension (+ 6.70m) is 18.25×9.50 m and base dimension on seabed (- 75.00m) is 28.50×30.00 m. The entire platform is considered supported and fixed to the sea bed by piled foundation system. Overall view of Offshore Platform in SACS software is shown in Fig. 4.

Steel material used in the platform has following properties; Density 7.85 t/m^3 , Young's Modulus 200 kN/mm^2 , Shear modulus 80 kN/mm^2 and Yield strength 248 MPa.

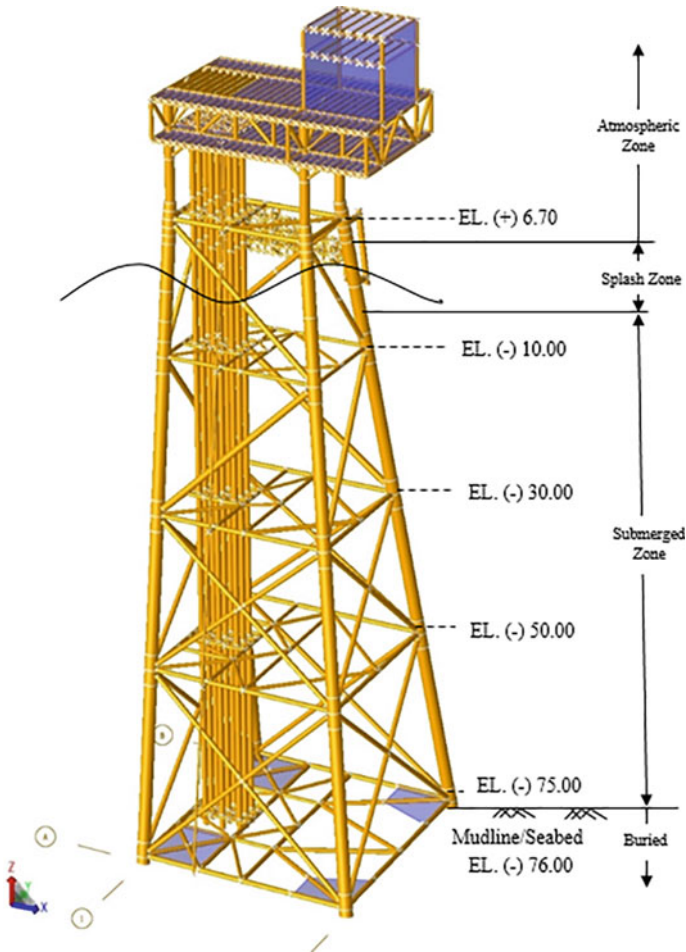


Fig. 4 SACS model of offshore platform

2.5 Design Environmental Conditions

The environmental loadings were applied to approach angles from 0 to 315° at 45° intervals as shown in Fig. 5. Still water depth has been taken as (Chart Datum) + (Lowest Astronomical Tide) + (50% of Astronomical Tide) + (Storm Surge) for Extreme Storm Environment condition. Metocean data [5] used for the In-Place and Pushover analysis of jacket structure are as shown in Tables 2 and 3.

Fig. 5 Wave approach directions for loading

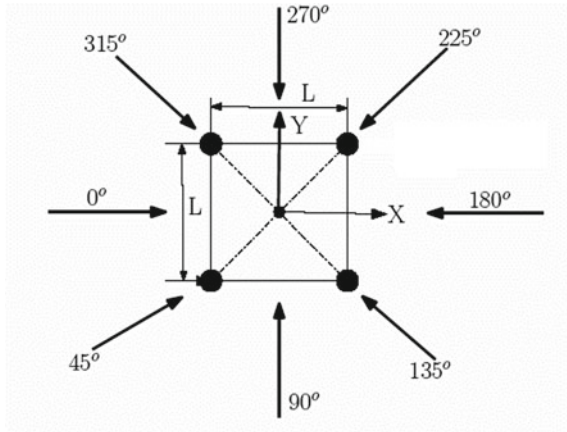


Table 2 Extreme storm wave and wind data

Wave and wind data								
Approach direction	0	45	90	135	180	225	270	315
100 year wave max. ht. (m)	15.09	16.77	17.07	17.68	18.00	14.48	13.26	16.00
100 year wave period (Sec)	13.00	13.70	13.90	14.20	14.40	12.50	11.80	13.80
Still water depth (m)	78.26	78.44	78.56	78.81	78.81	78.26	78.26	78.26
Design wind speed (m/sec)	51.90	49.70	48.90	50.60	53.30	53.30	53.30	53.30

Table 3 Extreme storm current profile

Elevation	Current speed (m/s)							
	Approach direction							
	0°	45°	90°	135°	180°	225°	270°	315°
Bottom	0.51	0.31	0.213	0.27	0.37	0.31	0.25	0.25
Y-1/4	0.97	0.69	0.609	0.66	0.81	0.72	0.65	0.65
Y-1/2	1.19	0.86	0.75	0.82	1.02	1.20	0.83	0.82
Y-3/4	1.40	1.02	0.90	0.99	1.21	1.08	0.95	0.98
Surface	1.64	1.23	1.09	1.18	1.45	1.27	1.16	1.22

Table 4 Design level analysis joint UC summary

Joint	Location	UC ratio
0101	Row-B, X-Brace Joint at EL. (-) 61.774	1.196
0063	Row-2, X-Brace Joint at EL. (-) 38.823	1.153
0104	Row-1, X-Brace Joint at EL. (-) 38.823	1.114
0062	X-Brace Joint at EL. (-) 61.774 on Row-A	1.049
0084	X-Brace Joint at EL. (-) 39.481 Row-A	1.014

3 Results and discussions

3.1 Design Level Analysis Results

It is seen from the results that no member has a UC value more than 1.0. However, few joints have seen with unity check value more than 1.0 shown in the following Table 4. These joints will further be checked in Ultimate strength analysis.

3.2 Ultimate Level Analysis Results

It is seen from the results that no member has a UC value more than 1.0. However, few joints have seen with Unity check value more than 1.0 shown in the following Table 5. These joints will further be checked in Ultimate strength analysis.

It is seen from the results that joints in Table 5 have a UC value more than 1.278 (33% increase in allowable stress is considered hence allowable UC for ultimate level is $1.7/1.33 = 1.278$).

Table 5 Ultimate level analysis joint UC summary

Joint	Location	UC ratio
0101	Row-B, X-Brace Joint at EL. (-) 61.774	1.393
0063	Row-2, X-Brace Joint at EL. (-) 38.823	1.348
0104	Row-1, X-Brace Joint at EL. (-) 38.823	1.316
0062	X-Brace Joint at EL. (-) 61.774 on face Row-A	1.222
0084	X-Brace Joint at EL. (-) 39.481 on face Row-A	1.168
0102	X-Brace Joint at EL. (-) 39.481 on face Row-B	1.035

Table 6 Reserve strength ratio

Sr. No.	Load case	Reserve strength ratio (RSR)
1.	101 (0°-extreme storm)	2.45
2.	102 (45°-extreme storm)	2.45
3.	103 (90°-extreme storm)	2.45
4.	104 (135°-extreme storm)	1.85
5.	105 (180°-extreme storm)	1.60
6.	106 (225°-extreme storm)	2.45
7.	107 (270°-extreme storm)	2.45
8.	108 (315°-extreme storm)	2.45

3.3 Pushover Analysis

As per API RP2A a minimum RSR of 1.60 is necessary for a high exposure category platform. From the above results it is observed that RSR is more than 1.60 for all the load cases and no members and joints are undergone plasticity at 100% environmental loading. Hence the jacket can withstand 100% environmental loading without collapse (Table 6).

3.4 Analysis Findings

In-place analysis has been performed to check that the platform structural member's capability to support the applied loads in extreme storm situation. The total Seastate loading on the jacket is converted into overturning moment and base shear at the seabed level. The Base Shear and Overturning Moment increases will be more for the direction of loading with maximum wave height. The maximum overturning moment and Base Shear are in load case 105. The obtained results may be summarised as follows:

- (a) The results of the design level analysis are shown in Section 3.1 from that it is observed that no members are having UC ratio more than 1.00 and five joints are having UC ratio more than 1.00.
- (b) The results of the Ultimate strength analysis are shown in Section 3.2 from that it is observed that no members are having UC ratio more than 1.278 and three joints are having UC ratio more than allowable UC ratio. These members will be further checked in pushover analysis.
- (c) The results of Pushover analysis are shown in Section 3.3 shows that RSR is more than 1.60 for all the load cases and no members and joints have undergone plasticity at 100% environmental loading (Fig. 6).

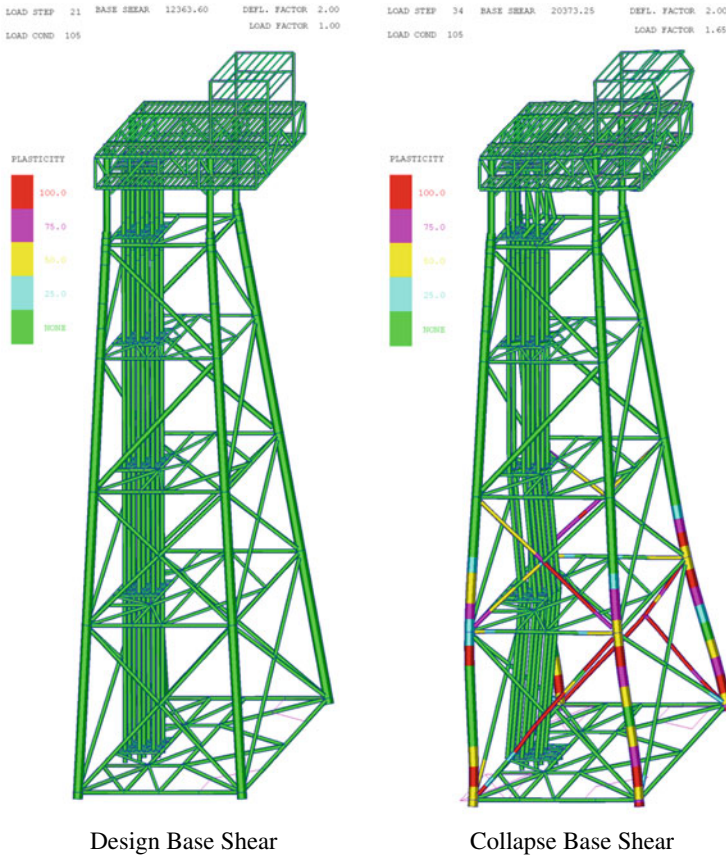


Fig. 6 Pushover analysis plots at design and collapse load condition

4 Conclusion

In this paper, the research studies on structural condition assessment of ageing offshore jacket platforms reported in the literature over the past few decades are presented and discussed. The structural response to the extreme conditions is expressed in terms of stresses in the structural members and it is quantified by using unity check ratio. The unity check summary for all members and joints satisfies the required condition of API RP 2A. The results of pushover analysis show that platform has sufficient reserve strength ratio for all the load cases and no members and joints have undergone plasticity at 100% environmental loading. The results showed that the platform has sufficient reserve strength and can resist the applied environmental load.

Accordingly, it can be concluded that Jacket structure is fit for purpose with recommendation that in future additional facilities/appurtenances like risers, riser guards etc. over and above the existing facilities which will enhance loading on the jacket shall be avoided.

References

1. Nallayarasu S (n.d.) Analysis and design of offshore structures. Department of Ocean Engineering, Indian Institute of Technology Madras
2. Wahab MMA, Kurian VJ, Liew MS, Kim DK (2020) Condition assessment techniques for aged fixed-type offshore platforms considering decommissioning: a historical review. *J Mar Sci Appl* 19:584–614
3. API RP 2A-WSD (2014) Recommended practice for planning, design and constructing fixed offshore platforms, 21st edn, Errata and Supplement 3, October 2007, Supplements October 3, 2007. API Publishing Services, Washington, DC
4. Chakrabarti S (2005) Handbook of offshore engineering. Elsevier Ltd.
5. Environmental data for Indian western offshore region is based on document “Notice Inviting Expression of Interest (EOI) for Hiring of Mobile Offshore Production Unit (MOPU) in Kutch Offshore” (2017)

Mechanical Properties and Micro Structure of Graphene Oxide (GO) Cement Composites: A Review



S. Arya and P. Seena

Abstract Ordinary Portland Cement (OPC) is the key ingredient in concrete, and it is the primary choice in the construction and building environment. OPC's superior technical qualities have made it a preferred choice for combining newly developed multi-functional materials. Because of its brittle nature, OPC resembles materials with weak resistance to crack formation, low tensile strength, and limited strain capacity. By virtue of their exceptional mechanical qualities, graphene and its derivatives, such as graphene oxide, carbon nanofibers, carbon nanotubes, and silica particles, have demonstrated a means to create a super concrete. Because of the outstanding interfacial interaction capabilities of graphene oxide, it can interface directly with cement particles. GO is a viable option for application as nano reinforcements in cement-based materials due to its outstanding mechanical capabilities, high aspect ratio, and good dispersibility in water. This paper conducts a thorough examination of the mechanical properties and microscopic structure of graphene oxide. Discussions will include matrix composition, pore structure, micro structure, workability, compressive, tensile, and flexural strength etc. In addition, the dispersion of graphene oxide in the cement paste, the improvement of GO dispersion with silica fume, the distribution of porosity and pore size, the solubility of water, the morphology and microstructure, the impact of hydration times on the microstructure, the regulation mechanism of GO in cement hydration products, and fluidity will all be observed and summarised. The composition, pore size distribution, and microstructure of concrete are studied using a variety of microstructure characterisation techniques, such as XRD, MIP, and SEM.

Keywords Graphene oxide · Matrix composition · Pore structure · Micro structure · Workability · Hydration products

S. Arya (✉) · P. Seena
Government Engineering College Thrissur, Thrissur, India
e-mail: dctr21jul003@gectcr.ac.in

© The Author(s), under exclusive license to Springer Nature Switzerland AG 2024
M. Nehdi et al. (eds.), *Proceedings of SECON'23*, Lecture Notes in Civil Engineering
381, https://doi.org/10.1007/978-3-031-39663-2_62

737

1 Introduction

Cement composites are the most significant and prevalent building material [1]. Its quasi-brittle character, which is to blame for its poor resistance to crack formation, low tensile strength, and low strain capacities, is the main drawback of concrete and cement-based materials [2, 3]. Adding admixtures and fibres to cement composites can improve their rheological characteristics, strength, durability, and other qualities [4]. The pre-existing porosity character of cement composite can be linked to the deficits in tensile and flexural strength [5]. Recent initiatives have sought to use nanoparticles into the manufacturing of cement concrete in an effort to increase its durability and mechanical qualities [6]. Recently discovered graphene oxide (GO) is a layered nanomaterial made of hydrophilic oxygenated graphene sheets that have carbonyl and carboxyl groups at the sheet edges and hydroxyl and epoxide functional groups on their basal planes. Oxidation and ultrasonic dispersion were used to create graphene oxide (GO) nanosheets [1]. Addition of graphene oxide (GO) to cement paste refines its microstructure and noticeably improves its water sorptivity and chloride penetration values [7]. When compared to SF pastes, GO encapsulated silica fume (GOSF) had better rheological qualities, showing that the addition of GO improved rheological properties [4]. A sufficient proportion of silica fume enhances compressive strength and GO dispersion in cement paste [2]. However, workability of cement paste was lowered due to water trapped in GO agglomerates, and hydration of cement paste was not considerably increased because GO was agglomerated [8]. Compressive strength was improved due to the effects of GO on porosity, hydration, and crack-bridging [9]. The GO sheet inside the cement composite specimen served as a bridge to improve the coherence within the cement. polycarboxylate-based superplasticizers show the most promise for dispersing GO in cement's alkaline environment [5]. In the presence of SF and PC-based superplasticizer, GO is successfully dispersed [10]. A detailed review of GO is conducted in this paper.

2 Mechanical Properties

By using GO in cement composites, numerous studies have obtained high compressive strength, tensile strength, and flexural strength. Lv [1] discovered that if GO concentration is 0.03% by weight of cement, displays 78.6% increment in tensile strength, 60.7% increment in flexural strength, and 38.9% gain in compressive strength. By adding 0.03% by weight of GO, Gong et al. [11] discovered nearly identical homogenous results. In this case, the 28-day compressive and tensile strengths had increased by more than 40%. Increased compressive strength of cement composites with GO incorporation was studied by Shang et al. [4]. A 15.1% increase is seen after adding 0.04% GO. Li et al. [3] also investigated the impact of graphene oxide and nano alumina on cement paste. The compressive and flexural strengths of Nano aluminates (NA) cement paste are better than those of normal cement paste. When

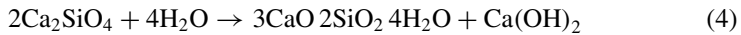
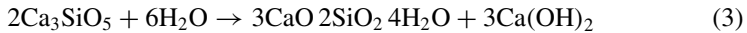
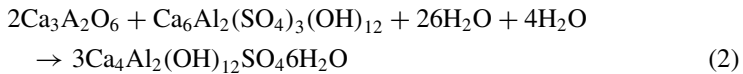
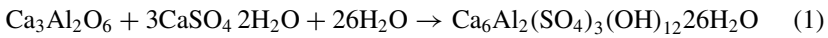
NA dosage is greater than 2%, flexural strength tends to improve less, which may be because NA agglomerates. However, when the GO dose exceeds 0.04%, the augmentation in flexural strength of GO-cement paste tends to decline by agglomeration. Li et al. [2] discovered that adding GO enhances the compressive strength of cement paste. A threshold for GO concentration was discovered to be roughly 0.03% by weight of cement. The influence of integrated GO is negligible when the GO content is below the threshold. The addition of GO raises the compressive strength when the GO content surpasses the threshold. Zhao et al. [12] created PC@GO (polycarboxylate superplasticizer (PC) modified GO), which exhibits improved mechanical properties due to the inclusion of 0.22 wt% PC and 0.022 wt% GO. Mokhtar et al. [13] investigated the mechanical characteristics and microstructure of GO reinforced cement. Results demonstrate the compressive strength gain by around 13% while the tensile strength increased by 41% at 0.03 wt% and 0.02% GONPs respectively. According to Kang et al. [9], GO cement mortar exhibits compressive, bending, and tensile strengths up to 32% (0.05 wt%), 20% (0.1 wt%), and 26% (0.01 wt%) higher than the typical values for regular cement mortar, respectively. Peng et al. [6] investigated how GO content and the w/c ratio affected GO-cement composites. Flexural strength is improved (21.86%) by 0.03wt% GO, while Compressive strength is strengthened (5.16%) by 0.01 wt% GO. When 0.05 wt% of GO is added, the compressive and flexural strengths also decline. Chintalapudi et al. [14] discovered that, at optimal dosages, adding graphene oxide to cement boosts compressive strength. After 28 days of curing, it was shown that the average increases in compressive strength for GO dosages of 0.02% and 0.03% were 28.5% and 46.4%, respectively. According to Devi et al. [15], adding GO to concrete at varying percentages by weight of cement reduced workability and significantly increased compressive strength (21–55%) and tensile strength (16–38%). GO cement paste was created by Akarsh et al. [10] using Silica fumes and M sand. According to the findings, the concrete with 0.15% GO and 7% silica fumes had a 29.54% higher compressive strength at 28 days than normal concrete. Changjiang et al. [16] examined the mechanical characteristics of GO-incorporated steel-fiber reinforced concrete. SFRC performs the best in terms of compression when the GO concentration is 0.05 wt%. Flexural strength and splitting tensile strength of SFRC were at their maximum when the GO concentration was 0.03 wt%.

3 Characterization of GO

3.1 Hydration Reaction

Tricalcium silicate C_3S (Ca_3SiO_5), dicalcium silicate C_2S (Ca_2SiO_4), tricalcium aluminate C_3A ($Ca_3Al_2O_6$), tetracalcium aluminoferrite C_4AF ($Ca_4AlnFe_{2-n}O_7$) as well as a small amount of clinker sulfate (Na_2SO_4 , K_2SO_4) and gypsum ($CaSO_4 \cdot 2H_2O$) are the major compounds of cement in unhydrated state. In the

hydration process, C_3A , C_4AF , C_3S and C_2S will carry out a complex hydration reaction to form ettringite ($Ca_6Al_2(SO_4)_3(OH)_{12} \cdot 26H_2O$, AFt), $Ca_4Al_2(OH)_2SO_4H_2O$ AFm), calcium hydroxide ($Ca(OH)_2$, CH) and calcium silicate hydrate ($3CaO \cdot 2SiO_2 \cdot 4H_2O$, C–S–H) gel, the corresponding chemical reactions of which are represented by Eqs. (1–4) respectively. Generally, CH, AFt and AFm typically display rod-like and needle-like geometries with disorder, which influences how brittleness of cement paste is [1].



A potential regulating mechanism for GO on cement hydration products can be suggested as depicted in Fig. 1 in light of the findings and discussion presented above. Numerous oxygen functional groups, including $-OH$, $-COOH$, and $-SO_3H$, are present on the surface of GO (Fig. 1a). While the hydration reaction is momentarily slowed down by PC (Fig. 1c), the active functional groups preferentially react with C_3S , C_2S , and C_3A to generate the growth sites of the hydration products (Fig. 1b). At the growing spots on the GO surface, the hydration reaction keeps on after the effect of retardation (Fig. 1d). The hydration products' growth points and development pattern are both regulated by GO, which is referred to as a template effect. GO can cause numerous nearby rod-like hydration crystals to coalesce into thick columns and flower-shaped crystals on the same GO surface (Fig. 1e). These column-shaped products, which are made up of rod-like AFt, AFm, CH, and C–S–H, grow forward from the GO surface in the same direction as a result of intense tension everywhere around them. The fully-bloomed flower-like crystals (Fig. 1f), which disseminate in pores and cracks as fillers and crack arrestors to slow crack development, are formed when the column-shaped crystals grow into a pore, crack, or loose structure [1, 17].

When the GO content is larger than 0.04%, the growth points are too dense to form single flower-like crystals, so the hydration crystals will adopt a polyhedron shape and form a compact structure. The flower-like crystals usually generated in holes and gap of the cement composites and forming cross-linking structure have great contributed to improving toughness of cement composites [1, 17]. The hydration of cement paste is accelerated due to the seeding effect of GO agglomerates which provide nucleation sites because of their small particle size and large surface area [8].

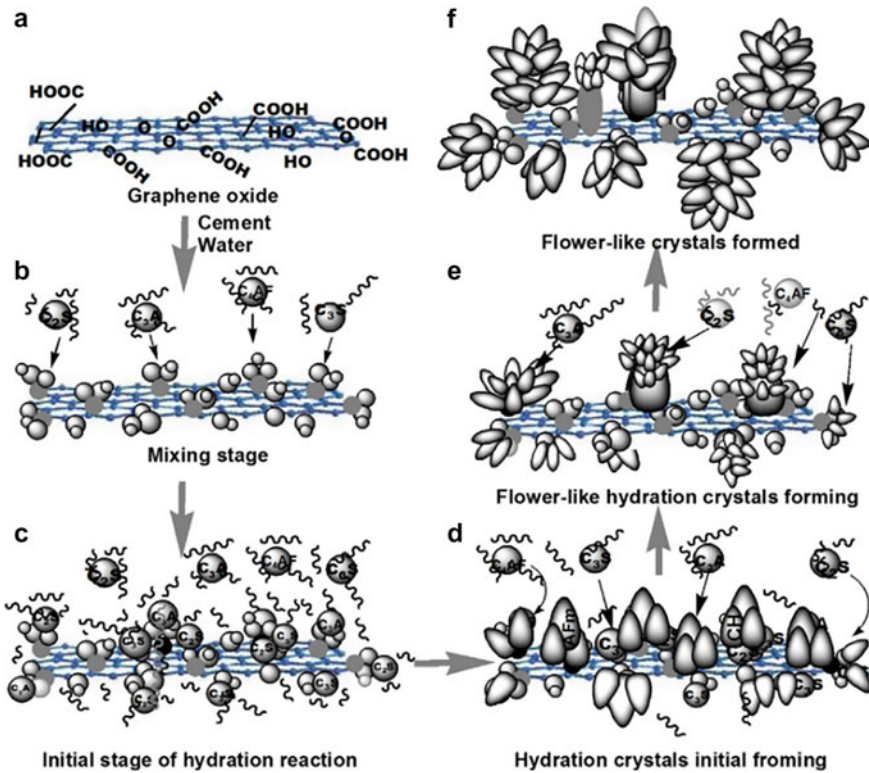


Fig. 1 Schematic diagram of regulation mechanism of GO on cement hydration crystal [17]

3.2 Chemical Composition and Properties of GO

Two-dimensional carbon allotrope known as graphene is composed of a single layer of carbon atoms organized in a hexagonal lattice. It has a special set of chemical properties that add to its extraordinary qualities. Table 1 displays the chemical composition of GO [5].

Due to its exceptional adsorption abilities, graphene can adsorb a wide range of molecules and nanoparticles on its surface [4]. The carbon atoms in graphene form solid covalent bonds and make up the entire material. In order to create a planar structure with sp^2 hybridization, each carbon atom is linked to three nearby carbon atoms [13]. By adding various chemical groups or molecules to the surface of graphene, different chemical functions can be added to it. Functionalization can alter

Table 1 Chemical composition of GO [5]

Elements	Carbon	Hydrogen	Nitrogen	Sulphur	Oxygen
Composition (%)	49–56	0–1	0–1	0–2	41–50

a substance's characteristics and improve its suitability for a particular purpose, such as enhancing the substance's solubility in solvents or generating particular reactive sites [10]. Because of its two-dimensional structure, graphene has an incredibly large surface area. This characteristic makes it appealing for a variety of applications, including catalysis and energy storage devices [16].

3.3 Micro Structure

The micro-structure of cement composites affects their mechanical characteristics. The matching SEM (Scanning Electron microscope) pictures of cement composites were also examined in order to clarify the connection between mechanical strength and microstructure. According to the findings, GO nanosheets were crucial in controlling the microstructure of hydration crystals, considerably lowering their brittleness and increasing their toughness [1]. The GNPs/GONPs and C–S–H gels precipitated and developed a stronger interfacial bond, according to the AFM scans and SEM photos. The microstructure of the graphene-reinforced cement paste becomes denser when the porous phase and low-density C–S–H gel diminish and the high-density C–S–H gel increases [18]. Figure 2 shows SEM pictures of crack patterns in samples of normal cement and 0.022% GO cement at a curing age of 28 days. Figure 2a illustrates the continuous microcracks that develop by slack hydration crystals in plain-cement composite. In the meantime, Fig. 2b depicts a sparse collection of thin fractures with considerable deflection and tortuosity in GO-cement composite. The presence of PC@GO nanosheets prevents cracks from spreading. As GO only makes up 0.022 wt% of the cement composite, it can be difficult to distinguish GO nanosheets in SEM pictures. While the compact structure predominates in the GO-cement sample (Fig. 2b), rod- and needle-shaped crystals with loose structures are frequently seen in plain-cement samples (Fig. 2a). The management of the shape and assembly of hydration products gives rise, with the inclusion of PC@GO, to the refined micro-structure [12].

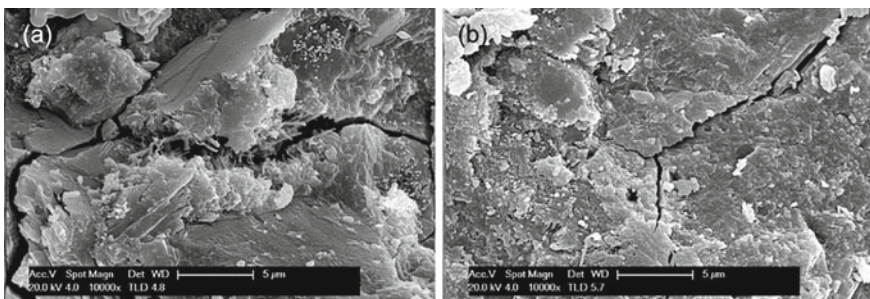


Fig. 2 SEM images of crack patterns in plain-cement sample, **a** and 0.022% GO-cement sample, **b** at curing time of 28 days [12]

3.4 Pore Size Distribution

Pore size distribution is assessed using the mercury intrusion porosimetry (MIP) test. Pore structure analysis' findings indicate a little modification in cement pore distribution as a result of GO addition [4, 12]. The inclusion of GO has improved the microstructure of cement paste and increased the number of gel holes [7, 7, 15].

3.5 Workability

The workability of cement composites is reduced by the addition of GO sheets. The minislump flow for the plain cement mixture's 0.03% by weight GO sheets is shown in Fig. 3a. The plain cement sample has a minispread diameter of about 130 mm. The diameter of the minislump was reduced to around 85 mm, which is 34.6% less than that of the plain cement sample, when 0.03% by weight GO was added. The shrinkage of the minislump diameter demonstrates how the workability of cement paste is affected by GO additions. It is typically linked to the fact that nanomaterials have a large specific surface area and so need more free water to moisten their surfaces [11].

The diameters of the mini-slump for C (without GO), CG2 (0.02 wt% GO), CG3 (0.03 wt% GO), and CG4 (0.04 wt% GO) are shown in Fig. 3b. The addition of 0.02% by weight GO marginally decreased the mini-slump diameter when compared to plain cement paste C. The mini-slump diameter, however, suddenly shrank to a level that was roughly 21% lower than that of the unmodified cement paste C when 0.03% by weight GO was added. The further increase in GO concentration to 0.04% had little effect on the slump diameter. The findings of the mini-slump test show that

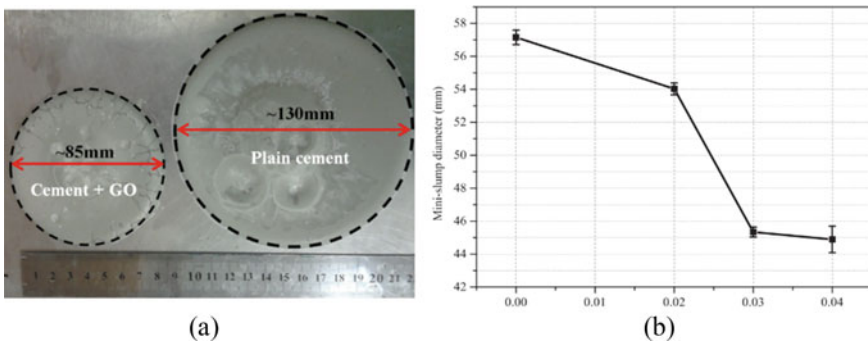


Fig. 3 **a** Minislump flow at 10 min after lifting up the minicore [11], **b** mini slump results of C, CG2, CG3 and CG4 [8]

the cement paste's workability was decreased by the addition of GO nanosheets. Furthermore, it is clear that 0.03% was the cutoff for the GO-incorporated cement paste's workability [8].

4 Conclusion

Structural characterization and mechanical behaviour of Graphene oxide (GO) in the cement composites is discussed meticulously in this article. Based on the literature survey, the following observations can be drawn.

- GO's impacts on porosity, hydration, and crack-bridging have greatly improved the cement composite's mechanical, chemical characteristics, and durability.
- GO nanosheets can regulate the development of crystals that resemble flowers in cement and significantly increases its hardness.
- The effects of GO and GO sheets encapsulating Silica Fume on the fluidity and rheological properties of cement pastes are different. The right amount of silica fume enhances the compressive strength and GO dispersion.
- The SEM images of microstructure shows that the addition of GO affects the morphology and distribution of cement hydration products.
- Workability of cement paste reduced due to water trapped in GO agglomerates. It can be coped up with addition of superplasticizers.
- Superplasticizers based on polycarboxylates show the best results for dispersing GO in an alkaline cement environment.

References

1. Lv S et al (2013) Effect of graphene oxide nanosheets of microstructure and mechanical properties of cement composites. *Comstr Build Mater* 49:121–127. <https://doi.org/10.1016/j.conbuildmat.2013.08.022>
2. Li X et al (2016) Incorporation of graphene oxide and silica fume into cement paste : a study of dispersion and compressive strength. *Constr Build Mater* 123:327–335. <https://doi.org/10.1016/j.conbuildmat.2016.07.022>
3. Li W et al (2017) Effects of nanoalumina and graphene oxide on early-age hydration and mechanical properties of cement paste. *J Mater Civ Eng* 29(9):1–9. [https://doi.org/10.1061/\(ASCE\)MT.1943-5533.0001926](https://doi.org/10.1061/(ASCE)MT.1943-5533.0001926)
4. Shang Y et al (2015) Effect of graphene oxide on the rheological properties of cement pastes. *Constr Build Mater* 96:20–28. <https://doi.org/10.1016/j.conbuildmat.2015.07.181>
5. Chuah S et al (2018) Investigation on dispersion of graphene oxide in cement composite using different surfactant treatments. *Constr Build Mater* 161:519–527. <https://doi.org/10.1016/j.conbuildmat.2017.11.154>
6. Peng H et al (2019) Mechanical properties and microstructure of graphene oxide cement-based composites. *Constr Build Mater* 194:102–109. <https://doi.org/10.1016/j.conbuildmat.2018.10.234>

7. Mohammed A et al (2015) Incorporating graphene oxide in cement composites: a study of transport properties. *Constr Build Mater* 84:341–347. <https://doi.org/10.1016/j.conbuildmat.2015.01.083>
8. Li X et al (2017) Effects of graphene oxide agglomerates on workability, hydration, microstructure and compressive strength of cement paste. *Constr Build Mater* 145:402–410. <https://doi.org/10.1016/j.conbuildmat.2017.04.058>
9. Kang D et al (2017) Experimental study on mechanical strength of GO-cement composites. *Constr Build Mater* 131:303–308. <https://doi.org/10.1016/j.conbuildmat.2016.11.083>
10. Akarsh PK et al (2021) Influence of graphene oxide on properties of concrete in the presence of silica fumes and M-sand. *Constr Build Mater* 268:121093. <https://doi.org/10.1016/j.conbuildmat.2020.121093>
11. Gong K et al (2015) Reinforcing effects of graphene oxide on Portland cement paste. *J Mater Civ Eng* 27(2):1–6. [https://doi.org/10.1061/\(ASCE\)MT.1943-5533.0001125](https://doi.org/10.1061/(ASCE)MT.1943-5533.0001125)
12. Zhao L et al (2017) Mechanical behavior and toughening mechanism of polycarboxylate superplasticizer modified graphene oxide reinforced cement composites. *Compos Part B: Eng* 113:308–316. <https://doi.org/10.1016/j.compositesb.2017.01.056>
13. Mokhtar MM et al (2017) Mechanical performance, pore structure and micro-structural characteristics of graphene oxide nano platelets reinforced cement. *Constr Build Mater* 138:333–339. <https://doi.org/10.1016/j.conbuildmat.2017.02.021>
14. Chintalapudi K et al (2019) Strength properties of graphene oxide cement composites. *Mater Today: Proc* 45:3971–3975. <https://doi.org/10.1016/j.matpr.2020.08.369>
15. Devi SC et al (2020) Effect of graphene oxide on mechanical and durability performance of concrete. *J Build Eng* 27(October 2019):101007. <https://doi.org/10.1016/j.jobe.2019.101007>
16. Liu C et al (2022) Studies on mechanical properties and durability of steel fiber reinforced concrete incorporating graphene oxide. *Cem Concr Compos* 130(July 2021):104508. <https://doi.org/10.1016/j.cemconcomp.2022.104508>
17. Lv S (2013) Regulation of GO on cement hydration crystals and its toughening effect. *Mag Concr Res* 65(20)
18. Tong T et al (2016) Investigation of the effects of graphene and graphene oxide nanoplatelets on the micro- and macro-properties of cementitious materials. *Constr Build Mater* 106:102–114. <https://doi.org/10.1016/j.conbuildmat.2015.12.092>

Engineering Properties of Geopolymer Concrete Incorporating Fly Ash and Clay



Sreedevi Lekshmi, J. Sudhakumar, and Khruvelu

Abstract It has been well known from the previous literature that the production process of one ton of cement contributes to the emission of nearly one ton of carbon dioxide gas to the atmosphere. Geopolymer concrete is completely devoid of cement and hence is considered as a sustainable alternative to the normal concrete. The key properties investigated in the present study include the compressive strength, flexural strength and water absorption of the fly ash clay based geopolymer concrete (GPC). Three types of clay were used in the study, viz., accumulated clayey soil (clay 1), surface clay (clay 2) and sub-surface clay (clay 3). The clays were incorporated in the system, in its raw state and after incorporating lime. It was observed that the engineering properties got enhanced after incorporating 3% of lime in the clays, when compared to that of raw clay based concrete specimens.

Keywords Compressive strength · Flexural strength · Water absorption · Fly ash · Lime

1 Introduction

1.1 General

The outstanding binding capacity of cement led to its elevated demand and hence its production. One ton of cement production ejects nearly one ton of CO₂ to the atmosphere. As a result of urbanization, the contribution of greenhouse gas by the cement production has reached its peak and hence became a grave concern. Geopolymer binder is a cement free concept which is attaining remarkable attention in the modern era as it make use of aluminosilicate rich waste products for its synthesis. Geopolymer was composed and developed in 1978 by Joseph Davidovits [1, 2]. The primary requirement for developing geopolymers include alumina and

S. Lekshmi (✉) · J. Sudhakumar · Khruvelu
Civil Engineering Department, National Institute of Technology Calicut, Calicut, India
e-mail: sreedevilekshminair@gmail.com

silica rich materials and an alkaline medium. Hence the geopolymerization process can be defined in simple terms as inorganic polymers developed by the blending of aluminosilicate rich industrial or agricultural waste with the combination of alkali hydroxide and alkali silicate [1]. The accepted alkaline solutions for developing the alkaline medium in geopolymers include combination of sodium silicate and sodium hydroxide or potassium silicate and potassium hydroxide. Studies reveal that the dissolution of alumina and silica species occur rapidly in sodium hydroxide than in potassium hydroxide [3]. The geopolymers have three-dimensional polymeric network of Si–O–Al with amorphous or semi crystalline structure [1]. The existing research performed in synthesizing geopolymers are based mainly on aluminosilicate surplus materials such as ground granulated blast furnace slag (GGBS), fly ash (class F and class C), rice husk ash, metakaolin, sugarcane bagasse ash and dolomite [4–10]. The properties and performance of geopolymers are influenced by the type of source material used and the alkaline medium, molar ratio of the solutions used, method of curing, etc. Based on these factors, the mechanical, chemical and thermal behaviour of geopolymer varies [11]. Few studies related to the use of clay or soil in geopolymers is tabulated in Table 1.

1.2 Research Significance

The study focusses on developing GPC using low calcium fly ash and different types of locally available clay as source material. The mechanical performance of GPC in terms of compressive strength (CS), flexural strength (FS) and water absorption has been evaluated. Lime was used to improve the performance of GPC, by partially replacing clay with lime, and compared with the results of raw clay based GPC specimens.

2 Materials and Methods

2.1 Materials

Three types of locally available clay of different source were used viz., accumulated waste clay, surface clay and sub-surface clay. The accumulated clay, surface clay and sub-surface clay were respectively, found to be non-plastic, medium plastic and highly plastic based on the plasticity index value. The high calcium fly ash collected from Neyveli thermal power plant was used as the primary source material. Sodium based alkaline activators were used, i.e., combination of sodium silicate and sodium hydroxide solution. Ratio of sodium silicate to sodium hydroxide (S/N) of 2.5 was chosen for the study. The molarity of NaOH considered was 7 M. Locally available

Table 1 Literature based on clay in geopolymers

References	Type of clay or soil used	Solutions and curing conditions	Remarks
[12]	Thermally treated Nigerian clay at 700 °C for 6 h	NaOH and Na ₂ SiO ₃ , Ambient temperature curing	The addition of calcined clay improved the dissolution of fly ash and hence improved the CS
[13]	Flood soil	NaOH and Na ₂ SiO ₃ , Oven curing at 75 °C	The curing temperature, molarity of NaOH and flood soil content influenced the geopolymer properties
[14]	Clays of low, medium and high plasticity	NaOH and Na ₂ SiO ₃ , Oven curing at 75 °C	The geopolymer properties were influenced by molarity of NaOH and plasticity of clay
[15]	Metakaolin and Tunasian natural clay, Calcined at 700 °C for 5 h	Phosphoric acid, Oven curing at 60 °C for 2 h	The crystalline phase of aluminum phosphate and monetite for both calcined and uncalcined based geopolymer was observed
[16]	Sidoarjo mud (Lusi)	NaOH and Na ₂ SiO ₃ , Steam curing at 60 °C for 6 h	Stronger matrix was achieved at 14M NaOH with steam curing
[17]	Dune sand	NaOH and Na ₂ SiO ₃ , KOH and K ₂ SiO ₃	Si/Al of GM increased with the addition of dune sand
[18]	Illitic clay (Friedland metaclay) heated to 875 °C	KOH and K ₂ SiO ₃	By heating better dissolution can be achieved by the distortion of the clay's structure. CS is influenced by surface area of clay

river sand was used as fine aggregate. The class C fly ash and clay content was taken in the ratio 75:25. The curing temperature in steam chamber was fixed as 75 °C.

2.2 Casting and Curing of GPC

For casting the concrete specimens, the materials were dry mixed for 3–4 min in a drum type mixer and then alkaline solution were added. The greased moulds were filled with the mix prepared and then vibrated with using a table vibrator. The specimens after vibrating were covered with polythene sheets to prevent the evaporation during curing. The specimens were kept in their moulds for 24 h and then they were removed and kept in a steam chamber for further curing. For GPC, heat curing substantially assists the chemical reaction in the concrete. Both curing time and curing temperature influence the CS of geopolymer concrete. The specimens were

steam cured for 24 h at 75 °C. They were taken out of the steam chamber and kept aside for 7 days for testing.

The GPC specimens after casting, specimens in steam chamber and cured specimens are shown in Figs. 1, 2 and 3, respectively.

Fig. 1 GPC specimens after casting



Fig. 2 GPC specimens kept in steam chamber



Fig. 3 Demoulded GPC specimens after curing



2.3 Experiments

2.3.1 Compressive Strength, Flexural Strength and Water Absorption

GPC cube specimens of size $150 \times 150 \times 150$ mm were used for testing CS (Fig. 4) and procedure was undertaken as per the guidelines of IS 513:1959 [19]. For evaluating FS, beam elements of size $150 \times 150 \times 500$ mm were used (Fig. 5). The test was performed as per IS 513: 1959 by adopting symmetrical two-point loading [19]. Water absorption was evaluated based on ASTM C642-82 on cube specimens of size 100×100 mm [20].

3 Results and Discussion

3.1 Compressive Strength, Flexural Strength and Water Absorption

The CS and FS improved with the incorporation of lime in clay by the partial replacement by 3% for clay 1, clay 2 and clay 3. The CS and FS improved by 20%, for clay 1, clay 2 and clay 3 based GPC after incorporating lime. The water absorption decreased by 8.5–10.5%, by the inclusion of lime in clay 1, clay 2 and clay 3 based GPC. The CS, FS and water absorption are reported in Tables 2, 3 and 4, respectively. The improvement in performance after the inclusion of lime in clay is attributed to the densification of microstructure due to the co-existence of C–S–H gel and aluminosilicate gel in GPC [4, 21–23].

Fig. 4 Compression testing of GPC



Fig. 5 Flexure testing of GPC



Table 2 Compressive strength of GPC

Properties	CS (MPa)		
	Clay 1	Clay 2	Clay 3
Raw clay GPC	33.78	39.65	36.22
Lime clay GPC	40.54	47.58	43.46

Table 3 Flexural strength of GPC

Properties	FS (MPa)		
	Clay 1	Clay 2	Clay 3
Raw clay GPC	4.05	4.56	4.35
Lime clay GPC	4.86	5.47	5.22

Table 4 Water absorption of GPC

Properties	Water absorption (%)		
	Clay 1	Clay 2	Clay 3
Raw clay GPC	9.36	9.81	10.67
Lime clay GPC	8.57	8.98	9.56

4 Conclusion

The development of GPC using low calcium fly ash and locally available clay was performed. The CS, FS and water absorption of GPC improved with the incorporation of lime in clay, for all the three types of clay based specimens. The incorporation of lime by partially replacing the clays results in the densification of the microstructure of the specimens due to the formation of C–S–H gel along with aluminosilicate gel (C–A–S–H and N–A–S–H gels). This resulted in the enhancement of CS and FS with the inclusion of lime into the system. A CS of 33–48 MPa was achieved with locally available clay-based GPC. The optimum proportion of fly ash and clay was obtained as 75:25, with 7 M NaOH solution and sodium silicate to sodium hydroxide ratio of 2.5 at 75 °C of curing temperature. Hence it can be concluded that locally available clays of any origin can be used in developing M30 and M40 grade GPC.

References

- Ming LY, Yong HC, Bakri MM, Hussin K (2016) Structure and properties of clay-based geopolymer cements: a review. *Prog Mater Sci* 83:595–629. <https://doi.org/10.1016/j.pmatsci.2016.08.002>
- Sakthidoss DD (2020) A study on high strength geopolymer concrete with alumina-silica materials using manufacturing sand. *Silicon* 12:735–746. <https://doi.org/10.1007/s12633-019-00263-wS>
- Parathi S, Naagarajan P, Pallikkara SA (2021) Ecofriendly 826 geopolymer concrete: a comprehensive review. *Clean Technol Environ Policy* 23:1701–1713. <https://doi.org/10.1007/s10098-828021-02085-082946>
- Saranya P, Nagarajan P, Shashikala AP (2021) Performance studies on steel fiber-reinforced GGBS-dolomite geopolymer concrete. *J Mater Civ Eng* 33(2):0899–1561. [https://doi.org/10.1061/\(asce\)mt.1943-5533.0003530](https://doi.org/10.1061/(asce)mt.1943-5533.0003530)
- Tenepalli SJ, Neeraja D (2018) Properties of class F fly ash based geopolymer mortar produced with alkaline water. *J Build Eng* 19:42–48. <https://doi.org/10.1016/j.jobbe.2018.04.031>

6. Chindaprasirt P, Chareerat T, Hatanaka S, Cao T (2011) High-strength geopolymer using fine high-calcium fly Ash. *J Mater Civ Eng* 23(3):264–270. [https://doi.org/10.1061/\(asce\)mt.1943-5533.0000161](https://doi.org/10.1061/(asce)mt.1943-5533.0000161)
7. Chiranjeevi K, Vijayalakshmi MM, Praveenkumar TR (2021) Investigation of fly ash and rice husk ash-based geopolymer concrete using nano particles. *Appl Nanosci*. <https://doi.org/10.1007/s13204-021-01916-2>
8. Fazil H, Yan D, Zhang Y, Zeng Q (2021) Effect of size of coarse aggregate on mechanical properties of metakaolin-based geopolymer concrete and ordinary concrete. *Materials* 14(12):3316. <https://doi.org/10.3390/ma14123316>
9. Akbar A, Farooq F, Shafique M, Aslam F, Alyousef R, Abduljabbar H (2021) Sugarcane bagasse ash-based engineered geopolymer mortar incorporating propylene fibers. *J Build Eng* 33:101492. <https://doi.org/10.1016/j.jobe.2020.101492>
10. Saranya P, Nagarajan P, Shashikala AP (2019) Development of ground-granulated blast-furnace slag-dolomite geopolymer concrete. *ACI Mater J* 116(6):235–243. <https://doi.org/10.14359/51716981>
11. Jithendra C, Elavenil S (2020) Effects of silica fume on workability and compressive strength properties of aluminosilicate based flowable geopolymer mortar under ambient curing. *Silicon* 12:1965–1974. <https://doi.org/10.1007/s12633-019-00308-0>
12. Ogundiran MB, Kumar S (2016) Synthesis of fly ash-calcined clay geopolymers: reactivity, mechanical strength, structural and microstructural characteristic. *Constr Build Mater* 125:450–457. <https://doi.org/10.1016/j.conbuildmat.2016.08.076>
13. Lekshmi S, Sudhakumar J (2021) Engineering and durability performances of fly ash based geopolymer mortar containing aluminosilicate rich flood soil waste with and without lime treatment. *Silicon* 14(11):6141. <https://doi.org/10.1007/s12633-021-01391-y>
14. Priyadharshini P, Ramamurthy K, Robinson RG (2017) Excavated soil waste as fine aggregate in fly ash based geopolymer mortar. *Appl Clay Sci* 146:81–91. <https://doi.org/10.1016/j.clay.2017.05.038>
15. Douiri H, Louati S, Baklouti S, Arous M, Fakhfakh Z (2017) Structural and dielectric comparative studies of geopolymers prepared with metakaolin and Tunisian natural clay. *Appl Clay Sci* 139:40–44. <https://doi.org/10.1016/j.clay.2017.01.018>
16. Ekaputri JJ, Triwulan I, Junaedi S, Fansuri, Aji RB (2015) Light weight geopolymer paste made with Sidoarjo mud (Lusi). *Mater Sci Forum* 803:63–74. <https://doi.org/10.4028/www.scientific.net/MSF.803.63>
17. Chuaha S, Duana WH, Panb Z, Huntera E, Korayemc AH, Zhaoa XL, Collinsd F, Sanjayane JG (2015) The properties of fly ash based geopolymer mortars made with dune sand. *Mater Des* 93:571–578. <https://doi.org/10.1016/j.matdes.2015.12.070>
18. Dietel J, Warr LN, Bertmer M, Steudel A, Grathoff GH, Emmerich K (2017) The importance of specific surface area in the geopolymerization of heated illitic clay. *Appl Clay Sci*. <https://doi.org/10.1016/j.clay.2017.01.001>
19. IS 513:1959 (n.d.) Methods of test of strength of concrete. Bureau of Indian Standards, New Delhi, p11
20. ASTM C 642 (n.d.) Standard test method for rate of water absorption. ASTM International, West Conshohocken, pp 1–4
21. Lekshmi S, Sudhakumar J (2022) An assessment on the durability performance of fly ash-clay based geopolymer mortar containing clay enhanced with lime and GGBS. *Cleaner Mater* 5:100129
22. Lekshmi S, Sudhakumar J (2022) Engineering and durability performances of fly ash based geopolymer mortar containing aluminosilicate rich flood soil waste with and without lime treatment. *Silicon* 14(11):6141–6156
23. Lekshmi S, Sudhakumar J (2022) Performance of fly ash geopolymer mortar containing clay blends. *ACI Mater J* 119(4):15–26

A Strategy Plan for Innovative and Sustainable Construction in Emerging Nations: A Case of India



Manisha Paul and Amit Kumar Jaglan

Abstract There is no question that the so-called “developing countries” require extensive infrastructure and built environment development. But these issues must be resolved in a way that is both socially and environmentally responsible. Instead of trying to change things after the fact, there is a pressing need to make sustainable interventions now, as these constructed environments are being produced. Yet, there are a number of obstacles to the adoption of sustainable construction technologies and practises, thus some enablers must be created to aid these nations in moving in that direction. There are two main strategies for addressing the financial difficulties of sustainable construction: market-oriented policies that affect the costs of specific types of construction and governance through standards, legal, and regulatory norms. In developed nations where the role of buildings in the economy is waning, sustainable construction goals are being implemented more aggressively on a macroeconomic level. In contrast, building is becoming increasingly significant in less developed or recently industrialised nations, yet sustainable building goals are more challenging to achieve. The adoption of sustainable construction development goals across the entire national economy is crucial for the construction industry at the meso-economic level. The management of sustainable building through legal and regulatory norms and practises and market-oriented policy that influences the costs of specific types of construction are the two complete strategies that are examined in this study. Also, to address some of these issues, the agenda 21 for Sustainable Building in Developing Countries recommended creating a research and development agenda based on a matrix of short-, medium and long-term technological, institutional, and value enablers. The current task is to create regional and national action plans that will allow these recommendations to be put into practise locally.

Keywords Sustainable · Construction · Development · Developing Countries · Policy

M. Paul (✉)

Department of Agronomy, Food, Natural Resources, Animals and Environment, University of Padova, Padova, Italy

e-mail: footprint1109@gmail.com

A. K. Jaglan

Department of Architecture, School of Planning and Architecture, New Delhi, India

1 Introduction

For the past few years, the fight against poverty, illiteracy, high infant mortality, short life expectancy, and other signs of low socioeconomic development has taken on a new urgency. Several levels of action are being taken in practise. These at the global level include the Millennium Declaration's adoption by all world leaders, the tracking of the goals and targets set forth in it, and the partial or whole cancellation of some nations' debts. The liberalisation of commerce and increasing aid are examples of bilateral initiatives. Additionally, some significant business organisations and individuals exhibit great altruism. It is the responsibility of building researchers to help end poverty for the billions of people who reside in developing nations. Certain important characteristics of the construction industry, its operations, and the interactions among them have been established because of the work done thus far. These characteristics demonstrate the value of and serve as a foundation for such study [16, 17, 18, 31, 38].

For developing nations to reap the most from construction's potential to contribute to national growth and development, it is urgent that study be done and recommendations be made for the immediate steps that must be followed. Construction engineering has increasingly used the idea of sustainability. Construction planning and management, building design, construction work, building maintenance, and building or infrastructure object restoration are all included in the field of construction engineering. Many nations around the world are paying more attention to the need for building renovation. This is due in part to an ageing building stock. The pressing need to lower energy use and greenhouse gas emissions in buildings is another factor. At COP 21, the United Nations Framework Convention on Climate Change (UNFCCC) reached an agreement to restrict the rise in global temperature to 1.5 °C over pre-industrial levels by 2050. This needs a swift switch to clean, renewable energy. Without reducing the energy consumption everywhere possible, including in buildings, achieving the target won't be attainable. In the world, the building industry handles about 28% of all energy-related CO₂ emissions [30].

Thus, upgrading the current stock's insulation and switching to carbon-free building services (heat, cold, ventilation, and electricity) must play a significant role in achieving emissions reductions. A special issue of *Energy and Buildings* offers insights on the energy efficiency of residential buildings in Europe and the tracking of repair efforts [37]. To ensure affordable housing and economic sustainability, it is simultaneously necessary to modernise numerous structures for social sustainability by raising quality of life standards. Moreover, more research is being done on sustainable building renovation (SBR). A suggestion for a research agenda for SBR based on a review article was included in an editorial article written by the first guest editor of this special issue [5, 21]. The pace of research on construction in developing nations has slowed practically to a standstill, despite the pressing need for it. This remark has long been made, and it was recognised that the direction of the field's study had changed [29, 28].

There are numerous explanations for this. First, the multilateral lending organisations and donor organisations from industrialised nations that once supported such studies have lost interest. Second, because so many of the field's previous articles are somewhat dated and no longer easily available, researchers today often revisit topics that were thoroughly covered many years ago, and not much new has been discovered in that time [34]. Researchers studying construction in emerging nations need to pay close attention to several fresh concerns that have surfaced. These include:

- (i) the private sector's participation in the provision of infrastructure and other significant construction projects.
- (ii) the internationalisation of construction with the advent of globalisation and the liberalisation of economic regimes.
- (iii) the formation of regional economic blocks and common markets, including among developing countries.
- (iv) the international recognition of the necessity of eradicating poverty; and
- (v) the concern of the international community with sustainable development, particularly environmental issues.

Given the increased political attention given to sustainable building renovation, it is crucial to examine and show the impact that sustainable building renovation can have on resolving significant societal challenges, such as those related to the Sustainable Development Goals of the United Nation, climate change, energy transition, circularity, industrialization, digital transformation, affordable housing provision and equality, heritage preservation, social value, and quality of life.

1.1 Language of Sustainable Building

As “construction” and “sustainable” are both extremely complicated concepts, there is an ongoing discussion regarding their definitions. The interpretive conundrum is made even more difficult by combining these two phrases to create a third. Without first addressing the questions of “sustainable for whom and sustainable in what way,” it is impossible to define “sustainable building” as merely “construction that is sustainable”. Additionally, there are specific and general definitions of construction.

In short, sustainable construction in developing countries plays a crucial role in fostering long-term environmental, social, and economic well-being. By integrating eco-friendly practices and innovative technologies, these countries can mitigate the negative impacts of construction on natural resources, reduce carbon emissions, and promote sustainable development. Emphasizing locally sourced materials not only decreases construction costs but also supports local economies. Additionally, incorporating energy-efficient designs, renewable energy systems, and improved waste management strategies can enhance the overall sustainability of buildings. Furthermore, sustainable construction practices can create job opportunities, improve living conditions, and enhance the resilience of communities, ultimately paving the way for a more sustainable future in developing countries. This part of the study aims

to describe the specific interpretations of these principles that guided the Agenda 21 Sustainable Building in Developing Countries because there are currently no agreed-upon common definitions [35].

1.1.1 Construction

Construction can be understood on four different levels, including site activities, the full project cycle, everything associated with the business of construction, and the overall process of developing human settlements [20]. The site operations that result in the realisation of a particular building or other construction project (such as a road, bridge, or dam) are the most frequent interpretation. Construction is seen as a particular stage in the project cycle at this most basic level. Intervention at this level, meanwhile, is only allowed in areas directly under the contractor's direct authority. The second interpretation of construction is the comprehensive cycle of a construction project, covering important stages like feasibility, design, building/construction, operation, decommissioning, demolition, and disposal [4].

Broader concerns must be addressed at stages earlier or later in the project cycle. Even though the interventions in the construction life cycle described above might significantly lessen the impact of the finished product, they do not encompass all related activities. Millions of employments and a sizable amount of GDP are generated by the construction industry alone, which forms a sizable portion of the global economy. When combined with other sectors and industries involved in the manufacturing and distribution of materials, as well as service industries like transportation, finance, and the real estate market, its effects on society, the environment, and the nature of our planet are profound. The creation of human settlements, including the planning, design, and execution phases, falls under the fourth level.

1.2 Sustainable Construction

Sustainable building and built environments are defined as “the contributions by buildings and the built environment to achieving components of sustainable development” and “the sustainable production, use, maintenance, demolition, and reuse of buildings and constructions or their components,” respectively, by the International Council for Research and Innovation in Building and Construction [1, 2]. Other definitions of sustainable construction are as follows: “Sustainable construction, in its own processes and products during their service life, aims at minimising the use of energy and emissions that are harmful to environment and health, and produces relevant information for customers to make their decision” [19].

Sustainable construction is described as “a holistic process seeking to restore and maintain balance between the natural and built ecosystems and develop settlements that recognise human dignity and support economic fairness” in Agenda 21 for Sustainable Construction in Developing Countries. This definition goes beyond the

prior definitions' inferred emphasis on minimising negative effects by specifically stating the aims of the social and economic components of sustainability, as well as incorporating the concept of environmental restoration [10]. All these definitions fall short in one way or another, but they do serve to identify three components of sustainable building. First, it calls for a broad definition of construction as a life-cycle activity including many more stakeholders than just those who are often associated with the construction business. Second, it emphasises on environmental preservation and raising people's and communities' quality of life. Finally, it encompasses non-technical factors of social and economic sustainability in addition to technological solutions.

People in underdeveloped nations experience the most environmental stress because many of them depend on natural ecosystems for their livelihoods. Furthermore, many nations' governments lack the resources to handle the pressure. To ensure that the significant amount of building that will be done in developing nations as part of the urbanisation process is done in ways that are "socially and ecologically appropriate," [10]. Du Plessis proposes that action should be started now.

A framework for a coordinated solution to the problem of reducing the social and ecological impact of construction is provided by the International Council for Research and Innovation in Building and Construction. The framework emphasises cooperation between all stakeholders. The framework will direct discussion between the various governmental levels, the larger construction industry, academic institutions, research facilities, and civil society at the national, regional, and international levels to develop and implement national and regional action plans for sustainable construction.

1.3 Industry Structure

Confusion is being caused by the growing variance in how "informal" construction activity is understood. The organisation of the construction industries in emerging nations is little understood, and the evolution of this organisation over time is even less well understood. Due of its size and importance, the informal sector is of particular interest to emerging nations, yet it is poorly understood. The informal sector of businesses, informal labour, the informal construction system, and informal buildings/settlements are the four "areas of informality" that are "often connected". Du Plessis [10] mentions evidence from numerous regions of the world (both developed and developing) that the building business is becoming more "informal". Wells investigates the different aspects of informality.

As construction is subject to a wide range of laws, she contends that since the absence of regulation is the core of informality, several interpretations of informality are unavoidable. To prevent misunderstandings and reap the full benefits of the sector for the construction industries in developing nations, it is crucial that the informal sector be clearly defined. The foundation for additional research on the industry, including the interaction between the formal and informal sectors, which might be

investigated to benefit from practical combinations of the two sectors, the causes and impacts of growing informality, and possible remedial actions.

2 Difficulties with Culture in Developing Nations

Many projects consist of both nationals of the host country and expats as employees. Wong investigates the leadership perceptions of and power relationships among Hong Kong Chinese and expatriate project managers from Western countries in the multinational construction firms in Hong Kong to gauge the potential impact of intercultural interactions among project participants on the working styles of professionals. Wong discovered that both management groups equally value both interpersonal relationships and work performance. Yet, there was a distinction between the two management groups in terms of how they interacted with their subordinates in terms of power [13, 33, 39].

Although both local and foreign project managers are adjusting their leadership perspectives to some extent across cultures, Wong concludes that some deeply ingrained cultural values and beliefs cannot be readily changed. The results of Wong's study are helpful for senior management of construction companies that operate in multicultural work environments because they would make it easier for them to appreciate and take into account culture in their interactions with their employees from different countries, as well as with staff from other companies and, equally important but rarely appreciated, with the local population in the host countries where they operate [39].

2.1 Design and Construction Methods for Social Sustainability in Developing Countries

We suggest that planning, designing, and building projects in the developing world start by adhering to these social sustainability processes by fusing research findings with examples of best practises.

2.1.1 Acquire Land Using Lawful Methods that Respect Local Customs

By assisting a person or group that does not own the property they are attempting to construct on, organisations run the risk of overextending themselves (or already occupy). Many people throughout the world who claim to own a home or piece of land but lack a land title. Local customs may make ownership issues even more difficult. Land disputes are a significant issue in India. As a result, before beginning any design work for a property, EMI, for instance, asks to examine the title [15, 26].

2.1.2 Include the Neighbourhood in All Phases of the Project

This idea is ingrained in how Engineers Without Borders runs. Engineers without Borders makes a five-year minimum commitment to the project community when it accepts a project. There are three phases to these projects: implementation, monitoring, and assessment. The community in need must apply with a formal letter asking assistance to Engineers without Borders before an Engineers without Borders chapter goes. Following its approval, the chapter will always make an assessment trip before beginning any construction. The chapter carries out health and need surveys and talks with local leaders about various implementation strategies. The community and the chapter ultimately settle on a project [14].

The community must also contribute at least 5% of the project's cost prior to construction to assure that there will be funds available for system maintenance and eventual replacement. On implementation trips, community members work on the project under the engineers' supervision and consult with the chapter frequently about implementation possibilities. Selected community members receive training in system maintenance and operation.

An established maintenance fee collection system, a strong relationship between the Engineers Without Borders chapter and an in-country NGO, and a signed memorandum of understanding regarding the community and chapter cooperation are additional requirements of Engineers Without Borders projects for the assisted communities [11].

2.1.3 Design with Consideration for the Culture of the Area

The usage of exposed brick serves as a representation of regional culture. Masonry is frequently used in construction in East Africa due to the accessibility of locally obtained clay and kilns controlled by families or communities. To hide the local brick, builders almost typically add painted plaster to interior walls. On the outer façade, brick or natural stone from a factory are added. It is deemed undesirable in this cultural setting to leave the native brick visible because doing so symbolises poverty (the same is often true in India). In one instance, EMI built the interiors and exteriors out of local brick. It appears stunning to western eyes. However, the Ugandan leadership at one nearby EMI-designed church opted to cover the exposed brick "feature" walls with drapery, demonstrating that owners and western designers may have differing perspectives on "excellent design" [8].

2.1.4 Consider Local Codes While also Adhering to International Standards When Designing for the Safety of the Building's Residents

In some places of the developing world, there could not be any building codes. Even if they do, it might not be feasible to construct to western-style standards. By pursuing

worldwide standards while considering the realities of locally accessible materials and construction techniques, building designers should seek to increase safety. For instance, standard building practise in India (and much of the developing world) is to first add several courses of brick to the external wall of the building, followed by a reinforced concrete ‘ring-beam’ at about 3 m high. Finally, the roof trusses are placed on top of the brick. Raising the height of the ring beam so that the trusses rest on it is an improved detail. Then, instead of relying on the questionable strength of the native clay brick, the trusses can be fixed to the building directly.

It’s a minor adjustment to a minor detail, yet it could increase building longevity and earthquake and wind safety. Even though the right detail is depicted in the plans, it could still need to be properly explained to construction workers and contractors [27, 36].

2.1.5 Design Initiatives that the Community May Safely Implement

Many developing nations’ educational systems could not adequately train local contractors to comprehend the implications of their choices, to exercise critical thought, or to ask questions. An EMI team was asked to assess the structural viability of adding a second floor to a newly built elementary school in a case from North India. Both the client and the neighbourhood builder had no prior experience with a structure of that size. In addition to the structure’s inability to support a second story, the EMI team discovered that it was also predisposed to collapsing in the case of an earthquake. They created a retrofit that was easy and affordable enough for a local builder to complete using standard information (in Hindi and English) from India’s Building Materials and Technology Development Council. “Innovations in earthquake-resistant construction in the developing world must be at a size that is realistic for the owners and builders to understand and apply” [23, 32].

3 Developing Countries’ Future Struggle with Sustainable Construction

Developing countries face several systemic issues, including rapid rates of urbanisation, extreme poverty, social inequality, a lack of institutional capacity, poor governance, an unstable economic environment, and environmental degradation, all of which by themselves create a difficult environment in which to work. Due to the complexity of this developmental problem, it can be difficult to distinguish between measures that try to promote development and those that ensure that the necessary development adheres to sustainable development principles. As a result, plans and strategies for sustainable development are wish lists supported by significant commercial and political interests that have a predetermined cultural interpretation of what constitutes development [3, 6, 7].

Globalization and environmental concerns are two areas where action is arguably most urgently needed. When it comes to globalisation, research should work to give developing-nation businesses the tools they need to respond strategically to the entry of foreign companies into their home markets so they can profit from doing business with them, learning from them, competing with them, collaborating with them, and using them as models and benchmarks. Regarding sustainability, efforts are needed to lessen the building industry's impact on environmental stress in developing nations, for instance by implementing the Agenda 21 for Sustainable Construction in Developing Countries.

To prevent the study of construction in developing nations from being ignored, researchers should work together. Most of these scholars, like me, have received their indirect taxes, levies, and other sacrifices to further their education, thus the poor people of developing nations have a right to expect more from them [25, 32, 40].

Nonetheless, it might be argued that sustainability lies more in the interactions between these realms than in acts within each of them. A sustainable development strategy that prioritises jobs over the environment or a renewable energy project that overlooks its effects on the environment and society, uproots thousands of people, and reduces biodiversity are ineffective in achieving their stated goals. The three pillars model has been effective in highlighting the need for a comprehensive approach; however, this model does not promote the integrative thinking required to address what is, at its core, a systems problem [9]. The idea that sustainable development should be viewed as an all-encompassing solution (the whole being more than the sum of its parts) to the complex systems challenges of the linked and interdependent linkages that dictate the interactions between humans, their society, economy, and technology, and the biosphere, is strongly supported in the literature [12, 22, 24].

Finding a comprehensive strategy to ensure that its contribution to the physical, economic, and human development of these countries complies with the requirements of sustainable development as defined by locally discernible needs and value systems represents the biggest challenge for the construction sector in developing countries (which may differ from the needs and values of the economic elite in these countries). The creation of a framework for such an all-encompassing approach was the goal of the Agenda 21 Sustainable construction in developing countries. Along with that, the following coordinated actions might be implemented:

- (i) formulation of, and agreement on, definitions of important terminology in construction in the context of developing nations
- (ii) establishment of, and agreement on, frameworks for researching national construction industries and aspects including human resource development, technological development, and corporate development
- (iii) implementation of these coordinated actions; and
- (iv) implementation of these coordinated actions [17].

4 Future Decisions to Make

The strategy's development of certain enablers is just one component. All the many parties involved in the development of the built environment must take specific steps to foster a supportive environment to ensure the development and adoption of these enablers. The following factors are the focal point of these actions:

- (i) Increasing capacity (internally and externally).
- (ii) Creating accessible and long-lasting financing sources and means of gaining access to them.
- (iii) Forming alliances and other forms of international and cross-sectoral collaboration.
- (iv) Internal reorganisation to align business processes with sustainability ideals.
- (v) Creating initiatives and systems to promote and aid implementation.
- (vi) Creating and utilising the best monitoring and evaluation systems and solutions for businesses and industries.

For research and education, the commercial sector, service providers, governments and regulatory stakeholders, and civil society, the actions under each of these groups will vary. Government will need to take a strong role in putting such a strategy into motion in developing nations where the business case for sustainable construction is still weak and civil society is focused on meeting immediate, survival requirements. Although it might be claimed that governments in developing nations are frequently weak, they do have the power to provide the institutional enablers required to strengthen the business case and raise the capacity and skill levels of the sector through their own procurement procedures, incentive programmes, and taxation.

5 Conclusion

Even though there has been a lot of research on the subject, social sustainability has not received as much attention as economic and environmental sustainability. This is particularly true in developing nations, where numerous local factors are disregarded by traditional sustainability criteria and grading systems. In the poor world, socially sustainable design and construction are being used, but there is still much space for development. The triple bottom line will be balanced by using the social sustainability methods described here as a starting checklist for initiatives in the poor world, which will help generate sustainable results. The building industry in emerging nations must play a crucial part in meeting this need as these nations will more and more often serve as the hub for industrial and infrastructure growth. There is currently a (restricted) window of opportunity due to the low levels of physical development to direct construction in a more sustainable direction. It is urgently necessary to respond in a clear and organised manner to take full advantage of this opportunity. A comprehensive framework to direct the development of such

a response is provided by the Agenda 21 Sustainable Construction in developing nations strategy. It has identified that several actions that need to be completed right now to address the most pressing issues preventing the transition to more sustainable construction:

- creating country-specific benchmark data, increasing awareness,
- gaining access to finance, establishing networks and collaborations, and
- building capacity.

From this perspective, it is obvious that a significant plan for sustainable construction in developing nations cannot be developed by a small group of experts sequestered in a conference room. It can only result from communication between the various levels of government, the larger construction sector, academic institutions, research facilities, and civil society on a global scale. Such a plan will need to be developed through a consultative process akin to that used in the creation of the Earth Charter, as well as at the national level through a process that places the global strategy in a local context and addresses local needs and priorities.

Thus, the implementation of Agenda 21 Sustainable Construction in developing nations holds tremendous potential for creating a more sustainable and resilient built environment. By adopting a holistic approach that addresses environmental, social, and economic aspects, these countries can transform their construction sectors into drivers of sustainable development. Through the utilization of eco-friendly materials, energy-efficient designs, renewable energy systems, and improved waste management practices, sustainable construction can significantly reduce the environmental footprint while improving the quality of life for communities. Furthermore, by promoting local sourcing, job creation, and building ability, sustainable construction contributes to the social and economic empowerment of developing nations. By embracing the principles of Agenda 21 Sustainable Construction, these countries can build a sustainable future that balances the needs of present and future generations.

Disclaimer Views expressed in the paper are personal and suggestive.

References

1. 50 years of international cooperation to build a better world. (2004). CIB, Rotterdam. <https://cibworld.org/member-benefits/>
2. Ahiabu MK, Emuze FA, Das DK (2022) A review of sustainable construction practices in Ghana. In: Climate emergency—managing, building, and delivering the sustainable development goals, pp 93–104. https://doi.org/10.1007/978-3-030-79450-7_9
3. Ali AH, Kineber AF, Elyamany A, Ibrahim AH, Daoud AO (2023) Modelling the role of modular construction’s critical success factors in the overall sustainable success of Egyptian housing projects. *J Build Eng* 106467. <https://doi.org/10.1016/J.JOBE.2023.106467>
4. Alsubeih MA (2013) A strategic framework for sustainable construction in Jordan. 3(2). www.iiste.org

5. Anker P, Brinkø J, Anker Jensen P, Maslesa E, Brinkø Berg J (2018) Sustainable building renovation: proposals for a research agenda. *Sustainability (Switzerland)* 10(12). <https://doi.org/10.3390/su10124677>
6. Assefa S, Lee HY, Shiue FJ (2022) A building sustainability assessment system (BSAS) for least developed countries: a case of Ethiopia. *Sustain Cities Soc* 87:104238. <https://doi.org/10.1016/J.SCS.2022.104238>
7. Bao Z (2023) Developing circularity of construction waste for a sustainable built environment in emerging economies: new insights from China. *Develop Built Environ* 13:100107. <https://doi.org/10.1016/J.DIBE.2022.100107>
8. Chawhan V, Kamal MA (2021) A study of planning, design and construction of buildings in Hilly regions of India. *Am J Civil Eng Architect.* 9(1):13–22. <https://doi.org/10.12691/AJCEA-9-1-3>
9. Daly HE (1990) Sustainable development: from concept and theory to operational principles. *Popul Dev Rev* 16:25. <https://doi.org/10.2307/2808061>
10. Du Plessis C (2002) Agenda 21 for sustainable construction in developing Countries. In: CSIR building and construction technology
11. EWB-USA, Principles of Development (2015). <https://volunteer.ewb-usa.org/s/article/EWB-USA-Common-Terms-and-Definitions#PMEL>
12. Gilbert R, Stevenson D, Girardet H, Stren R (1996) Making cities work: the role of local authorities in the urban environment. In *Making cities work: the role of local authorities in the urban environment* Earthscan. [https://doi.org/10.1016/s0264-2751\(97\)82707-2](https://doi.org/10.1016/s0264-2751(97)82707-2)
13. Giritli H, Oraz GT (2004) Leadership styles: some evidence from the Turkish construction industry. *Constr Manag Econ* 22(3):253–262. <https://doi.org/10.1080/01446190310001630993>
14. Hedborg S, Karrbom Gustavsson T (2020) Developing a neighbourhood: exploring construction projects from a project ecology perspective 38(10):964–976. <https://doi.org/10.1080/01446193.2020.1805479>
15. Hendry J, Tatum ML (2018) Building new traditions: drawing insights from interactive legal culture. *Palgrave Socio-Legal Studies*, pp 161–182. https://doi.org/10.1057/978-1-137-60645-7_11/COVER
16. Hillebrandt PM (2000a) Economic theory and the construction industry. *Econ Theory Constr Indust.* <https://doi.org/10.1057/9780230372481>
17. Hillebrandt PM (2000b) The construction industry and the economy. *Econ Theory Constr Indust* 19–28. https://doi.org/10.1057/9780230372481_3
18. Hillebrandt PM (2000c) The nature of construction economics. *Econ Theory Constr Indust* 3–8. https://doi.org/10.1057/9780230372481_1
19. Huovila P, H2ikkinen T, Aho I (n.d.) Sustainable construction in Finland: approach and best practices
20. Irurah DK (n.d.) Agenda 21 for sustainable construction in developing Countries Agenda for sustainable construction in Africa
21. Jensen PA, Maslesa E, Berg JB, Thuesen C (2018) 10 questions concerning sustainable building renovation. *Build Environ* 143:130–137. <https://doi.org/10.1016/J.BUILDENV.2018.06.051>
22. McDonough W, Braungart M (2002) Cradle to Cradle: remaking the way we make things. *Choice Rev Online* 40(02):40–0914. <https://doi.org/10.5860/CHOICE.40-0914>
23. Mike Eugene Collins (2007) EMI, architectural design guide, EMI East Africa. <https://www.scribd.com/document/395818349/eMiEA-Architectural-Design-Guide>
24. Mirzaie K, Fesharaki MN, Daneshgarb A (2012) Trust modeling based on Capra cognitive framework. *Proc Soc Behav Sci* 32:197–203. <https://doi.org/10.1016/J.SBSPRO.2012.01.030>
25. Molenaar AAA (2013) Durable and sustainable road constructions for developing Countries. *Proc Eng* 54:69–81. <https://doi.org/10.1016/J.PROENG.2013.03.007>
26. Mukherjee A (2018) Customary law and land rights: the Cautionary Tale of India, Jharkhand, and the Chotanagpur Tenancy Act. *Palgrave Socio-Legal Studies*, pp 97–109. https://doi.org/10.1057/978-1-137-60645-7_7/COVER
27. National Building Code - Bureau of Indian Standards. (2016). In: *National Building Code of India (NBC)*. <https://www.bis.gov.in/standards/technical-department/national-building-code/>

28. Ofori G (1994) Formulating a long-term strategy for developing the construction industry of Singapore. *Constr Manag Econ* 12(3):219–231. <https://doi.org/10.1080/01446199400000030>
29. Ofori G (2007) Construction in developing countries. 25(1):1–6. <https://doi.org/10.1080/01446190601114134>
30. Perspectives for the Clean Energy Transition—Analysis—IEA. (n.d.). Retrieved April 9, 2023, from <https://www.iea.org/reports/the-critical-role-of-buildings>
31. Pheng LS, Leong CHY (1992) A revisit to Turin’s paradigm. *Construction and development in the 1970s and 1980s. Habit Int* 16(3):103–117. [https://doi.org/10.1016/0197-3975\(92\)90067-9](https://doi.org/10.1016/0197-3975(92)90067-9)
32. Pocock J, Steckler C, Hanzalova B (2016) Improving socially sustainable design and construction in developing countries. *Proc Eng* 145:288–295. <https://doi.org/10.1016/J.PROENG.2016.04.076>
33. Rowlinson S, Ho TKK, Po-Hung Y (1993) Leadership style of construction managers in Hong Kong. *Constr Manag Econ* 11(6):455–465. <https://doi.org/10.1080/01446199300000051>
34. Ruddock L, Lopes J (2006) The construction sector and economic development: the “Bon curve.” *Constr Manag Econ* 24(7):717–723. <https://doi.org/10.1080/01446190500435218>
35. Sustainable buildings | UNEP - UN Environment Programme. (n.d.). Retrieved April 9, 2023, from <https://www.unep.org/explore-topics/resource-efficiency/what-we-do/cities/sustainable-buildings>
36. Vaughan E, Turner J (2013) Report | The Value and Impact of Building Codes | White Papers | EESI. Environmental and Energy Study Institute. <https://www.eesi.org/papers/view/the-value-and-impact-of-building-codes>
37. Visscher H, Sartori I, Dascalaki E (2016) Towards an energy efficient European housing stock: monitoring, mapping and modelling retrofitting processes: special issue of energy and buildings. *Energy Build* 132:1–3. <https://doi.org/10.1016/j.enbuild.2016.07.039>
38. Wells J (1986) The construction industry in developing countries: alternative strategies for development 184
39. Wong J, Wong P, Heng L (2007) An investigation of leadership styles and relationship cultures of Chinese and expatriate managers in multinational construction companies in Hong Kong. 25(1):95–106. <https://doi.org/10.1080/01446190600632573>
40. Ye K, Shen L, Zuo J (2013) Utilizing the linkage between domestic demand and the ability to export to achieve sustainable growth of construction industry in developing countries. *Habitat Int* 38:135–142. <https://doi.org/10.1016/J.HABITATINT.2012.05.008>

Behaviour of SFRC Filled Cold Formed Steel Built-Up Columns



Nanda S. Gopan and Ajai Thampy

Abstract Due to the appropriate composite action between the steel and concrete, steel concrete composites are gaining popularity in civil industry. Steel that are used in field is of different type. One such variety is Cold Formed Steel, CFS have comparatively high yield point and tensile strength making it suitable for wide range of applications. SFRC is claimed as modern cost-efficient building material as its exhibits more ductile failure. It eliminates the brittle failure in the concrete. In this study twelve built-up column is modelled in solid works and evaluated using ANSYS workbench software. 0.6, 1.2 and 1.8% of steel fibers are added to the infilled concrete and axial load is applied. It is further compared with the analysis of normal concrete filled built-up column. From the analysis report, SFRC filled built-up column has more bearing capacity than the ordinary concrete filled column. The columns filled with 1.8% of steel fiber possess more ductility index and ultimate load capacity. It has less lateral deformation compared to other models. In overall adding steel fibers to concrete increases the ductility and load bearing capacity of the column.

Keywords Concrete filled cold formed steel · Composite columns · ANSYS · Deformation · Ductility index · SFRC · Ultimate load

1 Introduction

Cold formed steel sections are applied in numerous engineering applications due to their low self-weight, altitude structural performance and outstanding material properties during the manufacturing process and construction stages. Thin sheets of cold-formed steel are produced, and these parts are frequently utilized in floor decking, built-up sections, columns, beams, and joists. They are also used in the

N. S. Gopan · A. Thampy (✉)
Amal Jyothi College of Engineering, Kanjirapally, Kottayam, India
e-mail: ajaihtampy@amaljyothi.ac.in

N. S. Gopan
e-mail: nandasgopan1997@gmail.com

construction of transmission poles, drainage systems, and railroad products. Panels and structural forms are the two main categories of CFS products. Open sections, closed sections, and built-up sections are some of the different structural shapes. C-sections, U-sections, Z-sections, E-sections, and I-sections are several CFS profiles is filled with steel fibers of various percentages. Concrete with steel fiber reinforcement is a composite material made of steel fibers and regular or specialty cements. When scientists recognized that SFRC could enhance the mechanical characteristics of concrete, including tensile strength, durability, fatigue life, toughness, impact resistance, and ultimate flexural strength capacity of the structural element, they discovered it to be beneficial. The mechanism of steel fibers in bringing the cracks in concrete is due to the pressure of shear stress at the interface between the steel fibers and the surrounding concrete materials. This shear stress transmission of force is due to SFRC there is combined section of concrete and steel through the combination action of bond components such as physical and chemical adhesion, the mechanical component of bond and fiber interlock.

A study on the buckling resistance of short columns made of concrete-filled cold-formed steel (CF-CFS) built up under compression was presented by Rahnavard et al. [1]. Twelve CF-CFS built-up specimens were used in the investigation, and four distinct cross section forms were assessed. FE conceptualization is carried out with Abaqus. The local and distortional buckling modes were present. Comparatively to CFS built-up sections without concrete, the bearing capacity of CFS built-up sections when employed in CF-CFS columns increased. The results from experimental tests and FE models showed a high degree of agreement. Test results to numerical analysis are compared in a range of 0.01–1.23. Due to the high concrete area and high confinement, the R-2U + 2C column has the maximum load bearing capacity [2].

A study on the buckling resistance of steel-fiber reinforced concrete encased steel composite columns was conducted by Venkateshwaran et al. [3]. The SFRHSC-encased steel composite columns were tested under eccentric compression loads to failure in order to establish its buckling resistance, as well as the behavior of the interaction between compression and moment strengths. The study findings demonstrated that the steel fiber-reinforced composite columns exhibited ductile behavior despite longitudinal steel reinforcements and were free of any debonding or early cover spalling indicators. According to test results, the steel fibers with hooked ends could successfully traverse the cracks as they widened [4].

Li et al. [5] researched about shear performance of steel fibers reinforced self-confinement and self-compacting concrete-filled steel tube stub columns. The failure mode of FSSCFST stub columns was demonstrated by experimental results to depend on the shear span-to depth ratio [6]. Steel fiber bridged the plastic cracks close to the shear failure plane, increasing the concrete's ductility and shear resistance. Bharkavi [7] researched about experimental and theoretical investigation on flexural member and analysis by ANSYS. Lu et al. [8] examined the axial compression behavior of steel fiber reinforced concrete-filled steel tube columns [9]. The study's objective was to assess the effects of steel fiber on the behavior of steel tube columns filled with varied concrete strengths and steel tube thicknesses. 36 specimens were tested using concrete with strengths of 50–70 MPa, steel tube thicknesses of 3, 4,

and 5, and steel fiber volume percentages of 0, 0.60, 0.90, and 1.20%. Comparing SFRCFST columns to PCFST columns of the same size, the ultimate loads on the SFRCFST columns are marginally greater. The addition of steel fibers, however, enhances the composite action between the steel tube and concrete core and enhances the concrete strength. Compressive stress–strain relationships of high strength steel fiber reinforced concrete were taken into consideration by Liao et al. [10]. The bond strength is taken into account in the proposed stress–strain model in this study. The empirical formulas for the suggested stress–strain model are produced by regressing 61 of the SFRC stress–strain curves. Compression tests on SFRC specimens are also used to validate the proposed stress–strain model.

A new type of built-up column proposed by Rahnavard et al. [1] is modified by incorporating the SFRC into the built-up column, the ultimate load and other strength parameters will change. A notable change in the ductility of the column can be witnessed [11]. In this study the behavior of the built-up column having 0.6, 1.2 and 1.6% of steel fibers [12]. This paper investigates the combined action of steel fiber and the cold formed steel in built up columns. The crack prevention property in steel fiber is combined with the high strength and tensile capacity of CFS to analyses the effect on the built-up columns [13].

2 Study of SFRC Filled Built-Up Column

Twelve specimens were tested to study the effect of steel fibers on the built-up column. Solid works is used for the modelling of column sections and analysis is done by ANSYS. The line tool is used in solid works further its extruded to obtain thickness. The position of the screws is as mentioned in Rahnavard et al. [1]. The built-up columns were made of high strength ductile CFS profiles and cross section used for study are square and rectangle (Figs. 1, 2 and 3; Tables 1 and 2).

SFRC filled CFS built up column is meshed using a square mesh of size 5 mm. Axial load is applied to the specimen with fixed as the end conditions [14]. The

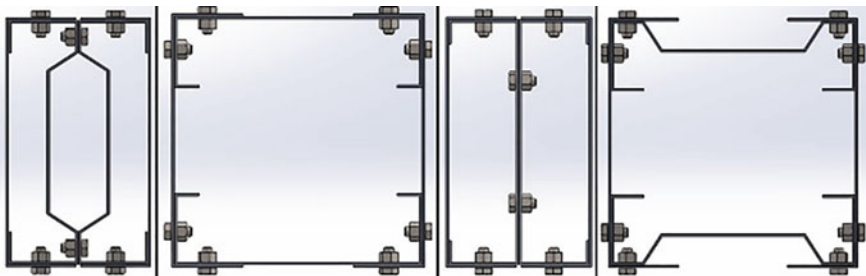


Fig. 1 Cross section of profiles

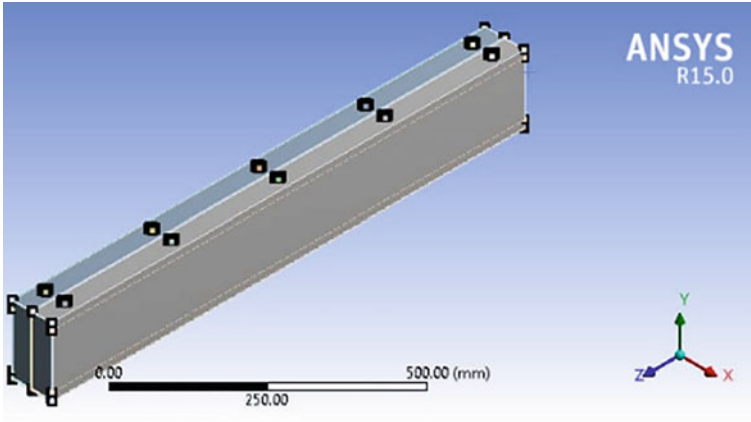


Fig. 2 Modelled column

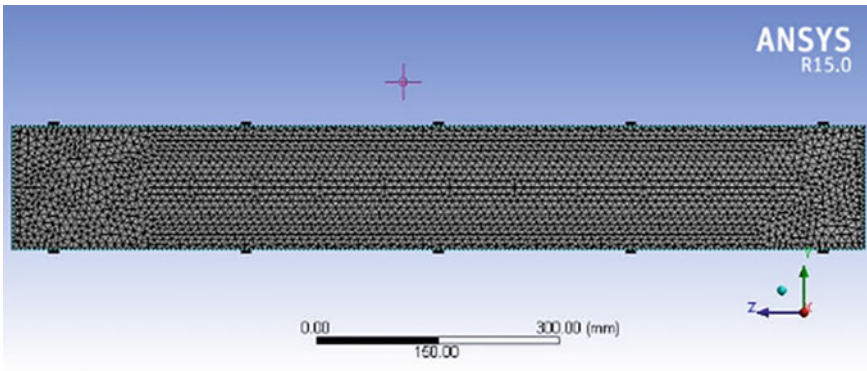


Fig. 3 Meshed column

Table 1 Dimensional details of CFS profiles [1]

Component	Length (mm)	Breadth (mm)	Thickness (mm)
C	150	43	1.5
U	153	43	1.5
Σ	150	43	1.5

Table 2 Material properties of steel fibers [8]

Type of fiber	Hooked end type
Length	30 mm
Diameter	0.52 mm
Aspect ratio	57.6
Density	7850 kg/m ³
Tensile strength	> 1060 MPa
Modulus of elasticity	2 × 10 ⁵ N/mm ²

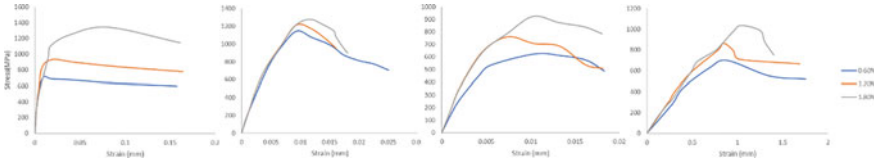


Fig. 4 Comparison of stress–strain graph of columns respectively as shown in Fig. 1

loading is increased at a particular time interval of 120 s [15]. Different loads of 100kN, 200kN, 400kN up to 1400kN are applied.

2.1 Analysis of Columns

Analysis is carried out to study the behavior of SFRC filled CFS built up column with different steel fiber percentages. Non-linear static structural analysis is carried out in ANSYS software [16]. Deformation, stress–strain relation w.r.t steel fibers [17] and ultimate loads are studied (Fig. 4).

The addition of steel fibers additionally decreased the column’s deflection. This improvement in the interfacial bond between the concrete matrix and steel fiber is what accounts for the increased ultimate load, ductility, and decrease in deformation. A greater energy dissipation capacity of the columns can be achieved as a result of higher deformation capacity of SFRC-filled CFS-built-up columns.

2.2 Result and Comparison

Ductility index is a measurement of ductility of the columns. Higher the value of DI more ductile the column. It is expressed as in Eq. 5.2 [10] (Figs. 5, 6 and 7).

$$\delta_{\text{ultimate load}} = \frac{\text{Ductility index (DI)}}{\delta_{\text{yield load}}}$$

From the comparison of the graphs, ductility index of M2 that is S-2C + 2U is highest in all steel fiber percentages. It is due to high confinement and larger concrete area. SFRC eliminated the brittle failure thus delays the failure making it ductile. The values of other all models follow a same trend of having highest DI for column having 1.8% of steel fiber. The increased bond and action between the concrete and steel fibers make it more ductile [18]. When the loads acts crack occurs, the steel fibers present in it prevents the propagation of the cracks. As the steel fiber volume fraction increases the maximum deformation also decreases which clearly depicts the role steel fibers in the built-up column. Due to the increase in the deformation capacity of SFRC filled CFS built-up columns energy dissipation capacity of the

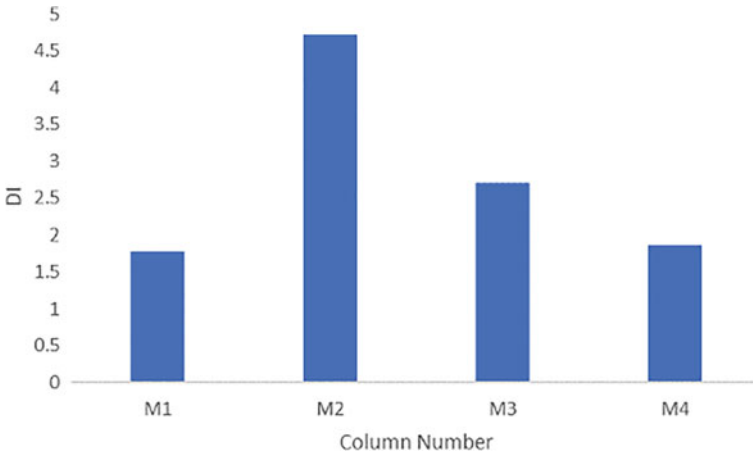


Fig. 5 Comparison of DI of columns having 1.8% steel fibers

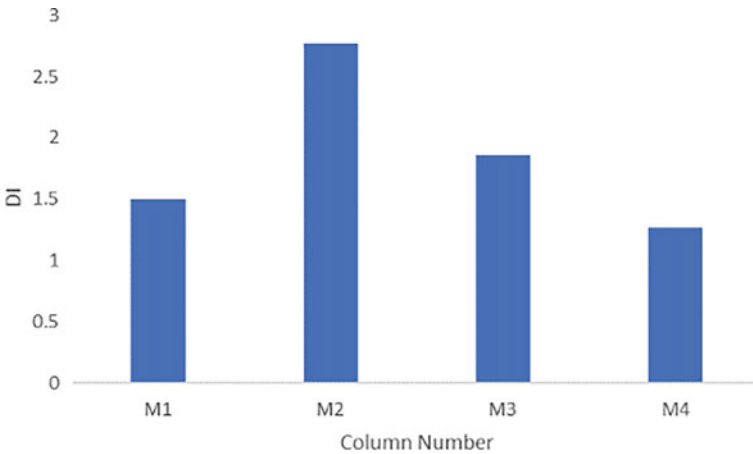


Fig. 6 Comparison of DI of columns having 1.2% steel fibers

columns can be increased. Steel fibers increase the dissipation capacity due to high lateral strain capacity imparted during pull out of fibers (Figs. 8, 9 and 10).

In all comparison plots built-up column made of 2U and 2Cs have greater load carrying capacity and DI which indicates the better performance. The main reason for the greater values is higher concrete area compared to other built-up columns. The effect of SFRC in concrete is visible only after the microcracks developed. It prevents the propagation of the microcracks in the concrete, thereby increasing the load capacity.

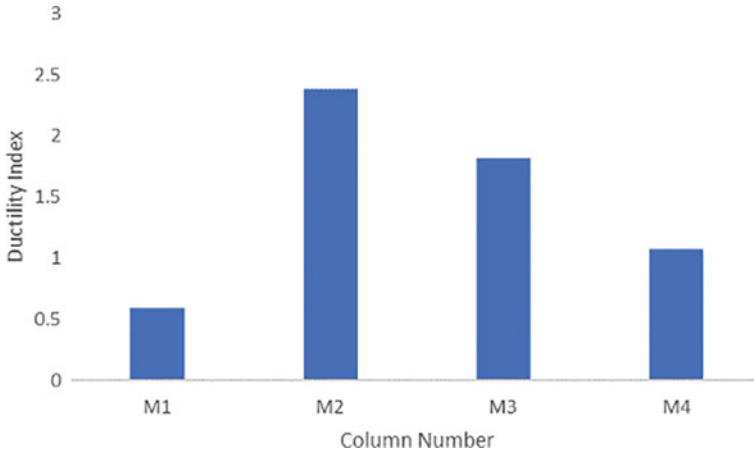


Fig. 7 Comparison of DI of columns having 0.6% steel fibers

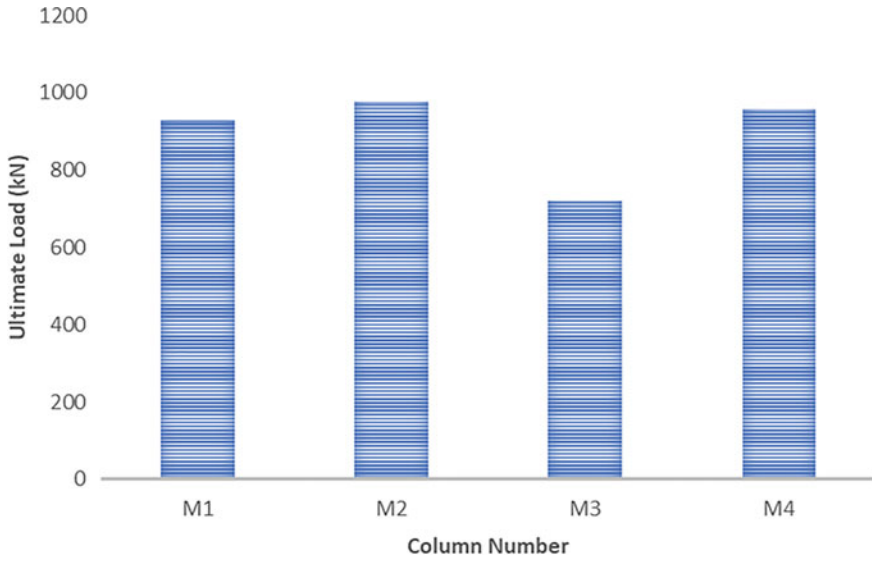


Fig. 8 Comparison of ultimate load of columns having 0.6% steel fibers

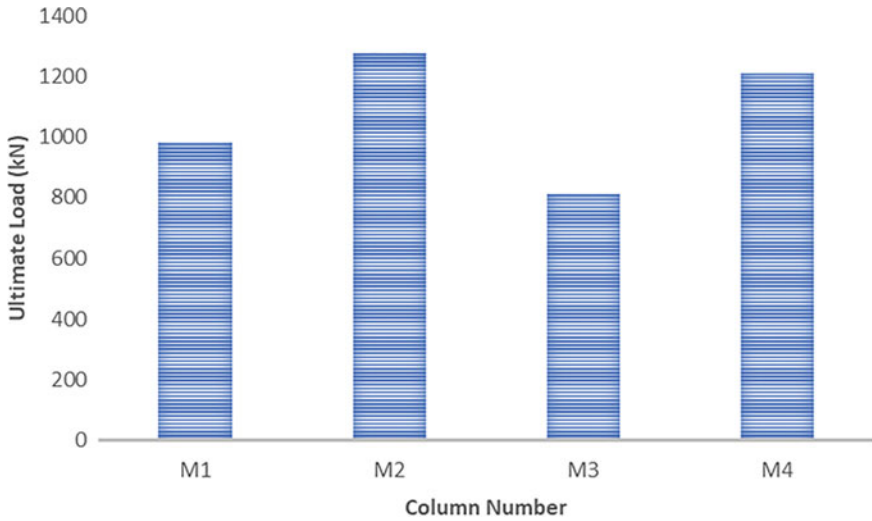


Fig. 9 Comparison of ultimate load of columns having 1.2% steel fibers

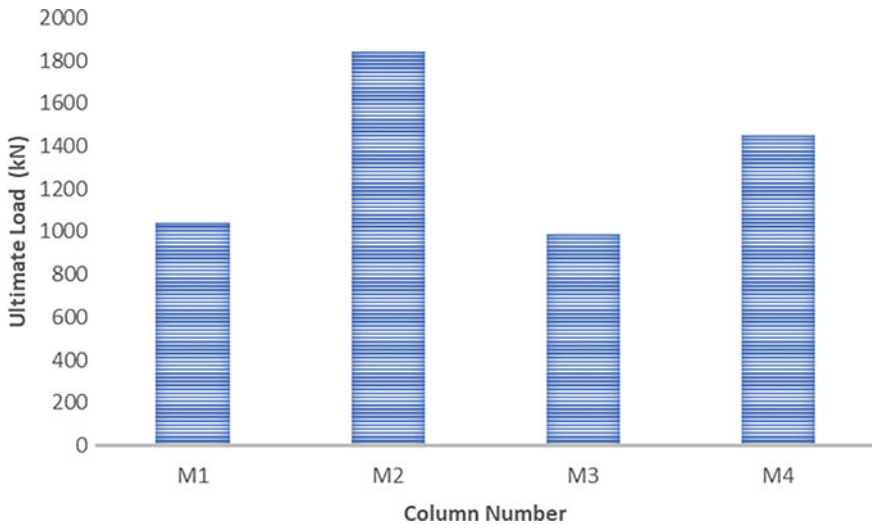


Fig. 10 Comparison of ultimate load of columns having 1.8% steel fibers

3 Conclusion

Steel fiber filled CFS built-up column is modelled using solid works and analyzed using ANSYS software. Steel fibers are added in three different percentage i.e., 0.6, 1.2 and 1.8%. The material properties will vary according to the percentage. The analysis is studied on the basis of ultimate load capacity and maximum deformation.

The conclusions from the study are:

- (1) In R-2U + 2C built-up column, maximum ductility and ultimate load is achieved when the column has 1.8% of steel fibers. The maximum deformation is also evident in the same column.
- (2) In S-2C + 2U the same trend of having maximum ductility index and ultimate load is seen on columns having steel fiber 1.8%. It is due to increased interaction between the steel fiber and concrete matrix.
- (3) In R-2U + 2 Σ and S-2U + 2 Σ maximum DI and ultimate load occurs in column having 1.8% steel fibers. The local reinforcing capability of steel fibers present in the mortar matrix and the web-like structural network formed by these fibers around the surfaces of coarse particles in the mix significantly enhances the post-cracking characteristics of the concrete.
- (4) On comparing the columns on the basis of steel fibers percentages, maximum ultimate load and DI occurs in S-2U + 2C column which is due to, the larger concrete area and more confinement.
- (5) In R-2U + 2C there is an increase of 31%, 39%, 47% on addition of 0.6%, 1.2% and 1.8% in the ultimate load capacity respectively.
- (6) In S-2U + 2C there is an increase of less than 10%, 30.64%, 84% on addition of 0.6%, 1.2% and 1.8% steel fibers in the ultimate load capacity respectively.
- (7) In R-2U + 2 Σ , on addition of steel fibers of 0.6%, 1.2% and 1.8% an increase of 19%, 34% and 63% is evident in ultimate load respectively.
- (8) In S-2U + 2 Σ , an increase of 11%, 41% and 69% is visible on addition of 0.6%, 1.2% and 1.8% of steel fibers respectively.

By the addition of the steel fiber and the use of highly ductile cold formed steel had improved the overall performance of the built-up column. From the analysis the column with two U and C sections having 1.8% of steel fiber depicts a better performance compared to all other columns. It is evident from the results of ductility index, maximum ultimate load carrying capacity and deformation pattern. Further studies can be performed with varying steel fiber percentages, different cross section of column and with another reinforced material.

References

1. Rahnavard R, Craveiro HD, Simões RA, Laím L, Santiago A (2022) Buckling resistance of concrete-filled cold-formed steel (CF-CFS) built-up short columns under compression. *Thin-Walled Struct* 170. <https://doi.org/10.1016/j.tws.2021.108638>
2. Usman M, Farooq SH, Umair M, Hanif A (2020) Axial compressive behavior of confined steel fiber reinforced high strength concrete. *Constr Build Mater* 230. <https://doi.org/10.1016/j.conbuildmat.2019.117043>
3. Venkateshwaran A, Lai BL, Liew JYR (2022) Buckling resistance of steel fibre- reinforced concrete encased steel composite columns. *J Constr Steel Res* 190. <https://doi.org/10.1016/j.jcsr.2022.107140>
4. Ting C, Huon T, Ho LH (n.d.) Compression test on cold-formed steel built-up back-to-back-channels stub columns

5. Li S, Liu Z, Lu Y, Zhu T (2017) Shear performance of steel fibers reinforced self-confinement and self-compacting concrete-filled steel tube stub columns. *Constr Build Mater* 147:758–775. <https://doi.org/10.1016/j.conbuildmat.2017.04.192>
6. Taufiq H, Lawson RM (2020) Composite columns using perforated cold formed steel sections. *J Constr Steel Res* 167. <https://doi.org/10.1016/j.jcsr.2020.105935>
7. Bharkavi D (2015) Experimental and theoretical investigation on flexural member and analysis by ANSYS. www.ijert.org
8. Lu Y, Li N, Li S, Liang H (2015) Behavior of steel fiber reinforced concrete-filled steel tube columns under axial compression. *Constr Build Mater* 95:74–85. <https://doi.org/10.1016/j.conbuildmat.2015.07.114>
9. Singh H (n.d.) Steel fiber reinforced concrete, behavior, modelling and design. Springer transactions in civil and environmental engineering. <http://www.springer.com/series/13593>
10. Liao WC, Perceka W, Liu EJ (2015) Compressive stress-strain relationship of high strength steel fiber reinforced concrete. *J Adv Concr Technol* 13(8):379–392. <https://doi.org/10.3151/jact.13.379>
11. Gandhi S, Shinde S, Kulkarni M (2020) Finite element analysis of steel fibre reinforced concrete composite panels subjected to combined effect of fire and blast. *Int Res J Eng Technol*. www.irjet.net
12. Liu Z, Lu Y, Li S, Zong S, Yi S (2020) Flexural behavior of steel fiber reinforced self-stressing recycled aggregate concrete-filled steel tube. *J Cleaner Prod* 274. <https://doi.org/10.1016/j.jclepro.2020.122724>
13. Shewalul YW (2021) Numerical and FEA investigation of sectional capacity and moment redistribution behavior of steel fiber reinforced concrete (SFRC) beam. *Heliyon* 7(6). <https://doi.org/10.1016/j.heliyon.2021.e07354>
14. Ayough P, Ibrahim Z, Sulong NHR, Hsiao PC (2021) The effects of cross-sectional shapes on the axial performance of concrete-filled steel tube columns. *J Constr Steel Res* 176. <https://doi.org/10.1016/j.jcsr.2020.106424>
15. El-Taly B, El-shami M (2021) Structural performance of cold-formed steel face-to-face and back-to-back beams. *Int J Civ Eng* 19(12):1427–1444. <https://doi.org/10.1007/s40999-021-00606-y>
16. Babu SS, Selvan SS (2020) State of the art of cold formed steel members. *Mater Today: Proc* 37(Part 2):3069–3073. <https://doi.org/10.1016/j.matpr.2020.09.013>
17. el Hady AM, el Aghoury MA, Ibrahim SM, Amoush EA (2022) Experimental investigation of steel built-up beam-columns composed of tracks and channels cold-formed sections. *J Build Eng* 51. <https://doi.org/10.1016/j.jobbe.2022.104295>
18. Altun F, Kişi Ö, Aydın K (2008) Predicting the compressive strength of steel fiber added lightweight concrete using neural network. *Comput Mater Sci* 42(2):259–265. <https://doi.org/10.1016/j.commatsci.2007.07.011>
19. Dar AR (2020) An experimental study on the flexural behavior of cold-formed steel composite beams. *Mater Today: Proc* 27:340–343. <https://doi.org/10.1016/j.matpr.2019.11.098>

Experimental Investigation on Mechanical Properties of Hybrid Polypropylene-Steel Fiber-Reinforced GGBS Mortar



Geethu Elsa Thomas, A. S. Sajith, and P. V. Indira

Abstract Research has shown that incorporating various types of fibers into a concrete mix can enhance the strength properties of cementitious matrices. Limiting the crack propagation in slab-like concrete structures, such as pavements, airport runways, and continuous slab-type sleepers for high-speed trains is critical. To achieve this, it is essential to address both crack propagation from loading and shrinkage. Distributed short fiber reinforcing, such as polypropylene fibers, is a smart solution in this scenario. The present study uses hybrid combinations of steel and polypropylene fibers in a mortar mix containing 50% cement and 50% Ground Granulated Blast Furnace Slag (GGBS). Fibers are randomly distributed as 0.5% of the volume of GGBS mortar. Five hybrid combinations of steel and polypropylene fibers are considered (25, 40, 50, 60, and 75%) to determine the mechanical properties. It is found that the addition of fibers enhances the mechanical properties of the mortar. The hybrid combination of 50% steel fiber and 50% polypropylene fiber in the GGBS mortar is optimum in terms of strength and economy. This study also promotes sustainable construction practices by utilizing GGBS as a raw material, which is an industrial byproduct.

Keywords Fiber-reinforced concrete · Steel fiber · Polypropylene fiber · Mechanical properties

1 Introduction

Hybrid fiber reinforced concrete is a new generation of building material with the primary advantages of its enhanced mechanical properties, such as higher compressive strength, toughness, and ductility [1]. The increasing need for construction materials has resulted in a substantial rise in cement consumption, leading to significant environmental concerns [2]. On the other hand, the utilization of high-strength

G. E. Thomas (✉) · A. S. Sajith · P. V. Indira
Department of Civil Engineering, National Institute of Technology, Calicut, Kozhikode, India
e-mail: geethuperayil@gmail.com

concrete can lead to higher construction costs due to the requirement of specific materials and additives to enhance the strength, along with specialized curing techniques [3, 4]. Consequently, several studies have been conducted to explore the possibility of producing them at a reduced cost [5]. The utilization of polypropylene fibers in such hybrid combinations can reduce the cost without compromising the strength of concrete. This study focuses on a hybrid combination of steel and polypropylene fibers (PP). The mechanical properties of different hybrid combinations are studied in terms of compressive strength (CS), flexural strength (FS), and split tensile strength (STS). The steel fibers provide high tensile strength and stiffness, while the polypropylene fibers contribute to improved crack resistance and durability. Studies show that utilizing PP fibers in concrete imparts resistance to shrinkage and toughness [6]. Hence they can be used for a wide range of applications, including the manufacturing of precast concrete elements such as precast panels, pipes, and poles, as well as in the production of concrete pavements and flooring systems.

The study additionally incorporates ground granulated blast furnace slag (GGBS), a byproduct of industrial processes, as a substitute for a portion of the cement. This method not only cuts down on construction expenses but also enhances the overall mechanical strength of the concrete, thereby fostering sustainable construction practices [7–9].

2 Experimental Investigations

2.1 Constituent Materials


The research utilized Ordinary Portland Cement which meets IS 12269:2013 [10] standard. GGBS conforming to IS 455-2015 [11] is another raw material used which contains 34.68% CaO, 33.11% SiO₂, 21.95% Al₂O₃, 9.50% MgO, 1.28% Fe₂O₃, and 0.10% SO₃ (as provided by the supplier). The GGBS has a specific gravity of 2.91, a specific surface of 400 m²/kg, and a particle size of 97.1 μm. M-sand is used as fine aggregate in accordance with the IS 383-1970 [12] guidelines. The M-sand falls under grading zone II and has a specific gravity of 2.68 and a fineness modulus of 2.81. The properties of Steel fibers and PP fibers are shown in Table 1. The mix was made workable with the use of Conplast SP430 as superplasticizer (SP), and potable water was used in the study.

2.2 Mix Proportions


The mix is prepared in accordance with IS 2250-1981 [13]. The current study utilizes a mix proportion of 1:1.5 (1 part binder and 1.5 part fine aggregate). The binder part consists of 50% cement and 50% GGBS, with a water to binder ratio of 0.35 and a

Table 1 Fiber properties

Fiber properties	Hooked-ended steel fiber	Polypropylene fiber
Diameter	0.5 mm	40 μm
Length	30 mm	12 mm
Aspect ratio	60	300
Tensile strength	1200 MPa	550–600 N/mm ²
Density	7960 kg/m ³	950 kg/m ³



Polypropylene fibers



Steel fibers

Table 2 Mix notations and proportions

Mix ID	Cement/ binder	GGBS/ binder	Fine aggregates/ binder	Water/ binder	Superplasticizer/ binder	Fiber content (volume ratio of 0.5%)	
						Steel (%)	Polypropylene (%)
G50	0.5	0.5	1.5	0.35	0.005	0	0
GHSP1	0.5	0.5	1.5	0.35	0.005	25	75
GHSP2	0.5	0.5	1.5	0.35	0.005	40	60
GHSP3	0.5	0.5	1.5	0.35	0.005	50	50
GHSP4	0.5	0.5	1.5	0.35	0.005	60	40
GHSP5	0.5	0.5	1.5	0.35	0.005	75	25
GS	0.5	0.5	1.5	0.35	0.005	100	0
GP	0.5	0.5	1.5	0.35	0.005	0	100

SP to binder ratio of 0.5. The detailed procedure for the preparation of GGBS mortar is published by the authors elsewhere [8]. Fibers were incorporated with a volume ratio of 0.5% [14]. Five hybrid combinations of steel and PP fibers are adopted in this study (25, 40, 50, 60, and 75%) to determine the mechanical properties. The details of the mix notations and the proportions are shown in Table 2.

2.3 Preparation of Test Specimens

The mixing procedure of fiber-reinforced GGBS mortar is shown in Fig. 1. The workability of the freshly prepared mix is estimated using the flow table test. To

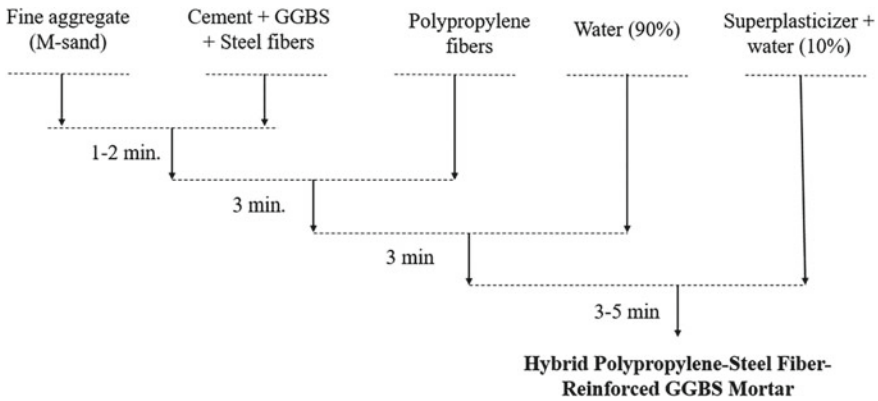


Fig. 1 Mixing procedure for fiber-reinforced GGBS mortar

investigate the hardened properties, samples were made in the form of standard cubes with a dimension of 70.6 mm, cylinders with a diameter of 100 mm and a height of 200 mm, and prisms with a size of 40 mm × 40 mm × 160 mm. After removing the molds, the specimens were left to cure in water at a temperature of 27 °C for 28 days. The results taken in this study are an average value of three samples.

3 Study on Mechanical Properties

3.1 Workability

The workability of the fresh mortar mix was assessed through a Flow table test following the guidelines outlined in IS 4031 (part-7-1988) [15]. The recorded flow values can be found in Table 3. The incorporation of fibers in the mortar mix reduced workability when compared to the control mix (G50), the mix without fibers. As the replacement level of PP fiber increased, the workability was found to get reduced. The addition of PP fibers increases the viscosity of the mix [16], leading to reduced workability.

3.2 Compressive Strength

Cubes (70.6 mm) from each mix were tested for CS after 28 days curing period. The test is conducted as per IS4031 part 6-1988, and the results are tabulated in Table 4. The hybrid mixes have an enhanced CS value. The CS value for GS mix (100% steel fiber) was 57 MPa, 11.76% higher than the control mix. GHSP3 mix

Table 3 Workability for different mixes

Mix	Flow (%)
G50	106
GHSP1	89
GHSP2	91
GHSP3	99
GHSP4	90
GHSP5	91
GS	98
GP	87

Table 4 Compressive strength for different mixes

Mix	Cube compressive strength (MPa)
G50	51
GHSP1	49
GHSP2	50
GHSP3	55
GHSP4	53
GHSP5	53
GS	57
GP	46

(50% steel fiber + 50% PP fiber) had the highest CS value compared to the other hybrid combinations. GHSP3 mix obtained a CS value of 55 MPa, which is greater than almost 3.77–12.24% of the other four hybrid mixes. GP mix (100% PP fiber) exhibited 46 MPa, the lowest CS value. The findings are consistent with past literature [17, 18], which indicates that the inclusion of PP fibers decreases CS. Overall, the hybrid blend of steel and PP fibers does not significantly enhance the CS.

3.3 Flexural Strength

Prisms of dimension 160 mm × 40 mm × 40 mm were taken after a curing period of 28 days and tested for FS (ASTMC-348-08) [19] using a deformation controlled UTM. The prisms were subjected to a three-point bending test under monotonic loading. Table 5 depicts the results obtained for different mixes. The addition of fibers has improved the FS, especially the hybrid combinations GHSP3, GHSP4, and GHSP5 are found to have greater FS values than the remaining mixes. The GHSP3 mix has the highest FS value of 8.72 MPa. Figure 2 is a plot for the load–deflection curves for the mixes. From the plot, it can be inferred that the hybrid combination

Table 5 Flexural strength for different mixes

Mix	Flexural strength (MPa)
G50	7.23
GHSP1	7.11
GHSP2	7.84
GHSP3	8.72
GHSP4	8.42
GHSP5	8.54
GS	7.97
GP	7.29

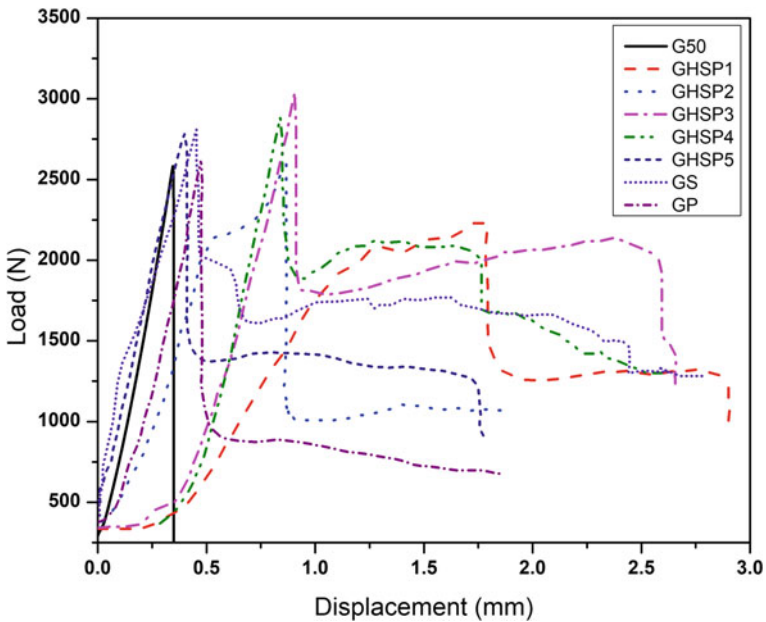


Fig. 2 Load–displacement plot for different mixes

of steel and PP fibers control crack propagation. The synthetic PP fibers bridge the micro-cracks and delay the system’s fracture generation [20].

3.4 Split Tensile Strength

Cylinders of diameter 100 mm and length 200 mm were tested for the STS in accordance with IS 5816:1999 [21]. The results are tabulated in Table 6. The hybrid mixes have exhibited greater values for STS. The mix GHSP3 is found to have a STS value

Table 6 Split tensile strength for different mixes

Mix	Split tensile strength (MPa)
G50	3.50
GHSP1	3.81
GHSP2	4.53
GHSP3	5.15
GHSP4	4.84
GHSP5	4.75
GS	4.90
GP	3.91

of 5.15 MPa, which is found to be greater than all other mixes. A combination of 50% steel fibers and 50% PP fibers has improved the STS values by reducing crack formation and enhancing the toughness of the system [17].

4 Conclusions

This research is an experimental investigation to study the mechanical characteristics of a hybrid combination of steel and PP fibers in a GGBS mortar. Tests were conducted to determine the CS, FS, and STS of different hybrid mixes. As GGBS is used in the study, it promotes sustainability. From the results, the following conclusions are made:

1. The inclusion of fibers in the mix reduces workability. Generally, it is found that a greater percentage of PP fiber in the mix increases the viscosity and reduces the flow value.
2. GS mix (100% steel fiber) had the highest compressive strength value, and this is due to the high Young's modulus value of steel fiber. The mix GHSP3 (50% steel fiber and 50% pp fiber) showed improved compressive strength value than other hybrid mixes.
3. The flexural strength value for the GHSP3 mix is 8.72 MPa, which is the highest value compared to other mixes. Hybrid combinations have improved flexural strength by arresting the cracks and delaying the fracture of the matrix.
4. The highest STS value was obtained for the GHSP3 mix when compared with the remaining mixes. The addition of PP fibers has improved tensile properties by preventing wider cracks.
5. It can be noted that the GHSP3 mix is found to have enhanced mechanical characteristics, indicating that the combination of 50% steel fibers and 50% PP fibers can be taken as an optimum mix in light of the mechanical properties determined by this study.

5 Future Scope

Hybrid steel-polypropylene fiber-reinforced concrete has a wide range of applications in various industries, including construction, infrastructure, and transportation. Further studies should be conducted on the ductility, impact resistance, and durability features of this hybrid mix. Also, studies on the applicability of this construction material for the construction of high-rise buildings, bridges, tunnels, and underground structures should be explored. The numerous advantages of this hybrid mix and the applications mentioned thereof make it a promising material for the future of concrete technology.

References

1. Qian CX, Stroeven P (2000) Development of hybrid polypropylene-steel fiber-reinforced concrete. *Cem Concr Res* 30(1):63–69
2. Lima C, Caggiano A, Faella C, Martinelli E, Pepe M, Realfonzo R (2013) Physical properties, and mechanical behavior of concrete made with recycled aggregates and fly ash. *Constr Build Mater* 47:547–559
3. Wille K, Naaman AE, El-Tawil S, Parra-Montesinos GJ (2012) Ultra-high-performance concrete, and fiber reinforced concrete: achieving strength and ductility without heat curing. *Mater Struct* 45:309–324
4. Chan YW, Chu SH (2004) Effect of silica fume on SF bond characteristics in reactive powder concrete. *Cem Concr Res* 34:1167–1172
5. Wang DH, Shi CJ, Wu ZM, Xiao JF, Huang ZY, Fang Z (2015) A review on ultra-high-performance concrete: part II. Hydration, microstructure, and properties. *Constr Build Mater* 96:368–377
6. Tawfik M, El-said A, Deifalla A, Awad A (2022) Mechanical properties of hybrid steel-polypropylene fiber reinforced high strength concrete exposed to various temperatures. *Fibers* 10:53
7. Thomas GE, Indira PV, Sajith AS (2022) Experimental investigations on durability characteristics of ground granulated blast furnace slag mortar. In: *E3S web of conferences*, vol 347, p 02007
8. Thomas GE, Indira PV, Sajith AS (2022) Enhancement of mechanical properties of cement mortar using ground granulated blast furnace slag as a partial replacement. In: *Recent trends in civil engineering*. Springer Nature Singapore, Singapore, pp 171–180
9. Thomas GE, Indira PV, Sajith AS (2022) Structural performance of ground granulated blast furnace slag mortar under impact loading. In: *Recent advances in structural engineering and construction management*. Springer Nature Singapore, Singapore, pp 813–820
10. IS 12269-2013 (2009) Ordinary portland cement, 53 grade-specification, 1st rev. Bureau of Indian Standards, New Delhi
11. IS 455-2015, Portland slag cement specifications, 5th rev. Bureau of Indian Standards, New Delhi
12. IS 383-1970 (reaffirmed in 2002) (2009) Specification for coarse and fine aggregates from natural sources for concrete, 9th reprint. Bureau of Indian Standards, New Delhi
13. IS 2250-1981 (reaffirmed 2000) (2009) Code of practice for preparation and use of masonry mortars, 5th rev. Bureau of Indian Standards, New Delhi
14. Thomas GE, Indira PV, Sajith AS (2023) Shape memory alloy fiber reinforced concrete/mortar—a review. *Mater Today Proc*

15. IS 4031-7 (1998), (reaffirmed 2005) (2009) Methods of physical tests for hydraulic cement, 2nd rev. Bureau of Indian Standards, New Delhi
16. Li XK, Sun L, Zhou YY, Zhao SB (2012) A review of steel-polypropylene hybrid fiber reinforced concrete. *Appl Mech Mater* 238:26–32
17. Jiao C, Sun W, Qin H (2004) Experimental study on bending performance of high-strength concrete of steel-propylene hybrid fiber. *Archit Technol* 1:48–50
18. Jiao C, Zhan Z (2007) Experimental study on compressive strength performance of concrete of steel-propylene hybrid fiber. *J Guangzhou Univ* 4:70–73
19. ASTM C348-08, Standard test method for flexural strength of hydraulic-cement Mortars
20. El-Hamrawy MI, Saba AM, Sherbini A, Metawei M, Sallam H (2007) Fracture energy of hybrid fiber reinforced concrete. In: Regional conference on civil engineering technology and international hydrology, pp 3–5
21. IS 5816:1999 (reaffirmed 2004), Splitting tensile strength of concrete—method of test. Bureau of Indian Standards, New Delhi

Spatial Analysis and Comparative Study of Noise Pollution at Ernakulam City Before and During COVID-19 Using GIS



Meera Varghese and A. H. Amalpriya

Abstract Traffic noise is one of the major environmental pollutants that are encountered in our daily life and it also affects the human health. Due to increase in the vehicular number on roads noise associated with roads has also been considerably rising in recent years. This causes alarming noise pollution. Considering Kerala, which is quite famous for its urbanization even in the remotest areas there is significant rise in number of vehicles and nature of traffic. Due to this, today many cities are witnessing the problem of noise pollution. In order to implement effective measures against traffic noise, the information about its distribution is imperative. The present study undertaken analyzes the spatial characteristics of urban environmental noise by using noise maps produced at different noise monitoring locations in the study area. Noise data was collected at varying intervals viz morning, afternoon, and evening. The spatial distributions of the noise levels during each time interval were evaluated and visualized by preparing noise maps using QGIS software. Covid lockdown has been one of it's kind situation and hence any works associated with the same has relevance in current context. This study attempts to investigate the impacts of COVID lockdown on the changes in noise pollution levels before and during the lockdown restrictions in different residential, commercial, industrial, and silence zones of the city of Ernakulam, Kerala. A noise prediction model was generated from the data obtained.

Keywords Geographic information systems · Lockdown · Noise maps · COVID

M. Varghese (✉) · A. H. Amalpriya
SCMS School of Engineering and Technology, Cochin, India
e-mail: meeravarghese@scmsgroup.org

© The Author(s), under exclusive license to Springer Nature Switzerland AG 2024
M. Nehdi et al. (eds.), *Proceedings of SECON'23*, Lecture Notes in Civil Engineering
381, https://doi.org/10.1007/978-3-031-39663-2_67

789

1 Introduction

Noise pollution refers to sounds in the environment that are caused by humans and that threaten the health or welfare of human or animal inhabitants. Noise pollution as a result of growing urbanisation and industrialisation is regarded as an environmental hazard and it has a negative impact on human health and well-being. The World Health Organization (WHO) has identified noise pollution as one of the primary environmental factors to public health issues. Among all sources of noise pollution, road vehicle traffic noise has a significant impact on the quality of urban areas [1]. It is one of the most common environmental contaminants that people are exposed to daily. It has a direct impact on human health. Traffic related noise pollution accounts for nearly two-third of the total noise pollution in an urban area [2]. Noise is a common problem in urban areas as compared to the villages because of the mechanization and more vehicles on the road.

The goal of the present study is to look at how noise levels change before and during lockdown, to look at noise exceedance levels in different zones and their impact, and to propose effective noise mitigation strategies to reduce the overall negative effects of noise.

In the present study Noise maps are used as a tool to understand the spatial characteristics of ambient noise levels in Ernakulam town. Noise data are collected at morning, afternoon and evening on working days. For visualization of noise pollution, noise mapping is done. Geographic Information System (GIS) was used to assess and visualise the spatial distributions of noise levels for each time interval. The novel approach to view noise pollution is through noise mapping. A noise map is rather similar to a weather map, it shows the hotspots (where it is loud) and the cooler areas (where it is calm). LIMA, FAA, Arc GIS, QGIS are some of the software that are used for producing noise maps [3]. Noise pollution has always been a global concern affecting both the public's health and the planet's fragile ecosystems. In order to tackle the ever increasing problem of noise pollution, particularly traffic pollution in the country, the Government of India came up with The Noise Pollution (Regulation and Control) Rules, 2000. One of the major objectives of the rule is to maintain the ambient air quality standards in respect of noise (Table 1).

1. Day time shall mean from 6.00 a.m. to 10.00 p.m.
2. Night time shall mean from 10.00 p.m. to 6.00 a.m.
3. Silence zone is an area comprising not less than 100 m around hospitals, educational institutions, courts, religious places or any other area which is declared as such by the competent authority.
4. Mixed categories of areas may be declared as one of the four above mentioned categories by the competent authority.

Table 1 Ambient air quality standards in respect of noise

Area code	Category of area or zone	Limits in dB (A) L_{eq}	
		Day time	Night time
(A)	Industrial area	75	70
(B)	Commercial area	65	55
(C)	Residential area	55	45
(D)	Silence zone	50	40

Source CPCB

1.1 Noise Study in Kochi

Kochi has been experiencing growth in urban spread. As per census 2001, urban population of Kerala is 25.9% of the state’s population among which the percentage for Kochi district was 48. Ashly et al. [4] in their study measured the environmental noise levels to assess the noise pollution in Ernakulam city. This data was used in the project for the noise level comparison before and during COVID. Measurements occurred between 30 and 130 dB (A). The measured noise levels were compared to the basic noise levels that were set by the Central Pollution Control Board (CPCB) for various zones, including commercial (55–60 dB), silent (40–50 dB), residential (50–55 dB), and industrial (65–70 dB), during the day and night. ArcGIS 9.3.1 software was used to create a noise map in order to better visualise Ernakulam’s city’s noise environment and its daily fluctuations. It was observed that the amount of traffic in these areas significantly affects the noise levels.

Sampath et al. [5] measured the noise levels within the city of Kochi. There were 26 locations where measurements were made, with two being in silence zones, one being in a residential zone, and the other twenty-six being in commercial zone. In the commercial zone, noise levels were generally 78.5 dB, which is 26.55 dB above the permissible level. Residential zone measured 40.7, 15 dB below the threshold. Equal noise levels were observed in both the commercial and silence zones, and they were significantly greater than the permissible level.

1.2 GIS Based Approach for Road Traffic Noise Mapping

The study conducted by Sonaviya [6] demonstrates the various GIS methodologies used for the noise mapping. A GIS-based noise mapping is advantageous for a more accurate depiction of noise pollution on a map. The main approach used for noise mapping is interpolation (kriging), and noise level contours can be created using this method. Kriging is possible by using an interpolation technique while taking into account the topographical region’s acoustic behaviour. It is possible to build noise contour maps that display how the ambient noise in an urban area changes during the time of day. A better outcome for the area with high traffic and noise properties

can be achieved using GIS. It also identifies the most exposed zones under the noise pollution bluster.

Obaidat [7] used the potential of Geographic Information Systems (GIS) to spatially map noise levels caused by traffic movements at relatively high traffic volume signalized intersections by combining field data with an analytical approach. In Amman, Jordan's capital, discrete mapping was used to collect noise data at 29 signalized intersections, between intersections, and in their respective neighborhood areas. In order to locate the appropriate noise level boundaries for the zone areas in accordance with local and international standards, spatial modeling was used to simulate the spread of traffic noise levels. Spatial maps are imperative for city planning and traffic engineers to zone and land use, land estimating, and traffic management.

The study's findings suggested that the created GIS maps would be valuable for applications in city planning and other types of environmental management for the following reasons:

- (1) Development of an online noise information system.
- (2) Temporal monitoring and queries of noise level changes as a function of time.
- (3) Spatial queries to find the location with the maximum noise disturbance and the time of day.
- (4) Using spatial maps based on noise levels as indications of changes in land prices.
- (5) Prediction and present evaluation of the acoustic environment in urban regions.

1.3 Gap Identified in Literature

Based on extensive literature review it has been noticed that noise maps can function as an effective tool for urban planners in management of noise pollution [8]. As the world was struck with Covid-19 pandemic there has been a drastic change in living conditions of the people. The pandemic has affected the general pattern and behavior of people. An extensive study on how the Covid lockdown and associated restrictions has affected the traffic distribution and noise characteristics of the Ernakulam city area has not been done. Hence an attempt is made to identify the spatial variation of noise pollution and compare the same with the conditions before pandemic. This can play a great role in suggesting traffic reduction as an effective noise reduction mechanism. The uniqueness of the study is that such kind of real time data with traffic restrictions is very difficult to obtain unless due to government imposed restrictions.

1.4 Objectives of the Study

The present work is carried out with the following objectives:

- To compare the noise levels in Ernakulam city, before and during the COVID pandemic.

- To analyse the impact of traffic volume on noise pollution.
- To collect the traffic noise data on different locations.
- To determine applications of QGIS in creating noise maps.
- Zoning based on available data using QGIS software.
- To develop a mathematical traffic noise model.

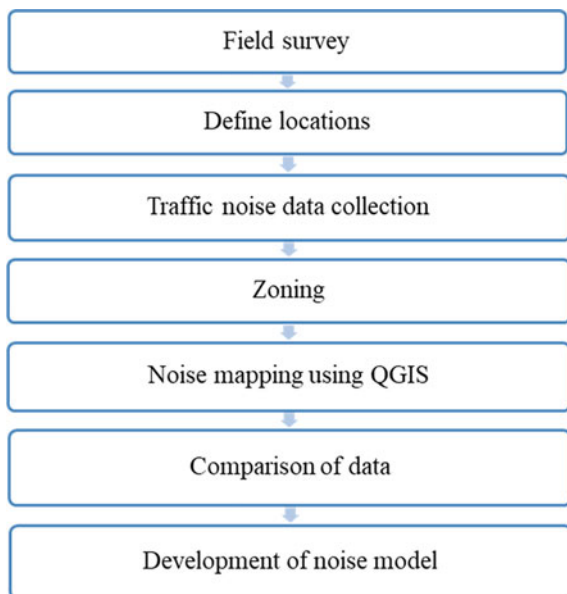
2 Materials and Methodology

The study area selected for the present work is based on the different zones in Ernakulam region. Commercial zone, industrial zone, residential zone and sensitive zones were identified based on reference from previous data. Traffic noise data as well as no. of vehicles was collected from 1st June 2021 to 8th June 2021. Based on the data collected Noise maps were prepared using QGIS and a mathematical model was also developed (Fig. 1).

2.1 Study Area

Ernakulam city was chosen as the study area. It covers an area of 94.88 km². It is the central portion of the city of Kochi. Ernakulam is a major financial and commercial hub of Kochi city, which is widely known as the commercial capital of the state.

Fig. 1 Schematic representation of the methodology



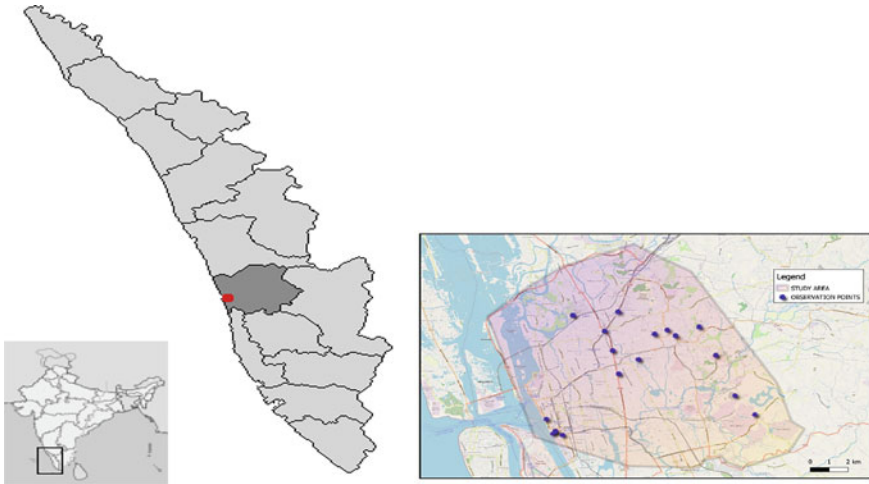


Fig. 2 A plot of study area

Ernakulam, also known as the CBD (Central Business District) of Kochi, has seen high urbanization in the past few decades, thus turning it into an economic hub of the city. The Ernakulam region, being at the heart of Kochi city, is well served by private/government buses, auto rickshaws, long and short-distance trains and ferries, and even the new metro rail. The city has the highest district wise growth of motor vehicles with 2,055,842 numbers. People largely dependent on city buses, metro rail, taxis and auto rickshaws for public transport. Traffic jams are usual in the area (Fig. 2).

2.2 Defining Locations

For assessing the noise levels, seventeen observation points were chosen over the study area and noise levels were monitored. To select the observation points, special care was taken to ensure that the locations chosen as observation points has considerable traffic and the points lay within an area for the purpose of mapping. Noise monitoring was done in good weather conditions to reduce the effects of wind and rain (Table 2).

2.3 Traffic Noise Data Collection

The city's significant areas were first determined, and measurement locations in the area were chosen based on two criteria: one, the location is accurately representative

Table 2 Study area locations and coordinates

Observation stations	Latitude	Longitude
Medical Trust Hospital	9.96408	76.28743
School of Marine Science	9.96497	76.28276
Lakshmi Hospital	9.9663	76.2838
ICA	9.96613	76.284
BPCL	9.97607	76.3805
FACT	9.98703	76.37092
Kakkanad West	10.008	76.32417
Infopark	10.01047	76.36162
Oberon Mall	10.01319	76.31169
Mavelipuram Colony	10.0219	76.34207
NGO Quarters	10.02293	76.33194
LuLu Mall	10.0245239	76.3077252
Thrikkakara	10.02523	76.33808
Fort Valley Township	10.02704	76.35355
AIMS Cochin	10.03372	76.29244
Pathadipalam	10.03587	76.31431

of the spatial distribution of noise in the area, and two, the noise field at the point is not affected by structures or other obstructions [9]. So, the Traffic noise at Medical Trust Hospital, School of Marine Science, District and Session Court, Lakshmi Hospital, Institute of Chartered Accountants (ICA), BPCL, FACT, Kakkanad West, Infopark, Oberon Mall, Mavelipuram Colony, NGO Quarters, AIMS Cochin, Thrikkakara, Fort Valley Township, LuLu Mall Edappally, and Pathadipalam, was collected. The noise levels were collected for seven continuous days i.e., from 1 June, Tuesday to 8 June Tuesday. The traffic noise data was collected during morning, afternoon and evening using the mobile application (sound level meter). A study on “Assessment of noise pollution at Ernakulam by GIS” was conducted by Ashly et al. [4]. The traffic details during the year 2016 was obtained from this study. The mean value of traffic noise collected was calculated. Working of the application was supervised throughout the days so as to prevent interruption. In case of interruption of working, it may lead to loss of recorded data. The traffic noise data collected was transferred to a system. The traffic noise data collected from 1st June 2021 to 8th June 2021 were analysed. From the data transferred to the system, analysis was carried out for the number of times. Earlier (2016), the noise level was above the maximum permissible limit (75 dB). During this period there was considerable reduction in traffic volume.

The data regarding the number of vehicles in each class, like two wheelers, cars, heavy vehicles, etc. should be known for the traffic modelling [10]. For obtaining the traffic density data, videos were shot in mobile camera to record the traffic in the selected locations. The video recording of 10-min samples were taken during the peak time and was then interpolated. Here, it is assumed that the traffic density does not

Table 3 Zoning of Areas

Residential zone	Commercial zone
NGO Quarters	AIMS
Infopark	Pathadipalam
Mavelipuram Colony	Kakkanad West
Fort Valley Township	LuLu and Oberon Mall
<i>Sensitive zone</i>	Thrikkakara
ICA	
School of Marine Science	<i>Industrial Zone</i>
Medical Trust Hospital	BPCL
Lakshmi Hospital District and Sessions Court	FACT

vary much within the period of traffic noise collection. The video was played back in slow mode and traffic density was estimated by counting the number of vehicles.

The seventeen selected locations were divided into four categories: commercial, silence, residential and industrial zone. Noise pollution rules have defined the acceptable level of noise in different zones for both daytime and night time. Commercial zone consisted of shopping malls, tourist attractive spots etc. It covers LuLu Mall, Oberon Mall, Pathadipalam, Amrita institute of medical science (AIMS), Thrikkakara Shiva temple and Kakkanad West. The silent zone is incorporated with educational institutions, hospitals etc. Medical trust hospital, Lakshmi hospital, District and session court, Institute of chartered account (ICA) and School of marine science are zoned under this. Residential zone is mainly incorporated by housing, as opposed to industrial and commercial areas. Residential zone covers the areas of NGO quarters, Infopark, Mavelipuram Colony and Fort Valley Township. Industrial Zone incorporates industrial type properties related to manufacturing, production etc. Bharat petroleum limited (BPCL) and Fertilizers and Chemicals Travancore Ltd (FACT) comes under this zone (Table 3).

2.4 Mapping of Data Using QGIS

QGIS known as Quantum GIS is a free desktop geographic information system (GIS) application that supports viewing, editing, and analysis of geospatial data. It is a GIS framework for working with maps and geographic information [11]. Using the data collected, noise mapping was done using QGIS 3.16.7 software. Eight noise maps, corresponding to each zone were prepared. QGIS software used to plot the noise levels contours using interpolation technique. The noise levels maps were created using QGIS to display the varying levels of noise during the course of the day in the city of Ernakulam. QGIS, effectively, provides better visual information of the places with larger traffic accumulations and noise levels, and it also indicates the

areas most at risk from noise pollution. Noise level data of each zone during 2016 and during COVID lockdown was plotted and represented using noise maps. The same was analyzed using bar-charts and a decline in noise levels was seen under COVID restrictions.

2.5 Development of Noise Model

In the present study, a road traffic noise prediction model for Indian conditions was developed using regression analysis. The developed model was based on Calixto model [12]

$$L_{eq} = 10 \log(Q_{ep}) \tag{1}$$

$$Q_{ep} = Q(1 + (n \times VP)/100) \tag{2}$$

$$L_{eq} = 10 \log Q(1 + (n \times VP)/100) \tag{3}$$

where Q_{ep} is the traffic flow, Q is the real hourly vehicle flow, VP is the Percentage of heavy vehicles and n is the weightage factor ($n = 4$ to $n = 10$) (Fig. 3).

To check whether Calixto equation could be used for the present study, a correlation study was carried out. First graphs were drawn between observed equivalent noise levels at x-axis and traffic flow and percentage of heavy vehicles at y-axis respectively to check whether the equivalent noise level have a positive relationship with the mentioned parameters. From the graphs a positive correlation was observed between the observed equivalent noise level and traffic flow. Hence Calixto equation was found to be fit to develop equation that satisfies the roads in Indian conditions (Fig. 4).

Since the road on which the present study conducted is a straight road, straight line equation can be applied to Calixto equation [13]

$$L_{eq} = a 10 \log Q(1 + (n \times VP)/100) + k \tag{4}$$

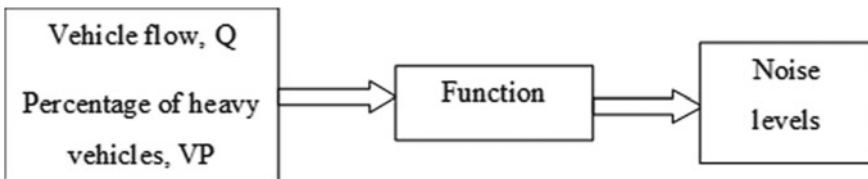


Fig. 3 Graphical representation of Calixto model [12]

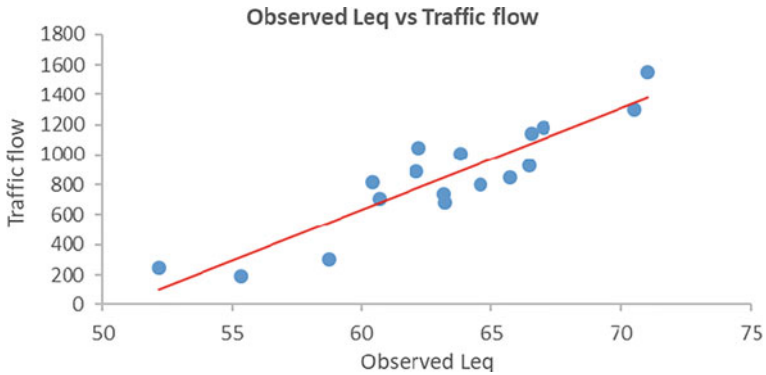


Fig. 4 Graph between observed L_{eq} and traffic flow

where Q_{ep} is the traffic flow, Q is the real hourly vehicle flow, VP is the Percentage of heavy vehicles, n is the weightage factor ($n = 10$), a and k are the constants.

In order to find the values of a and k to develop the equation that fits the roads in Indian conditions Microsoft Excel software was used (Table 4).

From the graph (Fig. 5) plotted above, a linear straight line was obtained and the values of constants ‘ a ’ and ‘ k ’ was found out to be 1.6432 and 14.638 respectively.

Table 4 Data used to find values of ‘ a ’ and ‘ k ’

S. No.	Location	Traffic flow, Q	No. of heavy vehicles	% of heavy vehicles, VP	z	Observed L_{eq}
1.	Medical Trust Hospital	1140	32	2.8	31.64	66.53
2.	Lakshmi Hospital	1050	15	1.43	30.79	62.2
3.	District and Session Court	820	25	3.04	30.29	60.4
4.	School of Marine Science	680	20	2.94	29.44	63.2
5.	Infopark	800	20	2.32	29.94	64.58
6.	Fort Valley Township	190	6	3.16	23.98	55.35
7.	LuLu Mall	1550	50	3.22	33.12	71.03
8.	Pathadipalam	1180	34	2.88	31.82	67.01
9.	AIMS Cochin	1010	22	2.17	30.90	63.78
10.	Oberon Mall	1300	32	2.46	32.09	70.5
11.	Thrikkakara	850	22	2.58	30.29	65.7
12.	Kakkanad West	740	15	2.02	29.49	63.15

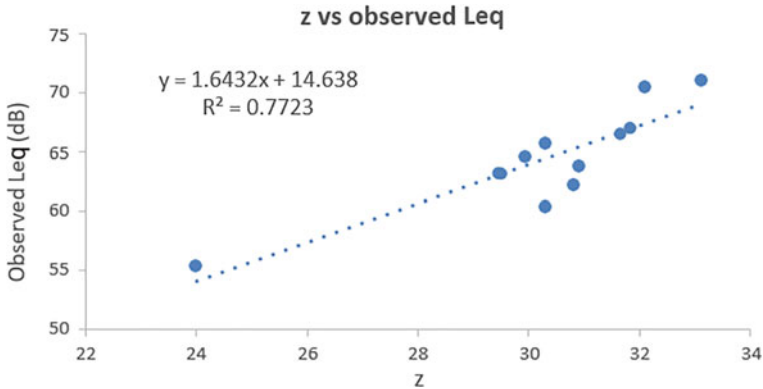


Fig. 5 Graph to find out values of constants 'a' and 'k'

Regression analysis was done for the same and the value for R^2 was found out to be 0.7723. Equivalent traffic noise levels of June 1st, Tuesday was considered to develop the model. Traffic noise regression analysis was carried between the observed equivalent noise levels and noise levels calculated by using Eq. (4).

From the result obtained a new equation was developed to fit Indian conditions.

$$L_{eq} = 1.6432 \times 10 \log(Q(1 + (10 \times VP)/100)) + 14.638 \quad (5)$$

Noise levels were calculated using the newly derived equation that fits the roads in Indian conditions and was compared with the observed noise levels. Model Validation was carried out by drawing a graph of observed noise level on x-axis and calculated noise level on y-axis. Regression analysis of the graph was done using Microsoft Excel software and R^2 value was found out. The noise prediction model can be used as an effective tool to understand the impact of heavy vehicles in noise pollution. The model can be used to predict the noise pollution in an area where there is very high heavy vehicular traffic [14].

3 Results and Discussion

3.1 Preparation of Noise Maps Using QGIS

From the noise survey carried out, noise mapping was done with the help of QGIS software. Interpolation method was used to carry out the noise mapping. Noise mapping for each zone, before COVID pandemic and the noise maps during the COVID pandemic were prepared using QGIS. IDW interpolation was used for this purpose. IDW will use the measured values around the prediction location for predicting a value for any unmeasured location. Values that are nearby to the predicted

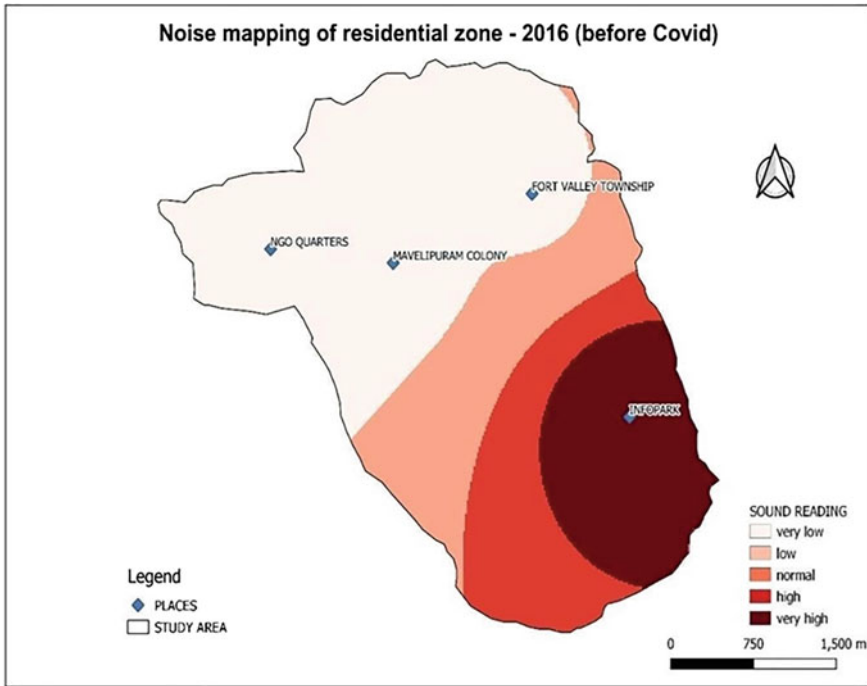


Fig. 6 Interpolated noise mapping for residential zone before COVID

location will have a greater impact on the anticipated value than values that are far away. Using this condition noise mapping was carried out [15].

To check the effect of lockdown and the impact COVID has caused on traffic noise, noise maps were prepared for values taken during June 2021 (during COVID restrictions) (Figs. 6, 7, 8, 9, 10, 11, 12 and 13).

3.2 Comparison of Noise Before and During Covid

Mapping of noise levels clearly shows that there is considerable reduction in noise levels during the COVID pandemic. The state has been under lockdown since May 8 following the sharp rise in coronavirus cases. Lockdown restrictions in Ernakulam, which comes under Orange A category, was eased from April 2021. The relaxations were mostly applicable to health and agriculture sectors. Traffic restrictions has also been made in this regard like Vehicles bearing odd registration numbers were allowed on the roads on Monday, Wednesday, and Friday while vehicles with even numbers were allowed to ply on Tuesday, Thursday and Saturday. Transport buses were limited in number and Kochi Metro was not operational. So people used private vehicles for their day to day activities. Also, as it was lockdown on Saturday and Sunday, people

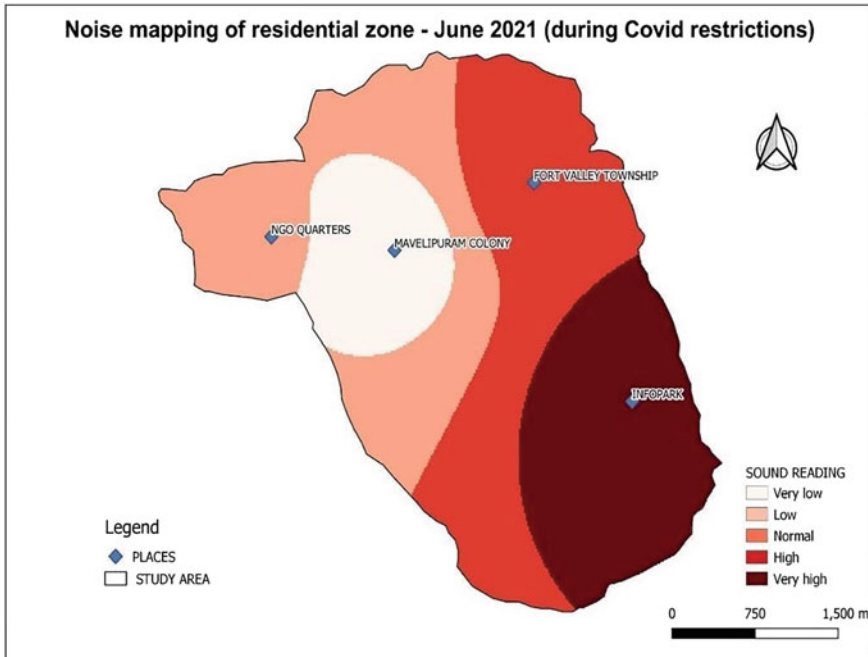


Fig. 7 Interpolated noise mapping for residential zone during COVID restrictions

came out in numbers for shopping on other days. In order to effectively compare the variation in noise levels, bar charts were plotted for each zone district was not allowed.

The chart clearly shows that there is considerable reduction in all four locations chosen under residential zone even though the results are a bit higher than the prescribed noise level. Among the locations, the noise levels from Infopark region have the highest variation. The noise levels were decreased to 64.58 dB during the COVID pandemic. The Infopark region is surrounded by flats and most of these are occupied by people working in Information Technology (IT) firms as it is near to Infopark, CSEZ Cochin and Smart City Kochi. Due to COVID pandemic, the Government had imposed lockdowns and there was prohibition from social gatherings. So, most of the IT companies had to switch to work from home mode, which allowed their employees to work from their home without going to office. This travel restriction had a positive result in decrease of vehicles on road and thus the noise pollution. Noise levels in Mavelipuram Colony reduced to 52.2 dB and was lower than the prescribed noise level (55 dB) (Fig. 14).

During 2016, before COVID, the highest sound level was recorded at LuLu mall with a dB of 123.45 followed by Pathadipalam and Oberon Mall. COVID pandemic had hindered the commercial activities in the city. Since COVID cases were rising in the city, both LuLu and Oberon Malls were shut as a measure to lower social gatherings and unnecessary mall visits. These malls are the main attractions in the

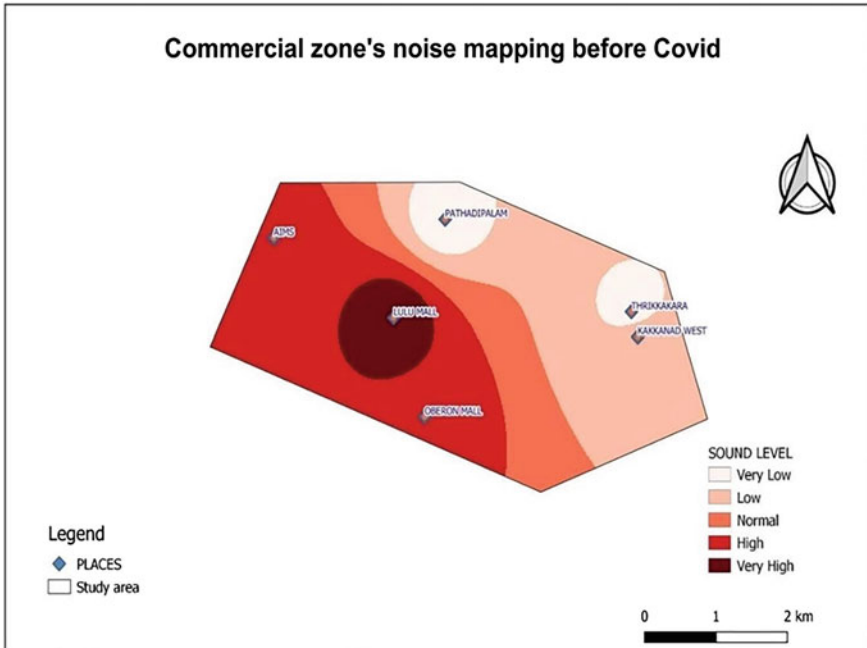


Fig. 8 Interpolated noise mapping for commercial zone before COVID

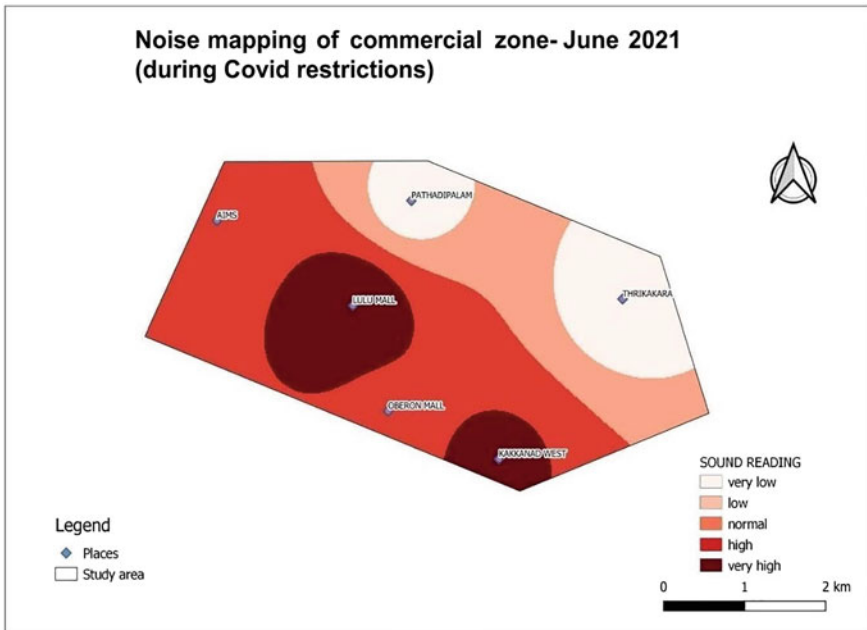


Fig. 9 Interpolated noise mapping for commercial zone during COVID restrictions

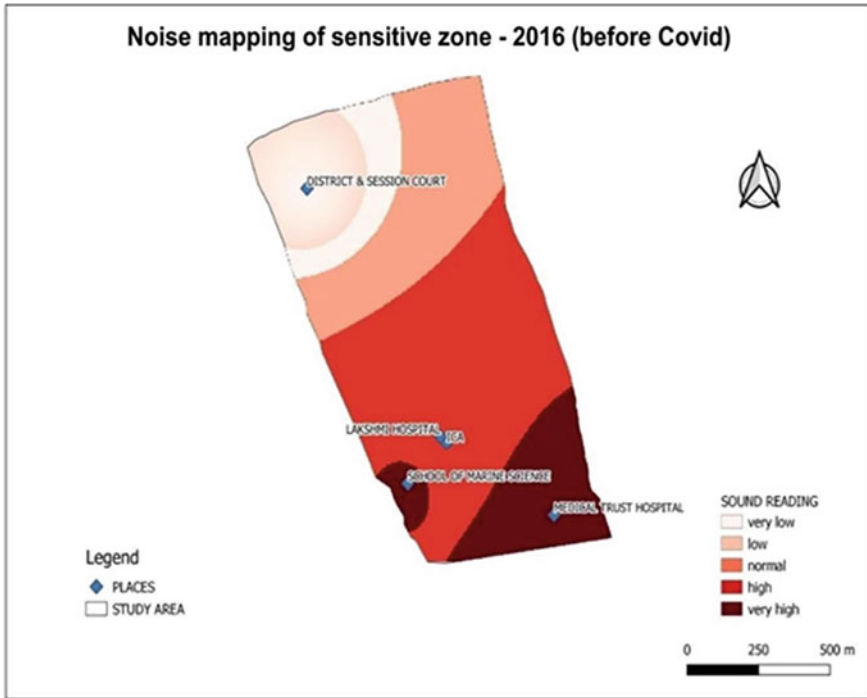


Fig. 10 Interpolated noise mapping for sensitive zone before COVID

city and traffic snarls are a usual sight at these roads. Shutdown of the malls has reduced the traffic rush and so the noise levels. AIMS Hospital, Cochin is one of the hospitals that witness usual rush and since the COVID cases were on surge, it had no difference even during this period. The hospital was a center for COVID vaccination drive. Thrikkakara civil station lays close to the noise monitoring point and this area usually experiences a rush on working days. But COVID restrictions had brought a reduction to this by lowering the noise levels to an extent of 65.7 dB which is closer to acceptable noise level. Noise level at Kakkanad West also meets the prescribed noise level. The noise levels measured in four out of six locations in the zone were above the prescribed limits, even under the COVID restrictions. But shows a significant decline when compared to the previous noise levels (Fig. 15).

All the five locations chosen under silence zone experienced very high noise levels from the prescribed noise level. The highest noise level was recorded at Medical Trust hospital with a dB of 66.53 which is higher than the prescribed level (50 dB). School of Marine Science recorded the second highest value with a dB of 63.2 Pallimukku junction in which the hospital lies is one of the busiest junctions in the city. There is a traffic signal at the junction and honking of vehicles is a common plight. Lakshmi hospital recorded third highest value with 60.4 dB. The operation of emergency medical services near that location and the sirens of ambulances reaching the hospital

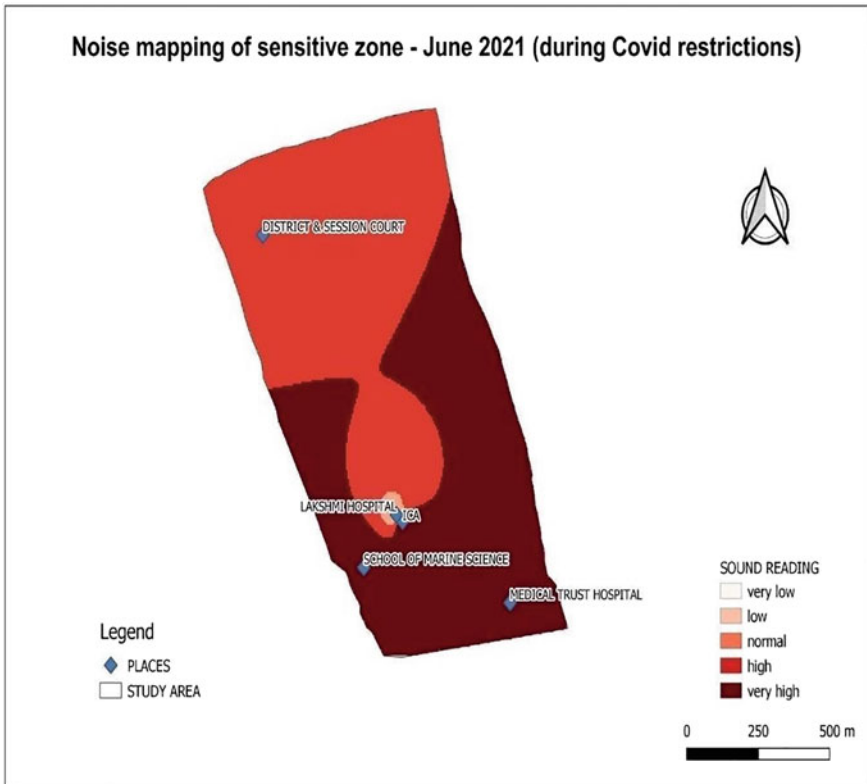


Fig. 11 Interpolated noise mapping for sensitive zone during COVID restrictions

has also resulted in noise levels. Lowest noise level was recorded at District and Session Court. Even during the COVID restrictions, the noise levels recorded are very much higher in all the locations. Noise levels under silence zone area should be kept under control as this includes hospitals, educational institutions and session court.

There was significant reduction in noise levels among both the locations zoned under industrial zone. The noise levels in BPCL declined by 21.57% and in FACT by 19.5%. Both the values were well below the prescribed levels. Partial shutdown of industrial activities has helped achieve this reduction (Figs. 16 and 17).

3.3 Control Measures that Can Be Adopted

Considering the reduction in traffic and thereby noise pollution during lock down period, the aspects during lockdown period can be considered for implementing traffic noise reduction. Although traffic restrictions can be implemented it will not

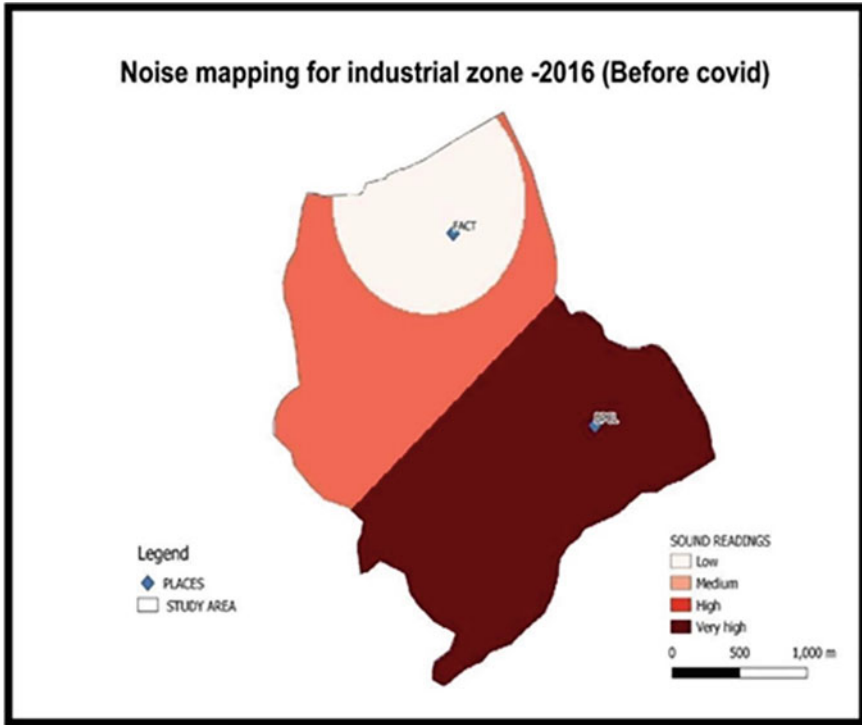


Fig. 12 Interpolated noise mapping for industrial zone before COVID

be possible to eliminate traffic in cities. Therefore, effective traffic management measures can help to mitigate the detrimental impacts of noise pollution. This study's findings have a few policy suggestions which are detailed below:

- Promoting environmentally friendly modes of transport: This study's findings show that strict traffic reduction measures can significantly reduce noise levels. Noise pollution can be reduced through a variety of measures, including a no honking policy, switching from motorized private transportation to walking and cycling for short distances, parking management and limiting access for the noisiest cars.
- Adoption of a greener environment: Building features like neighbourhood access to green spaces can lessen aggravation and the adverse effects of noise from traffic. There are a number of ways to reduce noise exposure, including planting trees, adding greenery to cities, creating green belts around roadways, and installing green roofs.
- Road infrastructure: Noise levels in areas with high sound levels can be reduced by installing noise-reducing pavements, traffic noise impedance walls, and quieter automobiles, as well as installing natural or artificial noise barriers, no-horn signs, and other traffic-calming measures.

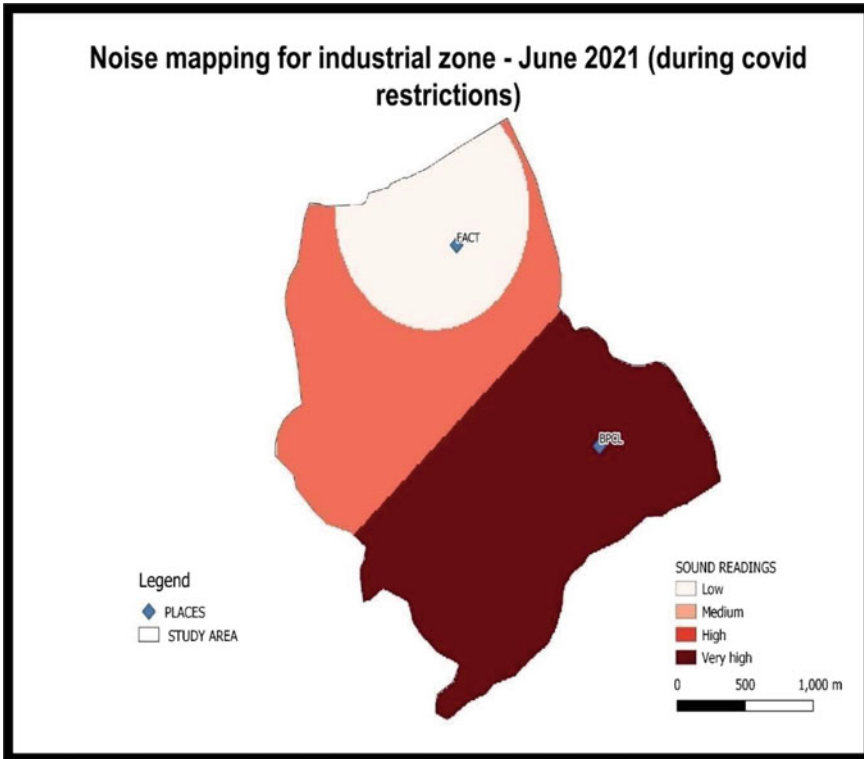


Fig. 13 Interpolated noise mapping for industrial zone during COVID restrictions

- **Development of a noise-monitoring database:** The development of a large sound monitoring network can aid in evaluating increased sound levels as well as the effectiveness of initiatives to reduce noise pollution. The placement of sound monitoring stations around cities and the creation of an appropriate noise monitoring database can help pinpoint the negative impacts of noise exposure in various locations and pinpoint neighbourhoods that may be particularly vulnerable to noise pollution.
- “Honk more, wait more” policy installed in Mumbai shall be implemented in the City, which rests the red traffic signal every time when the sound of horns goes above 85 decibels [16].
- **Noise emission reduction:** by source modification by changing tyre profiles and change in engine properties

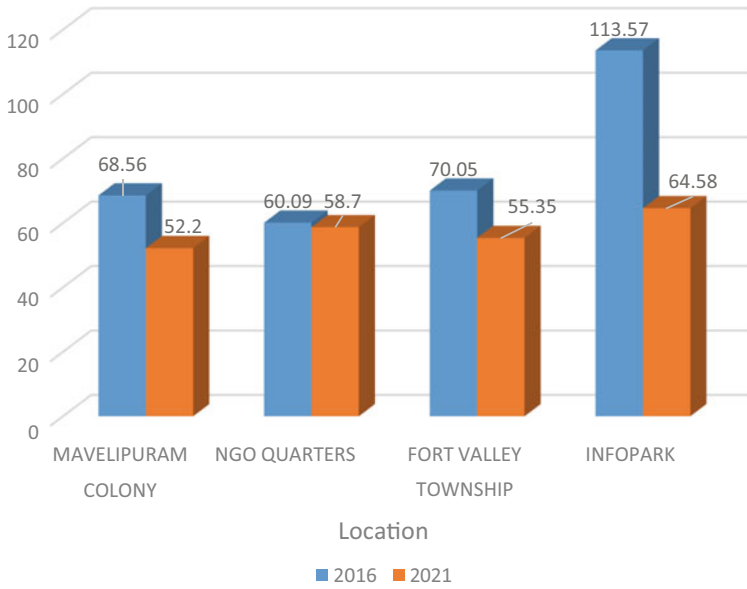


Fig. 14 Comparison chart for residential zone

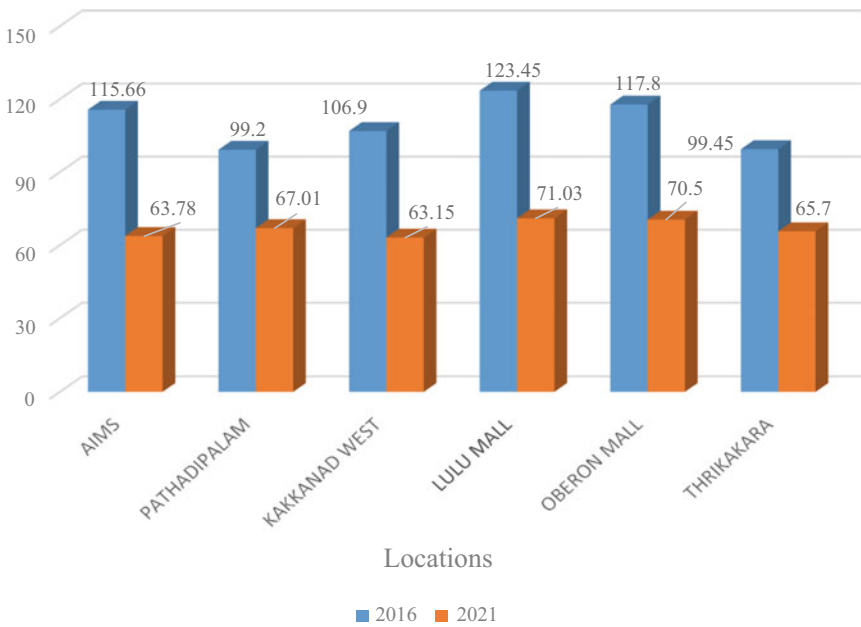


Fig. 15 Comparison chart for commercial zone

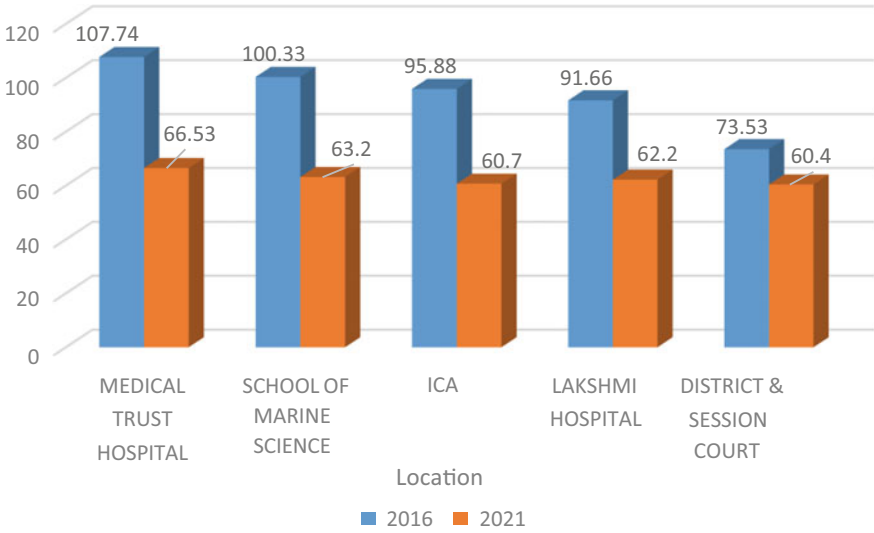


Fig. 16 Comparison chart for sensitive zone

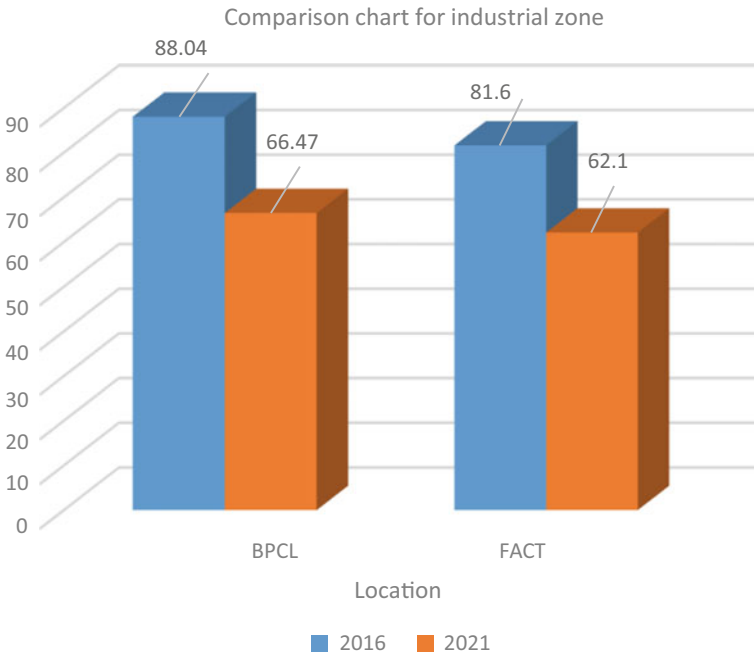


Fig. 17 Comparison chart for industrial zone

4 Conclusion

This study attempted to investigate to what extent the COVID-19 lockdown has impacted exposure to noise pollution levels in the city of Ernakulam, Kerala. The societal lockdown and behavioral shifts in the transportation industry have had a positive impact on local and regional pollution levels. In this context, this study contributed to a better understanding of sound level patterns and variations before and during the lockdown. The present study can be considered as a reference to understand how vehicle restrictions alone can significantly reduce the noise pollution.

The reduction in traffic is due to Government restrictions and noise level data in such a scenario is otherwise very hard to get because such a study with real time data is almost impossible if the Government restrictions were not applicable. The magnitude of changes in sound levels in the residential, industrial, commercial, and silence zones were evaluated, and noise maps were prepared for each zone using QGIS. Noise maps were prepared for the sound levels before and during the COVID restrictions.

The results showed a significant reduction in sound levels during lockdown compared to that of before lockdown at majority of the monitoring locations. Industrial and commercial zones saw a considerably greater decline than silence and residential zones. Except for the industrial zone, all other zones had recorded sound levels that were substantially higher than the recommended noise limits by the Central Pollution Control Board (CPCB) of India. This is indeed a subject of serious concern as continuous noise exposure can have long-term effects on a person's well-being such as annoyance and sleep disruption.

A mathematical traffic noise model was developed to fit the Indian road conditions and regression analysis was carried out. An R^2 value of 0.8149 was obtained and the model was validated. This indicates that the model could be used for similar works in future. This model can be used as a tool for understanding the impact of noise pollution due to heavy vehicles. This indeed helps in prediction of noise pollution and helps decision makers in carefully planning when developing an urban area. Since the model developed is on restricted traffic conditions due to Covid, the same can be used for urban planning to understand to what extent traffic reduction can reduce noise pollution quantitatively. Strict noise pollution mitigation techniques and appropriate policy measures could benefit public health and also ensures a long-term sustainable transportation infrastructure [17]. As a result, a number of feasible noise mitigation measures were also suggested in the study.

References

1. Sisodiya S, Mathur AK (2020) Comparative assessment of noise models for Kota city. *Mater Today Proc*
2. Mutalib NHA, Mashros N, Aminudin E, Zakaria R, Haron Z, Abd Talib MH, Hamid ARA (2018) Disturbance of traffic noise: evaluation on the effects and management on road corridors. *IOP Conf Ser Ear Environ Sci* 143(1):012049
3. Bocher E, Guillaume G, Picaud J, Petit G, Fortin N (2019) Noise modelling: an open-source GIS based tool to produce environmental noise maps. *ISPRS Int J Geo Inf* 8(3):130
4. Ashly S, Anilkumar B (2016) Assessment of noise pollution at Eranakulam by GIS. *Int J Adv Inf Sci Technol (IJAIST)* 5(10)
5. Sampath S, Das SM, Kumar VS (2004) Ambient noise levels in major cities in Kerala. *J Ind Geophys Union* 8(4):293–298
6. Sonaviya D, Tandel B (2019) A review on GIS-based approach for road traffic noise mapping. *Indian J Sci Technol* 14(12):1–6
7. Obaidat MT (2011) Spatial mapping of traffic noise levels in urban areas. *J Transp Res Forum* 47(2)
8. Pulakesh S (2014) Noise pollution assessment in greater Agartala city: a case study. *Int J Res Eng Technol* 03(09):402–407
9. Mishra A, Das S, Singh D, Maurya AK (2021) Effect of COVID-19 lockdown on noise pollution levels in an Indian city: a case study of Kanpur. *Environ Sci Pollut Res* 1–13
10. Kumar K, Katiyar VK, Parida M, Rawat K (2011) Mathematical modeling of road traffic noise prediction. *Int J Appl Math Mech* 7(4):21–28
11. Wawa EA, Mulaku GC (2015) Noise pollution mapping using GIS in Nairobi, Kenya. *J Geogr Inf Syst* 7(05):486
12. Calixto A, Pulsides C, Zannin PHT (2008) Evaluation of transportation noise in urbanised areas. A case study. *Arch Acoust* 33(2):185–199
13. Banerjee D, Chakraborty SK, Bhattacharyya S, Gangopadhyay A (2008) Modeling of road traffic noise in the industrial town of Asansol, India. *Transp Res Part D Transp Environ* 13(8):539–541
14. Maya MS, Sreedevi C (2015) Analysis of traffic noise pollution in Thiruvananthapuram city using mapping and modelling. *Int J Eng Res Technol (IJERT)* 1–5
15. Kurakula V, Skidmore A, Kluijver H, Stoter J, Dabrowska Zielinska K, Kuffer M (2007) A GIS based approach for 3D noise modelling using 3D city models. *Enschede, ITC, The Netherlands*
16. Vijay R, Sharma A, Chakrabarti T, Gupta R (2015) Assessment of honking impact on traffic noise in urban traffic environment of Nagpur, India. *J Environ Health Sci Eng* 13(1):1–10
17. Abo-Qudais S, Alhiary A (2005) Effect of traffic characteristics and road geometric parameters on developed traffic noise levels. *Can Acoust* 33(1):43–50

Sustainable Pervious Pavement Block with 3D Printed PETG Frame



Keerthana Ranjith  and M. V. Varkey 

Abstract Due to the impervious features of conventional pavements and increasing road coverage areas, the heat island effect is becoming more severe, and many environmental problems have appeared [1]. Since, conventional interlocks have a disadvantage of being non-pervious and hindering the chances of water to seep in to the ground we are introducing a pavement block, whose central core portion can withstand the load applied with an M30 concrete mix (IS 15658) and 45% of natural coarse aggregate in this concrete grade is substituted by recycled concrete coarse aggregate (RCCA). The perviousness is achieved by attaching a 3D printed PETG (Polyethylene terephthalate glycol) frame structure with lofted circular holes for water to trickle down. The pavement blocks are subjected to visual inspection, dimension tolerance, compressive strength, water absorption and flexural strength test (three-point test) according to IS 15658. The tests were done on factory made pavement block, pavement block without frame and with frame, for all these tests to get accuracy. The test results showed that pavement block with frame has remarkable strength and the aim of perviousness can be achieved easily. It is identified that the interlock block with 3D printed PETG frame attached for perviousness have more compressive strength compared to interlock block without frame and factory-made block. It is also understood that the block without frame has the least strength compared to other two pavement blocks. The strength of pavement block with frame has a significant increase in strength due to 3D PETG frame.

Keywords PETG · Perviousness of pavement block · Recycled concrete coarse aggregate

K. Ranjith (✉) · M. V. Varkey
Amal Jyothi College of Engineering, APJ Abdul Kalam Technological University, University in Thiruvananthapuram, Koovappally, Kanjirappally, Kerala 686518, India
e-mail: keerthanaranjith@ce.ajce.in

M. V. Varkey
e-mail: mvarkey@amaljyothi.ac.in

1 Introduction

Since 1950, 3D printing has been making inroads into the building sector. In addition to using concrete to 3D print the construction business also uses plastic fibers such as geopolymer, foams, PETG, and ABS thermoplastics. Since 3D printing is the process of building three-dimensional things layer by layer using a computer-generated design, the bonding performance of each layer deposited is being called into question in the case of 3D printing concrete. In order to improve the strength of permeable pavement, the concept of 3D printing is combined with the study of permeable pavement. In the light of imparting sustainability in the manufacturing of blocks the recycled concrete coarse aggregates are used [2].

Due to the limited availability of natural aggregates, it is mandatory to find alternate of NA [3]. In this study, the paver blocks are constructed by substituting 45% natural coarse aggregates by recycled concrete coarse aggregate. The study followed the method suggested by Kumar et al. [3]. The recycled concrete coarse aggregate (4.75–10 mm) was separated by using required sieve size [3]. In areas with minimal vehicular traffic, such as bike paths, service lanes, emergency access lanes, road shoulders, airports, and private sidewalks and driveways, permeable pavement is frequently used [4]. Permeable paving systems, in contrast to conventional impervious paving materials like concrete and asphalt, permit stormwater to percolate and infiltrate through the surface and into the aggregate layers and/or dirt beneath. Permeable paving systems can capture suspended solids and filter pollutants from stormwater in addition to decreasing surface runoff [1]. Permeable pavements are achieved generally through porous asphalt, pervious concrete and by providing wide gap between interlocks. The problem with porous asphalt is that it is slightly expensive than traditional paving also the need of special skills etc. Similarly pervious concrete requires longer curing time, specialized construction practice, conventional tests like slump and compaction factor are not applicable etc. Also, the load bearing capacity of these pavements are questionable. When it comes to interlock block with wide gap between them, the major problem is the interlocking of blocks itself is lacking there, also the chances of weeds to grow and things to get stuck between the gaps, aesthetics of the pavement etc. is a concern. After a while the interlock starts to get sinking and since there is not interlocking due to gaps i.e., The stability of paver block depends upon the presence of compacted sand in its joint to provide and maintain interlocking. We cannot suggest interlock block with gap between them as a feasible solution for ingress of water into the ground.

A thermoplastic thread used in 3DP is PETG filament. PETG is extremely strong, flexible, and nontoxic. It does not shrink or distort. It does not take in atmospheric humidity [5]. It does not degrade in water. It is suitable for outdoor uses because it is UV-resistant. It is also impervious to chemicals. Soleyman et al. [6], introduced a novel shape memory polymer (SMP) for the first time, which exhibits highly controlled self-coiling and tensile shape memory characteristics in 3D printed PETG thermoplastic structures [6], which helped to gain more confidence regarding the use of PETG for frame of concrete block.

The perviousness here is achieved through attaching a frame with lofted circular holes in it, so that the water could seep into the ground. The design is done in Fusion 360 and is printed using Ender 3S1. The frames have to be attached with the concrete paver block and for this purpose interlocking configurations and mix suggested by Wang et al. [7] was used. In order to maximize the mechanical integrity and capacity of prefabricated constructions with mechanical bite and adhesive forces Epoxy-based composite were used [7]. The pavement block thus casted adopting all these methods are subjected to tests according to IS 15658:2021 [8].

2 Research Framework

The methodology is divided in to parts such as Material collection, 3D printing, Assembling/ Casting, and Experimental Study (Fig. 1).

The materials for manufacturing such as Cement (PPC 43), Sand, and PETG has to be purchased. The lattice structure of pervious edges for pavement block is designed and sliced using Fusion 360 and Prusa Slicer. The design STL file and the PETG filaments are both feed in to the 3D printer and printed.

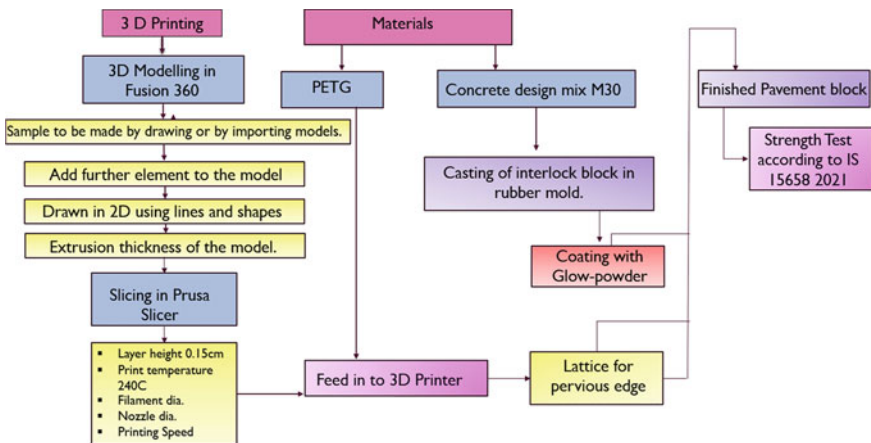


Fig. 1 Flow chart showing methodology followed

The pavement block is then casted with M30 concrete mix as of IS 15658:2021 and IS 2185:2005 [8, 9]. The percentage of natural coarse aggregates to be replaced by demolished building wastes (recycled concrete coarse aggregate—RCCA) is determined by casting M30 cubes with coarse aggregates replaced in 30, 45 and 60%.

After demoulding the pervious edges printed has to be attached with the blocks using epoxy-based cement. The quality of the pavement blocks has to be ensured by following IS 15658:2021 provisions.

3 Analysis and Discussion

3.1 Determining Percentage of RCCA

To determine percentage of the natural coarse aggregates to be substituted by RCCA cubes were casted; with 30, 45, 60 of RCCA in M30 mix. The 7th day and 28th day strength of each percentage cube is measured in CTM. The RCCA was processed by, collecting demolished cube wastes from civil lab and crushing it in the shredder. The shredded pieces are then passed through sieve sizes 12, 10, 6.3 and 4.75 mm. RCCA should pass through 12 mm sieve and retained in every other mentioned sieve (Fig. 2).

The RCCA were tested for properties such as Fineness modulus (7.074), Specific Gravity (2.594), Bulk density of loosely packed aggregate (1.394 g/cm³), Bulk



Fig. 2 a Building wastes, b hammered and collected in pan, c into the shredder, d sieving to correct grade sizes, e cube casted for strength tests, f compression testing, g interlock mold-zig-zag ant shape, h interlock block casted

density of compacted aggregate (1.573 g/cm^3). Similarly for natural coarse aggregate; Fineness modulus (7.968), Specific Gravity (2.639), Bulk density of loosely packed aggregate (1.534 g/cm^3), Bulk density of compacted aggregate (1.663 g/cm^3) and for fine aggregate; Fineness modulus (3.674), Specific Gravity (2.95), Bulk density of loosely packed aggregate (1.517 g/cm^3), Bulk density of compacted aggregate (1.69 g/cm^3) and is of grading zone II. For PPC 43; Setting time-initial 45 min and final 420 min. Soundness 5 mm, specific gravity 2.93 with fineness 7%. The tests were done based on IS 2386 Part 1, 1963 [10].

Figure 3 ,strength versus % RCCA Replaced graph shows the compressive strength of cubes in 7th day (blue line) and 28th day (red line). Concrete cube of M30 grade where the natural coarse aggregates are substituted with 30, 45 and 60% of recycled concrete coarse aggregate are subjected to compressive strength test to find out which percentage of RCCA replacement shows better strength performance. As the graph shows the cubes with 45% (33 N/mm^2 —28th day strength) of RCCA have higher compressive strength than cubes with 30% (27 N/mm^2 —28th day strength) and 60% (29 N/mm^2 —28th day strength) RCCA. Thus, the interlock blocks were casted with M30 concrete mix, 45% RCCA. The blocks are of Zig-zag ant shape with 50 mm height according to IS 15658. The cement used for cube casting as well as the interlock blocks in later stages are all selected based on IS 1489;1991 and tested according to IS 4031, Part 1, 4, 11;1996 for its properties [11, 12].

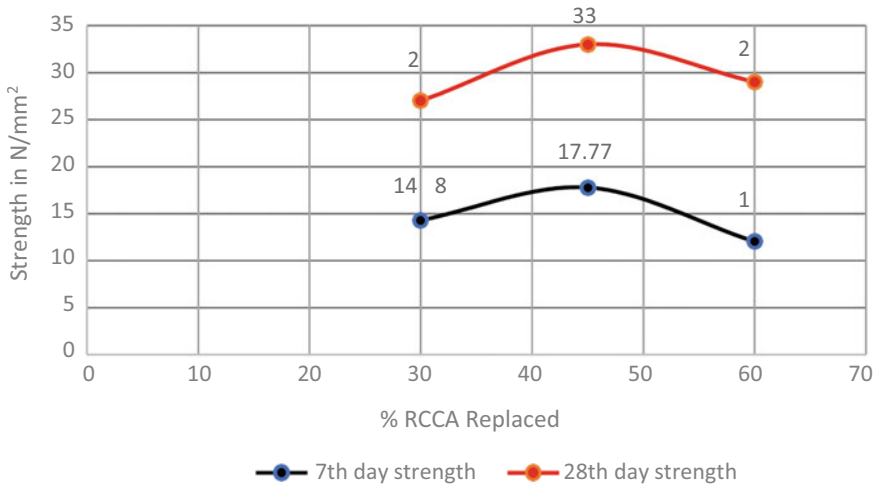


Fig. 3 Strength versus % RCCA replaced

3.2 3D Printing of PETG

The frame is designed to attach on the edges of the concrete block with lofted circular holes to avoid clogging and for the easiness of water to trickle down. The preliminary designing is done in AutoCad and then designed in Fusion 360 (Fig. 4). The file is saved as 'stl' format and is printed in Ender 3S1 printer. The printing temperature is 235 ± 10 °C. PETG filament and 3D printing in Ender 3S1 is shown in Fig. 5.

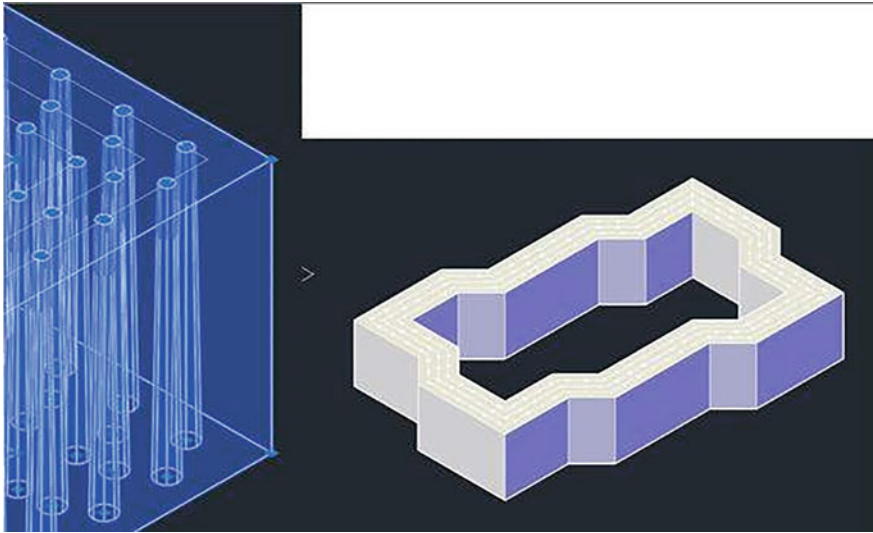


Fig. 4 Pervious edges 3D printed with lofted holes X-ray and Conceptual images (AutoCad and Fusion 360)

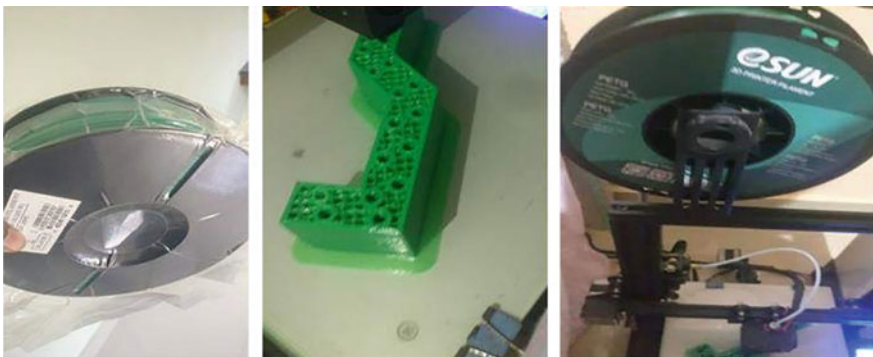


Fig. 5 PETG filament and 3D printing in Ender 3S1

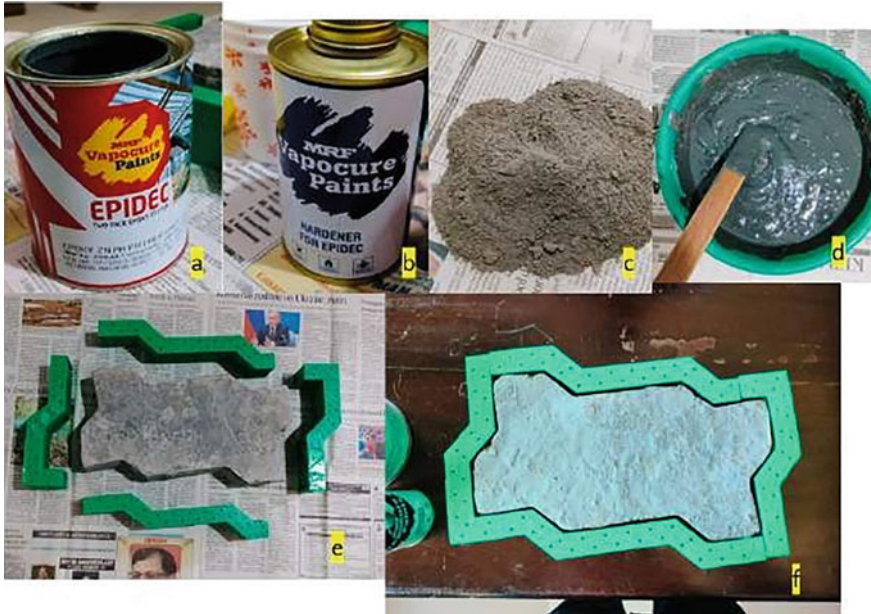


Fig. 6 a Epoxy resin, b hardener, c cement-sand mix, d cement based epoxy composite, e interlock block and 3D printed PETG frames, f frames attached with Interlock block

3.3 Attaching of Frames with Concrete Block

Cement-based composite for interlocking binding; The preparation process is as follows: first the epoxy resin and a water-borne epoxy resin are uniformly mixed and stirred, and a white emulsion liquid is formed. Subsequently, cement and sand are mixed separately, and the mixture is poured into the white emulsion liquid, and thereafter water is added for full mixing. The final bonding composite is applied on one end of the specimen owing to the poor fluidity, and subsequently the other end is compacted and bonded together. The coating thickness of the interface bonding material is approximately 5 mm [7] (Fig. 6).

3.4 Testing and Results

Compressive Strength. Compressive Strength is tested and compared for three different types of interlock block. (i) Factory made interlock block, (ii) Interlock block without frame, (iii) Interlock block with frame. Compressive strength test is done according to IS 15658:2021. Plan area have to be calculated for this test (Table 1).

Table 1 Compressive strength

	Factory made	Block without frame	Block with frame
W_a = Weight of specimen (kg)	7.254	4.525	5.580
W_w = Weight of specimen after removing from water (kg)	7.256	4.527	5.581
Thickness of block (cm)	6	6	6
Plan area (mm ²)	4×10^{-8}	3.33×10^{-8}	1.66×10^{-8}
Load (KN)	2400	1900	2800
Area (mm ²)	43,332	32,189.62	47,427
Compressive strength (N/mm ²)	60.001	59.026	61.557
Corrective compressive strength (N/mm ²)	60.001	59.026	61.557

Plan Area = $\frac{w_w - w_a \times 10^{-3}}{T}$ and for Compressive Strength = $\frac{\text{Load (KN)}}{\text{Area (mm}^2\text{)}}$ are the equations followed here. The correction factor is 1 for pavement blocks since the thickness is 6 cm. Generally, for M30 grade of paver block the height suggested is 50 mm, but since we are using RCCA and the block has pervious attachment the blocks have 60 mm thickness. Also, the factory-made block of M30 grade also had a depth of 60 mm.

It is identified that the interlock block with 3D printed PETG frame attached for perviousness have more compressive strength compared to interlock block without frame and factory-made block. It is also understood that the block without frame has the least strength compared to other two pavement blocks. The strength of pavement block with frame has a significant increase in strength due to PETG. The block barely had any visible crack, also the crack on the surface did not develop towards the core portion of the block (Figs. 7 and 8).

Water absorption. PETG material is water repellent and it does not absorb water by nature. For the water absorption test the block cannot be placed in oven since the service temperature of PETG is 70 °C and for this test the sample should be placed in oven for 24 ± 2 h in 105 ± 1 °C. Thus, only the pavement block without frame is tested for water absorption. Water Absorption = $\frac{w_1 - w_2}{w_2} \times 100$ (Table 2).

According to IS 15658:2021 for individual blocks water absorption should be less than 7% and for average it should be less than 6%. The pavement blocks casted satisfies both criteria.

Flexural strength—Three-point test. Flexural Strength is tested and compared for three different types of interlock block. (i) Factory made interlock block, (ii) Interlock block without frame, (iii) Interlock block with frame. Flexural strength test is done according to IS 15658:2021. The test is done in UTM. The flexural strength of the specimen shall be calculated as follows:

Flexural Strength, F_b (N/mm²) = $\frac{3Pl}{2bd^2}$; P = Maximum load in NI = distance between central lines of supporting rollers, in mm; b = average width of block,



Fig. 7 a1 Factory made block, a2 block without frame, a3 block with frame, b weighing factory made block, c weighing block without frame, d weighing block with frame, e factory made block in CTM, f block without frame in CTM, g block with frame in CTM



Fig. 8 a The only visible crack is on the surface, b no vertical crack in the sides, c block after loading in CTM

Table 2 Water absorption

Weight of the specimen (W1) (kg)	Weight of the specimen after taking from oven (W2) (kg)	Water absorption (%)
4.257	4.242	0.353
4.259	4.241	0.424

measured from both Faces of the specimen, in mm; and d = average thickness, measured from both ends of the fracture line, in mm (Table 3).

It was found that the paver block without frame has higher flexural strength than the other two blocks. Even though, the paver block with frame has lesser flexural strength than the other two paver blocks the crack only occurred at the surface and did not develop into the core of the block. This is due to the attachment of PETG frame on the edges of paver block. Even though the flexural strength values differ for three specimens, they satisfy the suggested values of minimum breaking load for paver blocks according to IS 15658 which is 2 KN (Figs. 9 and 10).

Table 3 Flexural strength

	Factory-made block	Block without frame	Block with frame
P (KN)	20	17	19
L (mm)	245	200	250
b (mm)	140	120	160
d (mm)	120	97	123
Flexural strength (N/mm ²)	3.645	4.516	2.943

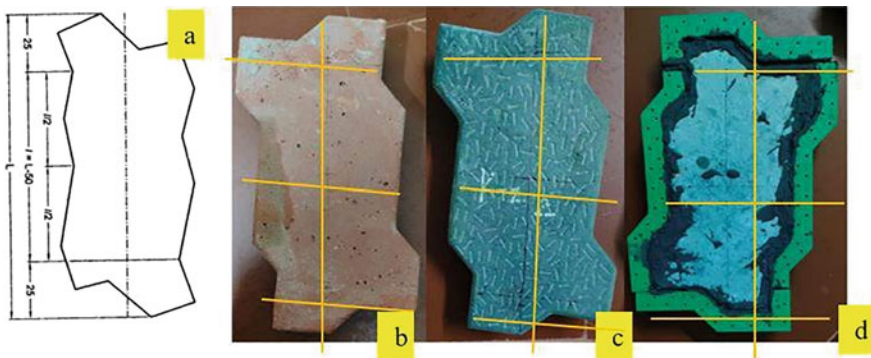


Fig. 9 Loading points for flexural strength test **a** according to IS 15658, **b** factory made block, **c** and **d** paver block without and with PETG frame



Fig. 10 a–c Three-point test setup of factory-made block, paver block with and without PETG frame, d–g crack pattern of factory-made block, paver block with and without PETG frame

4 Conclusion

The aim of this work is to achieve perviousness in concrete block without affecting the strength of concrete block. The required perviousness is achieved through 3D printed PETG copolymer frame attached to the concrete block. The lofted circles help in easy trickling of water into the ground and helps to avoid clogging of these holes. The PETG frame plays a significant role in increasing the overall strength of concrete block. The use of RCCA in casting of interlock block does not diminish

the strength of concrete and it turned out to be a sustainable and promising way of reusing demolished building wastes.

The comparison study of factory-made interlock block, interlock block without frame and with frame showed that, the compressive strength of interlock block without frame where 45% NA is replaced with RCCA has comparatively lesser compressive strength. The same interlock block when attached with PETG frame to achieve pervious edges also contributed in the strength performance of the interlock block. In case of flexural strength, the paver block with RCCA showed higher performance than the other two specimens. This needs to be further analysed and studied. The epoxy-based cement composite held the frame with the block; the bond was intact throughout all the experiment.

The introduced paver block thus, shows satisfactory performance in strength category and perviousness.

References

1. Lu G, Wang Y, Li H, Wang D, Oeser M (2019) The environmental impact evaluation on the application of permeable pavement based on life cycle analysis. *Int J Transp Sci Technol* 8(4):351–357
2. Sha A, Liu Z, Jiang W, Qi L, Hu L, Jiao W, Barbieri DM (2021) Advances and development trends in eco-friendly pavements. *J Road Eng* 1:1–42
3. Kumar G, Shrivastava S, Gupta RC (2020) Paver blocks manufactured from construction & demolition waste. *Mater Today Proc* 27:311–317
4. Kayhanian M, Li H, Harvey JT, Liang X (2019) Application of permeable pavements in highways for stormwater runoff management and pollution prevention: California research experiences. *Int J Transp Sci Technol* 8(4):358–372
5. Kluczyński J, Szachogłuchowicz I, Torzewski J, Śnieżek L, Grzelak K, Budzik G, Przeszlowski Ł, Małek M, Łuszczek J (2022) Fatigue and fracture of additively manufactured polyethylene terephthalate glycol and acrylonitrile butadiene styrene polymers. *Int J Fatigue* 165:107212
6. Soleyman E, Aberoumand M, Rahmatabadi D, Soltanmohammadi K, Ghasemi I, Baniassadi M, Abrinia K, Baghani M (2022) Assessment of controllable shape transformation, potential applications, and tensile shape memory properties of 3D printed PETG. *J Market Res* 18:4201–4215
7. Wang L, Liu Y, Yang Y, Li Y, Bai M (2021) Bonding performance of 3D printing concrete with self-locking interfaces exposed to compression–shear and compression–splitting stresses. *Addit Manuf* 42:101992
8. IS 15658:2021, Precast concrete blocks for paving-specifications
9. IS 2185 (Part 1): 2005, Concrete masonry units—specification (hollow and solid concrete blocks)
10. IS 2386 Part 1:1963, Methods of test for aggregates for concrete
11. IS 1489:1991, Portland—Pozzolana cement specification
12. IS 4031 Part 1,4,11:1996 of methods of physical tests for hydraulic cement

Experimental Study on Properties and Performance of Fibre Roofing Tile



Mariamol Kuriakose, Arju M. Tomy, Ajay Emmanuel, Alwin Biju, and Roshan Benny

Abstract Roof tiles have proven to be the latest home improvement trend. Homes or other structures in high-rainfall locations are more likely to have such tiles. The strength, beauty, and hardness of roof tiles are the main factors contributing to their rising popularity. In our project, we propose a light weight and heat-resistant roofing tile and panel made up of glass fibre. We used polyol and isocyanate to make the product heat-resistant. In locations with low-bearing capacity soil, fibre roofing tile is more useful as it reduces the structure's weight. Our roofing tile is lighter when compared to ordinary roofing tile. In this paper, we observe the methodology, experiment conducted, result, and cost of fibre roofing tile. The methodology explains the procedure to prepare the fibre roofing tile. The final product is obtained by following different steps. After manufacturing the product, different experiments are conducted to check the properties of the roofing tile. Break load test, water absorption test, permeability test, and heat resistance test are the experiments conducted. The results obtained are compared with other ordinary roofing tiles.

Keywords Fibre roofing tile · Clay roofing tile · Ceramic roofing tile · Liquid form

1 Introduction

Here we are conducting an experimental study on the properties and performance of the fibre roofing tile. Nowadays, available roofing tiles are made of clay, ceramic, metal, concrete, etc. Here we are introducing a new type of roofing tile that is made up of glass fibre. The primary characteristics of fibre roofing tile are its heat resistance and light weight. Our fibre roofing tile will be much more heat-resistant than standard roofing tiles available on the market. Because of their light weight, these can be used on structures built on low-bearing capacity soil. We are conducting experiments

M. Kuriakose · A. M. Tomy (✉) · A. Emmanuel · A. Biju · R. Benny
St. Joseph's College of Engineering and Technology, APJ Abdul Kalam Technological University,
Palai, Thiruvananthapuram 686579, India
e-mail: arjutomy@gmail.com

Fig. 1 Glass fibre

to test the strength and durability of the roofing tile. The obtained results will be compared to the properties of common roofing tiles. In order to produce these fibre roofing tiles, we are using glass fibre and resin as the main components. Here, we follow the same design as the traditional roofing tile for convenience. Since we are using fibre as the raw material, the resulting product, which is fibre roofing tile, must be checked in various ways in order to prove its stability. So, we conducted water absorption tests, breaking load tests, permeability tests, and heat resistance tests.

2 Material

2.1 Glass Fibre

Glass fibre is a substance made up of many, incredibly fine glass fibres. One of the most adaptable industrial materials available today is the product. Its mechanical characteristics are equivalent to those of other fibres like carbon fibre and polymers. We are using this glass fibre as the main raw material in our roofing tile. Glass fibre is moulded into the shape of a roofing tile using resin. Fibre is a light weight material, so fibre makes the roof tile light weight (Fig. 1).

2.2 Resin

The overall objective for use in laminating, polyester resin is an unsaturated polyester resin that cures quickly and is based on orthophthalic raw ingredients. It is unaccelerated. Suitable for both hand lay ups and gun spray-ups. The resin offers excellent mechanical properties, impact resistance, and water resistance. Here, resin is added to the glass fibre to make it loose and take the shape of the mould [1].

Fig. 2 Product obtained by mixing polyol and isocyanate



2.3 Liquid Foam

Liquid foam is used to make the roof tiles heat-resistant. The inner space of the roof tile is filled with liquid foam. The foam is obtained by mixing two liquids, namely polyol and isocyanate. Both liquids combined to make foam and give more strength to the roof tiles.

A polyol is an organic molecule with many hydroxyl groups, according to organic chemistry. Not all polyols have the same properties. However, polyols are usually viscous at room temperature due to hydrogen bonding. Isocyanates are a group of low-molecular-weight, extremely reactive compounds. They are widely used in the manufacture of flexible and rigid foams, fibres, coatings, etc. [1] (Fig. 2).

2.4 Pigment and Gelcoat

Pigment and gelcoat are the first layers of materials placed in the mould for the preparation of roof tiles. The main purpose of this material is to provide colour to the roof tile. We can give any colour to the tile, depending on the pigment. We tried different colours, such as brown, white, green, and dark yellow. This material also helps to detach the roof tile from the mould (Fig. 3).



Fig. 3 Different color fibre roof tiles

3 Methodology

3.1 Design and Manufacturing of Suitable Mould

For roofing tiles, various designs are available on the market. We have taken the design of clay roofing tile as the design of our fibre roofing tile because of the presence of grooves in the shape. The presence of grooves enables easy passage for rainwater. Also, this design enables a locking system for the roofing tile.

Based on the selected shape, we manufactured the mould using fibre mat, resin, and clay roofing tile. Place the fibre mat above the clay roofing tile and apply resin to it. After applying resin, the fibres get loose, and it takes on the shape of clay roofing tile. Again, a layer of fibre mat was coated above it to give it enough strength. The fibre gets hardened for 1 h and forms the mould. Some maintenance work is done to the mould using putty to get a good finish. Two moulds are prepared for the two sides of the roofing tile.

3.2 Creating Fiber Roofing Tile and Panel Using Glass Fibre

From the mould made of glass fibre, we can make roofing tiles. First, take the mould and clean it thoroughly using water. Add a small amount of PVA and polish it as a layer above the mould. It is helpful for the easy removal of fibre roofing tile from the mould. Then make a layer using 100 g of gelcoat and pigment. It gives colour to fibreglass roofing tile. Then we take a 325-g fibre mat, cut it into the proper shape to fit in the mould, and add resin to it. 1 mm of fibre mat is layered, and resin is added; this process is done for two moulds simultaneously. Allow the tiles one hour of rest. After preparing both sides of the roof tile, joint it by using putty. Also, do

some finishing work using putty. Fill the inner space of a roofing tile using liquid foam.

3.3 Determine the Properties of the Tile by Conducting Suitable Test

Various tests are performed on the completed fibre roofing tile to determine its properties. They are.

- Break Load Test
- Water Absorption Test
- Permeability Test
- Heat resistance.

From the weight load test, we can determine the load-carrying capacity of the roofing tile. The greater the load-carrying capacity, the greater the strength of the roofing tile. From the water absorption test, we can find the water absorption capacity of the roofing tile. A decrease in the water absorption value indicates that the material is good for roofing tile. A permeability test is conducted to determine the permeability value of the tile. The permeability value gives the amount of water permeable through the roofing tile.

4 Experimental Investigation

4.1 Break Load Test

Three tiles were tested after being soaked in water for 24 h in a wet condition. The tiles were placed evenly flat-wise on the bearer set with a span of 27 cm, resting on the bottom surface (Fig. 4). The load was applied in a direction perpendicular to the span at a uniform rate of 450–550 N/min Figure 4. Testing of specimens in break-load apparatus The individual breaking loads of the three tiles were recorded in wet conditions separately, and the average was taken as the load carrying capacity. Test results are shown in Table 1. Break load tests of other types of roofing tile were also conducted and noted in Table 2 [2–5].

4.1.1 Fibre Roofing Tile

See Table 1.

Fig. 4 Sample is placed in the apparatus

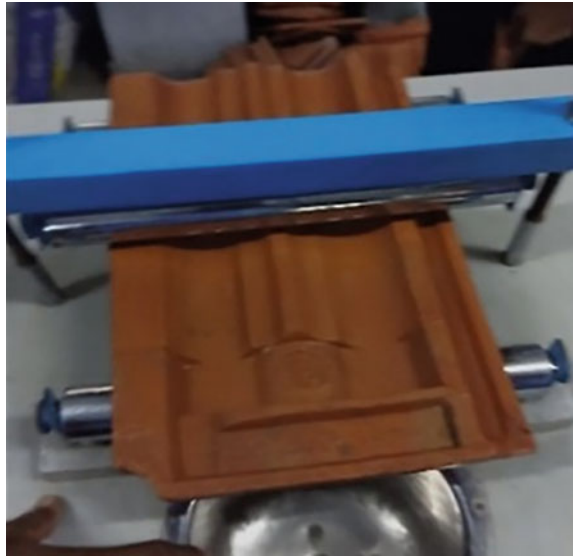


Table 1 Break load test value of fibre roofing tile

Sample No.	Dimensions (cm)	Weight of the lead shots (g)	Load (weight * 9.81) (N)	Break load (load * 12) (N)
1	40 × 23	23,580	231.32	2775.84
2	40 × 23	22,980	225.43	2705.16
3	40 × 23	23,300	228.57	2742.84

Table 2 Break load test value of other roofing tile

Type of sample	Dimension (cm)	Weight of the lead shots (g)	Load (weight * 9.81) (N)	Break load (load * 12) (N)
Clay	40.5 × 23.5	10,270	100.7	1208.4
Ceramic	39 × 30	20,320	199.3	2391.6

4.1.2 Other Roofing Tile

From the experiment, it is observed that fibre roofing tiles have higher strength. The average break load test strength of the fibre roofing tile is 2741.27 N. The break load strength of other roofing tiles, such as clay and ceramic are 1208.4 N and 23,916 N respectively. While comparing fibre roofing tile with other roofing tiles, it is observed that fibre tile have more strength.

4.2 Water Absorption Test

The test specimens were dried in an oven at a temperature of about 105–110 °C prior to the test. Dry weights were measured after atmospheric cooling and immersed in clean water at room temperature (24–30 °C) for about 24 h (Fig. 5). The specimen was then removed from the water, surface dried, and weighed. The increase in weight with respect to the original dry weight was taken as the water absorption for that sample. The mean water absorption of the three samples was taken. A sample set of results obtained is given in Table 3. The water absorption of other types of roofing tiles was also examined and noted in Table 4 [2–5].

4.2.1 Fibre Roofing Tile

See Table 3.

Fig. 5 Sample is placed for water absorption



Table 3 Water absorption value of fibre roofing tile

Sample No.	Wt. of dry tile W1 (g)	Wt. of wet tile W2 (g)	Water absorption (%)
1	610	610	0
2	620	620	0
3	620	620	0

Table 4 Water absorption value of other roofing tile

Type of sample	Wt. of dry tile W1 (g)	Wt. of wet tile W2 (g)	Water absorption (%)
Clay	2040	2321	13.77
Ceramic	2470	2580	4.45

Table 5 Permeability test values

Initial head (cm)	Final head (cm)	Time (h)	Permeability
5	5	24	Pass
5	5	24	Pass
5	5	24	Pass

4.2.2 Other Roofing Tile

The water absorption value of fibre roofing tile is zero. Clay and ceramic roofing tiles have water absorption values of 13.77% and 4.45%, respectively. The quantity of moisture that a particular type of tile is likely to absorb over time is measured by its water absorption. If the moisture penetration is too great, the tile may crack. In general, a tile's strength and durability are greater if it has a low water absorption rate.

4.3 Permeability Test

The test was conducted in a rectangular trough, open at the bottom, with the dimensions equal to the size of the tile under test. The tile was fitted at the bottom of the trough, and the space between the tile and the sides of the trough was plugged watertight with a suitable material like wax, bitumen, etc. Water was poured into the mould so that it stood over the lowest tile surface to a height of 5 cm. The water in the trough was allowed to stand for 24 h. The bottom of the tile was carefully examined to see whether the water had seeped through [5] (Table 5).

The permeability test is conducted on soil to determine the rate at which the material allows water to flow through it. Permeability depends on the grain structure and void space. Fibre roofing tile passes the permeability test due to the absence of moisture content at the bottom of the tile after 24 h. Here, for fibre roofing tile, the permeability value is zero. That means the amount of void space is less.

4.4 Heat Resistance Test

The heat resistance of the roofing tile was examined by placing it in the sunlight. Solar radiation from the sun heats the sample, and the amount of heat is measured using lasers. The amount of heat at the outer side of the sample (the surface in contact with the sun's rays) and the inner side of the sample is measured. The sample's heat resistance is determined by the difference in heat amounts [6] (Table 6; Fig. 6).

Table 6 Heat resistance test values

Type of sample	Amount of heat		Atmospheric temperature (°C)	Difference in heat
	Outer	Inner		
Fiber	48.6	42.6	35	6
Clay	53.4	53	35	0.4
Concrete	62.1	55.4	35	6.7

Fig. 6 Testing heat resistance using lacer



In the experiment, it was observed that concrete resists heat better. The intensities of heat at the top surface and bottom surface are 62.1 °C and 55.4 °C, respectively. But fibre tile feels less heat at the top surface, which is 48.6 °C. Fibreglass tiles resist some amount of heat falling on them due to the presence of liquid foam, which helps them resist heat. After the heat resistance of the foam, the amount of heat on the bottom of the fibre tile is 42.6 °C. 42.6 °C is the lowest amount of heat felt at the lower surface when comparing clay, fibre, and concrete.

5 Cost Analysis

The above-mentioned materials are mainly used for the preparation of roof tiles. The quantity and price for a single-fibre roof tile are mentioned in Table 7. The total price of a single roof tile is Rs. 85. It can be reduced to 60–70 while large-scale manufacturing is done [5].

Table 7 Cost analysis

Material	Quantity (g)	Rate (Rs.)
Fiber mat	125	21
Resin	325	15
Pigment and gelcoat	100	24
Foam	100	20
Other material		5
Total		85

6 Conclusion

In this project, we made a roofing tile using glass fibre, which is very lightweight. And we made the roofing tile heat-resistant by adding liquid foam to it. Materials used in the manufacturing of roofing tiles are glass fibre, liquid foam, gelcoat, polish, PVA, Harner, and cobalt. We conducted some experiments to test the properties of the roofing tile. Break load tests, water absorption tests, permeability tests, and heat resistance tests are the tests conducted. From the break load test, we observed that fibre roof tiles have more strength when compared to other ordinary roof tiles. 2741.27 N is the strength of the fibre roof tile, and it is enough for an entire roof tile. Water absorption and permeability tests are the next experiments to be conducted. The values obtained from both experiments are zero. That means fibreglass roof tiles are more resistant to water. So the fibre roof tile is a water-resistant roof tile, and moisture does not influence the fibre tile. The heat resistance test is the final test conducted. According to the test, fibre roof tiles have enough heat resistance. In comparison to other types of roof tiles, fibre roof tiles absorb less heat. The presence of liquid foam on it makes the roof tile heat-resistant. As a result of the experiments, we discovered that fibre roof tiles have sufficient strength, light weight, water resistance, and heat resistance.

From our studies, we understood that it is possible to make roofing tiles using fibre and also be able to achieve our objectives, such as low weight, heat resistance, and high strength in our roofing tiles. It also provides advice on what challenges should be anticipated during construction. The challenges are price, durability, serviceability, etc. Remedies for each problem can be obtained by the experimental method. The final product obtained after a lot of procedures should be the best among the roofing tiles. Fibreglass roofing tiles will compete in the market with other ordinary roofing tiles.

References

1. Topacio A, Arkuino RC, Romano KV, Abutin JC (2018) Development of hydrophobic composite roof tiles utilizing recycled plastic materials. *Mater Eng Dev*
2. Aravind S, Vinyas GP (2020) An experimental study on cement and fiber based roofing tile as an alternative to Mangaluru tile. *Int Res J Eng Technol* 7
3. Atoyebi OD, Orogbade BO, Olayanju TMA, Okunola AA, Oyetayo AJ (2020) Effect of coir fiber and clayey soil on the strength of unglazed roofing tiles. *Earth Environ Sci* 445
4. Saravanan J, ImthiyasAhame S, Muniyasamy X, Muthu Ganesh P, Sait RIA (2017) Low-cost roofing tiles using agricultural waste. *SSRG Int J Civ Eng* 4
5. Darsana P, Abraham R, Joseph A, Jasheela A, Binuraj PR, Sarma J (2015) Development of coir-fiber cement composite roofing tiles. *Proc Technol* 24
6. Michels C, Güths S, Marinoski DL, Lamberts R (2020) Thermal performance and thermal resistance of fiber cement roof tiles: experimental study. *Energy Build* 231

Studies on Seismic Performance of RC Framed Buildings Using Pseudo-optimization Method



G. Priyusha , C. Shreyasvi , and K. Venkataramana 

Abstract Most of the RC framed buildings which are designed for seismic prone regions have to follow the ductile detailing procedure outlined in earthquake resistant design code IS 13920(2016) while the infill wall in the RC frames must follow the procedure outlined in IS 1893 (Part 1): 2016. Earthquake resistant design aims to completely utilize the ductile behaviour of the members and its constituent materials. Nonlinear analysis is frequently used to explore the ductile behaviour of the structure which is visible only beyond the yield limit/the linear range of the material behaviour. However, nonlinear dynamic analysis can be time consuming and resource intensive. Therefore, the goal of the present study is to utilise the material strength to full potential while keeping the analysis simple and robust. Hence, a pseudo optimization technique was adopted to improve the existing analysis and seismic design methods. The adopted method employs linear models of a structure whose seismic design has been enhanced and optimised based on modal energy. The pseudo-optimized design is a three-step process. The first step is to perform Pushover analysis to evaluate the seismic capacity of the existing building. In the next step, the variation of storey stiffness, storey strength and modal energy shall be examined along the height of the building considering the in-plane stiffness and strength of unreinforced masonry (URM) infill walls. As a last step, based on the modal energies observed in various structural members, the design is optimised. This method is practitioner friendly and has potential for industry level applications.

Keywords Pseudo-optimization method · Pushover analysis · Equivalent diagonal strut · RC frame building · Modal energy

G. Priyusha (✉)

National Institute of Technology Karnataka, Surathkal, Karnataka 575025, India
e-mail: priyushag.203st006@nitk.edu.in

C. Shreyasvi · K. Venkataramana
Global Earthquake Model, Pavia, Italy

1 Introduction

Buildings with reinforced concrete frames (RCFs) are widely used all over the world because they are an economical construction technology with the use of easily accessible materials. RCF has previously shown itself to be a reliable seismic performer. In order to analyse a RCF, majority of structural designers today use finite element based software. This involves employing elastic models and analysing them for lateral force in addition to the existing vertical loads. Due to competitive pricing and other financial aspects involved in execution of a seismic design, engineers tend to keep the design of RC structures as close to the minimum code requirements as is practical. This study outlines a design method that practitioners can use to enhance their designs of bare and infilled RCF, with these benefits: (a) The data is used from the elastic models that are typically created in design practises and, therefore, requires no additional time in building modelling; (b) When compared to a traditional design, the building's construction costs are just slightly more and (c) The suggested design procedure needs little extra effort. Without substantially altering the way design offices now operate, the suggested design technique attempts to encourage safer structures.

1.1 Literature Review

Researchers have suggested a number of design techniques to create cost-effective seismic designs that meet or exceed code minimum performance due to the emergence of RCF. The efforts on the optimal configuration under various constraints are shown in [1–3]. These approaches were put out by many scholars, considerably streamlining the analysis [4–6]. Another popular approach is performance-based design (PBD) [7], which is based on FEMA P-58. The main goal of this study is to apply the pseudo-optimization technique [8] to an infilled RC frame design for residential applications using linear elastic models. The lateral stiffness and strength of the frame element are increased by the presence of infills [9, 10]. For bare RC frame and infilled RC frame buildings, a 3D model has been generated using structural analysis software, and analysis has been done in accordance with Indian norms.

2 Methodology

Proposed Design Method

This method imposes two restrictions on the system. In the first place, the method must use a linear elastic model, as is customary for the design process, to avoid increasing the amount of modelling effort that is required. Second, the design method must be easy to implement with the help of the software tools that are readily

available in design offices (such as software for structural design and analysis and spreadsheets).

After the conventional process of designing a building, you will need to complete the following three steps to follow the proposed method:

Step 1. In each independent (lateral) direction, apply seismic load patterns proportional to the prevailing mode of vibration to the building's linear elastic model. The modal energy is evaluated directly from the existing design software ETABS or SAP2000.

Step 2. Based on the visual examination of higher normalized modal energy (NME) values, dimensions of structural elements have been modified.

- a. For Columns, the area of cross-sections shall be increased for the top 25% of the NMEs list. Similarly, the bottom 25% of NMEs shall be reduced in cross-sections.
- b. For Beams, increase the depth of the section with higher NME values and it is performed floor-wise for ease of construction.
- c. As per practice in the Indian region, the higher dimensions are chosen as per the standard available sizes onsite.

Step 3. A similar increase in reinforcement is made based on the model's original RC design's safe evaluation.

3 Modeling and Analysis in ETABS Software

A five-story RC residential structure in seismic zone III is taken into consideration for the current analysis. Below is a picture of the building's plan and elevation (Fig. 1a, b). The soil type is medium stiff, and the plan comprises four orthogonal bays of 3 m each. 3 and 2 kN/m² are the superimposed dead load and live load. It has been designed in accordance with the IS 1893 (Part 1):2016 and IS 13920:2016 standards, respectively.

Four models are considered in this study, the first two models (model 1, 2) are of traditional design and remaining two models (model 3, 4) are of proposed design. To know the effectiveness of proposed design, model 1 (bare frame) and model 2 (infilled frame) are designed by conventional method later proposed methodology is applied on them and the results are obtained in models 3 and 4 respectively.

Model 1: Traditional Design of Bare RC Frame (TD Bare)

Beams are 230 × 300 mm² having a top and bottom reinforcement of 250 mm² at the joints. Columns are of 300 × 300 mm² with uniform reinforcement on all sides ($p_t = 1.0\%$) are assigned to model 1 and 2.

The Normalized Modal Energy of the beam in frame A for storeys 1 and 2 is higher than that of the remaining storeys, as can be seen in Fig. 2a, hence these floors are given the B1 230 × 350 dimension. Storeys 3 and 4 have been allocated for the B2 230 × 300 beams. Due to its lower NME values, the top floor B3 has 230 × 230

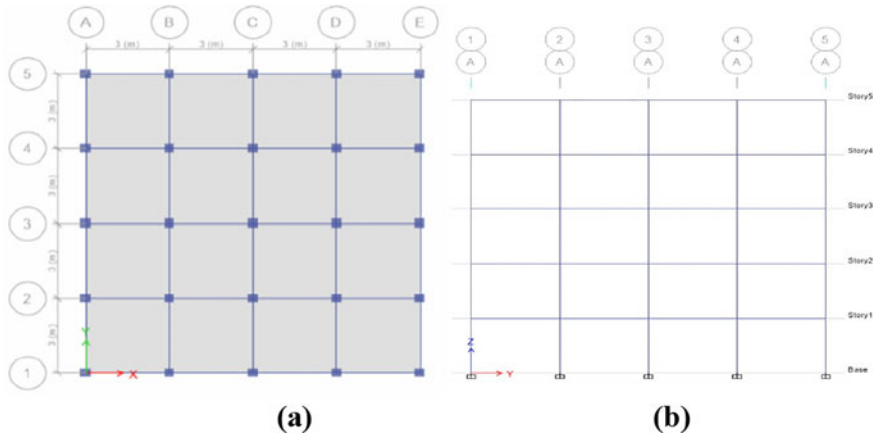


Fig. 1 a Plan and b elevation of proposed building

beams assigned to it. Figure 2b shows that, in the case of columns, higher NME is observed in the ground and first floor and lower NME for the roof level. As a result, the columns on the ground and first floors are given the C1 350 × 350 dimension, and the remaining levels 3, 4, and 5 are given C2 300 × 300 columns. It is noted that the NME of the top storey is lower than intermediate stories and the dimension could be further reduced. Since the IS 13920:2016 [11] code specifies the minimum dimension of the column to be 300 mm we have adopted the same.

As mentioned above the updated dimensions are used in models 3 and 4, refer to Table 1.

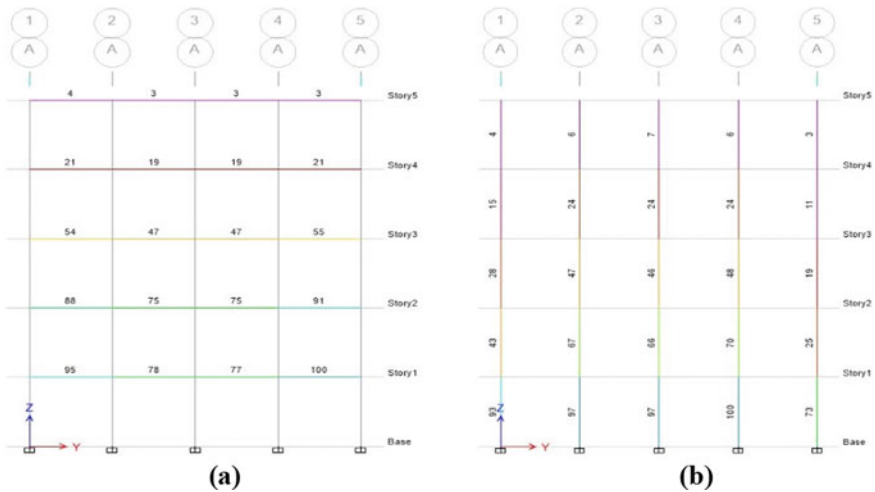


Fig. 2 Normalized modal energies (NME) of a beams b columns

Table 1 Proposed model’s structural details for columns and beams

Column dimension (mm)	Reinforcement (mm ²)	Beam dimension (mm)	Top and bottom reinforcement (mm ²)
C1 350 × 350	1020 ($p_t = 0.83\%$)	B1 230 × 350	300
C2 300 × 300	804 ($p_t = 0.89\%$)	B2 230 × 300	230
		B3 230 × 230	230

Model 2: Traditional Design Infilled RC Frame (TD Infilled)

The uniformly distributed load applied on peripheral beams of the floors and roof is 13.8 and 4.8 kN/m. The NME for the beams and columns is shown in Fig. 3a, b, for bracings it is shown in Fig. 3c.

Properties of Equivalent Diagonal Strut

Compressive strength of brick (f_b) = 10.3 MPa (First class brick as per IS:3495 (Part 1)-1992).

Compressive strength of mortar (f_{mo}) = 7.5 MPa (H2 grade as per IS:1905-1987).

The modulus of elasticity E_m (in MPa) of masonry infill shall be taken as

$$E_m = 550 f_m \tag{1}$$

where f_m is the compressive strength of masonry prism (in MPa) obtained as per IS 1905 or given by the expression:

$$\begin{aligned} f_m &= 0.433 f_b^{0.64} f_{mo}^{0.36} \\ &= 3.98 \text{ MPa} \end{aligned} \tag{2}$$

Substituting the value of Eq. (2) in Eq. (1), we get $E_m = 2188$ MPa.

The width of the diagonal strut of unreinforced masonry (URM) without openings as shown in Fig. 4. shall be taken as:

$$\begin{aligned} w_{ds} &= 0.175 \alpha_h^{-0.4} L_{ds} \\ &= 409.46 \sim 410 \text{ mm} \end{aligned} \tag{3}$$

where,

$$\alpha_h = h \sqrt{\frac{E_m t \sin 2\theta}{4 E_f I_c h}} = 3.4.$$

$L_{ds} = 3818$ mm and $t = 230$ mm.

E_m and E_f are the moduli of elasticity of the materials of the URM infill and RC frame.

I_c is the moment of inertia of the adjoining column, t is the thickness of the infill wall and θ is the angle of the diagonal strut with the horizontal.

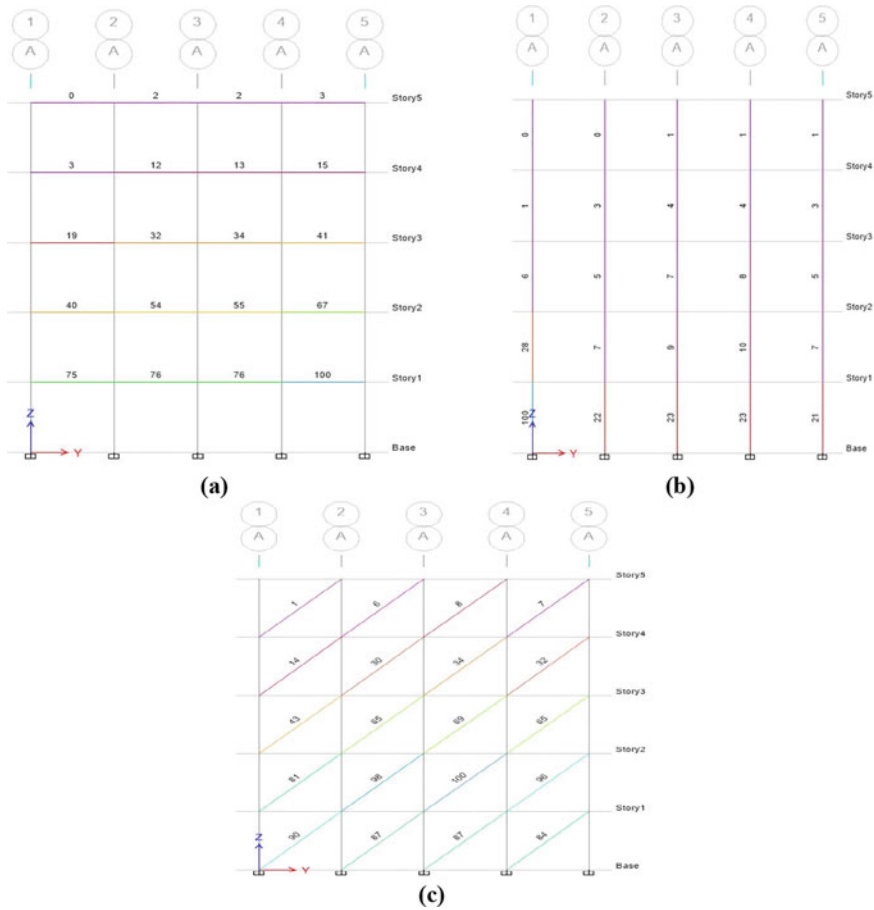


Fig. 3 Normalized modal energies (NME) for infilled RC frame of a beams b columns c bracings/strut

Model 3: Proposed Design Bare RC Frame (PD Bare)

The results from the normalized NME of Fig. 5a, b for the beams and columns of the redesigned building show that the work undertaken by structural members is on average higher compared to model 1 due to the application of the proposed methodology in the Pseudo-optimization case (PSO case).

Model 4: Proposed Building Infilled RC Frame (PB Infilled)

In this model, the infilled walls have been modeled as the diagonal strut element which helps in resisting the lateral load. The proposed methodology is applied for this building and the NME is shown in Fig. 6a, b.

The NME values of the beams and columns for the infilled case have been decreased due to the fact that the lateral load is being shared by the strut elements

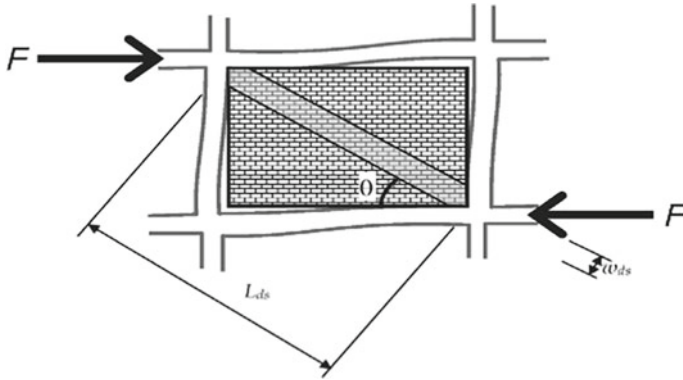


Fig. 4 Equivalent diagonal strut of URM infill wall [12]

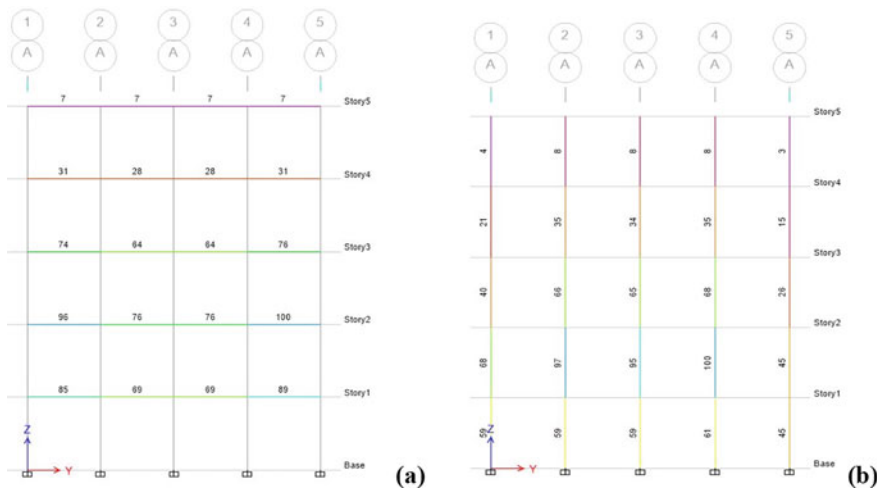


Fig. 5 PSO case NME a beams b columns

as shown in Fig. 6c, hence the work undertaken by structural elements has been reduced. The pattern of the optimization remains the same as it is been followed in model 3.

4 Results and Discussions

The results obtained by the seismic responses are plotted below for the various models considered for the study. The lateral load carrying capacity for model 4 is increased after applying the proposed method as shown in Fig. 7. It can be noted that

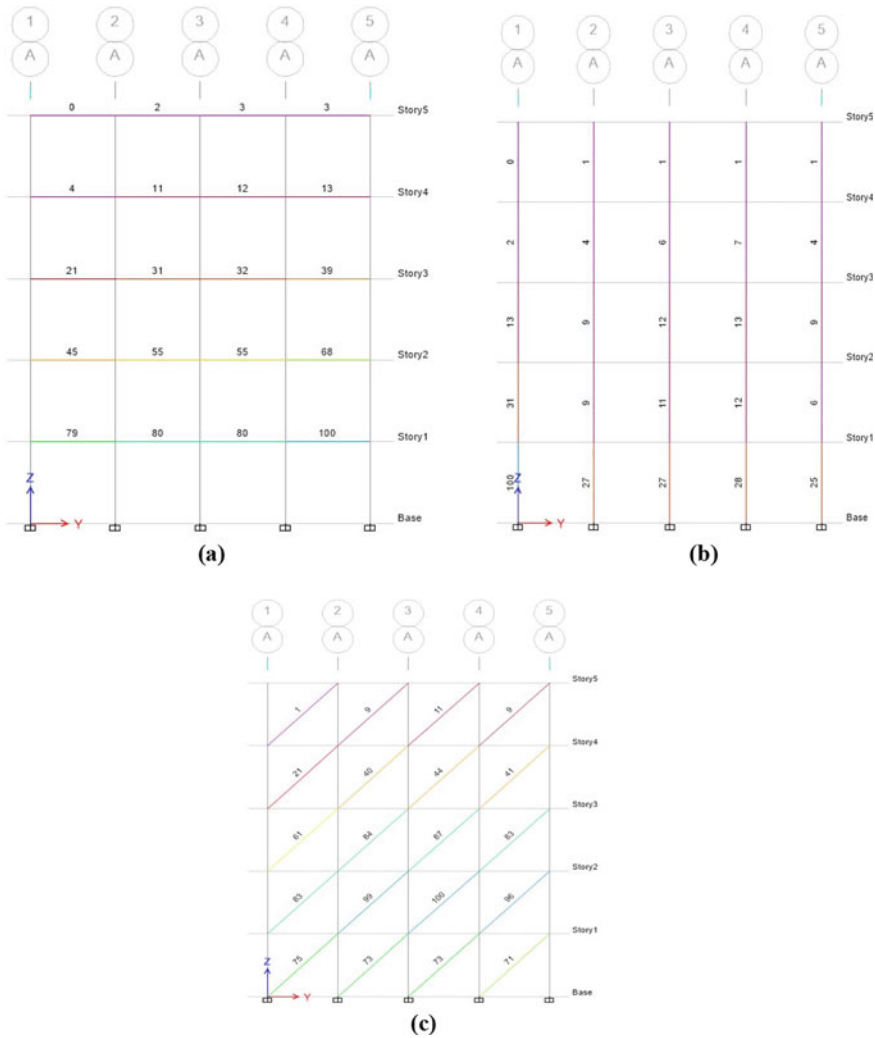


Fig. 6 PSO case NME for a beams b columns c bracings/strut

the load-carrying capacity for the proposed building (M3, M4) has been increased compared to traditional buildings (M1, M2). It can be concluded the proposed method of optimization has shown better load carrying capacity under seismic loads.

The maximum storey displacement for model 4 is less compared to the remaining models and it is shown in Fig. 8. The displacement values for models 1 and 3 for bare frames and models 2 and 4 for infilled frames where the storey displacement has been reduced to some extent after the application of the proposed method which can be regarded as advantageous. Storey displacement is the absolute value of displacement of the storey under the action of lateral load.

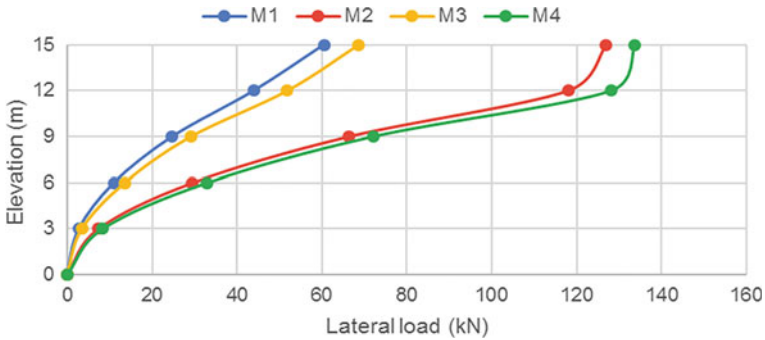


Fig. 7 Lateral load distribution along with storey height

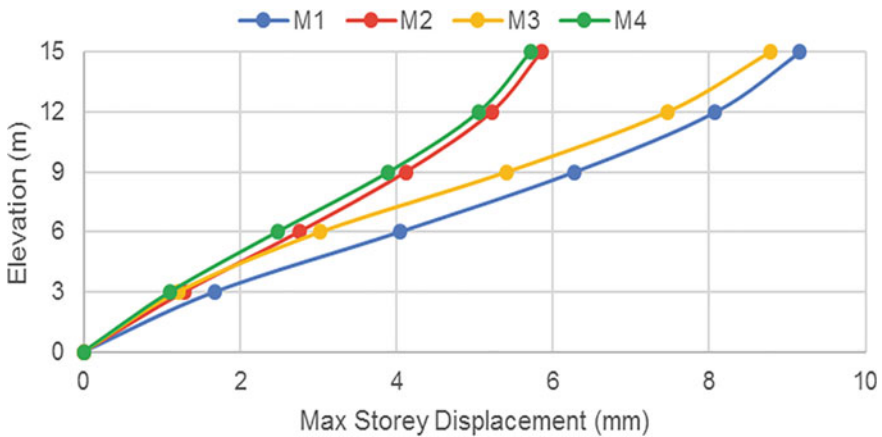


Fig. 8 Maximum storey displacement for various models

The storey drift plotted for various models is shown in Fig. 9, it is observed that after applying the proposed method there is a shift in the drift from storey 2 to storey 3 as seen for model 3 and model 4. As per IS 1893, storey drift in any storey shall not exceed 0.004 times the storey height and the values observed are within the limits specified in the standard.

The storey stiffness is highly affected by the influence of infills (M2 and M4), also it is evident from Fig. 10 that there is a further increase in stiffness values after applying the proposed method (M3 and M4). It can be observed that the lateral stiffness of infilled frame (M2, M4) is approximately increased by three to four times that of bare frame (M1, M3) indicating the role played by masonry infills contributing to the overall stiffness of the building.

Table 2 summarizes the results obtained after the earthquake analysis and pushover analysis.

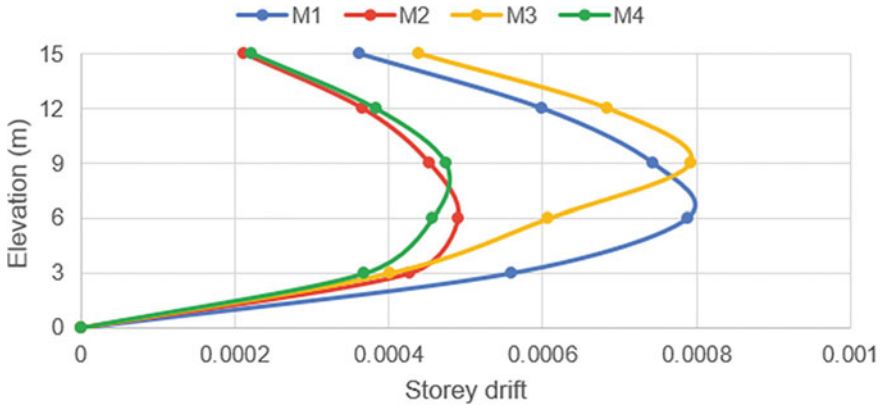


Fig. 9 Maximum storey drift for various models

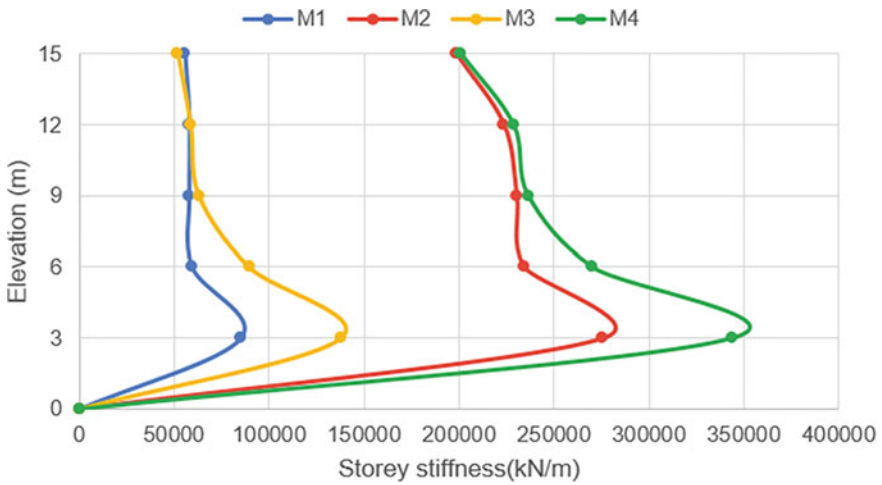


Fig. 10 Storey stiffness for various models

The maximum storey displacement is reduced significantly from model 3 to model 4 due to the additional lateral stiffness of masonry elements. Also, this accounted for the reduction in maximum storey drift by an amount of 40% from model 3 to model 4 after the application of the proposed method. The storey stiffness for infilled RC frame building is higher due to the additional lateral stiffness of the masonry. The overstrength factor and displacement ductility ratio are calculated from the results of the pushover analysis.

Table 2 Dynamic response parameters obtained from the earthquake analysis

Parameters	Model 1 (TD bare)	Model 2 (TD infilled)	Model 3 (PD bare)	Model 4 (PD infilled)
Time period (s)	0.983	0.618	0.894	0.581
Max story displacement (mm)	9.16	5.86	8.78	5.71
Max story drift	0.000788	0.000491	0.000792	0.000474
Story stiffness (kN/m)	85,295	275,680	138,108	343,700
Design base shear (kN)	141.44	348.00	156.66	374.07
Overstrength factor (Ω)	1.18	4.02	1.13	3.20
Displacement ductility ratio (μ)	1.62	4.13	1.29	3.24

Table 3 Concrete volume of structural elements

Model	Column (kN)	Beam (kN)	Total weight (kN)	Volume (m ³)
Model 1 and 2	843.50	931.22	1774.72	70.98
Model 3 and 4	965.33	941.80	1907.14	76.28

Material Quantity

- The increase in the material quantity of M30 grade concrete from model 1 to model 3 is 7.46% as shown in Table 3.
- The approximate increase in steel is 5.75% from model 1 to model 3 (9130–9655 kg).

5 Conclusions

The proposed design procedure aims to provide safer structures with the least amount of interference to the current operations of the design office. A term called overstrength is used to measure the discrepancy between a material, component, or structural system's required and actual strength. The overstrength ratio is, in other words, extra or reserve strength above the design strength. The ratio of peak elastic (yield) displacement to peak inelastic (target) displacement is known as the displacement ductility ratio. It provides a more accurate assessment of the structure's ductile capacity. For the pushover analysis, 4% of the building height, or 600 mm for all models, is used as the monitored displacement.

- The maximum story drift for infilled RC frame building is reduced by 40% compared to the bare RC frame building which is designed by the proposed methodology (models 3 and 4).
- The base shear is increased from 157 to 374 kN indicating the load resisting capacity to be increased from model 3 to model 4.
- The storey stiffness for the bare and infilled frame as per the proposed method are 138,108 and 343,700 kN/m which indicates that the masonry infills played a major role in increasing the lateral stiffness of the building. Hence, the effect of infills has a major impact on increased stiffness.
- The overstrength factors for the bare and infilled RC frames in the proposed designs are 1.13 and 3.20, respectively, highlighting the significance of the suggested method in utilising the building's reserve strength.
- The displacement ductility ratio for the proposed designs for the bare and infilled RC frame are 1.29 and 3.24 respectively. This implies that the ductility of the building is increased upon applying the proposed methodology.
- Brick infill walls present in RC frame buildings reduce the structural drift by 40% but increase the strength and stiffness by 138 and 148% respectively from models 3–4. The time period for the infilled RC frame building is lower than the bare RC frame building.
- The increase in material quantities between the traditional and proposed designs is approximately 7% for M30 grade concrete and 5% for Fe415 grade steel. As the optimization was primarily performed on columns and beams, the aforementioned variations only apply to them.

References

1. Arroyo O, Gutiérrez S (2017) A seismic optimization procedure for reinforced concrete framed buildings based on eigenfrequency optimization. *Eng Optim* 49(7):1166–1182. <https://doi.org/10.1080/0305215X.2016.1241779>
2. Arroyo O, Liel A, Gutiérrez S (2018) A performance-based evaluation of a seismic design method for reinforced concrete frames. *J Earthq Eng* 22(10):1900–1917. <https://doi.org/10.1080/13632469.2017.1309605>
3. Fragiadakis M, Lagaros ND (2011) An overview to structural seismic design optimisation frameworks. *Comput Struct* 89(11–12):1155–1165. <https://doi.org/10.1016/j.compstruc.2010.10.021>
4. Naeim F, Performance based seismic engineering (Chapter 15)
5. Papavasileiou GS, Charmpis DC (2016) Seismic design optimization of multi-storey steel-concrete composite buildings. *Comput Struct* 170:49–61. <https://doi.org/10.1016/j.compstruc.2016.03.010>
6. Zou XK, Chan CM, Li G, Wang Q (2007) Multiobjective optimization for performance-based design of reinforced concrete frames. *J Struct Eng* 133(10):1462–1474. [https://doi.org/10.1061/\(asce\)0733-9445\(2007\)133:10\(1462\)](https://doi.org/10.1061/(asce)0733-9445(2007)133:10(1462))
7. Kappos AJ, Ellul F (2000) Seismic design and performance assessment of masonry infilled R/C frames. In: Proceedings of 12th world conference on earthquake engineering, Auckland, New Zealand, pp 1–8 [Online]. Available: <http://www.iitk.ac.in/nicee/wcee/article/0989.pdf>

8. Arroyo O, Liel A, Gutiérrez S (2021) Practitioner-friendly design method to improve the seismic performance of RC frame buildings. *Earthq Spectra* 37(3):2247–2266
9. Sukrawa M (2015) Earthquake response of RC infilled frame with wall openings in low-rise hotel buildings. *Proc Eng* 125:933–939. <https://doi.org/10.1016/j.proeng.2015.11.118>
10. Priyusha G, Shreyasvi C, Venkataramana K (2022) Seismic performance of infilled RC frames by pseudo-optimization method. In: Marano GC et al (eds) *Lecture notes in civil engineering*, vol 284. Springer, Cham, pp 127–136. https://doi.org/10.1007/978-3-031-12011-4_11
11. IS 13920:2016 (2016) Indian standard ductile design and detailing of reinforced concrete structures subjected to seismic forces-code of practice, first rev. Bureau of Indian Standards, New Delhi, 2016. www.standardsbis.in
12. IS 1893 (Part 1):2016 (2016) Indian standard criteria for earthquake resistant design of structures, part 1 general provisions and buildings, sixth rev. Bureau of Indian Standards, New Delhi. www.standardsbis.in

Assessing the Predictability in Rainfall Time Series—A Case Study in Wisconsin Basin



P. Saravanan and C. Sivapragasam

Abstract Understanding the trend of rainfall series is necessary to manage water resources and to plan future development activities, especially during the construction of large-scale hydraulic structures. In many reported works, trend is estimated using Mann–Kendall test and persistence of the trend in future is estimated using the value of Hurst exponent. But the Hurst exponent only shows the nature of persistence ($H > 0.5$ persistence, $H < 0.5$ anti-persistence and $H = 0.5$ have equal probability), but it doesn't say for sure that the series is predictable even if it is persistent. In this study, a method is proposed to check how predictable a time series is. Annual and seasonal rainfall series for a period of 20 years (2002–2021) for 15 rain gauges located in Wisconsin river basin (Wisconsin State of USA) is used which covers almost 20 counties. It is seen that for annual data, increasing trend is found in all the 15 stations. Further, the Hurst exponent indicates the increasing trend is persistent in future also. In seasonal data, 13 stations have increasing trend with Hurst exponent value more than 0.5 in all the stations. Then, the Hurst exponent values are explored for 14 different sizes of the series starting from 7th year to 20th year for all the stations. Finally, the relation between predictability and oscillation (in term of standard deviation) of the 14 Hurst exponents is demonstrated. Prediction is performed using Artificial Neural Network to see how the oscillation in the 14 different Hurst exponents of series influences the prediction. The prediction performance with annual data of Reedsburg station is not good (NRMSE = 0.30) when compared to Lac Vieux Desert (NRMSE = 0.08) as evident from the standard deviation values. The Standard deviation in the 14 Hurst exponents of Reedsburg and Lac Vieux Desert are 0.22 and 0.08. Later, the same analysis is done on seasonal data which also corroborates that there is a relation between the oscillation of 14 different Hurst exponents and predictability.

P. Saravanan (✉)

Department of Civil Engineering, Vedavyasa Institute of Technology (Formerly Kalasalingam Academy of Research and Education, Srivilliputhur), Malappuram, India
e-mail: coveda@vedavyasa.org

C. Sivapragasam

Department of Civil Engineering, Kalasalingam Academy of Research and Education, Srivilliputhur, India

Keywords Predictability · Artificial neural network · Trend · Hurst exponent · Mann Kendall test · Rainfall prediction

1 Introduction

Construction of hydrological structures like dams, retention basins, levees, urban drainages etc., require information on the expected pattern of future rainfall. Rainfall pattern also influences the flood and drought. Hence, understanding on the future rainfall pattern is inevitable. To find the future rainfall pattern both statistical methods and machine learning based models have been used by researchers. Statistical methods include detection of trend and its persistence using tests like MK test, student t -test, Spearman rank correlation test, of which MK test have been widely used. For example, Sivapragasam et al. [1] calculated trend using MK test in Tamirabaruni river basin of Tamil Nadu in 14 stations with the historical records from the year 1971–2000. Barua et al. [2] found the trend in the rainfall series of past 50 years in Yarra river basin. They reported that trend calculation is more suitable for regional level when compared to global level. The report of Kumar et al. [3] also corroborated the same in 135 years of historical record in Indian stations. Before calculation of trend, the trend change year need to be calculated using CUSUM test to get meaningful result from trend. In MK test, the trend in any series is calculated using past data. But the result of MK test does not give any idea on the persistence of trend in future. The value of Hurst exponent can be used for better clarity about the future persistence. Hurst exponent is a statistical parameter which ranges between 0 and 1. If the Hurst exponent value of a series is near to 1, the trend in the series is persistent in future. When the value is near to 0, the trend in the series is anti-persistent (Anti-persistent denotes that if the calculated trend in the series is increasing, the future trend will be a decreasing trend and vice versa). If it is near to 0.5, the series is completely random [4]. Mukherjee et al. [5] used Hurst exponent to detect the persistence of a time series. Similarly Tatli [6] found the persistence of trend using Hurst exponent in a drought time series. The work of Suman et al. [7] also used Hurst exponent to find persistence in a hydrometeorological series.

Prediction of future rainfall is complex due to its dependence on many meteorological parameters like temperature, humidity, evaporation etc. To reduce the complexity of the prediction and to improve prediction performance, researchers have resorted to many techniques like hybridization [8], pre-processing of input [9], wavelet method [10] etc., in which assessment of predictability of the time series is prominent. Hurst exponent can also be used as a predictability measure in addition to the measure of persistence [6]. Using Hurst exponent, predictability of the series is determined before prediction to accept or reject a series for prediction. Peyghami and Khanduzi [11] calculated Hurst exponent to select time series for prediction. They accepted a series having Hurst exponent value more than 0.96 for prediction. Qian and Rasheed [12] reported the importance of checking predictability before

prediction. A series having Hurst exponent value near to 0 or 1 is predictable, near to 0.5 is non predictable series [13].

From the foregoing discussion, it is found that Hurst exponent is used as indicator for both predictability and persistence, which communicates that all the persistent series are predictable. But report by Sivapragasam et al. [14] is not fully in agreement with this. Hence, this study intended to demonstrate the relationship between the persistence and predictability of time series by predicting a persistent series. Also, it is intended to check how the oscillation in Hurst exponents of various sizes affects the predictability. Since, Artificial Neural Network (ANN) is popular in prediction of rainfall [15, 16] it is adopted for prediction in this study. Rainfall series of 15 stations located in Wisconsin basin has been used.

2 Study Area

The study area is chosen as Wisconsin river basin of USA (see Fig. 1) which is a fairly large basin and for which historical rainfall data are easily available. The length of the river is 700 km and the area of basin is 31,805 km². The average discharge and flood discharge in this basin is 200 cumec and 1000 cumec respectively. The basin is divided into three regions based on the hydrologic properties which are northern highland region, central plain region and western upland region. Soil in the northern highland region is silt and have poor drainage property. This region contains 27 dams. The central plain region is comparably flat and contains sandy soils with good drainage. Urban and agricultural lands are predominated in this region. In the western upland region, the river is very wide and have shallow depth. Consequently, this region has no dams. Lime stone is predominate in this region. The average temperature in this basin is 4–9 °C. The annual average precipitation is 75–85 cm. One can refer Predick and Turner [17] for more details of the basin.

3 Methodology

In this study, MK test is used to find the trend of the rainfall series, CUSUM test is used to find the trend change year, R/S analysis method is used to find the Hurst exponent and ANN is used to predict the rainfall.

3.1 CUSUM Test

Before calculation of trend, the trend jump year need to be calculated. Data from the trend change year only need to be given as input to find trend. The jump year of trend can be identified using Eq. (1). The procedure explained here is based on

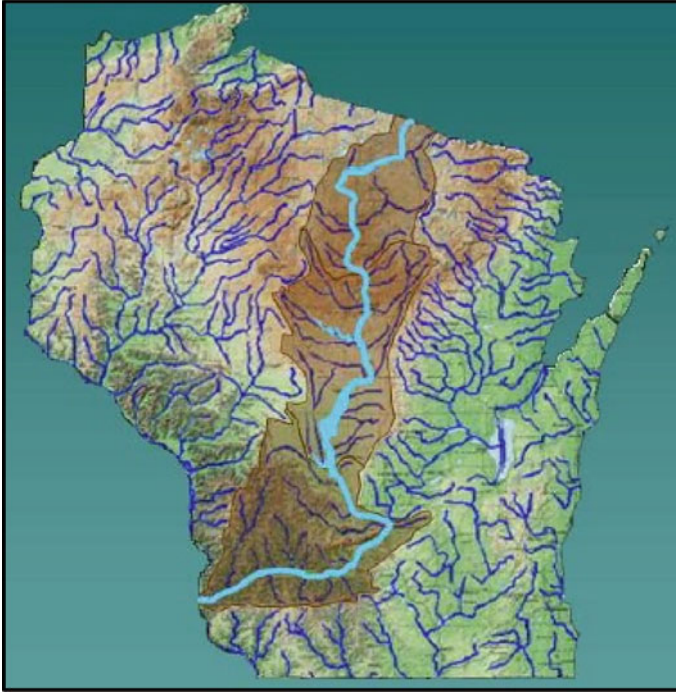


Fig. 1 Wisconsin basin

Chowdhury and Beecham [18].

$$y_i = (x_i + x_{i-1} + x_{i-2} + \dots + x_n) - i \cdot \bar{x} \quad (1)$$

Here, y_i is the CUSUM value at a time step i , x_i, \dots, x_n is the time series, n is the number of points in the sample, \bar{x} is the mean of the time series.

If there is no significant trend change, the plot between of y_i and i oscillates around x -axis. In case the oscillation deviates from its normal pattern, that point of change in pattern is identified as trend change point.

3.2 Mann-Kendal Test

MK test is used to find the trend of any series. Though a series can have outliers, MK test is unaffected. This test is more popular test to identify trend in hydrological series. In MK test two series x_i (ranked from $i = 1, 2, \dots, n - 1$) and x_j (ranked from $j = 2, 3, \dots, n$) is compared. From the comparison sgn value is obtained using Eq. (2),

$$sgn(x_j - x_i) = \{ +1 \text{ if } x_j > x_i, \quad 0 \text{ if } x_j = x_i, \quad -1 \text{ if } x_j < x_i \} \tag{2}$$

By using Eq. (3) Kendall’s statistics S is calculated,

$$S = \sum_{i=1}^{n-1} \sum_{j=i+1}^n sgn(x_j - x_i) \tag{3}$$

Here, n is the number of sample points. If the n is significantly more, the S is normally distributed near to zero mean. Equation (4) given below is used to find the Variance of S .

$$Var(S) = \frac{n(n - 1)(2n + 5) - \sum_{p=1}^g t_p(t_p - 1)(2t_p + 5)}{18} \tag{4}$$

Here, t_p is total number of data in the p th tie group and g is the total number of tied groups. Then the statistics of MK test is calculated using Eq. (5) given below,

$$Z = \begin{cases} \frac{s - 1}{\sqrt{var(s)}} \text{ if } s > 0, & 0 \text{ if } s = 0, & \frac{s + 1}{\sqrt{var(s)}} \text{ if } s < 0 \end{cases} \tag{5}$$

If the obtained Z is positive the trend is considered as increasing. For negative Z , the trend is considered as decreasing.

3.3 R/S Analysis Method

R/S method is widely used to estimate the value of Hurst exponent. The procedure of the method is given below.

- a. The time series has to be organized as different size. The rescaled range of each size need to be calculated as per Eq. (6) given below,

$$\left(\frac{R}{S}\right) = \frac{R_t}{\sigma_t} \text{ for } t = 1, 2, 3, \dots n \tag{6}$$

Here, $\left(\frac{R}{S}\right)$ is the rescaled range, σ_t is the standard deviation for the range

$$R_t = [\max(y_1, y_2, \dots y_t) - \min(y_1, y_2, \dots y_t)] \text{ for } t = 1, 2, \dots n \tag{7}$$

In Eq. (7) R_t is the highest size in each range

$$y_t = \sum_{i=1}^t (x_i - \mu) \text{ for } t = 1, 2, 3 \dots n \tag{8}$$

In Eq. (8), y_t is the modified series altered for deviations from the average, x_t is any value in the particular range, μ is the average of the range.

- b. Then, log of each size and its rescaled range need to be calculated and the log of each size and its rescaled ranges need to be plotted in horizontal and vertical axis respectively. The slope of the plot is the Hurst exponent value.

3.4 Artificial Neural Network

The concept of ANN is emerged from the function of human brain nerve cells. In ANN architecture, set of interconnected neurons are available in three different layers which are input layer, hidden layer and output layer. Each neurons have local memory. Neurons of hidden layer receives information from the neurons of input layer and sends modified information to the neurons of output layer. The information modification is based on the pattern of relation between input and output of the given observed data. Initially in each connection, weight is assigned randomly. At the end of modification process, the architecture gives the output for a given input as per the pattern available in the observed time series data, the weight is adjusted accordingly. Thus, ANN solves problems by automatic learning from the data. They obtain intelligence from the pattern of data given. Back propagation algorithm is the popular and widely used by many researchers [19].

Here, the performance of prediction is measured by Normalized Root Mean Squared Error (NRMSE) which is the ratio between Root Mean Squared Error (RMSE) and the average of the observed values. In the present study the sample size is very less (19 data). Performance of ANN does depend on the sample size besides other important parameters such as the quality and quantity of input information, the training algorithm and the complexity of network architecture. In some unavoidable cases, where there were data limitations, researchers have reported reasonably good performance by ANN. For instance, Aditya Mukerji [20] used ANN for prediction flood employing only 20 data. Sivapragasam et al. [21] predicted the flash flood using ANN by employing only 15 data points. Hence, ANN is applied in this study.

4 Result and Discussion

The analysis done on the Annual data and Seasonal data are discussed separately in this section. The trend and the persistence of trend in annual and seasonal rainfall series of all the stations are calculated initially. A series having persistent trend is also believed to be predictable. In this study, it is demonstrated that all the series having persistent trend are not necessarily predictable. Also, it is found that though a series have persistent trend, it needs a special property to have predictability.

4.1 Annual Data

In this study, to find the trend, MK test is used. But before applying it to any series, the year of change in trend need to be found using CUSUM test. The result of CUSUM test is given in Table 1 as “year of jump”.

The stations Stevens Point, Summit Lake, Merrill, Minocqua, and Stratford have significant change point year on 2013, 2012, 2009, 2012, and 2012 respectively. Other stations also have a mild change point year. Hence, the data before these years are not considered in the calculation of trend in the respective stations. After calculation of change year or jump year, the trend in the series is estimated from the change point year which are given as “Nature of trend” in Table 1. From the table it is found that Viroqua and Summit Lake stations have significant increasing trend. However, the trend in rainfall series of all other stations show a mild increase.

To find the persistence of trend in the series, the value of Hurst exponent is also calculated which is given as “Hurst exponent” in Table 1. From the table, one can observe that the Hurst exponent is more than 0.5 in all the stations. Hence, the available trend in all the series is persistent in future also.

To establish the relationship between persistence and predictability, investigation is extended further. It is suspected that though a series is persistent, the oscillation in Hurst exponent with the increase of size may influence the predictability. Hence,

Table 1 Results of CUSUM test, MK test and Hurst exponent in annual series

Name of the station	Year of jump (CUSUM test)	Z-statistics (MK test)	Nature of trend	Hurst exponent
Stevens Point	2013-Significant	0.313	Increasing-Mild	0.95
Wisconsin Dells	2014-Mild	1.525	Increasing-Mild	0.86
Viroqua	2014-Mild	1.849	Increasing-Significant	0.86
Lone Rock	2014-Mild	1.006	Increasing-Mild	0.72
Reedsburg	2012-Mild	1.525	Increasing-Mild	0.83
Baraboo	2014-Mild	0.811	Increasing-Mild	0.77
Rice Reservoir	2019-Mild	0.811	Increasing-Mild	0.85
Lac Vieux Desert	2015-Mild	0.876	Increasing-Mild	0.88
Boscobel Airport	2006-Mild	1.006	Increasing-Mild	0.89
Summit Lake	2012-Significant	0.894	Increasing-Significant	0.97
La Farge	2014-Mild	1.265	Increasing-Mild	0.84
Merrill	2009-Significant	0.915	Increasing-Mild	0.95
Hancock	2014-Mild	1.525	Increasing-Mild	0.83
Minocqua	2012-Significant	0	Increasing-Mild	0.99
Stratford	2012-Significant	0.537	Increasing-Mild	0.98

Hurst exponent for various sizes of data from 7 to 20 is calculated (see Table 2). In addition, to find the oscillation of Hurst exponent, standard deviation of Hurst exponents of various sizes (σ_h) is also calculated (shown in last column of Table 2). For analysis, a sample of two stations are selected such that while Hurst exponent for full size do not differ much, the standard deviation does differ. With same level persistence one station should represent lower oscillation and the other should represent higher oscillation. The stations Reedsburg and Lac Vieux Desert satisfied this selection criteria which is given as bold in Table 2. Hence analysis is done with these stations. One lead prediction is done in both the station. The annual rainfall of the years 2016, 2017, 2018, 2019 and 2020 is predicted using the annual rainfall of the past (2002–2015) by employing ANN. For both the predictions Logistic activation function and 4neurons in the hidden layer are found as optimal architecture with 36%, 36% and 28% of data in training, test and validation sets respectively. The comparison of actual and predicted data of Reedsburg and Lac Vieux Desert are given in Fig. 2a, b. As expected, the rainfall of Lac Vieux Desert station seems to have been better predicted when compared to that of Reedsburg station. Prediction in Reedsburg station is failed with NRMSE of 0.30 and the prediction of on Lac Vieux Desert seems good with NRMSE of 0.08.

The reason for the failure of prediction in Reedsburg station may be the oscillation ($\sigma_h = 0.22$) in Hurst exponents with the addition of every next year data. It is understood that if the Hurst exponent is changing every year the self-similar fractal character is weak, consequently the predictability of the series is also expected to be weak. Since the oscillation in the Hurst exponents are less ($\sigma_h = 0.05$) in Lac Vieux Desert series, it is predictable. To corroborate the understanding the same analysis has been done in seasonal data also.

4.2 Seasonal Data

In seasonal data also, the change point year of trend, trend and the persistence of trend is estimated by CUSUM test, MK test and Hurst exponent respectively. The results are given in Table 3. Except Boscobel Airport and Minocqua, all other stations show increasing trend in MK test. In all the stations the Hurst exponent is more than 0.5. This indicates the available increasing or decreasing trend in the stations is persistent in future also. However, in the Viroqua station the persistence is weak with the Hurst exponent value of 0.59. To corroborate the conclusions of previous section, the Hurst exponents of different sizes (see Table 4) and the standard deviation (σ_h) of the same (see last column of Table 4) are calculated for each station. From Table 4, two sample stations are selected based on the same selection criteria adopted in annual data. In this case, Baraboo and Lac Vieux Desert stations satisfied the selection criteria appropriately where Hurst exponent value of 0.73 and 0.74 and the standard deviation are 0.14 and 0.08 respectively, the same is given as bold in Table 4. One lead prediction is done with the seasonal data of Baraboo and Lac Vieux Desert stations using ANN. For the prediction of both stations, Logistic activation function,

Table 2 Hurst exponent values for different time series length for the annual data

Name of the station	Number of Years considered from the year 2002																				σ_h
	7	8	9	10	11	12	13	14	15	16	17	18	19	20							
Stevens Point	0.78	0.78	0.97	0.86	0.75	0.55	0.81	0.91	0.93	0.93	0.95	1	0.97	0.95	0.12						
Wisconsin Dells	0.63	0.81	0.8	0.68	0.82	0.57	0.68	0.61	0.62	0.76	0.82	0.87	0.88	0.86	0.11						
Viroqua	1	0.95	0.91	0.78	0.92	0.69	0.84	0.75	0.7	0.83	0.84	0.86	0.88	0.86	0.09						
Lone Rock	0.85	0.84	0.72	0.51	0.56	0.38	0.5	0.5	0.53	0.68	0.7	0.7	0.72	0.72	0.14						
Reedsburg	0.84	0.96	0.54	0.36	0.68	0.45	0.35	0.34	0.44	0.69	0.81	0.83	0.83	0.83	0.22						
Baraboo	0.5	0.77	0.66	0.56	0.76	0.59	0.79	0.74	0.6	0.75	0.75	0.75	0.78	0.77	0.10						
Rice Reservoir	0.53	0.8	0.88	0.51	0.58	0.47	0.71	0.67	0.75	0.91	0.89	0.94	0.92	0.85	0.17						
Lac Vieux Desert	1	1	1	0.85	0.97	0.87	1	0.95	0.98	1	0.99	1	1	0.88	0.05						
Boscobel/Airport	1	1	1	0.94	1	0.78	0.94	0.91	0.7	0.81	0.82	0.82	0.87	0.89	0.10						
Summit Lake	1	1	1	0.62	0.65	0.49	0.75	0.83	0.88	0.97	0.99	1	1	0.97	0.17						
La Farge	0.91	0.85	0.83	0.69	0.85	0.62	0.78	0.74	0.56	0.74	0.76	0.82	0.85	0.84	0.10						
Merrill	0.69	0.78	1	0.93	0.92	0.84	1	1	1	0.99	0.96	0.97	0.97	0.95	0.09						
Hancock	0.78	0.78	0.84	0.47	0.59	0.46	0.58	0.52	0.56	0.79	0.85	0.91	0.89	0.83	0.16						
Minocqua	1	1	1	0.8	0.88	0.77	0.94	1	1	1	1	1	1	0.99	0.08						
Stratford	0.77	0.85	1	0.93	0.79	0.75	0.92	0.93	0.98	0.98	0.98	1	0.99	0.98	0.09						

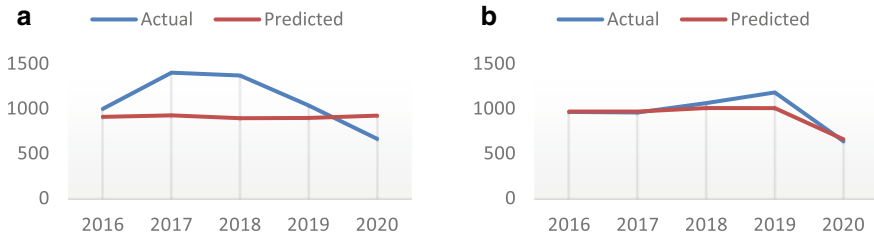


Fig. 2 **a** Comparison of actual and predicted annual rainfall in Reedsburg station. **b** Comparison of actual and predicted annual rainfall in Lac Vieux Desert station

3 hidden layer neurons are optimal with 36%, 36% and 28% of data in training, test and validation sets respectively.

The comparison of actual and predicted rainfall series is given in Fig. 3a, b for the Baraboo and Lac Vieux Desert stations respectively. The NRMSE of Baraboo and Lac Vieux Desert stations are 0.24 and 0.07. As expected, the series which has less standard deviation in Hurst exponents (σ_h) have more predictability than the series which has more standard deviation in Hurst exponents. This corroborate that all the series having persistence are not necessarily predictable. For a series to be

Table 3 Results of CUSUM test, MK test and Hurst exponent in seasonal series

Name of the station	Year of Jump (CUSUM test)	Z-statistics (MK test)	Nature of trend	Hurst exponent
Stevens Point	2013-Significant	0.73	Increasing-Significant	0.85
Wisconsin Dells	2015-Mild	1.136	Increasing-Mild	0.65
Viroqua	2015-Mild	1.2	Increasing-Mild	0.59
Lone Rock	2015-Mild	0.422	Increasing-Mild	0.63
Reedsburg	2015-Mild	0.422	Increasing-Mild	0.72
Baraboo	2015-Mild	0.522	Increasing-Mild	0.73
Rice Reservoir	2015-Mild	1.849	Increasing-Significant	0.8
Lac Vieux Desert	2015-Mild	0.552	Increasing-Mild	0.74
Boscobel Airport	2019-Mild	- 0.292	Decreasing-Mild	0.67
Summit Lake	2011-Significant	1.557	Increasing-Significant	0.95
La Farge	2015-Mild	0.941	Increasing-Mild	0.66
Merrill	2009-Mild	1.72	Increasing-Significant	0.88
Hancock	2015-Mild	1.136	Increasing-Mild	0.81
Minocqua	2012-Significant	- 0.179	Decreasing-Mild	0.97
Stratford	2015-Significant	1.202	Increasing-Significant	0.9

Table 4 Hurst exponent values for different time series length for seasonal data

Name of the station	Number of Years considered from the year 2002														σ_h
	7	8	9	10	11	12	13	14	15	16	17	18	19	20	
Stevens Point	0.94	0.87	0.94	0.81	0.61	0.42	0.61	0.74	0.73	0.83	0.84	0.85	0.85	0.85	0.14
Wisconsin Dells	0.56	0.81	0.55	0.6	0.82	0.65	0.76	0.75	0.64	0.74	0.7	0.65	0.67	0.65	0.08
Viroqua	0.64	0.8	0.77	0.63	0.79	0.57	0.71	0.71	0.62	0.72	0.65	0.62	0.67	0.59	0.07
Lone Rock	0.74	0.84	0.79	0.52	0.52	0.45	0.52	0.47	0.47	0.64	0.68	0.68	0.71	0.63	0.13
Reedsburg	0.62	0.81	0.72	0.44	0.71	0.62	0.69	0.72	0.67	0.78	0.8	0.79	0.78	0.72	0.10
Baraboo	0.41	0.79	0.46	0.49	0.78	0.65	0.77	0.78	0.72	0.78	0.8	0.75	0.77	0.73	0.14
Rice Reservoir	0.58	0.74	0.69	0.51	0.7	0.57	0.7	0.69	0.77	0.87	0.81	0.82	0.81	0.8	0.11
Lac Vieux Desert	0.83	1	1	0.8	0.9	0.75	0.82	0.81	0.83	0.89	0.88	0.85	0.79	0.74	0.08
Boscobel Airport	0.68	0.74	0.81	0.7	0.84	0.59	0.74	0.73	0.57	0.7	0.67	0.66	0.7	0.67	0.07
Summit Lake	1	1	1	0.61	0.58	0.64	0.8	0.86	0.92	0.99	0.99	0.99	0.99	0.95	0.16
La Farge	0.63	0.69	0.62	0.5	0.68	0.49	0.68	0.68	0.58	0.68	0.7	0.69	0.7	0.66	0.07
Merrill	0.47	0.73	0.92	0.89	0.92	0.85	1	1	1	0.96	0.92	0.93	0.89	0.88	0.14
Hancock	0.76	0.75	0.91	0.39	0.45	0.33	0.54	0.5	0.49	0.7	0.78	0.81	0.81	0.81	0.19
Minocqua	0.86	0.95	0.88	0.79	0.92	0.86	1	1	1	1	1	0.99	0.99	0.97	0.07
Stratford	0.69	0.84	1	0.9	0.82	0.68	0.87	0.88	0.89	0.92	0.93	0.95	0.93	0.9	0.09

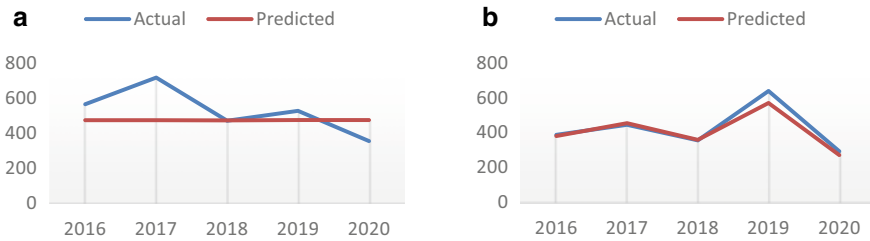


Fig. 3 **a** Comparison of actual and predicted seasonal rainfall in Baraboo station. **b** Comparison of actual and predicted seasonal rainfall in Lac Vieux Desert station

predictable, the Hurst exponents of the different sizes of the series need to have less oscillation or standard deviation.

5 Conclusion

1. Due to climate change, the trend in rainfall series is increasing in all the 15 stations in the annual series and 13 stations in the seasonal series.
2. Since the Hurst exponents in all the annual and seasonal series are more than 0.5, the trend is persistent in future also.
3. All the persistent series are not necessarily predictable.
4. If there is no oscillation of Hurst exponent in every year with the addition of latest data, then there is more chance for the series to be predictable.

References

1. Sivapragasam C, Balamurli S, Deepak M, Prakhar A, Muttill N (2013) Trends in rainfall patterns over the Tamarabarani basin in Tamil Nadu, India. In: Proceedings—20th international congress on modelling and simulation, MODSIM 2013. MODSIM, Australia, pp 2583–2589
2. Barua S, Muttill N, Ng AWM, Perera BJC (2013) Rainfall trend and its implications for water resource management within the Yarra River catchment, Australia. *Hydrol Proces* 27(12):1727–1738
3. Kumar V, Jain SK, Singh Y (2010) Analysis of long-term rainfall trends in India. *Hydrol Sci J* 55(4):484–496
4. Saravanan P, Sivapragasam C, Balamurali S, Priya MM (2016) Analysis of variations of trend in precipitation in Vellar river basin, Tamil Nadu, India. In: Proceedings of ICDMSDR. NIT Trichy, India, 22–24 Feb 2016, p 38
5. Mukherjee S, Sadhukhan B, Das AK, Chaudhuri A (2023) Hurst exponent estimation using neural network. *Int J Comput Sci Eng* 26(2):157–170
6. Tatli H (2015) Detecting persistence of meteorological drought via the Hurst exponent. *Meteorol Appl* 22(4):763–769

7. Suman A, Sindhu AD, Nayak AK, Namboothiri AS, Biswal B (2023) Unveiling the climatic origin of streamflow persistence through multifractal analysis of hydro-meteorological datasets of India. *Hydrol Sci J* 68(2):290–306
8. Nourani V, Komasi M, Alami MT (2012) Hybrid wavelet-genetic programming approach to optimize ANN modeling of rainfall-runoff process. *J Hydrol Eng* 17(6):724–741
9. Wu CL, Chau KW, Fan C (2010) Prediction of rainfall time series using modular artificial neural networks coupled with data-preprocessing techniques. *J Hydrol* 389(1–2):146–167
10. Goyal MK (2014) Monthly rainfall prediction using wavelet regression and neural network: an analysis of 1901–2002 data, Assam, India. *Theoret Appl Climatol* 118(1–2):25–34
11. Peyghami MR, Khanduzi R (2012) Predictability and forecasting automotive price based on a hybrid train algorithm of MLP neural network. *Neural Comput Appl* 21(1):125–132
12. Qian B, Rasheed K (2004) Hurst exponent and financial market predictability. In: *Proceedings of the second IASTED international conference on financial engineering and applications*. International Association of Science and Technology for Development, Cambridge, USA, pp 203–209
13. Rangarajan G, Sant DA (1997) Climate predictability index and its applications Govindan. *Geophys Res Lett* 24(10):1239–1242
14. Chandrasekaran S, Poomalai S, Saminathan B, Suthanthiravel S, Sundaram K, Abdul Hakkim FF (2019) An investigation on the relationship between the Hurst exponent and the predictability of a rainfall time series. *Meteorol Appl* 26(3):511–519
15. Hudnurkar S, Neela R (2023) On the performance analysis of rainfall prediction using mutual information with artificial neural network. *Int J Electr Comput Eng* 13(2):2101–2113
16. Tran Anh D, Duc Dang T, Van Pham S (2019) Improved rainfall prediction using combined pre-processing methods and feed-forward neural networks. *Multidiscip Sci J* 68(2):65–83
17. Predick KI, Turner MG (2008) Landscape configuration and flood frequency influence invasive shrubs in floodplain forests of the Wisconsin River (USA). *J Ecol* 96(1):91–102
18. Chowdhury RK, Beecham S (2010) Australian rainfall trends and their relation to the southern oscillation index. *Hydrol Process* 24(4):504–514
19. Sivapragasam C, Vanitha S, Muttill N, Suganya K, Suji S, Thamarai Selvi M, Selvi R, Jeya Sudha S (2014) Monthly flow forecast for Mississippi River basin using artificial neural networks. *Neural Comput Appl* 24(7–8):1785–1793
20. Mukerji A, Chatterjee C, Raghuvanshi NS (2009) Flood forecasting using ANN, neuro-fuzzy, and neuro-ga models. *Hydrol Eng* 14(6):647–652
21. Sivapragasam C, Malathy A, Ishwarya D, Saravanan P, Balamurali S (2020) Modelling the elements of flash flood hydrograph using genetic programming. *Indian J Geo Mar Sci* 49(06):1031–1038

Numerical Investigation on the Behaviour of Horizontally Curved Steel Box Girder Under Patch Loading



S. P. Fathima and M. S. Ajith

Abstract To get around topographical barriers, curved girders are frequently employed in bridge construction. Due to high flexural and torsional rigidity, girders with box cross-section are preferred over I-girders in these circumstances. Patch loading is one of the most typical loads a girder is subjected to. The present study carried out a numerical investigation of horizontally curved box girder under patch loading condition using a finite element model developed in ABAQUS CAE®. The existing experimental data in literature were used to validate the models. The study's primary goal is to examine the behaviour of the curved box girder under patch load and to analyse how patch load length affect its ultimate strength. The main parameters considered in this study are curvature angle, aspect ratio and web slenderness ratio.

Keywords Curved box girder · Steel · Patch loading · Numerical · ABAQUS

1 Introduction

Curved bridges are employed to build traffic interchanges or gangways, when site space and locations for piers are limited. Box girders are utilized in these situations due to their high flexural and torsional rigidity. A variety of heavy loads act upon them. In a particular load condition known as patch loading or partially distributed load, plate and box girders are subjected to localised compressive edge stresses. They are partially distributed load over a small length on the top or bottom flange of the girder. These loads are common in deep crane runway bridges, which are acted upon by the wheel loads from the crane. Another condition when a girder is subjected to a

S. P. Fathima · M. S. Ajith (✉)
Department of Civil Engineering, Government College of Engineering Kannur, Kannur 670563,
India
e-mail: ajithms83@gmail.com

S. P. Fathima
e-mail: er.fathimasp@gmail.com

high-intensity patch loading scenario is the incremental launching of bridge girders [1].

Due to the coupled bending and torsion along with the warping effects of non-uniform torsion, distortion, and shear lag, the structural behaviour of curved bridges demonstrates complexity. In a study conducted by Marcello et al. [2], it is observed that curvature causes only slight non-uniform torsion effects and a moderate increase in the magnitude of shear lag stress for longitudinally and transversely distributed loads, but it causes a large increase in axial warping stresses due to distortion. According to their findings, eccentric point loads applied to the internal web of curved girders greatly increase deflections, warping, and tangential stresses.

Yanling et al. [3] present an analytical solution for modelling the coupled bending-torsion behaviour of a curved girder in the elastic stage under arbitrary loads. Shear deformation of steel webs was shown to have a considerable effect on flexural deflection of the curved girder but no effect on torsional angle or normal stress in their investigation. In the study conducted by Nassr et al. [4] it is found that the central angle, aspect ratio, and diaphragm spacing are important parameters that greatly affect the distortional warping normal stress that is brought about in the curved box girders. In the study conducted by Frankl et al. [5] it has been inferred that shear buckling capacity and ultimate shear strength increases as horizontal curvature increase. Also, it has been seen that girder curvature increases web stability for horizontally curved steel plate girder.

The experimental investigation by Zhu et al. [6] found that deflection, transverse, and longitudinal displacements increase with the central angle. Furthermore, it has been observed that for girders with large curvature, the stress is not linearly distributed along the transverse direction due to the influence of the initial curvature and shear lag effect, and that there is a significant difference in normal stress between the inside and outside of the curved girder. As a result, the influence of curvature should be considered when analysing curved girders. Lee et al. [7] conducted a study for identifying optimum diaphragm spacing for horizontally curved box girders in which different loading conditions are considered. And it can be observed from their study that position and type of loading have significant influence on total stress and deflection in curved girders.

Several experimental studies have been conducted on the behaviour of plate girder under patch loading. Studies conducted by Kovacevic et al. [8, 9], Markovic et al. [10] and Ceranic et al. [11] experimentally considered the effect of length of patch load on girders of different web panel aspect ratios. From a detailed literature review it has been seen that study related to curved girder under patch loading is limited. Since loading condition have significant influence in the case of curved girders, it is of important to analyse the behaviour of curved girders under patch loading. Thus, the current study is intended to analyse the behaviour of curved box girders under patch load. Geometric parameters such as curvature angle and aspect ratio are the key parameters considered in the present study.

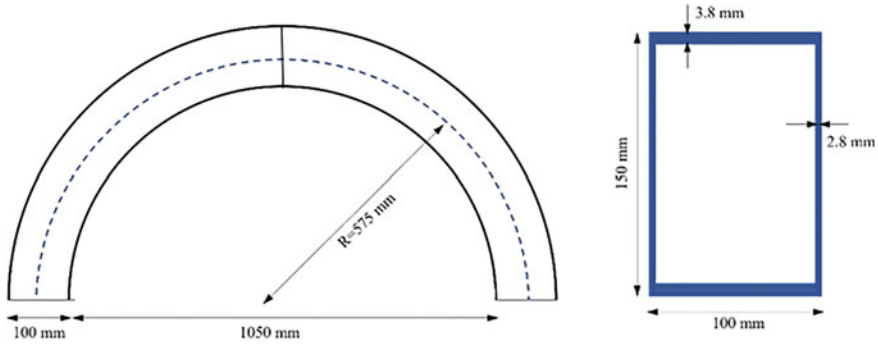


Fig. 1 Geometry and properties of the tested girder [12]

2 Numerical Modelling

Numerical model was developed using commercial finite element analysis software ABAQUS CAE®. The developed numerical model was validated against experimental data given by Hamza et al. [12]. Loading condition is simulated using experimental data from Kovacevic et al. [8].

2.1 Geometric Modelling

In order to simulate the behaviour of horizontally curved steel box girder, a two-span continuous girder having dimension shown in Fig. 1 is used. Both ends of the girder are fixed, and the test was carried under two-point load at midspan [12]. Bilinear material model having yield strength of 320 MPa is used. Figure 2 shows the model developed in ABAQUS.

2.2 Finite Element Modelling

Four noded shell elements with six degrees of freedom at each node (S4R) the elements were used for modelling, it is resilient to shell problems and has excellent adaptability. After a detailed mesh convergence study, the mesh size of 25 mm is fixed for further analysis. Eigen value buckling analysis is carried out and first buckling mode is used as imperfection for nonlinear analysis for which static Riks method is used. Loading is applied by using rigid body tie constraint.

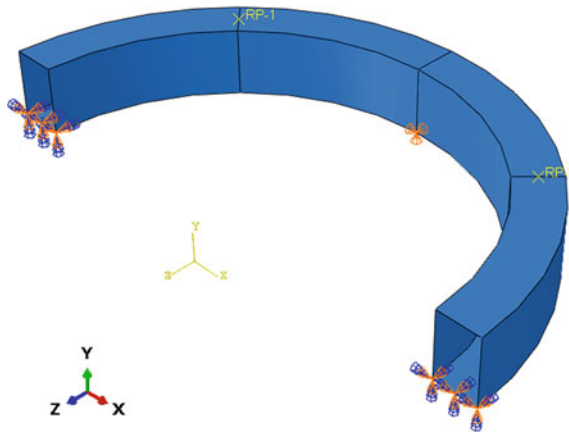


Fig. 2 Model developed in ABAQUS

2.3 Validation

The numerical model developed is validated using test result obtained by Hamza et al. [12]. The finite element method results were compared to the test results using the load–deflection curve and ultimate load. In general, there is good agreement between the finite element analysis results and the experimental data, as illustrated in Fig. 3.

Patch loading condition is effectively simulated using test data from Kovacevic et al. [8]. Both test results and finite element results are in good agreement, which

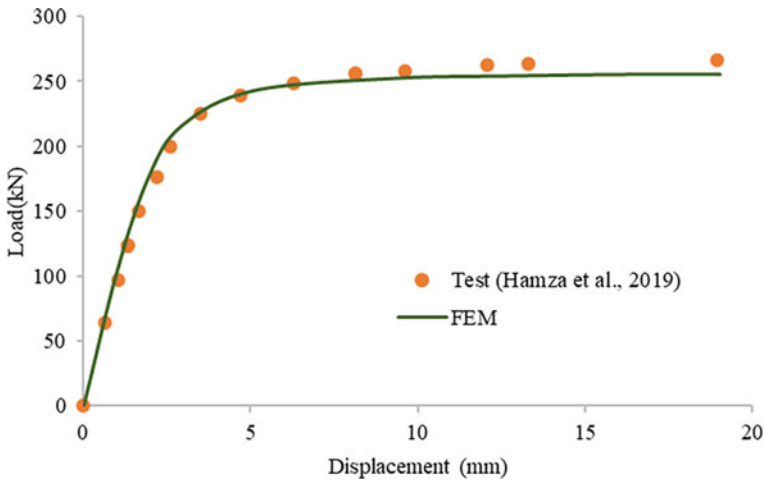


Fig. 3 Load versus displacement curve for curved girder

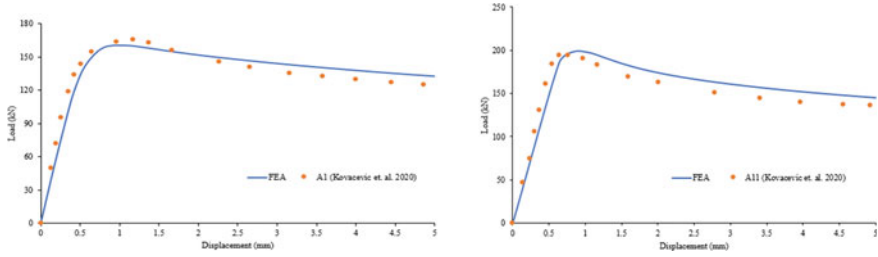


Fig. 4 Load versus displacement curve for girder under patch loading

is given in Fig. 4. Specimen under 50 and 100 mm patch load length is used for validation.

3 Parametric Study

To conduct parametric study, single-cell single-span box girder with both end fixed is developed using validated model. Curvature angle considered in this study is taken as per AASHTO [13] guidelines and the cross-sectional dimensions are fixed as per the guidelines from IRC:24-2010 [14]. Geometry of the girder and notations used for parametric study are shown in Fig. 5.

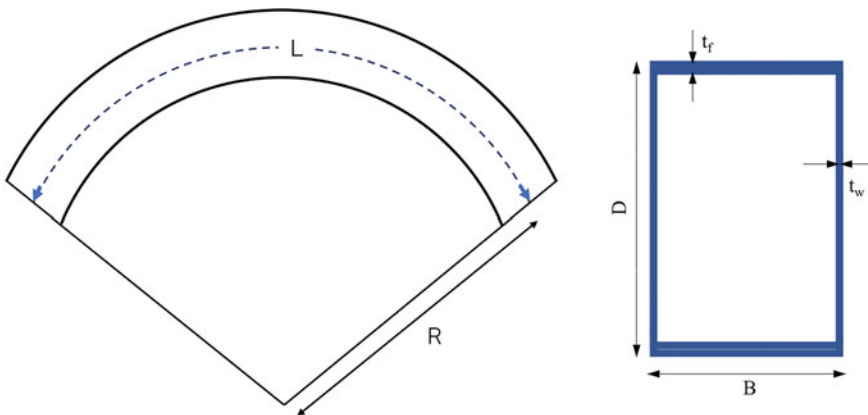


Fig. 5 Geometry and notations for girder used for the study

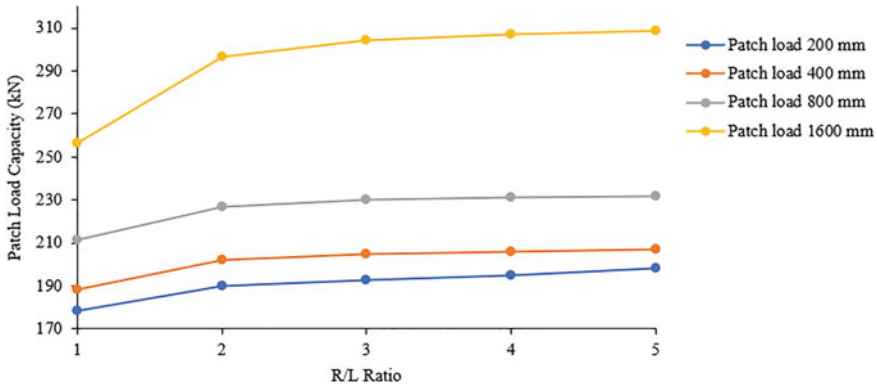


Fig. 6 Variation in patch load carrying capacity with R/L ratio

3.1 Effect of Curvature Angle

To study the effect of curvature angle under patch load of varying length, girders having radius to span ratio (R/L) 1–5 is considered by keeping the span of the girder constant ($L = 4000$ mm). Radius of curvature (R) varied from 4 to 20 m. Models with B/D ratio 1 were considered for this study.

Patch load carrying capacity for different R/L ratio under patch load of length 200, 400, 800, and 1600 mm is shown in Fig. 6. Patch load capacity increases as the angle of curvature decreases. This is due to the increase in torsional moment when the eccentricity from end support increase. It has been observed that patch load carrying capacity increased by 10% as R/L ratio increases from 1 to 5 in the case of patch load of length 200, 400, and 800 while there is an increase in patch load capacity of 20% under 1600 mm patch load. The increase in patch load capacity is marginal for R/L ratio 2–5 but a sharp increase is observed for R/L ratio 1–2. This increase is higher for higher patch load length.

3.2 Effect of Aspect Ratio

In order to analyse the effect of breadth to depth ratio (B/D) under patch load, girders having same cross-sectional area and constant width ($B = 180$ mm) is studied by varying the depth.

Analysis is conducted under patch load of varying length for girder having R/L ratio 1–5. Figure 7 shows the load–deflection curve for B/D ratios ranging from 1 to 5. The variation of patch load capacity for different B/D ratio under patch load length of 200, 400 and 800 mm is shown in Fig. 8.

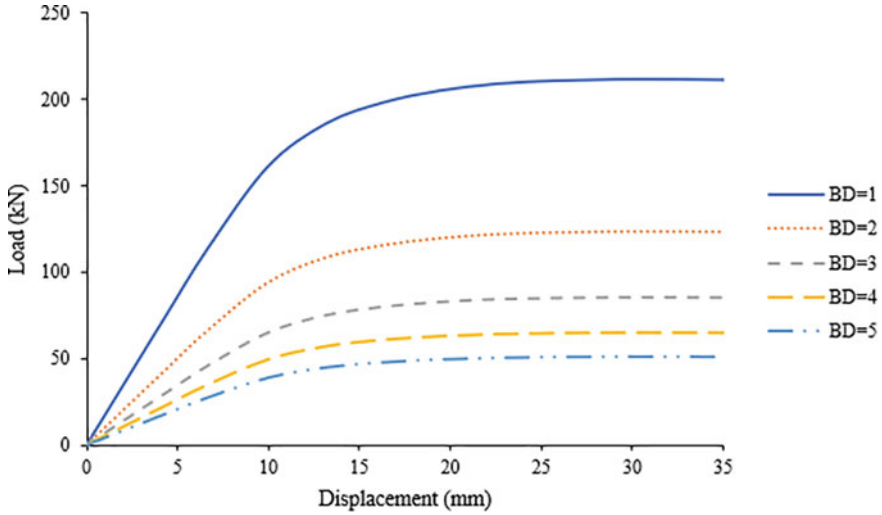


Fig. 7 Load versus displacement curve for different B/D ratio

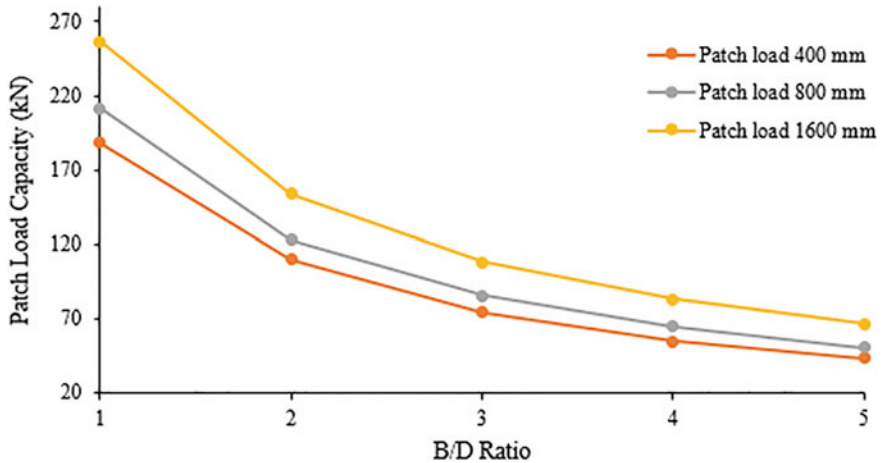


Fig. 8 Variation in load capacity for different patch load

Patch load capacity decreases by 75% when B/D ratio increases from 1 to 5. Similar trend is observed in the case of girder having lesser curvature angle. It is also notable that (Fig. 8) there is a sharp decrease in the load carrying capacity for lesser B/D ratio. As the B/D ratio increases effect of patch load length become insignificant.

3.3 Effect of Web Slenderness Ratio

The web plate thickness was varied to study the effect of web slenderness on patch loading by keeping web depth constant. The thickness was selected so that the web slenderness varied from 10 to 30. Slenderness ratio is the ratio of the web's depth (D) to the web's thickness (t_w), as shown in Fig. 5. Specimens were modelled with varying patch load lengths of 200, 400, 800 and 1600 mm. The load versus displacement curve is shown in Fig. 9. The variation in patch load capacity with different patch load length is shown in Fig. 10. The thickness of the web plate had a significant impact on the patch load capacity of the curved box girder.

As the thickness was increased, corresponding to the slenderness of 30–10, an increase in patch load capacity of around 83% was observed. This remained almost the same for all the patch load lengths considered. Hence it can be concluded that using a stockier web is one of the most effective ways to increase the patch load capacity of the girder.

A sharp decrease in patch load capacity was observed as the thickness of the web plate was reduced, corresponding to the slenderness ratio of 10–30. A similar trend was observed for all patch load lengths. An increase in patch load capacity was seen for higher patch load lengths as the area of the web resisting the load increased.

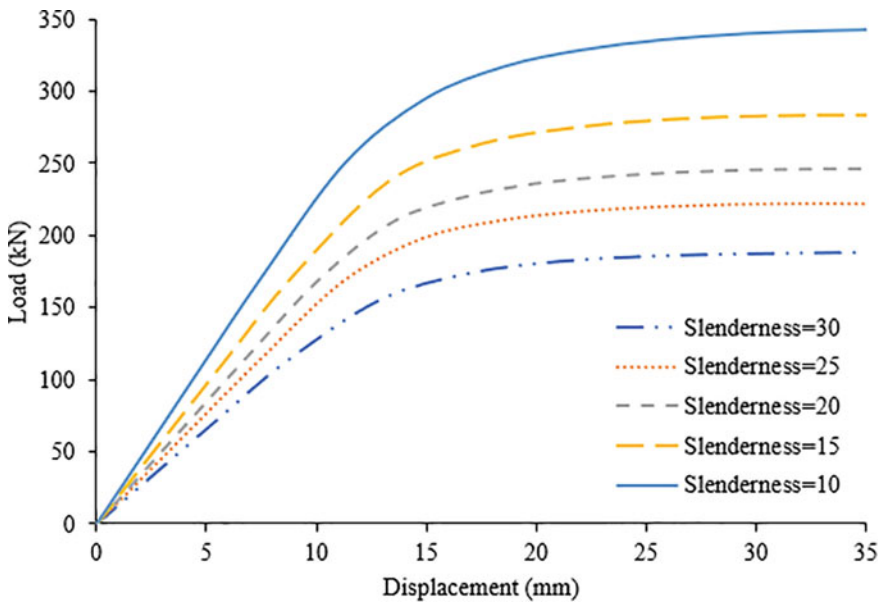


Fig. 9 Load versus displacement curve for varying slenderness ratio

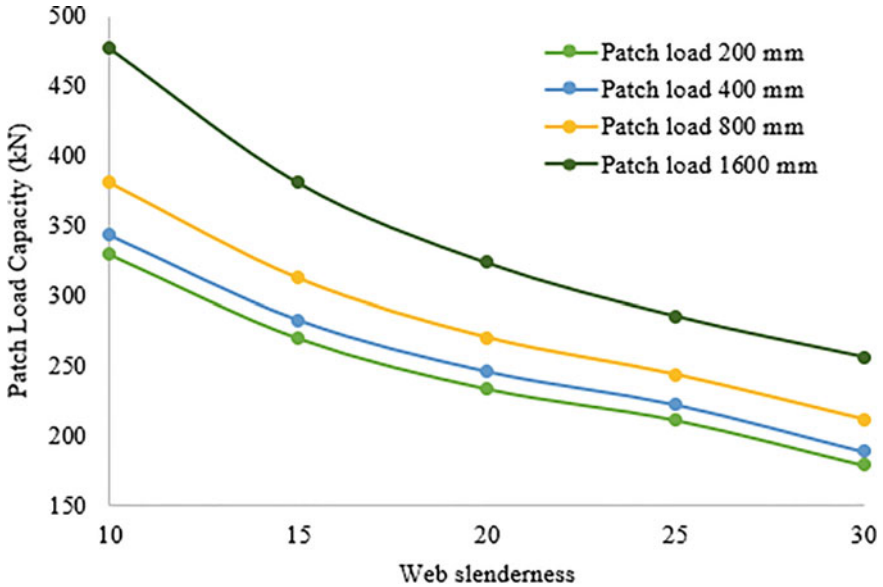


Fig. 10 Variation of patch load capacity with web slenderness

4 Conclusions

Steel girders are subjected to patch load in different situations in bridge construction and runway beams. Geometric parameters such as curvature angle and aspect ratio were investigated. Also, the effect of spacing between patch loads was analysed. The major conclusion from the parametric study conducted is listed below.

- i. The load carrying capacity of the girder decreases as the angle of curvature increases, this is due to increase of torsional moment. As the patch load length increases, load carrying capacity increases with decrease in curvature angle and is more significant for higher patch load length.
- ii. As the radius of curvature increases from 4 to 20 m, the load capacity increased by 10% for patch load length upto while there is an increase in load capacity of 20% for 1600 mm patch load.
- iii. Increase in patch load capacity is marginal for R/L ratio 2–5 but there is a sharp increase in load capacity for R/L ratio 1–2. Thus, curved girder having R/L ratio 1 can be critical in practical scenarios.
- iv. The panel aspect ratio has a significant effect on patch load capacity of the girder. The patch load carrying capacity decreases significantly for higher patch load length as the aspect ratio increases.
- v. Increase in web plate thickness is significant to patch load capacity. Increase in web thickness corresponding to slenderness of 30–10 increases patch load by 83%. This is because buckling of narrow webs is the most common mode of

failure in girders subjected to patch loads. As a result, one of the most effective strategies to improve the load-carrying capacity of girders subjected to patch loading is to use a stockier web.

- vi. The system's capacity can be increased significantly either by increasing the patch load length or by increasing the thickness of web plate.

References

1. Johnson DV (2017) Essentials of bridge engineering. Oxford and IBH Publishing
2. Arici M, Granata MF, Longo G (2022) Analysis of thin-walled curved box girders with torsion, distortion, and shear lag warping effects. *Thin Wall Struct* 175:109244
3. Wang C, Zhang Y, Zhang X, Li Y, Wei X (2022) Coupled bending-torsion behaviour of single-box multi-cell curved box-girders with corrugated-steel-webs. *J Constr Steel Res* 196:107411
4. Nassr AA, Abd-el-Rahim HH, Kaiser F, El-Sokkary AEH (2022) Topology optimization of horizontally curved box girder diaphragms. *Eng Struct* 256:113959
5. Granata MF (2014) Analysis of non-uniform torsion in curved incrementally launched bridges. *Eng Struct* 75:374–387
6. Zhu L, Su RKL, Li MJ (2021) Finite beam element with 26 DOFs for curved composite box girders considering constrained torsion, distortion, shear lag and biaxial slip. *Eng Struct* 232:111797
7. Lee J, Kim S, Kang YJ (2022) Improved design of intermediate diaphragm spacing in horizontally curved steel box bridges. *J Constr Steel Res* 198:107488
8. Kovacevic S, Markovic N (2020) Experimental study on the influence of patch load length on steel plate girders. *Thin Wall Struct* 151:106733
9. Kovacevic S, Markovic N, Sumarac D, Salatic R (2019) Influence of patch load length on plate girders. Part II: numerical research. *J Constr Steel Res* 158:213–229
10. Markovic N, Kovacevic S (2019) Influence of patch load length on plate girders. part I: experimental research. *J Constr Steel Res* 157:207–228
11. Ceranic A, Bendic M, Kovacevic S, Salatic R, Markovic N (2022) Influence of patch load length on strengthening effect in steel plate girders. *J Constr Steel Res* 195:107348
12. Hamza BA, Radhi AR, Al-Madhloom Q (2019) Effect of (B/D) ratio on ultimate load capacity for horizontally curved box steel beam under out of plane concentrated load. *Eng Sci Technol Int J* 22(2):533–537
13. AASHTO (2003) Guide specification for horizontally curved highway bridges. American Association of State Highway and Transportation Officials, Washington, DC
14. IRC 24-2010, Standard specifications and code of practice for road bridges. Indian Road Congress, Bureau of Indian Standards, New Delhi, India

Prediction of Shear Strength of Beam-Column Joint with Glass Fiber Reinforced Polymer Bars Using Response Surface Methodology



Regalla Tejaswi and Greegar George

Abstract The beam-column joints (BCJs) are one of the critical elements in reinforced concrete structures, having a significant impact on the seismic response of structures. Traditionally, the strong column-weak beam concept has been used during design, which assumes the BCJ as a rigid connection. However, this approach can lead to brittle shear failure at the joint under seismic loads, highlighting the importance of accurately estimating the joint shear strength (JSS) of BCJs to ensure structural safety. There has been a growing interest in replacing steel reinforcement with sustainable alternatives such as glass fiber reinforced polymer (GFRP) bars. The advantages of GFRP bars include reduced corrosion, improved service life, and lower maintenance costs. While some studies have evaluated the seismic behaviour of BCJs reinforced with GFRP bars, limited research has been conducted on determining the JSS of GFRP reinforced BCJs. The current design codes for estimating JSS rely solely on empirical formulae that consider the effect of concrete strength. However, this approach neglects the influence of other critical factors such as geometry, yield strength of steel, and longitudinal and transverse reinforcements, which are crucial for accurately predicting JSS. This paper proposes a novel approach for predicting JSS in BCJs reinforced with GFRP bars using the response surface methodology. To achieve this, finite element models of BCJs are developed using ABAQUS software, and their JSS at failure is evaluated. The experimental data from the literature are also incorporated to perform surrogate modelling of GFRP reinforced BCJs. The efficiency of the surrogate model is statistically evaluated using the coefficient of determination. Overall, this study presents more accurate approach for predicting shear strength of GFRP reinforced BCJs by considering all possible influencing parameters. This will help in preventing brittle shear failure and improving the durability of structure.

R. Tejaswi (✉) · G. George
Department of Civil Engineering, National Institute of Technology Tiruchirappalli,
Tiruchirappalli, India
e-mail: tejaregalla456@gmail.com

G. George
e-mail: greegar@nitt.edu

Keywords Response surface methodology · Beam-column joint · Joint shear strength · GFRP bars · Surrogate modelling

1 Introduction

The beam-column joint (BCJ) is a crucial element in ensuring the stability and integrity of structures during earthquakes. Failure of these joints can lead to significant deformations or even the collapse of the entire structure. From the catastrophic failures that occurred during the past earthquakes, it was observed that most of the failures were attributed to the joint failure. This is due to excessive shear demand caused by seismic excitation when the joint is inadequately designed for shear. Designers must calculate the shear strength of BCJs to prevent brittle shear failure at the joint region. The conventional strong column-weak beam design philosophy for seismic-resistant reinforced concrete (RC) structures assumes a rigid connection at the BCJ. However, this approach focuses only on providing adequate anchorage for the longitudinal reinforcement in beams, neglecting the BCJ as the most critical and vulnerable part of the structure. Consequently, even seismically resistant structures may experience shear failures in the BCJ region.

Numerous experimental, empirical, and analytical research have been conducted to understand the behaviour of BCJ. For instance, Ehsani et al. [4] investigated high-strength RC BCJs and found that higher concrete compressive strength leads to increased shear capacity while reducing ductility. Kaku et al. [8] studied the ductile behaviour of exterior BCJs with different axial loads and found that joint shear strength increases with axial loads. Fujii et al. [5] compared the joint behavior of interior and exterior BCJs, and found that exterior joints exhibit lower shear strength than interior BCJs. LaFave et al. [11] conducted tests on three exterior wide BCJs with slabs under quasi-static cyclic loading and found that wide beams provide extra confinement and increased joint shear strength. LaFave et al. [10] investigated the impact of various factors, including concrete compressive strength, joint reinforcing, and axial load on joint shear strength. Additionally, Saravanan et al. [14], Vollum et al. [15], and Bakir et al. [1] developed empirical formulae for shear strength of BCJs based on regression analysis using experimental databases. The design provisions of BCJs in most of the codes and literature consider the compressive strength of concrete and effective joint area for predicting the joint shear strength while neglecting column axial load, confinement, and other relevant parameters. This has been investigated by Kotsovou et al. [9] to incorporate all significant factors and develop an empirical formula using soft computing techniques.

The corrosion of steel bars is a critical factor that can significantly reduce the life expectancy and capacity of structures, especially in harsh environments. Several solutions, such as increasing concrete cover, applying epoxy coating protection to reinforcement, and galvanizing steel, have been proposed to mitigate corrosion. However, none of these solutions have demonstrated long-term effectiveness, highlighting the

need to explore alternatives such as non-corrodible fiber-reinforced polymers (FRPs) as a reinforcement for concrete structures.

Although FRP rebars offer several advantages over conventional steel including high strength-to-weight ratio and fatigue performance, the linear elastic behaviour until failure is a concern, particularly when used as a reinforcement in seismic active zones. However, in framed structures with shear walls in corrosive environments, the shear walls resist seismic loads, and steel reinforcement can be replaced with glass fiber reinforced polymer (GFRP) bars to prevent corrosion. For structures with shear wall in harsh environment, by replacing steel with GFRP, corrosion problem can be prevented, hence there is need to study the seismic behaviour of BCJs with GFRP reinforcement.

Ghomi et al. [6] and Hasaballa et al. [7] conducted research on the feasibility of using GFRP RC frames in seismic regions and studied the parameters affecting the seismic performance of GFRP-RC BCJs, such as joint shear stress, reinforcement anchorage type, concrete strength, and joints configuration. They used shear stress, reinforcement form, and concrete compressive strength as test variables for the seismic performance of T-shaped GFRP-RC concrete BCJs. The results showed that GFRP-RC BCJs do not undergo brittle failure and can withstand high transverse deflection. Mady et al. [12] demonstrated that GFRP-RC BCJs can achieve their design capacity under cyclic loading, with energy dissipation lower than that of RC concrete frames. Safdar et al. [13] tested three GFRP-RC BCJs under reversed cyclic loading to determine the influence of the anchorage type at the end of the longitudinal bars of the beam. Saravanan et al. [14] conducted experimental studies on BCJs with three different types of GFRP bars and determined the joint shear strength of BCJs. They also validated their results using a numerical model developed in ANSYS.

Although the design codes only account for shear strength of BCJ as a function of compressive strength of concrete, it is crucial to develop an empirical formula that considers all relevant parameters influencing joint shear strength. While there exist regression and analytical models for estimating joint shear strength in BCJs reinforced with conventional steel, these models are not applicable to BCJs reinforced with GFRP bars due to the significant differences in material characteristics. Therefore, there is a need to develop an empirical formula that accounts for all important parameters to predict joint shear strength in BCJs with GFRP reinforcement. This study proposes a novel approach to predicting joint shear strength in GFRP-reinforced BCJs using response surface methodology (RSM).

2 Methodology

For predicting the joint shear strength model of BCJs with GFRP bars, an experimental model is selected from the literature and its numerical model is developed in the ABAQUS software. The joint shear strength of this numerical model is determined and validated against with the experimental joint shear strength obtained from the literature. Subsequently, various models of BCJs are analysed in ABAQUS and

respective joint shear strengths are determined. The experimental data from different literature sources are also collected and consolidated with the ABAQUS results. This comprehensive dataset is used to predict joint shear strength using response surface methodology by selecting important parameters that can influence the joint shear strength.

3 Numerical Modelling in ABAQUS

For modelling the BCJ in ABAQUS, the entire concrete is represented as a single unit as shown in Fig. 1 with Kent-Park concrete damage plasticity model used to model the concrete, and GFRP bars modelled as an anisotropic material. A reduced integration eight-noded brick element (C3D8R) with three degrees of freedom at each node is employed to model the concrete. The rebars are modelled as truss element (T3D2) with three degrees of freedom at each node. For perfect bonding between GFRP bars and concrete, embedded interaction is chosen. The multi-point constraint is used for loading surfaces and support conditions.

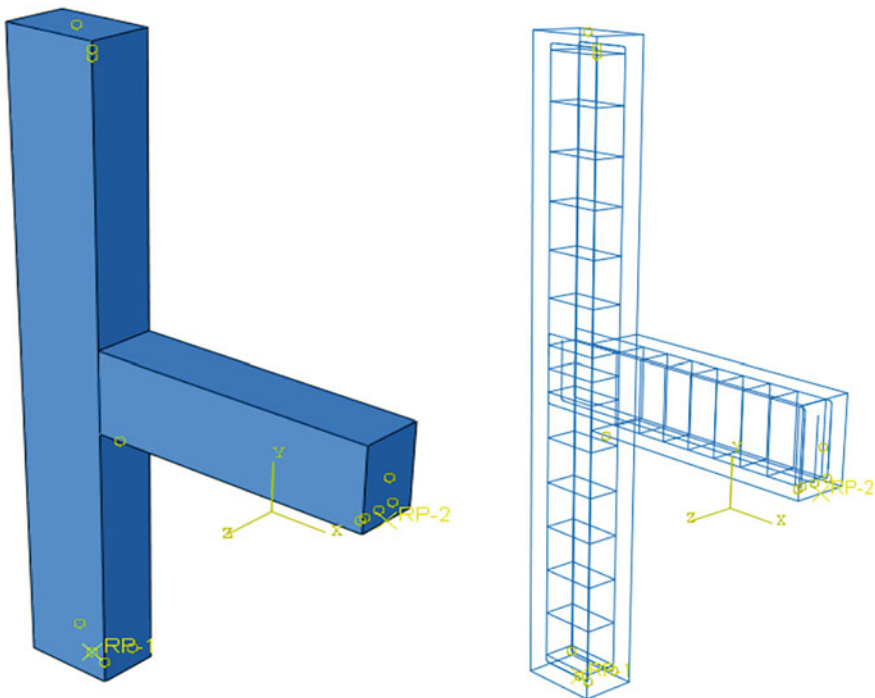


Fig. 1 Finite element model of beam column joint developed in ABAQUS

Table 1 Material properties

Material	Property	Value
Concrete	Density	2400 kg/m ³
	Modulus of elasticity	34 GPa
	Poisson’s ratio	0.2
	Concrete damage property model	Kent-Park model
GFRP bars	Longitudinal modulus of elasticity	47 GPa
	Poisson’s ratio	0.15
	Tensile strength	525 MPa

A model BCJF_g-M₃B with material properties listed in Table 1 as presented by Saravanan et al. [14] is selected and modelled in ABAQUS. The column is subjected to a constant axial load of 0.1 $f_{ck} \times A_g$, while a displacement-controlled loading is applied at the free end of the beam. The base of column is pinned, while the top of the column is supported by a roller that is free to move in the vertical axis. The beam end is subjected to free support conditions. Individual meshing is performed for each part with different mesh sizes until convergence. A load–deflection curve with respect to the free end of beam is plotted and joint shear strength is calculated using the methodology proposed by Del Vecchio et al. [3]. This joint shear strength obtained from ABAQUS model is compared with the experimental results of Saravanan et al. [14]. For this validated model, the parameters such as the compressive and tensile strengths of rebar are varied to obtain different numerical models, with respective joint shear strengths. These results are used to predict the joint shear strength of BCJ with GFRP reinforcement using the RSM technique.

3.1 Validation of ABAQUS Model

The load–deflection curve shown in Fig. 2, indicates a peak load of approximately 14 kN (rounding to integer) at the beam end. This value is in close agreement with the experimental peak beam load of 14.25 kN reported by Saravanan et al. [14] for BCJF_g-M₃B model and thus validating the ABAQUS numerical model. From this peak load, joint shear strength is calculated as per Eq. (1) proposed by Del Vecchio et al. [3].

$$V_{jh} = V_b \left(\frac{L_b}{d_b} - \frac{L_b}{L_c - H_c} \right) \tag{1}$$

Here, V_b is the maximum recorded shear forced on beam, L_b denotes beam length, L_c denotes column height, H_b denoted beam internal lever arm (considered as 0.75 H_b

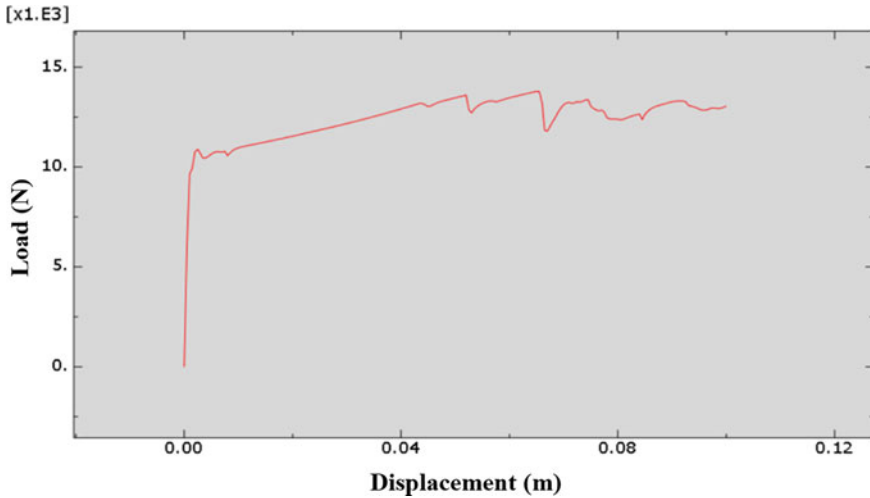


Fig. 2 Plot of load versus deflection graph at beam free end for the BCJ modelled in ABAQUS

as per Del Vecchio et al. [3], and H_c is the depth of column. For the aforementioned model, $V_b = 14$ kN as per Fig. 2 and using Eq. (1), joint shear force is estimated as 60 kN. From the experimental results of Saravanan et al. [14] the joint shear force is estimated as 69.15 kN.

4 Response Surface Methodology

Response surface methodology (RSM) is a collection of statistical and mathematical techniques used for empirical modelling and optimizing the response. RSM was first developed to model experimental responses and then applied into modelling the numerical experiments. The application of RSM is to model optimized response by reducing the cost of expensive analysis methods (i.e., finite element modelling or CFD analysis).

The relationship between response and design variables is unknown in the majority of real-world issues. In such problems, numerous experiments or computer simulations are run to establish the relationship between independent factors and response. Once the relationship has been established, it is possible to estimate the problem's optimal solution.

4.1 General RSM Equations

As per Nuran Bradley [2], if a model has output variable y as function of k independent variables, then mathematically it is represented as Eq. (2), where $x_i; i = 1, 2, \dots, k$ are independent input variables and y is the output response, ε is the noise associated with the system.

$$y = f(x_1, x_2, x_3, \dots, x_k) + \varepsilon \tag{2}$$

After performing enough experiments or numerical simulations, it is needed to determine the output as a function of independent inputs. This involves choosing a trail polynomial of suitable order for instance first order model is represented as Eq. (3) where $\beta_i; i = 0, 1, \dots, k - 1$ unknown coefficients of assumed polynomial are, x_{ik} represents the value of input variable x_k for i th model and y_i represents the output response of i th model.

$$y_i = \beta_0 + \beta_1 x_{i1} + \dots + \beta_{k-1} x_{ik} \tag{3}$$

The matrix representation of Eq. (3) is mentioned in Eq. (4), where Y denotes output vector, β denotes column vector of unknown coefficients, X denotes the matrix of values of input variables of different models as mentioned in Eq. (5).

$$Y = X\beta \tag{4}$$

where,

$$Y = \begin{pmatrix} y_1 \\ y_2 \\ \vdots \\ y_n \end{pmatrix}, \quad \beta = \begin{pmatrix} \beta_1 \\ \beta_2 \\ \vdots \\ \beta_{k-1} \end{pmatrix}, \quad X = \begin{bmatrix} 1 & x_{11} & x_{12} & \dots & x_{1k-1} \\ 1 & x_{21} & x_{22} & \dots & x_{2k-1} \\ \vdots & \vdots & \vdots & \vdots & \vdots \\ 1 & x_{n1} & x_{n2} & \dots & x_{nk-1} \end{bmatrix} \tag{5}$$

Error vector of assumed polynomial denoted as e , is calculated by Eq. (6), where $\hat{\beta}$ is the column vector of coefficients of assumed polynomial which is obtained by method of least squares and \hat{Y} is output of fitted polynomial as mentioned in Eq. (7).

$$e = (Y - \hat{Y}) \tag{6}$$

$$\hat{Y} = X\hat{\beta} \tag{7}$$

Sum of squares of residuals denoted as SS_{res} is obtained by using Eq. (8) where e_i denotes the error of i th model.

$$SS_{res} = \sum_{i=1}^n e_i^2 = \mathbf{e}^T \mathbf{e} = \mathbf{Y}^T \mathbf{Y} - 2\hat{\boldsymbol{\beta}}^T \mathbf{X}^T \mathbf{Y} + \hat{\boldsymbol{\beta}}^T \mathbf{X}^T \mathbf{X} \hat{\boldsymbol{\beta}} \tag{8}$$

By differentiating Eq. (8) with $\hat{\boldsymbol{\beta}}$ as mentioned in Eq. (9), SS_{res} is minimized thereby obtaining the column vector of coefficients for fitted polynomial represented in Eq. (10). Here T represents transpose of the respective matrices.

$$\frac{\partial SS_{res}}{\partial \hat{\boldsymbol{\beta}}} = 0 \tag{9}$$

$$\hat{\boldsymbol{\beta}} = (\mathbf{X}^T \mathbf{X})^{-1} \mathbf{X}^T \mathbf{Y} \tag{10}$$

4.2 Important Parameters Considered for RSM

Response quantity of interest in current study is joint shear strength of BCJ denoted by τ . Important parameters which affect the joint shear strength are yield strength of GFRP bar f_y , longitudinal modulus of elasticity of GFRP bar E_{long} , compressive strength of concrete f_{ck} , effective joint width b_j , percentage of beam bar reinforcement ρ_b , percentage of column bar reinforcement ρ_c , beam bar index x_b , joint shear reinforcement Index φ_s , column index P_y . These variables are considered as independent variables for RSM.

These input variables are calculated by using Eqs. (11)–(15) as per Bakir et al. [1] and mathematical representation of shear strength of BCJ is represented in Eq. (16) where $\bar{\tau}$ is column vector of joint shear strengths of all data from literature, $\boldsymbol{\beta}$ column vector obtained by Eq. (10) is represented in Eq. (18) and \mathbf{X} denotes the matrix of values of input variables of different models as mentioned in Eq. (5).

$$b_j = \frac{b_b + b_c}{2} \tag{11}$$

$$\varphi_s = \frac{A_{sh} f_y + A_{sv} f_y}{b_j h_c f_c} \tag{12}$$

$$P_y = \frac{N}{b_j h_c f_c} \tag{13}$$

$$x_b = \frac{n_b d_{sc} h_c}{b_b h_b} \tag{14}$$

$$\tau = \frac{V_j}{b_j \times h_c} \tag{15}$$

$$\bar{\tau} = \mathbf{X}\beta \tag{16}$$

where b_b and b_c represent width of beam and column respectively, A_{sh} and A_{sv} denote area of horizontal and vertical joint shear reinforcement, h_c and h_b are height of column and beam respectively, N is axial load on column, n_b is maximum number of top or bottom beam bars, d_{sc} is average beam bar diameter, V_j is joint shear force and τ is the joint shear strength of BCJ of i th model.

4.3 Results of RSM Linear Model

The experimental data of joint shear strengths of ten BCJs collected from [7, 14] are combined with the three FE models developed in Abaqus for performing RSM to predict the shear strength of beam column joint. Table 2 details the parameters of the three Abaqus models used in this study. The shear strengths of these models obtained while analyzing in Abaqus are also mentioned in this Table 2.

Linear model is assumed with 9 inputs mentioned in Sect. 4.2 and 1 output response as joint shear stress, τ , where τ represents joint shear stress of i th model.

$$\begin{aligned} \tau = & \beta_0 + \beta_1(f_y) + \beta_2(E_{long}) + \beta_3(f_{ck}) + \beta_4(b_j) \\ & + \beta_5(\rho_{col}) + \beta_6(\rho_{beam}) + \beta_7(x_b) + \beta_8(\varphi_s) + \beta_9(P_y) \end{aligned} \tag{17}$$

$$\begin{aligned} \beta = & [-14.16 \ 0.0048 \ 0.0447 \ 0.0128 \ -0.0078 \\ & -0.4775 \ 3.7328 \ 4.0798 \ 4.9416 \ 19.7605]^T \end{aligned} \tag{18}$$

4.4 Validation of RSM Model

For checking the significance of assumed polynomial sum of squares of residuals, total Sum of squares, sum of squares of regression denoted as SS_{res} , SS_{Total} , SS_{reg} respectively and then coefficient of determination denoted as R^2 for fitted model are calculated by Eqs. (19)–(22) respectively, where \bar{Y} is average of values in $\bar{\tau}$ vector.

$$SS_{res} = \sum_{i=1}^n e_i^2 = 14.246 \tag{19}$$

$$SS_{Total} = \sum_{i=1}^n (Y_i - \bar{Y})^2 = 101.76 \tag{20}$$

$$SS_{reg} = SS_{Total} - SS_{res} = 87.522 \tag{21}$$

Table 2 Parameters of the three models of beam column joint analysed in Abaqus

Model No.	f_y (MPa)	E_{long} (GPa)	f_{ck} (MPa)	b_j (mm)	ρ_{col}	ρ_{beam}	x_b	ϕ_s	P_y (kN)	Shear strength (kN)
1	525	47	46.23	230	0.4	0.86	0.104	0.224	250	60.12
2	580	59.5	35	230	0.4	0.86	0.104	0.224	250	62.15
3	690	69.8	40	230	0.4	0.86	0.104	0.224	250	67.23

$$R^2 = \frac{SS_{\text{reg}}}{SS_{\text{total}}} = 0.865 \quad (22)$$

The final proposed joint shear strength model for BCJ with GFRP bars by RSM is represented in Eq. (23)

$$\begin{aligned} \tau = & -14.16 + 0.0048(f_y) + 0.0447(E_{\text{long}}) + 0.0128(f_{ck}) - 0.0078(b_j) \\ & - 3.7328(\rho_{\text{col}}) + 0.4775(\rho_{\text{beam}}) + 4.0798(x_b) + 4.9416(\varphi_s) + 19.4605(P_y) \end{aligned} \quad (23)$$

5 Conclusions

In this study, reinforced concrete beam column joint with GFRP bars is modelled in ABAQUS by considering Kent-Park model for concrete and GFRP bar as anisotropic element. Joint shear strength is found from the numerical model and validated with the literature experimental result. To predict joint shear strength of beam column joint with GFRP bars RSM model is proposed by considering all the important parameters affecting the joint shear strength. This proposed formula can be used for all types of GFRP bars like grooved bars, sand coated bars and threaded bars but cannot be used for beam column joint with conventional steel. Coefficient of determination of proposed RSM model is found to be 0.865, which is satisfactory performance of the proposed model. By application of RSM, simulation cost and time can be saved in predicting the joint shear strength of beam column joint with GFRP bars.

References

1. Bakir PG, Boduroglu HM (2002) A new design equation for predicting the joint shear strength of monotonically loaded exterior beam-column joints. *Eng Struct* 24(8):1105–1117
2. Bradley N (2007) The response surface methodology. Indiana University South Bend
3. Del Vecchio C, Di Ludovico M, Prota A, Manfredi G (2015) Analytical model and design approach for FRP strengthening of non-conforming RC corner beam-column joints. *Eng Struct* 87:8–20
4. Ehsani MR, Alameddine F (1991) Design recommendations for type 2 high-strength reinforced concrete connections. *ACI Struct J* 88(3):277–291
5. Fujii S, Morita S (1991) Comparison between interior and exterior reinforced concrete beam-column joint behavior. *Spec Publ* 123:145–166
6. Ghomi SK, El-Salakawy E (2016) Seismic performance of GFRP- reinforced concrete exterior beam-column joints with lateral beams. *J Compos Constr* 20(1):04015019
7. Hasaballa M, El-Salakawy E (2016) Shear capacity of exterior beam-column joints reinforced with GFRP bars and stirrups. *J Compos Constr* 20(2):04015047
8. Kaku T, Asakusa H (1991) Ductility estimation of exterior beam-column sub assemblages in reinforced concrete frames. *Spec Publ* 123:167–186

9. Kotsovou GM, Cotsovos DM, Lagaros ND (2017) Assessment of RC exterior beam-column Joints based on artificial neural networks and other methods. *Eng Struct* 144:1–18
10. LaFave JM, Kim JH (2011) Joint shear behavior prediction for RC beam-column connections. *Int J Concr Struct Mater* 5(1):57–64
11. LaFave JM, Wight JK (1999) Reinforced concrete exterior wide beam-column-slab connections subjected to lateral earthquake loading. *Struct J* 96(4):577–585
12. Mady M, El-Ragaby A, El-Salakawy E (2011) Seismic behavior of beam-column joints reinforced with GFRP bars and stirrups. *J Compos Constr* 15(6):875–886
13. Safdar M, Sheikh MN, Hadi MN (2022) Cyclic performance of GFRP-RC T-connections with different anchorage and connection details. *J Compos Constr* 26(3):04022022
14. Saravanan J, Kumaran G (2010) Strut and tie model for the analysis of RC beam-column joints reinforced with non-metallic reinforcements. In: *Proceedings of the seventh structural engineering convention*, pp 1221–1230
15. Vollum RL, Newman JB (1999) Strut and tie models for analysis and design of external beam-column joints. *Mag Concr Res* 51(6):415–425

Environmental Assessment of Admixtures and Stone Powder in Cement Concrete



Kiran Devi , Amit Kumar, Babita Saini, and Paratibha Aggarwal

Abstract Concrete, being a versatile building material, is employed in a wide range of applications. Under normal circumstances, it performs satisfactorily but deteriorates under extreme situations. To attain the desired characteristics during construction, admixtures are used in cementitious materials. Accelerating admixtures fasten the setting and development of early age strength of the cement composites. Stone, on the other hand, is another significant building material used in the construction industry. The stone industry is also expanding with the construction industry's rise, generating tonnes of debris every year. Stone wastes in various forms, such as slurry, dust/powder, broken slabs, and aggregates, have been dumped on valuable land and watersheds. It creates a nuisance to the ecosystem, thereby becoming a potential environmental threat. In the present study, stone powder, along with accelerating admixtures has been utilized in concrete mixtures to examine its feasibility in terms of ecological and economic aspects. The study aimed to investigate the environmental impact of different additives i.e., stone powder, calcium nitrate, and triethanolamine individually and in combination for various cement concrete mixes. The environmental impact of concrete mixtures was evaluated in terms of embodied energy, carbon footprint, and cost analysis of different concrete mixes and compared with the plain mix. The performance index of different mixtures of concrete was also assessed. Results showed that stone powder was found to be very efficient in lowering the cost, energy use, and CO₂ emission among all additives. Compared to other additives, using stone powder in concrete enhanced the performance effectively.

K. Devi (✉) · A. Kumar · B. Saini · P. Aggarwal
Departemnt of Civil Engineering, National Institute of Technology, Kurukshetra, India
e-mail: kiranbimbhra@gmail.com

A. Kumar
e-mail: amit_6160040@nitkkr.ac.in

B. Saini
e-mail: bsaini@nitkkr.ac.in

K. Devi
Department of Civil Engineering, SGT University, Gurugram, India

Keywords Additive · Ecological · Economic analysis · Performance index · Sustainability

1 Introduction

Concrete is a versatile material due to its low cost, easy availability of ingredients, and higher compressive strength. Under various environmental conditions, concrete has several advantages and disadvantages. Researchers work to increase the efficiency of concrete by adding new components or materials to lessen its drawbacks. The accelerating admixtures can speed up or slow down the setting time. Accelerators are an additive added to grout, mortar, or concrete to hasten the setting process and speed up the hydration, hardening, or development of strength. Calcium nitrate (CN) and triethanolamine (TEA) are used as accelerators in the mortar and concrete [1, 2].

India is the largest producer and exporter of different types of stone in various textures worldwide. Dimension stones used frequently in Indian construction include marble and Kota stone. A siliceous limestone known as “Kota stone” is quarried in the Rajasthani town of Kota. The waste is created in the forms of slurry, dust, powder, and stone chips, which are dumped on open ground and harm the ecosystem [2, 3]. Also, cement production emits a huge amount of carbon dioxide and need alternate materials. These industrial wastes can be used cement or aggregates substitution in the construction sector. Singh et al. [4] studied that marble slurry in concrete lowered the cost, low energy use and lessened the carbon footprint. Khodabakhshian et al. [5] reported that blended marble powder and silica fume enhanced the strength of concrete while minimizing the negative impact on the environment. Devi et al. [6] investigated that using marble powder in mortar cut costs and energy use and lowered carbon emission.

In the present study, environmental and economic analysis of different additives i.e., CN, TEA and stone powder (SSP) in various concrete mixtures was carried out along with the strength. The ecological analysis of different concrete mixtures was determined in terms of energy consumption and carbon emission. The normalized energy consumption, carbon emission and cost of different eight concrete mixes was evaluated. The individual performance index of concrete mixtures was also evaluated. The aim of the present study to examine the economic and ecologic feasibility of different additives such as CN, TEA and stone powder in eight different concrete mixtures for the sustainable construction.

2 Methodology

In the present study, 43 grade of Portland cement and aggregate was used in the cement concrete. Cement was replaced by SSP by 7.5%; CN and TEA were used as cement additive at the dosages of 1% and 0.05% by the weight of cement respectively [7]. The mix detail has been given in the table [7].

The embodied energy (EE) and embodied carbon dioxide (ECO₂) of concrete can be used to analyse its ecological impact, while cost can be used to analyse its economic impact. The values of EE and ECO₂ for used materials have been taken from previous study and given in Table 1 [6, 8, 9]. The cost of all raw materials as per local market prices was taken and has also been given in Table 2.

The values in Table 2 have been used to calculate the value of EE, ECO₂, and cost for concrete using Eq. (1). The normalized energy consumption, carbon emission, or cost was evaluated using Eq. (2).

$$EE/ECO_2/Cost = \sum g_i m_i \tag{1}$$

where g_i = EE per unit mass of materials and m_i indicates the mass of concrete ingredients ‘i’ per unit cubic meter.

Table 1 Mix proportions for different concrete mixtures [7]

Mix No.	Cement, k/m ³	Sand, k/m ³	Aggregates, k/m ³	Water, k/m ³	CN, k/m ³	TEA, k/m ³	SSP, k/m ³
CC1	390	503.1	1088.1	167.7	0	0	0
CC2	360.75	503.1	1088.1	167.7	0	0	29.25
CC3	390	503.1	1088.1	167.7	0	0.195	0
CC4	390	503.1	1088.1	167.7	3.9	0	0
CC5	390	503.1	1088.1	167.7	3.9	0.195	0
CC6	360.75	503.1	1088.1	167.7	0	0.195	29.25
CC7	360.75	503.1	1088.1	167.7	3.9	0	29.25
CC8	360.75	503.1	1088.1	167.7	3.9	0.195	29.25

Table 2 EE, ECO₂, and cost of raw materials [6]

S. No.	Material	EE (MJ/kg)	E-CO ₂ (kgCO ₂ /kg)	Cost (INR/kg)
1	Cement	4.8	0.93	6
2	Sand	0.081	0.0051	1
3	Coarse aggregate	0.0083	0.0008	1.8
4	Water	0.2	0.0002	0.05
5	CN	0.1368	0.481	430
6	TEA	–	–	1060
7	SSP	–	–	–

$$\begin{aligned} & \text{Normalized Energy consumption or carbon emission or cost} \\ & = EE \text{ or } EC O_2 \text{ or } \frac{\text{cost}}{28\text{Days}} \text{Compressive Strength} \end{aligned} \quad (2)$$

The performance index (PI) tool promotes determining the SSP content to create the best combinations that adhere to the necessary performance standards. Equation 3 was used to compute the numeric index (R_i), and the highest numeric index was chosen as 5.00 [10, 11].

$$R_i = \frac{\text{Measured performance for each mixture}}{\text{Best measure performance}} \times 5 \quad (3)$$

3 Results and Discussion

3.1 Environmental Analysis

The influence of different materials i.e. CN, TEA and SSP on the environmental impact was assessed along with their normalized values. The variation of EE, ECO₂ and cost of different concrete mixes has been compared with reference to the control mix (CC1) and illustrated in Fig. 1. Figure 1 demonstrates the percentage variation of different parameters for various mix proportions. The mixes containing stone powder (CC2) had the minimum impact on the environment in terms of energy consumption and carbon emission; and cost compared to other concrete mixes. Figure 1 illustrate the reduction in the EE, ECO₂ and cost value due to the inclusion of stone waste below the axis. Adding admixtures in concrete hiked the construction price due to their high cost. The values of EE, ECO₂ and cost of concrete varied from 1896.2 to 2037.1 MJ/m³, 343.4 to 372.5 kgCO₂e/m³ and 4664 to 6487 INR/m³, respectively for all the mix proportions. The inclusion of SSP reduced the value of EE, ECO₂ and cost of concrete construction by 7%, 7% and 4%, respectively whereas, CN insignificantly enhanced all slightly. Since the TEA quantity was very low, therefore, its effect was not considered.

The inclusion of SSP and CN in concrete mixtures enhanced the 28 days compressive strength due to its pore-filling effect resulting in dense formation and better bonding between the constituents of solid phase [7]. TEA reduced the strength due to its regarding effect of C₃S hydration. The combination of CN and SSP enhanced the strength due to their predominant nature as reported by Devi et al. [7]. The percentage variation of compressive strength for the different concrete mixtures with reference to control mix have been illustrated in Fig. 2. Figure 2 illustrates the addition of TEA in concrete mixtures has the maximum reduction in the strength (downward direction) and SSP had the maximum increase in strength (upward direction).

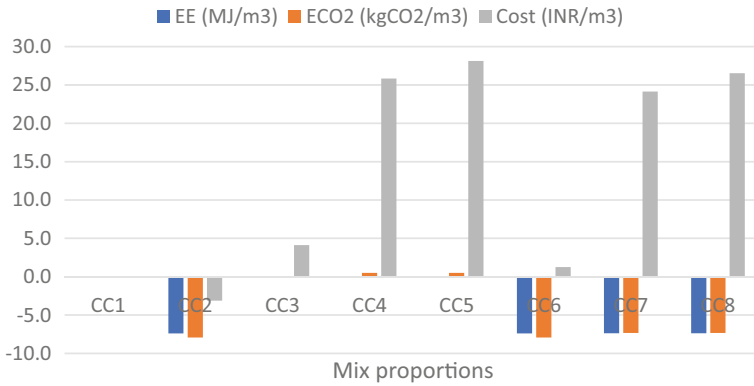


Fig. 1 Percentage variation in ecological and economic aspects of concrete with additives

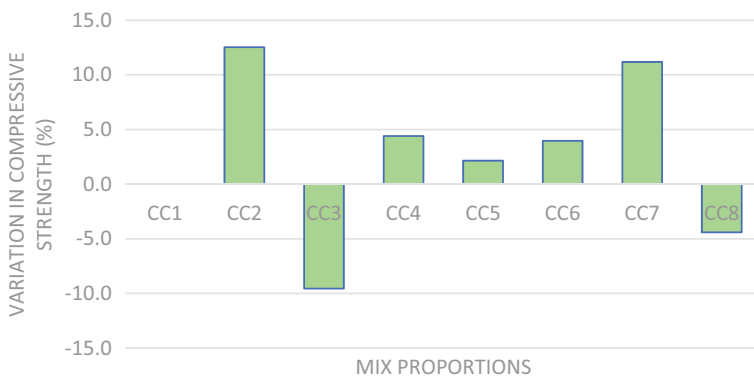


Fig. 2 Percentage variation in 28 days compressive strength

The normalized value for EE, ECO₂ and cost for the different mix proportions have been shown in Fig. 3. Normalized EE, ECO₂ and cost of concrete containing admixtures CN was higher than the control mix and TEA in concrete mixtures hiked the cost compared to other mixes due to its high price as illustrated in Fig. 3. The value of normalized EE, ECO₂ and cost of concrete mixtures containing stone powder was lower due to high strength among all the mix proportions. The concrete mixtures containing TEA had the highest value due to lower strength among all mixes.

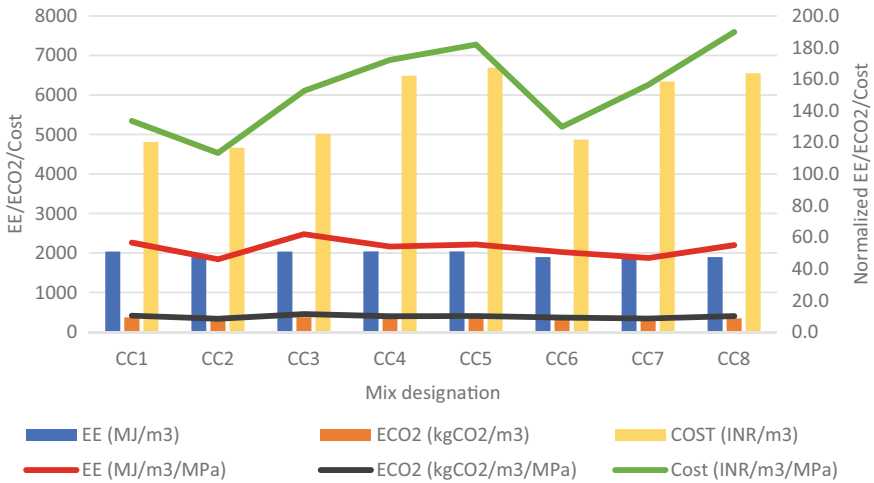


Fig. 3 Normalized energy consumption, normalized carbon emission and normalized cost

3.2 Performance Evaluation

The performance index for different concrete mixes in terms of sustainability have been evaluated and given in Table 3. The highlighted mixes had the optimum performance according to the properties i.e., mechanical strength, cost and ecological aspect. The mix CC2 i.e., SP at 7.5% was found the most suitable mix which can be preferred for various requirements such as economic or cost, environmental (energy consumption and carbon emission) and mechanical strength. The highest and lowest value were considered for the strength; and ecological and cost criteria, respectively for the performance index of different concrete mixtures. The lower values for economic and ecological aspects indicate the best performance because waste material is used to reduce cost and environmental impact. Therefore, SSP had the best strength, cost and ecological performance.

Table 3 Individual performance indices of concrete

Mix No	28D CS (MPa)	EE, (MJ/m ³)	ECO ₂ , (kg CO ₂ e/m ³)	Cost, (INR/m ³)
CC1	4.37	5.00	4.97	3.59
CC2	5.00	4.65	4.61	3.48
CC3	4.11	5.00	4.97	3.75
CC4	4.45	5.00	5.00	4.85
CC5	4.83	5.00	5.00	5.00
CC6	4.55	4.65	4.61	3.64
CC7	4.92	4.66	4.63	4.74
CC8	4.07	4.66	4.63	4.89

The bold value shows the optimum mix proportion in different aspects such as 28 days compressive strength, Embodied energy (EE), Embodied carbon dioxide (ECO₂) and cost among all mixes

4 Conclusion

In the present study, the feasibility of the chemical admixtures i.e., calcium nitrate and triethanolamine as cement additive; and stone powder as cement substitution in the eight different concrete mixtures was evaluated in terms of strength, ecological and economic aspects. The normalized energy consumption, carbon emission and cost of different mix proportions was also evaluated. The conclusions are given as.

- The addition of calcium nitrate and stone powder enhanced concrete's 28 days compressive strength, whereas the triethanolamine in the concrete mixtures declined the strength.
- Incorporating stone powder in the concrete mixtures reduced energy consumption and carbon emission by 7% each because it is an industrial by-product, freely available and used without any pre-processing.
- The chemical admixtures i.e. CN and TEA hiked the cost, energy consumption and carbon emission compared to the control mix. CN had more impact than TEA due to addition of a larger quantity.
- The mix CC2 i.e., SSP at 7.5% was found the most economical, eco-friendly and strength intensive among all the mixes.
- Therefore, SSP was proved as the best performer in terms of strength, cost and ecological aspects.

References

1. Aggoun S, Cheikh-Zouaoui M, Chikh N, Duval R (2008) Effect of some admixtures on the setting time and strength evolution of cement pastes at early ages. *Constr Build Mater* 22:106–110

2. Devi K, Saini B, Aggarwal P (2018) Combined use of accelerators and stone slurry powder in cement mortar” ICSWMD 2019. LNCE 21:1–8. https://doi.org/10.1007/978-3-030-02707-0_25
3. Hussain A (2015) Kota stone slurry problem and possible solutions (Online). Available: <https://www.slideshare.net/AkhtarHussain10/kota-stone-slurry-problem-and-possible-solutions>
4. Singh M, Srivastava A, Bhunia D (2017) An investigation on effect of partial replacement of cement by waste marble slurry. *Constr Build Mater* 134:471–488
5. Khodabakhshian A, de Brito J, Ghalehnovi M, Shamsabadi EA (2018) Mechanical, environmental and economic performance of structural concrete containing silica fume and marble industry waste powder. *Constr Build Mater* 169:237–251
6. Devi K, Saini B, Aggarwal P (2021) Economic and ecological feasibility of marble powder in cement mortar. In: Kalamdhad AS (ed) *Integrated approaches towards solid waste management*. Springer, Cham. https://doi.org/10.1007/978-3-030-70463-6_7
7. Devi K, Saini B, Aggarwal P (2019) Utilization of Kota stone slurry powder and accelerators in concrete. *Comput Concrete* 23(3):189–201. <https://doi.org/10.12989/cac.2019.23.3.189>
8. Flower DJM, Sanjayan JG (2007) Green-house gas emissions due to concrete manufacture. *Int J Life Cycle Assess* 12:282. <https://doi.org/10.1065/lca2007.05.327>
9. Siddique S, Chaudhary S, Shrivastava S, Gupta T (2019) Sustainable utilisation of ceramic waste in concrete: exposure to adverse conditions. *J Clean Prod* 210:246–255
10. Devi K, Saini B, Aggarwal P (2021) Impact of high temperature on mortar mixes containing additives. *J Eng Res* 10. <https://doi.org/10.36909/jer.10477>
11. Devi K, Saini B, Aggarwal P (2023) Performance evaluation of concrete using different additives. In: Marano GC, Rahul AV, Antony J, Unni Kartha G, Kavitha PE, Preethi M (eds) *Proceedings of SECON'22*. SECON 2022. Lecture notes in civil engineering, vol 284. Springer, Cham. https://doi.org/10.1007/978-3-031-12011-4_7

Evaluation of Disputes in Kerala Construction Industry



U. A. Devangana and Anu V. Thomas

Abstract Disputes are an inevitable part of the construction industry. Every year a huge amount of money and time is wasted on the settlement of disputes in construction projects. There can be different causes for the disputes to arise in construction projects. Prevention of disputes can be possible through proper identification and analysis of the factors causing them. This paper is a study on the identification of construction disputes from literature and through a questionnaire survey in Kerala public projects. The responses from the survey were logically analysed using fuzzy-DEMATEL analysis and Relative Importance Index (RII). Fuzzy-DEMATEL categorizes the factors as causes and effects. RII scaling is used to scale the factors that cause disputes causing cost overrun in Kerala public works. Thus, this study intends to find the factors affecting disputes, their inter-relationships and effects on Kerala construction sector.

Keywords Relative importance Index (RII) · Kerala public works · Fuzzy-DEMATEL · Disputes

1 Introduction

Disputes has always had its close acquaintance with construction projects. When the project goals are not met, limitations in the project's implementation will arise. It is necessary to handle the potential for conflicts or disagreements among the stakeholders in the project. Conflict is the result of there being a discrepancy in the values or objectives that must be met, both personally and in relation to others. Conflict can result from numerous sources, which include project scope, human resources, contracts, owners, contractors, consultants, and outside factors. These

U. A. Devangana (✉) · A. V. Thomas
Department of Civil Engineering, TKM College of Engineering, APJ Abdul Kalam Technological University, Thiruvananthapuram, India

A. V. Thomas
e-mail: anuvthomas@tkmce.ac.in

elements have an impact on the effectiveness and productivity of work, which can be disruptive [1]. The occurrence of disputes can be controlled to a certain limit by proper identification of the causes of disputes. This paper aims to find out all possible sources of disputes from literature review, conduct a survey to determine the disputes and its effects on the construction sector, and finally analyse the survey results with fuzzy logics.

2 Identification of Factors Causing Disputes in Construction

2.1 Identification and Classification of Cost Overrun Factors

There are plenty of factors that cause disputes in construction industry. Francis et al. [2] stated that disputes are costly both in terms of time and money and are often accompanied by the destruction of individual and good working relationships. Sinha and Wayal [3] pointed out that changes to scope occur not only due to the client but due to the stakeholder needs, the physical location, and the prevailing economic environment. Mante et al. [4] suggested that poor communication is one of the salient features of traditionally procured projects, thereby increasing the possibility of disputes. Cakmak and Cakmak, [5] in their work discussed disputes due to design errors. Osman et al. [6], stated that substantial amounts of money and time are spent annually in pursuing differing site conditions (DSC) claims. Naji et al. [7] in their research specified the top 10 sources of disputes as, poorly addressing the impact or effect of changes related to time and cost, EOT, escalation in price, payment failure in reference to contract conditions, suspension of work, defective work, tender evaluation, risk imposed by the contractor or owner, quality of work on-site. Francis et al. [2] and Tabish and Jha [8] stressed the importance of identifying these sources of disputes so that they can be managed more efficiently and effectively. From literature review, nine categories of factors having 52 sub-factors have been identified. A pilot study was conducted with 5 arbitrators and engineers from Kerala Public Works Department. The factors were reduced to 43 under nine different categories. Table 1 shows the identified factors causing disputes in construction projects.

3 Questionnaire Survey

The target group for the questionnaire survey was construction professionals in public sector projects, here, engineers from different departments of Kerala public works department were selected. A total of 30 responses were collected for the survey. The designation of respondents varied from chief engineers, executive engineers and

Table 1 Factors causing disputes

Sl. No	Main factors	Sub-factors
1	Owner related	Delay in contractor's bill settlement for completed work
2		Slow decision making
3		Delay in handing over site/right of way
4		Administration issues on client side
5		Unrealistic time targets
6	Contractor related	Improper planning and scheduling
7		Poor quality of work
8		Cash flow difficulties
9		Improper site management
10		Technical inadequacy and insufficient experience of contractor
11		Extra charges due to rework
12	Consultant related	Incorrect estimation of cost and time
13		Delay and improper inspection
14		Lack of professionalism
15		Quality assurance and quality control
16	Design related	Modification/change in design
17		Delay in design approval
18		Lack of clarity in specification and drawings
19	Coordination related	Change in scope of work
20		Extra work
21		Exceptionally low bid
22	Material labour equipment related	Price escalation related issues
23		Material shortage
24		Delay in material procurement
25		Modification in material specifications
26		Labour shortage
27		Dispute and strike
28		Poor qualification of labour
29		Labour charge
30		Equipment deficiency
31		Higher cost of equipment and machines
32		Contract related
33	Lack of clarity, inconsistency and overlapping of contractual provisions	
34	Coordination related	Delay in progress of work

(continued)

Table 1 (continued)

Sl. No	Main factors	Sub-factors
35		Lack of proper coordination between contractor and labour
36		Gaps in communication between client and contractor
37	External factors	Changes in rules and regulations of state and central government
38		Force majeure-act of God
39		Adverse weather conditions
40		Differing site conditions
41		Accidents and casualties
42		Insurance charges
43		Fraudulent and kickbacks

Table 2 Experience of respondents in construction field

Total experience	Number	Percentage (%)
Less than 2 years	2	6.67
2–5 years	5	16.67
6–10 years	2	6.67
11–15 years	4	13.33
Above 15 years	17	56.67

assistant engineers of different Kerala public works department. From the respondents, 56.67% had more than fifteen years of experience. The demographics of the survey is given in Table 2. The responses of the survey were used to perform DEMATEL Analysis as well as, to rank the factors with RII scale.

3.1 Fuzzy DEMATEL Analysis

The Decision-Making Trial and Evaluation Laboratory (DEMATEL) method is used to visualize a structure of complicated casual relationships through matrices or digraphs. Kumaraswamy [9] stated that the varied opinions of project participants regarding the reasons for the issues prevailing in a project is one of the major challenges in tracing the cause-effect links between given categories of claims, specific proximate causes, and root causes.

Fuzzy technique methodologies provide a viable tool for modeling subjective information, and handling uncertainty where comprehensive data sets are not available for modeling [7]. Thus, Fuzzy DEMATEL can be applied to problems that

involve group decision making. The procedure adopted for Fuzzy DEMATEL analysis to determine the cause-and-effect relationship between the main category of factors is as given below [10]:

- Step 1: The problem elements are formed in this step, along with the extent of their interrelationships. Thus 43 factors were collected from literature survey for questionnaire preparation.
- Step 2: The importance of the measurement scales is specified as 0–4, before the preparation of the questionnaire survey. The fuzzy scale adopted in the study is given in Table 3.
- Step 3: The responses in a direct relation matrix are defuzzified, using Eq. (1), which is called the central area method.

$$\text{Center of area} = \frac{a + b + c}{3} \tag{1}$$

where a, b, c are the corresponding TFNs

- Step 4: Average matrix(X) is calculated where each element is the average of corresponding elements from all the responses with its diagonal elements zero. Refer Eq. (2)

$$X = \begin{bmatrix} 0 & \dots & a_{1n} \\ \vdots & \ddots & \vdots \\ a_{1n} & \dots & 0 \end{bmatrix} \tag{2}$$

- Step 5: A normalized direct relation matrix (N) is built from direct relation matrix using Eqs. (3) and (4)

$$\lambda = \frac{1}{\max_{1 < i < n} \sum_{i=1}^n x_{ij}} \quad (i, j = 1, 2, \dots, n) \tag{3}$$

$$N = \lambda X \tag{4}$$

- Step 6: The Total relation matrix (T) is calculated based on Eq. (5)

Table 3 Fuzzy linguistic scale [11]

Linguistic phrases	Influence score	Triangular fuzzy numbers
No influence	0	(0, 0, 0.25)
Very low influence	1	(0, 0.25, 0.50)
Low influence	2	(0.25, 0.50, 0.75)
High influence	3	(0.50, 0.75, 1.00)
Very high influence	4	(0.75, 1.00, 1.00)

$$T = \lim_{k \rightarrow \infty} (N + N^2 + \dots + N^k) = N(1 - N)^{-1} \tag{5}$$

Step 7: From the total relation matrix the sum of all rows and columns are calculated. D_i shows the sum of the i th row and R_j shows the sum of the j th column D_i shows the sum of the i th row and R_j shows the sum of the j th column, which in turn denotes the direct and indirect influences between factors Eqs. (6) and (7).

$$D_i = \sum_{j=1}^n t_{ij} (j = 1, 2, \dots, n) \tag{6}$$

$$R_j = \sum_{i=1}^n t_{ij} (j = 1, 2, \dots, n) \tag{7}$$

Step 8: This step involves initial stages of making of the casual diagram or cause—effect digraph. $D + R$ and $D-R$ are calculated. Maximum $D + R$, prominence value shows that the corresponding factor has more relationships with other factors. They have more influence over other factors. Positive $D-R$, relation value however shows that they are cause groups or despatchers, and the negative valued factors are effect groups or receivers.

Step 9: The cause-effect diagram is drawn.

3.2 Relative Importance Index

As stated by Gebrehiweta and Luo [12], using a five-point Likert scale, the Relative Importance Index (RII) is used to assess the relative importance of the various causes of disputes due to cost overrun. The more significant the cause, the higher the value of the relative important index (RII), and vice versa. Equation (8) is used for calculation of RII.

$$RII = \frac{\sum W_i F_i}{A * N} \tag{8}$$

where

i —response category index, W_i —is the weight given by respondents, F_i —is the frequency of respondent for each weight, A —is the highest weight and N —is the total number of respondents. The relative important index (RII) ranges from 0 to 1 (0 not inclusive).

4 Results and Analysis

4.1 Fuzzy DEMATEL Analysis

- Step 1: The factors were identified and all the responses were collected from respondents.
- Step 2: All the collected responses are cross checked for any mistakes or missing data.
- Step 3: Using Eq. (1) the responses were defuzzified. A sample is shown in Table 4. In Table 4, Owner Related is V1, Contractor Related-V2, Consultant Related-V3, Design Related-V4, Project Related-V5, Material, Labour and Equipment Related-V6, Contract Related-V7, Coordination Related-V8 and External Factors is V9.
- Step 4: Average matrix(X) is calculated with all its diagonal elements zero as shown in Table 5.

Table 4 Defuzzified sample response

Main factors	V1	V2	V3	V4	V5	V6	V7	V8	V9
V1	0.083	0.250	0.750	0.500	0.250	0.250	0.500	0.500	0.500
V2	0.750	0.083	0.750	0.500	0.750	0.250	0.250	0.250	0.250
V3	0.250	0.500	0.083	0.500	0.750	0.250	0.083	0.083	0.083
V4	0.917	0.750	0.250	0.083	0.250	0.250	0.500	0.250	0.083
V5	0.250	0.500	0.500	0.500	0.083	0.250	0.250	0.250	0.083
V6	0.083	0.917	0.500	0.250	0.250	0.083	0.250	0.250	0.250
V7	0.250	0.500	0.500	0.917	0.500	0.250	0.083	0.500	0.250
V8	0.750	0.500	0.500	0.250	0.750	0.250	0.083	0.083	0.500
V9	0.750	0.500	0.083	0.917	0.250	0.250	0.500	0.500	0.083

Table 5 Average matrix (X)

Main factors	V1	V2	V3	V4	V5	V6	V7	V8	V9
V1	0	0.769	0.572	0.640	0.666	0.481	0.651	0.666	0.473
V2	0.666	0	0.553	0.598	0.659	0.837	0.719	0.776	0.602
V3	0.522	0.602	0	0.522	0.564	0.511	0.435	0.534	0.378
V4	0.556	0.590	0.590	0	0.602	0.401	0.500	0.488	0.443
V5	0.530	0.666	0.560	0.583	0	0.606	0.500	0.621	0.484
V6	0.553	0.803	0.340	0.412	0.628	0	0.568	0.590	0.564
V7	0.609	0.708	0.386	0.416	0.606	0.572	0	0.439	0.488
V8	0.575	0.690	0.534	0.553	0.553	0.625	0.530	0	0.522
V9	0.446	0.484	0.348	0.424	0.473	0.587	0.397	0.393	0

- Step 5: Normalised direct relation matrix(N) is calculated as per Eqs. (3) and (4). The λ value is 0.184. The N matrix is as shown in Table 6.
- Step 6: Total relation matrix(T) is calculated with Eq. (5) and is shown in Table 7.
- Step 7: The D + R and D-R values are calculated as per Eqs. (6) and (7). The respective prominence (D + R) and relation (D-R) values are given in Table 8.
- Step 8: Maximum prominence value was for contractor related factors, followed by, owner related, project related, material, coordination, contract, design, consultant and external factors. The greater the D + R values, greater will be the factor’s influence on other factors. Whereas the more the D-R value, the more those factors have chance to get influenced by other factors. Positive relation values are called cause group or despatchers. The cause group includes owner, contractor, consultant, design and coordination related factors. While, the effect group with negative D-R value includes, project related factors, material, labour, equipment related, contract and external factors.

Table 6 Normalised direct relation matrix (N)

Main factors	V1	V2	V3	V4	V5	V6	V7	V8	V9
V1	0	0.142	0.105	0.118	0.123	0.088	0.120	0.123	0.087
V2	0.123	0	0.102	0.110	0.121	0.154	0.132	0.143	0.111
V3	0.096	0.111	0	0.096	0.104	0.094	0.080	0.098	0.069
V4	0.102	0.110	0.109	0	0.111	0.074	0.092	0.090	0.081
V5	0.097	0.123	0.103	0.107	0	0.111	0.092	0.114	0.089
V6	0.102	0.148	0.062	0.076	0.116	0	0.104	0.109	0.104
V7	0.112	0.130	0.071	0.076	0.111	0.105	0	0.081	0.090
V8	0.106	0.128	0.098	0.102	0.102	0.115	0.097	0	0.096
V9	0.082	0.089	0.064	0.078	0.087	0.108	0.073	0.072	0

Table 7 Total relation matrix (T)

Main factors	V1	V2	V3	V4	V5	V6	V7	V8	V9
V1	0.491	0.700	0.529	0.566	0.629	0.592	0.586	0.610	0.521
V2	0.642	0.625	0.560	0.597	0.671	0.687	0.635	0.667	0.578
V3	0.502	0.585	0.365	0.475	0.532	0.51	0.477	0.511	0.437
V4	0.515	0.594	0.471	0.396	0.547	0.508	0.495	0.512	0.454
V5	0.546	0.645	0.496	0.524	0.483	0.575	0.529	0.567	0.492
V6	0.544	0.65	0.457	0.493	0.581	0.470	0.535	0.558	0.501
V7	0.531	0.620	0.445	0.474	0.555	0.542	0.419	0.513	0.469
V8	0.556	0.654	0.495	0.523	0.579	0.582	0.537	0.468	0.501
V9	0.439	0.508	0.380	0.412	0.465	0.475	0.422	0.438	0.327

Table 8 Prominence and relation values

Main factors	D	R	Prominence (D + R)	Relation (D - R)
Owner related	5.228517	4.770444	9.998962	0.4580
Contractor related	5.666903	5.594502	11.26141	0.0724
Consultant related	4.404167	4.200418	8.604586	0.2037
Design related	4.495964	4.464698	8.960663	0.0312
Project related	4.860745	5.046109	9.906853	- 0.1853
Material, labour, equipment related	4.802331	4.950724	9.753055	-0.1483
Contract related	4.570609	4.638693	9.209302	- 0.0680
Coordination related	4.900181	4.848728	9.748909	0.0514
External factors	3.870328	4.285431	8.155759	- 0.4151

Step 9: The cause-effect diagram is shown in Fig. 1.

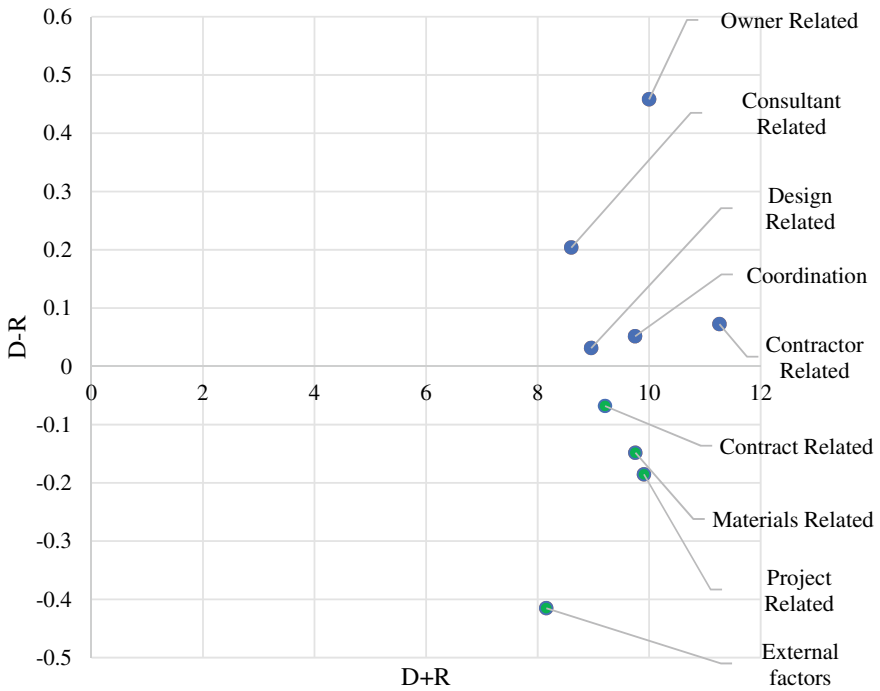


Fig. 1 Cause-effect diagram

4.2 *Relative Importance Index*

This section of study includes analysis of factors that influences the disputes due to cost overrun in Kerala public projects. The frequency of each factor from the collected responses were calculated. A total of 30 responses were collected from the industrial engineers. Equation (8) was used to determine the weightage of each factor. The factors were then arranged in descending order of their weightages. The top 5 factors that came in the list were, material shortage and poor quality of work was weighed 0.808, price escalation related issues with a weight of 0.768, extra charges due to rework with a weight of 0.744, cash flow difficulties from contractor were 0.736, while, unrealistic time targets by owner, improper site management by contractor, delay in handing over of site, and extra works in project have been weighed 0.728. Table 9 shows the weightages of other factors. However, the weights of their corresponding main categories varied as shown in Table 10.

4.3 *Validation*

The validation of the study was conducted with another questionnaire survey, where a team of 10 practising arbitrators, responded to the same questionnaire. Their responses were analysed using Relative Importance Index and the corresponding weights for each category were calculated as discussed before. The weights of main factors are shown in Table 11.

5 *Conclusion*

Disputes in the construction sector have a long-lasting impact on the progress of work, money and time involved. Thus, identification and prevention of disputes becomes a necessity in construction industry. In the case of public projects, the delay in establishment of a project affects the goodwill and trust of the public in government. Disputes cause a huge loss of money and time for all the stakeholders involved in a project; thus, it is necessary to identify all the probable causes of disputes and eliminate them at the early stages of construction itself.

Forty-three factors causing disputes in construction industry were identified from extensive literature review. A questionnaire survey was conducted with 30 engineering professionals from different departments in Kerala Public Works Department. The responses were analysed with Fuzzy-DEMATEL approach to determine the cause and effects of disputes. The maximum prominence value ($D + R$) was calculated for contractor, followed by, owner, project, material, coordination, contract, design, consultant and external factors. The contractor related factors had more prominence, i.e., they are more connected with other factors. Thus, controlling its

Table 9 Weightages of sub-factors from RII scaling

Sl. No	Sub-factors	Weightages
1	Material shortage	0.808
2	Price escalation related issues	0.768
3	Extra charges due to rework	0.744
4	Cash flow difficulties	0.736
5	Unrealistic time targets	0.728
6	Improper site management	0.728
7	Extra work	0.728
8	Improper planning and scheduling	0.720
9	Technical inadequacy and insufficient experience of contractor	0.720
10	Delay in design approval	0.720
11	Delay in material procurement	0.712
12	Delay in progress of work	0.712
13	Delay in handing over site/right of way	0.704
14	Slow decision making	0.696
15	Modification/change in design	0.696
16	Change in scope of work	0.696
17	Incorrect estimation of cost and time	0.672
18	Labour shortage	0.648
19	Labour charge	0.648
20	Gaps in communication between client and contractor	0.648
21	Delay in contractor's bill settlement for completed work	0.632
22	Adverse weather conditions	0.624
23	Lack of professionalism	0.616
24	Poor quality of work	0.608
25	Equipment deficiency	0.608
26	Lack of clarity in specification and drawings	0.600
27	Modification in material specifications	0.600
28	Differing site conditions	0.600
29	Administration issues on client side	0.592
30	Dispute and strike	0.592
31	Lack of proper coordination between contractor and labour	0.592
32	Exceptionally low bid	0.584
33	Poor qualification of labour	0.576
34	Delay and improper inspection	0.552
35	Higher cost of equipment and machines	0.552
36	Lack of clarity in tender and agreement clauses and drawings	0.544
37	Force majeure-act of God	0.528

(continued)

Table 9 (continued)

Sl. No	Sub-factors	Weightages
38	Lack of clarity, inconsistency and overlapping of contractual provisions	0.512
39	Changes in rules and regulations of state and central government	0.512
40	Quality assurance and quality control	0.504
41	Accidents and casualties	0.464
42	Fraudulent and kickbacks	0.432
43	Insurance charges	0.384

Table 10 Weights of the main factors from the study

Main factors	Weights
Owner	0.653
Contractor	0.66
Consultant	0.621
Design	0.653
Project	0.651
Material	0.652
Contract	0.542
Coordination	0.649
External	0.534

Table 11 Weights of the main factors from validation

Main factors	Weights
Owner	0.632
Contractor	0.792
Consultant	0.52
Design	0.64
Project	0.584
Material	0.712
Contract	0.52
Coordination	0.616
External	0.48

occurrence can control the chances of disputes to a greater extent. The cause group included owner, contractor, consultant, design and coordination related factors with owner related factors having more influence over other categories. The effect group had project related factors, material, labour, equipment related, contract and external factors. Therefore, external factors have more chances of getting influenced by other factors.

The top-rated factors in RII ranking were, material shortage, price escalation related issues, extra charges due to rework, cash flow difficulties from contractor, unrealistic time targets by owner, improper site management by contractor, and extra works in project. From both the study as well as the validation results, the top-rated main factors were contractor related, owner related, design related and material, labour and equipment related factors. Thus, prevention of occurrence of these factors and their associated sub-factors can control the occurrence of cost overrun in public projects and their related disputes efficiently.

Mitigation measures, to prevent the disputes and litigation due to the top-rated factors like, owner related, contractor related and material, labour equipment related and design related factors in public projects can be as follows:

- i. Tender documents or agreements shall clearly elaborate the responsibilities and obligations of both the parties to the agreement.
- ii. Tender documents or agreements shall specify the time of starting of work and time of completion of work (TOC), which may reduce chances for unrealistic time targets and delay in progress of work.
- iii. The obligations of owner such as supply of power to the site, getting sanction for project from statutory authorities, timely handing over of the site, and ensuring the law-and-order at the site should be fulfilled.
- iv. Bidder or contractor shall study the site conditions such as access to site facility for transport and storage of materials, availability of water and power, etc. before tendering for the work and make provisions for them in their offer.
- v. Better administration and planning by both contractor and client can reduce most of the issues related to material, labour and equipment.
- vi. Pre-contract negotiations, formulation of sound contract agreements, project schedule, documentation and records can help for easier settlement of claims.
- vii. Better contractor selection process, reconfiguration of payment schedules, and escalation payments based on market price can reduce the financial difficulties of contractors to a greater extent.
- viii. Financial difficulties at the client's side can be solved by flexible payment plans and securing the supplies with bank security.
- ix. A few of the measures for design changes can be thorough pre-bid studies, site visits, a clear design philosophy and design management methodology, and deadlines for design delivery.
- x. Usage of advanced tools such as Building Information Modelling (BIM) along with 3D/4D systems can also reduce possible chances of design changes.
- xi. A proper plan for the Resettlement & Rehabilitation (R&R) of project-affected individuals and families may reduce disruptions for the general public, and it also helps to build goodwill of the public.

Hence, this study has identified potential causes of disputes in construction projects. It can help professionals in the early identification of the factors causing disputes thus eliminating every chance of dispute so that projects can be implemented easily, without time or cost overrun.

References

1. Rauzana A (2016) Causes of conflicts and disputes in construction projects. *IOSR J Mech Civil Eng* 13(05):44–48
2. Francis M, Ramachandra T, Perera S (2022) Disputes in construction projects: a perspective of project characteristics. *J Leg Aff Disput Resolut Eng Constr* 14(2):04522007
3. Sinha M, Wayal AS (2007) Dispute causation in construction projects. *IOSR J Mech Civil Eng (IOSR-JMCE)*
4. Mante J, Ndekugri I, Ankrah N, Hammond F (2012) The influence of procurement methods on dispute resolution mechanism choice in construction. In: *Proceedings on 28th annual ARCOM conference*, pp 979–988
5. Cakmak E, Cakmak PI (2014) An analysis of causes of disputes in the construction industry using analytical network process. *Proc Soc Behav Sci* 109:183–187
6. Osman I, Ataei H, Seyrfar A (2022) Differing site conditions: clarifying misunderstandings to reduce costly litigation. *J Leg Aff Disput Resolut Eng Constr* 14(2):04522002
7. Naji KK, Mansour MM, Gunduz M (2020) Methods for modeling and evaluating construction disputes: a critical review. *IEEE Access* 8:45641–45652
8. Tabish SZS, Jha KN (2023) Dispute avoidance in public construction projects. *J Leg Aff Disput Resolut Eng Constr* 15(1):04522033
9. Kumaraswamy MM (1997) Conflicts, claims and disputes in construction. *Eng Constr Archit Manag* 4(2):95–111
10. Seker S, Zavadskas EK (2017) Application of fuzzy DEMATEL method for analyzing occupational risks on construction sites. *Sustainability* 9(11):2083
11. Sun WY, Lin WT (2011) Application fuzzy DEMATEL to develop a cause-and-effect model of risk in supply chain. In: *2011 International conference on management and service science*. IEEE, pp 1–4
12. Gebrehiwet T, Luo H (2017) Analysis of delay impact on construction project based on RII and correlation coefficient: empirical study. *Proc Eng* 196:366–374

Investigating the Characteristics of Bitumen Treated with Textile Pyrolysis Oil



Yugaj G. Chaudhari, Saurabh E. Shinde, and Namdao A. Hedao

Abstract As the population explodes, the amount of Municipal solid waste generated is also increasing while an effort is made to mitigate the problem of plastic and rubber, Textile waste is often neglected; nearly 16–20 tons per day is disposed of by burning or landfilling. However, it can be utilized in various sustainable applications, such as modifying bitumen. In this study, Textile Pyrolysis Oil (TXPO) modified bitumen was produced by incorporating TXPO at concentrations of 1, 2, and 3% of the total blend weight. The effects of TXPO on the binder were analyzed through tests measuring penetration grade, softening point, apparent viscosity, and mixing and compaction temperatures. Results indicate that adding TXPO to the base bitumen increased penetration values and slightly decreased the softening points of the modified bitumen. Based on dynamic viscosity tests, it was observed that viscosity increased with increasing TXPO concentration. Furthermore, the mixing and compaction temperatures decreased as the modifier content increased. The TXPO-modified bitumen exhibited suitable properties for use as an alternative to base bitumen in pavement applications in low-temperature regions. Additionally, it is a sustainable solution as it incorporates Municipal solid waste into the production of the modifier.

Keywords Textile pyrolysis oil · Municipal solid waste · Modified bitumen · Pyrolysis oil · Textile waste etc.

Y. G. Chaudhari (✉) · S. E. Shinde · N. A. Hedao
COEP Technological University, Pune, Maharashtra, India
e-mail: yugajgc21.civil@coep.ac.in

1 Introduction

As the world's population continues to grow, municipal waste is becoming an increasingly significant environmental problem. In addition, the construction industry is known for its substantial carbon footprint and impact on the environment. Therefore, finding sustainable practices for road construction is essential. One way to address these issues is by using recycled materials in pavement construction. The use of modifiers in pavement construction is a well-established practice to enhance the performance of bitumen. It can be modified with various additives to improve its physical and mechanical properties, such as increasing its flexibility, durability, and resistance to ageing and cracking. Pyro-oil, a byproduct of pyrolysis, is one such modifier that has shown promise in the modification of bitumen [10]. Pyrolysis is a process of heating organic materials in the absence of oxygen, producing a liquid product called pyro-oil.

Hadole et al. [10] attempted to mix High density polyethylene (HDPE) pyrolysis oil with Viscosity Grade (VG) 30 which resulted in improvements in surface free energy of the binder and it also improved the polarity of the base binder. Ageing of base bitumen decreases the work of adhesion but addition of HDPE pyro oil restricted the same. Zhang et al. [13] modified bitumen with bio-oil obtained from pyrolysis process, and conducted various tests such as penetration test, softening point, ductility test and viscosity test as well. Bio oil modified asphalt has lower softening point and lower viscosity as compared to base asphalt, the performance of Bio oil modified asphalt was much better in cold environment than in high temperature zones.

Kulkarni and Ranadive [11] produced pyro oil obtained from Low density polyethylene (LDPE) plastics which was sourced from municipal solid waste and mix into VG10 bitumen and testes were conducted at various temperatures. It was observed that addition of 20% pyro oil extracted using LDPE plastic waste to VG10 bitumen was best suited to make modified cutback and can be used as track coat between 2 layers of bituminous pavements. Al-Sabaeei et al. [1] examined the physical and high temperature rheological performance of Crude palm oil (CPO) and Tyre pyrolysis oil (TPO) composite by conducting various physical tests as well as rheological tests on the modified bitumen. The results for physical properties showed that addition of upto 5% CPO and varying TPO content resulted in higher softening point and dynamic viscosity but the penetration values were found to be decreasing.

Almost all the major waste materials which are produced in large quantities and fill up the landfills are being pyrolyzed and the oils are being used to modify or rejuvenate bitumen. Textile waste is a significant environmental concern, with millions of tonnes of textiles being discarded every year. Recycling textile waste to modify bitumen can help to reduce the environmental impact of both the waste and the pavement construction industry. In this study, we aim to investigate the use of textile waste in pavement construction, specifically in the modification of bitumen using Pyrolysis oil. The objective of this study is to examine the short-term aging behavior of textile pyrolysis oil modified bitumen by evaluating various physical properties, and effect of addition of textile pyrolysis oil on mixing and compaction temperature of binder.

2 Experimental Investigation

2.1 Material

2.1.1 Bitumen

VG 30 grade bitumen was used as base bitumen as this is widely used in India for paving applications. This bitumen was obtained from Yeravada hot mix plant, Pune.

2.1.2 Textile Pyrolysis Oil

The textile waste required for the Pyrolysis process was sourced from local tailors and dumping yards near Pune. Textile Pyrolysis-Oil (TXPO) was extracted at pilot pyrolysis plant installed in the Civil Engineering Department, COEP Technological University, Pune. The process of pyrolysis was carried out at 450–500 °C [12]. The oil obtained after the pyrolysis process was used as a modifier for bitumen.

2.2 Preparation of Modified Binder

To ensure fluidity of the bitumen the samples were placed in oven at 160 °C before mixing it with TXPO. The specific content of TXPO was added to the base bituminous binder gradually at first then it was mixed at the rate of 3000 rpm for 15 min and 5000 rpm for 5 min at the temperature of 140–160 °C using a high shear mixer to ensure a homogenous mixture [10]. Three Samples were prepared at dosages of 1, 2 and 3% of TXPO by total weight of the base bitumen [8, 9].

3 Experimental Research

3.1 Physical Properties

The physical properties of bitumen such as softening point, penetration value, ductility, viscosity carried out in laboratory using ASTM D36 [5], ASTM D5 [7], ASTM D113 [2] and ASTM D 4402 [6] respectively.

3.2 Rolling Thin Film Oven Test

Rolling Thin Film Oven Test is an extensively used laboratory test carried out to replicate the short-term ageing of asphalt binders. It assesses the susceptibility of binders when subjected to oxidative ageing and hardening when exposed to high temperatures and air over time. This test is an important tool for assessing the ageing process underwent while mixing, transportation and compaction of the bituminous mix. This test is carried out for 85 min at the temperature of 163 °C in accordance with ASTM D2872 [4]. Table 1 represents the physical properties of Textile Pyrolysis Oil modified bitumen while Table 2 shows the physical properties of modified bitumen after short term ageing process.

Table 1 Physical properties of unaged bitumen

Binder type	Penetration at 25 °C (1/10th of mm)	Softening point (°C)	Ductility (mm)	Viscosity at 135 °C (Cp)
VG30	50	47.5	75	500
VG30 + 1% TXPO	53	47.7	84	425
VG30 + 2% TXPO	60	47	88	375
VG30 + 3% TXPO	84	46.5	91	350

Table 2 Physical properties of bitumen after short term aging

Binder type	Penetration at 25 °C (1/10th of mm)	Softening point (°C)	Ductility (mm)	Mass change after RTFO test
VG30	45	70	70	0.00
VG30 + 1% TXPO	47	71	81	0.00
VG30 + 2% TXPO	54	60	84	0.58
VG30 + 3% TXPO	75	58	87	0.57

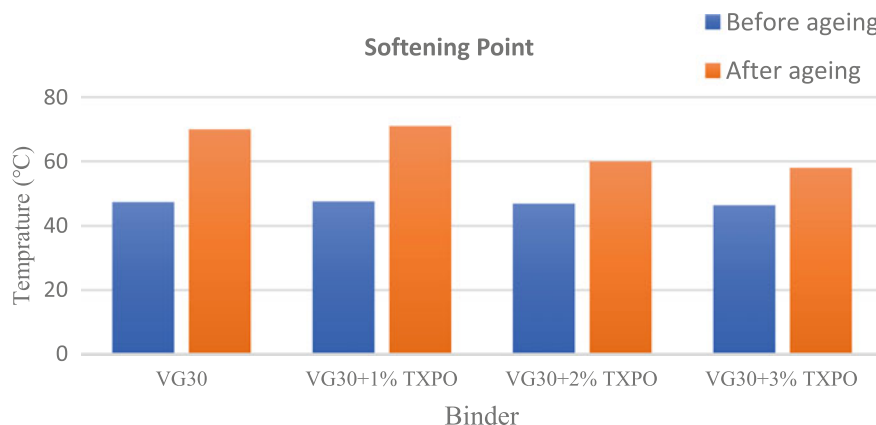


Fig. 1 Softening points of aged and unaged bitumen

4 Results and Discussion

4.1 Softening Point

The softening point test was carried out in the laboratory under conditions given in the ASTM [5] code and the results are presented in the bar chart in Fig. 1.

When the base binder is modified with 1% TXPO the softening point increases slightly before ageing and after short term ageing. It can be noted that the results start to decline as we increase the amount of TXPO to 2 and 3% both before ageing and also after short term ageing. It is also observed that as the TXPO content increases the softening point decreases after the short-term ageing process. This can be attributed to increased workability and enhanced low-temperature properties.

4.2 Penetration Test

The results of Penetration test are shown in Fig. 2.

It is observed that the penetration values decrease by 10–12% after RTFO test. The base binder and 1% TXPO modified A show almost the same values both before and after short term ageing but as the binder content is increased to 2 and 3% a sharp spike can be seen before ageing as well as after short term ageing of the base binder. As the TXPO content increases, the penetration also increases along with it. Due to these properties like adhesion and cohesion with materials are improved, and it also enhances the low-temperature performance of the base bitumen.

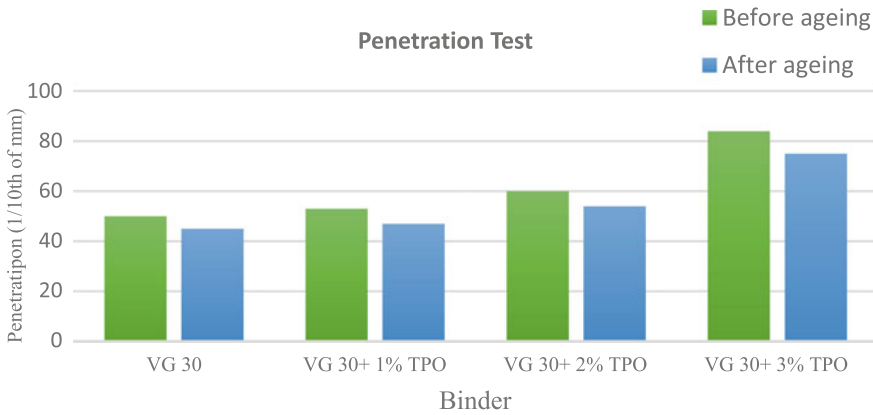


Fig. 2 Penetration values before and after short-term ageing

4.3 Ductility Test

Ductility test was carried out before ageing as well as after ageing and the results of both are compared below in Fig. 3.

Constant increase can be seen in the ductility of the TXPO modified bitumen whether it may be 1, 2 or 3% before short term ageing process. A reduction in ductility is observed in the base binder as well as the modified binder after the ageing process (Rolling Thin Film Oven test) for 1, 2 and 3%. It can be observed that the ductility increases due to the addition of TXPO in the base bitumen. It enhances the performance of pavement due to variations in temperature.

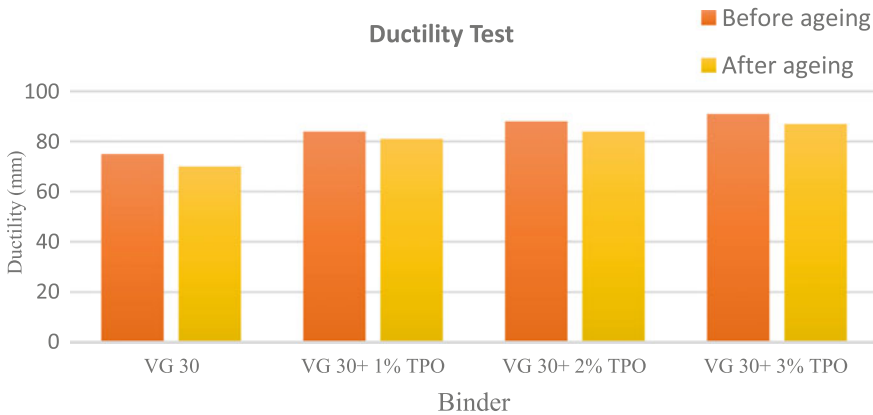


Fig. 3 Comparison between ductility of the un-aged and aged binder

Table 3 Viscosity of modified bitumen at 135 and 165 °C

Binder Type	Viscosity at 135 °C (cP)	Viscosity at 165 °C (cP)
VG30	500	125
VG30 + 1% TXPO	425	125
VG30 + 2% TXPO	375	100
VG30 + 3% TXPO	325	75

4.4 *Dynamic Viscosity*

This test was carried out on Brookfield Viscometer with respect to ASTM [6] standards, the results of this tests are shown in Table 3.

According to Table 3, the viscosity at 135 °C is decreasing constantly when the modifier content is increased from 1 to 3% uniformly. No change was observed between base binder and 1% TXPO modified bitumen at 165 °C but when the modifier content was further increased to 2 and 3% a decrease was observed in the viscosity. Overall, the reduction in viscosity can significantly positively affect performance and workability in asphalt pavements.

4.5 *Determination of Mixing and Compaction Temperature*

The mixing and compaction temperature of base bitumen and modified bitumen was calculated as per guidelines given in ASTM D2493 [3]. Viscosity observed at 135 °C and 165 °C plotted against temperature in Fig. 4. Mixing and compaction temperature calculated using range specified in ASTM D 2493 [3].

Mixing and compaction temperatures obtained from Fig. 4 are tabulated below.

Figure 4 and Table 4 show that mixing and compaction temperature decreases with respect to the base binder. It is also observed that the mixing and compaction temperature decreases as we increase the content of TXPO.

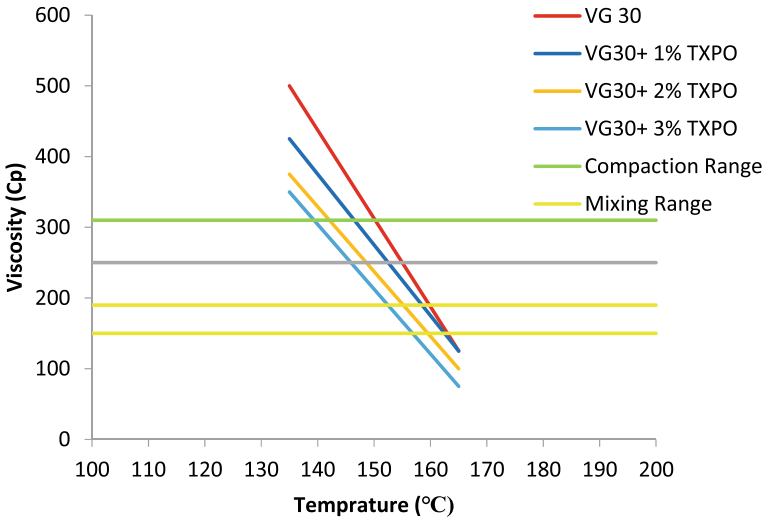


Fig. 4 Graphical representation of mixing and compaction temperature

Table 4 Mixing and compaction Temperature

Binder type	Mixing temperature range (°C)	Compaction temperature range (°C)
VG30	160–164	150–155
VG30 + 1% TXPO	158–163	146–153
VG30 + 2% TXPO	155–159	142–149
VG30 + 3% TXPO	152–157	140–146

5 Conclusion

This study was aimed towards the investigation of short-term ageing and mixing and compaction temperature of VG 30 grade bitumen, with and without the addition of Textile Pyrolysis Oil. All experiments were carried out in the laboratory in accordance to ASTM standards. Dosages of 1, 2 and 3% by the weight of the binder were utilized to create the modified binder used for the tests.

Several alterations in the bitumen’s properties were seen after the modifier and binder had been properly mixed. The mixture’s stiffness was reduced due to the addition of Textile Pyrolysis Oil, making it considerably easier to work with. Furthermore, no appreciable mass loss was found during the mixing and compaction processes brought on by heat and air, even after the mix had undergone brief aging.

The modifier makes the binder more flexible, which can improve fracture resistance because of its higher penetration than the base bitumen. Furthermore, as the modifier dosage grew, the viscosity of the binder reduced dramatically. This decrease in viscosity contributed to better bitumen-aggregate adhesion and cohesiveness.

Another noteworthy finding was that the use of textile pyrolysis oil derived from textile waste brought about a drop in mixing and compaction temperature. As a result, the energy used during pavement construction can be reduced. This not only provides a sustainable option to minimize textile waste but also makes the construction of sustainable pavements simpler.

The addition of 1% of TXPO to the base bitumen gives almost the same properties as the base bitumen in both unaged phase and also after short term ageing. The mixing of 2 and 3% of TXPO to the base binder can enhance the performance of binder in cold weather conditions.

In conclusion, the use of VG 30-grade bitumen treated with Textile Pyrolysis Oil demonstrated a variety of favorable impacts. The mixture grew less rigid and more malleable, with good adhesion and cohesiveness. Furthermore, the use of the modifier lowered energy consumption during construction and gave a sustainable solution to dealing with textile waste while building environmentally friendly pavements.

Author's Contributions Yugaj C. and Saurabh S. have carried out all the experimentation works as mentioned in ASTM standards under the guidance of Dr. N. A. Hedao. The manuscript was written by Yugaj C., Saurabh S. and Dr. N. A. Hedao.

References

1. Al-Sabaei A, Napiah M, Sutanto M, Alaloul W, Bala N (2021) Effects of tire pyrolysis oil (TPO) on the rheological properties of bitumen. *IOP Conf Ser Mater Sci Eng* 1144(1)
2. ASTM D113–17 A (2017) Standard method of test for ductility of asphalt materials. ASTM International 11(2016)
3. ASTM D2493 (2016) Standard practice for viscosity—temperature chart for asphalt binder. ASTM International
4. ASTM D2872 (2012) Standard test method for effect of heat and air on a moving film of asphalt (rolling thin-film oven test). In ASTM International
5. ASTM D36/D36M (2014) Standard test method for softening point of bitumen (ring-and-ball apparatus). In ASTM International
6. ASTM D4402–2015 (2015) Standard test method for viscosity determination of asphalt at elevated temperatures using a rotational viscometer. ASTM International, West Conshohocken, PA 4
7. ASTM D5/D5M-20 (2020) Standard test method for penetration of bituminous materials. In ASTM International, West Conshohocken
8. Bhagat NT, Hadole HP, Ranadive MS (2023) Oxidative aging characterization of pyro-oil modified binders using Fourier transform infrared spectroscopy. *Adv Sci Technol Res J* 17(1):140–149
9. Hadole HP, Suryawanshi SD, Ranadive MS (2021) Evaluation of moisture susceptibility of pyro-oil modified bitumen by surface free energy approach. *Lecture Notes Civil Eng 118 LNCE*
10. Khapne V, Hadole H, Ranadive M (2020) Assessment of anti-stripping property of pyro-oil modified bituminous mixes using surface free energy approach. In: International conference on transportation and development 2020: highway and airfield pavements—selected papers from the international conference on transportation and development 2020, pp 127–137
11. Kulkarni SB, Ranadive MS, Asce M (2020) Modified cutback as tack coat by application of pyro-oil obtained from municipal plastic waste: experimental approach. [https://doi.org/10.1061/\(ASCE\)](https://doi.org/10.1061/(ASCE)1061)

12. Miranda R, Sosa-Blanco C, Bustos-Martínez D, Vasile C (2007) Pyrolysis of textile wastes: I. Kinetics and yields. *J Anal Appl Pyrol* 80(2):489–495
13. Zhang X, Zhang K, Wu C, Liu K, Jiang K (2020) Preparation of bio-oil and its application in asphalt modification and rejuvenation: a review of the properties, practical application and life cycle assessment. In: *Construction and building materials*, vol 262. Elsevier Ltd. <https://doi.org/10.1016/j.conbuildmat.2020.120528>

Adaptive Neuro-Fuzzy Systems and Ensemble Methods in Joint Shear Prediction and Sensitivity Analysis



Shruti Shekhar Palkar and T. Palanisamy

Abstract In the absence of ductile design, beam-column joints form weak links in the frame during seismic activities, hence jeopardizing the entire structure. Deducing from the views of researchers, estimation of joint shear strength of RC beam-column joint is a necessity with a complexity. This complexity highlights the importance of machine learning models due to their data handling and predictive capabilities. This study used 233 beam-column joints with 132 exterior and 101 interior joints for training and testing the ensemble machine-learning models and an Adaptive neuro-fuzzy inference system. The performance indices of the models built and their comparison is carried out to find the optimum model to be deployed. The sensitivity analysis of the features considered was conducted to infer the differences in exterior and interior beam-column joints' behavior.

Keywords Beam column joint · Machine learning · ANFIS · Sensitivity analysis · Joint shear

1 Introduction

Inaccessibility to the area where crucial force mechanism takes place resulted in the assumption of rigidity of the beam-column joint. However, the account of seismic action highlighted the importance of ductility in the structure, which ensures that inelastic rotations dissolve the energy. The formation of these inelastic rotations, namely plastic hinges, is crucial to be absent in beam-column joints, as the failure of the beam-column joint jeopardizes the stability of the entire structure.

S. S. Palkar (✉) · T. Palanisamy
Department of Civil Engineering, National Institute of Technology Karnataka, Surathkal, India
e-mail: shrutipalkar586@gmail.com

T. Palanisamy
e-mail: tpalanisamycivil@nitk.edu.in

The strut and truss mechanism can justify the shear stress field in the joint core due to compression and tension forces in seismic action. The strut mechanism justifies the formation of a diagonal strut with a diagonal compressive force resulting from concrete compressive force and bond forces due to vertical and horizontal joint shear reinforcement. In a stress field, a central diagonal band in compression results in tension in a diagonal band across perpendicularly. The shear contribution of stirrups is negligible till the joint core can resist the diagonal compressive stress across the joint. However, the increase in load and cycles will cause softening effect and crack splitting in concrete, making the stirrups and column bars come into action. Hence joint shear force is a sum of the contribution of the strut and truss mechanism. With an increase in the shear strength contribution of the diagonal strut mechanism, the shear strength contribution of the truss mechanism tends to decrease, indicating the transformation of stresses in a joint. The complex combination of multiple mechanisms in beam column joints, along with the behavior of surrounding materials, makes it difficult to predict joint shear strength. The models considering empirical assumptions and simplifications using parameters based on the mechanisms justified by the theoretical analysis exhibit varied importance of parameters affecting shear strength. To address this, identifying patterns in input and output parameters is crucial for joint design. Machine learning helps to find these patterns and determine the importance of parameters in achieving the desired output [1].

2 Database Development

2.1 Dataset

The dataset used in this endeavor is derived from literature and consists of 233 beam-column joints, which include 101 interior and 132 exterior beam-column joints. All the beam-column joint data was chosen to be without eccentricity and subjected to monotonic or cyclic loading [2–38].

2.2 Input and Output

The variables used for the training and testing of data to predict the joint shear strength of beam-column joints are the percentage of beam bottom reinforcement ratio, cubic compressive strength of concrete, axial load factor, Bond Index, and column reinforcement percentage (Tables 1, 2 and 3).

$$\text{Area of joint} = b_j \times h_c \tag{1}$$

$$\text{where, } b_j = \begin{cases} \min(bc; bb + 0.5hc) \text{ if } bc > bb \\ \min(bb; bc + 0.5hc) \text{ if } bb > bc \end{cases}$$

$$\text{Stress} = \frac{\text{Experimental shear force at joint}}{\text{Area of joint}} \tag{2}$$

Table 1 Input features

No	Variable	Symbol	Formula
1	Bottom reinforcement ratio percentage of beam	Pb	$\frac{Astb \times 100}{bb \times hb}$
2	Concrete compressive strength	fc	fc
3	Axial load factor	P	$\frac{Pu}{bc \times hc \times fc}$
4	Column reinforcement percentage	Pc	$\frac{Astc \times 100}{bc \times hc}$
5	Bond index	B	$\frac{fy \times db}{2 \times hc \times \sqrt{fc}}$

Here $Astb$ —bottom reinforcement area of beam, bb —width of beam, hb —depth of beam, fc —cubic compressive strength of concrete, Pu —axial load on column, hc —height of column, bc —width of column, db —average diameter of bars used, fy —yield strength of reinforcement, $Astc$ —area of column reinforcement

Table 2 Properties of interior beam column joint dataset

No	Variable	Mean	Standard deviation	Median	Min	Max
1	Pb	1.46	1.38	1.38	0.67	3.09
2	Fc	36.46	14.61	32	18.20	81.2
3	P	0.14	0.14	0.11	0	0.6
4	Pc	2.97	1.3	2.91	0.65	7.56
5	B	2.42	0.98	2.16	1.23	6.46

Table 3 Properties of exterior beam column joint dataset

No	Variable	Mean	Standard deviation	Median	Min	Max
1	Pb	1.05	0.47	0.88	0.3	3
2	Fc	34.36	15.96	31.60	15	96.5
3	P ara>	0.1	0.1	0.08	0	0.4
4	Pc	1.76	0.69	1.81	0.21	3.77
5	B	2.41	0.81	2.28	1.14	5.29

3 Methodology

3.1 Machine Learning Models

The exterior and interior beam-column joint dataset is split into 70–30% for training and testing. Optimal parameters for each model were found using the grid search technique and cross-validation. The grid search technique involves specifying a grid of hyper-parameter values to search over and then training and evaluating the model with all possible combinations of these hyper-parameter values to find optimal parameters.

Decision Tree The decision tree starts with a root node with a feature to split the data set into two parts to minimize the mean square error further by iteratively calculating the mean squared error for all splits and choosing the split with the most negligible mean square error value. However, reducing to the leaf node till the mean square error is zero causes overfitting, which is avoided by cross-validation. The maximum depth in the decision tree model for the dataset in this study is 15. A slight change in data may lead to an entirely different decision tree. This sensitivity to data results in locally optimal solutions rather than a generalized model (Figs. 1 and 2).

Ensemble Methods Ensemble methods combine multiple models to improve predictive power and hence significantly improve performance. It fundamentally works on creating strong learners from a set of individual weak learners. Bagging and Boosting are the two types of ensemble modeling. Bagging (Bootstrap Aggregating): Bagging involves training multiple instances of the same model on different subsets of the training data obtained by random sampling with replacement (i.e., bootstrapping) from the original training data. The predictions of these individual

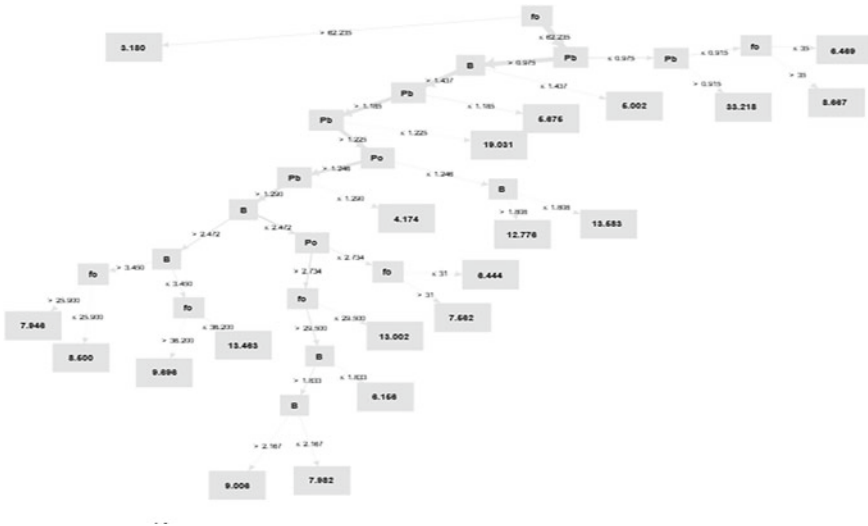


Fig. 1 Decision tree: exterior beam column joint

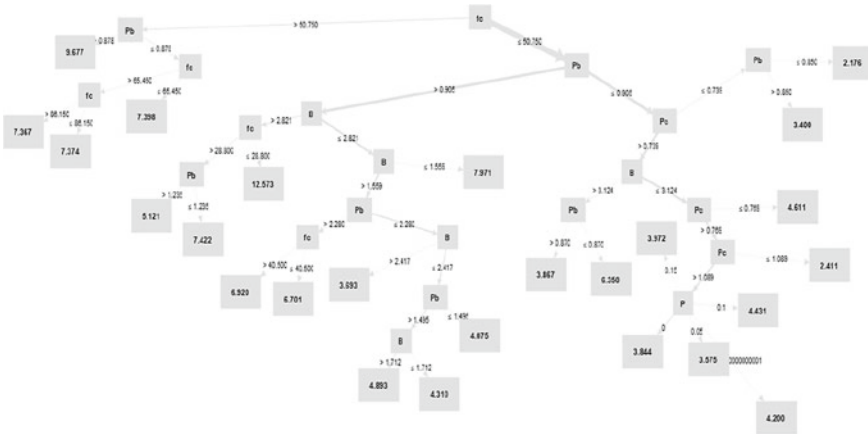


Fig. 2 Decision tree: interior beam column joint

models are combined by taking a majority vote or averaging to make the final prediction. Boosting: Boosting is an iterative technique that adjusts the weights of training instances to give more importance to misclassified instances, thereby focusing on complex examples.

Random Forest Random Forest modeling constructs multiple decision trees by randomly selecting subsets of the training data (with replacement) and subsets of features. These subsets are used to train individual decision trees. Each decision tree is grown using a criterion such as mean squared error (MSE), which measures the variability in the target values. The final prediction is the average of the predicted values from all the decision trees. Random Forests for regression are particularly useful when dealing with nonlinear relationships between features and the target variable, as they can capture complex interactions and patterns in the data. The optimized number of trees for the interior and exterior beam column joint dataset is 140 and max depth of 7 is achieved.

Gradient Boosted Trees In gradient boosting target outcomes for each case are set based on the gradient of the error with respect to the prediction. After creating first decision tree second model tree is created based on the learning from previous model tree. Hence reducing the prediction from each case an optimized model is built. The optimal parameters achieved for the interior and exterior beam column joint dataset are 150 trees, with a maximum depth of 4 at learning rate 0.1.

ANFIS (Adaptive Neuro Fuzzy Inference System) ANFIS, which stands for Adaptive Neuro-Fuzzy Inference System, is a hybrid model that integrates fuzzy logic (FL) and artificial neural networks (ANN) to overcome the limitations of FL’s subjective membership function and rule selection, as well as ANN’s black box nature. ANFIS combines the fuzzy reasoning capability of FL with the learning and generalization capabilities of ANN to create a neuro-fuzzy system capable of providing transparent and interpretable outputs while also being adaptable and

capable of capturing complex patterns in data through data-driven learning during training.

The ANFIS architecture can be fundamentally expressed in 5 layers:

Layer 1: Input node with membership functions—The input data is fuzzified using membership functions in this layer. The Gaussian membership function was applied to fuzzify the input data in this specific model. The Gaussian membership function is a bell-shaped curve that assigns a membership value to each input data point based on its proximity to a center and a spread parameter.

Layer 2: Fuzzy rule application and firing strength calculation—In this layer, the fuzzy rules, defined in the “if” and “then” format, are applied to the fuzzy sets obtained from Layer 1. The firing strength of each rule is calculated using a product operation, which is the multiplication of the membership values of the input data points associated with that rule (Figs. 3, 4 and 5).



Fig. 3 Schematic diagram of ANFIS

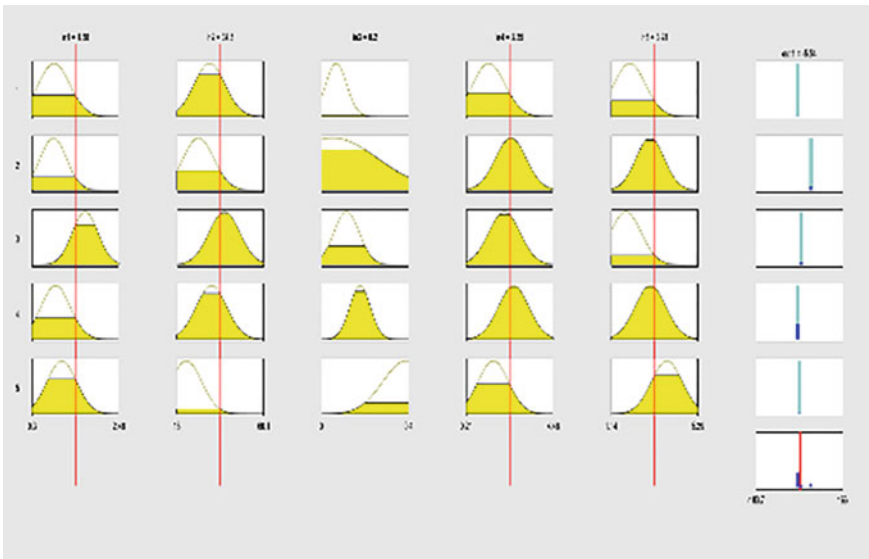


Fig. 4 Rules for EBCJ

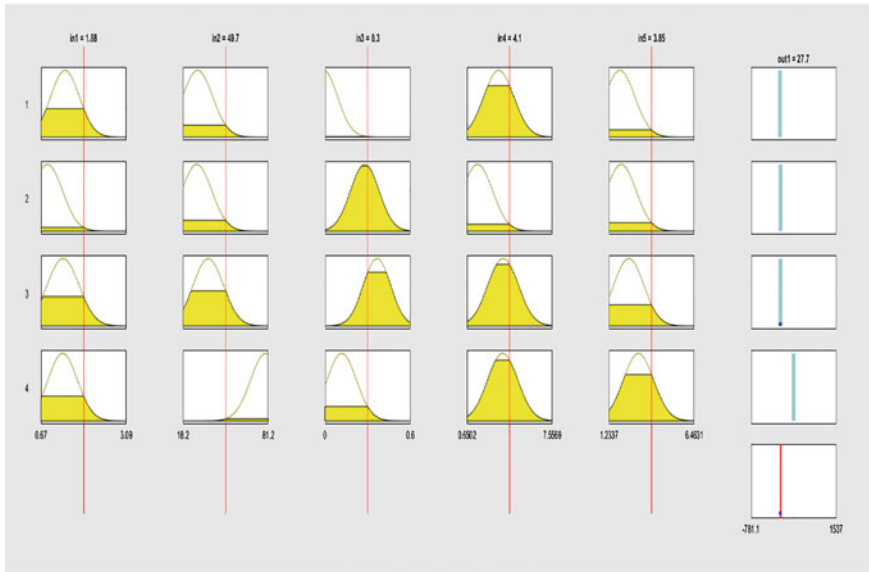


Fig. 5 Rules for IBCJ

Layer 3: Normalization of firing strength—The firing strengths calculated in Layer 2 are then normalized using weights.

Layer 4: Adaptive function with normalized firing strength—In this layer, an adaptive function is applied to the normalized firing strengths obtained from Layer 3. This adaptive function adjusts the parameters of the fuzzy logic rules based on the error between the predicted output and the actual output. It uses a learning algorithm to update the parameters during the training process.

Layer 5: Output generation after de-fuzzification—The final output is generated in this layer after de-fuzzification, which converts the fuzzy output obtained from Layer 4 into a crisp value. De-fuzzification methods such as centroid or weighted average can obtain a single output value from the fuzzy output (Fig. 6).

The membership functions in MATLAB were generated using a sub-clustering algorithm with specific training parameters, including a range of influence of 0.5, a squash factor of 1.25, an accept ratio of 0.5, and a reject ratio of 0.15, as the grid partitioning method produced an overfitting solution resulting high error in test data set. ANFIS model for exterior beam column joint was generated using 524 nodes, 1458 linear parameters, 30 nonlinear parameters and 243 fuzzy rules. ANFIS model for interior beam column joint was generated using 56 nodes, 24 linear parameters, 40 nonlinear parameters and 4 fuzzy rules.

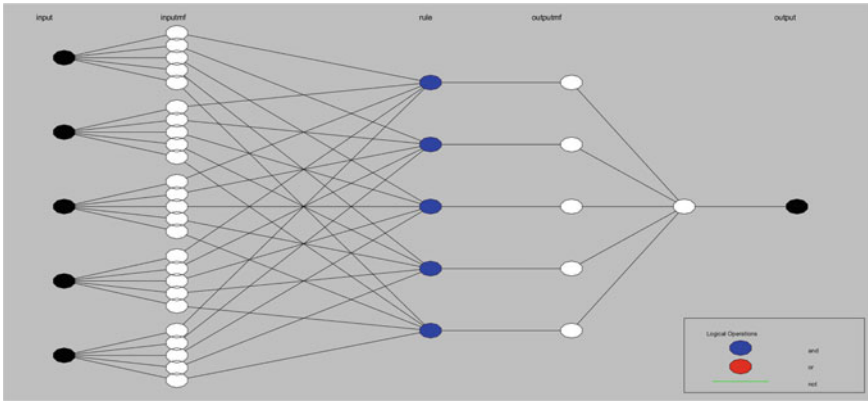


Fig. 6 ANFIS Architecture

4 Results and Conclusion

4.1 Performance of Models

Table 4 gives Root mean square error (Eq. 3) values of the model and Fig. 7a–h provide the visual representation of actual and predicted values from the respective models using Lift chart.

$$RMSE = \sqrt{\frac{\sum_{i=1}^N (x_i - \hat{x}_i)^2}{N}} \tag{3}$$

The Lift Chart is a useful visualization tool in machine learning for assessing the effectiveness of a predictive model in identifying positive outcomes and understanding its performance compared to random chance or a baseline model. Regression analysis determines the best-fitting line on a scatter plot by minimizing the sum of squared differences between observed data points and predicted values. Scatter plot with regression line assesses the line’s fit to the data: close points and clear pattern suggest a good fit, while significant deviations or lack of pattern indicate a poor

Table 4 Performance Index of Machine learning models

ML model	RMSE (Root mean squared error)	
	EBCJ	IBCJ
Decision tree	1.872	2.729
Random forest	1.411	3.446
Gradient boosted trees	1.939	3.126
ANFIS	3.448	4.206

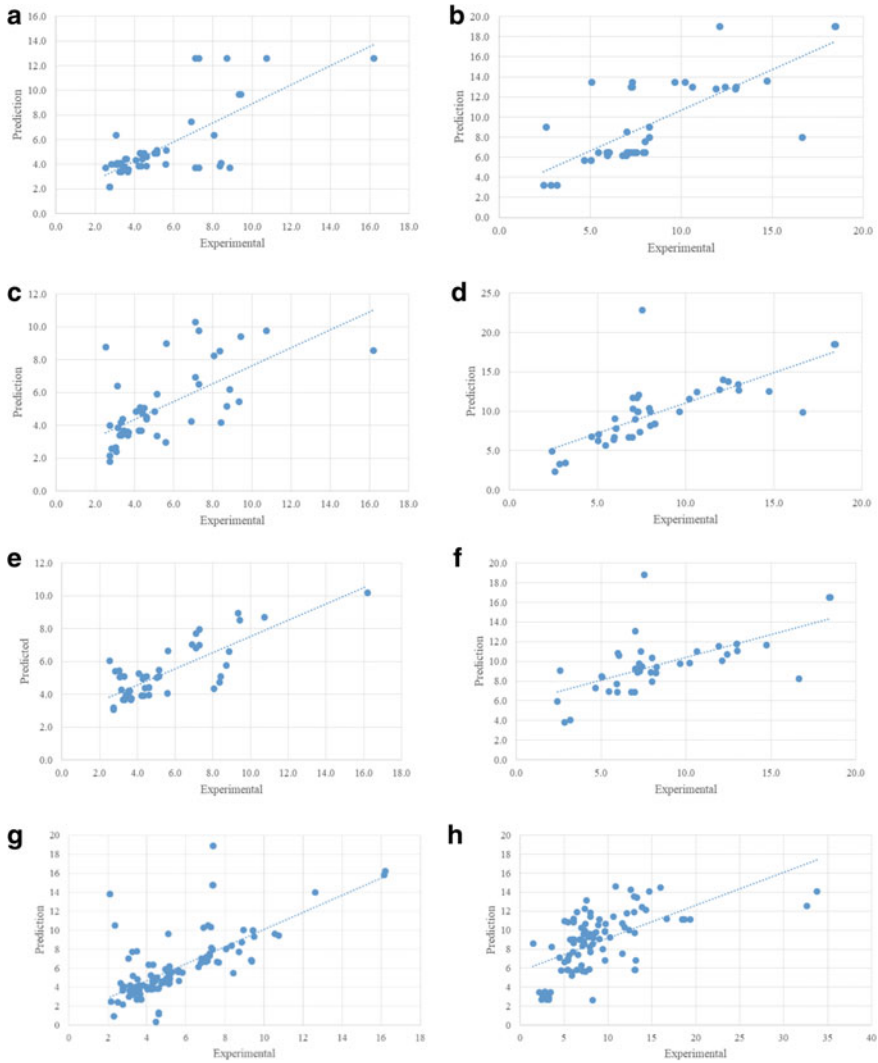


Fig. 7 a Decision Tree for EBCJ. b Decision Tree for IBCJ. c Gradient Boosted Tree for EBCJ. d Gradient Boosted Tree for IBCJ. e Random Forest for EBCJ. f Random Forest for IBCJ. g ANFIS for EBCJ. h ANFIS for IBCJ

fit. Considering the RMSE values and Lift chart, Random Forest model gives better results for EBCJ and Decision tree gives better results for IBCJ; which highlights the extensive dependency of ML model on dataset.

4.2 Importance of Input Features

The significance of the input feature is evaluated by assigning it a weight, which is determined by summing the improvements it contributes to splitting data at nodes in decision tree-based algorithms. This improvement can be measured using criteria such as information gain, Gini index, or least squares. The feature with more significant total improvements, considering all nodes where it is utilized for splitting, and weighted by the number of samples, is considered more important for predicting the target variable. The specific method for calculating feature importance varies depending on the algorithm and criterion used. The weights from all the models were considered for a cumulative and generalized effect and hence determine the important features (Figs. 8 and 9).

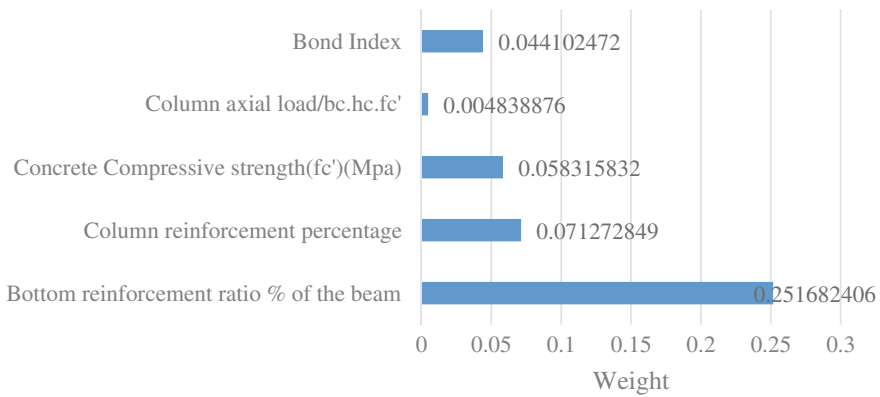


Fig. 8 Feature importance for EBCJ

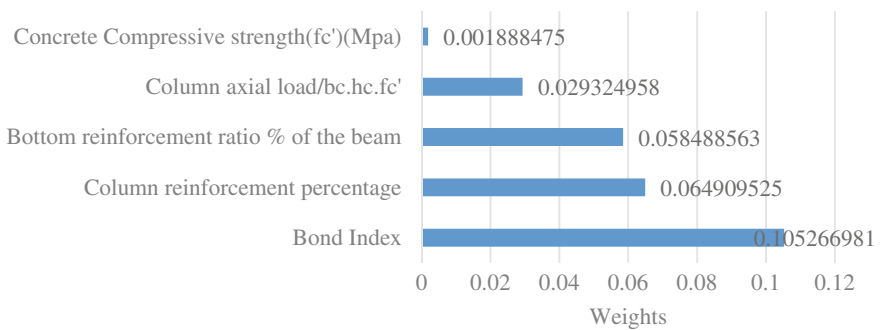


Fig. 9 Feature importance for IBCJ

4.3 Conclusions

In an interior beam-column joint within the core, high bond stresses are developed as confinement of the concrete perpendicular to the beam bar is always present. The confinement can be achieved in the form of axial load or reinforcement. Bond forces induced in concrete at four sides generate a diagonal compressive field; hence it is necessary to estimate the distribution of bond forces to assign joint shear force for strut and truss mechanisms [16]. This justifies the feature importance of the Bond Index and features involving reinforcement values.

The Joint shear stress values at exterior joints were less than that of an interior beam-column joint due to the presence of a single beam joined to the column. The beam reinforcement detailing plays a crucial role in exterior beam-column joint shear mechanisms, as during seismic action, the plastic hinge is assumed to be in the beam. Consequently the deduced feature importance of the bottom reinforcement percentage can be justified.

The performance of a machine learning model depends on a combination of factors including data quality and size, feature engineering, model training, model evaluation, computational resources, and data preprocessing. With a dataset enough to deduce and then recur the same results with increase in number of data points will definitely provide a better feature engineering and empirical models particular to the specific joint in the structure. Finding important features is crucial for both understanding and improving model performance. It helps identify the key factors driving predictions, guides model refinement, and enables accurate and practical recommendations. Additionally, the process of finding important features plays a pivotal role in understanding the underlying mechanism of the model and providing guidance for design guidelines.

References

1. Thai HT (2022) Machine learning for structural engineering: a state-of-the-art review. Structures 38(January):448–491. <https://doi.org/10.1016/j.istruc.2022.02.003>
2. Antonopoulos CP, Triantafyllou TC, Asce M (2003) Experimental investigation of FRP-strengthened RC beam-column joints. J Compos Construct 7(1):39–49
3. Baker JW (2007) Measuring bias in structural response caused by ground motion scaling. Pac Conf Earthq Eng 056:1–6. <https://doi.org/10.1002/eqe>
4. Mohammad R, Ehsani FA (1991) Design recommendations to joints ehsani e alamedine.PDF. ACI Struct J 88(3):277–291
5. El Amoury and To ghobarah (2002).pdf. (nd)
6. Faleschini F, Hofer L, Zanini MA, dalla Benetta M, Pellegrino C (2017) Experimental behavior of beam-column joints made with EAF concrete under cyclic loading. Eng Struct 139:81–95. <https://doi.org/10.1016/j.engstruct.2017.02.038>
7. Hwang S, Lee H, Wang K (2004) Seismic design and detailing of exterior reinforced concrete beam-column joints. In: 13th world conference on earthquake engineering, vol 397, pp 1–12
8. Karayannis C, Sirkelis K (2005) Response of columns and joints with spiral shear reinforcement. Comput Methods Exp Measur 41:455–463

9. Khan MI, Al-Osta MA, Ahmad S, Rahman MK (2018) Seismic behavior of beam-column joints strengthened with ultra-high performance fiber reinforced concrete. *Compos Struct* 200(July 2017):103–119. <https://doi.org/10.1016/j.compstruct.2018.05.080>
10. Le-Trung K, Lee K, Lee J, Lee DH, Woo S (2010) Experimental study of RC beam-column joints strengthened using CFRP composites. *Compos B Eng* 41(1):76–85. <https://doi.org/10.1016/j.compositesb.2009.06.005>
11. Liu C (2006) Seismic behaviour of beam-column joint subassemblies. MSc thesis, p 213
12. Megget LM (1974) Cyclic behaviour of exterior reinforced concrete beam-column joints. *Bull N Z Soc Earthq Eng* 7(1):27–47. <https://doi.org/10.5459/bnzsee.7.1.27-47>
13. Pantelides CP, Clyde C, Reaveley LD (2002) Performance-based evaluation of reinforced concrete building exterior joints for seismic excitation. *Earthq Spectra* 18(3):449–480. <https://doi.org/10.1193/1.1510447>
14. Varum H, Rossetto T, Costa A (2012) Cyclic response of RC beam-column joints reinforced with plain bars: an experimental testing campaign. 15Wcee, May 2014
15. Paulay T, Priestley MJN (1992) Seismic design of reinforced concrete and masonry buildings
16. Paulay T, Scarpas A (1981) The behaviour of exterior beam-column joints. *Bull N Z Soc Earthq Eng* 14(3):131–144
17. Rajagopal S, Prabavathy S (2014) Exterior beam-column joint study with non-conventional reinforcement detailing using mechanical anchorage under reversal loading. *Sadhana Acad Proc Eng Sci* 39(5):1185–1200. <https://doi.org/10.1007/s12046-014-0229-6>
18. Realfonzo R, Napoli A, Pinilla JGR (2014) Cyclic behavior of RC beam-column joints strengthened with FRP systems. *Constr Build Mater* 54:282–297. <https://doi.org/10.1016/j.conbuildmat.2013.12.043>
19. Shrestha R, Smith ST, Samali B (2009) Strengthening RC beam-column connections with FRP strips. *Proc Inst Civ Eng Struct Build* 162(5):323–334. <https://doi.org/10.1680/stbu.2009.162.5.323>
20. Tsonos AG (2005) Cyclic load behaviour of reinforced concrete beam-column subassemblages of modern structures. *WIT Trans Built Environ* 81(1999):439–449. <https://doi.org/10.14359/18777>
21. Vatani-Oskouei A (2010) Repairing of seismically damaged RC exterior beam-column connection using CFRP. *J Reinf Plast Compos* 29(21):3257–3274. <https://doi.org/10.1177/0731684410371407>
22. Wang and lee (2004).pdf. (nd)
23. Allam SM, Elbakry HMF, Arab ISE, Dhakal RP, Pan TC, Irawan P, Tsai KC, Lin KC, Chen CH, Gao F, Tang Z, Hu B, Chen J, Zhu H, Ma J, Hwang HJ, Eom TS, Park HG, Noguchi, Hiroshi, Fu J (2017) Seismic performance of strengthened reinforced concrete beam-column joints using FRP composites. *Eng Struct* 10(1):543–557. <https://doi.org/10.1016/j.engstruct.2015.04.021>
24. Zhang X, Li B (2020) Seismic performance of RC beam-column joints constructed with engineered cementitious composites. *J Struct Eng* 146(12):1–15. [https://doi.org/10.1061/\(asce\)st.1943-541x.0002824](https://doi.org/10.1061/(asce)st.1943-541x.0002824)
25. Bindhu KR, Sukumar PM, Jaya KP (2009) Performance of exterior beam-column joints under seismic type loading. *ISET J Earthq Technol* 46(2):47–64
26. Cheung PC, Paulay T, Park R (1993) Behavior of beam-column joints in seismically-loaded RC frames. *Struct Eng Lond* 71(8):129–137
27. Uma SR (2015) Seismic behavior of beam column joints in reinforced concrete moment resisting frames. *Earthquake* 2(7):1–36. <http://www.iitk.ac.in/nicee/IITK-GSDMA/EQ32.pdf>; <http://www.iitk.ac.in/nicee/IITK-GSDMA/EQ31.pdf>
28. Joshi PK (2014) Behaviour of beam-column joint under cyclic loading. *Int J Res Eng Technol* 03(15):749–751. <https://doi.org/10.15623/ijret.2014.0315140>
29. Gopi raju GD, Parthiban P, Student Mt, Professor A (2022) Comparative study on Rc beam column joint using both analytical and experimental method. *Int Res J Eng Technol* 1186–1189. www.irjet.net

30. Choudhury AH, Laskar AI (2020) Effect of hoop reinforcement yielding on the cyclic behavior of beam-column joint. *J Earthquake Eng* 26(6):1–18. <https://doi.org/10.1080/13632469.2020.1784317>
31. Lam E, Shu S, Xue Z, Fang S, Masqood S (2020) Interior beam column joints with nominal joint shear reinforcement versus unsymmetrical chamfers. *Eng Struct* 220(May):110907. <https://doi.org/10.1016/j.engstruct.2020.110907>
32. Prasanth R, Silambarasan G, Chandrikka V (2019) Review on reinforced concrete beam-column joint. *Int Res J Eng Technol* 6(May):509–514
33. Joint ACI-ASCE Committee 352 (2002) Recommendations for design of beam-column connections in monolithic reinforced concrete structures (ACI-ASCE 352-02). Technical report. <http://www.concrete.org/Publications/InternationalConcreteAbstractsPortal.aspx?m=details&i=10333>
34. Pauletta M, Di Marco C, Frappa G, Somma G, Pitacco I, Miani M, Das S, Russo G (2020) Semi-empirical model for shear strength of RC interior beam-column joints subjected to cyclic loads. *Eng Struct* 224(August):111223. <https://doi.org/10.1016/j.engstruct.2020.111223>
35. Chetchotisak P, Arjsri E, Teerawong J (2020) Strut-and-tie model for shear strength prediction of RC exterior beam-column joints under seismic loading. *Bull Earthq Eng* 18(4):1525–1546. <https://doi.org/10.1007/s10518-019-00756-4>
36. Thandavamoorthy TS (2017) Theoretical and experimental investigation of RC beam-column joint 4(August):29–41
37. Au FTK, Huang K, Pam HJ (2005) Diagonally-reinforced beam-column joints reinforced under cyclic loading. *Proc Inst Civ Eng Struct Build* 158(1):21–40. <https://doi.org/10.1680/stbu.2005.158.1.21>
38. Tran MT (2016) Influence factors for the shear strength of exterior and interior reinforced concrete beam-column joints. *Procedia Eng* 142:63–70. <https://doi.org/10.1016/j.proeng.2016.02.014>
39. IS-13920 (2016) Ductile design and detailing of reinforced concrete structures subjected to seismic forces-code of practise
40. Naderpour H, Mirrashid M (2019) Shear failure capacity prediction of concrete beam-column joints in terms of ANFIS and GMDH. *Pract Period Struct Des Constr* 24(2):1–18. [https://doi.org/10.1061/\(asce\)sc.1943-5576.0000417](https://doi.org/10.1061/(asce)sc.1943-5576.0000417)

Technology Landscape for BIM in Construction Site Safety Management



Hire Shalaka , Sandbhor Sayali , and Ruikar Kirti 

Abstract The development of Industry 4.0 has caused the global construction sector to move towards digitization. However, site safety is still one of the ignored aspects in terms of digitizing construction practices. The usage of technology-assisted solutions to support current practices is expanding. Building Information Modelling (BIM) is a noteworthy invention in the construction industry. Based on an intelligent model, BIM combines structured, cross-disciplinary data to provide a digital representation of an asset that lasts the duration of its life. With BIM's potential advantages, safety procedures can be enhanced, and superior safety solutions can be offered. To do so, assessing the prior research and current trends in BIM based site safety management is crucial. The paper aims to provide a technology landscape for BIM in construction site safety through a detailed patentometric analysis using leading database Espacenet. The patent data from the year 2016–2023 is considered for analysis. The selected data is analyzed for country-wise, year-wise patents and it also discusses the IPC, CPC codes for the patents in the arena of BIM for construction safety. Currently, China is leading the forefront of patenting BIM based construction safety solutions. The landscaping has unfolded the fact that BIM based site safety management is an emerging domain. The thorough patentometric analysis presented in this paper summarizes cutting edge innovations. It highlights the prior art as well as provides a pathway for strategic patenting with improved chances of publication and granting of patent thereof.

Keywords Patents · BIM · Safety · Hazards · Construction

H. Shalaka (✉) · S. Sayali

Department of Civil Engineering, Symbiosis Institute of Technology (SIT), Symbiosis International (Deemed University), Lavale, Pune, Maharashtra, India
e-mail: shalaka.hire@sitpune.edu.in

R. Kirti

School of Architecture, Building and Civil Engineering, Loughborough University,
Loughborough, UK

1 Introduction

The Indian construction industry has been one of the fastest-growing sectors in the country, contributing significantly to the economy. According to a report by the Department for Promotion of Industry and Internal Trade (DPIIT), the Indian construction industry is expected to reach a market size of \$1 trillion by 2025, with a projected CAGR of 15.7% during the period 2019-2025 [1]. With the growing scale of construction projects, the complexity is also increasing and handling such a large project requires effective management. One of the critical elements of construction project management is safety. The Indian construction industry has made significant progress in recent years in terms of safety practices and regulations. However, the number of onsite accidents is yet increasing. Every day, 38 individuals in the construction industry in India die as a result of workplace accidents (Indian Express, 2019) [2]. The minimum annual number of fatalities in the Indian construction industry between 2008 and 2012 was 11,614 [3]. These statistics show that it's important to prioritize worker safety and take steps to prevent construction accidents from occurring. However, as the number of construction accidents is continuously rising, it is evident that traditional safety methods are inefficient, and it is necessary to embrace new safety practices [4].

On the other hand, there's a paradigm shift in construction process with Industry 4.0 [5]. The global drive of automation in construction has the potential to revolutionize industry and bring many benefits. Industry.4.0, Artificial Intelligence (AI), big data, automation, the Internet of Things (IoT), blockchain, Building Information Modelling (BIM), and many other recent trends, tools, and technologies have the ability to close the gaps created by inefficient construction techniques [4]. BIM is one of the amazing developments, and its application has improved automation and produced superior competitive advantages as compared to conventional approaches. BIM is "a systematic process for managing and disseminating holistic information generated throughout the development and operation of building design" [6]. BIM includes the information sharing and information management among various project stakeholders [7]. There are several benefits of BIM that span throughout the lifecycle of the construction project. With BIM's potential advantages, safety procedures can be enhanced, and superior safety solutions can be offered. To do so, assessing the prior research and current trends in BIM based site safety management is crucial. The paper aims at providing technology landscape for BIM in construction site safety through a detailed patentometric analysis using Espacenet database.

2 Search Strategy

Discovering the most important records from a dataset is mostly dependent on keyword searches. The combination "AND" and "OR" performs an important part in the classification of records [8]. Table 1 represents set of keywords use for the

Table 1 Keyword strategy for Espacenet database

S. No	Keyword sets
I	BIM OR building information modeling AND construction
II	BIM AND construction AND safety
III	BIM OR building information modeling AND construction AND safety AND hazards

Source <https://worldwide.espacenet.com/accessed> on 3rd April 2023

study. Keyword set ‘BIM’ OR ‘Building Information Modeling’ AND ‘construction’ is searched initially with consideration of broad research area. The next keyword set is searched with the reflection of BIM for safety. Further, Lastly, the keyword set ‘BIM’ OR ‘Building Information Modeling’ AND ‘construction’ AND ‘safety’ AND ‘Hazards’ is searched for more specific results.

The third keyword set provides far fewer search results than the first two since the first keyword set is a generic search and excludes documents pertaining to safety. The study is therefore restricted to the findings of the keyword set III, which imparts an essential survey among all results, including Safety and risks linked studies, to produce a more particular and relevant analysis.

There are a couple ways to retrieve the necessary patents out of the database as well. Only one keyword set from the Espacenet database is examined in this article. Only the results of keyword set found in the Espacenet database are included in this search, regardless of where those keywords appear in the patent application.

3 Patent Landscape

The patent analysis is important to empathize the extent of research and innovation [9]. The keywords set III, BIM’ OR ‘Building Information Modeling’ AND ‘construction’ AND ‘safety’ AND ‘Hazards’ is used in a thorough patent analysis to identify the trend of innovation in BIM for safety. For the selected set of keywords, a workflow is designed as shown in Fig. 1.

Firstly, the data is retrieved from Espacenet database related to the keyword set II and the initial results were obtained. A total of 254 patent publications were observed, and all these 254 documents are published in the time span of year 2016 to 2023, hence no filter was provided to obtain the latest documents. Further, the analysis of the retrieved data is carried out and that includes year-wise, country-wise publications. It also includes analysis of patents by inventors and applicants followed by patent classification. All patents in the BIM for safety sector are available in English as well, however the Chinese scholars have made the most contributions in the novelty of the field. Lastly, as an output, the findings of the study are classified into 3 categories followed by commenting on scope and need in the domain.

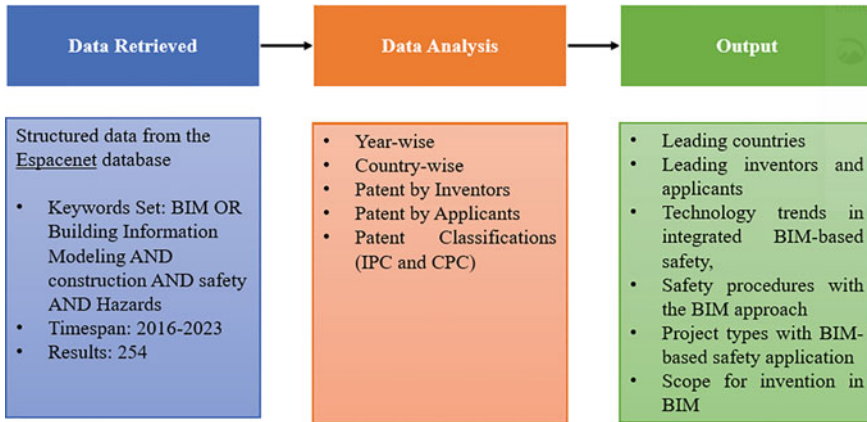


Fig. 1 Workflow for patent landscape in BIM in Construction Site Safety Management

3.1 Year-Wise Analysis

The year of the patent publication helps to recognize when the research is conducted in a precise area as well as years increase or decrease in that discipline [10]. The results obtained with the selected set of keywords III show that the first patent in this domain was published in year 2016. Henceforth this data was considered for analysis as all the results obtained are most recent, i.e., from span 2016 to 2023. Fig. 2. shows the Year-wise patent publications in the respective search.

Till 2016, there were fewer papers in the domain; nevertheless, starting in 2017, several patents gradually increased until 2022, when the number of patents peaked. In addition, seven documents have already been released at the start of 2023. The pattern

Fig. 2 Year-wise patent publication. Source <https://worldwide.espacenet.com/>

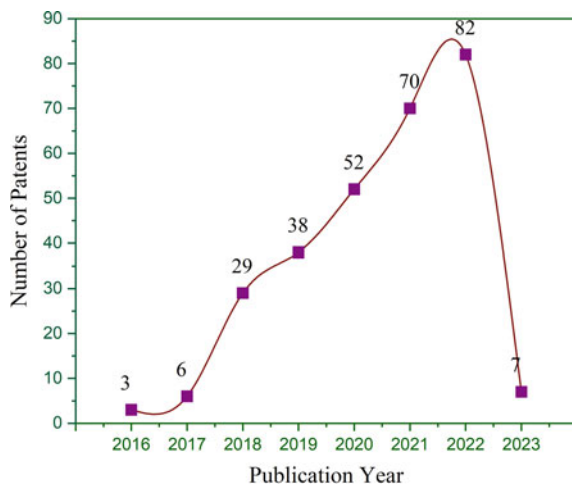


Table 2 Country Code (CC) and number of patents documents

Country code	Country name	Number of patent documents
CN	China	253
KR	Republic of Korea	1
WO	World Intellectual Property Organization	2

Source <https://worldwide.espacenet.com/>

indicates an ongoing expansion of research into BIM applications for construction safety.

3.2 Country-Wise Analysis

Analyzing the nation with the most patents in the BIM field, a sign of BIM research, involves an analysis of the statistics of global BIM adoption for safety. A total of 254 documents are published in three countries. Specific country codes are used to represent the patent distribution per country. The country code is made up of 2 letters that stand in for the nation that the patent is issued in. The data is reported from Espacenet for BIM for safety differentiated by patent issuing country and its country code in Table 2.

Table 2 demonstrates China's significant involvement in the relevant field. The leading nation working in this area is China with 253 number of publications contributing 98% of publication among all. In addition, the Republic of Korea and World Intellectual Property Organization have 01 and 02 publications. These statistics illustrate that India, along with a few other countries, has a significant research opportunity in BIM implementation for construction safety.

3.3 Patent by Inventors

To better comprehend the contribution of inventors, Fig. 3 depicts the leading inventors by patent count who have made contributions to the field of BIM for construction safety.

3.4 Patent by Applicants

The leading applicants contributing to the area of BIM for construction safety are depicted in Fig. 4 to appreciate the contribution of applicants.

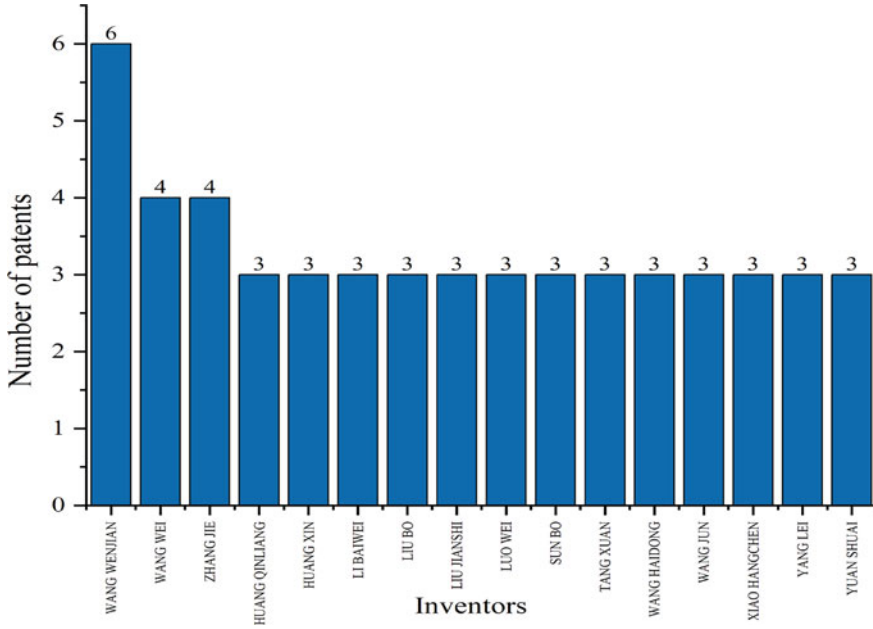


Fig. 3 Patents by Inventors. Source <https://worldwide.espacenet.com/>

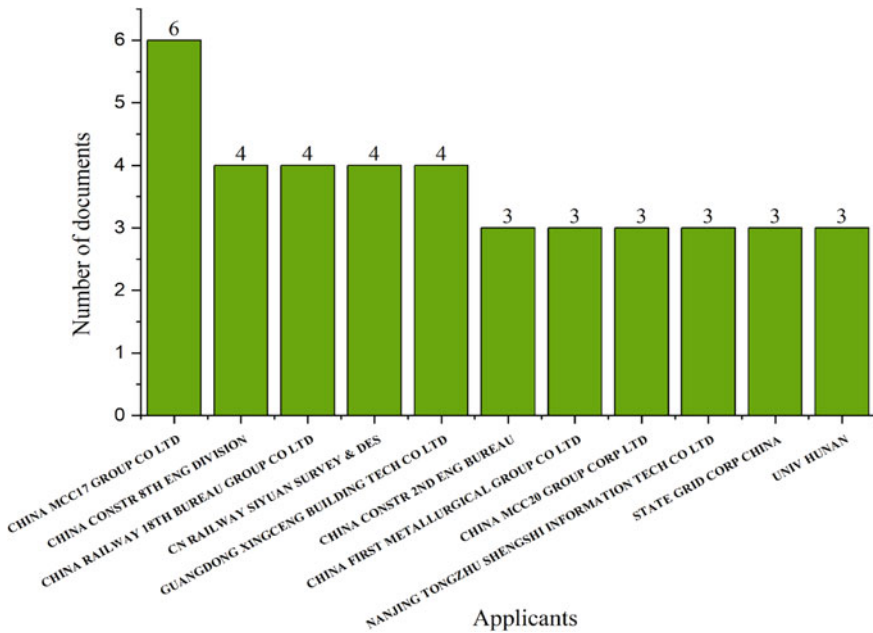


Fig. 4 Patent by Applicants. Source <https://worldwide.espacenet.com/>

3.5 Patent Classification

Sections (Technical Field) A through H and Y are included in the intellectual property classification (IPC) and corporate property classification (CPC) schemes. Human necessities are covered in Section A, operations and transportation are covered in Section B. Section D—Textiles and Paper, Section C—Chemistry and Metallurgy • Fixed Constructions in Section E, • Mechanical Engineering, Lighting, Heating, Weapons, and Blasting • Physics in Section G, • Electricity, Section H • Section Y—General tagging of newly developed technologies, cross-sectional technologies ranging across many IPC sections, and technical topics covered by the previous USPC. IPC class and CPC class data representations are based primarily on the topic or subject of the investigation, and they provide distinct information to an investigator through a particular domain [11, 12].

For example, G06F30 (Fig. 5) describes that the patent section is associated with Physics, 06 denotes that patent class implies instruments (calculating or counting), F signifies the electric digital data processing and 30 as Computer Aided Design (CAD). The IPC group and CPC group’s specification of code is mostly dependent on the subject or discipline in which the research is conducted, and it aids in the data extraction for a researcher from a certain domain. Figures 5 and 6 represent the number of patents under IPC and CPC classification.

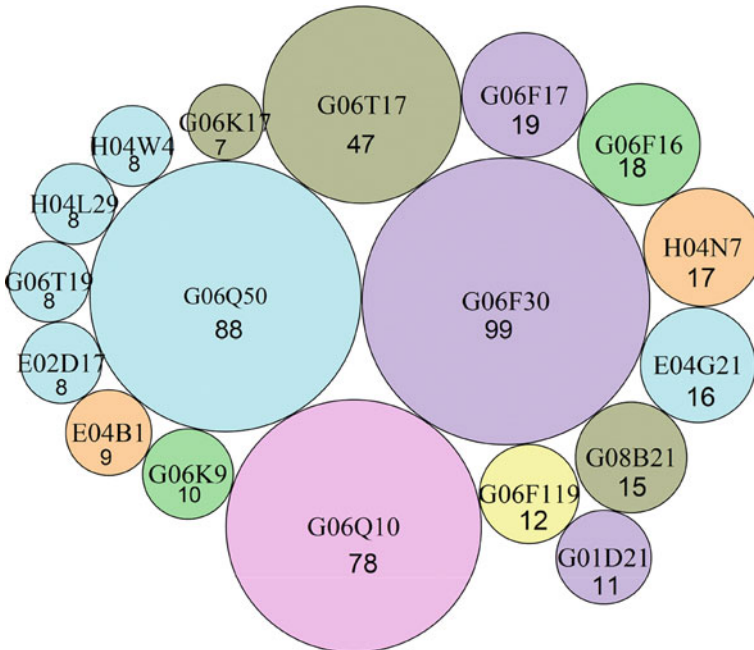


Fig. 5 Patent publication in IPC main group. Source <https://worldwide.espacenet.com/>

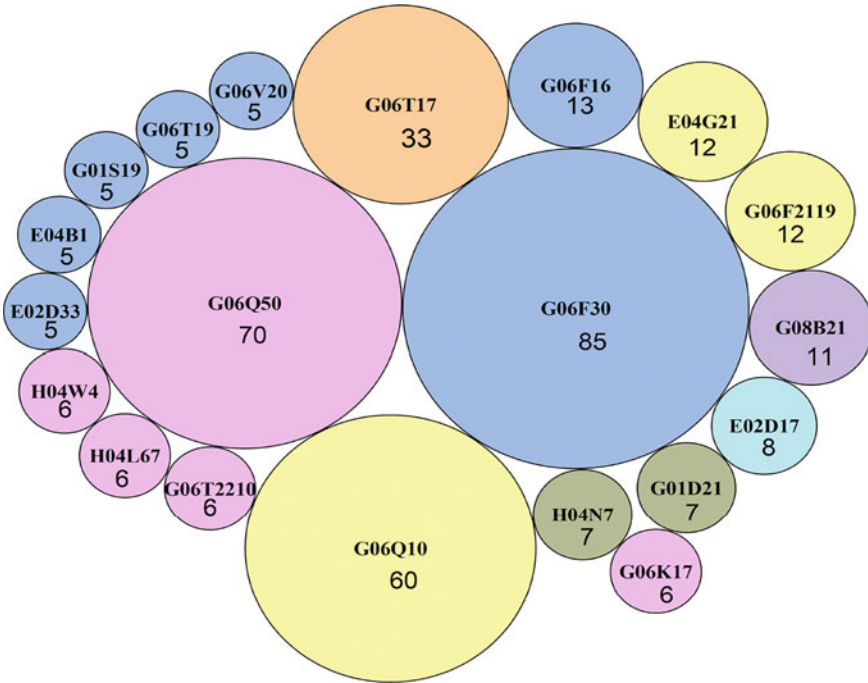


Fig. 6 Patent publication in CPC main group. Source <https://worldwide.espacenet.com/>

According to the sections designated by Patent classification, the patents pertaining to BIM and safety are directed toward the Physics domain. Both CPC and IPC data show that physics researchers are making significant contributions to the field. There are 156 patent documents classed in CPC and 197 patent documents classified in IPC under the physics division. Both the groups have highest documents in G06F30 with 99 documents in IPC and 85 documents in CPC.

4 Notable Findings and Discussion

This section summarizes the findings and provides the possible future scope in the domain. The results observed from the patent search are divided into three categories namely A. Technology trends in integrated BIM based safety, B. Safety procedures with BIM approach and C. Project types with BIM based safety application. All these categories are interrelated to each other. For category A, a total of 28 documents are observed. It is noted that BIM has been integrated with different technologies such as Geographic Information System (GIS) [13–16], Global Positioning System (GPS) [17, 18], Virtual Reality (VR) [19–21], Unmanned Arial Vehicle (UAV) [22, 23], Radio Frequency Identification (RFID) [24, 25], AI [26, 27], Ultra-Wide Bands

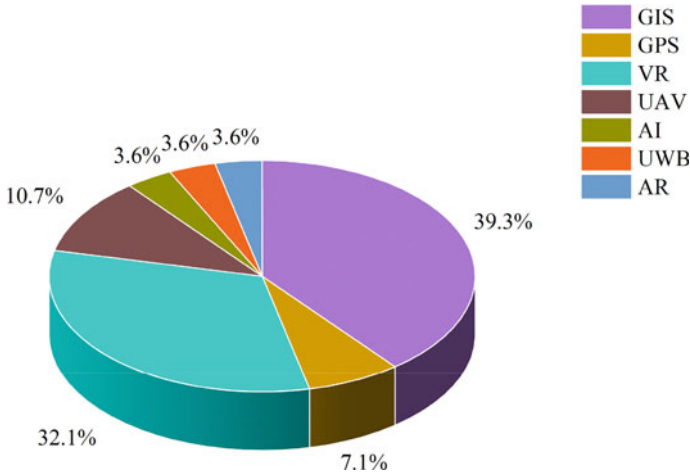


Fig. 7 % Patents from category A—technology trends in integrated BIM based safety

(UWB) [28] and Augmented Reality [30]. Fig. 7 depicts the trends in integrated BIM based safety. The Highest number of studies are related to GIS integration with BIM followed by VR Fig. 7.

For category B of BIM based safety procedures, a total of 77 documents are observed. This category includes safety procedures such as early warning, safety inspection, safety monitoring, and operations and maintenance. Early warning studies mainly include hazard identification and prevention with alarm systems and methods. It is observed that BIM is highly used for Safety monitoring followed by early warning. Also, some of the studies are jointly related to monitoring and inspection. It shows that there is a need to focus on early detection of hazards i.e., at preconstruction stage. It will help to reduce the rework, cost, time and minimize the hazards occurring at later stages of construction. Fig. 8 illustrates the BIM based safety procedures.

The category C is about Project specific BIM based safety and total 39 documents are observed in this category. It shows that BIM is majorly used for safety of infrastructure projects such as bridge and roads. Figure 9 illustrates Project types with BIM based safety application. The potential of BIM also needs to be utilized for some other kinds of projects including residential as the scale of residential projects is increasing and it needs advanced safety solutions which BIM is capable of. This will help to reduce the accidents on residential projects pertaining to safer environment on site.

It is also observed that the steel structures are mainly considered for the safety with BIM application. Some plumbing and electromechanical related studies are also observed. There are several hazards that are related construction structures such as scaffolding, formwork and some are related to machines like tower crane. Very limited studies are observed in this domain, where the safety of objects is taken care of.

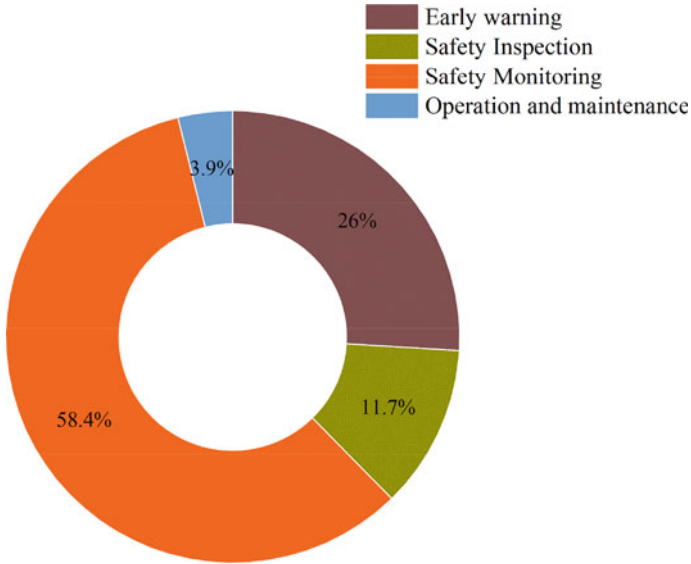


Fig. 8 % Patents from category B—safety procedures with BIM approach

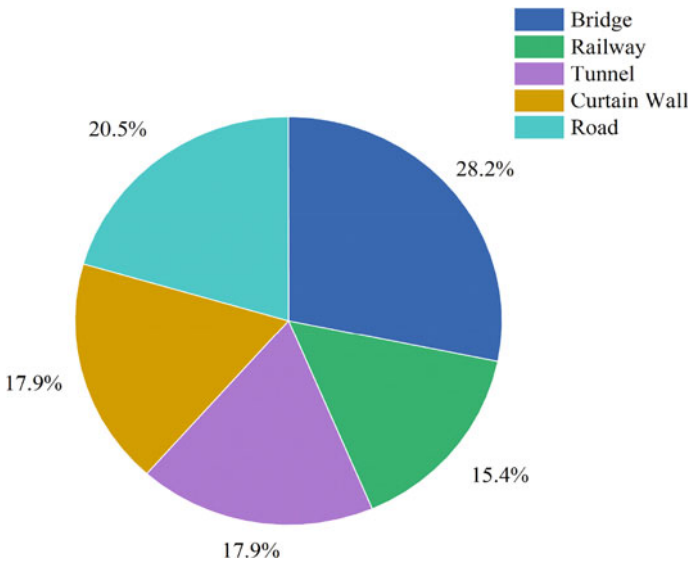


Fig. 9 % Patents from category C—Project types with BIM based safety application

In addition, more emphasis should be given on hazard specific BIM applications such as for fall hazard, stuck by an object hazard. It would help to apply the solution as per the occurrence of hazard as and when needed by different sites.

5 Conclusion

The level of research being conducted on BIM applications for construction safety is constantly escalating. However, from the standpoint of patentability, there are just a few studies and a few nations that offer them. In the search and analysis process, the data pertaining to the intended domain, no Indian patents were discovered. Additionally, Indian researchers were not included in inventor trend analyses, which suggests that for a developing nation like India to compete globally, it needs to enter this field.

It is true that BIM applications for safety have not been properly investigated both globally and in India. It shows there is a lot of scope for Indian researchers to explore this area.

The study reveals that BIM based safety management mainly adopts an integrated approach involving cutting-edge technologies such as GPS, GIS, AI, UAV, VR and more. The potential of these technologies when combined with BIM, the ultimate safety solutions can be achieved, whereas it is difficult to achieve them with conventional safety practices. It additionally reveals the noble compatibility of BIM to integrate with other technologies, and it may significantly enhance safety procedures to deliver effectual safety solutions.

The categorization presented in this study helps to understand the technological trends in integrated BIM, utilization of BIM for safety procedures and its adoption status as per project type. The safety domain is crucial in every construction project, requiring special consideration from the beginning. It is observed that studies mainly include real time monitoring which is while construction is ongoing, however the need to adopt BIM for preconstruction stage is essential. Moreover, safety management is important for all the construction projects despite its type. Major studies focused on utilization of BIM for infrastructure projects, and it shows there is need to adopt BIM benefits for different kind of projects such as residential and commercial.

References

1. India Brand Equity Foundation (IBEF) (2022) Homepage: <https://www.ibef.org/>
2. Express News Service (2017) Accidents at workplaces in India ‘under reported’; 38 per day in construction sector : Study,” Indian Express, pp 1–13
3. Patel DA, Jha KN (2016) An estimate of fatal accidents in Indian construction. In: Proceedings 32nd annual ARCOM conference ARCOM 2016, no. September, pp 539–548
4. Hire S, Ranjan A, Ruikar K, Sandbhor S (2022) AI-driven safety checks for ladders used on construction sites. IOP Conf Ser Earth Environ Sci 1101:092040. <https://doi.org/10.1088/1755-1315/1101/9/092040>

5. Sayali S, Ruikar K, Hire S (2021) Paradigm shift in construction processes with industry 4.0. In: Kotecha K, Kumar S, Bongale A, Suresh R (eds) *Industry 4.0 in small and medium-sized enterprises (SMEs)*, 1st edn. CRC Press, pp 33–52. <https://doi.org/10.1201/9781003200857>
6. Gerrish T, Ruikar K, Cook M, Johnson M, Phillip M, Lowry C (2017) BIM application to building energy performance visualisation and management challenges and potential. *Energy Build* 144:218–228. <https://doi.org/10.1016/j.enbuild.2017.03.032>
7. Hire S, Sandbhor S, Ruikar K, Amarnath CB (2021) BIM usage benefits and challenges for site safety application in Indian construction sector. *Asian J Civ Eng* 22(7):1249–1267. <https://doi.org/10.1007/s42107-021-00379-8>
8. Ghule B, Laad M, Tiwari AK (2021) Poly-4-methyl-1-pentene a dielectric material: patent landscape. *J Energy Storage* 36(1):102335. <https://doi.org/10.1016/j.est.2021.102335>
9. Raturi MK, Sahoo PK, Mukherjee S, Tiwari AK (2012) *Patinformatics—an emerging scientific discipline*
10. Hire S, Sandbhor S, Ruikar K (2021) Bibliometric survey for adoption of building information modeling (BIM) in construction industry—a safety perspective. *Arch Comput Methods Eng* 0123456789. <https://doi.org/10.1007/s11831-021-09584-9>
11. European Patent Office and United States Patent and Trademark Office (2018) CPC scheme and CPC definitions. *Coop Pat Classif*, pp 2–5 (Online). Available: <https://www.cooperativepatentclassification.org/cpcSchemeAndDefinitions/table.html>
12. USPTO, Classification Resources, pp 1–7 (2021) (Online). Available: <https://www.uspto.gov/web/patents/classification/>
13. Qingxue Z, Jiajia J, Guangfan J, Ning L, Yuanwei L (2022) BIM (Building Information Modeling)-based piping shaft installation construction method, CN114215309A
14. Wen Z, Zujie H, Xiaolong L, Siming L, Shufeng S, Yi H, Heng Z, Hua W, Xinwen N, Dengke F (2019) A railway tied-arch bridge construction simulation system and method based on a 3D GIS and a BIM. CN109783851A
15. Jun W (2020) Engineering management platform based on BIM model and 3D GI, CN211959405U
16. Youfu T, Xing G, Zhong Z, Xiong R, Yuanyuan T, Hongbin S, Zhenhua Y, Lingling F (2021) Railway construction site positioning management system based on BIM and GIS, CN112597578A
17. Xiangping Z, Min G, Yang L, Shaolin Z, Liuping L (2018) Safety management and control system and method based on GPS positioning and BIM model, CN108469752A
18. CN108470105A_Original_document_20230402201251.pdf. Haidong W (2018) BIM (Building Information Modeling) +3S (RS (Remote Sensing) +GIS (Geographic Information System) +GPS (Global Positioning System)) +VR (Virtual Reality) technique and underground engineering case knowledge base system-based method for compiling dynamic construction schemes, CN108470105A
19. Ziren W, Jun J, Xudong P, Xia L, Yadong Y, Qianya Y, YaNqi W (2020) Construction safety education device based on BIM and VR technology, CN110648564A
20. Yanhao H, Yuhu M, Jia J, Zuozhong M, Shuan L, Yilei L, Peng X, Nan Y, Jianyun Z, Dong W, Min Z (2022) System and method for realizing power debugging test and inspection work scene based on BIM + VR technology, CN115188231A
21. Jiahua L, Jie T, Liangzh C, Liang H, Qing L, Yong H, Chunyong S, Jing W, Liwei X, Yiping Y, Liming H, Qiao W, Biao Y, Hao S, Liyua N (2022) Engineering safety education method and system based on virtual reality, CN115268657A
22. Yong Z, Shiyu Z, Linlin L, Junjie X, Ruibin Y (2020) Construction safety management method and device based on unmanned aerial vehicle and computer equipment, CN110991282A
23. Chaoyang L, Yuqi Z, Peng G, Zhu Y, Wang Z, Zheng Y, Anming W, Rui L (2022) Steel structure monitoring method based on BIM and unmanned aerial vehicle technology, CN115376030A
24. Aimin Y, Zidi Z, Leilei S, Mingyu P, Shuo J, Zhongyu Z, Fengming Z, Zhaofeng J, Shengqi W (2019) Underground space intelligent constructor management system based on RFID and BIM technologies, CN110189106A

25. Qing Z, Lina Z (2018) Construction site security monitored control system based on RFID and BIM are integrated, CN207249677U
26. Jung-Won L, Xianyang K, Youning S, Zhen P, Renkuan F, Zhengxue Z, Wei Z (2022) Fire early warning and post-disaster floor damage prediction method and system based on BIM and deep learning, CN114444386A
27. Zhenguo H, Haiying H, Zhongshan Z, Jianan L, Weitao Y, Hongjie X, Dongyang Y (2021) Construction site safety management system based on BIM and AI, CN113688459A
28. Jiangtao M, Quanxi B, Baofeng Y, Xinwei X, Haohao Z, Mingming Z, Lujun M (2021) Near-edge opening construction management and control method based on BIM, UWB and AR technologies, CN113404318A
29. Sheng X, Jiaqi L, Shaofeng Q, Yu G, Gaokun L, Jingwei L, Hui Y (2020) Railway emergency cooperative support and inspection system based on AR technology, CN110995660A

Numerical Analysis of Floor to Column Pounding in Series



C. K. Fathima Hassan and C. Nijesh

Abstract Numerous studies conducted on the recent and past earthquake incidents shows that, around 40–50% of the failures of the structures is due to the collision between adjacent structures. The out of phase vibration caused by the lateral loads leads to collision, if sufficient separation is not provided. Studies on pounding of two adjacent buildings shows, the more flexible of the two gets affected more. Whereas the studies on 3 buildings arranged in a series shows opposite phenomena, that is the stiffer structure is affected more during pounding. Also, it was observed that the floor of one building hitting column of other building is more critical than the floor-to-floor collision; since it can lead to the brittle failure of the column. This study is focused on the behaviors of buildings under floor to column pounding when arranged in series. 3 MRF buildings arranged in series with different floor height were analyzed using ETABS Software. The effects of pounding depend on building characteristics, separation gap distance, ground motion characteristics and the characteristics of underlying soil.

Keywords Pounding · Floor to column pounding · Buildings in series · Earthquake · Numerical analysis

1 Introduction

The increase in demand for better lifestyle has increased the need of large number of buildings. Usually, the provision of high-rise building was confined to commercial buildings such as hospitals, universities, office buildings etc., however nowadays this demand has been extended to residential building also. The increase of demand in structures and decrease in available space has led to the phenomenon of ‘building at proximity’ [1]. When lateral load hit two or more structures at proximity, collision occur among the structures, and this phenomenon is known as pounding. If two

C. K. Fathima Hassan (✉) · C. Nijesh
Government College of Engineering Kannur, Department of Civil Engineering, Kannur 670563,
India
e-mail: ckfathi003@gmail.com

structures have same dynamic property or have sufficient separation gap among each other, the ground motion leads to in phase vibration among them, and there won't be any sign of pounding. But, if the ground motion results in out of phase vibration, the chances of collision is high if there is insufficient separation gap among the same. The effects of pounding may range from slight non-structural to structural failures and can even led to total collapse of the buildings. This out-of-phase vibration can be triggered by lateral deflections caused by lateral loads such as earthquake, extreme wind gusts, hurricanes, tsunamis, cyclones, and tornados. Due to its unpredictable occurrences, earthquake pounding has received the greatest attention from researchers. Therefore, in order to avoid structure pounding, either provide sufficient gap among each other, or design the structure for additional force which can result from the pounding.

There are two types of pounding [2]. Floor to floor pounding occurs in building with same storey height when slabs of each buildings collide each other. In a study by Filiatrault et al. [2] on pounding between 8 and 3 storey building frames, very large acceleration peak was observed at the 3rd floor level of 3 storey building, and even more hike was observed when floor hits the column of tall building. Studies by Jankowski [3] shows that, the amplification of response was in lighter and more flexible structure than heavier and stiffer structure. Also, the response amplification of flexible structure is more sensitive towards the parameters (gap size, storey mass, structural stiffness, and yield strength) considered; whereas, the response of stiffer structure has negligible variation. When slab of a building collides with column of adjacent building during out-of-phase vibration, the resulting phenomenon is known as floor-to-column pounding. It is the most damaging pounding, since the ductility and shear demand may exceed the strength [3], making their analysis a necessary. Karayannis and Favvata [4] found that during slab-to-column pounding, column's ductility requirements are higher where-the gap is smaller, mainly-in the columns-of the tallest building. If the shear developed exceeds the strength, brittle failure of structure can occur [4, 5].

The pounding among buildings in series is one of the main topics of discussions for recent years. It was observed that the rigid structure shows more amplification of response compared to flexible structure during pounding in series [5]. Anagnostopoulos [6] concluded that, the exterior building almost always shows higher increase in seismic performance compared to interior one. Later other researchers concluded that, the extent of effects of seismic pounding among buildings in series depends on dynamic characteristics of adjacent buildings, input excitation characteristics and the position of building, i. e., whether the building undergo one-sided or two-sided impacts [7–9]. It is evident that the studies regarding the seismic pounding response of buildings in series is minimal. So, this study aims to study the seismic pounding behavior of buildings in series with different floor levels along with a detailed parametric study.

2 Modelling

3 buildings (3 storey, 6 storey and 12 storey buildings), with all floors 3 m height and bays 5 m width, were selected for the modelling in ETABS Software. To introduce floor to column pounding, the first storey height of interior building was provided as 4.5 m inducing pounding at 1/2nd height of impacted column. All the buildings were designed according to capacity design rules such that the brittle failure is avoided. All the beams were 0.3 m × 0.7 m and slabs were 15 cm thick. The nonlinear dynamic analysis of 3 buildings arranged in series with different configurations and gap sizes were analysed using ETABS software, considering the material and geometric nonlinearities. In the Finite Element (FE) model, Mander-stress-strain relation was assigned to-concrete material for both unconfined and confined tension and compression stress-strain relation (Fig. 1a). The steel material was assigned a bilinear stress strain model, which considers the strain hardening (Fig. 1b). The geometric nonlinearity was modelled using plastic hinges. In this study, concrete with 30 MPa compressive strength, 25 kN/m³ unit weight and 24 GPa modulus of elasticity and reinforcing steel with yield strength of 360 MPa were used.

All buildings were acted upon by a live load of 2 kN/m². The dead load includes self-weight along with 1.5 kN/m² and panel-wall load of 10 kN/m² on all-beams. The seismic design of the considered buildings-were done according-to ECP-201 with design parameters: earthquake zonem5B (based on Egyptian zoning system), importance factor = 1, peak ground-acceleration PGA = 0.3 g, Type-2 design response spectrum, and-soil class D with-soil factor S = 1.8. The total-seismic mass was calculated as dead-load plus 25% of live-load based on ASCE7-210. The nonlinear-dynamic time history analysis was conducted using 9 ground motion data that are absolutely in compatible with design spectrum. The ground motion time histories were extracted from PEER Ground motion data, then matched to the proposed elastic design spectrum using SeismoMatch software. The selected ground motion along

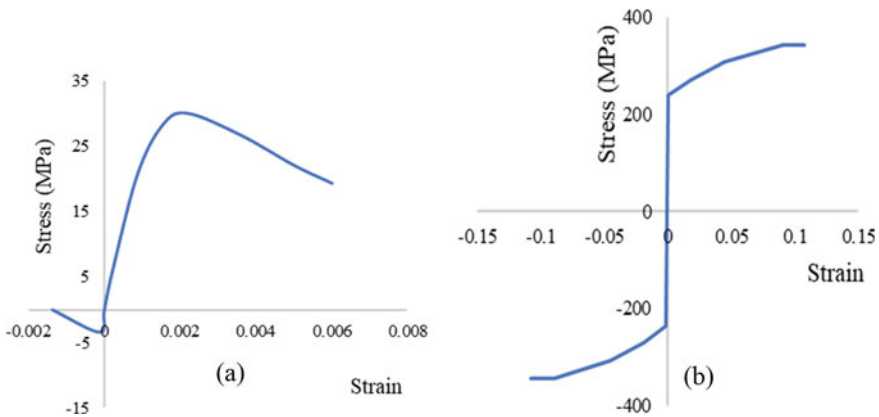


Fig. 1 Stress-strain relation of a concrete and b steel

Table 1 Ground motion characteristics

Earthquake	Magnitude	PGA (g)
San Simeon	6.52	0.13
Morgan Hill	6.19	0.19
Christchurch	6.20	0.29
L' Aquila	6.30	0.52
Loma Prieta	6.93	0.65
Imperial Valley	6.53	0.60
Bam	6.60	0.81
Kobe	6.90	0.83
Chi-Chi	7.62	0.86

with characteristics were tabulated in Table 1. The structural impact among the buildings were modelled using compression only gap element. The pounding force of impact model F is determined as:

$$F = \begin{cases} 0, & \delta \leq G \\ k\delta + c\dot{\delta}, & \delta \geq G \end{cases} \tag{1}$$

where k and c-are stiffness and-damping coefficient and G is-the separation gap size. $\delta = u_i - u_j - G$ and $\dot{\delta} = \dot{u}_i - \dot{u}_j$ are the relative-displacement and velocity between colliding structural elements. u_i, u_j and \dot{u}_i, \dot{u}_j are the displacement and velocity of the element's nodes i, j. When two nodes come into contact, this element becomes active and otherwise will be inactive. In current study, the-impact stiffness of-the gap element-k was determined as the greater value-of either the-axial stiffness of-the-collided floors-or the lateral-stiffness of the-stiffer building-at the impact level.

$$k = \gamma \frac{EA}{B} \quad \text{or} \quad \gamma \frac{3EI}{h^3} \tag{2}$$

where, A is the-area of the impact surface, E is the modulus of elasticity, and b is building-width in the impact direction, I is the moment of inertia of equivalent cantilever model of the stiffer building, h is the height building-up to the impact level. The-value of γ was taken-as 50 for the current study.

2.1 Verification of Modelling

To analyse the floor to column pounding of buildings in series, floor to column pounding results were validated against Miari et al. [1]. 3 pounding cases (pounding at 1/2nd, 1/3rd and 2/3rd height of impacted column) were verified and only 0.2% deviation was observed in column shear force of impacted column. The verification is

followed by validation of pounding of buildings in series for 3 different configuration and different ground motion against Raheem et al. [8, 9], and almost exact match was observed with deviation of 0.1%.

3 Parametric Study

The floor to column pounding in series was introduced by increasing the first storey height of interior building by 1.5 m inducing floor to column pounding at the 1/2nd height of impact column. A total of 135 FE analysis was carried out to study 4 different parameters such as impact height, alignment configuration, gap distance and ground motion characteristics.

3.1 Effect of Configuration

The pounding of buildings in series greatly depends upon the configuration in which the buildings are arranged, i. e., whether the building undergoes one sided or two sided impact. In this study, 3 arrangements namely, 12-6-3 (Configuration I), 3-12-6 (Configuration II) and 6-3-12 (Configuration III) were considered for comparison. The comparison of mean variation of storey displacement in different configurations along with no pounding response is represented in Fig. 2.

In configuration I (12-6-3), the displacement response requirements for the 6-story interior building and the 3-story exterior short building are significantly reduced, whereas the 12-story exterior high building experiences an increase in the response

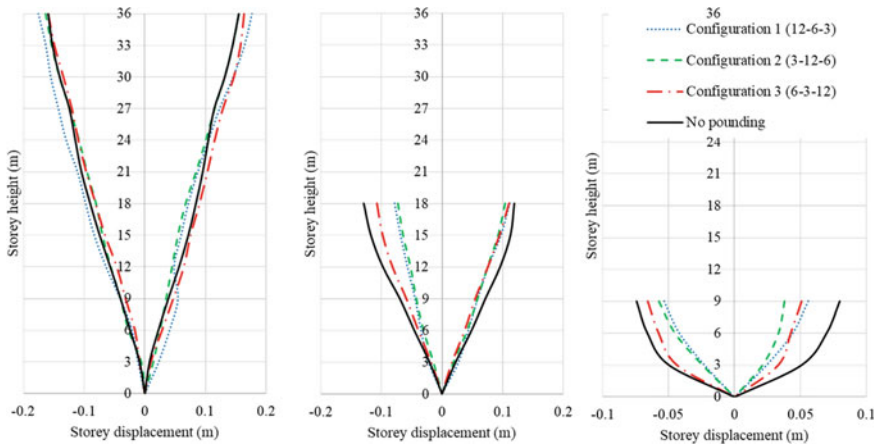


Fig. 2 Comparison of mean storey displacement of different configurations

over the height above the impact level in the rebound direction and a decrease in the response in the impact direction. When compared to the no-pounding scenario, Configuration II (3-12-6) shows that pounding has increased the middle high building's peak absolute displacement above the impact level. The peak displacement of the left and right relative short structures, however, has decreased because of floor to column pounding. Configuration III (6-3-12) reduces the short building's pounding response and its impact on the two adjacent structures. Therefore, because of floor to column pounding in series, the response of shorter structures decreases, while it increases in taller structures. Even though the floor to column pounding in series benefits the shorter buildings, it considerably increases the response of taller buildings and increases the column shear force to many folds resulting in detrimental rather than beneficial effects.

3.2 Effect of Height of Impact

The effects of floor to column pounding depends on the height at which the collision occurs in the impacted column. i. e., whether the impact occurs at above or below the center or at the mid height, inducing pounding at 1/3rd, 1/2nd, and 2/3rd height (by providing first storey height of 4 m and 4.5 m, and first two stories of 4 m on the inner 3 storey building respectively). These three different pounding scenarios were analysed for configuration III and the variation of storey displacement and storey shear force compared in Figs. 3 and 4.

When the three buildings are undergoing floor to column pounding in series, the response of the shorter building is amplified more compared to the floor-to-floor pounding, but the effect is less visible in the case of the taller building. This effect depends on the ground motion, configuration, and the height of impact. The response of all three buildings were almost similar when the collision is at 1/3rd and 2/3rd

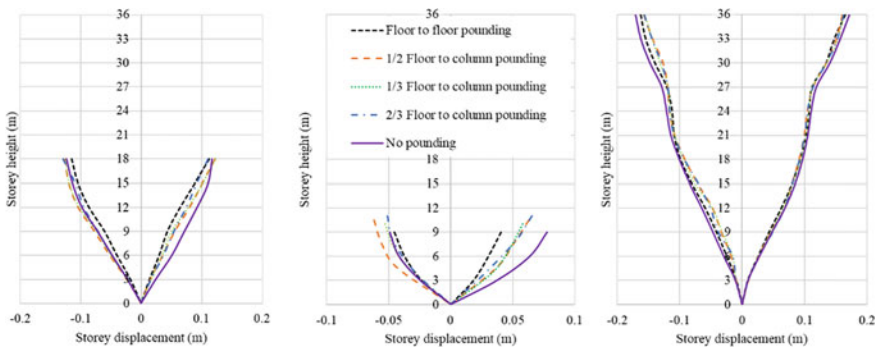


Fig. 3 Comparison of mean storey displacement response of Configuration III

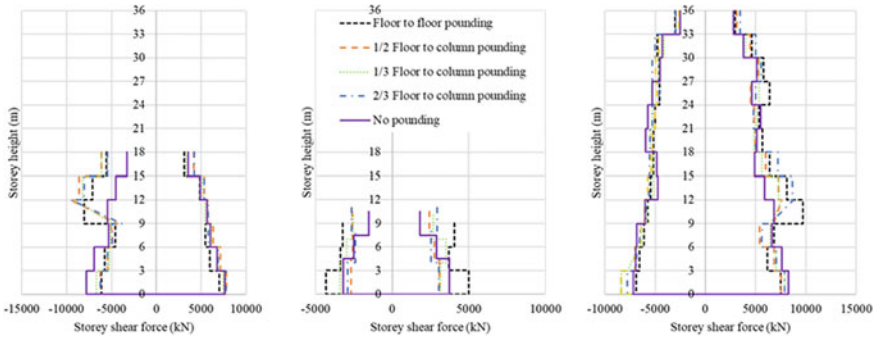


Fig. 4 Comparison of mean storey shear force response of Configuration III

height and the effects are less critical than the 1/2nd collision. The storey displacement responses of shorter buildings were reduced compared to the no pounding case, but the response is higher than the floor-to-floor pounding. Besides, the response of taller buildings at stories higher than shorter building is amplified both in impact and rebound directions in all configurations.

3.3 Effect of Gap Distance

The effect of gap distance was studied considering 6 different gap distances (2, 4, 6, 8, 10 and 12 cm) along with the in-contact condition (gap distance = 0 cm) and was compared with no pounding condition. This effect was studied considering 9 different ground motions. The mean storey displacement distribution along the height of the three buildings for configuration III is represented in the following figure (Fig. 5).

As gap distance increases, the storey displacement and storey shear force approaches to the response at no pounding case. The variation of response depends on gap distance, building and ground excitation characteristics along with the alignment position of buildings. Minimum of 8 cm gap distance is required to avoid pounding between 6 and 3 storey building, while 10 cm is necessary for 3 and 12 storey building. But the same was observed to be only 6 and 10 cm respectively to avoid floor to floor pounding. Therefore, the minimum separation gap depends on the building characteristics and providing them avoid pounding only if it is adequate. It was observed that the pounding force first increases with increase in gap distance and then decreases with increase in gap distance, finally leading to zero pounding force. And the increase in gap distance reduces the number of occurrences of collision between structures in both the cases.

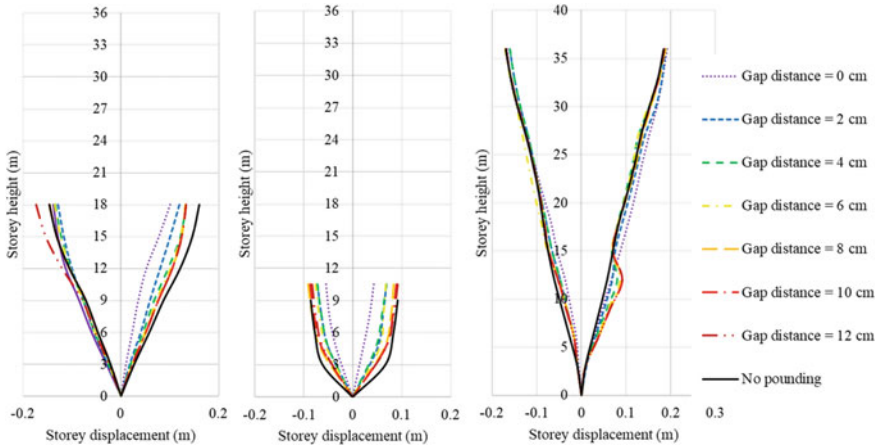


Fig. 5 Comparison of effect of gap distance in Configuration III

3.4 Effect of Ground Motion Characteristics

The response of all buildings under pounding depends on the ground motion characteristics along with the building characteristics. The shear force experienced by columns at impact level in Configuration III under different ground motion are tabulated below (Table 2). As the intensity of ground motion increases, column shear force and pounding forces at impact level increases. For PGA (Peak Ground Acceleration) between 0.13 and 0.86, the column shear force at impact increases by 3–4 times in both exterior 6 and 12 storey buildings in Configuration III. The potential pounding force increases as the storey height increases and the pounding force at impact increases when the magnitude and PGA of ground motion increases.

4 Conclusions

The study on floor to column pounding of buildings in series was conducted considering 3 storey, 6 storey and 12 storey building arranged in 3 different configurations, separation gap distances and different storey heights by conducting nonlinear time history analysis using 9 time histories that are absolutely compatible with the design spectrum. It was observed that the response of buildings under floor to column pounding depends on, height of impact, building characteristics, position of the building whether it has one sided or two-sided impacts, separation gap distances and input ground motion characteristics. Irrespective of the position, the tallest building (12 storey building) undergoes more amplification in response compared to shorter building. It was also evident that the building in interior position is affected less compared to the exterior buildings. The pounding above or below the mid height of

Table 2 Column shear force under different ground motion (Configuration III)

Earthquake	PGA (g)	Column shear force (kN) at different storey height					
		6 storey building			12 storey building		
		P	N P	Times	P	N P	Times
San Simeon	0.13	793.1	248.3	3.2	818.7	256.8	3.2
Morgan Hill	0.19	1086	269.8	4	1477.9	340.3	4.3
Christchurch	0.29	1052.3	269.7	3.9	1497.9	365.8	4.1
L Aquila	0.52	941.7	229.5	4.1	1395.3	346.7	4
Loma	0.65	1010.2	326.5	3.1	1116.6	299.9	3.7
Imperial Valley	0.6	1045.2	301.5	3.5	1048	290.2	3.6
Bam	0.81	866.7	272.9	3.2	1264.3	374.6	3.4
Kobe	0.83	1042.2	286.6	3.6	1144	283.5	4
Chi-chi	0.86	976.4	303.8	3.2	1321.8	339.8	3.9

impacted column has almost similar responses and is more critical than pounding at mid height. Floor to column impact increases the column shear force by 3–6 times, and if exceeded the column shear strength results in brittle failure. The increase of gap distance reduces the effects considerably, but it will avoid pounding failure only if it is sufficient. The necessary gap distance to avoid floor to column pounding in series was found to be more compared to the same for floor to floor pounding in series. Besides, sufficient gap distance depends on building characteristics, configuration, and input excitation characteristics. As a result, it is strongly advised to include requirements and provisions in the codes for the evaluation of the minimum necessary seismic separation and the pounding risk of structures. Many of the conclusions are extremely relevant to many other nearby structures, even if some of them will be case study specific. In order to give the engineering design profession useful tools for assessing and mitigating the very dangerous impacts of pounding, more research is urgently required.

References

- Miari M, Jankowski R (2022) Analysis of floor-to-column pounding of buildings founded on different soil types. *Bull Earthq Eng* 1–22
- Filiatrault A, Wagner P, Chery S (1996) An experimental study on the seismic pounding of buildings. In: Eleventh world conference on earthquake engineering
- Jankowski R (2008) Earthquake-induced pounding between equal height buildings with substantially different dynamic properties. *Eng Struct* 30(10):2818–2829
- Karayannis CG, Favvata MJ (2005) Earthquake-induced interaction between adjacent reinforced concrete structures with non-equal heights. *Earthq Eng Struct Dynam* 34(1):1–20
- Jankowski R, Seleemah A, El-Khoriby S, Elwardany H (2015) Experimental study on pounding between structures during damaging earthquakes. In: *Key engineering materials*, vol 627. Trans Tech Publications Ltd., pp 249–252

6. El-Khoriby S, Seleemah A, Elwardany H, Jankowski R (2015) Experimental and numerical study on pounding of structures in series. In: *Advances in structural engineering*. Springer, New Delhi, pp 1073–1089
7. Anagnostopoulos SA (1988) Pounding of buildings in series during earthquakes. *Earthq Eng Struct Dynam* 16(3):443–456
8. Abdel Raheem SE, Fooly MY, Abdel Shafy AG, Taha AM, Abbas YA, Abdel Latif M (2019) Numerical simulation of potential seismic pounding among adjacent buildings in series. *Bull Earthq Eng* 17(1):439–471
9. Raheem SEA, Fooly MY, Shafy AG, Abbas YA, Omar M, Latif M, Mahmoud S (2018) Seismic pounding effects on adjacent buildings in series with different alignment configurations. *Steel Compos Struct* 28(3):289–308

Nonlinear Finite Element Modelling of Prestressed Concrete Railway Sleeper Using ABAQUS



Kamble Yash Vijay and Greegar George

Abstract Railway sleepers are essential components of railway tracks that support the rails, maintain their position, and transfer weights to the track ballast. Nowadays, prestressed concrete sleepers are commonly used due to their improved endurance during high-cycle fatigue, which increases their durability. However, the accumulation of damage to a concrete sleeper over its service life can result in failure, especially from rail loads that have the potential to cause cracking in the sleepers. To study this failure pattern, a three-dimensional nonlinear finite element model of prestressed concrete railway sleepers is developed using Abaqus software, based on the geometry of the Mainline Broad-Gauge sleeper (RDSO/T-2496). The model incorporates a concrete damage plasticity model to simulate the behaviour of high-strength concrete, with solid elements used to model the prestressing strands. The static analysis was performed according to IRS-T39 to estimate the moment of resistance and fracture. This study provides a comprehensive and realistic model for the analysis of prestressed concrete railway sleepers undergoing fatigue. The results of this study will help in the design and maintenance of railway tracks, leading to improved durability and reduced maintenance costs.

Keywords Finite element analysis · Prestressed railway sleeper · ABAQUS software · Static analysis · Four-point bending test

K. Y. Vijay (✉) · G. George
Department of Civil Engineering, National Institute of Technology Tiruchirappalli,
Tiruchirappalli, India
e-mail: yash.kamble1998@gmail.com

G. George
e-mail: greegar@nitt.edu

1 Introduction

Railway transportation is one of the safest, most economical, and most comfortable transports for passengers as well as goods. The largest railway network in Asia is Indian Railways, which uses about 350 million concrete sleepers annually. Railway sleepers are an essential part of railway systems. When compared to the utilization of traditional teak wood sleepers, which are now obsolete and only have limited use, the critical demand for concrete sleepers for the Indian Railways is much greater. Sleepers are a crucial part of ballasted railway tracks because they support the rails transversely to preserve the right gauge width while distributing the train axle loads to the ballast and subgrade. The requirements for rail operations have increased significantly. The ordinary concrete sleepers, which have a 40 to 50-year expected service life, are no longer usable before that time. Prestressed concrete sleepers are the most typical type of railway sleeper. Because of the slow train speeds and light axle loads at the time the sleepers were constructed, only static loads were considered. However, given the high running speeds and axle loads of today, it is essential to take dynamic loads into account when designing. Since it is known that dynamic loads can harm rails, numerical analysis has become more and more popular over the past 20 years.

El-sayed et al. [2] studied the influence of coupling lateral and vertical loads on sleepers. Two finite element (FE) models have been developed, namely the global and detailed models. The global model was developed to quantify the realistic boundary condition and the global load distribution on the sleepers. The detailed model was developed to study the local response of sleepers and fasteners under loading. Dan et al. [1] studied fatigue analysis of sleepers. The methodology adopted was the damage accumulation method for fatigue life assessment. They also did a parametric study on the sleepers considering five types of support conditions, impact load distribution, and track stiffness. The finite element results were validated with the static experimental results [1]. Parvez and Stephen [6] studied the efficiency of prestressed concrete sleepers with the addition of steel fibres for cyclic and static loading and compared the results with the conventional prestressed sleeper. Three cases were considered with fibre contents of 0, 0.25, and 5% by volume. The minimum requirement of steel fibres was estimated for a better life span of the sleeper. Sakdirat et al. [7] studied a brittle cracking model of sleepers. The numerical analysis results were compared with the experimental results. Evaluation of crack propagation was studied in this research on the prestressed concrete sleepers. Yang et al. [10] studied dynamic wheel-rail rolling contact behaviour on the sleepers where the sleeper hanging defects were considered along with rail surface irregularity. You et al. [11] studied the structural capacity of the sleeper using nonlinear finite element method. Rail seat abrasion was considered in this study, where the loss of fastening toe load, improper rail cant, and gauge variation was included. Three types of abrasion were considered and compared. You and Sakdirat [12] studied the fatigue life of concrete sleeper considering field loading conditions. The maximum positive bending moment and maximum negative bending moment for various field conditions were presented in

this research. Prestress loss and cracking load were estimated. Simonava et al. [8] studied the influence of ageing and material properties on fatigue life of prestressed sleepers. Two types of sleepers were considered, one with the age of 28 days and one used on the site for 17 years. Static and cyclic loads were applied, and the response of the sleeper was estimated from these tests. Khan [4] did experimental studies on geopolymer prestressed sleepers and compared with conventional sleepers. The moment of resistance and fracture were estimated from the static testing. The failure loads for both sleepers were also estimated.

This paper aims to develop a numerical model of prestressed concrete sleepers that satisfies the structural and durability requirements for sleeper manufacturing as well as the relevant and essential static tests performed on the sleepers to determine whether they are good after manufacturing. This paper includes numerical testing on sleepers while considering solid elements for prestressing strands for a more realistic view. By considering solid elements for prestressing strands will give a more detailed results as it will reflect on site conditions. This model will behave as an accurate representation of the sleeper.

2 Methodology

The geometry of the prestressing tendons and the sleepers are developed using AutoCAD 3D. The geometry is then imported into ABAQUS, where a finite element model is made for further analysis. A four-point bending test is simulated in ABAQUS to determine the deflection of the sleeper and the failure load. The testing methodology adopted is accordance with the Indian Railway Standards (IRS) [3, 6, 9].

2.1 *Geometry Details of Monoblock Concrete Sleepers*

Monoblock prestressed concrete sleepers are of two types i.e., pre-tensioned and post-tensioned. Nowadays, the sleepers used are of pre-tensioned types. The pre-tensioned sleeper has an overall length of 2750 mm and weighs approximately 286.5 kg. The sleeper has a trapezoidal cross-section with a top width of 150 mm, bottom width of 249 mm, and a depth of 210 mm at the rail seat, as shown in Fig. 1. A cant of 1 in 20 has been provided on the top surface of the sleeper for 175 mm on either side of the centre line to cover the area of rail fittings. The sleeper is prestressed with 18 number of high-tensile steel strands. The material properties adopted for the constitutive model of concrete and steel is shown in Table 1.

Fig. 1 Cross-sectional dimensions of the sleeper at the rail seat and centre of the sleeper

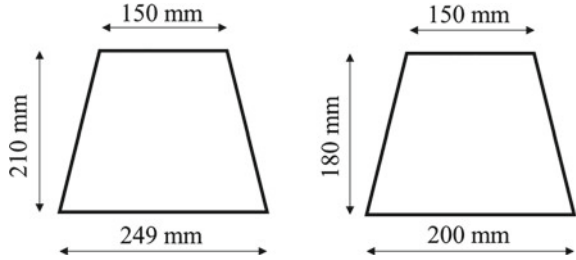


Table 1 Material properties

Material	Property	Value
Concrete	Density	2400 kg/m ³
	Modulus of elasticity	37.08 GPa
	Poisson's ratio	0.2
	Concrete damage property model	Kent-Park model
Steel	Modulus of elasticity	200 GPa
	Poisson's ratio	0.3

2.2 AutoCAD Modelling

The prestressed railway sleeper geometry was made with the help of AutoCAD 3D shown in Fig. 2. Since the twisted strand geometry was hard to model in ABAQUS, AutoCAD was used for this purpose.

2.3 Finite Element Formulation

The geometry of concrete and prestressing strands was imported individually from AutoCAD 3D in ABAQUS as shown in Fig. 3. The FE modelling of the geometry was done in ABAQUS.

The interaction between prestressing steel and the concrete was provided as embedded interaction. There were 18 strands of which one strand consisted of 3–3 mm intertwined wires which were embedded in the whole region of concrete. A C3D8R an 8-node linear brick, reduced integration, hourglass control element was used for meshing of concrete and steel.

The boundary conditions were kept simply supported in which 2 edges were created on the surface and those two edges were made to be simply supported by using pinned boundary conditions in ABAQUS. Loading was provided according to the test procedure of 30 kN/min, but this loading was converted to pressure and was applied on the surface. The amplitude was provided with an equal interval to increase the load gradually with time. In the loading module, prestress was applied as

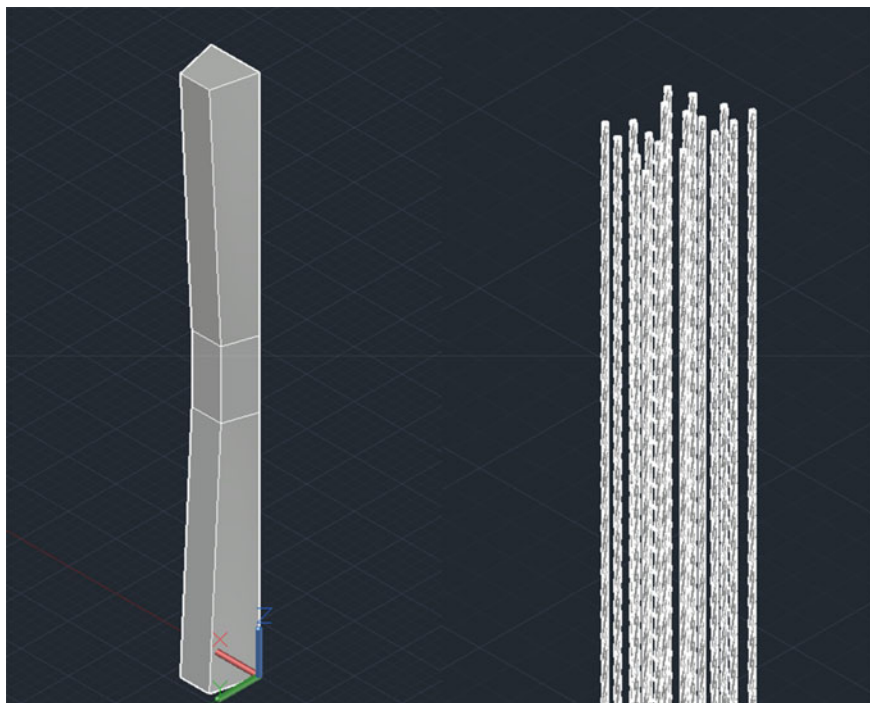


Fig. 2 Modelling of the concrete and the prestressing strands using AutoCAD 3D

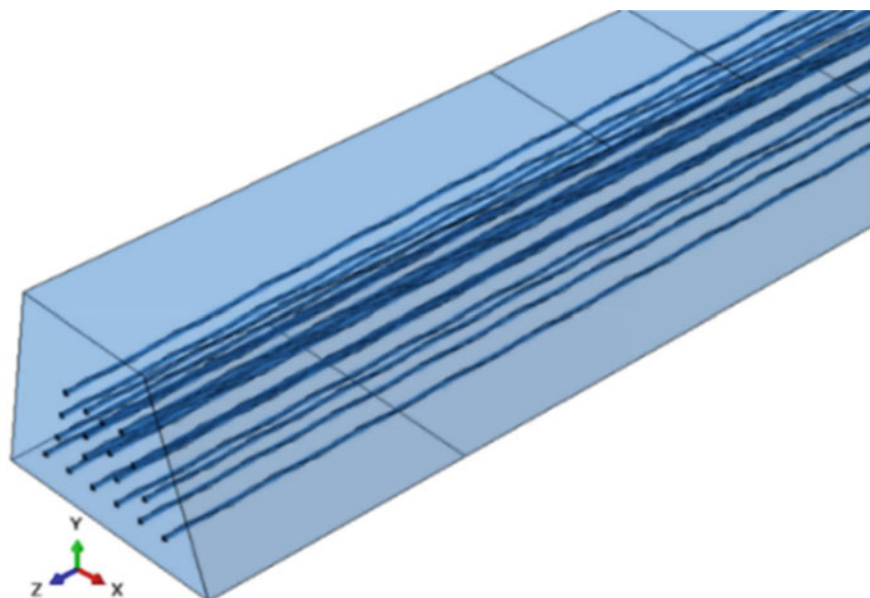


Fig. 3 Assembled model of prestressed sleeper in ABAQUS imported from AutoCAD 3D

an initial stress of -1286 N/mm^2 . The negative sign here indicates the compressive force that will be transferred to the concrete after the assembly.

The mesh size of concrete adopted for this study was 100 mm, while prestressing steel mesh size was taken to be 30 mm. Two steps were created along with the initial step. In the initial step, prestressing was introduced in the initial step in ABAQUS. The boundary conditions were provided in the first step as static, and general. The loading conditions were provided in the second step as static, and general. The second step consisted of 800 s over which the load was applied gradually according to the test procedure.

2.4 Static Testing

In the static analysis, the four-point bending test is simulated in Abaqus for this sleeper and is checked for the moment of resistance and moment of failure. The test setup for this test is shown in Fig. 4.

The test methodology adopted is as follows:

1. The sleepers are loaded gradually (at the rate of 30–40 kN/min) up to the specified load, which will be retained at this level for three minutes for observing cracks, if any. For this purpose, a crack is defined as one which is barely visible to the naked eye and is at least 15 mm long from the tension edge of the sleeper. However, if a crack appears smaller than the specified load, that value shall be recorded [3].
2. For the ‘Moment of Resistance’ (MR) test, the sleeper shall be deemed to have passed the test if it sustains the loads specified in the relevant sleeper drawing without cracking. While loading, the load can be applied up to 5 kN more than the specified load.
3. For the ‘Moment of failure’ (MF) test, the sleeper shall be deemed to have passed the test if it can take a load beyond the specified test load. The initial cracking loads shall also be recorded for rail seat bottom, centre top and/or centre bottom (as the case be) for further statistical analysis of data during the MF test.

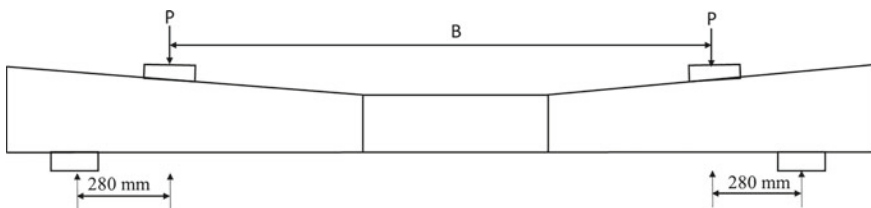


Fig. 4 Test setup for four-point bending test on the sleeper

3 Results and Discussion

The results obtained for the deflection and moment of resistance and moment of fracture test are as follows.

3.1 Deflection

The numerical model of a sleeper has been tested for four-point bending under a load of 147.15 kN for two cases: one with prestressing and one without prestressing. The deflection detected in the sleeper without prestressing was 6.69 mm and the deflection in the sleeper with prestressing was 4.38 mm, as shown in Fig. 5a, b. The permissible deflection for sleeper according to Indian standards is 20 mm [3].

3.2 Moment of Failure and Moment of Resistance Test

The sleeper was loaded at a rate of 30 kN/min for 800 s. For the moment of resistance test, a crack of 15 mm should appear after 230 kN [6]. Minor cracks have been observed at 130 kN, but for the crack to propagate up to 15 mm, a far larger load is required, thus we can conclude that the sleeper is safe for the moment of resistance test. Since the sleeper did not fail up to a load of 370 kN, it can be concluded that it is safe for moment of resistance test according to Indian standards [6]. The load deflection curve is plotted for the four-point bending test and is shown in Fig. 6.

4 Conclusions

Based on the geometry of the Mainline Broad-Gauge sleeper (RDSO/T-2496), a three-dimensional nonlinear finite element modelling of prestressed concrete railway sleepers is done using ABAQUS software. To simulate the behaviour of high-strength concrete, the model considered a concrete damage plasticity model and for prestressing strands, solid elements were used. Following are the conclusions from this paper.

- In this study, solid elements were used instead of beam elements for prestressing strands, which produced reliable results.
- The sleeper was tested under four-point loading and verified with sleeper manufacture checks.
- The first crack in the prestressed sleeper was observed at the load of 130 kN.
- The prestressed sleeper did not fail up to 370 kN indicating that it is safe for the moment of fracture test according to IRS-T39.

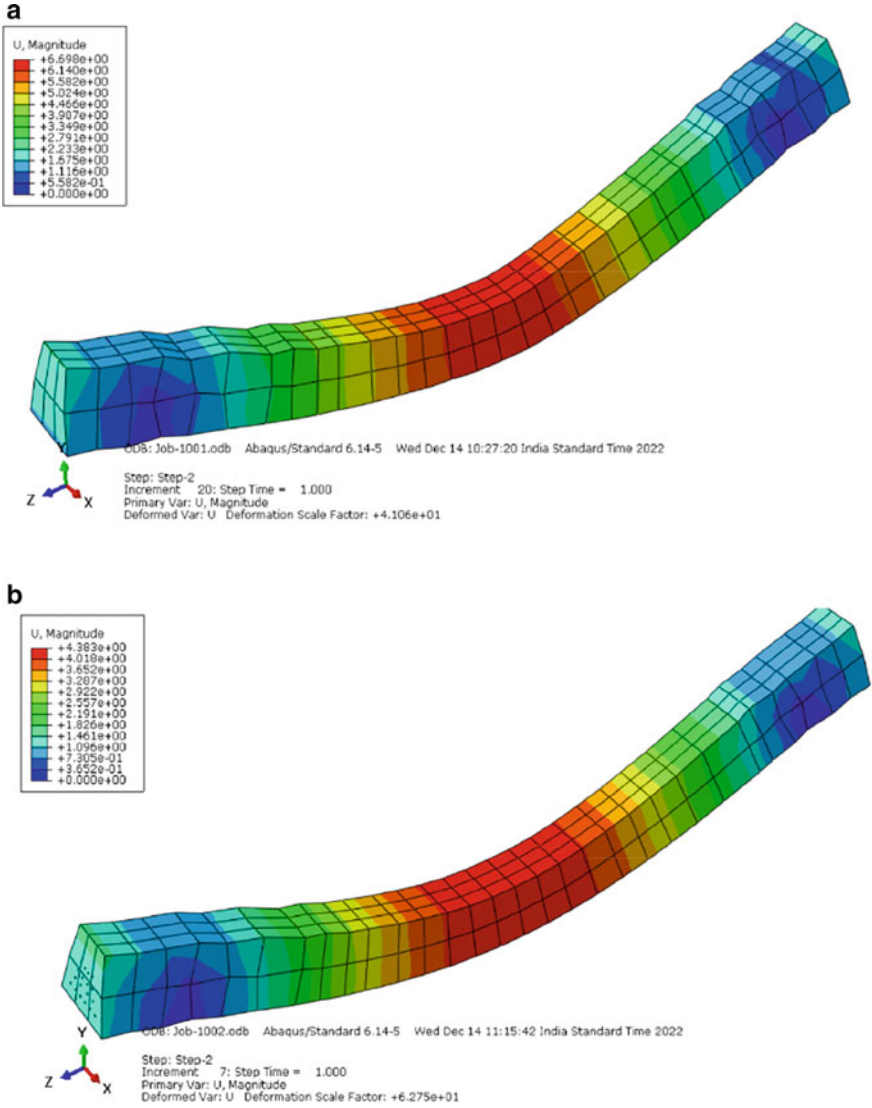


Fig. 5 a Deflection of sleeper under four-point bending test excluding prestressing in the strands. **b** Deflection of sleeper under four-point bending test including prestressing in the strands

- From the numerical analysis of prestressed sleeper, the maximum value of deflection is found to be 4.38 mm which is within the permissible limit 20 mm as per Indian standards.

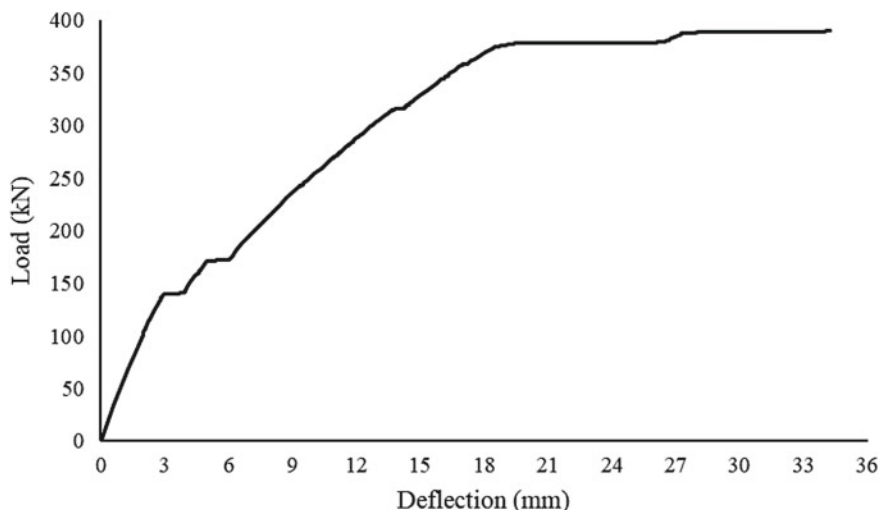


Fig. 6 Load deflection curve of the prestressed sleeper under four-point loading

References

1. Dan L, Sakdirat K, You R, Liu P (2022) Fatigue life modelling of railway prestressed concrete sleepers. *Structures* 41:643–656
2. El-sayed M, Zohny H, Riad H, Nour M (2021) A three-dimensional finite element analysis of concrete sleepers and fastening systems subjected to coupling vertical and lateral loads. *Eng Failure Anal* 122:105236
3. Indian Railway standard specification for pre-tensioned prestressed concrete sleepers for broad gauge, metre gauge and narrow gauge. T-39 October 2020. Research designs and standards organisation
4. Khan I (2021) Mechanical performance of geopolymer prestressed railway sleepers. *Mater Today Proc* 47:414–423
5. Parvez A, Stephen F (2017) Fatigue of steel-fibre-reinforced concrete prestressed railway sleepers. *Eng Struct* 141:241–250
6. Quality assurance planning for manufacturing of PSC Sleepers—August 2017 (CAMTECH/C/2017/QA-PSC Sleeper/1.0). Ministry of Railways
7. Sakdirat K, Fu H, Ye C (2021) Numerical studies to evaluate crack propagation behaviour of prestressed concrete railway sleepers. *Eng Failure Anal* 131:105888
8. Šimonová H, Veselý V, Keršner Z, Culík L, Mosler T, Bilek V (2014) Influence of the age and level of concrete fatigue on prestressed railway sleeper response: parametric study and experiment. *Adv Mater Res* 969:218–221. Trans Tech Publications, Switzerland
9. Technical Diary 2020–21, Indian Railways Civil Engineering Portal
10. Yang F, Wei Z, Sun X, Shen C, Núñez A (2021) Wheel-rail rolling contact behavior induced by both rail surface irregularity and sleeper hanging defects on a high-speed railway line. *Eng Fail Anal* 128:105604
11. You R, Goto K, Ngamkhanong C, Sakdirat K (2018) Nonlinear finite element analysis of structural capacity of railway prestressed concrete sleepers with rail seat abrasion. *Eng Failure Anal* 95
12. You R, Sakdirat K (2019) Evaluation of remaining fatigue life of concrete sleeper based on field loading conditions. *Eng Failure Anal* 105

A Machine Learning Based Model to Assess Flexural Strength of Corroded Reinforced Concrete Beams



Arjun Sharma , Somain Sharma , and Kuldeep Kumar 

Abstract Corrosion in members is a significant durability problem in reinforced concrete; it reduces load-carrying capacity. This study collected corroded reinforced concrete beam specimens tested under flexural loads from the published literature. The whole database comprises 177 corroded beam specimens. A few parameters of the corroded beams, such as width, beam depth, compressive strength of concrete, yield strength of steel reinforcement, percentage weight loss etc., were collected from the literature. Two different machine-learning-based model was trained to predict the residual flexural strength of the corroded beam. K-Nearest Neighbor (KNN) and Support Vector Machine (SVM), were used to train the models for predictions. Comparative analysis of the models was done using six statistical indices R^2 , Mean Absolute Percentage Error (MAPE), Mean Absolute Error (MAE), Root Mean Square Error (RMSE), $a-20$ index, and Nash Sutcliffe, to propose the best of the two model for prediction. The results from the SVM model show an R^2 -value of 0.989 and that of the KNN model show 0.809. The proposed ML models are reliable, accurate, fast, and cost-effective. This model can be utilized as a structural health-monitoring tool to detect the early damages in the RC beams.

Keywords Corroded beams · Residual flexural strength · KNN · SVM · ML

1 Introduction

Reinforced Concrete (RC) was considered to be a highly durable material, but, soon corrosion of RC members was discovered has a major durability problem in the RC structures [1, 2]. RC structures have four major structural components the slab, beam, columns and footings. The beams are responsible for the transfer of the live load imposed on the slab to the columns, therefore plays a crucial part load transfer in RC structure. RC beams are anticipated to fail in flexure rather than to shear because

A. Sharma · S. Sharma (✉) · K. Kumar
Department of Civil Engineering, Punjab Engineering College (Deemed to Be University),
Chandigarh 160012, India
e-mail: somainsharma@gmail.com

shear failure is a brittle failure with no warnings [3]. However, during the service period of the beam it may be deteriorated by the effect of chloride ions or carbonates, present in the external atmosphere of the beam [4]. These carbonates tend to enter the RC environment through the presence of voids in RC surface [4]. Other variables that contribute to the deterioration of embedded reinforcement include concrete cracks and inadequate covering [5]. The most common cause of structural deterioration and catastrophic collapse during a structure's lifetime is corrosion of reinforcement bars embedded in concrete [4, 5].

Sectional losses of both steel and concrete occur as a result of corrosion in the steel reinforcement, creating a high stress zone in the reinforcement (due to reduction in the effective cross sectional area). An iron oxide layer that forms on the surface of reinforcement typically shields the reinforcement [6], but it is not very effective in shielding from corrosion initiation. The bond strength, which is the adhesive force between the concrete and steel is also reduced considerably, due to the volumetric expansion inside the RC beam [7]. The volumetric expansion in the RC member, can be attributed to the new products formed after the chemical reaction of corrosion. The corrosion initiation is possible either due to the attack of Calcium hydroxide ($\text{Ca}(\text{OH})_2$), or Chloride ions (Cl^-). Calcium hydroxide ($\text{Ca}(\text{OH})_2$) in the concrete reacts with atmospheric carbon dioxide (CO_2), which seeps through voids and concrete with poor consistency, to produce regions of low pH near to the reinforcement. Low pH and Calcium Hydroxide attack cause damage to the reinforcement's passive protective iron oxide layer, which eventually causes the reinforcement to corrode [8, 9]. The activity of chloride ion can damage the shielding oxide layer that surrounds the reinforcement. Free chloride ion, may be present in the water which was used during construction and curing processes. It can also seep into concrete during the service period from the atmosphere such as through action of rain or the presence of humid conditions [10]. The combined effect of all of this lowers the RC Beams' ability to support flexural loads. Additionally, corrosion in RC beams causes the failure mode to transition from pure shear failure to flexure failure [11]. Thus, it is crucial to predict the flexural strength of corroded RC beams in order to guarantee the durability of the beams over the course of their entire life-cycle.

A lot of research has been done on the methods of retrofitting for the rehabilitation of the structure [12–16]. The common aspect of these retrofitting techniques is to accurately predict the residual strength of the element. Therefore, this work attempts to predict the residual flexural load carrying capacity of the beam.

Emerging fields of computer science such as artificial intelligence (AI) and machine learning (ML) enable the development of machine learning models that simulate human intelligence and the development of data-based descriptive models that are effective at handling extremely complex problems seamlessly. For engineering applications, a well-built ML model reveals dependency connections between the input parameters and the predicted variable. There is a lot of possibility for ML to be used in the development of expert tools in the field of engineering.

The development of a machine learning-based method to forecast the flexural strength of corroded reinforced concrete (RC) beams is discussed in the article [17]. To choose the most accurate predictive model, the study comprised training and

assessing various single and ensemble machine learning models. The best model was then put into a graphical user interface (GUI) for real-world application, enabling quick, precise, and knowledgeable forecasting of the flexural capacity of corroded RC beams. The created tool is simple to use and can let the created machine learning model be used in real-world applications. The gradient-boosting algorithm, with an R^2 value of 97.30%, was suggested by the authors as the proposed model since it produced the best results on the training dataset.

This research makes use of machine learning (ML) to provide predictions regarding the seismic failure mode of corroded RC columns as well as their maximum bearing capacity [18]. There are 180 corroded RC column cycle tests contained within a huge database. The predictive model makes use of a total of six different machine learning (ML) techniques, including three single learning techniques (k-Nearest Neighbours, Decision Tree, and Artificial Neural Network) and three ensemble learning techniques (Random Forest, AdaBoost, and CatBoost). A case-study column demonstrates ML-based seismic performance assessment of RC columns. With 89% accuracy, the Random forest and CatBoost models predict seismic failure modes best. The CatBoost model predicts bearing capacity better than mechanism-based coding models, with an R^2 of 0.92.

This article proposes an RC beam lifetime flexural strength forecasting model. For predictive model development, k-nearest neighbour (KNN) and Support Vector Machine (SVM) methods are employed to train experimental data. To begin, a database consisting of 177 corroded RC beam samples tested under flexural loads were compiled from the relevant published research. Based on nine different input parameters, indicating geometric measurements, material qualities, reinforcement details, and the degree of beam corrosion, the models are trained to forecast the ultimate flexural strength. Later to compare the two models, six different statistical parameters (Coefficient of determination (R^2), Mean Absolute Percentage Error (MAPE), Mean Absolute Error (MAE), Root Mean Square Error (RMSE), Nash Sutcliffe (NS) and a20-index) were considered.

2 Research Significance

For the purpose of corroded degraded beam repair and rehabilitation, it is crucial to ascertain the residual flexural strength of the corroded beams. It is important to ascertain the strength to choose the most suitable rehabilitation technique. The evaluation of the residual strength of corroded beams is thus not covered by the current norms of procedure. So, it becomes crucial to precisely assess the strength of the corroded beams. Due to the complexity of the corrosion process and the numerous dependent factors, it might be challenging to determine the residual flexural strength of corroded RC Beams. The axial load-carrying capability of RC Beams has been determined in this study using a potent ML-based approach to handle this issue.

3 Methods

The data set of 177 experimentally tested beam samples that was used for training includes the compressive strength of concrete (f_c), the width (b) and depth (h) of the beam section, the section ratio of the longitudinal steel reinforcement (rl), the shear span-to-depth ratio of the beam (l), the corrosion degree of the longitudinal reinforcement, which was expressed as the weight loss ratio (η_{wrt}) and the section loss ratio of the longitudinal reinforcement (η_{lsn}), and the ultimate flexural strength from tests at failure (M_{fx}). This corroded beam dataset was collected from multiple published literatures [19–29], in total, the dataset was collected from 10 published literature. Out of these parameters, the models were trained to predict the M_{fx} , rest all parameters were the input parameters. Input parameters were carefully selected, and also depended on the enough availability of data to create the proposed model in the best way possible. The range of input parameters and predicted parameter from each of the literature for the dataset is shown in Table 1 below. It shows that the η_{wrt} , of the specimens from Jin and Zhao et al. are in the range of 0.47–6.05% and similarly for other parameters. The number of specimens needed to propose any ML-based model should be larger than ten times the input parameters [30, 31], therefore the algorithms that were developed for calculating the residual flexural strength of the corroded RC Beam is sufficient. The minimum, maximum, mean, and standard deviation of the collected database are displayed in Table 2.

3.1 Normalisation

The act of Normalisation renders the data unitless, making it simple for artificial or machine learning algorithms to comprehend. Using the Normalisation technique, all values are distributed between a range of two numbers, in this case, 0 and 1. Without normalisation, large-value neurons have a considerably greater training impact than small-value neurons; this could cause the model's precision training to deviate and produce erroneous results. As a result, data normalization was required for our investigation. The mathematical expression used for the standardisation is described in Eq. (1) [7].

$$Z_{normalized} = \frac{(y - y_{min})}{(y_{max} - y_{min})} \quad (1)$$

where $Z_{normalized}$ is the result that has been normalised, y is the value that has to be normalised in the given dataset, y_{min} is the lowest value and y_{max} is the highest value in the given dataset.

Table 1 Range of parameters from the collected database

References	Strength of concrete (Mpa)	B (mm)	H (mm)	Pl (%)	σ_y (MPa)	λ	η_{wt} (%)	η_{st} (%)	M_{fx} (KN.m)
Jin and Zhao [19]	22.13	150	150	1.33	427	2.65	0.47-6.05	1.76-7.27	7.89-10.27
Hui et al. [20] (24 tests)	31.4-39.6	151-176	249-256	0.58-1.52	293-495	3-3.3	0-10.99	0-16.42	17.74-38.95
Cao et al. [21] (12 tests)	34.4	120	200	1.08	470-500	2.78	0-13.05	0-18.35	12.9-26.73
Xia et al. [22] (20 tests)	25.9-35.6	150	200	1.49-1.72	425-575	2.06	0-10.36	0-11.55	18.34-38.5
Azad et al. [23] (36 tests)	28	200	215-315	0.78-1.61	575-593	1.35-2.2	1.39-26.29	2.67-35.8	16.1-65.98
Azad et al. [24] (24 tests)	33.4-46.49	150	150	0.92-1.54	520-590	3.1-3.57	5.4-34.8	6.63-47.77	6.48-12.76
Shang et al. [25] (8 tests)	42.78-44.9	150-152	200	0.89-1.61	313-321	3.53-3.64	0-19.32	0-29.73	9.21-21.37
Rodriguez et al. [26] (16 tests)	42.58-62.62	150	200	0.63-1.84	575-585	4.85-4.88	0-13.35	0-18.64	10.1-39.4
Chen et al. [27] (7 tests)	30	120	200	0.83	335	2.55	0-24	0-33.8	2.84-8.82
Zhang et al. [28] (13 tests)	23.56	120	180	0.87	335	3.44	0-6.91	0-8.12	6.08-7.1

Table 2 Details of collected database

Description	Symbol	Unit	Min	Max	Average	Standard deviation
Strength of concrete	f_c	Mpa	22.13	62.62	33.78	9.42
Width of beam section	b	mm	120.00	200.00	156.37	25.63
Depth of beam	h	mm	150.00	315.00	207.25	46.09
Sectional ratio of longitudinal steel reinforcement	p_l	%	0.58	1.84	1.21	0.34
Shear span-to-depth ratio of beam	λ	–	1.35	4.88	2.87	0.91
Weight loss ratio	η_{wt}	%	0.00	34.80	7.71	7.16
Section loss ratio	η_{sn}	%	0.00	47.77	10.40	10.03
Ultimate flexure strength	M_{fx}	kN m	2.84	65.98	21.12	12.77

4 Performance Criteria

Post the formulation of two different ML models, it is important to put forward the best technique out of the two for better use and wider acceptability. This was done using the six, most commonly used statistical parameters/statistical indices, namely coefficient of determination (R^2), Mean Absolute Percentage Error (MAPE), Mean Absolute Error (MAE), Root Mean Square Error (RMSE), Nash Sutcliffe (NS) and a20-index. These statistical parameters are widely used in the literature [7, 32, 33]. The idea behind the use of these parameters is to evaluate the performance of the model in the most comprehensive manner, i.e. analysing both the errors in the predicted results as well as the range in which the predicted value lie in respect to the experimental values. An R^2 value of 1 denotes a strong association, while a value of 0 denotes a random relationship, and it evaluates the correlation between outputs and targets. A statistical forecasting method’s prediction accuracy is measured by the mean absolute percentage error [34]. Nash–Sutcliffe values that are near to 1 indicate that the model is doing well and diminish the accuracy of the model towards zero [35]. The Nash–Sutcliffe efficiency (NSE) is equal to one (NSE 1) for a model that is flawless and has an error variance of zero, and vice versa. The a-20 index, a modern statistical engineering indicator, shows the percentage of samples that match estimation values with a 20% deviation from experimental values and may be used to evaluate AI models [45–47]. Values of NSE, R^2 and a20 index is considered best at 1 and worst at 0. Whereas, for the MAPE, MAE and RMSE lower the value, the lower the errors and hence better-predicted results. The mathematical equations of the discussed indices are shown in Eqs. (2–7).

$$R^2 = \left[\frac{\sum_{i=1}^N (E_i - \bar{E})(S_i - \bar{S})}{\sqrt{\sum_{i=1}^N (E_i - \bar{E})^2 (S_i - \bar{S})^2}} \right]^2 \quad (2)$$

$$MAPE = \frac{1}{N} \sum_{i=1}^N \left| \frac{E_i - S_i}{E_i} \right| \times 100 \quad (3)$$

$$MAE = \frac{1}{N} \sum_{i=1}^N |E_i - S_i| \quad (4)$$

$$RMSE = \sqrt{\frac{\sum_{i=1}^N (E_i - S_i)^2}{N}} \quad (5)$$

$$NS = 1 - \frac{\sum_{i=1}^N (E_i - S_i)^2}{\sum_{i=1}^N (E_i - \bar{S}_i)^2} \quad (6)$$

$$a20 - index = \frac{m20}{N} \quad (7)$$

5 Artificial Intelligence

In its simplest form, artificial intelligence is the study of how to solve problems by integrating computer science with massive databases. In addition, it covers the topics of machine learning and deep learning, which are commonly brought up while talking about artificial intelligence. These disciplines create forecasting or data categorization systems using artificial intelligence (AI) algorithms based on input [36, 37].

A subfield of artificial intelligence called “machine learning” (ML) uses algorithms to systematically identify the connections between data and information [38]. It incorporates concepts from a variety of academic fields, including logic, computer science, information theory, probability and statistics, and artificial intelligence [37].

There are various machine learning algorithms, including supervised, unsupervised, and reinforcement learning. Supervised learning involves labelled data and model training. Unsupervised learning includes training a model using unlabelled data so the algorithm can discover patterns and relationships. Machine learning employs a model to find patterns and relationships in data. The model then makes predictions or decisions based on those patterns [38]. A portion of the data used to train a machine learning model is “held back” and utilised to test its accuracy. How well the model matches the image to its label on this test dataset determines its accuracy [36].

5.1 KNN

K-nearest neighbor (KNN) is a simple yet powerful non-parametric algorithm used for both classification and regression tasks in machine learning [39]. KNN is a lazy learning algorithm, which means it does not learn a model from the training data but instead stores the entire training dataset in memory [40]. It speeds up training but slows prediction, especially for huge datasets. KNN’s simplicity and interpretability are advantages. KNN doesn’t need a training phase or make any data distribution assumptions. This makes KNN a versatile algorithm that can handle linear and non-linear input–output relationships. KNN is an interpretable algorithm [40, 41], which means it is easy to understand how the algorithm is making predictions. KNN handles noisy and incomplete data well. It can handle irregular and outlier datasets as it requires no assumptions about data distribution. Furthermore, KNN is a flexible algorithm that can be used for a variety of machine learning tasks. It can be used for both classification and regression problems, and it can handle datasets with many input variables [42].

The KNN regression method extrapolates the output values of the training set’s nearest neighbors to forecast the output value. The hyperparameter k , which is the number of neighbor, is specified prior to training. To determine the closest data points, the distance between a query point and the other point must be calculated. By creating decision boundaries, which divide query points into various regions, these distance metrics help in the division of query points. The distance function in the shape of the Minkowski measure is given by Eq. (8) which determines the distance between the neighbours

$$D(X, Y) = \left(\sum_{i=1}^k |x_i - y_i|^p \right)^{\frac{1}{p}} \tag{8}$$

where, p is the power parameter, k is the number of neighbors and x_i, y_i are the coordinates of points respectively. By assigning the power measure, p , equal to 1 and 2, respectively, it is possible to derive the Minkowski distance from the Euclidean and Manhattan distances, two additional common distance metrics which calculated distance for neighbors.

Equation 9 calculates the average of the k closest neighbours with similar properties, while Eq. 10 calculates an inverse distance weighted average [43]. Nearby neighbours have more of an impact on the target than far away neighbours.

$$\hat{f}(x) = \frac{1}{k} \sum_{x_i \in N_k(x)} y_i \tag{9}$$

$$\hat{f}(x) = \frac{\sum_{x_i \in N_k(x)} \frac{1}{d_i} y_i}{\sum_{x_i \in N_k(x)} \frac{1}{d_i}} \tag{10}$$

where, $N_k(x)$ is the neighborhood of x defined by the k closest points and d_i is the distance from the i th point to the estimated point x_i in the training data.

5.2 SVM

A popular machine learning approach for classification and regression applications is called Support Vector Machine (SVM). SVM’s primary goal is to identify a hyperplane that maximally separates data points belonging to different classes. In other words, SVM seeks to find the best decision boundary that can accurately classify new data points. SVM hyperplanes divide the input space into two sections. SVM finds the hyperplane that maximises the margin between two closest data points from distinct classes. A flat, $n-1$ -dimensional subset of an n -dimensional Euclidean space that divides the space into two disjointed sections is known as a hyperplane. SVM employs a variety of kernel functions, including linear, polynomial, and radial basis function (RBF) kernels, to determine the ideal hyperplane for the data. In SVM, the support vectors define the hyperplane, and the margin is computed based on the distance between the support vectors. SVM works well in high-dimensional spaces, which makes it ideal for solving complex problems where there are many input variables. In addition, it can identify the most important variables and ignore the irrelevant ones, which helps to improve the overall accuracy and efficiency of the algorithm. SVM is robust to outliers and works well with small datasets, unlike other ML methods. Despite a feed of small dataset, it can still identify the underlying patterns in the data even if there are a few outliers present. SVM is a well-established and well-understood algorithm that has been extensively studied and used in a wide range of applications. The prediction of the SVM algorithm is given by Eq. (11) [44]

$$f(x) = \sum_{i \in SV} (\alpha_i - \alpha_i^*) K(x_i, x) + b \text{ subject to } \alpha_i, \alpha_i^* \in [0, C] \quad (11)$$

where, $K(x_i, x)$ is the kernel function, b is a bias, C is the regularization parameters, α_i and α_i^* are the Lagrange multipliers of the lower and upper Support Vector.

6 Results and Discussions

This section discusses the results obtained from the developed models, both KNN and SVM. The results from the performance indices are discussed in this section.

The difference of predicted value from the actual value varies from -11.99 to 25.03 kN m in the KNN model. The mean and standard deviation of errors generated from the KNN model are 3.75 and 5.75 respectively. The difference of predicted value from the actual value varies from -11.20 to 5.07 kN m in the SVM model. The mean and standard deviation of the errors generated from the SVM model are

-0.02 and 1.30 respectively. The errors from the KNN and SVM model are shown here in Table 3.

Figure 1 shows the regression plot and the error plot from the developed KNN model. In the regression plot, experimental values are shown on the x-axis and predicted values are shown on the y-axis of the graph. The regression plot also shows the $\pm 10\%$ line. In case of the regression plot, most of the values lie below the 45° line, which means that the experimental value are greater than the predicted values from the KNN model. In the error plot, the x-axis shows the Number of Specimen and y-axis denotes the numerical value of error in each of the sample. In this work, error is defined as the difference between the experimental value and predicted value. The horizontal black line in the error plot, shows the zero error line. Most of the errors are numerically positive, which confirms that the predicted values from the KNN model are less than the experimental values for the corroded beam specimens.

Figure 2 shows the regression plot and error plot for the proposed SVM model. As evident from the regression plot, the most of the values lie on the 45° line. It shows that for most of the specimens the predicted values from the SVM model are equal to the experimental values collected from the literature. It can be seen that only 3 specimens outliers the range of $\pm 10\%$ error line. In the error plot, shown in Fig. 2b of the points lie on the horizontal zero error line, confirming that for most of the specimens the predicted values from the SVM model are equal to the experimental

Table 3 Details of errors in the developed KNN and SVM model

Errors in proposed model	Min (predicted value-actual value)	Max (predicted value-actual value)	Average	Standard deviation	Range
KNN	- 11.99	25.03	3.75	5.75	37.02
SVM	- 11.20	5.07	- 0.02	1.30	16.27

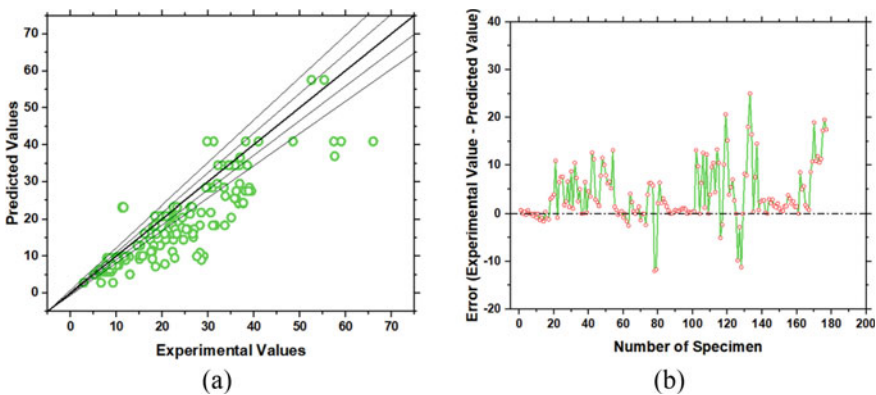


Fig. 1 Results from the developed KNN model **a** regression **b** error plot

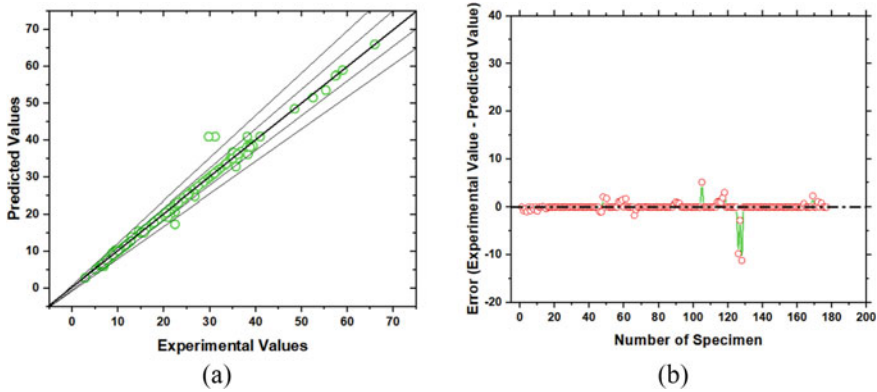


Fig. 2 Results from the proposed SVM model **a** regression plot **b** error plot

Table 4 Performance indices of the developed KNN and SVM models

Predictive model	R ²	MAPE (%)	MAE(kN m)	RMSE (kN m)	NS	a20-index
KNN	0.809	20.085	4.489	6.842	0.734	0.533
SVM	0.989	1.598	0.342	1.299	0.990	0.977

value collected from the literature. There are very few observed deviations from the zero error horizontal line in the graph.

Results from the six performance metrics are shown in Table 4. The R²-value from the KNN model is 0.809, while that from the SVM model is 0.989. The MAPE and MAE values from the KNN model are 20.085% and 4.489 kN m, respectively. The values of MAPE and MAE from the SVM model are 1.598% and 0.342 kN m, respectively. RMSE, NS and a20-index values of the KNN model are 6.842 kN m, 0.734 and 0.533, respectively. From the SVM model, the values of RMSE, NS and a20-index are 1.299 kN m, 0.990 and 0.977, respectively.

7 Conclusion

This work develops two machine learning based models, namely k-nearest neighbour and support vector machine to predict the residual flexural strength of corroded reinforced concrete beams. A total of 177 corroded reinforced concrete beam samples were collected from the literature, to train the machine learning models. The data set of 177 experimentally tested beam samples which was used for training which consists of the compressive strength of concrete (f_c), width of beam section (b), depth of beam section (h), section ratio of longitudinal steel reinforcement (rl), shear span-to-depth ratio of beam (l), corrosion degree of longitudinal reinforcement were

expressed as weight loss ratio (η_{wt}) and the section loss ratio of longitudinal reinforcement (η_{sn}), ultimate flexural strength from tests at failure (M_{fk}). The comparison of the two developed model is done based on the six statistical indices, coefficient of determination (R^2), Mean Absolute Percentage Error (MAPE), Mean Absolute Error (MAE), Root Mean Square Error (RMSE), Nash Sutcliffe (NS) and a20-index:

1. The SVM model outperformed the developed KNN model, in all the six statistical indices. It had an R^2 -value of 0.989 which is better than the R^2 -value of KNN model 0.809. Similarly, the MAPE, MAE and RMSE also had the difference of 18.487, 0.342 and 5.543 respectively.
2. The KNN model has a poor precision compared to that of the SVM model as for only 73.4% of specimens the predicted value lied between the range of 0.8–1.2 times of the experimental value. The precision of the SVM model is 99%.
3. Since the anticipated values for the majority of the specimens are lower than the experimental values, the constructed KNN model is conservative in its outcomes prediction.

The proposed SVM model is robust in predicting the residual flexural strength of corroded RC beams. The developed model can be widely used, as it showed promising results with very high precision. The developed model is also easy to use, compared to that of the existing analytical models available which require more significant level of effort. The proposed model can further be advanced by adding more and more corroded beams specimens, to create a larger dataset for the training purposes.

References

1. Yépez F, Yépez O (2017) Role of construction materials in the collapse of R/C buildings after Mw 7.8 pedernales—Ecuador earthquake, April 2016. *Case Stud Struct Eng* 7:24–31
2. Sharma K, Deng L, Noguez CC (2016) Field investigation on the performance of building structures during the April 25, 2015, Gorkha earthquake in Nepal. *Eng Struct* 121:61–74
3. Punmia BC (1992) Reinforced concrete structures vol 1, 1st edn. Laxmi Publication Pvt Ltd
4. Castel A, François R, Arliguie G (2000) Mechanical behaviour of corroded reinforced concrete beams—part 1: experimental study of corroded beams. *Mater Struct* 33:539–544
5. Shaikh FUA (2018) Effect of cracking on corrosion of steel in concrete. *Int J Concr Struct Mater* 12:1–12
6. Wang J, Basheer PAM, Nanukuttan SV, Bai Y (2015) Influence of cracking caused by structural loading on chloride-induced corrosion process in reinforced concrete elements: a review. In: Durability of reinforced concrete from composition to protection: selected papers of the 6th international RILEM PhD workshop held in delft, The Netherlands, July 4–5, 2013. Springer, pp 99–113
7. Sharma S, Arora HC, Kumar A, Kontoni DPN, Kapoor NR, Kumar K, Singh A (2023) Computational intelligence-based structural health monitoring of corroded and eccentrically loaded reinforced concrete columns. *Shock and Vibration*
8. Nguyen TH, Nguyen DT, Nguyen DH, Tran DH (2022) Evaluation of residual strength of corroded reinforced concrete beams using machine learning models. *Arab J Sci Eng* 47(8):9985–10002

9. Ahmad S (2003) Reinforcement corrosion in concrete structures, its monitoring and service life prediction—a review. *Cement Concr Compos* 25(4–5):459–471
10. Zhou Y, Gencturk B, Willam K, Attar A (2015) Carbonation-induced and chloride-induced corrosion in reinforced concrete structures. *J Mater Civ Eng* 27(9):04014245
11. Fu B, Feng DC (2021) A machine learning-based time-dependent shear strength model for corroded reinforced concrete beams. *J Build Eng* 36:102118
12. Bossio A, Lignola GP, Protà A (2018) An overview of assessment and retrofit of corroded reinforced concrete structures. *Procedia Struct Integrity* 11:394–401
13. Aquino W, Hawkins NM (2007) Seismic retrofitting of corroded reinforced concrete columns using carbon composites. *ACI Struct J* 104(3):348
14. Meda A, Mostosi S, Rinaldi Z, Riva P (2016) Corroded RC columns repair and strengthening with high performance fiber reinforced concrete jacket. *Mater Struct* 49:1967–1978
15. Triantafyllou T (2011) Innovative textile-based composites for strengthening and seismic retrofitting of concrete and masonry structures. In: *Advances in FRP composites in civil engineering: proceedings of the 5th international conference on FRP composites in civil engineering (CICE 2010)*, Sep 27–29, 2010, Beijing, China. Springer, Berlin, pp 3–12
16. Bhattacharjee J (2016) Rehabilitation/retrofitting of concrete structures along with case study. *Civil Eng Urban Plann Int J* 3(2):1–11
17. Abushanab A, Wakjira TG, Alnahhal W (2023) Machine learning-based flexural capacity prediction of corroded RC beams with an efficient and user-friendly tool. *Sustainability* 15(6):4824
18. Xu JG, Hong W, Zhang J, Hou ST, Wu G (2022) Seismic performance assessment of corroded RC columns based on data-driven machine-learning approach. *Eng Struct* 255:113936
19. Jin WL, Zhao YX (2001) Test study on bending strength of corroded reinforced concrete beams. *Ind Construct* 31(5):9–11
20. Hui YL, Li R, Lin ZS, Quan MY (1997) Experimental studies on the property before and after corrosion of rebars in basic concrete members. *Ind Construct* 27(4):14–18
21. Cao FB, Wang CX, Liu LG, Xin YD, Li JH, Tian ZG (2015) Experimental study and rigidity analysis on corroded reinforced recycled concrete beams. *Build Struct* 45(10):49–55
22. Xia J, Jin WL, Li LY (2012) Effect of chloride-induced reinforcing steel corrosion on the flexural strength of reinforced concrete beams. *Mag Concr Res* 64(6):471–485
23. Azad AK, Ahmad S, Al-Gohi BHA (2010) Flexural strength of corroded reinforced concrete beams. *Mag Concr Res* 62(6):405–414
24. Azad AK, Ahmad S, Azher SA (2007) Residual strength of corrosion damaged reinforced concrete beams. *ACI Mater J* 104(1):40–47
25. Shang DF (2005) Study on flexural behavior of corroded reinforced concrete beams. Dissertation for the doctoral degree. Tongji University, Shanghai (in Chinese)
26. Rodriguez J, Ortega LM, Casal J (1997) Load carrying capacity of concrete structures with corroded reinforcement. *Constr Build Mater* 11(4):239–248
27. Chen J (2013) Study on degradation regularity of bearing capacity of RC beams under corrosive conditions. *J Disaster Prev Mitig Eng* 33:83–87 (in Chinese)
28. Zhang Z (2010) Experimental study of bending behavior of corroded reinforced concrete beams. Dissertation for the Doctoral Degree. Shanghai: Shanghai Jiao Tong University
29. Abu-Mostafa YS, Magdon-Ismail M, Lin HT (2012) Learning from data: AML Book: AML Book
30. Kumar A, Arora HC, Kumar K, Mohammed MA, Majumdar A, Khamaksorn A, Thinnukool O (2022) Prediction of FRCM–Concrete bond strength with machine learning approach. *Sustainability* 14(2):845
31. Kapoor NR, Kumar A, Kumar A, Kumar A, Mohammed MA, Kumar K, Kadry S, Lim S (2022) Machine learning-based CO₂ prediction for office room: a pilot study. *Wirel Commun Mob Comput* 2022
32. Singh R, Arora HC, Bahrami A, Kumar A, Kapoor NR, Kumar K, Rai HS (2022) Enhancing sustainability of corroded RC structures: estimating steel-to-concrete bond strength with ANN and SVM algorithms. *Materials* 15(23):8295

33. Kim S, Kim H (2016) A new metric of absolute percentage error for intermittent demand forecasts. *Int J Forecast* 32(3):669–679
34. Wang WC, Chau KW, Cheng CT, Qiu L (2009) A comparison of performance of several artificial intelligence methods for forecasting monthly discharge time series. *J Hydrol* 374(3–4):294–306
35. Du-Harpur X, Watt FM, Luscombe NM, Lynch MD (2020) What is AI? Applications of artificial intelligence to dermatology. *Br J Dermatol* 183(3):423–430
36. Clark D (2020) *Artificial intelligence for learning: How to use AI to support employee development*. Kogan Page Publishers
37. Awad M, Khanna R (2015) *Efficient learning machines: theories, concepts, and applications for engineers and system designers*. Springer, p 268
38. Cunningham P, Delany SJ (2021) k-nearest neighbour classifiers-a tutorial. *ACM Comput Surv (CSUR)* 54(6):1–25
39. Kataria A, Singh MD (2013) A review of data classification using k-nearest neighbour algorithm. *Int J Emerg Technol Adv Eng* 3(6):354–360
40. Hautamaki V, Karkkainen I, Franti P (2004) Outlier detection using k-nearest neighbour graph. In: *Proceedings of the 17th international conference on pattern recognition, 2004. ICPR 2004, vol 3*. IEEE, pp 430–433
41. Batista GE, Monard MC (2002) A study of K-nearest neighbour as an imputation method. *His* 87(251–260):48
42. Brownlee J (2016) *Machine learning algorithms from scratch with Python. Machine Learning Mastery*
43. Degtyarev VV, Tsavdaridis KD (2022) Buckling and ultimate load prediction models for perforated steel beams using machine learning algorithms. *J Build Eng* 51:104316
44. Yu H, Kim S (2012) SVM tutorial-classification, regression and ranking. *Handbook Nat Comput* 1:479–506
45. Li Y, Hishamuddin FNS, Mohammed AS et al (2021) The effects of rock index tests on prediction of tensile strength of granitic samples: a neuro-fuzzy intelligent system. *Sustainability* 13(19) Article ID 10541
46. Xu H, Zhou J, Asteris PG, Jahed Armaghani D, Tahir MM (2019) Supervised machine learning techniques to the prediction of tunnel boring machine penetration rate. *Appl Sci* 9(18) Article ID 3715
47. Kumar A, Arora HC, Mohammed MA, Kumar K, Nedoma J (2022) An optimized neuro-bee algorithm approach to predict the FRP-concrete bond strength of RC beams. *IEEE Access* 10:3790–3806

Numerical Investigation on the Behaviour of Blind-Bolted Steel Beam to CFST Column Connections



K. Aparna and K. N. Rajesh

Abstract Due to several benefits provided by the combined contribution of steel and concrete the usage of steel–concrete composite structures has been extensively accepted in the building industry for decades. In order to transfer loads from one member to another, connections are an essential component of a structure. The failure criteria of the bolted beam to column connections vary due to the strength and mechanical properties of individual components. In the present study, the cyclic load carrying capacity of steel beam to bolted concrete filled steel tube connection is evaluated using finite element software ANSYS. The failure modes, strength and overall behaviour of the specimens have been studied. Blind bolted concrete filled steel tube was numerically validated and a comprehensive parametric study was conducted to determine the effect of the following parameters. The infill concrete, tube wall thickness of the steel tube connections and thickness of plate used in the beam column connection are selected as parameters for the current study. The effect of these parameters on the seismic behaviour and corresponding changes in failure mode is detailed in this study. The blind bolted CFST connections has improved strength, stiffness, moment capacities and lateral resistance and thus it has broad applications and future scopes in various fields.

Keywords Blind bolted connection · Concrete filled steel tube · Seismic behaviour · Failure mode

1 Introduction

Today, steel constructions are the material of choice for building of all sizes, from modest homes to skyscrapers. This is due to the material's numerous positive characteristics, including strength, homogeneity, elasticity, ductility, toughness, etc. In comparison to reinforced concrete columns of comparable size, CFSTs also have better lateral stiffness, higher strength, increased ductility, improved fire resistance,

K. Aparna · K. N. Rajesh (✉)
Government College of Engineering, Kannur, India
e-mail: 21m445@gcek.ac.in

© The Author(s), under exclusive license to Springer Nature Switzerland AG 2024
M. Nehdi et al. (eds.), *Proceedings of SECON'23*, Lecture Notes in Civil Engineering
381, https://doi.org/10.1007/978-3-031-39663-2_82

979

and superior aesthetics. The complexity of the beam-to-column connections and the lack of construction expertise have limited the usage of CFSTs, despite the fact that they can be a cost-effective form of composite construction. Typically, welds, bolts, or a mix of the two are used to join the CFST columns to the open section steel beams. A better understanding of the inelastic behaviour of connections is needed to make concrete-filled tube columns a viable alternative in composite construction.

Bolted connections are the most prevalent type of connection. Compared to rivets or welds, blind bolts are a form of fastener that is meant to be more durable and sturdier. Since they are entered from just one side of the material to be bonded, they are known as “blind” fasteners and are very useful in production and repair processes. Additionally, these bolts were made to be used in limited spaces where using hexagonal nuts or regular rivets would be difficult. To install a blind bolt, a normal hole must first be predrilled. The blind side expands when the joint is tightened, forming a sturdy joint.

Pouring concrete into the steel tube columns could significantly improve the stiffness and strength of a connection. The tensile behaviour of headed anchored hollow-bolts in connections between hollow steel tubes filled with concrete was investigated by Debnath et al. [1].

When concrete was present inside the hollow steel tube, the tensile pull-out behaviour of the connection was less likely to cause the connection to deform when used with CFST column connections. The strength and rigidity of the connections have also been greatly enhanced by the length of the bolt embedded into the concrete core. The performance of blind bolted connections to stainless steel tubular columns loaded with concrete was examined by Zhong et al. [2], who discovered that the blind bolts function well without shank fracture.

Liu et al. [3] conducted experimental study on cyclic behaviour of a novel steel beam-to-prefabricated CFST column connection with threaded sleeve bolts. Connection behaves as being rigid and of full-strength for non-sway frame, stiffness of connections improved due to blind bolts and the component based approach provides good estimations.

Cabrera et al. [4] conducted a thorough research for a concrete-filled column using extended hollow bolt connections. The study’s findings led them to the conclusion that the grade of bolts and concrete’s strength are the main determinants of the stiffness and strength of connections. These connections displayed rigid and semi-rigid behaviour when subjected to cyclic loading. Each component exhibits a distinct behaviour, such as bending or stress. As a result, they recommended outlining the need for in-depth research on the combined action of components as a joint.

Similar studies were performed by Wang et al. [5] on blind bolted CFST columns for low-rise structures. They had put forward some measures in the panel region like local thickening of the tube wall to increase the initial stiffness. Also, the anchorage length of the bolt was extended to improve the tensile performance. But it had no significant effect on the moment capacity. They proposed an anchorage length ratio of 0.25 for the design.

In their investigation of the behaviour of stainless steel blind bolted T-stub to stainless steel tube connections filled with concrete; Li et al. [6] discovered that the concrete infill significantly increased the initial stiffness and load-carrying capacity of CFSSTs by preventing the inward deformation of tube side walls and achieving a fixed boundary condition for tube face walls.

2 Numerical Modelling

A numerical model was developed using the commercial finite element software ANSYS Workbench R22 [7] to determine the effect of cyclic loading on bolted steel beam to CFST column connection. The validation of the generated model was done with the experimental results obtained by Liu et al. [3].

2.1 Geometry of the Connection

The dimensions of the model and material properties of the components of the model adopted in the experimental study conducted by Liu et al. [3] are used for the modelling of the FE model. The steel beam model of span 1160 mm on both sides and width 150 mm, the column of width 250 mm and height 1715 mm, the end plate of width 200 mm and depth 460 mm and bolt of shank diameter 16 mm for connection are dimensions of the components of the model used for the modeling purpose. The detailed geometry of every part in the connection is given in Fig. 1.

2.2 Material Model

In the present study the constitutive model of the steel components developed by Liu et al. [2] was used based on the tensile coupon test conducted by them for finite element modelling. Figure 2 shows the constitutive models of stress strain characteristics of steel tubes, bolt, beam flange, beam web and end plate used in the present study. The stress- strain characteristics of the steel material were input using the bilinear stress strain curve. The Poisson's ratio was taken as 0.3.

The isotropic hardening model is selected for concrete. SOLID186 element with stress-strain curve is employed for modelling concrete in the FEA. The confined uniaxial stress-strain curve is applied to define the concrete material property. Tests have been shown that the stress strain relationship for concrete confined by suitable arrangement is different from that of unconfined concrete.

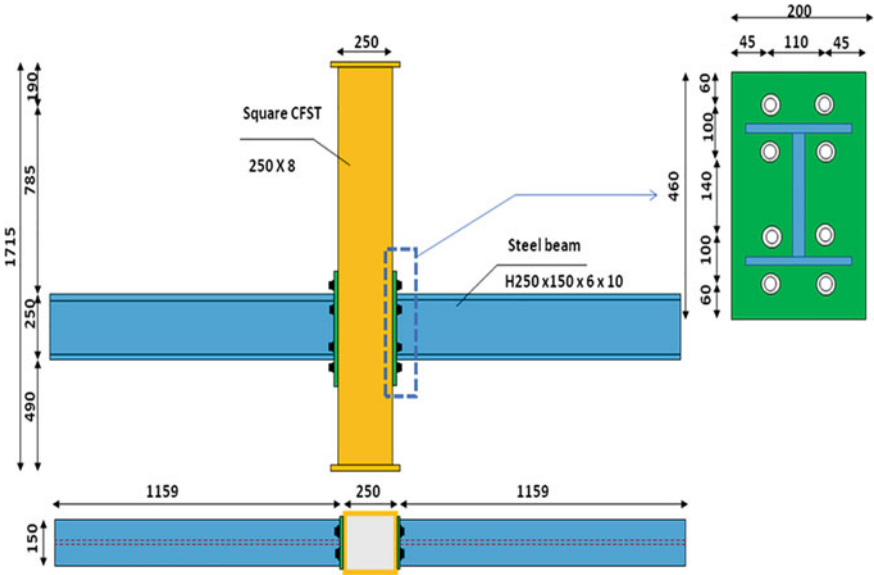


Fig. 1 Geometry of the connection

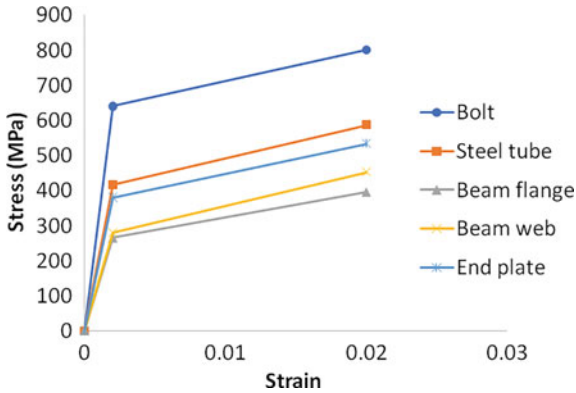


Fig. 2 Stress strain curve of components used in the model [3]

2.3 Finite Element Modelling

The solid 186 element was used for meshing. It is a higher order 3-D, 20-node solid element that exhibits quadratic displacement behaviour. The element is defined by 20 nodes having three degrees of freedom per node: translations in the nodal X, Y, and Z directions. In the specimen the column was hinged at bottom hence horizontal displacement in the directions of X, Y, and Z are all restricted. The beam was hinged on both sides. Load was applied as cyclic through column top in the horizontal X

direction. Figure 4 shows the loading protocol. The loading process is displacement-controlled. Analysis was carried out using the static general method in ANSYS Workbench till the peak load as observed in the experiment test. Displacement was predominantly load controlled throughout the experiment. Figure 3 shows the model generated in ANSYS software with the loading directions and boundary conditions.

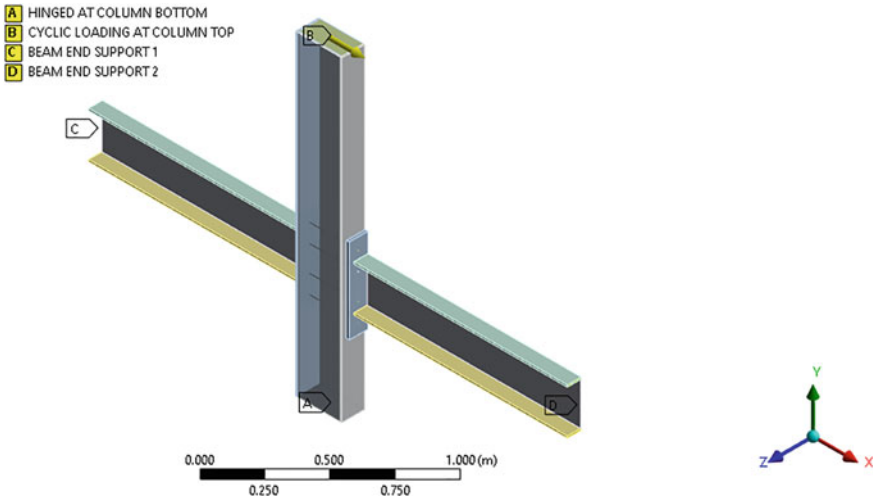


Fig. 3 Model generated in ANSYS

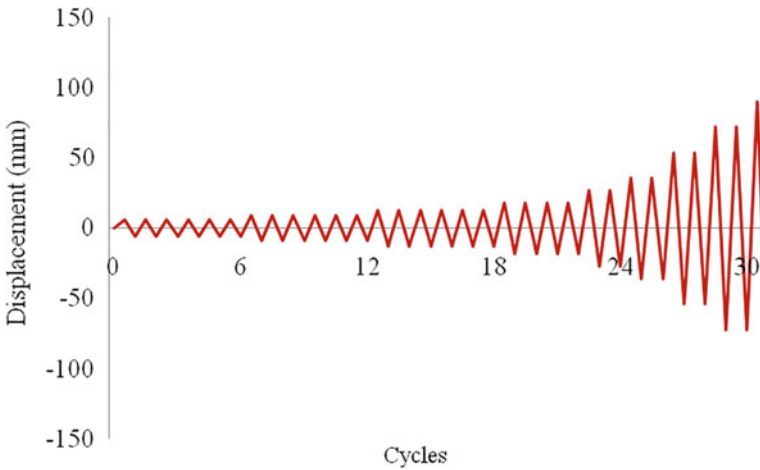


Fig. 4 Loading protocol- SAC-97

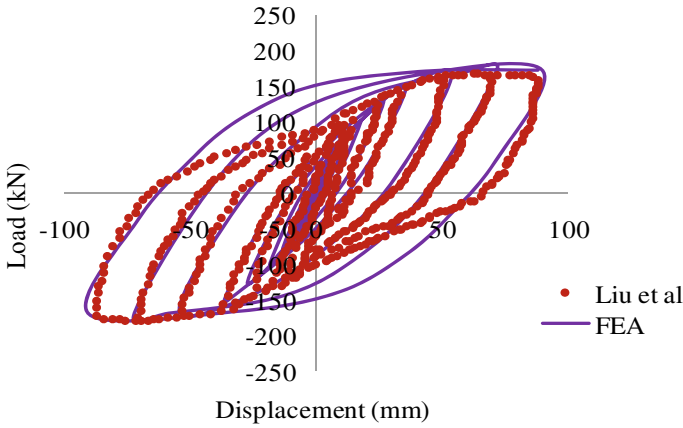


Fig. 5 Load- displacement curve of model

2.4 Validation of Model

The numerical model developed was validated using result obtained by Liu et al. [3]. The deviation observed was 2.01% respectively Fig. 5 represents the load displacement curve of the samples obtained.

3 Parametric Study

3.1 Effect of change in thickness of end plate

The effect of change in thickness of the end plates used in the connection was chosen as the thickness of end plate had a significant influence on the connection strength and ductility. A total of 5 models were developed varying the thickness of the end plates and the material properties of all the parts of the model were kept constant. Figure 6 shows the Load-deformation curve of different thickness of end plate.

It was observed that increase in the thickness of the end plate improved the lateral load carrying capacity of the connection. Table 1 shows the variation of load with end plate thickness.

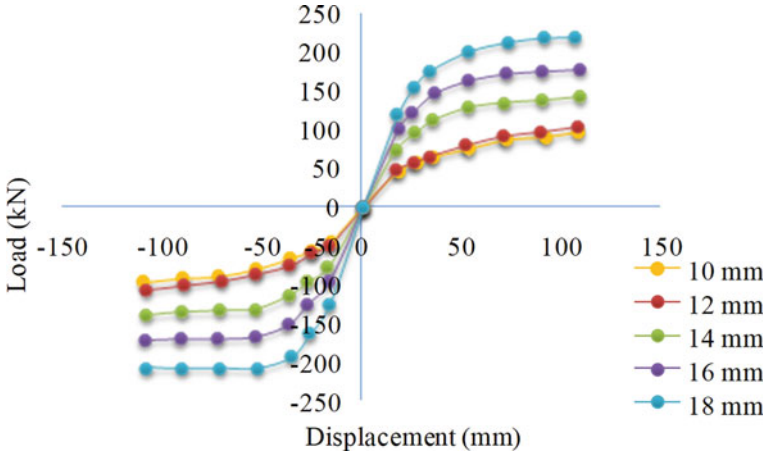


Fig. 6 Load- deformation curve of different thickness of end plate

Table 1 Variation of load with end plate thickness

Model	Thickness of end plate (mm)	Peak load obtained (kN)
2	10	96.523
3	12	105.92
4	14	137
5	16	171.712
6	18	206.0496

3.2 Effect of Change in Thickness of Steel Tubes

The effect of change in thickness of steel tube of the CFST column was chosen as another parameter which influences the connection under applied cyclic displacement. The material properties for steel tube, concrete, endplate, bolt and beam are kept constant. Table 2 shows the variation of load with thickness of steel tube. As the thickness of tube increases the area of region yielded in the tube decreases considerably and also the stress induced in concrete decreases. Figure 7 shows the Load-deformation curve of different thickness of steel tube.

3.3 Effect of Infill Concrete

The effect of infill concrete in the connection is studied to see the importance of concrete in the connection. The presence of infill concrete improved the lateral load carrying capacity by 15.5% (Fig. 8).

Table 2 Variation of load with steel tube thickness

Model	Thickness of steel tube (mm)	Peak load obtained (kN)
7	6	153.8
5	8	171.712
8	10	197.5
9	12	206.1
10	14	223.3

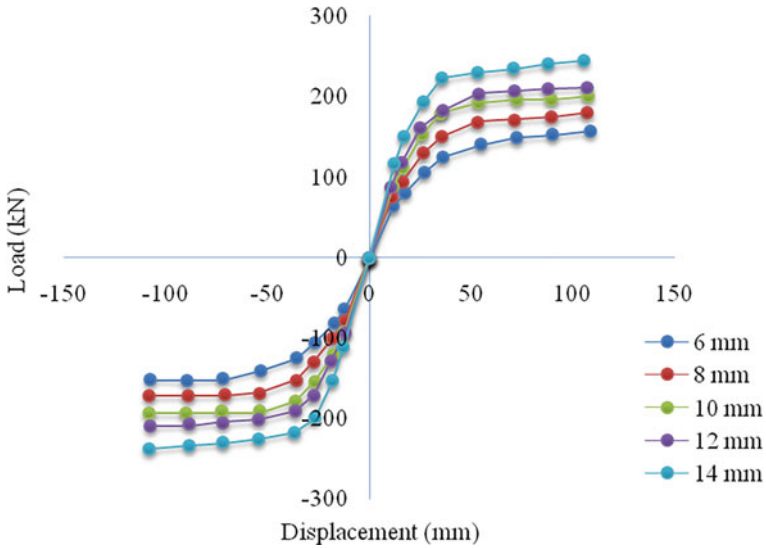


Fig. 7 Load-deformation curve of different thickness of steel tube

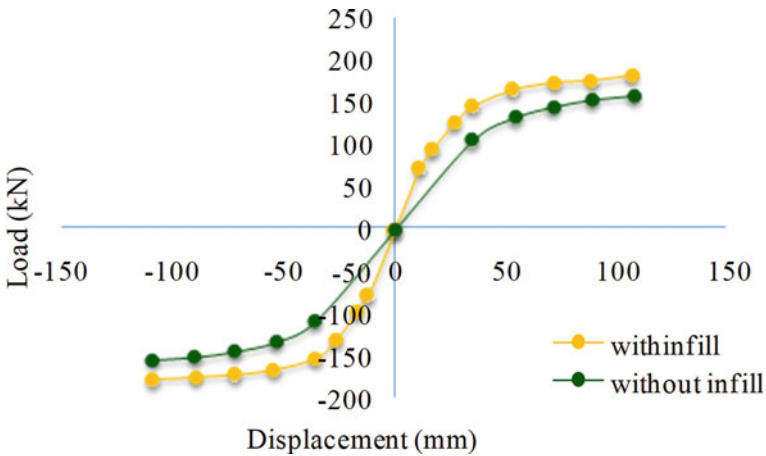


Fig. 8 Load-deformation curves showing effect of infill concrete

4 Conclusions

The finite element model in ANSYS developed was able to represent the bolted connection of CFST column and Steel beam.

The previous studies indicate that in such connection joint failure comes in to picture. To control that some of the parameters were chosen. The major conclusions of arrived after different parametric study are listed.

- The connection's ability to carry lateral loads increased as end plate thickness increased. An optimum thickness of 12 mm can be adopted as its displacement ductility is high among other thicknesses.
- The area of the zone surrendered significantly lowers with an increase in steel tube thickness, and the stress created in the concrete likewise decreases.
- Therefore, it is important to choose the steel tube thickness in a CFST column-steel beam connection by lowering the likelihood of column failure while also taking cost into account.
- By 15.5%, the lateral load carrying capacity was increased by the addition of infill concrete. As a result, when concrete is present, the member's strength improves.

The present study concentrated only on cyclic loading. Studies may be conducted including monotonic loading and also axial loading for determining the effect of axial load ratio.

References

1. Debnath PP, Chan TM (2022) Tensile behaviour of headed anchored hollow-bolts in concrete filled hollow steel tube connections. *Eng struct.* 234
2. Zhong Tao MD, Hassan K, Song T-Y, Han L-H (2018) Experimental study on blind bolted connections to concrete-filled stainless-steel columns. *J Constr Steel Res* 128:825–838
3. Liu HQ, Liu YZ, Huo JS, Zhu DJ (2021) Cyclic behavior of a novel steel beam-to-prefabricated CFST column connection with threaded sleeve bolts. *Structures* 34:615–629
4. Cabrera M, Tizani W, Ninic J (2021) A review and analysis of testing and modeling practice of extended Hollow-Bolt blind bolt connections. *J Constr Steel Res.* 183
5. Wang J, Zhanga N, Guo S (2017) Experimental and numerical analysis of blind bolted moment joints to CFTST columns. *Thin Walled Struct.* 109:185–201
6. Li YL, Zhao XL (2022) Study on stainless steel blind bolted T-stub to concrete-filled stainless steel tube connections. *Eng Struct.* 257:114107
7. Jiao W, Wang W, Chen Y, The LH (2022) Seismic performance of concrete-filled SHS column-to-beam connections with slip-critical blind bolts. *J Constr Steel Res* 170:106075

Numerical Investigation on the Behavior of Bent Shear Panel Damper on Eccentrically Braced Composite Frames



Reshma and K. N. Rajesh

Abstract In modern buildings, seismic loading is an added important factor to account in safe structural design. Seismic dissipation systems are utilized to protect critical components in the structure from the energy released during earthquakes. Metallic yield dampers are low-cost components providing energy dissipation through yielding. Steel dampers have indeed gained significant attention and research due to their stable hysteretic behaviour, as well as their ease of availability and construction compared to other metals. Steel possesses excellent mechanical properties, such as high strength, ductility, and toughness, making it an attractive material for structural damping applications. Bent shear panel dampers (BSPD) are shear panel dampers (SPD) with bent in the middle and connected to the web of the composite beam in the frame to overcome the drawbacks of traditional SPDs a relatively new addition to the yielding metallic damper, with the properties of easy assembly and low cost. The bent panel can help maintain the lateral stiffness and energy dissipation capability of the frame. In the present study behavior of BSPD is to be evaluated using finite element software ANSYS Workbench to enhance the ductility and thereby to improve the energy dissipation capacity. The failure modes, strength and overall behavior of the specimens need to be studied. Some parameters which include effect of slits and the effect of low yield materials mainly aluminum. Number of slits is a crucial parameter that defines the stiffness and compactness. Slits proves to be an innovative energy dissipation technique which not only reduces cost but also gains sufficient ductility by plastic hinge formation at the slits. Slit improves the ductile behavior and energy dissipation by more than 100%.low yield material aluminum improves the energy dissipation capacity and improves the ductility of the material slightly and shows high improvement in stiffness. Perforations lessen elastic stiffness and yield strength in comparison to unperforated specimens.

Keywords Low yield point steel · Bent shear panel dampers · Cyclic behavior · Ductile behavior · Energy dissipation

Reshma · K. N. Rajesh (✉)

Department of Civil Engineering, Government College of Engineering Kannur, Kannur 670563, India

e-mail: knrajesh74@gcek.ac.in

1 Introduction

Building structures need to have sufficient capacity to resist the dynamic forces exerted by strong earthquakes and hurricanes. Enhancing the mechanical parameters, such as strength, stiffness, and ductility, is indeed crucial for improving the seismic performance of traditional buildings. Seismic dampening is an important aspect for buildings, especially for buildings of greater heights and importance. Seismic damping systems aim to protect the building by absorbing and dissipating the seismic energy imparted during an earthquake.

Among the conventional lateral load-bearing systems, such as the concentrically braced frame (CBF), eccentrically braced frame (EBF), and moment resisting frame (MRF), the CBF system exhibits the highest lateral elastic stiffness and ultimate strength. However, it has the lowest ductility. The low ductility of the CBF system is primarily due to the buckling of the diagonal members of the braces. Moreover, in the inelastic zone, the buckling further leads to degradation of lateral stiffness and strength. As a result, the CBF system is not suitable for high seismic risk zones due to these inherent limitations and the need for structures to have adequate ductility and energy dissipation capacity in such areas. Eccentrically braced frames (EBFs) are widely recognized as a preferred lateral load-resisting system for steel buildings in high seismicity areas. They are considered a hybrid solution that combines the advantages of both moment resisting frames (MRFs) and concentrically braced frames (CBFs) while minimizing their respective disadvantages. EBFs aim to provide high levels of ductility, like MRFs, which allows the structure to deform and dissipate energy during seismic events. At the same time, EBFs can also offer high levels of elastic stiffness, akin to CBFs. This stiffness helps control lateral displacements and provides stability to the structure under normal loading conditions. An eccentrically braced composite frame with a low-yield-point (LYP) steel shear link is a highly efficient energy dissipation system that exhibits excellent mechanical properties. The shear link in eccentrically braced composite frames is crucial for determining their seismic performance.

Various strategies have been proposed to enhance the energy dissipation and deformation capacity of traditional steel structures. Among these strategies, shear panel dampers (SPDs) have gained significant popularity as energy dissipation devices, particularly for improving the seismic performance of structures. Low yield point steel, which performs excellently in terms of ductility, is utilized as the material for hysteretic dampers to get over this restriction. [1]. To efficiently increase their stiffness and strength and disperse input energy through plastic deformation in seismic situations, shear panel dampers (SPDs) are frequently utilized in eccentrically braced composite frames (EBCFs). Rahnavard et al. [2] evaluated the single shear panel and double shear panel models and proves the twin shear panel system showed a stronger tendency to develop shear linkages after applying acceleration to the structure and performing a time history analysis, leading to a better capacity for dissipation in the plastic zone. Deng et al. [3] testing revealed that restraining plates with sufficient stiffness and strength can successfully prevent the energy dissipation plate from

bowing out of plane. Yao et al. [4] conducted a study with low-yield-point steel core plates with a nominal yield stress of 225 MPa are stiffened out-of-plane using square steel tubes (named LYP225 steel). The test findings demonstrate that square tubes effectively prevent the bulking of the core plates, and all specimens display a full hysteretic response and an adequate capacity for releasing energy. The decreased plate sections enhance the ultra-low cycle fatigue performance by lowering the possibility of fracture propagation developing at the flange end. Several researchers have developed and studied metallic dampers that take advantage of the plastic behavior of metals. Dampers have been made of steel, aluminum, and shape memory alloys. Low point yield steel, which increases the deformation capacity and energy dissipation capacity, is the most economical and readily accessible metal. [5] There has been a lot of research on shear yielding dampers and other dampers that use metallic yielding. The composite beam in the frame may be subjected to additional bending moments and axial forces from vertically positioned SPDs, which could damage the concrete slab supporting the frame. To get over the limitations of conventional SPDs, the SPDs used in this study were bent in the middle and attached to the web of the composite beam in the frame. As a result, the axial force and bending moment produced by the SPDs can be reduced managing the concrete slab's damage.

The low yield strength of aluminum in shear offers advantages in the design of shear links, particularly in terms of reducing the chances of web buckling and allowing for greater participation of the material in plastic deformation. Deepak Yadav et al. [6] investigated the cyclic behavior of aluminium shear yielding damper. AI-SYDs can be used to improve existing structures' seismic performance or to retrofit structures that have been damaged by earthquakes. Aspect and slenderness ratios of web plates have been found to have a significant impact on their energy dissipation potential. Zhao et.al [1] investigated the properties of BSPDs and how they are arranged in EBCFs. And examined BSPDs have good energy dissipation capabilities and a ductile behavior after yielding. And proves the deformation capacity and energy dissipation effectiveness of such dampers can be improved by using link flanges and steel with a low yield point. Seyed Saeed Askariani et.al [7] used slit link beams in eccentrically braced frames. He used butterfly shaped links throughout the link beams with tapered sections at corners. Slits transferred the failure point from link ends to the end of slits. Slits increased the plastic strain capacity thus utilizing the plastic capacity of material. He investigated the effect of fillet radius and different link spans on eccentrically braced frame. Fillet radius improved the behaviour by avoiding stress concentration at corners. A fillet radius of 2–5 mm improved the failure characteristics avoiding stress continuity caused by straight corner edges. Slits increased the plastic strain capacity thus increasing the dissipation capacity. Slender links with more height/ thickness ratio performed well rather than slits with larger openings. Increasing the thickness of link beams improved the stiffness properties which undergo degradation when slits are provided. Ahmadi et.al [8] conducted a study on parabolic shaped slit shear walls to attain efficient slit geometry and to reduce the effect of strain concentration in shear wall. He proposed parabolic shaped slits along the shear walls, with multilevel arrangement to increase stiffness properties of shear wall. No pinching behavior was observed, and slits enhanced the drift

ratio by almost 6% which ensures ductility and plastic rotation capacity. The slits enhanced plastic hinge creation which prevents early damage of shear walls. This study focusses on improving the ductile behavior and energy dissipation by incorporating slits in BSPD to achieve better seismic performancee and includes the effect of low yield material which is aluminum in improving ductility of BSPD.

2 Numerical Modelling

The BSPD under cyclic loading is modelled in finite element software ANSYS Workbench 2022 R2. The experimental data from Zhao et al. [1] must be compared with the FEM models to proceed into the parametric study. BSPD is modelled as shell element with multilinear kinematic hardening model.

2.1 Material Modelling

The Low Yield Point (LYP) steel, LY160, which has a yield strength of 160 MPa and is used to give the best material support for energy dissipation devices, was used to design the damper. Material property obtained from the tensile coupon test conducted by zhao et al. BSPD2 made up of BLY160 is used in this study. Figure 1 depicts the real stress strain curves of the steel grade obtained from the study conducted by Zhao et al. [1]. Multilinear kinematic hardening was taken for the study. Material property of bly160 obtained from coupon test is listed in Table 1. Poisson ratio of 0.3 is taken. Dimensions of the modelled is also explained in Table 2.

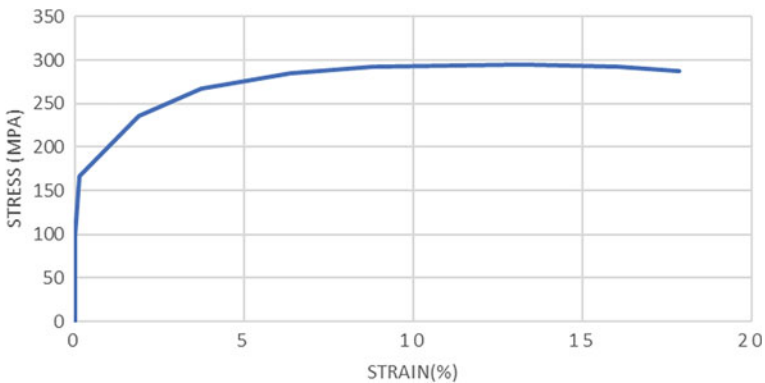


Fig. 1 Stress strain curve of BLY160

Table 1 Material property of BLY160

Grade	Elastic modulus (GPa)	Yield strength (MPa)	Ultimate strength (MPa)	Elongation (%)
BLY160	203	154	295	37.2
Q345	203	285	455	25.5

Table 2 Dimension of model

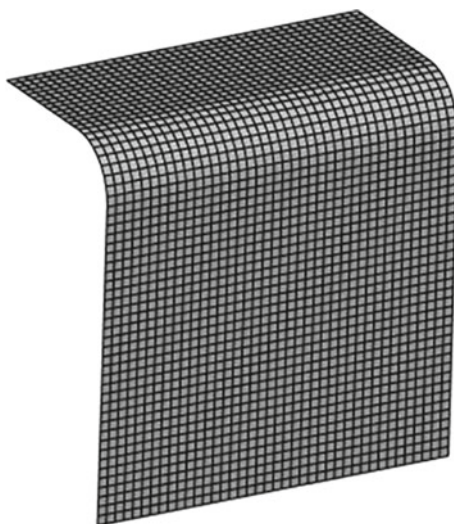
Specimen	BSPD length (mm)	Thickness of web (mm)	Depth of web panel (mm)	Bent radius
BLY160	200	16	200	50

2.2 Finite Element Modelling

For modelling reasons, shell 181 is use as the element type. SHELL 181 is suitable for analysing thin to moderately thick shell structures. It is a four noded 2D element with six degrees of freedom at each node. Which is translations in the x, y, z directions, rotations about the x, y, z axes. A mesh convergence study is to be conducted by fixing a mesh element and running simulations with different mesh sizes. Upon observation of convergence of results a suitable mesh size is to be adopted for later studies. The mesh size is selected by considering the computational time for simulations without compromising the accuracy of the results. Meshed model is shown in Fig. 2.

Each loading level increase is equal to 1% of the typical specimen's 2.0 mm BSPD length, and the loading process is displacement controlled. Each loading level underwent two cycles, as displayed in Fig. 3. The applied force was reduced to 85%

Fig. 2 Meshed model obtained in ansys



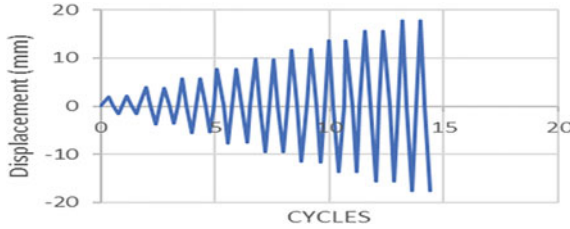


Fig. 3 loading protocol

C: BDSP 1
Static Structural
Time: 1. s
10-02-2023 11:18
A LOADING
B SUPPORT

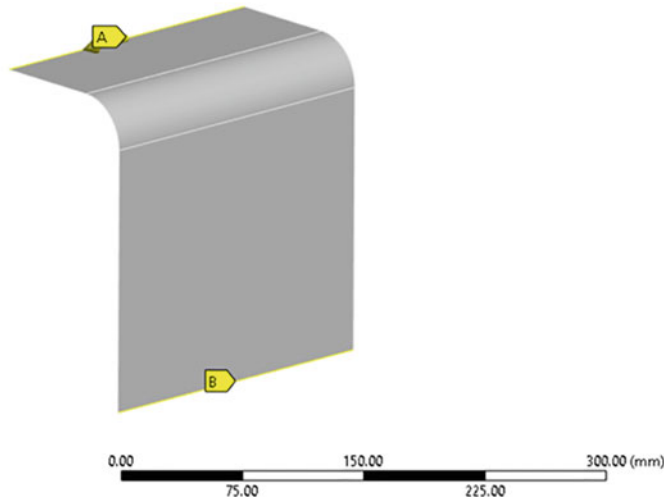


Fig. 4 Model created in ansys with loading and boundary condition

of the maximum load or a fatal fracture was noticed, at which point the loading operation was stopped. The typical static loading rate of 10- 5 m/s is set to prevent the yield strength and energy dissipation capacity of the BSPD from growing with increasing loading rate. The details of various boundary conditions applied to the model are given in Table 2. Figure 4 shows the model with boundary conditions and loading pattern.

2.3 Validation

The peak load of the model obtained is compared with the experimental results of Zhao et al. The model is validated against the experimental model. Figure 5 shows the comparison between hysteresis curve obtained from FEM and experimental setup. The ultimate load obtained from experimental results were 299.13kN and that from

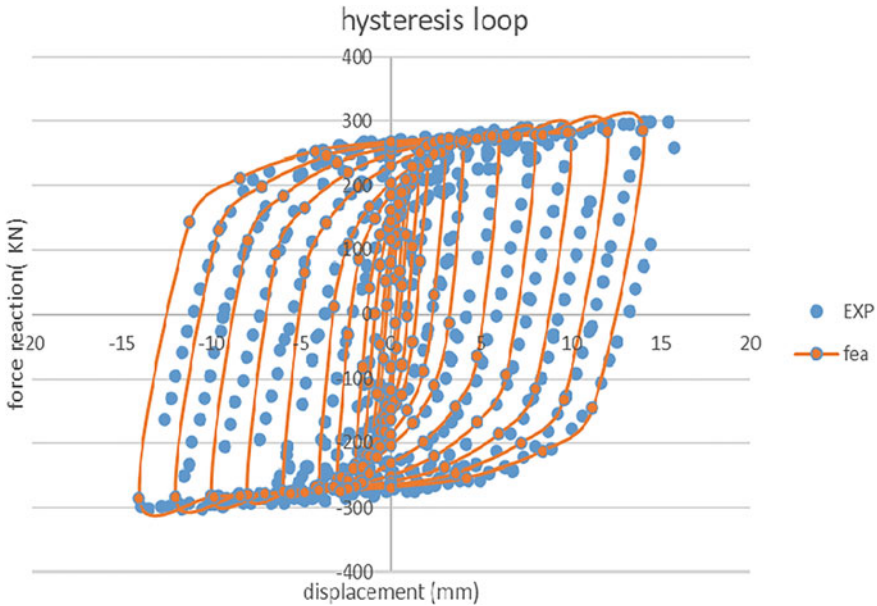


Fig. 5 Load displacement curve

FE analysis was 284.5 kN. A percentage error of 4.89% was observed. This 4.89% deviation between the experimental and numerical model for steel dampers indicates a reasonably good agreement, but it also highlights the need for ongoing research, calibration, and refinement. The implications of this deviation should be carefully considered in terms of validation confidence, design considerations, sensitivity analysis, model calibration, reliability, and future research to ensure the accuracy and applicability of the numerical model in practical engineering applications. As the hysteresis curve obtained from FE analysis matches with the experimental results the model was validated and further used for parametric studies.

3 Parametric Study

The validated model is extended to obtain further parametric study. The first parameter considered is the effect of number of slits and the second parameter is the effect of thickness of the plate of the BSPD with slit to improve stiffness. the third parameter is the effect of low yield material aluminum.

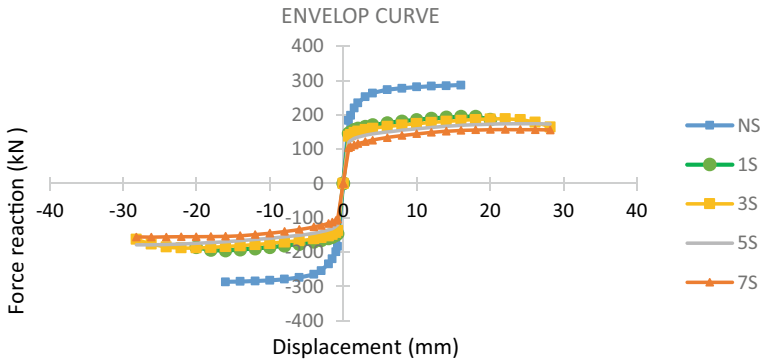


Fig. 6 Number of slits effect

3.1 Effect of Number of Slit

Slit numbers is chosen according to the spacing of the BSPD. A fillet radius of 2 mm is chosen and select the dimension of slit as 50×5 mm. A total of 4 model is chosen for the analysis. Which is 1 s, 3 s, 5 s, 7 s. As the number of slits increases ultimate shear force of the BSPD decreases. Failure is observed at the slit ends. The cumulative energy dissipation capacity increases for one slit (1 s) and 3 slit model with a percentage of 78.56% and 94.5% respectively then it shows a slight decrease in the cumulative energy dissipation. For 5 slit (5 s) it shows 75.50% improvement in energy dissipation compare no slit model. Ductility of the BSPD increases as number of slit increases by a percentage of 76.24% as compared to no slit model. Figure 6 shows effect of number of slits. To improve the strength of BSPD with slit further parameter is to be done properly, which include increasing the thickness of the BSPD plate.

3.2 Effect of Thickness of BSPD Plate

As the number of slits is improved ductility of the model improved but the stiffness of the model decreased gradually. So, in order to improve the performance of the model having ductility thickness of the model is increased from 16 mm to 20,22,24,26 and 28 mm. Increasing the thickness shows a significant improvement in stiffness. Thus, seismic performance of the model is improved. As thickness increased load carrying capacity also increased with a percentage ductility of 76.4%. It also increased the energy dissipation capacity up to 333.42 kJ. Figure 7 shows the effect of thickness whereas Fig. 8 shows the thickness to energy dissipation capacity.

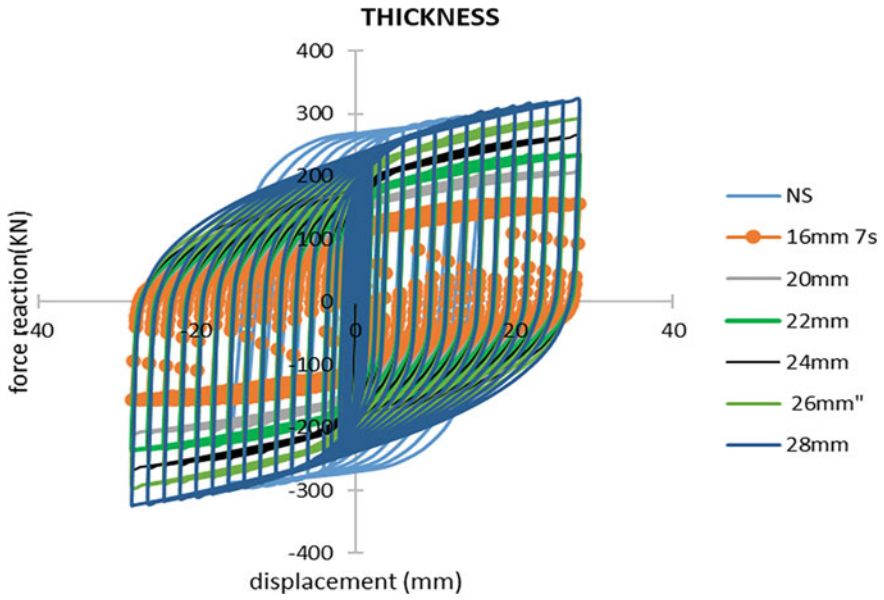


Fig. 7 Effect of thickness

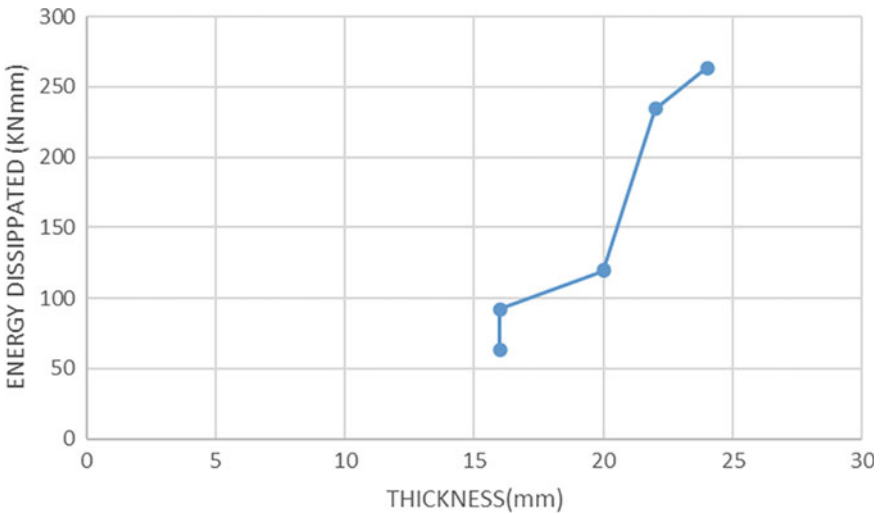


Fig. 8 Variation of thickness with energy dissipation.

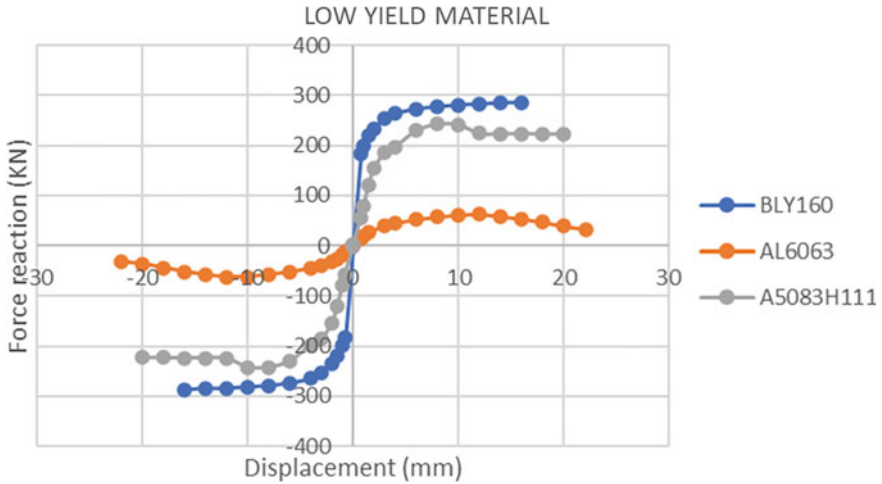


Fig. 9 Effect of aluminum on BSPD

3.3 Effect of Low Yield Material Aluminium

Low yield material aluminum is considered here instead of low yield steel and the result obtained is compared with the low yield material. Mainly 2 type of aluminum alloy which is used in braces is considered which is AL6063 and A 5083H111. Stiffness of the material is increased by using aluminum instead of low yield steel from 168.66 kN/mm to 298.85 kN/mm. Ductility increased by 24. 78% by using aluminum alloy instead of low yield steel. For pure aluminum alloy percentage ductility is improving. Energy dissipation capacity of the material increased by 83.99 kJ using aluminum. Figure 9 shows the effect of aluminum in BSPD.

4 Conclusion

The study investigates the effect of number of slit and thickness of plates to improve ductility and energy dissipation capacity of the material. From this the following conclusions can be made.

1. Slits in BSPD improves the seismic performance by increasing the ductility and energy dissipation.
2. As the number of slits increased the ductility of the BSPD increases gradually from 12.53 to 76.24%.
3. Number of slits shows an increase in energy dissipation up to 3 number of slits then suddenly drops. Unstable seismic behavior is obtained by decreasing the force carrying ability of the BSPD.

4. Increasing the thickness of plate improves the stiffness and energy dissipation capacity of BSPD.
5. Using a low yield material aluminum improves the energy dissipation capacity and improves the ductility of the material slightly and shows high improvement in stiffness.

This study helps in improving the ductility and energy dissipation capacity of BSPD. Stiffness and ultimate load carrying capacity is also improved thus, improving the overall seismic performance.

References

1. Zhao JZ, Tao MX, Zhuang LD (2022) Development of bent shear panel dampers for eccentrically braced composite frames. *J constr steel struct*
2. Rahnavard R, Hassanipour A, Suleiman M et al. (2017) Evaluation on eccentrically braced frame with single and double shear panels. *J Build Eng.* 10:13–25
3. Deng K, Pan P, Li W, et al. (2015) Development of a buckling restrained shear panel damper. *J Constr Steel Res.*106:311–321
4. Yao Z, Wang W, Yazhi Z (2021) Experimental evaluation and numerical simulation of low-yield-point steel shear panel dampers. *Eng Struct.* 245:112860
5. Lina X, Wua KA, Skalomenos KA, Lu L, Zhao S (2019) Development of a buckling-restrained shear panel damper with demountable steel-concrete composite restrainers. *Soil Dyn Earthq Eng.* 118:221–230
6. Guo L, Wang J, Wang W, Wang H (2021) Experimental, numerical and analytical study on seismic performance of shear-bending yielding coupling dampers. *Eng Struct* 244
7. Askariani SS, Garivani S, Aghakouchak AA (2020) Application of slit link beam in eccentrically braced frames. *J Construct Steel Res.*170
8. Ahmadi Z, Aghakouchak AA, Mirghaderi SR (2021) Steel slit shear walls with an efficient geometry. *Thin-Walled Struct.* 159:107296

Effect of Length of Free Ends of Flamingo Shear Reinforcing Technique on Shear Capacity of Reinforced Concrete



Asmaa Shaker Mahmood, Suhad M. Abd, and Hadee Mohammed Najm

Abstract An alternative shear reinforcement technique has been proposed which is the flamingo technique, instead of the traditional vertical stirrup, it is made prefabricated. Five reinforced concrete beams were used with dimensions (200 × 300 × 1800) mm, two reference (with stirrups and without stirrups) and three beams using flamingo technique having diameter with (8 mm), and free ends by constant inclination angle (45°). This study aims to determine how a change in length of free ends affects the Flamingo technique. The length of free ends was used (50–50%), (75–50%) and (60–80%) from the effective depth of beam. According to the results, found that the beams showed an improvement in shear strength of by (108.3, 116.7 and 153.7%) when compared with beam without stirrup, and by 25, 30 and 52.2% over the reference beam with stirrup, as well as, it was observed that the beam containing ratios of 50 and 50% exceeded other ratios by 17.9 for the beam 80–60 and by 11.9 for the beam 75–50%, on other hand, the deflection improved by (10.01%, 10.9%, and 30%) respectively, compared to reference beam with stirrup.

Keywords RC beam · Shear failure · Flamingo technique

A. S. Mahmood (✉)

Department of Civil Engineering College of Engineering, University of Diyala, Diyala, Iraq

e-mail: Gk4071@myamu.ac.in

S. M. Abd

Department of Highways and Airports Engineering College of Engineering, University of Diyala, Diyala, Iraq

H. M. Najm

Civil Engineering Department, Zakar Hussein Engineering College Aligarh Muslim, University, Aligarh 202002, India

Department of Civil Engineering, Bilad Alrafdain University College, Diyala 32001, Iraq

1 Introduction

Despite its high compressive strength, concrete has a low tensile strength. Because of this, it is essential to employ ductile shear reinforcement, which boosts the concrete's capacity for withstanding strain while simultaneously lowering its brittleness. It was common practice to use traditional steel reinforcement in reinforced concrete members as shear reinforcement (stirrups) [1]. Reinforced concrete beams behave very differently when they fail in shear than when they bend, which is considered an unsafe mode of failure by the industry. Excessive shear forces cause diagonal cracks to develop that are much wider than flexural cracks, which usually occur without much advance warning before the beams shear. Reinforced concrete beams were re-examined after shear reinforcement became prohibitively expensive and risky. Beams are supported by internal moments and shears. When designing a reinforced concrete part, flexure is typically taken into account first, which then dictates the size and arrangement of reinforcing bars [2, 3]. Mohammed [4] studied swimmer bars and typical steel stirrups for shear reinforcement. Ten beams (1600 long, 150 wide, and 250 mm high) were tested for concrete compressive strength, swimmer bar shape, and number of planes. The 10 beams are divided into two groups: the first consists of five standard concrete beams with a constant flexural reinforcement area, and the second consists of five high-strength concrete beams with an identical flexural reinforcement area but higher strength than the first group. One beam from each group employed typical steel stirrups with the same area and spacing, whereas the other four beams were strengthened in shear with swimmer bars with varying numbers of bars, spacing, and number of planes. For both high-strength and conventional concrete, as the number of swimmer bar planes with the same shape increases, so does shear strain. As a result of its increased load-carrying capacity, one of the best forms proposed in this study is the shape one of three swimmer bar planes with 166.67 mm space between them. Crack width, propagation, and quantity were all reduced in comparison to high-strength concrete [4–7]. De Corte and Boel [8] studied the effect of shear helical rings on reinforced concrete beams under static load and four loading points. The study was conducted on 24 models of concrete beams, 12 with self-compacting concrete and 12 with ordinary compressed concrete. Both types had a vertical rib reference beam and continuous helical ring beams. The beams are designed to ensure shear failure and bending strength. Shear space to depth ratio (2.5–3) Using helical rings increases shear bearing capacity by 5%, increases the shear area-to-depth ratio, and reduces crack width. Due to overlap, this technique is more cost-effective [8]. Abdul-Razzaq and Farhood [9] examined the shear behavior of (100 * 150 * 1200) mm beams reinforced with standard steel in flexure and with CFRP strips in shear. He studied the effect of adding waste plastic fibers (PET) on beam shear behavior (0.25, 0.5, 0.75, 1, 1.25, and 1.5%). This project is intended to reduce stirrup rusting. The insertion of PET fibers into standard steel stirrups boosted the shear strength of beams with CFRP strips. Increased PET fibers enhanced beam shear ductility. FRP materials' brittleness and unidirectionality impede shear reinforcement (stirrup) manufacture [10]. Colyvas et al. [11] examined wire ropes as shear reinforcements.

Due to its high flexibility, low weight, and robustness, it's a cheaper alternative to standard rectangular concrete stirrups. This work aims to improve our understanding of the shear behavior of concrete beams reinforced by spiral wire rope. To do this, six beam samples were tested under four loads. DIM technology Examine beam crack formation and spread. According to tests, the strong shear strength of continuous spiral rope favors controlling diagonal cracks. Spiral wire rope samples had a higher serviceability crack width than standard stirrup beam samples [12]. By pouring 8 concrete models in 2020, Isam explored carbon textile yarns. All beams (200 * 300 * 1500 mm), two as references, one with steel passengers and one without. The rest of the samples used carbon fiber at varying lengths (100, 60 and 30 % of the packaging's effective depth). At a 45° angle and varying distances, the interference lift extends the final load by 100 by 24.5% and reduces the deviation compared to steel compounds. Reducing distancing between interconnected passengers to 90 mm without further shearing enhancement increased the final load by 26% while reducing deviation by 30.1% compared to ordinary steel passengers. Moreover, the tilting of fabric threads increased the final load by 45° by 55% while reducing deviation by 3% compared to steel passengers. Steel fiber impregnated mortars increased maximum load by 3% and reduced deviation by 13.6%. The last two beams contain flamingo reinforcement with upper limbs and angled bottom. The beams increased shearing capacity, cutting flexibility, final deviation, and breaking behavior. The researcher also studied flamingo technology. Pour four models and study the effect of changing the angle of the free limbs of this technique, as well as the length of these limbs, and discover that they improve the final load and elasticity of the shear capacity when compared to the standard package [13, 14].

2 Experimental Program

2.1 Material

2.1.1 Cement

This study employs standard Portland cement (type I) supplied by the Tasluja factory in Iraq. The chemical makeup and physical attributes adhere to the Iraqi Standard Specification (I.Q.S. No. 5, 1984) (I.Q.S. No. 5, 1984) [15].

2.1.2 Fine Aggregates

The natural sand used for this project's fine aggregate was found in the Al-Sidor area. It has a 2.38 fineness modulus. Conformity of the fine aggregate's grading and physical characteristics to the Iraqi Specification's limitations (I.Q.S. No. 45, 1984) [16].



Fig. 1 Head stud

2.1.3 Coarse Aggregate

In this investigation, coarse aggregates consist of natural gravel with a maximum particle size of (12.5 mm). The natural gravel came from the Al-Sidor area. After being cleaned, the gravel was dried by air. The physical properties and grading of the aggregates met the requirements (Iraqi standard No. 45, 1984) [16].

2.1.4 Steel Reinforcement

Deformed steel bars are used to reinforce beams in shear and bending, as shown in Table 1 6, 8 and 10 mm stirrups were used in the Flamingo technique, as well as 2 Ø 12 in the compression zone to stabilize steel and 4 Ø 16 for flexural reinforcement whereas Ø 8 @ 130 mm were used as traditional vertical stirrups.

2.1.5 Head Stud

They are attached at the head of free endings by welding (double head) as shown in Fig. 1, where they interfere with concrete and prevent slipping.

2.1.6 Concrete Mix

A concrete mix with 39 MPa and mix constituents shown in Table 2 was used through this. Cylinders of 300 heights and 150 mm diameters were used to obtain compressive strength of concrete at (7 and 28) days. After demanding the samples were cured in water tanks for 28 days [17].

Specimens Descript

The samples in this study used molds with dimensions (200 × 300 × 1800 mm), the first control beams (RCWS) (see Fig. 2a, b) was reinforced with conventionally vertical steel stirrups in the shear zone, second reference beam without stirrup (RCWOS) and other beams with flamingo technique with different length of free end

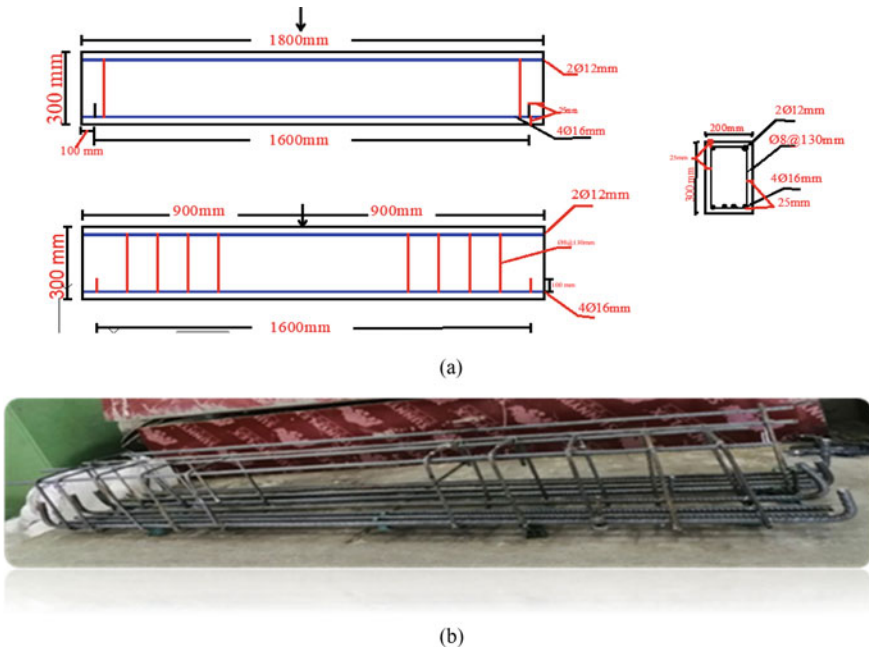


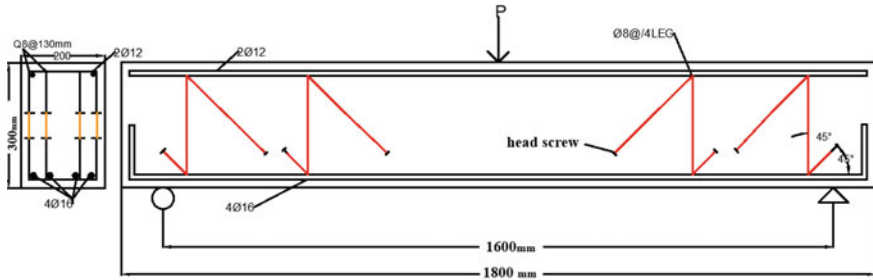
Fig. 2 a, b Reference beams

(80–60, 75–50 and 50–50%) from the effective of depth of beam (as a main variable to study their effect on shear capacity), the diameter used 8 mm and the angle of inclination was fixed at 45°. The shape of a flamingo is roughly Z-shaped with legs (see Fig. 3 a, b), and its surface area is equivalent to that of vertical stirrup. They were tested in one–point load at mid beams in order to determine the shear capacity and other properties as shown in Table 3.

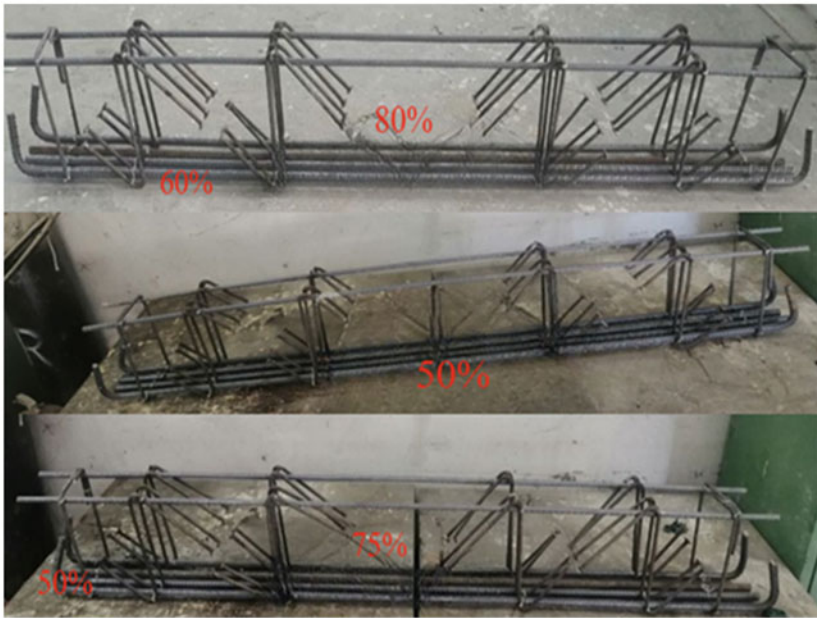
This pre–fabrication is installed using normal splicing as in normal stirrup, thereby reducing manual work on site and easing of application

3 Conclusion and Discussion

- This section compares the load-bearing capacity, load deflection, shear ductility index, and crushing behavior of the flamingo and control beams. The comparison focuses on the most efficient usage of steel stirrups or flamingo technique which is done by using the same area steel in the control beam. Table 1 results of beams after tested.



(a)



(b)

Fig. 3 a, b Flamingo reinforcing technique

Table 1 Properties of reinforcing steel bar

Type	Diameter (mm)	Yield stress f_y (MPa)	Ultimate Strength f_u (MPa)	Elongation (%)
Main reinforcement	16	580	683	10.24
	12	635	728	9.04
Shear reinforcement	8	330	528.1	21.52

Table 2 Concrete mix constituents

Cement (kg/m ³)	450
Sand (kg/m ³)	860
Gravel (kg/m ³)	860
Water (kg/m ³)	207
S.P	0.46%
w/c	46%
Slump (mm)	140 mm

Table 3 Details of the tested beams

Specimen	Description
RCWOS	Reinforcement concrete beam without stirrup
RCWS	Reinforcement concrete beam with stirrup with diameter 8 mm
FL (80, 60%)	With 60% upper end length and 80% lower end length with 45°angle of inclination, diameter 8 mm
FL (50, 50%)	With 50% upper end length and 50% lower end length with 45 angle of inclination, diameter 8 mm
FL (75, 50%)	With 50% upper end length and 75% lower end length with 45 angle of inclination, diameter 8 mm

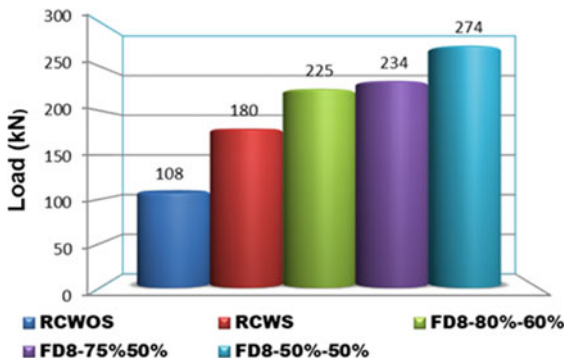
A. Load Carrying Capacity

Figure 4 shows that the shear capacity of the beams used in the (FL-80–60%, FL-75–50%, and FL-50–50%) beams increases by (108.3, 116.7 and 153.7%) when compared with beam without stirrup and by (25, 30 and 52.2), compared to the RCWS reference sample respectively. Furthermore, the ends which are 50% of the effective section depth used in the FL-50–50% model are increased by 17.9 and 14.6% compared to the two beams used. This increase was due to the improvement of the internal stress distribution of the beam when using this technique. It seems that equal length for the free ends of flamingo units might led to uniform distribution increases load carrying capacity by increasing resistance of R.C. beam for longer time.

B. Load Deflection Behavior

Due to the results in Table 4, the deflection at yield load increased with decrease the percentage of the length ends, when compared with reference (RCWS) beam by (48.4, 42.9 and 25.4%) for (FL-50–50%, FL-50–75%, and FL-80–60%),but at ultimate load, deflection was decreased by (10.01,10.9, and 30%) for beams (FL-50–50%, FL-50–75%, and FL-80–60%) compared with reference beam (RCWS) as shown Fig. 5, on the other hand, the deflection decreased as the length of the

Fig. 4 Ultimate load capacity of tested beams



ends increased, and the increase in the length of the end led to a greater interception diffused shear failure from the support to mid beam.

C. Shear Ductility

Table 4 Test results of the beam

Specimen	Py* (kN)	% diff in Py	Pu kN	% Diff in Pu	y** (mm)Δ	% Diff in Δy	Deflection Δu mm	% Diff. of Δu	Ductility $\frac{\Delta u}{\Delta y}$	% Diff.in ductility
RCWOS			108	-40			6.5			
RCWS	126		180		5.5		12.8		2.33	
FL-50-50%	190	50.8	274	52.2	8.16	48.4	11.5	-10.01	1.4	-39.9
FL-50-75%	166	31.7	234	30	7.86	42.9	11.4	-10.9	1.45	-37.8
FL-80-60%	160	22.2	225	25	6.9	25.4	8.95	-30	1.3	-44.2

* Py: Yield load of longitudinal reinforcement when it reached its yield strain

** Δy: Deflection at yield load

Fig. 5 Load deflection curves for the flamingo specimens

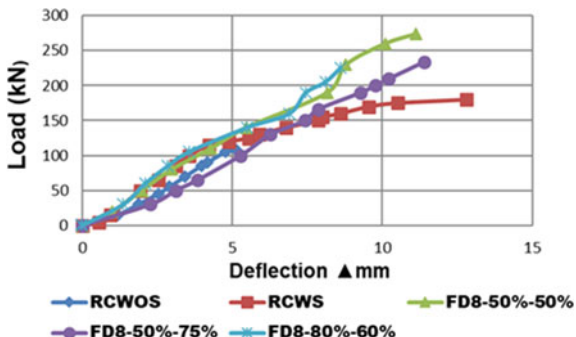


Table 5 Detail of load crack and crack width

Specimen	Crack load Pcr (kN)	Ultimate load Pu (kN)	Pcr/Pu (%)	%Increase in cracking load	Crack width @ 160 kN	%Decrease crack width @ 160 kN
RCWOS	60	108	64.8			
RCWS	70	180	38.9		0.6	
FL-80-60%	110	225	62.2	36.4	0.2	- 66.6
FL-50-75%	127	234	54.3	81.4	0.4	- 33.3
FL-50-50%	135	274	49.3	92.9	0.5	- 16.7

Table 4 shows that the shear ductility ($\Delta u/\Delta y$) in beams (RCWS, FL-50-50%, FL-50-75%, and FL-80-60%), from results found that the ductility shear decreased when used flamingo technique compared with stirrup normal (RCWS) by 39.9, 37.8 and 44.2% for (FL-50-50%, FL-50-75%, and FL-80-60%), which is decreased due to not completely enclosing or confining the concrete and leaving it loose at the ends of this technique compared with stirrup. On other hand, it found that beam with longer length decrease more because of distribution of stress at stage yield for beams.

D. Crack Behaviour

Table 5 shows the final load and the initial load that caused cracks in the shear zone of the beams (RCWOS, RCWS, FL-80-60%, FL-50-75%, and FL-50-50%) where the load appears cracking as a percentage of final load (64.8, 38.9, 62.2, 54.3, 49.3%), respectively. When compared to the normal stirrup reference beam (RCWS), crack load values increased (36.4, 81.4, 92.9%) for beams (FL-80-60%, FL-50-75%, and FL-50-50%), respectively. It is also found that the crack width decreased by (66.6, 33.3, and 16.7%) when comparing the flamingo technique with the beam with stirrup normal due to increase the efficiency this technique. On the other hand, the crack load increased with the decrease in the length of the free ends as a result of the stress distribution in the first stage on the beams with the same length, but the crack width increased, and at the load of 160 kN it was found that the crack width increased by one and a half times for beams (FL-80-60%) from (FL-50-50%). The reason is the objection with crack development in the later stages of the higher length beams. According to the Plate 1, the failure pattern was different due to the change in the ratio of the length of the free ends, where in the ratio (50-50%) the failure pattern was dowel action failure, and in the ratio (50-75% and 60-80%) were shear flexure.

4 Conclusions

As a result of this research, it was discovered that:

- Beams with the flamingo technique, the load-deflection, stiffness and cracking behavior were all superior to the traditional steel stirrups.

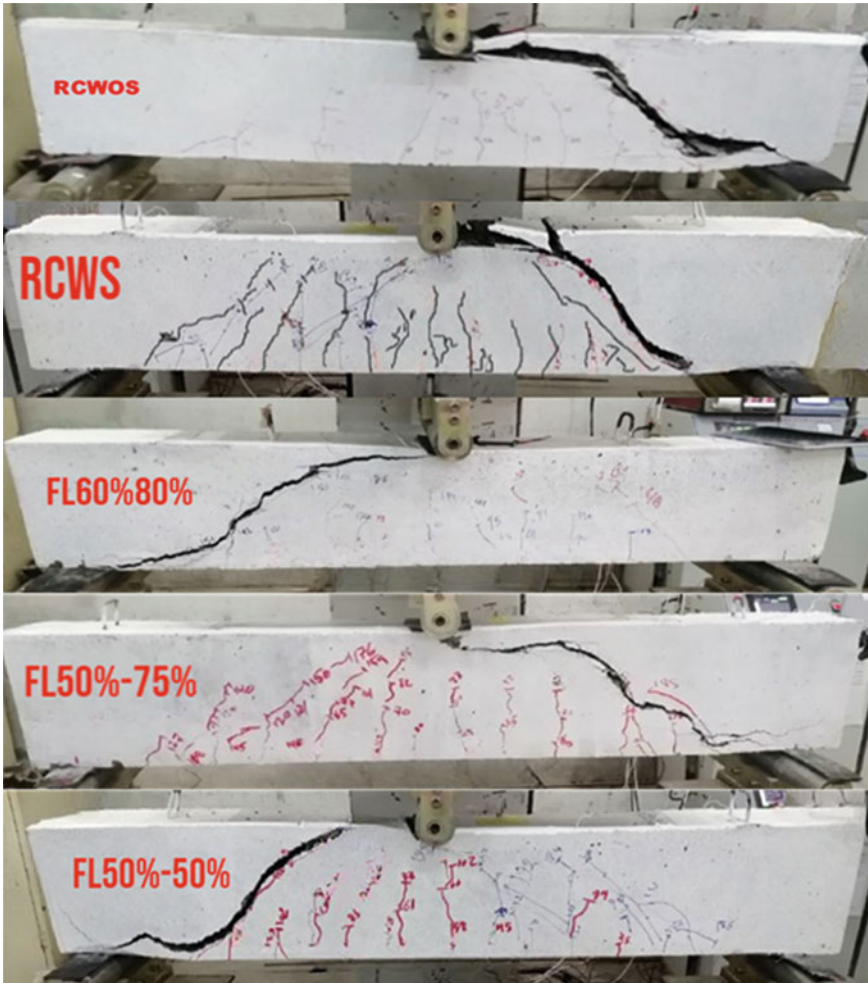


Plate 1 Crack patter of beams with different of length free ends

- Flamingo technique with change the length of the free ends from effective beam depth (FL-50-50%, FL-50-75%, and FL-80-60%),The beams showed an improvement in shear strength of by (108.3,116.7 and 153.7%) when compared with beam without stirrup, and by 25, 30 and 52.2% over the reference beam with stirrup, as well as, it was observed that the beam containing ratios of 50 and 50% exceeded other ratios by 17.9% for the beam 80 – 60 and by 11.9% for the beam 75 – 50%,on other hand, the deflection improved by (10.01,10.9, and 30%) respectively, compared to reference beam with stirrup.

- The crack loads of the (FL-80–60, FL-50–75%, and FL-50–50%) beams were by (36.4, 81.4, and 92.9%) greater than those of the reference beam with stirrup. While the crack width was reduced by (66.6, 33.3, and 16.7%) compared to the reference beam with stirrup, but the shear ductility decreased by (44.2, 39.9, and 37.8%) for beams respectively.
- The mode of failure of reference beam (RCWS) was shear failure and beams with flamingo was shear failure and dowel action.

References

1. Abdulsalam B (2014) Behaviour of shear critical FRP reinforced concrete one-way slabs. <https://doi.org/10.13140/RG.2.1.2783.1844>
2. Bazant ZP, Sun H–H (1987) Size effect in diagonal shear failure: influence of aggregate size and stirrups. *ACI Mater J* 84(4):259–272
3. Committee CI (2019) ACI 318–19: building code requirements for structural concrete and commentary. Am Concr Inst Farmingt Hills, MI, USA
4. Mohamed HA (2017) Effect of using swimmer bars on the behavior of normal and high strength reinforced concrete beams. *Ain Shams Eng J* 8(1):29–37. <https://doi.org/10.1016/J.ASEJ.2015.07.007>
5. Hemanthkumar M (2016) Effect of swimmer bars on reinforced concrete beams. *Int J Emerg Technol Eng Res* 4 [Online]. Available: www.ijeter.everscience.org
6. Al–Nasra MM, Asha NM, Najmi AS (2013) Investigating the use of swimmer bars as shear reinforcement in reinforced concrete beams 2013 [Online]. Available: www.irjes.comwww.irjes.com
7. Al–Nasra M (2019) The use of swimmer bars as shear reinforcement in reinforced concrete structures. *J Eng Appl Sci* 14(9):2775–2782. <https://doi.org/10.36478/jeasci.2019.2775.2782>
8. De Corte W, Boel V (2013) Effectiveness of spirally shaped stirrups in reinforced concrete beams. *Eng Struct*.52:667–675. <https://doi.org/10.1016/J.ENGSTRUCT.2013.03.032>
9. Abdul-Razzaq KS, Farhood MA (2019) Design-oriented testing and modeling of reinforced concrete pile caps. *KSCE J Civ Eng* 23:3509–3524
10. Hadithia AI AI, Abbasa MA (2018) Innovative technique of using carbon fibre reinforced polymer strips for shear reinforcement of reinforced concrete beams with waste plastic fibres. <http://www.tandfonline.com/loi/tece20>
11. Colyvas GM, Malecot Y, Sieffert Y, Aboudha S, Kanali C (2020) Behavior of reinforced concrete beams using wire rope as internal shear reinforcement. *Eng Technol Appl Sci Res* 10(4):5940–5946
12. Yang KH, Kim GH, Yang HS (2011) Shear behavior of continuous reinforced concrete T–beams using wire rope as internal shear reinforcement. *Constr Build Mater* 25(2):911–918. <https://doi.org/10.1016/j.conbuildmat.2010.06.093>
13. Mhaimed S, Abd SM (2021) Shear capacity of concrete beams reinforced with textile carbon yarns and flamingo reinforcing system, In: 2021 4th Int. Iraqi Conf Eng Technol Their Appl (IICETA) pp 212–217. 1109/IICETA51758.2021.9717950
14. Mhaimed AS, Abd SM (2021) Improved shearing capacity of reinforced concrete thresholds using arming techniques using new proposed steel arming techniques, Republic of Iraq ministry of planning central organization for standardization and quality control, Diyala, Jul 04 2021
15. S No (1984) Portland Cement, the Iraqi Central organization for standardization and quality control, Baghdad-Iraq

16. S No (1984) 45, Natural Sources for Gravel that is Used in Concrete and Construction Baghdad
17. Standard test method for compressive strength of cylindrical concrete specimens 1. https://doi.org/10.1520/C0039_C0039M-16

Effect of Ultrafine Materials on Drying Shrinkage of Concrete



Jerison Scariah James, Jibin Joy Ponnappal, Aiswarya Jayan,
and Elson John

Abstract The utilization of ultrafine materials in concrete has gained significant notice in modern times for its potential to enhance the properties of concrete. The drying shrinkage of concrete, which happens when concrete loses moisture and contracts, is one of the main issues in the workplace's building. If this is not handled correctly, it may result in cracks and damage. This study examined the impact of ultrafine materials on the drying shrinkage of concrete, and the results are presented in this report. The research involved using ultrafine slag and ultrafine fly ash as partial replacements of cement in concrete for a grade of M35. The specimens were prepared with ultrafine of 10% replacement with cement as optimal, and the drying shrinkage was measured and compared to a control specimen without ultrafine materials. In the investigation, the hardened properties, including compressive strength and flexural strength, as well as the shrinkage test, were carried out. The findings revealed that the utility of ultrafine materials decreased the drying shrinkage of concrete, with ultrafine slag being more effective than ultrafine fly ash. The pozzolanic reaction of these materials contributed to the formation of additional calcium silicate hydrate (C-S-H) gel, which packed any voids and reduced the overall porosity of the concrete, resulting in a reduction in drying shrinkage. In conclusion, the study suggests that the utilization of ultrafine materials in concrete can effectively decrease the drying shrinkage of concrete, with ultrafine slag being more effective than ultrafine fly ash. However, further research is recommended to investigate the long-term effects of using these materials on the endurance of concrete. This investigation highlights the potential of ultrafine materials as a sustainable solution to boost the properties of concrete, particularly the drying shrinkage of concrete.

Keywords Drying shrinkage · Ultrafine GGBFS · Ultrafine fly ash

J. S. James (✉)

Research Scholar, APJ Abdul Kalam Technological University, Thiruvananthapuram,
Kerala 695016, India

e-mail: p18cep01@mace.ac.in

J. S. James · J. J. Ponnappal · A. Jayan · E. John

Department of Civil Engineering, Mar Athanasius College of Engineering, Kothamangalam, India

e-mail: elson@mace.ac.in

1 Introduction

1.1 General

Adding significant industrialised wastes such as GGBFS, fly ash, silica fume, copper slag, husk ash, etc. to concrete has allowed researchers to comprehensively analyse its mechanical and durability properties. A key factor that affects the lifespan and endurance of concrete constructions is durability. One of the properties that significantly persuade the concrete's longevity is shrinkage [1]. Although shrinkage cracks are inevitable, the width, expansion, and start of the fracture all significantly affect the concrete's strength. It results in the diffusion of chloride ions, acids, and alkalis into the concrete's core structure, interfering with the inner compact bonding of different raw ingredients and lowering the strength [2].

When concrete loses moisture content, it shrinks, which is characterised as a change in size. Concrete experiences three types of shrinkage: plastic, drying, and autogenous. Plastic shrinkage develops from moisture loss while the concrete is still wet. Drying shrinkage results from moisture loss from concrete after it has dried [3]. Other types of shrinkage include carbonation shrinkage and thermal shrinkage. Shrinkage can induce tensile stresses in concrete, which when exceeding the tensile strength of concrete, can lead to deterioration problems [4]. Shrinkage is a significant concern when there is a high evaporation rate resulting due to lack of moisture, high water temperature and high windy conditions during curing of concrete. Drying shrinkage is also a major concern in buildings with high surface to volume ratio. Some of the most effective ways to reduce shrinkage involves use of mineral admixtures [5].

Mineral admixtures, also known as supplementary cementitious materials are industrial derivatives having finely divided particles having pozzolanic and cementitious properties [6]. Fly ash produced from the combustion of pulverized coal, GGBFS (ground granulated blast furnace slag) resulting from the rapid cooling of slag from furnaces producing pig iron and steel are examples of SCMs [5]. They can be added in the range of 20–50% of cement by mass replacement and provide various benefits other than performance improvement such as cost reduction, sustainable development, ecological benefits etc. [7]. This study investigates the effect of various ultrafine materials on compressive strength, flexural strength, and drying shrinkage of concrete.

2 Drying Shrinkage in Concrete

Drying shrinkage describes to the contraction of hardened concrete due to the loss of capillary water. It happens when the surface-absorbed water in the calcium silicate hydrate (C-S-H) gel and the hydrostatic tension in tiny pores are diminished [8]. As concrete ages, all types of Portland cement concrete experience drying shrinkage



Fig. 1 Drying shrinkage in concrete [12]

or volume change. Initially, excess water in the mixture evaporates and escapes as bleed water on the concrete surface. Once the bleed water is gone, additional water is drawn out from the interior of the concrete mass [9]. This shrinkage primarily results from the deformation of the cement paste, although the stiffness of the aggregates can also influence it. This process, which occurs after the concrete has set, is known as drying shrinkage [10]. Most drying shrinkage occurs within the first few months of the concrete's lifespan. Drying shrinkage is produced by the removal of water from unsaturated air voids present in concrete. However, a portion of this shrinkage can be recovered by submerging the concrete in water for a specific time, called moisture movement [11] (Fig. 1).

When the water-cement ratio is extremely low, nearly all the water is consumed during cement hydration. In such cases, if the relative humidity within the concrete drops below 80%, there is minimal interchange of moisture between the concrete and the regular exterior environment [13]. Additionally, high-strength concrete has a low permeability, which means that any drying that does occur is minimal. Consequently, the drying shrinkage experienced with high-strength concrete is substantially lower compared to normal-strength concrete [12].

3 Experimental Program

3.1 Materials Used

Cement. The cement used was ordinary Portland Cement-Grade 53, certified with IS: 12269-1987. Table 1 lists the cement's characteristics.

Aggregates. The study employed fine aggregate in the form of locally accessible manufactured sand, which had a maximum size of 4.75 mm. This sand exhibited a specific gravity of 2.62 and a water absorption rate of 1.31%. Additionally, crushed

Table 1 Properties of the cement

Si no	Properties	Test Results
1	Specific gravity	3.15
2	Standard consistency	28%
3	Setting time-initial	130 min
4	Setting time-final	245 min
5	Fineness	5%
7	7th—day compressive strength	20.6
8	28th—day compressive strength	53.5

stone with a maximum size of 20 mm was utilized, possessing a specific gravity of 2.8% and a water absorption rate of 0.62%.

Ultrafine Ground Granulated Blast Furnace Slag. The study utilized two distinct sources to acquire Ground Granulated Blast Furnace Slag (GGBFS), which adheres to the IS 1727—1967 standard and possesses a specific gravity of 2.9. These specific sources were selected based on their wide popularity in the market, easy accessibility, and established reactivity [14].

Ultrafine Fly Ash. For the study, fly ash conforming to Grade 1 of IS 3812 was used, provided uniform blending with the cement is ensured [15]. Ultrafine fly ash, consisting of highly fine particles with an average size varying between 2 and 4 microns and having a specific gravity of 2.2, was used in the investigation.

Water. Portable water with pH values lying between 6 and 8 is used for the study.

Superplasticizer. Superplasticizer is a chemical admixture, also used as a high range water reducer. At low water content, superplasticizers can be treated to increase the workability of the mixture. In this research, a pc-based superplasticizer with the relative density of 1.08 ± 0.01 at 25 °C is used as the superplasticizer.

3.2 Concrete Mix Proportions

Concrete mixes were prepared with Supplementary Cementitious Materials as per IS 10262:2019. SCMs used include ultrafine fly ash and ultrafine GGBFS (Ground Granulated Blast Furnace Slag) by replacing cement content by 10% by weight as per previous studies. Superplasticizer was varied accordingly to obtain the required slump in the range of 100–120. The mixes prepared are CM: Control Mix, UF1: a slag based ultrafine material (source 1), mix UF2: ultrafine material based on ultrafine fly ash, mix UF3: a slag based ultrafine material (source 2). The constituent proportions of concrete mixtures employed for assessing the drying shrinkage of concrete are demonstrated in Table 2.

Table 2 Mix combinations with varying SCMs

Name	Cement (kg/m ³)	SCM (kg/m ³)	Coarse aggregate (kg/m ³)	Fine aggregate (kg/m ³)	Water (kg/m ³)	Superplasticizer (kg/m ³)
CM	380	–	1145	776	154	1.39
UF 1	342	38	1145	776	154	1.24
UF 2	342	38	1145	776	154	1.21
UF 3	342	38	1145	776	154	1.21

Table 3 Slump values of concrete mixes

Name	Slump (mm)
CM	120
UF1	125
UF2	110
UF3	110

3.3 *Mixing and Placing*

The concrete mix for the research was prepared using machine mixing. The raw materials were loaded into the mixer and mixed for 3 min. The workability of the concrete was then assessed by computing the slump, and the results were tabulated in Table 3. The mixture was then vibrated and cast into test specimens in moulds. The specimens were demoulded after one day and cured in water for 28 days. The properties of the hardened concrete, including compressive strength and drying shrinkage, were then investigated.

4 Testing Methods

4.1 *Compressive Strength Test*

The specimens were tested as per IS: 516—1959. 150 × 150 × 150 mm concrete cubes were used as specimens to determine the compressive strength. The load was applied at a uniform rate without shock. Compressive strength was found at 7th-day 14th-day and 28th-day respectively [16].

4.2 Flexural Strength Test

The test was carried out as per as per IS 516: 1959. Specimen of size $150 \times 150 \times 700$ mm were cast. The load was applied at a rate of loading of 400 kg/min after a curing period of 28 days [16].

4.3 Slump Test

The slump test is used to measure the consistency and workability of cement. The slump test shows the workability of concrete, and the ease with which the concrete flows. The slump test was done on fresh concrete and workability was found as per IS 1199—1959 [17].

4.4 Drying Shrinkage Test

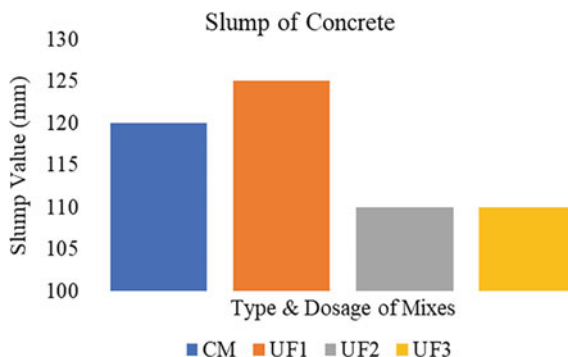
The length changes of concrete prisms were measured in millimeters using a mechanical dial gauge-length comparator, following the guidelines outlined in ASTM C157 [18]. To facilitate the measurement process, each concrete specimen was equipped with a steel stud featuring rounded tips on both ends. The sensitivity of the measurements was set at 1/1000 mm. For each concrete mixture, three prisms were cast, and once demolded, these specimens were placed in a curing room maintained at a relative humidity of 65% and a temperature of 20 °C. The initial measurement was taken on the same day the specimens were demolded, and subsequent measurements were recorded for four months from the initial measurement [10]. Three specimens were utilized for each time interval, and the average value of the three measurements was considered the concrete's shrinkage. The shrinkage results obtained from the laboratory investigation are graphically presented.

5 Results and Discussion

5.1 Slump

The workability of concrete, which denotes the level of internal work needed to attain thorough compaction, holds significant importance. This attribute is influenced by several factors, including the composition of materials, mix proportions, and prevailing environmental conditions. The slump test is employed as a means of assessing the workability of fresh concrete. By adjusting the superplasticizer content as mentioned in Table 3, the target slump range of 100 to 120 was achieved, and the

Fig. 2 Slump of concrete mixes with and without ultrafine materials



results are presented in Table 3 and Fig. 2. The study shows that all mixes containing ultrafine materials have superior workability and cohesiveness compared to the control mix with less amount of superplasticizer. However, to gain a deeper understanding of the impact of ultrafine materials on workability, further investigations are required.

Concrete workability is essential because it affects the ease of placement, compaction, and finishing. A concrete mix that is too stiff will be challenging to handle and causes shrinkage problems, and a mix that is too fluid will result in segregation, bleeding, and an uneven surface. Therefore, it is crucial to achieve optimal workability for a particular application. As observed in earlier studies, ultrafine elements including ultrafine fly ash and ultrafine slag are also known to enhance the workability of concrete [19].

In conclusion, the study shows that the addition of ultrafine materials can enhance the workability and cohesiveness of fresh concrete. However, further research is necessary to understand the underlying mechanisms and optimize their usage.

5.2 Compressive Strength

Compressive strength for the mixes was found at 7th, 14th and 28th day respectively. The results are provided in Table 4 and plotted in Fig. 3 as graphically. Mixes UF1, UF2 and UF3 show higher compressive strength than the control mixture. According to the study findings, on the 7th day, the mixture UF1, which incorporates ultrafine ground granulated blast furnace slag (GGBFS), exhibits the highest strength. However, on the 14th day, the mixture UF2, where ultrafine fly ash is used as an alternative material, demonstrates the highest strength. Furthermore, on the 28th day, the mix UF2 continues to exhibit the highest strength gain. These results align with the conclusions drawn by Kandie et al. [20].

The higher compressive strength of UF1, UF2 and UF3 could be due to the higher fineness and higher pozzolanic reactivity of ultrafine material. Both ultrafine slag and ultrafine fly ash are highly reactive pozzolanic materials. They react with calcium

Table 4 Compressive strength of blends with and without ultrafine materials

Name	7th day cube strength (MPa)	14th day cube strength (MPa)	28th day cube strength (MPa)
CM	23	31	38
UF1	30	34	42
UF2	26	38	45
UF3	27	36	44

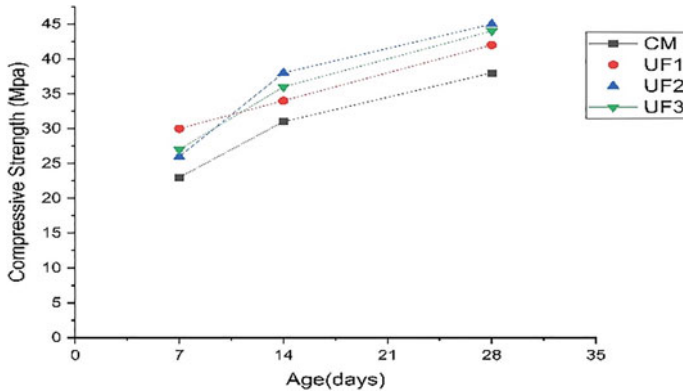


Fig. 3 Compressive strength of ultrafine blends along with control mix

hydroxide present in the concrete to make additional calcium silicate hydrates (C-S-H), which contribute to the development of a denser and more cohesive matrix [21, 22]. This increased hydration and formation of additional C-S-H gel results in improved compressive strength [23].

5.3 Flexural Strength

The findings of the flexural strength test, which was performed following a 28-day curing period, are illustrated in Table 5. The flexural strength of all mixes that contained ultrafine materials was found to be superior to that of the control mixture.

Table 5 Flexural strength of blends with and without ultrafine materials

Mix designations	Flexural strength (MPa)
CM	4.71
UF1	5.2
UF2	5.3
UF3	5.56

Fig. 4 Flexural strength of concrete blends with and without ultrafine materials

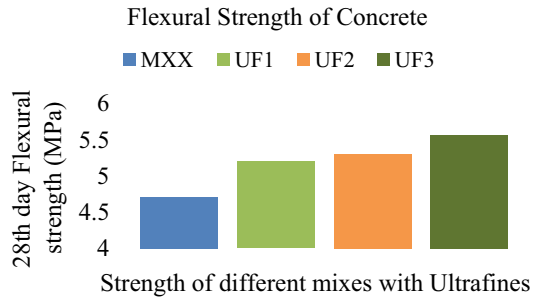


Figure 4 graphically represents the same results. Among all the mixes tested, Mix UF3, prepared by replacing cement with ultrafine GGBFS obtained from source 2, exhibited the highest flexural strength. This indicates that the addition of ultrafine materials, particularly ultrafine GGBFS, can improve the flexural strength of the mix.

The ultrafine particles of slag and fly ash fill the gaps between coarser aggregate particles, resulting in improved particle packing. This denser packing leads to enhanced interlocking and improved load transfer, ultimately improving the flexural strength of the concrete. The findings, as shown in previous studies, indicate that enhancing the flexural capacity of structures by utilizing ultrafine materials in construction could be a viable approach to increase their strength [24, 25].

5.4 Drying Shrinkage

The drying shrinkage was determined using length comparator. The results are plotted in the figures shown below. The shrinkage behavior of concrete mixes containing ultrafine materials (UF1, UF2, and UF3) was investigated and compared with a control mix (CM) in this study. Figures 5, 6, and 7 display the shrinkage comparison of the mixes with ultrafine materials against the control mix.

The results showed that all mixes containing ultrafine materials exhibited significantly lower shrinkage than the control mix. Figure 8 depicts a comparison of the shrinkage strains of the three ultrafine materials along with control mix. Compared to the other two materials, UF3 exhibited the highest strain, although in the initial days, the strains were more or less within the same range of values. UF2, which is an ultrafine material based on fly ash, showed lower shrinkage strain in the later days. The ultrafine slag and fly ash act as fillers, occupying the voids between the cement particles [26]. This filler effect contributes to the overall densification of the concrete matrix, reducing the potential for crack propagation [27]. UF1 and UF2 displayed almost similar values until 90 days. However, after 90 days, the rate of shrinkage increase in UF2 was significantly less than that of UF1.

In summary, the use of ultrafine fly ash and ultrafine GGBFS can have varying effects on the resistance to shrinkage in concrete structures. As an example, when

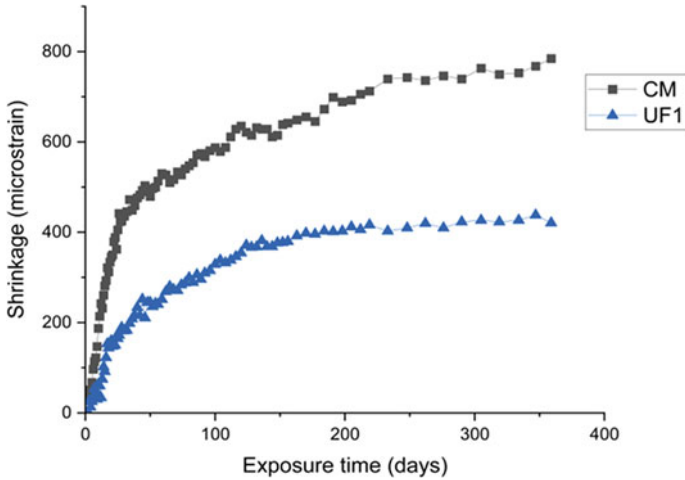


Fig. 5 Shrinkage strain of UF1 and CM

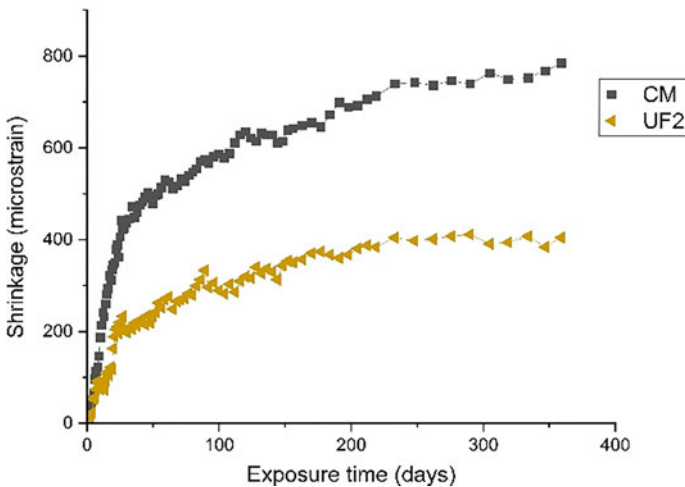


Fig. 6 Shrinkage strain of UF2 and CM

210 days had passed, the variation in strain between the three ultrafine materials was merely 35 microstrains. So, the choice of material may depend on specific project requirements, such as the desired level of crack resistance on particular days or limits on shrinkage strain. The pozzolanic activity of fly ash, along with its capacity to react with calcium hydroxide in the presence of water, is attributed to the presence of reactive silica and alumina. This reaction leads to the formation of additional C-S-H gel. Better strength growth and less drying shrinkage result from this interaction

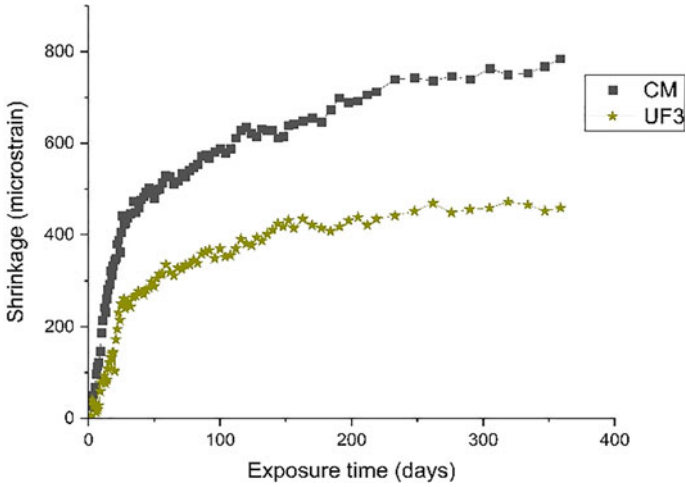


Fig. 7 Shrinkage strain of UF3 and CM

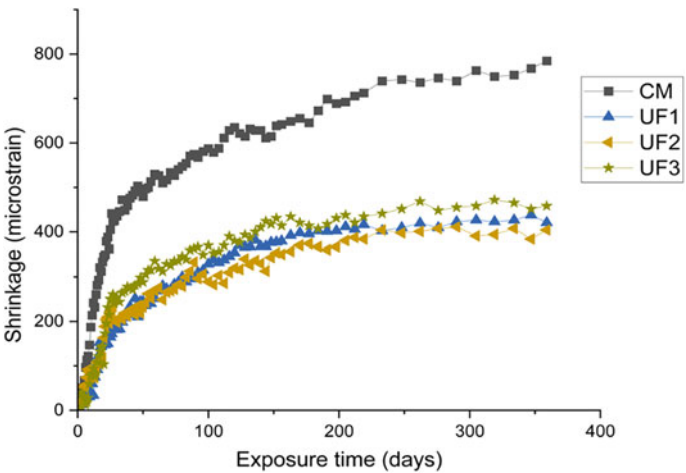


Fig. 8 Shrinkage strain of different ultrafine materials with control mix

[28]. Based on the results, the use of ultrafine materials, particularly UF2, can be recommended for applications where higher shrinkage strain resistance is required.

The conclusions of this research help to clarify the behaviour of ultrafine materials in concrete mixtures with regard to shrinkage and their potential for usage in construction applications.

6 Conclusion

The utilization of supplementary cementitious materials (SCMs), specifically ultrafine fly ash and ultrafine GGBFS, can significantly decrease drying shrinkage in concrete. During the initial 28-day age of the specimens, the specimens made with ultrafine fly ash exhibit a marginally elevated value than those made with slag-based materials. However, in the subsequent ages of around 90–120 days, the ultrafine fly ash demonstrates approximately 50 microstrains less shrinkage than the ultrafine slag. Over the course of a year, the values become almost equivalent, but UF2 displays less shrinkage compared to the other materials. The shrinkage of ultrafine incorporated concrete is only around 40% of the shrinkage observed in the control mix. The enhanced packing density due to the fineness of these materials leads to a reduction in the number of pores, thereby increasing density and reducing drying shrinkage. Additionally, the higher pozzolanic reactivity of these materials also contributes to the shrinkage reduction. In comparison, ultrafine fly ash exhibited superior shrinkage resistance than ultrafine slag materials, accompanied by a slightly higher compressive strength.

In conclusion, the integration of ultrafine SCMs in concrete can effectively reduce drying shrinkage, improve compressive strength, and promote sustainable development. To assess these materials' overall performance and long-term durability, more analysis and testing are required.

References

1. James JS, Rose A, John E, Paul S (2021) A review on the influence of shrinkage reducing admixtures on concrete. *Sustain Agri Food Environ Res* 10:1
2. Tazawa E, Miyazawa S (1997) Influence of constituents and composition on autogenous shrinkage of cementitious materials. *Mag Concr Res* 49(178):15–22
3. Wu SY, Wu YF, Huang J (2013) Effect of ultrafine ground-granulated blast-furnace slag on shrinkage of high-performance concrete. *J Wuhan Univ Technol Mater Sci Ed* 28(1):67–71
4. Sahinagic-Isovic M et al (2012) Shrinkage strain of concrete-causes and types. *Gradevinar* 64(9):727–734
5. Subramaniam KV, Gromotka R, Shah SP, Obla K, Hill R (2005) Influence of ultrafine fly ash on the early age response and the shrinkage cracking potential of concrete. *J Mater Civ Eng* 17(1):45–53
6. James J, John E (2020) The effectiveness of shrinkage reducing admixture and fly ash on plastic shrinkage of concrete. CRC Press, pp 101–107
7. Liu J, Tian Q, Wang Y, Li H, Xu W (2020) Evaluation method and mitigation strategies for shrinkage cracking of modern concrete. Elsevier
8. Atis CD (2003) High-volume fly ash concrete with high strength and low drying shrinkage. *J Mater Civ Eng* 15(2):153–156
9. Aly T, Sanjayan JG (2008) Shrinkage cracking properties of slag concretes with one-day curing. *Mag Concr Res* 60(1):41–48
10. Jianyong L, Yan Y (2001) A study on creep and drying shrinkage of high-performance concrete. Elsevier
11. Heikal M, Ghani RA, Abd EM (2021) The effect of ultra-fine ground granulated blast furnace slag on the properties of self-compacting concrete. *J Mater Eng Perform* 30(3):1513–1523

12. <https://www.constrofacilitator.com/concrete-shrinkage-causes-types-and-itsprevention/>
13. Al-Saleh SA (2014) Comparison of theoretical and experimental shrinkage in concrete. Elsevier
14. IS 1727—1967 Methods of tests for pozzolanic
15. IS 3812—Specification for fly ash for use as pozzolana
16. IS 516—1959 Methods of tests for strength of concrete
17. IS 1199—1959 Methods of sampling and analysis of concrete
18. ASTM C157 Standard test method for length change of hardened hydraulic cement, mortar & concrete
19. Smith JD, Johnson AB (2022) The influence of ultrafine slag and ultrafine fly ash on concrete workability. *J Sustain Constr Mater* 45(2):123–135
20. Kandie B, Börs E (2021) Ultra-fine fly ash concrete. In: *Advances in construction materials and systems*. Taylor & Francis, pp 371–388
21. Anderson CR, Lee KW (2021) Workability of ultrafine slag and fly ash in self-consolidating concrete. *J Constr Mater Tech* 68(3):201–214
22. Gupta S, Sharma V (2020) Effect of ultrafine slag and fly ash on workability of concrete: a comparative study. *Int J Sustain Constr* 32(1):45–52
23. Patel RK, Singh R (2019) Workability enhancement of concrete using ultrafine slag and fly ash. *J Adv Concr Technol* 78(4):301–315
24. Chen L, Wang Z (2018) Investigation of workability of ultrafine slag and fly ash concrete. *Constr Build Mater* 92(2):187–194
25. Johnson AB, Smith JD (2023) Flexural strength of ultrafine slag and ultrafine fly ash in concrete. *J Adv Concr Technol* 68(3):201–214
26. Adams PJ et al (2017) Reduction of drying shrinkage in ultrafine slag and fly ash concrete. *Concr Res Lett* 26(3):109–116
27. Brown LR, Smith EM (2016) Drying shrinkage behavior of ultrafine slag and fly ash concrete. *J Concr Technol* 52(1):78–86
28. Bilodeau A, Malhotra VM (1993) Influence of chemical composition of slag on its reactivity and the performance of slag cement. *Cem Concr Res* 23(2):397–404

Effects of Vertical Irregularities on Seismic Response and Vulnerability of RCC Framed Structure



Mohd Ubaid and Rehan Ahmad Khan

Abstract The effects of vertical irregularities on the response of a structure cannot be underestimated. The presence of vertical irregularities will change the overall response of a structure. In this study effects of different types of vertical irregularities on seismic response and seismic vulnerability of a structure have been analyzed. A six-story reinforced cement concrete building is used as a benchmark building and 28 new models are made by incorporating vertical irregularities in the benchmark model for analysis. The response of all the models is analyzed by using the pushover analysis. SPO2FRAG software is used for the assessment of the seismic vulnerability of models. From the analysis results, it is observed the change in stiffness, mass and position of irregularities in a structure will have a significant effect on the overall response of a structure. The results of the study are presented in terms of story displacements, inter story-drift ratios, capacity curves and median capacity plots.

Keywords SPO2FRAG · Vulnerability · Fragility · Vertical irregularity · Non-linear static · Pushover · Framed structure

1 Introduction

The irregularities may be provided for aesthetics and architectural purposes in a structure. The irregularities in a structure may broadly be classified as plan irregularity or vertical irregularity or a combination of both. Siva Naveen et al. [1] analyzed irregular structure under earthquake loads. They analyzed structures with a single irregularity and combination of irregularities. They found that the irregularities do not always increase the seismic response of the structure. Among all the structures having single irregularity only, vertical irregularities have shown maximum response. Özmen et al. [2] studied the torsional irregularities in a multi-story building. From their study, they found that the torsional irregularity coefficient increases, and the floor rotation decrease as the number of stories decreases. The effect of vertical

M. Ubaid · R. A. Khan (✉)

Department of Civil Engineering, Aligarh Muslim University, Uttar Pradesh, Aligarh, India
e-mail: rehan_iitd@rediffmail.com

irregularities on the seismic response may be very significant, this is why it becomes necessary to do the seismic vulnerability assessment of the structure. Zentner et al. [3] have reviewed the existing approaches and application of four fragility analysis methods, namely the Safety Factor method, Numerical Simulation in conjunction with linear Regression (LR) and maximum likelihood estimator (MLE) and the Incremental Dynamic Analysis [4] method. From the analysis, they have found that the median capacities determined with different methods are very close. Bhosale et al. [5] have studied the vertical irregularities of the building considering the regularity index and seismic risk. They have studied 4 frames having different types of vertical irregularities along with a regular frame. From the fragility, analysis using the probabilistic seismic demand model (PSDM) method, they found that the setback and stepped buildings are better than a regular frame while the open ground story and floating column frame are more vulnerable than their regular counterpart. Moon et al. [6] have focused on fragility analysis of space reinforced concrete frame structures with structural irregularity in the plan. They have used an integrated computational framework using MATLAB (FERUM) and ZEUS-NL. From the fragility curves obtained they found that the structural irregularity considerably affects the seismic vulnerability and the PGA/PGV ratio of ground motion also affects the fragility. Rajeev and Tesfamariam [7] have investigated the effect of construction quality and soft story on the probabilistic seismic demand model (PSDM) and seismic fragility of three reinforced cement concrete structures. They have found that the soft story and construction quality significantly affect the seismic fragility. For developing the fragility curves incremental dynamic analysis is very accurate but computationally expensive as well. To overcome this computational effort involved in incremental dynamic analysis Vamvatsikos and Cornell [8] proposed a new approach called SPO2IDA which provides a direct connection between the static pushover curve and the results of incremental dynamic analysis. Baltzopoulos et al. [9] developed a software named SPO2FRAG which works on the SPO2IDA algorithm to generate the fragility curve directly from the static pushover curve of a structure. This software reduces the efforts involved in incremental dynamic analysis. Pavel and Carale [10] have done the seismic assessment for a typical soft-story reinforced concrete structure. They have used the SPO2FRAG method and Incremental Dynamic Analysis for the seismic fragility analysis. The median capacities obtained from the SPO2FRAG results were close to the incremental dynamic analysis (IDA).

In this study, 28 vertically irregular and one regular reinforced concrete frame have been analyzed. The effect of different types of vertical irregularity on the responses of the structure has been assessed by performing a pushover analysis of different frames. The seismic fragility assessment has been done by using the SPO2FRAG software. The results from pushover analysis are presented in terms of the percentage change in story displacement and percentage change in the inter-story drift ratio for each model. Capacity curves are also plotted for each model to see the effect of vertical irregularities on the capacity of a structure.

2 Modelling and Analysis

2.1 Description of Models

According to IS 1893:2016 (Part-1) [11], a structure has stiffness irregularity if there is a story whose lateral stiffness is less than that of the story above, a structure has mass irregularity if the seismic weight of any floor is 150% more than the floor below, a structure has vertical geometrical irregularity if the horizontal dimension of lateral force resisting in any story is more than 125% of the story below and in-plane discontinuity in vertical elements resisting lateral force when the in-plane offset of the lateral force-resisting element is greater than 20% of the plan length of those elements. In this study, a six-story reinforced cement concrete frame has been taken as a benchmark (BM). The isometric view of the model created in ETABS [12] is shown in Fig. 1. The benchmark model has 6 bays at 3 m length in both X and Y directions. The story height is 2.8 m for all the stories in the benchmark model. The size of the beams is 300 mm × 450 mm and the size of the column is 500 mm × 500 mm for the benchmark model. For including the vertical irregularities, changes are made in the benchmark (BM) model. All these building models are created in ETABS. The characteristic strength of concrete is taken as M25 for all the structural members. The rebar grade is taken as Fe415 for use as reinforcement. The slab thickness is taken as 130 mm. The dead loads and live loads are taken from IS875:1987 Part-1 [13] and Part-2 [14] respectively. All the frames have been analyzed and designed in ETABS. All the models have been designed as a special moment-resisting frame (SMRF), located on soil type II, situated in zone 5, and having importance factor 1 as per IS1893:2016 (Part-1). IS 456:2000 [15] is used for reinforced concrete design and IS13920 [16] is used for the ductile detailing of the structures. In this study models having mass irregularity, stiffness irregularity, vertical geometrical irregularity, and a model with floating columns along with a benchmark model having no irregularity have been studied. The description of the models is given in Table 2.

2.2 Pushover Analysis

The response of different models has been analyzed by using pushover analysis. For including these non-linearities plastic hinges are provided in beams and columns. P-M2-M3 hinges are provided at both the ends of all the columns. M3 hinges are provided at both the ends of the beams. The base of all the models is assumed to be fixed. The lateral load for pushover analysis was applied based on the first mode shape of the building. The results of the pushover analysis will be used in SPO2FRAG software for seismic vulnerability assessment of models.

Fig. 1 Isometric view of the benchmark model

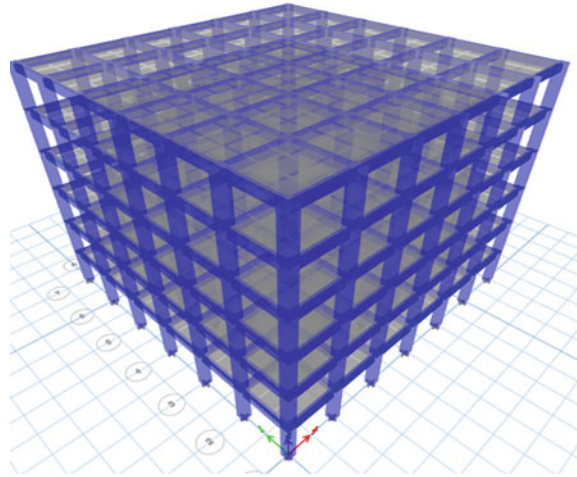


Table 1 Displacement limit states [17]

Damage state	Displacement threshold
Slight	$0.7D_y$
Moderate	D_y
Extensive	$D_y + 0.25 (D_u - D_y)$
Complete	D_u

2.3 Seismic Vulnerability Analysis

The seismic fragility curve is a graphical representation between the probability of exceeding a particular limit state for a structure and the ground motion intensity. For the seismic vulnerability assessment of the structure SPO2FRAG software has been used. This software is very easy to use for developing the fragility curves as compared to incremental dynamic analysis. Two important parameters for generating a fragility curve are intensity measure (IM) and engineering demand parameter (EDP). Different parameters may be used as intensity measures i.e. peak ground acceleration or fundamental mode spectral acceleration. SPO2FRAG uses the fundamental mode spectral acceleration $S_a (T_1)$ as the intensity measure. The structural damping was taken as 5%.

2.4 Definition of Limit States

In SPO2FRAG software the limit states for a structure can be defined in terms of inter-story drift ratio or roof drift ratio. In this study, the roof drift ratio is considered as the engineering demand parameter. The threshold values for the engineering demand

parameter are defined for different damage states. For determining the roof drift ratio, first, the displacement at the roof is determined according to the displacement limit states given by Penna et al. [17] as given in Table 1.

where D_y and D_u are yield and ultimate displacement respectively.

After determining the roof displacements these values are converted into roof drift ratio by dividing the displacements with the height of the building. Then these values are used as the threshold roof drift ratios for different limit states.

3 Results and Discussion

3.1 Story Displacement and Inter-story Drift Ratio

The percentage change in story displacement and inter-story drift ratio for each model has been plotted. The change in each of these responses is calculated with respect to the benchmark model.

3.1.1 Effect of Mass Irregularity on Story Displacement and Inter-story Drift Ratio

Figure 2 shows the change in story displacement and inter-story drift ratio for M-2F2M, M-3F2M, M4F2M, M-5F2M models. Here in these models, the floor mass increased by 2 times on the respective floor as shown in the Table 2. This is done to access the effect of mass irregularity at different story levels. From the change in displacement plot, it can be seen that the story displacement decreases significantly in M-3F2M and M-4F2M models. The maximum decrease of 37.48% is observed in model M-4F2M on the first floor. However, in the case of M-5F2M and M-6F2M, there is a slight increase in the story displacement, the maximum value being 3.62% for M-6F2M. As the increased mass of the story is shifted from second to sixth story the time period of the building increases and becomes more than the time period of BM model. The increase in the mass can be beneficial if the mass is increased at lower stories as compared to upper stories.

From the inter-story drift ratio plot in Fig. 2 it clear that the M-3F2M and M-4F2M models show a maximum decrease in the inter-story drift ratios. The maximum decrease (39.38%) in the inter-story drift ratio was found out to be in M-4F2M on the fifth floor. In the M-2F2M model, there is a significant decrease in inter-story drift ratio up-to third floor after which the decrease in value is not very significant. There is a sudden decrease in the inter-story drift ratio at the fifth and sixth floor in M-5F2M. M-6F2M shows a slight increase in the inter-story drift ratio at each story level except on the first floor.

Figure 3 shows the plots of the percentage change in story displacement and inter-story drift ratio for M-3F1.5M, M-3F2M, M-3F2.5M, and M-3F3M models. In

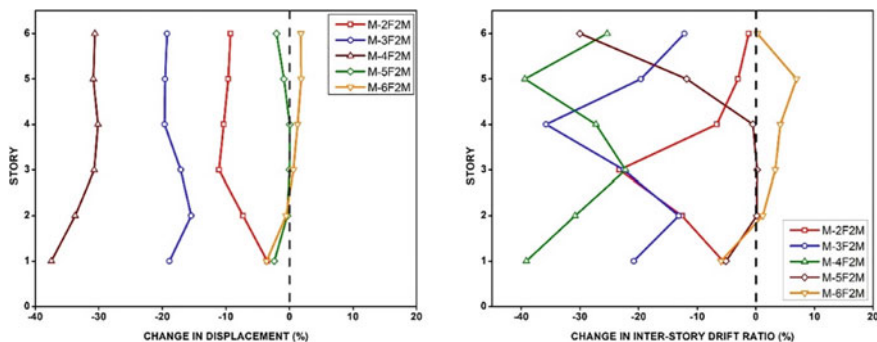


Fig. 2 Percentage change in story displacement and inter-story drift ratio

these models the behavior of the benchmark model has been assessed by increasing the floor mass on the third floor by a factor of 1.5, 2, 2.5, and 3 in M-3F1.5M, M-3F2M, M-3F2.5M, and M-3F3M models respectively. All the models show a decrease in story displacement and inter-story drift ratio. M-3F2M shows a maximum decrease in story displacement of 19.66% on the fourth floor. However, M-3F1.5M, M-3F2.5M, and M-3F3M show a percentage maximum decrease in story displacement of 6.91%, 12.29%, and 16.04% on the sixth floor respectively. The increase of mass on the second floor will affect the story displacement significantly. Figure 3 also shows the percentage change in the inter-story drift ratio for M-3F1.5M, M-3F2M, M-3F2.5M, and M-3F3M models. Among the four models, M-3F3M shows the maximum decrease of 49.98% in the inter-story drift ratio on the fourth floor. All the models show a sudden decrease in the inter-story drift ratio on the third and fourth floors, the maximum displacement being on the fourth floor.

3.1.2 Effect of Stiffness Irregularity on Story Displacement and Inter-story Drift Ratio

Figure 4 shows the percentage in story displacement and inter-story drift ratio for models S-GF25C, S-1F25C, S-2F25C, S-3F25C, S-4F25C and S-5F25C. The model S-1F25C shows the maximum decrease of 82.28% in story displacement on the first floor while the S-4F25C model shows a minimum decrease of 3.68% in story displacement on the first floor. From the inter-story drift ratio plot in Fig. 4, it is seen that the inter-story drift ratio suddenly increases at the junction of the story where the number of columns is reduced to 25 from 49 and the story above i.e. S-3F25C model the number of columns is reduced and the inter-story drift ratio of the fourth floor increases up-to 193.78% which is maximum among these six models having reduced number of columns. This trend is the same for all the models but the increase in inter-story drift ratio is not the same. The reduction in the numbers of column reduces the stiffness of that story as compared to other stories which results in the reduced performance of the structure as compared to BM models. If it is necessary to reduce

Table 2 Description of models

Model	Irregularity	Period (sec) (fundamental mode)
BM	No irregularity	0.669
M-2F2M	2 times floor mass on the second floor	0.627
M-3F2M	2 times floor mass on the third floor	0.645
M-4F2M	2 times floor mass on the fourth floor	0.668
M-5F2M	2 times floor mass on the fifth floor	0.687
M-6F2M	2 times floor mass on the sixth floor	0.697
M-3F1.5M	1.5 times floor mass on the third floor	0.656
M-3F2.5M	2.5 times floor mass on the third floor	0.638
M-3F3M	3 times floor mass on the third floor	0.634
S-GF25C	Number of columns reduced to 25 at ground floor	0.724
S-1F25C	Number of columns reduced to 25 on the first floor	0.724
S-2F25C	Number of columns reduced to 25 on the second floor	0.709
S-3F25C	Number of columns reduced to 25 on the third floor	0.691
S-4F25C	Number of columns reduced to 25 on the fourth floor	0.674
S-5F25C	Number of columns reduced to 25 on the fifth floor	0.663
S-GF3.2SH	Story height increased from 3 to 3.2 m at ground floor	0.694
S-1F3.2SH	Story height increased from 3 to 3.2 m on the first floor	0.702
S-2F3.2SH	Story height increased from 3 to 3.2 m on the second floor	0.698
S-3F3.2SH	Story height increased from 3 to 3.2 m on the third floor	0.689
S-4F3.2SH	Story height increased from 3 to 3.2 m on the fourth floor	0.68
S-5F3.2SH	Story height increased from 3 to 3.2 m on the fifth floor	0.674
S-3F3.6SH	Story height increased from 3 to 3.6 m on the third floor	0.712
S-3F4SH	Story height increased from 3 to 4 m on the fourth floor	0.737
S-1.2CS	Column size increased to 120%	0.64
S-1.5CS	Column size increased to 150%	0.61
S-1.8CS	Column size increased to 180%	0.588

(continued)

Table 2 (continued)

Model	Irregularity	Period (sec) (fundamental mode)
VG-1	A setback at the second and fourth floor	0.427
VG-2	A setback on the second floor and continues up-to-the sixth floor	0.557
FC	Floating columns at ground floor	0.834

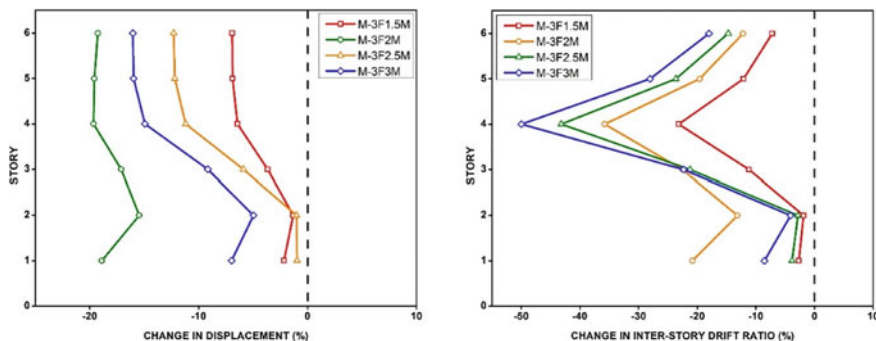


Fig. 3 Percentage change in story displacement and inter-story drift ratio

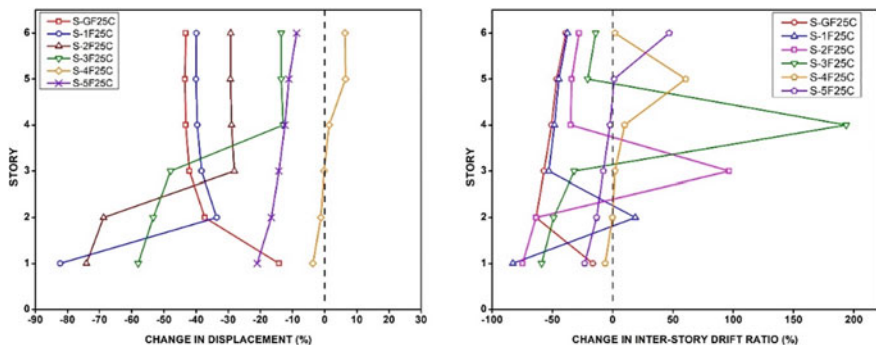


Fig. 4 Percentage change in story displacement and inter-story drift ratio

the numbers of columns at a particular level in the building, proper stiffness should be added at that level using some other alternatives (braces, shear walls, etc.) for better performance of the structure.

Figure 5 shows the percentage change in story displacement and inter-story drift ratio for S-GF3.2SH, S-1F3.2SH, S-2F3.2SH, S-3F3.2SH, S-4F3.2SH and S-5F3.2SH models. S-GF3.2SH shows an increase in story displacement on the first floor but the change in the story displacement decreases as we move to the upper floors. Model S-3F3.2SH and S-5F3.2SH show a somewhat similar percentage

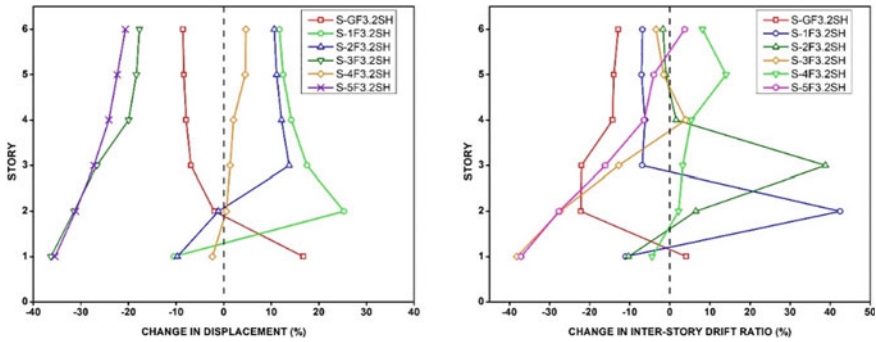


Fig. 5 Percentage change in story displacement and inter-story drift ratio

decrease at the first, second and third floors and there are a slight change between the change for two S-3F3.2SH and S-5F3.2SH models at the fourth, fifth and sixth floors. S-1F3.2SH shows a maximum increase in story displacement of 25.27%. The maximum decrease in story displacement is seen in S-3F3.2SH which is 36.29%. S-1F3.2SH shows a sudden increase in inter-story drift ratio of 42.48% on the second floor but on the third floor and onward this change decrease and is nearly equal. As can be seen from the plot of the percentage in the inter-story drift ratio that the change increases suddenly at the junction of the floor having reduced stiffness due to increased column height from 2.8 to 3.2 m and the above floor joining it.

From the plot of story displacement in Fig. 6, model S-3F4SH shows the maximum increase in story displacement of 48.39% on the fourth floor. However, the story displacement decreases in S-3F3.2SH and S-3F3.6SH and the maximum decrease is seen in S-3F3.2SH which is 36.29%. As the stiffness is decreased on the third floor by increasing the story height from 2.8 m to 3.2 m, 3.6 m, and 4 m in the respective models, there is a sudden increase in story displacement on those floors. The inter-story ratio also increases as the stiffness decreases. The maximum increase is in the S-3F4SH model where the story height is increased to 4 m from 2.8 m (Fig. 6).

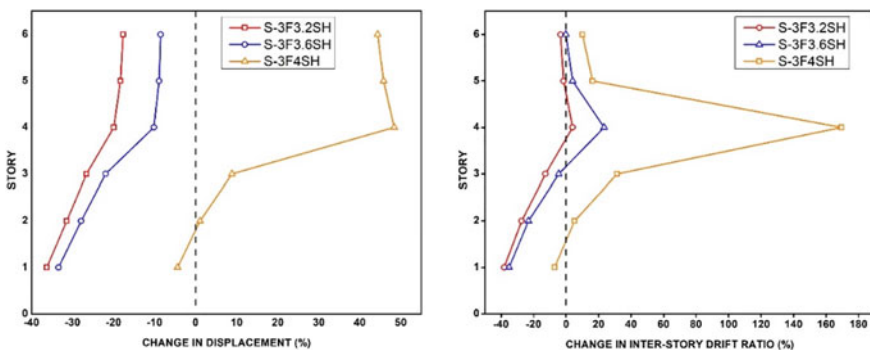


Fig. 6 Percentage change in story displacement and inter-story drift ratio

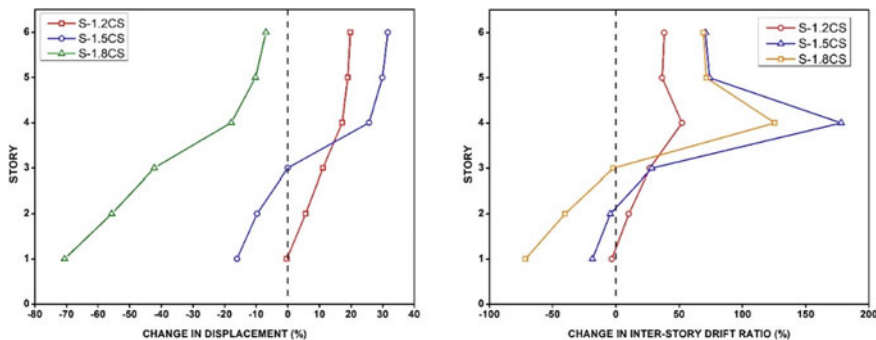


Fig. 7 Percentage change in story displacement and inter-story drift ratio

Among the three models S-1.2CS, S-1.5CS and S-1.8CS, S-1.8CS shows the maximum decrease in story displacement of 36.29% on the first floor which is due to the increased size of columns by a factor of 1.8 (Fig. 7). This increase in size in the column increases the stiffness and results in decreased story displacements. The story displacement increases significantly on the fourth floor because the column size is not increased above the third floor resulting in an abrupt change in stiffness. S-1.5CS shows more decrease in story displacement relative to S-1.2CS which is due to increased stiffness but from the fourth floor onward S-1.5CS shows more increase in story displacement relative to S-1.2CS. All three models show a significant increase in the inter-story drift ratio on the fourth floor. Maximum inter-story displacement in the S-1.5CS model which is 178.07% on the fourth floor. S-1.8CS shows a significant decrease in the inter-story drift ratio on the first floor of 71.48%.

3.1.3 Effect of Vertical Geometrical Irregularity on Story Displacement and Inter-story Drift Ratio

Figure 8 shows the change in story displacement and inter-story drift ratio plots for models VG-1 and VG-2. VG-2 shows a maximum decrease in displacement on the first floor of 70.73%. VG-1 and VG-2 show a significant decrease of 57.7% and 71.59% respectively in the inter-story drift ratio on the first floor. This percentage decrease starts decreasing up-to-the-second floor and there is an abrupt change in the inter-story drift on the third floor which is due to vertical geometrical irregularity available on the second floor in both VG-1 and VG-2 model. In the third story, the percentage increase is 68.19% and 85.18% for VG-1 and VG-2 respectively. Vertical geometrical irregularity is more in the VG-2 model, due to the sudden reduction in the horizontal dimension of lateral load resisting elements at the second-floor relative to the VG-1 model on the second and third floors but on the fourth and fifth floors, the value is the same. The most common way to improve the performance of a structure having irregularities is to use bracings as discussed by Ubaid and Khan [18, 19].

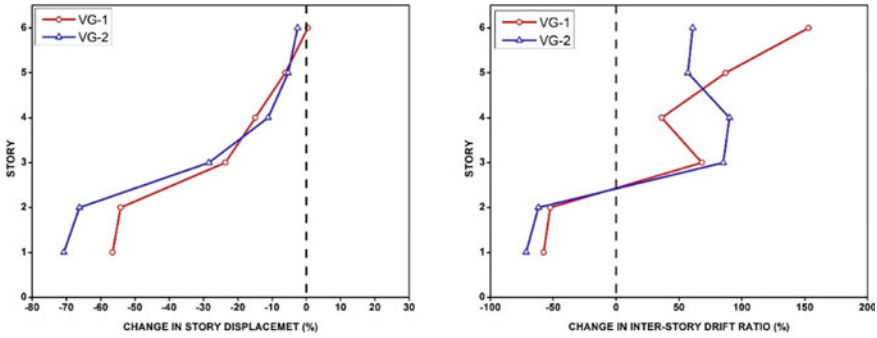


Fig. 8 Percentage change in story displacement and inter-story drift ratio

3.1.4 Effect of Floating Columns on Story Displacement and Inter-story Drift Ratio

FC model which has floating columns shows a significant reduction in story displacement and inter-story drift ratio as shown in Fig. 9. FC shows a 29.13% and 40.56% decrease in story displacement on the first and second floor as shown in Fig. 9. The FC shows a maximum decrease in inter-story displacement on the second floor and the inter-story drift ratio gradually increases up-to sixth floor.

3.2 Seismic Vulnerability Assessment

SPO2FRAG software needs many input values of a building to generate the fragility data. Story displacement vs base shear data is needed in the first step. Story displacement may be in terms of roof displacement or it may be the displacement of different stories in separate columns. Capacity curves for different vertically irregular models

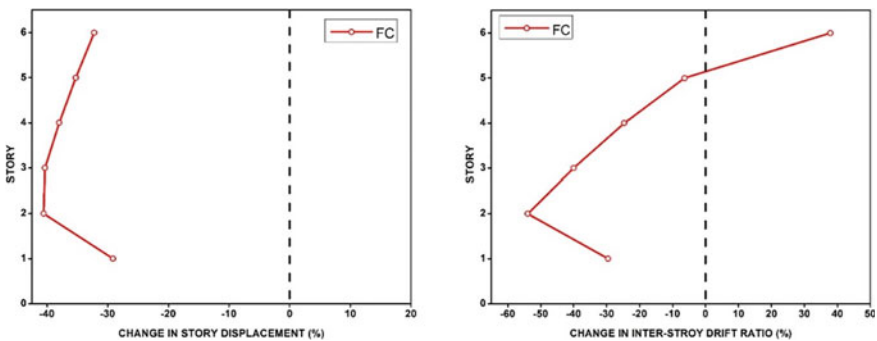


Fig. 9 Percentage change in story displacement and inter-story drift ratio

have been plotted along with the capacity curve of the benchmark model to understand the effect of vertical irregularity on the capacity curve. The median capacities of different models for slight, moderate, extensive, and complete limit states are also plotted in separate plots. The median capacity corresponds to the probability of a fifty percent exceedance of a particular limit state.

3.2.1 Effect of Mass Irregularity on Seismic Vulnerability

Figure 10 shows the capacity curve and median capacity plot for BM, M-2F2M, M-3F2M, M-4F2M, M-5F2M, and M-6F2M models. From the capacity, the curve plot is very clear that the capacity curves of M-2F2M, M-3F2M, M-4F2M, M-5F2M lies above the benchmark (BM) which means that the overall stiffness has increased for these four models by introducing the mass irregularity. However, the capacity curve of M-6F2M lies a little below of BM. The median capacity curve in Fig. 10 shows that after introducing the mass irregularity the median capacities decrease for all the models. Model M-4F2M has the lowest median capacity values for all the limit states. For complete damage state in M-4F2M, the median capacity is 0.522 g however for BM it is 0.704 g. The difference between the median capacity increases as we go from slight to moderate, moderate to extensive, and extensive to complete for all the models. M-2F2M shows slightly increased median capacities for slight, moderate, and extensive damage relative to the benchmark model but for complete damage, it is slightly low (0.669 g) relative to the benchmark model (0.704 g).

The capacity curves for M-3F1.5M, M-3F2M, M-3F2.5M, and M-3F3M lie above the capacity curve for the benchmark model as shown in Fig. 11. As the mass of the third floor is increased the capacity curve shifts upward and the maximum shift is shown by the M-3F3M model having three times more floor mass at the third story relative to other stories. This shift in capacity curve influence the overall behavior of the building. In Fig. 11 the median capacity curve is also shown for BM, M-3F1.5M, M-3F2M, M-3F2.5M, and M-3F3M. M-3F2M shows the minimum median capacities for all the damage limit states. The behavior of the building is affected very

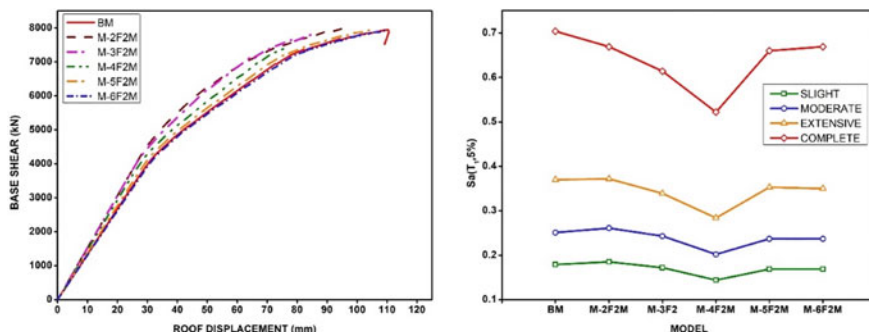


Fig. 10 Capacity curve and median capacity plot

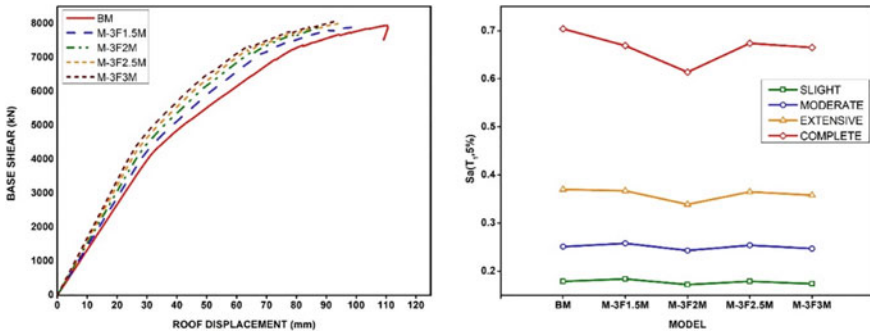


Fig. 11 Capacity curve and median capacity plot

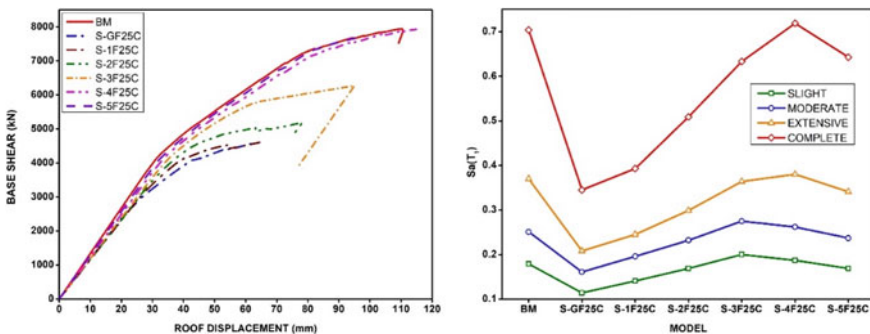


Fig. 12 Capacity curve and median capacity plot

much when the mass irregularity is introduced on the third floor by two times. M-3F1.5M gives slightly increased median capacities for slight and moderate damage relative to the benchmark and a very small decrease for extensive and complete damage limit states.

3.2.2 Effect of Stiffness Irregularity on Seismic Vulnerability

Figure 12 shows the capacity curve and median capacity plot for BM, S-GF25C, S-1F25C, S-2F25C, S-3F25C, S-4F25C, and S-5F25C models. When the stiffness irregularity is introduced in models one by one at different floors by decreasing the column numbers from 49 to 25, the maximum shift in the capacity curve below to the benchmark (BM) model is shown by the S-GF25C model having only 25 columns at ground floor. This is a very critical problem in some buildings where the numbers of columns are reduced suddenly on the ground floor for clear space requirements. S-5F25C shows the minimum shift in the capacity curve below the benchmark model. Model S-GF25C also shows the least median capacity values for

each damage limit state. This is why S-GF25C is the most critical case from all the six models having reduced numbers of columns at different stories. S-4F25C gives slightly higher median capacities for all damage capacities relative to the benchmark model.

Among S-GF3.2SH, S-1F3.2SH, S-2F3.2SH, S-3F3.2SH, S-4F3.2SH, S-5F3.2SH, the capacity curve of S-GF3.2SH shows the maximum shift below the capacity curve of the benchmark (BM) model as shown in Fig. 13. From this plot, it is clear the influence of reduced stiffness by increasing the story height is very significant in S-GF3.2SH. However, this effect is minimum in S-5F3.2SH. From the fragility analysis data, the S-3F3.2SH model shows the least median capacities for all limit states which means this model is the most vulnerable.

From Fig. 14, as the stiffness is reduced by increasing the story height on the third floor from 2.8 m in BM to 3.2 m, 3.6 m, and 4 m in S-3F3.2SH, S-3F3.6SH, S-3F4SH respectively, the capacity curve shifts below the benchmark capacity curve significantly. The maximum shift is observed in S-3F4SH. The maximum roof displacement for S-3F4SH is quite high (158.36 mm) relative to the benchmark (109.71 mm). The median demand capacity increases at the story height are increased. The maximum median capacities being observed in S-3F4SH. The median capacity at complete damage state is 0.856 g and for the benchmark, it is 0.704 g showing a significant increase in median capacity. The median capacities for S-3F3.2SH, S-3F3.6SH are low relative to the benchmark model for all the damage states. The lowest median capacities are shown by the S-3F3.2SH model.

Figure 15 shows the capacity curves and median capacity curves for S-1.2CS, S-1.5CS, and S-1.8CS in which the column size is increased by a factor of 1.2, 1.5, and 1.8 respectively up-to second floor relative to the benchmark model. This increase in the size of columns increases the stiffness of the ground, first and second floor. The effect of this increased stiffness can be seen very clearly in the capacity curve plot in Fig. 15. As the stiffness increases the capacity curve shifts upward relative to the benchmark capacity curve. S-1.8CS shows a maximum shift in the capacity curve relative to the benchmark model. All the models show increased median capacities

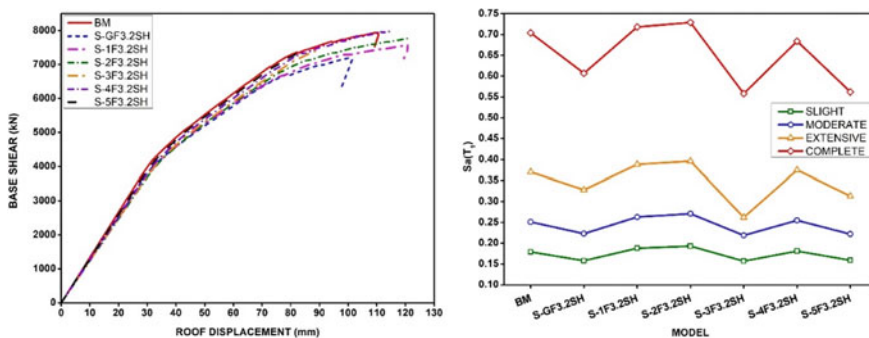


Fig. 13 Capacity curve and median capacity plot

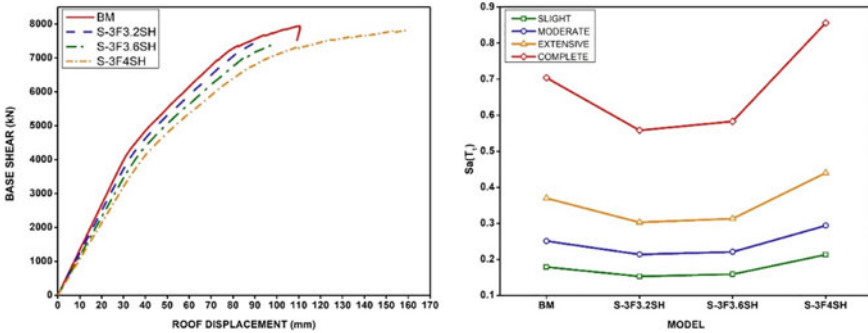


Fig. 14 Capacity curve and median capacity plot

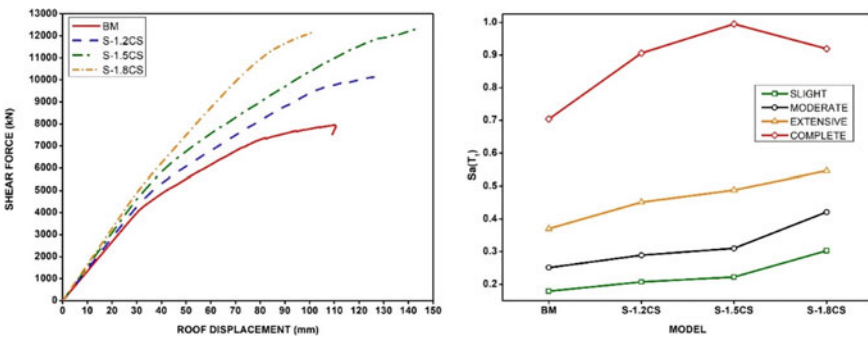


Fig. 15 Capacity curve and median capacity plot

for all damage states relative to the benchmark model. S-1.5CS shows a slightly increased median capacity at a complete damage state relative to S-1.8CS.

3.2.3 Effect of Vertical Geometrical Irregularity on Seismic Vulnerability

The percentage capacity curve and median capacity plot for VG-1 and VG-2 are shown in Fig. 16. Both the capacity curves lie below the capacity curve of the benchmark structure. VG-1 shows less shift in the capacity curve than VG-2 because in VG-2 the horizontal dimension of the lateral load resisting system is reduced on the second floor and it is kept constant up-to fifth floor but in VG-1 this reduction is done in steps first at the second floor and the then at the fifth floor. The effect of the reduction in the horizontal dimension of the lateral load resisting system can also be seen from the median capacity curve for VG-1 and VG-2 model as shown in Fig. 16. The median capacity of VG-1 is more than the VG-2 but the median capacities for

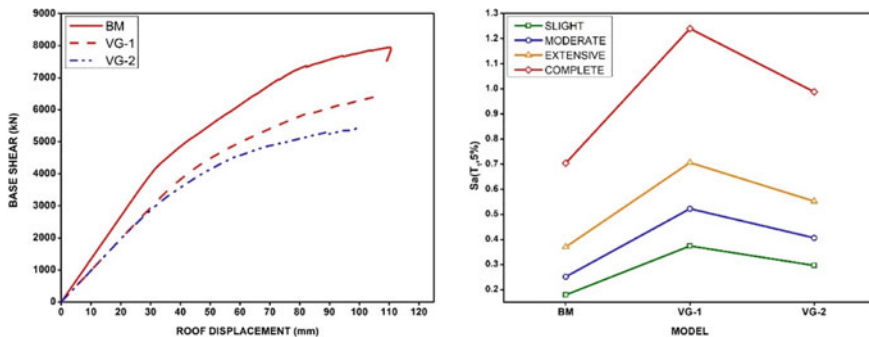


Fig. 16 Capacity curve and median capacity plot

both VG-1 and VG-2 are more than the median capacities for the benchmark frame for all the damage states.

3.2.4 Effect of Floating Columns Irregularity on Seismic Vulnerability

FC model which has floating columns shows a significant shift in the capacity curve below the capacity curve of the benchmark model as shown in Fig. 17. The presence of floating columns also affects the median capacities very much. From the median capacity plot in Fig. 17, it can be seen that the median capacity in the FC model reduces to 0.303 g from 0.704 g in the benchmark model for complete damage state. This significant reduction in median capacity shows that buildings having floating columns are very vulnerable.

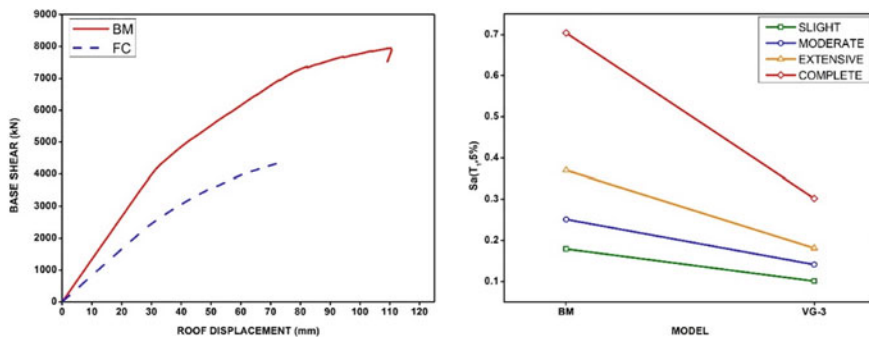


Fig. 17 Capacity curve and median capacity plot

4 Conclusion

The effects of vertical irregularities on the structural response have been analysed by using pushover analysis and the seismic vulnerability assessment has been done by using SPO2FRAG software. A total of 29 models, 28 models with vertical irregularity, and one regular frame have been analyzed. The regular frame has been used as a benchmark to compare the results of vertically irregular models. The effect on structural response and seismic vulnerability is increased in some models and decreased in some models depending upon the placing of vertical irregularity in models. Among all the cases investigated maximum decrease in percentage story displacement and maximum seismic vulnerability is in the model where the number of columns is reduced on the ground floor. The presence of floating columns in a building significantly increases the seismic vulnerability of the structure which is why the floating columns should not be used in a building as a part of the lateral load resisting system.

References

1. Siva Naveen E, Abraham NM, Anitha Kumari SD (2019) Analysis of irregular structures under earthquake loads. *Procedia Struct Integr* 14:806–819. <https://doi.org/10.1016/j.prostr.2019.07.059>
2. Özmen G, Girgin K, Durgun Y (2014) Torsional irregularity in multi-story structures. *Int J Adv Struct Eng* 6:121–131. <https://doi.org/10.1007/s40091-014-0070-5>
3. Zentner I et al (2016) Fragility analysis methods: review of existing approaches and application. *Nucl Eng Des*. <https://doi.org/10.1016/j.nucengdes.2016.12.021>
4. Vamvatsikos D, Cornell CA (2002) Incremental dynamic analysis. *Earthquake Engng Struct Dyn* 31:491–514. <https://doi.org/10.1002/eqe.141>
5. Bhosale AS, Davis R, Sarkar P (2017) Vertical irregularity of buildings: regularity index versus seismic risk. *ASCE-ASME J Risk Uncertainty Eng Syst Part A Civ Eng* 3(3):04017001. <https://doi.org/10.1061/AJRUA6.0000900>
6. Moon D-S, Lee Y-J, Lee S (2018) Fragility analysis of space reinforced concrete frame structures with structural irregularity in plan. *J Struct Eng* 144(8): 04018096. [https://doi.org/10.1061/\(ASCE\)ST.1943-541X.0002092](https://doi.org/10.1061/(ASCE)ST.1943-541X.0002092)
7. Rajeev P, Tesfamariam S (2012) Seismic fragilities for reinforced concrete buildings with consideration of irregularities. *Struct Saf* 39:1–13. <https://doi.org/10.1016/j.strusafe.2012.06.001>
8. Vamvatsikos D, Cornell CA (2006) Direct estimation of the seismic demand and capacity of oscillators with multi-linear static pushovers through IDA. *Earthquake Engng Struct Dyn* 35:1097–1117. <https://doi.org/10.1002/eqe.573>
9. Baltzopoulos G, Baraschino R, Iervolino I, Vamvatsikos D (2017) SPO2FRAG: software for seismic fragility assessment based on static pushover. *Bull Earthquake Eng* 15:4399–4425. <https://doi.org/10.1007/s10518-017-0145-3>
10. Pavel F, Carale G (2019) Seismic assessment for typical soft-storey reinforced concrete structures in Bucharest, Romania. *Int J Disaster Risk Reduct* 41:101332
11. IS 1893: Part 1: 2016. Criteria for earthquake resistant design of structures—part 1: general provisions and buildings. Bureau of Indian Standards
12. ETABS v18. Computers and Structures, Inc. (CSI), America

13. IS 875: Part 1: 1987. Code of practice for design loads (other than earthquake) for buildings and structures: part 1 dead loads—unit weights of building materials and stored materials (Second Revision). Bureau of Indian Standards
14. IS 875: Part 2: 1987. Code of practice for design loads (other than earthquake) for buildings and structures: part 2 imposed loads (Second Revision). Bureau of Indian Standards
15. IS 456: 2000. Plain and reinforced concrete—code of practice (Fourth Revision). Bureau of Indian Standards
16. IS 13920: 2016. Ductile design and detailing of reinforced concrete structures subjected to seismic forces—code of practice (First Revision). Bureau of Indian Standards
17. Penna A, Cattari S, Galasco A, Lagomarsino S (2004) Seismic assessment of masonry structures by non-linear macroelement analysis. In: IV international seminar on structural analysis of historical construction—possibilities of numerical and experimental techniques, vol 2. A.A. Balkema Publishers, Padova, pp 1157–1164
18. Ubaid M, Khan RA (2023) Effect of bracing configuration on the seismic response of buildings with re-entrant corners. *Innov Infrastruct Solut* 8:56. <https://doi.org/10.1007/s41062-022-01029-x>
19. Ubaid M, Khan RA (2022) Performance assessment of vertically irregular steel buckling-restrained braced frame with different bracing configurations. In: Fonseca de Oliveira Correia JA, Choudhury S, Dutta S (eds) *Advances in structural mechanics and applications*. ASMA 2021: structural integrity, vol 19. Springer, Cham. https://doi.org/10.1007/978-3-030-98335-2_23

Experimental Investigation on Microstructure-Based Quality Assessment of TMT Reinforcing Bars



Ansa Varghese  and Bino I. Koshy 

Abstract It has been several decades since mild steel and cold twisted deformed bars got replaced by Thermo Mechanically Treated (TMT) bars or otherwise called Quenched and Self Tempered (QST) bars. Though TMT bars are manufactured with the supreme technologies of tempcore, thermex, etc., researchers have indicated a lack of quality in rebars. The present study is conducted on 12 mm TMT steel rebars. The rebars of different chemical compositions were collected from construction sites for assessing the quality of the rebars based on their microstructure. The present state of affair at the construction site on quality checks on rebars are very much lacking. The study also emphasizes the need for better and expanded checks on quality standards for steel rebars used in concrete structures before embedment. An optical microscope-based characterization of rebar microstructure is conducted. A chemical test, the nital TM ring test is done to estimate the microstructure phase distribution in the collected rebars. The specimens collected were from different sites in the state of Kerala. The use of TMT rebars in the construction sector has undoubtedly enhanced construction quality in many ways. Proper quality checks play a pivotal role in further quality enhancement of reinforced concrete.

Keywords TMT rebars · Nital TM ring test · Microstructural assessment · Optical microscopic imaging

1 Introduction

Reinforced concrete plays a salient role in the construction industry across the world. Regardless of that, structural distresses are very common in structures and the exact diagnosis of the reason behind the damage is often difficult [1]. Hence, quality is to be

A. Varghese (✉) · B. I. Koshy
Amal Jyothi College of Engineering, Kanjirapally, Kottayam, Kerala, India
e-mail: ansavarghese@ce.ajce.in

B. I. Koshy
e-mail: binoikoshy@amaljyothi.ac.in

ensured on every material used in the construction to ensure durable structures. Steel rebar quality predominantly depend on the manufacturing process adopted. The tempcore process is employed to produce high-strength rebars at low cost. The process if done with proper quality control, produce an outer Tempered Martensite (TM) layer and an inner Ferrite Pearlite (FP) core. The tempcore process comprise of three different processes and is detailed by [2]. Initially, the steel rebars supplied by hot rolling mill is passed through a special water-cooling chamber; termed as tempcore box, where the rebar is cooled with pressurized water. A constant temperature is maintained so as to ensure that martensite state is not reached. Thickness of TM depends on exposure time and flow rate of water. From the cooling box, the air-cooled steel dissipates heat from center to periphery forming TM [3]. Finally, rebar is cooled in a cooling bed and austenite core is converted to FP based on chemical composition of rebar and cooling rate. It was found that air-cooled steel had an absence of TM ring formation with the help of a software called thermocalc [2]. But, tensile strength was higher when rebar was air-cooled during the manufacturing process. Different compositions are being used by manufactures for steel production apart from differences in cooling.

2 Materials and Methods

The collection process employed was random samples collected from different sites in Kerala. The rebars collected included those with two different chemical compositions, composition-1 and composition-2, which are detailed in Table 1. The rebars collected were with less than 3 months of purchase and kept at construction sites prior to construction.

The methodology adopted include nital TM test analysis on the cross section of the specimen and optical microscopic studies on the cross-sectional surface of the collected surface.

Table 1 Composition of the rebars collected

Element	Composition as per IS 1786:2008	Composition-1 of collected rebar	Composition-2 of collected rebar
C	0.03	0.22–0.27	0.23
S	0.055	0.014–0.028	0.035
P	0.045	0.017–0.047	0.035
Mn	–	0.75–1.15	≥ 60
Al	–	0.008–0.071	-
Cr	–	0.01–0.032	-

2.1 Nital TM Ring Test

Nital TM ring test, a qualitative test suggested by [4] and given as a check to be used for TMT bars before usage. The test is contemplated as a field test. The procedure adopted is cutting the rebar along the cross-section and polishing the specimen with sand papers of different grades of 320, 600, 800, 1000, 1500 and 2000 in the respective order and subsequent clothing so as to obtain a mirror like finish. The specimen is then poured with nital solution on the top of the cross-sectional area of the specimen. The TM ring becomes visible by naked eye and could be then photographed. A quality light is to be ensured while photographing the TM and FP regions obtained.

2.2 Optical Microscopy

The microstructure was analyzed using an optical microscope. The procedure for specimen preparation is to be taken with great care for obtaining accurate microstructure [4]. The sample is initially grinded for obtaining a leveled surface as shown in Fig. 1a. Then, the specimen cross section is polished with sandpapers of grade 320, 400, 600, 800, and 1500 in order with a glass plate at the bottom as shown in Fig. 1b. Specimen is rotated at right angle every time the sand paper grade is changed. The scratch-free mirror-like finish is obtained as given in Fig. 1c. Finally, clothing is done with the help of clothing machine given in Fig. 1d. The specimen is then etched with 5% nital for the proper reveal of the metal microstructure. Nital is the solution prepared with the proportion of 95 ml ethanol or ethyl alcohol and 5 ml concentrated nitric acid, as per ASTM E407. The art of specimen preparation is to be excelled in obtaining a proper microstructure of the metal. Otherwise, damage to specimens unnecessarily occurs.

3 Results and Discussions

3.1 Nital TM Ring Test

Nital TM ring test was done to infer the distribution of tempered martensite and ferrite pearlite distribution in the cross-section of the TMT rebar. Two extreme phase distributions were obtained from the test. As reported by [5], there is a definite difference in the obtained TM-FP regions based on manufactures. Specimen with composition-1 revealed no TM region at all. While the specimen with composition-2 showed a clearly defined TM-FP region.

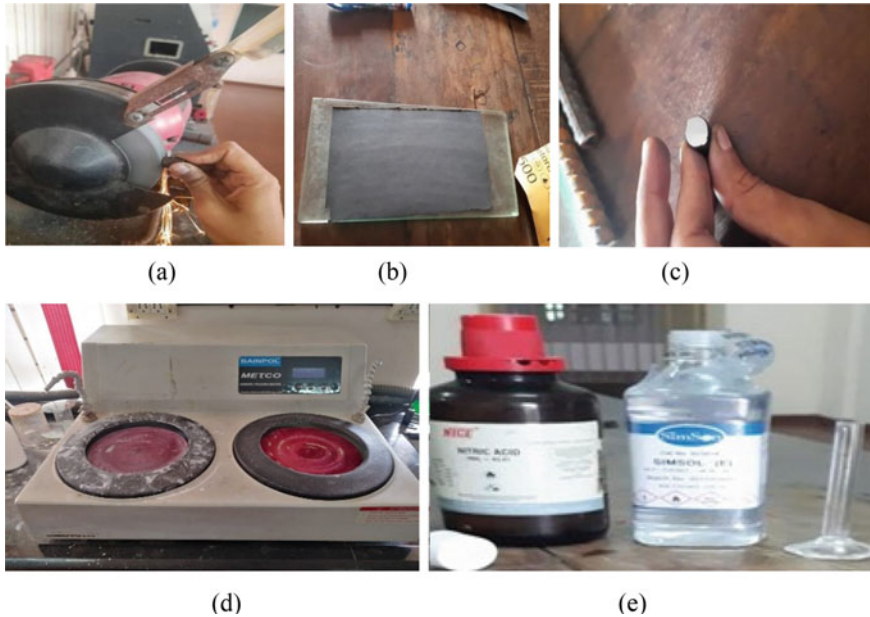


Fig. 1 Test specimen preparation steps **a** Grinding of specimen for surface leveling **b** Polishing specimen with sandpapers kept on a glass plate to obtain a **c** Mirror-like finished specimen **d** Clothing machine **e** Etching done using nitric acid and ethanol

The TM region in the etched microstructure gives a higher yield and the FP region gives ductility to the TMT bar. So, for obtaining desirable quality in rebars with proper strength and ductility, both FP and TM ring is to be present in the rebar in the specimen with composition-2. The composite action is detailed by [6]. Maximum hardness is reported to be obtained at the periphery which is in the TM ring area and gradually decreases inwards as we reach the core area [7]. The discontinuous and non-uniform tempered martensitic peripheral ring increase corrosion susceptibility in the reinforcing bars [8]. Phase distribution is chiefly governed by the cooling and tempering process adopted during the rebar manufacturing [9]. The manufacturing process is to be monitored precisely by all manufactures so as to provide reliable rebars at the market. The nital TM ring test result obtained in the present study is germane to the rebar quality available in the market (Fig. 2).

3.2 *Microstructure Based on Optical Imaging*

Optical microscopic images were taken after specimen preparation as explained in Sect. 2.2. The optical microscopic images were captured using QS-17 AT, QS Metrology and MIAS software. The magnifications of 10x and 20x were taken. The



Fig. 2 Nital TM ring test results of collected samples with **a** Composition-1 and **b** Composition-2

etched specimen was washed thoroughly and air dried using a drier before observing the microstructure under the microscope. The etching time was kept strictly 2 s. Higher etching time resulted in over etched samples with distorted microstructure. While specimen without etching did not reveal a proper microstructure.

The collected specimens revealed an altered microstructure in the cross-sectional area when observed with the optical microscope. The actual microstructure of the core was obtained only in freshly cut specimen which was in par with the microstructure as reported by [10, 11] and is given in Fig. 3a. All other specimens showed localized variations in the microstructure. This could possibly be due to atmospheric exposure. The optical microstructural imaging (OMI) of rebar microstructure of specimen with composition-1 showed localized deformations and pits as seen in Fig. 3c, d.

A green color was visible in the OMI of the rebar with composition-2 and slightly in microstructure of composition-1 as seen in Fig. 3e and b respectively. Green rust or $\text{Fe}(\text{OH})_2$ is an unstable corrosion product but, when oxidized forms Fe_2O_3 , forming a multilayer of rust [12]. This green rust formation is possibly due to the rebar exposure to environment. Rebars at sites are in proximity of such exposures [13]. These observed changes in microstructure can influence corrosion rate of carbon steel [14].

Tempcore is said to be a better alternative than thermex for corrosion resistance [15]. It is the cooling stage in the steel manufacturing process that control the microstructure of steel rebars. While TM-FP microstructure is given much important in literature, the actual microstructure obtained in the microscope is often given lesser importance. This is addressed in this work.

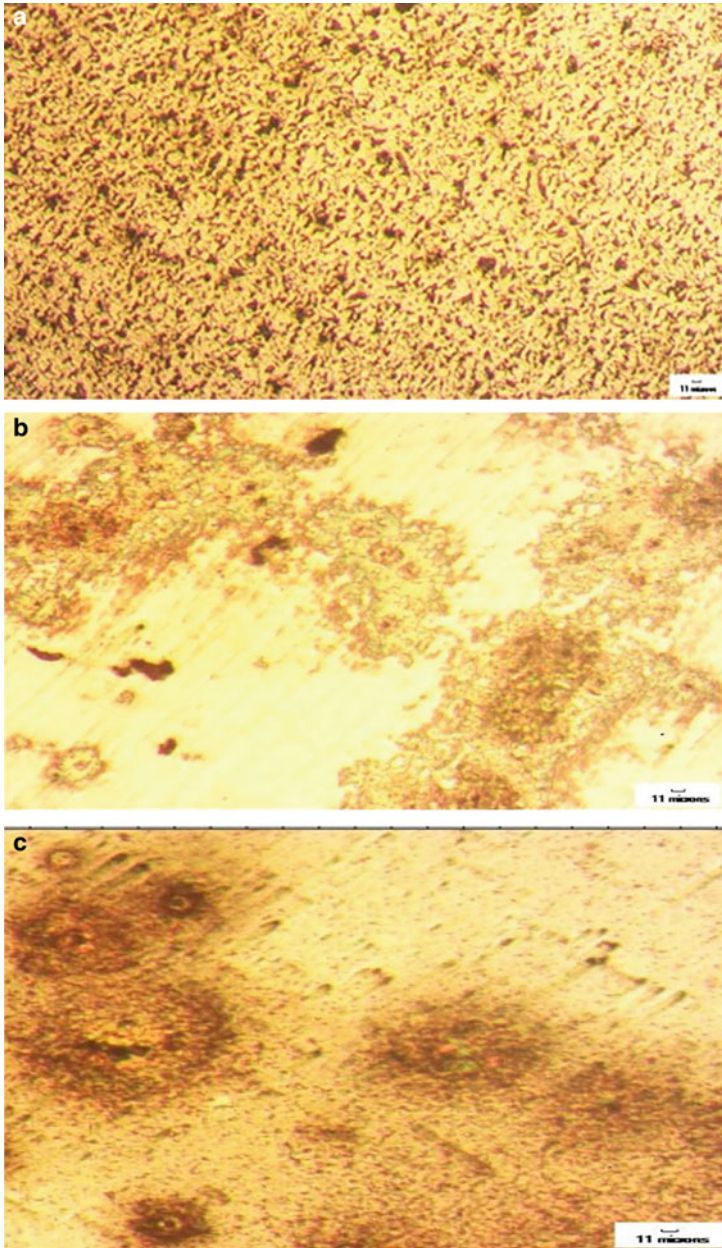


Fig. 3 a Cross-sectional microstructure of the core of a freshly cut TMT rebar under optical microscope in 10x magnification b Optical image of the core area of rebar with chemical composition-1 in 10x magnification c Optical microscopic imaging of core of rebar with composition-2 in 10x magnification d Optical image of the core area of rebar specimen with composition-1 in 20x magnification e Optical image of core area of rebar specimen with composition-2 with 10x magnification

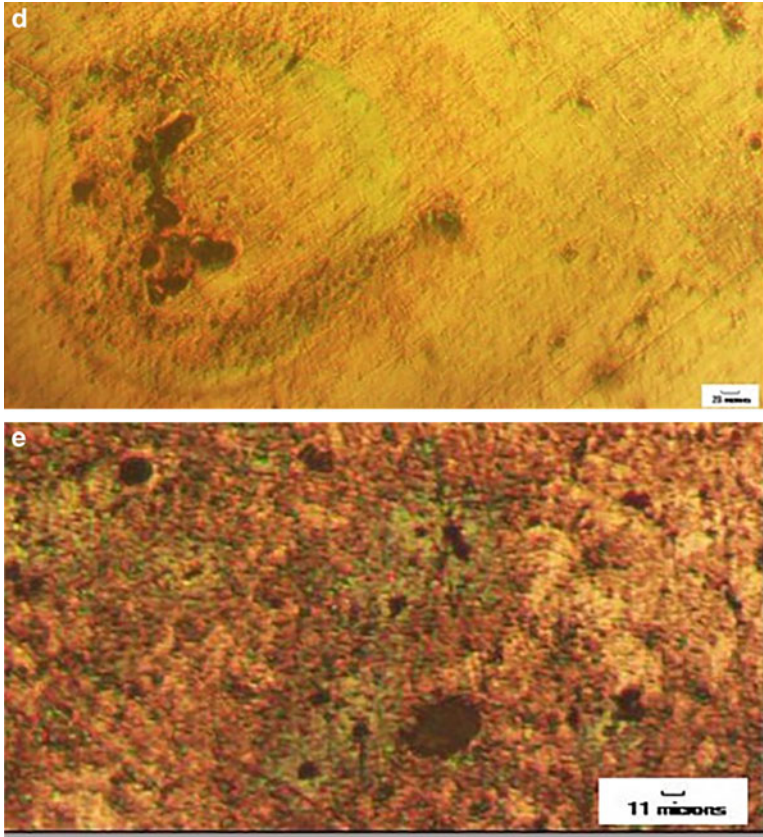


Fig. 3 (continued)

4 Conclusion

The study emphasized on the quality of rebar available at sites. Rebars with two different elemental composition were taken for the study. Some of the important takeaways from the work include:

- (1) The TM ring available in the market of the two rebar compositions considered were obtained in its extremities. Composition-1 showed no TM ring at all. While composition 2 showed fully adequate TM ring.
- (2) The optical microscopic image showed critical alterations in the microstructure. The ferrite region in the microstructure was seen to be distorted in the microscopic images.
- (3) The presence on green rust that would initiate pitting corrosion on the surface was seen in the surface of rebar on mere period of atmospheric exposure.

- (4) In addition to the manufacturing process, the difference in elemental composition among different rebars were also found.
- (5) The need for elemental composition control was also found necessary, as the difference between the two set of rebar selected were only in elemental composition other than the manufacturing process.
- (6) Earlier studies have highlighted the need for proper control on manufacturing process in terms of cooling time in the thermal mechanical treatment process, but little have been emphasized on the adherence to elemental composition.

References

1. Varghese A, Koshy BI (2022) Structural health monitoring aided by neural networks. In: Second international conference on next generation intelligent systems (ICNGIS). Kottayam, India, pp 1–6. <https://doi.org/10.1109/ICNGIS54955.2022.10079879>
2. Bandyopadhyay K, Lee J, Shim JH, Hwang B, Lee MG (2019) Modeling and experiment on microstructure evolutions and mechanical properties in grade 600 MPa reinforcing steel rebar subjected to TempCore process. *Mater Sci Eng* 745:39–52. <https://doi.org/10.1016/j.msea.2018.12.079>
3. Noville JF (2015) TEMP CORE®, the most convenient process to produce low cost high strength rebars from 8 to 75 mm. In: Proceedings of the METEC and 2nd European steel technology and application days (ESTAD) conference. Düsseldorf, Germany, pp 15–19
4. Nair SAO, Pillai RG (2017) TM-ring test-A quality control test for TMT (or QST) steel reinforcing bars used in reinforced concrete systems. *Indian Concr Inst J* 18(1):27–35
5. Al-rubaiey SI, Anoon EA, Hanoon MM (2013) The influence of microstructure on the corrosion rate of carbon steels. *Eng Technol J* 31(10):1825–1836
6. Nair SA, Mohandoss P, Ram K, Adnan T, Pillai RG (2023) Mechanical characteristics of quenched and self-tempered (QST or TMT) steel reinforcing bars used in concrete structures. *Constr Build Mater* 11(363):129761
7. Nandi SK, Tewary NK, Saha JK, Ghosh SK (2016) Microstructure, mechanical properties and corrosion performance of a few TMT rebars. *Corros Eng Sci Technol* 51(7):476–488
8. Nair SA, Pillai RG (2016) Effect of phase distributions on the corrosion of quenched and self-tempered (QST) steel rebars. In: Proceedings of 70th RILEM week and international conference on materials, systems and structures in civil engineering, 15–29 Aug. Lyngby, Denmark
9. Li CH, Chen CY, Tsai SP, Yang JR (2019) Microstructure characterization and strengthening behavior of dual precipitation particles in CuTi microalloyed dual-phase steels. *Mater Des* 166:107613
10. Doi K, Hiromoto S, Shinohara T, Tsuchiya K, Katayama H, Akiyama E (2020) Role of mill scale on corrosion behavior of steel rebars in mortar. *Corros Sci* 177:108995. <https://doi.org/10.1016/j.corsci.2020.108995>
11. Kabir IR, Islam MA (2014) Hardened case properties and tensile behaviours of TMT steel bars. *Am J Mech Eng* 2(1):8–14
12. Bautista A, Pomares JC, González MD, Velasco F (2019) Influence of the microstructure of TMT reinforcing bars on their corrosion behavior in concrete with chlorides. *Constr Build Mater* 229:116899

13. Varghese A, Koshy BI (2023) Risk perception on building construction safety. *Mater Today Proc.* <https://doi.org/10.1016/j.matpr.2023.04.070>
14. Clover D, Kinsella B, Pejcic B, De Marco R (2005) The influence of microstructure on the corrosion rate of various carbon steels. *J Appl Electrochem* 35:139–149
15. Pradhan B, Bhattacharjee B (2007) Role of steel and cement type on chloride-induced corrosion in concrete. *ACI Mater J* 104(6):612

BaFNet: A Soil Erosion Control Net Using Banana Pseudo-stem Fibers



Rolando Bitagun Jr., Angelo Lui Agustin, Noel Frederick Figueroa, Vaneza Lapangan, Princess Anne Layugan, Lester Ramirez, Marc Aeron Reyes, Frances Lorane Calapini, and Ertie Abana

Abstract Soil erosion is a naturally occurring process that affects all landforms determined by four fundamental factors: soil characteristics, vegetative cover, topography, and climate. Various soil erosion control is processed to lessen and delay from happening using different parts of a plant. Hence, this study aimed to produce BafNet and compare it to Coconet in terms of water absorption capacity, tensile strength, and net efficiency or soil reduction efficiency. It was revealed that the banana pseudo-stem fiber (BPSF) rope could absorb more water than the coco fiber rope by 39%. Also, it is stronger than the coco fiber rope by 165.2 N and 5.85 MPa for a one-meter rope having a diameter of 6 mm. For torrential rain on a silty type of soil at a 30° slope, the results exhibited that BafNet is more efficient than the Coconet by 11%.

Keywords Banana pseudo-stem fiber · Erosion control net · Soil erosion · Soil reduction efficiency · Tensile strength · Water absorption capacity

1 Introduction

Soil erosion is a natural process and form of soil degradation when the upper layer of soil is displaced by the dynamic activity of erosive agents such as wind, water, and mass movement. It has been an increasingly recognized problem due to expanding population and growing concern for food supply and water resources every year. This condition causes great destruction to soil characteristics and its properties and fertility, affecting countless numbers of individuals [1]. It also leads to a series of events, including the devastation of natural vegetation, loss of prime lands for

R. Bitagun Jr. · A. L. Agustin · N. F. Figueroa · V. Lapangan · P. A. Layugan · L. Ramirez · M. A. Reyes · F. L. Calapini

School of Engineering, Architecture, and Information Technology Education, University of Saint Louis, Tuguegarao City, Philippines

E. Abana (✉)

Center for Engineering Research and Technology Innovation, University of Saint Louis, Tuguegarao City, Philippines

e-mail: ertie04@gmail.com

food production, and the opening of ecologically fragile lands. In the Philippines, about 45% of the arable lands have been moderately to severely eroded, causing the movement of subsistence farmers to marginal lands with the hope of meeting their daily food requirements. Approximately 5.2 M ha have been eroded severely, while 8.5 M ha are moderately eroded, resulting in a 30-50% reduction in soil productivity and water retention capacity [2].

Because of its natural process, its occurrence is unpredictable; therefore, recent studies have focused on preventive measures for this problem by providing erosion control measures. One of the current solutions for soil erosion problems is using degradable geosynthetics to prevent soil loss from the seedbed and vegetation establishment for sufficient site protection [3]. The most common temporary, degradable systems are erosion control netting (ECN), open weave meshes (ECM), and erosion control blankets (ECB). This provides a non-eroding environment, effective, affordable, and compatible with sustainable land management practices [4]. For example, the Coconet [5] and Baconet—Banana Fiber and Coconut Coir [6] are used in the Philippines as effective soil erosion control.

On the other hand, banana is one of the major agricultural products of the Philippines, producing 9.36 million metric tons on 447,889 ha, with Cavendish cultivars accounting for about 53% of total banana production, Saba (28%), and Lakatan (10%) in the year 2018. Among the regions, Cagayan Valley is one of the major producers of Saba or Cardava Bananas [7]. However, banana pseudo-stem usually becomes biomass waste once the harvest time of banana fruit is finished [8]. Thus, many studies have been conducted on banana fibers to increase and promote an eco-friendly environment. Some of the products made from banana fibers are reinforcing materials, textiles, polymer matrix, packaging material, tablecloth, handicrafts, and paper sheets.

Based on the different studies, the banana pseudo-stem fibers (BPSF) are considered the high-quality fiber in terms of their physical properties. Specifically, the BPSF has a good modulus of elasticity, tensile strength, stiffness, low density, and strong moisture absorption quality, making it a promising fiber material [8–11]. The study [8] also shows that the durability of BPSF can stay up to three months of storage. However, if the storage period of the fiber is longer than three months, its tensile strength is considerably decreased. Moreover, By utilizing alternative natural fiber resources like BPSF, the accumulation of agricultural waste, including banana pseudo-stems, can be minimized. This approach helps address the problem associated with the disposal of biomass waste. In addition, properly designed and installed soil erosion control can significantly reduce soil erosion [12].

Although the combination of banana and coconut fibers [6] has been studied and used as slope protection, it is worthwhile to study the banana fiber as another soil erosion control material separately. The previous studies revealed different products made from banana fibers, but no one produced soil net using it. Therefore, this current study focused only on producing a soil net called BafNet fabricated from BPSF. The net was then subjected to a tensile strength test, water absorption capacity test, and surface run-off simulation to test its performance efficiency in mitigating soil erosion.

2 Methods

2.1 Fabrication of BafNet

The banana plantation was visited in Rizal, Cagayan, to ask permission from the owner to get some of the banana (Saba) trees that have been harvested. It was cut into one-meter lengths and transported to Tuguegarao City for preparation in Fig. 1. This process helped the owner reduce the agro-waste by converting it into more useful materials such as the net.

The collected banana pseudo-stems in Fig. 2 were cleaned up to remove impurities before the extraction process. Banana Pseudo-Stem Fibers (BPSF) were separated from the stems by a water retting process, soaking it within a 24-h duration. In Fig. 3, the fibers were extracted by scraping the soaked BPSF with a scraper tool to remove the remaining lignin and hemicellulose. Then, the fibers were collected and air-dried until the free water content was removed.

After extracting the BPSF, a single rope was manually fabricated. Figure 4 shows a single rope made by braiding two even lengths and sections of BPSF in the same direction. As the rope's tip approached, another pair of BPSF was joined to overlap the previous pair's tails and secure the connection between the ropes. This step was repeated until the desired length was achieved. After that, the BafNet was woven in the traditional open-weave design in Fig. 5 by intertwining the single rope at right angles to each other. The mesh opening size of the BafNet is 25mm \times 25mm and

Fig. 1 Collection of BPS



Fig. 2 Removing the impurities

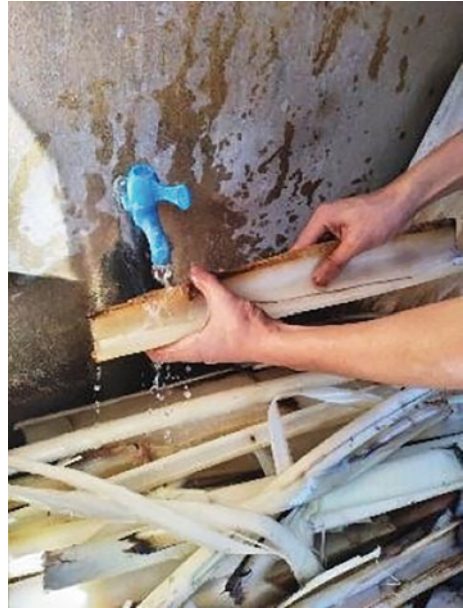


Fig. 3 Fiber extraction



dimensions of 825 mm \times 425 mm to match the commercially available Coconet sample.

2.2 BafNet Testing

Tests were performed to identify the physical properties of BafNet in terms of water absorption capacity and tensile test of the single rope made of fibers. These properties are essential in determining how much will the soil net uphold the soil from erosion.

Fig. 4 Braiding of a single rope



Fig. 5 Weaving of ropes



The water absorption capacity of the fiber ropes was determined using the method described in ASTM D570—98. A laboratory balance scale was used to record the dry mass (m_{dry}) of a single fiber rope. It was submerged in water for 24 h and the fiber rope was pat dry with a clean cloth to record its wet mass (m_{wet}) [13]. Five BPSF ropes and five coco fiber rope samples with a length of 500 mm and a diameter of 6 mm were used in this process. The water absorption capacity (WAC) of the fiber rope was computed as:

$$WAC = \frac{m_{wet} - m_{dry}}{m_{dry}} \times 100\% \tag{1}$$

The tensile strength test was performed manually because the Universal Testing Machine (UTM) for fiber ropes is not accessible in the locality. Figure 6 demonstrates a one-meter fiber rope carrying an empty bucket fastened to a horizontal rod 2 m above the ground. Before the test, the mass of the empty bucket was recorded (m_{bucket}). Weights (sands) were gradually added to the bucket until the rope broke. The mass of the bucket with the weights (sands) was measured (m_{total}) at the breaking point. This method was applied on five BPSF ropes and five coco fiber rope samples. The tensile stress (σ) was computed as:

$$\sigma = \text{net weight} / \text{cross-sectional area of the rope} \quad (2)$$

where

$$\text{net weight} = (m_{\text{total}} - m_{\text{bucket}})(9.81) \quad (3)$$

The measured time it took for the showerhead to fill up a 95 mm container with water was used to calculate the average rainfall intensity used in the soil run-off simulation. A surface run-off test was conducted on a soil testbed with a 30° slope to simulate a run-off scenario using water as the primary agent of weathering and erosion [14]. Three soil testbeds with 865mm (l) × 445mm (w) dimensions were created. In Fig. 7, soil bed A was the bare soil, soil bed B was the soil with Coconet, and soil bed C was the soil with BafNet. For the erosion control test, an artificial rainfall which was water coming from three shower heads (one for each soil testbed),

Fig. 6 BPSF rope carrying a bucket



Fig. 7 Experimental Test Beds: **a** Bare soil **b** with Coconet **c** with BafNet



was installed 1-foot above and perpendicular to the top of the soil testbed. For 25 min, the rainfall intensity remained constant. Surface run-off from the top of the soil was channeled to a catchment basin by a gutter (plastic) installed at the bottom of the slope. Every 5-min interval, the volume of the run-off in the basins was measured [14]. Before being measured (m_{dry}), the collected sediments were filtered out with a canvas cloth and sun-dried. The sediment yield was evaluated as the rate of sediment removal from the watershed per unit area during a specified time and was calculated as:

$$\text{Sediment Yield} = m_{dry} / (\text{surface area} \times \text{time}) \quad (4)$$

The performance efficiency of the BafNet and Coconet in mitigating soil erosion was evaluated using formula (5), where ($m_{dry, covered}$) represents the dry weight of the sediments eroded from the soil net-covered slope and ($m_{dry, uncovered}$) represents the dry weight of the sediments eroded from the bare soil-uncovered slope [14].

$$\text{Net efficiency} = m_{dry, uncovered} - m_{dry, covered} \times 100 \quad (5)$$

3 Results and Discussion

3.1 Properties of the Fibers

The water absorption capacity of the Coco Fiber rope and BPSF rope in Table 1 was calculated and recorded using formula (1). It shows that the coco fiber rope and BPSF rope have an average water absorption capacity of 220% and 259%, respectively. This implies that the BPSF rope can absorb more water than the coco fiber rope by 39%.

Table 1 Water absorption and tensile strength of CocoNet and BafNet

Sample	Water absorption (%)	Tensile Load (N)	Tensile stress (MPa)
CocoNet	220	179.92	6.36
BafNet	259	345.12	12.21

This behavior was explained in the study of [15] that banana fibers are hydrophilic, resulting in a high water absorption capacity.

Table 1 also records the results of the tensile strength test conducted on five samples of 6-mm diameter coco fiber ropes and BPSF ropes, using Formulas 2 and 3. The findings reveal that the coco fiber rope exhibited an average tensile load of 179.92 N and an average tensile stress of 6.36 MPa. In contrast, the BPSF rope demonstrated a higher average tensile load of 345.12 N and an average tensile stress of 12.21 MPa. This indicates that the BPSF rope is approximately 63% stronger than the coco fiber rope. Moreover, when compared to a 6-mm diameter bamboo rope [13], the BPSF rope surpassed it by 12%, with an average tensile load of 428.68 N and an average tensile stress of 10.65 MPa, as determined using a universal testing machine. Hence, these results highlight the enhanced durability of the BPSF rope, particularly in terms of tensile strength.

It is worth noting that while banana pseudo-stem fibers possess inherent biodegradability, utilizing them in this application with longer lifespans may require a balance between their biodegradable nature and the use of protective measures to extend their useful life. To promote a longer lifespan, it is important to consider appropriate treatments and coatings that can enhance their durability and resistance to degradation. Applying protective coatings, such as natural or synthetic polymers, can help increase their resistance to moisture, UV radiation, and microbial attacks, thereby extending their useful life.

3.2 *Sediment Yield Analysis and Soil Loss Reduction Efficiency*

The simulation's average rainfall intensity was 5307 mm/hr which falls under the category of torrential rain. According to Philippine Atmospheric, Geophysical, and Astronomical Services Administration (PAGASA), more than 30 mm of rain is observed in 1 h of torrential rain. Therefore, in low-lying areas, severe flooding is likely to occur. Surface run-off simulation was executed to compare erosion rates between bare and soil net-covered slopes. The first 5 min of the simulation was omitted to allow full saturation of the soil [14].

Table 2 summarizes the results of the sediment yield results from three testbeds. The results showed that the bare soil has an average of 10,730.53 (g/m².hr), Coconet has an average sediment yield of 1120.66 (g/m².hr), and BafNet has an average of 165.25 (g/m².hr) during torrential rain on a silty type of soil at 30° slope. The

Table 2 Sediment yield and net efficiency of CocoNet and BafNet

Rainfall Duration (minutes)	Sediment Yield (g/m ² ·hr)			Net Efficiency (%)	
	Bare soil	Coconet	BafNet	Coconet	BafNet
10	12,256.41	819.90	176.14	93	98
15	12,952.13	1116.46	319.02	91	97
20	11,562.77	768.46	112.23	93	99
25	6150.81	1778.22	53.62	71	99

Coconet accumulated 955.41 (g/m²·hr) more sediment yield than the BafNet. The lower the sediment yield, the more controlled the soil erosion. Thus, soil erosion is most controlled in the BafNet. Furthermore, soils with soil-net-cover consistently showed a significant reduction in sediment yield compared to the bare soil testbed. This is due to the water absorption property of the Coconet and BafNet, which lessens the impact of a raindrop on the soil surface layer. However, during the 25th minute of rainfall, the bare soil and soil with Coconet attained their maximum sediment yield of 6150.81 (g/m²·hr) and 1778.22 (g/m²·hr), respectively, which can be attributed to the scouring of the soil in testbed A and B. In contrast, the soil with BafNet reached the lowest sediment yield of 53.62 (g/m²·hr) during that period.

Calculating the net efficiency or soil loss reduction efficiency using formula (5) determines the effectiveness of soil net in reducing soil loss during run-off. The result of 5-min interval rainfall is tabulated in Table 2.

For torrential rain on a silty type of soil at a 30° slope, the results exhibited that BafNet has an average of 98% reduction efficiency while Coconet has an average of 87%. The BafNet is more efficient than the Coconet by 11%. Moreover, the net efficiency of BafNet is higher than that of Jute and Coir Erosion Control Blankets, with a net efficiency of 66% for 30° slopes and 78% for 60° slopes [14], Bambusa Blumeana Fiber Mat with 74% for 60° slope [13], and Water Hyacinth Fiber Mat (WHFM) with 78% for 30° slope [14]. The present study confirmed the findings in [10] about BafNet being a feasible replacement for commercially available soil nets.

4 Conclusion

The performance efficiency of the BafNet in mitigating soil erosion was investigated in this study in terms of water absorption capacity, tensile strength, and soil loss reduction efficiency using surface runoff simulation or rainfall simulation. The water absorption capacity of the BafNet reduced the damaging impact of raindrops, making it effective in mitigating surface erosion and subsequent slope failure. The BPSF rope is more flexible and can carry larger loadings. Also, the BafNet prevented significant mass runoff from the topsoil during the simulation.

To further validate the results of this study, it is recommended to conduct sediment runoff analysis on actual slopes, considering factors such as the diameter of the rope, mesh openings, dimension of the soil net area, degree of inclination, and different soil types. Additionally, utilizing a tensile testing machine for natural fiber and incorporating an anchoring system is highly advised. These modifications and additions will provide a more comprehensive understanding of erosion control techniques, their adaptability across various conditions, and the long-term effectiveness of the selected materials and measures.

References

1. Decano CS, Malamug VU, Agulto ME, Gavino HF (2016) Development of corn (*Zea mays* L.) stalk geotextile net for soil erosion mitigation. *Int J Mater TextE Eng* 10(10):618–623
2. Philippines department of agrarian reform: the Philippine national action plan to combat desertification, land degradation, drought, and poverty (2004)
3. Fortea-Verdejo M, Bumbaris E, Burgstaller C, Bismarck A, Lee KY (2017) Plant fibre-reinforced polymers: where do we stand in terms of tensile properties? *Int Mater Rev* 62(8):441–464
4. Guerra AJT, Bezerra JFR, Fullen MA, Mendonça JKS, Jorge MCO (2015) The effects of biological geotextiles on gully stabilization in São Luís, Brazil. *Nat Hazards* 75:2625–2636
5. Department of public works and highways: amendment to DPWH standard specification for item 622-coconet bio-engineering solutions (2016)
6. Hernandez CS, Almanzor N, Marcos MCM (2018) Properties and behavior of banana fiber and coconut coir (Baconet) Geotextile. In: *Advances in civil, environmental, & materials research (ACEM18)*. Songdo Convensia, Incheon, Korea
7. OpenSTAT—Philippine statistics authority. <https://openstat.psa.gov.ph/>. Accessed 18 Jan 2023
8. Subagyo A, Chafidz A (2018) Banana pseudo-stem fiber: preparation, characteristics, and applications. *Banana nutrition-function and processing kinetics*, pp 1–19
9. Mukhopadhyay S, Figueiro R, Arpaç Y, Şentürk Ü (2008) Banana fibers—variability and fracture behaviour. *J Eng Fibers Fabr* 3(2):155892500800300207
10. Jiyas N, Kumar B, John M (2016) Synthesis and mechanical characterization of woven banana and glass fiber reinforced epoxy composites. *IJSER* 7:32–38
11. Chen ML, Wu GJ, Gan BR, Jiang WH, Zhou, JW (2018) Physical and compaction properties of granular materials with artificial grading behind the particle size distributions. *Adv Mater Sci Eng*
12. Kavitha V, Aparna G (2021) A review on banana fiber and its properties. *Asian J Pharm Res Dev* 9(3):118–121
13. Valle SB, Albay RD, Montilla AM (2013) *Bambusa blumeana* fiber as erosion control geotextile on steep slopes. *IOP Conf Ser Mater Sci Eng* 513(1):12030
14. Chow MF, Hashrim H, Chong ST, Ng YJ (2019) Investigating the effectiveness of water hyacinth fiber mat for soil erosion control. *IOP Conf Ser Mater Sci Eng* 551(1):012008
15. Badyankal PV, Manjunatha TS, Vaggar GB, Praveen KC (2021) Compression and water absorption behaviour of banana and sisal hybrid fiber polymer composites. *Mater Today Proc* 35:383–386

Characterisation of Pyro-oil Modified EVA and SBS Bitumen Using Variation in MSCR Test



N. T. Bhagat, N. A. Hedaoo, and M. S. Ranadive

Abstract The multiple stress creep and recovery (MSCR) test is the most commonly used method to characterise the rutting resistance of bituminous binders. However, the stress levels of 0.1 and 3.2 kPa, employed in this test as per ASTM D7405 are insufficient to represent the non-linear viscoelastic behaviour of modified bitumen under practical traffic conditions. Therefore, the modified binders are required to be characterised at higher stress levels. The present study intended to analyse the permanent deformation behaviour of high-density polyethylene (HDPE) pyro-oil modified bitumen using variation in stress levels of the MSCR test. The base bitumen VG30 is modified using ethylene vinyl acetate (EVA) and styrene butadiene styrene (SBS) polymers. The base and polymer modified bitumen are further modified with HDPE pyro-oil which was obtained from the pyrolysis of HDPE plastic waste. MSCR test with additional stress levels of 5, 6.4, 10, 12.5, and 25 kPa is used to characterise the base, polymer, and pyro-oil modified bitumen. It was found that higher stress levels than the standard 3.2 kPa are required to obtain the non-linear behavior of polymer modified bitumen. The addition of pyro-oil increased the rutting resistance of EVA modified bitumen, whereas the same is found to be decreased for SBS modified bitumen.

Keywords Pyro-oil · EVA · SBS · MSCR · Stress levels · Rutting

N. T. Bhagat (✉)

Research Scholar, Department of Civil Engineering, College of Engineering, Pune 411005, India
e-mail: bhagat.nikita14@gmail.com

N. A. Hedaoo

Associate Professor, Department of Civil Engineering, College of Engineering, Pune 411005, India
e-mail: nah.civil@coep.ac.in

M. S. Ranadive

Department of Civil Engineering, College of Engineering, Pune 411005, India
e-mail: msrtunnel@yahoo.co.in

1 Introduction

Rutting is one of the most common distresses found in flexible pavements. It occurs in the form of permanent deformation due to the gradual accumulation of strain induced by traffic loadings. Rutting occurs as longitudinal depressions along the wheel path of a pavement. This reduces the service life of pavement and makes the ride uncomfortable and unsafe for the vehicles [1, 2]. The improvement of the rutting resistance of pavement is the topic of research for pavement engineers worldwide. It has been found that the rheological properties of bituminous binders are directly related to pavement distress [3, 4]. Therefore, enhancing the properties of bitumen by modification and characterizing their rheological response over a range of test conditions is necessary. The most important aspect of the pavement management system is evaluating the resistance to rutting and other pavement distress mechanisms, and using it to create an effective strategy regarding the maintenance and rehabilitation of pavement [5].

Modifying the bitumen using polymers is the most common technique used for increasing the rutting resistance of bitumen. The styrene–butadiene–styrene (SBS) and ethylene–vinyl–acetate (EVA) are the most commonly used types of polymers, i.e., elastomer and plastomer respectively for manufacturing polymer modified bitumen (PMB). Saboo et al. [6], investigated the rheological response of both EVA and SBS polymer modified binders. The study concluded that EVA modified binders show better performance at high temperatures, with lowest non recoverable creep compliance (J_{nr}), while the SBS modified binders performed well at the high and intermediate temperatures. High Density Polyethylene (HDPE) is also one of the polymers (Plastomer) that is used as a bitumen modifier. Piromanski et al. [7], used HDPE plastic as a bitumen modifier and evaluated the rutting performance of the modified binders using multiple stress creep and recovery (MSCR) test. The results showed that HDPE enhanced the rutting resistance of the modified binders. Hadole et al. [8], used HDPE pyro-oil for modification of VG30 bitumen and assessed its effect on the moisture damage susceptibility using surface free energy (SFE) approach. The study concluded that addition of HDPE pyro-oil, improved the moisture resistance of the bitumen. The influence of HDPE pyro-oil modification on characterization of oxidative aging of bitumen using FTIR spectra has also been done by Bhagat et al. [9], and the study revealed that HDPE pyro-oil helped in reduction of aging of the binders.

In the NCHRP 9–10 research program, based on the conducted creep studies during the program, a test named multiple stress creep and recovery (MSCR) test [10]. As per AASHTO T350 [11] and ASTM D7405 [12], this test is performed using dynamic shear rheometer, at 0.1 kPa and 3.2 kPa stress levels, for measuring the creep and recovery of the bituminous binders and mastics. Also, the linear and non-linear viscoelasticity of the binders and mastics is determined by this test. The parameter non recoverable creep compliance (J_{nr}) is calculated from the results of MSCR, as the ratio of average non-recovered strain of 10 cycles, to the applied stress for the 10 cycles. Another parameter called the recovery percent (%R) is determined

as the ratio of the average of recovered strain to that of the unrecovered strain for 10 cycles. It is an indicator of the degree of recovery when the bitumen or mastic sample is allowed to recover after repeated shearing. The rheological response of the bitumen is represented by both J_{nr} and %R, and are correlated well with the rutting performance of asphalt mixtures [13]. However, some researchers stated that the stress levels of 0.1 kPa and 3.2 kPa specified in the standards are arbitrarily selected and do not necessarily express the stresses at which the binder experiences and behaves non-linearly inside the pavement under heavy traffic loading [14, 15]. In some recent research [3, 15–17], recommended to use higher stress levels in MSCR test, as some modified binders show linear behaviour at standard stresses. Bahia et al. and Hossain et al. [18, 19], stated that the non-linear behaviour of the binders can be depicted if a stress level close to 12.8 kPa is added to the standard MSCR protocol and thus the rutting resistance of binders can be obtained more clearly. Saboo and Kumar [20], analysed the effect of different stress levels up to 30 kPa, on the virgin and polymer modified binders. From their research it was found that virgin binder behaves linearly at 0.1 kPa stress, and becomes very sensitive to change in stress after that, whereas the PMB does not show non-linear behavior up to as much as 10 kPa stress. From the above discussion, it becomes a necessity to assess the stress level at which bitumen modified with a new material, behaves non-linearly and represent the rutting resistant performance of the modified binders.

In the present study, HDPE pyro-oil has been used to modify the base bitumen VG30, SBS and EVA polymer modified binders. The effect of addition of pyro-oil on the rutting behavior of these binders is evaluated at different stress levels of 0.1, 3.2, 5, 6.4, 10, 12.8, and 25.6 kPa by varying the MSCR test conditions. The test is conducted at 50, 60, and 70 °C to analyse the effect of temperature on the variation on rutting performance of the binders.

2 Materials and Methodology

2.1 Materials

VG30 [21] bitumen was used as base bitumen for validating the proposed methodology. Three different modifiers are used for modification of the base bitumen consisting of two polymers SBS and EVA, and one pyrolysis oil named HDPE pyro-oil. HDPE pyro-oil is condensed from High Density Polyethylene (HDPE) by decomposition at high temperatures in the absence of oxygen. Here onwards the HDPE pyro-oil will be referred as 'pyro-oil'. HDPE plastic waste was collected from MSW plant at Sangavi, located in Pune City, Maharashtra, India. For the break down of plastic waste, the pilot pyrolysis reactor plant was developed at the Transportation Engineering Laboratory, Civil Department, College of Engineering, Pune, India. The HDPE plastic waste was pyrolysed at high temperatures of about 750°C. The working procedure of pyrolysis plant and the yield of plastic pyro-oils were

discussed by Kulkarni and Ranadive [22] in detail. The EVA, and SBS polymers in the form of pellets were procured from Rishiroop Polymers Pvt. Ltd., Mumbai, Maharashtra, India.

2.2 Methodology

The modified bitumen were prepared by mixing the base bitumen VG0 and the modifiers using a high shear mixer of the make T25 digital easy clean IKA instruments. 3% of SBS and 5% of EVA modifiers by weight of the base bitumen were selected for preparing the polymer modified binders. As per Bhagat and Ranadive [23], the three variables that are to be considered for modification of a bitumen are the shear rate, mixing temperature, and mixing time. For preparing the PMBs firstly, the base bitumen is heated at about 165–175 °C, then the respective polymers were added to the hot bitumen and mixed at a shear rate of about 6000 rpm for first 10 min and at 7500 rpm for 25 min. The base bitumen, SBS and EVA modified binders are then further modified with pyro-oil by adding 1% by weight of it to the binders. The pyro-oil modified binders were prepared by mixing the binders at about 150 °C with the pyro-oil at 5000 rpm for 15 min and at 3000 rpm for the last 5 min. The percentage of modifiers and the nomenclature of the binders is given in Table 1. Storage stability test was performed on the resulting PMBs and polymer plus pyro-oil modified binders as per ASTM D7131 [24]. The differences in softening points of the top and bottom samples after storage stability test were found to be less than 2.5 °C for all PMBs, indicating that the binders can remain stable at higher temperature. All the binders were tested for the physical properties like, penetration, softening point, ductility, viscosity, etc. The results of the physical properties of the base and modified binders are presented in Table 2.

The binders are subjected to short term aging using rolling thin film oven (RTFO) as per ASTM D 2872 [25]. The short term ageing of base bitumen, polymer and pyro-oil modified binder was carried out at 163 °C for 85 min in RTFO.

The rheological characterization is done using dynamic shear rheometer (DSR) of the made Discovery HR-1 of TA instruments. Temperature sweep test was performed using 25 mm parallel plate geometry of DSR at a constant angular frequency of 10 rad/

Table 1 Details of the modified binders

Sr. no	Modifier percentage	Name of binder
1	VG30	VG30
2	VG30 + 3% SBS	SBS3
3	VG30 + 5% EVA	EVA5
4	VG30 + 1% pyro-oil	VG30 + 1P
5	VG30 + 3% SBS + 1% pyro-oil	SBS3 + 1P
6	VG30 + 5% EVA + 1% pyro-oil	EVA5 + 1P

Table 2 Physical properties of binders

Binder	Penetration @25 °C (1/10th of mm)	Softening point (°C)	Ductility (cm)	Elastic recovery (%)	Viscosity @ 60 °C (poise)	Rotational viscosity at 135 °C (Pa.s)	Performance grade
VG30	55	50	10	–	2754	428	PG64—
SBS3	48	57	80	74	–	1655	PG70—
EVA5	47	58	85	72	–	1548	PG70—
VG30 + 1P	57	49	–	–	–	422	PG64—
SBS3 + 1P	50	53	–	72	–	1622	PG70—
EVA5 + 1P	44	60	–	73	–	1590	PG76—

s from 40 °C to 82 °C with an increment of 6 °C. This test is performed in order to determine temperature Performance Grade (PG grades) of the binders that are presented in Table 2.

The multiple stress creep and recovery (MSCR) test with stress levels of 0.1, 3.2, 5, 6.4, 10, 12.8, and 25.6 kPa is performed at the temperatures 50, 60, and 70 °C for all binders. The non-recoverable creep compliance (J_{nr}) and the recovery percentage (%R) are calculated by the following Eqs. 1 and 2.

$$J_{nr} = \frac{\sum_{i=1}^{10} \left(\frac{\varepsilon_{10}}{\sigma} \right)_i}{10} \tag{1}$$

$$R = \frac{\sum_{i=1}^{10} \left(\frac{\varepsilon_1 - \varepsilon_{10}}{\varepsilon_1} \right)_i}{10} \tag{2}$$

where,

σ = applied stress,

i = cycle number,

ε_1 and ε_{10} = strain accumulated in the creep period of one cycle and the strain accumulated in one creep and recovery cycle respectively and are calculated as follows using Eqs. 3 and 4.

$$\varepsilon_1 = \varepsilon_c - \varepsilon_0 \tag{3}$$

$$\varepsilon_{10} = \varepsilon_r - \varepsilon_0 \tag{4}$$

where,

ε_r = strain at the end of one cycle,

ε_c = strain at the end of the creep period of one cycle, and.

ϵ_0 = strain at the start of one cycle.

3 Results and Discussion

The effect of varying stress on the rutting performance of the base and modified binders is evaluated using non recoverable creep compliance (J_{nr}) and recovery percent (%R) values. The assessment of non-linear behaviour of all the binders is also done by observing J_{nr} variation with increasing stress. Figure 1a, b, c show the variation of J_{nr} with stress at 50, 60, and 70 °C respectively. The J_{nr} values show a general trend of increase with increase in stress for all binders irrespective of temperatures. This indicates that the binder becomes susceptible to rutting under heavier traffic loading. From the figure, it can be observed the EVA modified binders show the least J_{nr} values as compared to the SBS modified binder and base bitumen. Also, J_{nr} values increase after addition of pyro-oil for base bitumen VG30 and SBS3 binder, whereas it decreases for the EVA5 binder.

This indicates that the pyro-oil softens the base bitumen and is responsible for the breaking of polymer network in the SBS modified binder. However, the addition of pyro-oil stiffens the EVA modified binder, which may be due to the chemical interaction of plastomeric content in the HDPE pyro-oil with EVA as both HDPE and EVA are plastomers.

However, evaluation of only J_{nr} values is not sufficient, the recovery percent should also be taken into consideration as it is an indicator of the elasticity of binders. Higher the value of recovery percent, higher is the elasticity of the binder, which means after the removal of stress the strain recovery will be higher. Figure 2a, b, c shows the variation of recovery percent with varying the stress at 50, 60, and 70 °C respectively. It is found that EVA5 + 1P has the highest recovery percent as compared to other binders. This means that addition of 1% pyro-oil increased the elasticity of the EVA5 binder. However, the addition of pyro-oil to SBS3 and VG30 has reduced the recovery percent indicating the increase in viscous components in the modified binders. At 70 °C, the base bitumen VG30 and VG30 + 1P binders show negative recovery percent at higher stress. This is because of the development of very large strains due to high temperature and high stress. The high temperature performance grade of both VG30 and VG30 + 1P binders is 64 °C, which means that the binders cannot sustain above this temperature. Therefore, it could not recover at 70 °C, and lost the elastic property due to high stress. Such conditions make the binders enter the tertiary flow making them unstable [15].

The non-linear behaviour of the binders is assessed from the Fig. 3 which shows a semi-log line graph of J_{nr} values with variation in stress at 50 °C. The variation at all temperatures is similar, therefore only one graph at 50 °C is shown here. From the figure it can be observed that the base bitumen VG30 and the VG30 + 1P binder behave linearly only at 0.1 kPa stress, and enter the non-linear behaviour from 3.2 kPa. However, the non-linear behaviour of all the polymer modified binders starts after

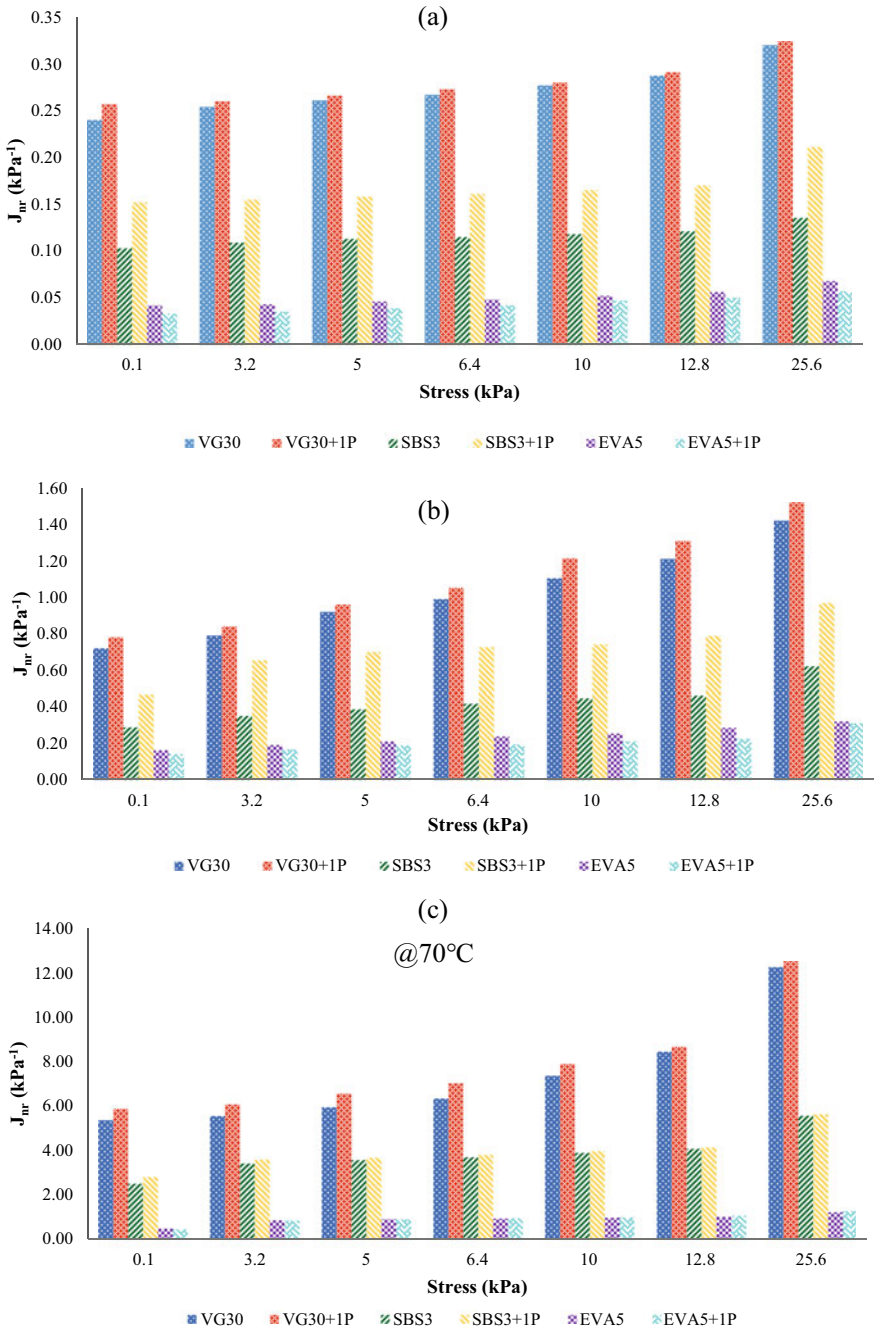


Fig. 1 Variation of J_{nr} values with stress at a $50\text{ }^{\circ}\text{C}$, b $60\text{ }^{\circ}\text{C}$, and c $70\text{ }^{\circ}\text{C}$

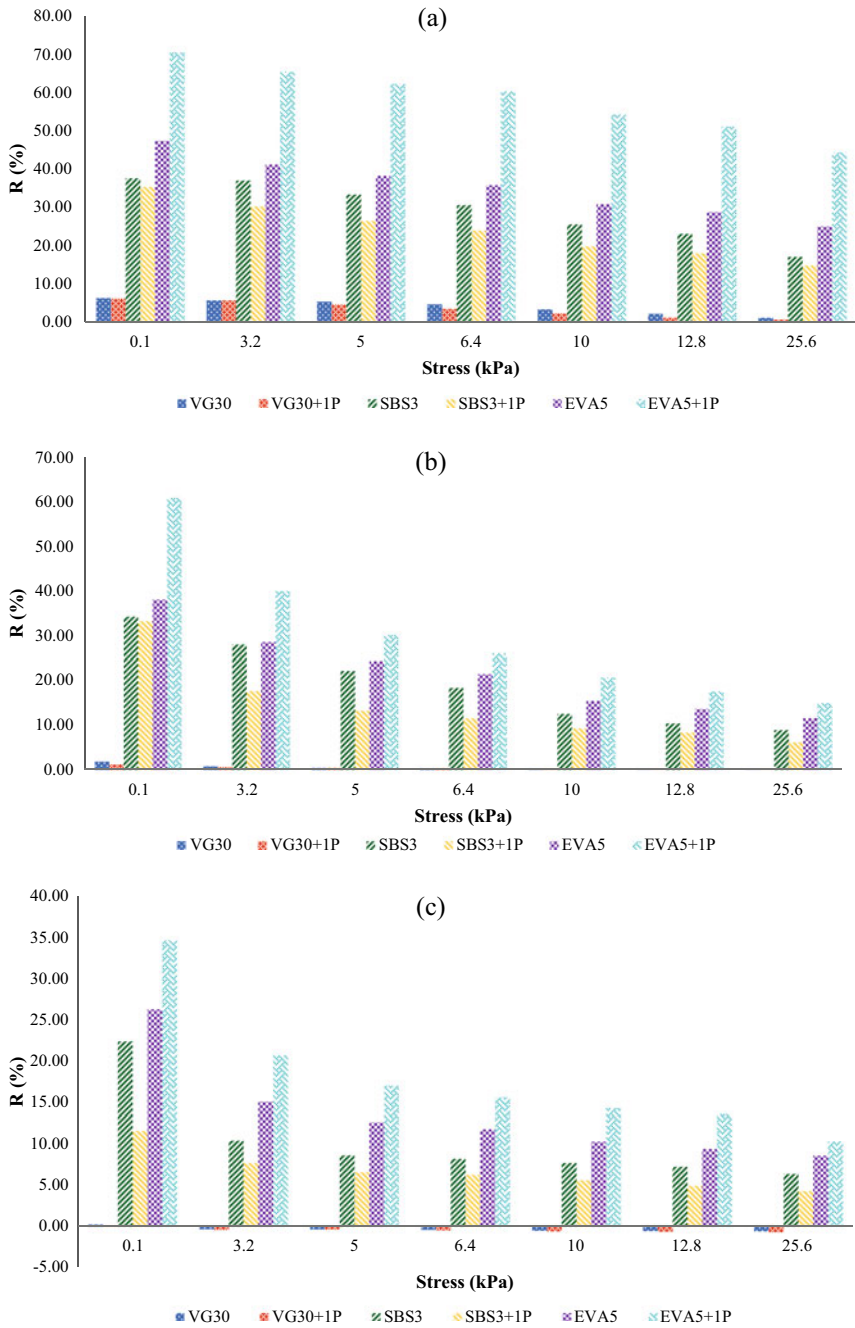


Fig. 2 Variation of %R with stress at a 50 °C, b 60 °C, and c 70 °C

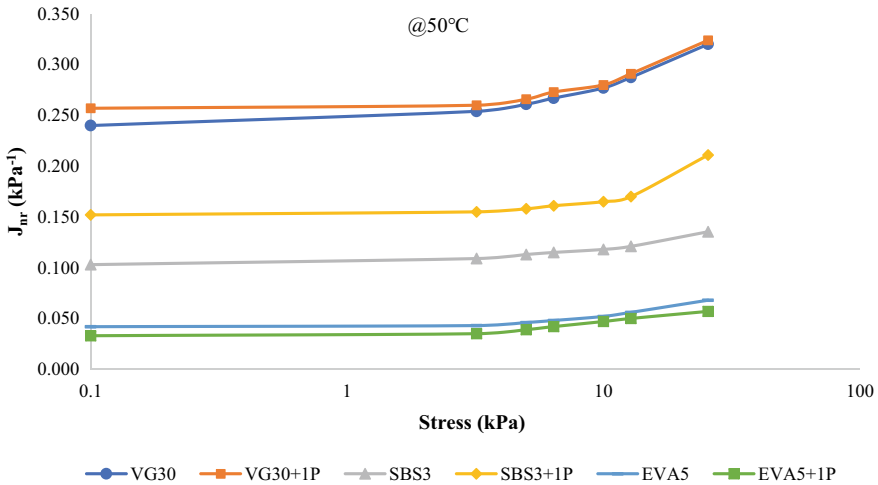


Fig. 3 Variation of J_{nr} vs. log of stress

12.5 kPa stress. This means that modified binders should be tested for additional stress levels in order to characterize the rutting resistance.

4 Conclusions

The study focussed on the rutting characterization of pyro-oil modified base and polymer modified bitumen by variation in stresses of the multiple stress creep and recovery test. HDPE plastic waste pyro-oil is used for modification of the base bitumen VG30 as well as polymer modified binders. The use of pyro-oil obtained from waste HDPE, helps reducing the plastic waste content from the municipal solid waste. These modified binders are then analysed for rutting behaviour using MSCR test including higher stresses like 5, 6.4, 10, 12.8, and 25.6 kPa. Following conclusions are drawn from the study:

- The bitumen, whether unmodified or modified behave non-linearly in the pavements under the various traffic loading and temperature conditions. It is necessary to test the binders in non-linear zone, i.e., under high stress levels. Additional stresses should be added to the MSCR test protocol in order to achieve this.
- The rutting resistance of EVA5 binder is enhanced by addition of 1% pyro-oil addition, whereas it reduced the rutting resistance for VG30 and SBS3 binders.
- The binders VG30 and VG30 + 1P starts showing non-linear behaviour 3.2 kPa onwards, while the polymer modified binders show non-linear behaviour after as high as 12.5 kPa stress.

References

1. Hajikarimi P, Rahi M, Moghadas Nejad F (2015) Comparing different rutting specification parameters using high temperature characteristics of rubber-modified asphalt binders. *Road Mater Pavement Des* 16:751–766. <https://doi.org/10.1080/14680629.2015.1063533>
2. Liu H, Zeiada W, Al-Khateeb GG, Shanableh A, Samarai M (2021) Use of the multiple stress creep recovery (MSCR) test to characterize the rutting potential of asphalt binders: a literature review. *Constr Build Mater* 269:121320. <https://doi.org/10.1016/j.conbuildmat.2020.121320>
3. Delgadillo R, Bahia HU (2010) The relationship between nonlinearity of asphalt binders and asphalt mixture permanent deformation. *Road Mater Pavement Des* 11:653–680. <https://doi.org/10.3166/RMPD.11.653-680>
4. Behnood A, Shah A, McDaniel RS, Beeson M, Olek J (2016) High-temperature properties of asphalt binders: comparison of multiple stress creep recovery and performance grading systems. *Transp Res Rec* 2574:131–143. <https://doi.org/10.3141/2574-15>
5. Domingos MDI, Faxina AL (2016) Susceptibility of asphalt binders to rutting: literature review. *J Mater Civ Eng* 28:04015134. [https://doi.org/10.1061/\(asce\)mt.1943-5533.0001364](https://doi.org/10.1061/(asce)mt.1943-5533.0001364)
6. Saboo N, Kumar R, Kumar P, Gupta A (2018) Ranking the rheological response of SBS- and EVA-modified bitumen using MSCR and LAS tests. *J Mater Civ Eng* 30. [https://doi.org/10.1061/\(asce\)mt.1943-5533.0002367](https://doi.org/10.1061/(asce)mt.1943-5533.0002367)
7. Piromanski B, Chegenizadeh A, Mashaan N, Nikraz H (2020) Study on HDPE effect on rutting resistance of binder. *Buildings* 10:1–12. <https://doi.org/10.3390/buildings10090156>
8. Hadole HP, Suryawanshi SD, Khapne VA, Ranadive MS (2021) Moisture damage resistance of short-term aged pyro-oil-modified bitumen using rolling thin film oven by surface free energy approach. *J Mater Civ Eng* 33:04021268. [https://doi.org/10.1061/\(asce\)mt.1943-5533.0003872](https://doi.org/10.1061/(asce)mt.1943-5533.0003872)
9. Bhagat NT, Hadole HP, Ranadive MS (2023) Oxidative aging characterization of pyro-oil modified binders using fourier transform infrared spectroscopy. *Adv Sci Technol Res J* 17:140–149
10. Bahia HU, Hanson DI, Zeng M, Zhai H, Khatri MA, Anderson RM (2001) Characterization of modified asphalt binders in superpave mix design
11. A. Standard, standard method of test for multiple stress creep recovery (MSCR) test of asphalt binder using a dynamic shear rheometer (DSR), T350-19 (2019)
12. A. D7405-20, Standard test method for multiple stress creep and recovery (MSCR) of asphalt binder using a dynamic shear rheometer (2020)
13. D'Angelo JA (2009) The relationship of the MSCR test to rutting. *Road Mater Pavement Des* 10:61–80. <https://doi.org/10.3166/RMPD.10HS.61-80>
14. Gopalipour A (2011) Modification of multiple stress creep and recovery test procedure and usage in specification, p 106. <http://144.92.161.87/handle/1793/56398>
15. Jafari M, Babazadeh A, Aflaki S (2015) Effects of stress levels on creep and recovery behavior of modified asphalt binders with the same continuous performance grades. *Transp Res Rec* 2505:15–23
16. Saboo N, Kumar P (2015) A study on creep and recovery behavior of asphalt binders. *Constr Build Mater* 96:632–640
17. D'Angelo J, Kluttz R, Dongre RN, Stephens K, Zanzotto L (2007) Revision of the superpave high temperature binder specification: the multiple stress creep recovery test (with discussion). *J Assoc Asph Paving Technol* 76
18. Bahia H, Tabatabaee HA, Mandal T, Faheem A (2013) Field evaluation of Wisconsin modified binder selection guidelines-Phase II. Wisconsin Highway Research Program
19. Hossain Z, Zaman M, Ghosh D (2015) Creep compliance and percent recovery of Oklahoma certified binder using the multiple stress recovery (MSCR) method, *Fhwa-Ok-14-19*, pp 1–5. https://www.researchgate.net/publication/313905146_CREEP_COMPLIANCE_AND_PERCENT_RECOVERY_OF_OKLAHOMA_CERTIFIED_BINDER_USING_THE_MULTIPLE_STRESS_RECOVERY_MSCR_METHOD

20. Saboo N, Kumar P (2018) Analysis of creep and recovery for modified binder. *Indian Highw* 46
21. I. 73-2013, Specification for paving bitumen. *Bur Indian Stand* (2013)
22. Kulkarni SB, Ranadive MS (2020) Modified Cutback as tack coat by application of pyro-oil obtained from municipal plastic waste: experimental approach. *J Mater Civ Eng* 32:04020100. [https://doi.org/10.1061/\(ASCE\)MT.1943-5533.0003079](https://doi.org/10.1061/(ASCE)MT.1943-5533.0003079)
23. Bhagat NT, Ranadive MS (2023) Review on mechanisms of bitumen modification: process and variables. *Recent Trends Constr Technol Manag*, 1185–1192
24. ASTM, ASTM D7131: Standard practice for determining the separation tendency of polymer from polymer modified asphalt (2005)
25. D. ASTM, Standard test method for effect of heat and air on a moving film of asphalt (rolling thin-film oven test), *USA Annu B ASTM Stand* (2012)